UC San Diego
UC San Diego Electronic Theses and Dissertations

Title

Synthesis and Reactivity Studies of Metallacyclobutenes and. eta. 4-Cyclopentadienes Derived Therefrom & Ruthenium Catalyzed Cyclizations of Conjugated tri-pi Systems

Permalink

https://escholarship.org/uc/item/48n2495k

Author

Qin, Pengjin

Publication Date

2020

Peer reviewed|Thesis/dissertation

UNIVERSITY OF CALIFORNIA SAN DIEGO

Synthesis and Reactivity Studies of Metallacyclobutenes and. eta. 4-Cyclopentadienes Derived Therefrom & Ruthenium Catalyzed Cyclizations of Conjugated tri-pi Systems

A dissertation submitted in partial satisfaction of the requirements for the degree Doctor of Philosophy

in

Chemistry

by

Pengjin Qin

Committee in charge:

Professor Joseph M. O'Connor, Chair
Professor Carlo Ballatore
Professor Guy Bertrand
Professor Charles L. Perrin
Professor Haim Weizman

2020

The dissertation of Pengjin Qin is approved, and it is acceptable in quality and form for publication on microfilm and electronically:

Chair

University of California San Diego

2020

DEDICATION

This dissertation is dedicated to my family,

to 覃非平,

to 肖中玉,

to 覃君烈,

to 舒秀珍,

to 王德延,

and to 肖伯胜.

EPIGRAPH

博学之，审问之，慎思之，明辨之，笃行之

《中庸》

TABLE OF CONTENTS

LIST OF SCHEMES

xvii

LIST OF FIGURES

xxvii

LIST OF TABLES

LIST OF ABBREVIATIONS

Å = Angstrom (10^{-10} m)

AIBN = azobisisobutyronitrile

Anal. = elemental analysis

atm = unit of pressure

Ar = aryl

bis = prefix of two identical ligands

bs = broad singlet

calcd. = calculated

C_n = n-carbon isomer

CO = carbon monoxide

Cp = cyclopentadienyl

Cp* = pentamethylcyclopentadienyl

cm^{-1} = wavenumber

Cmpd. = compound

Cnt = centroid

°C = degrees Celsium

D = deuterium

d = doublet

$\Delta G°$ = Gibbs free energy

DFT = Density Functional Theory

δ = chemical shift, delta

η^n = hapticity of a ligand with n contiguous atoms bound to a metal center

E = energy

EI = electron impact

equiv. = equivalents

esd = estimated standard deviation

Et = ethyl

Et_2O = diethyl ether

EtOAc = ethyl acetate

g = grams

HMBC = Heteronuclear Multiple Bond Quantum Correlation

HRMS = High Resolution Mass Spectrometry

HSQC = Heteronuclear Single Quantum Coherence

Hz = Hertz (s^{-1})

h = hours

^{i}Pr = isopropyl

IR = Infrared

^nJ = nth bond NMR coupling constant

κ^n = hapticity of a ligand

K = degrees Kelvin

K_{eq} = equilibrium constant

kcal = kilocalories

IR = infrared

L_n = ligand set of a metal complex

λ = wavelength

m = meter, multiplet

m = *meta* position

M = transition metal, molar (mol/L)

Me = methyl (CH_3)

MeCN = acetonitrile

min = minutes

mp = melting point

mol = moles

NOE = nuclear overhauser effect

NMR = Nuclear Magnetic Resonance

ν = infrared stretching frequency

OTs = tosylate

o = *ortho* position

ORTEP = Oak Ridge Thermal Ellipsoid Plot

PPh_3 = trephenylphosphine

Ph = phenyl (C_6H_5)

p = *para* position

ppm = parts per million

π = pi

q = quartet

R = alkyl group

r.t. = room temperature

SO_2Ph = phenylsulfone

s = singlet, seconds

σ = sigma

T = temperature

t = triplet

THF = tetrahydrofuran

TIPS = triisopropylsilyl

Tol = tolyl

tris = prefix of three identical ligands

TS = transition state

^tBu = tertiary-butyl ($C(CH_3)_3$)

UV = ultraviolet

TMS = trimethylsily

ACKNOWLEDGEMENTS

First, I would especially like to thank my advisor, Professor Joseph O'Connor. Thank you for offering me the opportunity to join your lab. Thanks for believing me at the beginning even though I didn't have much experience in making molecules before. You shaped me from the scratch, helped me switch to chemistry major, and led me into a research area I've never thought about. To be honest, coming to the U.S. to pursue my Ph.D. was like an adventure for me, and I was always a little anxious about how well I can do and how far I can go. You have always praised me and encouraged me, which tremendously built up my confidence and helped me get on the right track rapidly. I think I'm very lucky to get you as my advisor, and sometimes I don't even know how to show my appreciation. I really like those days when you, Ryan and I ate meal together in the apartment while we were talking a lot about our chemistry. I miss those days when you invited us to your house, and you cooked the steak and burger with Barbara for us. I also miss those days we have a lot of fun in Tianjin when both of us went to China in the summer. I appreciate that you trust me and offer me the chance to participate into both metallacyclobutene project and ruthenium project, which really helped me gain a lot of research experiences and confidence. Please forgive my occasional impatience and anxiety for publishing papers. Sometimes I'm a little emotional and just cannot stop myself from thinking about it. I'm extremely grateful for your guidance, support and everything you did for me in the past 6 years, and this experience has profound effects on my future career and is invaluable for my entire life!

I would like to thank Professor Charles Perrin, who always attends our group meetings and has seen my presentations since I started my graduate school. He is a

very knowledgeable professor and gave me a lot of thoughtful comments and insightful suggestions when I met problems. I also took the two graduate-level courses he was teaching, Kinetics and Spectroscopy, from which I learned considerable practical knowledge and skills that I can apply into my research. Thank you for offering me the opportunity to learn form you.

I would also like to thank my other doctoral committee members over the years. Thanks for Professor Guy Bertrand served as the chair of my second-year exam. He picked a literature about gold agostic interaction as my exame topic, which is a very interesting paper and left a very deep impression on me. I would like to appreciate Professor Haim Weizman for his comments and encouragement after my second-year exam. I am grateful for the learning experiences I obtained from him by serving as the teaching assistant in his organic chemistry class and organic chemistry laboratory class. I am thankful to Professor Carlo Ballatore for serving on my committee, for inspiring me and helping me in my research.

Anther person who offered me a lot of help on my research is Dr. Ryan Holland. He was my mentor and trained me with all kinds of lab techniques when I started my graduate school. He is a very nice and patient person, and whenever I have a question, he always has an answer. I don't think my graduate school would go through so smoothly without his help.

I appreciate all the previous and present lab members who offered me help and friendship, including Dr. Marissa Aubrey, Dr. Stephen Cope, Dr. Kate Veccharelli, Dr. Christina Hoong, Dr. Pauline Olsen, Han Steger, Li-An Wang, Yifan Li, and Burak Tufekci. I also appreciate the help provided from many individuals who are in charge of

UCSD falicilites. Thanks Dr. Arnold Rheingold and Dr. Curtis Moore for the help on the X-ray crystallography. Dr. Yongxuan Su helped us acquire a lot of HRMS and GCMS data. I would like to thank Dr. Anthony Mrse for training me with a variety of NMR techniques and assisting me with many specialized NMR experiments.

I would also like to appreciate Professor Kim Baldridge for all the computational work she has done for us over the years in the two research projects.

Last but not leat, I would like to express my great gratitude to my parents. I appreciate the education and cultivation from my father, Feiping Qin, on me to be an upright, brave, thoughtful, hardworking and ambitious young man. He always puts me first, provides me the best education, and supports me unconditionally. Nothing woud have been possible without his guidance and help for the past 28 years. My mother, Zhongyu Xiao, is a very caring person who offers me unlimited love, emotionally encourages me, and always believes that I can accomplish anything that I'm aiming for. I'm very lucky to be your son and thank you for everything you did for me. I really really love both of you, dad and mom!

Chapter 2 contains a full reptrint of publication "Metal-Alkyne and Metallacyclobutene Reactivity toward a Diazoacetamide: Conversion to Highly Functionalized 1,3-Diene Complexes and Oxametallacyclopentadienes" Qin, P.; Holland, R. L.; Moore, C. E.; O'Connor, J. M. *Organometallics* **2019**, *38*, 863-869. The dissertation author is the first author on this paper.

Chapter 2 contains the material being prepared for the publication "Coupling of Metal-Alkyne Complexes with *α*-Diazocarbonyl Compound: An Efficient Way to Synthesize Highly Functionalized Metallacyclobutenes". Qin, P.; Bunker, K. D.; Holland,

R. L.; Rheingold, A. L.; O'Connor, J. M. The dissertation author is the first author on this paper.

Chapter 2 contains the material being prepared for the publication "Thermal Reactivity of Late-metal Metallacyclobutene Complexes: Reversible Formation of Dicobalt Propendiyl Complexes". Qin, P.; Bunker, K. D.; Holland, R. L.; Rheingold, A. L.; O'Connor, J. M. The dissertation author is the first author on this paper.

Chapter 3 contains the material being prepared for the publication "Redox-induced ligand fragmentations: One-electron oxidation triggers carbon-carbon bond cleavage in π-ligands: Synthesis of trisubstituted cobaltocenium salts". Qin, P.; Baldridge, K. K.; Melaimi, M.; Cenzano-Fong B. S.; Holland, R. L.; O'Connor, J. M. The dissertation author is the first author on this paper.

Chapter 3 contains the material being prepared for the publication "Ring-Expansion Reactions of Highly Substituted η^4-Cyclopentadiene Ligands Generate Functionalized Aromatics". Qin, P.; O'Connor, J. M.; Cenzano-Fong B. S.; Holland, R. L.; Rheingold, A. L. The dissertation author is the first author on this paper.

Chapter 4 is a full reprint of the publication "Acid-Induced Liberation of Polysubstituted Cyclopentadiene Ligands from Cyclopentadienyl Cobalt: A [2 + 2 + 1] Cycloaddition Route Toward 1, 2, 4-Trisubstituted Cyclopentadienes" Qin, P.; Holland, R. L.; Bunker, K. D.; O'Connor, J. M.; Baldridge, K. K.; Rheingold, A. L. *J. Org. Chem*. **2019**, *84*, 13992-14004. The dissertation author is the first author on this paper.

Chapter 5 is a full reprint of the publication "Photoactivated Transition-Metal Triggers for Ambient Temperature Enediyne and Dienyne Cyclization: Ruthenium-η^6-Naphthalene Complexes" Qin, P.; Cope, S. K.; Steger, H.; Veccharelli, K. M.; Holland,

R. L.; Hitt, D. M.; Moore, C. E.; Baldridge, K. K.; O'Connor, J. M. *Organometallics*, **2017**, *36*, 3967-3973. The dissertation author is the first author on this paper.

Chapter 6 contains the material being prepared for the publication "Chemoselective Ruthenium-Catalyzed Cycloisomerization of Conjugated Dienynes". Qin, P.; Steger, H.; O'Connor, J. M.; Baldridge, K. K.; Cope, S. K. The dissertation author is the first author on this paper.

Chapter 6 contains the material being prepared for the publication "Ambient Temperature Aitken Cycloisomerization of Dienynes: Partitioning between Hopf and Aitken Pathways". Hitt, D. M.; Qin, P.; Steger, H.; Baldridge, K. K.; Rheingold, A. L.; O'Connor, J. M. The dissertation author is the co-author on this paper.

Chapter 7 contains the material being prepared for the publication "Enediyne Cycloaromatization with Incorporation of Chlorine from Chloroform and Hydrogen from 1,4-Cyclohexadiene". Qin, P.; O'Connor, J. M.; Baldridge, K. K.; Perrin, C. L.; Hitt, D. M.; Veccharelli, K. M.; Cope, S. K.; Holland, R. L.; Raub, A. The dissertation author is the first author on this paper.

Chapter 8 contains the material that is accepted for the publication "Transition-Metal Catalysis of Triene 6π Electrocyclization: The π-Complexation Strategy Realized". *Angew. Chem. Int. Ed*. **2020**, *accepted*. Qin, P.; Wang, L. A.; O'Connor, J. M.; Baldridge, K. K.; Li, Y.; Tufekci, B.; Chen, J.; Rheingold, A. L. The dissertation author is the first author on this paper.

CURRICULUM VITAE

Education

2015 – 2020   University of California San Diego
                   Doctor of Philosophy, Chemistry

2014 – 2015   University of California San Diego
                   Master of Science, Materials Science and Engineering

2010 – 2014   Harbin Institute of Technology
                   Bachelor of Science, Chemistry

Research Experiences

2014 – 2019   Research assistant, University of California San Diego

                   Ph.D. Advisor: Prof. Joseph M. O'Connor

   1. Creatively designed and conducted numerous multi-step syntheses of various target polyunsaturated organic molecules, including stereospecific acyclic enediynes, dienynes, and trienes. Explored the ruthenium-mediated/catalyzed cyclization of conjugated tri-π systems with high regio- and stereoselectivity via various metal-π interactions.

   2. Prepared a wide range of acetylenes, diazocarbonyls, and vinyl diazo molecules as building blocks to assemble highly functionalized metallacyclobutene (MCB) complexes, as well as explored the reactivities of MCB towards various organic substrates.

2012 – 2014   Research assistant, Harbin Institute of Technology, China

                   B.S. Thesis Advisor: Prof. Xiaohong Wu

   Applied ball-milling technique to prepare CNT-coated sulfur partilcles for the use as the cathode material to improve the cycle stability of lithium-sulfur batteries. Also served as the group leader of a Problem-Based Learning Project to review the literature and optimize the conditions necessary to assemble morphology-controlled cathodes materials

2010 – 2012	Research assistant, Harbin Institute of Technology, China
	Advisor: Prof. Qun Wang

Explored the performance of different organic ligands utilized in the hydrothermal synthesis of silver doped PbTe nanomaterials. Analyzed and evaluated the properties of the hydrothermally derived products with XRD, SEM, TEM and CV, as well as optimized the solvent components for the reaction accordingly.

Laboratory Manager

Responsible for equipment maintenance and troubleshooting issues in the laboratory, including glove box installation, building and maintaining vacuum and Schlenk line systems, equipment repair, calibration of the public gas chromatography system, writing protocols and training students in the use of NMR and FT-IR instruments.

Teaching Assistantships

Organic Chemistry I (4 times)

Organic Chemistry II (8 times)

Organic Chemistry III (twice)

Organic Chemistry Laboratory I (twice)

Organic Chemistry Laboratory II (twice)

General Chemistry Laboratory (once)

Mentorships

Trained two master students and five undergraduate students on proper laboratory techniques, use of characterization facilities, and documentation of research results.

Directed a collaboration of four students to complete and publish experimental work. Edited and shaped dissertations and oral discourses of laboratory members.

Publications

Qin, P.; Wang, L. A.; O'Connor, J. M.; Baldridge, K. K.; Li, Y.; Tufekci, B.; Chen, J.; Rheingold, A. L. Transition-Metal Catalysis of Triene 6π Electrocyclization: The π-Complexation Strategy Realized. *Angew. Chem. Int. Ed*. **2020**, *accepted*.

Qin, P.; Holland, R. L.; Bunker, K. D.; O'Connor, J. M.; Baldridge, K. K.; Rheingold, A. L. Acid-Induced Liberation of Polysubstituted Cyclopentadiene Ligands from Cyclopentadienyl Cobalt: A [2 + 2 + 1] Cycloaddition Route Toward 1, 2, 4-Trisubstituted Cyclopentadienes. *J. Org. Chem.* **2019**, *84*, 13992-14004.

Qin, P.; Holland, R. L.; Moore, C. E.; O'Connor, J. M. Metal-Alkyne and Metallacyclobutene Reactivity toward a Diazoacetamide: Conversion to Highly Functionalized 1,3-Diene Complexes and Oxametallacyclopentadienes. *Organometallics*. **2019**, *38*, 863-869.

Qin, P.; Cope, S. K.; Steger, H.; Veccharelli, K. M.; Holland, R. L.; Hitt, D. M.; Moore, C. E.; Baldridge, K. K.; O'Connor, J. M. Photoactivated Transition-Metal Triggers for Ambient Temperature Enediyne and Dienyne Cyclization: Ruthenium-η^6-Naphthalene Complexes. *Organometallics*, **2017**, *36*, 3967-3973.

Holland, R. L.; O'Connor, J. M.; Bunker, K. D., **Qin, P**.; Cope, S. K.; Baldridge, K. K.; Siegel, J. S. Stereospecific Oxidative Demetallation of Highly Functionalized CpCo (1, 3-Diene) Complexes: An Experimental and Computational Study. *Synlett*, **2015**, *26*, 2243-2246.

Presentations

Qin, P., Cenzano-Fong, B., Baldridge, K. K., Holland, R. L., O'Connor, J. M. "Conversions of a Metallacyclobutene to Conjugated Dienes" *Abstracts*, 251st ACS National Meeting, San Diego, CA, Mar 13 – 17, **2016**; INOR-1311.

Qin, P.; O'Connor, J. M.; Wang, L.; Li, Y.; Veccharelli, K.; Baldridge, K. K.; Chen, J.; Tufekci, B. Transition Metal-catalyzed Cycloaromatization of Conjugated Trienes. *Abstract*, 258th ACS National Meeting, San Diego, CA, Aug 25 – 29, **2019**; ORGN-0066.

Qin, P.; O'Connor, J. M.; Hitt, D.; Steger, H.; Baldridge, K. K. Chemo-and Regioselective Ruthenium-catalyzed Cycloaromatization of Conjugated Dienynes. *Abstract*, 258th ACS National Meeting, San Diego, CA, Aug 25 – 29, **2019**; ORGN-0065.

ABSTRACT OF THE DISSERTATION

Synthesis and Reactivity Studies of Metallacyclobutenes and. eta. 4-Cyclopentadienes
Derived Therefrom & Ruthenium Catalyzed Cyclizations of Conjugated tri-pi Systems

by

Pengjin Qin

Doctor of Philosophy in Chemistry

University of California San Diego, 2020

Professor Joseph M. O'Connor, Chair

This work is mainly composed of two parts. The first part talks about synthesis and reactivity studies of metallacyclobutenes (MCB) and η^4-cobalt-cyclopentadienes derived therefrom, which includes chapter 1, 2, 3, and 4. The second part talks about ruthenium-mediated/catalyzed cyclizations of conjugated tri-π molecules, which includes chapter 5, 6, 7, and 8.

Chapter 1 is a review of historical development of metallacyclobutenes and η^4-cyclopentadienes with numerous literature-reported representative examples. Chapte 2 talks about preparation of new cobaltocyclobutenes, reversible thermolysis of MCB to

dicobalt propendiyl complex, formation of η^4-diene complexes from MCB, photochemical isomerization of MCB, and the reactivities of MCB/cobalt-alkyne complexes towards dizaoacetamide. Chapter 3 presents syntheses of η^4-cyclopentadienes and vinylmetallacyclobutene complexes, as well as further reactivity study of η^4-cyclopentadienes to produce highly functionalized cobaltocenium cations and arenes. Chapter 4 introduces a Brønsted acids triggered demetallation of η^4-cyclopentadiene to give fulvenol, cyclopentenone, and cyclopentadienes as products.

Chapter 5 talks about an air-stable ruthenium-naphthalene complex Cp*Ru(Nap)PF$_6$ as trigger of "Cp*Ru$^+$" under photochemical conditions to cycloaromatize enediyne in the presence of 1,4-cyclohexandiene at ambient temperature. Chapter 6 describes a chemoseletive ruthenium-mediated cycloaromatization of dienynes with phenyl goup. A noval ruthenium-catalyzed cyclization mode was also discovered on a chlorine and methyl incorporated dienyne, whose regioselectivity is controlled by the size of a nearby fused ring. Chapter 7 is a clean-up work of an unprecedented cycloaromatization mode of enediynes. Both vinyl chloride intermediates and arene products were resynthesized from a modified method with higher yields, and products were furtherly purified and fully characterized. Mechanistic studies were carried out via deuterium labelling experiments. Chapter 8 introduces ruthenium-mediated/catalyzed conjugated trienes. The reactions of Cp*Ru(NCMe)$_3$PF$_6$ with trienes at ambient temperature give η^6-arene complex with excellent yields. VT NMR experiments allows the observation and isolation of variable metal-triene intermediates at low temperature. Furthermore, the first example of metal-π complexation catalyzed 6π electrocyclization of conjugated trienes was discovered.

CHAPTER 1

Metallacyclobutenes and η^4-Cyclopentadienes

A. Introduction

Metallacycles have been widely proposed to play a crucial role in a variety of metal-catalyzed processes, especially in metathesis and polymerization reactions of olefins[1] and acetylenes,[2] which have been vastly applied in total synthesis to construct new frameworks through carbon-carbon bond formation reactions.[3] In particular, metallacyclobutene, different from well-studied metallacyclopropene, metallacyclobutane or metallacyclopentadiene complexes, has a metal center simultaneously coordinated to both a sp^2 carbon and a sp^3 carbon (Figure 1-1). Benefiting from this unique unsymmetrical coordination mode, in our lab, we discovered that late-metal metallacyclobutene or its tautomer η^3-vinylcarbene exhibits rich reactive patterns with highly regio-and steroselectivities towards various unsaturated substrates, such as carbenes, alkenes, alkynes, carbon monoxide, and nitroso molecules to generate η^4-1,3-dienes[4], η^4-1,4-dienes[5], η^4-cyclopentadiene[6], η^4-ketene[7], η^2(N,O)-hydroxylamido complexes[8], respectively (Scheme 1-1).
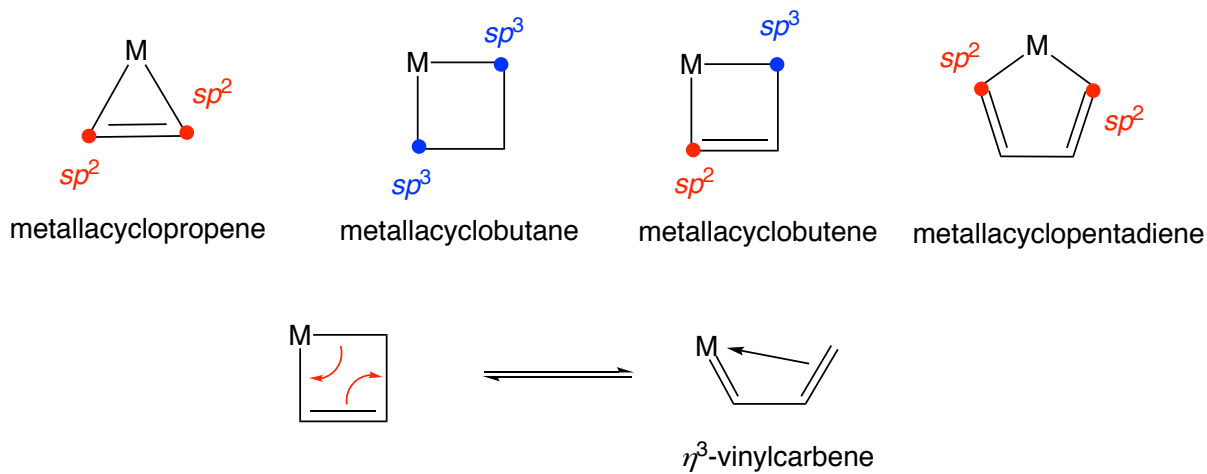
Figure 1-1. Structures of different metallacycles that have been reported in literature.
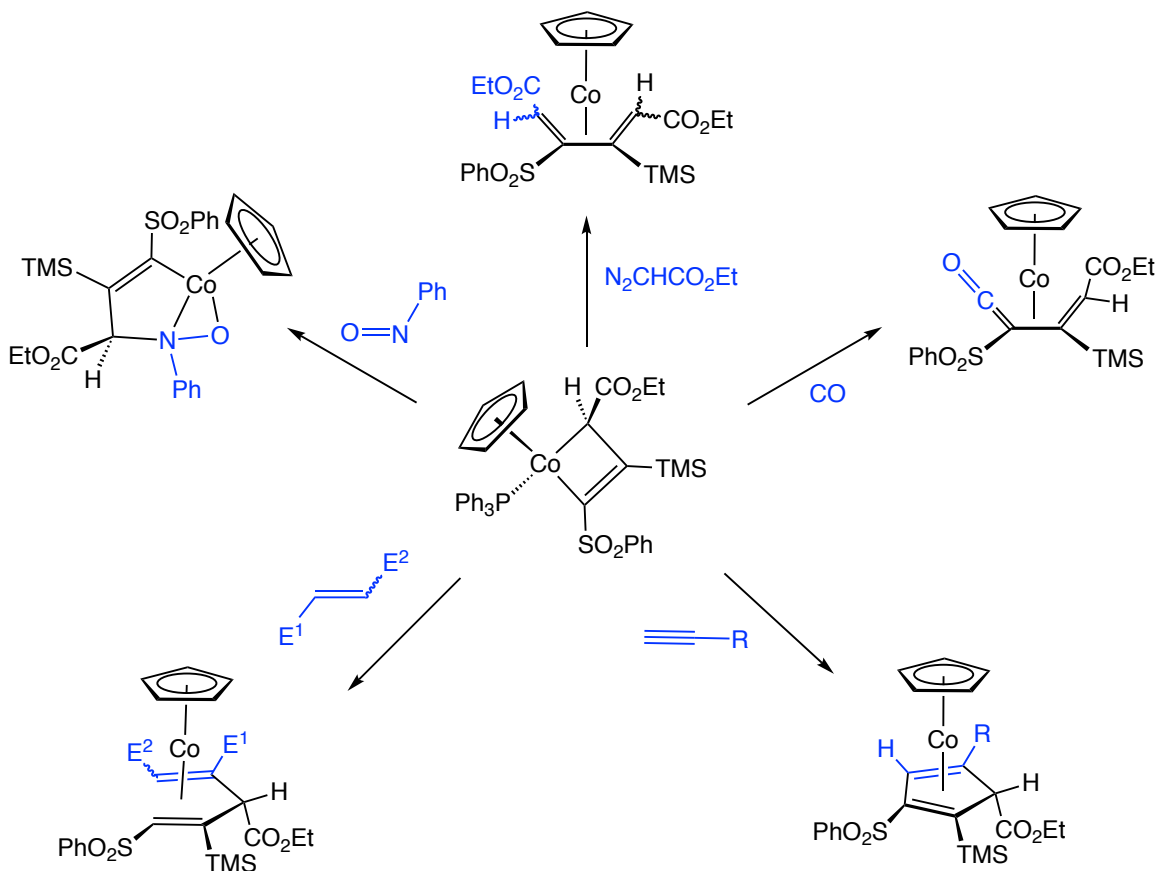
Scheme 1-1. Reactivities of a late-metal metallacyclobutene towards different substrates.

Since the first ferrocene molecule was synthesized[9] and structurally characterized[10] in 1950s, η^5-cyclopentadienyl ligand has rapidly become one of the most common ligands that appears in the literature of organometallic chemistry, for the reason that it can be employed as ancillary ligand to control both electronic effect and steric hindrance of the metal center,[11] as well as that the versatile hapticity (η^1 or η^3) provides crucial intermediates for the mechanisms of a wide variety of transition metal-mediated reactions.[12] As a result, the derivatives, η^4-cyclopentadienyl complexes, have also attracted considerable attentions for their facial interconversions with η^5-cyclopentadienyl complexes through a oxidation/reduction process. In addition, upon

demetallation, the η^4-cyclopentadienyl complexes can serve as precursors to uncomplexed five-membered carbocycles, which is valuable in organic synthetic strategy.

B. Metallacyclobutene serves as intermediate and/or transition state

Historically, metallacyclobutenes were extensively proposed as intermediates and/or transition states in a lot of metal-mediated reactions involving formations of new carbon-carbon bonds with a number of different transition metals, including tantalum, chromium, molybdenum, tungsten, manganese, ruthenium, rhodium, and platinum. Here, some of the representative examples are exhibited below.

Specifically, in 1979, R. R. Schrock's group reported that a tantacyclobutene complex serves as an intermediate in a reaction of tantalum carbene complex with diphenylacetylene.[13] Mechanistically, they proposed that diphenylacetylene firstly coordinates to the metal center of the carbene complex **1**, which is subsequently attacked by the neopentylidene α-carbon to generate the tantacyclobutene intermediate **2**. A followed rearrangement gives an observable vinylcarbene intermediate **3** (Scheme 1-2). Even though the stereochemistry of the metallacyclobutene **2** is not clear, the rearranged vinylcarbene intermediate is confirmed to be a single isomer by both ^{1}H and ^{13}C NMR, and it can be trapped by addition of ethylene to give a single diene molecule **4**.
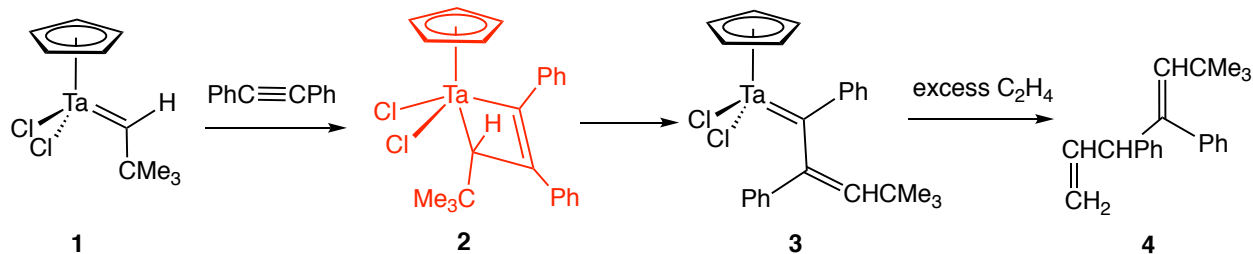
Scheme 1-2. Coupling of tantalum alkylidene with diphenylacetylene.

Since Dötz discovered the benzannulation reaction by employing vinylic alkoxy pentacarbonyl chromium carbene complex coupled with acetylenes in the late 1970s,[14] chromacyclobutenes and the rearranged vinylcarbene complexes have been extensively proposed as crucial intermediates in these cycloaromatization reactions.

In 1988, William D. Wulff's group conducted mechanistic studies on the benzannulation reactions, in which a Fisher type chromium carbene complex was allowed to couple with acetylenes.[15] They commented that despite there was a conflict between the mechanism that has been proposed by Dötz involving the η^4-vinylketene complex intermediate **10** and the mechanism that has been proposed by Casey involving a chromacyclohexadiene intermediate **9**, they both have the same chromacyclobutene and vinylcarbene complex intermediates **7** and **8** (Scheme 1-3). The ring opening of the chromacyclobutene have been simply assumed to produce the *E* isomer of the vinylcarbene intermediate **8** since the necessity of this configuration for both formation of the chromacyclohexadiene in Casey's mechanism and electrocyclic ring closure of the η^4-vinylketene in Dötz's mechanism.

5
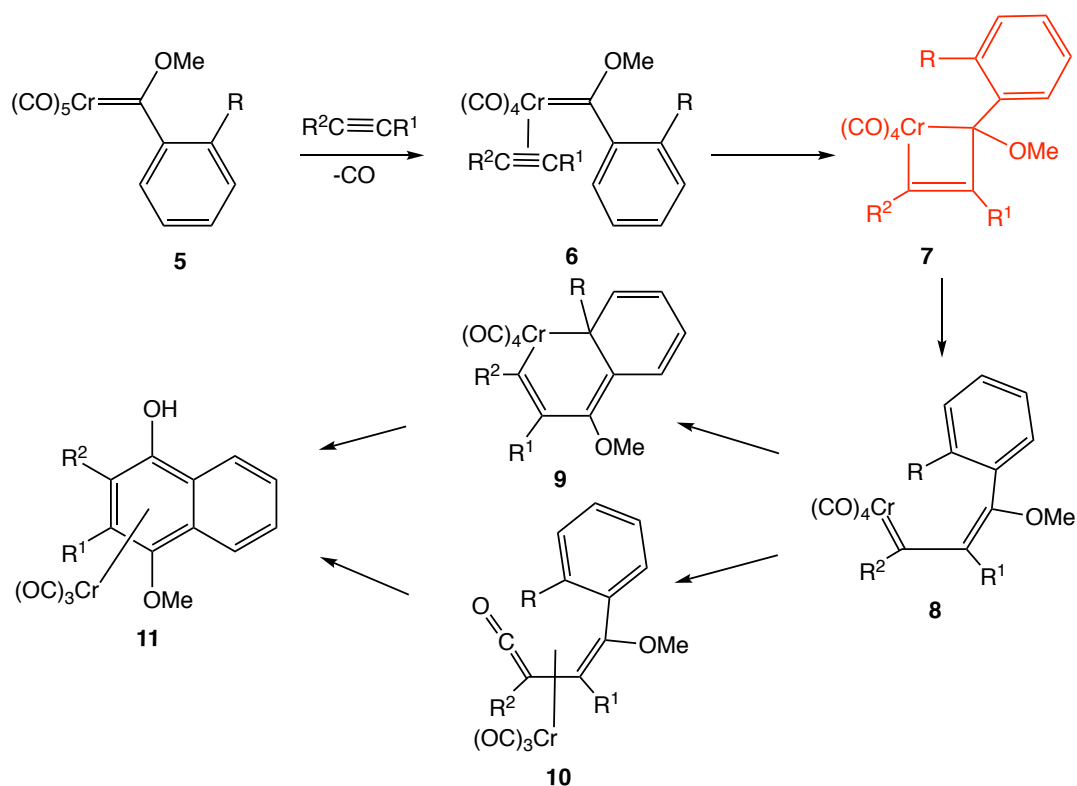
Scheme 1-3. Proposed mechanisms of benzannulation reaction.

James Herndon reported a versatile [4 + 2 + 1 - 2] cycloaddition for the constructions of cyclopentenones by employing cyclopropylcarbene-chromium and alkynes in 1992.[16] The mechanism they proposed is very similar to the Dötz reaction, in which the alkyne is inserted to the chromium carbene to generate a chromacyclobutene intermediate **14** that is followed by further rearrangements to produce the cyclopentenone (Scheme 1-4).
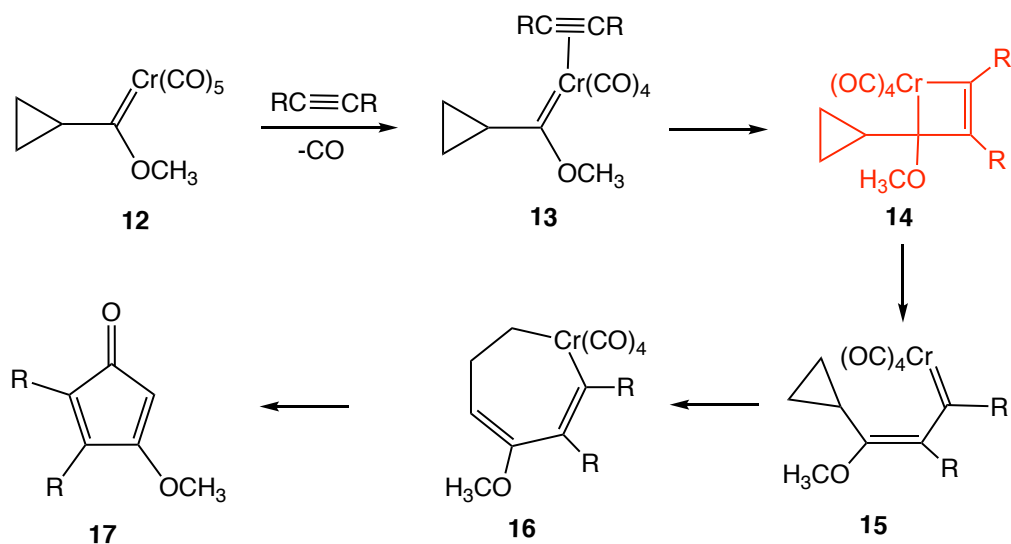
Scheme 1-4. [4 + 2 + 1 - 2] cycloaddition to form cyclopentenone.

Under photochemical conditions, chromium iminecarbene complex was found able to couple with alkynes to generate dendralene molecules instead of 2*H*-pyrrole derivatives. Sampedro reported this result in 2005 with a proposed mechanism that a metallacyclobutene intermediate **19** is involved, that is followed by a special ring opening process with a hydride abstraction path to give the acyclic dendralene **21** (Scheme 1-5).[17]
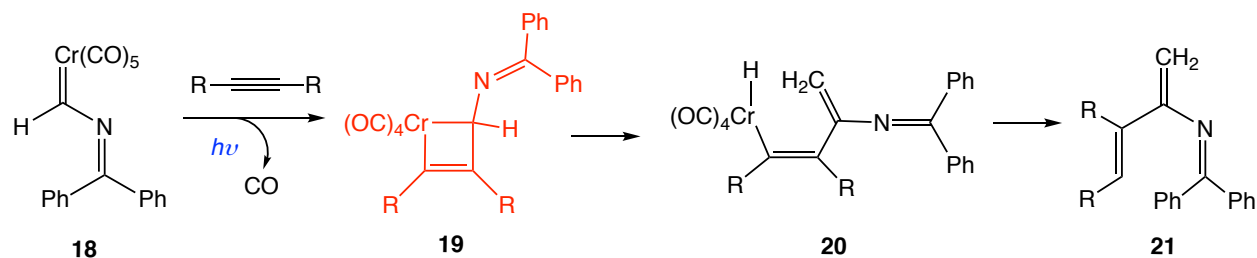
Scheme 1-5. Formation of dendralene products.

In 2007, R. R. Schrock discovered a ring-closing metathesis reaction catalyzed by a series of high oxidation state monoalkoxide monopyrrolyl molybdenum complex.[18] They proposed that the different metathesis products **26** and **30** arise from initial insertion of the triple bond into an intermediate alkylidene complex to produce α- or β- substituted metallacyclobutenes **23** and **27**, followed by further rearrangements through ring formation and extrusion of alkylidene complex (Scheme 1-6).
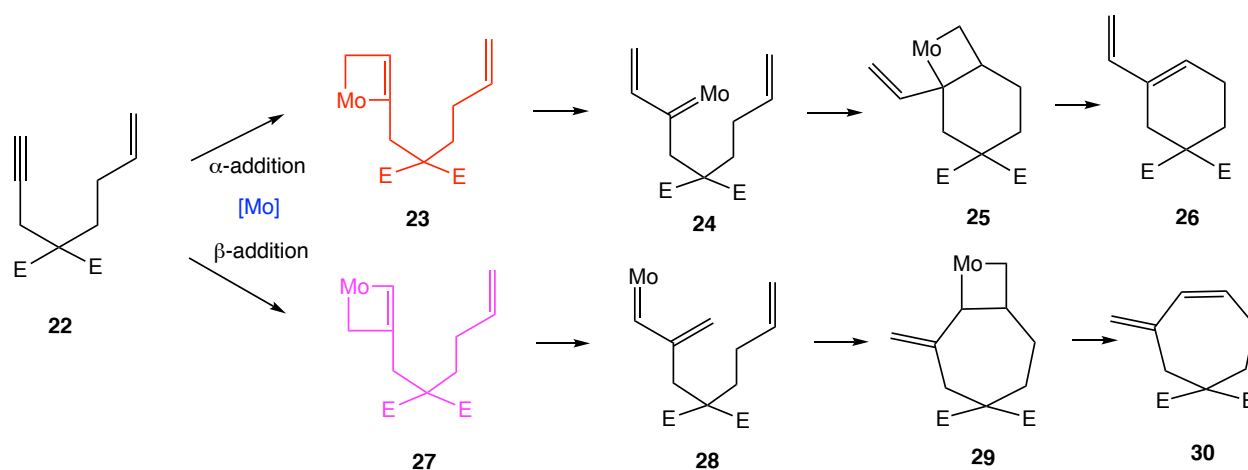
Scheme 1-6. Molybdenum mediated ring-closing metathesis reaction.

In 2014, Xavier Solans-Monfort conducted a DFT study on the reaction mechanism of the ring closing enyne metathesis catalyzed by molybdenum alkylidene complexes,[19] which indicates that the metal is energetically more favorable to react with alkyne first to undergo an *yne-then-ene* pathway to produce metallacyclobutene intermediate than undergo the *ene-then-yne* mechanism to generate metallacyclobutane intermediate, even though metallacyclobutenes are computed to be very short-living intermediate.

The intermediacy of a tungstacyclobutene **33** was proposed by Charles Casey in 1979 when they used ethoxyacetylene reacting with a tungsten alkylidene pentacarbonyl complex that is generated in situ by employing $N(CH_2CH_3)_4^+(CO)_5WCH(OCH_3)C_6H_5^-$ with trifluoroacetic acid.[20] They proposed that the reaction proceeds via an initial formation of a tungstacyclobutene followed by a ring opening to produce the styrylethoxycarbene complex **33** (Scheme 1-7).
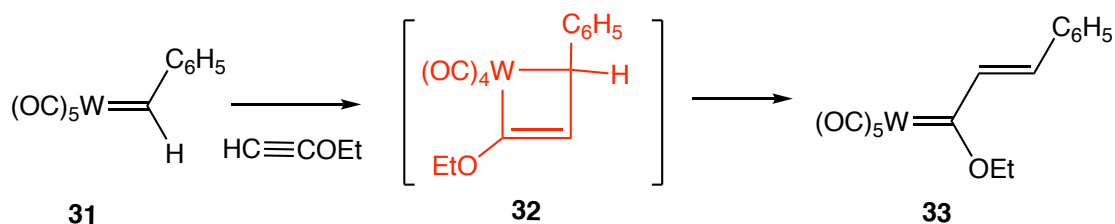
Scheme 1-7. Reaction of ethoxyacetylene with tungsten alkylidene complex.

A stereoselective ring closing enyne metathesis reaction was reported by Thomas Katz in 1984 by employing tungsten catalyst,[21] which shows that the ring opening fashion of tungstacyclobutene intermediate dictates the stereochemistry of the final olefin products (Scheme 1-8).
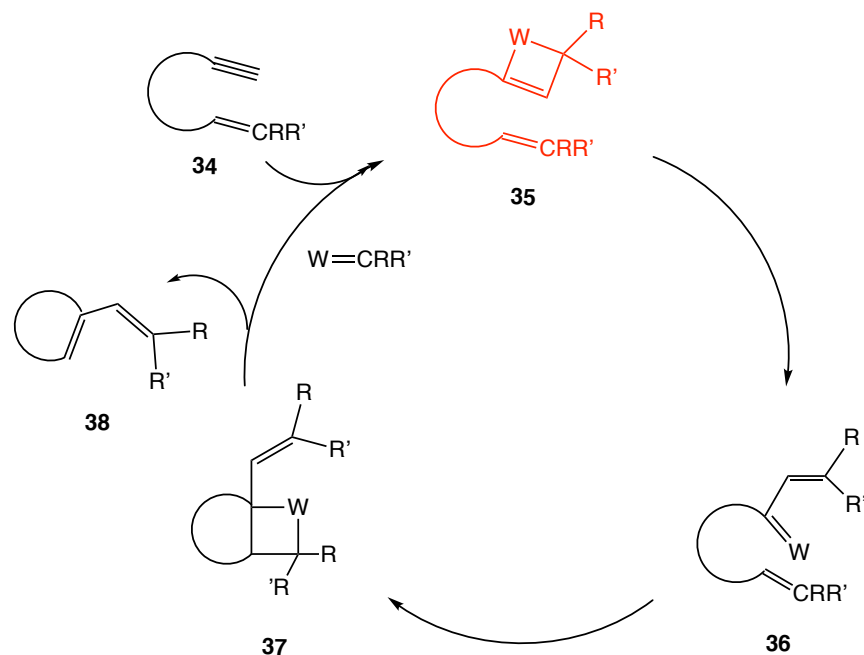
Scheme 1-8. Tungsten catalyzed ring closing enyne metathesis.

Wataru Ando reported a mangacyclobutene intermediated reaction of polysilacycloalkynes with a manganese vinylidene complex in 1996.[22] When they treated the metallallene complex **39** under photochemical condition in the presence of polysilacycloalkyne, an alkyne vinylidene complex **40** was generated by the dissociation of a carbonyl ligand from complex **39**, that is followed by formation of metallacyclobutene **41**. The generation of organic triene **42** was proposed by the reductive elimination of metallacyclobutene concomitant with a 1,2-dilyl shift (Scheme 1-9).
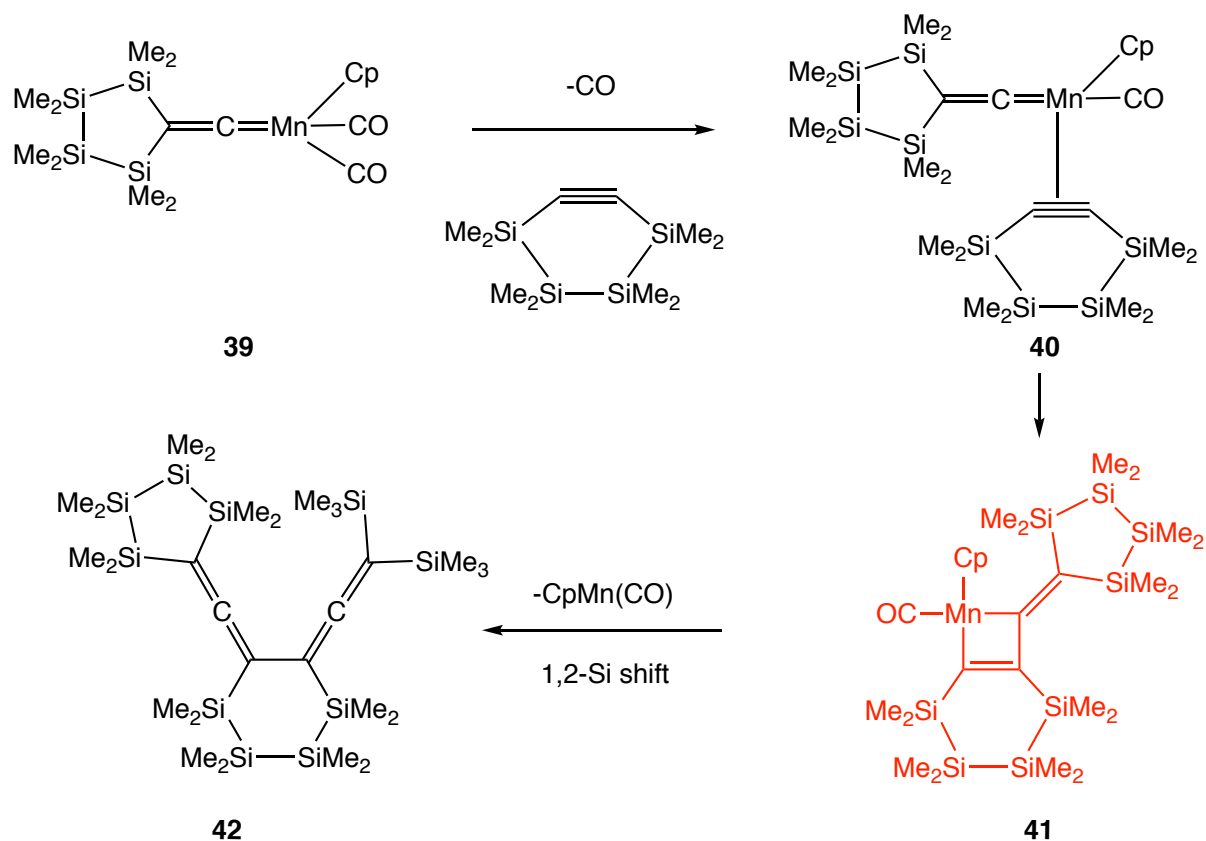
Scheme 1-9. Polysilacycloalkynes couple with manganese vinylidene complex.

Buchmeiser conducted a DFT calculation study on the ruthenium alkylidene catalyzed cyclopolymerization of 1,6-heptadiynes in 2012.[23] The computational results indicate that the formation of the two types of ruthenacyclobutene intermediate **45** and **46** is the rate-determining step, and thus the α-insertion pathway to generate metallacyclobutene **45** with lower activation barrier is more favorable. The energy difference dictates the regioselectivity and cyclization fashion of the metathesis process (Scheme 1-10).

11
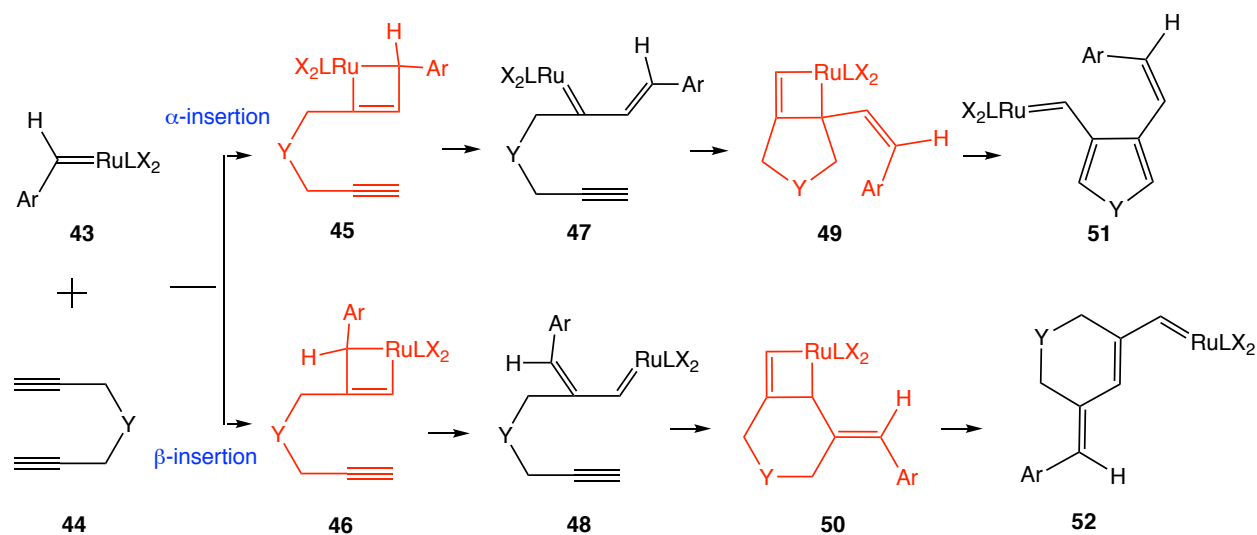
Scheme 1-10. Ruthenium catalyzed cyclopolymerization of heptadiynes.

More recently, in 2017, Suresh reported a mechanistic study on the cyclotrimerization of acetylenes that is catalyzed by Grubbs first and second generation catalysts.[24] The DFT calculation exhibits that the activation barriers of all steps are moderate in the three successive cross metathesis pathways, in which three ruthenacyclobutenes are proposed as intermediates (Scheme 1-11).
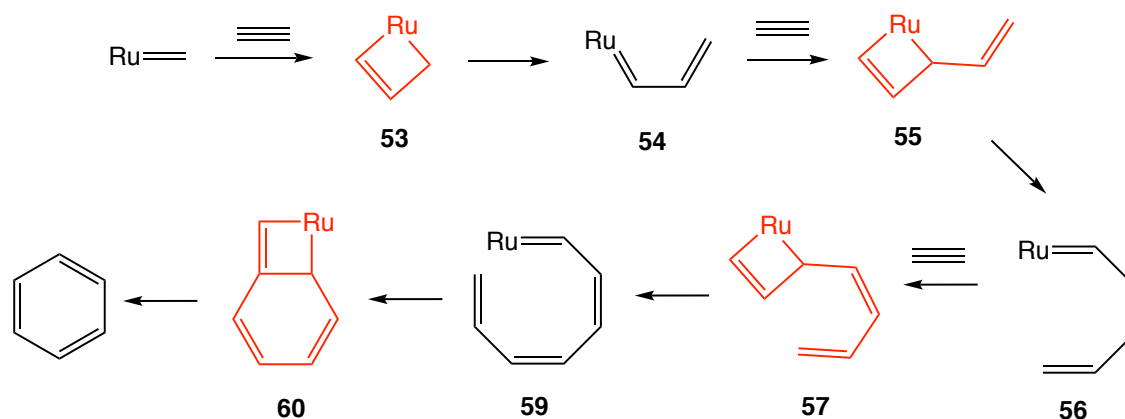
Scheme 1-11. Trimerization of alkynes catalyzed by Grubbs catalyst.

At the same time, in 2017, a rhodacyclobutene intermediate was proposed by Xiaoguang Bao in the $Rh_2(OAc)_4$ catalyzed transannulation of triazole molecule with phenylacetylene.[25] The [2 + 2] cycloaddition of rhodium carbenoid with acetylene was proposed to form a metallacyclobutene intermediate **64** followed by reductive elimination to afford cyclopropene (Scheme 1-12).
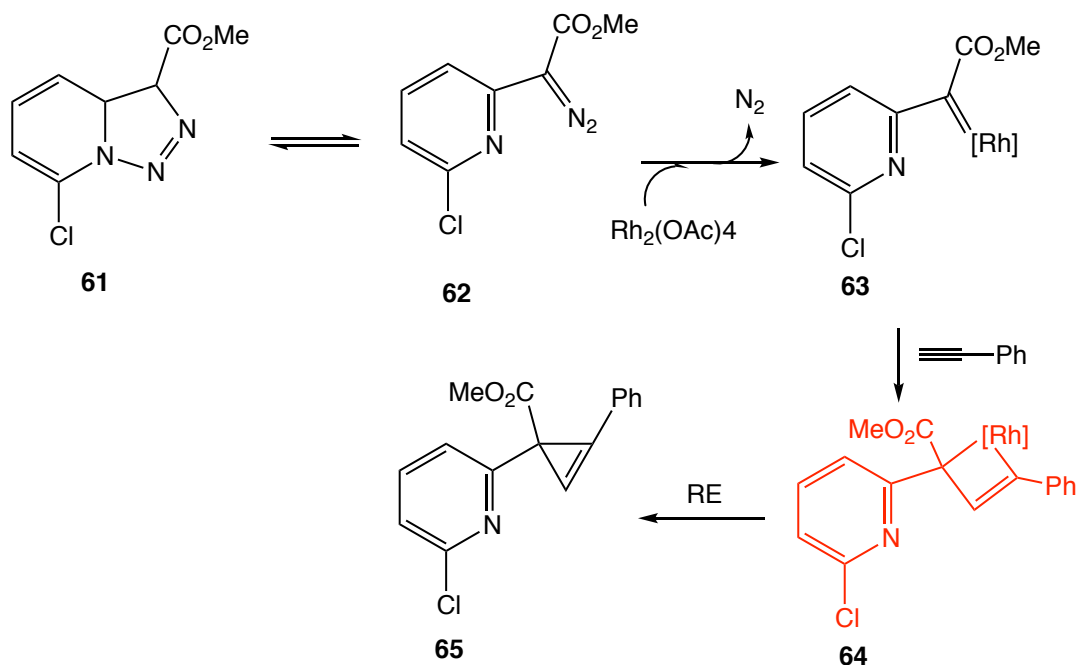
Scheme 1-12. Rhodium catalyzed transannulation of triazoimine with acetylene.

In addition, another example of late metallacyclobutene intermediate is the platinacyclobutene, that was reported by Ai-Jan Chen in an electrophilic aromatic substitution by an organoplatinum η^3-allenyl/propargyl complex.[26] They proposed that the electrophilic η^3-allenyl/propargyl complex **66** replaces an aryl proton to generate the

metallacyclobutene intermediate that is subject to the ensuing protonation to afford the arylallyl complex **68** (Scheme 1-13).
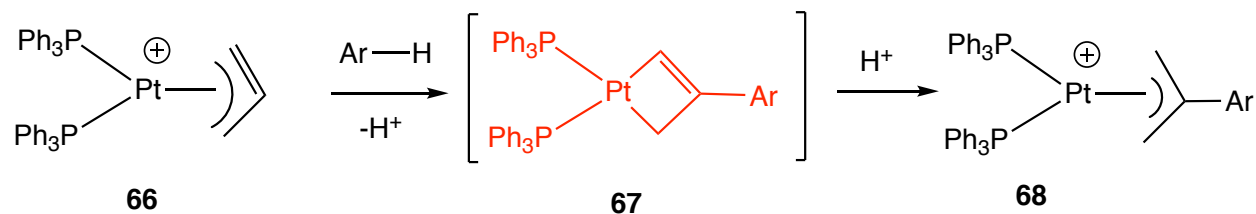
Scheme 1-13. Electronic aromatic substitution of organoplatinum η^3-allenyl complex.

C. Characterized/Isolated Metallacyclobutenes

Since Tebbe and co-workers reported the first isolated metallacyclobutene that was prepared from the reaction of $Cp_2TiCH_2AlClMe_2$ with acetylenes in 1980 (Scheme 1-14),[27] other examples of isolated and characterized transition-metal metallacyclobutene complexes were successively reported with highly varied structures and synthetic pathways by employing a large variety of transition metals, such as titanium, zirconium, vanadium, tantalum, molybdenum, rhenium, cobalt, rhodium, and iridium. Some of the representative examples are shown below.
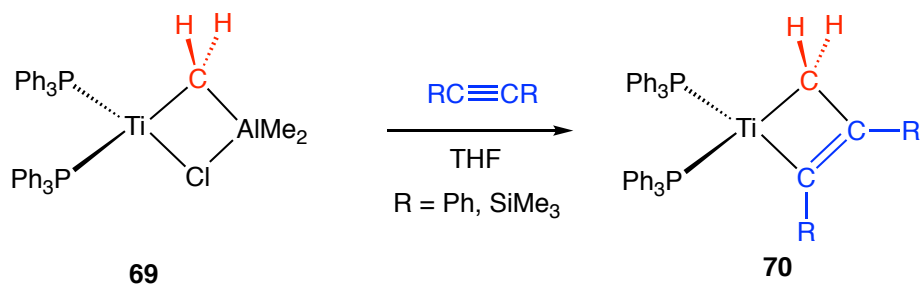
Scheme 1-14. Coupling of Tebbe's reagent with alkyne.

Specifically, in 1991, Paul Binger reported a titanacyclobutene which is prepared from an insertion reaction of $Cp_2Ti(PMe_3)_2$ into 1,2-diphenylcyclopropene via loss of two PMe$_3$ ligands (Scheme 1-15).[28] The resulting metallacyclobutene **72** was characterized by both ^{1}H and ^{13}C NMR spectroscopy. In a similar fashion, they also isolated a zirconacyclotuene by employing a vinyl zirconocene complex **73** reacting with 1,2-diphenylcyclopropene. The structure of metallacyclobutene **74** was studied by X-ray analysis. In later work, they also showed a matallabicyclohexane, that is made from coupling of zirconocene acetylene complex with 1,1-dimethylcyclopropene, can rearrange to a vinyl metallacyclobutene **76** (Scheme 1-16).[29]
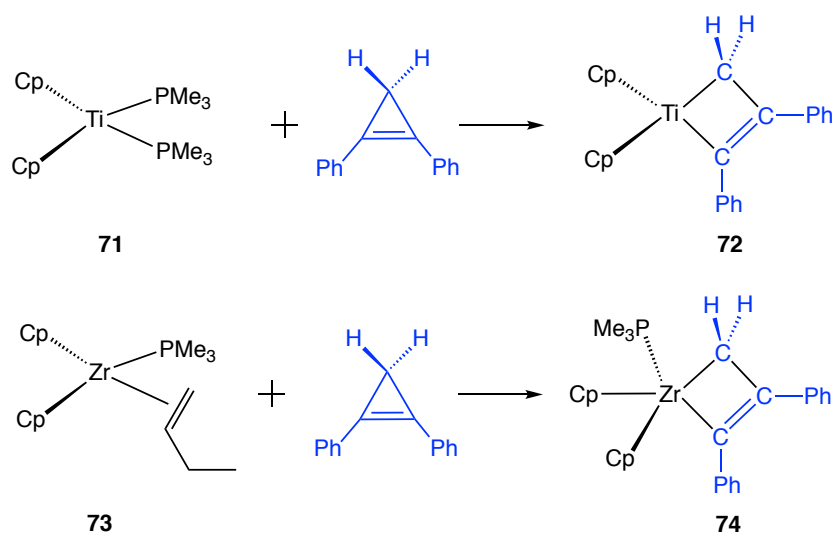
Scheme 1-15. Formation of metallacyclobutenes via oxidative additions.
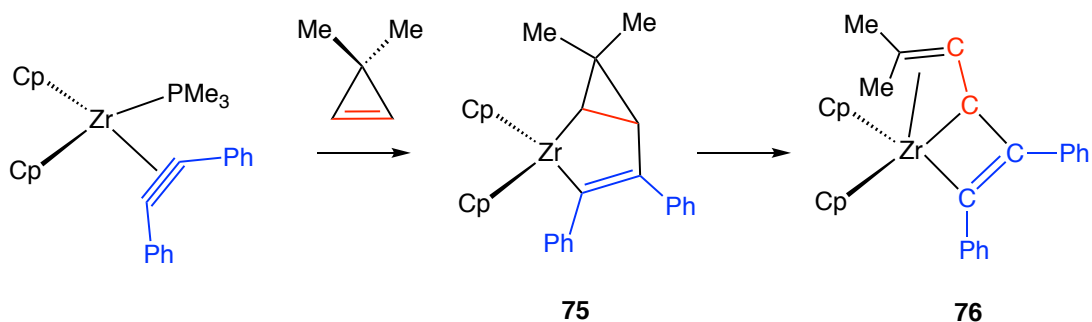
Scheme 1-16. Formation of vinyl metllacyclobutene from zirconocene.

In 1993, Doxsee's group conducted a reaction between Tebbe's reagent with a conjugated enyne, which afforded three isomeric metallacyclobutene complexes. Despite the mixture of the three titanacyclobutenes are inseparable, analysis of ^{1}H and ^{13}C NMR spectroscopy, aided by 2D COSY studies, allowed unambiguous structural assignments for the three metallacycles (Scheme 1-17).[30]
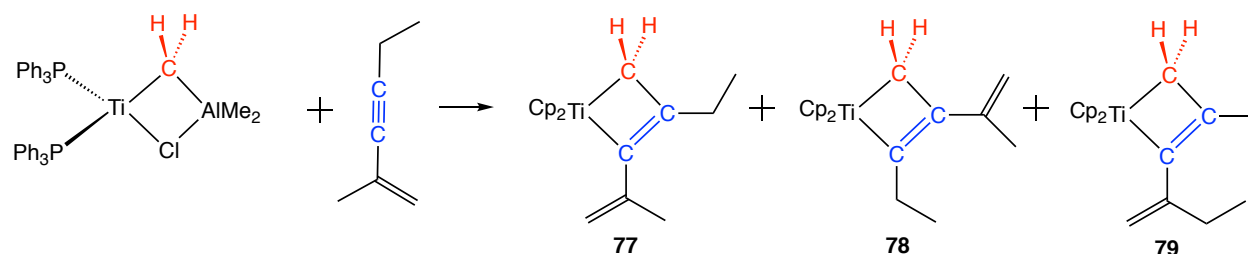
Scheme 1-17. Formation of three isomeric titanacyclobutenes.

Another interesting example of isolated titanacyclobutene was reported by Richard Ernst in 2006.[31] They used a half-open titanocene complex **80** coupled with four equivalents of phenyltrimethylsilyl acetylene to afford a metallacyclobuene complex **81** (Scheme 1-18), in which a carbon-carbon titanium agostic interaction is involved. The structure was confirmed by X-ray crystallography.
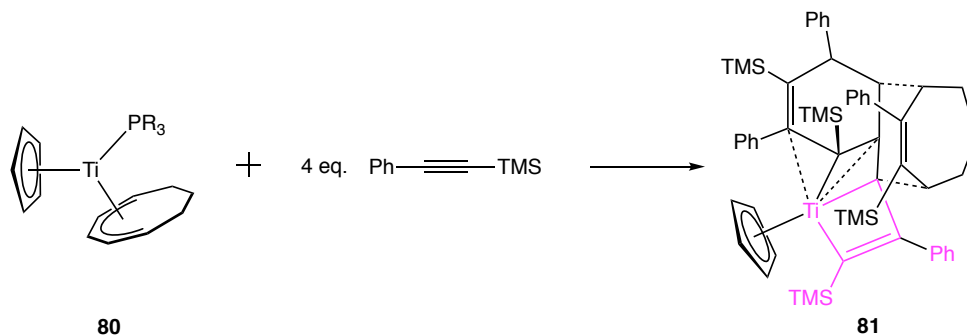
Scheme 1-18. Formation of titanacyclobutene with carbon-carbon agostic interaction.

Some of IV metals are also found capable to form stable metallacyclobutenes for isolation. In 2008, Kotohiro Nomura reported a vanadacyclobutene that was prepared by treating the (arylimido)vanadium-alkylidene complex **82** with diphenylacetylene at -30 ˚C (Scheme 1-19).[32] The resulting metallacyclobutene was identified based on ^{1}H, ^{13}C, ^{51}V NMR spectroscopy, which indicates that complex **83** is a mixture of two isomers for the reason that the diphenylacetylene can potentially insert via both *syn* and *anti* fashion.
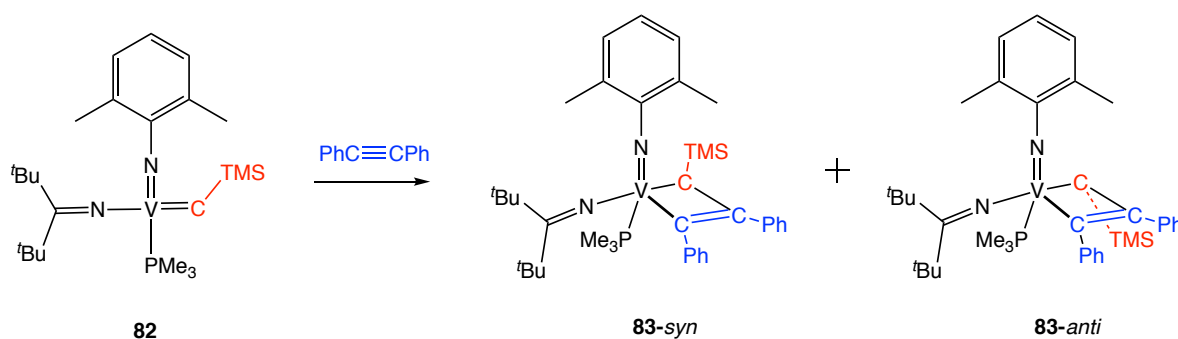
Scheme 1-19. Formation of vanadacyclobutene from vanadium alkylidene complex.

Tantalacyclotuenes were prepared by R. R. Schrock in 1988 from the reaction between tantalum alkylidene complex and symmetric acetylenes (Scheme 1-20).[33] The alternative possible structure of vinylalkylidene complexes formed by rearrangement of the metallacyclobutene can be ruled out based on the α-H chemical shift at 3-4 ppm and the splitting pattern in the NMR spectrum.

84

85

R = Me, Ph, TMS
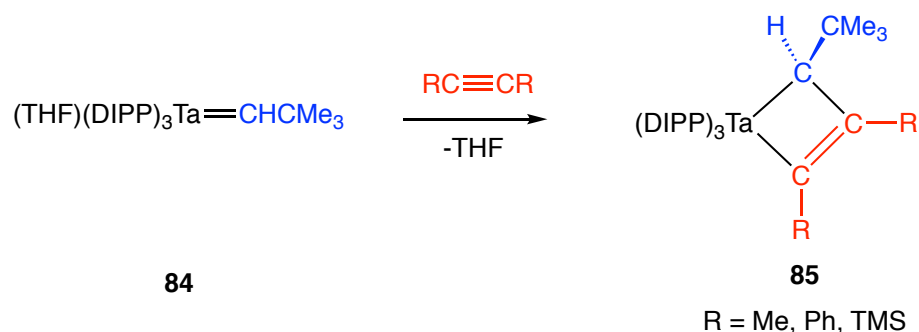
Scheme 1-20. Tantalum alkylidene complexes couple with acetylene.

In 2001, Adams reported that an iminium molybdacyclobutene can be obtained via a ring rearrangement that is triggered by protonation of metallacyclopentene concomitant with an isocyanide shift (Scheme 1-21).[34] The metallacyclobutene was isolated and confirmed by X-ray crystallography.

86

87
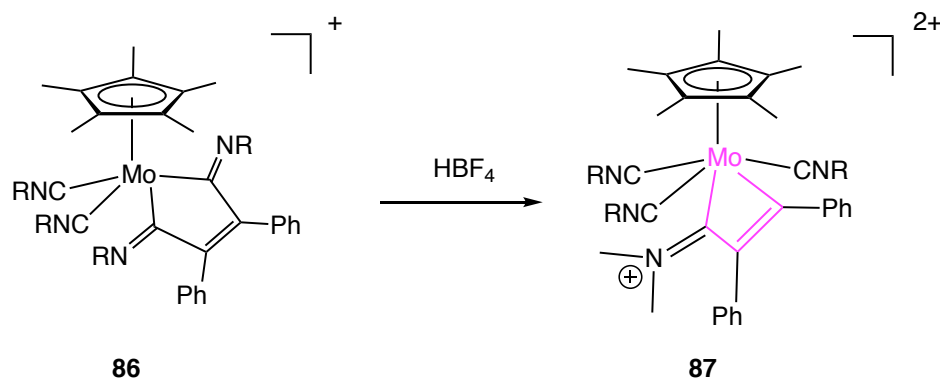
Scheme 1-21. Formation of molybdacyclobutene complex from metallacyclopentene.

Casey described rhenacyclobutene formations via hydride abstraction of rhenium-alkyne complex **88** with trityl cation to generate (η^3-propargyl) rhenium complex, that is followed by nucleophilic attacking at the center carbon by PMe$_3$ or alkyl lithium reagents (Scheme 1-22).[35,36]
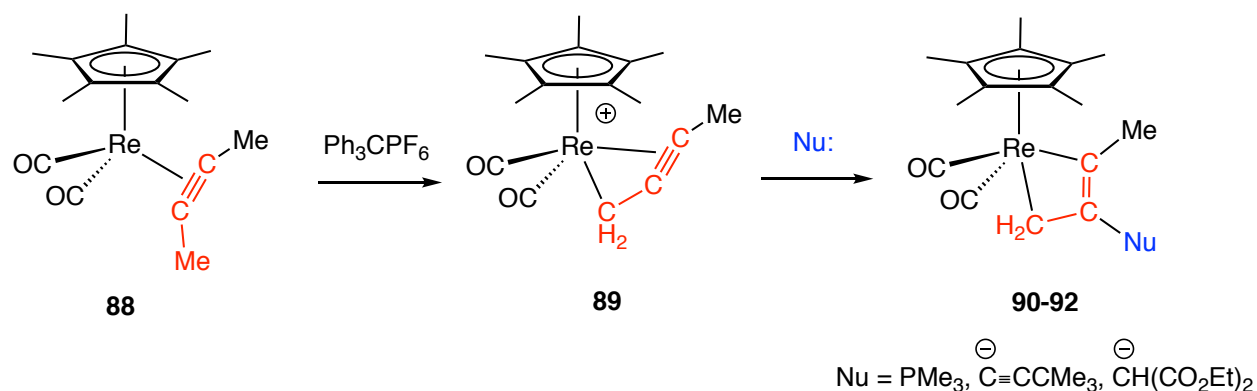
Scheme 1-22. Synthesis of rhenacyclobutene from η^3-propargyl rhenium complex.

Iminium cobaltacyclobutenes were assembled by Wakatsuki's lab via coupling of cobalt-alkyne complexes with isocyanide with highly regioselectivities (Scheme 1-23).[37] In a similar fashion, insertion of alkylisocyanide into the rhodium-alkyne complex can produce rhodacyclobutene complex[38] (Scheme 1-24) whose structure was subsequently confirmed by X-ray crystallography.

R^1= Ph, H, Me
R^2 = Ph, CN, CO_2Me

R^3 = p-MeC$_5$H$_4$, Ph, 2,6-Me$_2$C$_6$H$_3$
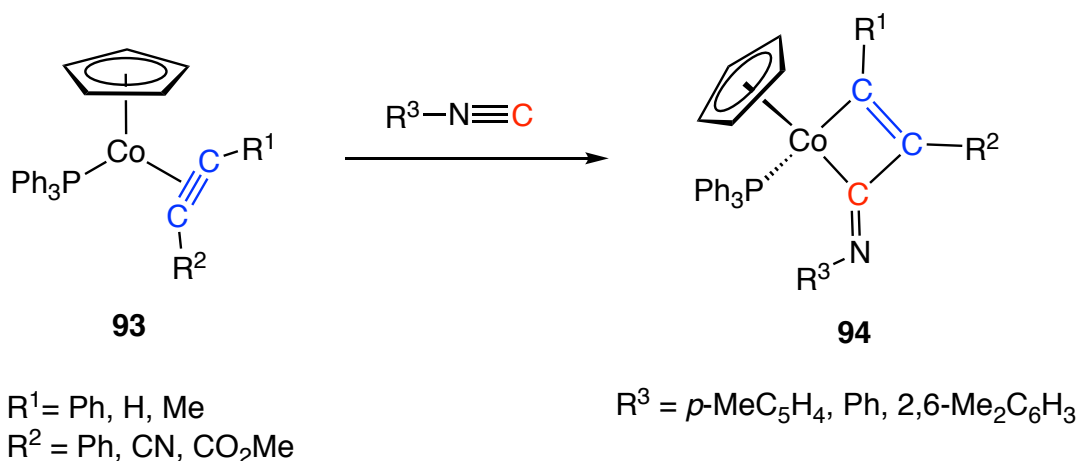
Scheme 1-23. Formation of iminium cobaltacyclobutene from cobalt-alkyne complex and isocyanide.
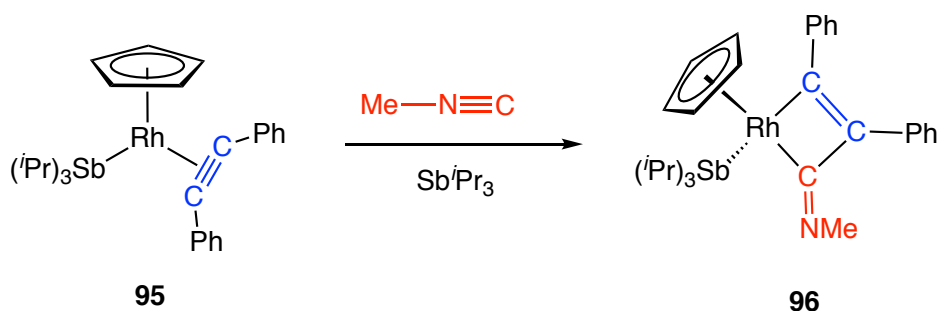
Scheme 1-24. Formation of iminium rhodacyclobutene from rhodium-alkyne complex and isocyanide.

O'Connor's lab described the formation of an air-stable highly functionalized cobaltacyclobutene from the reaction of cobalt-alkyne complex and ethyl diazoacetate in 1992. (Scheme 1-25)[39] The resulting metallacyclobutene turns out to be very regio- and stereo-selective. The steric hindrance between ester group and triphenyl phosphine dictates the *trans* configuration, and the electron-withdrawing sulfone substituent located on the α-carbon help stabilize the ring structure.

Scheme 1-25. Metallacyclobutene formation from cobalt-alkyne complex and diazocarbonyl.

More recently, in 2017, Tom Baker's group reported an isolable highly fluorinated cobaltacyclobutene complex which is derived from the coupling of cobalt alkylidene complex **99** with phenyacetylenes (Scheme 1-26).[40] The experimental results suggest

that terminal acetylenes with electron-withdrawing groups are crucial to stabilize the four-membered ring framework, and DFT calculations indicate that the rate limiting step is the formation of a 1,4-diradical intermediate **100**.
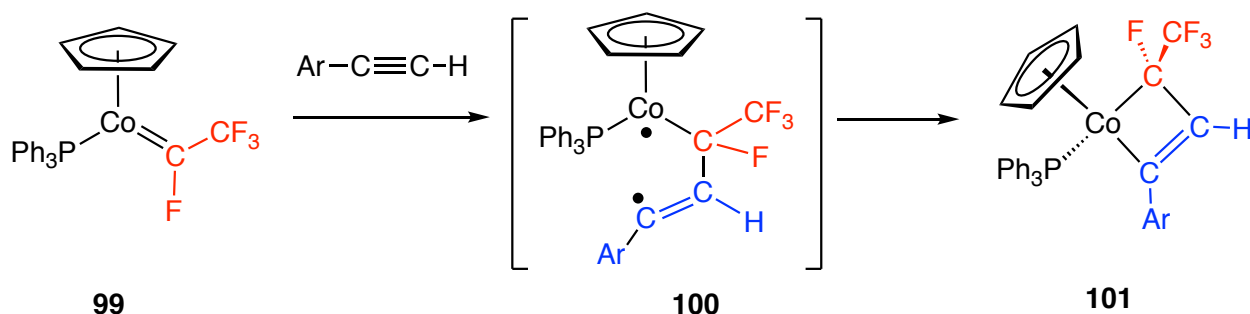
Scheme 1-26. Coupling of acetylene with cobalt alkylidene complex.

The first isolated and structurally characterized iridacyclobuene was reported by Thorn in 1983.[41] They conducted a carbon-oxygen bond cleavage on a (methoxymethyl)iridium acetylene complex **102** by employing an electrophilic reagent (BrSiMe₃). They proposed that once losing the methoxy group, an iridium alkylidene acetylene intermediate was generated followed by annulation to form the metallacyclotuene **104** (Scheme 1-27).
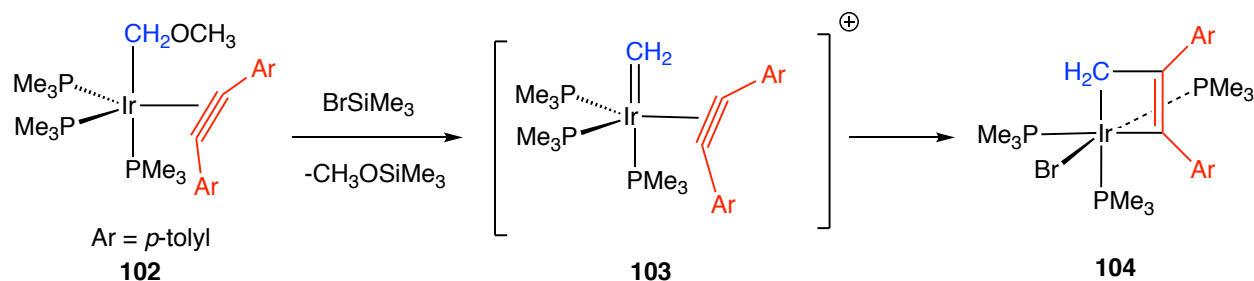
Scheme 1-27. Synthesis of iridacyclobutene via carbon-oxygen bond cleavage.

Another example of isolated iridacyclobutene was synthesized by O'Connor's lab in 1990 through a rearrangement of a metallacyclopentadiene alkylidene complex **105**.[42] The formation of metallacyclobuene was proposed to proceed via a migratory coupling of the carbene with carbon metal bond (Scheme 1-28). The structure of the iridacyclobutene was unambiguously determined by X-ray diffraction study.
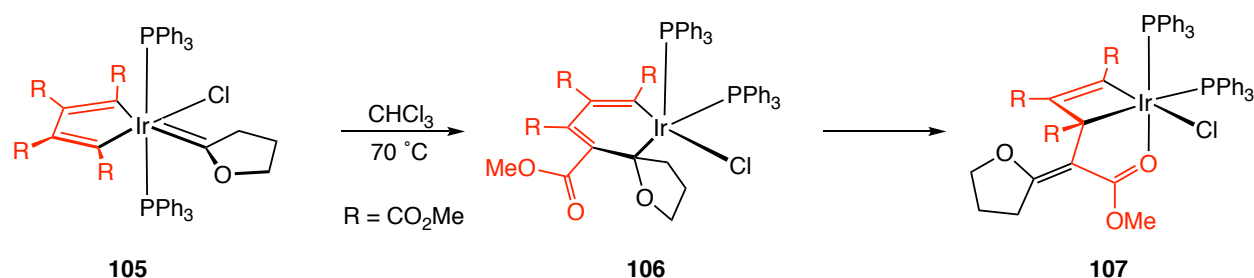
Scheme 1-28. Cobaltacyclobutene from rearrangement of a metallacyclopentadiene.

Platinacyclobutenes were reported by Hughes's group in 1988 via oxidative addition of perfluorocyclopropene to platinum (0) complex (Scheme 1-29).[43] The resulting metallacyclobutene was isolated and characterized by ^{19}F, ^{31}P, ^{1}H, ^{13}C NMR spectroscopy as well as single-crystal X-ray diffraction.
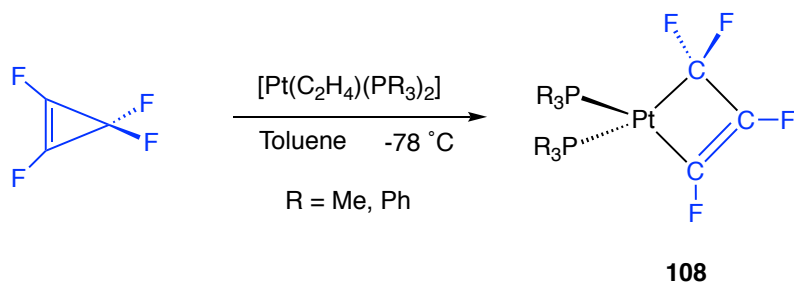
Scheme 1-29. Formation of platinacyclobutene from metal-insertion reaction.

Analogous to synthetic strategy of Casey's rhenacyclobutene, platinacyclobutenes were also prepared by Chen's lab in 1997 by employing NEt_3, PPh_3, and pyridine as nucleophiles to attack the center carbon of cationic (η^3-propargyl) platinum complex (Scheme 1-30).[44]

$$ER_3 = NEt_3, PPh_3$$

109　　　　　　　　　　**110**
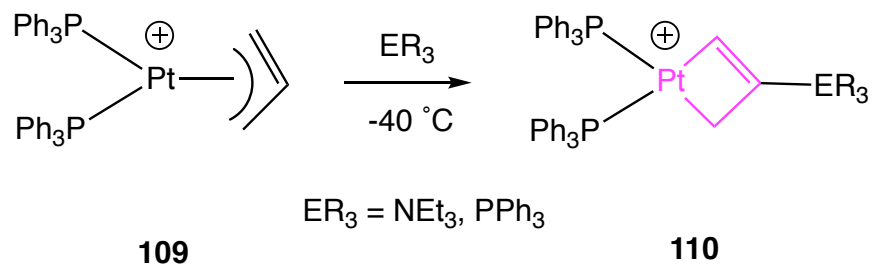
Scheme 1-30. Synthesis of platinacyclobutene from (η^3-propargyl) platinum complex.

D. η^4-Cyclopentadiene Complexes

Cyclopentadienyl ligand is one of the most significant ancillary ligands in organometallic chemistry. As an important coordination mode, η^4-cyclopentadiene complexes have been largely studied since the discovery of its η^5-cyclopentadienyl complex analogues. Nucleophilic additions of the η^5-cyclopentadienyl complexes have been widely employed as the major method to synthesize η^4-cyclopentadiene complexes. However, despite η^5-cyclopentadienyl metallic complex is ubiquitous in both early and late transition metals, the corresponding η^4-cyclopentadiene ligands are mostly found bearing high affinity to late transition metals.

The first η^4-cyclopentadiene complex was reported by Wilkinson in 1959.[45] They discovered that when the cobaltocenium halides were treated with sodium borohydride

or lithium aluminum hydride, a neutral compound was obtained, in which one of the Cp ligands has been reduced to cyclopentadiene (Scheme 1-31). Also, a monomethyl derivative, $(\eta^5\text{-}C_5H_5)Co(\eta^4\text{-}5\text{-methylcyclopenta-1,3-diene})$ **114** was prepared by the reaction between methyl iodide and cobaltocene. The structures of the two η^4-cyclopentadiene cobalt complexes were supported by the ^1H NMR spectra, in which the two sets of shielded vinyl hydrogens were observed at about 5.2 and 2.5 ppm, while the ring hydrogen attached on the sp^3 carbon is located at 2.0 or 2.6 ppm.
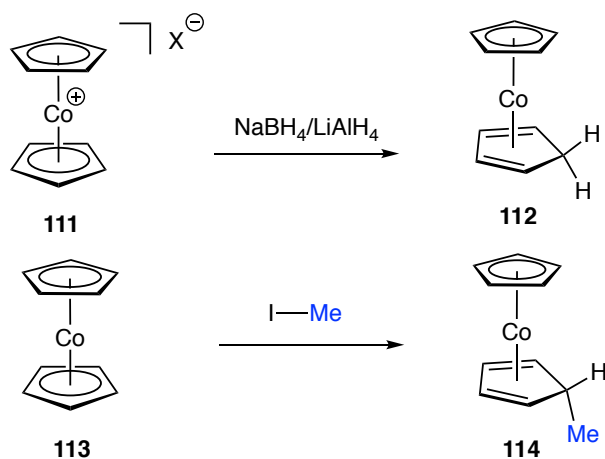
Scheme 1-31. The first reported synthesis of η^4-cyclopentadiene complexes.

Since then more and more examples of η^4-cyclopentadienyl cobalt (I) complexes were synthesized by nucleophilic attack of Grignard reagents at the unsaturated hydrocarbon ring of cobaltocenium cations (Scheme 1-32).[46] X-ray single crystallography has also been utilized to study the structures of isolated η^4-cyclopentadiene cobalt (I) complexes,[47,48] which reveals that two possible stereoisomers, *exo* and *endo*, can exist in this system.
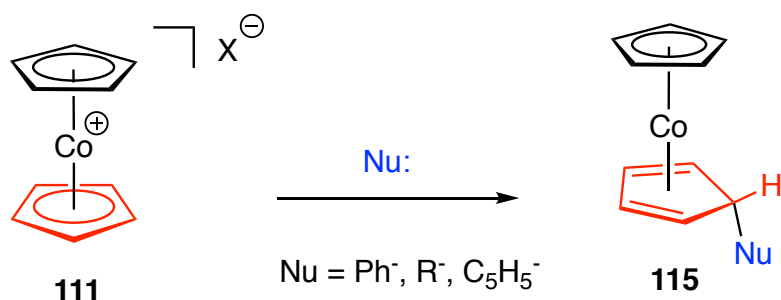
Scheme 1-32. Formation of η^4-cyclopentadiene complexes from cobaltocenium cation.

The reactions of cobaltocene with organocadmium compounds were also reported to make the (η^5-cyclopentadienyl)(η^4-cyclopentadiene) cobalt complexes.[49, 50] Mechanistically, they proposed that after the cobaltocene activates the R-Cd bond within the coordination sphere of the cobalt atom, two transition states **116** and **117** can be given followed by formation of the *exo* isomer of η^4-cyclopentadienyl product, as well as the metallic cadmium as side product (Scheme 1-33).
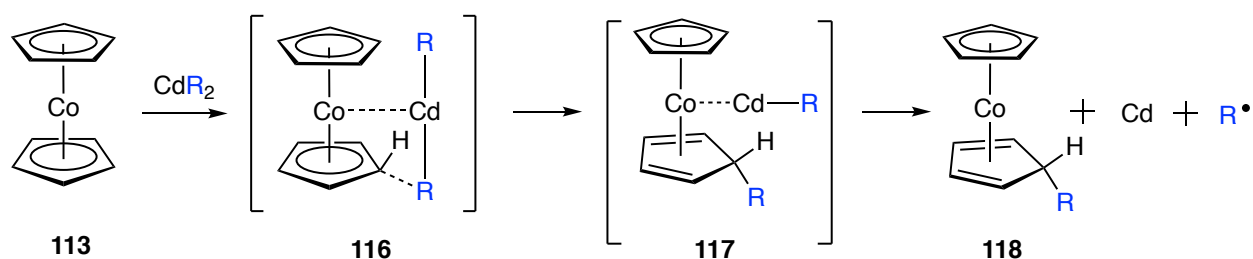
Scheme 1-33. Organocadmium assisted formation of η^4-cyclopentadiene complex.

In 1988, O'Connor described a coupling of carbene with two alkynes to generate highly substituted η^4-cyclopentadiene products.[51] Three different metallacyclopentadiene complexes (**119**, **120**, **121**) that were prepared from coupling of CpCo(PPh₃)₂ with two alkynes are employed as precursors to react with ethyl

25

diazoacetate. After extrusion of dinitrogens, metallacycles **119** and **121** selectively generated the *exo-η⁴*-cyclopentadiene products **122** and **124**, respectively, while both *endo* and *exo* isomers were obtained in the case of metallacyclopentadiene **120** (Scheme 1-34). Followed by this work, they reported oxidations of the *η⁴*-cyclopentadiene cobalt (I) complex derived therefrom to produce uncomplexed cyclopentadienes and cobaltocenium cations.[52]
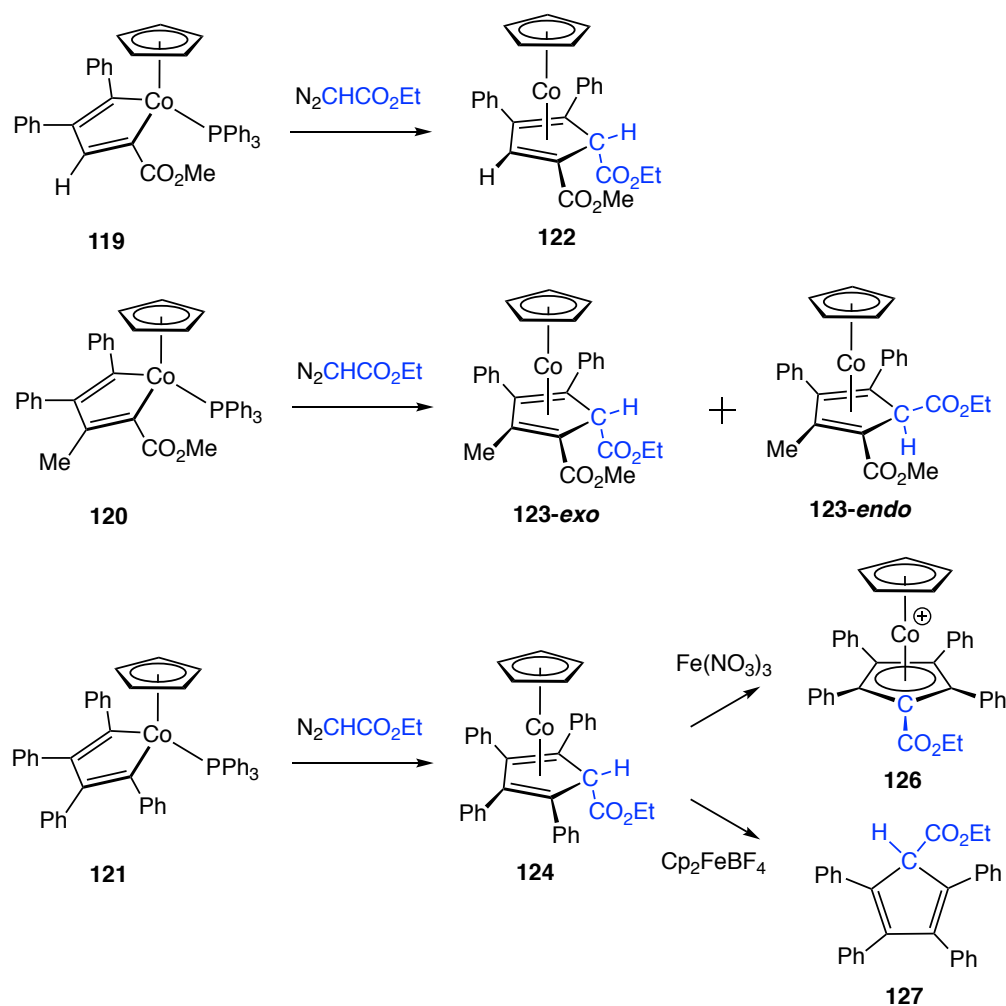
Scheme 1-34. Carbene insertion of metallacyclopentadienes.

P. Fehlner reported a very interesting cluster structure of cobaltopentaborane complex **128** of which the steric demands of the external ligands on metal center compete effectively with the electronic requirement of the core, in which a η^4-cyclopentadiene cobalt substructure is incorporated (Scheme 1-35).[53]
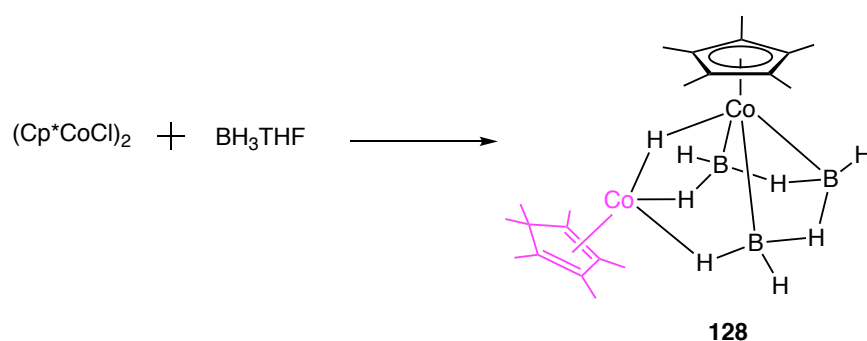
Scheme 1-35. Formation of a η^4-cyclopentadiene cluster.

In 1995, O'Connor 's lab reported that when a cobaltocyclobutene was treated with numerous alkynes, η^4-cyclopentadiene products can be generated with high regio- and stereoselectivites (Scheme 1-36).[6] They proposed that the steric hindrance of the alkyne substrate dictates the distributions of *exo* and *endo* isomers.

R^1 = CO_2Me, Ph, CMe_3, CH_2OCH_3
R^2 = H, CO_2Me, COMe
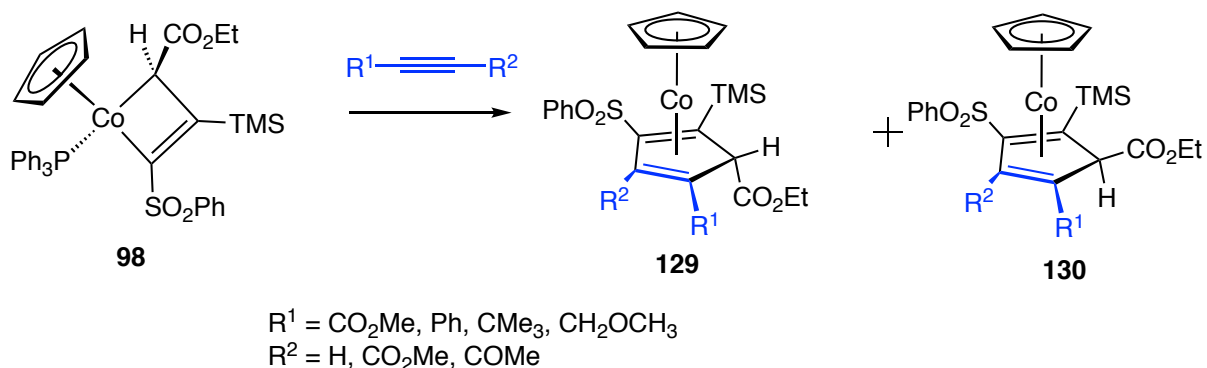
Scheme 1-36. Cobaltacyclobutene to η^4-cyclopentadiene complexes.

In 2009, Wang prepared two *exo-η^4*-cyclopentadiene cobalt complexes by employing cobaltocene reacting with ethyl 2-bromoisobutyrate and AIBN (Scheme 1-37).[54] By conducting kinetic studies, they discovered that the *exo*-substituted η^4-cyclopentadiene cobalt complexes are the actual catalyst for the atom transfer radical polymerization process of methyl methacrylate (MMA).
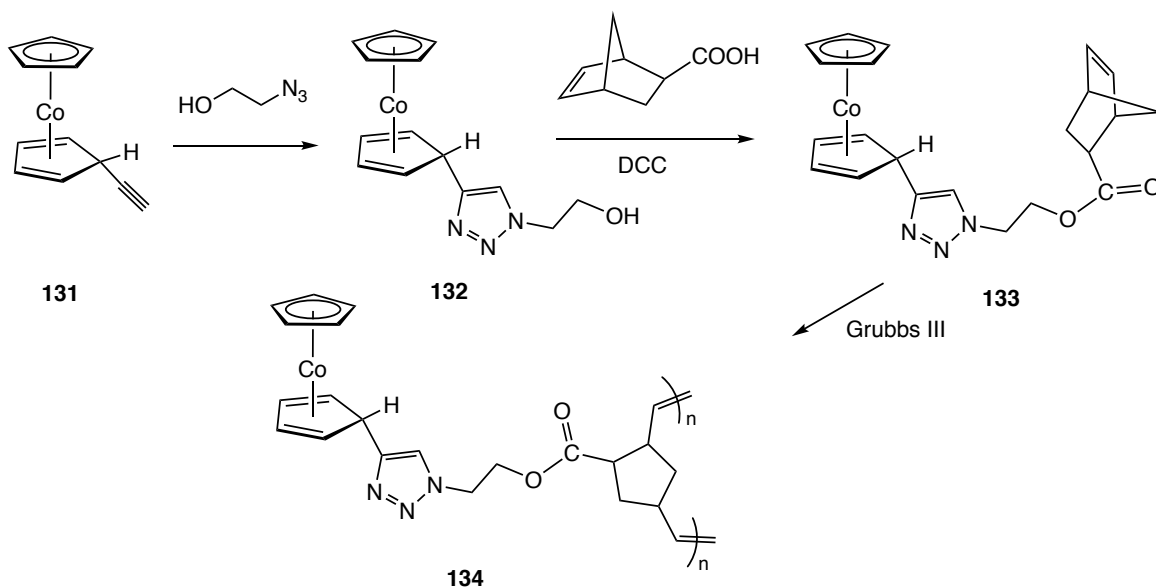
Scheme 1-37. η^4-Cyclopentadiene cobalt complex catalyzed polymerization.

A neutral *exo*-substituted η^4-cyclopentadiene CpCo(I) unit-containing polymer was synthesized by Tang' lab in 2014.[55] The monomer was prepared by copper-catalyzed azide-alkyne cycloaddition followed by esterification to incorporate a norbornene group (Scheme 1-37). After treating the monomer with Grubbs catalyst III, metallopolymer **134** can be prepared as light orange powders. They also found that the resulting metallopolymer can be applied as heterogenous macromolecular catalyst for atom transfer radical polymerization of methyl methacrylate and styrene.

Besides cobalt, iron is the second largest studied transition metal that bears the η^4-coordination mode to cyclopentadiene. The first η^4-cyclopentadiene iron complex was prepared by P. L. Pauson in 1956 via the reaction between cyclopentadiene and iron tricarbonyl dimer (Scheme 1-38).[56] In1974, Whitesides reported a alternate route to η^4-cyclopentadiene Fe(CO)$_3$ complex by employing sodium cyanoborohydride to reduce the CpFe(CO)$_3$BF$_4$.[57]

135   **136**   **137**
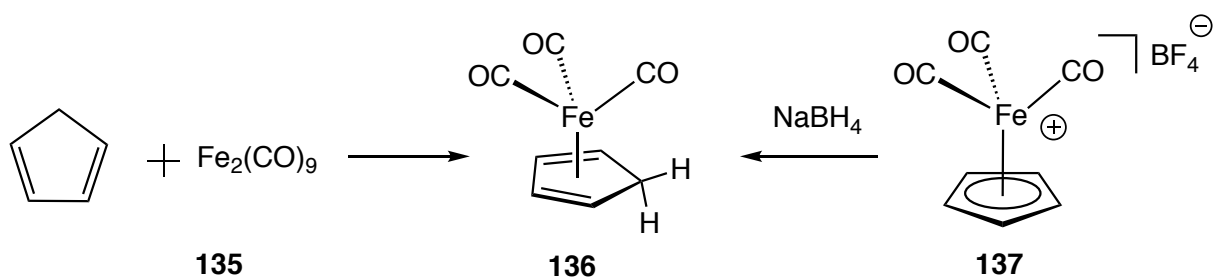
Scheme 1-38. The first reported η^4-cyclopentadiene iron complex.

Weber synthesized novel 5-*exo*-phoshino-η^4-cyclopentadiene complexes (η^4-C$_5$H$_5$PR^{1}R^2)Fe(CO)$_3$ by employing PR^{1}R^2 as nucleophile to attack the carbocyclic ligand of the cationic CpFe(CO)$_3$ complex (Scheme 1-39).[58] However, it is interesting to find that it failed when the cationic Cp*Fe(CO)$_3$ analogue was utilized, in which the carbon monoxide that is attached on the metal was attacked by the nucleophile instead of the carbocyclic ligand.
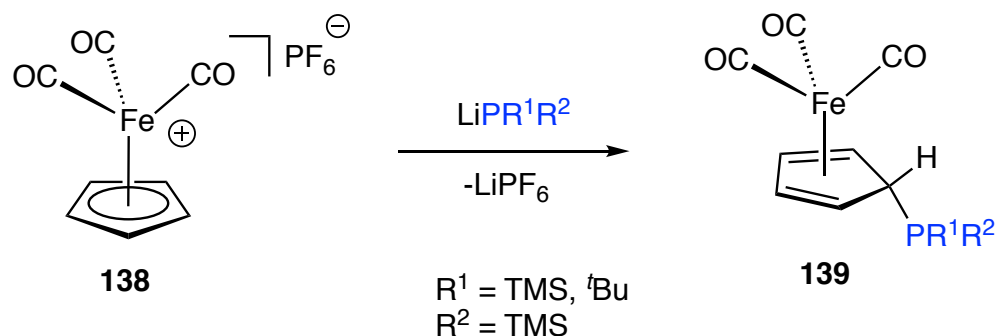
Scheme 1-39. Phosphine substituted η^4-cyclopentadiene iron complex.

Liu described a ring alkylation reaction by employing MeLi as nucleophile to attack $(\eta^5\text{-Cp})Fe(CO)_2I$ in the presence of bis(diphenylphosphino)methane (dppm) as coordination ligand to yield a novel monodentate dppm complex $(\eta^4\text{-}MeC_5H_5)Fe(CO)_2((\eta^1\text{-dppm})$ (Scheme 1-40).[59]
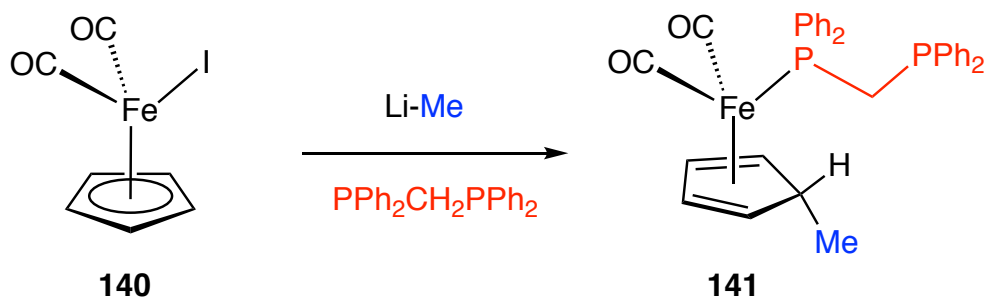
Scheme 1-40. Formation of a novel monodentate η^4-cyclopentadiene complex.

Valerio Zanotti demonstrated that a variety of carbon nucleophiles, such as Grignard and alkyl lithium reagents, can be applied to do the nucleophilic addition on the bridged iron dimetallic complex **142** to produce the η^4-cyclopentadiene iron complexes **143** (Scheme 1-41).[60]
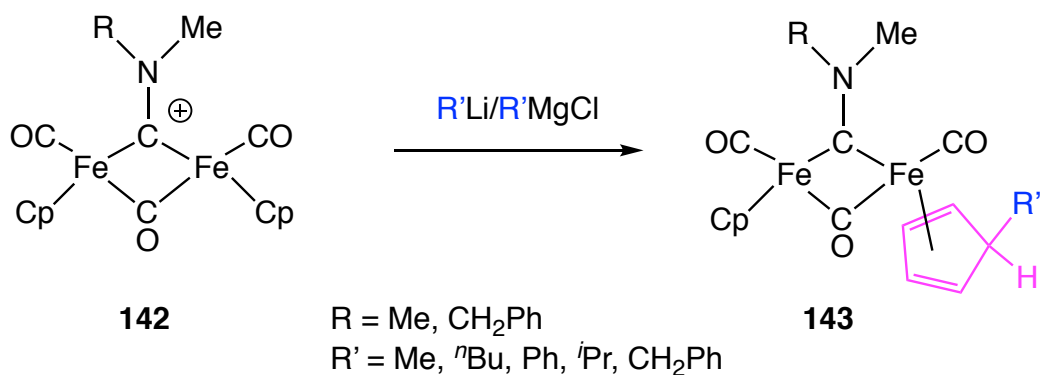
Scheme 1-41. Nucleophilic attack on the rion dimetallic complex.

At the same time, in 1997, Cutler exhibited a manganese carbonyl catalyzed reactions of PhMe$_2$SiH with methoxycarbonyl iron complexes Cp(CO)$_2$FeCO$_2$Me to yield the η^4-cyclopentadiene iron complex **145** (Scheme 1-42).[61] Mechanistically, they proposed that the manganese inserted into the Si-H bond followed by delivering the hydride to carbocyclic ligand of the iron complex, and then the ester group fragments to carbon monoxide and methoxysilane.
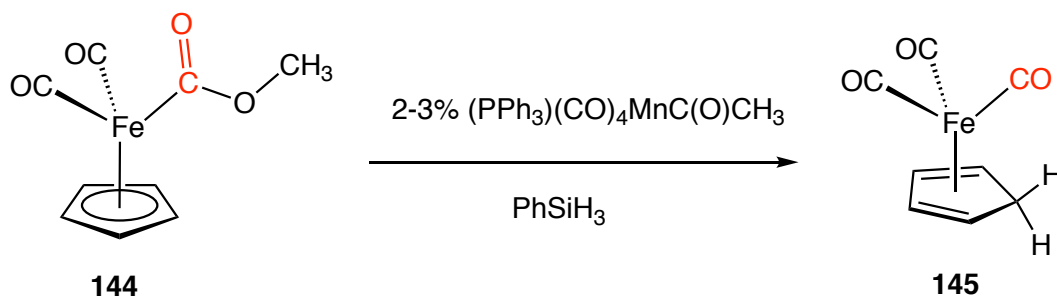
Scheme 1-42. Manganese catalyzed formation of η^4-cyclopentadiene iron complex.

Prout's lab reported a crystal structure of η^4-(1-*endo*-ethyl)cyclopentadiene-η^5-cyclopentadienyl(triehtylphosphine)-chloromolybdenum (II) **147**, which is synthesized by

treating $Cp_2Mo(C_2H_5)Cl$ with trialkylphosphine (Scheme 1-43).[62] It was found that the ethyl group that was attached on the metal center migrates to the cyclopentadienyl ring, in which a Cp ring slippage mechanism might be involved.

$R_3 = (C_2H_5)_3, (C_6H_5)_2CH_3, C_6H_5(CH_3)_2$
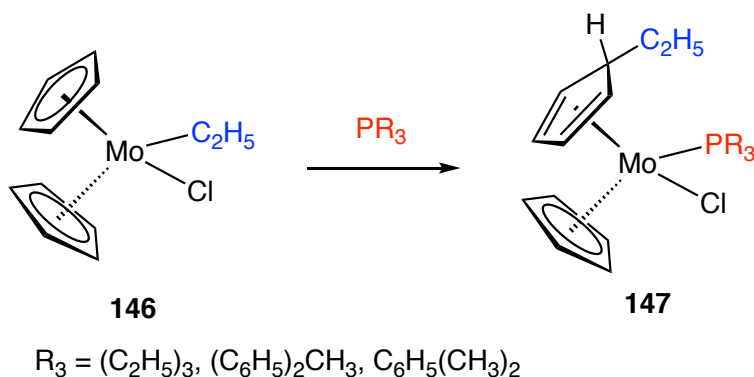
Scheme 1-43. Ethyl migration to form the molybdenum η^4-cyclopentadiene complex.

A novel α-hydrogen elimination reaction was discovered by Guy Orpen in 1986 that a four-electron alkyne-molybdenum complex was treated with diphenylacetylene to yield a η^4-cyclopentadiene molybdenum complex.[63] They proposed that after the α-hydrogen elimination, an alkylidene hydride complex **149** was generated followed by coupling with alkyne to form a hydridomolybdenacyclobutene intermediate **150**, which can be trapped by another equivalent of diphenylacetylene to form a metallacyclohexadiene **151**. After reductive elimination and molybdenum assisted hydride transfer, the final η^4-cyclopentadiene complex can be afforded (Scheme 1-44).
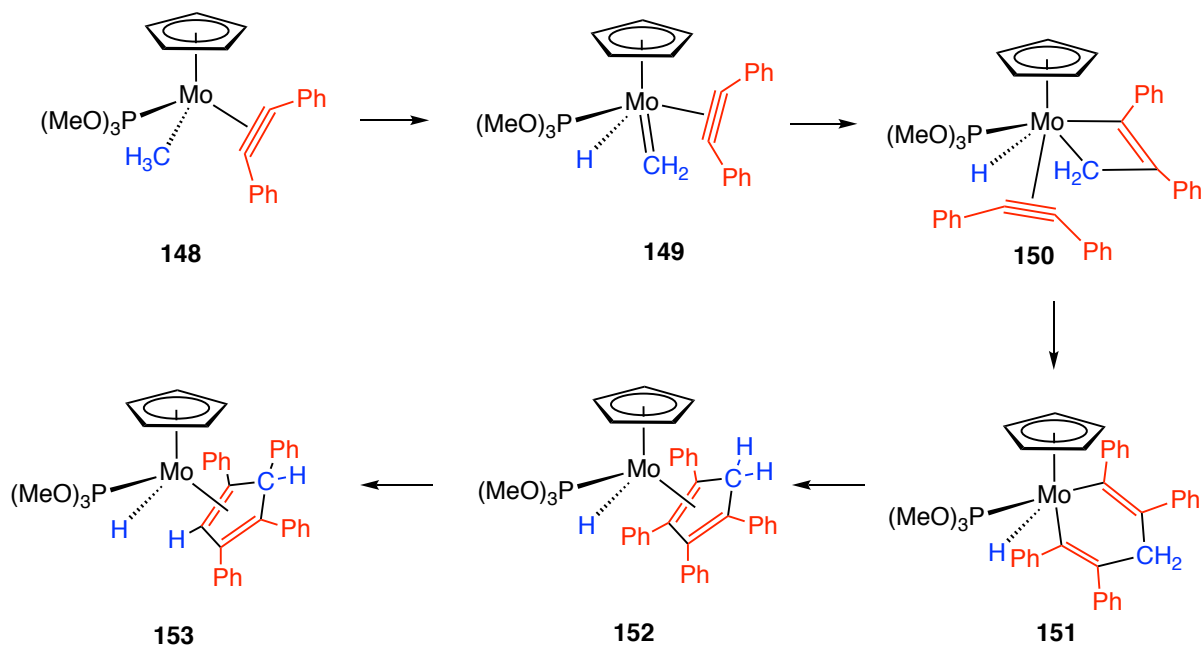
Scheme 1-44. Synthesis of η^4-cyclopentadiene complex via α-hydrogen elimination.

Hydride reduction[64,65] and nucleophilic addition[65] of the carbocyclic ligand were also demonstrated to be applicable to η^5-cyclopentadienyl molybdenum moiety. When the η^5-Cp indenyl molybdenum dication complex **154** was treated with sodium borohydride, the η^4-cyclopentadiene indenyl complex **155** was generated, whearas various nucleophiles can selectively attack the cyclopentadienyl ligand in the dimetallic molybdenum complex **156** (Scheme 1-45).
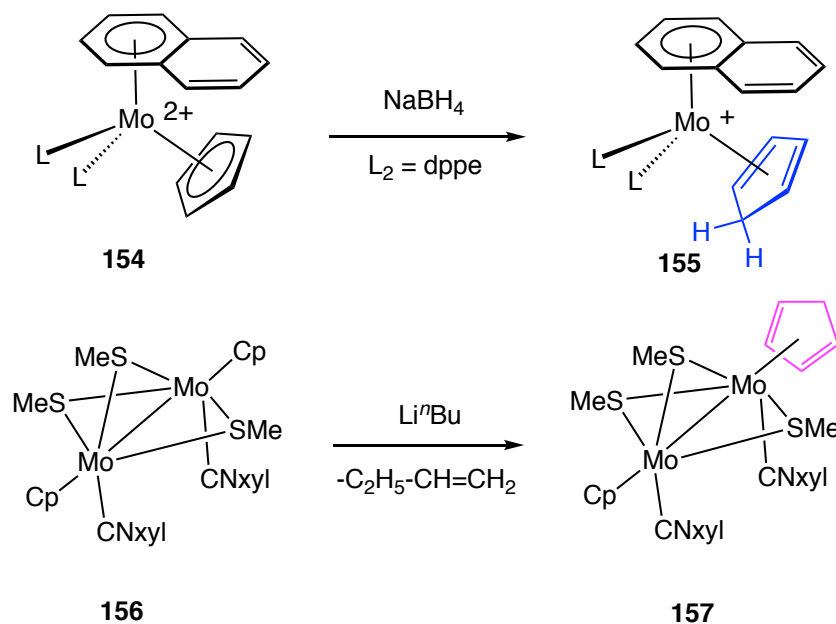
Scheme 1-45. Hydride reduction and nucleophilic addition on the cyclopentadiene.

In 1996, John Cooper discovered an electrophilic addition of CCl_4 to the cyclopentadienyl ligand in the tungstenocene carbonyl complex to produce the *exo-η^5-*CpW(η^4-C_5H_5-CCl_3)(CO)Cl complex.[66] It was postulated that two steps are getting involved in the mechanism: 1) electron transfer from the metal to fragment the CCl_4 into a radical and chloride anion. 2) *exo* addition of the trichloromethyl radical on the cyclopentadienyl ligand (Scheme 1-46).
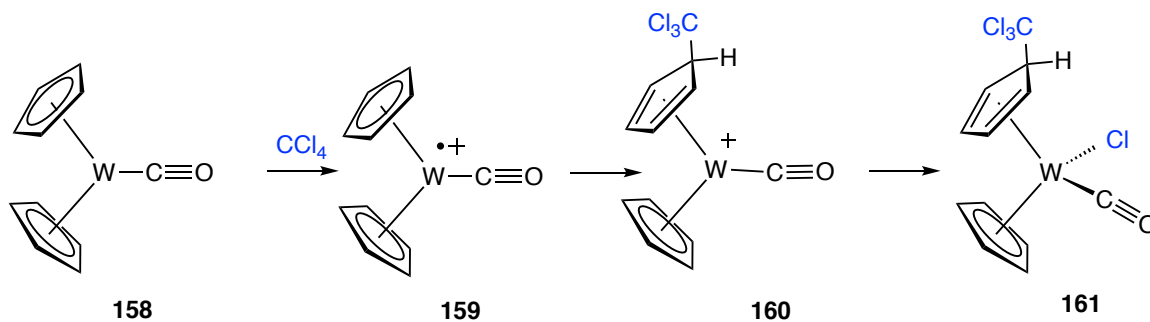
Scheme 1-46. CCl_4 incorporated formation of tungsten η^4-cyclopentadiene complex.

34

More lately, in 2003, John Cooper also synthesized a η^4-cyclopentadiene manganese anion complex **164** by utilizing excess of cyclopentadiene monomer at 195 K to trap [Mn(η^4-C$_6$H$_6$)(CO)$_3$]$^-$ that was prepared from anthracenide reduction of [Mn(η^6-C$_6$H$_6$)(CO)$_3$]PF$_6$ (Scheme 1-47).[67] The structure of the resulting product was studied by X-ray crystallography.
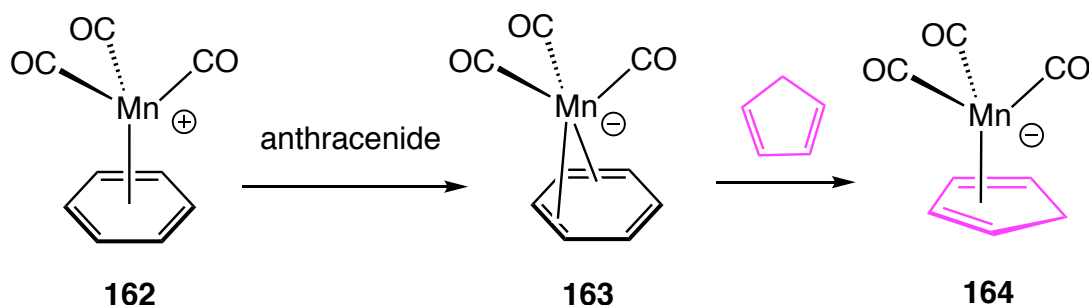
Scheme 1-47. Synthesis of manganese η^4-cyclopentadiene complex.

The first η^4-cyclopentadiene rhenium complex was prepared by N. W. Alcock in 1965, in which the bis-η^5-cyclopentadienyl rhenium hydride complex was treated with excess of *n*-butyl lithium followed by excess of methyl iodide (Scheme 1-48).[68] Despite the detailed mechanism was not given, the resulting *exo-η^4*-cyclopentadiene rhenium complex was demonstrated by X-ray studies.
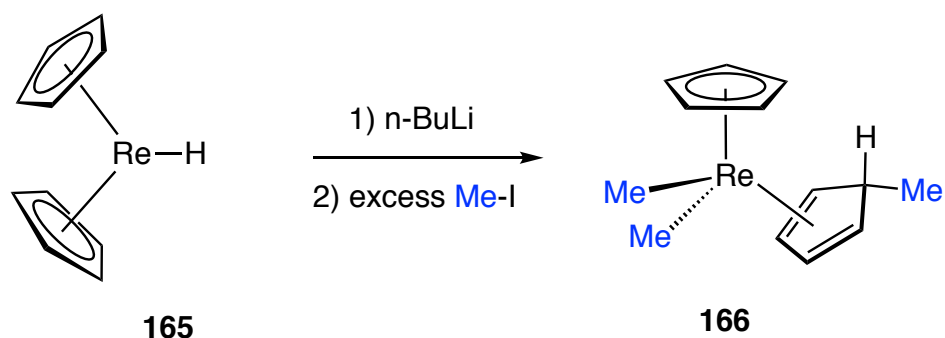
Scheme 1-48. Rhenium hydride complex to *exo*-η^4-cyclopentadiene.

Another η^4-cyclopentadiene rhenium complex was reported by Willian Jones.[68,69] They employed the rhenium triphenylphosphine hydride as precursors, either under thermal condition or photochemical condition in the presence of excess of cyclopentadiene, the η^4-cyclopentadiene rhenium trihydride complex **167** was obtained (Scheme 1-49).
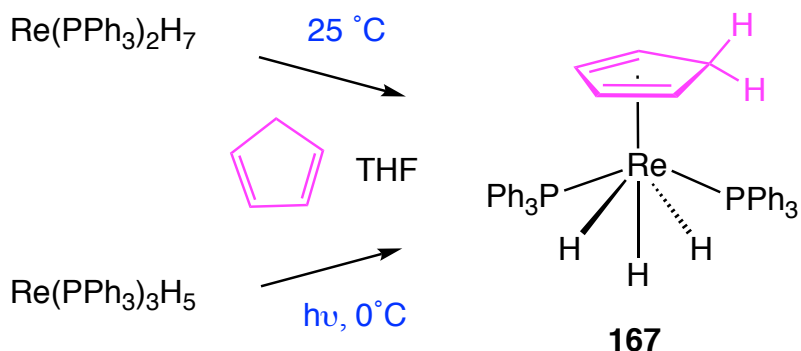
Scheme 1-49. Synthesis of rhenium η^4-cyclopentadiene under thermal and photochemical conditions.

Related to what John Cooper did on tungsten complex, Gladysz described a formation of *exo*-substituted η^4-cyclopentadiene rhenium complex by using a phenylphosphido complex (η^5-C$_5$H$_5$)Re(NO)(PPh$_3$)(PPhCl) reacting with CCl$_4$ (Scheme

1-50).[70] They proposed that the reaction was achieved by a charge transfer followed by a radical chain mechanism that is supported by the fact that the formation of final η^4-cyclopentadiene product was dramatically inhibited in the presence of radical trap duroquinone.
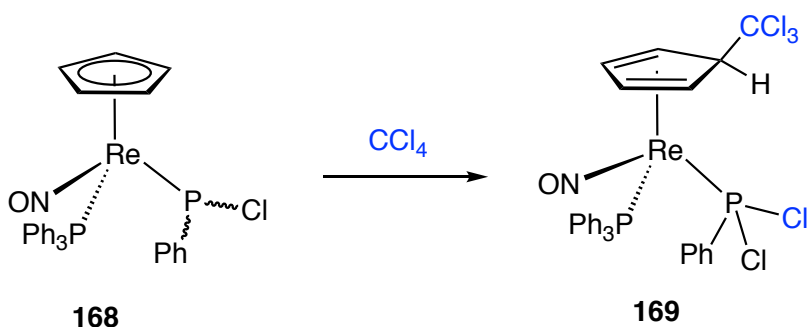
Scheme 1-50. CCl$_4$ incorporated formation of rhenium η^4-cyclopentadiene complex.

In comparison to iron carbonyl analogue, the ruthenium η^4-cyclopentadiene complex can be prepared from reflux mixture of Ru$_3$(CO)$_{12}$ with cyclopentadiene in hexanes (Scheme 1-51).[71] Even though quantitative conversion into CpRu(CO)$_2$H was observed after prolonged heating, the η^4-cyclopentadiene intermediate can be isolated as pale yellow liquid whithin a short reaction time.
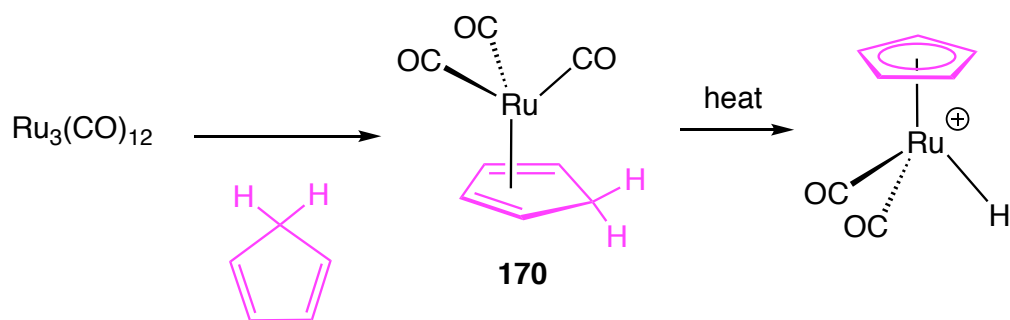
Scheme 1-51. Synthesis of ruthenium η^4-cyclopentadiene complex.

The ruthenium η^4-cyclopentadiene complex was also found prepared from hydride reduction of Cp ligand on the ruthenium cationic molecule. Stephen Davies reported that the triphos or tripod ruthenium cations **171**, **172** can be reduced to the corresponding *exo* η^4-cyclopentadiene complexes that is confirmed by deuterium labelling study (Scheme 1-52).[72]
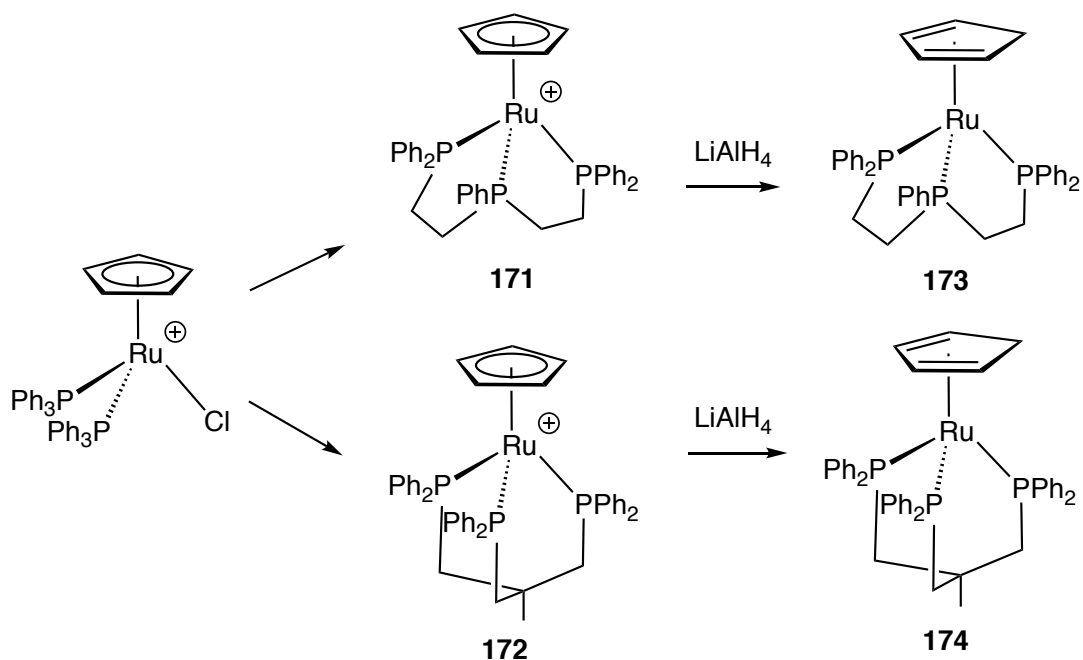
Scheme 1-52. Hydride reduction to form ruthenium η^4-cyclopentadiene complex.

Hughes reported a formation of rhodium η^4-cyclopentadiene complex by treating the 1,2,3-triphenyl-3-vinylcycloprop-1-ene **175** with η^4-indenyl-Rh(η^2-C$_2$H$_2$)$_2$ complex **176**.[73] They proposed that a metallacyclohexadiene complex **177** serves as the intermediate after a formal oxidative addition of the vinylcyclopropene to the metal, that is followed by reductive elimination to afford the final η^4-cyclopentadiene product (Scheme 1-53). Another example they reported later in 1993 is that when the *t*-butyl

analogue of vinylcyclopropene was employed as precursor to react with [Rh-η^2-(C$_2$H$_2$)$_2$-Cl]$_2$, a vinyl metallacyclobutene complex **180** can be isolated, and after longer reaction time at room temperature, the vinyl metallacyclobutene intermediate can be converted to the η^4-cyclopentadiene complex **181**.[74,75] This observation further supported the mechanism they proposed in the former reaction.
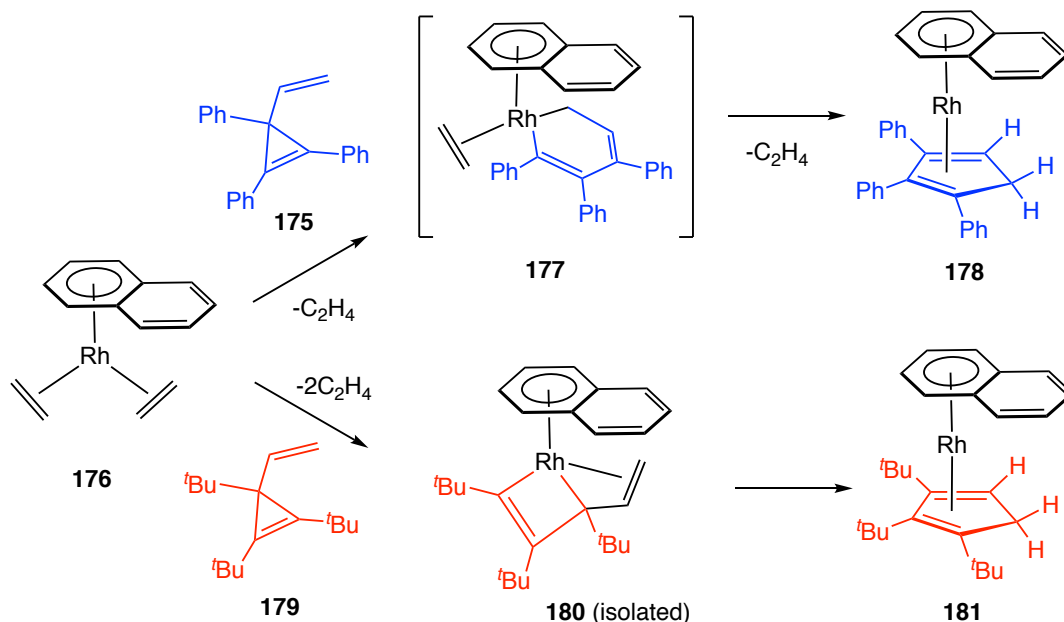
Scheme 1-53. Synthesis of rhodium η^4-cyclopentadiene complexes.

The earliest iridium η^4-cyclopentadiene complex was synthesized by Fisher in 1959, in which they treated the IrCl$_3$ with KC$_5$H$_5$ to produce a pale-yellow solid that was proposed as a η^5-C$_5$H$_5$-Ir-η^4-C$_5$H$_6$ complex **183**.[76] More lately, in 1991, Shapley reported an unexpected acquisition of the same complex **183** via the reaction of [(η^2-C$_8$H$_{14}$)$_2$IrCl]$_2$ with thallium cyclopentadienide (Scheme 1-54).[77]
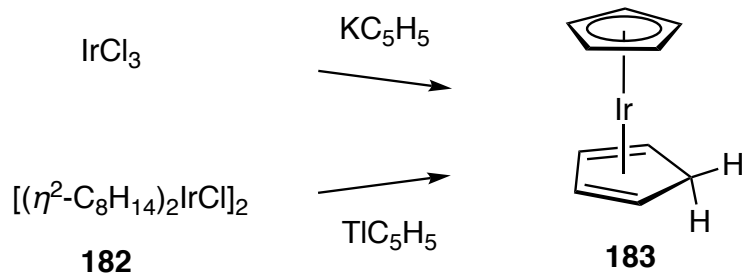
Scheme 1-54. Synthesis of iridium η^4-cyclopentadiene complex.

Furthermore, the synthesis of platinum η^4-cyclopentadiene complexes were described by Maitlis 1994.[78] They discovered that when a suspension of K_2PtCl_4 in methanol was treated with the mixture of pentamethylcyclopentadiene, $SnCl_2$, and concentrated hydrochloric acid, a mixture of two isomeric (*exo* and *endo*) platinum η^4-cyclopentadiene complexes (**184-a** and **184-b**) can obtained after refluxing in methanol for 4 hours (Scheme 1-55).
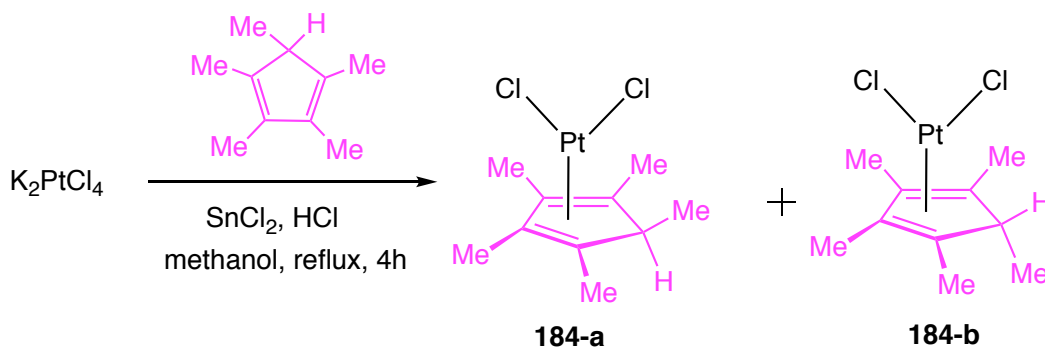
Scheme 1-55. Synthesis of platinum endo and exo-η^4-cyclopentadiene complexes.

E. Conclusion

A number of proposed metallacyclobutenes were described to serve as key intermediates or transition states in a large variety of transition metal-mediated reactions to construct new carbon-carbon bonds, including cyclopropenation, acetylene polymerization, and enyne metathesis. Despite extensive studies have been conducted on synthesis and characterization of metallacyclobutenes from a wide range of different transition metals, sufficiently stable metallacyclobutenes for isolation are still found subject to combinational factors of metal, ring substituents, and ancillary ligands. Most of the reported metallacyclobutene complexes were found lack of functional-group tolerance. Also, despite a lot of different types of substrates were explored to react with metallacyclobutene in O'Connor's lab, the reactivity studies of late transition-metal metallacyclobutene were still rare in the literature. Hence, more investigations are still needed to unveil these subtle structurally stable metallacyclobutenes as well as their reactivities. Furthermore, as one of oldest discovered organometallic compounds, η^4-cyclopentadiene complexes were largely reported in the literature, and a number of representative examples with various transition metals are presented in this chapter. However, only a few reactivity studies with very limited description of mechanisms were found on these molecules, and therefore, more reactive patterns and mechanistic studies of η^4-cyclopentadiene complexes need to be furtherly developed.

F. References

1. (a) McGuinness, D. S. Olefin oligomerization via metallacycles: dimerization, trimerization, tetramerization, and beyond. *Chem. Rev.* **2010**, *111*, 2321-2341. (b) Hoveyda, A. H. Evolution of catalytic stereoselective olefin metathesis: from ancillary transformation to purveyor of stereochemical identity*. J. Org. Chem.* **2014**, *79*, 4763-4792.

2. (a) Fürstner, A.; Mathes, C.; Lehmann, C. W. Mo [N(*t*-Bu)(Ar)]₃ complexes as catalyst precursors: in situ activation and application to metathesis reactions of alkynes and diynes. *J. Am. Chem. Soc.* **1999**, *121*, 9453-9454. (b) Fürstner, A.; Mathes, C.; Lehmann, C. W. Alkyne metathesis: development of a novel molybdenum-based catalyst system and its application to the total synthesis of epothilone A and C. *Chem. Eur. J.* **2001**, *7*, 5299-5317. (c) Tsai, Y. C.; Diaconescu, P. L.; Cummins, C. C. Facile synthesis of trialkoxymolybdenum (VI) alkylidyne complexes for alkyne metathesis. *Organometallics* **2000**, *19*, 5260-5262. (d) Fürstner, A.; Seidel, G. Ring-Closing Metathesis of Functionalized Acetylene Derivatives: A New Entry into Cycloalkynes. *Angew. Chem. Int. Ed.* **1998**, *37*, 1734-1736. (e) Zhang, W.; Moore, J. S. Synthesis of poly (2, 5-thienyleneethynylene)s by alkyne metathesis. *Macromolecules* **2004**, *37*, 3973-3975.

3. Nicolaou, K. C.; Bulger, P. G.; Sarlah, D. Metathesis reactions in total synthesis. *Angew. Chem. Int. Ed.* **2005**, *44*, 4490-4527.

4. (a) O'Connor, J. M.; Chen, M. C.; Holland, R. L,; Rheingold, A. L. Addition of Dissimilar Carbenes across an Unsymmetrically Substituted Alkyne: Regio-and Stereoselective Synthesis of Trisubstituted 1,3-Dienes. *Organometallics* **2011**, *30*, 369-371. (b) O'Connor, J. M.; Chen, M. C.; Frohn, M.; Rheingold, A. L.; Guzei, I. A. Diazoketones Undergo Reaction with a Cobalt Alkyne Complex to Give Highly Functionalized Conjugated Dienes. *Organometallics* **1997**, *16*, 5589-5591. (c) Holland, R. L.; O'Connor, J. M.; Bunker, K. D.; Qin, P.; Cope, S. K.; Baldridge, K. K.; Siegel, J. S. Stereospecific Oxidative Demetallation of Highly Functionalized CpCo (1,3-Diene) Complexes: An Experimental and Computational Study. *Synlett* **2015**, *26*, 2243-2246.

5. Holland, R. L.; Bunker, K. D.; Chen, C. H.; DiPasquale, A. G.; Rheingold, A. L.; Baldridge, K. K.; O'Connor, J. M. Reactions of a Metallacyclobutene Complex with Alkenes. *J. Am. Chem. Soc.* **2008**, *130*, 10093-10095.

6. O'Connor J. M.; Fong, B. S.; Ji, H. L.; Hiibner, K.; Rheingold, A. L. A New Metal-Mediated Cyclization: Conversion of a Metallacyclobutene and Alkyne Substrates to η^4-Cyclopentadiene Products. *J. Am. Chem. Soc.* **1995**, *117*, 8029-8030.

7. O'Connor, J. M.; Ji, H. L.; Rheingold, A. L. Late metal metallacyclobutene chemistry: conversion to η^4-vinylketene, η^4-vinylketenimine, and furan products. *J. Am. Chem. Soc.* **1993**, *115*, 9846-9847.

8. Holland, R. L.; O'Connor, J. M. Nitroso Compounds Serve as Precursors to Late-Metal η^2(N,O)-Hydroxylamido Complexes. *Organometallics* **2008**, *28*, 394-396.

9. Kealy, T. J.; Pauson, P. L. A new type of organo-iron compound. *Nature*, **1951**, *168*, 1039.

10. Dunitz, J. D.; Orgel, L. E.; Rich, A. The crystal structure of ferrocene. *Acta Crystallogr.* **1956**, *9*, 373-375.

11. (a) Gassman, P. G.; Mickelson, J. W.; Sowa Jr, J. R. 1,2,3,4-Tetramethyl-5-(trifluoromethyl) cyclopentadienide: a unique ligand with the steric properties of pentamethylcyclopentadienide and the electronic properties of cyclopentadienide. *J. Am. Chem. Soc.* **1992**, *114*, 6942-6944. (b) Gassman, P. G.; Sowa Jr, J. R.; Hill, M. G.; Mann, K. R. Electrochemical Studies of Organometallic Complexes with Tetra-*n*-butylammonium Tetrakis [3,5-bis (trifluoromethyl) phenyl] borate as the Electrolyte. X-ray Crystal Structure of $[C_5(CF_3)Me_4]Fe(C_5H_5)$. *Organometallics* **1995**, *14*, 4879-4885. (c) Evju, J. K.; Mann, K. R. A facile route to 1-trifluoromethyl-2,3,4,5-tetramethylcyclopentadienyl ruthenium half-and mixed-sandwich compounds. *Organometallics* **2002**, *21*, 993-996.

12. O'Connor, J. M.; Casey, C. P. Ring-slippage chemistry of transition metal cyclopentadienyl and indenyl complexes. *Chem. Rev.* **1987**, *87*, 307-318.

13. Wood, C. D.; McLain, S. J.; Schrock, R. R. Multiple metal-carbon bonds. 13. Preparation and characterization of monocyclopentadienyl mononeopentylidene complexes of niobium and tantalum including the first details of an α-abstraction process. *J. Am. Chem. Soc.* **1979**, *101*, 3210-3222.

14. (a) Dötz, K. H. Synthesis of the Naphthol Skeleton from Pentacarbonyl-[methoxy (phenyl) carbene] chromium (0) and Tolan. *Angew. Chem. Int. Ed.* **1975**, *14*, 644-645. (b) Heinz Dötz, K.; Dietz, R.; von Imhof, A.; Lorenz, H.; Huttner, G. Reaktionen von Komplexliganden, IV. Stereoselektive Synthese substituierter Naphthaline: Darstellung und Struktur eines Tricarbonyl (naphthalin) chrom (0)-Komplexes. *Chem. Ber.* **1976**, *109*, 2033-2038. (c) Timko, J. M.; Yamashita, A. Synthesis of 2-Substituted Naphthalenediol Derivatives using Chromium Carbene Complexes: 1-Acetoxy-2-Butyl-4-Methoxynaphthalene. *Organic Syntheses* **2003**, *71*, 72-72.

15. McCallum, J. S.; Kunng, F. A.; Gilbertson, S. R.; Wulff, W. D. Mechanistic studies on the reaction of chromium carbene complexes with acetylenes. Furan formation and the dependence of the product distribution on the stereochemistry of reaction intermediates. *Organometallics* **1988**, *7*, 2346-2360.

16. Tumer, S. U.; Herndon, J. W.; McMullen, L. Reaction of alkynes with cyclopropylcarbene-chromium complexes: a versatile [4+2+1-2] cycloaddition reaction for the construction of cyclopentenones. *J. Am. Chem. Soc.* **1992**, *114*, 8394-8404.

17. Sampedro, D.; Caro, M.; Rodríguez, M. A.; Campos, P. J. Irradiation of imine-group VI carbene complexes in the presence of alkynes. 2. control of product distribution. *J. Org. Chem.* **2005**, *70*, 6705-6713.

18. Singh, R.; Schrock, R. R.; Müller, P.; Hoveyda, A. H. Synthesis of Monoalkoxide Monopyrrolyl Complexes Mo (NR)(CHR')(OR")(pyrrolyl): Enyne Metathesis with High Oxidation State Catalysts. *J. Am. Chem. Soc.* **2007**, *129*, 12654-12655.

19. Solans-Monfort, X. DFT study on the reaction mechanism of the ring closing enyne metathesis (RCEYM) catalyzed by molybdenum alkylidene complexes. *Dalton Trans.* **2014**, *43*, 4573-4586.

20. Casey, C. P.; Polichnowski, S. W.; Shusterman, A. J.; Jones, C. R. Reactions of benzylidene pentacarbonyltungsten with alkenes. *J. Am. Chem. Soc.* **1979**, *101*, 7282-7292.

21. Katz, T. J.; Sivavec, T. M. Metal-catalyzed rearrangement of alkene-alkynes and the stereochemistry of metallacyclobutene ring opening. *J. Am. Chem. Soc.* **1985**, *107*, 737-738.

22. Hojo, F.; Fujiki, K.; Ando, W. Reaction of Polysilacycloalkynes with $CpCo(CO)_2$ and $CpMn(CO)_3$. *Organometallics* **1996**, *15*, 3606-3610.

23. Naumov, S.; Buchmeiser, M. R. Regioselectivity of Insertion and Role of the Anionic Ligands in the Ruthenium Alkylidene Catalyzed Cyclopolymerization of 1,6-Heptadiynes. *Organometallics* **2012**, *31*, 847-856.

24. Remya, P. R.; Suresh, C. H. Mechanistic studies on acetylene cyclotrimerization catalyzed by Grubbs first and second generation catalysts. *Molecular Catalysis* **2017**, *441*, 63-71.

25. Wang, C.; Zhou, Y.; Bao, X. Mechanistic Insights into the Rh-Catalyzed Transannulation of Pyridotriazole with Phenylacetylene and Benzonitrile: A DFT Study. *J. Org. Chem.* **2017**, *82*, 3751-3759.

26. Chen, J. T.; Hsu, R. H.; Chen, A. J. Addition of Aromatic C−H Bonds to η^3-Allenyl/Propargyl Complexes. Organoplatinum-Induced Electrophilic Aromatic Substitution Reactions. *J. Am. Chem. Soc.* **1998**, *120*, 3243-3244.

27. (a) Tebbe, F. N.; Harlow, R. L. Titanacyclobutenes. *J. Am. Chem. Soc.* **1980**, *102*, 6149−6151. (b) McKinney, R. J.; Tulip, T. H.; Thorn, D. L.; Coolbaugh, T. S.; Tebbe, F. N. Sub-stituent Effects in Metallacyclobutenes. Contributions from a Metal-methylene-acetylene Adduct form. *J. Am. Chem. Soc.* **1981**, *103*, 5584−5586

28. Binger, P.; Müller, P.; Herrmann, A. T.; Philipps, P.; Gabor, B.; Langhauser, F.; Krüger, C. Metallacyclobutene aus η^3-Cyclopropen-Komplexen des Titanocens und Zirkonocens. *Chem. Ber.* **1991**, *124*, 2165-2170.

29. Binger, P.; Müller, P.; Langhauser, F.; Sandmeyer, F.; Philipps, P.; Gabor, B.; Mynott, R. Metallabicyclo[3.1.0]hexene und deren Umlagerung zu Vinylmetallacyclobutenen (M = Ti, Zr). *Chem. Ber.* **1993**, *126*, 1541-1550.

30. Doxsee, K. M.; Juliette, J. J.; Mouser, J. K.; Zientara, K. Metallacyclobutene-metallabutadiene (vinylcarbene complex) interconversions: ring opening of titanacyclobutenes. *Organometallics* **1993**, *12*, 4742-4744.

31. Harvey, B. G.; Arif, A. M.; Ernst, R. D. Coupling reactions of alkynes with half-open titanocenes: Agostic (C-C)→Ti interactions in a tetra(alkyne) coupling product with the Ti(C_5H_5)(c-C_8H_{11}) fragment. *J. Organomet. Chem.* **2006**, *691*, 5211-5217.

32. Zhang, W., Yamada, J.; Nomura, K. Reactions of an (Arylimido)vanadium(V)-Alkylidene, V($CHSiMe_3$)(N-2,6-$Me_2C_6H_3$)(N=C^tBu_2)(PMe_3), with Nitriles, Diphenylacetylene, and Styrene. *Organometallics* **2008**, *27*, 5353-5360.

33. Wallace, K. C.; Liu, A. H.; Davis, W. M.; Schrock, R. R. Living polymerization of 2-butyne using a well-characterized tantalum catalyst. *Organometallics* **1989**, *8*, 644-654.

34. Adams, C. J.; Anderson, K. M.; Bartlett, I. M.; Connelly, N. G.; Orpen, A. G.; Paget, T. J.; Phetmung, H.; Smith, D. W. Molybdenum-based alkyne–isocyanide coupling reactions: synthesis of a reactive diiminometallacyclopentene complex. *J. Chem. Soc., Dalton Trans.* **2001**, 1284-1292.

35. Casey, C. P.; Yi, C. S. Nucleophilic attack at the central carbon of a cationic (η^3-propargyl) rhenium complex. *J. Am. Chem. Soc.* **1992**, *114*, 6597-6598.

36. Casey, C. P.; Boller, T. M.; Samec, J. S.; Reinert-Nash, J. R. Quantitative Determination of the Regioselectivity of Nucleophilic Addition to η^3-Propargyl Rhenium Complexes and Direct Observation of an Equilibrium between η^3-Propargyl Rhenium Complexes and Rhenacyclobutenes. *Organometallics* **2008**, *28*, 123-131.

37. Wakatsuki, Y.; Miya, S. Y.; Ikuta, S.; Yamazaki, H. Metallacyclobutene formation from a substituted-acetylene complex of cobalt and an isocyanide. Regioselectivity and rearrangement. *J. Chem. Soc., Chem. Commun.* **1985**, 35-37.

38. Werner, H.; Heinemann, A.; Windmüller, B.; Steinert, P. Stepwise Insertion of Alkylisocyanides into the Metal-Alkyne Bond of Half-Sandwich Type Rhodium Complexes: Synthesis and Structural Characterization of Metallacyclobutenes and Metallacyclopentenes. *Chem. Ber*. **1996**, *129*, 903-910.

39. O'Connor, J. M.; Ji, H.; Iranpour, M.; Rheingold, A. L. Formation of a stable metallacyclobutene complex from. α-diazocarbonyl and alkyne substrates. *J. Am. Chem. Soc*. **1993**, *115*, 1586-1588.

40. Lee, G. M.; Leung, A. S.; Harrison, D. J.; Korobkov, I.; Hughes, R. P.; Baker, R. T. Experimental and computational evidence for 1, 4-diradical intermediates in reactions of cobalt fluorocarbene complexes with terminal aryl-alkynes to give metallacyclobutenes. *Organometallics* **2017**, *36*, 2853-2860.

41. Calabrese, J. C.; Roe, D. C.; Thorn, D. L.; Tulip, T. H. Conversion of a (methoxymethyl) iridium (I) acetylene complex to a metallacyclobutene iridium(III) complex. Crystal and molecular structures of Ir(CH_2OMe)(p-tol-C≡C-p-tol)(PMe_3)$_3$ and *fac*-Ir[CH_2C(p-tol)=C(p-tol)]Br(PMe_3)$_3$. *Organometallics* **1984**, *3*, 1223-1230.

42. O'Connor, J. M.; Pu, L.; Woolard, S.; Chadha, R. K. Carbene ligand insertion into a metallacycle ring: a metallacyclopentadiene to metallacyclobutene conversion. *J. Am. Chem. Soc*. **1990**, *112*, 6731-6732.

43. (a) Hemond, R. C.; Hughes, R. P.; Robinson, D. J.; Rheingold, A. L. Activation of a fluorinated carbon-carbon bond by oxidative addition of tetrafluorocyclopropene to platinum (0). The first example of a perfluorometallacyclobutene. *Organometallics* **1988**, *7*, 2239-2241. (b) Hughes, R. P.; King, M. E.; Robinson, D. J.; Spotts, J. M. Stereoselective oxidative additions of a carbon-carbon σ-bond in tetrafluorocyclopropene to iridium (I) complexes. *J. Am. Chem. Soc.* **1989**, *111*, 8919-8920.

44. Cheng, Y. C.; Chen, Y. K.; Huang, T. M.; Yu, C. I.; Lee, G. H.; Wang, Y.; Chen, J. T. Synthesis of Metallacyclobutenes of Late Transition Metals via Nucleophilic Addition of Allenyl or Propargyl Complexes. *Organometallics* **1998**, *17*, 2953-2957.

45. Green, M. L. H.; Pratt, L.; Wilkinson, G. A new type of transition metal–cyclopentadiene compound. *J. Chem. Soc.* (Resumed), **1959**, 3753-3767.

46. Davies, S. G.; Green, M. L.; Mingos, D. M. P. Nucleophilic addition to organotransition metal cations containing unsaturated hydrocarbon ligands: A survey and interpretation. *Tetrahedron* **1978**, *34*, 3047-3077.

47. Churchill, M. R.; Mason, R. The crystal and molecular structure of π-cyclopentadienyl 1-phenylcyclopentadiene cobalt. *Proc. Roy. Soc. Ser. A.* **1964**, *279*, 191-209.

48. Churchill, M. R. The structure and bonding of a cobalt-cyclopentadiene complex. *J. Organomet. Chem.* **1965**, *4*, 258-260.

49. Razuvaev, G. A.; Mar'in, V. P.; Andrianov, Y. A.; Vyshinskaya, L. I.; Smirnov, A. S. New derivatives of (η^5-cyclopentadienyl)(η^4-cyclopentadiene)cobalt. *Russ. Chem. Bull.* **1987**, *36*, 423-423.

50. Razuvaev, G. A.; Mar'in, V. P.; Andrianov, Y. A.; Vyshinskaya, L. I.; Druzhkov, O. N. Synthesis and mass spectra of derivatives of (η^5-cyclopentadienyl)(η^4-cyclopentadiene) cobalt. *J. Organomet. Chem.* **1988**, *346*, 403-412.

51. O'Connor, J. M.; Pu, L.; Rheingold, A. L.; Uhrhammer, R.; Johnson, J. A. A new mode of carbene reactivity: coupling with two alkynes to generate highly substituted cyclopentadiene products. *J. Am. Chem. Soc.* **1989**, *111*, 1889-1891.

52. O'Connor, J. M.; Johnson, J. A. Selective Oxidation of a Highly-Substituted η^4-Cyclopentadiene Cobalt Complex: Partitioning Between Uncomplexed Diene and Cobalticinium Cation Products. *Synlett* 1989, 57-59.

53. Nishihara, Y.; Deck, K. J.; Shang, M.; Fehlner, T. P. Cluster chemistry driven by ligand bulk. Significance of the synthesis of *nido*-1-(η^5-C$_5$Me$_5$)Co-2-(η^4-C$_5$Me$_5$H) CoB$_3$H$_8$ and its dehydrogenation to *nido*-2,4-{(η^5-C$_5$Me$_5$)Co}$_2$B$_3$H$_7$. *J. Am. Chem. Soc.* **1993**, *115*, 12224-12225.

54. Zhao, X.; Yu, Y.; Xu, S.; Wang, B. Controlled/"living" radical polymerization of methyl methacrylate catalyzed by CpCo(I) complexes conveniently generated from cobaltocene in situ. *Polymer* **2009**, *50*, 2258-2263.

55. Yan, Y.; Zhang, J.; Wilbon, P.; Qiao, Y.; Tang, C. Ring-Opening Metathesis Polymerization of 18-e Cobalt(I)-Containing Norbornene and Application as Heterogeneous Macromolecular Catalyst in Atom Transfer Radical Polymerization. *Macromol. Rapid Commun*. **2014**, *35*, 1840-1845.

56. Hallam, B. F.; Pauson, P. L. Ferrocene derivatives. Part III. Cyclopentadienyliron carbonyls. *J. Chem Soc.* (Resumed), **1956**, *588*, 3030-3037.

57. Whitesides, T. H.; Shelly, J. Thermolysis and photolysis of (cyclopentadiene) iron tricarbonyl. Evidence for a radical mechanism involving iron(I). *J. Organomet. Chem.* **1975**, *92*, 215-226.

58. Weber, L.; Reizig, K. Synthese und Reaktivität von [5-*exo*-Phosphino-η^4-cyclopentadien]-tricarbonyleisenkomplexen/Synthesis and Reactivity of [5-*exo*-Phosphino-η^4-cyclopentadiene] Tricarbonyliron Complexes. *Zeitschrift für Naturforschung B* **1984**, *39*, 1350-1354.

59. Liu, L. K.; Luh, L. S.; Wen, Y. S.; Eke, U. B.; Mesubi, M. A. Synthesis of heterobimetallic complexes from (η^4-MeC$_5$H$_5$)Fe(CO)$_2$(η^1-PPh$_2$CH$_2$PPh$_2$). *Organometallics* **1995**, *14*, 4474-4482.

60. Busetto, L.; Camiletti, C.; Castellari, C.; Monari, M.; Zanotti, V. Selective C-C bond formation at diiron μ-aminocarbyne complexes. *J. Chem. Soc., Dalton Trans.* **1997**, 4671-4676.

61. Cavanaugh, M. D.; Gregg, B. T.; Chiulli, R. J.; Cutler, A. R. The reactions of hydrosilanes with the methoxycarbonyl complexes Cp(L)(CO) MCO$_2$Me (M = Fe, Ru; L = CO, PPh$_3$) and (L)(CO)$_x$MCO$_2$Me (M = Co, Mn; L = CO, PPh$_3$; x= 3, 4, with and without catalysis. *J. Organomet. Chem.* **1997**, *547*, 173-182.

62. Cannillo, E.; Prout, K. η^4-(1-*endo*-Ethyl)cyclopentadiene-η^5-cyclopentadienyl (triethylphosphine)-chloromolybdenum(II). *Acta Cryst.* **1977**, *33*, 3916-3918.

63. Feher, F. J.; Green, M.; Orpen, A. G. The role of α-hydrogen elimination reactions in the formation of η^3-cyclopropenyl-and η^4-cyclopentadiene-molybdenum complexes. *J. Chem. Soc., Chem. Commun.* **1985**, 291-293.

64. Gamelas, C. A.; Herdtweck, E.; Lopes, J. P.; Romão, C. C. Redox-Induced Indenyl Slippage in [IndCpMoL$_2$]$^{2+/+/0}$ Complexes. *Organometallics* **1999**, *18*, 506-515.

65. Cabon, N.; Pétillon, F. Y.; Orain, P. Y.; Schollhammer, P.; Talarmin, J.; Muir, K. W. Controlled nucleophilic activation of different sites in [Mo$_2$Cp$_2$L$_2$ (μ-SMe)$_2$(μ-L')]$^+$ cations (L= Bu^{t}NC, xylNC, CO; L' = SMe or PPh$_2$). *J. Organomet. Chem.* **2005**, *690*, 4583-4601.

66. Jernakoff, P.; Fox, J. R.; Cooper, N. J. Electrophilic addition of CCl$_4$ to a cyclopentadienyl ligand in the tungstenocene carbonyl [W(η^5-C$_5$H$_5$)$_2$(CO)] to give [W (η^5-C$_5$H$_5$)(η^4-C$_5$H$_5$-*exo*-CCl$_3$)(CO)Cl]. *J. Organomet. Chem.* **1996**, *512*, 175-181.

67. Shao, L.; Geib, S. J.; Cooper, N. J. A potassium cryptate-2,2,2 salt of tricarbonyl (η^4-cyclopentadiene) manganese. *Acta Cryst*. **2003**, *59*, m69-m71.

68. Alcock, N. W. The moleculer structure of dimethyl-π-cyclopentadienyl-methylcyclopentadienerhenium. *Chem. Commun.* (London), **1965**, 177-178.

69. Jones, W. D.; Maguire, J. A. Preparation and reaction dynamics of (η^4-C$_5$H$_6$) Re (PPh$_3$)$_2$H$_3$. A structurally characterized η^4-cyclopentadiene complex. *Organometallics* **1985**, *4*, 951-953.

70. Jones, W. D.; Maguire, J. A. Preparation, dynamic behavior, and C-H and C-C cleavage reactions of (η^4-4-C$_5$H$_6$)Re(PPh$_3$)$_2$H$_3$. Structures of (η^4-C$_5$H$_6$)Re(PPh$_3$)$_2$H$_3$, CpRe(PPh$_3$)$_2$H$_2$, and CpRe(PPh$_3$)H$_4$. *Organometallics* **1987**, *6*, 1301-1311.

71. Buhro, W. E.; Arif, A. M.; Gladysz, J. A. Synthesis and reactivity of functionalized rhenium phosphido complexes (η^5-C$_5$H$_5$)Re(NO)(PPh$_3$)(PXX'): an unusual carbon tetrachloride 1,3-addition leading to an *exo*-substituted η^4-cyclopentadiene complex. *Inorg. Chem.* **1989**, *28*, 3837-3845.

72. Humphries, A. P.; Knox, S. A. Reactions of cyclopentadiene with carbonyl-ruthenium and -osmium complexes. *J. Chem. Soc., Dalton Trans.* **1975**, 1710-1714.

73. Davies, S. G.; Felkin, H.; Fillebeen-Khan, T.; Tadj, F.; Watts, O. Hydride reduction of the cations {(η^5-C$_5$H$_5$)Fe[(Ph$_2$PCH$_2$)$_3$CMe]}PF$_6$, {(η^5-C$_5$H$_5$)-Ru[(Ph$_2$PCH$_2$CH$_2$)$_2$PPh]}PF$_6$, and {(η^5-C$_5$H$_5$)Ru[(Ph$_2$PCH$_2$)$_3$CMe]}PF$_6$: regioselectivity and mechanism. *J. Chem. Soc., Chem. Commun.* **1981**, 341-342.

74. Grabowski, N. A.; Hughes, R. P.; Jaynes, B. S.; Rheingold, A. L. Stepwise transition metal promoted ring expansion reactions of vinylcyclopropenes to give cyclopentadienes and cyclohexa-2,4-dienones. The first example of a 1-metallacyclohexa-2,4-diene complex, {[Pt-CH$_2$-CH=C(Ph)-C(Ph)=C(Ph)](PPh$_3$)$_2$}. *J. Chem. Soc., Chem. Commun.* **1986**, 1694-1695.

75. Donovan, B. T.; Hughes, R. P.; Kowalski, A. S.; Trujillo, H. A.; Rheingold, A. L. Stereoselective rhodium-promoted ring closure of an η^4-1,3-pentadienediyl ligand to an η^4-1,3-cyclopentadiene, with subsequent regiospecific *endo*-H migration: molecular structure of [Rh(η^5-C$_5$H$_5$)(1-4-η)-C$_5$H$_3$-1,2-*exo*-5-^{t}Bu$_3$)]. *Organometallics* **1993**, *12*, 1038-1043.

76. Hughes, R. P.; Trujillo, H. A.; Gauri, A. J. Stereoselective ring expansion of 3-vinyl-1-cyclopropenes to give (η^5-cyclopentadienyl)ruthenium and (η^4-cyclohexadienone) iron complexes. Exclusion of planar metallacyclohexadiene intermediates and relevance to the Dötz reaction. *Organometallics* **1995**, *14*, 4319-4324.

77. Fischer, E. O.; Zahn, U. Über Aromatenkomplexe von Metallen, XXVIII. Cyclopentadienyl-rhodium(I)-cyclopentadien und Cyclopentadienyl-iridium(I)-cyclopentadien. *Chem. Ber.* **1959**, *92*, 1624-1628.

78. Szajek, L. P.; Shapley, J. R. Unexpected synthesis of CpIr(η^4-C$_5$H$_6$) and a ^{1}H and ^{13}C NMR comparison with its cobalt and rhodium congeners. *Organometallics* **1991**, *10*, 2512-2515.

79. Gusev, O. V.; Morozova, L. N.; Tat'yana, A. P.; Petrovskii, P. V.; Ustynyuk, N. A.; Maitlis, P. M. Synthesis of η^5-1,2,3,4,5-pentamethylcyclopentadienyl-platinum complexes. *J. Organomet. Chem.* **1994**, *472*, 359-363.

CHAPTER 2

Synthesis and Reactivity Studies of Metallacyclobutenes

A. Introduction

Metallacyclobuenes, as stated in chapter 1, have been largely reported as key intermediates for a lot of transition metal triggered metathesis reactions, and a number of isolated metallacyclobutenes were synthesized by employing various strategies with different transition metals in the literature. However, late transition metal metallacyclobutenes are still rare, and only a few isolated examples were reported in the literature for the reason that stable metallacyclobutene for isolation was found dictated by the combinational factors of ring substituents, ancillary ligands, and types of transition metals.

Inspired by Hong's work in 1978,[1] in which a cobalt diphenylacetylene complex **1** was treated with ethyl diazoacetate in benzene at ambient temperature to generate two η^4-1,3-diene complexes as well as two dicobalt complexes with the proposed intermediacy of metallacyclobutene **2** (Scheme 2-1), O'Connor lab successfully synthesized a stable cobaltacyclobutene **8** with high regio-and stereoselectivity by employing a plolarized cobalt-alkyne complex **7** that bears sulfone as electron withdrawing group and trimethylsilane as sterically protecting group (Scheme 2-2).[2] Since then, a lot of reactivity studies of metallacyclobutene with different unsaturated substrates have been successively explored in our lab.[3] Also, more recently in 2014, it was found that when a more sterically hindered cobalt-alkyne complex **9** was used as precursor[4], an equilibrium can be observed between the isolated metallacyclobutene **10** and an η^3-vinylcarbene complex **11** who has been widely proposed as intermediate in Dötz type reactions.
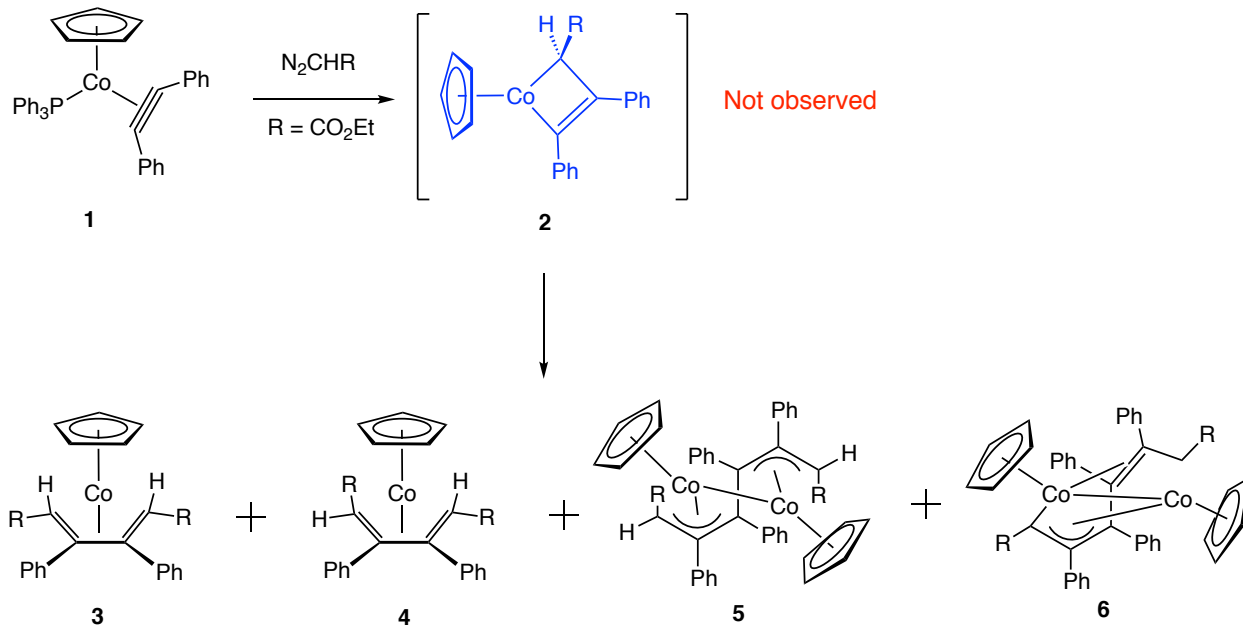
Scheme 2-1. Reaction of $(C_5H_5)(PPh_3)Co\{\eta^2\text{-}C(Ph)=C(Ph)\}$ with ethyl diazaoacetate.
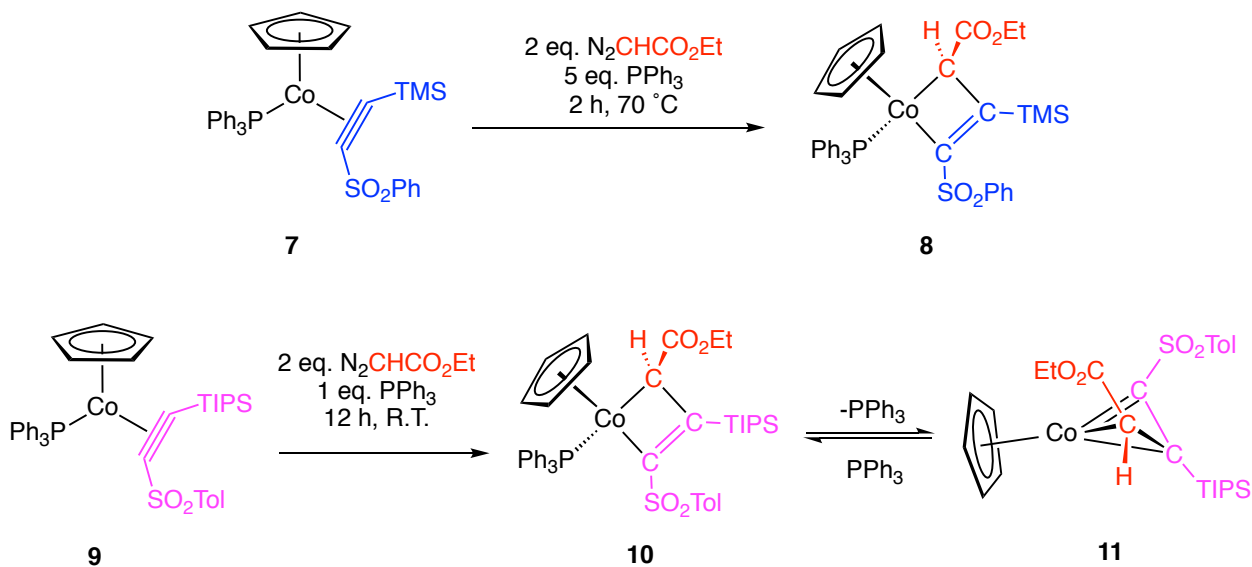
Scheme 2-2. Isolated metallacyclobutenes and observation of η^3-vinylcarbene complex.

Hence, by following the same synthetic strategy of previous work of assembling metallacyclobutenes via couplings of metal-alkyne complexes with carbene, here we explored the effects of ring substituents on the stability of metallacyclobutene by employing different alkyne precursors coupling with α-diazocarbonyl compounds. The factors of ancillary phosphine ligand were studied under photochemical conditions. Furthermore, the thermolysis and reactivity studies of the isolated metallacyclobutene were also explored.

B. Synthesis of Cobalt-alkyne Complexes

1. Synthesis of Precursors

As one of the key precursors to assemble metallacyclobutene, the cobalt-alkyne complexes can be prepared from the reaction between $CpCo(PPh)_2$ with various acetylenes, and we developed an ideal synthetic method of $CpCo(PPh)_2$ with decent yields within two steps in the scale of 20 g by modifying multiple procedures that were reported in the literature.[5] The synthesis starts with dissolving commercially available $CoCl_2 \cdot 6H_2O$ (9.6g, 40.4 mmol) with triphenylphosphine (32 g, 122.1 mmol) in 200 proof ethanol (600 mL) in a nitrogen flushed three-neck round-bottom flask at 60-70 °C. After vigorously stirring the mixture for 30 minutes, a light blue solution with white suspended fine powder of triphenylphosphine was obtained, which was slowly cooled down to ambient temperature. Then 1.28 g (33.8 mmol) of $NaBH_4$ was introduced in 10 minutes, and the color of the solution was observed changing from blue to dark green, and finally

to brown. After filtering the powder and washed with ethanol, water, ethanol, and hexanes, 24.5 g (68.9% yield) of CoCl(PPh$_3$)$_3$ was obtained as slightly air-sensitive dark brown solid (Scheme 2-3).

It was found that the temperature and rate of NaBH$_4$ addition are crucial to the success of synthesizing CoCl(PPh$_3$)$_3$. The temperature of the CoCl$_2$ and triphenylphosphine mixture need to be fully cooled down below 30 °C before introducing NaBH$_4$, otherwise the intense reaction between CoCl$_2$ with NaBH$_4$ could over reduce cobalt and lead to undesired side products. Also, if NaBH$_4$ is loaded too fast to the solution, some green unknown compounds will be generated to drop down the yield. The crude brown CoCl(PPh$_3$)$_3$ powders are slight air sensitive, but they can be worked up quickly in the fume hood, and stored under inert atmosphere or vacuum for several months. However, slowly decomposition to green unknown complexes was observed upon exposed to air for 10 hours.
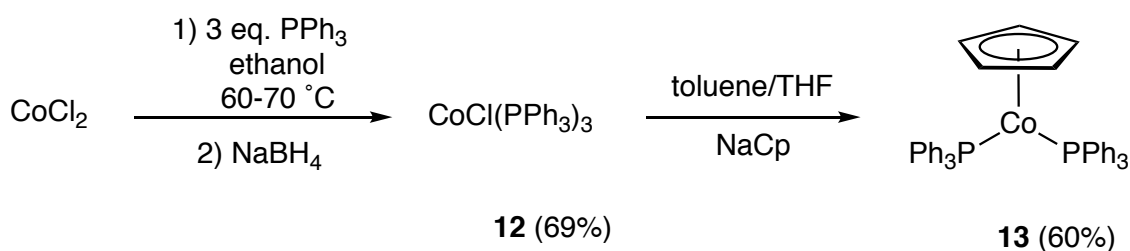
Scheme 2-3. Synthesis of (C$_5$H$_5$)Co(PPh$_3$)$_2$ complex.

For the second step, 49 g (55.6 mmol) of CoCl(PPh$_3$)$_3$ were dried on high vacuum line for 12 hours, and subsequently dissolved in 200 mL of toluene in the glove box. After stirring vigorously for 90 minutes and treated with NaCp, the solution was allowed to filtered through celite and then layered with hexanes to slowly afford

CpCo(PPh$_3$)$_2$ (21.6 g, 60% yield) as air-sensitive dark purple crystalline solids. It is crucial to carry out all the procedures in the glove box to prevent massive decomposition of air-sensitive starting materials and product.

Based on the comparison of our previous work with Hong's result, we reasoned that the stability of metallacyclobutene **8** was largely supported by the sulfone group of the alkyne, which behaves as an electron-withdrawing group to strengthen the C-Co bond, and thus stabilizes the ring structure. However, one might argue that the phenyl sulfone substituent, as a bulky functional group, could also sterically affect the structure. In order to unambiguously explain the electron effects on the stability of metallacyclobutene, carbonyl group was accepted as an ideal candidate for the small size and electron-demanding feature. We were pleased to find that Min-Tsang Hsieh reported a systematic synthetic procedure of acetylenes bearing a trifluromethylacetyl group.[6]
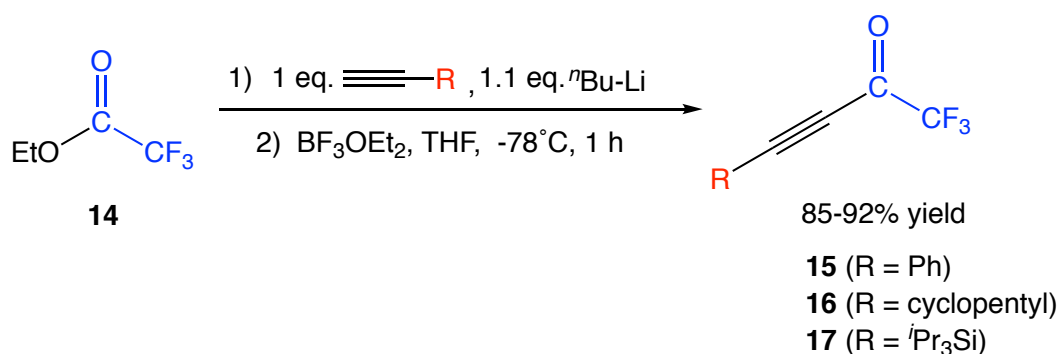
Scheme 2-4. Synthesis of trifluromethylacetyl group substituted alkynes.

By employing the modified literature procedure to phenylacetylene, ethynylcyclopentane, and ethynyltriisopropylsilane, alkynes **15**-**17** can be obtained with

85-92% yield. For instance, 5 g (27.4 mmol) of ethynyltriisopropylsilane was deprotonated by ^{n}Bu-Li (12.5 mL, 2.5 M in hexanes) in anhydrous THF (40 mL) at -78 °C for 1 hour, that is followed by loading a mixture of ethyl trifluoromethylacetate (4.88 g, 31.26 mmol) and BF_3OEt_2 (4.44 g, 31.28 mmol) dropwisely. After concentrated and chromatography on silica gel, 6.8 g (89% yield) of **17** can be harvested as clear oil (Scheme 2-4). The carbon-carbon triple bond stretch was observed in IR spectrum at 2163 cm^{-1}, while the carbonyl stretch is located at 1710 cm^{-1}. The presence of triisopropylsilane group is confirmed by the resonance of ^{1}H NMR at δ 1.11 (d, J = 6.2 Hz, 18H) and 1.19 (m, 3H), and the trifluromethylacetyl group was observed in ^{13}C{^{1}H} NMR via the two prominent quartets at δ 114.8 (q, J_{CF} = 289 Hz, CF_3) and 166.8 (q, J_{CF} = 42 Hz, CO). The other two alkynes **15** and **16** were both synthesized in a similar fashion, and all the new alkynes were fully characterized by IR, HRMS, ^{1}H NMR, and ^{13}C NMR spectroscopy (Table 2-1, vide infra).

2. Synthesis of Cobalt-Alkyne Complex 18

The synthesis of cobalt-alkyne complexes begins with treating readily available $(C_5H_5)Co(PPh_3)_2$ with the organic acetylenes, which was reported by Yamazaki and co-workers to assemble variable cobalt-alkyne complexes and metallacyclopentadienes.[7] When 1,1,1-trifluoro-4-phenylbut-3-yn-2-one **15** (0.84 g, 4.24 mmol) was introduced into the stirring benzene (25 mL) solution of $(C_5H_5)Co(PPh_3)_2$ (2.5 g, 3.85 mmol) under nitrogen, the color of the reaction mixture gradually changed from red to purple. After stirring at ambient temperature for 12 hours, the solution was layered with hexanes to

slowly afford dark purple crystalline solid of **18** with 80.9% yield. The resulting solids are stable in the air, and it can be stored on bench for more than 2 years. However, it slowly decomposes in benzene or chloroform solution to some unknown polar paramagnetic complexes. The integration of the ^{1}H NMR (CDCl$_3$) spectrum of **18** in the aromatic region with 20 hydrogens indicates that only one triphenylphosphine ligand was substituted by the alkyne (Scheme 2-5), which contrasts with Yamazaki's work that metallacyclopentadiene was obtained as the major product when they employed other alkynes as precursors to react with (C$_5$H$_5$)Co(PPh$_3$)$_2$, such as diphenyl acetylene, dimethyl acetylene, and methyl propiolate. We reasoned that this difference might be ascribed to the strong electron withdrawing effect of the trifluromethylacetyl group that stabilizes the cobalt-alkyne complex through strong π-back bonding, and thus prevents the further reaction of **18** with more acetylenes.
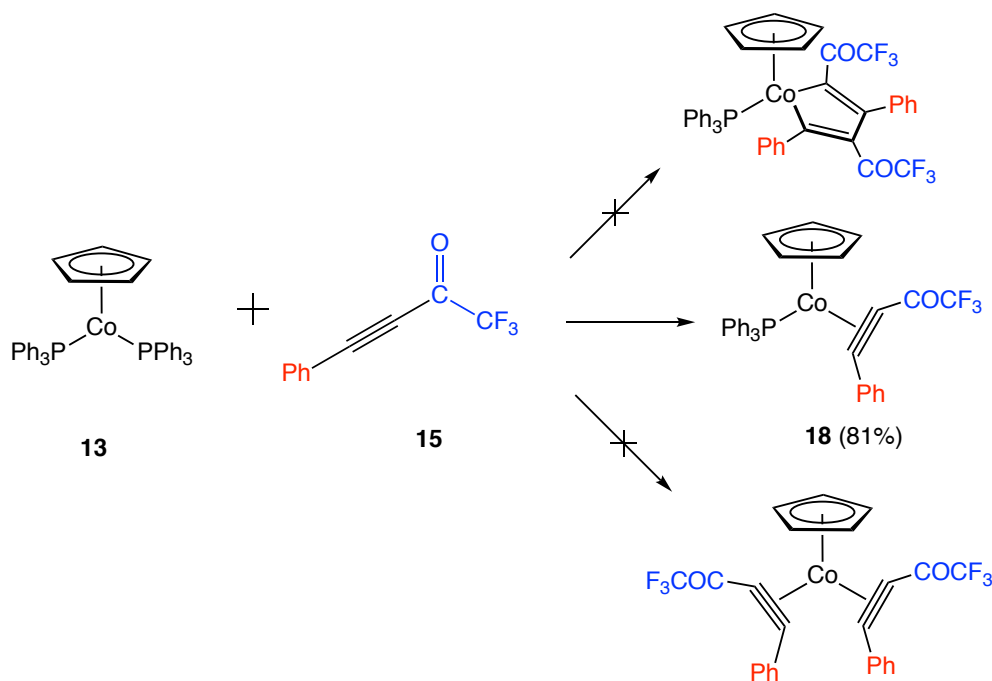
Scheme 2-5. Formation of cobalt-alkyne complex Cp(PPh$_3$)Co{η^2-C(Ph)=C(COCF$_3$)}.

57

The coupling of phosphorus with two acetylene carbons were observed in ^{13}C {^{1}H} NMR spectrum (CDCl$_3$, 125 MHz) at δ 82.8 (d, J_{CP} = 9.2 Hz) and 155.7 (d, J_{CP} = 9.4 Hz) with a remarkable difference in the chemical shift, which might be attributed to a stronger back-bonding between cobalt and the more electron-poor carbon bearing phenyl substituent than the more electron-rich carbon bearing carbonyl group. The prominent splitting of carbonyl carbon by fluorine was observed at δ 172.1 (q, J_{CF} = 34.7 Hz), while the trifluoromethyl group was detected at δ 116.4 (q, J_{CF} = 292 Hz). In the IR spectrum, the C=O stretching frequency of **18** was detected at 1616 cm^{-1}, and the C≡C bond exhibits a stretch frequency at 1776 cm^{-1}, which is 419 cm^{-1} weaker than the corresponding free alkyne **15**.

Complex **18** has been furtherly characterized by X-ray crystallography, and the structure was confirmed to exhibit a trigonal η^2-coordination mode (Figure 2-1). The significantly longer C1–C2 bond distance (1.290(4) Å) than the regular C≡C bond distance (1.20 Å) is consistent with the strong back donation effect from the metal center. The bend-back angle of the cobalt-alkyne complex can be affected by both steric and electronic factors. In the case of **18**, the phenyl substituent is bulkier than the trifluoromethylacetyl group based on the A value in the context of cyclohexane that shows a 1.56 kcal/mol difference,[8] Also, the β carbon (C1) that is attached on a phenyl group is more electronically poor than the α carbon (C2) that is attached on the carbonyl group. The shorter Co–C1 distance (1.926(3) Å) compared to Co–C2 distance (1.932(2) Å) is consistent with the stronger back donation from cobalt to the β-carbon than α-carbon. Therefore, both electric and steric effects tune the bend-back angle on C1 (31.5(3)°) a little greater than on C2 (31.1(3) °).
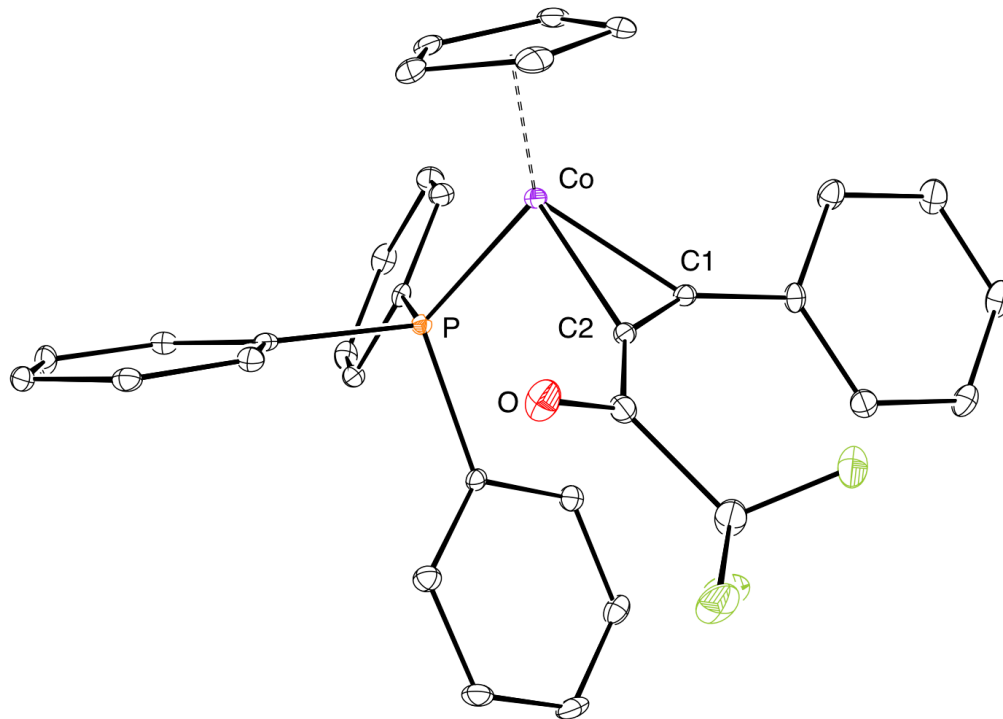
Figure 2-1. ORTEP drawing of complex **18** with ellipsoids shown at 30% probability.

3. Synthesis of Cobalt-Alkyne Complex 19

In order to explore the electronic effects of arene substituent versus alkyl substituent, 4-cyclopentyl-1,1,1-trifluorobut-3-yn-2-one **16** with a cyclopentyl group was employed as the precursor to synthesize the cobalt-alkyne complex. In a similar fashion, 3.1 g (4.8 mmol) of $(C_5H_5)Co(PPh_3)_2$ was allowed to react with 1 g (5.3 mmol) of 4-cyclopentyl-1,1,1-trifluorobut-3-yn-2-one in dry toluene in a glove box for 12 hours at ambient temperature, during which period, the color of the solution changed from red to dark (Scheme 2-6). The crystallization was triggered by drawing a layer of hexanes and keeping the solution at -20 °C, and 2.48 g (82% yield) of complex **19** was obtained as

dark crystalline solids after one week. The compound was found stable at ambient temperature in the presence of air. However, massive decomposition was observed after keeping in dry chloroform solution for 2 days.
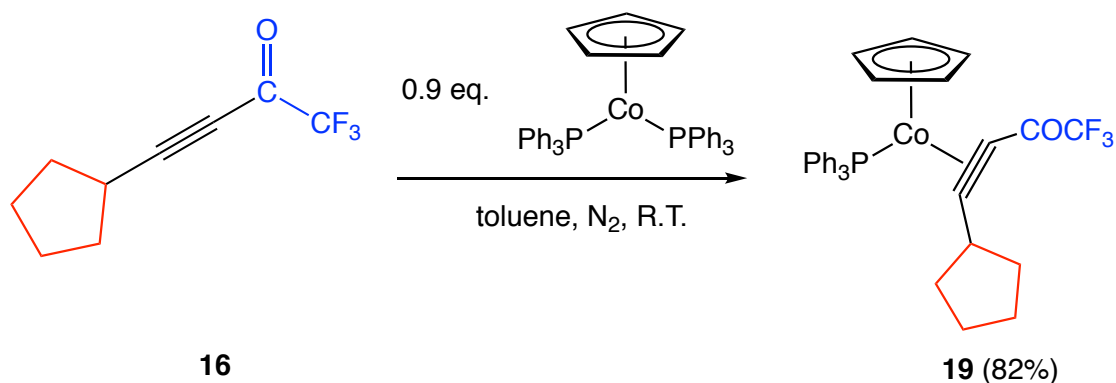
Scheme 2-6. Synthesis of cobalt-alkyne complex $Cp(PPh_3)Co\{\eta^2\text{-}C(C_5H_9)=C(COCF_3)\}$.

The presence of cyclopentyl group in the ^1H NMR (400 MHz, $CDCl_3$) spectrum is manifested by the multiplets of 9 hydrogens in the aliphatic region, while the integration of 15 hydrogens in the aromatic region is consistent with the proposed cobalt-alkyne complex structure that only one triphenylphosphine is substituted by the alkyne. The two acetylene carbons are observed in the ^{13}C $\{^1H\}$ NMR spectrum ($CDCl_3$, 125 MHz) at δ 71.9 (d, J_{CP} = 9.2 Hz) and 172.5 (bs), respectively, which also exhibits an abnormal deshielding β carbon (C1). The couplings between fluorine and carbons in the trifluoromethylacetyl moiety were observed at δ 116.0 (q, J_{CF} = 292 Hz, CF_3) and 171.8 (q, J_{CF} = 35.2 Hz, CO). The C=O stretching frequency of complex **19** was detected in IR spectrum at 1624 cm^{-1}, while the C≡C resonance is observed at 1777 cm^{-1}, with 430 cm^{-1} weaker than the free alkyne **16**.

The structure of complex **19** was confirmed by using single X-ray crystallography (Figure 2-2), which is consistent with the trigonal η^2-coordination mode. The strong back donation from the metal center is manifested by the extended C≡C distance (1.290(3) Å). Despite the cyclopentyl group is bulkier than the trifluoromethylacetyl group, the Co–C1 distance (1.918(2) Å) is significantly shorter than the Co-C2 distance (1.9528(19) Å), which might be attributed to the electronic effect that the β carbon is more electron withdrawing than the α carbon. The bend-back angle on the two acetylene carbons are detected very similar to each other (C1: 32.81 (19) ° and C2: 32.68 (19) °).
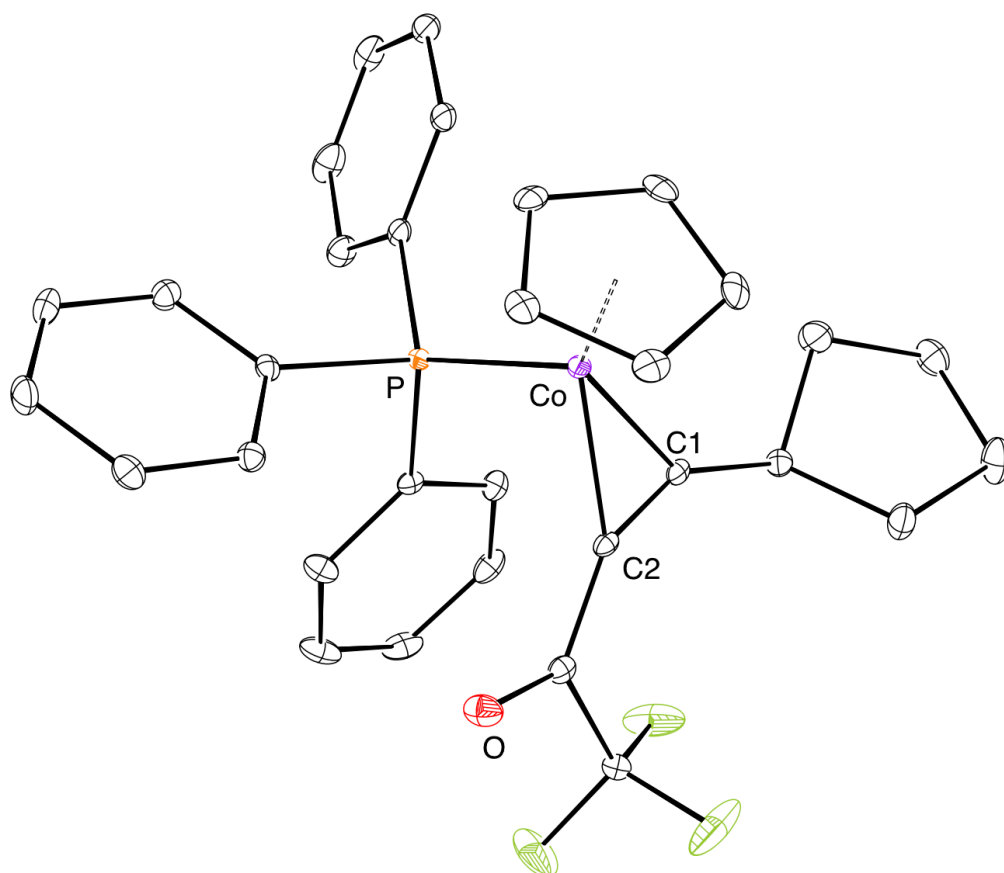
Figure 2-2. ORTEP drawing of complex **19** with ellipsoids shown at 30% probability.

4. Synthesis of Cobalt-Alkyne Complex 20

In order to compare with our previously reported metallacyclobutene that bears a bulky trimethylsilyl or triisopropylsilyl group, 1,1,1-trifluoro-4-(triisopropylsilyl)but-3-yn-2-one was synthesized and employed as the cobalt-alkyne complex precursor. Specifically, 1.42 g (5.1 mmol) of the alkyne **17** was allowed to mix with 3.0 g (4.6 mmol) of $(C_5H_5)Co(PPh_3)_2$ in dry toluene under inert atmosphere for 12 hours (Scheme 2-7). A crystallization process was subsequently conducted by layering hexanes at -20 °C, and 2.3 g (74% yield) of complex **20** was obtained as dark crystalline solids after washing with cold hexanes. This cobalt-alkyne complex was found much more sensitive to air than complex **18** and **19**, and it slowly decomposed to some unknown paramagnetic compounds even in solid form when exposed to air. In addition, it was found that complex **20** start to decompose in dry chloroform after 10 hours in a sealed J.Y. NMR tube under vacuum.
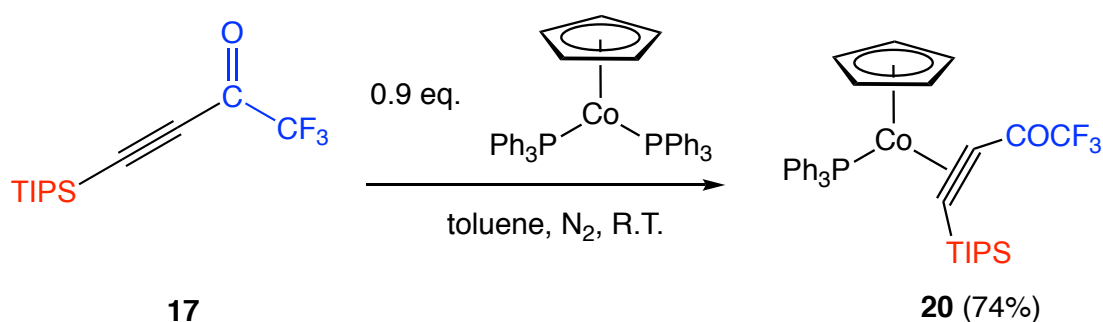
Scheme 2-7. Synthesis of cobalt-alkyne complex $Cp(PPh_3)Co\{\eta^2\text{-}C(TIPS)=C(COCF_3)\}$.

In the ^{1}H NMR (400 MHz, C_6D_6) spectrum, the prominent resonances of triisopropylsilyl group were observed at δ 1.02 (m, 3H) and 1.16 (m, 18H), and the relative integration of TIPS to Cp (21 : 5) excludes the metallacyclopentadiene structure. The two acetylene carbons were observed in the ^{13}C {^{1}H} NMR spectrum (C_6D_6, 125 MHz) at δ 104.4 (d, J_{CP} = 7.0 Hz) and 118.5 (bs), while the trifluoromethylacetyl group exhibits two quartets at δ 117.8 (q, J_{CF} = 292 Hz, CF_3) and 180.6 (q, J_{CF} = 35.0 Hz, CO), respectively. The C≡C stretching frequency of complex **20** was detected at 2035 cm^{-1} in the IR spectrum, which is 128 cm^{-1} weaker than the corresponding organic alkyne, and the carbonyl resonance was observed at 1633 cm^{-1}.

X-ray quality crystals were successfully grown from benzene/hexanes at -40 °C, and the structure was confirmed to be the expected trigonal cobalt-alkyne complex (Figure 2-3). The elongated C≡C distance caused by the back bonding from the metal center was measured as 1.265(4) Å. The bend-back angle on the C1 site (23.7(3) °) is significantly smaller than the bend-back angle on the C2 site (35.3(3) °), which is ascribed to the torsion of the bulky triisopropylsilyl group, and this large steric hindrance is also manifested by the abnormally longer Co–C2 distance (2.011(4) Å) than the Co–C1 distance (1.975(4) Å).
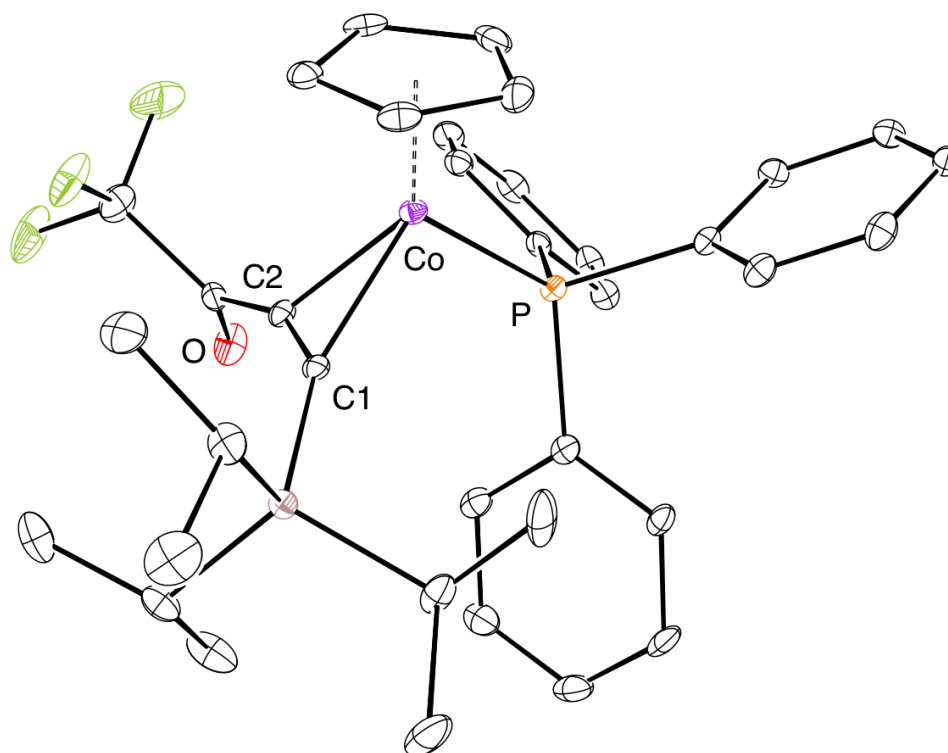
Figure 2-3. ORTEP drawing of complex **20** with ellipsoids shown at 30% probability.

5. Comparisons of Results

Based on the synthetic scope, we made a large progress on developing a more efficient and highly yielded one-pot synthetic strategy, in which a direct crystallization was conducted on the reaction mixture instead of the chromatography that was employed by most of the other work in the literature. The elimination of chromatography helps prevent massive decomposition of the desired cobalt-alkyne complexes when running through silica gel/aluminum in the solution, and thus provides better yields. The formations of all the cobalt-alkyne complexes are proposed to share the same straightforward mechanism, which involves dissociation of a triphenylphosphine ligand to generate an unsaturated 16-electron intermediate **21** followed by trapped with an

acetylene to afford the η^2-alkyne complex (Scheme 2-8). However, it was found that most of the cobalt-alkyne complexes that were reported in the literature are air-sensitive or could easily react with another equivalent of alkyne to generate metallacyclopentadiene, whearas complex **15** and **16** are very stable to air in solid phase, and were found inert to further reactions in the presence of excess alkynes. This unusual stability can be attributed to the strong electron-withdrawing trifluoromethylacetyl group that strengthens the cobalt-carbon bonds.
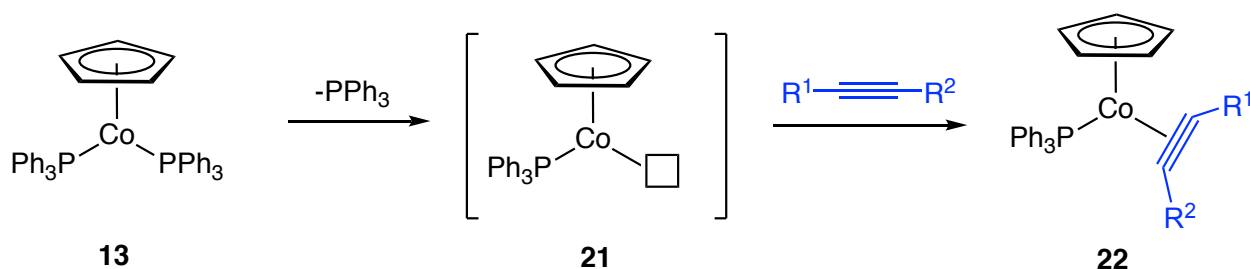
Scheme 2-8. Proposed mechanism for the formation of cobalt-alkyne complexes.

Since Yamazaki and co-workers developed a systematic way to assemble cobalt-alkyne complexes by utilizing readily available $(C_5H_5)Co(PPh_3)_2$ with corresponding alkynes,[7] a number of cobalt-alkyne complexes have been assembled in a similar fashion and reported in the literature (Figure 2-4).[9] It will be interesting to compare our cobalt-alkyne systems with others that are attached with various different functional groups, which will provide insight understandings of this cobalt involved trigonal η^2-coordination mode of alkyne complexes.
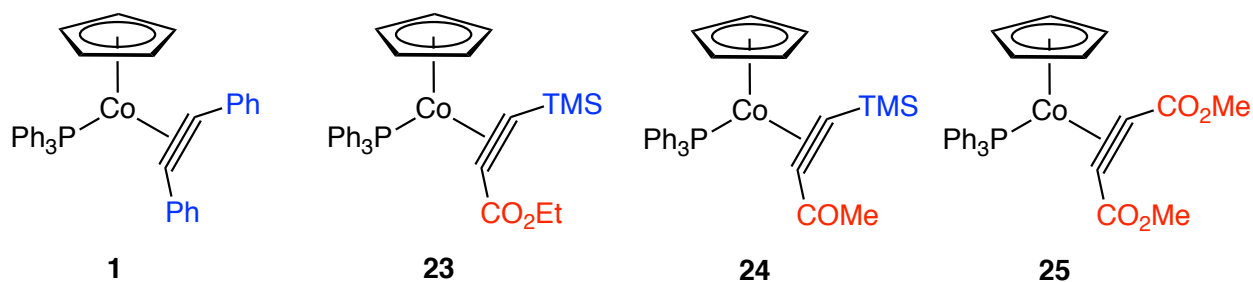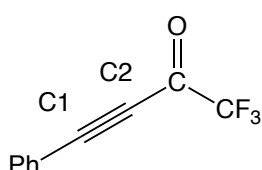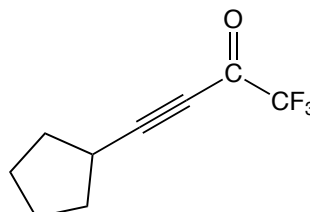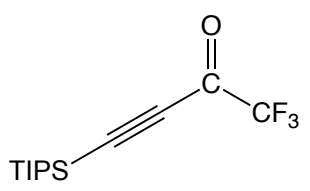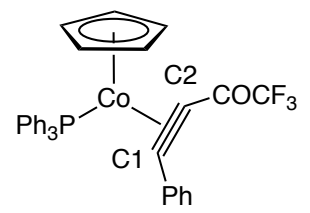
Figure 2-4. Cobalt-alkyne complexes in the literature.
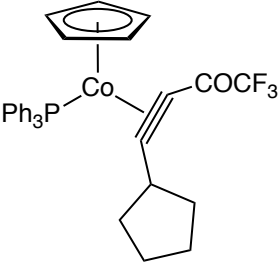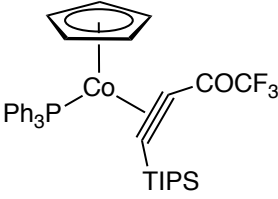
In these cobalt-alkyne complexes, there are a few prominent spectroscopical characters that are ascribed to the coordination of a metal center. Firstly, in both our newly prepared trifluoromethylacetyl system and those were reported by Yamazaki and Bunker, the C≡C bonds are drastically weakened by the π back donation from the metal, which is manifested by the large red shift of the C≡C bond stretching frequency (Δ = 338 – 430 cm⁻¹) in IR spectrum (Table 2-1). The only exception is complex **20** whose C≡C stretching resonance is only 128 cm⁻¹ shorter than the corresponding free alkyne, which might be attributed to the steric congestion of the bulky TIPS group that weakens the metal-π bond interaction. Secondly, a special character is notable in the trifluoromethylacetyl alkyne systems that the C=O bond stretch of the carbonyl groups are all weakened (Δ = 77 – 82 cm⁻¹) in complex **18**, **19**, and **20**. These diminished resonances can be ascribed to the hyperconjugation of the carbonyl groups to cobalt.[10] Furthermore, in consistent with the IR spectra, the partially double-bond character of alkyne is also reflected by the more downfield resonances of acetylene carbons in ¹³C {¹H} NMR spectra relative to the organic alkynes. However, it was noted that the extent of difference of chemical shift changes drastically with different substituents, and remarkable deshileding effect was exhibited in the trifluoromethylacetyl cobalt-alkyne

systems. For instance, in complex **18** and **19**, the most downfield acetylene carbon was observed 55 – 63 ppm more deshielded than the corresponding free alkynes, while only 17 ppm difference was detected in complex **7** and 21 ppm in complex **25**.

Table 2-1. Spectroscopic characterizations of trifluoromethylacetyl substituted alkynes and corresponding cobalt-alkyne complexes.

Complex	^{1}H NMR, (δ) & IR (cm^{-1})	^{13}C{^{1}H} NMR, (δ)
15	7.4 – 7.7 (m, 5H, Ar) 2195 (C≡C) 1698 (C=O)	84.3 (C1) 100.5 (C2) 114.8 (q, J_{CF} = 286 Hz, CF_3) 167. 2 (q, J_{CF} = 41 Hz, CO)
16	1.65 – 2.05 (m, 8H, pentyl) 2.90 (m, 1H) 2207 (C≡C) 1709 (C=O)	75.8 (C1) 109.6 (C2) 114.8 (q, J_{CF} = 288 Hz, CF_3) 167. 5 (q, J_{CF} = 42 Hz, CO)
17	1.11 (m, 18H, TIPS) 1.19 (m, 3H, TIPS) 2163 (C≡C) 1710 (C=O)	98.6 (C1) 109.2 (C2) 114.8 (q, J_{CF} = 289 Hz, CF_3) 166.8 (q, J_{CF} = 42 Hz, CO)
18	4.79 (s, 5H, Cp) 1776 (C≡C) 1616 (C=O)	82.8 (d, J_{Cp} = 9.2 Hz, C1) 84.2 (s, Cp) 116.4 (q, J_{CF} = 292 Hz, CF_3) 155.7 (d, J_{Cp} = 9.4 Hz, C2) 177. 1 (q, J_{CF} = 35 Hz, CO)

Table 2-1. Spectroscopic characterizations of trifluoromethylacetyl substituted alkynes and corresponding cobalt-alkyne complexes (continued).

Complex	^{1}H NMR, (δ) & IR (cm^{-1})	^{13}C{^{1}H} NMR, (δ)
19	4.66 (s, 5H, Cp) 1777 (C≡C) 1624 (C=O)	71.9 (d, J_{Cp} = 9.2 Hz, C1) 83.7 (s, Cp) 116.0 (q, J_{CF} = 292 Hz, CF_3) 171.8 (q, J_{CF} = 35 Hz, CO) 172.5 (bs, C2)
20	4.60 (s, 5H, Cp) 2035 (C≡C) 1633 (C=O)	83.0 (s, Cp) 104.4 (d, J_{Cp} = 7.0 Hz, C1) 118.5 (bs, C2) 117.8 (q, J_{CF} = 292 Hz, CF_3) 180.6 (q, J_{CF} = 35 Hz, CO)
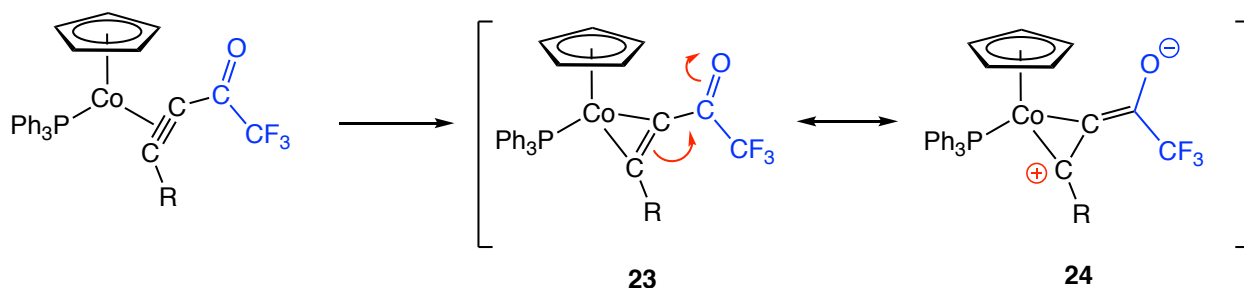
Scheme 2-9. Resonance structures of triflouromethylacetyl group substituted cobalt-alkyne complexes.

X-ray crystallographic analysis of the isolated cobalt-alkyne complexes allows for a comparison of structural characteristics to those cobalt-alkyne analogues that were reported in the literature. The selected bond distances and angles are summarized in

Table 2-2. The most prominent character of this trigonal η^2-coordination mode is the σ donation and π back donation between the acetylene and metal center, which can be reflected by the elongated C≡C bond distance in the cobalt-alkyne complexes (1.257 – 1.290 Å). It was found the C≡C bond distances in complex **18** (1.287(4) Å) and **19** (1.290(3) Å) are significantly longer than in complex **1** (1.2779(19) Å) and **7** (1.257 (4) Å), primarily due to the presence of resonance structure **24** in both complex **18** and **19** that weakens the π bond in the cobalt-alkyne complex (Scheme 2-9). The distances between cobalt and acetylene carbons are affected by both electronic effects and steric effects, i.e., when a stronger electron-withdrawing substituent is attached on the carbon, the cobalt-carbon distance will be shorter, whearas a bulky substituent can elongate the cobalt-carbon bond.[11] This phenomenon can be illustrated by a comparison of cobalt-alkyne complex **1**, **18** and **20**. Owing to the presence of resonance structure showed in Scheme 2-9, the carbon bearing a phenyl group in complex **18** is more electron poor than the acetylene carbon in complex **1** that has two phenyl substituents, and echoing to this electron effect, the Co–C1 bond (1.921(3) Å) in complex **18** is observed considerably shorter than complex **1** (1.9614(13) Å). Despite the C1 is more electron deficient than C2 in both complex **18** and **20** because of the resonance structure, the steric hindrance brought by the bulky TIPS group tunes the Co–C1 bond longer than the Co–C2 bond in complex **20** (Δ = 0.036 Å), while the opposite trend was observed in complex **18** (Δ = -0.015 Å).

When a comparison is made between the two acetylene carbons within a cobalt-alkyne complex, a percentage slippage value Ω was defined by O'Connor to evaluate the different chemical environments of the two alkyne carbons in the unsymmetrical coordination mode (Figure 2-5).[9] For instance, as expected, if the symmetrical cobalt-alkyne complexes **1** and **25** are applied in the equation, very small value of 0.4% and 0.2% of Ω are obtained, respectively, while 22% was detected in the unsymmetrical complex **7**. Surprisingly, the slippage value of unsymmetrical complex **18** (1.4%) and **19** (2.0%) were considerably small relative to the ester analogue **23** and **24** (16% and 10.2%), which might be due to the strong inductively electron-withdrawing effect of trifluoromethylacetyl group that competes the effect of resonance structure. The slippage value of complex **20** was detected as negative (-2.2%), primarily ascribed to the steric hindrance between TIPS group and tripenylphosphine. Furthermore, the bend-back angle showed in Figure 2-5 can be defined to describe the interaction of each acetylene carbon with metal center. The bend-back angle is also dictated by both electron effects and steric factors. For instance, in cobalt-alkyne complex **7** whose two substituents (TMS group and SO_2Ph group) have similar size, the bend-back angle on the sulphone site (35.7 °) is prominently greater than the trimethylsilane site (21.7 °) because of the electron-withdrawing effect of the sulfone group, whereas the bend-back angle on the C1 site of complex **20** (35.3(3) °) is larger than the corresponding C1 bend-back angle of complex **18** (31.2(3) °) and **19** (32.68(19) °) owing to the presence of steric hindered TIPS group in complex **20**.

Table 2-2. Selected bond distances (Å), angles (°), and percentage slippage Ω value of cobalt-alkyne complexs.

Complex	Co–C1	Co-C2	C1-C2	α	β	Ω
18	1.921(3)	1.936(3)	1.287(4)	31.2	30.7	1.4
20	2.011(4)	1.975(4)	1.265(4)	35.3	23.7	-2.2
19	1.918(2)	1.9528(19)	1.290(3)	32.68	32.81	2.02
1	1.9614(13)	1.9548(13)	1.2779(19)	31	32	0.4
7	1.911(4)	2.008(3)	1.257(4)	35.7	21.7	24
23	1.936(4)	2.001(4)	1.280(6)	37.6	27.4	16
24	1.945(2)	1.988(2)	1.279(3)	36.1	27.4	10.2
25	1.9387(14)	1.9396(14)	1.277(2)	27.8	33.1	0.2
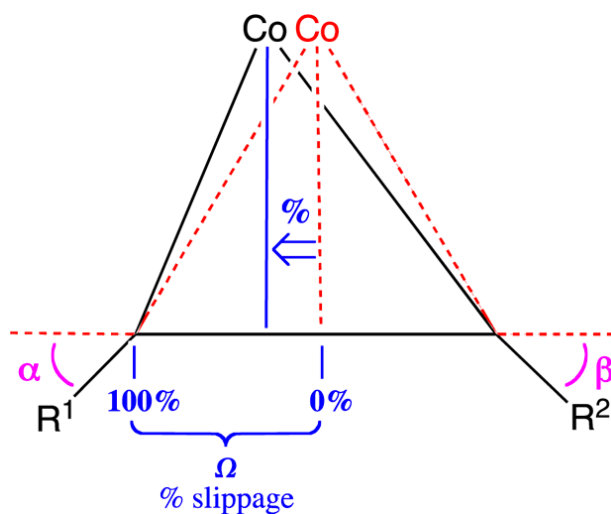
Figure 2-5. Percentage slippage value Ω and bent-back angles of cobalt-alkyne complexes.

C. Reactions of Cobalt-Alkyne Complexes with Ethyl Diazoacetate

1. Synthesis of Metallacyclobutene From Complex 18

By comparing the stable metallacyclobutene **8** that O'Connor lab obtained in 1993 with the work reported by Yamazaki and coworkers that when $(C_5H_5)(PPh_3)Co\{\eta^2\text{-}[C(Ph)\equiv C(Ph)]\}$ was treated with ethyl diazoacetate, two dicobalt complexes and two η^4-diene complexes were produced via an unobserved metallacyclobutene intermediate (Scheme 2-1), we reasoned that the electron-withdrawing sulfone group stabilizes the metallacyclobutene intermediate by strengthening the Co-C bond, and the bulky trimethylsilyl group inhibits the formation of bimetallic products. To verify the electronic factors that influence the stability of metallacyclobutene, we were firstly attracted by cobalt-alkyne complex **18** that replaces one of the phenyl groups of Yamazaki's metal-alkyne complex **1** with a strong electron-withdrawing trifluoromethylacetyl group.

When ethyl diazoacetate (1.0 g, 15% in toluene) were introduced into a stirring dry toluene solution of **18** (0.51 g, 0.87 mmol) over 10 hours at ambient temperature under inert gas atmosphere, the color of the reaction mixture gradually changed from purple to red. After concentrated, chromatography on silica gel, and recrystallization (toluene/hexane) in the air under dark, complex **25** was obtained as an air-stable crystalline solid with 40.3% yield (Scheme 2-10). It is noted that complex **25**, as the major product, is the first compound that comes through the column, following which one more red band was also observed. It was collected and identified by using ^1H NMR spectroscopy as a mixture of two η^4-diene complexes **26** and **27** with 1:1 ratio based on

the integration of their Cp resonances, and the isolated yield is calculated as 16% for each. The structural confirmations of the **26** and **27** were conducted by an independent synthesis of the two η^4-diene complexes from the reaction of metallacyclobutene **25** with ethyl diazoacetate (vide infra).
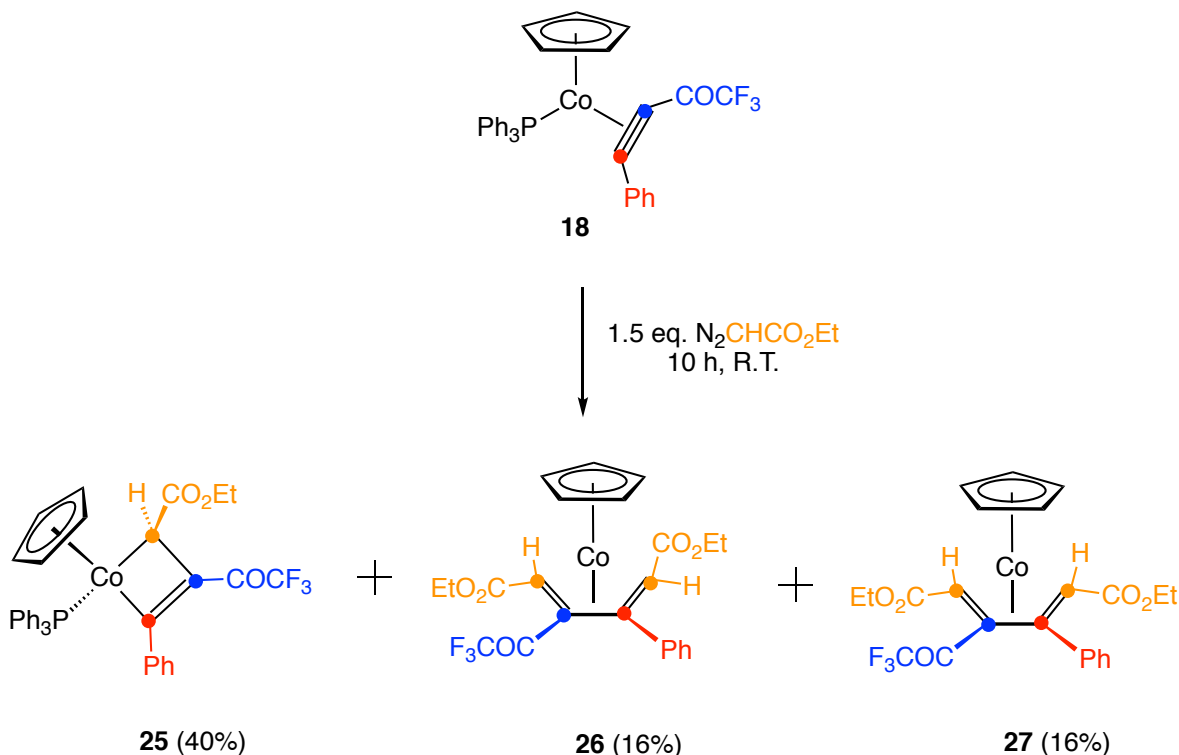
Scheme 2-10. Reaction between cobalt-alkyne complex **18** with ethyl diazoacetate.

Based on the ^{1}H NMR spectrum (CDCl$_3$, 400 MHz) of isolated complex **25**, the ester group from ethyl diazoacetate was found incorporated into the product, which exhibits a methyl resonance at δ 1.39 (t, 3H, J = 7.2 Hz) with two diastereotopic hydrogen resonances at δ 4.19 (m, 1H) and 4.29 (m, 1H), respectively. The ring hydrogen on the sp^3 carbon was observed coupled with phosphorus at δ 1.52 (d, 1H,

J_{PH} = 7.6 Hz), which excludes the possibilities of η^2-vinyl carbene complex **28**, η^3-vinyl carbene complex **29**, and oxa-metallabenezen complex **30** (Figure 2-6). In addition, the integration of 20 hydrogens from triphenylphosphine ligand and phenyl group in the aromatic region also supports the metallacyclobutene structure instead of a bimetallic complex. In the ^{13}C {^1H} NMR spectrum (CDCl$_3$, 125 MHz), a doublet at δ -0.38 (d, J_{CP} = 13.8 Hz) is assigned to the sp^3 ring carbon, which is strongly shielded by the metal center. The couplings between phosphorus and the two sp^2 ring carbons were detected at δ 198.8 (d, J_{CP} = 21.4 Hz) and 130.9 (d, J_{CP} = 2.5 Hz), which are assigned to the two carbons bearing phenyl group and trifluoromethylacetyl group, respectively, based on the chemical shifts. The smaller carbon-phosphorus coupling on the carbon bearing trifluoromethylacetyl group than the carbon bearing phenyl group suggests the regiochemistry that the phenyl substituent is closer to the metal center. Compared to the cobalt-alkyne precursor **18**, these two significantly lower-field vinyl carbon resonances (Δ = 48.1 and 43.1 ppm) in **25** are consistent with the proposed metallacyclobutene structure. In the IR spectrum, the two carbonyl groups of the ester and ketone moieties are observed at 1682 and 1690 cm^{-1}, and the weakened C=O stretching frequency is attributed to the hyperconjugation of carbonyl to the cobalt.
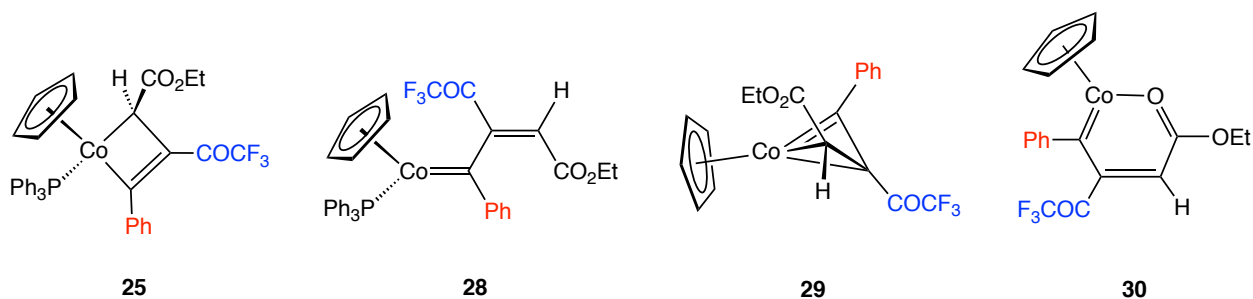
Figure 2-6. Possible products from coupling of cobalt-alkyne complex with ethyl diazoacetate.

The structure of **25** has been furtherly studied by X-ray crystallography, which reveals **25** as a single regio- and stereoisomeric cobaltacyclobutene (SS, RR) with two stereocenters at Co and C3 (Figure 2-7). This stereoselectivity matches what we expected that the ester substituent is more favorable to be located *anti* to the bulky triphenylphosphine ligand. The C1–C2 bond distance (1.356(4) Å) and C2–C3 bond distance (1.507(3) Å) indicate a double bond character and single bond character, respectively, which confirms the metallacyclobutene formulation (Table 2-3). The four-membered metallacycle structure is essentially planar with the largest deviation of planarity on C2 (0.008(2) Å) (the distance between C2 and the mean plane of the four-membered ring). Echoing with the ^{13}C NMR spectrum, the structure shows that more electron-poor carbon bearing phenyl group is located closer to metal center than the carbon bearing trifluoromethylacetyl group. It is consistent with what we observed before on metallacyclobutene **8**, in which the carbon with a strong electron-withdrawing sulfone group is closer to the cobalt than the carbon with an electron-donating trimethylsilyl group. We reason that this high regioselectivity is related to the electron-withdrawing effect that leads to a stronger Co–C bond, and also help stabilize the η^3-vinylcarbene intermediate on the way to form metallacyclobutene (vide infra).
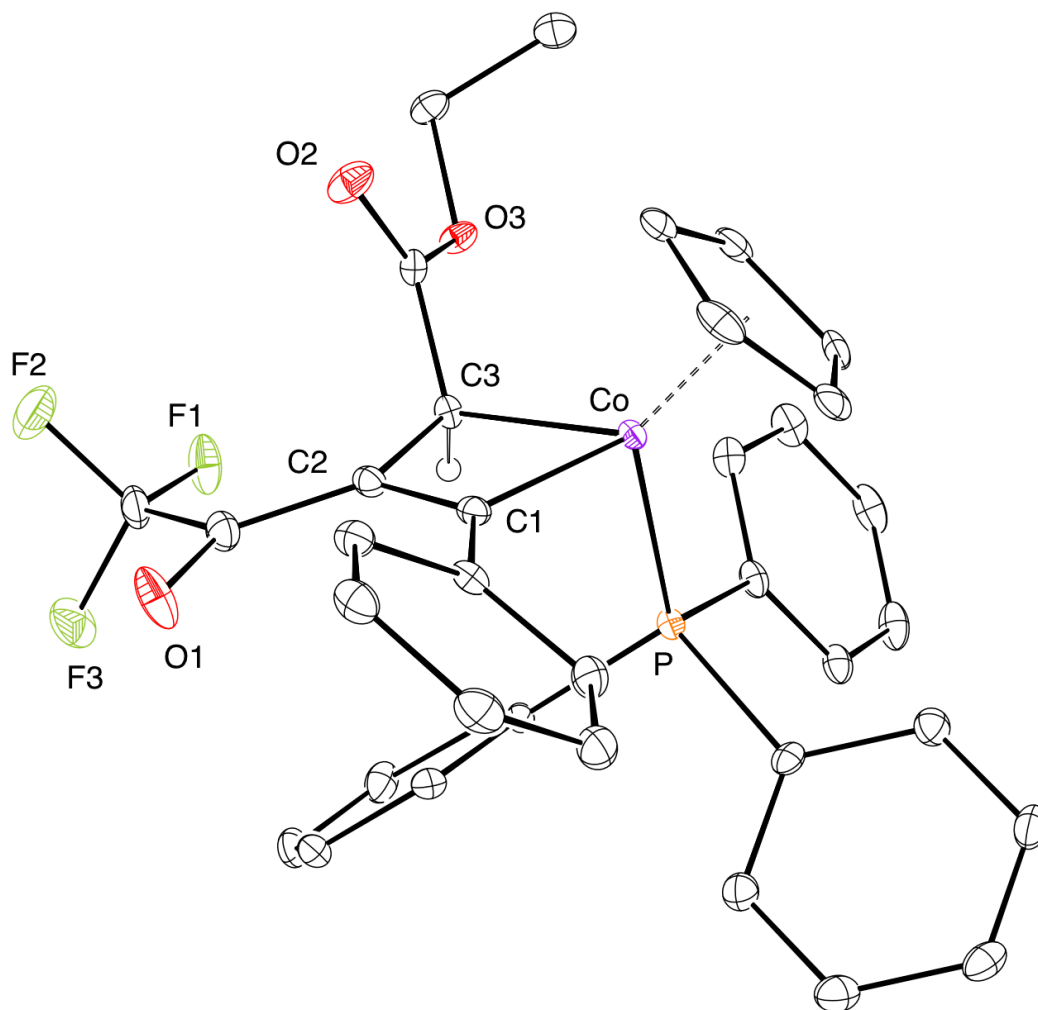
Figure 2-7. ORTEP drawing of complex **25** with ellipsoids shown at 30% probability.
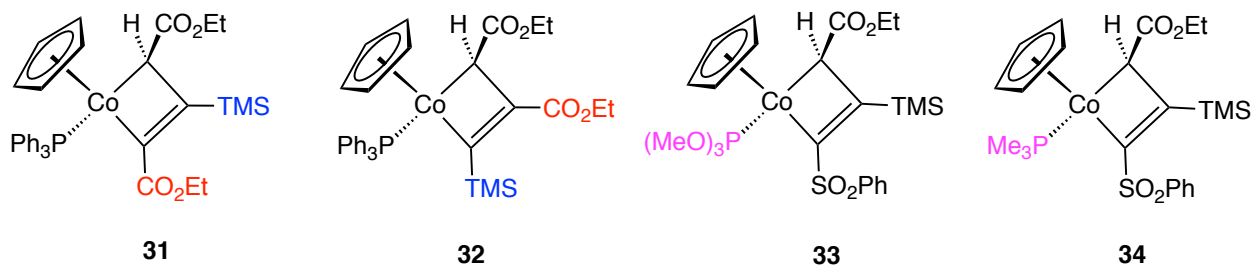
Figure 2-8. Metallacyclobutene synthesized by Mingchou Chen and Kevin Bunker.

The crystallographic characters of metallacyclobutene **25** are also allowed to be compared with our previously reported metallacyclobutenes **8** and **10**, and with those

ester substituted analogues that were synthesized by Kevin Bunker[12] and Mingchou Chen[13] (Figure 2-8). A conspicuous difference of the metallacycle **25** from others that bearing triphenylphosphine ligand is the significantly shorter Co–C1 bond distance (Δ = 0.02 – 0.05 Å), that is ascribed to the most electron-poor C1 carbon on complex **25** that strengthens the Co–C1 bond. Also, the double bonds distances (C1-C2) of metallacycles **8**, **31**, **32**, **33**, and **34** (1.334-1.338 Å) are very similar to each other, whereas the C1–C2 distance (1.356 (4) Å) of **25** is significantly longer, which might be attributed to that the stronger electron-withdrawing trifluoromethylacetyl group on **25** amplifies the back-donation effect from metal center to the double bond. Besides the π back bond, another reason for the elongated C1–C2 distance is the contribution from the resonance structure **35** (Scheme 2-11), which is either absent (in **8**, **33**, and **34**) or weaker (in **31** and **32**) due to the lack of inductively electron-pulling CF_3 moiety. Compared to complex **8**, the C1–C2–C3 angle in **25** is slightly greater (3.4 °), primarily due to the steric hindrance of the bulky TMS group in metallacycle **8**.

Table 2-3. Selected bond distances (Å) and angles (°) of metallacyclobutene complexes with different substituents.

Complex	8	11	25	31	32	33	34
Co-C1	1.938(2)	1.938(3)	1.906(2)	1.9262(16)	1.9569(17)	1.9187(15)	1.915(3)
Co-C3	2.0501(19)	2.055(3)	2.048(2)	2.0625(16)	2.0506(17)	2.0633(15)	2.055(2)
Co-P	2.1991(7)	2.2009(17)	2.2016(7)	2.1667(4)	2.1831(5)	2.1255(5)	2.1648(8)
C1-C2	1.336(3)	1.345(3)	1.356(4)	1.337(2)	1.336(2)	1.337(2)	1.338(4)
C2-C3	1.525(3)	1.515(3)	1.507(3)	1.510(2)	1.495(2)	1.521(2)	1.513(4)
C3-C4	1.470(3)	1.465(3)	1.471(3)	1.470(2)	1.476(2)	1.476(2)	1.466(4)
C4-O1	1.212(2)	1.211(3)	1.213(3)	1.214(2)	1.211(2)	1.2121(19)	1.218(3)
C1-Co-C3	66.95(8)	65.77(11)	69.45(9)	64.24(7)	69.61(7)	66.32(6)	66.62(11)
Co-C1-C2	101.89(15)	102.93(17)	98.69(16)	101.05(11)	95.48(12)	103.43(10)	102.83(19)
C1-C2-C3	100.43(17)	98.6(3)	103.83(19)	101.77(13)	107.72(15)	99.31(12)	99.8(2)
C2-C3-Co	90.72(12)	91.99(18)	88.02(14)	89.55(10)	86.94(10)	90.84(9)	90.79(15)
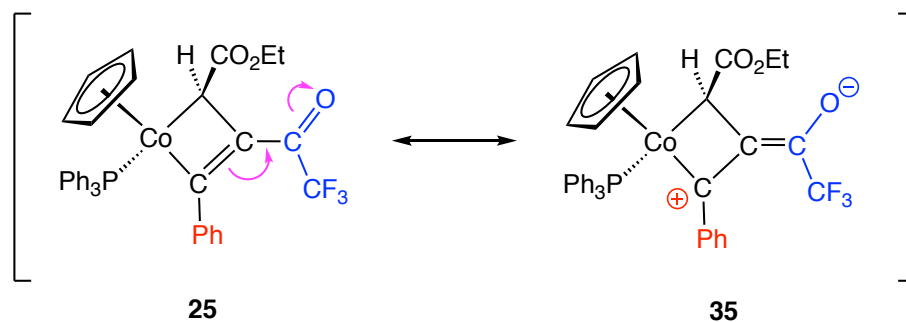
Scheme 2-11. Resonance structures of metallacyclobutene **25**.

Mechanistically, we propose that upon the dissociation of labile triphenylphosphine ligand from cobalt-alkyne complex **18**, the metal center is attacked by the α-carbon of ethyl diazoacetate to generate a highly reactive intermediate **36** (Scheme 2-12). Extrusion of a N_2 from complex **36** produces a cobalt-alkylidene intermediate **37**, which is followed by a migratory insertion of alkyne to form two isomeric η^3-vinylcarbene intermediates **29**-*E* and **29**-*Z*. Alternatively, the two η^3-vinylcarbene complexes can be generated by dissociation of N_2 from intermediate **36** via a nucleophilic attack of acetylene to the α-carbon of ethyl diazoacetate. Previously, we reported an equilibration can be observed by employing a more sterically hindered metallacyclobutene complex with a TIPS (^{i}Pr$_3$Si) substituent on the alkyne.[4] It should be noted that these 18-electron η^3-vinylcarbene intermediates are more stable than the unsaturated 16-electron metallacyclobutene intermediate **2** that was proposed by Yamazaki.[1] Based on these two facts, we believe the η^3-vinylcarbene is more likely to serve as intermediate instead of the unsaturated 16-electron metallacyclobutene. In addition, another possible intermediate other than η^3-vinylcarbene is the 18-electron oxa-metallacyclobenzene **30**, in which the metal center is coordinated to the carbonyl oxygen instead of the alkene. After the two η^3-vinylcarbene intermediates or oxa-metallacyclobenzene are trapped by triphenylphosphine, a pair of diasteromeric metallacyclobutenes is generated, in which the ester group stays *trans* to the bulky triphenylphosphine ligand to release steric hindrance.
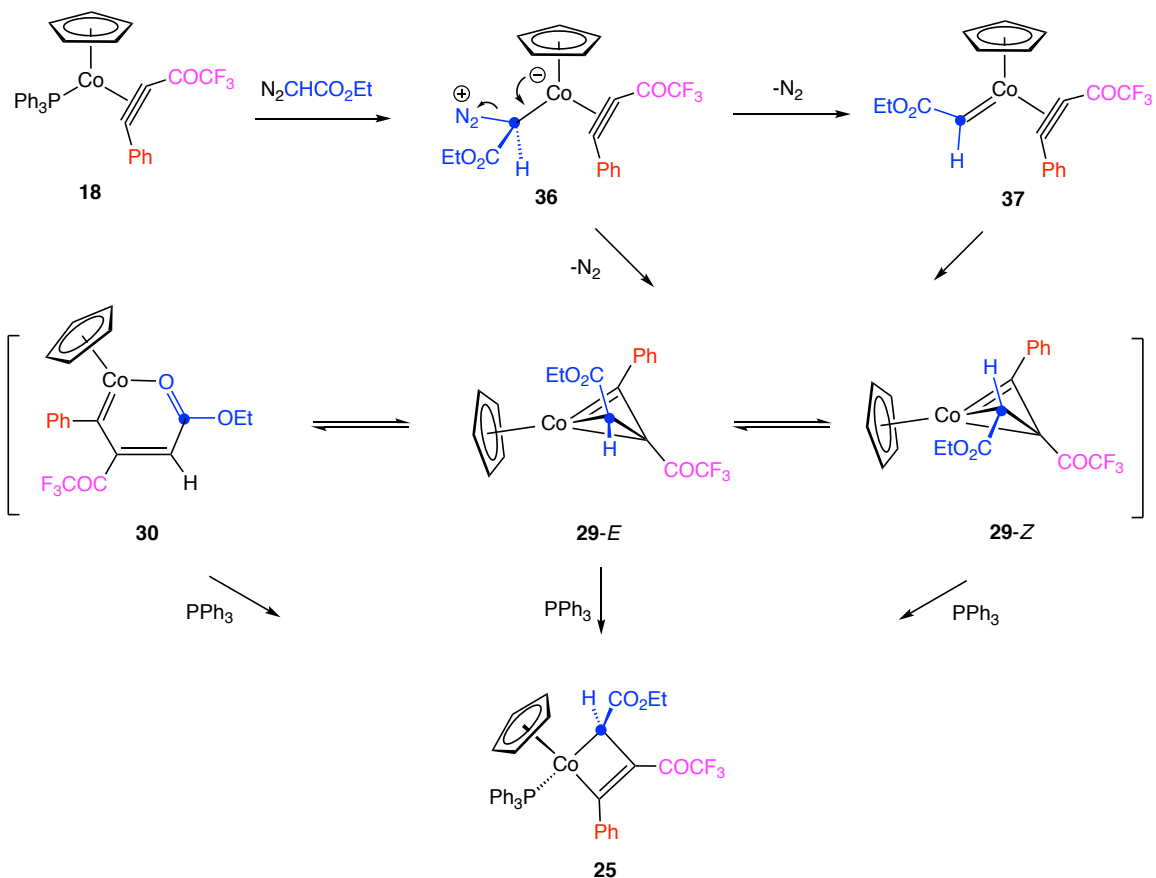
Scheme 2-12. Proposed mechanisms of formation of metallacyclobutene **25**.

2. Reactions of Other Cobalt-alkyne Complexes with Ethyl Diazoacetate

Based on the formation of metallacyclobutene **25** from complex **18**, the other two cobalt-alkyne precursors **19** and **20** were also employed to react with ethyl diazoacetate. However, the desired corresponding metallacyclobutenes have not been observed.

An NMR scale reaction was conducted between cobalt-alkyne complex **19** (5 mg, 0.0087 mmol) with ethyl diazoacetate (1.2 mg, 0.001 mmol) in a J.Y. NMR tube under inert atmosphere in C₆D₆ (0.75 mL) solvent. The reaction mixture was monitored by

using ^{1}H NMR (400 MHz) spectroscopy. It was noted that the cobalt-alkyne complex **19** can cause large decomposition of the ethyl diazoacetate, and after 1 hour at ambient temperature, all the ethyl diazoacetate were consumed with 70% of unreacted complex **19**. However, there is no evidence for the formation of expected metallacyclobutene complex because of the absence of the characteristic sp^3 ring hydrogen that was always observed as a doublet at around 1.5 ppm for the metallacyclobutene structure. In order to convert all the cobalt-alkyne complex to product, five more equivalents of ethyl diazoacetate was introduced in the reaction mixture, and after 90 minutes, all the cobalt-alkyne complexes were consumed with observance of multiple new Cp resonances at δ 4.47 (11.6%), 4.66, 4.72 (15.3%), 4.82, 4.84 (20.5%), 4.94, and 4.97. Isolation of any of these products was not successful due to the complexity of the reaction.

Extra triphenylphosphine was loaded into the reaction mixture beforehand with the hope that it can kinetically stabilize the metallacyclobutene. However, large inhibition effect was observed, and the reaction was sluggished and leads to massive decomposition of ethyl diazoacetate during the long reaction time. In addition, trimethyl phosphate, as a better σ donor than triphenylphosphine, was also employed into the reaction mixture in a separate NMR reaction. It was found that trimethyl phosphate substituted triphenylphosphine to generated complex **39** within 10 minutes (Scheme 2-13) with 86% of NMR yield based on the integration of new Cp resonance at δ 4.67 relative to internal standard. However, a large decomposition of ethyl diazoacetate was caused by the slow reaction rate, and no evidence of formation of desired metallacyclobutene **41** was observed.
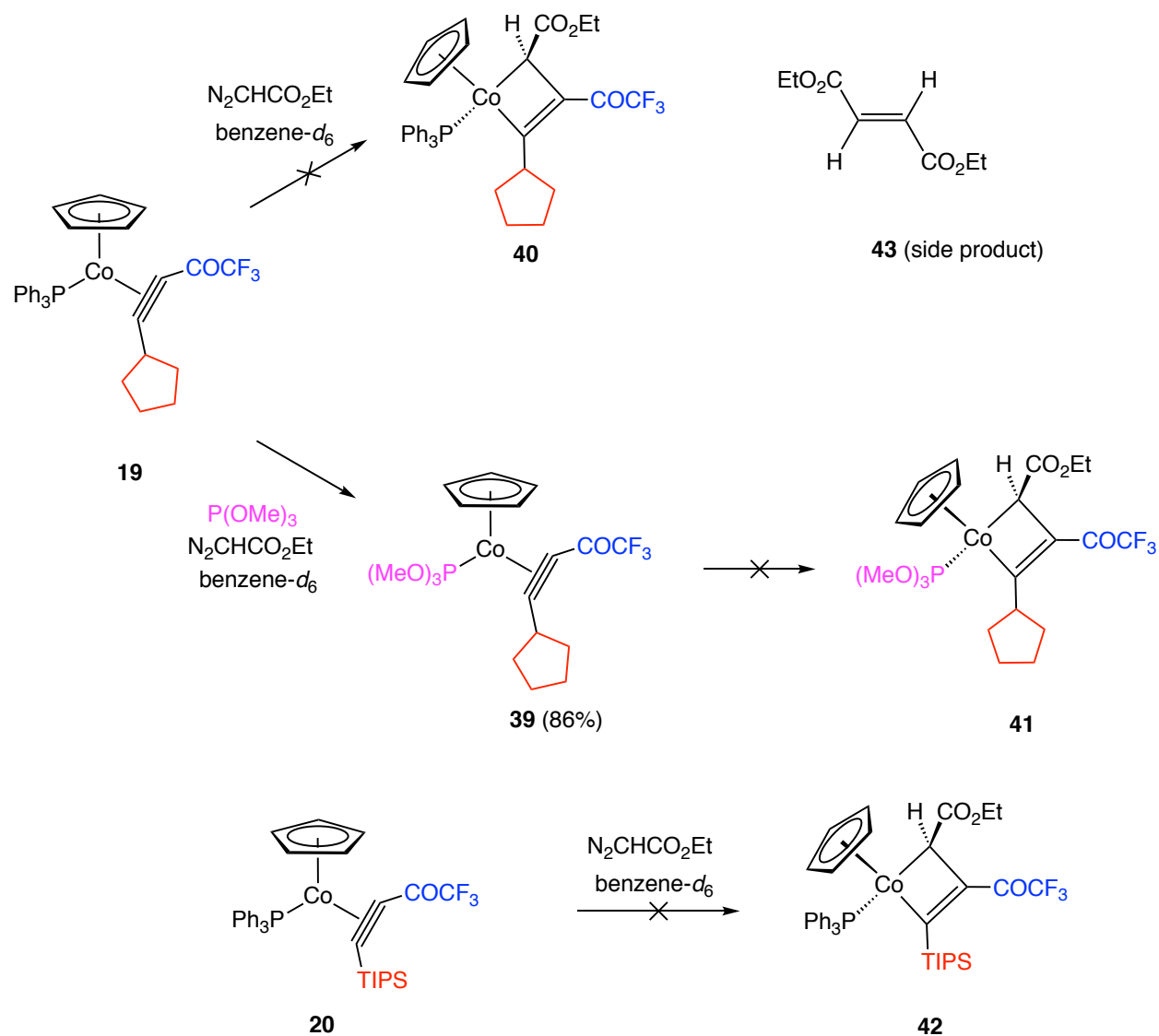
Scheme 2-13. Reactions of cobalt-alkyne complex **19** and **20** with ethyl diazoacetate.

A similar NMR reaction was carried between cobalt-alkyne complex **20** and ethyl diazoacetate. Two equivalents of ethyl diazoacetate was slowly introduced into the C_6D_6 solution of complex **20** over three times to prevent possible quick further reactions of the metallacyclobutene with the α-diazocarbonyl molecules. However, multiple Cp resonances were also observed at δ 4.44, 4.87, 4.54, and 4.91 in ^1H NMR after 2 hours

at ambient temperature, and there is no evidence for the formation of desired metallacyclobutene **42**.

The remarkable different reactivities of these three cobalt-alkyne complexes towards ethyl diazoacetate might be attributed to that extended conjugation is constructed in the metallacyclobutene complex **25** among the trifluoromethylacetyl group, double bond of alkene, and phenyl group, which tunes the metallacyclic structure more thermodynamically stable, whereas such extended π systems are absent with cyclopentyl or TIPS groups. For future direction, it would be interesting to explore the electron effects on stability of metallacyclobutene by employing various arene substituents on the cobalt-alkyne complex.

D. Metal-Alkyne and Metallacyclobutene Reactivity Toward a Diazoacetamide[15]

We previously reported the reactions of cobalt-alkyne complexes **7** and **8** with ethyl diazoacetate to give metallacyclobutenes, **8** and **10**, respectively (Scheme 2-14).[2,4] Reaction of the metallacycles with additional ethyl diazoacetate produced cobalt-1,3-diene complexes **43** and **44**, respectively. In the case of **7**, diastereomeric diene complexes **45** and **46** were also formed. The related reactions of **7** with the diazoketones $N_2CHCOMe$ and $N_2CHCOPh$ generated 1,3-(*Z*,*E*)-diene complexes **47** and **48**, respectively, with no spectroscopic evidence for the formation of metallacyclobutenes.[14]
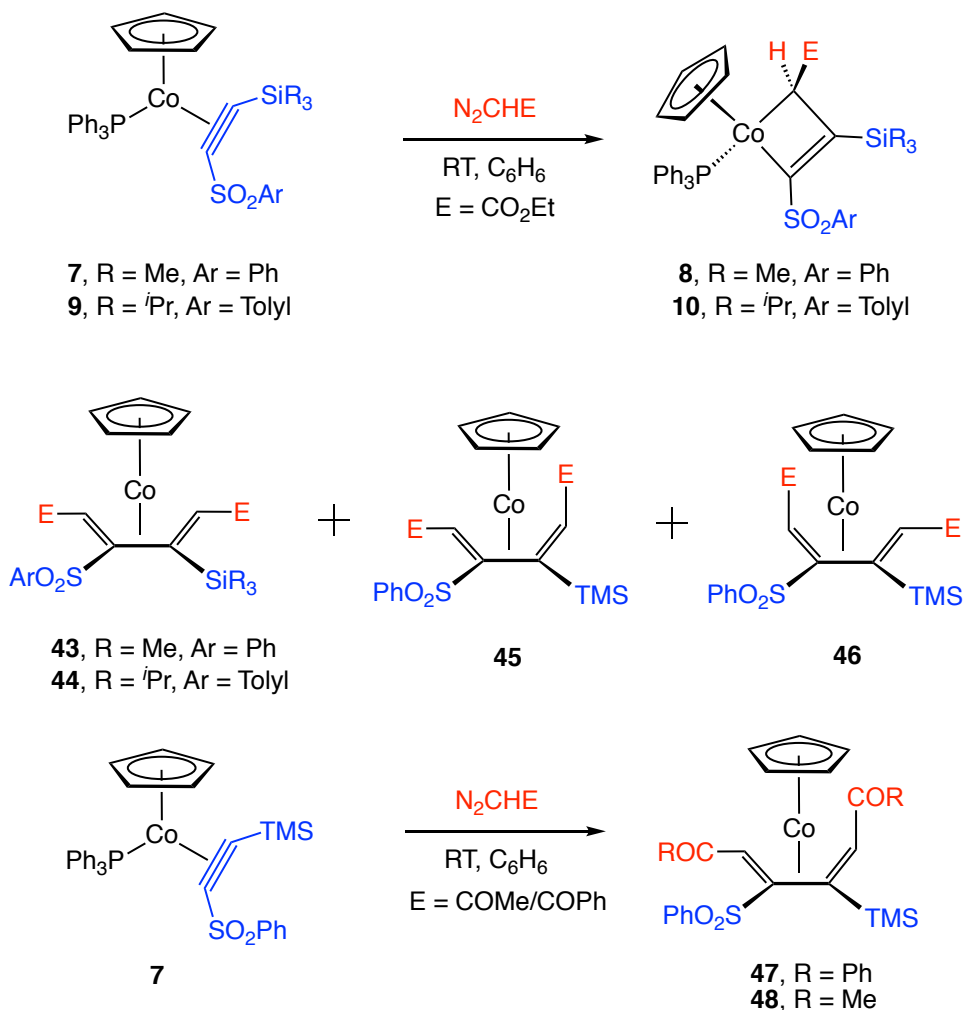
Scheme 2-14. Reactions of cobalt-alkyne complexes **7** and **9** with diazoacetate and diazoketones.

We have now examined the reactivity of the relatively electron-rich diazocarbonyl, 2-diazo-N,N-dimethylacetamide,[15,16] toward cobalt-alkyne complexes **7** and **9**. Unexpectedly, the reactions of **7** and **9** with 2-diazo-N,N-dimethylacetamide generate oxametallacyclopentadiene-sulfinato products $(\eta^5\text{-}C_5H_5)(SO_2Ar)Co[\kappa^2\text{-}\{O=C(NMe_2)CH=C(SiR_3)\}]$ (**49**, R = Me, Ar = C_6H_5 and **50**, R = $CH(CH_3)_2$, Ar = $p\text{-}C_6H_4CH_3$), which have been characterized by X-ray crystallography. The diphenylacetylene complex **1** and cobaltacyclobutene **8** undergo reaction with 2-diazo-

N,N-dimethylacetamide to produce the respective cobalt-(*Z,E*)-1,3-diene complexes, (η^5-C$_5$H$_5$)Co[η^4-(ECH=CPhCPh=CHE)] (**51**; E = CONMe$_2$) and (η^5-C$_5$H$_5$)Co{η^4-[ECH=C(SO$_2$Ph)C(TMS)=CH(CO$_2$Et)]} (**52**; E = CONMe$_2$).[17]
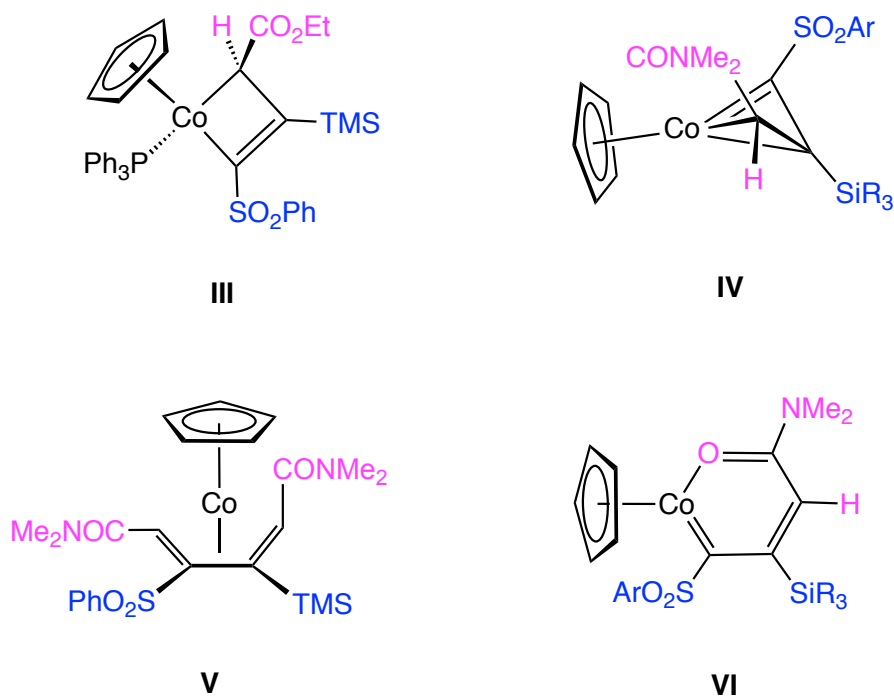
Figure 2-9. Spectroscopic data eliminate **III**−**VI** as viable structures for **49** and **50**.

The cobalt-alkyne complexes **7** and **9** underwent reaction with 2-diazo-*N,N*-dimethylacetamide (2 equiv) in dry toluene under an inert atmosphere to produce **49** (34% yield) and **50** (30%), respectively (Scheme 2-15). The spectroscopic data suggest very similar structures for the two isolated products. In the ^{1}H NMR (CDCl$_3$) spectrum of **49**, downfield resonances are observed at δ 7.5 − 8.1 (m, 5H) and 6.44 (s, 1H), indicating the presence of a phenylsulfonyl group and a vinyl hydrogen. Incorporation of an amido group is supported by two singlets at δ 2.88 (3H, NMe) and 2.91 (3H, NMe),

and the presence of a low energy carbonyl IR absorption at 1590 cm^{-1} (CDCl$_3$). The low energy IR absorption is consistent with coordination of the amide oxygen to cobalt. For comparison, the rhodium oxametallacycle, (P^{i}Pr$_3$)$_2$Rh(Cl)(H)[κ^2-(CH=CHCONH$_2$)], exhibits ν(C=O) at 1567 cm^{-1} (KBr).[18] On the basis of the ^{1}H NMR and IR spectroscopic data, it is possible to rule out cobaltacyclobutene (**III**), η^3-vinylcarbene (**IV**), and cobalt-diene (**V**) structures for **49** (Figure 2-9). Unexpectedly, the ^{13}C{^{1}H} NMR (CDCl$_3$) spectroscopic and mass spectrometry data for **49** indicated the presence of only nineteen carbon atoms, thereby ruling out oxametallabenzene structure **VI**.

7, R = Me, Ar = Ph
9, R = ^{i}Pr, Ar = Tolyl

49, R = Me, Ar = Ph
50, R = ^{i}Pr, Ar = Tolyl

53, R = CH$_2$SO$_2$Ph
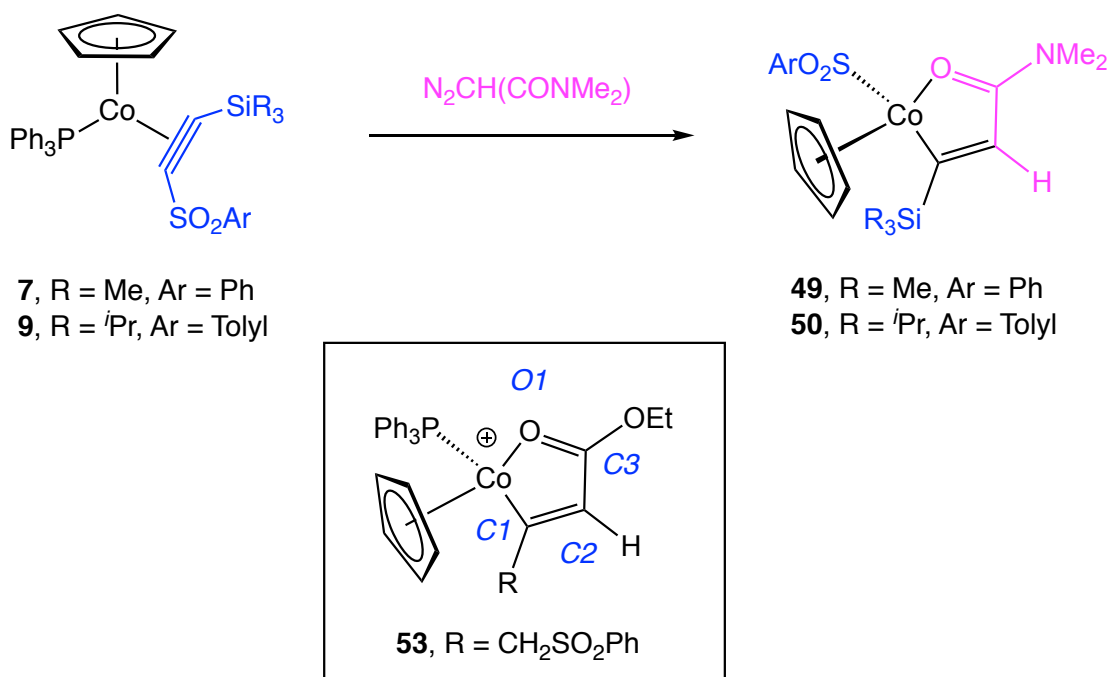
Scheme 2-15. Reactions of diazoacetamide with cobalt-alkyne complexes **7** and **9** generates oxametallacyclopentadiene products.

Ultimately, single-crystal X-ray analyses revealed **49** and **50** to be oxametallacyclopentadiene-sulfinato complexes (Figure 2-10, Figure 2-11, and Table 2-4).[19,20] Structurally characterized oxacobaltacyclopentadiene complexes are relatively rare,[21] and **49/50** appear to be the first examples that involve an amide oxygen. The Co-C(1)-C(2)-C(3)-O(1) rings in oxacobaltacyclopentadienes are nearly planar, with the largest displacements of a ring-atom from the mean plane being O(1) (-0.0350(18) Å) for **49** and C(1) (+0.0274(14) Å) for **50**. The conformation about the C(3) − N bond places the C(9)-N-C(10) mean plane parallel to the metallacycle ring plane, with a plane − plane dihedral angle of 7.3(2)° for **50** and 9.2(3)° for **49**. In **49**, the 1.348(5) Å C(1) − C(2) distance and 1.469(5) Å C(2) − C(3) distance indicate significant carbon-carbon double bond character at C(1) − C(2). Similar bond metrics are observed for **50**, with the most notable difference being a more acute Co − C(1) − Si angle in **49** (129.5(2)°) relative to that in **50** (135.5(2)°).
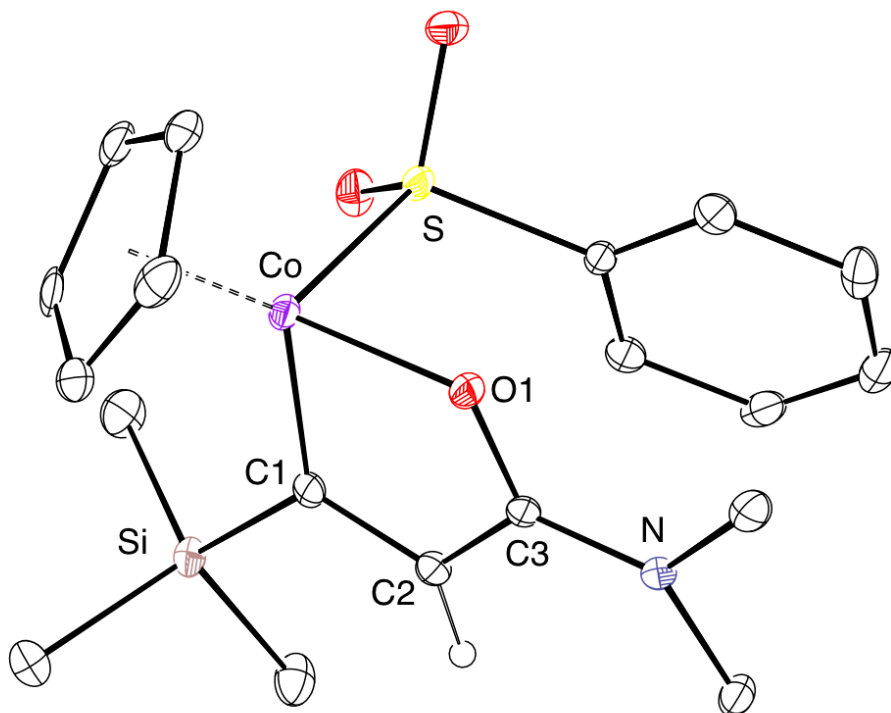
Figure 2-10. ORTEP drawing of **49** with ellipsoids shown at 30% probability.
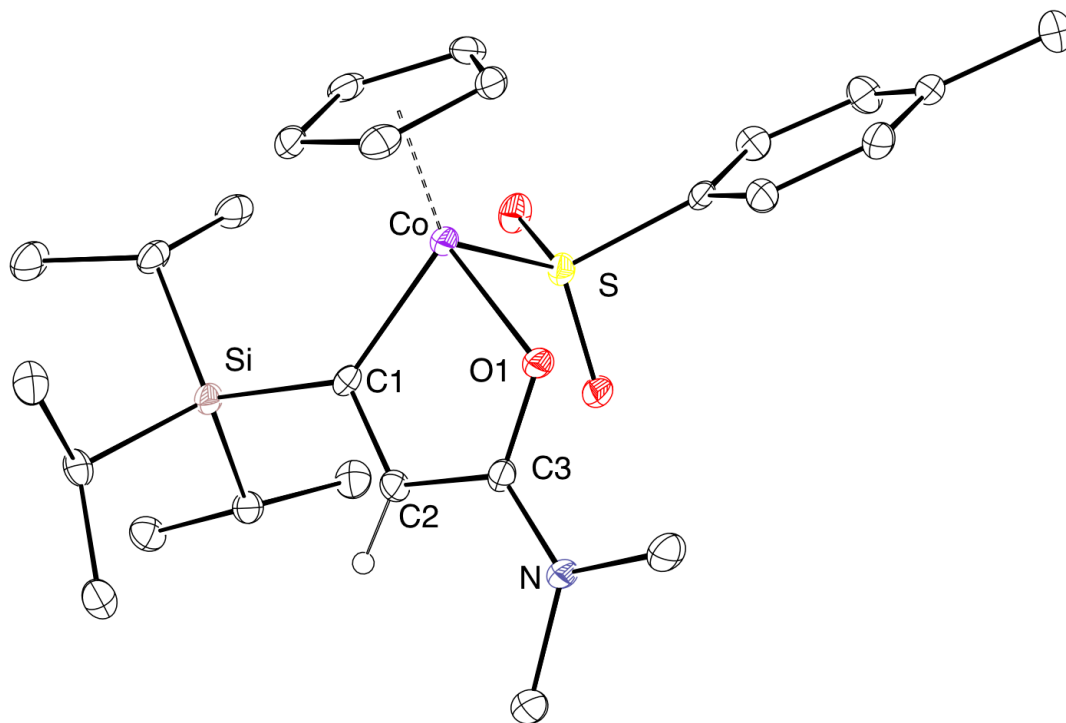
Figure 2-11. ORTEP drawing of **50** with ellipsoids shown at 30% probability.

Table 2-4. Distances (Å) and angles (deg) from crystallographic data for **49**, **50**, and **53**.

	49	50	53
Co-Cp^{cnt}	1.699(2)	1.702(2)	1.667(1)
Co-C(1)	1.937(4)	1.954(4)	1.914(2)
Co-S	2.190(1)	2.192(1)	-
Co-O(1)	1.935(2)	1.923(2)	1.950(2)
C(1)-C(2)	1.348(4)	1.346(5)	1.338(3)
C(2)-C(3)	1.457(4)	1.462(5)	1.434(3)
C(3)-O(1)	1.283(3)	1.273(4)	1.239(3)
C(1)-Si	1.880(3)	1.914(4)	-
C(3)-N	1.328(3)	1.328(4)	-
Co-O(1)-C(2)	113.4(2)	113.2(2)	110.9(2)
C(1)-Co-O(1)			84.4(1)
Co-C(1)-C(2)	110.6(2)	109.2(2)	111.0(2)
C(1)-C(2)-C(3)	115.9(2)	116.2(3)	114.2(3)
C(2)-C(3)-O(1)	115.5(2)	116.1(3)	119.4(2)
S-Co-C(1)	90.6(1)	89.7(1)	-
S-Co-O(1)	93.4(1)	90.5(1)	-

The structural data for **50** indicate a major resonance contribution from charge-separated resonance structure **50**-*II*, with a relatively minor contribution from metallafuran structure **50**-*III* (Figure 2-12). This contrasts markedly with the data for literature oxacobaltacycle **53**,[21b] which exhibits a significantly longer Co – O(1) distance and significantly shorter C(3) – O(1) and Co – C(1) distances. Thus, carbene (metallafuran) resonance structure **III** is a more significant contributor for **53** than for **50**. We attribute this difference in the relative resonance contributors for **50** and **53** primarily to the better pi-donor ability of nitrogen relative to oxygen.
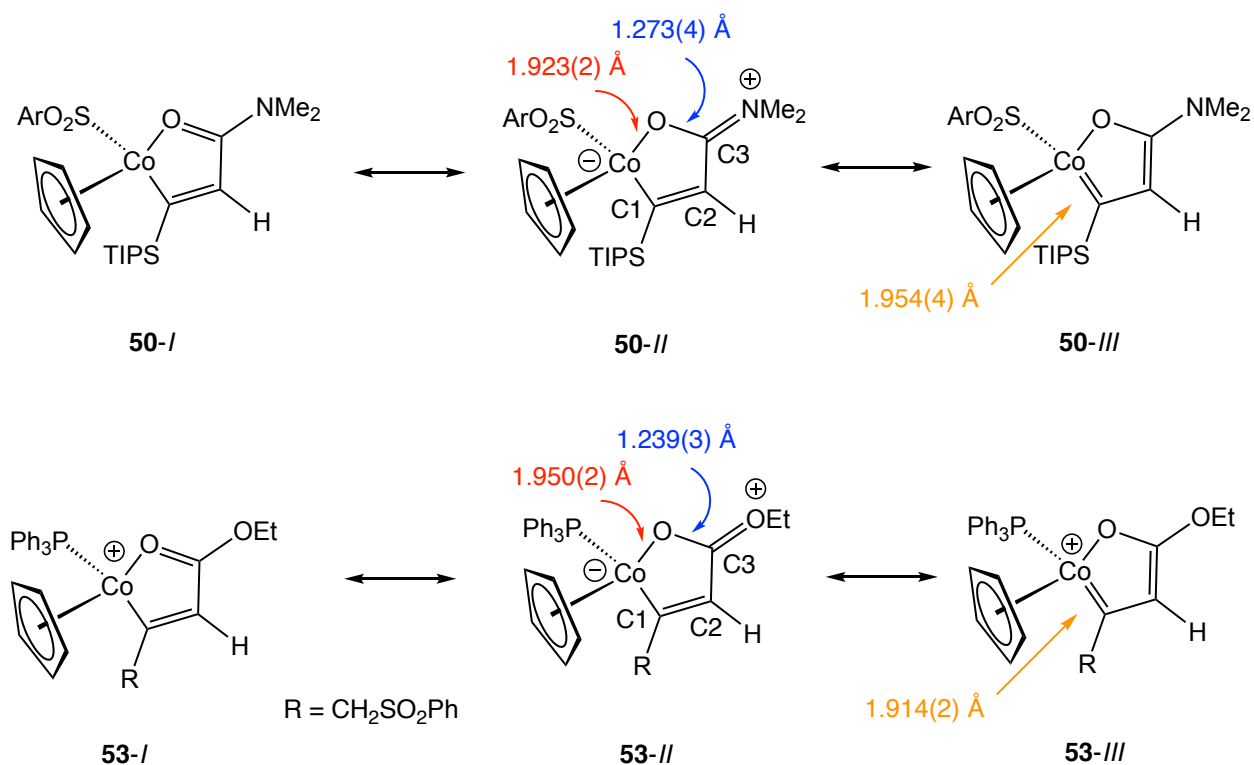
Figure 2-12. Comparison of resonance contributors for **50** and **53**.

The mechanism of formation for **49/50** must be complex. In an effort to determine the fate of the missing carbon atom, a reaction of **7** and diazoacetamide in dry, degassed benzene-d_6 was monitored by ^{1}H NMR spectroscopy. After 16 h at ambient temperature, analysis indicated the expected formation of **49**, as well as a 27% yield of a second cyclopentadienyl-cobalt product (δ 4.61, s). Additional resonances attributed to trace amounts of uncharacterized byproducts were observed at δ 4.40, 4.68, 4.71, 4.76, 4.84, 4.88, 5.11, 5.38, and 6.27. Our initial speculation that the δ 4.61 resonance is due to (η^5-C$_5$H$_5$)(PPh$_3$)Co(CO) (**54**) was confirmed by comparison of the NMR and IR spectroscopic data to those for an authentic sample of **54** prepared from CpCo(PPh$_3$)$_2$ (**13**) and CO (Scheme 2-16).[22] Notably, treatment of **7** with 1 atm of CO at room

temperature also led to the formation of **54** in 78% isolated yield. Thus, the missing carbon atom appears to have been converted to CO.
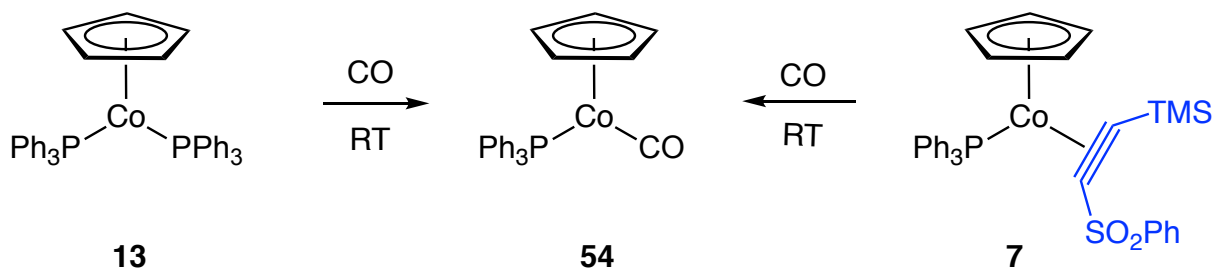
Scheme 2-16. Formation of $(\eta^5\text{-}C_5H_5)(PPh_3)Co(CO)$ from **13** and **7**.

The 27% yield of **54** makes it unlikely that the CO oxygen originated from adventitious oxygen or water in the reaction mixture. Furthermore, in solution, the alkyne complexes **7** and **9** decomposed upon exposure to air, and the reaction of **7** with diazoacetamide in $^{18}OH_2$-saturated C_6D_6 resulted in decomposition of **7**, with no formation of **49** or **54**.[23] An alternative source for the oxygen in byproduct **54** is the sulfone group of an organometallic complex (e.g., **7**), or an organic compound such as $TMSC\equiv CSO_2Ph$.[24] Scheme 2-17 provides a mechanism for incorporation of a sulfone oxygen into the CO ligand of **54**. Attack of the sulfone oxygen at the carbene carbon of VI15 would generate zwitterion VII followed by fragmentation to intermediate VIII and an alkynyl sulfoxide. Subsequent decarbonylation would lead to IX from which CO dissociation produces **49**. Reaction of liberated CO with **7** provides a reasonable explanation for the formation of byproduct **54**. This mechanism is highly speculative and efforts to increase the yield of **49** by the addition of DMSO or dimethylsulfone were

unsuccessful. Reaction of the liberated sulfoxide with other species (e.g., **7**, diazoacetamide, IV, VI, etc.) may lead to the trace amounts of unidentified byproducts.[25]
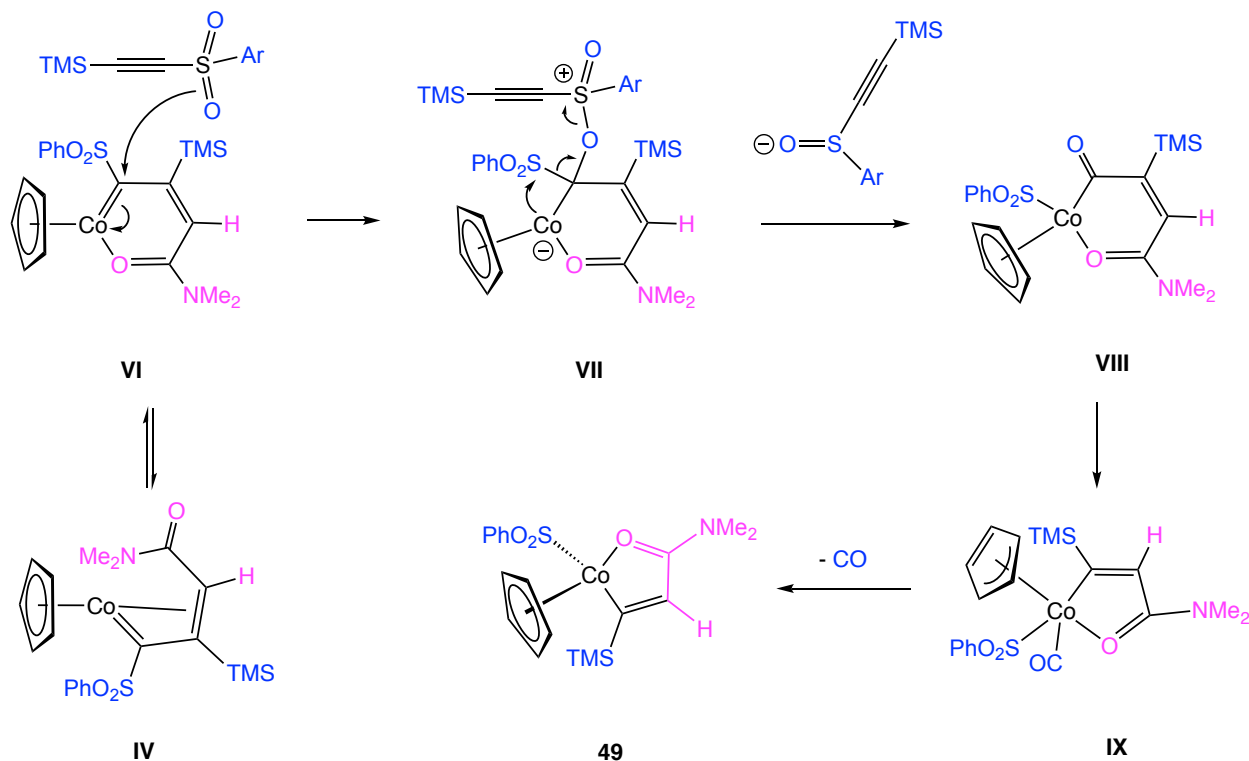
Scheme 2-17. Mechanistic speculation for the conversion of **7** to **49**.

The disparate outcomes observed for the reaction of **7** with diazoacetamide vs. diazoester reagents may be a consequence of differences in the relative stabilities and reactivity of the corresponding vinylcarbene intermediates (e.g. **IV** and **VI** vs. analogues derived from a diazoester).

Regardless of the mechanism by which **49** forms, it is clear that the diazo reagent has coupled to a carbon of the alkyne ligand in diazoacetamide. In an effort to establish the reactivity of diazoacetamide toward a complex that is less capable of alkyne fragmentation, we turned to the reaction of **1** and diazoacetamide. Treatment of

a toluene solution of **1** with 5 equiv. of diazoacetamide at ambient temperature led to formation of the cobalt-diene complex **55** as a single diastereomer in 81% isolated yield (Scheme 2-18). In the ^{1}H NMR spectrum (CDCl$_3$) of **55**, singlets at δ 1.73 (1H) and 3.54 (1H) are attributed to the *anti* and *syn* hydrogens of the diene ligand, respectively. For comparison, the analogous diene complex, (η^5-C$_5$H$_5$)Co[η^4-(*Z,E*)-CH(CO$_2$Et)=CPhCPh=CH(CO$_2$Et)], derived from **1** and ethyl diazoacetate, exhibits resonances in CDCl$_3$ at δ 1.70 (s, H^{anti}) and 3.70 (s, H^{syn}).[1] The structure of **55** was confirmed by an X-ray crystallographic analysis (Figure 2-13).
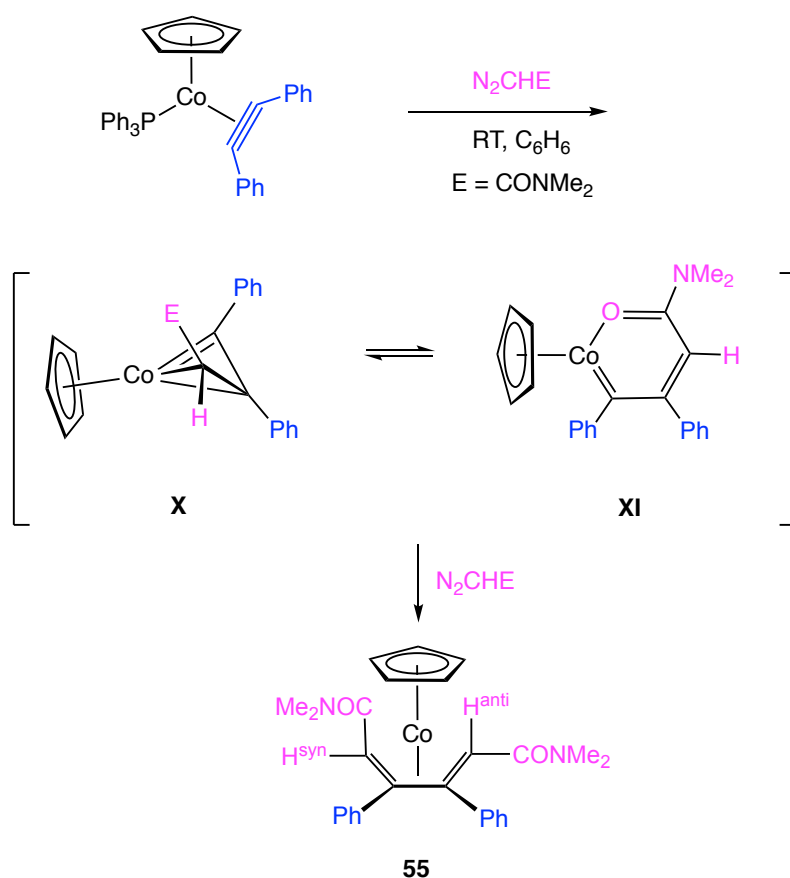
Scheme 2-18. Reaction of diazoacetamide with cobalt-alkyne complex **1**.

We previously found that **10** exists in equilibrium with the η^3-vinylcarbene complex **11** (Scheme 2-19), and calculations indicated that **13**-*TIPS* is more stable than the unsaturated cobaltacyclobutene analogue.[4] We therefore propose that **55** is formed via the intermediacy of a vinylcarbene intermediate (e.g. **X** or **XI**) which undergoes reaction with a second equivalent of diazoacetamide (Scheme 2-18).
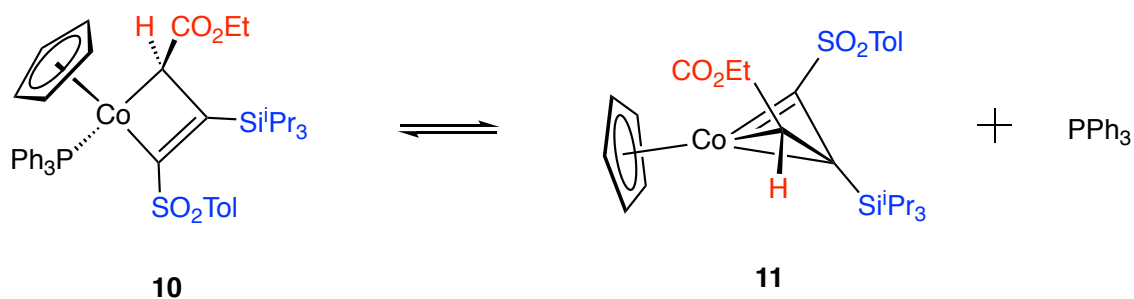
Scheme 2-19. Equilibrium between metallacycle **10** and vinylcarbene **11**.
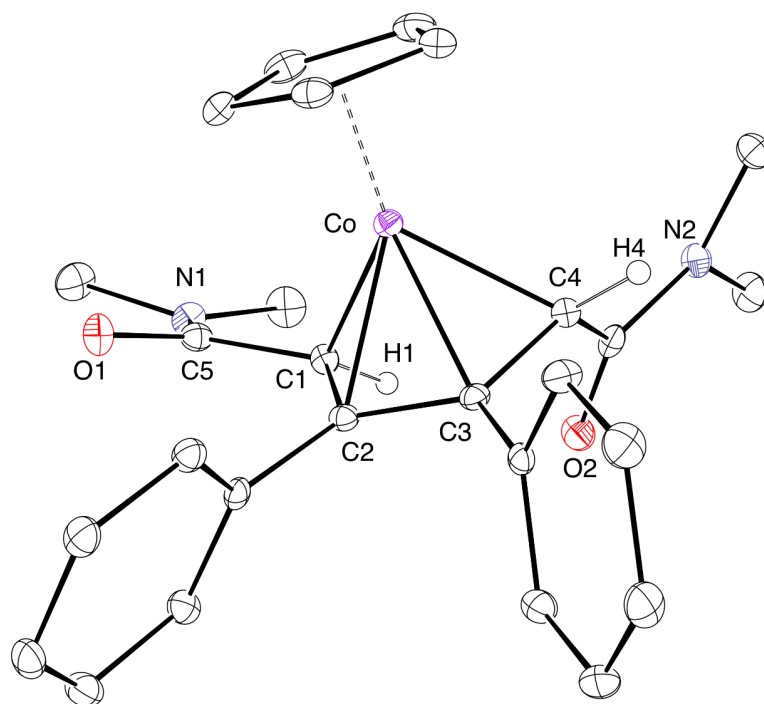
Figure 2-13. ORTEP drawing of **55** with ellipsoids shown at 30% probability.

The proposed formation of η^3-vinylcarbene **X**, and our previous observation that

8 underwent reaction with diazoketones to give dienes,[14b] The above results suggested

that diazoacetamide may undergo a regio- and stereoselective reaction with an η^3-

vinylcarbene derived from **8** to give a 1,3-diene bearing four different functional groups.

In the event, reaction of **8** with 1.5 equivalents of diazoacetamide proceeded at 70 °C (6

h) to give a 53% yield of **57** (Scheme 2-20). In the ^{1}H NMR spectrum (CDCl$_3$) of **57**,

resonances at δ 1.44 (s, 1H, H^{anti}) and 3.53 (s, 1H, H^{syn}) indicate *ZE* stereochemistry, as

was observed for cobalt-diene complexes **47, 48** and **55**.[26] A single-crystal X-ray

analysis confirmed that the amide-substituted carbene had coupled to the

metallacyclobutene carbon bearing the sulfone substituent, and that the amide and

sulfone groups are *syn* (Figure 2-14). This stereochemical outcome is consistent with

that observed from reaction of **8** with diazoketones. We propose the intermediacy of a

η^3-vinylcarbene (**XII**) for the conversion of **8** to **57** (Scheme 2-20). Mechanistic

possibilities for the conversion of η^3-vinylcarbene intermediate **XII** to cobalt-diene **57**

products include either direct attack of the diazo reagent at the carbene carbon and

initial diazoacetamide attack at cobalt followed by carbon – carbon bond formation, as

shown in Scheme 2-21.
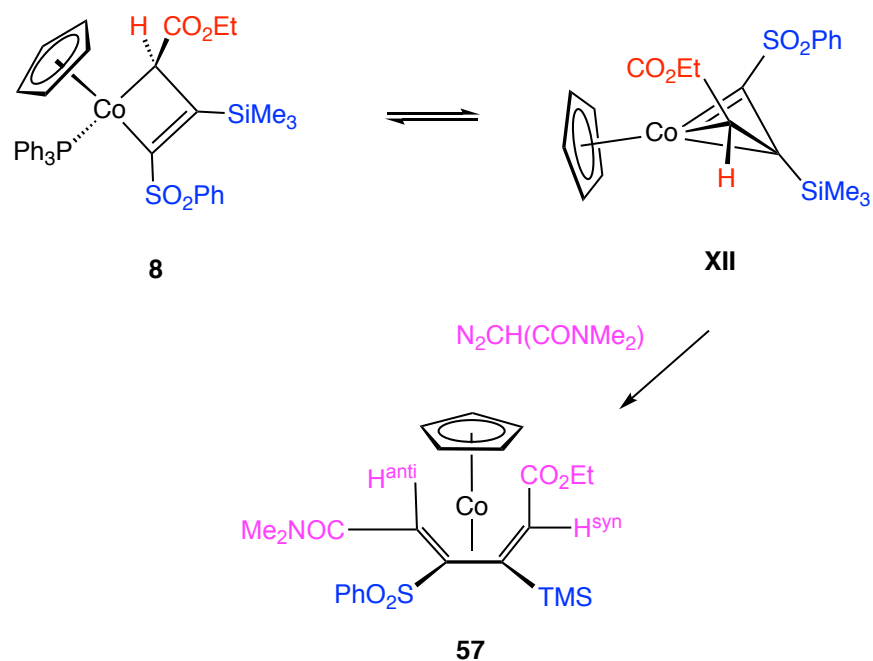
Scheme 2-20. Reaction of diazoacetamide with cobaltacyclobutene **8**.
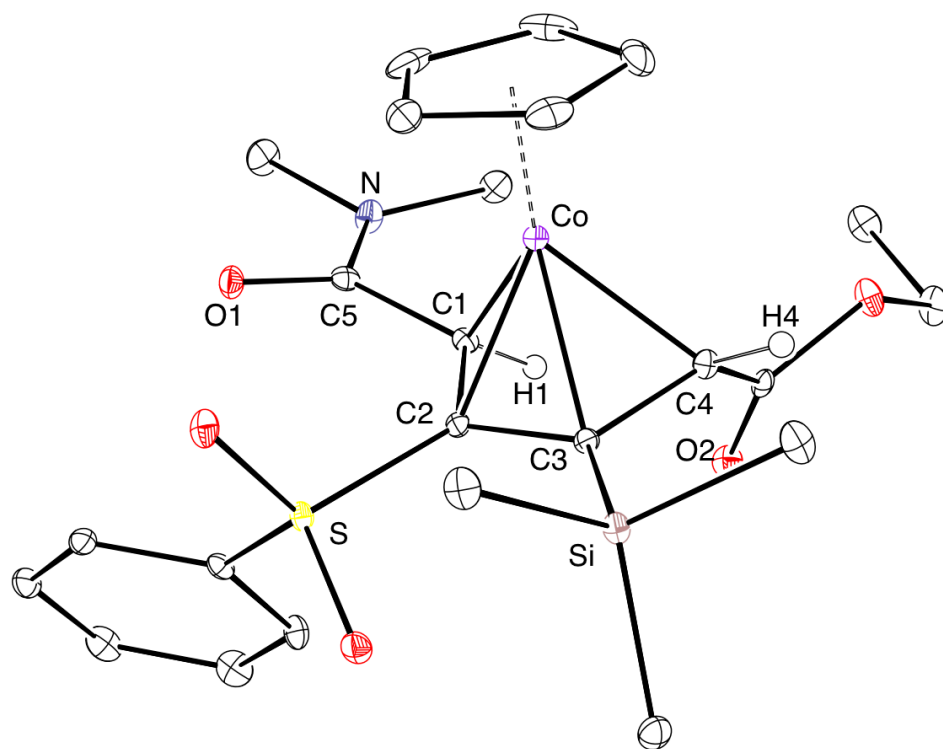
Figure 2-14. ORTEP drawing of **57** with ellipsoids shown at 30% probability.
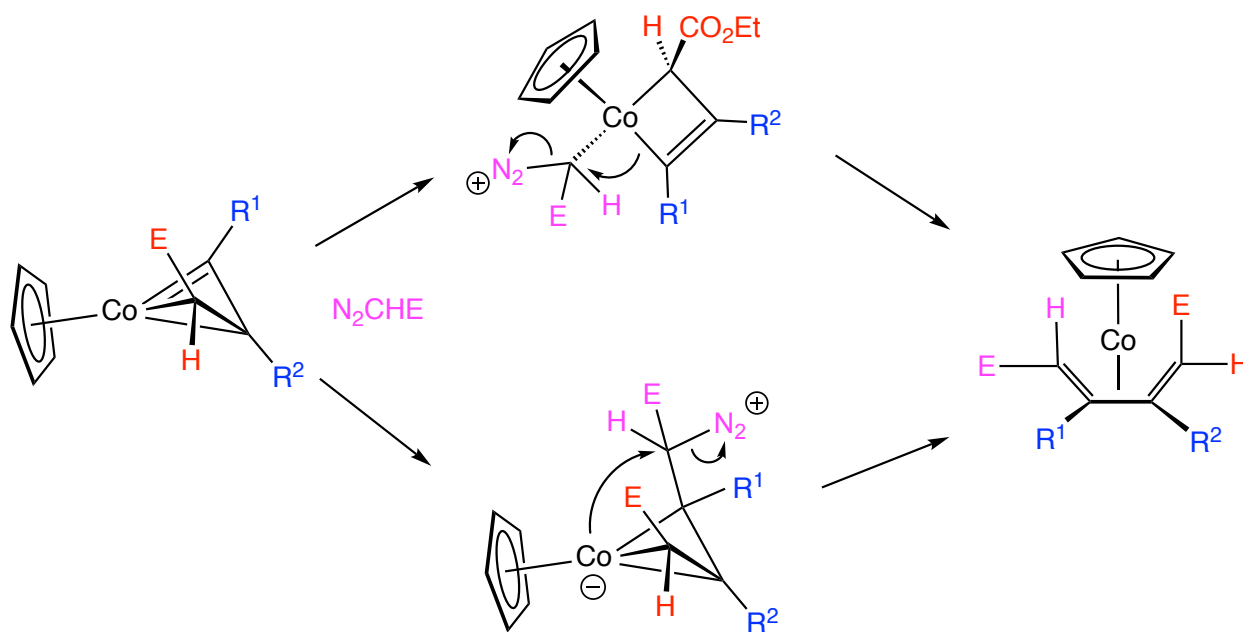
Scheme 2-21. Mechanistic possibilities for the conversion of vinylcarbene intermediates to metal-diene products.

In comparison, a control experiment was carried out by employing the diazoacetamide with free alkyne (TMS)C≡C(SO$_2$Ph) in the absence of metal. When 5 mg (0.02 mmol) of trimethyl((phenylsulfonyl)ethynyl)silane and 2.5 mg (0.022 mmol) of diazoacetamide was added into a J.Y. NMR tube with 0.4 mL of dry benzene-d_6, a new set of resonances formed cleanly within 12 hours. After the reaction is done, a 98% NMR yield of a new product was obtained based on the integration of the new TMS resonance located at δ 0.32 relative to internal standard. A followed preparation scale reaction allowed for the isolation and characterization of the product (Scheme 2-22). In the ^{1}H NMR spectrum (CDCl$_3$, 400 MHz), the two methyl resonances of amide are

observed at δ 2.86 (s, 3H) and 3.11 (s, 3H). It is notable that a very deshielded hydrogen located at δ 10.52 is observed as a broad singlet, which matches a typical chemical shift of pyrazole molecule.[27] A high-resolution mass spectrometry analysis indicates the chemical formula of the product as $C_{15}H_{21}N_3O_3SSi$ that rules out the cyclopropene structure **58**. A further crystallization of the product in hexanes/methylene chloride afforded white crystalline solids that is suitable for single X-ray crystallography study (Figure 2-15), revealing a diaza-cyclopentadiene structure, in which the carbon bearing TMS group is selectively bonded to the nitrogen atom. The double bond between C1 and C2 is only slightly shorter (Δ = 0.011 Å) than the single bond between C2 and C3, which is attributed to the steric hindrance between the bulky TMS and sulfone group. The aromatic five-membered heterocycle is essentially planar with the largest deviation of planarity at N1 (0.029(2) Å). The disturbance of aromaticity from π-π bond interaction of the amide group with the heterocycle is excluded due the large torsion angle of O1 – C4 – C3 – N2 (85.1 (3) °). In addition, an intermolecular hydrogen bond (1.928 Å) is detected between the ring hydrogen and carbonyl oxygen in the crystal lattice, which is consistent with low-field resonance of the ring hydrogen in the ^{1}H NMR.
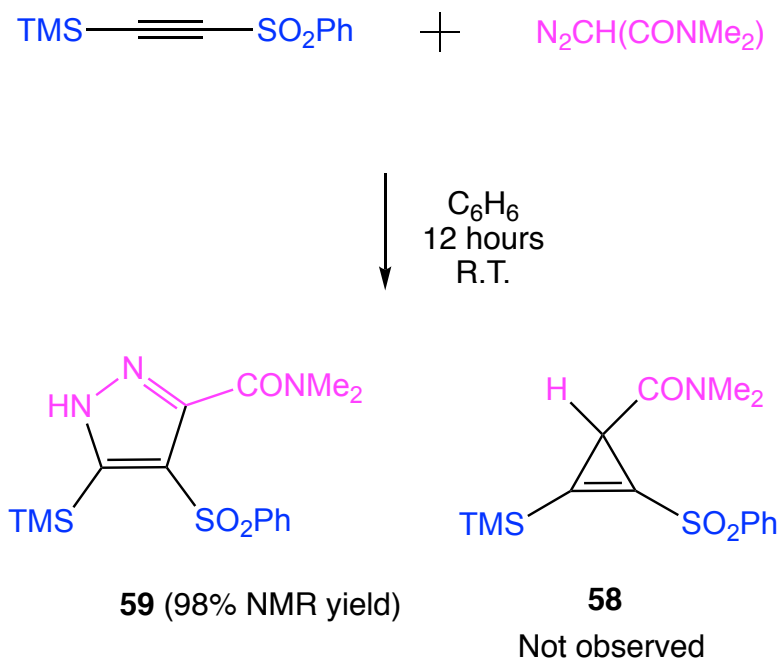
Scheme 2-22. Reaction of alkyne (TMS)C≡C(SO₂Ph) with diazoacetamide.
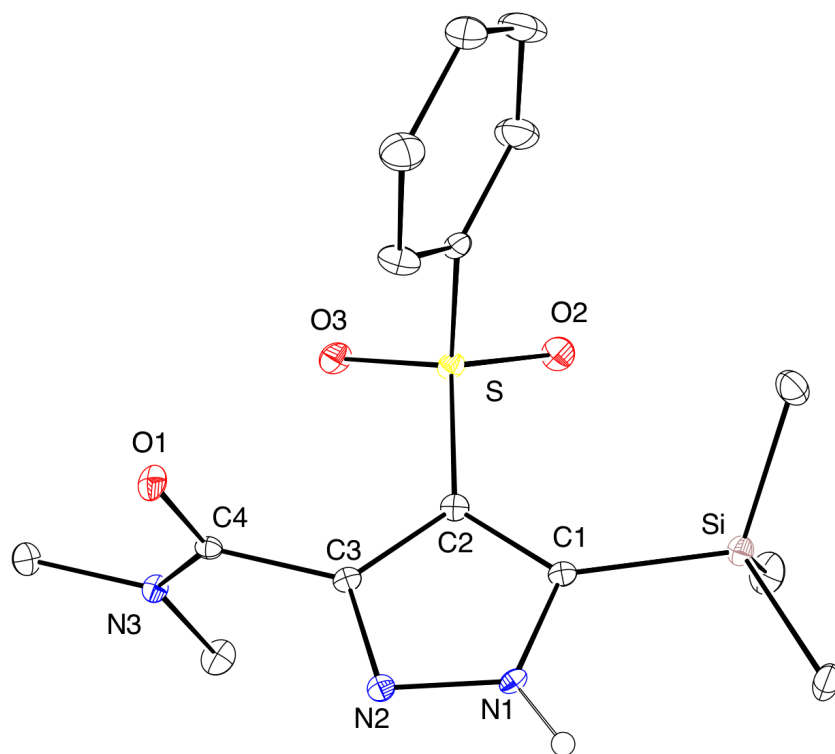
Figure 2-15. ORTEP drawing of **59** with ellipsoids shown at 30% probability.

The pyrazole product **59** was subsequently allowed to react with CpCo(PPh₃)₂ in benzene-d_6. After 8 hours, when all the CpCo(PPh₃)₂ was consumed, a lot of dark green paramagnetic green precipitate was generated without any evidence of formation of oxametallacyclopentadiene **49** or complex **54** (Scheme 2-23).
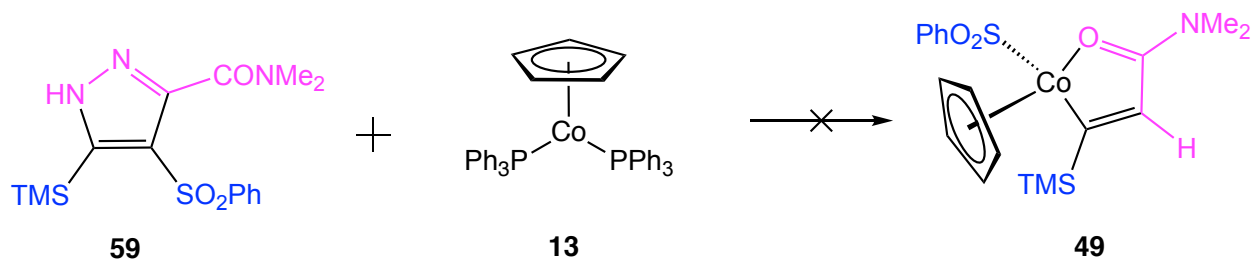
Scheme 2-23. Reaction of pyrazole **59** with CpCo(PPh₃)₂.

Mechanistically, for the formation of pyrazole **59**, we proposed that the more electron rich carbon that is attached to the TMS group selectively attack the terminal nitrogen N1 of diazoacetamide (Scheme 2-24), and a followed nucleophilic attack of the carbon bearing sulfone group by the α carbon of diazoacetamide generates the five-membered ring intermediate **60**. The final pyrazole product **59** is produced via a deprotonation/protonation process by trace amount of base in the reaction mixture with the intermediacy of aromatic cyclic anion **61**.
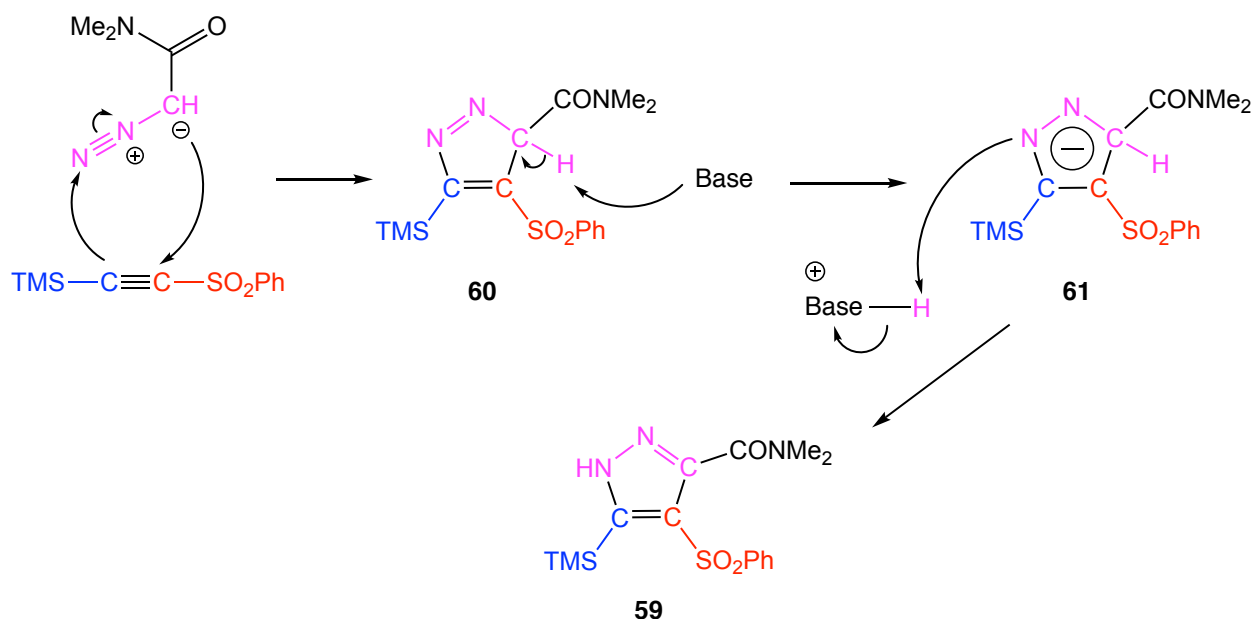
Scheme 2-24. Proposed mechanism for the formation of **59**.

In summary, a surprising carbon-extrusion reaction has been uncovered for the reaction of sulfone-substituted alkyne complexes with a diazoacetamide. The reaction mechanism must be highly complex, involving the cleavage of a carbon – sulfur bond and the loss of a single carbon atom, which appears to be incorporated into the carbon monoxide ligand of the (η^5-C$_5$H$_5$)Co(PPh$_3$)(CO) byproduct. In comparison, without the incorporation of metal, a highly regio selective pyrazole compound **59** was generated exclusively. Notably, the diphenylacetylene complex **1** undergoes reaction with diazoacetamide to give a high yield of cobalt-diene complex **55**, with no evidence for diastereomeric diene isomers. Alternatively, the metallacyclobutene complex **8** undergoes reaction with diazoacetamide to give a single diastereomer of the tetra-functionalized 1,3-diene complex **57**. The formation of both diene complexes is proposed to involve the reaction of diazoacetamide with an unobserved η^3-vinylcarbene intermediate.

E. Reactivity Studies of Metallacyclobutenes

1. Thermal Reactivity of Cobaltacyclobutene: Reversible Formation of Dicobalt Propendiyl Complex

In order to compare with Hong's dicobalt complexes that were generated from the reaction between cobalt-alkyne complex (η^5-C$_5$H$_5$)Co(Ph)C≡C(Ph) and ethyl diazoacetate, a thermolysis reaction was carried out on the newly isolated metallacyobutene **25**. After 5 mg (0.007 mmol) of cobaltocyclobutene **25** was added into a J.Y. NMR tube with 1,4-bis(trimethylsilyl)benzene as internal standard, 1.2 mL of dry benzene-d_6 was distilled into the NMR tube and the reaction mixture was heated at 70 °C in an oil bath under dark, during which process, the color of the solution slowly changed from red to dark. After 3 hours, all the starting metallacyclobutene **25** was consumed based on the Cp resonance at δ 4.47, and two Cp resonance with equal intensity were observed at δ 4.28 (s, 5H, Cp) and 4.76 (s, 5H, Cp), respectively, which suggests that a bimetallic complex was generated. Integration of the two Cp resonance relative to internal standard gives a 91% NMR yield (Scheme 2-25). A preparation scale reaction was conducted in the glove box, in which 0.32 g (0.477 mmol) of complex **25** was heated in toluene at 70 °C for 3 hours. After concentrated and chromatography on aluminum oxide with hexanes/ethyl acetate inside the glove box, 0.102 g (80% yield) of complex **62** was isolated as air-sensitive dark oil.
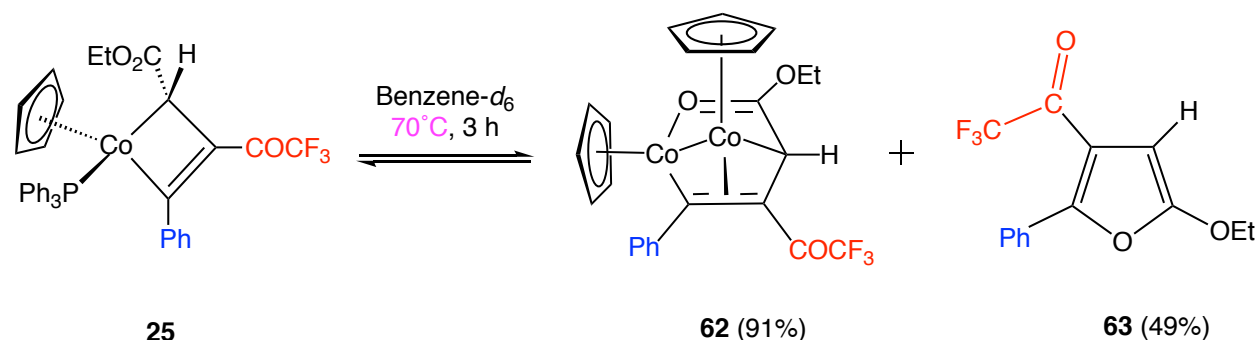
Scheme 2-25. Thermolysis of metallacyclobutene **25**.

In the ^{1}H NMR spectrum (CDCl$_3$, 400 MHz) of complex **62**, the two Cp resonances were observed at δ 4.28 (s, 5H) and 4.76 (s, 5H), respectively. Two diastereotopic hydrogens on the ester group exist at δ 3.46 (m, 1H) and 3.3 (m, 1H). The integration of ester group relative to the Cp resonance indicates that only one ester group is incorporated, and the integration of 5 hydrogens in the aromatic region suggests that the triphenylphosphine is no longer coordinated to the cobalt in the product. Compared to metallacyclobutene **25**, the chemical shift of C2 on **62** in the ^{13}C {^{1}H} NMR spectrum moved from δ 198 to 88.8, which indicates a very strong shielding effect from the two metal centers of the dicobalt complex. Also, the movement of C3 from δ -3.8 to 26.6 suggests that C3 is no longer coordinated to the metal center. The characteristic carbon-fluorine coupling of trifluoromethylacetyl group was observed at δ 115.9 (q, J = 294 Hz, CF$_3$), and 187.5 (q, J = 33.6 Hz, COCF$_3$). The relatively low carbonyl stretch frequency (1700 cm^{-1}) of ester in IR of **62** is consistent with the back-donation effect from the metal center.

The X-ray quality crystals of **62** was obtained from recrystallization of the dark oil in toluene and hexanes at -20 °C under inert atmosphere. The crystallography study of

complex **62** exhibits a dicobalt propendiyl complex (Figure 2-16), in which the two cobalt connect to each other with a distance of 2.5485 (4) Å that fits the range of other dicobalt propendiyl complex (2.54 – 2.57 Å) synthesized in our lab before.[4, 12] It is noticed that the Co1 – C1 (1.8968(16) Å) and C2 – C3 (1.452(2) Å) distances in complex **62** are shorter than the corresponding bond distances in the starting metallacyclobutene **25** (Co-C1 (1.906(2) Å) and C2-C3 (1.507(3) Å)), whereas the C2 – C3 distance is significantly longer (Δ = 0.074 Å) in complex **62**. These bond distance differences can be ascribed to the existence of resonance structure in dicobalt complex **62** that provides complex **62** more vinylcarbene character (Scheme 2-26). The C4 – O1 distance in the carbonyl of ester group in complex **62** was detected much shorter (Δ = 0.028 Å) than the corresponding carbonyl distance in complex **25**, which is attributed to the strong back donation effect from the metal center that weakens the carbon-oxygen double bond. The conjugation of phenyl group or the trifluoromethylacetyl group to the diene moiety in the ring structure are excluded due to the large torsion angle of C2 – C1 – C5 – C6 (112.13(18) °) and of O2 – C7 – C2 – C1 (43.4(2) °).
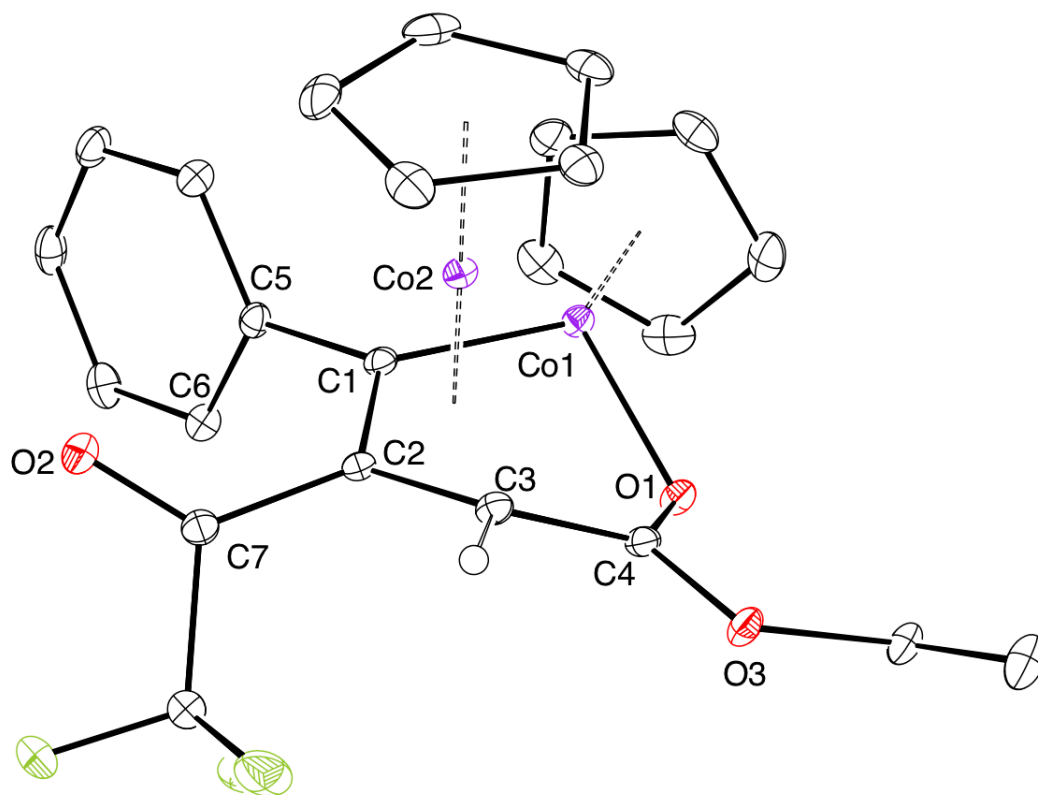
Figure 2-16. ORTEP drawing of **62** with ellipsoids shown at 30% probability.
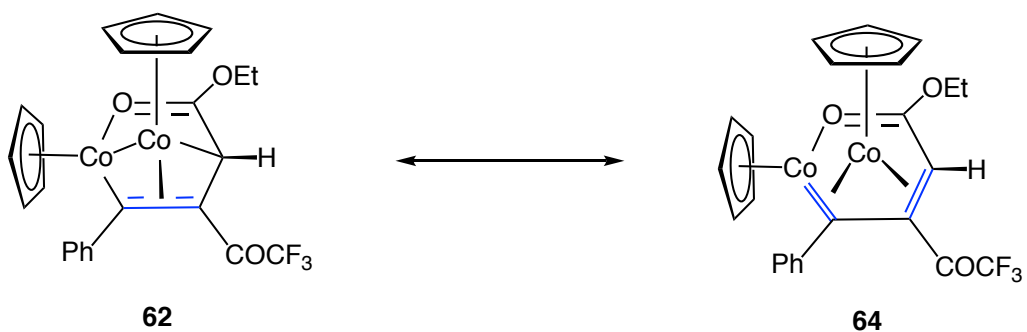
Scheme 2-26. The resonance structures of complex **62**.

In order to compare complex **62** to other similar dicocalt propendiyl complexes that are derived from metallacyclobutenes with different substitutents (Figure 2-17), a structural comparison and analysis was conducted among dicocalt propendiyl complexes **62**, **65**, **66** and **67** (Table 2-5). The Co1 – Co2 distances of the four complexes are in the range of 2.54 – 2.57 Å, which are slightly longer than some other reported cobalt-cobalt bond length (2.33 – 2.49 Å) in different systems in the literature[28]. Compound **67** has the shortest Co1 – C1 distance (1.873(7) Å) among the four dicobalt complexes due to the least steric congestion between C1(R) and "CpCo", whereas the steric hindrance of TMS on C3 is manifested by the longer Co2 – C3 distance (Δ = 0.06 – 0.08 Å) and smaller C2 – C3 – C4 angle (Δ = 6 – 7.5˚) than the rest three complexes. The bond length of C1 – C2 in all the four complexes are between 1.414 and 1.435 Å, which indicates the double bond character in the propendiyl ring. The C4 – O1 distances (1.237 – 1.244 Å) and Co1 – O1 distances (1.933 – 1.944 Å) of **65**, **62** and **66** are consistent with other examples of ester coordinated to cobalt that were reported in the literature[29]. It is noted that, however, complex **67** has a significantly shorter Co1-O1 bond (Δ = 0.03 – 0.04 Å) and longer C4 – O1 bond (Δ = 0.02 – 0.025 Å) than the other three, which might imply that a stronger σ-donation and π-back donation effect between the ester group and metal center exists in **67**. The large steric hindrance of TIPS in **66** is reflected by the elongated Co2 – C2 distance (2.009(2) Å) relative to the counterpart of the rest three compounds (1.952 – 1.987 Å). Additionally, it is observed that Co2 – C1 distances of **65** and **66** are 0.015 – 0.04 Å longer than **62** and **67**, which might be attributed to the electron withdrawing effect of the sulfone group.
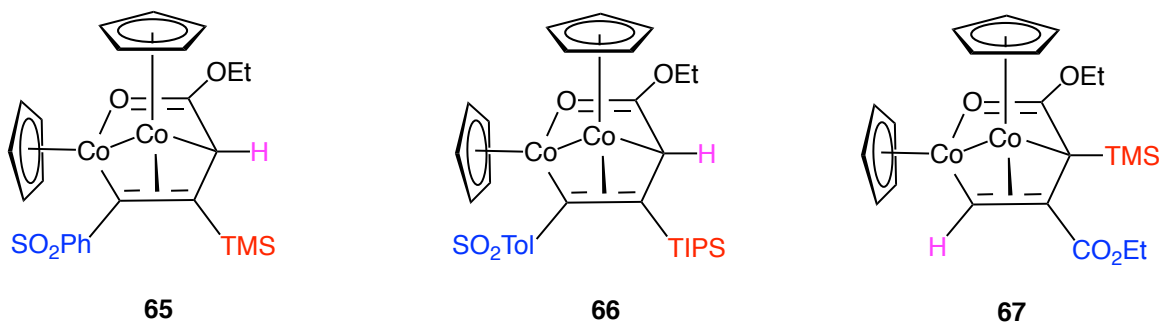
Figure 2-17. Other dicobalt propendiyl complexes synthesized by O'Connor group.

Besides the dicobalt complex **62**, an air-stable yellow oil that is proposed as furan derivative was also isolated with a 49% yield by the flash chromatography. The furan derivative **63** was fully characterized with ^{1}H NMR, ^{13}C NMR, IR, and HRMS. The vinyl hydrogen resonance was observed in ^{1}H NMR (500 MHz, CDCl$_3$) at δ 5.66 (s, 1H), and the ethyl group from the ester shows at δ 1.48 (t, 3H, J = 7.0 Hz) and 4.22 (q, 2H, J = 7.0 Hz). The integration of 5 hydrogen in the aromatic region indicates the absence of triphenylphosphine. In the ^{13}C{^{1}H} NMR spectrum (125 MHz, CDCl$_3$), the four ring carbons of furan were observed at δ 81.6, 115.3, 152.8, and 160.0, respectively. The characteristic C-F couplings of trifluoromethylacetyl group were detected at δ 116.7 (q, J_{CF} = 289.7 Hz, CF_3) and 175.5 (q, J_{CF} = 35.5 Hz, $COCF_3$). The C=O stretch shows at 1712 cm^{-1} in IR spectrum.

Table 2-5. Distances (Å) and angles (deg) from crystallographic data of dicobalt propendiyl complexes **62**, **65**, **66**, and **67**.

	65	62	66	67
Co1-C1	1.909(2)	1.8968(16)	1.928(2)	1.873(7)
C1-C2	1.432(3)	1.430(2)	1.435(3)	1.414(10)
C2-C3	1.461(3)	1.452(2)	1.460(3)	1.448(9)
C3-C4	1.444(3)	1.443(2)	1.440(3)	1.439(9)
C4-O1	1.237(2)	1.241(2)	1.244(3)	1.262(8)
O1-Co1	1.9437(14)	1.9361(11)	1.9330(17)	1.904(4)
Co1-Co2	2.5584(4)	2.5485(4)	2.5659(5)	2.5558(13)
Co2-C1	1.958(2)	1.9906(16)	1.951(2)	1.972(7)
Co2-C2	1.987(2)	1.9663(15)	2.009(2)	1.952(6)
Co2-C3	1.998(2)	2.0196(15)	2.000(2)	2.078(6)
Co1-C1-C2	122.97(15)	117.75(11)	122.54(17)	120.6(5)
C1-C2-C3	111.60(18)	118.40(14)	111.64(19)	121.1(6)
C2-C3-C4	123.10(19)	122.00(14)	121.6(2)	115.6(6)

The generation of furan derivative **63** indicates that a demetallation process occurred on the metallacyclobutene during the thermolysis, from which the liberated "CpCo" fragment was employed as the second metal source to form dicobalt complexes in the followed steps. Analogous demetallation reactions can be found by using rhodium-mediated coupling of alkynes and diazocarbonyls to generate furan products, in which a metallacyclobutene was proposed as intermediate[30]. There are two possible mechanisms for the formation of furan **63** from the starting metallacyclobutene **25** (Scheme 2-27): a) rearrange of metallacyclobutene to form a η^1-vinylcarbene complex **68**. Then nucleophilic addition of the ester carbonyl oxygen to the carbene carbon generates an oxacyclopentene intermediate **69**, that is followed by elimination of cobalt gives product **63** with the 'CpCoPPh$_3$' moiety; b) 1,3-cobalt shift from the sp^3 hybridized

ring-carbon to the ester carbonyl oxygen gives an oxametallacycle complex **30**, which

subsequently undergoes reductive elimination to produce furan **63**.
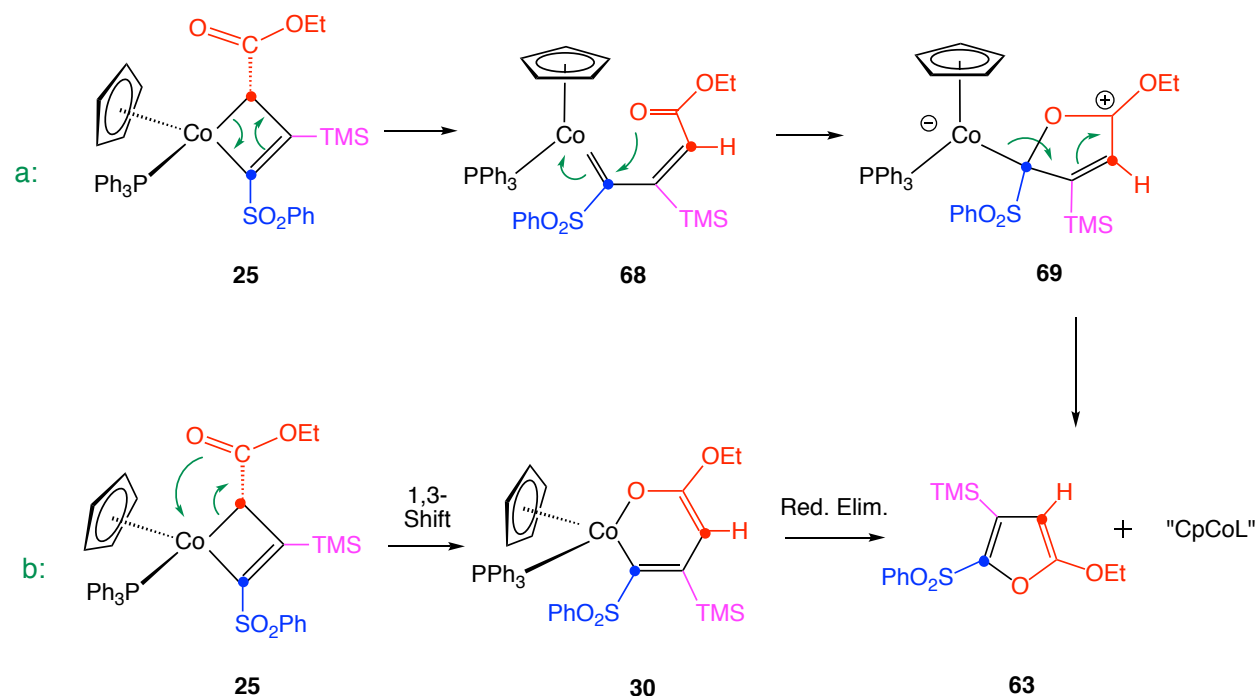
Scheme 2-27. Proposed mechanisms of furan formation.

In order to increase the yield of complex **63** and to explore how the two cobalt

atoms binding together, a NMR scale reaction was carried out between (η^5-

C$_5$H$_5$)Co(PPh$_3$)$_2$ (**13**) and metallacyclobutene **25** (Scheme 2-28). After 5 mg (0.007

mmol) of complex **25** and 1.2 equivalents of **13** were added into to J.Y. NMR tube with

bis(trimethylsilyl)benzene as internal standard in benzene-d_6 solvent. The tube was

heated at 70 °C for 2 hours under inert atmosphere, which generated the desired

dicocalt propendiyl complex **62** with 94.5% NMR yield. As expected, the furan derivative

63 was not observed.
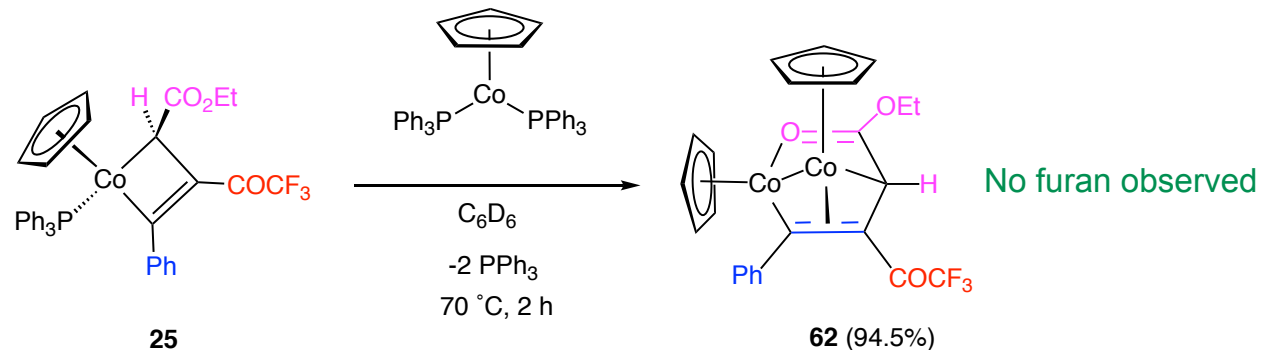
Scheme 2-28. Reaction of metallacyclobutene **25** with CpCo(PPh₃)₂.

Based on the experimental results obtained above, for the formation of dicocalt propendiyl complex **63**, we propose that upon the dissociation of triphenylphosphine ligand from metallacyclobutene **25** under heat, an equilibrium can be established among three possible intermediates: *E*-vinylcarbene **29**-*E*, *Z*-vinylcarbene **29**-*Z*, and oxametallabenzene **30**. The 'CpCoPPh₃' moiety that was generated from Scheme 2-27 can be stabilized via coordination to the carbonyl oxygen of vinylcarbene intermediate **29**-*E* and **29**-*Z*, which is followed by insertion of the cobalt into the alkylidene double bond as well as loss of the triphenylphosphine to produce the dicobalt complex. Alternatively, the 'CpCoPPh₃' moiety can also bind to the double of the oxametallabenzene intermediate **30**, and the substitution of triphenylphosphine by the alkylidene double bond can afford the dicobalt complex **62**. It should be noted that the dicobalt product that is generated from vinylcarbene intermediate is essentially the same as the product produced from oxametallabenzene intermediate, with the only difference that the two 'CpCo' fragments are switched (Scheme 2-29).
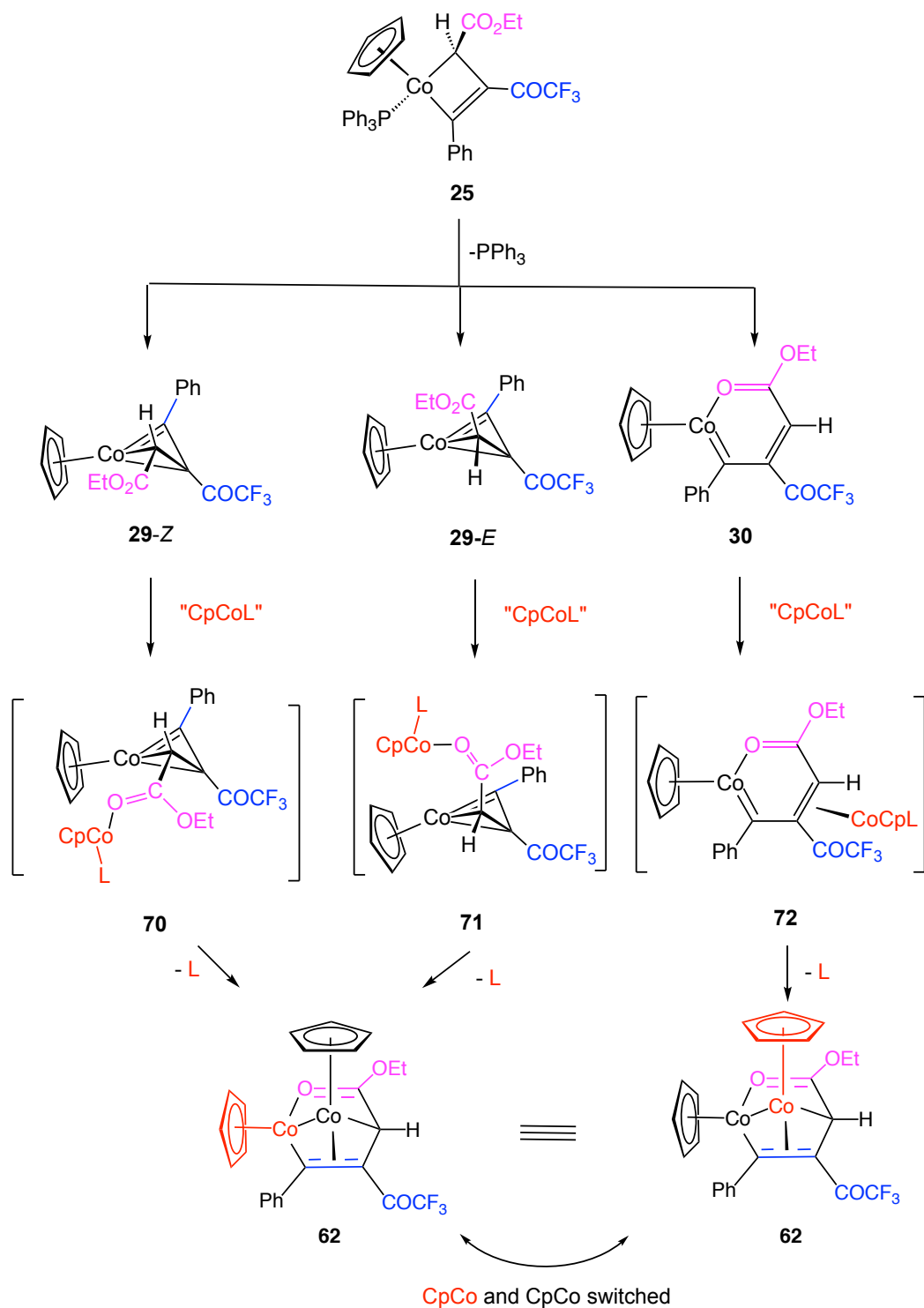
Scheme 2-29. Proposed mechanisms of dicobalt propendiyl complex **62** formation.

Furthermore, it is noteworthy that when a benzene-d_6 solution of dicobalt propendiyl complex **62** was allowed to expose to air in the presence of PPh$_3$, complex **62** started to decompose, and the color of solution slowly changed from dark to red with the formation of some green precipitates. After keeping on the bench overnight, the solution was filtered through a Pasteur pipet with cotton, and the subsequent ^{1}H NMR spectrum of the resulting solution indicates that all the complex **62** disappeared, and a 94% yield of recovery of metallacyclobutene **25** was detected based on the integration of Cp resonance at δ 4.47 relative to internal standard. Despite the oxidation mechanism is not clear yet, this reversible transformation of metallacyclobutene and dicobalt propendiyl complex shed light on the intrinsic interconversions character between η^3-vinylcarbene/ oxametallabenzene and metallacyclobutene complex.

2. Reaction of metallacyclobutene 25 with ethyl diazoacetate

As mentioned earlier, two η^4-diene complexes were generated when Yamazaki treated cobalt-alkyne complex (η^5-C$_5$H$_5$)Co(Ph)C$\equiv$C(Ph) **1** with ethyl diazoacetate in the intermediacy of metallacyclobutene (Scheme 2-1), and in our lab, we investigated the reactivity of metallacyclobutene **8** towards ethyl diazoacetate to produce 3 stereoisomers of η^4-diene complexes (Scheme 2-30). Herein, we explored the reactivity of newly synthesized metallacyclobutene **25** with ethyl diazoacetate.
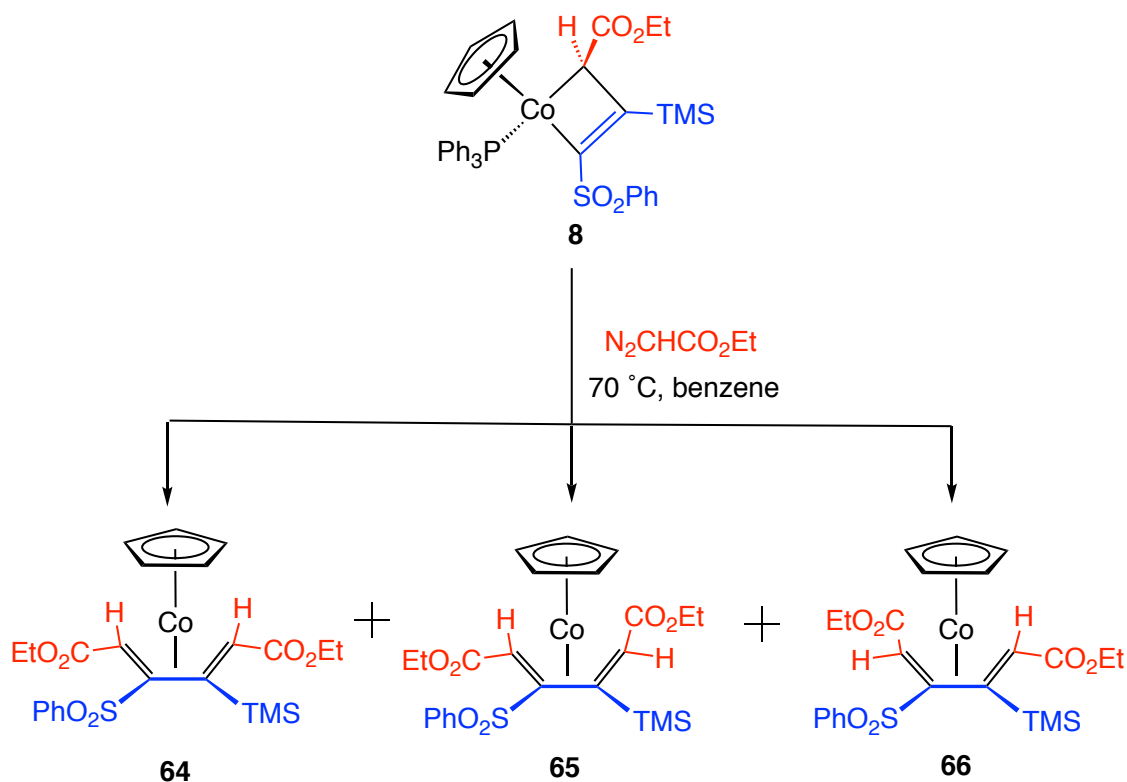
Scheme 2-30. Reaction of metallacyclobutene **8** with ethyl diazoacetate.

When 5 mg (0.007 mmol) of cobaltocyclobutene **25** was treated with 10 equivalents of ethyl diazoacetate in benzene-d_6 at 70 °C in a sealed NMR tube under inert atmosphere, the color of the solution slowly changed from red to orange. After 40 minutes, all the complex **25** disappeared based on the resonance of Cp at δ 4.46 (s, 5H), and two new Cp resonances were observed at δ 4.77 (s, 5H) and 4.70 (s, 5H) with 40% and 12% yield, respectively, based on the integration relative to internal standard. Unfortunately, a massive decomposition of ethyl diazoacetate brought a lot of overlaps in the spectrum that make it difficult for the further analysis of the spectrum, and therefore, a preparation scale reaction was conducted by employing the same ratio of starting materials under same reaction conditions in dry toluene. When the reaction is

done, the solution was concentrated and chromatographed on silica gel with 10% of ethyl acetate in hexanes to afford the mixture of two diene complexes as air-stable red oil (Scheme 2-31). Unfortunately, further attempts of separating the two diene complexes via chromatography failed due to the very similar polarities of the two complexes. However, some pure samples of the diene product **26** was successfully isolated from the partial crystallization from the mixture in ethyl acetate and hexanes at -20 °C.
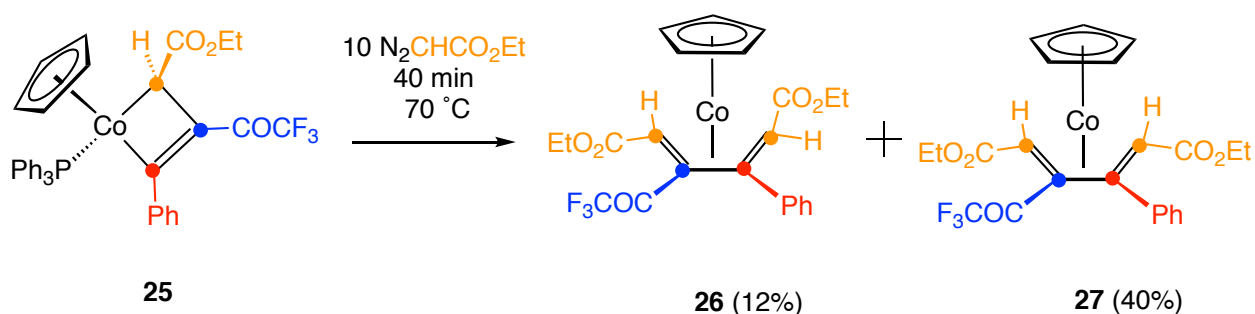
Scheme 2-31. Reaction of metallacyclobutene **25** with ethyl diazoacetate.

In the ^1H NMR spectrum of complex **26** (C_6D_6, 400 MHz), the Cp resonance located at δ 4.70 (s, 5H) indicates that complex **26** is actually the minor product in the reaction. Two sets of ethyl ester resonances were observed at δ 0.90 (t, 3H, J = 7.0 Hz, Me), 0.98 (t, 3H, J = 7.0 Hz, Me), and 3.90 (m, 4H, CH_2CH$_3$). The two vinyl hydrogens were detected at δ 2.42 (s, 1H) and 3.60 (s, 1H), and these abnormally up-field chemical shifts are owing to the shielding effect from the metal center. The integration of the aromatic region with 5 hydrogens indicates that the triphenylphosphine is no longer coordinated to the cobalt. In the $^{13}C\{^1H\}$ NMR spectrum (CDCl$_3$, 125 MHz) of complex

26, the two carbonyl carbon resonances of the two ester groups were observed at δ 171.9 and 177.4, respectively. The characteristic carbon-fluorine couplings of trifluoromethylacetyl group were observed at δ 115.3 (q, J = 291 Hz, CF_3), and 186.0 (q, J = 36.3 Hz, $COCF_3$). The four up-filed vinyl carbon resonances exist at δ 60.6, 61.3, 97.3, and 102.3, which is ascribed to the back-donation effect from the metal center. The carbonyl stretches of trifluoromethylacetyl group and ester groups in IR spectrum were detected at 1743 cm^{-1} and 1690 cm^{-1}, respectively.

The structure of diene complex **26** was confirmed by single X-ray crystallography, which reveals an unsymmetrical coordination mode on the two ester sites to give an *EZ* isomer (Figure 2-18). The back-donation effect from the metal center on the conjugated diene is manifested by the elongated C=C bond distances of C1 – C2 (1.429(8) Å) and C3 – C4 (1.431(8) Å). Compared to diene complex **55** that was synthesized from diphenylacetylene, the Co – C3 bond distance is significantly shorter (Δ = 0.026 Å), which is attributed to the strong electron-withdrawing effect of the trifluoromethylacetyl group (Table 2-6). The four carbons on the two conjugated C=C bonds are essentially planar with a small torsion angle of C1 – C2 – C3 – C4 (4.9(8) °), whereas the $\pi - \pi$ interaction between phenyl substituent and the diene is impossible due to the large plane – plane angle (84.53 °) of the phenyl ring and diene plane. In addition, a hydrogen bond with 2.144(5) Å was observed between the carbonyl oxygen (O1) of ester group and the vinyl hydrogen (H4).
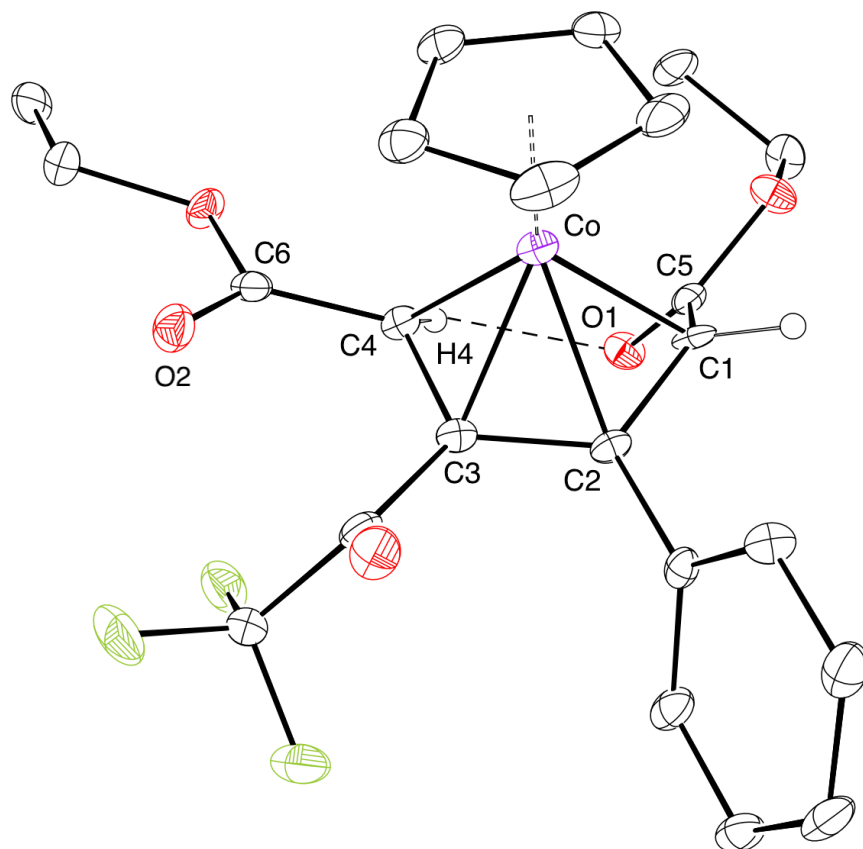
Figure 2-18. ORTEP drawing of **26** with ellipsoids shown at 30% probability.

Table 2-6. Selected bond distances (Å) and angles (deg) from crystallographic data of η^4-diene complex **26**.

C1 – C2	1.429(8)	C1---C4	2.799(8)
C2 – C3	1.452(8)	O1---H4	2.144(5)
C3 – C4	1.431(8)	C1-C2-C3	118.5(5)
Co – C1	2.021(6)	C2-C3-C4	117.6(5)
Co – C2	1.999(6)	C1-C2-C3-C4	4.9(8)
Co – C3	1.976(5)	O1-C5-C1-C2	10.0(10)
Co – C4	2.048(5)	O2-C6-C4-C3	11.0(9)

In contrast to complex **26**, very similar resonance patterns were displayed in the

^{1}H NMR spectrum of complex **27** (C$_6$D$_6$, 400 MHz). The Cp peak of **27** was observed at

δ 4.77 (s, 5H), which indicates that complex **27** is the major product of the previous

NMR reaction. Two sets of ethyl ester resonances were observed at δ 0.79 (t, 3H, J =

7.0 Hz, Me), 0.97 (t, 3H, J = 7.0 Hz, Me), 3.71 (m, 2H, CH_2CH$_3$), and 3.80 (m, 2H,

CH_2CH$_3$). The two vinyl hydrogen resonances are detected at δ 0.61 (s, 1H) and 0.75

(s, 1H), respectively. The structure of **27** (*ZZ* isomer) was speculated by comparing the

corresponding chemical shifts of the two vinyl hydrogen resonances with complex **26**. It

was observed that both vinyl hydrogens in complex **27** are more up field, which

indicates that both vinyl hydrogens are strongly shielded by metal center, and hydrogen

bond interaction that is shown in complex **26** should be absent in this scenario. Further

purification of complex **27** failed due to the facial interconversion to complex **26** at

ambient temperature (vide infra).

When a similar reaction of metallacyclobutene **25** with ethyl diazoacetate was

carried out at ambient temperature, no reaction was observed within 10 hours, which

suggests that a thermal dissociation of triphenylphosphine ligand is involved in the

reaction. Mechanistically, we propose that upon losing triphenylphosphine at high

temperature, a η^3-vinyl carbene intermediate **29**-*E* was generated, that is followed by

nucleophilic attack from the α-carbon of dizaocarbonyl compound at the alkylidene

carbon to give the metallacyclobutane **67** (Scheme 2-32). After ring opening and loss of

a nitrogen gas, a metallacyclopentene intermediate **69** can be generated, and a

subsequent reductive elimination gives the η^4-diene products.
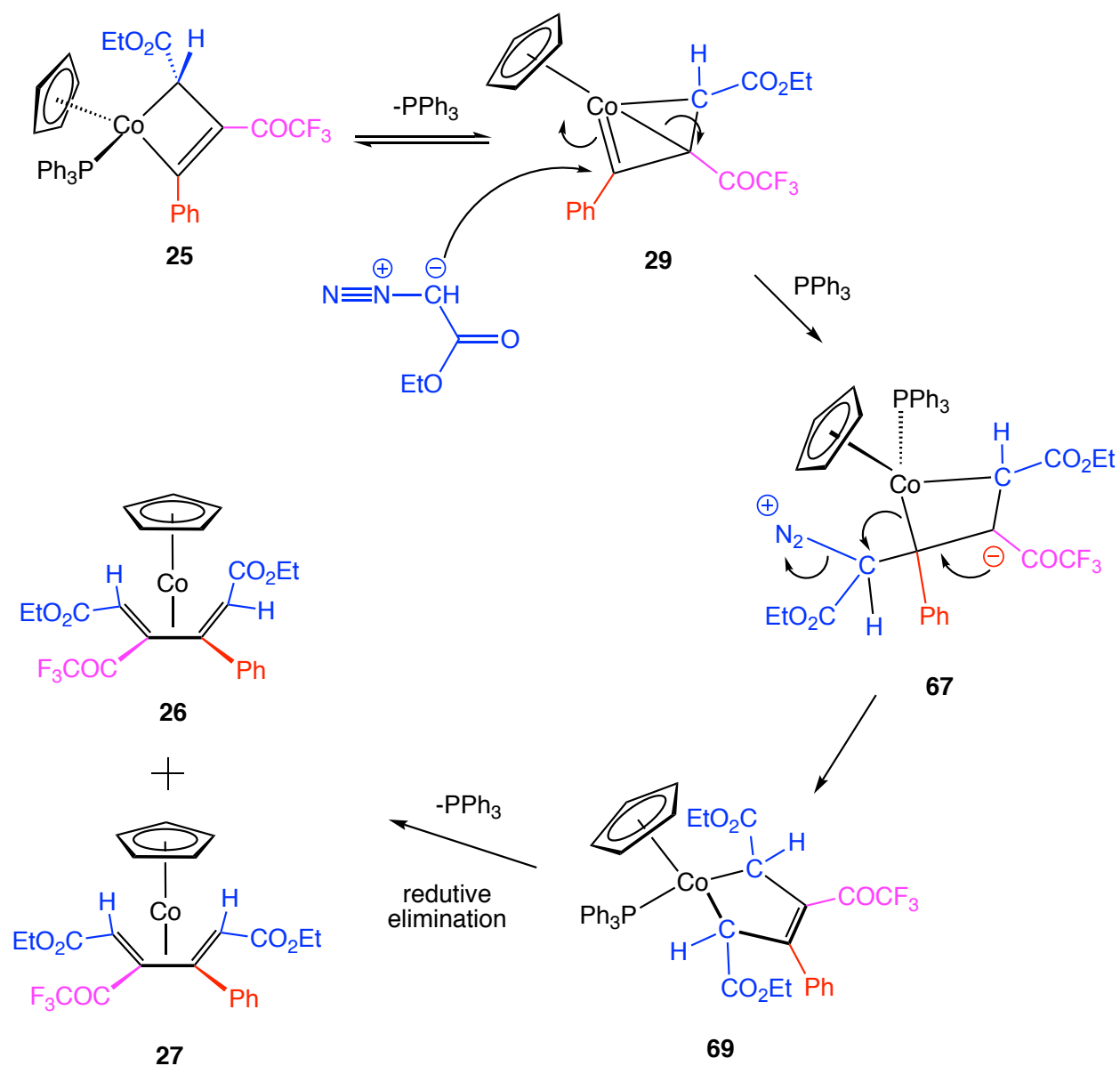
Scheme 2-32. Proposed mechanism of η^4-diene complex formations.

It was found that after exposing the inseparable mixture of **26** and **27** in bezene-d_6 to lab light, a new set of ^{1}H NMR resonances were observed at δ 0.77 (t, 3H, J = 7.0 Hz, Me), 1.14 (t, 3H, J = 7.0 Hz, Me), 4.06 (m, 4H, CH_2CH$_3$), 4.51 (s, 5H, Cp), 5.72 (s, 1H, vinyl-H), and 5.97 (s, 1H, vinyl-H). The two comparatively down field vinyl hydrogen

resonances suggest the formation of *EE* isomer **70** (Scheme 2-33). An equilibrium was established among those three isomers after exposure to lab light for 40 days, and the ratio (**27**: **26** : **70** = 1 : 9.8 : 2.1) was calculated by the integration of Cp resonances at δ 4.77, 4.70, and 4.51, respectively. In a control experiment, when the pure sample of complex **26** in bezene-d_6 solution was kept in the dark for 14 days with internal standard, no decomposition or interconversion of diene isomers was observed. The same NMR tube was subsequently exposed to lab light, and the equilibrium with the same ratio of three diene isomers was obtained after 40 days. We reason that the relatively large quantity of complex **26** is ascribed to the presence of hydrogen bond that stabilizes the structure, and more steric congestions from the two ester groups lead complex **27** least favorable.
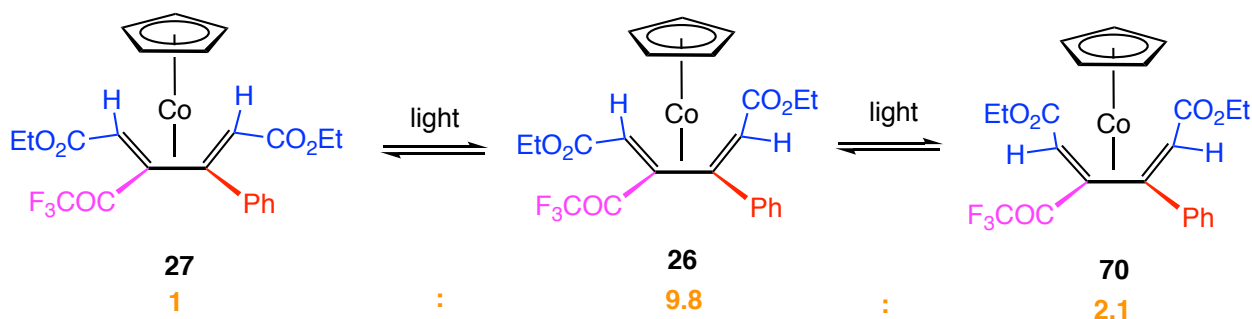
Scheme 2-33. Interconversion of η^4-diene complexes under photochemical conditions.

In comparison, a similar photochemical isomerization process of cobalt η^4-diene complexes was reported by Vollhardt's group.[31] They observed that upon the irradiation of η^4-diene complex **68**, a rapid isomerization occurs on both alkene sites to give the complex **72**, and they proposed that a metallacyclopentene **71** serves as the

intermediate to establish the equilibrium (Scheme 2-34). However, this so-called "envelope flip" process can not well explain the formations of complex **27** and **70** from photochemical isomerization of complex **26**, in which only one alkene is isomerized while the other one retains. One possible alternate mechanism would be the generation of cobalt radical intermediate **73** and **75** under photochemical condition, followed by a rotation of the single bond and regeneration of η^4-diene complexes **27** and **70** (Scheme 2-35). More mechanistic studies need to be conducted in the future to reveal the mechanism of this remarkable isomerization process.
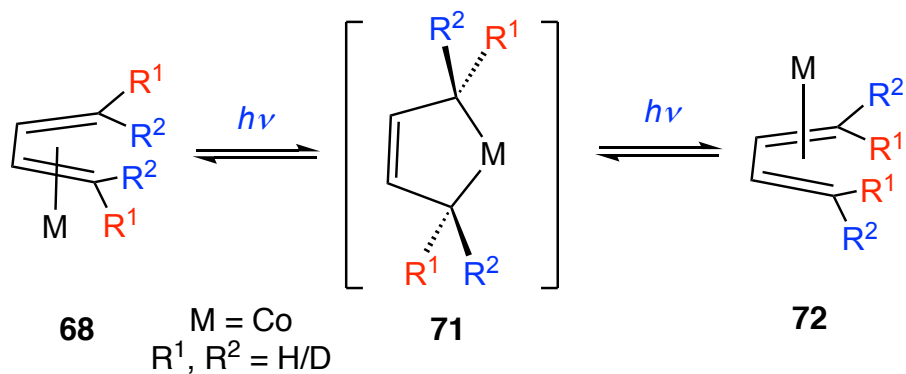
Scheme 2-34. Photochemical isomerization of cobalt η^4-diene complexes.
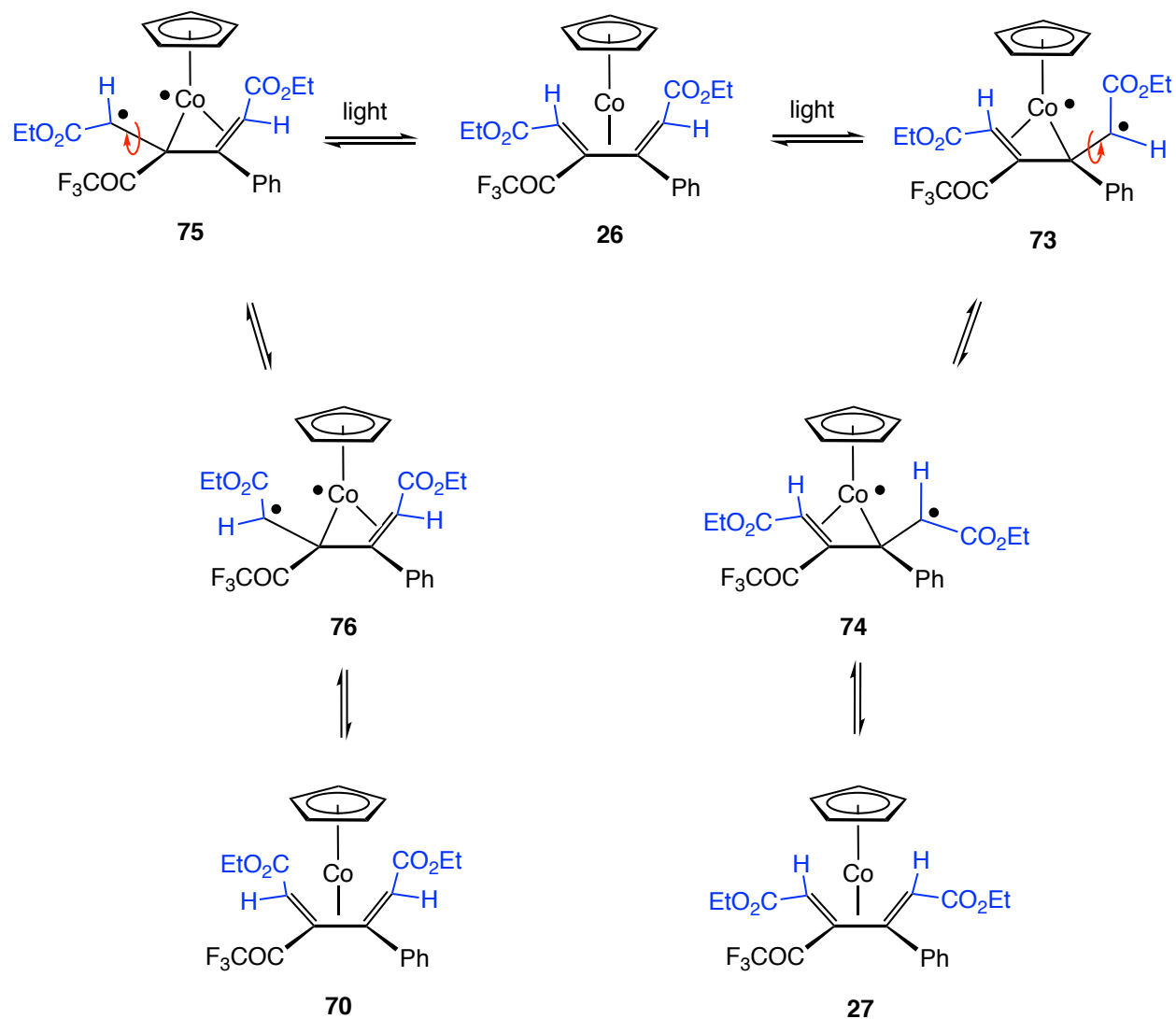
Scheme 2-35. Proposed radical mechanism of photochemical isomerization of η^4-diene complex.

3. Photochemical isomerization of metallacyclobutene

Since we reasoned that the steric hindrance between phosphine ligand and ester group is the key factor that controls the stereochemistry of metallacyclobutene **8**,[2] in order to explore how the ancillary phosphine ligand affects the formation of cobaltocyclobutene and to obtain the other possible diastereomers, thermal phosphine

121

exchanging reactions were conducted to prepare new metallacycles. Trimethyl phosphine was selected as an ideal candidate for its strong electron-donation effect. Also, the relative size of PMe$_3$ and PPh$_3$ have been addressed in the context of cone angles, with the latter exhibiting a 27 ° greater in the cone angle,[32] and we expect this diminished cone angle of PMe$_3$ can help release the steric congestion with ester group. Metallacyclobutene **8** was treated with 5 equivalents of trimethyl phosphine in a Teflon-sealed reaction tube at 70 °C in toluene solvent under inert atmosphere for 4 hours. After flash chromatography on silica gel with ethyl acetate/hexane under dark in the fume hood, two red bands were collected with 50% and 15.7% yields, and they were characterized as two diastereomers **77** and **78**, respectively (Scheme 2-36). The structure of the two isomers were unambiguously confirmed by using X-ray crystallography by previous students.
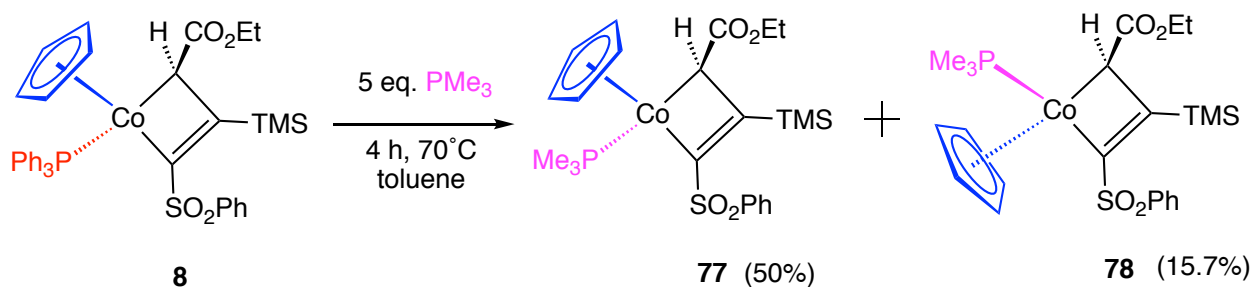
Scheme 2-36. Metallacyclobutene **8** reacts with PMe$_3$.

It was found that the two PMe$_3$ substituted diastereomeric metallacyclobutenes **77** and **78** can interconvert at 70 °C. In order to explore the relative stability of the two isomers, an acetone-d_6 solution (0.7 mL) of pure complex **77** (0.003 mmol) was heated at 70 °C with 1,3,5-tri-*tert*-butylbenzene as internal standard under dark, and the

reaction mixture was monitored by using [1]NMR spectroscopy. After 27 hours, the appearance of complex **78** was observed, and an equilibrium was established between **77** and **78** (4.8 :1), and the ratio didn't change anymore. When a similar reaction was carried out by employing complex **78** as starting material, the same ratio was obtained after 30 hours. Accordingly, the complex **77** bearing ester group *anti* to the phosphine ligand is more thermodynamically favorable than the isomer **78** with a calculated ΔG = 1.07 kcal/mol (Scheme 2-37).
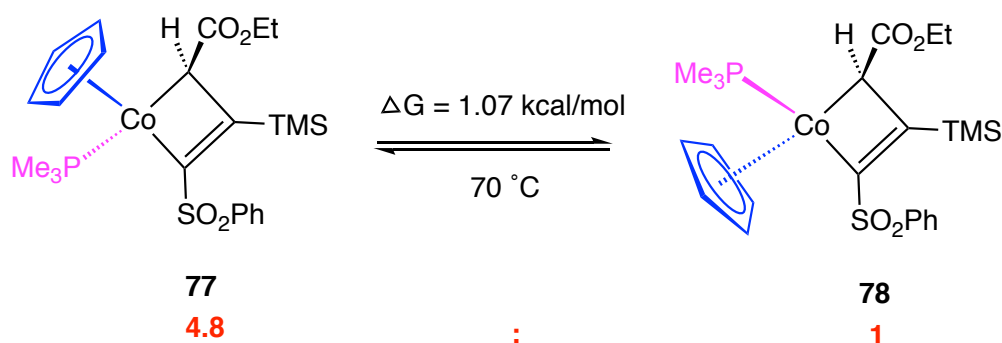
Scheme 2-37. Thermal equilibrium between metallacycles **77** and **78**.

Besides thermal conditions, dissociation of phosphine ligands from transition metals that is triggered under photochemical conditions have been widely reported in the literature.[33] We noted that the PMe$_3$ substituted metallacyclobutene **77** and **78** can rapidly interconvert to each other under UV-vis light to achieve the epimerization on the metal center. Photolysis of acetone-d_6 solution of **77** with 1,3,5-tri-*tert*-butylbenzene (internal standard) in an oven-dried J. Yang tube was carried out in a Rayonette photoreactor equipped with UV broadband lamps that is centered at 254 nm. The reaction was monitored by ^{1}H NMR spectroscopy, and during the course of reaction,

new resonances of **78** were observed at δ 0.16 (s, 9H, Si(CH_3)$_3$) and 4.45 (s, 5H, C$_5H_5$) with the consumption of **77**. After 10 minutes, an equilibrium was observed between **77** and **78**, and the ratio (0.75:1) didn't change anymore after longer irradiation. Integration of the Cp resonances relative to internal standard indicates a 61% conversion of **77** and an 85% yield of **78** based on the converted **77**. In a similar fashion, when **78** was employed as starting material, the equilibrium with same ratio of the two diastereomers was also observed after 10 minutes under the same UV lamps (Scheme 2-38). A dynamic plots of NMR spectra at different time points under UV light for the interconversion between **77** and **78** is shown in Figure 2-19.
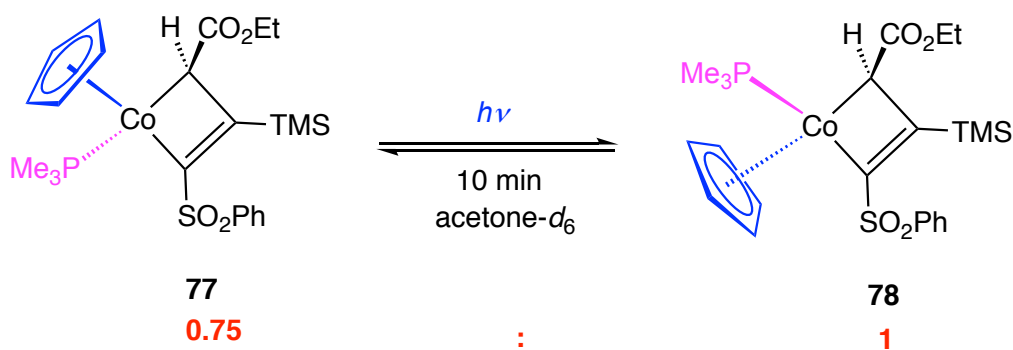
Scheme 2-38. Equilibrium established between metallacycles **77** and **78** under photochemical condition.
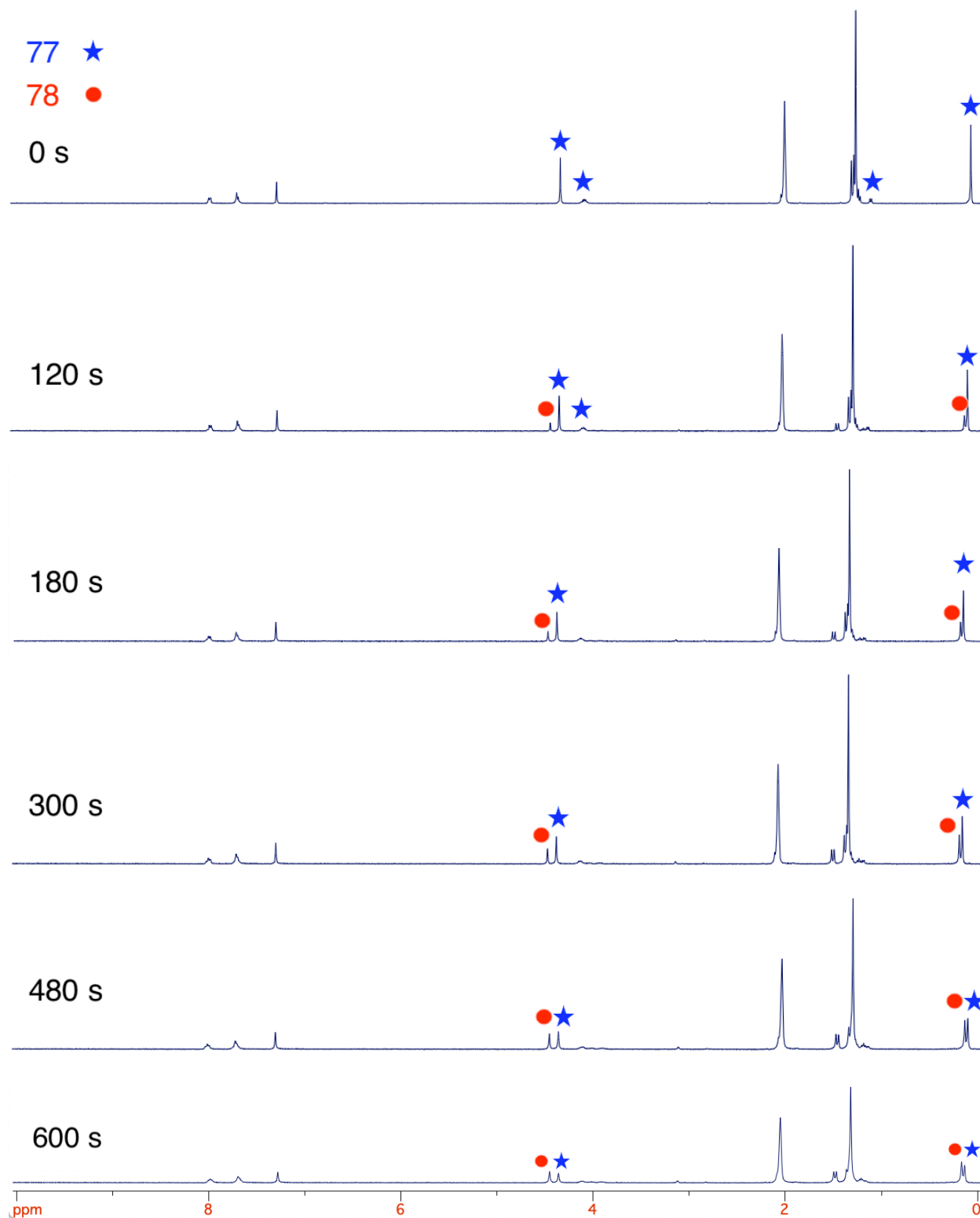
Figure 2-19. Dynamic NMR spectra with different time points of irradiating complex **77**.

125
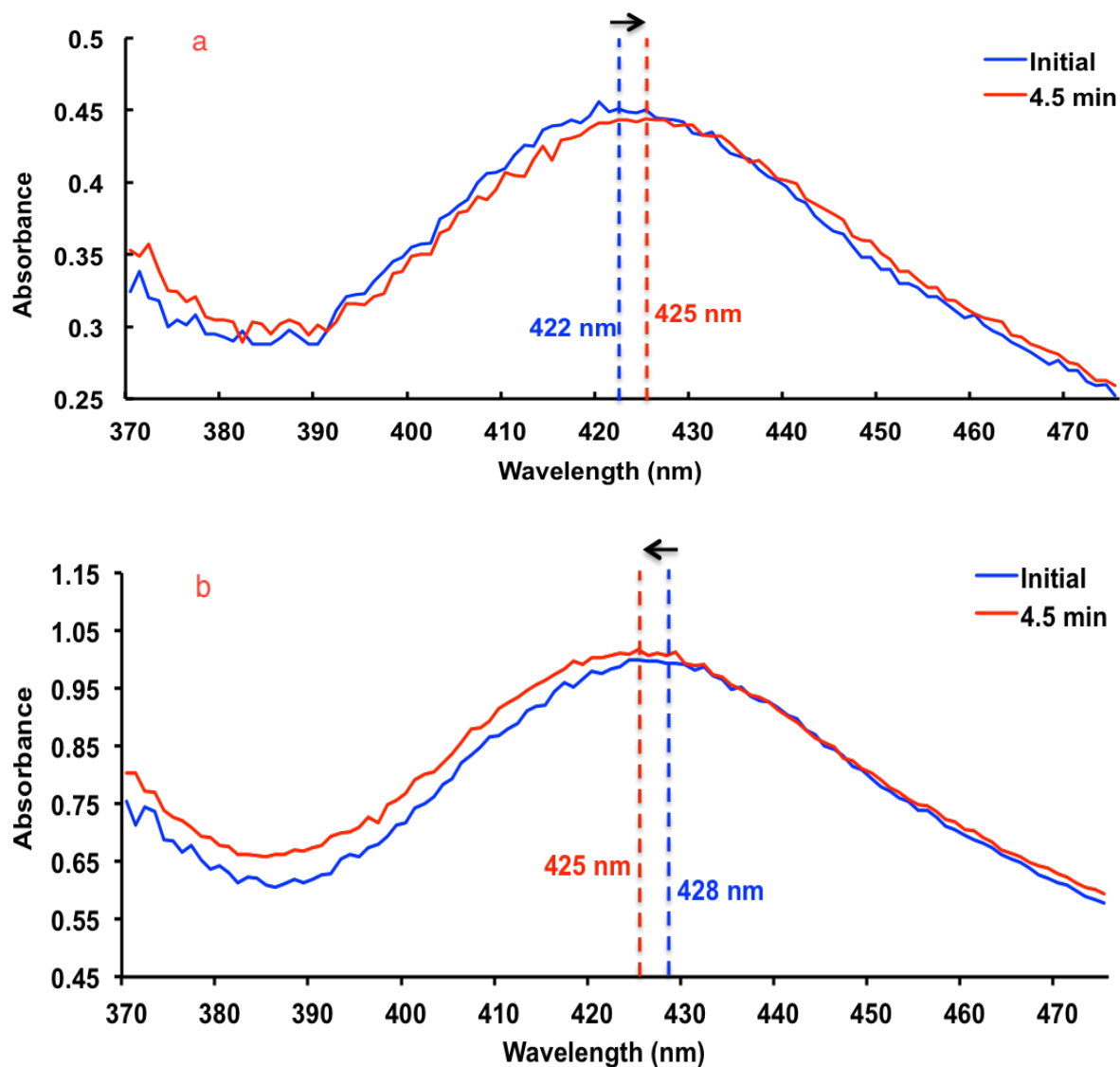
Figure 2-20. UV-vis absorption spectra of photolyzing **77** under UV broadband lamps centered at 254 nm (a); UV-vis absorption spectra of photolyzing **78** under the same UV lamps (b).

This reversible light-triggered epimerization process has also been monitored by utilizing UV-visible spectroscopy (Figure 2-20). In a Shimadzu UV-3600 UV/vis/NIR spectrometer, **77** in dry acetone exhibits a λ_{max} at 422 nm with a molar absorptivity of 1127.5 $M^{-1}cm^{-1}$ while **78** shows a λ_{max} at 428 nm with a molar absorptivity of 1169.4 M^-

[1]cm^{-1}. After photolyzing acetone solution of **77** in a sealed quartz cell under UV broadband lamps for 4.5 minutes, the equilibrium was established, and λ_{max} was observed to shift from 422 to 425 nm. Alternatively, λ_{max} was observed to shift from 428 to 425 nm when **78** acetone solution was subjected to the same UV lamps for 4.5 minutes to reach an equilibrium. The resulting solutions were both detected by ^{1}H NMR spectroscopy, which gives the same ratio of **77** and **78** (0.75 : 1).

Two possible mechanisms were proposed for this observed epimerization process: (a) adventitious amount of base that presents in the solution can potentially deprotonate the ring hydrogen of complex **77** to form an enolate, that is followed by a reprotonation to produce the diastereomer **78**; (b) an η^3-vinyl carbene is generated as intermediate, in which the dissociation of phosphine ligand is involved (Scheme 2-39).
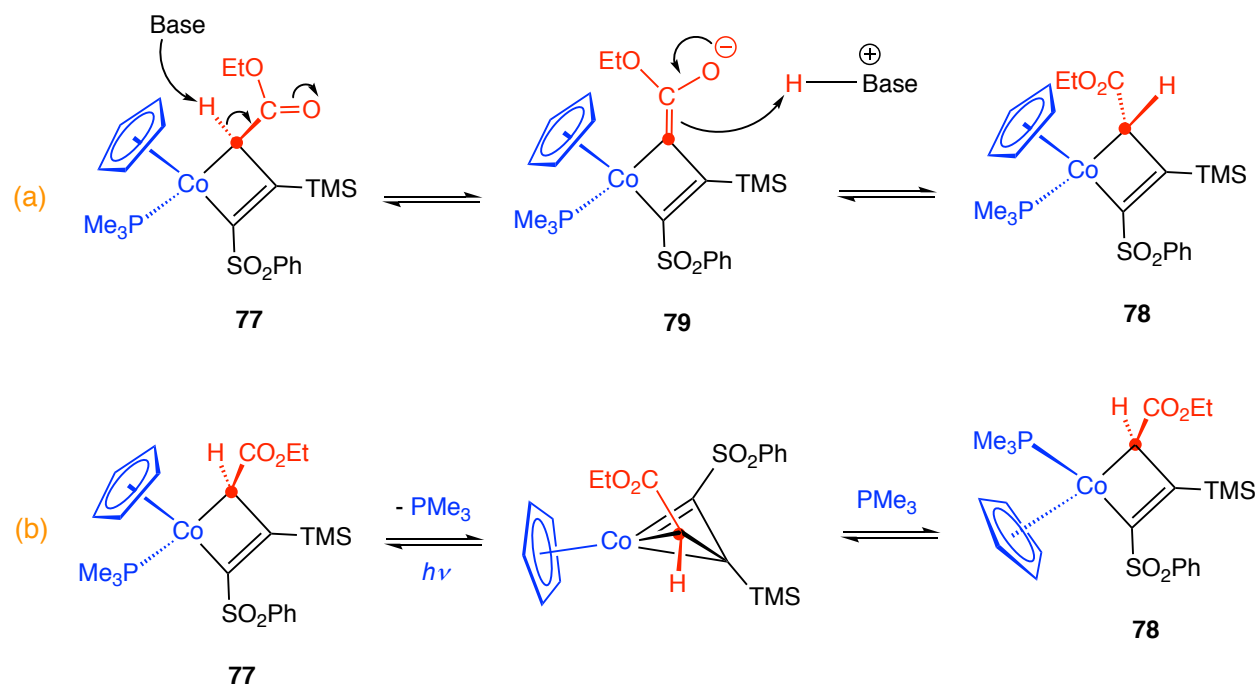
Scheme 2-39. Proposed mechanisms of photochemical isomerization of metallacyclobutenes **77** and **78**.

To examine the first mechanism, 1.2 equivalents of D_2O was loaded in the NMR tube with keeping other reaction conditions the same. However, after photolyzing the reaction mixture for 10 minutes, there is no observance of the deuterium enrichment on either complex **77** or **78**, which provides a strong negative evidence for the proposed mechanism (a). An inhibition reaction was subsequently conducted by loading 8 equivalents of free PMe_3 in the solution with complex **77** as starting material. A prominent longer reaction time (30 minutes) was observed to reach the same equilibrium compared to the original reaction (10 minutes) without adding extra trimethyl phosphine, which suggests that the epimerization necessitates the dissociation of PMe_3. Further reactions to trap the proposed η^3-vinyl carbene intermediate under photochemical conditions might need to be carried out in the future to support the mechanism (b).

A similar photochemical epimerization reaction was also conducted on metallacyclobutene **8**. The acetone-d_6 (0.45 mL) solution of complex **8** (5 mg, 0.007 mmol) in a J.Y. NMR tube was irradiated by UV light under inert atmosphere, and the reaction mixture was monitored by ^1H NMR spectroscopy. It was found a new set of Cp and TMS resonances of complex **80** started to grow at δ 0.19 (s, 9H, TMS) and 4.60 (s, 5H, Cp). The characteristic ring hydrogen resonance of metallacyclobutene was observed at δ 3.46 (d, 1H, J_{PH} = 2.8 Hz). After 45 minutes, a equilibrium was established with a 1.5 : 1 ratio of complex **8** and **80** (Scheme 2-40). The reaction was also monitored by using UV-visible spectroscopy in a Shimadzu UV-3600 UV/vis/NIR spectrometer. Cobaltacyclobutene **8** initially showed a λ_{max} at 445 nm in dry acetone-d_6 (0.0156 M), and the λ_{max} shifted to 428 nm after photolyzing for 45 minutes with the

formation complex **80** (Figure 2-21). However, it was found that complex **80** slowly

converted back to complex **8** under dark, and after keep the same NMR tube under dark

for 14 hours, all the complex **80** disappeared giving an 85% yield of the original

metallacycle **8**. Compared to metallacyclobutene **77**, we reason that larger steric

hindrance between triphenylphosphine and ester group on complex **8** causes this back-

conversion behavior.
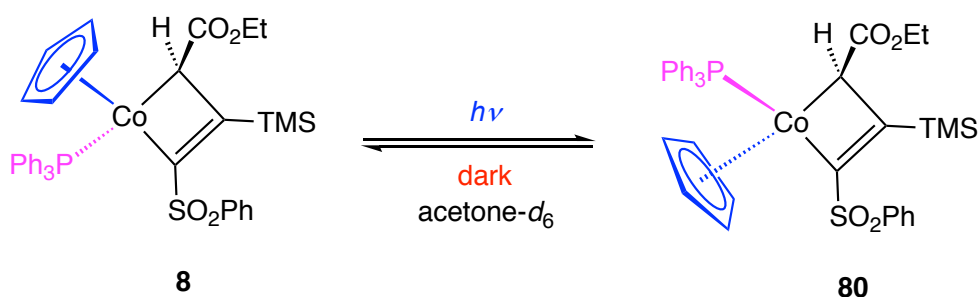
Scheme 2-40. Interconversion between **8** and **80**.
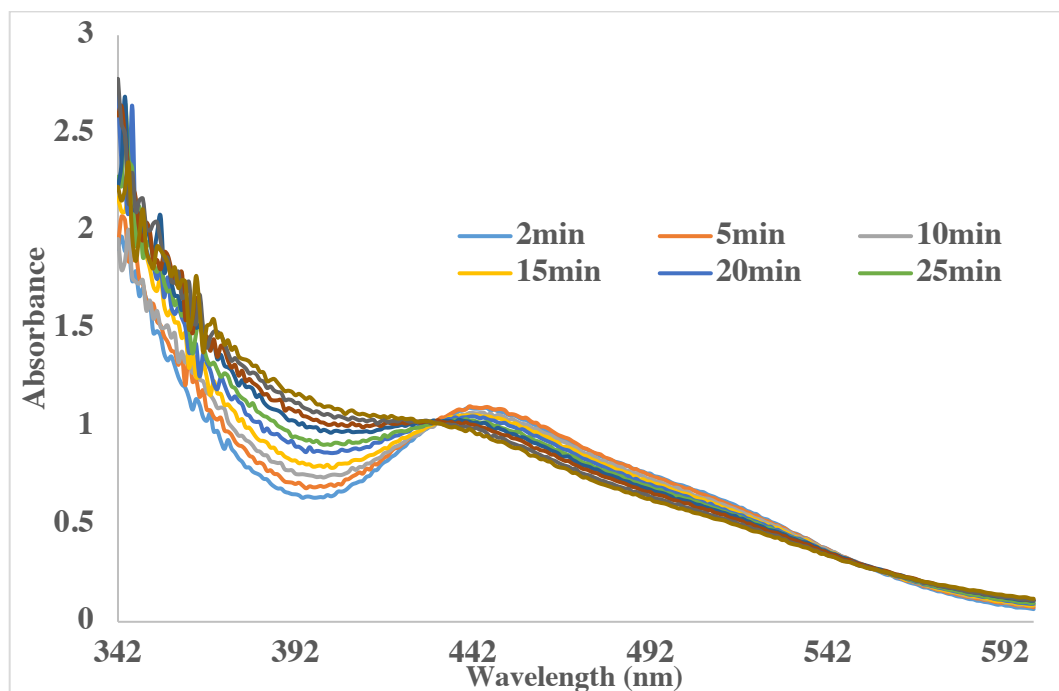
Figure 2-21. UV-vis absorption spectra of photolyzing **8** under UV broadband lamps centered at 254 nm at different time points.

F. Conclusions

In summary, three different electron-deficient cobalt-alkyne complexes bearing trifluoromethylacetyl group were synthesized from the reaction of $(\eta^5\text{-}C_5H_5)Co(PPh_3)_2$ with corresponding acetylenes, and the coupling of ethyl diazoacetate with complex $(\eta^5\text{-}C_5H_5)(PPh_3)Co[\eta^2\text{-}(Ph)C{\equiv}C(COCF_3)]$ leads to an air-stable metallacyclobutene complex $(\eta^5\text{-}C_5H_5)(PPh_3)Co[C(Ph)=C(COCF_3)CH(CO_2Et)]$, that was isolated and fully characterized. It was found that an electron-withdrawing group on the α position and extended conjugation of the alkene are both very important factors for the stabilization of cobaltacyclobutene in our system.

A remarkable carbon-extrusion reaction has been uncovered by employing sulfone-substituted cobalt-alkyne complexes reacting with dizaoacetamide, which contrasts with the formation of a pyrazole molecule without the intermediacy of transition metal. The single carbon that is lost via the C – S bond cleavage appears to be incorporated into carbon monoxide of $(\eta^5\text{-}C_5H_5)Co(PPh_3)(CO)$ byproduct. In comparison, the reaction of dizaoacetamide with cobalt-alkyne complex $(\eta^5\text{-}C_5H_5)(PPh_3)Co[\eta^2\text{-}(Ph)C{\equiv}C(Ph)]$ and cobaltacyclobutene $(\eta^5\text{-}C_5H_5)(PPh_3)Co[C(SO_2Ph)=C(TMS)CH(CO_2Et)]$ generates two η^4-diene complexes with high regio-and stereoselectivity.

The thermolysis studies were conducted on the isolated cobaltacyclobutene to generate dicobalt propendiyl complex and furan derivative, in which a η^3-vinylcarbene complex was proposed as intermediate. The dicobalt complex was also made independently from the reaction between $(\eta^5\text{-}C_5H_5)Co(PPh_3)_2$ and metallacyclobutene

with 95% yield, and was subsequently characterized by X-ray crystallography. The transformation from dicobalt propendiyl complex back to metallacyclobutene via an air oxidation in the presence of PPh$_3$ manifests the intrinsic reversible interconversional character between metallacyclobutene and η^3-vinylcarbene.

The reactivity of metallacyclobutene towards ethyl diazoacetate was explored, which produces two isomeric η^4-diene complexes (*EZ* and *ZZ*). It was found that a photochemical isomerization can occur to generate *EE* η^4-diene isomer under lab light, and an equilibrium is established among the three isomers. Two diastereomers of PMe$_3$ substituted metallacyclobutenes were synthesized from phosphine ligand exchange reaction of the corresponding PPh$_3$ substituted metallacyclobutene under thermal conditions. Rapid interconversions among the two metallacyclobutene diastereomers can be achieved by UV-light-triggered photodissociation of phosphine ligand, which was monitored by utilizing both NMR and UV-vis spectroscopy.

G. Experimentals

1. General information

All the organometallic reagents were handled under inert gas atmosphere or using the Schlenk technique, unless otherwise noted. The commercially available acetonitrile-d_3, chloroform-d were refluxed over CaH$_2$ for two days and freeze-pump-thaw to degas on Schlenk line. Benzene-d_6 was dried over sodium/benzophenone ketyl and freshly distilled prior to use. All the dry solvents were flushed through an aluminum

column under inert gas atmosphere via a solvent distilling system. Solution ^{1}H and ^{13}C{^{1}H} NMR were recorded on Mercury 400 MHz spectrometer and Varian X-Sens 125 MHz spectrometer, respectively. ^{1}H and ^{13}C{^{1}H} NMR chemical shifts were reported in ppm which is referenced to CHCl$_3$ (^{1}H, 7.26 ppm), CDCl$_3$ (^{13}C, 77.16 ppm), C$_6$H$_6$ (^{1}H, 7.16 ppm), C$_6$D$_6$ (^{13}C, 128.06 ppm), CNCH$_3$ (^{1}H, 1.94 ppm), and CNCD$_3$ (^{13}C, 1.32 ppm). All the IR spectra of the isolated compounds were recorded on a Thermo-Nicolet iS10 FTIR spectrometer at room temperature. The high-resolution mass spectra were recorded on an Agilent 6230 Accurate-Mass TOFMS instrument by using positive ion mode. Combustion analysis was performed by NuMega laboratories of San Diego, CA (USA) or MIDWEST MICROLAB of Indianapolis, IN (USA).

2. Preparation and characterization data

16
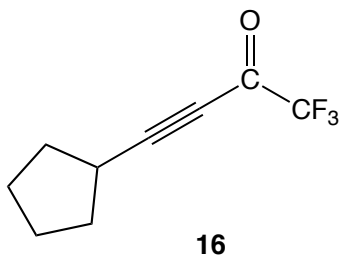
Preparation of 4-cyclopentyl-1,1,1-trifluorobut-3-yn-2-one (16): 12.2 ml of n-BuLi (2.5M in hexane) was added dropwisely into a stirred solution of ethynylcyclopentane (2.5 g, 26.55 mmol) in anhydrous THF (40 ml) at -78°C. The resulting solution was allowed to stirred for 1 hour while warm up to room temperature and then a mixture of ethyl trifluoromethylacetate (4.2 g, 26.90 mmol) and BF$_3$OEt$_2$ (3.77 g, 26.56 mmol) were

introduced dropwise. After stirring for 2 hours, 20 ml saturated solution of NH$_4$Cl was added, and the aqueous layer was extracted by pentane 3 times (3*30 ml). The combined organic extracts was washed with brine and dried over MgSO$_4$. After chromatography on silica gel with 10% Ethyl acetate/hexane, 4.6 g (yield = 91.1 %) of **16** was obtained as clear oil. IR (CDCl$_3$) 2968, 2877, 2207, 1709, 1454, 1319, 1216, 1161, 1117, 959, 749 cm^{-1}; ^{1}H NMR (CDCl$_3$, 400 MHz) δ 1.646 (m, 2H), 1.784 (m, 4H), 2.046 (m, 2H), 2.898 (m, 2H); ^{13}C{^{1}H} NMR (CDCl$_3$, 125 MHz) δ 25.5, 30.4, 33.1, 75.8, 109.6, 114.8 (q, J_{CF} = 288 Hz), 167.5 (q, J_{CF} = 42 Hz). HRMS for [C$_9$H$_{10}$F$_3$OCH$_3$OH]$^+$: 223.0940 (Theo. Mass), 223.0939 (Mass Measured), Delta (-0.5 ppm).

17
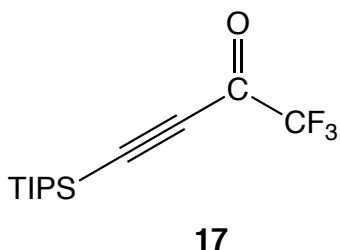
Preparation of 1,1,1-trifluoro-4-(triisopropylsilyl)but-3-yn-2-one (17): 12.5 ml of n-BuLi (2.5M in hexane) was added dropwisely into a stirred solution of ethynyltriisopropylsilane (5.0 g, 27.42 mmol) in anhydrous THF (40 ml) at -78 °C. The resulting solution was allowed to stirred for 1 hour while warm up to room temperature and then a mixture of ethyl trifluoromethylacetate (4.88 g, 31.26 mmol) and BF$_3$OEt$_2$ (4.44 g, 31.28 mmol) were introduced dropwise. After stirring for 2 hours, 20 ml saturated solution of NH$_4$Cl was added, and the aqueous layer was extracted by

pentane 3 times (3*30 ml). The combined organic extracts was washed with brine and dried over MgSO$_4$. After chromatography on silica gel with 10% Ethyl acetate/hexane, 6.8 g (yield = 89 %) of **17** was obtained as clear oil. IR (CDCl$_3$) 2948, 2870, 2162, 1710, 1463, 1382, 1307, 1216, 1160, 1066, 882, 791 cm^{-1}; ^{1}H NMR (CDCl$_3$, 400 MHz) δ 1.112 (d, J = 6.2 Hz, 18H), 1.15-1.22 (m, 3H); ^{13}C{^{1}H} NMR (CDCl$_3$, 125 MHz) δ 11.0, 18.5, 98.6, 109.2, 114.8 (q, J_{CF} = 289 Hz), 166.8 (q, J_{CF} = 42 Hz). HRMS for [C$_{13}$H$_{21}$F$_3$OSiNa]$^+$: 301.1406 (Theo. Mass), 301.1406 (Mass Measured), Delta (0 ppm).

18
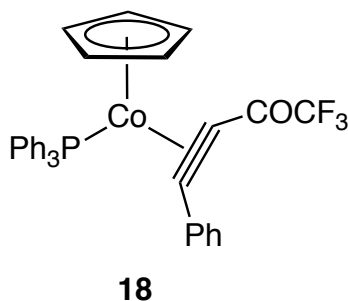
Preparation of (η^5-C$_5$H$_5$)(PPh$_3$)Co[η^2-(Ph)C≡C(COCF$_3$)] (18): 2.5 g (3.85 mmol) of CpCo(PPh$_3$)$_2$ were added into a reaction tube with 25 mL dry toluene inside a glove box. After stirring for 30 minutes, 840 mg (4.24 mmol) of 1,1,1-trifluoro-4-phenylbut-3-yn-2-one was introduced and the color of the solution slowly changed from red to purple. The resulting solution was allowed to stirred overnight and then layered with 100 ml of hexane to trigger crystallization. After one week, 1.82 g (80.9% yield) of **18** was obtained by filtration and air stable purple crystals were washed with dry hexanes. Mp: 165.6 °C; IR (CDCl$_3$) 3075, 3056, 2251, 1776, 1746, 1615, 1482, 1432, 1307, 1204,

1193, 1135, 1091, 1049, 907, 810 cm^{-1}; ^{1}H NMR (CDCl$_3$, 400 MHz) δ 4.79 (s, 5H), 7.26-

7.40 (m, 18H, PPh$_3$ and Ph), 7.969 (m, 2H, Ph); ^{13}C{^{1}H} NMR (CDCl$_3$, 125 MHz) δ 82.8

(d, J_{CP} = 9.2 Hz, CCO), 84.2 (C_5H_5), 116.4 (q, J_{CF} = 292 Hz, CF_3), 127.9 (d, J_{CP} = 9.4

Hz, C_m, PPh$_3$), 128.2 (C_m, Ph), 129.6 (C_p, Ph), 129.7 (C_p, PPh$_3$), 132.1 (C_o, Ph), 132.3

(C_i, Ph), 133.8 (d, J_{CP} = 10.2 Hz, C_o, PPh$_3$), 133.9 (d, J_{CP} = 40.2 Hz, C_i, PPh$_3$), 155.7 (d,

J_{CP} = 9.4 Hz, C-Ph), 172.1 (q, J_{CF} = 34.7 Hz, COCF$_3$). HRMS for [C$_{33}$H$_{26}$CoF$_3$OP]$^+$:

585.1000 (Theo. Mass), 585.0999 (Mass Measured), Delta (-0.2 ppm). Elemental

Analysis: C% (67.82); H% (4.31). Found: C% (67.80); H% (4.70).

19
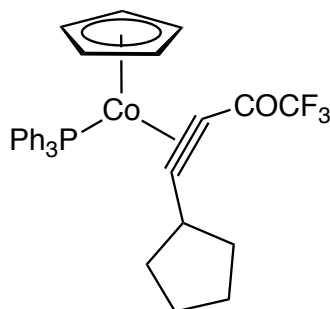
Preparation of (η^5-C$_5$H$_5$)(PPh$_3$)Co[η^2-(C$_5$H$_9$)C≡C(COCF$_3$)] (19): 3.1 g (4.78 mmol) of

CpCo(PPh$_3$)$_2$ were added into a reaction tube with 20 mL dry toluene inside a glove

box. After stirring for 30 minutes, 1g (5.26 mmol) of alkyne 4-cyclopentyl-1,1,1-

trifluorobut-3-yn-2-one were introduced and the color of the solution slowly changed

from red to dark. The resulting solution was allowed to stirred overnight and then

layered with 100 ml of hexane to trigger crystallization at -20°C. After one week, 2.48 g

(81.7% yield) of **19** was obtained by filtration and air stable dark crystals were washed

with dry hexanes. Mp: 143.5 °C; IR (CDCl$_3$) 3057, 2956, 2869, 1777, 1624, 1481, 1435, 1303, 1189, 1135, 1092, 909, 809 cm^{-1}; ^{1}H NMR (CDCl$_3$, 400 MHz) δ 1.52-2.2 (m, 8H), 4.658 (s, 5H), 7.346 (m, 9H), 7.493 (m, 6H); ^{13}C{^{1}H} NMR (CDCl$_3$, 125 MHz) δ 25.9, 26.0, 33.5, 34.9, 42.8, 71.9 (d, J_{CP} = 9.7 Hz), 83.7, 116.0 (q, J_{CF} = 292 Hz), 129.9 (d, J_{CP} = 9.4 Hz), 129.6, 133.9 (d, J_{CP} = 10.3 Hz), 134.4 (d, J_{CP} = 40.7 Hz), 155.7 (d, J_{CP} = 9.4 Hz), 171.8 (q, J_{CF} = 35.2 Hz), 172.5 (bs). HRMS for [C$_{32}$H$_{30}$CoF$_3$OP]$^+$: 577.1313 (Theo. Mass), 577.1308 (Mass Measured), Delta (-0.9 ppm). Elemental Analysis: C% (66.67); H% (5.07). Found: C% (66.59); H% (5.31).

20
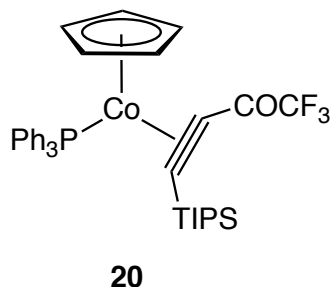
Preparation of (η^5-C$_5$H$_5$)(PPh$_3$)Co[η^2-(TIPS)C≡C(COCF$_3$)] (20): 3.0 g (4.63 mmol) of CpCo(PPh$_3$)$_2$ were added into a reaction tube with 10 mL dry toluene inside a glove box. After stirring for 30 minutes, 1.416 g (5.09 mmol) of alkyne 1,1,1-trifluoro-4-(triisopropylsilyl)but-3-yn-2-one were introduced and the color of the solution slowly changed from red to dark. The resulting solution was allowed to stirred overnight and then layered with 10 ml of hexane to trigger crystallization at -20˚C. After two weeks, 2.3 g (74% yield) of **20** was obtained by filtration and air sensitive dark crystals were washed with dry hexanes under inert atmosphere. Mp: 104.5°C; IR (CDCl$_3$) 3056, 2942,

2861, 2035, 1633, 1437, 1188, 1120, 1092, 1053, 882 cm^{-1}; ^{1}H NMR (C$_6$D$_6$, 400 MHz) δ 1.017 (m, 3H), 1.159 (m, 18H), 4.600 (s, 5H), 7.013 (m, 9H), 7.647 (m, 6H); ^{13}C{^{1}H} NMR (CDCl$_3$, 125 MHz) δ 12.2, 19.1, 19.3, 83.0, 90.5, 104.4 (d, J_{CP} = 7.0 Hz), 118.5, 117.8 (q, J_{CF} = 292 Hz), 128.1, 129.6, 134.4, 180.6 (q, J_{CF} = 35.0 Hz). HRMS for [C$_{36}$H$_{41}$CoF$_3$OPSiNa]$^+$: 687.1841 (Theo. Mass), 687.1840 (Mass Measured), Delta (-0.1 ppm). Elemental Analysis: C% (65.05); H% (6.22). Found: C% (64.68); H% (6.6).

25
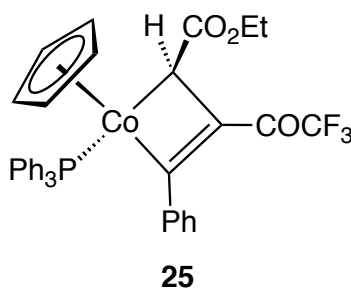
Preparation of (η^5-C$_5$H$_5$)(PPh$_3$)Co[C(Ph)=C(COCF$_3$)CH(CO$_2$Et)] (25): 0.51g (0.87 mmol) of (η^5-C$_5$H$_5$)(PPh$_3$)Co[η^2-(Ph)C≡C(COCF$_3$)] were added in a reaction tube with dry toluene (40 ml) as solvent in a glove box. After stirring the solution for 30 minutes, 0.995 g ethyl diazoacetate (15% in toluene) were introduced over 10 hours under inert gas atmosphere. The color of the solution changed from purple to red gradually and the resulting solution was allowed to stir for 5 more hours at room temperature. The solvent was then evaporated under reduced pressure and chromatography on silica gel with 20% EtOAc/hexanes yielded 235.7 mg (40.3% yield) of **25** an air stable red crystalline solid. Mp: 142.1 °C; IR (CDCl$_3$) 3056, 2975, 2251, 1690, 1596, 1538, 1479, 1435, 1365, 1307, 1171, 1091, 1043 cm^{-1}; ^{1}H NMR (CDCl$_3$, 400 MHz) δ 1.39 (t, 3H, J = 7.2 Hz,

CH_3), 1.52 (d, 1H, J_{PH} = 7.6 Hz, CHCO$_2$), 4.19 (m, 1H, CHHCH$_3$), 4.29 (m, 1H, CHHCH$_3$), 4.47 (s, 5H, C$_5$H$_5$), 7.2-7.5 (m, 20H); ^{13}C{^{1}H} NMR (CDCl$_3$, 125 MHz) δ -3.8 (d, J_{CP} = 13.8 Hz, CHCO$_2$), 15.0(CH$_3$), 59.4 (CH$_2$CH$_3$), 89.6 (C_5H$_5$), 116.5 (q, J_{CF} = 293 Hz, CF$_3$), 127.1 (C_p, Ph), 127.4 (d, J_{CP} = 66 Hz, C_i, PPh$_3$), 127.68 (d, J_{CP} = 5.8 Hz, C_m, PPh$_3$), 127.7 (C_m, Ph), 128.4 (d, J_{CP} = 9.5 Hz, C_p, PPh$_3$), 130.7 (C_o, Ph), 130.9 (d, J_{CP} = 2.5 Hz, CCOCF$_3$), 134.2 (d, J_{CP} = 5.7 Hz, C_o, PPh$_3$) , 147.1 (C_i, Ph), 162.6 (dq, J_{CP} = 5.9 Hz, J_{CF} = 32.8 Hz, COCF$_3$), 181.5 (CO$_2$Et), 198.8 (d, J_{CP} = 21.4 Hz, C-Ph). HRMS for [C$_{37}$H$_{32}$CoF$_3$O$_3$P]$^+$: 671.1368 (Theo. Mass), 671.1367 (Mass Measured), Delta (-0.1 ppm). Elemental Analysis: C% (66.27); H% (4.66). Found: C% (66.38); H% (4.70).
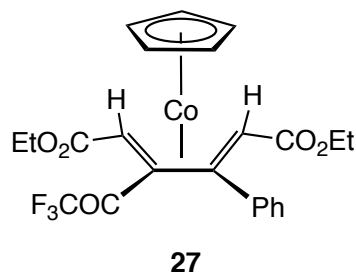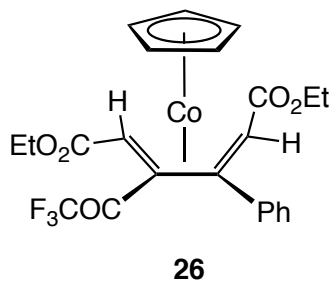
26   **27**

Preparation of (η^5-C$_5$H$_5$)Co[η^4-CH(CO$_2$Et)=C(COCF$_3$)C(Ph)=CH(CO$_2$Et) (26/27): When the same procedure of synthesizing metallacyclobutene **25** was conducted, a red band in the chromatography before **25** was collected (138 mg, 32% combined yield), and ^{1}H NMR spectrum indicates 1:1 ratio of **26** and **27**. Pure **26** was isolated from partial crystallization of the mixture in ethyl acetate/hexane under -20˚C. Further purification of complex **27** failed due to the close polarities of **26** and **27** upon chromatography.

For **27**: ^{1}H NMR (C$_6$D$_6$. 400 MHz) δ 0.61 (s, 1H, H^{anti}), 0.75 (s, 1H, H^{anti}), 0.79 (t, 3H, J = 6.8 Hz, CH_3), 0.97 (t, 3H, J = 7.2 Hz, CH_3), 3.87 (m, 4H, CH_2CH$_3$), 4.77 (s, 5H, Cp), 6.9-7.8 (m, 5H, C$_6H_5$).

For **26**: Mp 128.5 °C; IR (KBr, thin film) 3062, 2984, 2900, 1743 (C=O), 1690 (C=O), 1412, 1312, 1205 cm^{-1}; ^{1}H NMR (CDCl$_3$, 400 MHz): δ 1.26 (t, 3H, J = 7.2 Hz, CH_3), 1.34 (t, 3H, J = 7.2 Hz, CH_3), 1.86 (s, 1H, H^{anti}), 3.68 (s, 1H, H^{syn}), 4.05 (q, 2H, J = 7.2 Hz, CH_2CH$_3$), 4.22 (q, 2H, J = 7.2 Hz, CH_2CH$_3$), 5.10 (s, 5H, Cp), 7.3-7.5 (m, 5H, C$_6H_5$). ^{13}C{^{1}H} NMR (CDCl$_3$, 125 MHz): δ 14.5 (CH$_3$), 14.7 (CH$_3$), 38.0 (CCO$_2$), 40.5 (CCO$_2$), 60.6 (OCH$_2$CH$_3$), 61.3 (OCH$_2$CH$_3$), 84.6 (Cp), 97.3 (CPh), 102.3 (CCOCF$_3$), 115.3 (q, J_{CF} = 291 Hz, CF$_3$), 128.2 (C$_m$, Ph), 128.5 (C$_p$, Ph), 130.5 (C$_o$, Ph), 136.4 (C$_i$, Ph), 171.9 (CO$_2$Et), 177.4 (CO$_2$Et), 186.0 (q, J_{CF} = 32.8 Hz, COCF$_3$). HRMS for [C$_{23}$H$_{23}$CoF$_3$O$_5$]$^+$: 495.0824 (Theo. Mass), 495.0817 (Mass Measured), Delta (-1.4 ppm). Elemental Analysis: C% (55.88); H% (4.49). Found: C% (56.07); H% (4.76).

49
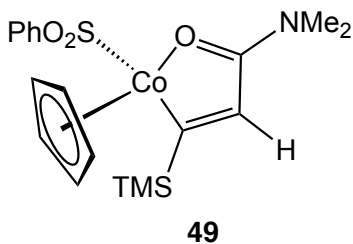
Preparation of (η^5-C$_5$H$_5$)(SO$_2$Ph)Co[κ^2-O=C(NMe$_2$)CH=C(SiMe$_3$)] (49): 221 mg (0.352 mmol) of cobalt-alkyne complex **7** and 62 mg (0.549 mmol) of N,N-dimethyldiazoacetamide were added into a reaction tube with 100mL dry toluene inside

a glove box. After dissolving them by stirring for 10 minutes, it was sealed with teflon cap as well as electrical tape. Then the solution was heated at 70°C for 3 hours. Via chromatography on silica gel with 60% Acetone/hexane, 56 mg (yield = 36.5 %) of **49** was obtained as an air stable dark brown crystalline solid after recrystallization from hot toluene and hexane. Mp: 135.5 °C; IR (CDCl$_3$) 2947, 2892, 1590, 1442, 1417, 1402, 1240, 1279, 1086, 1041, 919, 844 cm^{-1}; ^{1}H NMR (CDCl$_3$, 400 MHz) δ 0.442 (s, 9H), 2.880 (s, 3H), 2.908 (s, 3H), 5.093 (s, 5H), 6.441 (s, 1H), 7.5-8.1 (m, 5H); ^{13}C{^{1}H} NMR (CDCl$_3$, 125 MHz) δ 1.08, 35.53, 40.13, 87.36, 126.94, 127.13, 129.58, 136.87, 151.23, 177.09, 223.86. HRMS for [C$_{19}$H$_{26}$CoNO$_3$SSiNa]$^+$: 458.0627 (Theo. Mass), 458.0626 (Mass Measured), Delta (-0.2 ppm). Elemental Analysis: C% (52.40); H% (6.02). Found: C% (52.20); H% (6.40).

50
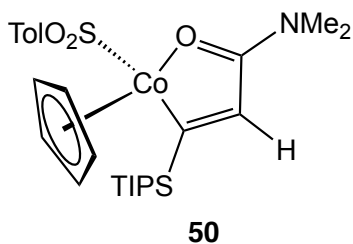
Preparation of (η^5-C$_5$H$_5$)(SO$_2$Ph)Co[κ^2-O=C(NMe$_2$)CH=C(SiMe$_3$)] (50): 460 mg (0.624 mmol) of cobalt-alkyne complex **9** and 110 mg (0.972 mmol) of N,N-dimethyldiazoacetamide were added into a reaction tube with 150mL dry toluene inside a glove box. After dissolving them by stirring for 10 minutes, it was sealed with teflon cap as well as electrical tape. Then the solution was heated at 70°C for 3 hours. Via

chromatography on silica gel with 80% ethyl acetate/hexane, 101 mg (yield = 30.3 %) of

50 was obtained as an air stable dark crystalline solid after recrystallization from hot

toluene and hexane. Mp: 150.2 °C; IR (CDCl$_3$) 2920, 2942, 2861, 1590, 1466, 1421,

1194, 1086, 1041, 1013, 919, 882, 814 cm^{-1}; ^{1}H NMR (CDCl$_3$, 400 MHz) δ 1.28 (d, 9H,

J = 7.6 Hz), 1.32 (d, 9H, *J* = 7.2 Hz), 1.50 (m, 3H), 2.41 (s, 3H), 3.00 (s, 3H), 3.13 (s,

3H), 4.94 (s, 5H), 6.74 (s, 1H), 7.21 (d, 2H, *J* = 8.0 Hz), 7.72 (d, 2H, *J* = 8.0 Hz); ^{13}C{^{1}H}

NMR (CDCl$_3$, 500 MHz) δ 13.42, 19.58, 19.91, 21.52, 35.57, 40.40, 87.41, 125.67,

128.42, 139.52, 140.52, 153.28, 176.79, 219.26. HRMS for [C$_{26}$H$_{40}$CoNO$_3$SSiNa]$^+$:

556.1722 (Theo. Mass), 556.1722 (Mass Measured), Delta (0 ppm). Elemental

Analysis: C% (58.51); H% (7.55). Found: C% (58.19); H% (7.94).

54
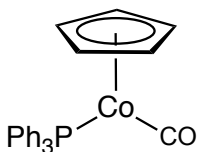
Preparation of (η^5-C$_5$H$_5$)Co(PPh$_3$)(CO) (54): 54 is made by slightly modifying the

known procedure in literature[34]. 150 mg (0.231 mmol) of CpCo(PPh$_3$)$_2$ was dissolved in

200 ml dry toluene under inert atmosphere. Carbon monoxide was bubbled through the

solution for 5 minutes while keep stirring the solution. The color of the solution changed

from red to orange brown immediately. After pulling off solvent under vacuum, some

brown powder stayed in the flask and then the powder was washed with hexane to get

rid of the triphenylphosphine residue. After filtration and drying under vacuum, 75 mg (yield = 78.4 %) of **54** can be obtained as brown air sensitive solid. The spectrum data matches what was reported in the literature.

NMR tube reaction of cobalt-alkyne complex 7 with 2-diazo-*N,N*-dimethylacetamide: 4 mg (0.006 mmol) of **7** were added into an oven dried J.Y. NMR tube with 1,3,5-Tri-*ter*-butyl-benzene as internal standard, then 0.75 mL of dry C_6D_6 was distilled into the NMR tube on the Schlenk line. After the sample was dissolved by shaking the tube on Vortex Mixer for 5 minutes, an ^{1}H NMR spectrum was recorded. Then 14.5 mg of 2-diazo-N,N-dimethylacetamide in hexane (10%, 0.012 mmol) was added into another oven dried J.Y. NMR tube. Hexane was pumped away on Schlenk line and 0.5 ml of dry C_6D_6 was distilled into the tube. Then the solution in the second NMR tube was transferred into the first tube by using a 9" extended tip pipet in a glove box. The reaction mixture was kept at room temperature and monitored by using ^{1}H NMR. After 16 hours, all the **7** were consumed based on the disappearance of TMS resonance at δ 0.136 (s, 9H), and the resonances of **49** were observed at δ 0.59 (s, 9H, TMS), 2.04 (s, 3H, Me), 2.32 (s, 3H, Me), 4.85 (s, 5H, Cp), and 6.48 (s, 1H, vinyl-*H*). The characteristic Cp resonance of **12** was observed at δ 4.61 (s, 5H). The NMR yields of **49** (38.5%) and **54** (27.1%) were calculated by the integration of Cp resonances at δ 4.85 (s, 5H) and 4.61 (s, 5H) relative to internal standard at δ 1.35.

55
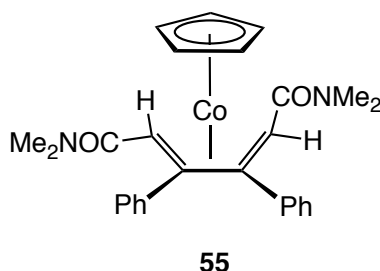
Preparation of (η^5-C$_5$H$_5$)Co[η^4-CH(CONMe$_2$)=C(Ph)C(Ph)=CH(CONMe$_2$) (55): 200 mg (0.354 mmol) of (η^5-C$_5$H$_5$)(PPh$_3$)Co{η^2-(Ph)C≡C(Ph)} and 200 mg (1.77 mmol) of N,N-dimethyldiazoacetamide were added into a round bottom flask with 50mL dry toluene inside a glove box. The reaction mixture was allowed to stir at room temperature for 48 hours under inert atmosphere. After chromatography on silica gel with 25% ethyl acetate/hexane, 136 mg (yield = 81.3 %) of **55** was obtained as an air stable dark red crystalline solid after recrystallization from toluene and hexane. Mp: 139.2 °C; IR (CDCl$_3$) 3084, 3056, 3022, 2925, 2237, 1624, 1607, 1488, 1421, 1257, 1146, 1063 921, 907 cm^{-1}; ^{1}H NMR (C$_6$D$_6$, 400 MHz) δ 2.26 (s, 1H), 2.58 (s, 3H), 2.73 (s, 6H), 2.80 (s, 3H), 3.38 (s, 1H), 4.93 (s, 5H), 6.9-7.6 (m, 10H); ^{1}H NMR (CDCl$_3$, 400 MHz) δ 1.73 (s, 1H), 2.80 (s, 3H), 2.85 (s, 3H), 3.02 (s, 3H), 3.31 (s, 3H), 3.54 (s, 1H), 5.07 (s, 5H), 6.9-7.4 (m, 10H); ^{13}C{^{1}H} NMR (C$_6$D$_6$, 125 MHz) δ 35.27, 37.69, 40.08, 47.75, 83.90, 94.75, 104.79, 126.81, 126.95, 127.30, 127.69, 131.44, 132.20, 138.44, 141.70, 171.74, 172.63. HRMS for [C$_{27}$H$_{30}$CoN$_2$O$_2$]$^+$: 473.1634 (Theo. Mass), 473.1626 (Mass Measured), Delta (-1.7 ppm). Elemental Analysis: C% (68.64); H% (6.19). Found: C% (68.76); H% (6.51).

57
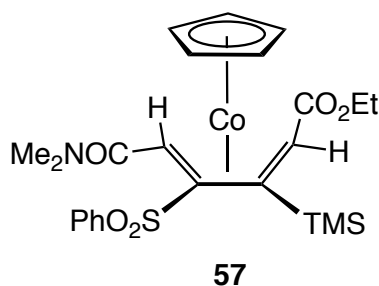
Preparation of (η^5-C$_5$H$_5$)Co[η^4-CH(CONMe$_2$)=C(TMS)C(SO$_2$Ph)=CH(CO$_2$Et) (57): 500 mg (0.70 mmol) of cobaltacyclobutene (η^5-C$_5$H$_5$)(PPh$_3$)Co{κ^2-C(SO$_2$Ph)=C(TMS)CHCO$_2$Et} and 120 mg (1.06 mmol) of N,N-dimethyldiazoacetamide were added into a reaction tube with 100mL dry toluene inside a glove box. The reaction tube was sealed with Teflon cap, and the reaction mixture was allowed to be heated at 70°C 6 hours. After chromatography on silica gel with 20% ethyl acetate/hexane, 197 mg (yield = 52.8 %) of **57** was obtained as a air stable dark red crystalline solid after recrystallization from ethyl acetate and hexane. Mp: 158.8 °C; IR (CDCl$_3$) 3059, 2978, 2951, 2898, 2251, 1677, 1668, 1531, 1481, 1434, 1365,1295, 1130, 1083 cm^{-1}; ^{1}H NMR (CDCl$_3$, 400 MHz) δ 0.50 (s, 9H), 1.22 (t, 3H, *J* = 7.2 Hz), 1.44 (s, 1H), 2.41 (s, 3H), 2.49 (s, 3H), 3.53 (s, 1H), 3.93 (m, 2H), 5.15 (s, 5H), 7.41 (t, 2H, *J* = 7.2 Hz), 7.49 (t, 1H, *J* = 7.2 Hz), 7.83 (d, 2H, *J* = 7.2 Hz); ^{13}C{^{1}H} NMR (CDCl$_3$, 500 MHz) δ 2.22, 14.52, 35.72, 37.60, 37.62, 46.63, 60.40, 83.54, 84.86, 113.85, 127.84, 128.45, 132.42, 142.06, 170.52, 173.77. HRMS for [C$_{24}$H$_{33}$CoNO$_5$SSi]$^+$: 534.1175 (Theo. Mass), 534.1170 (Mass Measured), Delta (-0.9 ppm). Elemental Analysis: C% (54.02); H% (6.04). Found: C% (53.88); H% (6.11).
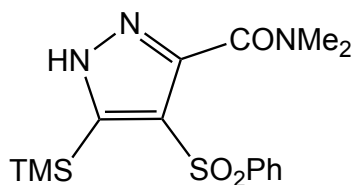
59

Preparation of N,N-dimethyl-4-(phenylsulfonyl)-5-(trimethylsilyl)-1H-pyrazole-3-carboxamide (59): To a benzene solution (100 ml) of 210 mg (0.88 mmol) of trimethyl((phenylsulfonyl)ethynyl)silane in a round bottom flask was added 100 mg (0.88 mmol) of 2-diazo-N,N-dimethylacetamide. The solution was allowed to stir at room temperature under dark for 24 hours. The solvent was then evaporated under reduced pressure to produce white solids. After recrystallization in DCM and hexanes, 0.286 g (92.4% yield) of **59** was obtained as white crystalline solid; Mp: 238.2 ˚C; IR (CDCl$_3$): 3214, 2950, 1643, 1526, 1446, 1392, 1315, 1253, 1149, 1095, 1060, 995, 910, 849 cm^{-1}; ^{1}H NMR (CDCl$_3$, 400 MHz) δ 0.42 (s, 9H, TMS), 2.86 (s, 3H, Me), 3.11 (s, 3H, Me), 7.4-7.6 (m, 3H, C$_6$H$_5$), 8.07 (d, 2H, J = 7.2 Hz, C$_6$H$_5$), 10.52 (bs, 1H, NH); ^{13}C{^{1}H} NMR (CDCl$_3$, 500 MHz) δ 1.16, 35.06, 38.90, 127.13, 127.68, 128.95, 133.20, 142.21, 147.79, 148.61, 163.75. HRMS (HR-ESI-TOFMS) for [C$_{15}$H$_{21}$N$_3$O$_3$SSiNa]$^+$: 374.0965 (Theo. Mass), 374.0961 (Mass Measured), Delta (-1.1 ppm).

145
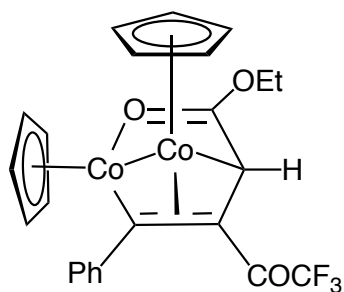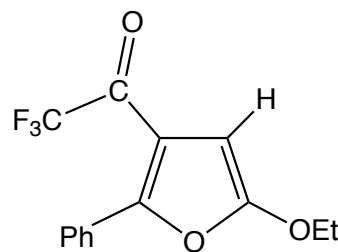
62   **63**

Preparation of dicobalt propendiyl complex 62 and furan 63: 320 mg (0.477 mmol) of metallacyclobutene **25** were added into a reaction tube with 50 mL dry toluene inside a glove box. After stirring for 10 minutes to dissolve all the solids, the tube was sealed with teflon cap as well as electrical tape. Then the solution was heated at 70°C for 3 hours. When the reaction is done, the color of the solution changed from red to dark brown. Via chromatography on silica gel inside the glove box with 2% ethyl acetate/hexane, 102 mg (yield = 80.3 %, NMR yield = 90.2 %) of **62** was obtained as an air sensitive dark crystalline solid after recrystallization from toluene and hexane at -20°C, and **63** (62 mg) was obtained as a yellow oil with 49% yield.

Characterization of 62: Mp 149.5 °C; IR (CDCl$_3$) 3094, 3007, 2984, 1727, 1700, 1592, 1442, 1303, 1246, 1161, 1143, 990, 909, 810, 699 cm^{-1}; ^{1}H NMR (CDCl$_3$, 400 MHz) δ 1.22 (t, 3 H, J = 7.2 Hz, CH_3), 2.83 (s, 1 H, CHCO$_2$), 3.80 (m, 1 H, CHHCH$_3$), 3.94 (m, 1 H, CHHCH$_3$), 4.36 (s, 5 H, Cp), 5.09 (s, 5 H, Cp), 7.0-7.6 (m, 5 H, Ph); ^{13}C{^{1}H} NMR (CDCl$_3$, 125 MHz) δ 14.05 (CH$_3$), 26.61 (CHCO$_2$), 62.85 (CH$_2$CH$_3$), 79.99 (Cp), 80.67 (Cp), 88.84 (Co-C-Ph), 115.89 (q, J_{CF} = 294.1 Hz, CF$_3$), 124.51 (C_o, Ph), 126.72 (CCOCF$_3$), 127.81 (C_m, Ph), 156.58 (C_p, Ph), 174.83 (C_i, Ph), 184.47 (CO$_2$Et), 187.45

146

(q, J_{CF} = 33.6 Hz, $COCF_3$); HRMS for $[C_{24}H_{21}Co_2F_3O_3]^+$: 532.0101 (Theo. Mass), 532.0102 (Mass Measured), Delta (0.2 ppm). Elemental Analysis: C% (54.16); H% (3.98). Found: C% (54.54); H% (4.38).

Characterization of 63: IR (Neat): 3155, 3062, 2984, 2928, 1713, 1620, 1548, 1489, 1388, 1315, 1013, 907, 883 cm^{-1}; ^{1}H NMR (CDCl$_3$, 500 MHz) δ 1.49 (t, 3 H, J = 7.2 Hz, CH_3), 4.22 (q, 2 H, J = 7.2 Hz, OCH_2), 5.68 (s, 1 H, =CH), 7.43 (m, 3 H, C_6H_5), 7.97 (m, 2 H, C_6H_5); ^{13}C{^{1}H} NMR (CDCl$_3$, 125 MHz) δ 14.64 (CH_3), 67.85 (OCH_2), 81.67 (=CH), 115.30 (C-Ph), 116.75 (q, J_{CF} = 291.4 Hz, CF_3), 128.31 (C_o, Ph), 128.43 (C_m, Ph), 128.66 (C_i, Ph), 130.42 (C_p, Ph), 152.81 (OCO), 160.04 ($CCOCF_3$), 175.50 (q, J_{CF} = 36.7 Hz, $COCF_3$).
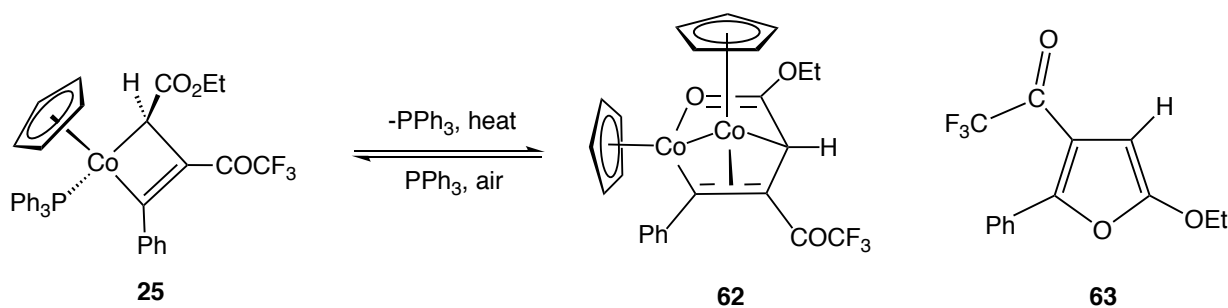
Reversible interconversion between 25 and 62: 5 mg (0.007 mmol) of **25** and 1,4-Bis(trimethylsilyl)benzene (internal standard) were added into a teflon top NMR tube. 1.2 ml of C$_6$D$_6$ was distilled into the NMR tube on the Schlenk line. After shaking the tube on Vortex Mixer for 5 minutes to dissolve all the solids, a ^{1}H NMR spectrum was recorded as initial one. Then the solution was heated at 70°C in an oil bath, and the reaction was subsequently monitored by ^{1}H NMR spectroscopy. After 3 hours, the color

of solution changed from red to dark, and **25** was totally consumed based on the Cp peak at δ 4.465. New ^{1}H NMR resonances for **62** were observed at δ 0.72 (t, 3H, J = 7.2 Hz), 3.29 (m, 1H), 3.46 (m, 1 H), 4.28 (s, 5 H, Cp) and 4.76 (s, 5 H, Cp). Percent yield was calculated from integration of the internal standard relative to the sum of two Cp resonance of **62**. (90.2 % yield). Another set of new resonances for a furan derivative was observed at δ 0.90 (t, 3 H, J = 7.2 Hz), 3.31 (q, 2 H, J = 7.2 Hz) and 5.40 (s, 1H). The percent yield of furan derivative was calculated from integration of the internal standard relative to the methyl group at 0.90 ppm. (98 % yield). Then the solution was transferred into a vial and opened to air. After one day, the color of the solution changed from dark to red and it generated some green precipitates. The solution was filtered through a pasteur pipet filter and a ^{1}H NMR spectrum was taken afterwards. **62** was totally consumed based on its Cp peak at δ 4.28 and δ 4.76 ppm. New ^{1}H NMR resonances for **25** were observed at δ 1.16 (t, 3 H, J = 7.2 Hz), 1.93 (d, 1 H, J = 6.8 Hz), 4.18 (m, 1 H), 4.26 (m, 1 H) and 4.46 (s, 5 H, Cp). Percent yield was calculated from integration of the new Cp peak of **25** and one of the Cp peaks of **62** at 4.28 ppm relative to internal standard (94 % yield).
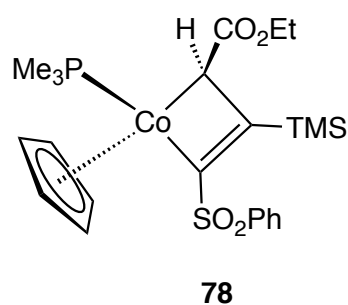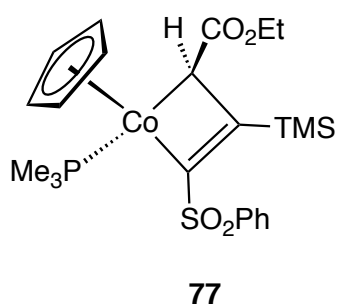
77   **78**

Preparation of (η^5-C$_5$H$_5$)(PMe$_3$)Co[C(SO$_2$Ph)=C(TMS)CH(CO$_2$Et)] (77/78): a 100-ml thick-walled reaction tube equipped with a threaded Teflon plug and o-ring, was charged with **25** (500 mg, 0.703 mmol), trimethylphosphine (300 mg, 3.94 mmol) and toluene (80 ml) under inert atmosphere. The flask was sealed and stirred on a vortex mixer to dissolve all the solids. After the solution was heated at 70 °C under dark for 4 hours, the reaction mixture was chromatographed on silica gel under dark with 30% EtOAc/hexanes yielded 58 mg (15.7% yield) of **78** and 184 mg (50% yield) of **77** both as red oil. Exposure of the oil to hexane vapors in the dark resulted in the formation of red-orange crystals suitable for solid-state analysis.

Characterization of 77: Mp 142.1 °C; IR (KBr, thin film) 1677 (C=O) cm^{-1}; ^{1}H NMR (CDCl$_3$, 400 MHz): δ 0.15 (s, 9H, Si(CH_3)$_3$), 1.19 (d, 1H, J = 7.2 Hz CHCO$_2$Et), 1.34 (t, 3H, J = 7.2 Hz, CH_3), 1.39 (d, 9H, J = 10.4 Hz, P(CH_3)$_3$), 4.15 (m, 2H, CH_2CH$_3$), 4.21 (s, 5H, C$_5$$H_5$), 7.57 (m, 3H, m,p-C$_6H_5SO_2$), 8.00 (d, 2H, J = 8.0 Hz, o-C$_6$H$_5$SO$_2$). ^{13}C{^{1}H} NMR (C$_6$D$_6$, 125 MHz): δ -2.32 (CHCO$_2$Et), 0.34 (Si(CH$_3$)), 15.53 (CH$_3$), 17.78 (d, J = 30.02 Hz, P(CH$_3$)$_3$), 59.37 (CH$_2$CH$_3$), 86.27 (C$_5$H$_5$), 128.31 (p-SO$_2$Ph), 129.43 (m-SO$_2$Ph), 132.35 (o-SO$_2$Ph), 144.03 (d, J = 34.20 Hz, C(SO$_2$Ph)), 144.23 ($ipso$-SO$_2$Ph), 170.10 (d, J = 5.01 Hz, C(Si(CH$_3$)$_3$)), 181.07 (CO$_2$Et). Elemental Analysis for C$_{23}$H$_{34}$CoO$_4$PSSi: C, 52.66%; H, 6.53%. Found: C, 52.75%; H, 6.57%.

Characterization of 78: Mp 138.4 °C; IR (KBr, thin film) 3093, 2975, 2942, 2910, 1674 (C=O), 1521, 1446 cm^{-1}; ^{1}H NMR (CDCl$_3$, 400 MHz): δ 0.19 (s, 9H, Si(CH_3)$_3$), 1.24 (t, 3H, J = 7.2 Hz, CH_3), 1.46 (d, 9H, J = 10.4 Hz, P(CH_3)$_3$), 3.09 (d, 1H, J = 2.0 Hz CHCO$_2$Et), 3.99 (m, 2H, CH_2CH$_3$), 4.35 (s, 5H, C$_5$$H_5$), 7.58 (m, 3H, m,p-C$_6H_5SO_2$), 7.97 (d, 2H, J = 8.0 Hz, o-C$_6$H$_5$SO$_2$). ^{13}C{^{1}H} NMR (CDCl$_3$, 125 MHz): δ -9.50 (d, J = 12.4 Hz,

*C*HCO₂Et), -0.25 (Si(*C*H₃)), 14.77 (*C*H₃), 18.13 (d, J = 29.8 Hz, P(*C*H₃)₃), 59.28 (*C*H₂CH₃), 84.80 (*C*₅H₅), 127.80 (*p*-SO₂Ph), 129.01 (*m*-SO₂Ph), 132.50 (*o*-SO₂Ph), 142.82 (*ipso*-SO₂Ph), 144.64 (d, J = 34.8 Hz, *C*(SO₂Ph)), 171.24 (d, J = 5.2 Hz, *C*(Si(CH₃)₃)), 180.47 (*C*O₂Et). HRMS for [C₂₃H₃₅CoO₄PSSi]⁺: 525.1089 (Theo. Mass), 525.1092 (Mass Measured), Delta (0.6 ppm). Elemental Analysis for C₂₃H₃₄CoO₄PSSi: C, 52.66%; H, 6.53%. Found: C, 52.87%; H, 6.48 %.
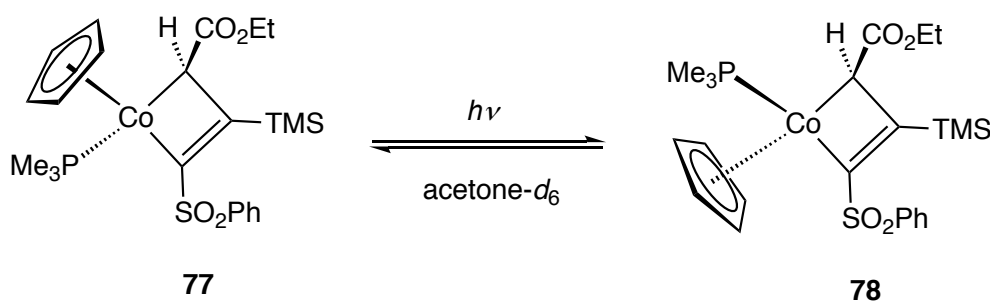
NMR tube reaction of 77/78 under UV-vis light to form equilibrium in acetone-*d₆*:
77 (2.5 mg, 0.005 mmol) and 1,3,5-tri-*tert*-butylbenzene (internal standard) were added to an oven dried J. Young tube. Then 0.7 ml of acetone-*d₆* was distilled into the NMR tube. The resulting solution was subsequently degassed via 3 cycles of freeze/pump/thaw/degas. An ¹H NMR spectrum was recorded immediately as the initial spectrum. The reaction tube was left in the dark for 6 h and another ¹H NMR was taken, indicating that no reaction had occurred. The J. Young tube was then placed in a Rayonette photoreactor equipped with UV broadband lamps that is centered at 254 nm. After 10 minutes, the reaction was monitored by ¹H NMR spectroscopy. A new set of ¹H NMR resonances for **78** were observed at δ 0.16 (s, 9H, Si(C*H*₃)₃), 1.21 (t, 3H, J = 7.2 Hz, C*H*₃), 1.35 (d, 9H, J = 10.4 Hz, P(C*H*₃)₃), 3.12 (d, 1H, J = 2.4 Hz C*H*CO₂Et), 3.96

(m, 2H, C*H₂*CH₃), 4.45 (s, 5H, C₅*H₅*), 7.68 (m, 3H, *m,p*-C₆H₅SO₂), 7.98 (d, 2H, *J* = 8.0 Hz, *o*-C₆H₅SO₂). The conversion of **77** (61%) was calculated by the integration of TMS peak at 0.13 ppm relative to internal standard. The ratio of **77** and **78** (0.75:1) was calculated by the integration of their Cp peaks at 4.36 ppm and 4.45 ppm, respectively. The NMR tube was then allowed to be photolyzed up to 30 minutes, indicating no change happened to the ratio of the two isomers (0.75:1). Then the NMR tube was kept in the dark for 5 hours, and another ^{1}H NMR spectrum was taken, which also showed no change happened to the ratio. A very similar reaction was conducted by using **78** as starting material. After photolizing the reaction under the same condition, a new set of ^{1}H NMR resonances for **77** were observed at δ 0.13 (s, 9H, Si(C*H₃*)₃), 1.16 (d, 1H, *J* = 6.8 Hz C*H*CO₂Et), 1.29 (t, 3H, *J* = 7.2 Hz, C*H₃*), 1.35 (d, 9H, *J* = 10.4 Hz, P(C*H₃*)₃), 4.11 (m, 2H, C*H₂*CH₃), 4.36 (s, 5H, C₅*H₅*), 7.68 (m, 3H, *m,p*-C₆H₅SO₂), 7.98 (d, 2H, J = 8.0 Hz, *o*-C₆H₅SO₂). The ratio of **77** and **78** (0.75:1) was calculated by the integration of their Cp peaks at 4.36 ppm and 4.45 ppm, respectively. No change was observed to the ratio of the two isomers when continue photolyzing the NMR tube or keep the reaction mixture under dark.

Using UV-vis absorption spectra to monitor interconversion of 77 and 78 under UV-vis light in acetone: UV−visible spectra were collected on a Shimadzu UV-3600 UV/vis/NIR spectrometer. 4.0 mM of **77** in dry acetone were prepared in glove box, and the solution was transferred into a quartz cell (1 mm path length) that was sealed by a screw cap with Teflon tape. For comparison, a same size cell with blank dry acetone was used as background. An initial spectrum was recorded, and it showed that **77** has a

λ_{max} at 422 nm with a molar absorptivity of 1127.5 $M^{-1}cm^{-1}$. Then the sample was placed into a Rayonette photoreactor equipped with UV broadband lamps that is centered at 254 nm. The reaction was monitored by using UV-vis spectroscopy. After 4.5 minutes, the reaction established a equilibrium and the spectrum didn't change any more. The λ_{max} of the reaction mixture moved to 425 nm. A very similar reaction was conducted by using **78**. 8.5 mM of **78** was prepared in the same way mentioned above, and the initial spectrum showed that **78** has a λ_{max} at 428 nm with a molar absorptivity of 1169.4 $M^{-1}cm^{-1}$. After 4.5 minutes, when the reaction reached the equilibrium, the λ_{max} of the reaction mixture also moved to 425 nm.

H. Appendix

1.646
1.784
2.036
2.055

2.881
2.898
2.916

7.260
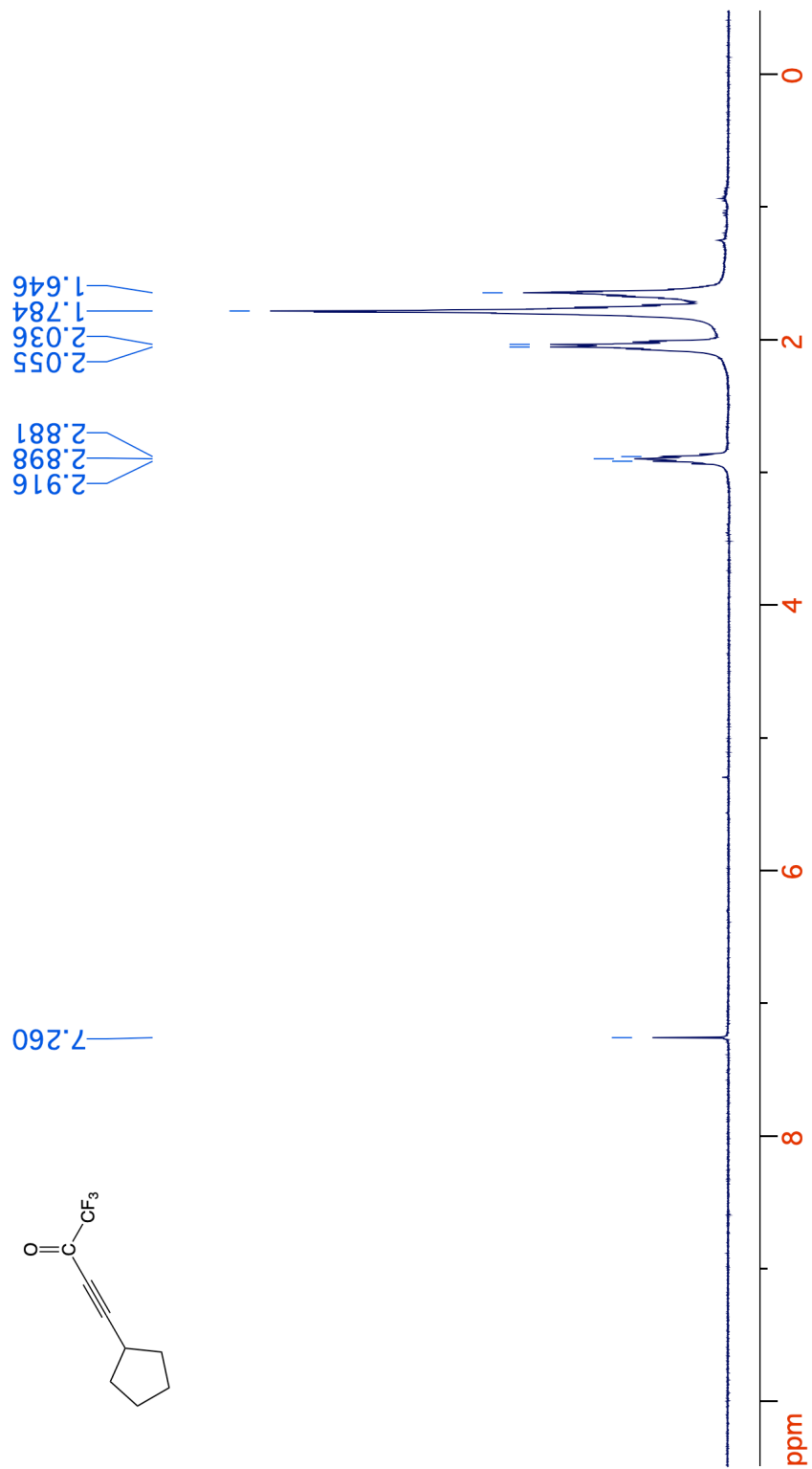
Figure 2-22. ^{1}H NMR spectrum (400 MHz, CDCl$_3$) of **16**.
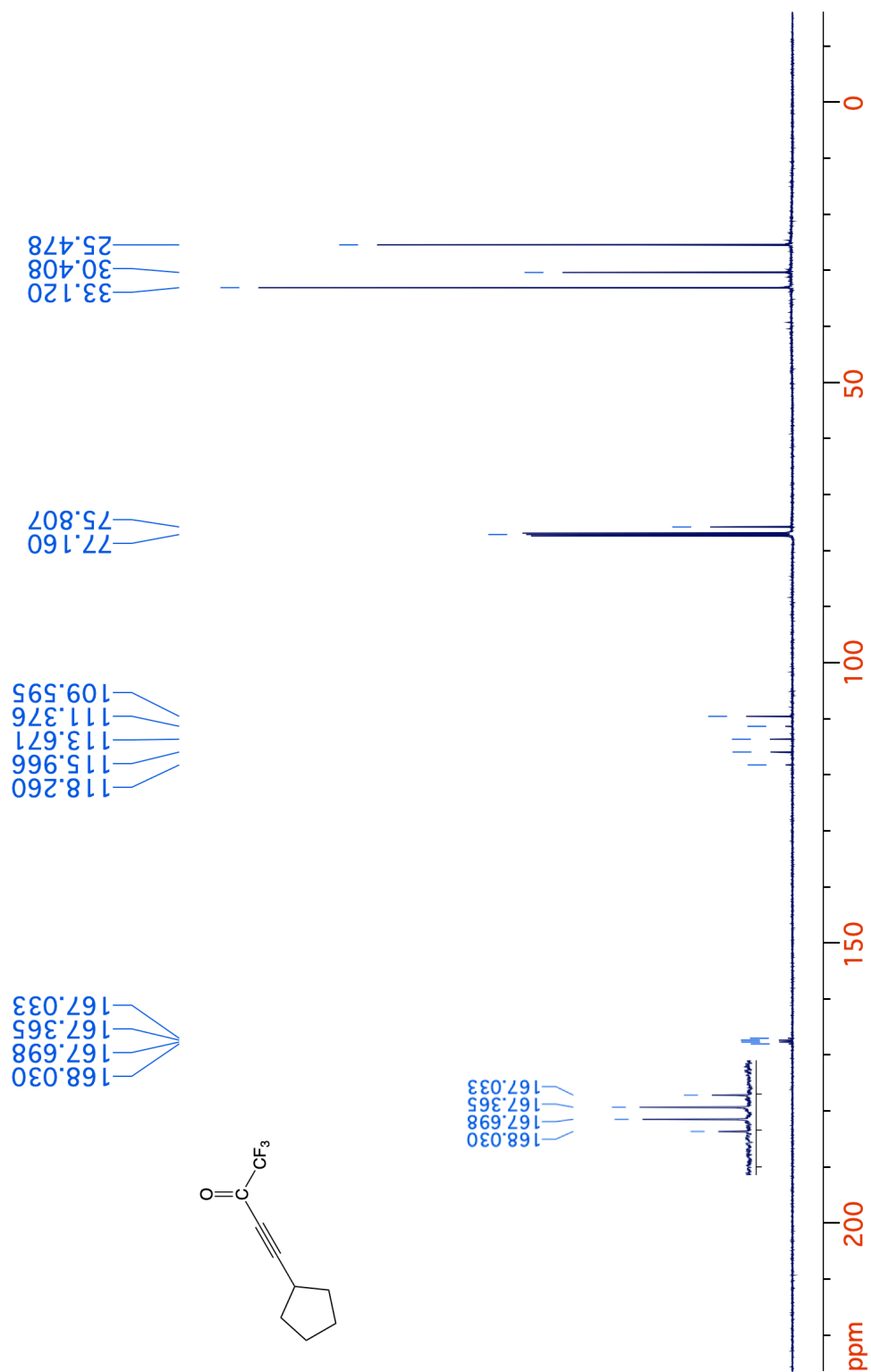
Figure 2-23. $^{13}C\{^1H\}$ NMR spectrum (125 MHz, CDCl$_3$) of **16**.

7.260

1.085
1.111
1.126
1.165
1.180
1.191
1.200
1.216

O=C—CF₃ (TIPS—C≡C—)

Figure 2-24. ¹H NMR spectrum (400 MHz, CDCl₃) of **17**.
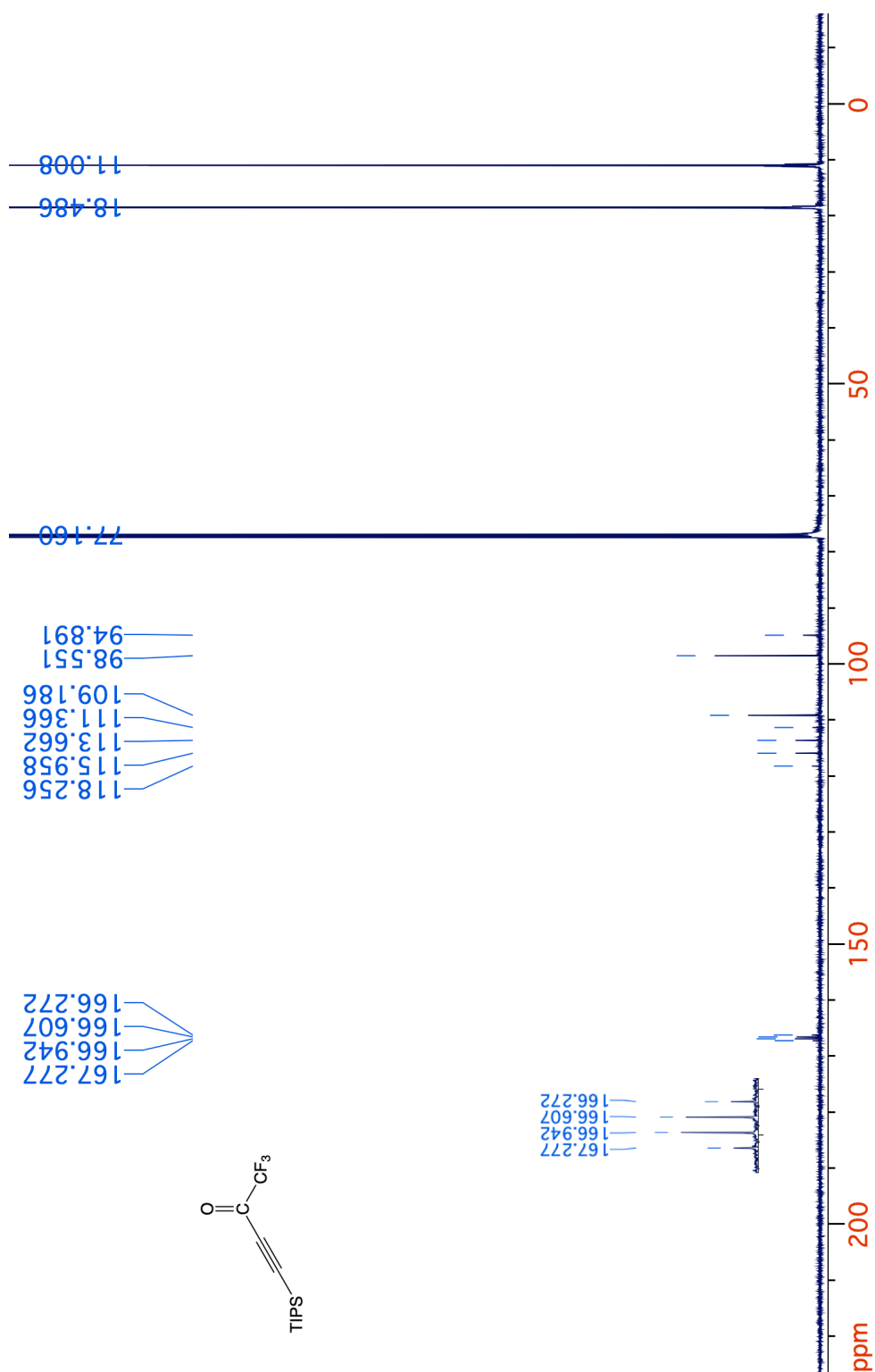
Figure 2-25. $^{13}C\{^1H\}$ NMR spectrum (125 MHz, CDCl$_3$) of **17**.
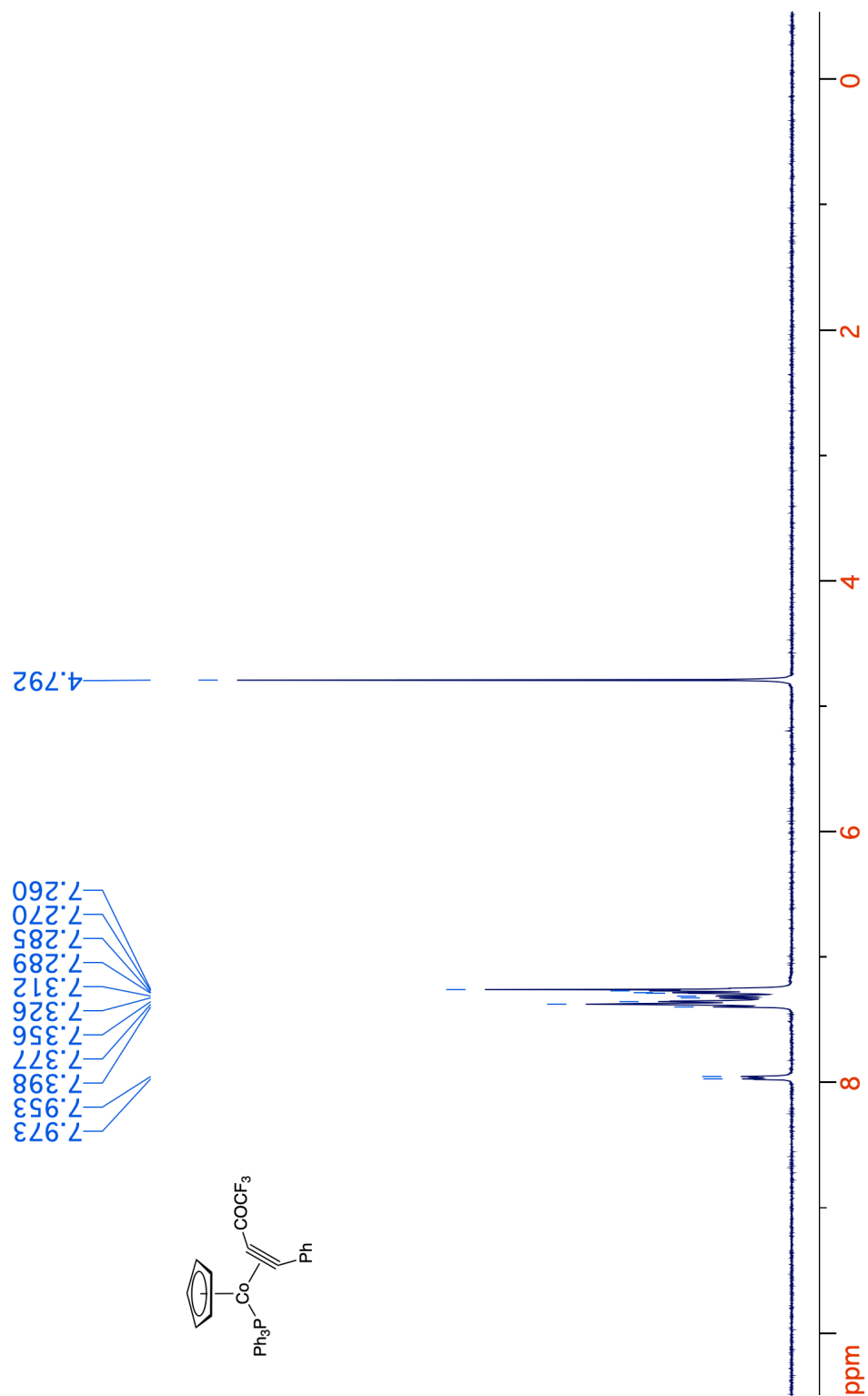
Figure 2-26. ^1H NMR spectrum (400 MHz, CDCl$_3$) of **18**.

Figure 2-27. $^{13}C\{^1H\}$ NMR spectrum (125 MHz, CDCl$_3$) of **18**.
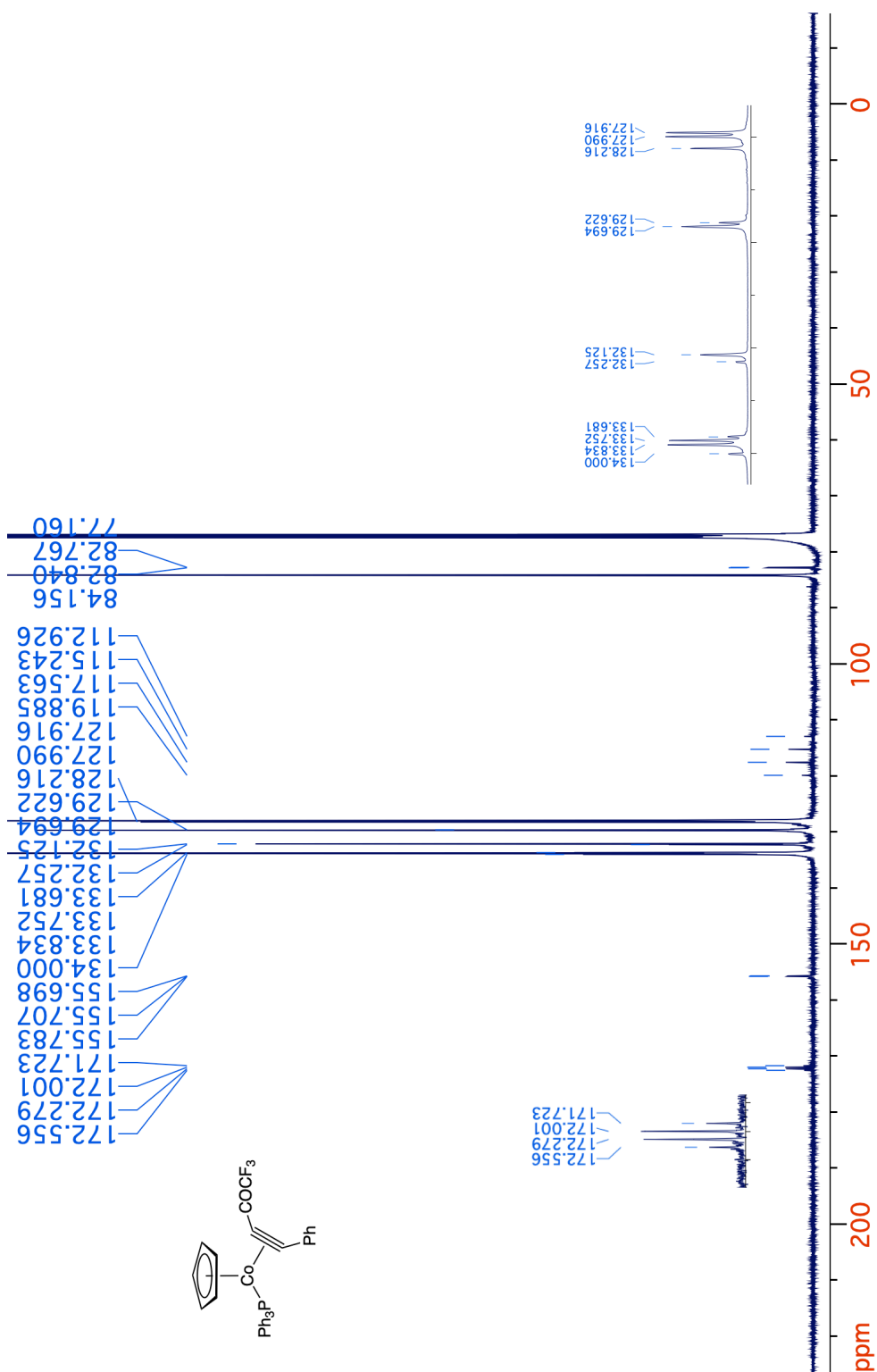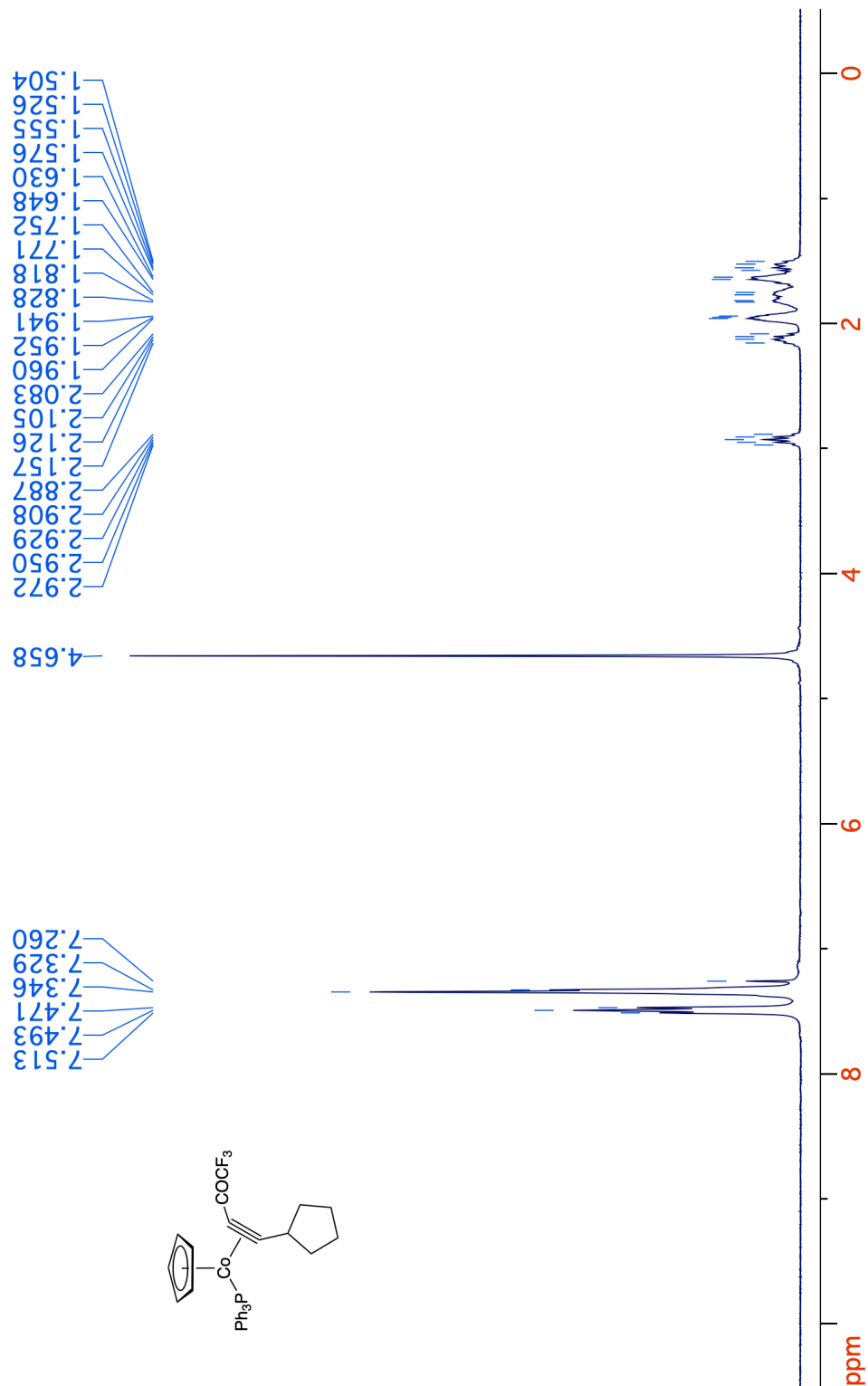
Figure 2-28. ^{1}H NMR spectrum (400 MHz, CDCl$_3$) of **19**.
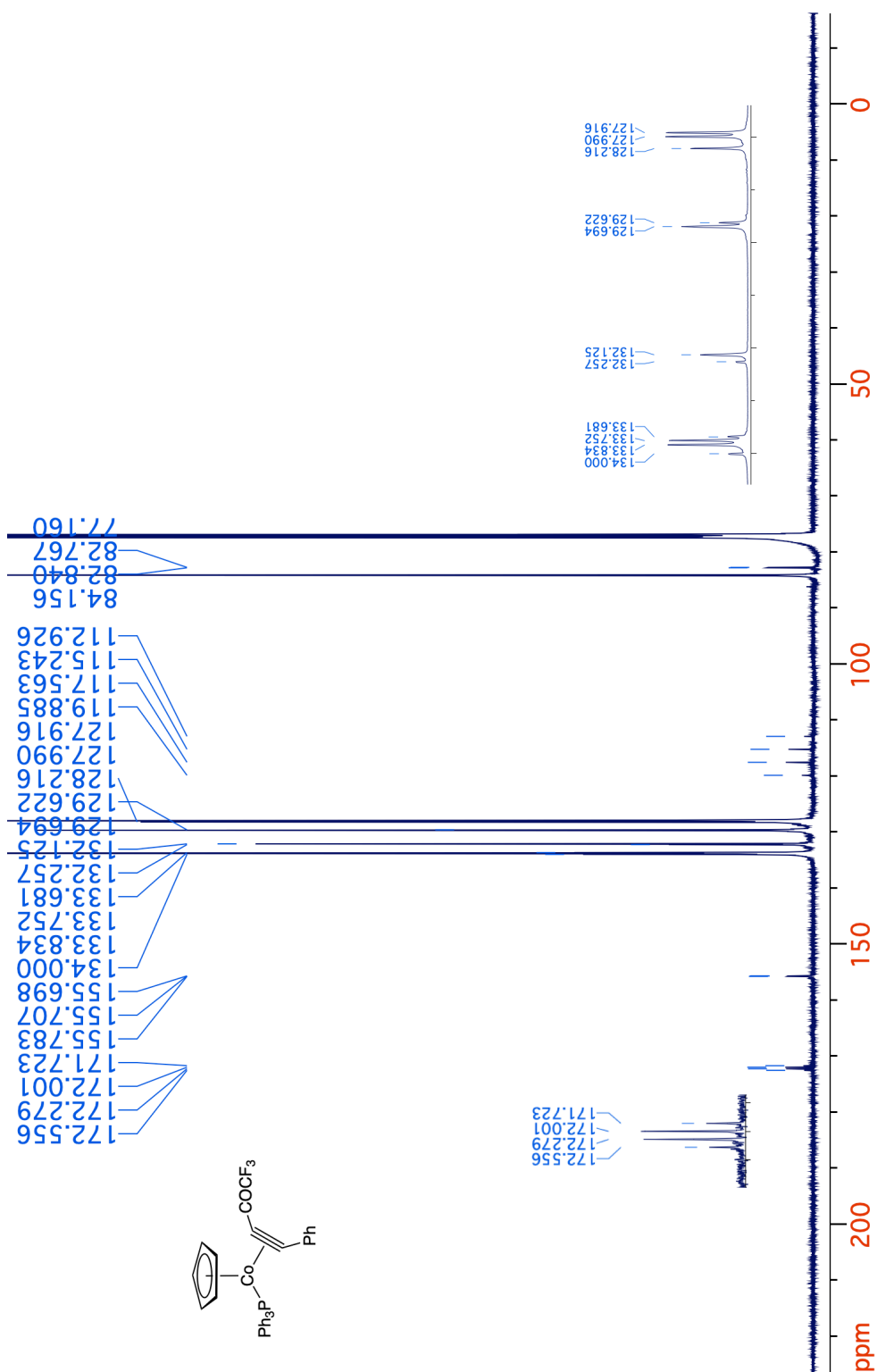
Figure 2-29. $^{13}C\{^1H\}$ NMR spectrum (125 MHz, CDCl$_3$) of **19**.

0.980
0.999
1.017
1.036
1.054
1.139
1.159
1.178
1.219
1.235

4.600

6.978
6.995
7.013
7.030
7.160
7.625
7.647
7.668
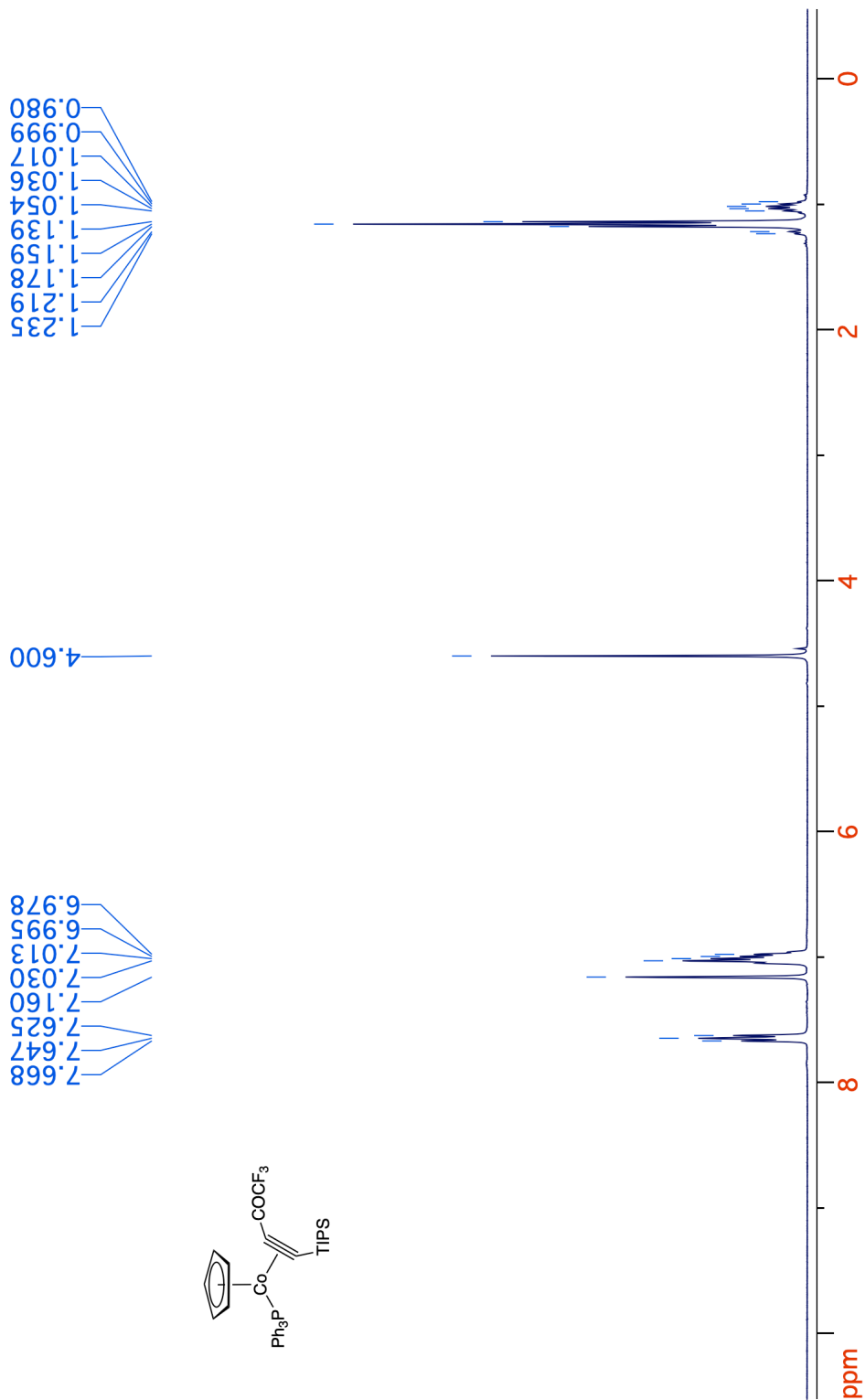
Figure 2-30. [^1]H NMR spectrum (400 MHz, C$_6$D$_6$) of **20**.

161
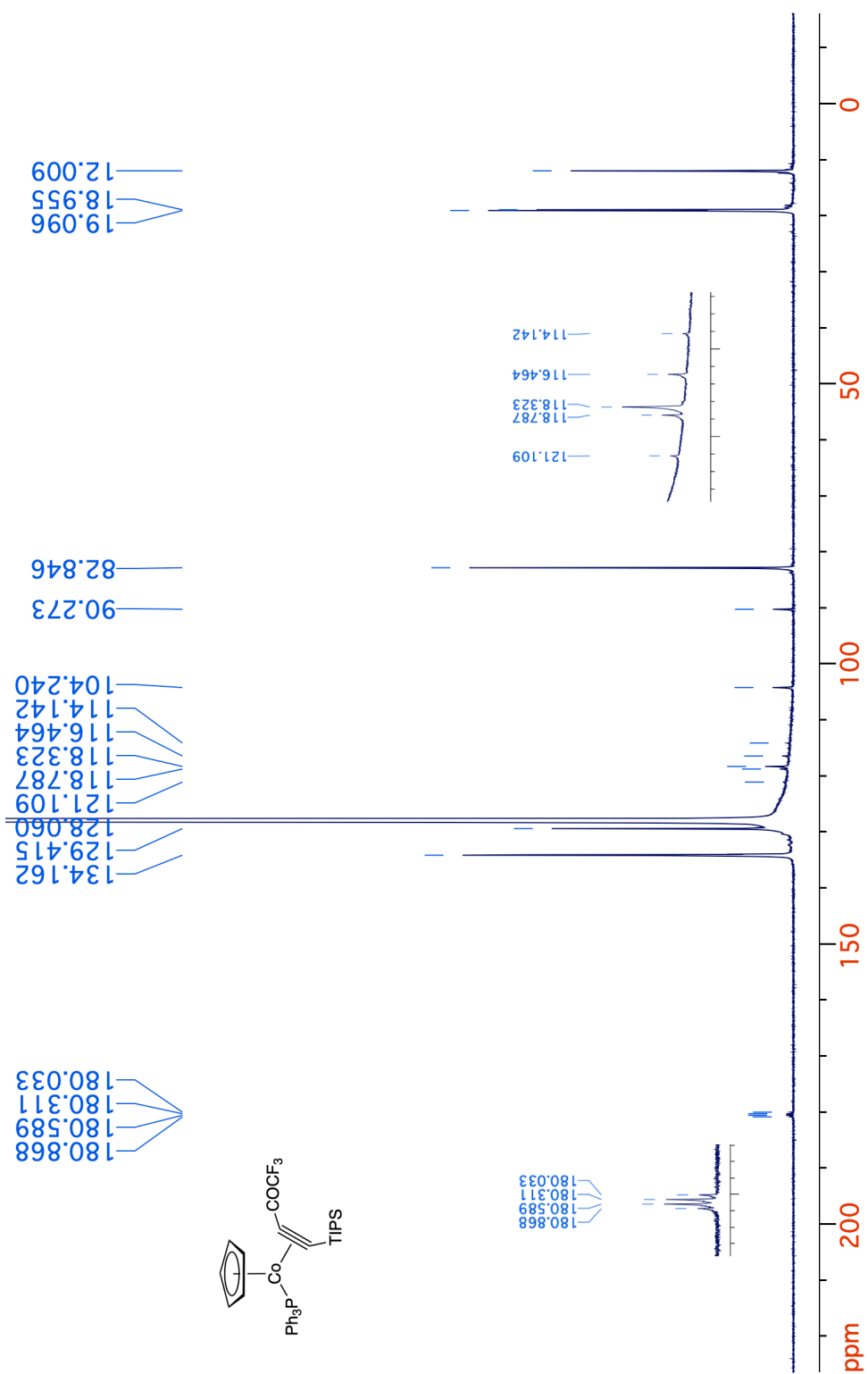
Figure 2-31. $^{13}C\{^1H\}$ NMR spectrum (125 MHz, C_6D_6) of **20**.
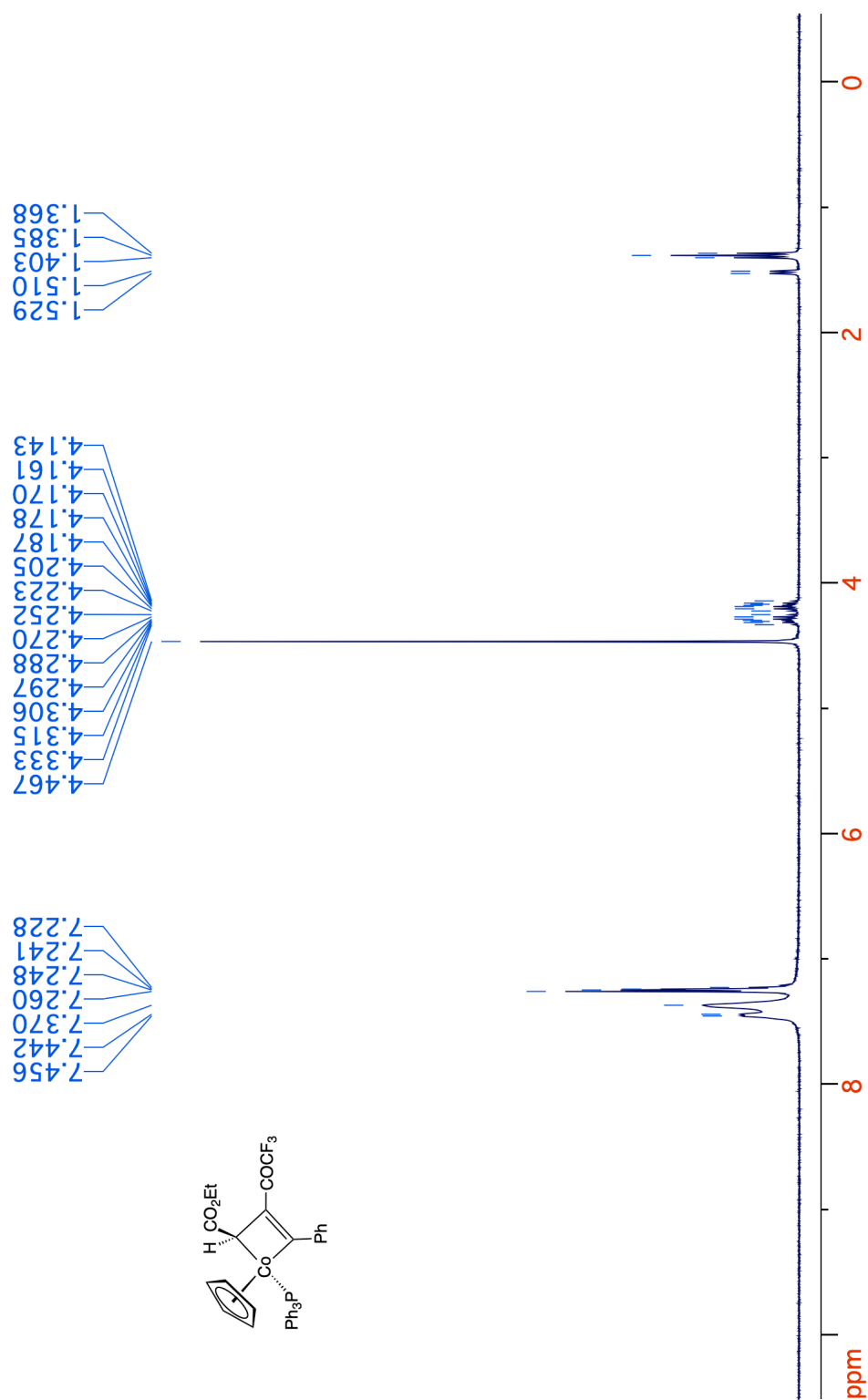
Figure 2-32. ^{1}H NMR spectrum (400 MHz, CDCl$_3$) of **25**.
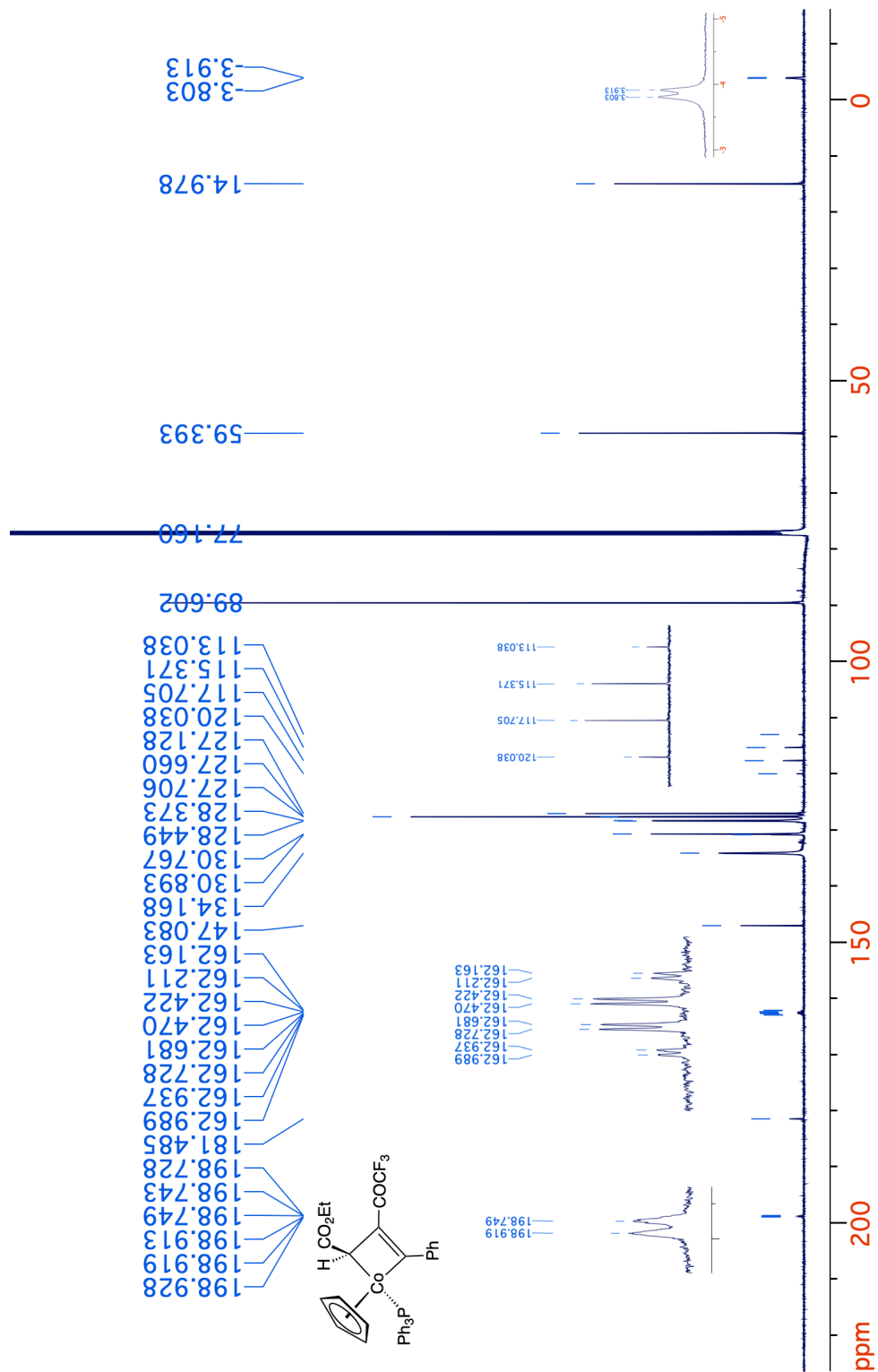
Figure 2-33. $^{13}C\{^1H\}$ NMR spectrum (125 MHz, CDCl$_3$) of **25**.
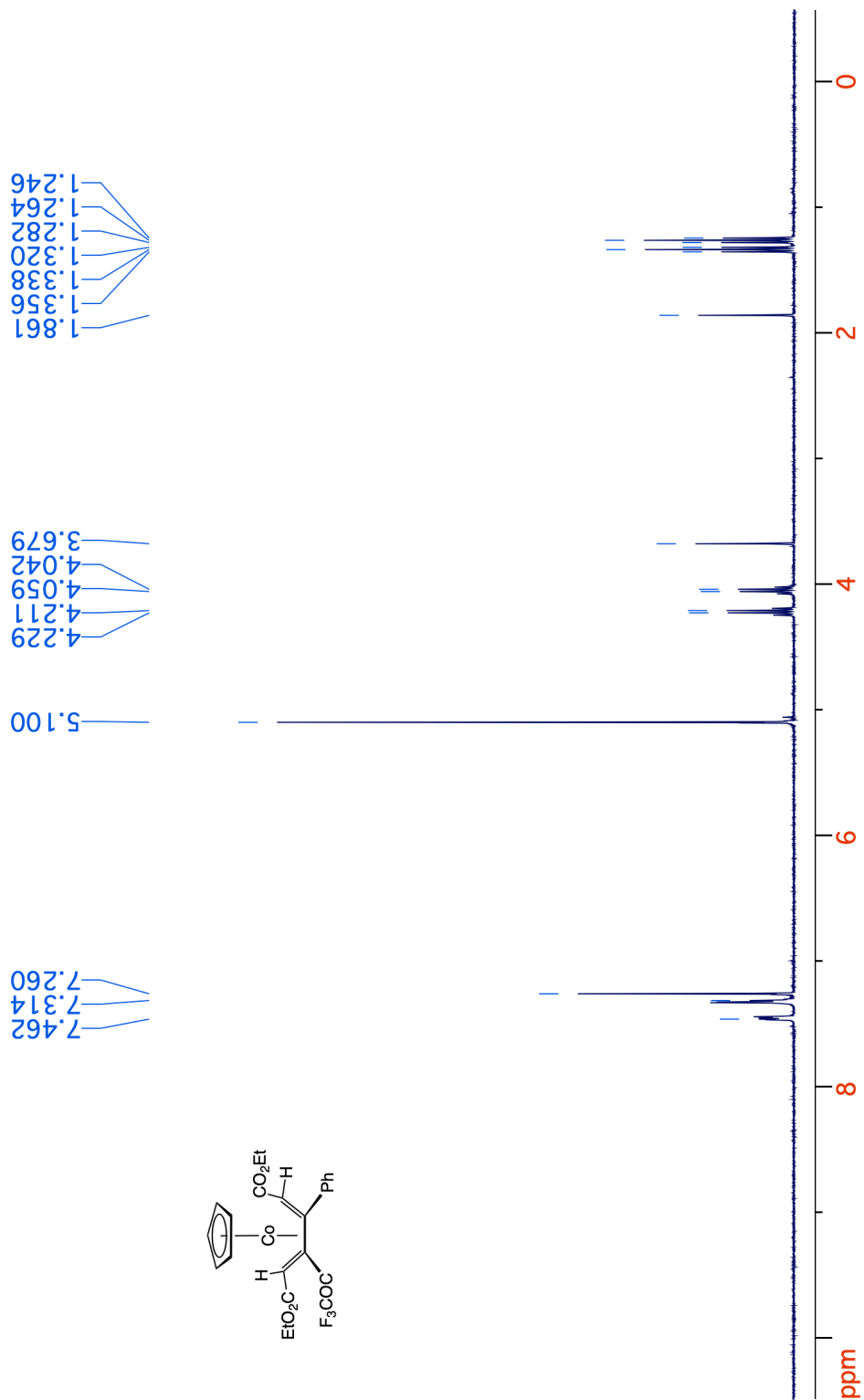
Figure 2-34. ^{1}H NMR spectrum (400 MHz, CDCl$_3$) of **26**.

Figure 2-35. $^{13}C\{^1H\}$ NMR spectrum (125 MHz, CDCl$_3$) of **26**.
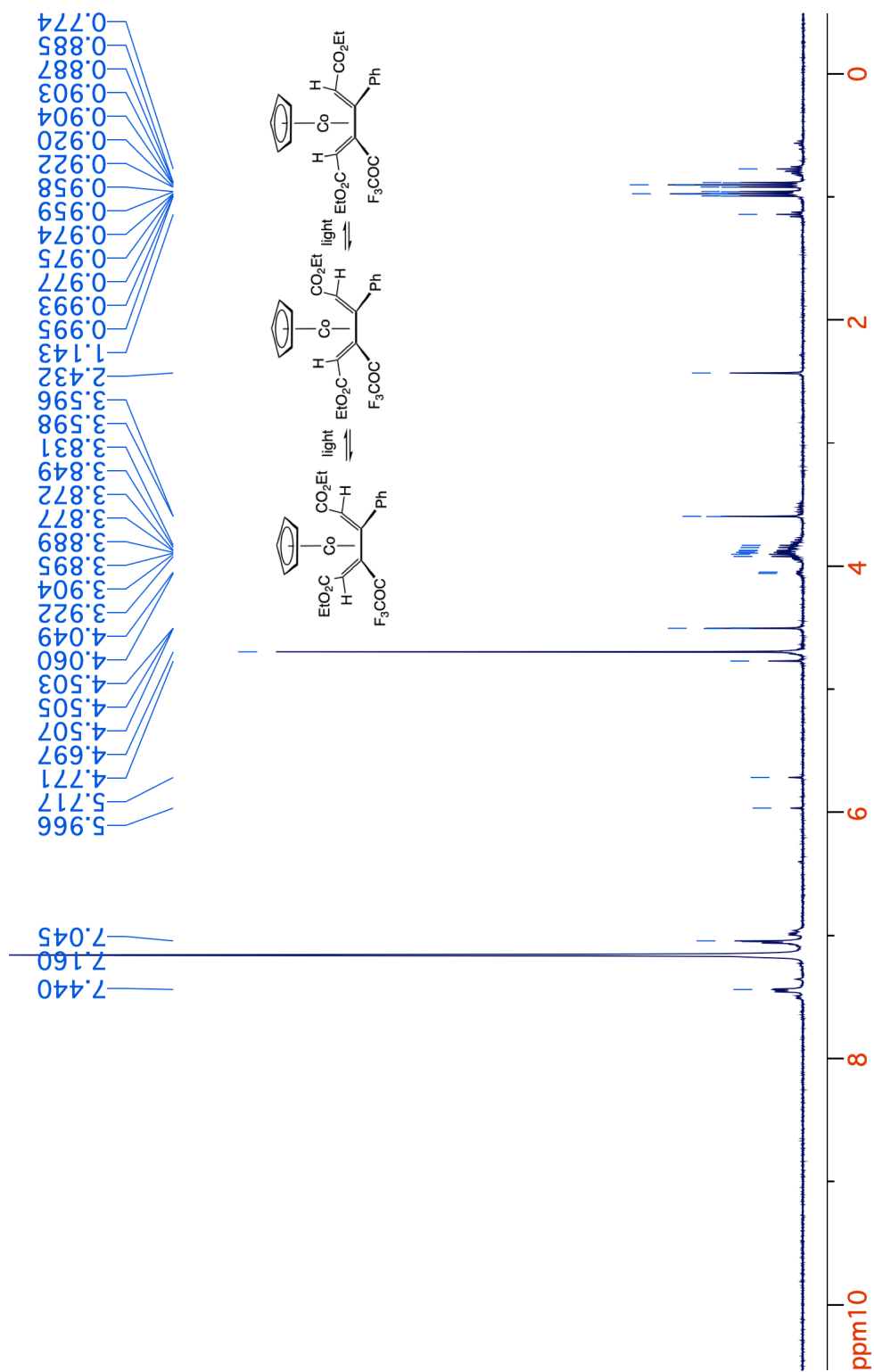
Figure 2-36. ^{1}H NMR spectrum (400 MHz, C_6D_6) of exposing **26** to light for 40 days.
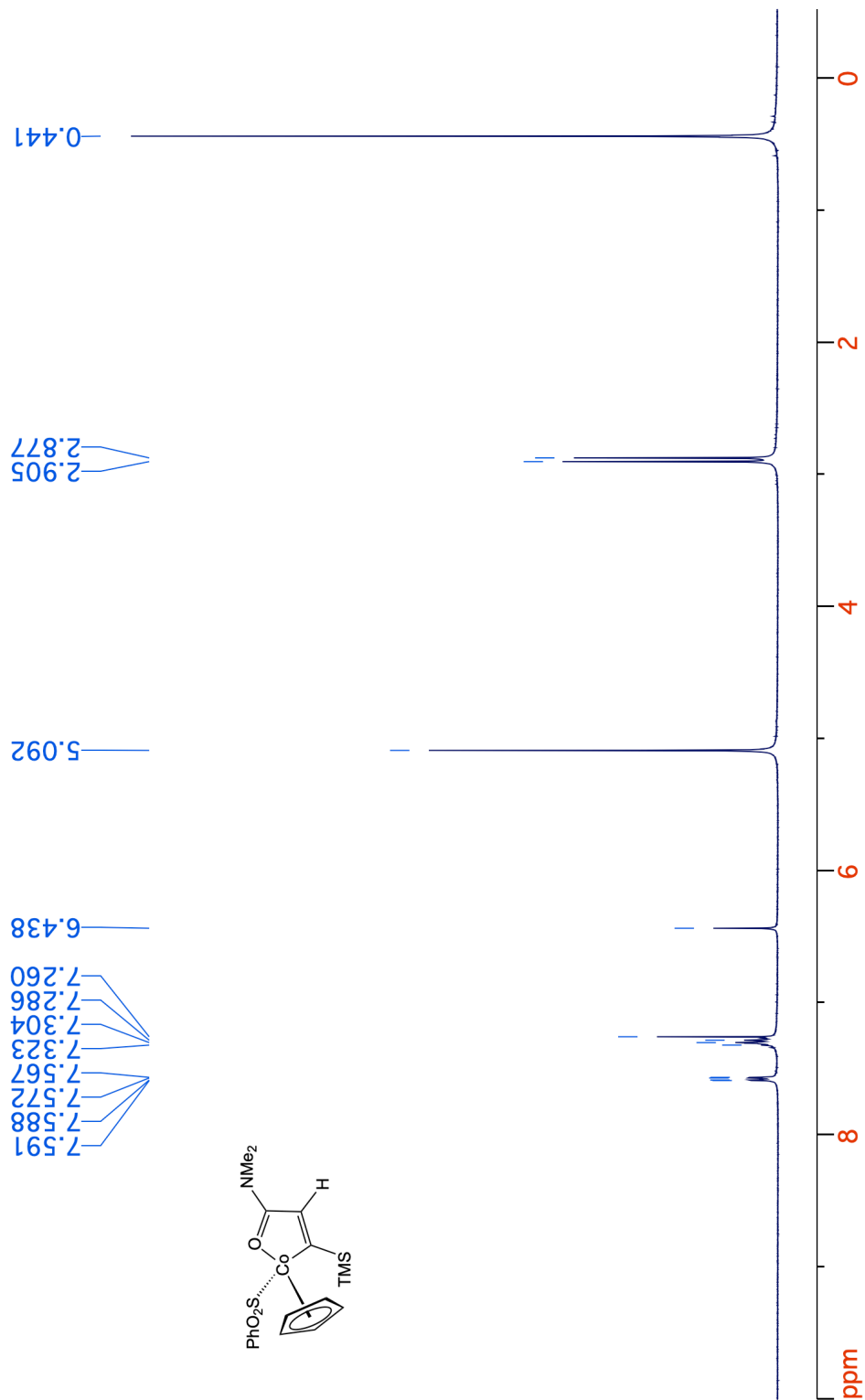
Figure 2-37. ^{1}H NMR spectrum (400 MHz, CDCl$_3$) of **49**.
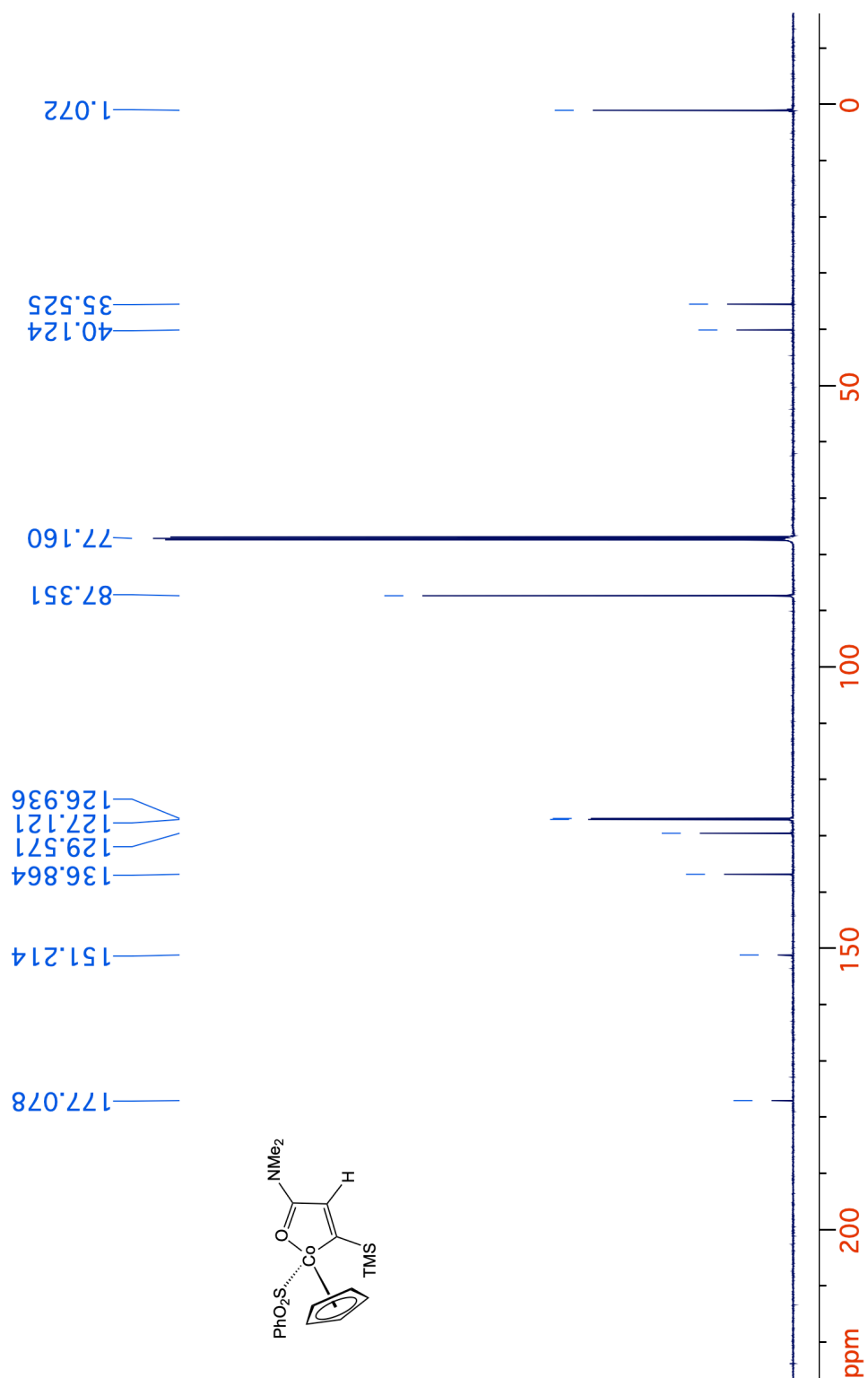
Figure 2-38. $^{13}C\{^1H\}$ NMR spectrum (125 MHz, CDCl$_3$) of **49**.

Figure 2-39. ^{1}H NMR spectrum (400 MHz, CDCl$_3$) of **50**.

1.268
1.287
1.313
1.331
1.357
1.361
1.461
1.479
1.498
1.517
2.414

3.002
3.129

4.936

6.742
7.203
7.222
7.223
7.260
7.713
7.733
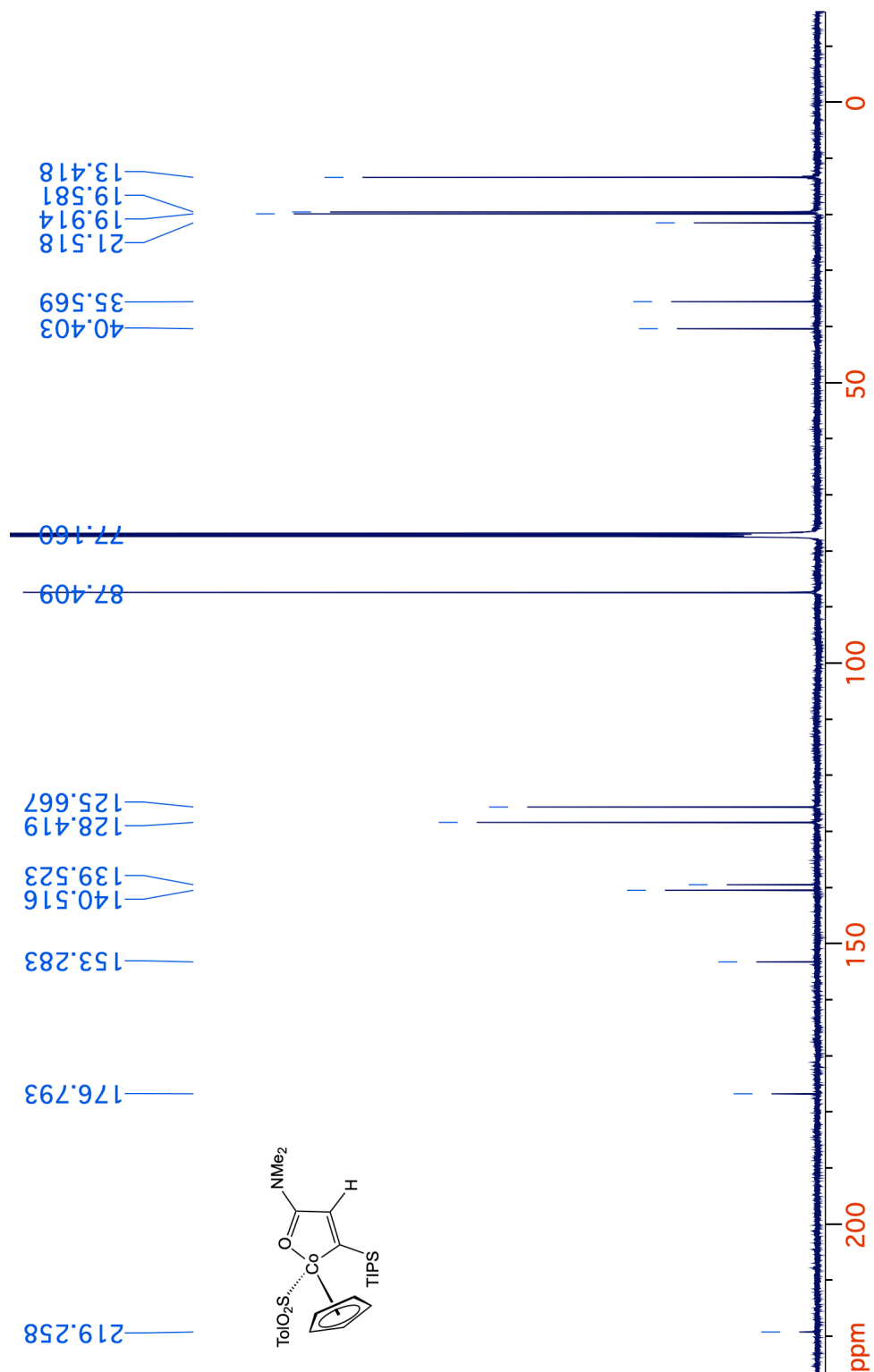
Figure 2-40. $^{13}C\{^1H\}$ NMR spectrum (125 MHz, CDCl$_3$) of **50**.
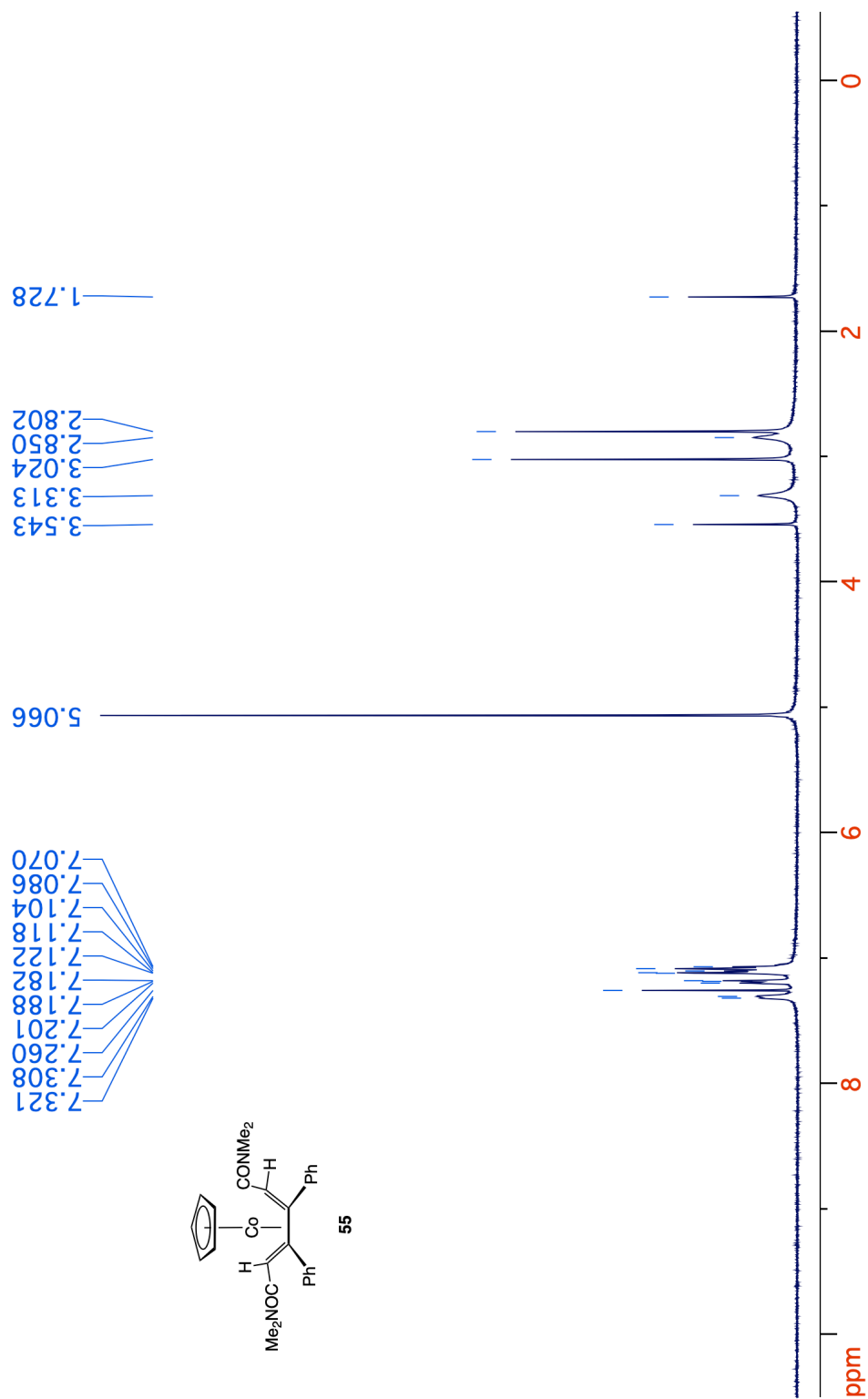
Figure 2-41. ^{1}H NMR spectrum (400 MHz, CDCl$_3$) of **55**.

35.833
37.886
40.644
43.158
77.160
83.848
95.573
104.399
126.590
126.823
127.017
127.565
130.587
131.629
137.654
140.650
172.426
173.746
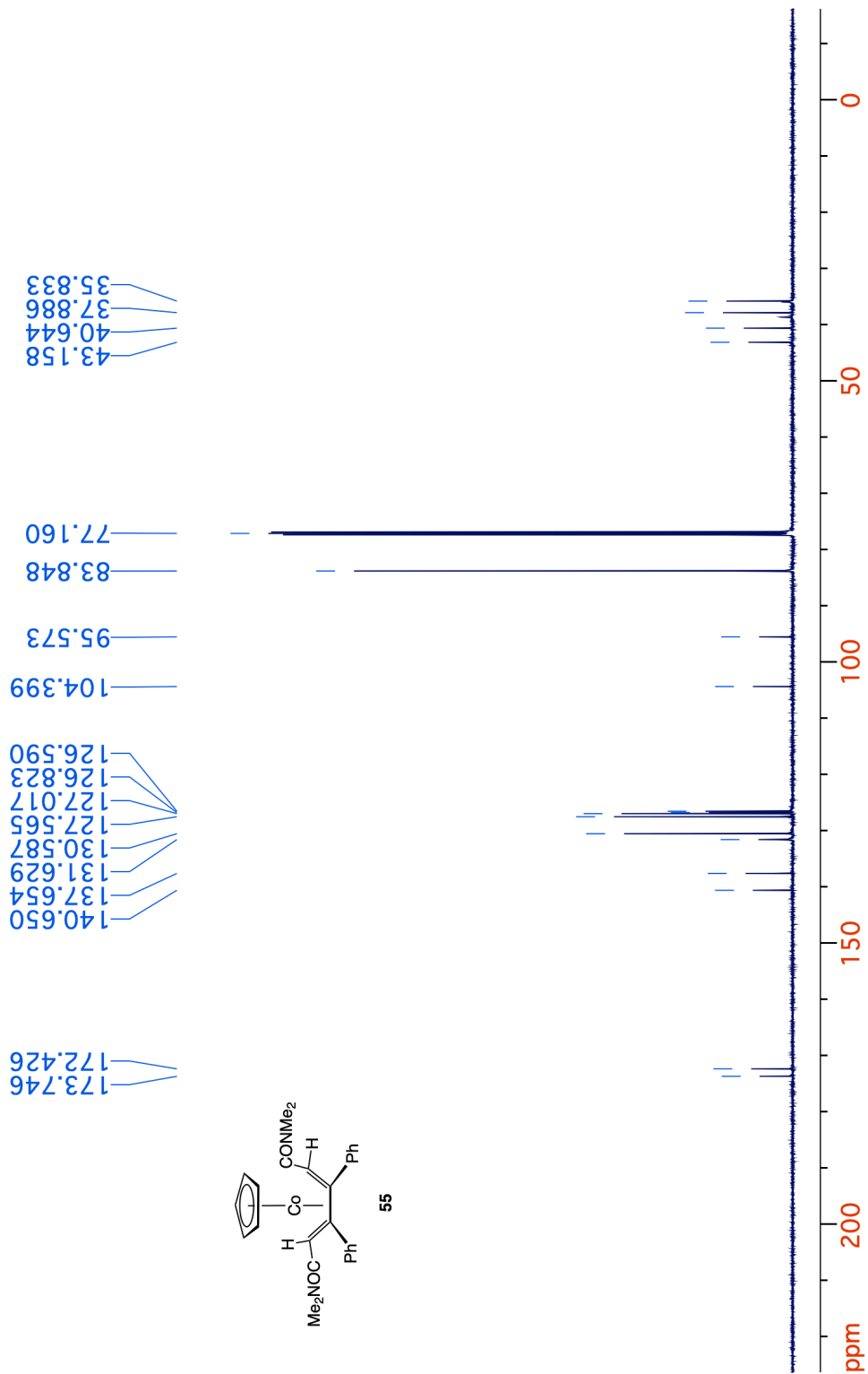
Figure 2-42. $^{13}C\{^1H\}$ NMR spectrum (125 MHz, CDCl$_3$) of **55**.

0.496

1.205
1.223
1.241
1.439

2.410
2.487

3.530
3.688
3.899
3.908
3.916
3.926
3.934
3.944
3.952
3.962
3.971

5.152

7.260
7.390
7.408
7.428
7.486
7.504
7.821
7.839
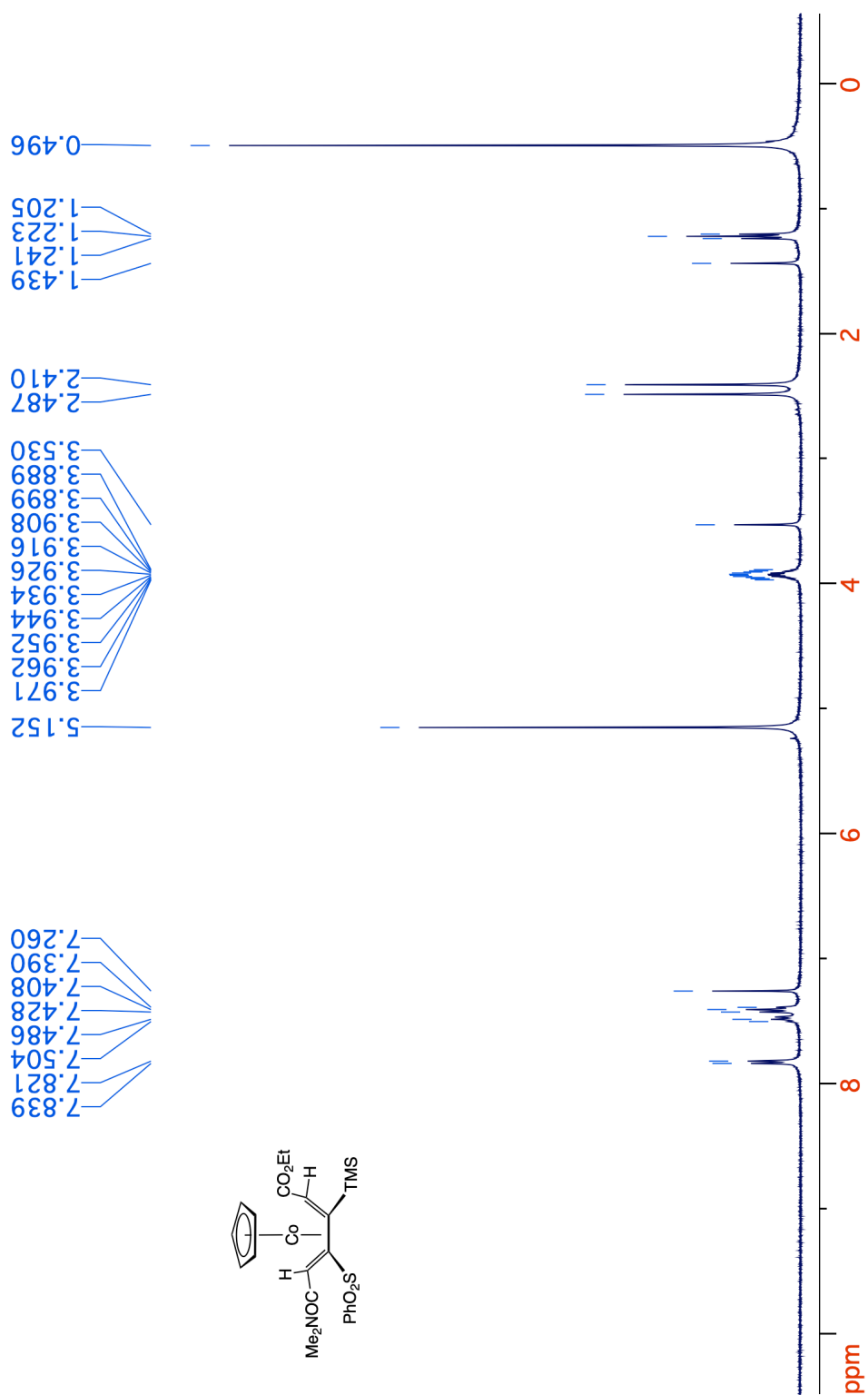
Figure 2-43. ^{1}H NMR spectrum (400 MHz, CDCl$_3$) of **57**.

174
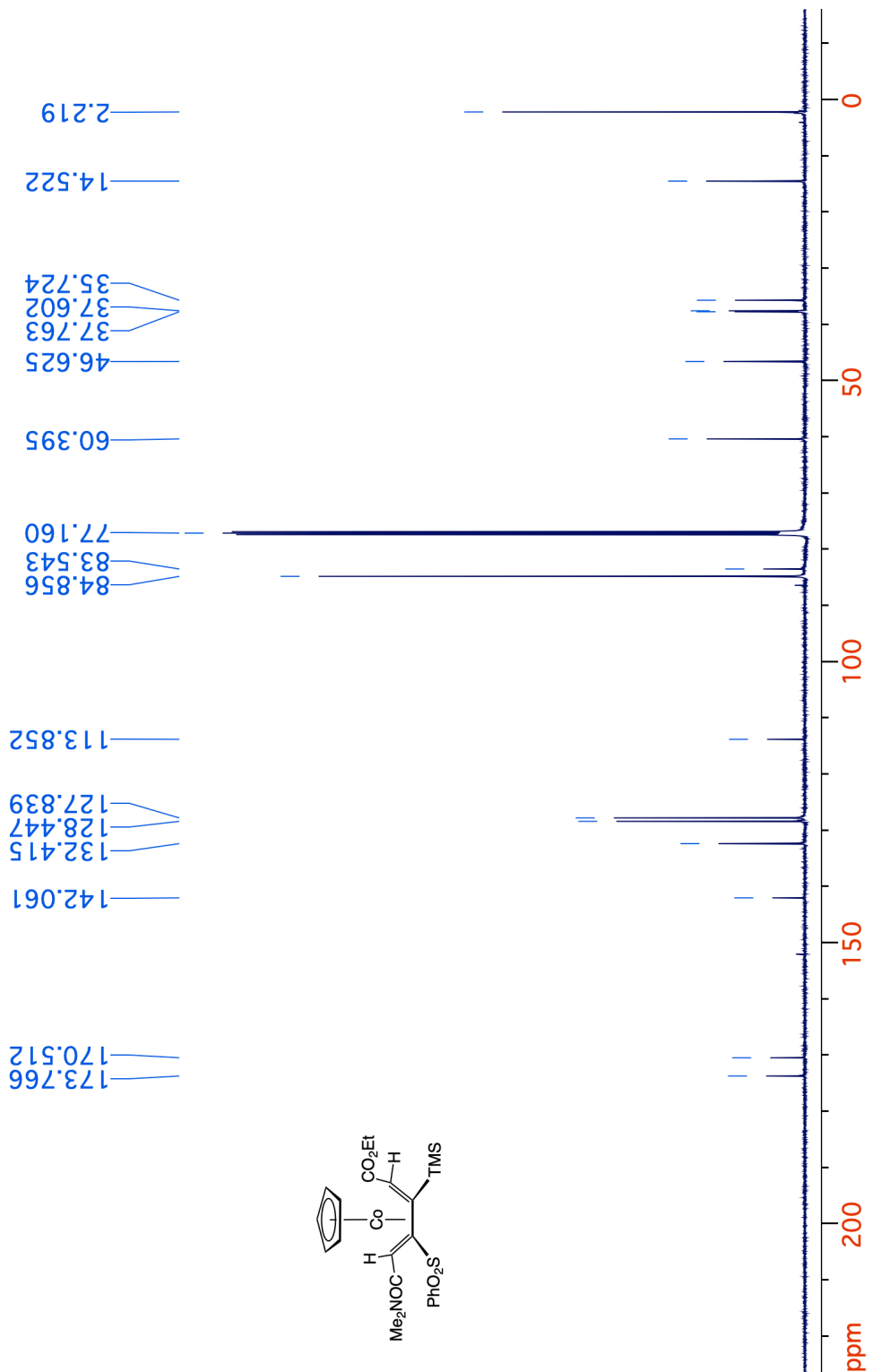
Figure 2-44. $^{13}C\{^1H\}$ NMR spectrum (125 MHz, CDCl$_3$) of **57**.

2.219
14.522
35.724
37.602
37.763
46.625
60.395
77.160
83.543
84.856
113.852
127.839
128.447
132.415
142.061
170.512
173.766
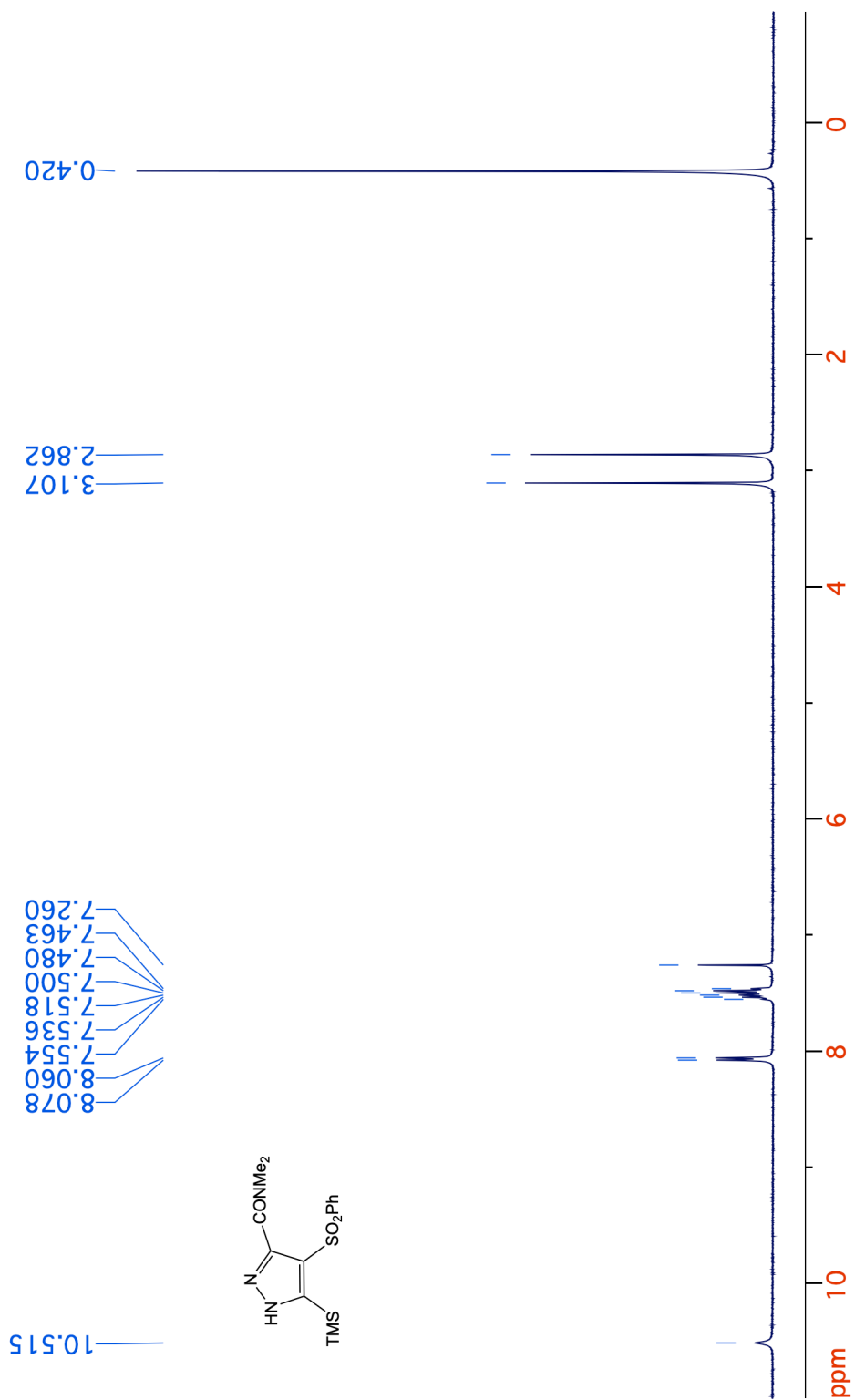
Figure 2-45. ^{1}H NMR spectrum (400 MHz, CDCl$_3$) of **59**.
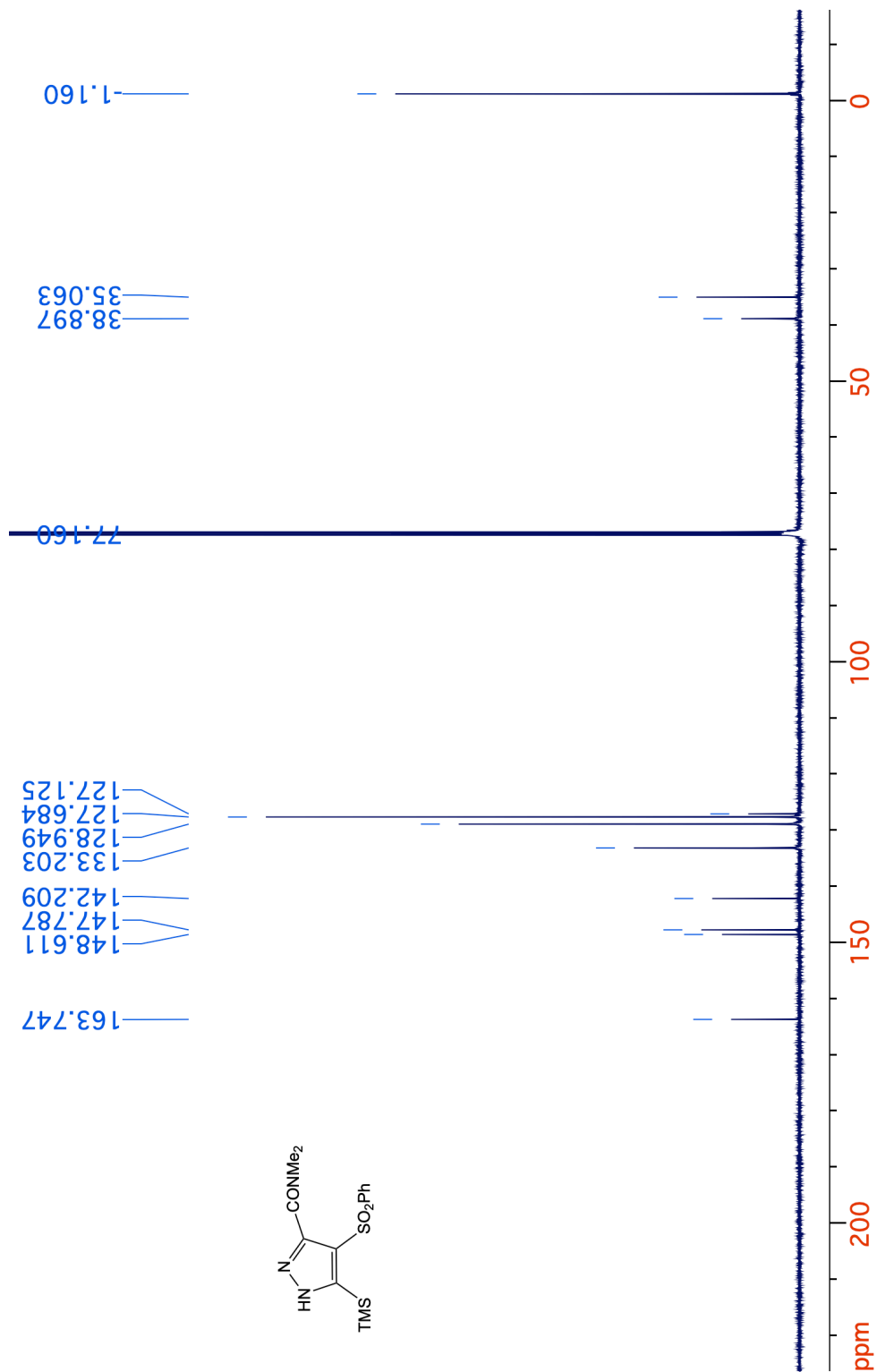
Figure 2-46. $^{13}C\{^1H\}$ NMR spectrum (125 MHz, CDCl$_3$) of **59**.

-1.160

35.063
38.897

77.160

127.125
127.684
128.949
133.203
142.209
147.787
148.611

163.747

CONMe$_2$
SO$_2$Ph
TMS
HN
N

1.203
1.221
1.238

2.824
2.827
2.831
2.834
3.752
3.770
3.779
3.787
3.797
3.805
3.814
3.832
3.901
3.919
3.928
3.937
3.946
3.955
3.964
3.981
4.360
5.088

7.260
7.264
7.384
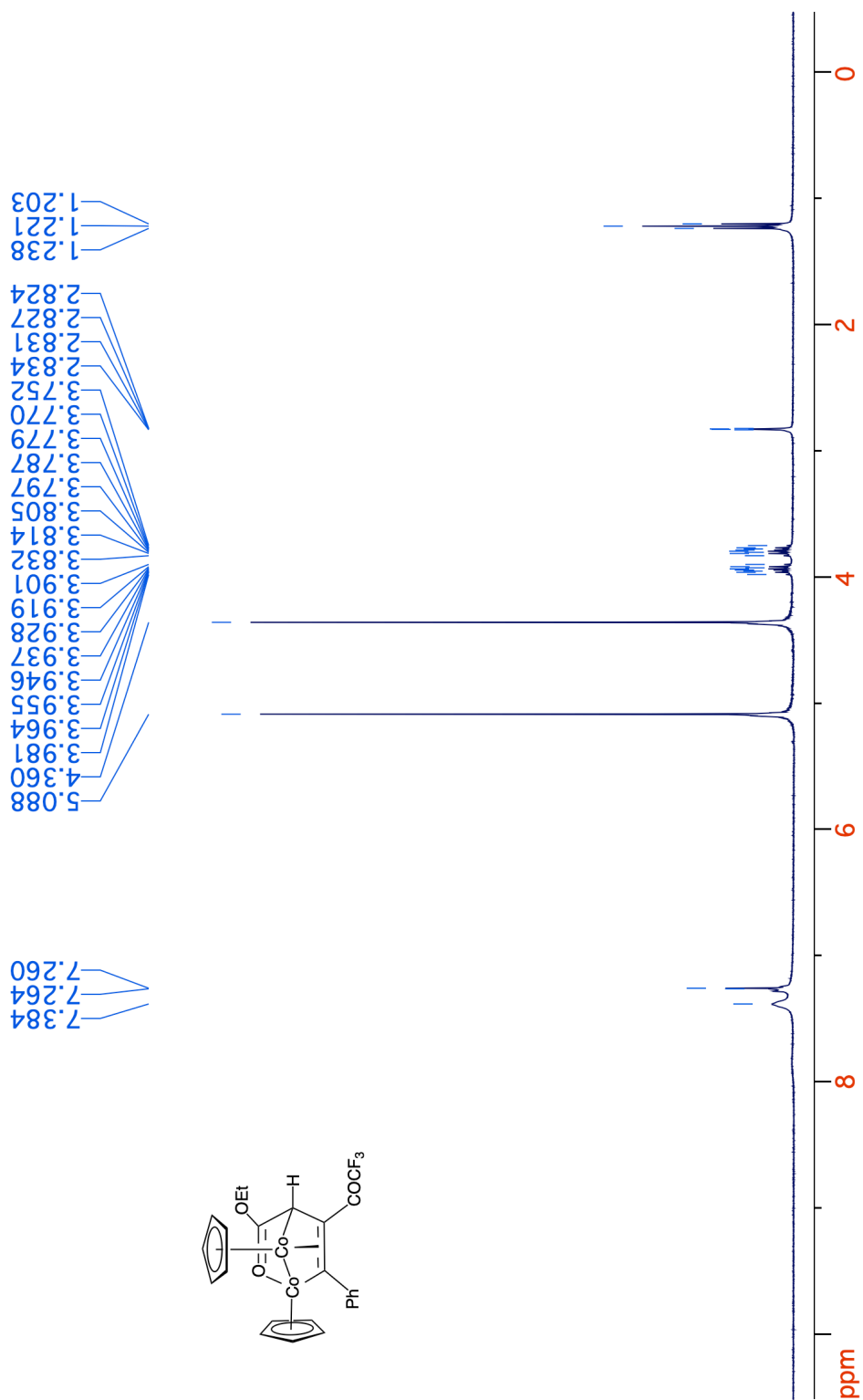
Figure 2-47. ^{1}H NMR spectrum (400 MHz, CDCl$_3$) of **62**.

14.045
26.609
62.845
77.160
79.985
80.667
88.837
112.387
114.726
117.063
119.402
124.507
126.718
127.806
156.584
174.827
184.465
187.048
187.316
187.583
187.851

112.387
114.726
117.063
119.402

187.048
187.316
187.583
187.851
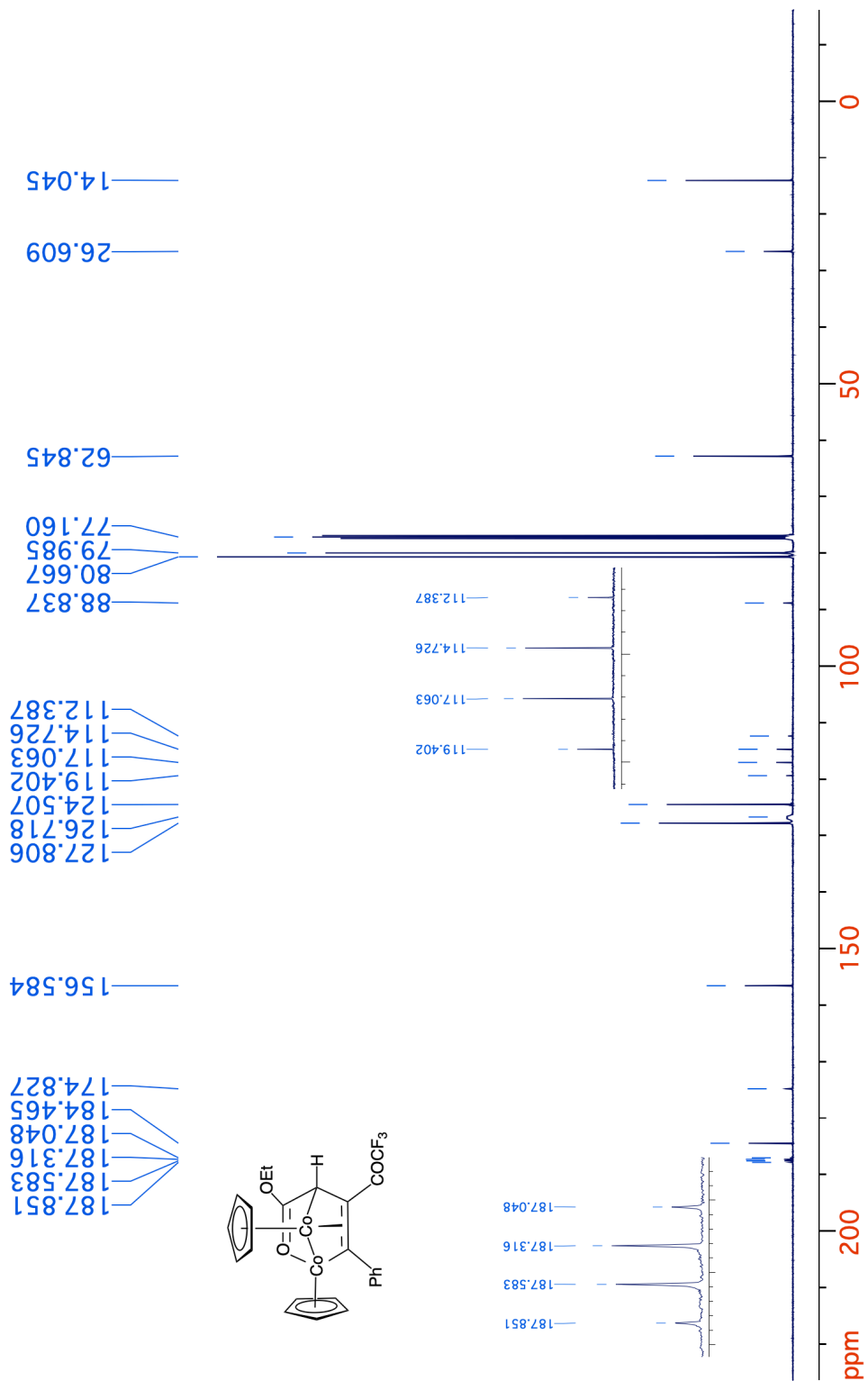
Figure 2-48. ^{13}C{^{1}H} NMR spectrum (125 MHz, CDCl$_3$) of **62**.
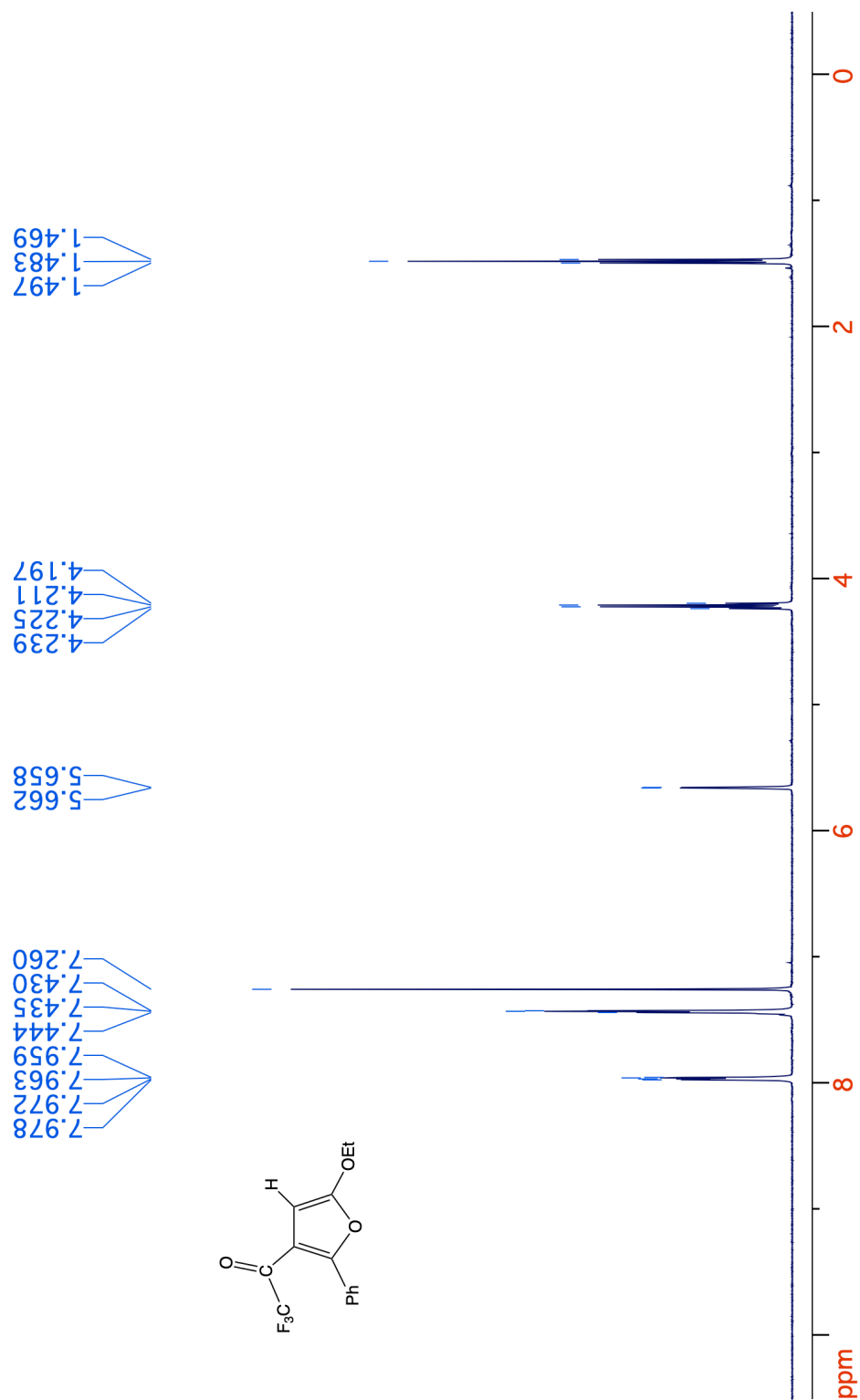
Figure 2-49. ^{1}H NMR spectrum (500 MHz, CDCl$_3$) of **63**.
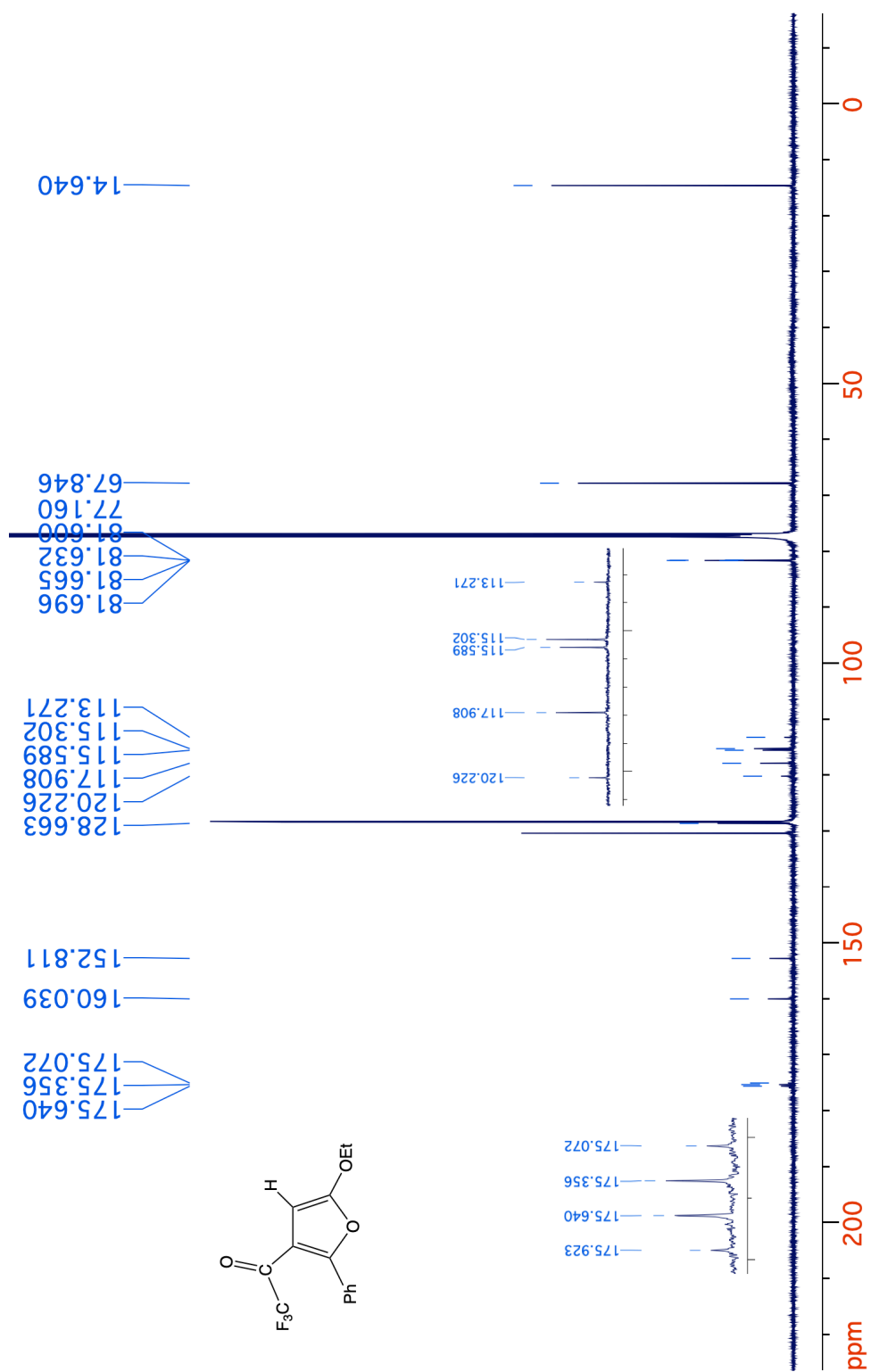
Figure 2-50. $^{13}C\{^{1}H\}$ NMR spectrum (125 MHz, CDCl$_3$) of **63**.

181
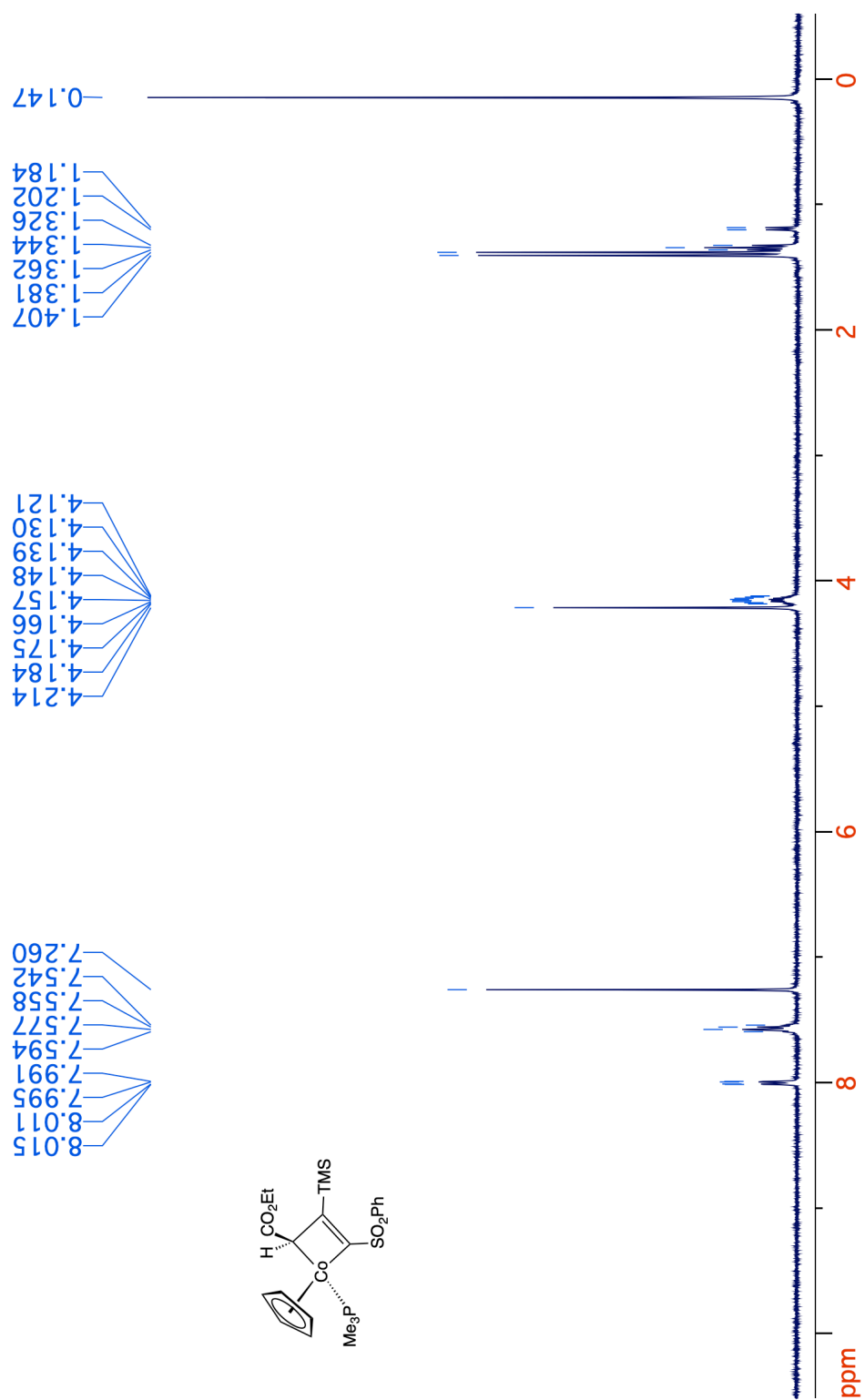
Figure 2-51. ^{1}H NMR spectrum (400 MHz, CDCl$_3$) of **77**.
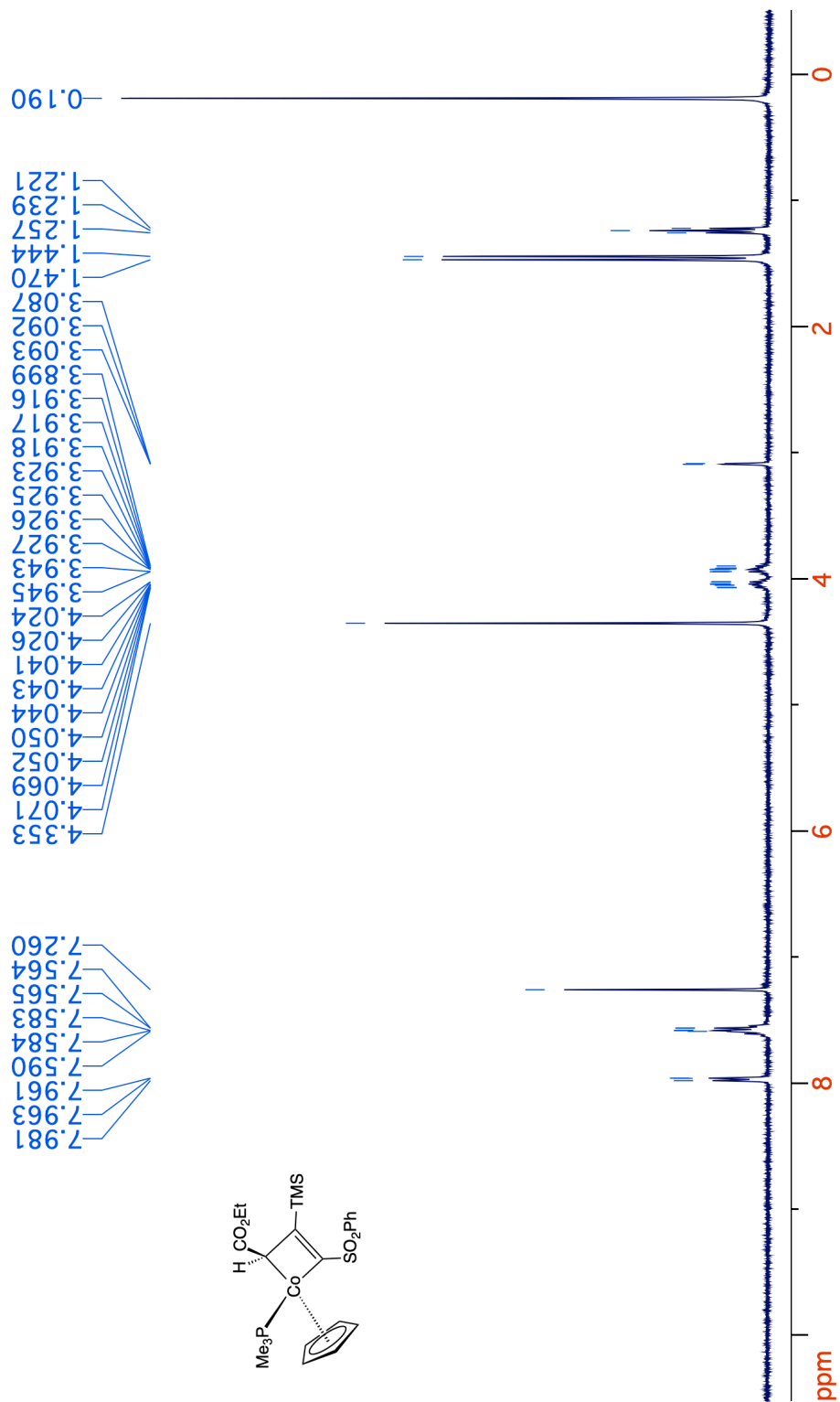
Figure 2-52. ^{1}H NMR spectrum (400 MHz, CDCl$_3$) of **78**.
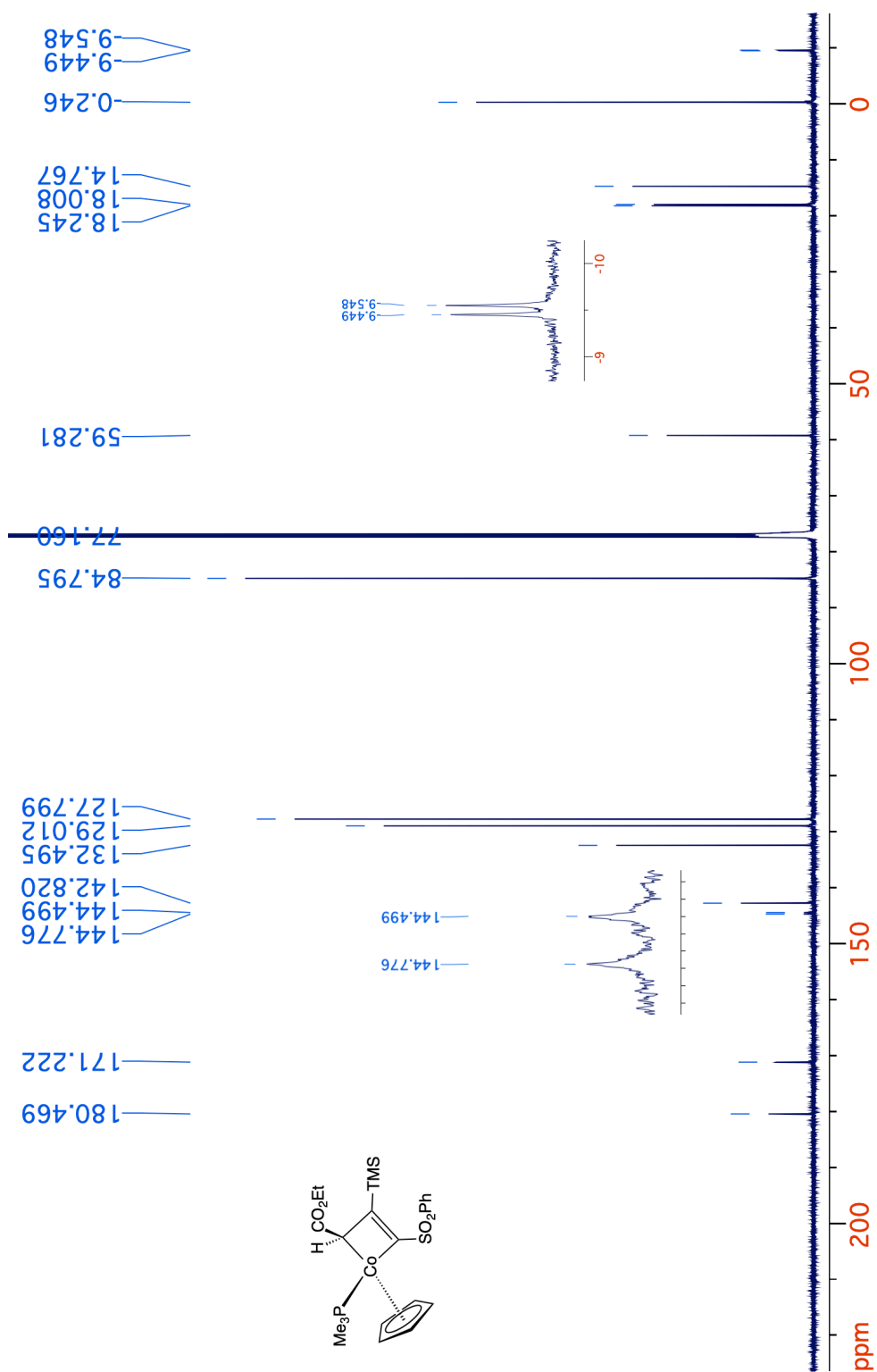
Figure 2-53. $^{13}C\{^1H\}$ NMR spectrum (125 MHz, CDCl$_3$) of **78**.
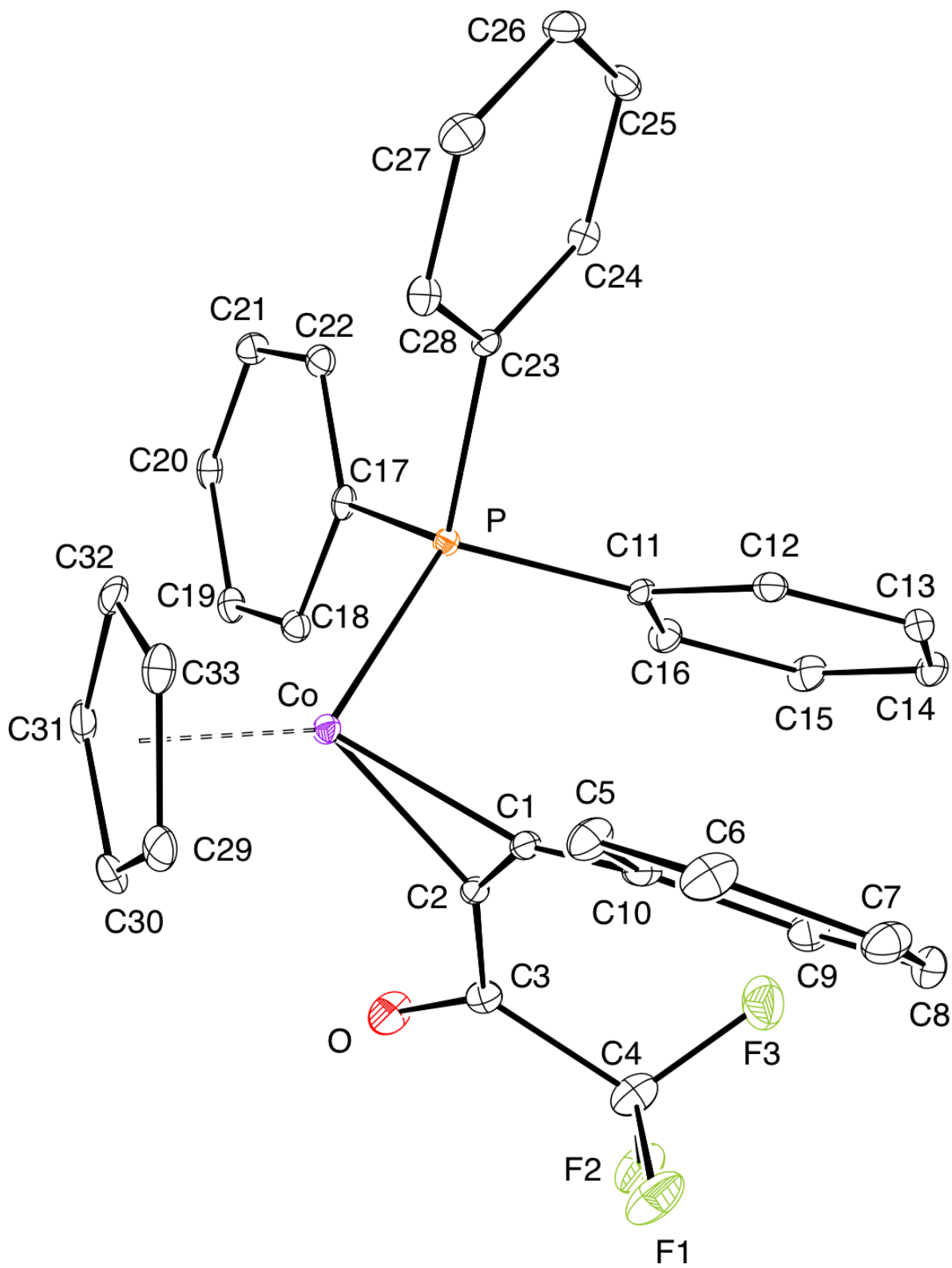
Figure 2-54. ORTEP view of complex **18**. Ellipsoids shown at 30% probability. Most hydrogens are omitted for clarity.

Table 2-7. Crystal data and structure refinement for complex **18**.

Identification code	pq_430_a
Empirical formula	C33 H25 Co F3 O P
Formula weight	584.43
Temperature	100.0 K
Wavelength	0.71073 Å
Crystal system	Monoclinic
Space group	P 1 21 1
Unit cell dimensions	a = 10.6429(4) Å $\alpha = 90°$.
	b = 15.8260(5) Å $\beta = 108.2950(10)°$.
	c = 16.6412(5) Å $\gamma = 90°$.
Volume	2661.27(15) Å^3
Z	4
Density (calculated)	1.459 Mg/m^3
Absorption coefficient	0.752 mm^{-1}
F(000)	1200
Crystal size	0.2 x 0.2 x 0.2 mm^3
Theta range for data collection	1.289 to 26.365°.
Index ranges	-13<=h<=13, -19<=k<=18, -20<=l<=20
Reflections collected	27284
Independent reflections	10388 [R(int) = 0.0232]
Completeness to theta = 26.000°	99.9 %
Absorption correction	Semi-empirical from equivalents
Max. and min. transmission	0.4908 and 0.4578
Refinement method	Full-matrix least-squares on F^2
Data / restraints / parameters	10388 / 1 / 703
Goodness-of-fit on F^2	1.041
Final R indices [I>2sigma(I)]	R1 = 0.0237, wR2 = 0.0591
R indices (all data)	R1 = 0.0249, wR2 = 0.0595
Absolute structure parameter	0.011(3)
Extinction coefficient	n/a
Largest diff. peak and hole	0.678 and -0.286 e.Å^{-3}
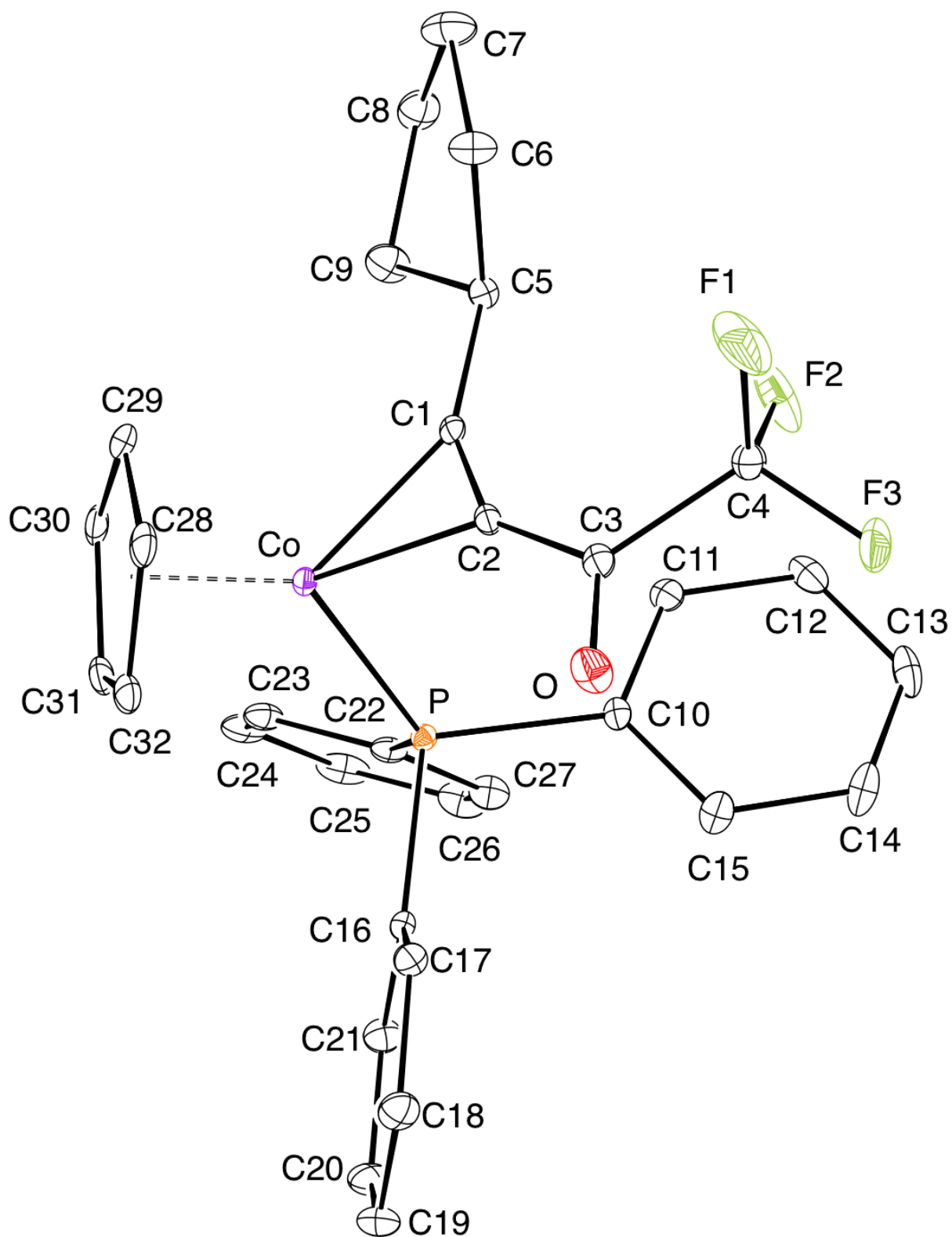
Figure 2-55. ORTEP view of complex **19**. Ellipsoids shown at 30% probability. Most hydrogens are omitted for clarity.

187

Table 2-8. Crystal data and structure refinement for complex **19**.

Identification code	pq_522_a
Empirical formula	C32 H29 Co F3 O P
Molecular formula	C32 H29 Co F3 O P
Formula weight	576.45
Temperature	100.0 K
Wavelength	0.71073 Å
Crystal system	Monoclinic
Space group	P 1 21/c 1
Unit cell dimensions	a = 8.2266(3) Å α = 90°.
	b = 16.6784(7) Å β = 93.204(2)°.
	c = 19.4513(9) Å γ = 90°.
Volume	2664.67(19) Å^3
Z	4
Density (calculated)	1.437 Mg/m^3
Absorption coefficient	0.750 mm^{-1}
F(000)	1192
Crystal size	0.2 x 0.2 x 0.075 mm^3
Crystal color, habit	violet plate
Theta range for data collection	3.158 to 25.349°.
Index ranges	-8<=h<=9, -20<=k<=19, -23<=l<=23
Reflections collected	22057
Independent reflections	4853 [R(int) = 0.0389, R(sigma) = 0.0341]
Completeness to theta = 25.242°	99.8 %
Absorption correction	Semi-empirical from equivalents
Max. and min. transmission	0.4903 and 0.4508
Refinement method	Full-matrix least-squares on F^2
Data / restraints / parameters	4853 / 0 / 343
Goodness-of-fit on F^2	1.020
Final R indices [I>2sigma(I)]	R1 = 0.0306, wR2 = 0.0644
R indices (all data)	R1 = 0.0416, wR2 = 0.0689
Extinction coefficient	n/a
Largest diff. peak and hole	0.368 and -0.288 e.Å^{-3}
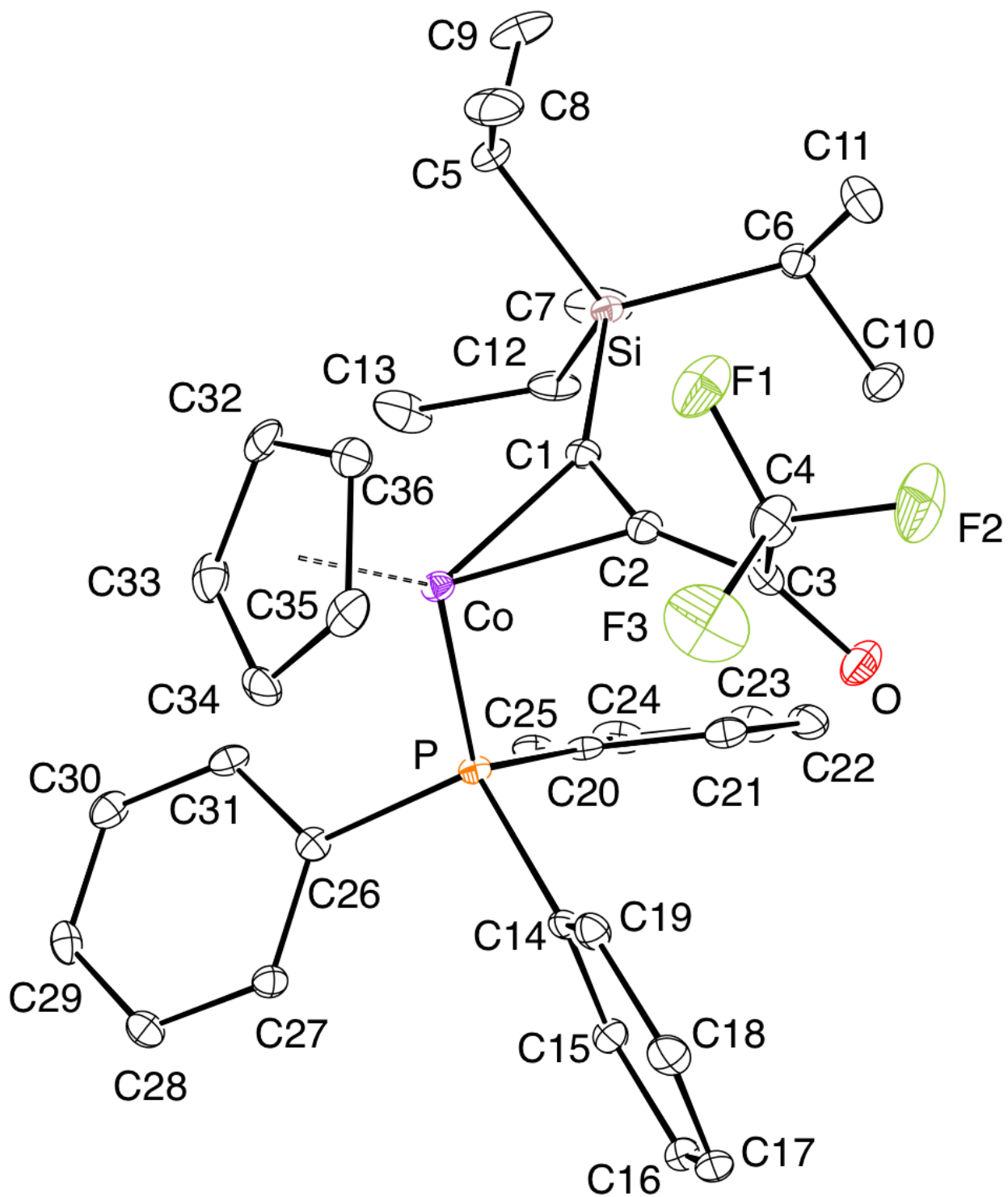
Figure 2-56. ORTEP view of complex **20**. Ellipsoids shown at 30% probability. Most hydrogens are omitted for clarity.

Table 2-9. Crystal data and structure refinement for complex **20**.

Identification code	oconn_pq_0527_0m_a
Empirical formula	C36 H41 Co F3 O P Si
Formula weight	664.68
Temperature	100.0 K
Wavelength	0.71073 Å
Crystal system	Monoclinic
Space group	C 1 2/c 1
Unit cell dimensions	a = 11.726(19) Å α = 90°.
	b = 17.60(3) Å β = 91.62(2)°.
	c = 32.30(5) Å γ = 90°.
Volume	6664(19) Å^3
Z	8
Density (calculated)	1.325 Mg/m^3
Absorption coefficient	0.643 mm^{-1}
F(000)	2784
Crystal size	0.2 x 0.3 x 0.07 mm^3
Theta range for data collection	1.261 to 25.414°.
Index ranges	-14<=h<=14, -18<=k<=21, -38<=l<=38
Reflections collected	61536
Independent reflections	6136 [R(int) = 0.0712]
Completeness to theta = 25.242°	99.9 %
Absorption correction	None
Max. and min. transmission	0.4901 and 0.4386
Refinement method	Full-matrix least-squares on F^2
Data / restraints / parameters	6136 / 0 / 414
Goodness-of-fit on F^2	1.078
Final R indices [I>2sigma(I)]	R1 = 0.0462, wR2 = 0.1277
R indices (all data)	R1 = 0.0697, wR2 = 0.1478
Extinction coefficient	n/a
Largest diff. peak and hole	0.449 and -0.439 e.Å^{-3}
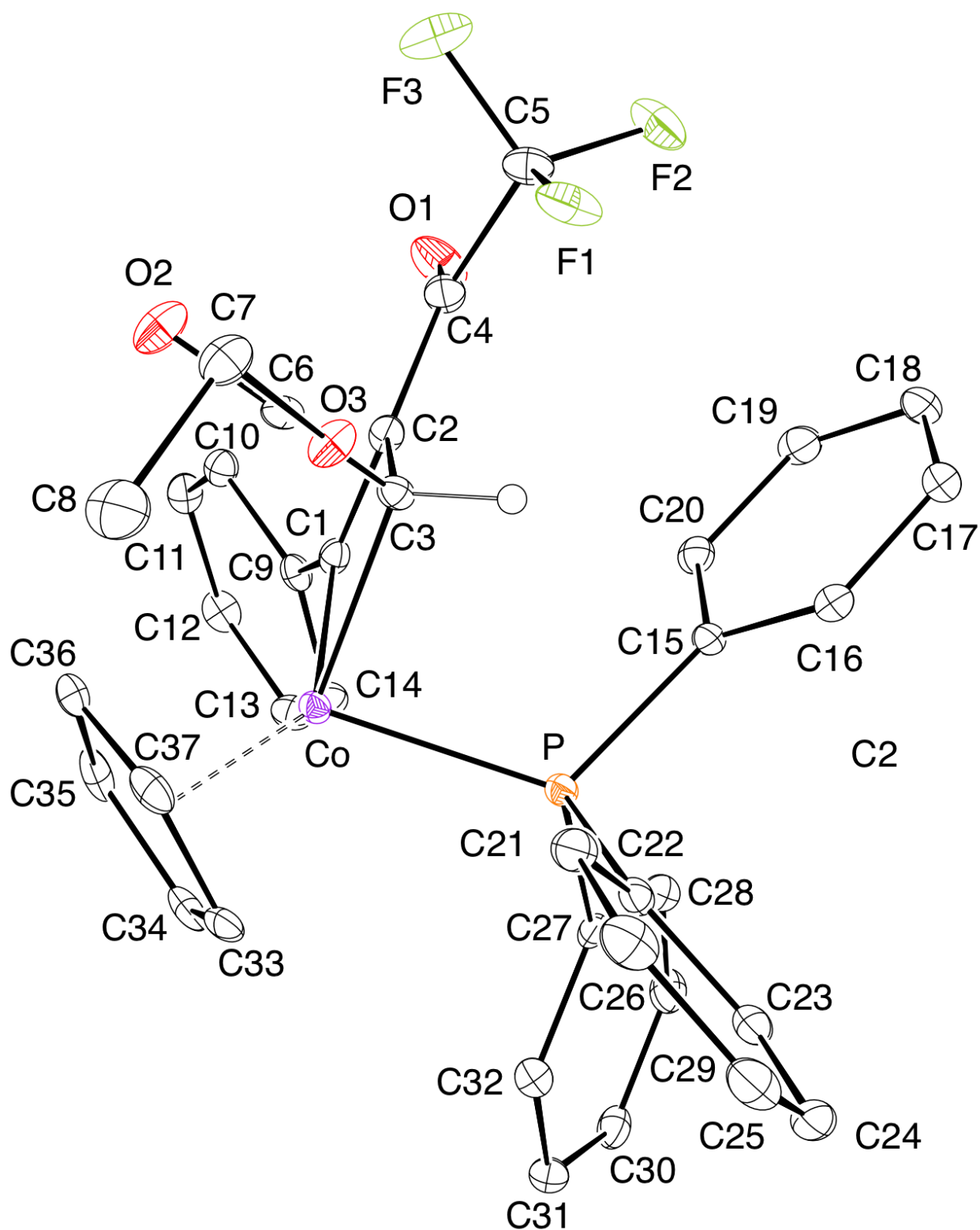
Figure 2-57. ORTEP view of complex **25**. Ellipsoids shown at 30% probability. Most hydrogens are omitted for clarity.

Table 2-10. Crystal data and structure refinement for complex **25**.

Identification code	cc_a
Empirical formula	C37 H31 Co F3 O3 P
Formula weight	670.52
Temperature	100.0 K
Wavelength	0.71073 Å
Crystal system	Monoclinic
Space group	C 1 c 1
Unit cell dimensions	a = 10.1042(3) Å $\quad\alpha = 90°$.
	b = 18.7596(6) Å $\quad\beta = 96.6680(10)°$.
	c = 16.2051(5) Å $\quad\gamma = 90°$.
Volume	3050.91(16) Å^3
Z	4
Density (calculated)	1.460 Mg/m^3
Absorption coefficient	0.671 mm^{-1}
F(000)	1384
Crystal size	0.231 x 0.087 x 0.076 mm^3
Theta range for data collection	2.171 to 26.390°.
Index ranges	-12<=h<=12, -23<=k<=23, -14<=l<=20
Reflections collected	22223
Independent reflections	4740 [R(int) = 0.0286]
Completeness to theta = 25.000°	100.0 %
Absorption correction	Semi-empirical from equivalents
Max. and min. transmission	0.2602 and 0.2287
Refinement method	Full-matrix least-squares on F^2
Data / restraints / parameters	4740 / 2 / 408
Goodness-of-fit on F^2	1.044
Final R indices [I>2sigma(I)]	R1 = 0.0207, wR2 = 0.0513
R indices (all data)	R1 = 0.0215, wR2 = 0.0518
Absolute structure parameter	0.000(11)
Extinction coefficient	n/a
Largest diff. peak and hole	0.341 and -0.142 e.Å^{-3}
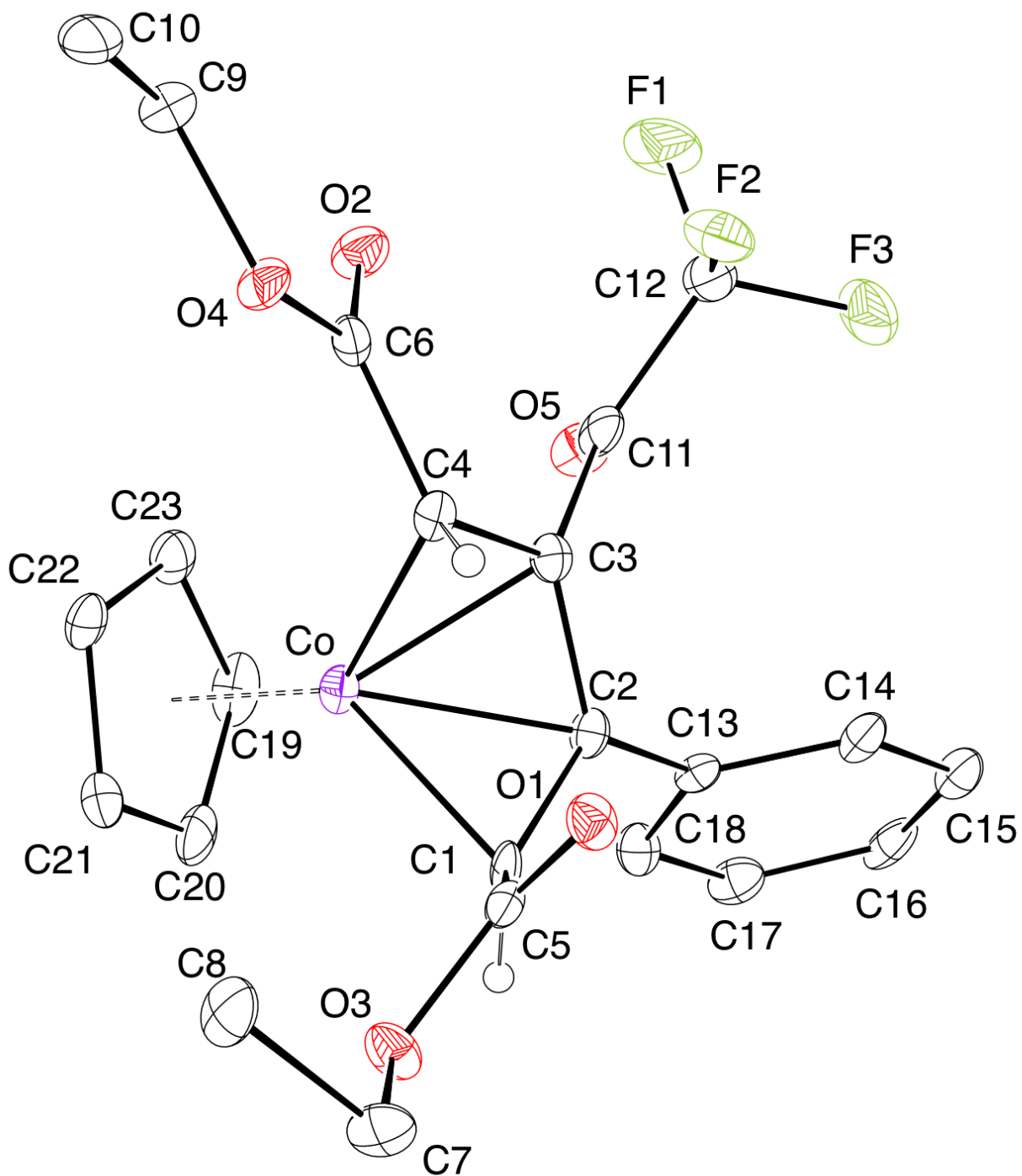
Figure 2-58. ORTEP view of complex **26**. Ellipsoids shown at 30% probability. Most hydrogens are omitted for clarity.

Table 2-11. Crystal data and structure refinement for complex **26**.

Identification code	pq_0444
Empirical formula	C23 H22 Co F3 O5
Molecular formula	C23 H22 Co F3 O5
Formula weight	494.33
Temperature	100.0 K
Wavelength	0.71073 Å
Crystal system	Monoclinic
Space group	P 1 21 1
Unit cell dimensions	a = 10.3761(4) Å $\quad \alpha = 90°$.
	b = 15.1059(7) Å $\quad \beta = 90.119(2)°$.
	c = 13.5255(5) Å $\quad \gamma = 90°$.
Volume	2119.99(15) Å^3
Z	4
Density (calculated)	1.549 Mg/m^3
Absorption coefficient	0.869 mm^{-1}
F(000)	1016
Crystal size	0.253 x 0.117 x 0.104 mm^3
Crystal color, habit	Red Block
Theta range for data collection	1.348 to 26.412°.
Index ranges	-12<=h<=12, -18<=k<=18, -16<=l<=16
Reflections collected	30814
Independent reflections	8574 [R(int) = 0.0402, R(sigma) = 0.0550]
Completeness to theta = 25.000°	100.0 %
Absorption correction	Semi-empirical from equivalents
Max. and min. transmission	0.0932 and 0.0667
Refinement method	Full-matrix least-squares on F^2
Data / restraints / parameters	8574 / 1 / 584
Goodness-of-fit on F^2	1.030
Final R indices [I>2sigma(I)]	R1 = 0.0351, wR2 = 0.0591
R indices (all data)	R1 = 0.0464, wR2 = 0.0628
Extinction coefficient	n/a
Largest diff. peak and hole	0.395 and -0.329 e.Å^{-3}
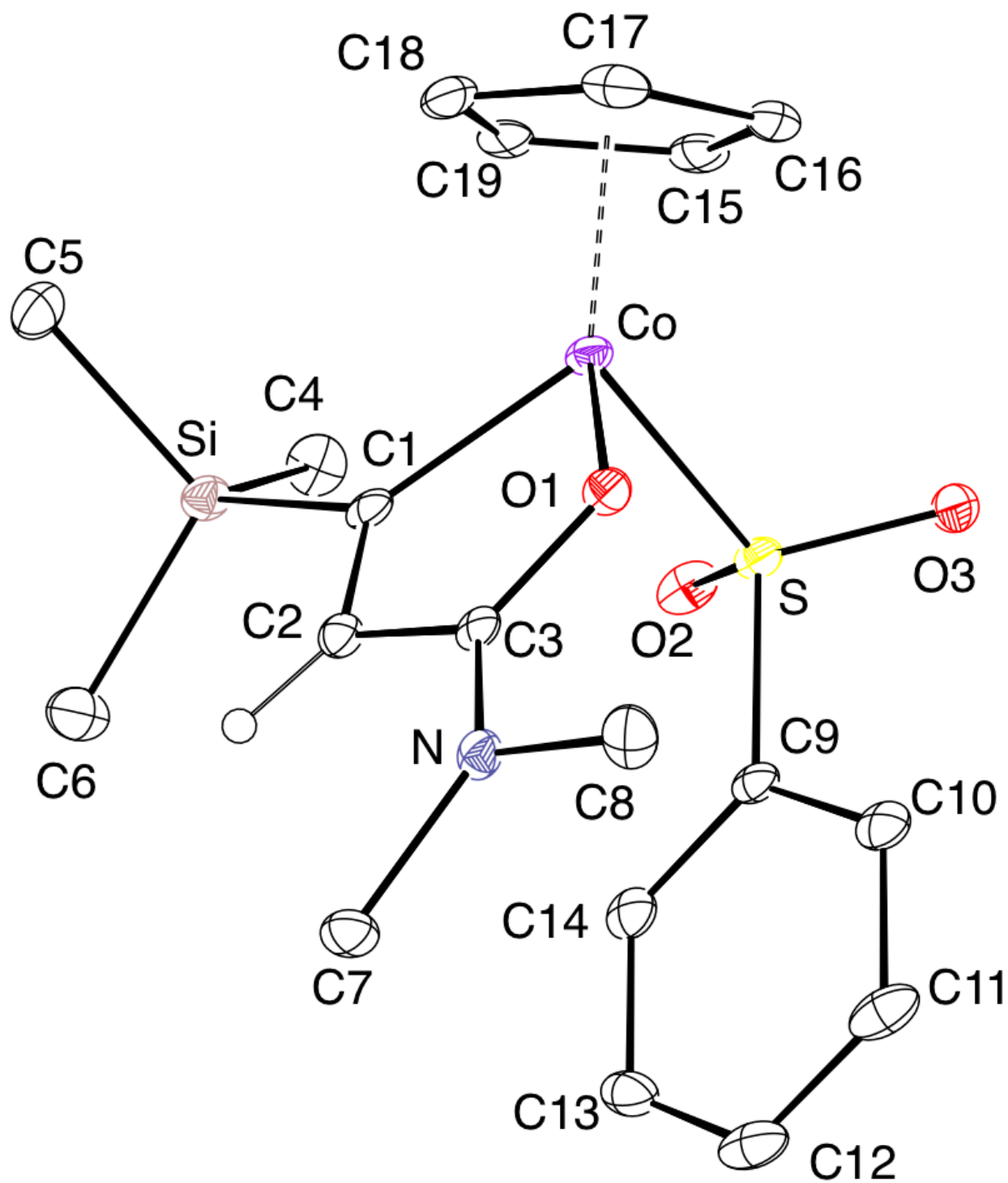
Figure 2-59. ORTEP view of complex **49**. Ellipsoids shown at 30% probability. Most hydrogens are omitted for clarity.

Table 2-12. Crystal data and structure refinement for complex **49**.

Identification code	PQ_0346
Empirical formula	C19 H28 Co N O4 S Si
Formula weight	453.50
Temperature	100.0 K
Wavelength	0.71073 Å
Crystal system	Monoclinic
Space group	P 1 21/c 1
Unit cell dimensions	a = 16.2803(15) Å $\quad \alpha = 90°$.
	b = 10.7770(9) Å $\quad \beta = 108.450(3)°$.
	c = 12.8021(12) Å $\quad \gamma = 90°$.
Volume	2130.7(3) Å^3
Z	4
Density (calculated)	1.414 Mg/m^3
Absorption coefficient	0.983 mm^{-1}
F(000)	952
Crystal size	0.127 x 0.087 x 0.064 mm^3
Theta range for data collection	2.304 to 25.341°.
Index ranges	-19<=h<=19, -12<=k<=12, -15<=l<=15
Reflections collected	18892
Independent reflections	3902 [R(int) = 0.0463]
Completeness to theta = 25.000°	100.0 %
Absorption correction	Semi-empirical from equivalents
Max. and min. transmission	0.7453 and 0.6427
Refinement method	Full-matrix least-squares on F^2
Data / restraints / parameters	3902 / 0 / 252
Goodness-of-fit on F^2	1.036
Final R indices [I>2sigma(I)]	R1 = 0.0386, wR2 = 0.0880
R indices (all data)	R1 = 0.0557, wR2 = 0.0964
Extinction coefficient	n/a
Largest diff. peak and hole	0.757 and -0.416 e.Å^{-3}
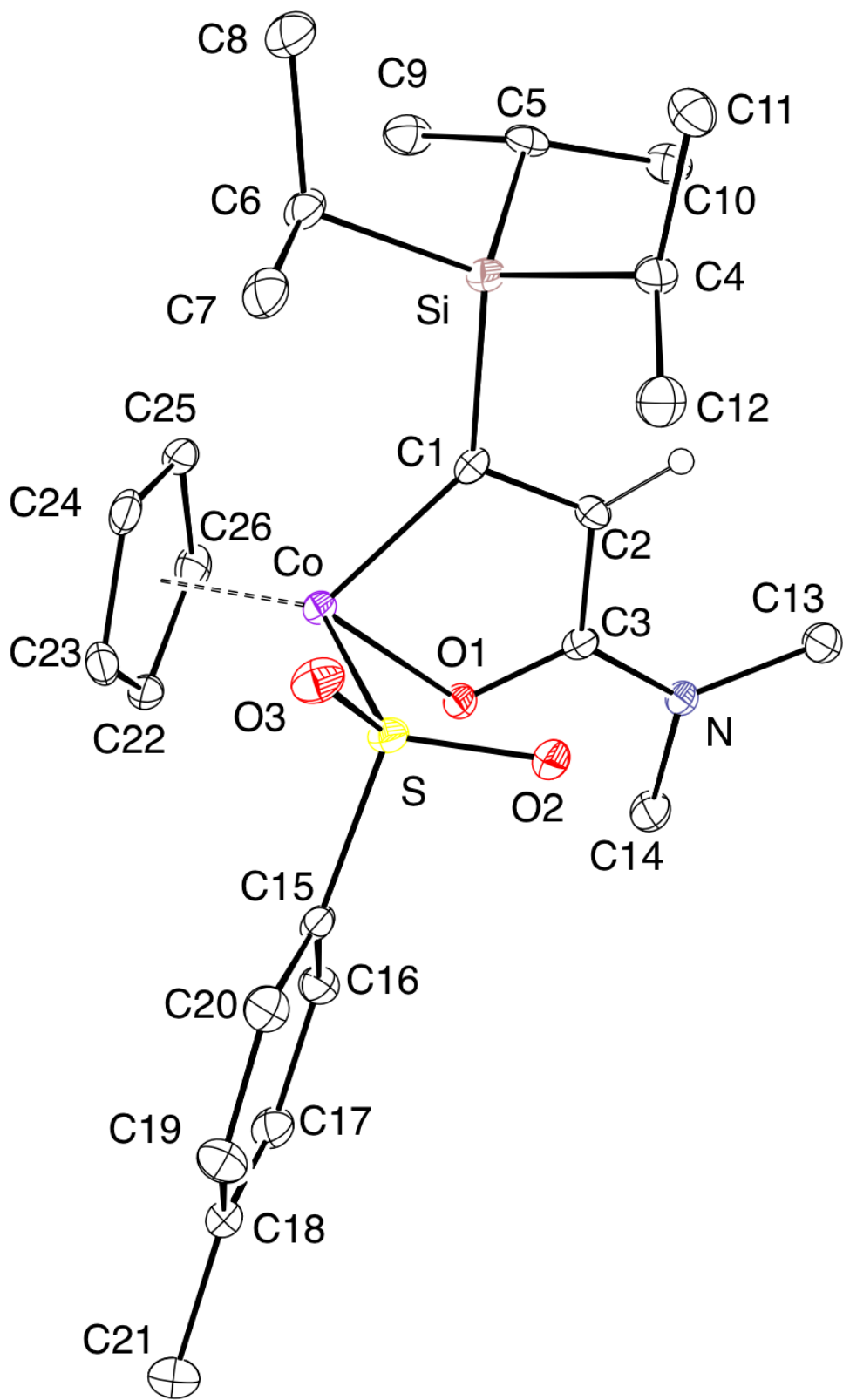
Figure 2-60. ORTEP view of complex **50**. Ellipsoids shown at 30% probability. Most hydrogens are omitted for clarity.

Table 2-13. Crystal data and structure refinement for complex **50**.

Identification code	PQ_0401
Empirical formula	C26 H40 Co N O3 S Si
Formula weight	533.67
Temperature	100.0 K
Wavelength	0.71073 Å
Crystal system	Triclinic
Space group	P-1
Unit cell dimensions	a = 7.643(2) Å α = 81.727(5)°.
	b = 10.748(3) Å β = 88.900(4)°.
	c = 16.521(5) Å γ = 85.548(4)°.
Volume	1338.9(7) Å^3
Z	2
Density (calculated)	1.324 Mg/m^3
Absorption coefficient	0.791 mm^{-1}
F(000)	568
Crystal size	0.157 x 0.131 x 0.082 mm^3
Theta range for data collection	1.246 to 25.388°.
Index ranges	-9<=h<=9, -12<=k<=12, -19<=l<=19
Reflections collected	24621
Independent reflections	8326 [R(int) = 0.0543]
Completeness to theta = 25.000°	99.9 %
Absorption correction	Semi-empirical from equivalents
Max. and min. transmission	0.091637 and 0.063680
Refinement method	Full-matrix least-squares on F^2
Data / restraints / parameters	8326 / 0 / 308
Goodness-of-fit on F^2	1.022
Final R indices [I>2sigma(I)]	R1 = 0.0494, wR2 = 0.0963
R indices (all data)	R1 = 0.0744, wR2 = 0.1058
Extinction coefficient	n/a
Largest diff. peak and hole	0.478 and -0.445 e.Å^{-3}
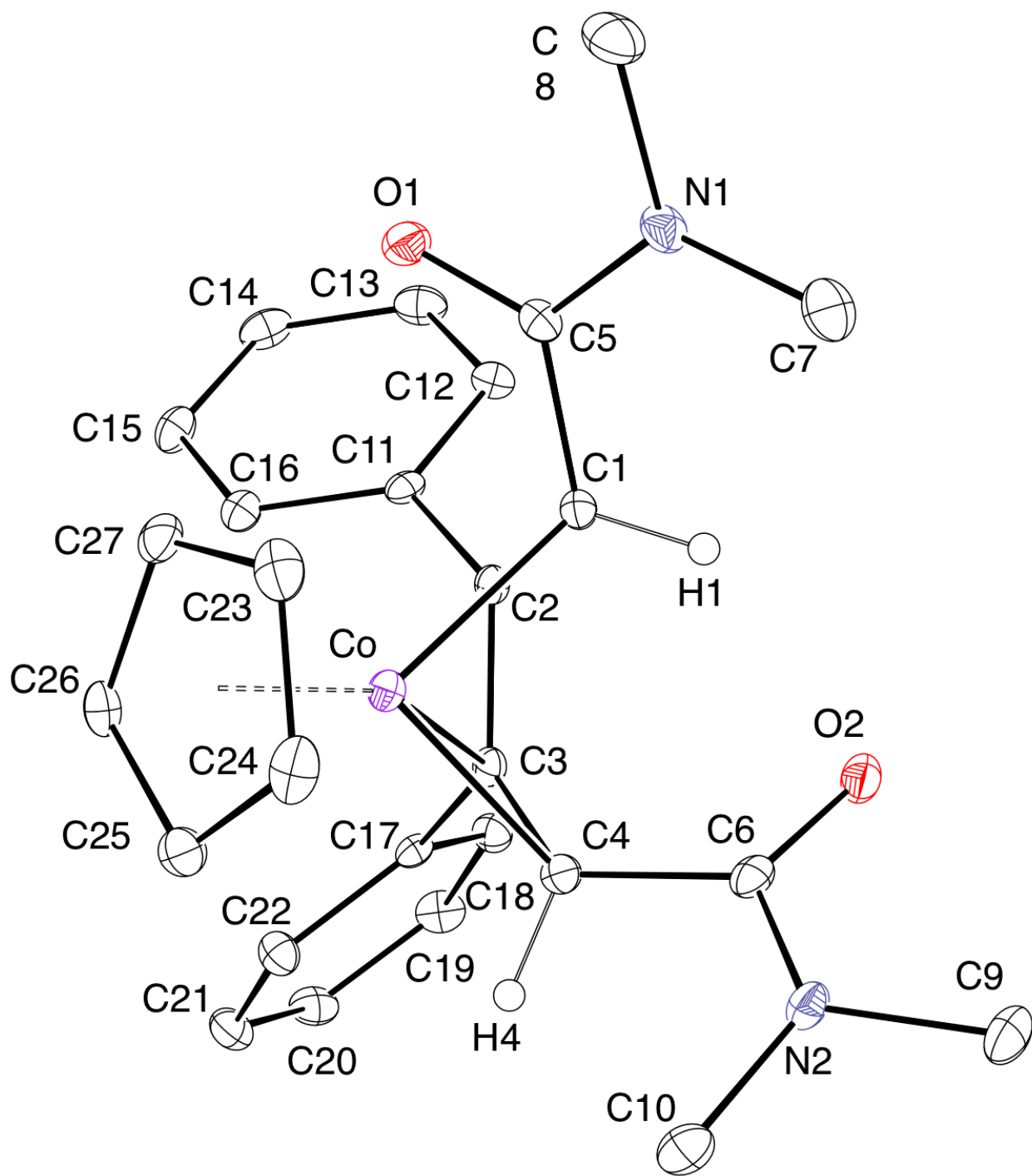
Figure 2-61. ORTEP view of complex **55**. Ellipsoids shown at 30% probability. Most hydrogens are omitted for clarity.

Table 2-14. Crystal data and structure refinement for complex **55**.

Identification code	PQ_0445
Empirical formula	C30.50 H33 Co N2 O2
Molecular formula	C27 H29 Co N2 O2, 0.5(C7 H8)
Formula weight	518.52
Temperature	100.0 K
Wavelength	0.71073 Å
Crystal system	Monoclinic
Space group	P 1 21/c 1
Unit cell dimensions	a = 34.70(2) Å α = 90°.
	b = 10.020(6) Å β = 108.896(7)°.
	c = 31.641(19) Å γ = 90°.
Volume	10409(11) Å^3
Z	16
Density (calculated)	1.323 Mg/m^3
Absorption coefficient	0.689 mm^{-1}
F(000)	4368
Crystal size	0.217 x 0.206 x 0.093 mm^3
Crystal color, habit	Dark Red Block
Theta range for data collection	1.917 to 25.584°.
Index ranges	-41<=h<=42, -12<=k<=12, -38<=l<=38
Reflections collected	139320
Independent reflections	19267 [R(int) = 0.0545, R(sigma) = 0.0340]
Completeness to theta = 25.000°	99.9 %
Absorption correction	Semi-empirical from equivalents
Max. and min. transmission	0.2590 and 0.2195
Refinement method	Full-matrix least-squares on F^2
Data / restraints / parameters	19267 / 0 / 1297
Goodness-of-fit on F^2	1.022
Final R indices [I>2sigma(I)]	R1 = 0.0335, wR2 = 0.0717
R indices (all data)	R1 = 0.0458, wR2 = 0.0767
Extinction coefficient	n/a
Largest diff. peak and hole	0.631 and -0.320 e.Å^{-3}
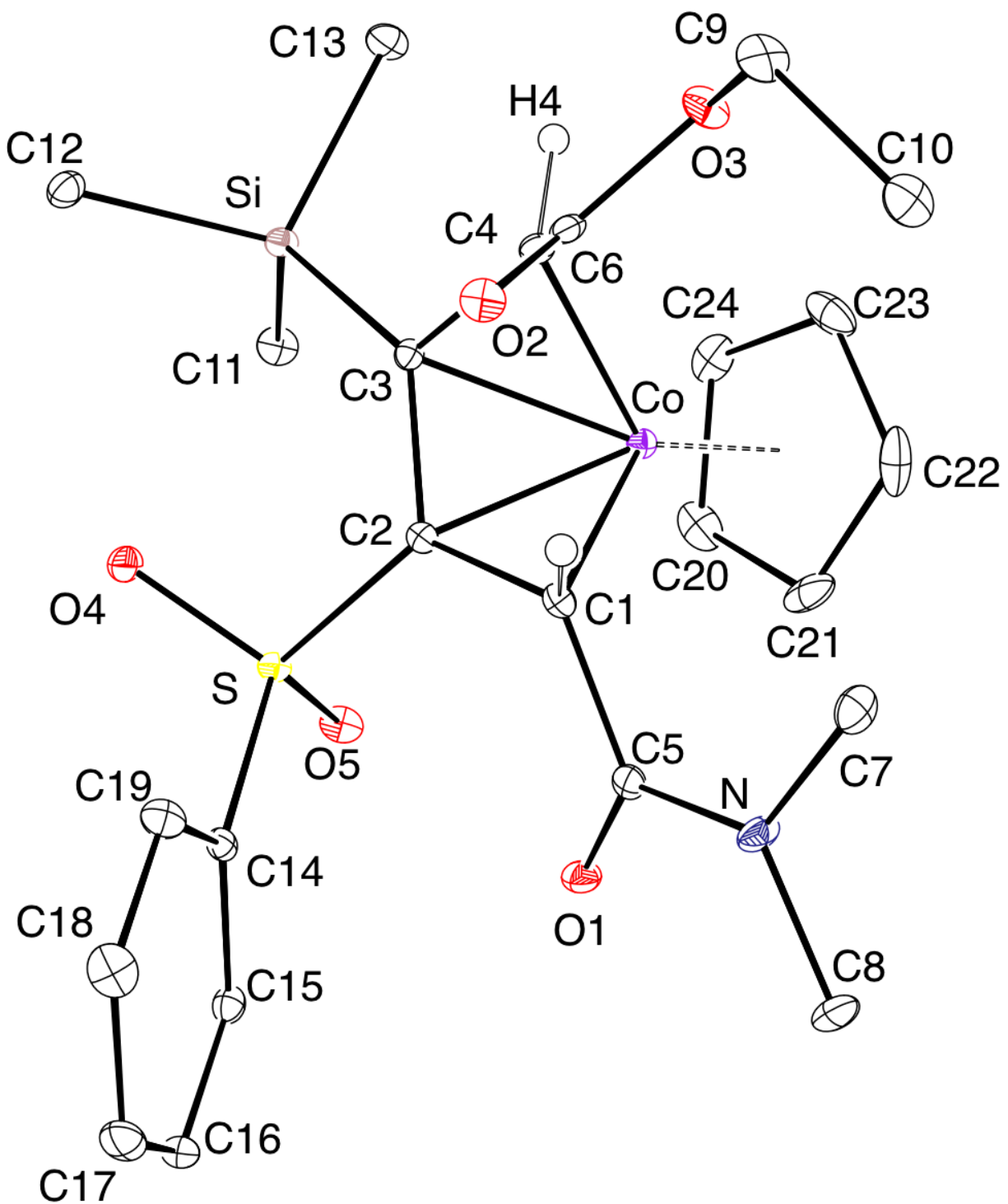
Figure 2-62. ORTEP view of complex **57**. Ellipsoids shown at 30% probability. Most hydrogens are omitted for clarity.

Table 2-15. Crystal data and structure refinement for complex **57**.

Identification code	RLH3182
Empirical formula	C24 H32 Co N O5 S Si
Molecular formula	C24 H32 Co N O5 S Si
Formula weight	533.58
Temperature	100.0 K
Wavelength	0.71073 Å
Crystal system	Triclinic
Space group	P-1
Unit cell dimensions	a = 8.1656(3) Å α = 97.133(2)°.
	b = 8.9372(4) Å β = 101.317(2)°.
	c = 17.7410(7) Å γ = 95.155(2)°.
Volume	1250.99(9) Å^3
Z	2
Density (calculated)	1.417 Mg/m^3
Absorption coefficient	0.852 mm^{-1}
F(000)	560
Crystal size	0.475 x 0.083 x 0.069 mm^3
Crystal color, habit	Red Needle
Theta range for data collection	1.183 to 25.404°.
Index ranges	-9<=h<=9, -10<=k<=10, -21<=l<=21
Reflections collected	31995
Independent reflections	4582 [R(int) = 0.0329, R(sigma) = 0.0236]
Completeness to theta = 25.000°	100.0 %
Absorption correction	Semi-empirical from equivalents
Max. and min. transmission	0.0916 and 0.0676
Refinement method	Full-matrix least-squares on F^2
Data / restraints / parameters	4582 / 0 / 304
Goodness-of-fit on F^2	1.042
Final R indices [I>2sigma(I)]	R1 = 0.0275, wR2 = 0.0638
R indices (all data)	R1 = 0.0343, wR2 = 0.0664
Extinction coefficient	n/a
Largest diff. peak and hole	0.343 and -0.333 e.Å^{-3}
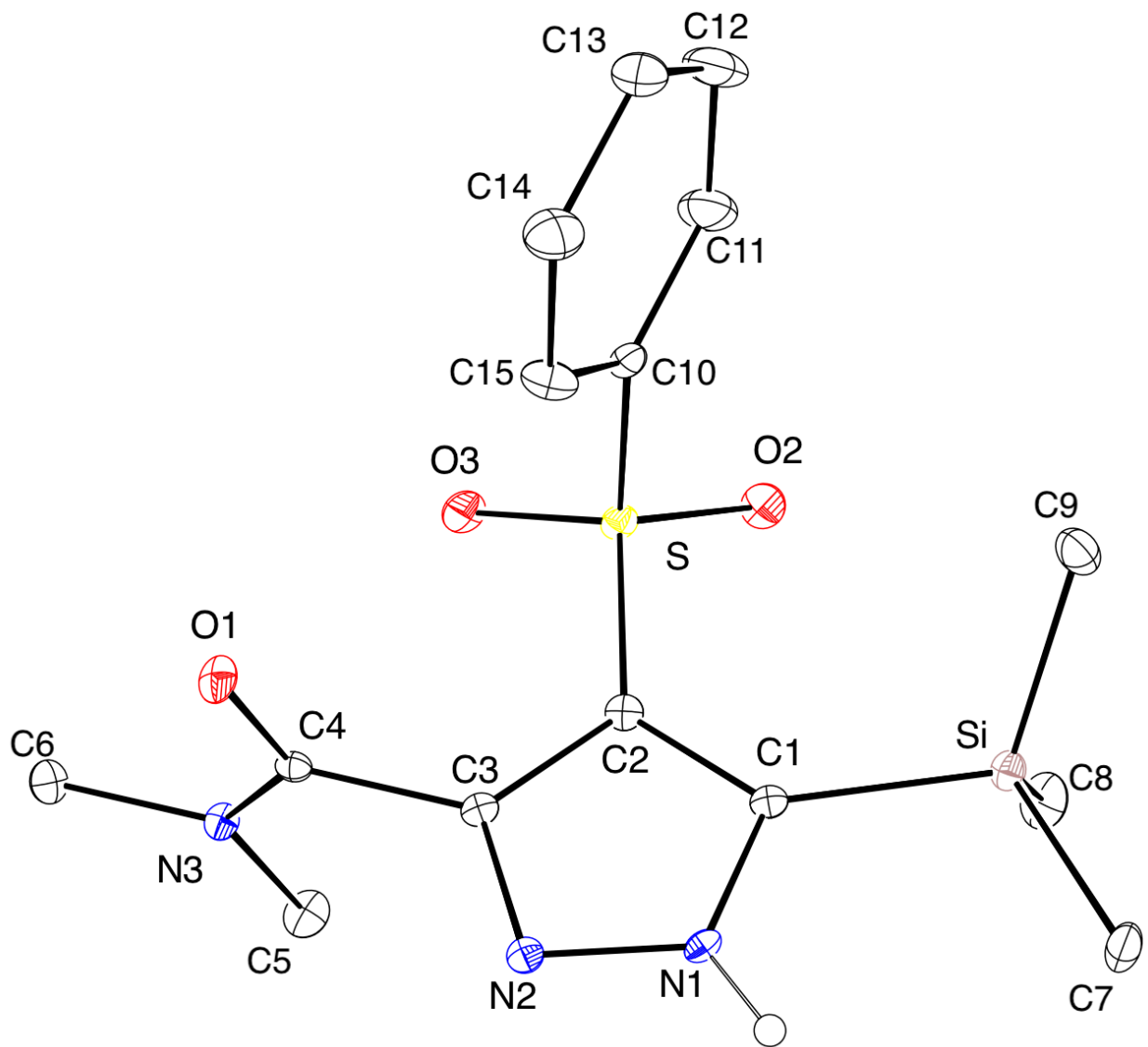
Figure 2-63. ORTEP view of complex **59**. Ellipsoids shown at 30% probability. Most hydrogens are omitted for clarity.

Table 2-16. Crystal data and structure refinement for complex **59**.

Identification code	pq679
Empirical formula	C H N O S Si
Formula weight	103.18
Temperature	100.0 K
Wavelength	0.71073 Å
Crystal system	Triclinic
Space group	P-1
Unit cell dimensions	a = 11.1932(16) Å α = 98.516(4)°.
	b = 12.2880(18) Å β = 98.660(4)°.
	c = 13.399(2) Å γ = 90.033(3)°.
Volume	1801.4(5) Å^3
Z	28
Density (calculated)	2.663 Mg/m^3
Absorption coefficient	1.409 mm^{-1}
F(000)	1456
Crystal size	0.5 x 0.4 x 0.07 mm^3
Theta range for data collection	1.555 to 26.188°.
Index ranges	-13<=h<=13, -15<=k<=15, -16<=l<=16
Reflections collected	7137
Independent reflections	7137 [R(int) = ?]
Completeness to theta = 25.242°	99.9 %
Absorption correction	None
Max. and min. transmission	0.4906 and 0.4162
Refinement method	Full-matrix least-squares on F^2
Data / restraints / parameters	7137 / 0 / 426
Goodness-of-fit on F^2	1.062
Final R indices [I>2sigma(I)]	R1 = 0.0562, wR2 = 0.1488
R indices (all data)	R1 = 0.0647, wR2 = 0.1561
Extinction coefficient	n/a
Largest diff. peak and hole	1.326 and -0.507 e.Å^{-3}
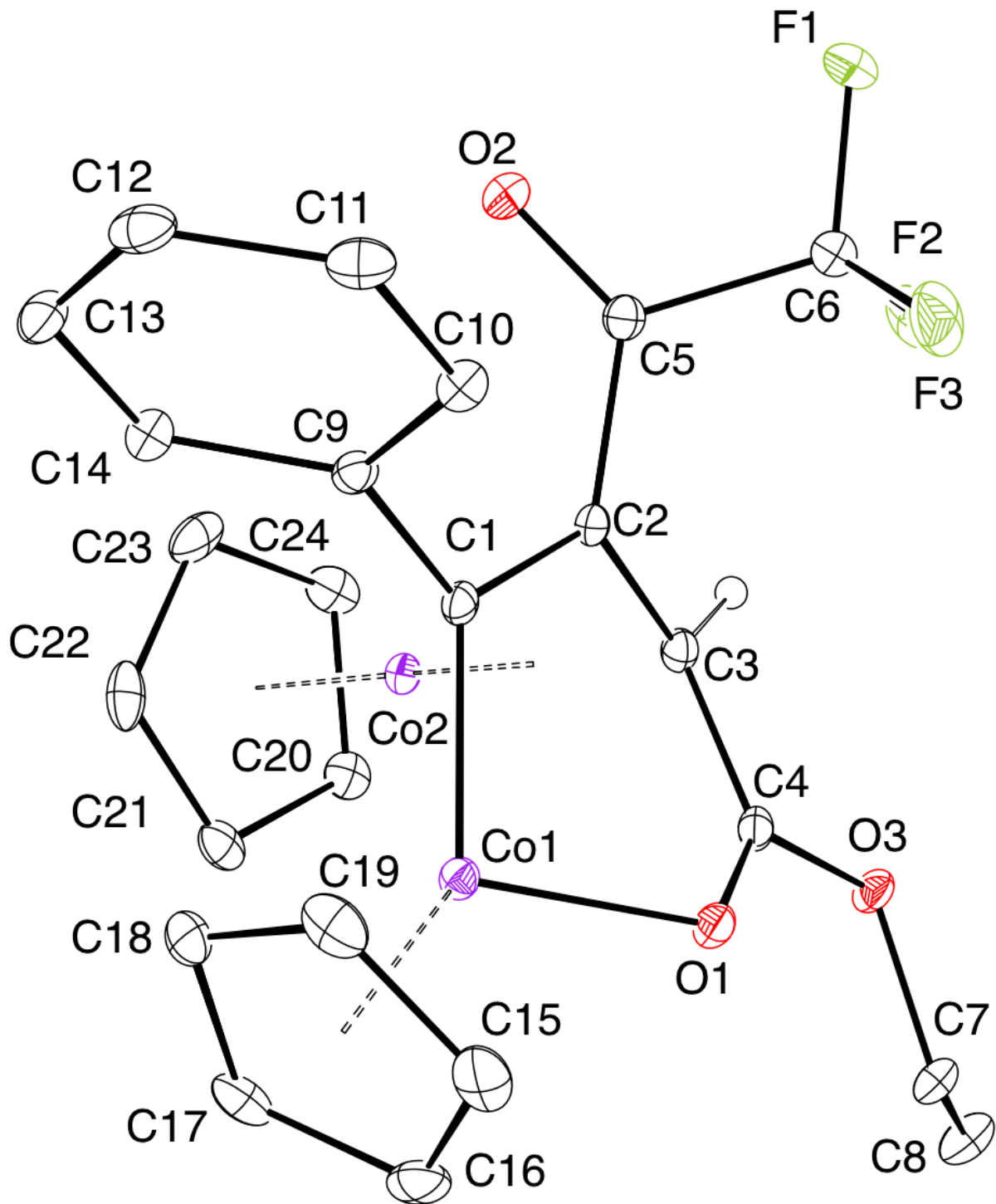
Figure 2-64. ORTEP view of complex **62**. Ellipsoids shown at 30% probability. Most hydrogens are omitted for clarity.

Table 2-17. Crystal data and structure refinement for complex **62**.

Identification code	pq_0467_a
Empirical formula	C24 H21 Co2 F3 O3
Formula weight	532.27
Temperature	100.0 K
Wavelength	0.71073 Å
Crystal system	Monoclinic
Space group	P 1 21/c 1
Unit cell dimensions	a = 8.7730(17) Å $\quad \alpha = 90°$.
	b = 8.5200(16) Å $\quad \beta = 98.608(2)°$.
	c = 29.033(6) Å $\quad \gamma = 90°$.
Volume	2145.7(7) Å^3
Z	4
Density (calculated)	1.648 Mg/m^3
Absorption coefficient	1.596 mm^{-1}
F(000)	1080
Crystal size	0.357 x 0.276 x 0.194 mm^3
Theta range for data collection	1.419 to 26.418°.
Index ranges	-10<=h<=10, -10<=k<=10, -36<=l<=35
Reflections collected	26433
Independent reflections	4398 [R(int) = 0.0296]
Completeness to theta = 25.000°	99.9 %
Absorption correction	Semi-empirical from equivalents
Max. and min. transmission	0.2602 and 0.2157
Refinement method	Full-matrix least-squares on F^2
Data / restraints / parameters	4398 / 0 / 290
Goodness-of-fit on F^2	1.078
Final R indices [I>2sigma(I)]	R1 = 0.0239, wR2 = 0.0568
R indices (all data)	R1 = 0.0261, wR2 = 0.0581
Extinction coefficient	n/a
Largest diff. peak and hole	0.394 and -0.221 e.Å^{-3}

Acknowledgement

Chapter 2 contains a full reptrint of publication "Metal-Alkyne and Metallacyclobutene Reactivity toward a Diazoacetamide: Conversion to Highly Functionalized 1,3-Diene Complexes and Oxametallacyclopentadienes" Qin, P.; Holland, R. L.; Moore, C. E.; O'Connor, J. M. *Organometallics* **2019**, *38*, 863-869. The dissertation author is the first author on this paper.

Chapter 2 contains the material being prepared for the publication "Coupling of Metal-Alkyne Complexes with *α*-Diazocarbonyl Compound: An Efficient Way to Synthesize Highly Functionalized Metallacyclobutenes". Qin, P.; Bunker, K. D.; Holland, R. L.; Rheingold, A. L.; O'Connor, J. M. The dissertation author is the first author on this paper.

Chapter 2 contains the material being prepared for the publication "Thermal Reactivity of Late-metal Metallacyclobutene Complexes: Reversible Formation of Dicobalt Propendiyl Complexes". Qin, P.; Bunker, K. D.; Holland, R. L.; Rheingold, A. L.; O'Connor, J. M. The dissertation author is the first author on this paper.

I. References

1. Hong, P.; Aoki, K.; Yamazaki, H. Reaction of a Diphenylacetylene-cobalt Complex with Alkyl Diazoacetates. *J. Organomet. Chem*. **1978**, *150*, 279-293.

2. O'Connor, J. M.; Ji, H.; Iranpour, M.; Rheingold, A. L. Formation of a Stable Metallacyclobutene Complex from α-Diazocarbonyl and Alkyne Substrates. *J. Am. Chem. Soc*. **1993**, *115*, 1586-1588.

3. (a) O'Connor J. M.; Fong, B. S.; Ji, H. L.; Hiibner, K.; Rheingold, A. L. A New Metal-Mediated Cyclization: Conversion of a Metallacyclobutene and Alkyne Substrates to η^4-Cyclopentadiene Products. *J. Am. Chem. Soc.* **1995**, *117*, 8029-8030. (b) Holland, R. L.; Bunker, K. D.; Chen, C. H.; DiPasquale, A. G.; Rheingold, A. L.; Baldridge, K. K.; O'Connor, J. M. Reactions of a Metallacyclobutene Complex with Alkenes. *J. Am. Chem. Soc.* **2008**, *130*, 10093-10095. (c) Holland, R. L.; O'Connor, J. M. Nitroso Compounds Serve as Precursors to Late-Metal η^2(N,O)-Hydroxylamido Complexes. *Organometallics* **2008**, *28*, 394-396. (d) Holland, R. L.; O'Connor, J. M.; Bunker, K. D.; Qin, P.; Cope, S. K.; Baldridge, K. K.; Siegel, J. S. Stereospecific Oxidative Demetallation of Highly Functionalized CpCo(1,3-Diene) Complexes: An Experimental and Computational Study. *Synlett* **2015**, *26*, 2243-2246.

4. O'Connor, J. M.; Baldridge, K. K.; Vélez, C. L.; Rheingold, A. L.; Moore, C. E. Chemistry at the Alkyne–Carbene Intersection: A Metallacyclobutene-η^3-Vinylcarbene Equilibration. *J. Am. Chem. Soc.* **2013**, *135*, 8826-8829.

5. Wakatsuki, Y.; Yamazaki, H., Lindner, E.; Bosamle, A. (1,3-Butadiene-1,4-Diyl)(η^5-Cyclopentadienyl)-(Triphenylphosphine) Cobalt with Various Substituents. *Inorg. Syn.* **1989**, *26*, 189-200.

6. Hsieh, M. T.; Kuo, S. C.; Lin, H. C. Solvent-and Transition Metal Catalyst-Dependent Regioselectivity in the [3+2] Cyclocondensation of Trifluoromethyl-α,β-ynones with Hydrazines: Switchable Access to 3-and 5-Trifluoromethylpyrazoles. *Adv. Synth. Catal.* **2015**, *357*, 683-689.

7. (a) Aresta, M.; Rossi, M.; Sacco, A. Tetrahedral complexes of cobalt(I.) *Inorg. Chim. Acta* **1969**, *3*, 227-231. (b) Wakatsuki, Y.; Yoshimura, H.; Yamazaki, H. Sur les Organometalliques Issus de Thioamides: II. Reaction avec les α-enones *J. Organomet. Chem.* **1989**, *266*, 215-221.

8. Eliel, E. L.; Manoharan, M. Conformational analysis. 40. Conformation of 1-methyl-1-phenylcyclohexane and Conformational Energies of the Phenyl and Vinyl Groups. *J. Org. Chem.* **1981**, *46*, 1959-1962.

9. (a) Baldridge, K. K.; Bunker, K. D.; Vélez, C. L.; Holland, R. L.; Rheingold, A. L.; Moore, C. E.; O'Connor, J. M. Structural Characterization of (C_5H_5)Co(PPh$_3$)(η^2-alkyne) and (C_5H_5)Co(η^2-alkyne) Complexes of Highly Polarized Alkynes. *Organometallics* **2013**. *32*, 5473-5480. (b) Bunker, K. D.; Rheingold, A. L.; Moore, C. E.; Aubrey, M.; O'Connor, J. M. Synthesis of the cobalt–alkyne complex (η^5-C_5H_5)(PPh$_3$)Co{η^2-(Me$_3$Si)CC(CO$_2$Et)} and structural characterization of trimethylsilyl substituted cobaltacyclopentadiene complexes derived therefrom. *J. Organomet. Chem.* **2014**, *749*, 100-105.

10. Traylor, T. G.; Berwin, H. J.; Jerkunica, J.; Hall, M. L. *Pure Appl. Chem.* **1972**, 599.

11. (a) Mana, J.; John, K.D.; Hopkins, M.D. *Adv. Organomet. Chem*. **1995**, *38*, 79-154. (b) Modern acetylene chemistry / edited by P.J. Stang and F. Diegerich; Weinheim. New York: VCH, c**1995**. (c) Priciples and applications of organotransition metal chemistry / James P. Collman; [2d ed.].; Mill Valley, Calif.: University Science Books, **1987**.

12. Bunker, K. Doctoral Dissertation, Late-Metal Metallacyclobutenes: Synthesis, Isolation, and Reactivity Studies of Cobaltacyclobutenes. University of California, San Diego, CA, USA, **2003**.

13. Chen, M. Doctoral Dissertation, University of California, Metallacyclobutenes as Reactive Intermediates: Conversion to Cobalt Diene and Cobalt Allene Complexes. San Diego, CA, USA, **1998**.

14. (a) O'Connor, J. M.; Chen, M.-C.; Frohn, M.; Rheingold, A. L.; Guzei, I. A. Diazoketones Undergo Reaction with a Cobalt Alkyne Complex to give Highly Functionalized Conjugated Dienes. *Organometallics* **1997**, *16*, 5589-5591; (b) O'Connor, J. M.; Chen, M.-C.; Holland, R. L.; Rheingold A. L. Addition of Dissimilar Carbenes across an Unsymmetrically Substituted Alkyne: Regio- and Stereoselective Synthesis of Trisubstituted 1,3-Dienes. *Organometallics* **2011**, *30*, 369-371.

15. Tomioka, H.; Kondo, M.; Izawa, Y. Substituent Effects on the Product Distribution in Diazo Amide Photochemistry. Role of Ground-State Conformation Populations. *J. Org. Chem.* **1981**, *46*, 1090-1094.

16. For leading references to the metal-mediated reactions of diazoamides, see: (a) Ring, A.; Ford, A.; Maguire, A. R. Substrate and Catalyst Effects in C-H Insertion Reactions of α-Diazoacetamides. *Tetrahedron Lett.* **2016**, *57*, 5399-5406; (b) Suárez, A.; Fu, G. C. A Straightforward and Mild Synthesis of Functionalized 3-Alkynoates. *Angew. Chem. Int. Ed.* **2004**, *43*, 3580-3582; (c) Doyle, M. P.; Winchester, W. R.; Protopopova, M. N. 151. Tetrakis[(4S)-4-phenyloxazolidin-2-one]dirhodium(II) and Its Catalytic Applications for Metal Carbene Transformations. *Helv. Chim. Acta* **1993**, *76*, 2227-2235.

17. For leading references to the synthesis of cobalt-diene complexes, see: (a) Aechtner, T.; Barry, D. A.; David, E.; Chellamallah, C.; Harvey, D. F.; de la Houpliere, A.; Knopp, M.; Malaska, M. J.; Pérez, D.; Schärer, K. A.; Siesel, B. A.; Vollhardt, K. P. C.; Zitterbart, R. Cobalt-Mediated [2+2+2] Cycloadditions of Alkynes to Benzo-[*b*]furans and Benzo[*b*]thiphenes: A Potential Route toward Morphanoids. *Synthesis* **2018**, *50*, 1053-1089; (b) Gandon, V.; Agenet, N.; Vollhardt, K. P. C.; Malacria, M.; Aubert, C. Cobalt-Mediated Cyclic and Linear 2:1 Cooligomerization of Alkynes with Alkenes: A DFT Study. *J. Am. Chem. Soc.* **2006**, *128*, 8509-8520; (c) Foerstner, J.; Kakoschke, A.; Stellfeldt, D.; Butenschön, H. Reactions of a Chelated Cyclopentadienylcobalt(I) Complex with 3,3-Disubstituted Cyclopropenes: Formation of Isoprene, Vinylcarbene, and 1-Phosphadiene Ligands at the Metal. *Organometallics* **1998**, *17*, 893-8966; (d) Wakatsuki, Y.; Aoki, K.; Yamazaki, H. Cobalt Metallocycles. 6. Preparation and Structure

of Cobaltacyclopentene Complexes and Their Reactions with Olefins and Acetylenes. *J. Am. Chem. Soc.* **1979**, *101*, 1123-1130.

18. Dirnberger, T.; Werner, H. Hydrido(vinyl)rhodium(III)-Komplexe aus [RhCl(P*i*Pr₃)₂] und Olefinen. *Chem. Ber.* **1992**, *125*, 2007-2014.

19. For CpCo-sulfinato complexes, see: (a) O'Connor, J. M.; Bunker, K. D.; Rheingold, A. L.; Zakhrov, L. Sulfoxide Carbon-Sulfur Bond Activation. *J. Am. Chem. Soc.* **2005**, *127*, 4180-4181; (b) Vélez, C. L.; Markwick, P. R. L.; Holland, R. L.; DiPasquale, A. G.; Rheingold, A. L.; O'Connor, J. M. Cobalt 1,3-Diisopropyl-1H-imidazol-2-ylidene Complexes: Synthesis, Solid-State Structures, and Quantum Chemistry Calculations. *Organometallics* **2010**, *29*, 6695-6702.

20. For leading references to metal-sulfinato complexes, see: (a) Grapperhaus, C. A.; Darensbourg, M. Y. Oxygen Capture by Sulfur in Nickel Thiolates. *Acc. Chem. Res.* **1998**, *31*, 451-459; (b) Sriskandakumar, T.; Behyan, S.; Habtemariam, A.; Sadler, P. J.; Kennepohl, P. Electrophilic Activation of Oxidized sulfur Ligands and Implications for the Biological Activity of Ruthenium(II) Arene Anticancer Complexes. *Inorg. Chem.* **2015**, *54*, 11574-11580; (c) Lefort, L.; Lachicotte, R. J.; Jones, W. D. Insertion of SO_2 into the Metal-Carbon Bonds of Rhodium and Iridium Compounds, and Reactivity of the SO_2-Inserted Species. *Organometallics* **1998**, *17*, 1420-1425.

21 (a) Niu, Q.; Zhang, S.; Li, X.; Sun, H.; Fuhr, O.; Fenske, D. Synthesis and Characterization of Diorganocobalt Chlorides by Aliphatic Vinylic C-Cl Bond Activation. *Z. Anorg. Allg. Chem.* **2016**, *642*, 866-869; (b) O'Connor, J. M.; Chen, M. C.; Holland, R. L. Protonation of Cobalt-Allene Constitutional Isomers: Highly Selective Formation of Cobalt-Allyl and Oxacobaltacyclopentadiene Complexes. *Organometallics* **2010**, *29*, 6161-6164; (c) Davies, J. E.; Mays, M. J.; Raithby, P. R.; Sarveswaran, V.; Shields, G. P. Nature of Previously Reported Thermally Unstable Products Derived from the Reaction of [Co₂(CO)₈] with PhSSPh, EtSSEt or PhSeSePh and of the Reactions of these Products with Alkynes or Isocyanides. *J. Chem. Soc., Dalton Trans.* **1998**, 775-779; (d) Yamamoto, Y.; Tanase, T.; Sugano, K. Reactions of Dicobalt Octa(isocyanide) with 2-Bromoacetophenone. *J. Organometal. Chem.* **1995**, *486*, 21-29.

22. King, R. B. Organometallic Chemistry of the Transition Metals. XI. Some New Cyclopentadienyl Derivatives of Cobalt and Rhodium. *Inorg. Chem.* **1966,** *5*, 82-87.

23. The crude reaction mixture from the reaction of **7** and diazoacetamide in the presence of ¹⁸OH₂-saturated C₆D₆ was also analyzed by ESI-MS with no evidence for the formation of unlabeled **54** or isotopically-enriched **54**-¹⁸O. Decomposition of starting material without formation of **50** and **54** was also observed in wet THF-d_8 solvent.

24. A similar mechanism would involve initial sulfone attack on the carbene carbon of **IV**.

25. Minor byproducts may include, cobalt-acetylides (ref 19a), dicobalt complexes (refs. 1, 4, 19a), cobalt-diene isomers (refs. 26), cobaltacyclopentadienes (ref. 9), and cobaltacyclobutenes (ref. 2).

26. For the interconversions of diastereomeric CpCo-1,3-diene complexes, see: (a) Eaton, B.; King, Jr. J. A.; Vollhardt, K. P. C. First Photochemical Envelope Isomerization of a Late-Transition-Metal 1,3-Butadiene Complex: A Triple Stereochemical Labeling Experiment. *J. Am. Chem. Soc.* **1986**, *108*, 1359-1360; (b) O'Connor, J. M.; Chen, M.-C.; Rheingold, A. L. Fluoride Induced Isomerization of Cobalt Diene Complexes. *Tetrahedron Lett.* **1997**, *30*, 5241-5244; (c) Baldridge, K. K.; O'Connor, J. M; Chen, M.-C.; Siegel, J. S. Envelope-flip Dynamics in CpCo(Diene) Complexes: An ab initio Quantum Mechanical Study. *J. Phys. Chem. A* **1999**, *103*, 10126-10131.

27. Chenon, M. T.; Coupry, C.; Grant, D. M.; Pugmire, R. J. Carbon-13 magnetic resonance study of solvent stabilized tautomerism in pyrazoles. *J. Org. Chem*. **1977**, *42*, 659-661.

28. (a) King Jr, J. A.; Vollhardt, K. P. C. Vinyl hydrogen activation in mono- and dinuclear (η^5-cyclopentadienyl)(hexatriene)cobalt complexes. Thermal and photochemical hydrogen shifts of complementary stereochemistry. *J. Am. Chem. Soc*. **1983**, *105*, 4846-4848. (b) King Jr, J. A.; Vollhardt, K. P. C. Photochemical synthesis and structure of (μ-η^4-syn-1,3-butadiene) (μ-carbonyl) bis(η^5-cyclopentadienyl) dicobalt(Co-Co), a dinuclear butadiene complex. *Organometallics* **1983**, *2*, 684-686. (c) Cirjak, L. M.; Ginsburg, R. E.; Dahl, L. F. Synthesis, stereochemistry, and bonding of cobalt-cobalt multiple-bonded (pentamethylcyclopentadienyl)- and cyclopentadienylcobalt carbonyl dimers, [Co$_2$ (η^5-C$_5$R$_5$)$_2$(μ-CO)$_2$]$_n$ (R= Me, n= 0, 1; R= H, n= 1): a comparative analysis of the antibonding dimetal nature of the unpaired electron in the monoanions and its structural effects upon oxidation. *Inorg. Chem*. **1982**, *21*, 940-957. (d) Werner, H.; Kolb, O.; Schubert, U.; Ackermann, K. Komplexe mit kohlenstoffsulfiden und-seleniden als liganden: X. Synthese und kristallstruktur von C$_5$H$_5$(PMe$_3$)Co(μ-CS)$_2$CoC$_5$H$_5$: Ein zweikernkomplex mit unsymmetrischen Co(CS)Co-brückenbindungen *J. Organomet. Chem*. **1982**, *240*, 421-428.

29. (a) Stolzenberg, A. M.; Scozzafava, M.; Foxman, B. M. Metallacyclopentene / metallaoxanorbornadiene chemistry. Synthesis, characterization, and reactivity of 1-(cyclopentadienyl)-1-cobalta-2-oxanorbornadiene complexes. *Organometallics* **1987**, *6*, 769-777. (b) Doherty, M. D.; Grant, B., White, P. S.; Brookhart, M. Reactions of H$_2$ and R$_3$SiH with Electrophilic Cobalt(III) Alkyl Complexes: Spectroscopic Characterization, Dynamics, and Chemistry of [Cp*Co(L)(H)(η^2-H$_2$)][B(Ar$_F$)$_4$] and [Cp*Co(L)(H)(η^2-HSiR$_3$)][B(Ar$_F$)$_4$] *Organometallics* **2007**, *26*, 5950-5960.

30. Padwa, A. Rhodium(II) mediated cyclizations of diazo alkynyl ketones. *J. Organomet. Chem*. **2000**, *610*, 88-101.

31. Eaton, B.; King, J. A.; Vollhardt, K. P. C. First photochemical envelope isomerization of a late transition metal 1, 3-butadiene complex: a triple stereochemical labeling experiment. *J. Am. Chem. Soc*. **1986**, *108*, 1359-1360.

32. Tolman, C. A. Steric Effects of Phosphorus Ligands in Organometallic Chemistry and Homogeneous Catalysis. *Chem. Rev*. **1997**, *77*, 313-348.

33. (a) Green, M. A.; Huffman, J. C.; Caulton, K. G. Photochemistry of Transition-metal Polyhydrides: Dimerization of Tris(dimethylphenylphosphine)pentahydrorhenium Following Photodissociation of Phosphine . *J. Am. Chem. Soc*. **1981**, *103*, 695-696. (b) Deo, C.; Bogliotti, N.; Retailleau, P.; Xie, J. Triphenylphosphine Photorelease and Induction of Catalytic Activity from Ruthenium-Arene Complexes Bearing a Photoswitchable o-Tosylamide Azobenzene Ligand. *Organometallics* **2016**, *35*, 2694-2700. (c) Wada, M.; Kumazoe, M. *J. Chem. Soc., Chem. Commun*. d-d Band Excitation of the Diorganonickel(II) Complexes *trans*-[Ni{2,6-(MeO)$_2$C$_6$H$_3$}$_2$L$_2$] (L = PMe$_3$ or PMe$_2$Ph) and Their Analogues causing Reversible Phosphine Dissociation and/or Organic Group Rotation about the Ni-C Bond. **1985**, 1204-1205. (d) Suzuki, H.; Miyazaki, Y.; Hoshino, M. Laser Photolysis Studies of Rhodium(III) Porphyrins. Photodissociation of Axial Phosphine Ligand in the Temperature Range 300-200 K. *J. Phys. Chem. A* **2003**, *107*, 1239-1245. (e) Mirbach, M. F.; Mirbach, M. J.; Wegman, R. W. Photochemical Ligand Dissociation, Electron Transfer, and Metal-Metal Bond Cleavage of Phosphine-Substituted Cobalt Carbonyl Complexes. *Organometallics* **1984**, *3*, 900-903.

34. Yamazaki, H.; Hagihara, N. Bis (triphenylphosphine)-pi-cyclopentadienyl-cobalt (I) and-rhodium (I). *Bull. Chem. Soc. Jpn*. **1971**, *44*, 2260-2261.

CHAPTER 3

Synthesis and Reactivity Studies of η^4-cyclopentadiene complexes

A. Introduction

As the derivative of metallocenes, η^4-cyclopentadiene complex is one of the oldest organometallic complexes that were discovered in the history, and it has been widely used as catalyst in materials sciences to synthesize polymers.[1] Cobalt, as one of the most common and cheapest transition metals on earth, is famous for its intermediacy in various cyclization reactions with alkynes to construct new carbon-carbon bonds, such as [2 + 2 + 2] cyclotrimerization of alkynes[2] (Scheme 3-1) and Pauson-Khand reaction[3] (Scheme 3-2).
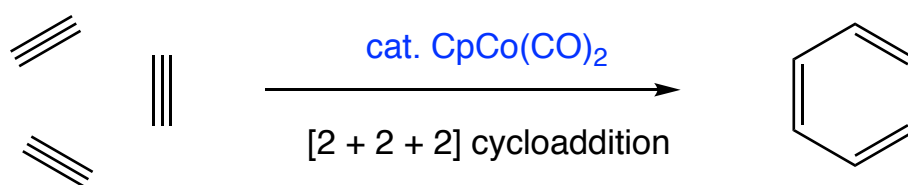
Scheme 3-1. Cobalt catalyzed cyclotrimerizaton of alkynes.
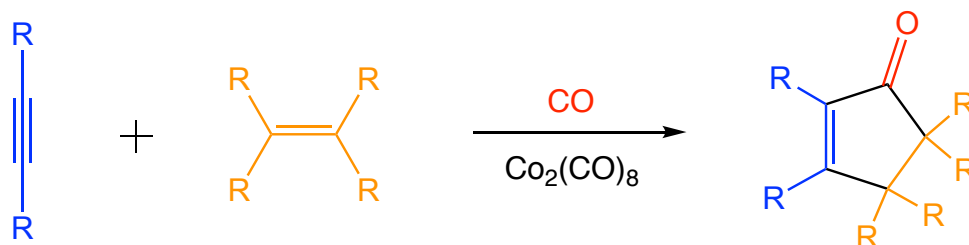
Scheme 3-2. Cobalt-mediated Pauson-Khand reaction.

In 1995, O'Connor's group discovered that cobalt incorporated η^4-cyclopentadiene complexes can be assembled with high regio-and stereoselectivity from a cycloaddition reaction, in which one carbene and two acetylenes are involved

(Scheme 3-3).[4] These reactions share the same metallacyclobutene intermediate **2** with different functional group located at C4 position. In principle, different multi-functionalized η^4-cyclopentadiene complexes can be synthesized in this fashion by modifying the substituents on metallacyclobutene and acetylenes, and therefore, in order to explore the scope of this [2 + 2 + 1] cycloaddition reaction, three different metallacyclobutenes were employed as precursors to react with various alkynes to prepare η^4-cyclopentadiene complexes in this chapter. In addition, by changing the loading order, when a cobalt-alkyne complex was treated with vinyl diazoacetate, a vinyl metallacyclobutene was generated, that is followed by thermolysis at high temperature to afford η^4-cyclopentadiene complexes.
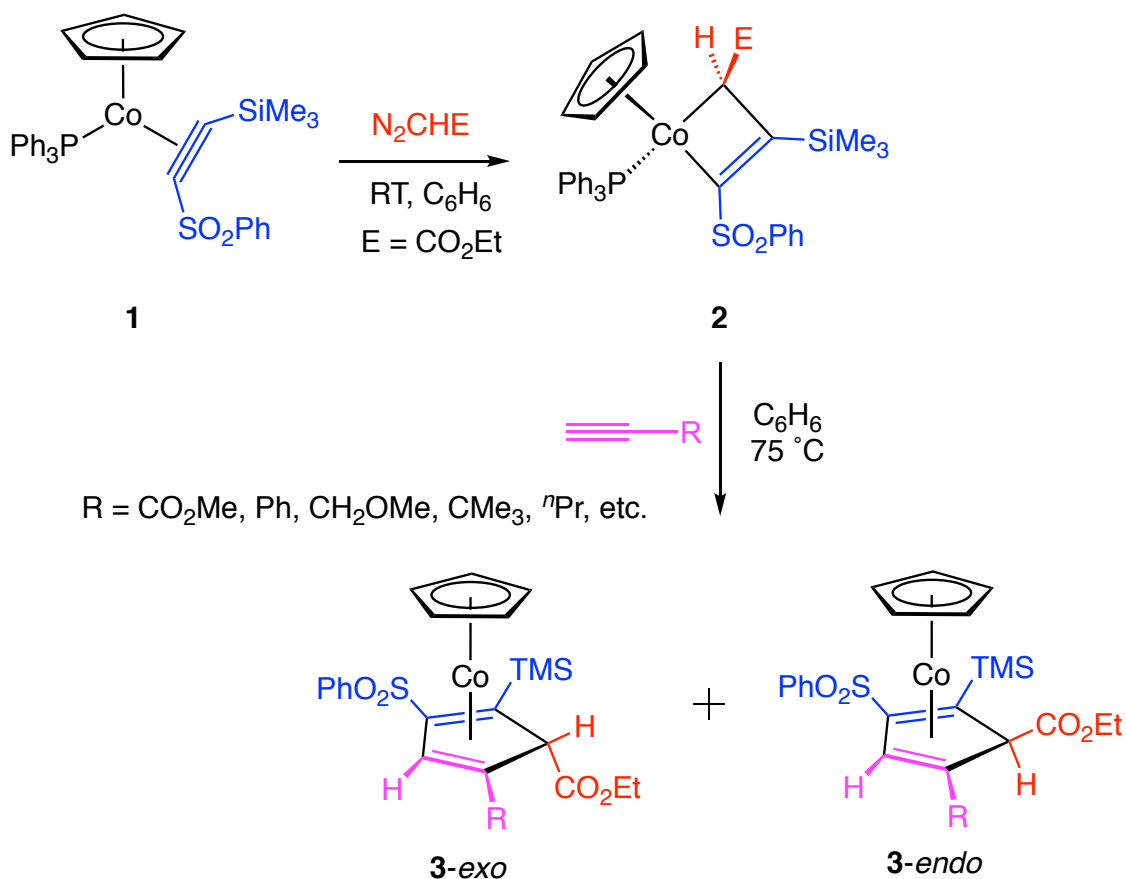
Scheme 3-3. Synthesis of η^4-cyclopentadiene complexes.

Furthermore, despite extensive studies have been conducted on synthesis of η^4-cyclopentadiene complexes with various transition metals in the literature,[5] The reactivity studies of η^4-cyclopentadiene complexes are still rare. Herein, in this chapter, we explored the reactivates of η^4-cyclopentadiene complexes under variable reaction conditions by manipulating the functional group attached on the ring, from which highly functionalized metallocens and arenes were generated with high regioselectivity.

B. Synthesis of η^4-Cyclopentadiene Complexes

1. Reaction of Metallacyclobutene 2 with various acetylenes

In order to explore the reactivity of metallacyclobutene with alkynes, a number of commercially available terminal acetylenes with various functional groups were employed as substrates to couple with cobaltacyclobutene **2**. Firstly, we carried out the reaction of complex **2** with propyne. The toluene (50 mL) solution of 0.2 g (0.284 mmol) metallacycle **2** was treated with 6 equivalents of propyne in a Teflon-sealed reaction tube under inert atmosphere. The reaction mixture was allowed to heat at 70 °C for 8 hours, and TLC analysis indicates that all the metallacyclobutene starting disappeared. After chromatography on silica gel in the air, two red bands were observed and collected separately, which affords two products with 61.3% and 33.3% yields, respectively (Scheme 3-4). The major product turned out to be an air-stable red oil, while the minor product formed an air-sensitive dark red crystalline solid.

216
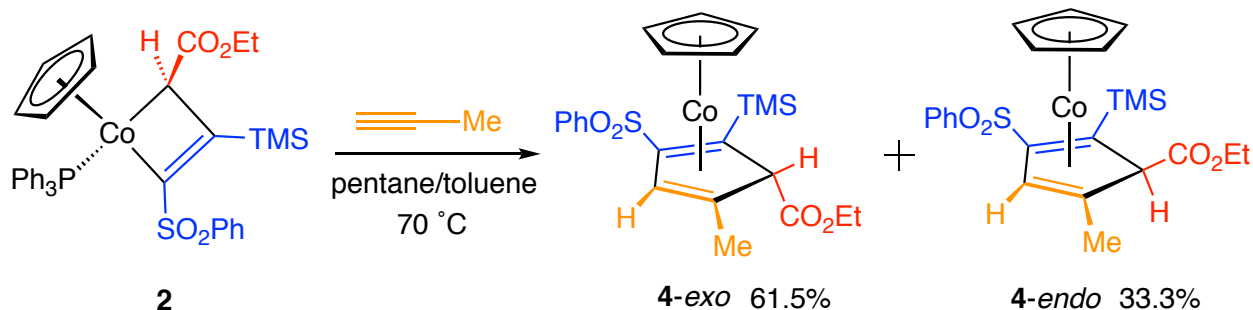
Scheme 3-4. Reaction of metallacyclobutene **2** with propyne.

In the ^{1}H NMR spectrum (400 MHz, CDCl$_3$) of the major product, the ester group and TMS group from the starting metallacyclobutene were still present and observed at δ 0.91 (t, 3H, J = 7.2 Hz, CH_3), 3.67 (m, 2H, CH_2CH$_3$), and 0.11 (s, 9H, TMS), respectively. One extra methyl resonance was observed at δ 1.27 (s, 3H) that is attributed to the incorporation of propyne. The characteristic shielded ring hydrogen of metallacyclobutene was no longer observed, and instead, two singlet hydrogen resonances were detected at δ 3.44 (s, 1H) and 5.63 (s, 1H). The integration of 5 hydrogen in the aromatic region indicates the absence of the triphenylphosphine ligand. In the ^{13}C{^{1}H} NMR spectrum (125 MHz, CDCl$_3$), the phenyl sulfone group shows at δ 127.3, 128.9, 132.8, and 142.9. There are 4 shielded vinyl-carbon resonances that were observed at 101.5, 82.7, 64.6, and 60.2, which is consistent with a η^4-diene structure. The carbonyl stretch was detected at 1718 cm^{-1} in the IR spectrum.

Since the spectra data is not sufficient to elucidate the stereochemistry of the structure, and therefore X-ray crystallography analysis was conducted after recrystallized the products in DCM/hexanes under -20 °C (Figure 3-1). As we anticipated, the structure of the major product was revealed as a η^4-cyclopentadiene

complex. The C1 – C5 and C4 – C5 bond distances were measured as 1.523(4) and 1.532(4) Å, which indicate the single bond characters, while the double bonds C1 – C2 and C3 – C4 were detected with 1.427(5) and 1.444(4) Å bond length, respectively. The two acetylene carbons of propyne is incorporated to form the vinyl carbons of the ring, and the sp^3 ring carbon is from the α carbon of ethyl diazoacetate. The structure of the η^4-cyclopentadiene complex has high regioselectivity that the terminal sp carbon of propyne selectively couples with the carbon bearing sulfone group, which might be ascribed the steric hindrance between the methyl substituent and the bulky sulfone group. The steric hindrance between phenyl sulfone and trimethylsilane group is manifested by the longer bond distance of C1 – C2 than C3 – C4 ($\Delta = 0.017$ Å). The five membered ring is puckered, and the plane-plane fold angle of (C1-C4-C5)-(C1-C2-C3-C4) is measured as 31.0(3)°. A staggered conformation was observed between the Cp ligand and the cyclopentadiene. The *exo* stereochemistry is defined by the ester substituent that is attached on the sp^3 ring carbon stays *anti* to the metal center.
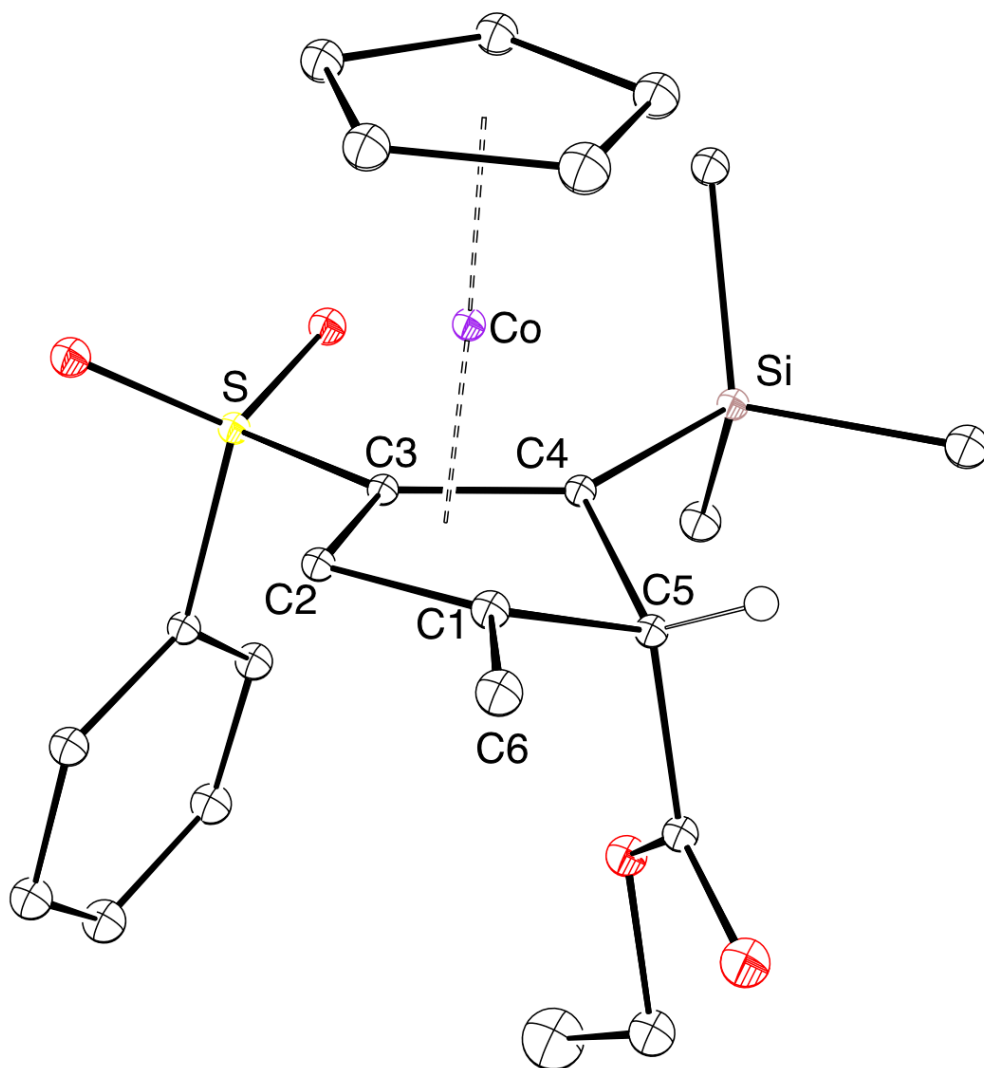
Figure 3-1. ORTEP drawing of **4**-*exo* with ellipsoids shown at 30% probability.

For the minor product, very similar patterns were observed in both ^{1}H and ^{13}C{^{1}H} NMR spectra. The two diastereotopic hydrogen resonances on the ester group shows at δ 4.17 (m, 1H, C*H*$_2$CH$_3$) and 4.22 (m, 1H, C*H*$_2$CH$_3$) in the ^{1}H NMR spectrum. The hydrogen attached on the sp^3 ring carbon shifts more up filed in the spectrum (Δ = 0.58 ppm), which fits the typical range of *endo* ring-hydrogen chemical shift in η^4-

cyclopentadiene complexes.[6] The presence of ester group is also confirmed by the C=O stretch (1738 cm^{-1}) in IR spectrum.

The X-ray quality crystal of the minor product is obtained from recrystallization in hexanes and ethyl acetate under inert atmosphere at ambient temperature, and a single X-ray crystallography study was conducted subsequently. As we expected, the structure of the minor product is unveiled as an *endo* isomer of η^4-cyclopentadiene complex that has the same connectivity as the *exo* isomer (Figure 3-2). To our knowledge, this is the first example of cobalt η^4-cyclopentadiene complexes whose *endo* and *exo* isomers are both structurally characterized. The comparison of the two complexes **4**-*exo* and **4**-*endo* is summarized in Table 3-1. Analogous to complex **4**-*exo*, the C3 – C4 bond distance is significantly longer (Δ = 0.051 Å) in complex **4**-*endo* due to the steric congestion between sulfone and TMS substituents. The strong back-donation effect that is caused by the electron-withdrawing sulfone group is manifested by the shorter Co – C3 bond (1.925(3) Å) compared to Co – C2 bond (1.976(3) Å). Compared to complex **4**-*exo*, the plane-plane fold angle of (C1-C4-C5)-(C1-C2-C3-C4) in complex **4**-*endo* is significantly greater (Δ = 7.7 °), which is attributed to the amplified steric hindrance between the ester group and the Cp ligand in the latter structure, and this greater steric congestion is also reflected by the longer nonbonding distance between Co and C5 (Δ = 0.078 Å) in complex **4**-*endo*.
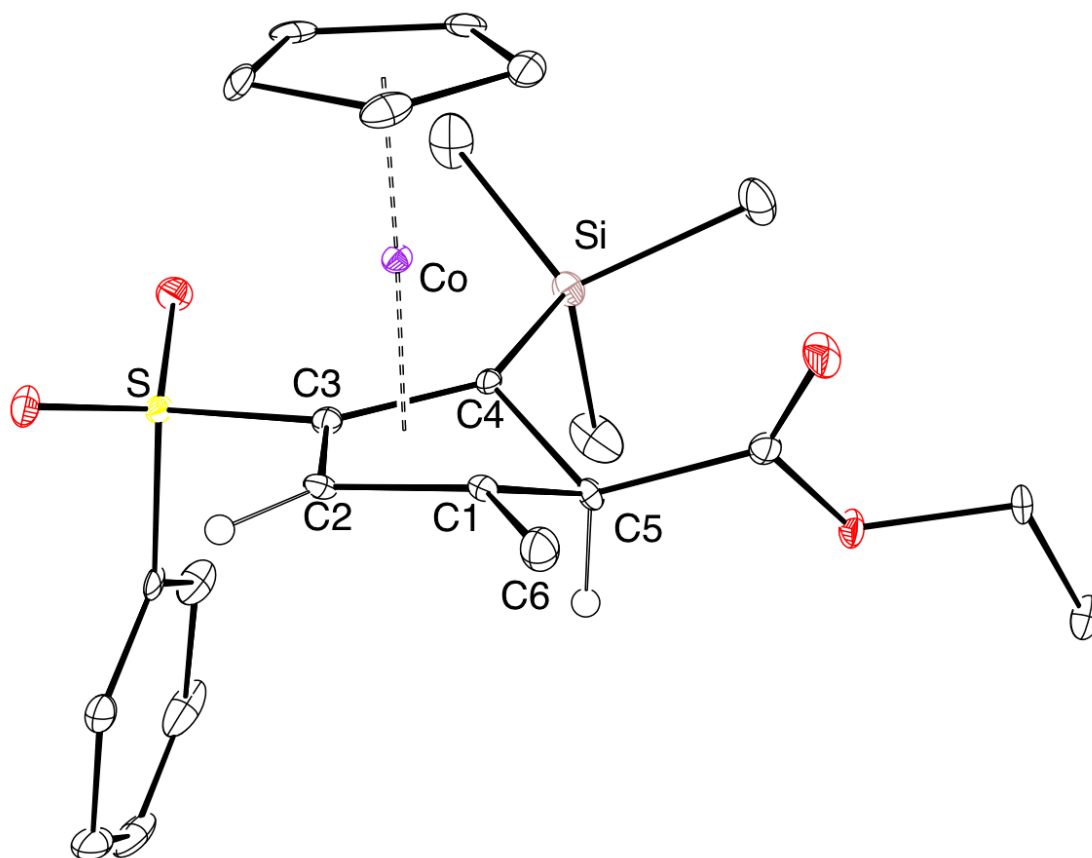
Figure 3-2. ORTEP drawing of **4**-*endo* with ellipsoids shown at 30% probability.

Table 3-1. Distances (Å) and angles (deg) from crystallographic data of η^4-cyclopentadiene complexes **4**-*exo* and **4**-*endo*.

	4-*exo*	**4**-*endo*		**4**-*exo*	**4**-*endo*
C1 – C2	1.427(5)	1.410(5)	Co – C4	2.061(3)	2.027(3)
C2 – C3	1.445(4)	1.429(5)	C1-C2-C3	105.7(3)	106.8(3)
C3 – C4	1.444(4)	1.461(5)	C2-C3-C4	109.4(3)	108.6(3)
C4 – C5	1.532(4)	1.561(5)	C3-C4-C5	106.3(3)	103.4(3)
Co – C1	2.054(3)	2.075(3)	C4-C5-C1	98.4(2)	96.5(3)
Co – C2	1.982(3)	1.976(3)	ring-fold angle	31.0(3)	38.7(3)
Co – C3	1.941(3)	1.925(3)	Co⋯C5	2.543(3)	2.621(4)

A computational study was carried out based on the two X-ray structures by Prof. Kim Baldridge to compare the relative stability of the two η^4-cyclopentadiene isomers. The results indicate that complex **4**-*exo* is 5.23 kcal/mol more stable than complex **4**-*endo* (Scheme 3-5). One might expect that the difference of 5 kcal/mol might be too large for the observance of *endo* isomer, and therefore we reason that the **4**-*endo* is more kinetically favorable. The isolated **4**-*endo* was allowed to heat up at 70 °C in CDCl$_3$ under inert atmosphere, and the reaction was monitored by ^{1}H NMR spectroscopy. However, it was found that complex **4**-*endo* slowly decomposed in the solution without any evidence of formation of complex **4**-*exo*, which indicates that the formation of the two η^4-cyclopentadiene complexes is irreversible.

Scheme 3-5. Computational energy difference between complex **4**-*exo* and **4**-*endo*.

Compared to Bella Fong's result that when phenylacetylene was employed as precursor,[7] a very similar 2 : 1 ratio of exo and endo isomers was obtained. In order to explore the electronic effects on the formation of η^4-cyclopentadiene complexes, the reaction of more electron-rich acetylene 4-ethynyl-*N*,*N*-dimethylaniline with metallacyclobutene **2** was conducted. After 3.0 mg (0.004 mmol) of cobaltacyclobutene

2 and 2.1 mg (0.014 mmol) of 4-ethynyl-*N,N*-dimethylaniline were mixed in a J.Y. NMR tube with 0.7 mL of dry CDCl$_3$ under inert atmosphere, the tube was heated at 70 °C and monitored by ^{1}H NMR spectroscopy. After 6 hours, when all of the starting metallacyclobutene was consumed, the *endo* and *exo* isomers of η^4-cyclopentadiene complexes were observed with 1 : 1 ratio based on the integration of TMS resonances at δ 0.01 (s, 9H) and 0.15 (s, 9H), respectively (Scheme 3-6). In the preparation scale reaction, 5 equivalents of the acetylene were treated with complex **2** in dry toluene at 70 °C for 5 hours, and after chromatography in silica gel, one isomer was isolated as an air-stable red crystalline solid. Unfortunately, the isolation of the other isomer failed owing to the instability, which led to the decomposition to some unknown purple paramagnetic complexes that gave broad signals in NMR spectrum.
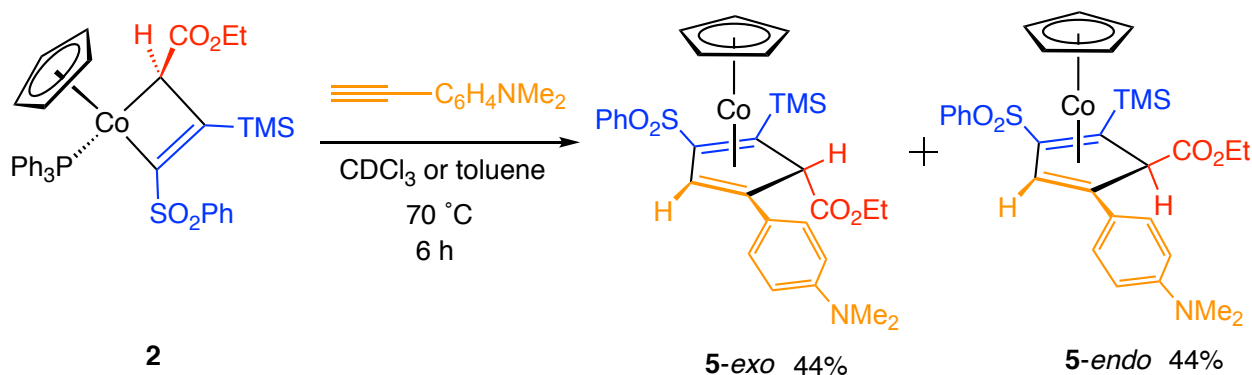
Scheme 3-6. Reaction of metallacyclobutene **2** with 4-ethynyl-N,N-dimethylaniline.

In the ^{1}H NMR spectrum (400 MHz, CDCl$_3$) of the isolated isomer, the NMe$_2$ moiety was observed at δ 2.92 (s, 6H). A vinyl hydrogen was detected at δ 6.24 (s, 1H), while another singlet at δ 6.24 (s, 1H) matches the typical chemical shift of ring

hydrogen in exo η^4-cyclopentadiene complexes.[6] The integration of 9 hydrogen in the aromatic region is consistent with the two phenyl ring from sulfone and 4-ethynyl-N,N-dimethylaniline. Four shielded vinyl carbon signals were observed at δ 60.26, 61.32, 78.42, and 101.91. The carbonyl stretch of ester group shows at 1710 cm^{-1} in the IR spectrum.

The structure of the isolated isomer was studied by X-ray crystallography, which reveals an *exo* configuration of η^4-cyclopentadiene complex **5**-*exo* (Figure 3-3). The bond distance and angles are summarized in Table 3-2, which are very similar to complex **4**-*exo.* The steric hindrance between the amino phenyl group and Cp ligand is manifested by the longer Co – C1 bond distance in complex **5**-*exo* (2.109(3) Å) than in complex **4**-*exo* (2.054(3) Å). The cyclopentadiene ring is also puckered with a (C1-C4-C5)-(C1-C2-C3-C4) plane-plane fold angle of 32.1(3) °. The Co····C5 nonbonding distance is measured as 2.584(4) Å. The phenyl dimethyl amino substituent is essentially planar with a small C10-N-C9-C8 torsion angle (3.4(4) °). Also, the small torsion angle of C7-C6-C1-C2 indicates that the diene moiety is delocalized well with the arene substituent.
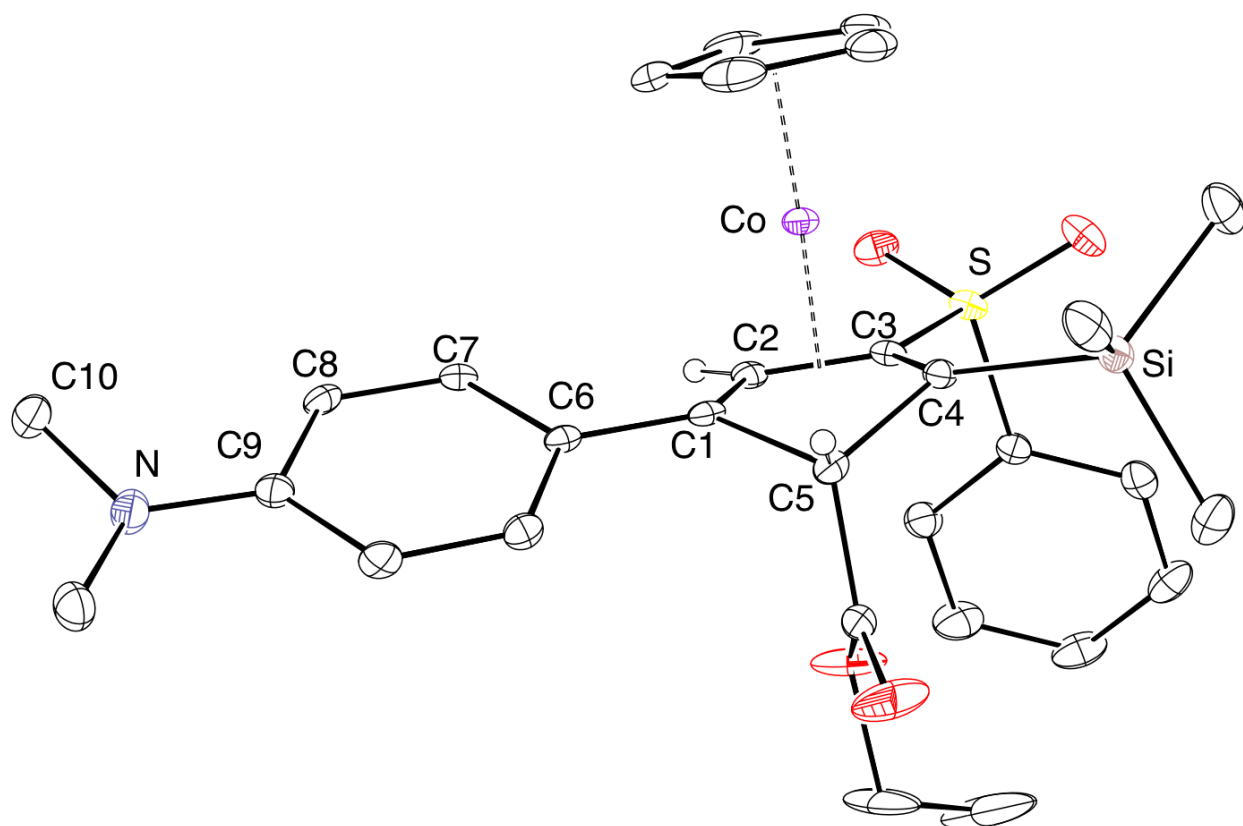
Figure 3-3. ORTEP drawing of **5**-*exo* with ellipsoids shown at 30% probability.

Table 3-2. Seletecd bond distances (Å) and angles (deg) of η^4-cyclopentadiene complex **5**-*exo*.

C1 – C2	1.422(5)	C1-C2-C3	107.2(3)
C2 – C3	1.424(5)	C2-C3-C4	109.1(3)
C3 – C4	1.452(5)	C3-C4-C5	105.2(3)
C4 – C5	1.552(5)	C4-C5-C1	98.2(3)
C1 – C5	1.519(5)	C10-N-C9-C8	3.4(4)
Co – C1	2.109(3)	C7-C6-C1-C2	27.1(3)
Co – C2	1.974(3)	ring-fold angle	32.1(3)
Co – C3	1.925(3)	Co····C5	2.584(4)

Despite the isolation of the other product failed, it can be identified as the *endo* isomer according to the similar resonances to complex **5**-*exo* in ^{1}H NMR spectrum (CDCl$_3$, 400 MHz) of the crude reaction mixture: The TMS and Cp signals were observed at δ 0.01 (s, 9H, TMS), and 5.00 (s, 5H, Cp). The dimethyl amino group shows at δ 2.90 (s, 6H, NMe$_2$). The ester group with two diastereotopic hydrogen resonances were detected at δ 1.33 (t, 3H, J = 7.0 Hz, OCH$_2$CH_3), 4.17 (m, 1H, OCH_2CH$_3$), and 4.30 (m, 1H, OCH_2CH$_3$). The two ring hydrogen resonances shows at δ 3.20 (s, 1H, CHCO$_2$) and 5.97 (s, 1H, vinyl-H). All the arene peaks were observed at δ 6.53 (d, 2H, J = 8.8 Hz, Ar), 6.80 (d, 2H, J = 8.8 Hz, Ar), 7.5-7.7 (m, 3H, Ar), and 8.05 (d, 2H, J = 7.2 Hz, Ar).

Based on the result above, one might argue that the different exo/endo products distribution caused by the amino phenyl substituent versus phenyl substituent can also be attributed to steric reasons since amino phenyl group is slightly bulkier than the phenyl group. In order to clarify this argument, less electron-rich acetylene 1-ethynyl-4-isopropylbenzene that has similar size of 4-ethynyl-*N,N*-dimethylaniline was employed as substrate to react with metallacyclobutene **2**. The result shows that upon treating complex **2** with 5 equivalents of 1-ethynyl-4-isopropylbenzene at 70 $^\circ$ C for 6 hours, a 1.7 : 1 ratio of **6**-*exo* and **6**-*endo* were generated (Scheme 3-7). Both stereoisomers were successfully isolated as slightly air-sensitive solids, and fully characterized via ^{1}H, ^{13}C NMR, IR, HRMS and elemental analysis (Table 3-4). Accordingly, despite the explanation behind the electronic effect is still unclear, it is safe to conclude that more electron-rich alkyne tends to give higher ratio of the endo product.
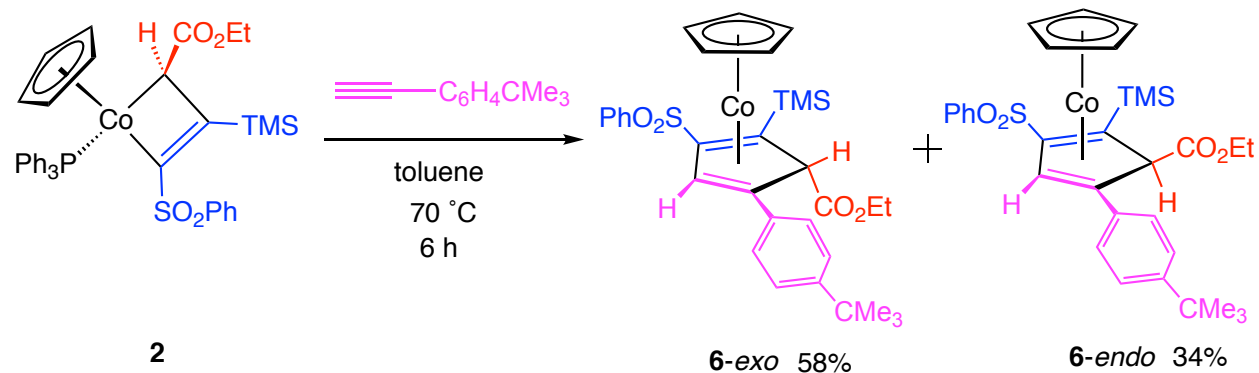
Scheme 3-7. Reaction of metallacyclobutene **2** with 1-ethynyl-4-isopropylbenzene.

To explore the electron-withdrawing effect on the formation of η^4-cyclopentadiene complexes, propargyl alcohol was ucsed as precursor to react with metallacyclobutene **2**. When the experiment of complex **2** and 5 equivalents of propargyl alcohol was conducted in a similar fashion, surprisingly, only one isomer was generated with 84% isolated yield. The product was identified as an *exo* isomer of η^4-cyclopentadiene complex (Scheme 3-8) based on the reason that the chemical shift of ring hydrogen that is attached on the sp^3 carbon (δ 3.47).[6] The two pairs of diatereotopic hydrogen resoances werer observed at δ 3.54 (m, 1H, CH_2CH$_3$), 3.74 (m, 1H, CH_2CH$_3$); and 3.64 (m, 1H, CH_2OH), 3.88 (m, 1H, CH_2OH). The stereochemistry is also confirmed by a subsequent X-ray crystallography analysis (Figure 3-4). The seleted bond angle and distances are summarized in Table 3-3. The exclusive formation of **6**-*exo* supports the point that electron-deficient alkyne tends to selectively produce *exo* isomer. However, more experiments with various acetylenes need to be carried out in the future for the further demonstration of this conclusion.
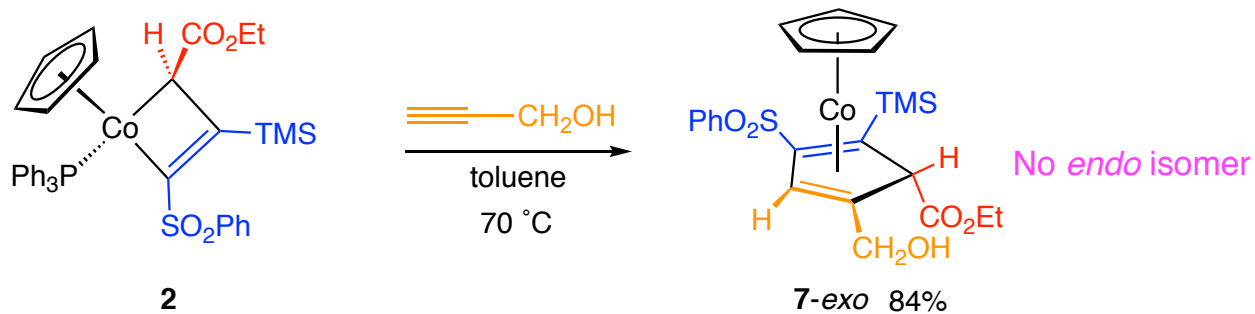
Scheme 3-8. Reaction of metallacyclobutene **2** with propargyl alcohol.
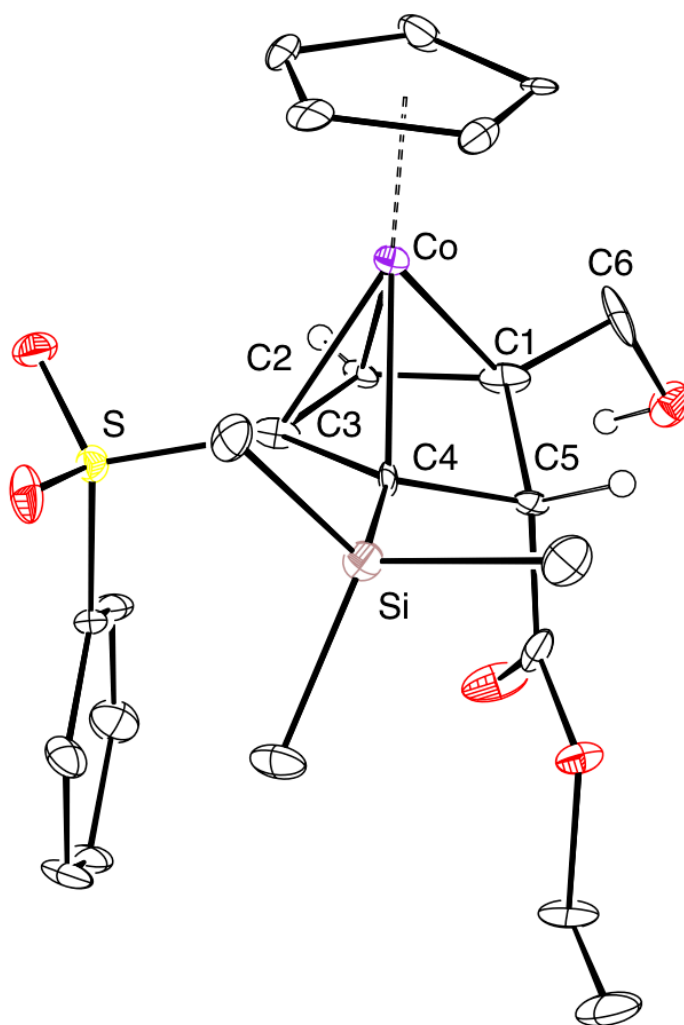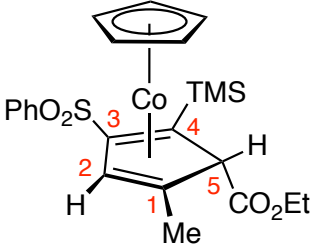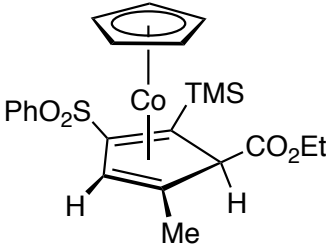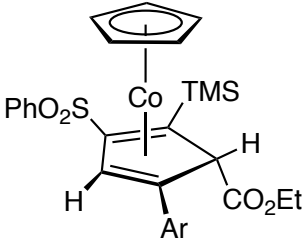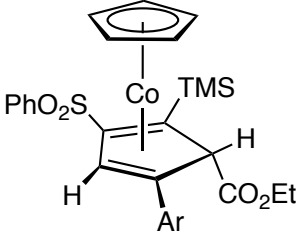
Figure 3-4. ORTEP drawing of **7-exo** with ellipsoids shown at 30% probability.

Table 3-3. Seletecd bond distances (Å) and angles (deg) of η^4-cyclopentadiene complex **7**-*exo*.
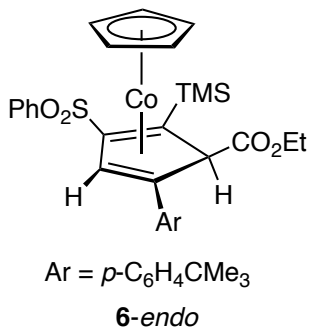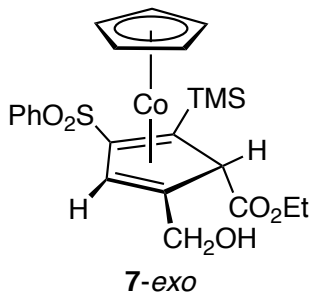
C1 – C2	1.38(2)	C1-C2-C3	107.3(11)
C2 – C3	1.497(17)	C2-C3-C4	105.8(11)
C3 – C4	1.488(16)	C3-C4-C5	105.9(10)
C4 – C5	1.536(18)	C4-C5-C1	96.8(9)
C1 – C5	1.560(16)	C1-Co-C4	70.1(5)
Co – C1	1.999(15)	C2-Co-C3	44.9(5)
Co – C2	1.970(13)	ring-fold angle	36.6(13)
Co – C3	1.950(13)	Co····C5	2.551(13)

Furthermore, I also cleaned up previous graduate students' work by repeating some of the alkynes Bella used to react with cobaltacyclobutene **2** (Scheme 3-9). The first one I repeated is utilizing tributyl(ethynyl)stannane as substrate, which produced 51% yield of **9**-*exo* and 37% yield of **9**-*endo*, respectively. In the original work, it states that the separation of the two isomers failed due to the close polarity of the two isomers. However, it is found that by using 8% ethyl acetate in hexanes as eluent in flash chromatography with long column, the mixture of *exo* and *endo* isomers can be successfully separated, and the exo isomer was fully characterized by ^{1}H, ^{13}C NMR, IR, HRMS and elemental analysis (see experimental and supporting information sections). The complex **9**-*exo* was also employed as precursor for the further reactivity studies of η^4-cyclopentadiene complexes (vide infra).

Table 3-4. Spectroscopic data of η^4-cyclopentadiene complexes (in CDCl$_3$).

Complex	^{1}H NMR, (δ); IR, (cm^{-1})	^{13}C{^{1}H} NMR, (δ)
4-exo	0.11 (s, 9H, TMS) 0.91 (t, 3H, J = 7.2 Hz, CH$_2$CH_3) 1.27 (s, 3H, Me) 3.44 (s, 1H, CHCO$_2$) 3.67 (m, 2H, CH_2CH$_3$) 4.95 (s, 5H, Cp) 5.63 (s, 1H, vinyl-H) 7.0 – 8.1 (m, 5H, Ar) IR: 1718 (C=O)	0.7 (TMS) 14.1 (CH$_2$CH$_3$) 18.2 (Me), 39.4 (C4) 56.6 (C1), 60.2 (CH$_2$CH$_3$) 64.6 (C5), 82.4 (Cp) 82.7 (C2), 101.5 (C3) 127.3 (C$_m$), 128.9 (C$_o$) 132.8 (C$_p$), 142.9 (C$_i$) 166.3 (CO$_2$Et)
4-endo	-0.04 (s, 9H, TMS) 1.01 (s, 3H, Me) 1.32 (t, 3H, J = 7.2 Hz, CH$_2$CH_3) 2.87 (s, 1H, CHCO$_2$) 4.20 (m, 2H, CH_2CH$_3$) 4.99 (s, 5H, Cp) 5.60 (s, 1H, vinyl-H) 7.0 – 8.1 (m, 5H, Ar) IR: 1710 (C=O)	0.6 (TMS) 14.3 (CH$_2$CH$_3$) 16.9 (Me), 34.3 (C4) 55.2 (C1), 60.1 (CH$_2$CH$_3$) 65.9 (C5), 81.6 (C2) 83.1 (Cp), 100.3 (C3) 127.1 (C$_m$), 129.1 (C$_o$) 132.9 (C$_p$), 143.2 (C$_i$) 172.9 (CO$_2$Et)
5-exo Ar = p-C$_6$H$_4$NMe$_2$	0.15 (s, 9H, TMS) 0.82 (t, 3H, J = 6.8 Hz, CH$_2$CH_3) 2.92 (s, 6H, NMe$_2$) 3.59 (m, 2H, CH_2CH$_3$) 4.12 (s, 1H, CHCO$_2$) 4.79 (s, 5H, Cp) 6.24 (s, 1H, vinyl-H) 6.5 – 8.1 (m, 9H, Ar) IR: 1713 (C=O)	0.8 (TMS), 14.0 (CH$_2$CH$_3$) 38.8 (C4), 40.5 (NMe$_2$) 59.1 (C5), 60.3 (CH$_2$CH$_3$) 61.3 (C1), 78.4 (C2) 83.0 (Cp), 101.9 (C3) 112.8 (C$_m$), 126.1 (C$_p$) 126.7 (C$_o$), 127.5 (C$_{m(s)}$) 128.9 (C$_{o(s)}$),132.8 (C$_{p(s)}$) 142.8 (C$_{i(s)}$), 148.9 (C$_i$), 165.9 (CO$_2$Et)
6-exo Ar = p-C$_6$H$_4$CMe$_3$	0.16 (s, 9H, TMS) 0.83 (t, 3H, J = 6.8 Hz, CH$_2$CH_3) 1.28 (s, 9H, CMe$_3$) 3.62 (m, 2H, CH_2CH$_3$) 4.07 (s, 1H, CHCO$_2$) 4.83 (s, 5H, Cp) 6.37 (s, 1H, vinyl-H) 7.0 – 8.2 (m, 9H, Ar) IR: 1718 (C=O)	0.6 (TMS), 14.2 (CH$_2$CH$_3$) 31.4 (CMe_3), 35.0 (CMe$_3$) 40.1 (C4), 56.5 (C1) 60.6 (CH$_2$CH$_3$) 61.5 (C5), 80.7 (C2) 83.4 (Cp), 103.0 (C3) 125.5 (C$_m$), 126.2 (C$_{m(s)}$) 127.8 (C$_{o(s)}$), 129.2 (C$_o$) 133.1 (C$_{p(s)}$), 136.1 (C$_p$) 143.0 (C$_{i(s)}$), 149.4 (C$_i$) 166.2 (CO$_2$Et)

Table 3-4. Spectroscopic data of η^4-cyclopentadiene complexes (continued)

Complex	^{1}H NMR, (δ); IR, (cm^{-1})	^{13}C{^{1}H} NMR, (δ)
Ar = p-C$_6$H$_4$CMe$_3$ **6**-*endo*	0.03 (s, 9H, TMS) 1.27 (s, 9H, CMe$_3$) 1.32 (t, 3H, J = 6.8 Hz, CH$_2$CH_3) 3.22 (s, 1H, CHCO$_2$) 4.25 (m, 2H, CH_2CH$_3$) 5.04 (s, 5H, Cp) 6.08 (s, 1H, vinyl-H) 6.8 – 8.2 (m, 9H, Ar) IR: 1710 (C=O)	0.7 (TMS), 14.4 (CH$_2$CH$_3$) 31.4 (CMe_3), 35.0 (CMe$_3$) 35.5 (C4), 56.3 (C1) 61.0 (CH$_2$CH$_3$) 64.3 (C5), 83.3 (C2) 84.0 (Cp), 101.4 (C3) 125.3 (C$_m$), 125.9 (C$_{m(s)}$) 127.4 (C$_{o(s)}$), 129.4 (C$_o$) 133.2 (C$_{p(s)}$), 136.4 (C$_p$) 143.4 (C$_{i(s)}$), 149.3 (C$_i$) 173.2 (CO$_2$Et)
7-*exo*	0.15 (s, 9H, TMS) 0.9 (t, 3H, J = 7.2 Hz, CH$_2$CH_3) 2.69 (bs, 1H, CH$_2$OH) 3.54 (m, 1H, CH_2CH$_3$) 3.64 (m, 1H, CH_2OH) 3.74 (m, 1H, CH_2CH$_3$) 3.88 (m, 1H, CH_2OH) 5.03 (s, 5H, Cp) 5.88 (s, 1H, vinyl-H) 7.5 – 8.1 (m, 5H, Ar) IR: 1720 (C=O) 3350 (O-H)	0.9 (TMS) 14.0 (CH$_2$CH$_3$) 40.8 (C4) 56.6 (C1) 60.9 (CH$_2$CH$_3$) 61.8 (CH$_2$OH) 63.2 (C5), 81.6 (C2) 82.2 (Cp), 102.6 (C3) 127.4 (C$_m$), 129.0 (C$_o$) 133.0 (C$_p$), 142.6 (C$_i$) 169.1 (CO$_2$Et)

8-*exo* (R^1 = Ph, R^2 = H) 62%   **8**-*endo* (R^1 = Ph, R^2 = H) 29%
9-*exo* (R^1 = SnBu$_3$, R^2 = H) 51%   **9**-*endo* (R^1 = SnBu$_3$, R^2 = H) 37%
10-*endo* (R^1 = R^2 = CO$_2$Me) 95%
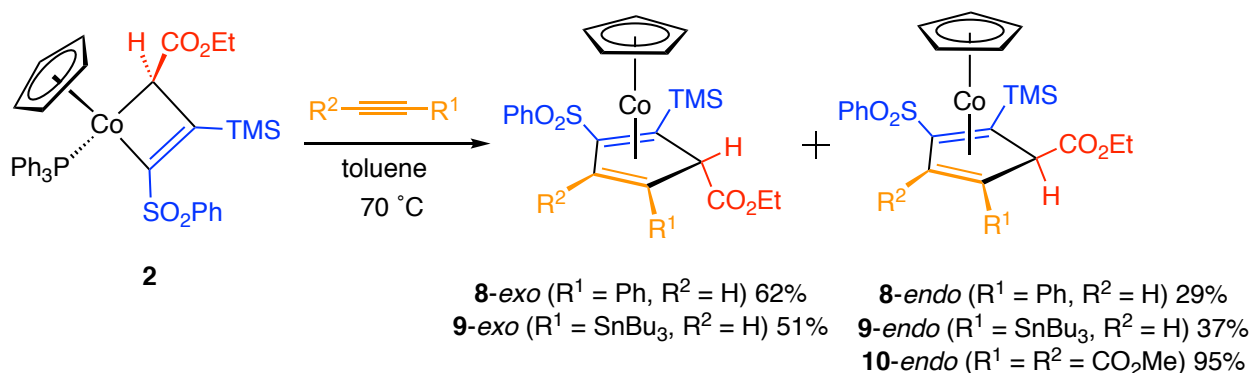
Scheme 3-9. Cleaned up work of metallacycle reacting some acetylenes.

The second substrate I repeated is dimethyl but-2-ynedioate (DMAD) for the reason that the sp^3 ring hydrogen resonance in ^{1}H NMR spectrum was observed at δ 3.03 (s, 1H), which fits the range of *endo* isomer; whereas a NOE experiment conducted before indicated an interaction between the Cp ligand and the sp^3 ring hydrogen, which suggests an *exo* structure. In order to clarify this confliction, I successfully grew some crystals that were suitable for X-ray crystallography analysis, and it unambiguously demonstrates the formation of *endo-η^4*-cyclopentadiene complex (Figure 3-5). The prominent feature of this structure is the exceptionally long C1 – C2 double bond distance (1.532(4) Å), which is attributed to the strong back-donation effect from the metal center, caused by the electron-withdrawing effects of the two ester groups (Table 3-5). The cyclopentadiene ring is puckered, and the steric congestion between ester group and Cp ligand is manifested by the large plane – plane angle [(C1-C4-C5) – (C1-C2-C3-C4), 36.2(4) °] and long Co····C5 distance (2.617(4) Å). The small torsion angle of O1-C6-C1-C2 (32.3(4) °) indicates that the ester group attached on C1 is well conjugated with the diene; whereas the ester group attached on C2 is localized due the large dihedral angle of O3-C7-C2-C1 (84.0(4) °).
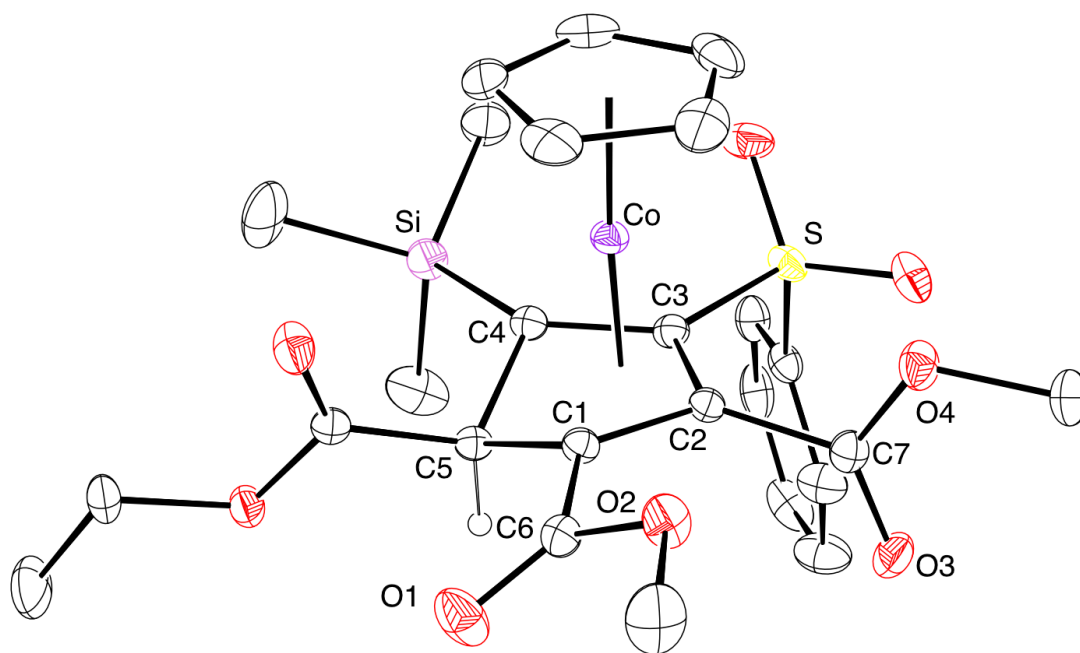
Figure 3-5. ORTEP drawing of **10**-*endo* with ellipsoids shown at 30% probability.

The third substrate I repeated is phenyl acetylene for couple of reasons. Firstly, η^4-cyclopentadiene products are subsequently used as precursor for the reactivity studies (vide infra); secondly, since example that has both structurally characterized *exo* and *endo* isomers is very rare, it is important to grow single crystals of both isomers for structural comparison (Figure 3-6, Figure 3-7). The two η^4-cyclopentadiene complexes both exhibit a staggered conformation between the Cp ligand and the cyclopentadiene ring. There is a greater steric hindrance between the ester and phenyl substituents in **8**-*endo*, which is reflected by the longer C4 – C5 (Δ = 0.019 Å) bond distance. As the same trend that was observed in **4**-*exo* and **4**-*endo*, the ring fold angle [(C1-C4-C5) – (C1-C2-C3-C4)] in **8**-*endo* (35.17(16) °) is larger than **8**-*exo* (32.8(4) °), and C1-C5-C4 angle in **8**-*exo* is wider (Δ = 0.73 °). The steric congestion between ester group and Cp ligand is released in **8**-*exo*, which is manifested by the shorter Co····C5 nonbonding

distance (Δ = 0.0498 Å). In addition, the conjugation of the phenyl substituent with the cyclopentadiene is better in the *exo* isomer due to the smaller C7-C6-C1-C2 dihedral angle (Δ = 20.74 °). Computational studies of the structures indicate that complex 8-*endo* is 6.96 kcal/mol less stable than **8**-*exo*, which suggests that 8-*endo* is more kinetically favorable (Scheme 3-10).
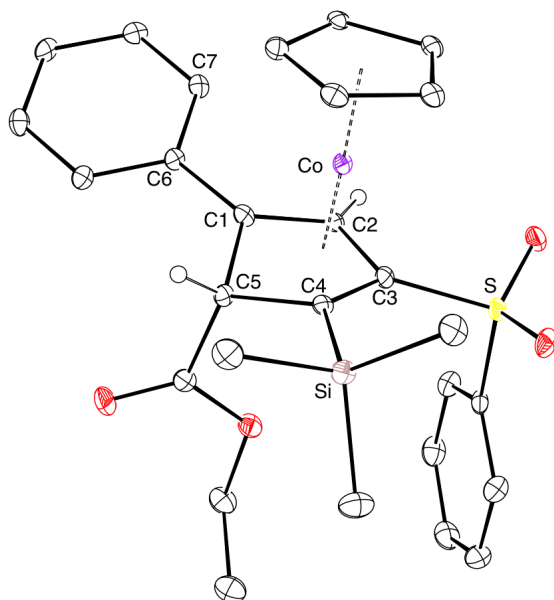
Figure 3-6. ORTEP drawing of **8**-*exo* with ellipsoids shown at 30% probability.
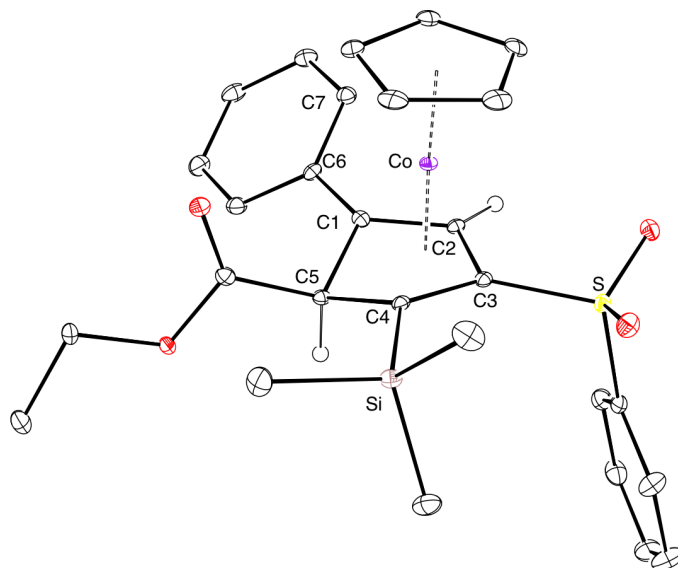
Figure 3-7. ORTEP drawing of **8**-*endo* with ellipsoids shown at 30% probability.

Table 3-5. Seletecd bond distances (Å) and angles (deg) of η^4-cyclopentadiene complexes **8**-*exo*, **8**-*endo*, and **10**-*endo*.

	10-*endo*	**8**-*exo*	**8**-*endo*
C1 – C2	1.532(4)	1.417(4)	1.420(3)
C2 – C3	1.427(5)	1.434(4)	1.435(2)
C3 – C4	1.447(5)	1.453(4)	1.453(3)
C4 – C5	1.463(4)	1.540(4)	1.559(2)
C1 – C5	1.551(5)	1.535(4)	1.527(2)
Co – C1	2.061(4)	2.088(3)	2.1071(17)
Co – C2	1.952(3)	1.979(3)	1.9779(17)
Co – C3	1.952(4)	1.943(3)	1.9307(18)
Co – C4	2.069(4)	2.043(3)	2.0386(17)
C1-C5-C4	96.6(3)	97.9(2)	97.17(14)
C5-C1-C2	109.3(3)	108.8(3)	108.49(17)
ring fold angle	36.2(4)	32.8(4)	35.17(16)
Co····C5	2.617(4)	2.567(3)	2.6168(18)

Scheme 3-10. Computational energy difference between complex **8**-*exo* and **8**-*endo*.

Mechanistically, we proposed that upon heating the metallacyclobutene **2**, triphenylphosphine ligand can dissociate to reversibly generate two vinyl carbene intermediates **12**-*E* and **12**-*Z* (Scheme 3-11).[8] To form the vinylmetallacyclobutene intermediates **12**-*E* and **12**-*Z*, the acetylene inserts into the cobalt alkylidene in a highly regioselective way that the carbon bearing functional group stays closer to the metal center to avoid steric congestion. After reductive elimination from C1 and C5, vinylmetallacyclobutene intermediate **12**-*E* selectively generates η^4-cyclopentadiene complex **13**-*exo*, while **13**-*endo* is produced by vinylmetallacyclobutene intermediate **12**-*Z*.
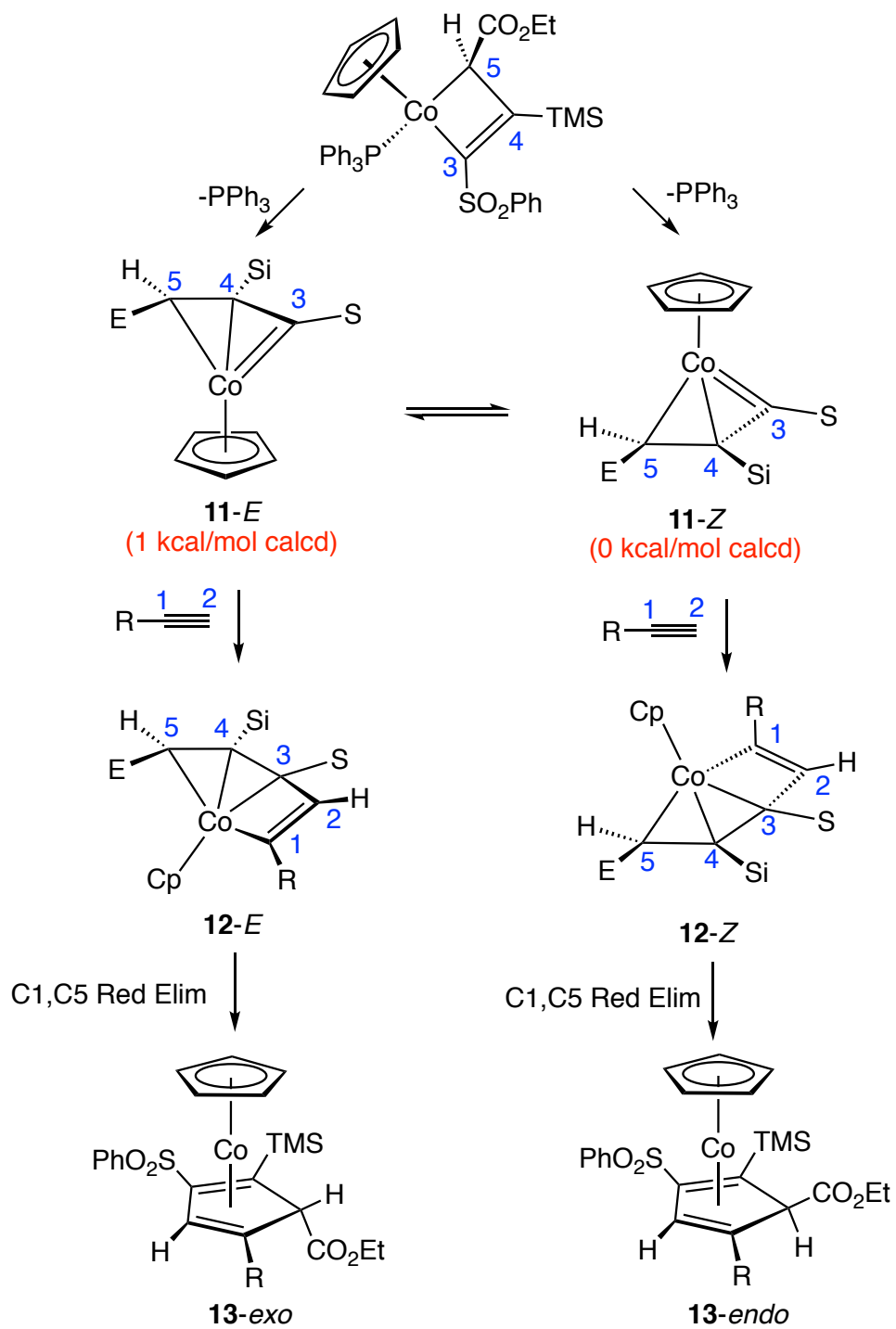
Scheme 3-11. Proposed mechanism of formation of η^4-cyclopentadiene complexes.

2. Formation of Vinylmatallacyclobutene and η^4-Cyclopentadiene Complexes

In order to explore the reactivity of other metallacyclobutenes towards alkynes, we carried out the reaction of phenylacetylene with metallacyclobutene (η^5-C_5H_5)(PPh$_3$)Co[C(CO$_2$Me)=C(CO$_2$Me)CH(CO$_2$Et)] (**15**). The cobaltacyclobutene **15** was firstly observed by Kevin Bunker. When he treated the cobalt-alkyne complex **14** with ethyl diazoacetate in benzene at ambient temperature, the formation of metallacyclobutene **15** with 74% yield was observed via ^{1}H NMR spectroscopy after 2 hours. However, it was found complex **15** is too unstable to be isolated.[9] Continued from his work, I utilized phenyl acetylene to trap the cobaltacyclobutene **15** to explore the reaction pattern of complex **15** with alkyne. The benzene solution of cobalt-alkyne complex **14** was treated with 1.5 equivalents of ethyl diazoacetate under inert atmosphere for 3 hours, and 5 equivalents of phenyl acetylene was subsequently loaded in the solution. The reaction mixture was heated up at 70 °C for 40 minutes under nitrogen, and the color of the solution gradually changed from dark brown to red. After chromatography on silica gel, complex **16** was obtained as a red air-stable solid with 46% yield (Scheme 3-12).
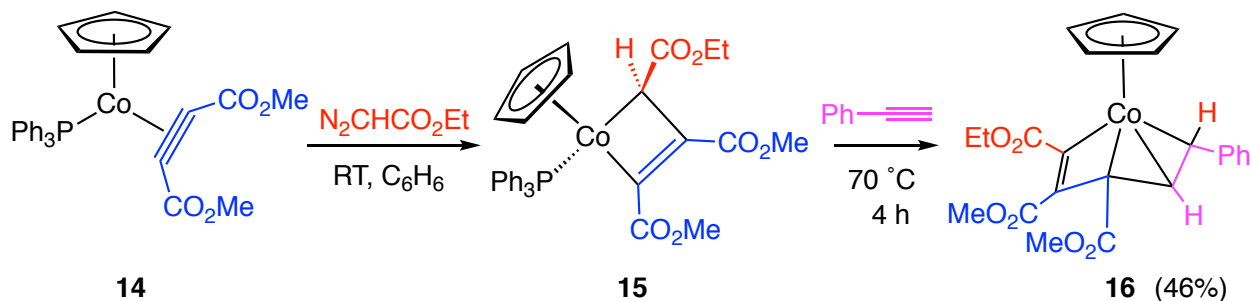
Scheme 3-12. Formation of vinylmetallacyclobutene complex **16**.

In the ^{1}H NMR spectrum (400 MHz, CDCl$_3$) of the isolated product, the ethyl ester group was observed as a methyl resonance δ 1.43 (t, 3H, J = 7.2 Hz) with two diastereotopic hydrogen resonances at δ 4.39 (m, 1H, CH_2CH$_3$) and 4.46 (m, 1H, CH_2CH$_3$). The two methyl esters were detected at δ 3.58 (s, 3H, Me) and 3.88 (s, 3H, Me), respectively. The integration of 5 hydrogen in the aromatic region indicates that phenyl acetylene is incorporated and triphenylphosphine ligand is no longer coordinated. The observance of the two vinyl hydrogen resonances at δ 4.01 (d, 1H, J = 11.2 Hz) and 6.59 (d, 1H, J = 11.2 Hz) suggests the presence of an internal disubstituted alkene, and thus excludes the η^4-cyclopentadiene structure. In the ^{13}C{^{1}H} NMR spectrum (125 MHz, CDCl$_3$), the 3 carbonyl carbon signals were observed at δ 160.6, 173.5, and 173.9, respectively. The C=O stretch was detected at 1702 cm^{-1} in the IR spectrum. High-resolution mass spectrum gives the chemical formula as C$_{23}$H$_{23}$CoO$_6$, which indicates that it is a structural isomer of η^4-cyclopentadiene.

Since the spectra data can't well define the structure, an X-ray crystallography analysis is urgent. The crystals were obtained from layering hexanes with saturated solution of the product in toluene at -20 °C, and the X-ray analysis reveals a single regio- and stereoiosmeric vinylmetallacyclobutene structure (SS, RR) with two stereocenters at Co and C3 (Figure 3-8). The C1 – C2 bond distance (1.318(7) Å) and C2 – C3 bond distance (1.509(7) Å) indicate a double-bond character and a single-bond character, respectively, which is consistent with the metallacyclobutene formulation (Table 3-6). The four-membered metallacycle structure is essentially planar with the largest deviation of planarity on C1 (0.002(2) Å) (the distance between C1 and the mean plane of Co-C1-C2-C3). The ester group attached on C2 is well conjugated with

metallacyclobuene with a small O3-C9-C2-C1 torsion angle (14.9(5) °); whereas the ester group attached on C1 is localized due the large dihedral angle of O1-C8-C1-C2 (82.6(7) °). The metallacyclobutene is welded by a metallacyclopropane with the phenyl substituent staying *trans* to the four-membered ring to release the steric congestion between the phenyl group and ethyl ester. The metallacyclopropane moiety was found essentially planar with a small dihedral angle of C4-C5-C6-C7 (8.2(8) °).
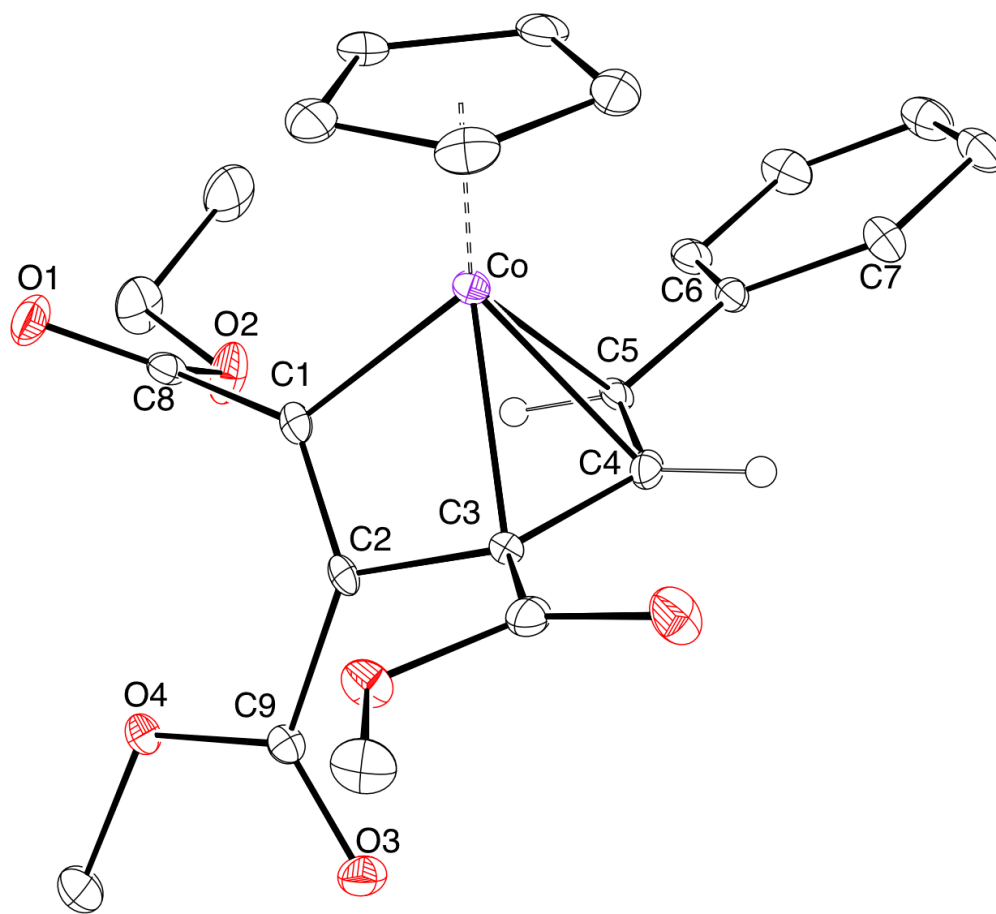
Figure 3-8. ORTEP drawing of complex **16** with ellipsoids shown at 30% probability.

Table 3-6. Seletecd bond distances (Å) and angles (deg) of vinylmetallacyclobutene **16**.

Co – C1	1.915(5)	Co – C4	1.995(6)
C1 – C2	1.318(7)	Co-C1-C2	99.1(3)
C2 – C3	1.509(7)	C1-C2-C3	105.3(4)
C3 – C4	1.429(6)	C2-C3-Co	86.9(3)
C4 – C5	1.397(8)	Co-C5-C4	65.8(3)
C5 – Co	2.109(5)	C4-C5-C6-C7	8.2(8)
C3 – Co	2.066(5)	O3-C9-C2-C1	14.9(5)

Since vinylmetallacyclobutene has been proposed as intermediate for the formation of η^4-cyclopentadiene,[4] complex **16** was allowed to heat at 70 °C in CDCl$_3$, and the reaction was monitored by ^{1}H NMR spectroscopy. However, after 48 hours, there was no reaction occurred to generate the desired η^4-cyclopentadiene (Scheme 3-13).

16
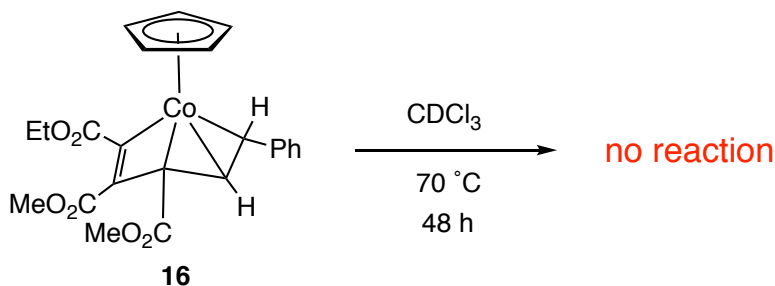
Scheme 3-13. No thermolysis reaction on complex **16**.

Mechanistically, for the formation of vinylmetallacyclobutene **16**, we proposed that upon the dissociation of triphenylphosphine from metallacyclobutene **15**, the vinyl carbene intermediate **17** is generated, that is followed by the insertion of phenyl acetylene to the alkylidene to give the metallacycle intermediate **18**, in which the phenyl

substituent selectively stays close to the cobalt to avoid steric congestion (Scheme 3-14). Oxidative addition of the cobalt agostic intermediate **19** generates the metallabenzene intermediate **20**, and after reductive elimination of the hydride and the carbon bearing phenyl group, a vinyl carbene intermediate **21** can be produced. The final vinylmetallacyclobutene complex **16** is afforded by a followed rearrangement of **21**. According to our previous metallacyclobutene examples, it is found that an electron-withdrawing group attached on the C1 position is helpful to stabilize the four-membered ring structure by strengthening the Co − C1 bond.[8,10] Compare vinylmetallacyclobutene **18** and 1**6**, one may expect that the latter is more stable for the reason that ester group is a better electron-withdrawing group than phenyl group, which serves as the driven force for the hydride shift of intermediate **18**.
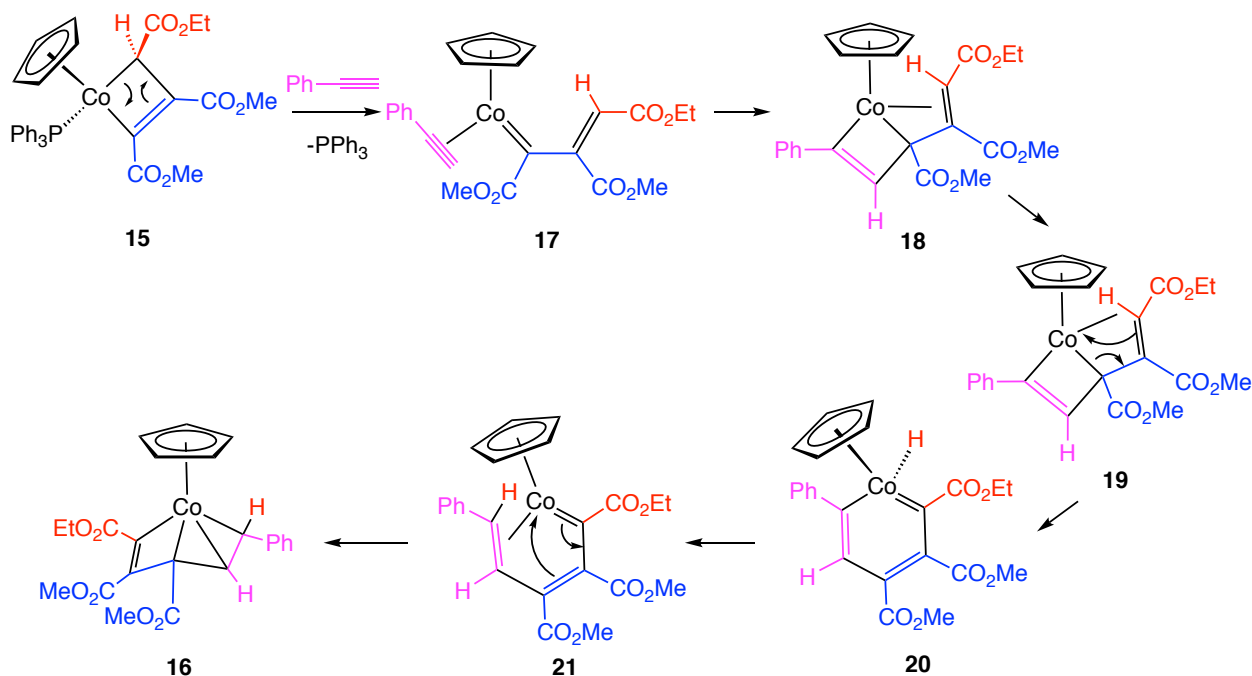
Scheme 3-14. Formation of complex **16** from metallacyclobutane **15**.

242

A similar reaction was also carried out with a different metallacyclobutene (η^5-C_5H_5)(PPh_3)Co[C(Ph)=C(COCF$_3$)CH(CO$_2$Et)] (**22**) and phenyl acetylene. Complex **22** (0.357 g, 0.532 mmol) was mixed with phenyl acetylene (0.272 g, 2.663 mmol) in 60 mL of dry benzene in a glove box (Scheme 3-15). The reaction mixture was heated at 70 °C, and reaction was monitored by TLC analysis. After 2 hours, when all the starting metallacyclobutene was consumed, chromatography on silica gel gave two products as air-stable solids: major product (dark red, 56.7% yield) and minor product (light green, 23.3% yield).
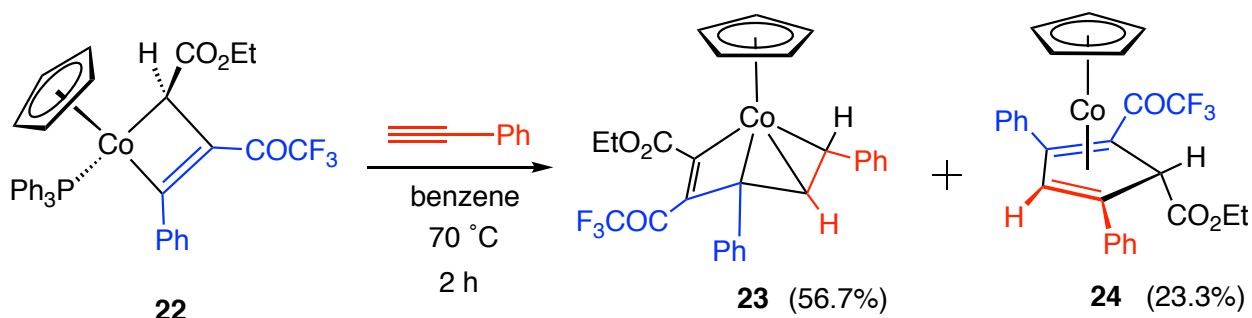
Scheme 3-15. Reaction of metallacyclobutane **22** with phenyl acetylene.

The ^{1}H NMR spectrum (400 MHz, CDCl$_3$) of the major product has very similar patterns to vinylmetallacyclobutene complex **16**. The ester group was observed at δ 1.48 (t, 3H, J = 7.2 Hz), 4.47 (q, 2H, J = 7.2 Hz). Two vinyl hydrogen resonances on the internal disubstituted alkene were detected at δ 3.89 (d, 1H, J = 10.8 Hz) and 6.25 (d, 1H, J = 10.8 Hz), respectively. The integration of 10 aromatic hydrogen signals is consistent with the two phenyl groups that are from cobaltacyclobutene **22** and phenyl acetylene. In the ^{13}C{^{1}H} NMR spectrum (125 MHz, CDCl$_3$), the characteristic C − F

couplings of trifluoromethylacetyl group shows at δ 116.3 (q, J_{CF} = 291 Hz, COCF_3) and 163.7 (q, J_{CF} = 35.4 Hz, COCF$_3$). An abnormally deshielded vinyl carbon resonance at δ 173.5 might be attributed to the strong electron-withdrawing effect of the adjacent trifluoromethylacetyl group. The carbonyl C=O stretch was exhibited at 1705 cm^{-1} in the IR spectrum, which is consistent with what was observed in vinylmetallacyclobutene complex **16**.

The single crystal of the major product was obtained from recrystallization in toluene and hexanes at -20 °C. As we anticipated, X-ray crystallography analysis gives a vinylmetallacyclobutene structure **23** (Figure 3-9). Complex **23** also turns out to be a single regio- and stereoiosmeric structure (SS, RR) with two stereocenters at Co and C3. The selected bond distances and angles are summarized in Table 3-7. The metallacyclobutene ring Co-C1-C2-C3 is essentially planar with the largest deviation of planarity on C2 (0.0006(14) Å). The phenyl group that sits *trans* to the four-membered ring is well conjugated with the alkene, with a small dihedral angle of C4-C5-C6-C7 (4.1(3) °). The delocalization of trifluoromethylacetyl group with cyclobutene is manifested by the small torsion angle of O3-C9-C2-C1 (4.4(2) °). Compared to complex **16**, the C1 – C2 bond distance is significantly longer in complex **23** (Δ = 0.34 Å), which might be attributed to the stronger contribution of resonance structure of the α,β-unsaturated moiety of the trifluoromethylacetyl group.
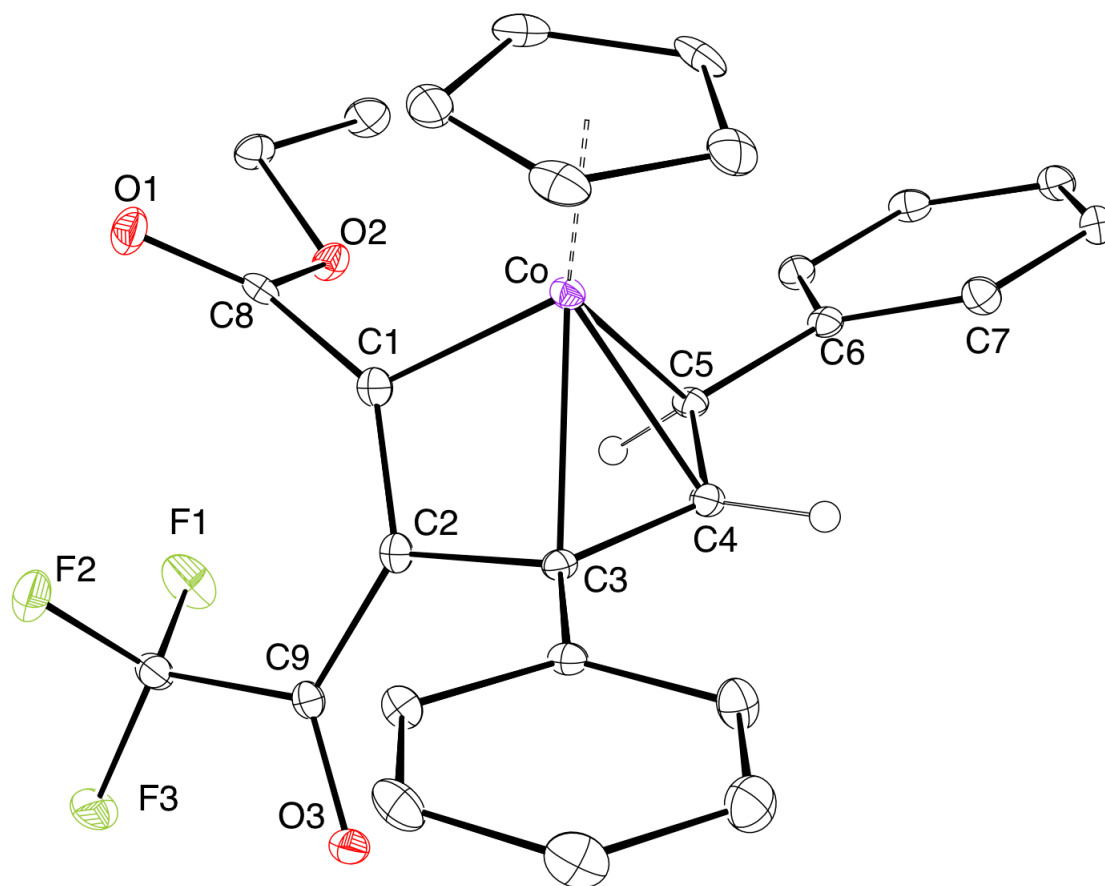
Figure 3-9. ORTEP drawing of complex **23** with ellipsoids shown at 30% probability.

Table 3-7. Seletecd bond distances (Å) and angles (deg) of vinylmetallacyclobutene **23**.

Co – C1	1.890(2)	Co – C4	2.003(2)
C1 – C2	1.352(3)	Co-C1-C2	100.0(2)
C2 – C3	1.509(3)	C1-C2-C3	104.8(2)
C3 – C4	1.421(3)	C2-C3-Co	86.23(19)
C4 – C5	1.421(3)	Co-C5-C4	73.68(16)
C5 – Co	2.099(2)	C4-C5-C6-C7	14.1(3)
C3 – Co	2.106(2)	O3-C9-C2-C1	4.4(2)

For the minor product, high-resolution mass spectrometry gave a chemical formula as $C_{27}H_{22}CoF_3O_3$, which is the same as the major product **23**. However, the signal patterns of the minor product in ^1H NMR spectrum (400 MHz, $CDCl_3$) are different from complex **23**. The two vinyl hydrogen resonances with doublets as in complex **23** are no longer present, but instead, two singlet signals were detected as δ 4.45 (s, 1H) and 6.14 (s, 1H), which highly matches the range of ring hydrogen resonances (both the vinyl hydrogen and hydrogen attached on the sp^3 ring carbon) that were observed in our previous η^4-cyclopentadiene systems.[4] In the $^{13}C\{^1H\}$ NMR spectrum (125 MHz, $CDCl_3$), four shielded vinyl carbon resonances are exhibited at δ 58.5, 61.0, 83.7, and 101.0, respectively. The characteristic trifluoromethylacetyl group was observed at δ 117.0 (q, J_{CF} = 292.5 Hz, $COCF_3$) and 186.0 (q, J_{CF} = 33.7 Hz, $COCF_3$). The carbonyl C=O stretch was measure at 1728 cm^{-1} in the IR spectrum.

The X-ray quality crystals of the minor product were also successfully obtained from recrystallization in toluene and hexanes at -20 °C. As we expected, the crystallography analysis reveals an exo-η^4-cyclopentadiene structure **24** (Figure 3-10). The phenyl group from phenyl acetylene is selectively attached on C1, which follows the same trend of other η^4-cyclopentadienes mentioned earlier, such as **4**-*exo*, **4**-*endo*, and **5**-*exo*. The representative bond distances and angles are summarized in Table 3-8. The cyclopentadiene ring is puckered with a (C1-C4-C5)-(C1-C2-C3-C4) plane-plane fold angle of 32.0(2) °, and the Co⋯C5 nonbonding distance is measured as 2.566(3) Å. A good $\pi - \pi$ interaction of the trifluoromethylacetyl group and diene moiety is manifested by the planar structure with a small dihedral angle of O1-C6-C4-C3 (4.7(3) °). Compared to complex **4**-*exo*, the smaller steric hindrance between trifluoromethylacetyl

group and Cp ligand in complex **24** is reflected by the shorter Co – C4 distance ($\Delta =$ 0.028 Å). Despite less steric congestion is present between C3 and C4 in complex **24** than in **4**-*exo* due to the different sizes of substituents attached on the two carbons, the C3 – C4 bond distance in **24** is detected longer ($\Delta = 0.01$ Å) than complex **4**-*exo*, which might be attributed to a stronger back-donation effect from the metal center on the alkene in **24**.
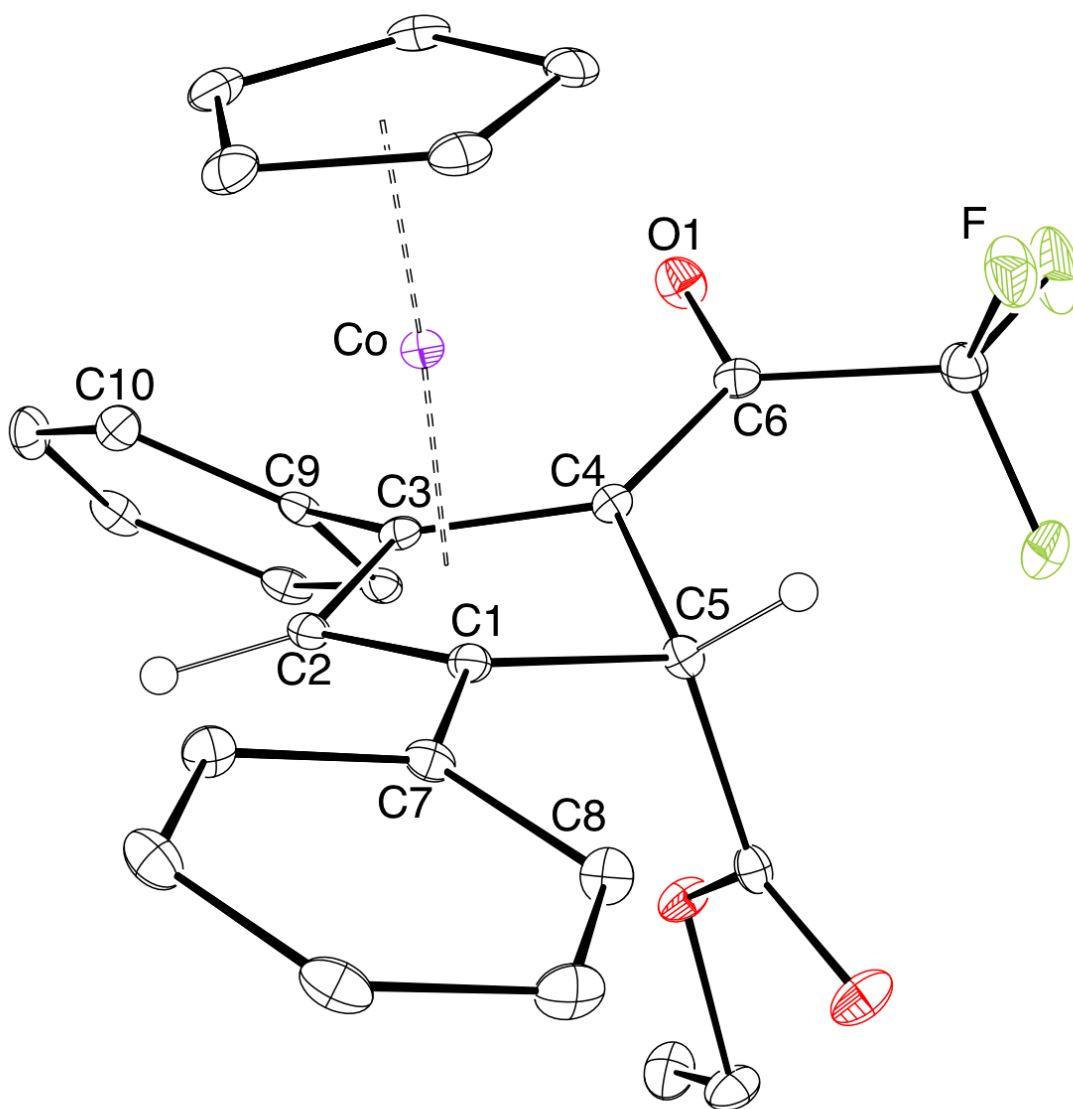
Figure 3-10. ORTEP drawing of **24** with ellipsoids shown at 30% probability.

Table 3-8. Seletecd bond distances (Å) and angles (deg) of complex **24**.

C1 – C2	1.430(3)	Co – C3	1.986(2)
C2 – C3	1.429(3)	Co – C4	2.033(2)
C3 – C4	1.454(3)	C1-C5-C4	95.61(18)
C4 – C5	1.535(3)	C2-C1-C8-C7	23.7(3)
C5 – C1	1.537(3)	O1-C6-C4-C3	4.7(3)
Co – C1	2.057(2)	ring fold angle	32.0(2)
Co – C2	1.986(2)	Co····C5	2.566(3)

When a benzene-d_6 solution of complex **23** was heated at 70 °C in an NMR tube under inter atmosphere, it was found that complex **23** could be slowly converted into complex **24**. The reaction was monitored by ^{1}H NMR spectroscopy. After 55 days, all the starting complex **23** was consumed, and 54.5% NMR yield of complex **24** was obtained based on the integration of the Cp resonance relative to internal standard (Scheme 3-16).
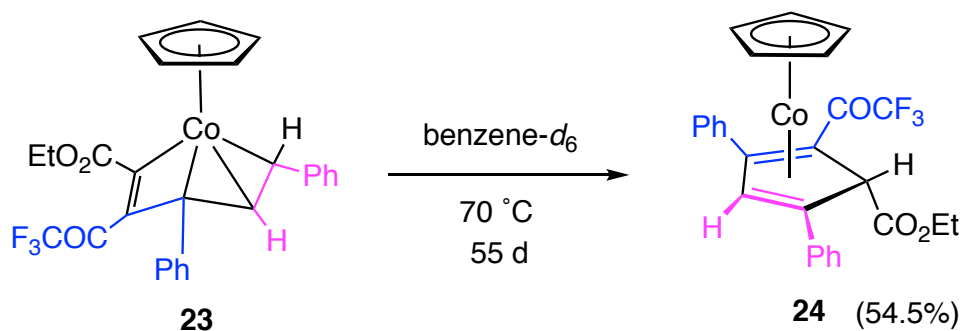
Scheme 3-16. Formation of complex **24** from vinylmetallacyclobutene **23**.

The mechanism of formation of vinylmetallacyclobutene **23** should be very similar as complex **16**. After dissociation of triphenylphosphine from metallacyclobutene **22**, a vinyl carbene intermediate **25** is generated, which couples with the phenyl acetylene to

produce vinylmetallacyclobutene intermediate **26**. Metallabenzene intermediate **27** is generated from oxidative addition of **26**, which is followed by a reductive elimination to afford complex **23**. Alternatively, rearrangement of intermediate **26** followed by coordination of a phosphine ligand can produce metallacyclohexadiene intermediate **28**, and after reductive elimination, the η^4-cyclopentadiene complex **24** is afforded (Scheme 3-17). It should be noted that the cobalt-mediated hydride transfer process from **26** to **23** should be reversible for the generation of complex **24** from **23**.
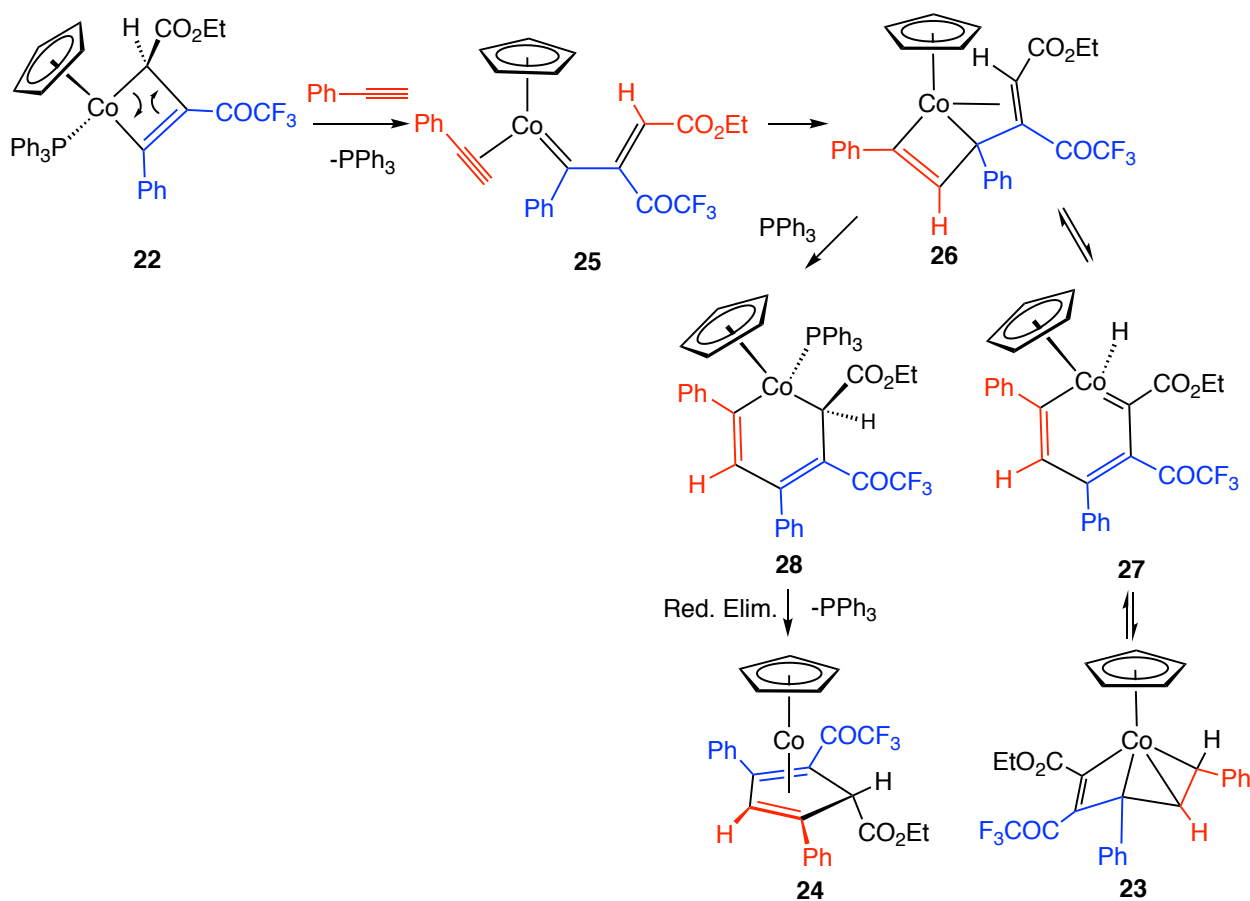
Scheme 3-17. Formation of complexes **23** and **24** from metallacyclobutane **22**.

3. Reaction of Vinyl Diazoacetate with Cobalt-Alkyne Complex

The method that has been employed to synthesize cobalt η^4-cyclopentadiene complexes in this chapter so far is all utilizing cobalt-alkyne complex reacting with a carbene to form metallacyclobutene intermediate followed by coupling with a second alkyne. However, the examples of cobaltacyclobutene are still very rare in the literature, and the stability of metallacyclobutene is found subjected to both ring substituents and ancillary ligands. Also, cobalt-alkyne complexes are more readily available and have higher functional group tolerance than metallacyclobutenes. Herein, we describe an alternative method to assemble cobalt η^4-cyclopentadiene complex by employing cobalt-alkyne complex **29** reacting with a vinyl carbene molecule **32** that is essentially the combination of a carbene and an acetylene (Scheme 3-18).
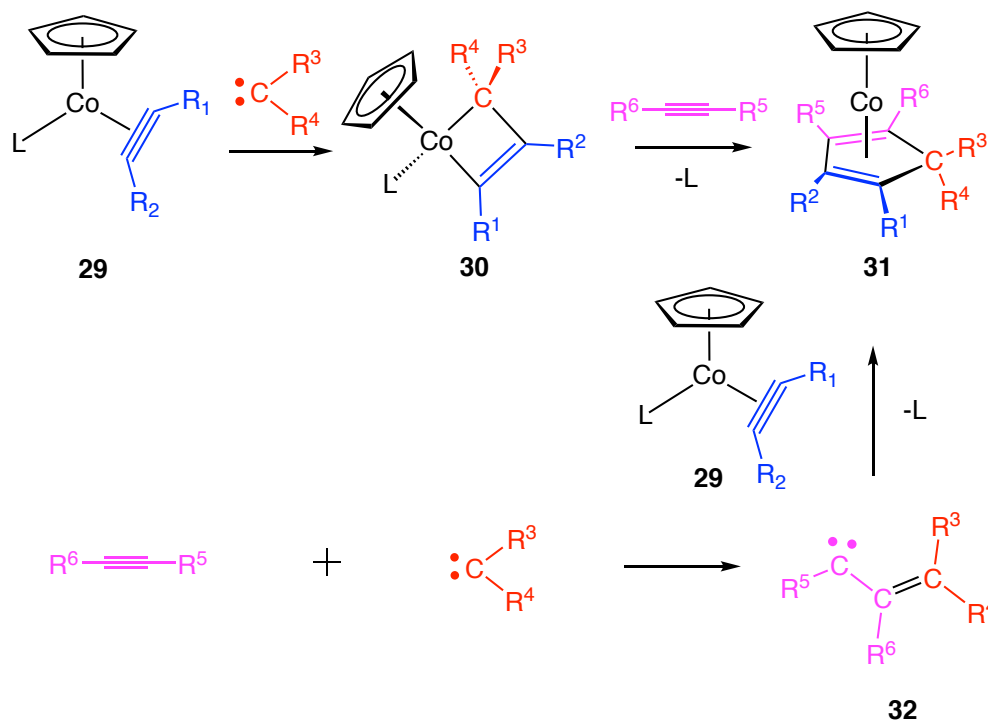
Scheme 3-18. Two possible ways to assemble η^4-cyclopentadiene complex.

In order to prepare the vinyl carbene starting material, we modified the literature reported procedure of synthesis of vinyl diazoacetate **36**.[11,12] An acetone (20 mL) solution of 4-acetylbenzenesulfonyl chloride (**33**, 3.85 g, 20 mmol) was added dropwise over 1 hour into a water (10 mL) solution of sodium azide (2 g, 30 mmol) at 0 °C. The reaction mixture was allowed to warm up to ambient temperature for another 11 hours. After extraction with ethyl acetate, the crude product **34** (92% yield) can be used without any further purification (Scheme 3-19). Then molecule **34** was treated with one equivalent of unsaturated ester **35** in acetonitrile at -20 °C with slowly loading of DBU as base. After keep stirring the reaction at 0 °C for 30 minutes, work up and chromatography on silica gel afforded vinyl diazoacetate **36** as a red oil with 80% yield. It was noted that molecule **36** needs to be stored at -20 °C, and slow decomposition of **36** was observed at ambient temperature via a self-annulation process to produce pyrazole derivative **37** (Scheme 3-20).

Scheme 3-19. Syntheis of vinyl diazoacetate **36**.

Scheme 3-20. Selft annulation of vinyl diazoacetate **36**.

Most of our previously synthesized η^4-cyclopentadiene complexes were prepared from metallacyclobutene **2**, which is made from the coupling of cobalt-alkyne complex **38** with ethyl diazoacetate. In order to compare to our previous results, the reaction of vinyl diazoacetate **36** with cobalt-alkyne complex **38** was carried out. The complex **38** was treated with 3 equivalents of vinyl diazoacetate **36** in benzene at ambient temperature under inert atmosphere. The reaction mixture was stirred in a glove box and monitored by using ^{1}H NMR spectroscopy (Scheme 3-21). The color of the solution gradually changed from dark to red. After 3 days, all the starting material **38** was consumed, and chromatography on silica gel gave a red air-stable solid (60% NMR yield).
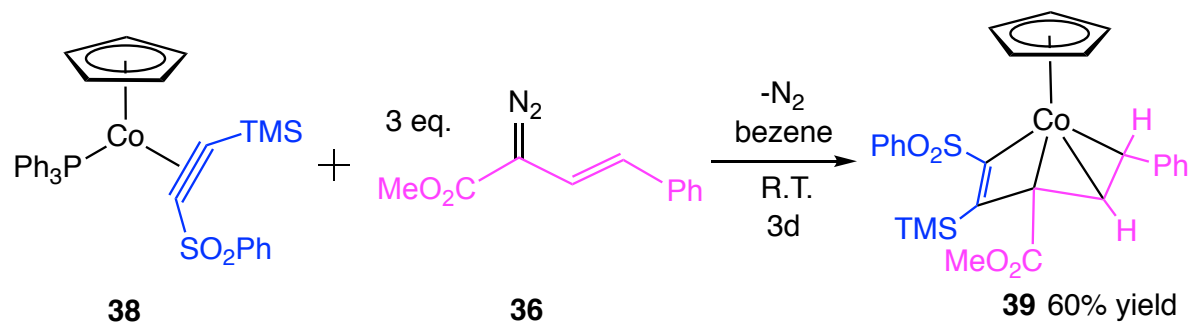
Scheme 3-21. Reaction of cobalt-alkyne complex **38** with vinyl diazoacetate **36**.

In the ^{1}H NMR spectrum (400 MHz, CDCl$_3$) of the product, the TMS and sulfone group are still present via the resonances at δ 0.12 (s, 9H, SiMe$_3$), 7.67 (t, 2H, J = 7.6 Hz, H$_m$), 7.76 (t, 1H, J = 7.2 Hz, H$_p$), 8.10 (d, 2H, J = 7.6 Hz, H$_o$). The incorporation of vinyl diazoacetate **36** is confirmed by the methyl ester at δ 3.91 (s, 3H). The integration of 10 hydrogens in the aromatic region indicates that the phosphine ligand is not coordinated anymore. Two vinyl hydrogen resonances were detected at δ 3.30 (d, 1H, J = 11.6 Hz) and 6.34 (d, 1H, J = 11.6 Hz), which excludes the possibility of η^4-cyclopentadiene structure. The carbonyl carbon of ester group was observed in the ^{13}C{^{1}H} NMR spectrum (125 MHz, CDCl$_3$) at δ 174.7, and the C=O bond stretch shows at 1707.3 cm^{-1} in the IR spectrum.

The crystals of the product were obtained from recrystallization in toluene and hexanes at -20 °C, and X-ray crystallography analysis reveals a vinylmetallacyclobutene structure (Figure 3-11). Analogous to other vinylmetallacyclobutene structures we obtained before, Complex **39** also turns out to be a single regio- and stereoiosmeric structure (SS, RR) with two stereocenters at Co and C3. The metallacyclobutene ring is essentially planar with the largest deviation from planarity is on C3 (0.00057(6) Å). The selected bond distances and angles are summarized in Table 3-9. Compared to vinylmetallacyclobutene **23**, the steric hindrance between sulfone group and Cp ligand is manifested by the longer C1 – Co distance (Δ = 0.0405 Å), and the steric congestion between TMS group and ester in complex **39** is reflected by the longer C2 – C3 bond distance (Δ = 0.01 Å). The sterical interaction among TMS group, sulfone group, and ester group also narrows down the C1-C2-C3 angle in complex **39** (Δ = 4.94 °) The small dihedral angle of C4-C5-C6-C7 (17.088(13) °) indicates that the phenyl

substituent is well conjugated with the C3-C4-C5 allylic system; whereas the double bond in the metallacyclobutene ring is localized from the allylic system by the large torsion angle of C1-C2-C3-C4 (63.745(7) °). The nonbonding C1····C5 distance is measured as 2.732(3) Å.
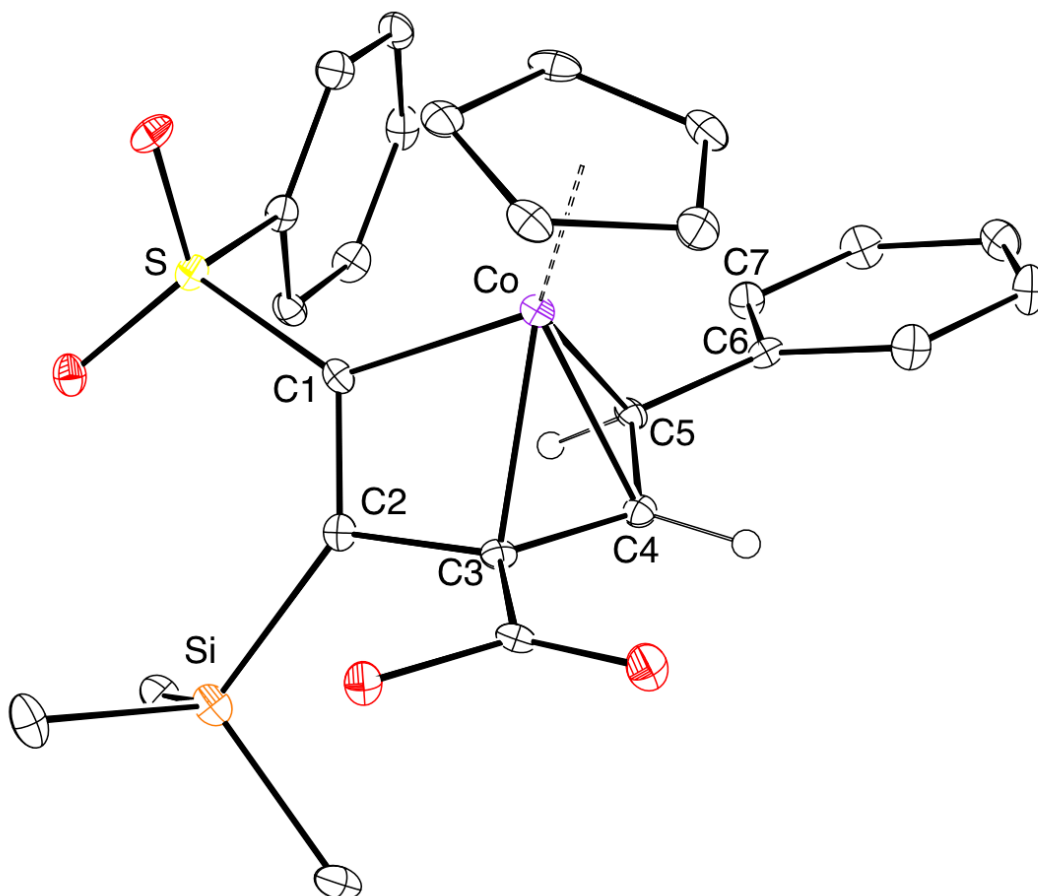
Figure 3-11. ORTEP drawing of **39** with ellipsoids shown at 30% probability.

Table 3-9. Seletecd bond distances (Å) and angles (deg) of complex **39**.

Co – C1	1.9305(3)	Co – C4	1.9966(3)
C1 – C2	1.33883(13)	Co – C5	2.1188(2)
C2 – C3	1.51850(17)	Co-C1-C2	102.731(7)
C3 – C4	1.42053(17)	C1-C2-C3	99.859(9)
C4 – C5	1.41482(18)	C2-C3-Co	90.964(10)
Co – C3	2.06094(19)	C4-C5-C6-C7	17.0881(13)
C1····C5	2.7324(2)	C1-C2-C3-C4	63.745(7)

For the mechanism of formation of complex **39**, we proposed that the α carbon of vinyl diazoacetate **36** undergoes a nucleophilic attack on the C2 position of cobalt-alkyne complex **38**, which is followed by loss of a triphenylphosphine ligand to generate the cobalt anion intermediate **40** (Scheme 3-22). Extrusion of a nitrogen gas via the nucleophilic attack from the anionic metal center produces the vinyl metallacyclobutene **39**. It is not clear why the α carbon of vinyl diazoacetate selectively attack the more electron-rich C2 instead of the C1 that bears an electron-withdrawing sulfone group. One possible reason is that Co – C1 bond is much stronger than the Co – C2 bond due to the more back-donation effect on the C1 site.
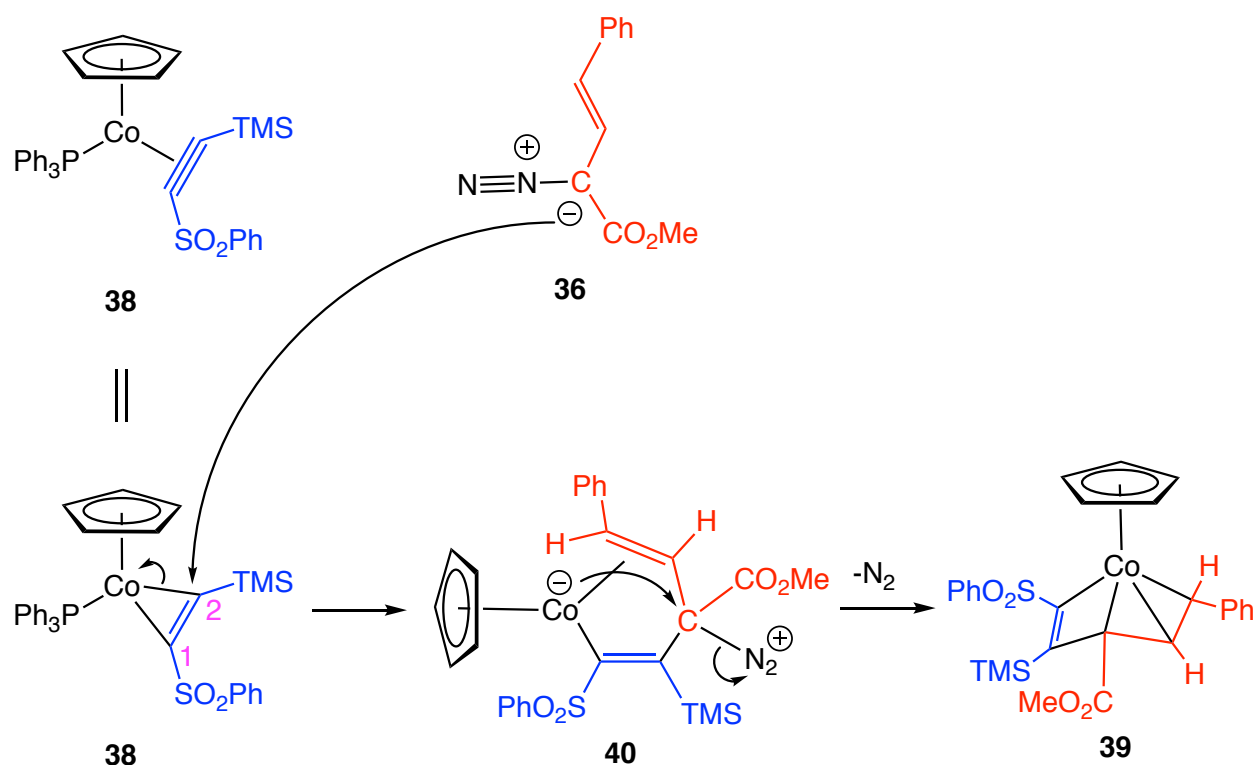
Scheme 3-22. Formation of vinylmetallacyclobutene complex **39**.

A thermolysis reaction was subsequently conducted on the isolated complex **39**. The toluene (20 mL) solution of complex **39** (100 mg, 0.186 mmol) was placed into a Teflon-sealed reaction tube under nitrogen. The reaction mixture was heated at 180 °C and monitored by ^{1}H NMR spectroscopy. After 90 minutes, all the starting complex **39** disappeared, and chromatography on silica gel afforded a red slightly air-sensitive oil (80% NMR yield).

The ^{1}H NMR spectrum (400 MHz, CDCl$_3$) of the product indicates that it is a mixture of two complexes with a 2 : 1 ratio (Scheme 3-23). Unfortunately, further attempt to isolate the two molecules failed due to the close polarities of the two isomers. Besides the Cp and TMS resonances of the two complexes, two sets of ring hydrogen signals located at δ 3.24 (s, 1H), 3.45 (s, 1H); and δ 3.92 (d, 1H, J = 2.8 Hz), 4.16 (d,

1H, J = 2.8 Hz) indicate the η^4-cyclopentadiene structure of the two molecules. The major product is assigned as *exo* isomer for the reason that the ring hydrogen resonances are more deshielded, which is the trend we observed on other η^4-cyclopentadiene complexes. The regiochemistry of the two isomers are speculated based on the mechanism we proposed for the formation of other η^4-cyclopentadiene complexes, i.e., a hydride shift occurs before the reductive elimination (see Scheme 3-17).
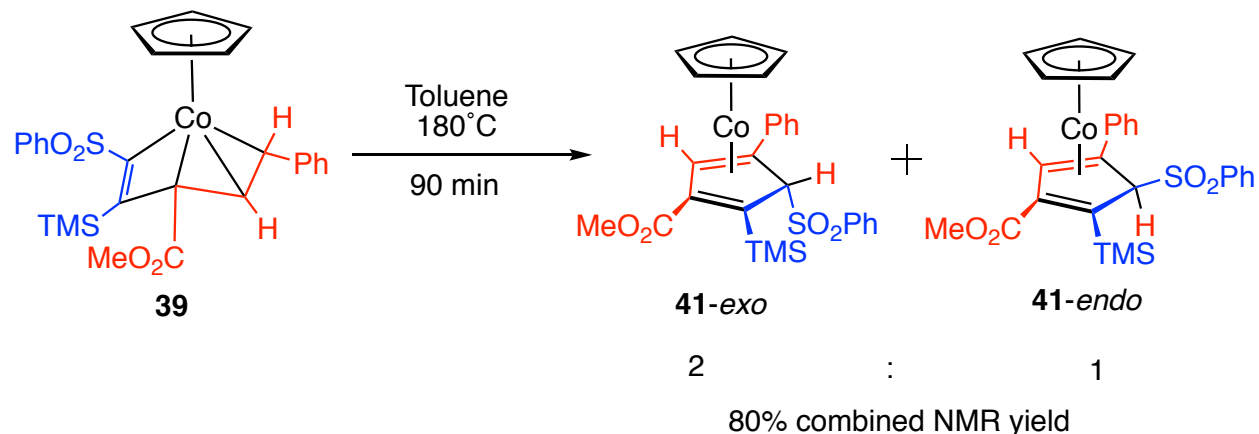
Scheme 3-23. Thermolysis of vinylmetallacyclobutene **39**.
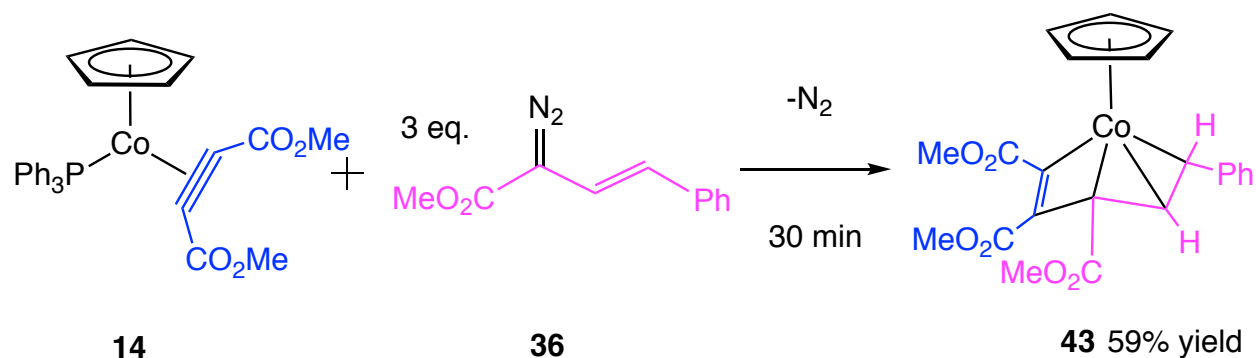
Scheme 3-24. Reaction of alkyne complex **14** with vinyl diazoacetate **36**.

In addition, another readily available cobalt-alkyne complex $(C_5H_5)(PPh_3)Co[C(CO_2Me)\equiv C(CO_2Me)]$ (**14**) was also employed to be examined with 5 equivalents of vinyl diazoacetate **36** in benzene-d_6 under inert atmosphere (Scheme 3-24). Different from the scenario of complex **38**, it was found that no reaction occurred at ambient temperature, and then the mixture was heated at 70 °C. After 30 minutes, all the starting cobalt-alkyne complex was consumed, and the product complex **43** was obtained with a 59% NMR yield based on the integration of Cp resonance at δ 4.32. The structure of complex **43** is supported by the ^{1}H NMR spectrum (400 MHz, C_6D_6). The three methyl resonances of ester groups were observed at δ 3.32 (s, 3H), 3.57 (s, 3H), and 3.69 (s, 3H). The two characteristic vinyl hydrogen signals located at δ 4.14 (d, 1H, J = 11.2 Hz) and 6.57 (d, 1H, J = 11.2 Hz) indicate the vinylmetallacyclobutene structure. Unfortunately, the further isolation of pure complex **43** failed due the close polarity to the pyrazole molecule **37**, which brought the difficulty to separate the two molecules in chromatography.

For the future direction: (1) More cobalt-alkyne complexes can be employed as precursors to examine the reaction with vinyl diazoacetate to assemble either vinylmetallacylobutene or η^4-cyclopentadiene complexes; (2) Vinyl diazoacetate **36** can be potentially used as a versatile building block to react with $CpCo(PPh_3)_2$, alkylidene complexes, metal-alkene complexes, and metallacyclobutenes to develop new reaction patterns; (3) The reactivity of vinylmetallacyclobutene can be further explored, such as demetallation, oxidation/reduction, and reactions with acid/base.

C. Formation of Cabaltocenium Cation From η^4-Cyclopentadiene Complexes

1. Introduction

Metallocene is one of the oldest organometallic species that was discovered in history, which has been attracted tremendous attentions in a lot of different research areas since 1950s, such as materials science, pharmaceutical industry, catalysis, etc. Ferrocene, in particular, serves as the leading member of the metallocene complex family,[13] and has been vastly explored on its great potentials in catalytic, optical, magnetic and biological applications.[13, 14]

As the analogue of ferrocene, cobaltocene has one more valence electron (19 e) than ferrocene, which makes it readily to lose one electron with a 5.56 eV ionization potential to generate the cobaltocenium cation.[15,16] Cobaltocenium salt, as the isoelectronic structure of ferrocene, has also been extensively studied in polymer chemistry[17] and biochemical functions.[18] A few examples of preparing functionalized cobaltocenium complexes can be found in the literature. For instance, Vanicek reported that a carboxylic acid derivative **45** can be obtained over 3 steps from cobaltocenium **44** via alkylation, hydride abstraction, and oxidation processes (Scheme 3-25).[19] Cobaltoceniumdiazonium **46** can be treated with various nucleophiles via Sandmeyer-type reactions to produce halogen substituted cobaltocenium.[20] Direct amination of cobaltocenium hexafluoridophosphate was reported by Bildstein via a "vicarious nucleophilic substitution" reaction.[21] The nitro group can be installed on the

cyclopentadienyl ring by the modification of carboxylic acid derivative **49** in multiple steps.[22]
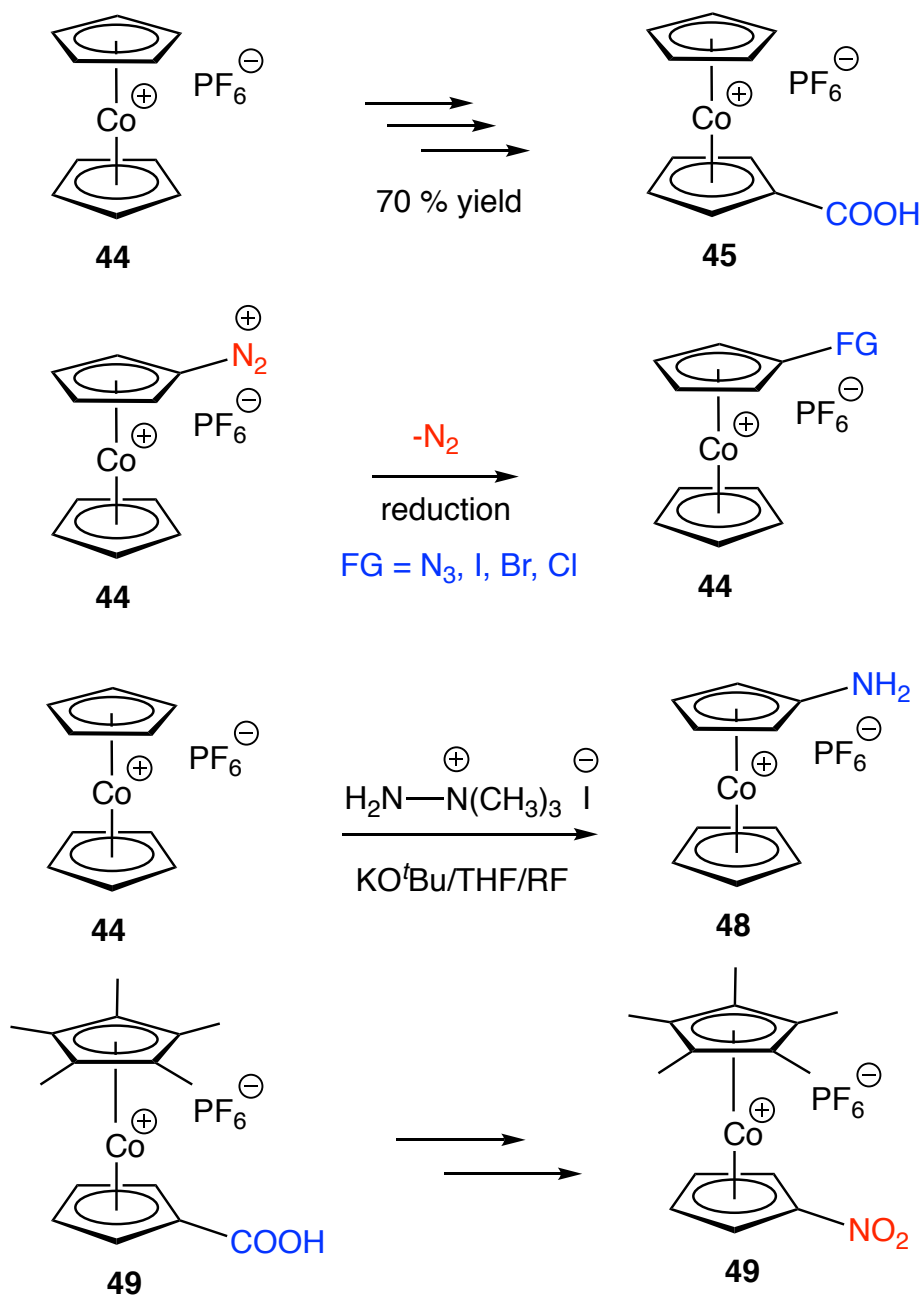
Scheme 3-25. Synthesis of functionalized cobaltocenium cations.

Despite some synthetic strategies of monosubstituted cobaltocenium derivatives have been developed, however, compared to ferrocene, cobaltocenium salts are highly polar, cationic species, which impedes their chemical functionalization by common organic reactions that are widely used in ferrocene. It was found extremely hard to synthesize multi-substituted derivatives of cobaltocenium salts.[23] Herein, we describe a novel way of preparing trisubstituted cobaltocenium salts with excellent yields and high regioselectivities by manipulations of cobalt η^4-cyclopentadiene complexes that are essentially synthesized from a formal [2 + 2 + 1] cycloadditon reaction. In addition, an unprecedented umpolung fragmentation was observed upon the oxidation of hydroxyl cobalt-η^4-cyclopentadiene complexes to form the final cobaltocenium salts.

2. Preparation of Hydroxyl Cobalt-η^4-cyclopentadiene Complexes

To synthesize the cobaltocenium cations, the first step is making the hydroxyl cobalt-η^4-cyclopentadiene complexes as precursors, in which the ester group on the sp^3 ring carbon is reduced to alcohol. It was found that diisobutylaluminium hydride (DIBAL-H) reducing agent gives the best yields in our η^4-cyclopentadiene systems, and it reacts cleanly with the *exo* isomers to afford the desired hydroxyl cobalt-η^4-cyclopentadiene complex, while the reactions to *endo* isomers produce multiple products.[7] Accordingly, seven different *exo*-η^4-cyclopentadiene complexes that were synthesized earlier in this chapter (R = Me, CH$_2$OCH$_3$, CH$_2$OH, Ph, p-C$_6$H$_4{}^t$Bu, p-C$_6$H$_4$NMe$_2$, SnBu$_3$) were employed as starting materials to carry out this reduction reactions.

The first one we examined is the methyl substituted *exo*-η^4-cyclopentadiene complex **4**-*exo*. A dry toluene (100 mL) solution of complex **4**-*exo* (200 mg, 0.40 mmol) was added into an oven-dried Teflon sealed reaction tube (Scheme 3-26). Then five equivalents of DIBAL-H (2.0 mmol, 1.2 M in toluene) were injected into the solution under argon at -78 °C while keeping it stirring. Some foaming was observed in the adding process. The reaction mixture was kept at -78 °C for 2 hours, then 0 °C for 4 hours before quenched with methanol. After aqueous work up and chromatography on silica gel, 88 % yield of products were obtained as slightly air-sensitive red solids.
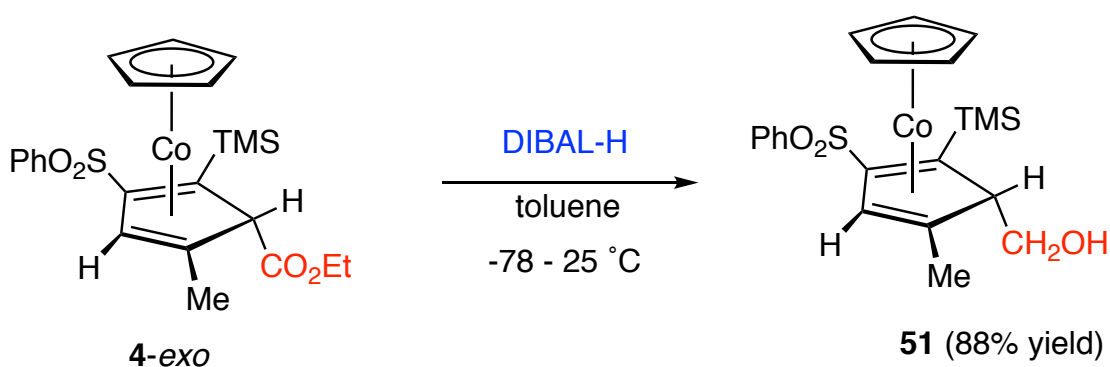
Scheme 3-26. Reduction of complex **4**-*exo* by DIBAL-H.

In the ^{1}H NMR spectrum (400 MHz, CDCl$_3$) of the isolated product, the methyl group, vinyl-ring hydrogen, and trimethylsilane group are still present, and have similar chemical shifts as the starting **4**-*exo* at δ 1.28 (s, 3H, Me), 5.44 (s, 1H, vinyl-H), and 0.16 (s, 9H, TMS), respectively. However, the ethyl group on the starting material is no longer present, and instead, the assumed hydroxyl methyl group shows two distereotopic hydrogen resonances at δ 2.43 (m, 1H) and 2.67 (m, 1H). The presence of the hydroxyl group was confirmed by the disappearance of the signal at δ 0.37 (dd, 1H,

J = 5.0 Hz, 7.0 Hz) upon adding D_2O. Also, the ring hydrogen attached on *sp*^{3} carbon was observed changing from a singlet to a triplet δ 2.88 (t, 1H, *J* = 4.0 Hz) due to the coupling with the hydroxyl methyl moiety. In the $^{13}C\{^1H\}$ NMR spectrum (125 MHz, CDCl$_3$), the carbonyl carbon of the ester group at δ 166.3 in complex **4**-*exo* is gone, and the 13 different carbon environments is consistent with the proposed hydroxyl cobalt-η^4-cyclopentadiene structure. Required by the NMR spectra data, the C=O stretch of complex **4**-*exo* at 1718 cm^{-1} in the IR spectrum is no longer present; whereas the emergent of a broad peak at 3517 cm^{-1} supports the existence of hydroxyl group.

The crystals of the product were obtained from recrystallization in toluene and hexanes at ambient temperature. As we anticipated, the X-ray crystallography analysis reveals a hydroxyl cobalt-η^4-cyclopentadiene structure (Figure 3-12), in which the phenylsulfone group remains without any reduction. The cyclopentadiene ring exhibits a staggered conformation to the Cp ligand through the cobalt. The bond angle and distances of complex **51** are very similar to the starting ester substituted η^4-cyclopentadiene complex **4**-*exo* (Table 3-10). The C3 – C4 bond distance (1.452(3) Å) is significantly longer than the C1 – C2 distance (1.418(3) Å), which is ascribed to the steric hindrance between the bulky TMS and phenylsulfone group, and the greater steric congestion of the hydroxylmethyl group with the TMS group than the methyl group is manifested by the longer C4 – C5 bond distance relative to C1 – C5 bond distance (Δ = 0.026 Å). Compared to complex **4**-*exo*, the cyclopentadiene ring of complex **51** has a larger deviation from planarity with a greater ring-fold angle [(C1-C4-C5)-(C1-C2-C3-C4) plane-plane fold angle)] (Δ = 3.2 °), which is consistent with the longer Co⋯C5 nonbonding distance in complex **51** (Δ = 0.049 Å).

Figure 3-12. ORTEP drawing of **51** with ellipsoids shown at 30% probability.

Table 3-10. Comparison of seletecd bond distances (Å) and angles (deg) of complex **4-exo** and **51**.

	4-exo	**51**		**4-exo**	**51**
C1 – C5	1.523(4)	1.519(3)	Co – C2	1.982(3)	1.971(2)
C4 – C5	1.532(4)	1.545(3)	Co – C3	1.941(3)	1.932(2)
C5 – C7	1.531(4)	1.525(3)	C1-C2-C3	105.7(3)	106.5(2)
Co – C1	2.054(3)	2.076(2)	C1-C5-C4	98.4(2)	97.49(18)
Co – C4	2.061(3)	2.052(2)	C2-C1-C5	109.2(3)	108.77(19)
C1 – C2	1.427(5)	1.418(3)	C3-C4-C5	106.3(3)	105.16(19)
C2 – C3	1.445(4)	1.432(3)	ring fold angle	31.0(3)	34.2(2)
C3 – C4	1.444(4)	1.452(3)	Co····C5	2.543(3)	2.592(2)

Interestingly, when complex **52**-*exo* that was prepared from the reaction between metallacyclobutene **2** with methyl prapagyl ether[7] was employed as precursor to carry out the DIBAL-H reduction (10 equivalents), the same hydroxyl η^4-cyclopentadiene complex **51** was obtained as the only product with 67% yield (Scheme 3-27). Hydrolysis of ether under acidic condition is a classic organic process. However, ether is notoriously inert to strong base, and it has been widely used as solvent for a variety of hydride reduction reactions. To our knowledge, this is the first example of hydride reduction of ether. Despite the mechanism of this remarkable transformation is still unclear, it provides us an alternate more optimal synthetic method towards complex **51** since only the *exo* isomer was generated in the reaction of metallacyclobutene **2** with methyl prapagyl ether.

Scheme 3-27. Reduction of complex **52**-*exo* by DIBAL-H.

The next *exo*-η^4-cyclopentadiene we examined with DIBAL-H is complex **7**-*exo*, which is trickier due to the presence of a hydroxyl functional group. When a dry toluene solution of complex **7**-*exo* (0.06 M) was treated with ten equivalents of DIBAL-H under inert atmosphere at -78 °C – 23 °C, 30% yield of complex **53** was isolated as red air-

stable crystalline solids after chromatography on silica gel (Scheme 3-28). The ^{1}H NMR spectrum (400 MHz, CDCl$_3$) of the isolated product shows two pairs of diastereotopic hydrogen resonances located at δ 2.45 (m, 1H, CHCH$_2$OH), 3.25 (m, 1H, CHCH$_2$OH); 2.82 (d, 1H, J = 11 Hz, CH$_2$OH), 3.99 (d, 1H, J = 11 Hz, CH$_2$OH). The two hydroxyl hydrogen signals were detected at δ 1.86 (t, 1H, J = 7.2 Hz, CHCH$_2$OH) and 2.73 (bs, 1H, CH$_2$OH), respectively, which were confirmed by the disappearance of the two peaks when treated with D$_2$O. The coupling between the hydrogen attached on the sp^3-ring carbon and hydroxylmethyl group was observed at δ 3.43 (dd, 1H, J = 7.2 Hz, 7.6 Hz, CHCH$_2$OH). The observance of 13 carbon environments in the ^{13}C{^{1}H} NMR spectrum (125 MHz, CDCl$_3$) is consistent with the dihydroxyl η^4-cyclopentadiene formulation. The four vinyl carbons were detected at δ 39.0, 60.5, 80.8, and 103.9, while the sp^3-ring carbon exists at δ 62.9. A broad signal at 3350 cm^{-1} in IR spectrum confirms the presence of hydroxyl groups.
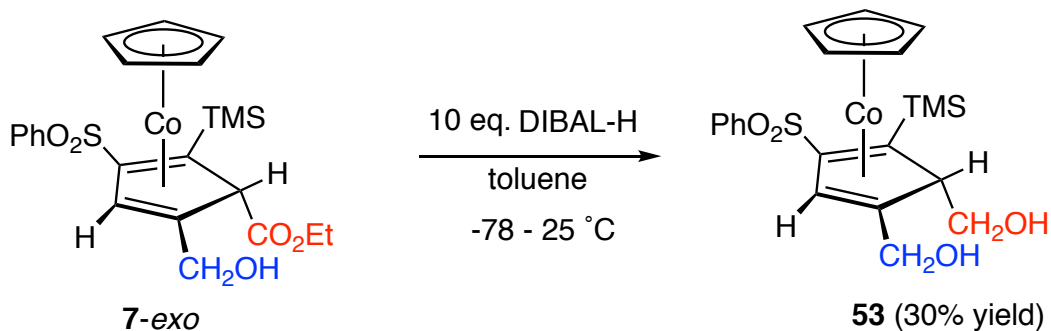
Scheme 3-28. Reduction of complex **7**-*exo* by DIBAL-H.

The X-ray quality crystals of complex **53** were obtained from recrystallization in methylene chloride and hexanes, and the subsequent crystallography analysis confirms the structure of hydroxyl cobalt-η^4-cyclopentadiene (Figure 3-13), in which the two

hydroxyl methyl groups are located at C1 and C5 positions, respectively. The selected bond distances and angles were summarized in Table 3-11. All the structural parameters of complex **53** are very similar to other η^4-cyclopentadiene complexes that have been described in this chapter. The cyclopentadiene ring also shows a staggered conformation relative to the Cp ligand through the metal center. Compared to hydroxyl η^4-cyclopentadiene **51**, the Co – C1 bond distance in complex **53** is shorter by 0.0235 Å owing to the fact that the electron-withdrawing hydroxylmethyl group attached on C1 strengthens the Co – C1 bond via a greater back donation effect. The (C1-C4-C5)-(C1-C2-C3-C4) plane-plane fold angle in complex **53** (35.07(15) °) is slightly bigger than complex **51** (34.2(2) °), which is attributed to the greater steric congestion between the two hydroxyl methyl groups in complex **53**.
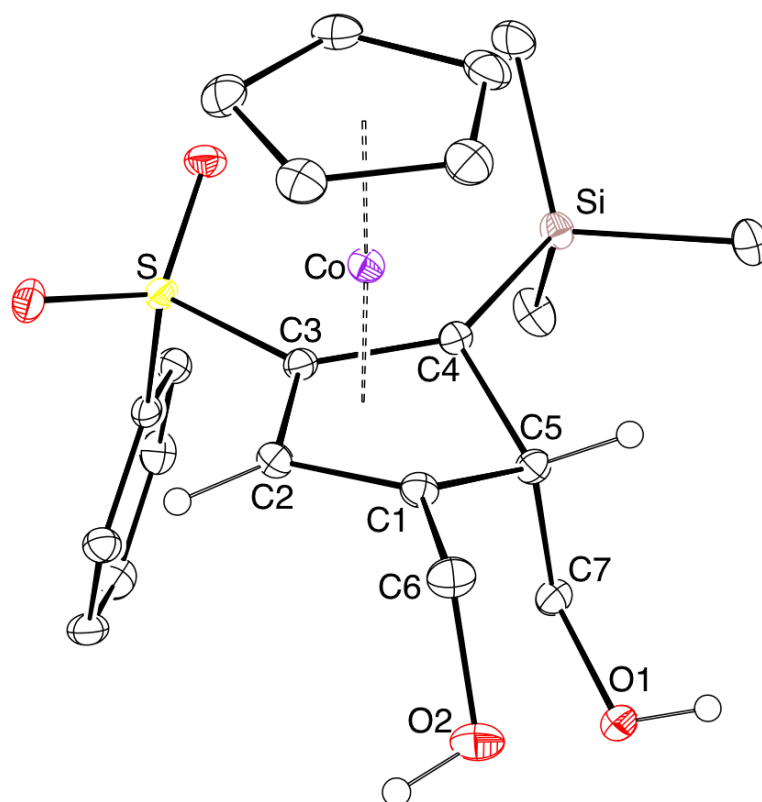

Figure 3-13. ORTEP drawing of **53** with ellipsoids shown at 30% probability.

Table 3-11. Seletecd bond distances (Å) and angles (deg) of complex **53**.

C1 – C2	1.419(2)	Co – C4	2.0480(16)
C2 – C3	1.435(2)	C6 – O2	1.434(2)
C3 – C4	1.454(2)	C7 – O1	1.434(2)
C4 – C5	1.540(2)	C1 – C6	1.497(2)
C5 – C1	1.518(2)	C1-C5-C4	97.18(13)
Co – C1	2.0350(18)	C2-C1-C5	108.57(14)
Co – C2	1.9732(17)	Co····C5	2.5647(17)
Co – C3	1.9462(17)	ring fold angle	35.07(15)

The comparatively low yields of complex **53** might be ascribed to some complex unknown side reactions with DIBAL-H, in which the hydroxylmethyl group on C1 is involved. Indeed, some insoluble dark precipitates were observed in the reaction mixture that must belong to the decomposed starting materials. One possible solution of this problem is to protect the hydroxylmethyl group before conducting the reduction reaction, which can be examined in future directions.

In order to expand this DIBAL-H reduction reaction to other η^4-cyclopentadiene complexes with different ring substituents, complexes **5**-*exo* (R = p-C$_6$H$_4$NMe$_2$), **6**-*exo* (R = p-C$_6$H$_4$^{t}Bu), **8**-*exo* (R= Ph), and **9**-*exo* (R = SnBu$_3$) were employed as precursors to carry out reactions under very similar conditions with 5 – 7 equivalents of DIBAL-H. After aqueous work up and chromatography on silica gel, good to excellent yields of corresponding hydroxyl cobalt-η^4-cyclopentadiene complexes **54** (R = p-C$_6$H$_4$NMe$_2$), **55** (R = p-C$_6$H$_4$^{t}Bu), **56** (R = Ph), and **57** (R = SnBu$_3$) were afforded, respectively. (Scheme 3-29). All the four hydroxyl η^4-cyclopentadiene products were isolated as red slightly air-

sensitive oil/solids with good to excellent yield. The relatively low yield of complex **54** is caused by its instability that led to decomposition during the work-up process.

5-*exo* (R = *p*-C$_6$H$_4$NMe$_2$)
6-*exo* (R = *p*-C$_6$H$_4$^{t}Bu)
8-*exo* (R = Ph)
9-*exo* (R = SnBu$_3$)

54 (R = *p*-C$_6$H$_4$NMe$_2$). 55%
55 (R = *p*-C$_6$H$_4$^{t}Bu), 93.6%
56 (R = Ph), 90.1%
57 (R = SnBu$_3$), 92.1%
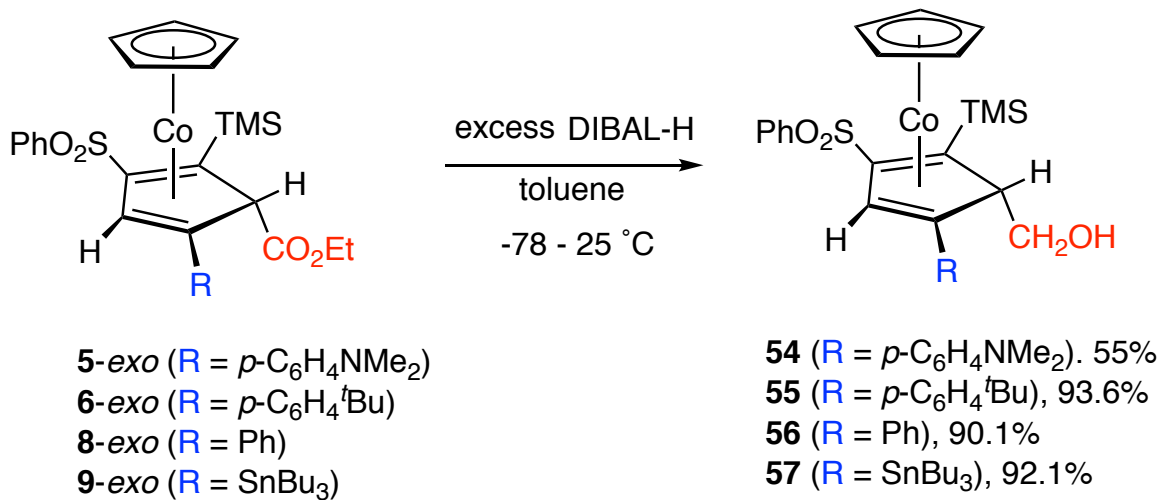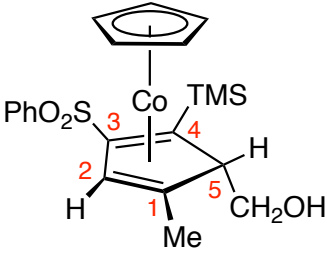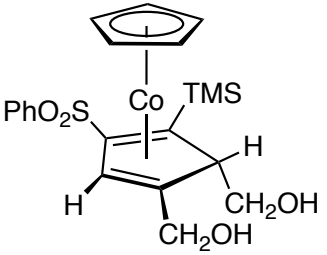
Scheme 3-29. Reduction of *exo*-η^4-cyclopentadiene complexes with DIBAL-H.
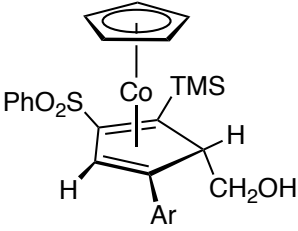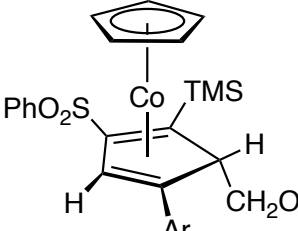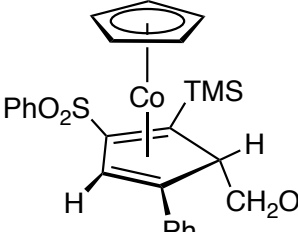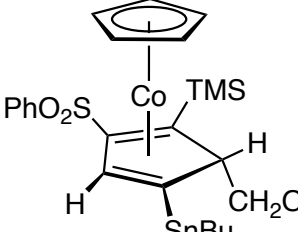
The five resulting complexes were fully characterized by IR, HRMS, elemental analysis, ^{1}H NMR and ^{13}C NMR spectroscopy, and the NMR spectroscopic data are summarized in Table 3-12. The resonances of the ring hydrogen attached on sp^3 carbon were observed at δ 2.86 − 3.59, which are slightly more upfield than the ester substituted η^4-cyclopentadiene complexes that exhibit a range of δ 3.44 − 4.12. The vinyl ring hydrogens that are β to the sp^3-ring carbon resonate in the range of δ 5.44 − 6.22, which are more downfield than the corresponding hydrogen (δ 5.37) in the parent complex, [(η^5-C$_5$H$_5$)Co(η^4-C$_5$H$_6$)],[24] owing to the inductive electron-withdrawing effect of sulfone group. The two diastereotopic hydrogens on the hydroxylmethyl group were observed abnormally upfield (δ 2.2 − 2.7), which might be attributed to the shielding effect from the metal center. The presence of hydroxyl group in all the six complexes

were observed by the IR spectra (broad peak at 3340 – 3360 cm^{-1}) and confirmed by the missing signals upon adding D_2O. The hydroxyl hydrogen resonance in complex **53** (δ 1.86) is detected more deshielded than the other 5 complexes (δ 0.25 – 0.46), which might be ascribed to the intramolecular hydrogen bond between the two hydroxyl groups in complex **53**. In the $^{13}C\{^{1}H\}$ NMR spectra, the vinyl carbons C2 (δ 75.4 – 89.1), C3 (δ 102.5 – 104.0), and C4 (δ 39.0 – 41.4) were observed shielded by the metal center via back-donation effects, and the chemical shifts of C1 (δ 49.4 – 61.7) are dictated by the variable ring substituents.

Table 3-12. Spectroscopic data of hydroxyl η^4-cyclopentadiene complexes (in CDCl$_3$).

Complex	^{1}H NMR, (δ)	^{13}C{^{1}H} NMR, (δ)
51	0.16 (s, 9H, TMS) 0.37 (dd, 1H, *J* = 5.0 Hz, 7.0 Hz, O*H*) 1.28 (s, 3H, Me) 2.55 (m, 2H, C*H*$_2$OH) 2.88 (t, 1H, *J* = 4.0 Hz, C*H*CH$_2$OH) 4.87 (s, 5H, Cp) 5.44 (s, 1H, vinyl-H) 7.5 – 8.1 (m, 5H, Ar)	1.4 (TMS) 18.3 (Me) 39.3 (C4) 61.3 (C1) 65.0 (OCH$_2$) 65.9 (C5) 81.2 (C2) 82.3 (Cp), 102.5 (C3) 127.7 (C$_m$), 129.4 (C$_o$) 133.3 (C$_p$), 143.0 (C$_i$)
53	0.15 (s, 9H, TMS) 1.86 (t, 1H, *J* = 7.2 Hz, CHCH$_2$O*H*) 2.45 (m, 1H, CHC*H*$_2$OH) 2.73 (bs, 1H, CH$_2$O*H*) 2.82 (d, 1H, *J* = 11 Hz, C*H*$_2$OH) 3.25 (m, 1H, CHC*H*$_2$OH) 3.43 (dd, 1H, *J* = 7.2 Hz, 7.6 Hz, C*H*CH$_2$OH) 3.99 (d, 1H, *J* = 11 Hz, C*H*$_2$OH) 4.95 (s, 5H, Cp) 5.72 (s, 1H, vinyl-H), 7.5 – 8.1 (m, 5H)	1.19 (TMS) 39.0 (C4) 60.5(C1) 62.9(C5) 63.0(OCH$_2$) 67.8 (OCH$_2$) 80.8 (C2) 103.9 (C3) 127.5 (C$_m$), 129.3 (C$_o$) 133.2 (C$_p$), 142.5 (C$_i$)

Table 3-12. Spectroscopic data of hydroxyl η^4-cyclopentadiene complexes (continuted)

Complex	^{1}H NMR, (δ)	^{13}C{^{1}H} NMR, (δ)
PhO$_2$S, Co, TMS, H, CH$_2$OH, H, Ar Ar = p-C$_6$H$_4$NMe$_2$ **54**	0.22 (s, 9H, TMS) 0.46 (dd, 1H, J = 4.8 Hz, 7.6 Hz, CH$_2$OH) 2.47 (m, 1H, CH$_2$OH) 2.67 (m, 1H, CH$_2$OH) 2.93 (s, 6H, NMe$_2$) 3.59 (t, 1H, J = 4.8 Hz, CHCH$_2$OH) 4.70 (s, 5H, Cp) 6.05 (s, 1H, vinyl-H) 6.5 – 8.2 (m, 9H, Ar)	1.2 (TMS) 39.4 (C4), 40.5 (NMe$_2$) 60.5 (C5), 61.7 (C1) 66.9(OCH$_2$), 75.4 (C2) 82.8 (Cp), 102.6 (C3) 112.9 (C$_m$), 126.3 (C$_p$) 126.9 (C$_o$), 127.5 (C$_{m(s)}$) 129.2 (C$_{o(s)}$),133.0 (C$_{p(s)}$) 142.8 (C$_{i(s)}$), 148.9 (C$_i$)
PhO$_2$S, Co, TMS, H, CH$_2$OH, H, Ar Ar = p-C$_6$H$_4$CMe$_3$ **55**	0.23 (s, 9H, TMS) 0.44 (dd, 1H, J = 4.8 Hz, 7.0 Hz, OH) 1.28 (s, 9H, CMe$_3$) 2.49 (m, 1H, CH$_2$OH) 2.66 (m, 1H, CH$_2$OH) 3.56 (t, 1H, J = 4.8 Hz, CHCH$_2$OH) 4.73 (s, 5H, Cp) 6.18 (s, 1H, vinyl-H) 7.2 – 8.2 (m, 9H, Ar)	1.4 (TMS), 31.4 (CMe_3) 35.0 (CMe$_3$) 41.0 (C4), 59.0 (C1) 60.8 (OCH$_2$),66.9 (C5) 83.2 (C4 and Cp) 103.7 (C3) 125.7 (C$_m$), 126.3 (C$_{m(s)}$) 127.7 (C$_{o(s)}$), 129.5 (C$_o$) 133.3 (C$_{p(s)}$), 136.5 (C$_p$) 142.9 (C$_{i(s)}$), 149.5 (C$_i$)
PhO$_2$S, Co, TMS, H, CH$_2$OH, H, Ph **56**	0.24 (s, 9H, TMS) 0.46 (dd, 1H, J = 4.8 Hz, 7.0 Hz, OH) 2.51 (m, 1H, CH$_2$OH) 2.67 (m, 1H, CH$_2$OH) 3.57 (t, 1H, J = 4.4 Hz, CHCH$_2$OH) 4.73 (s, 5H, Cp) 6.18 (s, 1H, vinyl-H) 7.1 – 8.2 (m, 10H, Ar)	1.4 (TMS) 41.4 (C4), 58.4 (C1) 60.6 (C5), 66.8 (OCH$_2$) 83.3 (C2 and Cp) 104.0 (C3) 126.0 (C$_m$), 126.4 (C$_{m(s)}$) 127.7 (C$_{o(s)}$), 129.4 (C$_o$) 129.5 (C$_{p(s)}$), 133.4 (C$_p$) 139.8 (C$_{i(s)}$), 142.8 (C$_i$)
PhO$_2$S, Co, TMS, H, CH$_2$OH, H, SnBu$_3$ **57**	0.14 (s, 9H, TMS) 0.25 (t, 3H, J = 6.0 Hz, OH) 0.92 (m, 15H, Bu) 1.2 – 1.6 (m, 12H, Bu) 2.24 (m, 1H, CH$_2$OH) 2.28 (m, 1H, CH$_2$OH) 2.86 (t, 1H, J = 4.8 Hz, CHCH$_2$OH) 4.95 (s, 5H, Cp) 5.82 (s, 1H, vinyl-H) 7.2 – 8.2 (m, 5H, Ar)	1.2 (TMS) 10.5 (Bu) 13.9 (Bu), 27.6 (Bu) 29.3 (Bu), 40.1 (C4) 49.4 (C1), 66.0(C5) 68.1 (OCH$_2$), 81.3 (Cp) 89.1 (C2), 103.8 (C3) 127.4 (C$_m$), 129.2 (C$_o$) 133.1 (C$_p$), 142.9 (C$_i$)

3. Reactions of Hydroxyl η^4-Cyclopentadiene Complexes with Brønsted acid

In the literature, the reactivity of cobalt-η^4-cyclopentadiene complexes with Brønsted acids has long been explored in history,[25] and there are mainly three types of results: 1) loss of a hydride from the sp^3-ring hydrogen to generate a cobaltocenium salt; 2) an acid triggered demetallation process occurs to produce free organic cyclopentadiene; 3) no reaction observed (Scheme 3-30). After we synthesized the hydroxyl η^4-cyclopentadiene complexes, we also subsequently examined their reactivities towards Brønsted acid.
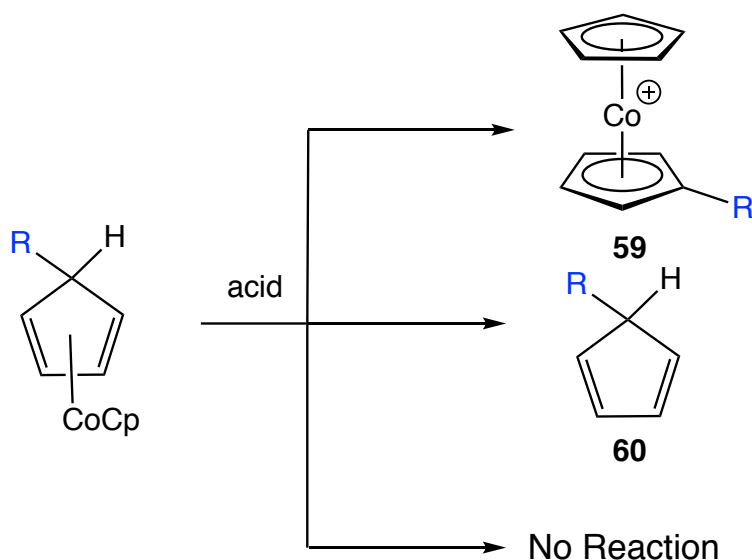
Scheme 3-30. Reaction of cobalt-η^4-cyclopentadiene with acid.

Firstly, an NMR scale reaction of the complex **51** with trifluoroacetic acid (TFAH) was carried out. After an initial NMR spectrum of complex **51** (4.7 mg, 0.01 mmol) with internal standard was recorded in CDCl$_3$, 0.2 mL of TFAH was added into the NMR

tube. A subsequent NMR spectrum indicates that all the starting **51** was consumed based on the TMS resonance at δ 0.16 (s, 9H), and a new set of TMS and Cp resonances were observed at δ 0.41 (s, 9H, TMS) and 5.88 (s, 5H, Cp). The integration of the new TMS signal relative to internal standard gives a 92.5% NMR yield.

In the preparation scale reaction, a diethyl ether (20 mL) solution of complex **51** (36 mg, 0.08 mmol) was treated with three equivalents of HBF$_4$•Et$_2$O under argon. The color of the solution slowly changed from red to yellow. After stirring at ambient temperature for 2 hours, solvent was evaporated and chromatography on silica gel with MeOH/methylene chloride afforded 88% yield of product as an air-stable orange crystalline solid (Scheme 3-31).
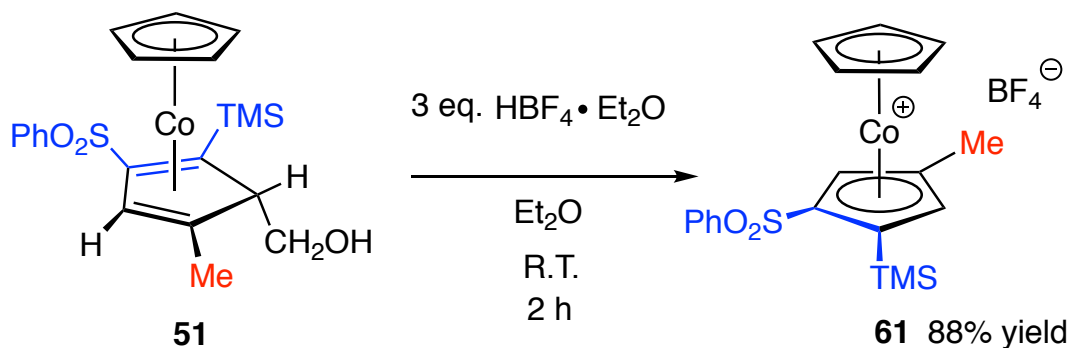
Scheme 3-31. Reaction of hydroxyl η^4-cyclopentadiene **51** with HBF$_4$.

In the ^{1}H NMR spectrum (400 MHz, CDCl$_3$) of the isolated product, the presence of TMS and Cp resonances excludes the possibility of demetallation reaction. However, the fact that the CH$_2$OH moiety is no longer present also rules out the hydride loss scenario. The vinyl hydrogen of the starting material at δ 5.44 also disappeared, and two new singlets were observed at δ 5.87 (s, 1H) and 6.14 (s, 1H), respectively. The

methyl resonance shifts from δ 1.28 to 2.29. The integration of five hydrogen in the aromatic region suggests that the sulfone group is still attached. In the $^{13}C\{^1H\}$ NMR spectrum (125 MHz, CDCl$_3$), the four vinyl carbon signals at δ 39.3, 61.3, 81.2, and 102.5 all disappeared with the sp^3-ring carbon at δ 65.9, and five new downfield carbon resonances were observed at δ 88.3, 92.9, 94.2, 109.4, and 109.6. The high-resolution mass spectrometry gives the chemical formula as $[C_{20}H_{24}CoO_2SSi]^+$, which is consistent with the ^1H NMR data that a CH$_2$OH moiety was extruded from the starting material. The broad peak of O – H stretch at around 3550 cm^{-1} in the IR spectrum is no longer present. The high polarity that was manifested by the insolubility in diethyl ether suggests that the product might be a cobaltocenium salt.

The crystals of the product were obtained from recrystallization in acetone/hexanes. The X-ray crystallography analysis reveals a structure of 1,3,4-trisubstituted cobaltocenium salt, in which the methyl group sits on the C1 position while the phenylsulfone and trimethylsilane groups are located at C3 and C4 sites, respectively (Figure 3-14). To our best knowledge, this is the first example of trisubstituted cobaltocenium cation. The steric congestion from the bulky TMS group is reflected by the longer C3 – C4 (1.438(2) Å) and C4 – C5 (1.443(2) Å) bond distances compared to the C1 – C2 (1.424(2) Å) and C1 – C5 (1.426(2) Å) bond distances. The Co – C3 bond distance (2.0133(16) Å) is measured significantly shorter than Co – C1 bond distance (2.0835(16) Å), which is attributed to the strong electron-withdrawing phenylsulfone group that strengthens the Co – C3 bond. The steric hindrance between phenylsulfone and TMS groups tune the C3-C4-C5 angle smaller than the C2-C3-C4 angle (Δ = 5.94 °). The distance between cobalt and the centroid of Cp ligand

(1.6479(8) Å) is very close to the distance between cobalt and the centroid of substituted Cp' (1.6476(8) Å), and both distances are slightly longer than the Co – Cp in parent complex (η^5-C$_5$H$_5$)$_2$CoBF$_4$ (1.634(3) Å).[26]
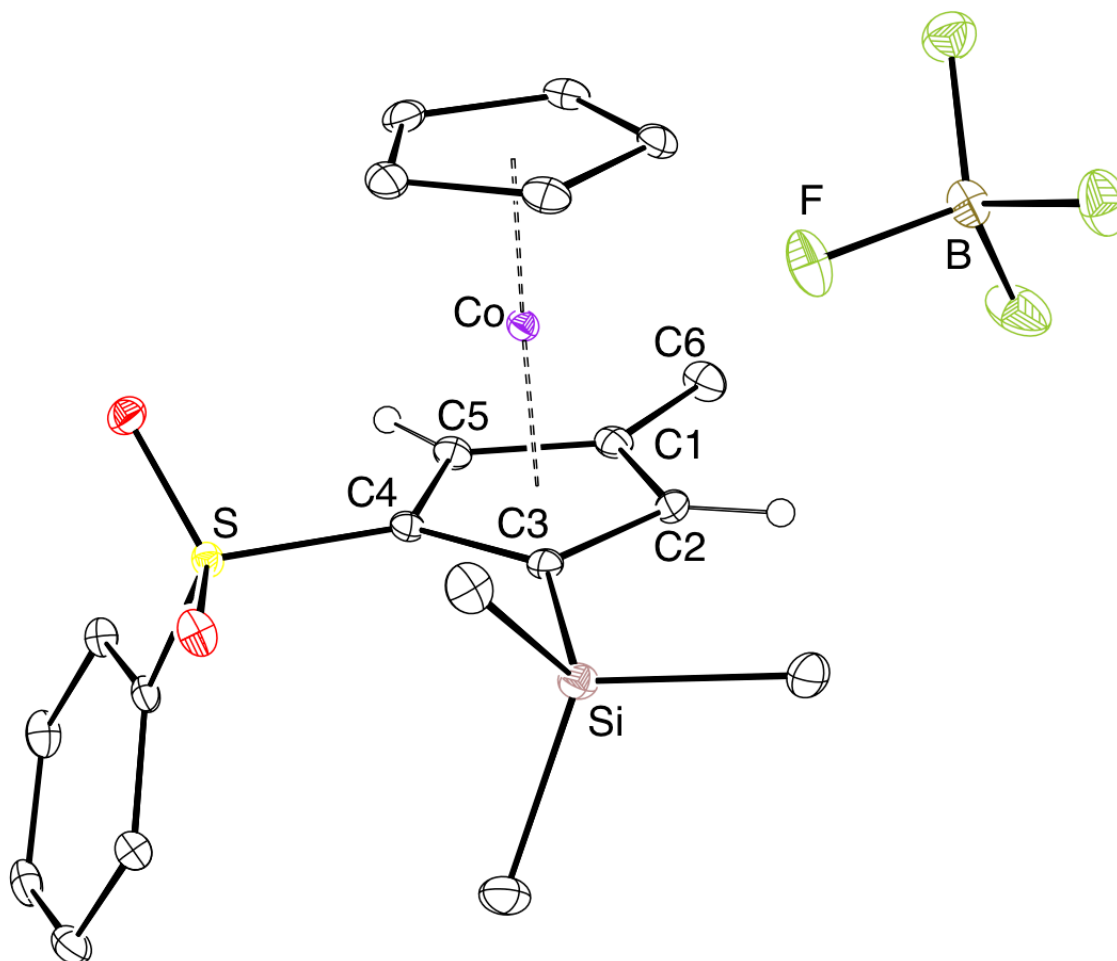
Figure 3-14. ORTEP drawing of **61** with ellipsoids shown at 30% probability.

In a similar fashion, the reactivities of three other hydroxyl η^4-cyclopentadiene complexes **54** (R = p-C$_6$H$_4$NMe$_2$), **55** (R = p-C$_6$H$_4$^{t}Bu), and **56** (R = Ph) towards acid were also explored. The reactions were conducted under very similar conditions with excess of HBF$_4$•Et$_2$O at ambient temperature in argon. After work up, cobaltocenium salts **62** (R = p-C$_6$H$_4$NMe$_2$, 83.4%), **63** (R = p-C$_6$H$_4$^{t}Bu, 86.9%), and **64** (R = Ph, 84.2%)

can be isolated as air-stable crystalline solids (Scheme 3-32). It was noted that complex **63** and **64** were not suitable for chromatography due to the large polarities, and in order to isolate the two complexes, direct crystallization was carried out after washing the reactions mixture with hexanes. An interesting phenomenon is that the color the complex **62** is deep purple while the other three cobaltocenium compounds bear yellow color, which might be ascribed to the extended conjugated π system by the NMe$_2$ moiety that changes the HOMO-LUMO gap and thus leads the compound adsorbing more orange lights.

54 (R = p-C$_6$H$_4$NMe$_2$), 55%
55 (R = p-C$_6$H$_4{}^t$Bu), 93.6%
56 (R = Ph), 90.1%

62 (R = p-C$_6$H$_4$NMe$_2$), 83.4%
63 (R = p-C$_6$H$_4{}^t$Bu), 86.9%
64 (R = Ph), 84.2%
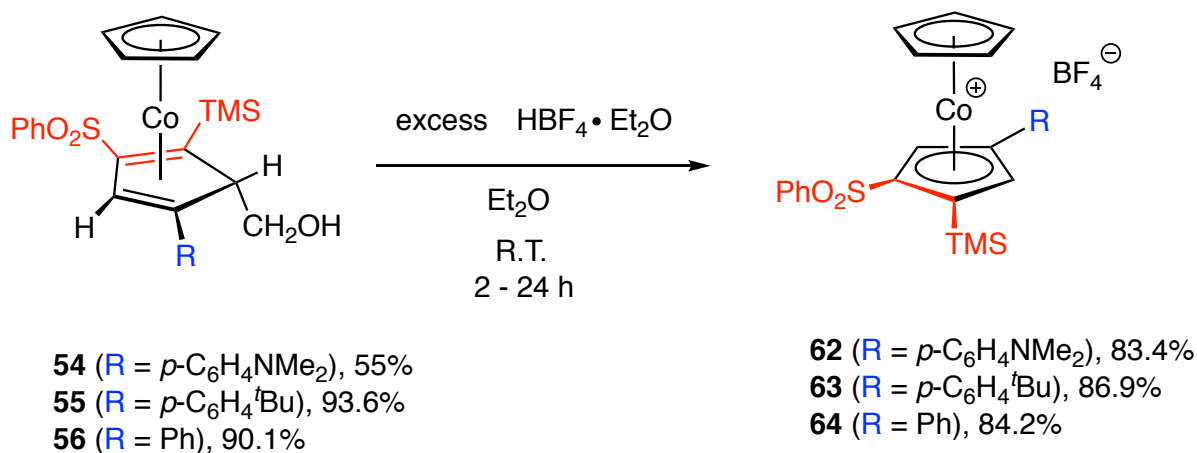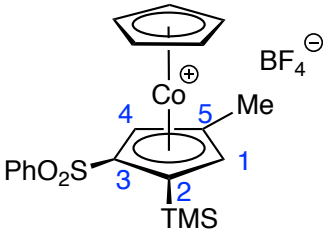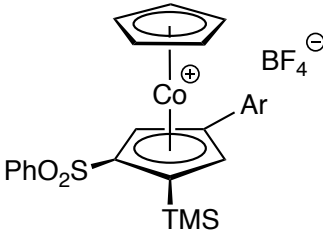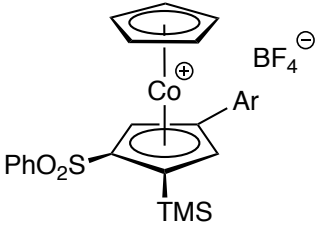
Scheme 3-32. Reactions of hydroxyl η^4-cyclopentadiene complexes with HBF$_4$.
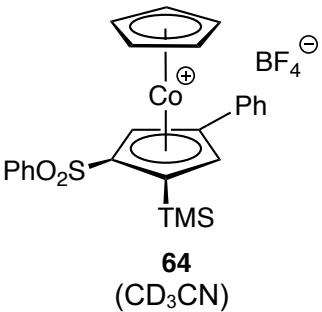
All the four cobaltocenium complexes were subsequently characterized by IR, HRMS, elemental analysis, ^{1}H NMR and ^{13}C NMR spectroscopy, and the NMR spectroscopic data are summarized in Table 3-13. In the ^{1}H NMR spectra, the ring hydrogen resonances on the substituted cyclopentadiene were observed in the range of δ 5.87 – 6.81, which share the same region with the Cp ligand (δ 5.70 – 5.98). The ring hydrogen attached on C2 was found a little more downfield than ring hydrogen on C5 (Δ

= 0.12 – 0.62), owing to the presence of adjacent electron-withdrawing phenylsulfone group. In the $^{13}C\{^1H\}$ NMR spectra, the five ring carbons of substituted cyclopentadiene are shielded by the metal center and sit in the range of δ 85.2 – 112.3. In comparison, the carbons in the Cp ligand was observed in the range of δ 87.6 – 88.8.

Table 3-13. Spectroscopic data of hydroxyl cobaltocenium complexes.

Complex	^1H NMR, (δ)	$^{13}C\{^1H\}$ NMR, (δ)
 61 (CDCl₃)	0.44 (s, 9H, TMS) 2.29 (s, 3H, Me) 5.87 (s, 1H, C(1)*H*) 5.98 (s, 5H, Cp) 6.14 (s, 1H, C(4)H) 7.5 – 8.0 (m, 5H, Ar)	0.6 (TMS) 13.8 (Me) 87.7(Cp) 88.5(C1) 93.1(C4), 94.4(C2) 109.6(C5), 109.8(C3) 128.2 (C$_m$), 130.3 (C$_o$) 135.3 (C$_p$), 139.0 (C$_i$)
 Ar = *p*-C₆H₄NMe₂ **62** (CDCl₃)	0.47 (s, 9H, TMS) 3.06 (s, 6H, NMe₂) 5.70 (s, 5H, Cp) 6.35 (s, 1H, C(1)*H*) 6.47 (s, 1H, C(4)*H*) 6.7 – 8.0 (m, 9H, Ar)	0.39 (TMS) 40.3 (N*Me₂*) 79.9 (C1), 85.2 (C4) 87.6 (Cp), 94.4 (C2) 108.5 (C5), 112.3 (C3) 112.9 (C$_m$), 113.4 (C$_p$) 127.9 (C$_{m(s)}$), 129.9 (C$_{o(s)}$) 130.0 (C$_o$),134.9 (C$_{p(s)}$) 139.2 (C$_i$), 152.8 (C$_{i(s)}$)
 Ar = *p*-C₆H₄CMe₃ **63** (CD₃CN)	0.45 (s, 9H, TMS) 1.37 (s, 9H, CMe₃) 5.72 (s, 5H, Cp) 6.19 (s, 1H, C(1)*H*) 6.81 (s, 1H, C(4)*H*) 7.5 – 8.1 (m, 9H, Ar)	0.01 (TMS) 31.1 (C*Me₃*) 35.6 (*C*Me₃) 85.3 (C1) 86.6 (Cp) 88.9 (C4), 94.9 (C2) 109.4 (C5), 110.2 (C3) 125.8 (C$_p$), 127.4 (C$_m$) 128.8 (C$_{o(s)}$), 129.0 (C$_o$) 130.9 (C$_{p(s)}$),136.0 (C$_p$) 139.8 (C$_i$), 156.1 (C$_{i(s)}$)

Table 3-13. Spectroscopic data of hydroxyl cobaltocenium complexes (continued).

Complex	^{1}H NMR, (δ)	^{13}C{^{1}H} NMR, (δ)
 64 (CD$_3$CN)	0.44 (s, 9H, TMS) 5.73 (s, 5H, Cp) 6.21 (s, 1H, C(1)*H*) 6.83 (s, 1H, C(4)*H*) 7.5 – 8.1 (m, 10H, Ar)	0.1 (TMS) 85.8 (C1) 88.8 (Cp) 89.3 (C4), 95.3 (C2) 109.1 (C5), 110.5 (C3) 128.9 (C$_p$ and C$_{m(s)}$) 129.2 (C$_o$), 130.5 (C$_m$) 131.0 (C$_{o(s)}$),132.4 (C$_{p(s)}$) 136.1 (C$_i$), 139.9 (C$_{i(s)}$)

The X-ray quality crystals of all the other three cobaltocenium complexes **62** (Figure 3-15), **63** (Figure 3-16), and **64** (Figure 3-17) were successfully obtained from recyclization in acetone/hexanes or slowly evaporation from methyl ethyl ketone. The selected bond distances and angles of all four cobaltocenium salts are summarized and compared in Table 3-14. The carbon – carbon bond distances in the substituted Cp ring were measured in the range of 1.383(12) – 1.453(13) Å. In comparison, the carbon – carbon bond distance in the parent complex (η^5-C$_5$H$_5$)$_2$CoBF$_4$ was detected as 1.397(4) Å.[26] The C1 – C5 bond distance in complex **61** is considerably shorter (0.013 – 0.027 Å) than in complex **62**, **63**, and **64**, which might be attributed to the extended conjugation of the arene substituents in the latter three complexes. The distances between the metal center and the substituted cyclopentadiene centroids were measured as 1.633(4) – 1.6655(14) Å, while the Co – Cp distances were found in the ranges of 1.641(7) – 1.6687(16) Å. Compare complex **62** and **64**, longer Co – C1 bond distance (Δ = 0.062 Å) was detected in the former due to the more electron-rich dimethyl phenyl amino functional group than the phenyl substituent. The presence of electron-withdrawing

278

phenylsulfone group tunes the Co – C3 bond distances significantly shorter (Δ = 0.038 – 0.076 Å) than the corresponding Co – C4 bonds in all the cobaltocenium complexes. Within the substituted Cp ring of each complex, the C3-C4-C5 angle is consistently measured as the smallest one (Δ = 4.5 – 8.3 °) among the five inner angles, which is ascribed to the steric hindrance between the bulky TMS group and metal center. The good conjugations between the cyclopentadiene with the arene substituents are manifested by the small torsion angles C2-C1-C6-C7 in complex **62** (17.7(3) °), **63** (6.1(9) °), and **64** (6.8(13) °), respectively. In addition, the dimethyl amino group is essentially planar to the adjacent phenyl group in complex **63** with a negligibly small dihedral angle of C8-C9-N-C10 (0.2(3) °).
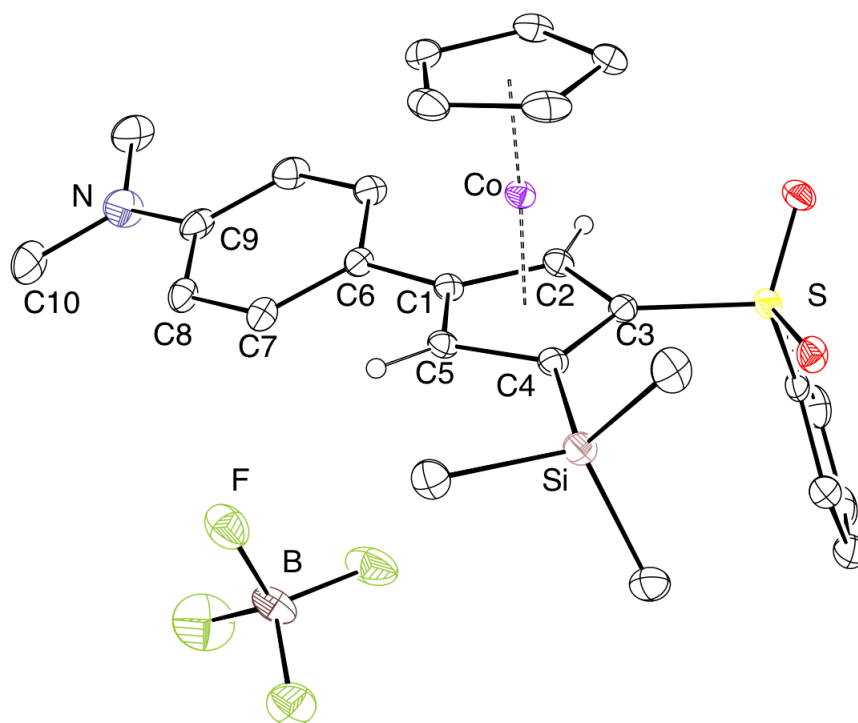
Figure 3-15. ORTEP drawing of **62** with ellipsoids shown at 30% probability.
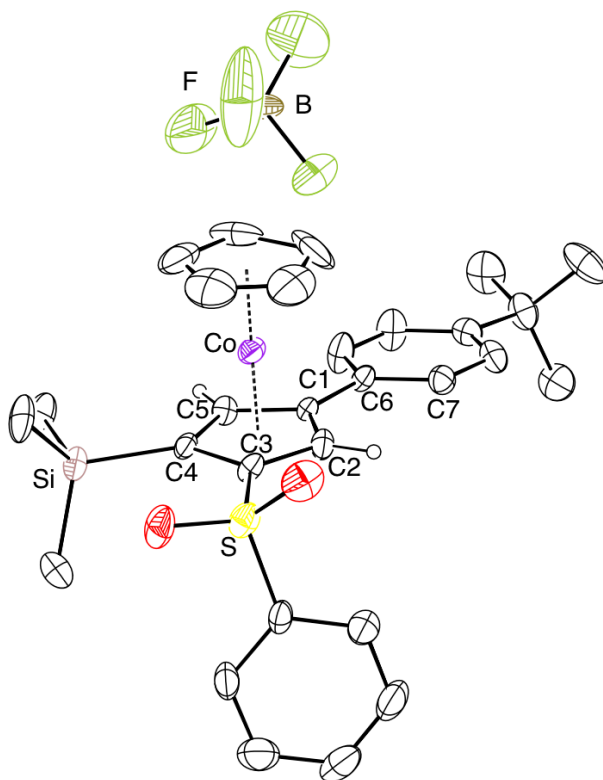
Figure 3-16. ORTEP drawing of **63** with ellipsoids shown at 30% probability.
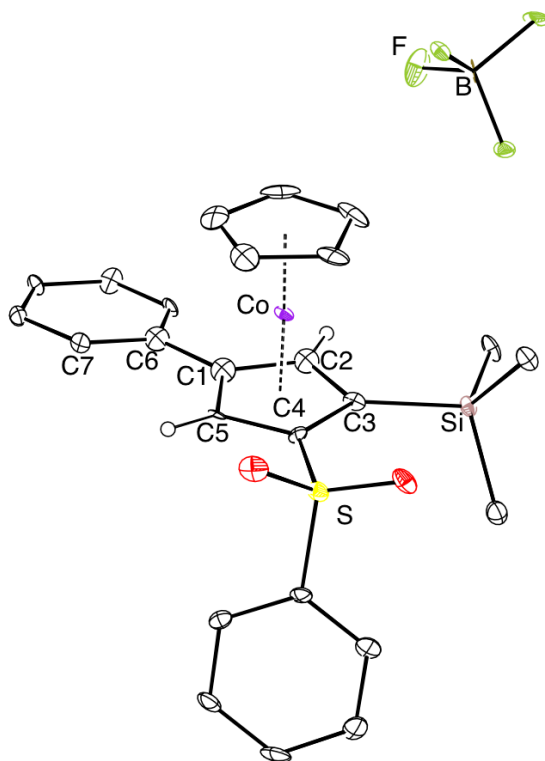
Figure 3-17. ORTEP drawing of **64** with ellipsoids shown at 30% probability.

Table 3-14. Seletecd bond distances (Å) and angles (deg) of cobaltocenium complexes **61**, **62**, **63**, and **64**.

	61	62	63	64
C1 – C2	1.424(2)	1.438(2)	1.386(12)	1.410(13)
C2 – C3	1.435(2)	1.443(4)	1.383(12)	1.438(14)
C3 – C4	1.438(2)	1.465(5)	1.451(12)	1.439(13)
C4 – C5	1.443(2)	1.452(4)	1.417(12)	1.439(14)
C5 – C1	1.426(2)	1.452(4)	1.439(12)	1.453(13)
C1 – C6	1.503(2)	1.480(4)	1.466(12)	1.481(14)
Co – Cp	1.6479(8)	1.6687(16)	1.644(8)	1.641(7)
Co – Cp'	1.6475 (8)	1.6655(14)	1.633(4)	1.636(5)
Co – C1	2.0835(16)	2.128(3)	2.056(8)	2.033(10)
Co – C3	2.0133(16)	2.0126(3)	1.980(9)	2.016(10)
Co – C4	2.0627(16)	2.075(3)	2.056(8)	2.054(10)
C2-C1-C5	106.67(15)	107.0(3)	106.4(8)	107.4(8)
C1-C2-C3	107.85(14)	107.6(3)	108.9(8)	108.1(9)
C2-C3-C4	110.13(14)	110.4(3)	110.0(7)	109.7(8)
C3-C4-C5	104.19(13)	104.2(3)	102.7(8)	105.4(9)
C2-C1-C6-C7	–	17.7(3)	6.1(9)	6.8(13)
C8-C9-N-C10	–	0.2(3)	–	–

When the dihydroxyl η^4-cyclopentadiene complex **53** was treated with HBF$_4$•Et$_2$O at the same reaction condition, however, the expected hydroxylmethyl substituted cobaltocenium complex **65** was not observed (Scheme 3-33). The reaction mixture turned from red to dark brown immediately upon adding the acid. The TMS and Cp resonances are absent in the ^{1}H NMR spectrum of the resulting product, and lots of

broad peaks in the spectrum suggests some paramagnetic complexes were generated. Isolation and crystallization of the product failed due to the complexity of the resulting mixture. It is still not clear how the extra hydroxylmethyl functional group on C1 position affected the reaction results.
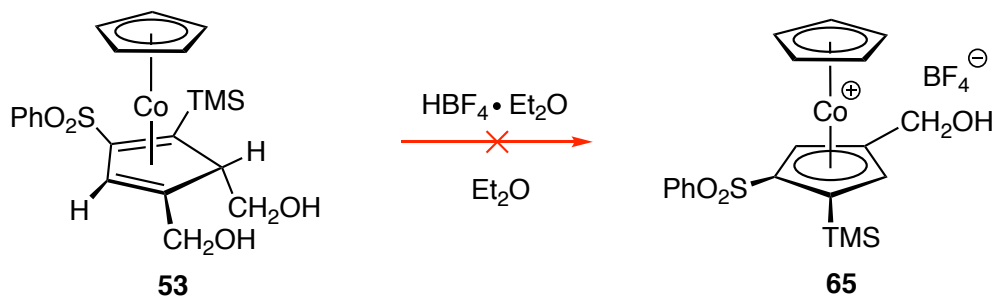
Scheme 3-33. Reaction of complex **53** with HBF$_4$•Et$_2$O.

The complex **57** with a ^{t}BuSn substituent was also employed as precursor to examine the reactivity towards HBF$_4$•Et$_2$O (Scheme 3-34). After adding the acid, the phenomenon was very similar to the formation of cobaltocenium salts, i.e., the color of the solution gradually changed from red to yellow. After concentrated and crystallization, the final product was isolated as an air-stable yellow crystalline solid. However, the X-ray crystallography analysis reveals a cobalt aquo complex **66** (Figure 3-18), without any observance of the desired cobaltocenium cation. The yield of complex **66** was estimated as 20 – 30% due to some impurities presenting in the products. It is not clear how the ^{t}BuSn substituent dramatically affected the reaction results either.
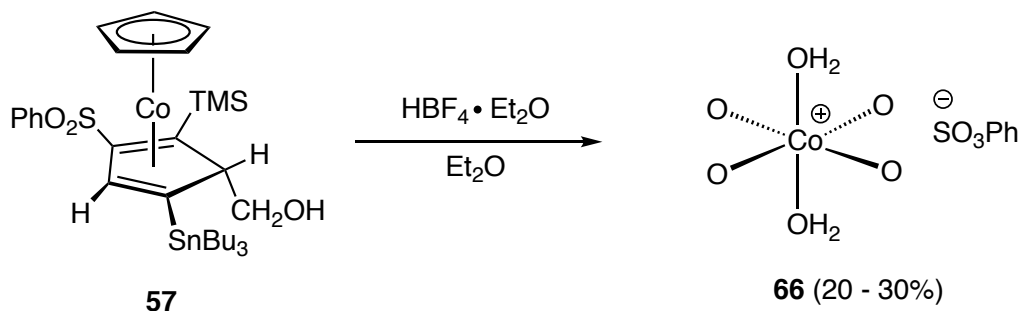
Scheme 3-34. Reaction of complex **57** with HBF₄•Et₂O.
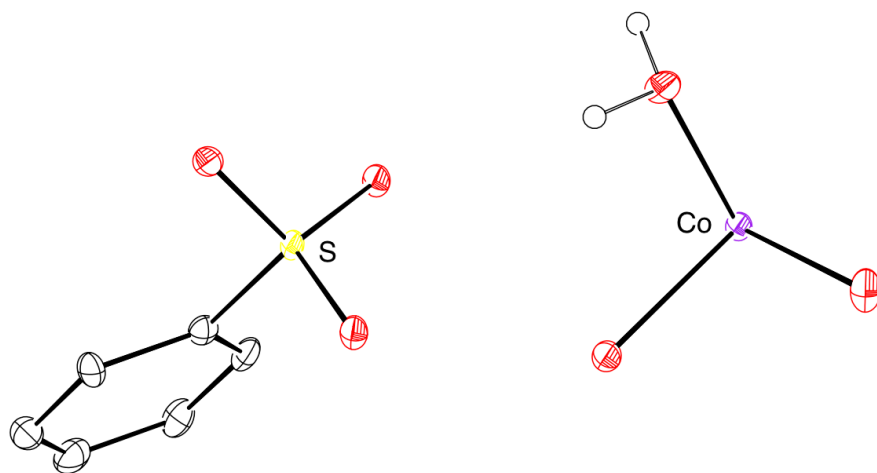
Figure 3-18. ORTEP drawing of **66** with ellipsoids shown at 30% probability.

4. Reactions of Hydroxyl η^4-Cyclopentadiene Complex with Ferrocenium Cation

Besides the Brønsted acid, in principle, we propose that any oxidant that is stronger than acid might also be able to trigger the same fragmentation to produce the cobaltocenium salt. Ferrocenium cation is a commonly used one-electron oxidant, which has a higher oxidation-reduction potential than regular Brønsted acids in polar solvent, and it generates a stable ferrocene compound after the reduction.[27] Herein, the NMR scale reaction of the hydroxyl η^4-cyclopentadiene was carried out with the commercially available $(\eta^5\text{-C}_5\text{H}_5)_2\text{FePF}_6$.

The complex **51** with methyl substituent (4.1 mg, 0.009 mmol) was added into a J.Y. NMR tube with 1,3,5-tri-*tert*-butylbenzene as internal standard in CDCl$_3$ (1.2 mL) solvent under argon. After the initial ^{1}H NMR was recorded, ferrocenium hexaflourophosphate (9.0 mg, 0.027 mmol) was added into the tube. The ferrocenium cation started to dissolve and the color of the reaction mixture immediately changed from red to yellow while shaking the tube. The subsequent ^{1}H NMR spectrum indicates that all the starting complex **51** was consumed based on the TMS resonance at δ 0.16 (s, 9H), and 89% yield of the cobaltocenium **61** was obtained based on the integration of the TMS resonance at δ 0.44(s, 9H) relative to internal standard (Scheme 3-35). Besides the formation of cobaltocenium product, there are two additional important information that can be obtained from the spectroscopic data: 1) the amount of ferrocene generated in the solution is as twice as the formation of cobaltocenium **61** based on the relative integration of Cp resonances of complex **61** (δ 5.87) and ferrocene (δ 4.16); 2) a prominent singlet located at δ 9.74 indicates a formation of 33% yield of formaldehyde, which was also confirmed by the carbonyl carbon resonance in ^{13}C NMR spectrum at δ 195. To rule out the effect of any possible acid in this reaction, another NMR tube reaction was carried out by adding one equivalent of triethyl amine at the beginning without changing any other procedures, which gave essentially the same result.
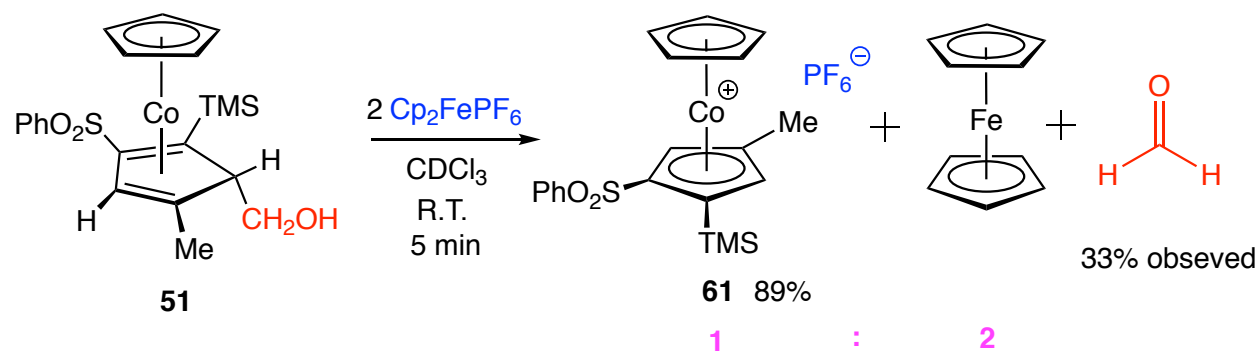
Scheme 3-35. Reaction of complex **51** with ferrocenium cation.

Based on the observations above, mechanistically, we propose that there are two possible fragmentation routes towards the cobaltocenium product (Scheme 3-36). In path A, one equivalent of ferrocenium cation firstly oxidizes the hydroxyl η^4-cyclopentadiene **51** to give the η^4-cyclopentadiene cobalt cation **67**, that is followed by a heterolytic cleavage to generate the cobaltocene **68** and formaldehyde. After a further oxidation of the cobaltocene **68** by one more ferrocenium cation, the final cobaltocenium salt can be afforded. However, an alternative path B could occur by a homolytic cleavage on η^4-cyclopentadiene cobalt cation **67** to generate the cobaltocenium cation **61** with the formaldehyde radical **69**, and one more ferrocenium cation can do a one-electron oxidation on the radical to produce the formaldehyde.
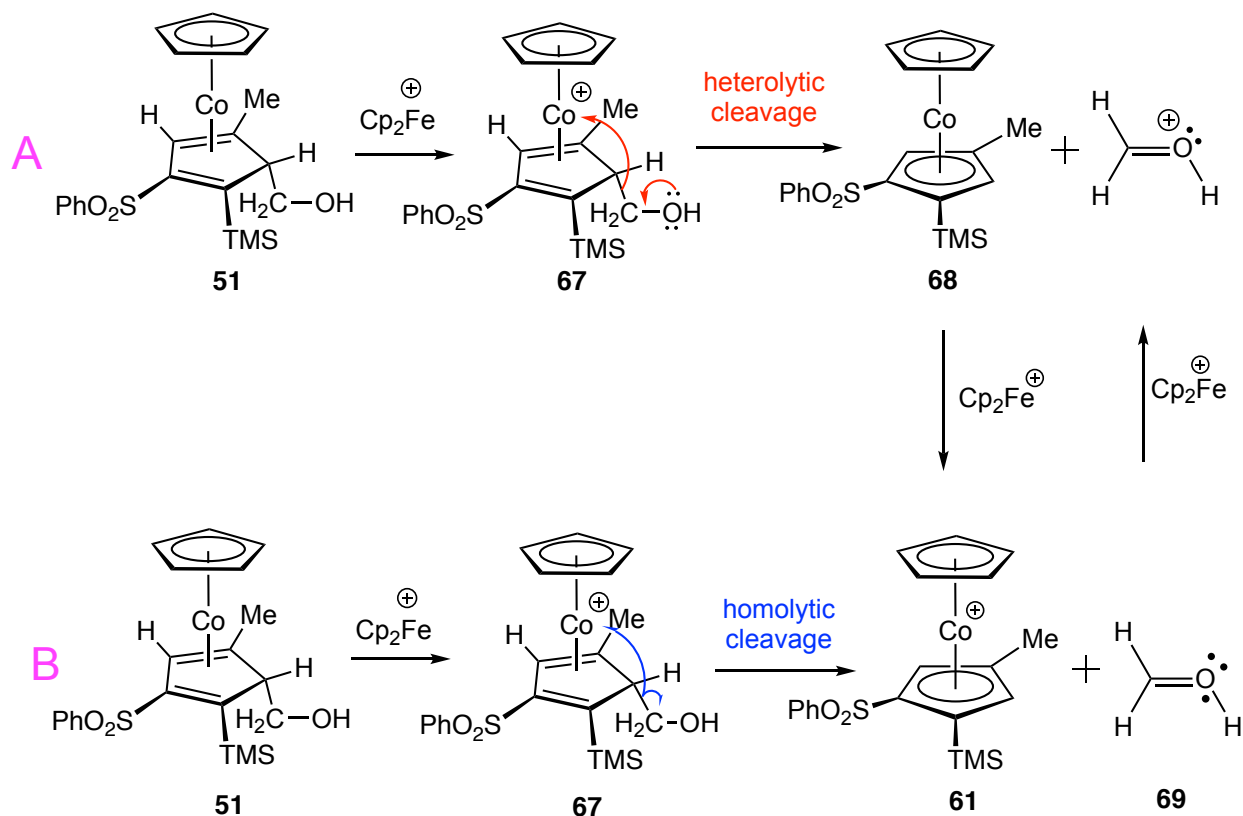
Scheme 3-36. Formaiton of cobaltocenium **61** and formaldehyde from complex **51**.

For the Brønsted acid triggered fragmentation, the mechanism can be essentially the same as the ferrocenium cation scenario by simply switching the oxidant to acid. We attributed the fact that the ring-hydride loss pathway doesn't apply to our system to the less hydridic feature of the sp^3 ring hydrogen of our systems in the presence of strong electron-withdrawing phenylsulfone group.

In order to evaluate the two possible mechanisms, a list of NMR reactions was attempted to trap the possible radical intermediates (Scheme 3-37). However, there are no evidence for the formation of methanol in the presence of 1,4-cylclohexadiene or tributylstannane, or by utilizing THF-d_8 as solvent. Photolyzing complex **51** in THF-d_8 without adding ferrocenium cation results no formation of the cobaltocenium cation **61**.

No evidence for the methanol radical trapped by the TMPO was observed either. All the negative evidence in these NMR reactions support the heterolytic cleavage (path a) as the more favorable mechanism. More computational studies are underway to furtherly elucidate the validity of the two mechanisms.
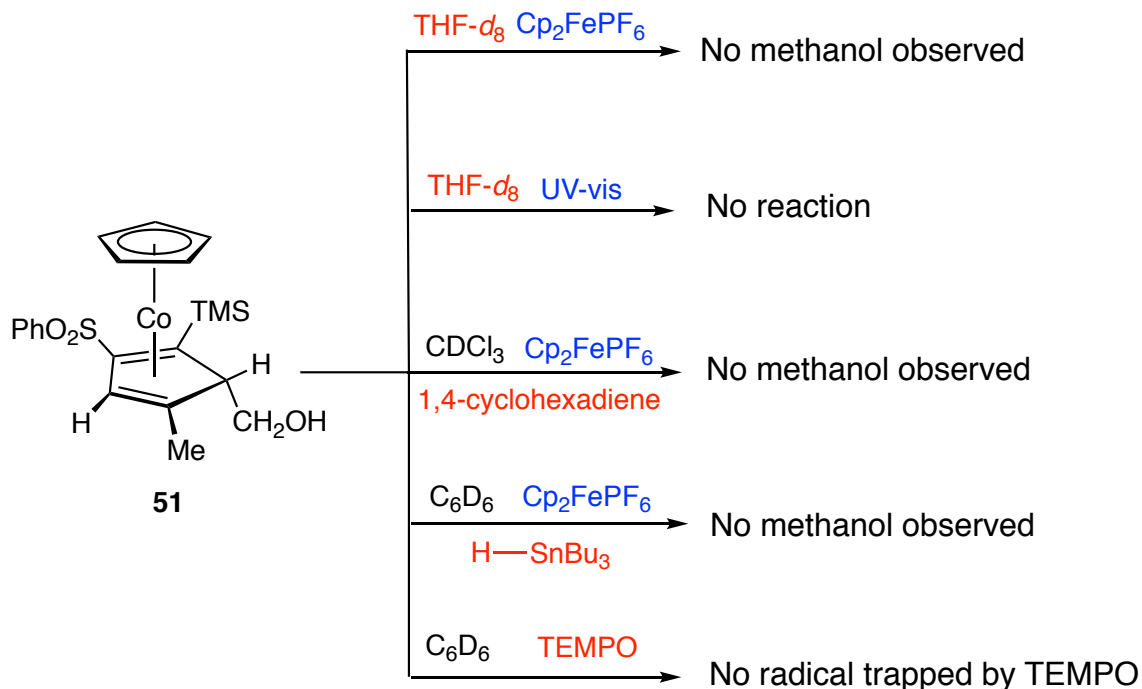
Scheme 3-37. Attemptations to trap possible radical intermediates.

5. Electrochemical and Biological Properties of Cobaltocenium Salt

As the isoelectronic structure of ferrocene, cobaltocenium has been widely explored by the electrochemical properties in the literature.[27] It would be interesting to also examine the electrochemical behaviors of the trisubstituted cobaltocenium salts that were synthesized above. In collaboration with Guy Bertrand group, an electrochemical analysis of the four cobaltocenium complexes were performed. The

cyclic voltammetry curves of all four compounds are shown in Figure 3-19. They all exhibit a reversable oxidation-reduction behavior, and the oxidation potentials were observed depending on the different ring substituents (R = Me, -1.01 V; R = Ph, -0.92 V; R = p-C$_6$H$_4$^{t}Bu, -0.94 V; R = OEt, -1.04 V).
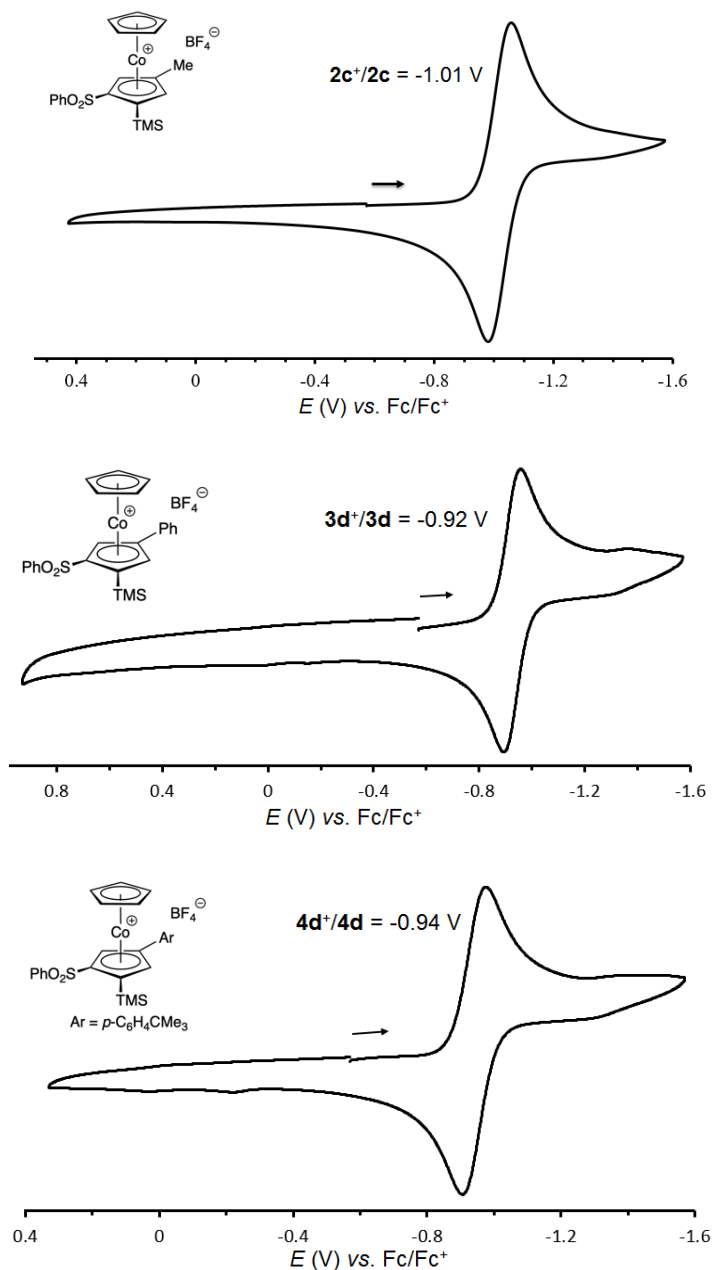
Figure 3-19. Cyclic voltammetry curves of cobaltocenium complexes.

Cytotoxicity of cobaltocenium cation to cancer cells has been discovered in the literature with conjunction to other transition metals, such as mercury and gold.[28, 29] However, the cytotoxicity of monosubstituted cobaltocenium cation solely was found very limited.[28] Our lab mate Pauline Olsen carried out a cytotoxicity analysis of the trisubstituted cobaltocenium complex **61** with HeLa cells, which demonstrates the first example of high cytotoxicity of cobaltocenium towards cancer cells with a IC_{50} value of 54.19 ± 3.10 (Figure 3-20). We attributed the high cytotoxicity of complex **61** to the incorporations of sulfone and TMS groups, which help strengthen the anticancer activities[30] and improve the lipophilicities of the cobaltocenium molecule.
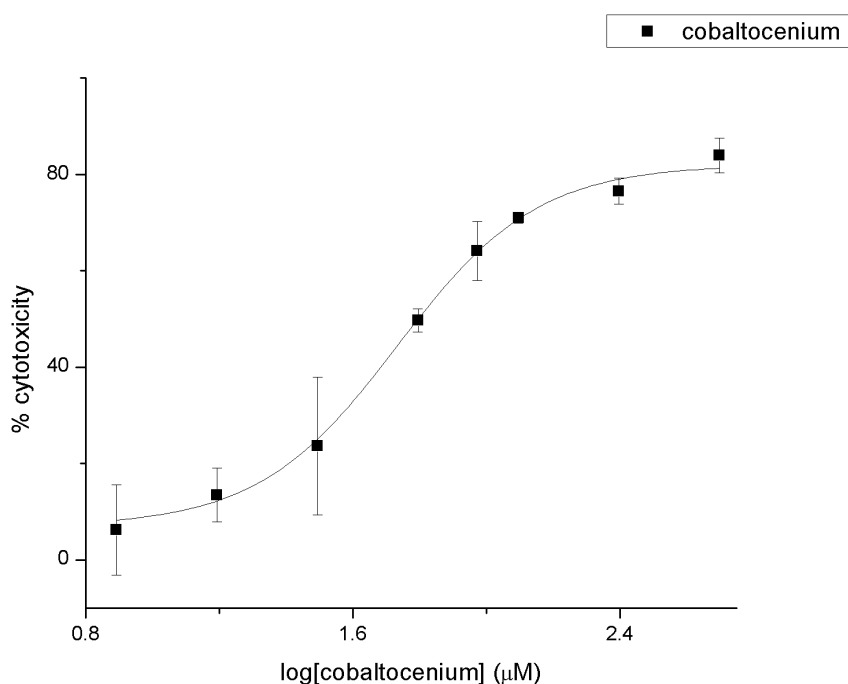
Figure 3-20. Cytotoxicity curve of different concentrations of cobaltocenium **61**.

D. Ring-expansion reactions on the η^4-Cyclopentadiene Complexes

1. Formation of Tosylate Complex and Subsequent Ring-expansion Reactions

As the most common connection mode in organic compounds, carbon-carbon σ-bond has its irreplaceable role in constructing molecules, and the reactions involving this type of bond are widespread in pharmaceutical science and petroleum industries. However, activation of carbon-carbon σ-bond by transition metal is still a challenging area and only limited examples have been reported.[31] Of particularly interesting ones are transition metal-mediated ring-expansion reactions in which cleavage and reform of carbon-carbon bonds are both involved to give an annulation product. Herberich and coworkers reported that a η^4-cyclopentadiene cobalt bearing 1-haloalkyl substituents can undergo ring expansion under mild conditions to form η^5-cyclohexadienyl cations (Scheme 3-38).[32] Stryker and coworkers reported a conversion of η^4-cyclopentadiene cobalt to a seven-membered ring cobalt cation via the reaction with alkyne in the presence of acid (Scheme 3-39).[33] Other successful examples are particularly through β-carbon eliminations.[34] However, most of these ring-expansion transformations lacks functional groups tolerance and potentially need a further demetallation step to obtain the desired organic products.
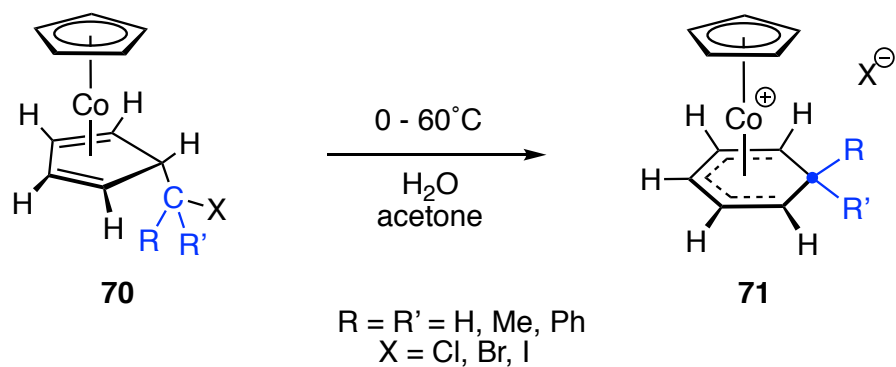
Scheme 3-38. Herberich's ring-expansion reacton of η^4-cyclopentadiene complexes.

R = Me, ^{t}Bu   R$_1$, R$_2$ = H, Me, ^{t}Bu, Ph, TMS
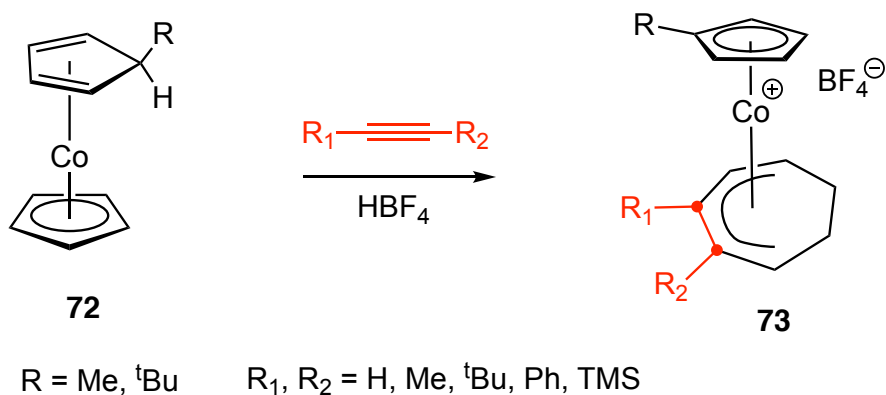
Scheme 3-39. Ring expansion of η^4-cyclopentadienes with acetylene incorporated.

As mentioned earlier in this chapter, we developed a systematic way to synthesize multisubstituted cobalt η^4-cyclopentadiene complexes with high regio- and stereoselectivities via the coupling of metallacyclobutane with various acetylenes. The presence of an ethoxycarbonyl substituent on the sp^3-ring carbon of our system suggests that these readily available cyclopentadiene complexes may serve as precursors to unsaturated six-membered ring carbocycles via a two-step sequence involving reduction of ethoxycarbonyl to a hydroxymethyl and conversion of hydroxyl group to a good leaving group, followed by a "Herberich ring-expansion". Here we

describe the first example of CpCo(η^4-cyclopentadiene) ring-expansion chemistry leading to highly regioselective trisubstituted metal-free benzenoid products without adding further oxidizing reagents for demetallation.

In order to trigger the ring-expansion reaction to occur in our η^4-cyclopentadiene complexes, a good leaving group must be placed on the carbon that is attached on the sp^3-ring carbon. One might expect a good strategy to achieve that is to reduce the ester group an alcohol, followed by protonation of the hydroxyl group. However, as mentioned earlier, the reactions between hydroxyl η^4-cyclopentadiene complexes and Brønsted acid generate high yielded cobaltocenium cations without any observation of the ring-expanded "Herberich products". To avoid the oxidation by the acid, another strategy to introduce a good leaving group would be tosylating the hydroxyl group.

The first complex we examined is the methyl substituted hydroxyl η^4-cyclopentadiene **51**. A dry chloroform solution of complex **51** (0.5 mmol, 50 mM), p-toluenesulfonyl chloride (4.0mmol, 0.4 M) and 2-dimethylaminopyridine (4 mmol, 0.4 M) was allowed to stir over 15 hours at 30˚C, during which time the reaction was monitored by TLC analysis. After aqueous workup and chromatography on silica gel, 229.5 mg (77.3%) of the product were isolated as dark crystalline solid after recrystallization from chloroform/hexane (Scheme 3-40). It was found that a suitable temperature is the key to make the reaction successful to give a decent yield. When temperature is above 40˚C, the product **74** was found start to decompose and formed some paramagnetic green precipitates. However, if sufficient heat is not given, the reaction rate would be too slow, and some starting material decomposed in the solution during the long reaction time and thus dropped down the yield.
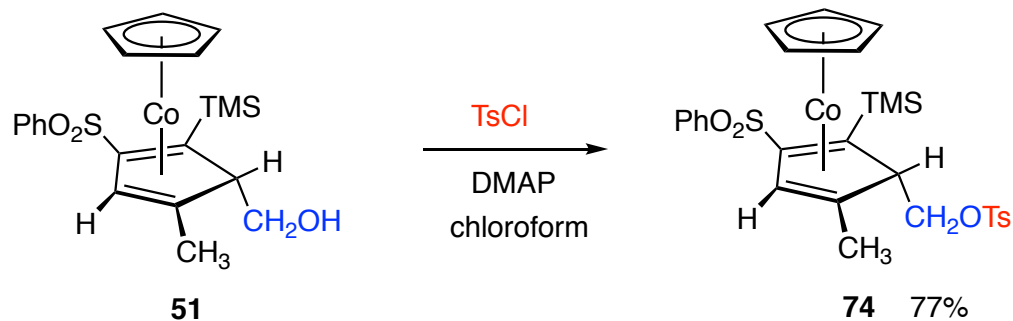
Scheme 3-40. Tosylating hydroxyl η^4-cyclopentadiene **51**.

In the ^{1}H NMR spectrum (400 MHz, CDCl$_3$) of the isolated product, the hydroxyl group at δ 0.37 (dd, 1H, J = 5.0 Hz, 7.0 Hz) is no longer present. The two diastereotopic hydrogen resonances were observed at δ 2.54 (dd, 1H, J = 6.8 Hz, 9.6 Hz) and 2.86 (dd, 1H, J = 4.8 Hz, 9.6 Hz), respectively. The incorporation of tosylate is confirmed by the appearance of a new methyl resonance at δ 2.43 (s, 3H), and the integration of nine hydrogen signals in the aromatic region is consistent with the two phenyl groups. The 18 carbon environments in the ^{13}C NMR spectrum also supports the tosylate formulation. In the IR spectrum, the broad O-H stretch at 3350 cm^{-1} is no longer observed.

The structure of complex **74** was confirmed by X-ray crystallography (Figure 3-21). The selected bond distances and angles were summarized in Table 3-15. The three bonds C1 – C2 (1.409(3) Å), C2 – C3 (1.446(3) Å), C3 – C4 (1.448(2) Å) of the conjugated diene moiety were detected very similar. The ring fold angle of the cyclopentadiene [(C1-C4-C5)-(C1-C2-C3-C4) plane-plane fold angle) was measure as 33.75(15) Å. Compared to the parent complex **51**, the larger steric hindrance of the tosylate group is manifested by the longer C5 – C7 distance (Δ = 0.003 Å) and shorter

Co····C5 nonbonding distance (Δ = 0.007 Å) in complex **74**. In addition, the distance of

C7 – O in complex **74** (1.468(2) Å) is distinctively longer than in complex **51** (1.425(3)

Å), which suggests the weaker C-O bond in tosylate than in hydroxyl group.
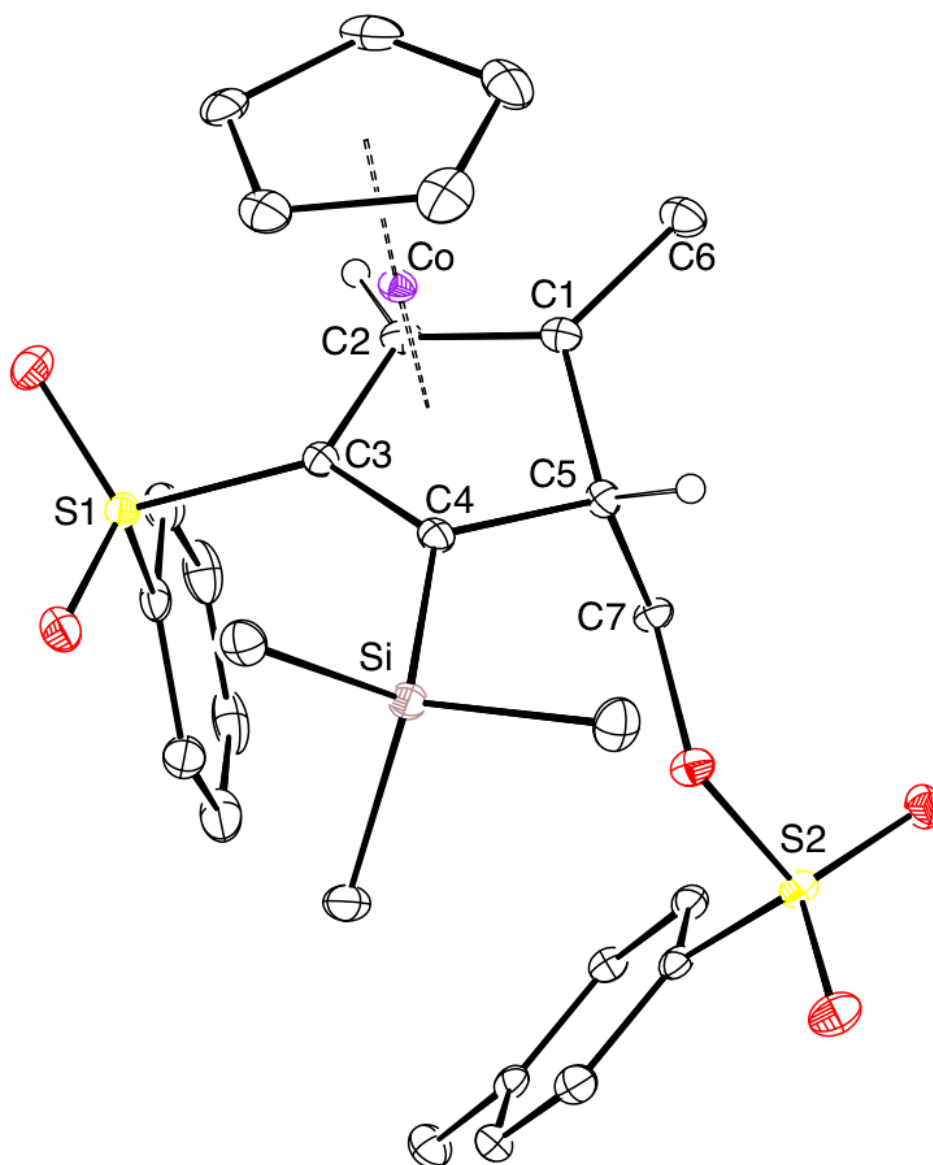
Figure 3-21. ORTEP drawing of **74** with ellipsoids shown at 30% probability.

Table 3-15. Seletecd bond distances (Å) and angles (deg) of complex **74**.

C1 – C2	1.409(3)	Co – C4	2.0704(17)
C2 – C3	1.446(3)	C5 – C7	1.528(2)
C3 – C4	1.448(2)	C2-C3-C4	108.75(17)
C4 – C5	1.542(2)	C3-C4-C5	105.69(14)
C5 – C1	1.530(2)	C2-C1-C5	108.96(16)
Co – C1	2.0466(18)	C1-C5-C4	97.31(14)
Co – C2	1.9595(17)	Co····C5	2.5846(15)
Co – C3	1.9360(17)	ring fold angle	33.73(15)

To conduct the ring expansion reaction, 229.5 mg (0.382 mmol) of complex **74** and 47 mg of DMAP (0.385 mmol) were dissolved in 10 ml dry chloroform in a schlenk flask under inert atmosphere (Scheme 3-41). The resulting solution was allowed to heat at 75°C, during which time the reaction mixture was monitored by TLC analysis. After 24 hours, all the starting materials disappeared, and some insoluble green precipitates crashed out. After filtration and chromatography on silica gel, 82 mg (70% yield) product was obtained as clear oil.
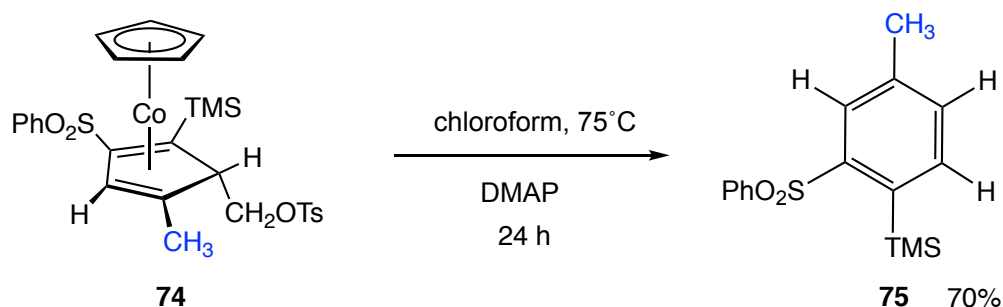
Scheme 3-41. Thermolysis of complex **74**.

High-resolution mass spectrometry provided the formula of the product as $C_{16}H_{20}O_2SSi$, which indicates that the metal is not binded to the product anymore. In ^1H NMR spectrum (400 MHz, CDCl$_3$), two singlet peaks at δ 0.41 (s, 9H) and 2.34 (s, 3H) indicates that TMS and methyl group are still attached on the product, but chemical shift of both signals are significantly more down field than the complexes **51** and **74** analogues. Eight hydrogens were detected by the integration of aromatic region between δ 7.3 and 7.9. Besides the signals of phenyl sulfone group, three signals at δ 7.34 (d, 1H, J = 7.6 Hz), 7.61 (bs, 1H), and 7.68 (d, 1H, ^{HH}J = 7.6 Hz) were observed, which indicates the formation of a new trisubstituted aromatic ring. In ^{13}C NMR spectrum (CDCl$_3$), six more new carbon environments in the aromatic region are also exhibited besides the phenyl sulfone group. All the spectroscopic data point to the arene strucuture **75**, which is generated from a ring-expanded aromatization of η^4-cyclopentadiene along with an automatic demetallation process.

In order to compare with Herberich's reactions, the same reaction condition was also used to conduct the ring expansion reactions. When 80% acetone/20% water solution of complex **74** (0.163 mmol, 8.2 mM) and pyridine (0.174 mmol, 8.7 mM) was heated at 40°C under N$_2$ for four days, 16.5 mg (36.2%) of **75** was the only compound isolated after chromatography without observing any η^5-cyclohexadienyl cobalt cation **76** (Scheme 3-42). We reason that the aqueous solvent might complicate the reaction and some side reactions could occur dropping down the yield.
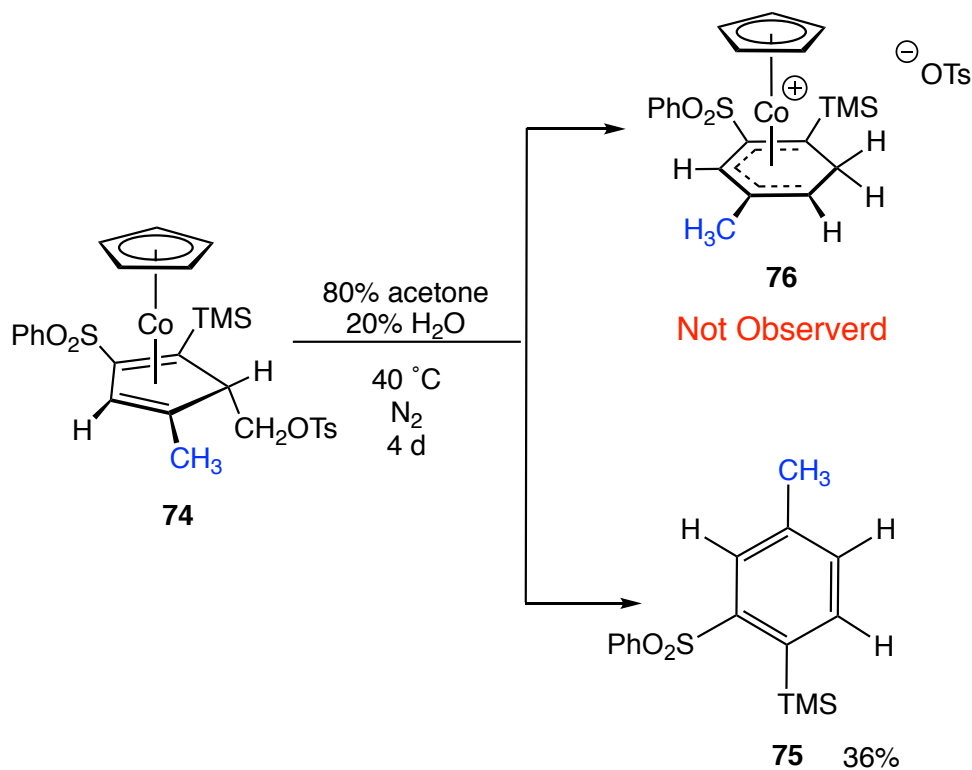
Scheme 3-42. Ring-expansion reaction of complex **74** in acetone/H$_2$O.

Furthermore, to clean up the work of previous graduate student, hydroxyl η^4-cyclopentadiene complexes **56** and **77** were also employed as precursors to conduct the ring-expansion reactions to afford arene derivatives **78** and **79**, respectively (Scheme 3-43, also see the spectra in Appendix section).
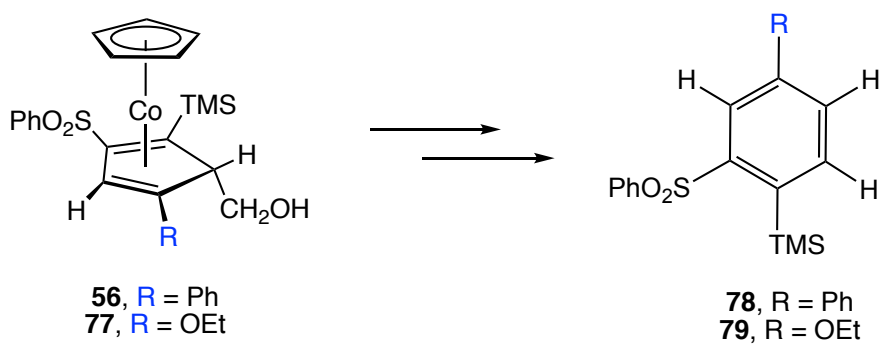
Scheme 3-43. Ring expansion on hydroxyl η^4-cyclopentadiene complexes **56** and **77**.

2. Deuterium Labelling Studies

Mechanisms for the formation of **75** have been proposed in scheme 3-44. During the ring-expansion aromatization process, the cyclopentadiene ligand can potentially rearrange in two different ways. If the single bond bearing the carbon with TMS substituent migrates, then η^5-cyclohexadienyl cobalt cation intermediate **80** forms, that is followed by deprotonation to generate the arene product, in which the newly incorporated ring carbon is *meta* to the methyl substituent (route a). Alternatively, if the single bond bearing the carbon with methyl substituent migrates, the newly incorporated ring carbon should be *ortho* to the R substituent in the final product (route b).

In order to distinguish these two mechanisms, an isotopic labeling study has been carried out (Scheme 3-45). Firstly, complex **52**-*exo* was allowed to treat with DIBAL-D. As mentioned earlier, both the ester group and methyl ether group can be reduced by DIBAL-D to provide complex **82** in which two deuterium were incorporated on the hydroxymethyl group and one deuterium on the methyl group, respectively. Then a one-pot reaction was employed to conduct the ring expansion reaction. 150 mg (0.323 mmol) of complex **82**, 93 mg (0.488 mmol) of tosyl chloride, and 60 mg (0.491 mmol) of DMAP were allowed to stir in dry chloroform at room temperature for 14 hours followed by heating at 75°C for 24 hours. After purification, 60 mg (60.6%) of **83** was obtained as clear oil without any observation of isomer **84**, which indicates that route a is the exclusive mechanism.
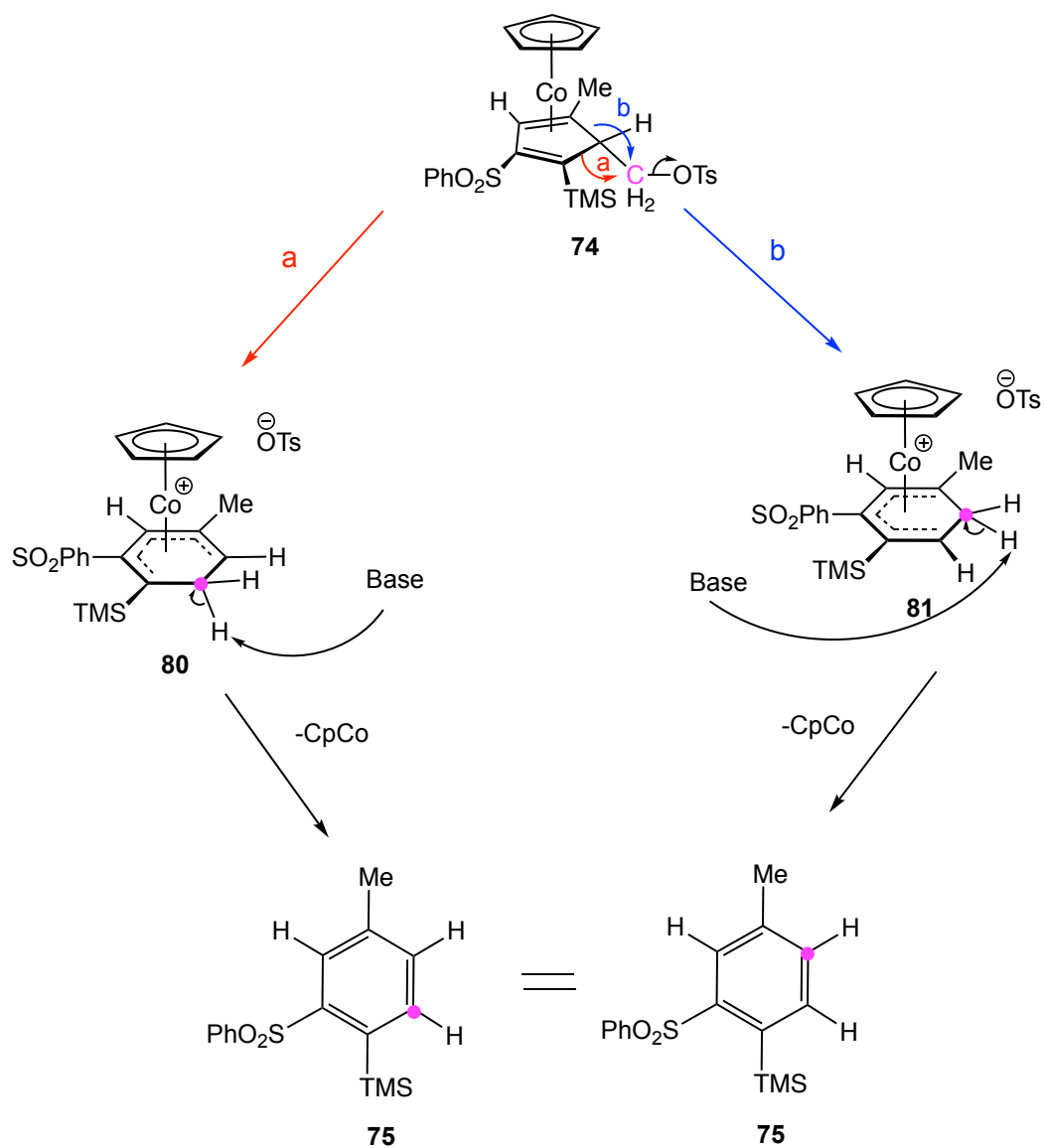
Scheme 3-44. Two possible mechanisms for the ring expansion of complex **74**.
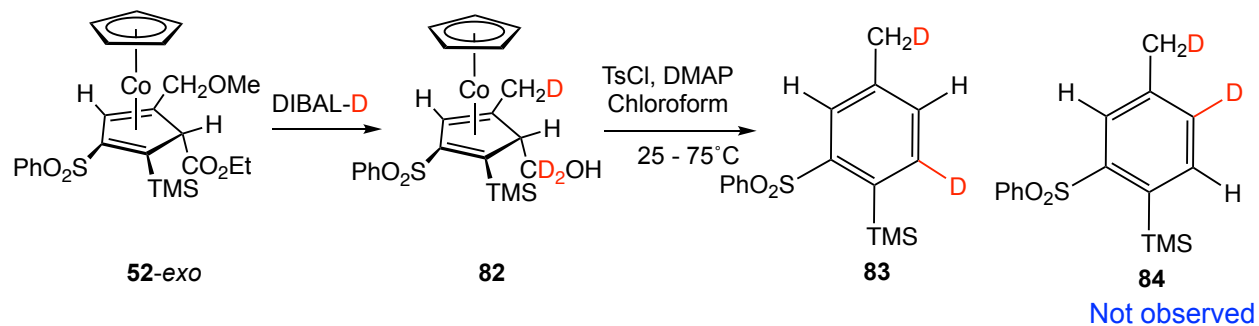
Scheme 3-45. Deuterium labelling studies of ring-expansion reactions.

The regiochemistry of **83** was confirmed by the comparison to **75** in ^{1}H NMR spectroscopy (400 MHz, CDCl$_3$) (Figure 3-22). The most distinctive changes are that the signal of proton c in **75** (δ 7.68, d, *J* = 7.6 Hz) was not observed in **83** at all, and proton b in **75** (δ 7.34, d, *J* = 7.6 Hz) changed from a doublet to singlet in **83**. These two differences indicate that the deuterium should be attached on the carbon that is *ortho* to TMS group, and thus compound **83** forms exclusively.
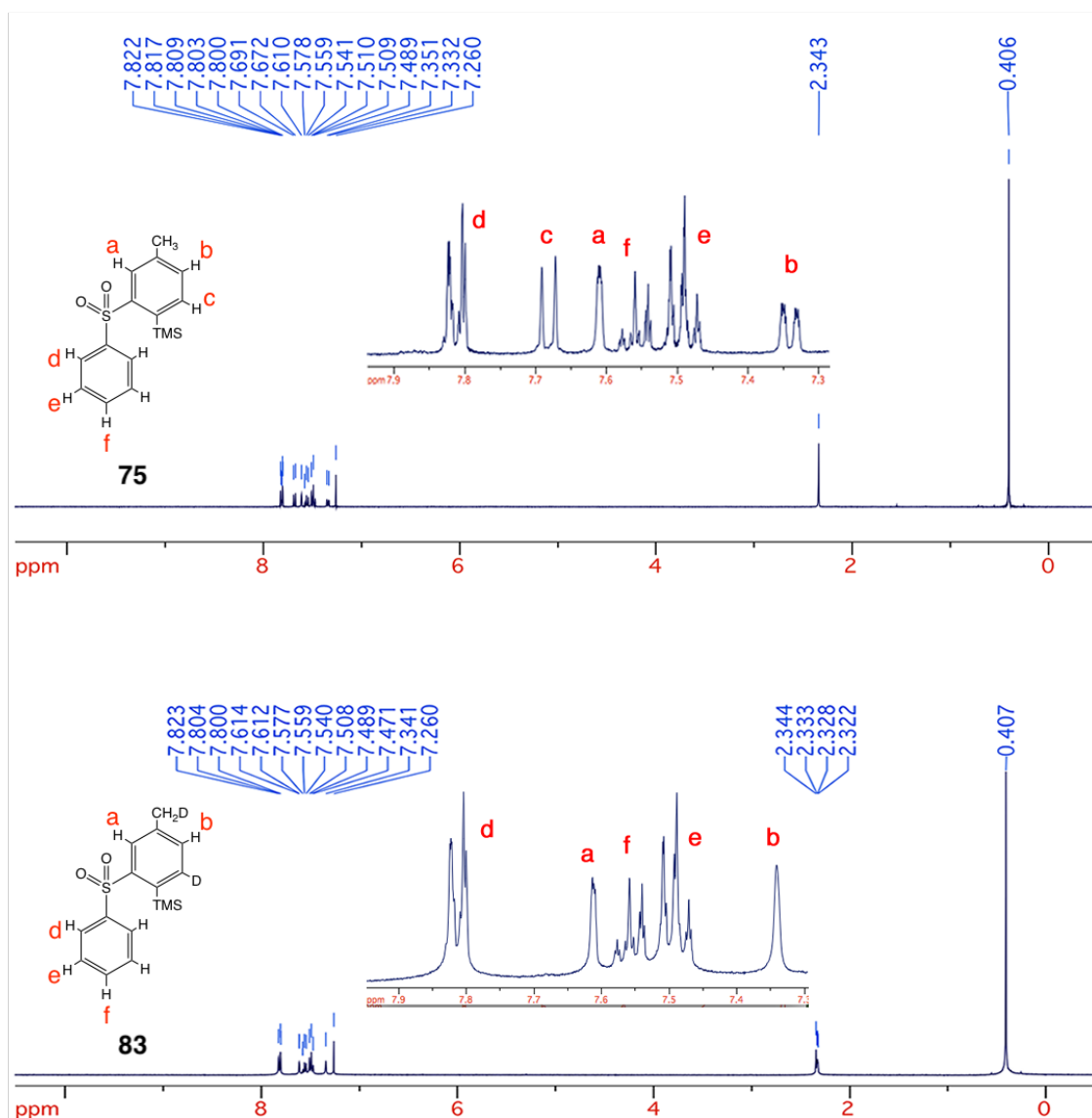
Figure 3-22. ^{1}H NMR sepctra (CDCl$_3$, 400 MHz) of compound **75** and **83**.

300

This remarkable regioselectivity might be caused by different electronic effect of substituents on ring carbons. Due to the electron-donating effect of TMS group, the carbon bearing TMS group should be more electron rich and thus can behave as a better nucleophile to undergo the S_N2 reaction than the carbon with methyl group. The chemical shift of the carbon bearing TMS (δ 60.05) and the carbon bearing methyl group (δ 71.63) in ^{13}C NMR spectrum (CDCl$_3$) also support the electron density difference. This behavior is analogous to the Baeyer-Villiger oxidation of unsymmetrical ketone, in which the more electron rich carbon has better migratory aptitude[35]. Additionally, this selective migration might also be ascribed to the energetical difference of variable conformations in transition state. If the leaving group is *anti* to TMS group by rotating the C5 – C7 bond, it can provide least steric congestion between TMS and leaving group, which will create a suitable geometry for the S_N2 reaction to proceed in route a. However, if the S_N2 reaction undergo in route b, TMS group must be *syn* to the leaving group, which will increase the energy and destabilize the transition state.

E. Conclusions

In summary, the treatment of metallacyclobutane (η^5-C$_5$H$_5$)(PPh$_3$)Co [C(SO$_2$Ph)=C(TMS)CH(CO$_2$Et)] (**2**) with a variety of terminal acetylenes HC≡CR (R = Me, CH$_2$OH, SnBu$_3$, *p*-C$_6$H$_4$NMe$_2$, and *p*-C$_6$H$_4$CMe$_3$) generate multi-functionalized cobalt η^4-cyclopentadiene complexes with high regioselectivity and good to excellent yields, which were characterized by ^{1}H, ^{13}C NMR, IR, HRMS, elemental analysis, and single crystallography. The existence of *endo* and *exo* isomers was found dictated by

the both electronic and steric effects of the substituents. To clean up previous work, the products from metallacyclobutane **2** with phenyl acetylene (both *endo* and *exo* isomers) and dimethyl but-2-ynedioate (*endo* isomer exclusively) were successfully crystallized and studied by X-ray crystallography.

Vinylmetallacyclobutene (η^5-C$_5$H$_5$)Co[C(CO$_2$Et)=C(CO$_2$Me)C(CO$_2$Me)CHCH(Ph)] (**16**) was obtained from trapping metallacyclobutene intermediate (η^5-C$_5$H$_5$)(PPh$_3$)Co [C(CO$_2$Me)=C(CO$_2$Me)CH(CO$_2$Et)] (**15**) with phenyl acetylene; whereas both vinylmetallacyclobutene (η^5-C$_5$H$_5$)Co[C(CO$_2$Et)=C(COCF$_3$)C(Ph)CHCH(Ph)] (**23**) and η^4-cyclopentadiene complex (η^5-C$_5$H$_5$)Co[η^4-C(COCF$_3$)=C(Ph)CH=C(Ph)CHCO$_2$Et] (**24**) were produced via the treatment of corresponding metallacyclobutene (η^5-C$_5$H$_5$)(PPh$_3$)Co [C(Ph)=C(COCF$_3$)CH(CO$_2$Et)] was with phenyl acetylene. Also, the first interconversion from vinylmatallacycle **23** to η^4-cyclopentadiene **24** was observed, which sheds light on the mechanism of this formal [2 + 2 +1] coupling. In addition, an alternative synthetic route of both vinylmetallacyclobutene and η^4-cyclopentadiene complexes were demonstrated by using a vinyl diazoacetate reacting with cobalt-alkyne complexes.

The first examples of trisubsitituted cobaltocenium cations were obtained by reducing the ester group of η^4-cyclopentadiene complexes with DIBAL-H followed by treatment with Brønsted acids, in which an unprecedented fragmentation takes place to generate formaldehyde as side product. The structures of different substituted cobatocenium salts were all confirmed by X-ray crystallography. The unique electrochemical and biological properties of cobaltocenium cations derived therefrom were also explored.

Furthermore, the hydroxyl cobalt-η^4-cyclopentadiene complexes can be furtherly tosylated and employed as precursors to achieve a novel ring-expansion reaction via a metal-mediated carbon-carbon bond activation, in which two alkynes and one ethyl diazoacetate are allowed to assemble multi-functionalized arenes in a highly regioselective manner. The selective migration mode that was dictated by both steric and electronic effects was confirmed by a deuterium labelling study. On the way to aromatization, the cyclopentadienyl cobalt substructure was found dissociating automatically without further addition of any oxidants.

F. Experimentals

4-*exo* 　　　　 4-*endo*
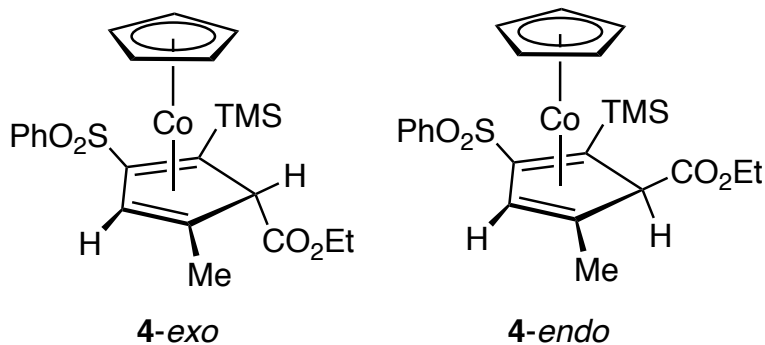
Preparation of [(η^5-C$_5$H$_5$)Co(η^4-C(TMS)=C(SO$_2$Ph)CH=C(Me)CH(CO$_2$Et)] *(4-exo and 4-endo)*: A 5% pentane solution of propyne (2.82 mL, 2.101 mmol) was added to a dry toluene solution (50 mL) of (η^5-C$_5$H$_5$)(PPh$_3$)Co[C(SO$_2$Ph)=C(TMS)CH(CO$_2$Et)] (**2**) (203 mg, 0.284 mmol) under a nitrogen atmosphere. The solution was heated at 70 °C for 8 h and chromatographic workup (silica gel, 10% EtOAc/hexanes), followed by

recrystallization from dichloromethane/hexanes, led to the isolation of **4**-*exo* (85.1 mg, 61.3% yield) and **4**-*endo* (46.2 mg, 33.3% yield) as red crystalline solids.

For **4**-*exo*: mp 92 °C; IR (CDCl$_3$) 3092, 3070, 2954, 2898, 1718, 1443, 1313, 1241, 1207, 1146, 1094, 1030 cm^{-1}. ^{1}H NMR (CDCl$_3$, 400 MHz): δ 0.11 (s, 9H), 0.91 (t, 3H, J = 7.2 Hz), 1.27 (s, 3H), 3.44 (s, 1H), 3.66 (m, 2H), 4.95 (s, 5H), 5.63 (s, 1H), 7.0-8.1 (m, 5H). ^{13}C{^{1}H} NMR (CDCl$_3$, 125 MHz): δ 0.7, 14.1, 18.2, 39.4, 56.6, 60.2, 64.6, 82.4, 82.7, 101.5, 127.3, 128. 9, 132.8, 142.8, 166.2. HRMS for [C$_{23}$H$_{29}$CoO$_4$SSiNa]$^+$: HRMS (ESI-TOF) *m/z*: [M+Na]+ Calcd for C$_{23}$H$_{29}$CoO$_4$SSiNa 511.0780; Found 511.0778. Anal. Calcd for C$_{23}$H$_{29}$CoO$_4$SSi: C, 56.54; H, 5.98. Found C, 56.37; H, 6.34.

For **4**-*endo*: mp 116 °C; IR (CDCl$_3$) 3072, 2976, 2942, 2898, 1738, 1713, 1446, 1313, 1244, 1149, 1093, 1024 cm^{-1}. ^{1}H NMR (CDCl$_3$, 400 MHz) δ − 0.04 (s, 9H), 1.01 (s, 3H), 1.32 (t, 3H, J = 7.2 Hz), 2.86 (s, 1H), 4.20 (m, 2H), 4.99 (s, 5H), 5.60 (s, 1H), 7.0-8.1 (m, 5H). ^{13}C{^{1}H} NMR (CDCl$_3$, 125 MHz): δ 0.5, 14.4, 16.9, 34.3, 55.2, 60.6, 65.9, 81.6, 83.1, 100.2, 127.1, 129.1, 132.9, 143.2, 172.9. HRMS (ESI-TOF) *m/z*: [M+Na]+ Calcd for C$_{23}$H$_{29}$CoO$_4$SSiNa 511.0780; Found 511.0776. Anal. Calcd for C$_{23}$H$_{29}$CoO$_4$SSi: C, 56.54; H, 5.98. Found C, 56.30; H, 6.18
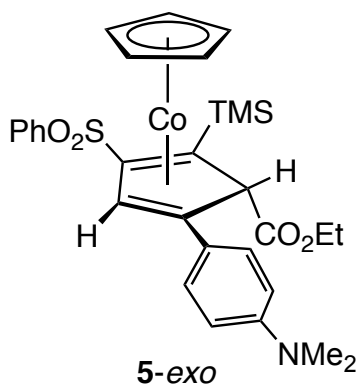
5-*exo*

Preparation of (η^5-C$_5$H$_5$)Co[η^4-C(TMS)=C(SO$_2$Ph)CH=C(*p*-C$_6$H$_4$NMe$_2$)CH(CO$_2$Et)] (5-exo): A dry toluene solution (80 mL) of (η^5-C$_5$H$_5$)(PPh$_3$)Co[C(SO$_2$Ph)=C(TMS)CH(CO$_2$Et)] (**2**) (202.0 mg, 0.284 mmol) and 4-ethynyl-*N*,*N*-dimethylaniline (194.0 mg, 1.350 mmol) was heated under a nitrogen atmosphere at 70 °C for 5 h. Chromatographic workup (silica gel, 15% EtOAc/hexanes), followed by recrystallization from hot ethanol, led to the isolation of air-stable **5**-*exo* (76.1 mg, 44.1% yield) as a red crystalline solid. mp 180.2 °C; IR (CDCl$_3$) 3062, 2951, 2895, 2801, 1710, 1610, 1542, 1443, 1305 cm^{-1}. ^{1}H NMR (CDCl$_3$, 400 MHz): δ 0.15 (s, 9H), 0.82 (t, 3H, *J* = 6.8 Hz), 2.92 (s, 6H), 3.59 (m, 2H), 4.12 (s, 1H), 4.79 (s, 5H), 6.24 (s, 1H), 6.58 (d, 2H, *J* = 8.8 Hz), 7.10 (d, 2H, *J* = 8.8 Hz), 7.57 (m, 3H), 8.11 (d, 2H, *J* = 7.2 Hz). ^{13}C{^{1}H} NMR (CDCl$_3$, 125 MHz): δ 0.6, 14.0, 38.8, 40.5, 59.1, 60.3, 61.3, 78.4, 83.0, 101.9, 112.8, 126.1, 126.7, 127.5, 128.9, 132.8, 142.8, 148.9, 165.9. HRMS (ESI-TOF) *m/z*: [M+H]+ Calcd for C$_{30}$H$_{37}$CoNO$_4$SSi 594.1539; Found 594.1536. Anal. Calcd for C$_{32}$H$_{36}$CoO$_4$SSi: C, 60.69; H, 6.11. Found C, 59.81; H, 5.71.

6-*exo*   6-*endo*
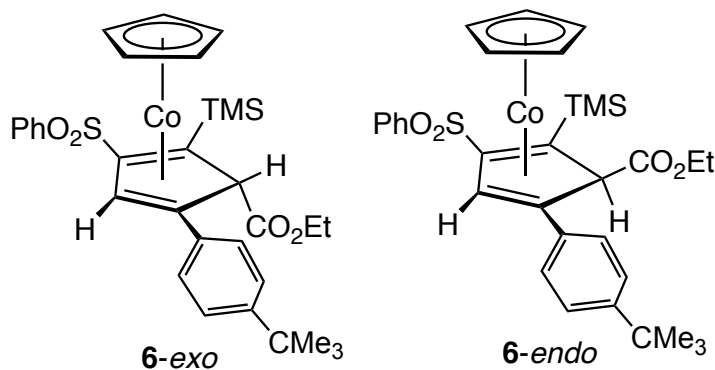
Preparation of (η^5-C$_5$H$_5$)Co[η^4-C(TMS)=C(SO$_2$Ph)CH=C(*p*-C$_6$H$_4$'Bu)CH(CO$_2$Et)] (6-exo and 6-*endo*): A dry toluene solution (100 mL) of (η^5-C$_5$H$_5$)(PPh$_3$)Co[C(SO$_2$Ph)=C(TMS)CH(CO$_2$Et)] (**2**) (520 mg, 0.732 mmol) and 1-(tert-butyl)-4-ethynylbenzene (578 mg, 3.653 mmol) was heated under a nitrogen atmosphere at 70 °C for 6 h. Chromatographic workup (silica gel, 10% EtOAc/hexanes), followed by recrystallization from EtOAc/hexanes, led to the isolation of air-stable **6**-*exo* (255.8 mg, 57.7% yield) and slightly air stable **6**-*endo* (149.1 mg, 33.6% yield) as red crystalline solids.

For **1**-*Ar'Bu*: mp 95.0 °C (deg); IR (CH$_2$Cl$_2$) 3093, 3058, 2965, 2899, 2865, 1718, 1442 cm^{-1}, ^{1}H NMR (CDCl$_3$, 400 MHz): δ 0.16 (s, 9H), 0.83 (t, 3H, *J* = 7.2 Hz), 1.28 (s, 9H), 3.59 (m, 1H), 3.64 (m, 1H), 4.07 (s, 1H), 4.83 (s, 5H), 6.37 (s, 1H), 7.0-8.2 (m, 9H). ^{13}C{^{1}H} NMR (CDCl$_3$, 125 MHz): δ 0.8, 14.2, 31.4, 35.0, 40.1, 56.5, 60.6, 61.5, 80. 7, 83.4, 103.0, 125.5, 126.2, 127.8, 129.2, 133.1, 136.1, 142.9, 149.4, 166.2. HRMS (ESI-TOF) *m/z*: [M+Na]+ Calcd for C$_{32}$H$_{39}$CoO$_4$SSiNa 629.1563; Found 629.1561. Anal. Calcd for C$_{32}$H$_{39}$CoO$_4$SSi: C, 63.35; H, 6.48. Found C, 63.10; H, 6.33.

For **6**-*endo*: mp 162-163 °C; IR (CH$_2$Cl$_2$) 2962, 2898, 2801, 1741, 1710 cm^{-1}. ^{1}H NMR (CDCl$_3$, 400 MHz): δ 0.03 (s, 9H), 1.27 (s, 9H), 1.32 (t, 3H, *J* = 7.2 Hz), 3.22 (s, 1H), 4.18 (m, 1H), 4.30 (m, 1H), 5.04 (s, 5H), 6.08 (s, 1H), 6.8-8.1 (m, 9H). ^{13}C{^{1}H} NMR (CDCl$_3$, 125 MHz): δ 0.7, 14.4, 31.4, 35.0, 35.5, 56.3, 61.0, 64.3, 83.3, 84.0, 101.4, 125.3, 125.9, 127.4, 129.4, 133.2, 136.4, 143.4, 149.2, 173.3. HRMS (ESI-TOF) *m/z*: [M+H]+ Calcd for C$_{32}$H$_{40}$CoO$_4$SSi 607.1743; Found 607.1743. Anal. Calcd for C$_{32}$H$_{39}$CoO$_4$SSi: C, 63.35; H, 6.48. Found C, 62.96; H, 6.48.
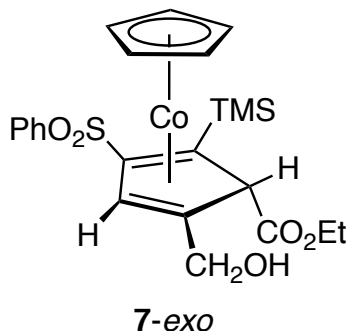
7-*exo*

Preparation of (η^5-C$_5$H$_5$)Co[η^4-C(TMS)=C(SO$_2$Ph)CH=C(CH$_2$OH)CH(CO$_2$Et)] (7-*exo*):

500 mg (0.70 mmol) of (η^5-C$_5$H$_5$)(PPh$_3$)Co[C(SO$_2$Ph)=C(TMS)CH(CO$_2$Et)] (**2**) and 196.2 mg (3.50 mmol) of propargyl alcohol were added into a reaction tube with 120mL dry toluene. After dissolving them by stirring for 10 minutes, it was bubbled with argon and sealed with Teflon cap as well as electrical tape. Then the solution was heated at 70°C for 6 hours. Via chromatography on silica gel with 30% EtOAc/hexane, 305.5 mg (yield = 84%) of **7**-*exo* was obtained as an air stable red crystalline solid after recrystallization from EtOAc/hexane; IR (CH$_2$Cl$_2$) 3350, 1720 cm^{-1}, ^{1}H NMR (CDCl$_3$, 400 MHz) δ 0.15 (s, 9H, TMS), 0.9 (t, 3H, J = 7.2 Hz, CH$_2$CH_3), 2.69 (bs, 1H, CH$_2$OH), 3.54 (m, 1H, CH_2CH$_3$), 3.64 (m, 1H, CH_2OH), 3.74 (m, 1H, CH_2CH$_3$), 3.88 (m, 1H, CH_2OH), 5.03 (s, 5H, Cp), 5.88 (s, 1H, vinyl-H), 7.5 – 8.1 (m, 5H, Ar); ^{13}C{^{1}H} NMR (CDCl$_3$, 125 MHz) δ 0.9 , 14.0, 40.8, 56.6, 60.9, 61.8, 63.2, 81.6, 82.2, 102.6, 127.4, 129.0, 133.0, 142.6, 169.1; HRMS for [C$_{23}$H$_{29}$CoO$_5$SSiNa]$^+$: 527.0735 (Theo. Mass), 527.0735 (Mass Measured), Delta (0.0 ppm). Elemental Analysis: C% (54.75); H% (5.79). Found: C% (54.39); H% (5.70).

8-*exo*   **8**-*endo*
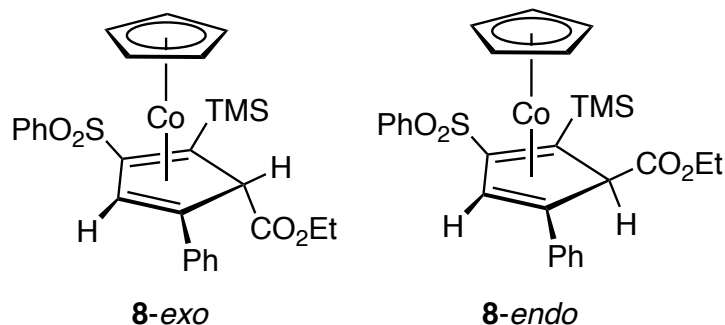
Preparation of (η^5-C$_5$H$_5$)Co[η^4-C(TMS)=C(SO$_2$Ph)CH=C(Ph)CH(CO$_2$Et)] (8-*exo* and

8-*endo*): A dry toluene solution (100 mL) of (η^5-C$_5$H$_5$)(PPh$_3$)Co [C(SO$_2$Ph)=C(TMS)CH(CO$_2$Et)] (**2**) (623.8 mg, 0.878 mmol) and ethynylbenzene (448.2 mg, 4.388 mmol) was heated under a nitrogen atmosphere at 70 °C for 6 h. Chromatographic workup (silica gel, 10% EtOAc/hexanes), followed by recrystallization from EtOAc/hexanes, led to the isolation of **8**-*exo* (299.7 mg, 62.0% yield) and **8**-*endo* (142.3 mg, 29.4% yield), as air-stable red crystalline solids.

For **8**-*exo*: mp 136-137 °C; IR (CH$_2$Cl$_2$) 3098, 3058, 2981, 2950, 2899, 2361, 2338, 1710, 1442, 1314 cm^{-1}, ^{1}H NMR (CDCl$_3$, 400 MHz): δ 0.16 (s, 9H), 0.83 (t, 3H, J = 7.0 Hz), 3.60 (m, 1H), 3.63 (m, 1H), 4.08 (s, 1H), 4.81 (s, 5H), 6.42 (s, 1H), 7.0-8.2 (m, 10H). ^{13}C{^{1}H} NMR (CDCl$_3$, 125 MHz): δ 0.8, 14.2, 40.5, 55.8, 60.6, 61.36, 80.8, 83.5, 103.3, 125.8, 126.4, 127.8, 129.19, 129.3, 133.2, 139.3, 142.8, 166.2. HRMS (ESI-TOF) *m*/*z*: [M+Na]+ Calcd for C$_{28}$H$_{31}$CoO$_4$SSiNa 573.0937; Found 573.0938. Anal. Calcd for C$_{28}$H$_{31}$CoO$_4$SSi: C, 61.08; H, 5.67. Found C, 60.97; H, 5.70.

For **8**-*endo*: mp 152-153 °C; IR (CH$_2$Cl$_2$) 3457, 3132, 3081, 3054, 2976, 2922, 2895, 2864, 1741, 1594, 1439, 1326 cm^{-1}, ^{1}H NMR (CDCl$_3$, 400 MHz): δ 0.03 (s, 9H), 1.30 (t, 3H, J = 7.2 Hz), 3.24 (s, 1H), 4.16 (m, 1H), 4.29 (m, 1H), 5.04 (s, 5H), 6.13 (s, 1H), 6.5-

8.1 (m, 10H). $^{13}C\{^1H\}$ NMR (CDCl$_3$, 125 MHz): δ 0.65, 14.38, 35.74, 55.94, 61.01, 64.51, 83.68, 84.1, 101. 7, 125.6, 126.2, 127.4, 128.8, 129.4, 133.3, 139.5, 143.3, 173.2. HRMS (ESI-TOF) *m/z*: [M+Na]+ Calcd for C$_{28}$H$_{31}$CoO$_4$SSiNa 573.0937; Found 573.0936. Anal. Calcd for C$_{28}$H$_{31}$CoO$_4$SSi: C, 61.08; H, 5.67. Found C, 61.26; H, 5.72.
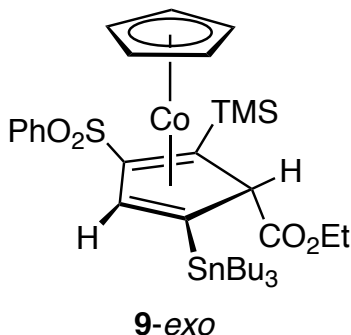
9-*exo*

Preparation of (η^5-C$_5$H$_5$)Co[η^4-C(TMS)=C(SO$_2$Ph)CH=C(SnBu$_3$)CH(CO$_2$Et)] (9-*exo*): 410 mg (0.577 mmol) of (η^5-C$_5$H$_5$)(PPh$_3$)Co[C(SO$_2$Ph)=C(TMS)CH(CO$_2$Et)] (**2**) were added into a reaction tube with 100mL dry toluene. After dissolving them by stirring for 10 minutes, it was bubbled with argon for 15 minutes and then 901 mg (2.86 mmol) of Ethylnyltributylstannane were added. The reaction tube was sealed with Teflon cap as well as electrical tape. Then the solution was heated at 70°C for 18 hours. Via chromatography on silica gel with 8% EtOAc/hexane, 223 mg (yield = 50.6 %) of **9**-*exo* was obtained as an air stable red oil; IR (CDCl$_3$) 2950, 2928, 2870, 2850, 1729, 1712, 1443, 1307, 1246, 1149, 1018, 841, 810 cm^{-1}, ^1H NMR (CDCl$_3$, 400 MHz) δ 0.06 (s, 9H), 0.88 (m, 18H), 1.28-1.52 (m, 12H), 3.51 (s, 1H), 3.57 (m, 2H), 4.99 (s, 5H), 6.00 (s, 1H), 7.54 (m, 3H), 8.55 (d, 2H, *J* = 7.2 Hz); $^{13}C\{^1H\}$ NMR (CDCl$_3$, 125 MHz) δ 0.6, 10.2, 13.9, 14.1, 27.6, 29.2, 38.9, 45.0, 60.1, 66.1, 81.7, 90.6, 103.8, 127.5, 128.9, 132.8,

142.8, 166.5. HRMS for $[C_{34}H_{53}CoO_4SSiSnNa]^+$: 787.1685 (Theo. Mass), 787.1685 (Mass Measured), Delta (0 ppm).

16
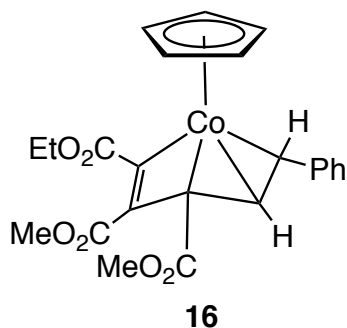
Preparation of (η^5-C$_5$H$_5$)Co[C(CO$_2$Et)=C(CO$_2$Me)C(CO$_2$Me)CHCH(Ph)] (16): 335 mg (0.633 mmol) of cobalt-alkyne complex (η^5-C$_5$H$_5$)(PPh$_3$)Co[η^2-(CO$_2$Me)C≡C(CO$_2$Me)] (**14**) and 723 mg (0.951 mmol, 15% in toluene) of ethyl diazoacetate were added into a reaction tube with 80mL dry toluene inside a glove box. After stirring for 3 hours at room temperature under nitrogen gas, 390 mg (3.82 mmol) of phenyl acetylene was added. Then it was sealed with Teflon cap as well as electrical tape. The solution was heated at 70°C for 40 minutes. When the reaction is done, the color of the solution changed from dark brown to red. Via chromatography on silica gel with 25% ethyl acetate/hexane, 132 mg (yield = 46 %) of complex **16** was obtained as an air stable dark red crystalline solid after recrystallization from toluene and hexane at -20°C. Mp: 137.4 °C; IR (CDCl$_3$) 3109, 2984, 29511, 1702, 1619, 1438, 1346, 1244, 1213, 1116, 1021, 819 cm^{-1}; ^{1}H NMR (CDCl$_3$, 400 MHz) δ 1.43 (t, 3H, J = 7.2Hz), 3.58 (s, 3H), 3.88 (s, 3H), 4.01 (d, 1H, J = 11.2 Hz), 4.42 (m, 2H), 4.61 (s, 5H), 6.59 (d, 1H, J = 11.2 Hz), 7.2-7.6 (m, 5H); ^{13}C{^{1}H}

NMR (CDCl$_3$, 125 MHz) δ 14.9, 47.5, 51.4, 52.8, 61.0, 65.8, 86.5, 91.3, 118.4, 127.1, 127.1, 129.4, 142.1, 156.3, 160.6, 173.5, 173.9. HRMS for [C$_{23}$H$_{24}$CoO$_6$]$^+$: 455.0899 (Theo. Mass), 455.0901 (Mass Measured), Delta (0.4 ppm). Elemental Analysis: C% (60.80); H% (5.10). Found: C% (60.54); H% (5.49).
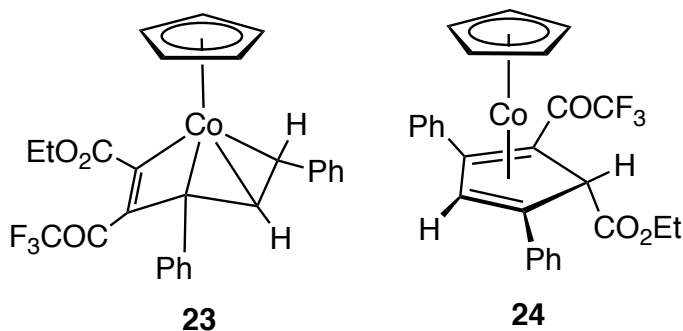
23 **24**

Preparation of (η^5-C$_5$H$_5$)Co[C(CO$_2$Et)=C(COCF$_3$)C(Ph)CHCH(Ph)] (23) and (η^5-C$_5$H$_5$)Co[η^4-C(COCF$_3$)=C(Ph)CH=C(Ph)CH(CO$_2$Et)] (24): 357 mg (0.532 mmol) of metallacyclobutene (η^5-C$_5$H$_5$)(PPh$_3$)Co[C(Ph)=C(COCF$_3$)CH(CO$_2$Et)] (**22**) and 272 mg (2.663 mmol) of phenyl acetylene were added into a reaction tube with 60 mL dry benzene inside a glove box. Then the tube was sealed with Teflon cap as well as electrical tape. After stirring the solution for 10 minutes to make all solid dissolved, the solution was heated at 70°C for 2 hours in an oil bath. Via chromatography on silica gel with 8% ethyl acetate/hexane, 154 mg (yield = 56.7 %) of **23** was obtained as an air stable dark red crystalline solid after recrystallization from toluene and hexane at -20°C, and complex **24** was obtained as an air stable green crystalline solid after recrystallization from toluene and hexane at -20°C.

For **23**: Mp: 113.5 °C; IR (CDCl$_3$) 3060, 3025, 2982, 1705, 1663, 1583, 1482, 1451, 1200, 1136, 1073, 1012, 906, 822, 760, 734, 692 cm^{-1}; ^{1}H NMR (CDCl$_3$, 400 MHz) δ 1.48 (t, 3H, J = 7.2 Hz), 3.89 (d, 1H, J = 10.8 Hz), 4.39 (s, 5H), 4.474= (q, 2H, J = 7.2 Hz), 6.25 (d, 1H, J = 10.8 Hz), 7.2-8.0 (m, 10H); ^{13}C{^{1}H} NMR (CDCl$_3$, 125 MHz) δ 14.8, 61.2, 63.6, 69.0, 84.3, 87.7, 116.3 (q, J_{CF} = 291 Hz), 124.8, 126.7, 127.0, 127.0, 128.5, 129.3, 129.4, 140.6, 142.7, 163.7 (q, J_{CF} = 35.4 Hz), 173.5, 193.4. HRMS for [C$_{27}$H$_{23}$CoF$_3$O$_3$]$^+$: 511.0926 (Theo. Mass), 511.0928 (Mass Measured), Delta (0.4 ppm). Elemental Analysis: C% (63.54); H% (4.34). Found: C% (63.29); H% (4.47).

For **24**: Mp: 120.8 °C; IR (CDCl$_3$) 3088, 3060, 2982, 1728, 1674, 1505, 1449, 1403, 1307, 1194, 1138, 1029, 973 cm^{-1}; ^{1}H NMR (CDCl$_3$, 400 MHz) δ 1.07 (t, 3H, J = 7.2 Hz), 3.91 (m, 2H), 4.45 (s, 1H), 4.57 (s, 5H), 6.14 (s, 1H), 7.2-8.0 (m, 10H); ^{13}C{^{1}H} NMR (CDCl$_3$, 125 MHz) δ 14.1, 34.0, 55.0, 58.5, 61.0, 81.8, 83.7, 101.0, 117.0 (q, J_{CF} = 292.5 Hz), 126.0, 126.7, 128.2, 128.3, 129.1, 130.1, 136.0, 138.8, 167.4, 186.0 (q, J_{CF} = 33.7 Hz). HRMS for [C$_{27}$H$_{23}$CoF$_3$O$_3$]$^+$: 511.0926 (Theo. Mass), 511.0920 (Mass Measured), Delta (-1.2 ppm). Elemental Analysis: C% (63.54); H% (4.34). Found: C% (63.78); H% (4.73).

23   **24** (54.5%)
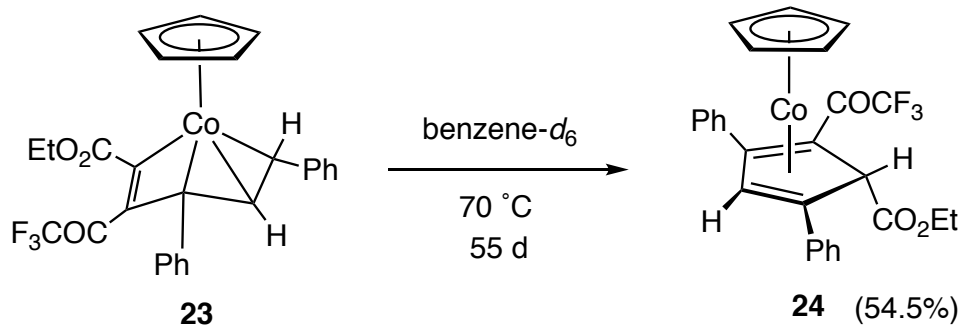
NMR scale reaction of conversion of complex 23 to 24: 4 mg (0.008 mmol) of **23** and 1,3,5-tri-*tert*-butylbenzene (internal standard) were added into a Teflon top NMR tube. Around 0.7 ml of C_6D_6 was distilled into the NMR tube on the Schlenk line. After shaking the tube on Vortex Mixer for 5 minutes to dissolve all the solids, the first ^{1}H NMR was recorded as initial one. Then the solution was heated at 70°C in an oil bath. The reaction was subsequently monitored by ^{1}H NMR spectroscopy and time points were taken at 2 h, 12 h, 48 h, 5 d, 40d, and 55d. After 55 days, **23** was totally consumed based on the Cp peak at 4.05 ppm. New ^{1}H NMR resonances for **24** were observed at δ 0.74 (t, 3H, *J* = 7.2 Hz), 3.69 (m, 2H), 4.13 (s, 5H, Cp), 4.64 (s, 1H) and 5.67 (s, 1H). Percent yield was calculated from integration of the internal standard relative to the Cp resonance of **24** at 4.13 ppm (54.5 % yield).

39
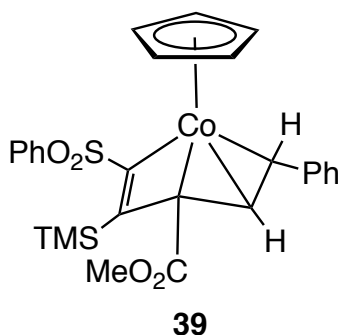
Preparation of (η^5-C$_5$H$_5$)Co[C(SO$_2$Ph)=C(TMS)C(CO$_2$Me)CHCH(Ph)] (39): 500 mg (0.78 mmol) of cobalt-alkyne complex (η^5-C$_5$H$_5$)(PPh$_3$)Co[η^2-(SO$_2$Ph)C≡C(TMS)] (**38**) was mixed with 473 mg (2.34 mmol) of vinyl diazoacetate **36** in a dry benzene solution

(150 mL) under N_2. The reaction mixture was allowed to stir at ambient temperature for 3 days. After chromatography on silica gel with 8% ethyl acetate/hexane, 226 mg (yield = 54 %) of **29** was obtained as an air stable dark red crystalline solid after recrystallization from toluene and hexane at -20°C. IR (CH_2Cl_2): 3062, 2950, 2256, 1707, 1529, 1449, 1282, 1234, 1138, 1083 cm^{-1}; ^{1}H NMR (CDCl$_3$, 400 MHz) δ 0.12 (s, 9H, TMS), 3.30 (d, 1H, J = 11.6 Hz, vinyl-H), 3.91 (s, 3H, Me), 4.56 (s, 5H, Cp), 6.34 (d, 1H, J = 11.6 Hz, vinyl-H), 6.8 – 8.1 (m, 10H, Ar); ^{13}C{^{1}H} NMR (CDCl$_3$, 125 MHz) δ 0.8, 45.7, 52.5, 67.3, 86.7, 89.6, 126.5, 126.8, 128.1, 129.3, 132.8, 142.2, 142.5, 150.9, 155.9, 174.7. HRMS for [C$_{27}$H$_{30}$CoO$_4$SSi]$^+$: 537.0961 (Theo. Mass), 537.0958 (Mass Measured), Delta (-0.6 ppm). Elemental Analysis: C% (60.21); H% (5.80). Found: C% (60.15); H% (5.72).
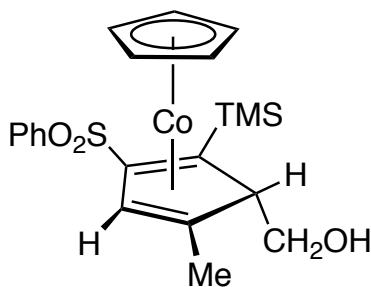
51

Preparation of (η^5-C$_5$H$_5$)Co[η^4-C(TMS)=C(SO$_2$Ph)CH=C(Me)CH(CH$_2$OH)] (51): 201 mg (0.386 mmol) of (η^5-C$_5$H$_5$)Co[η^4-C(TMS)=C(SO$_2$Ph)CH=C(CH$_2$OCH$_3$)CH(CO$_2$Et)] (**52**-*exo*) were dissolved in 30 mL dry toluene and bubbled with argon for 10 minutes. Then added 3.2 mL (3.2 mmol, 1.0 M in toluene) of DIBAL-H under -78° while keep it

stirring. Some foaming in the red solution was observed during the addition. The reaction was stirred at -78°C for 2 hours, then at 0˚C for four hours. Then quenched it with 5 mL MeOH and extracted three times with a saturated sodium potassium tartrate solution (30 mL each time). The organic layer was dried with magnesium sulfate. After chromatography on silica gel with 30% EtOAc/hexane, 114.6 mg (yield = 66.6%) of **51** was obtained as an air stable black crystalline solid via recrystallization from toluene/hexane. In a similar fashion, when 200 mg (0.40 mmol) of $(\eta^5\text{-}C_5H_5)Co[\eta^4\text{-}(C(TMS)=C(SO_2Ph)CH=C(CH_3)CH(CO_2Et)]$ (**4**-*exo*) was employed as starting material to be treated with DIBAL-H (2.0 mmol, 1.2 M in toluene), 88% yield of complex **51** can be obtained by using the same work-up procedure. mp 146-148°C; IR (CH$_2$Cl$_2$) 3517, 3089, 3064, 2954, 2898, 2856, 1582, 1443 cm^{-1}, ^{1}H NMR (CDCl$_3$, 400 MHz) δ 0.16 (s, 9H), 0.37 (dd, 1H, J = 5.0 Hz, 7.0 Hz), 1.28 (s, 3H), 2.43 (m, 1H), 2.67 (m, 1H), 2.88 (t, 1H, J = 4.0 Hz), 4.87 (s, 5H), 5.44 (s, 1H), 7.5-8.1 (m, 5H); ^{13}C{^{1}H} NMR (CDCl$_3$, 125 MHz) δ 1.4, 18.3, 39.3, 61.3, 65.0, 65.9, 81.2, 82.3, 102.5, 127.7, 129.4, 133.3, 143.0. HRMS for [C$_{21}$H$_{28}$CoO$_3$SSi]$^+$: 447.0855 (Theo. Mass), 447.0853 (Mass Measured), Delta (-0.5 ppm). Elemental Analysis: C% (56.49); H% (6.10). Found: C% (56.73); H% (6.47).

53

Preparation of (η^5-C$_5$H$_5$)Co[η^4-C(TMS)=C(SO$_2$Ph)CH=C(CH$_2$OH)CH(CH$_2$OH)] (53): 901 mg (1.803 mmol) of complex (η^5-C$_5$H$_5$)Co[η^4-C(TMS)=C(SO$_2$Ph)CH=C(CH$_2$OH)CH(CO$_2$Et] (**7**-*exo*) were dissolved in 30 mL dry toluene and bubbled with argon for 10 minutes. Then added 9.05 mL (10.82 mmol, 1.0 M in toluene) of DIBAL-H under -78° while keep it stirring. Some foaming in the red solution was observed during the addition. The reaction was stirred at -78°C for 2 hours, then at 0˚C for four hours. Then quenched it with 5 mL MeOH and extracted three times with a saturated sodium potassium tartrate solution (30 mL each time). The organic layer was dried with magnesium sulfate. After chromatography on silica gel with 50% EtOAc/hexane, 264 mg (yield = 29.5 %) of **53** was obtained as an air stable red crystalline solid via recrystallization from methylene chloride/hexanes; mp 198-199°C; IR (CH$_2$Cl$_2$) 3550, 3093, 3066, 2955, 2888, 1582, 1443 cm^{-1}, ^{1}H NMR (CDCl$_3$, 400 MHz) δ 0.15 (s, 9H, TMS), 1.86 (t, 1H, J = 7.2 Hz, CHCH$_2$O*H*), 2.45 (m, 1H, CHC*H*$_2$OH), 2.73 (bs, 1H, CH$_2$O*H*), 2.82 (d, 1H, J = 11 Hz, C*H*$_2$OH), 3.25 (m, 1H, CHC*H*$_2$OH), 3.43 (dd, 1H, J = 7.2 Hz, 7.6 Hz, C*H*CH$_2$OH), 3.99 (d, 1H, J = 11 Hz, C*H*$_2$OH), 4.95 (s, 5H, Cp), 5.72 (s, 1H, vinyl-H), 7.5-8.1 (m, 5H, Ar); ^{13}C{^{1}H} NMR (CDCl$_3$, 125 MHz) δ 39.0, 60.5, 62.9,

63.0, 67.8, 80.8, 81.7, 103.9, 127.4, 129.3, 133.2, 142.5. HRMS for [$C_{21}H_{27}CoO_4SSiNa$]$^+$: 485.0624 (Theo. Mass), 485.0622 (Mass Measured), Delta (-0.4 ppm). Elemental Analysis: C% (54.53); H% (5.88). Found: C% (53.85); H% (5.52).

Ar = *p*-$C_6H_4NMe_2$

54
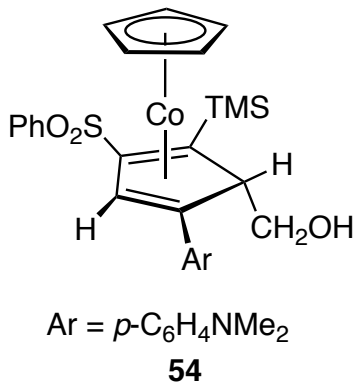
Preparation of (η^5-C_5H_5)Co[η^4-C(TMS)=C(SO_2Ph)CH=C(*p*-$C_6H_4NMe_2$)CH(CH_2OH)]

(54): 78.1mg (0.128 mmol) of (η^5-C_5H_5)Co[η^4-C(TMS)=C(SO_2Ph)CH=C(*p*-$C_6H_4NMe_2$) CH(CO_2Et] (**5-exo**) were dissolved in dry toluene and bubbled with argon for 10 minutes. Then added 0.43 mL (0.643 mmol, 1.2 M in toluene) of DIBAL-H under -78°C while keep it stirring. Some foaming in the red solution was observed during the addition. The reaction was stirred at -78°C for 2 hours, then at 0°C for four hours. Then quenched it with 1.5 mL MeOH and extracted three times with a saturated sodium potassium tartrate solution (10 mL each time). The organic layer was dried with magnesium sulfate. Via chromatography on silica gel with 20% EtOAc/hexane, 38.8 mg (yield = 54.9%) of **54** was obtained as an air sensitive red oil; IR (CDCl$_3$) 3525, 3092, 2950, 2898, 2853, 2800, 1607, 1524, 1446, 1357, 1299, 1152, 1082, 841 cm^{-1}, ^{1}H NMR

(CDCl$_3$, 400 MHz) δ 0.22 (s, 9H, TMS), 0.46 (dd, 1H, J = 4.8 Hz, 7.6 Hz), 2.47 (m, 1H), 2.67 (m, 1H), 2.93 (s, 6H), 3.59 (t, 1H, J = 4.8 Hz), 4.70 (s, 5H), 6.05 (s, 1H), 6.57 (d, 2H, J = 8.8 Hz), 7.12 (d, 2H, J = 8.4 Hz), 7.57 (m, 3H), 8.12 (d, 2H, J = 6.8 Hz); ^{13}C{^{1}H} NMR (CDCl$_3$, 125 MHz) δ 1.2, 39.4, 40.5, 60.5, 61.7, 66.9, 75.4, 82.8, 102.6, 112.9, 126.4, 126.9, 127.5, 129.2, 133.0, 142.8, 149.0. HRMS for [C$_{28}$H$_{34}$CoNO$_3$SSiNa]$^+$: 574.1253 (Theo. Mass), 574.1249 (Mass Measured), Delta (-0.7 ppm).
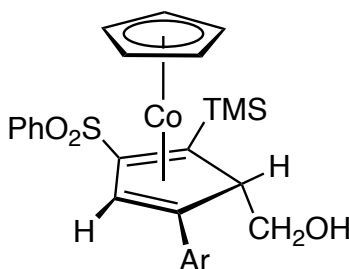
Ar = p-C$_6$H$_4$CMe$_3$

55

Preparation of (η^5-C$_5$H$_5$)Co[η^4-C(TMS)=C(SO$_2$Ph)CH=C(p-C$_6$H$_4$CMe$_3$)CH(CH$_2$OH)] (55): 189.0mg (0.3117 mmol) of (η^5-C$_5$H$_5$)Co[η^4-C(TMS)=C(SO$_2$Ph)CH=C(p-C$_6$H$_4$CMe$_3$) CH(CO$_2$Et] (**6-exo**) were dissolved in dry toluene and bubbled with argon for 10 minutes. Then added 1.17 mL (1.404 mmol, 1.2 M in toluene) of DIBAL-H under -78˚C while keep it stirring. Some foaming in the red solution was observed during the addition. The reaction was stirred at -78˚C for 2 hours, then at 0°C for four hours. Then quenched it with 1.5 mL MeOH and extracted three times with a saturated sodium potassium tartrate solution (20 mL each time). The organic layer was dried with

magnesium sulfate. Via chromatography on silica gel with 20% EtOAc/hexane, 164.7 mg (yield = 93.6%) of **55** was obtained as a slight air sensitive red crystalline solid after recrystallization from toluene/hexane; Decomposition Temperature 98°C; IR (CH$_2$Cl$_2$) 3527, 3089, 3058, 2958, 2903, 2865, 1520, 1442, 1302 cm^{-1}, ^{1}H NMR (CDCl$_3$, 400 MHz) δ 0.23 (s, 9H), 0.44 (dd, 1H, J = 4.8 Hz, 7.6 Hz), 1.28 (s, 9H), 2.49 (m, 1H), 2.66 (m, 1H), 3.56 (t, 1H, J = 4.4 Hz), 4.73 (s, 5H), 6.18 (s, 1H), 7.2-8.2 (m, 9H); ^{13}C{^{1}H} NMR (CDCl$_3$, 125 MHz) δ 1.4, 31.4, 35.0, 41.0, 59.0, 60.8, 66.9, 83.2, 103.7, 125.7, 126.3, 127.7, 129.5, 133.3, 136.5, 142.93, 149.5. HRMS for [C$_{30}$H$_{37}$CoO$_3$SSiNa]$^+$: 587.1457 (Theo. Mass), 587.1454 (Mass Measured), Delta (-0.5 ppm). Elemental Analysis: C% (63.81); H% (6.60). Found: C% (63.62); H% (6.56).

56
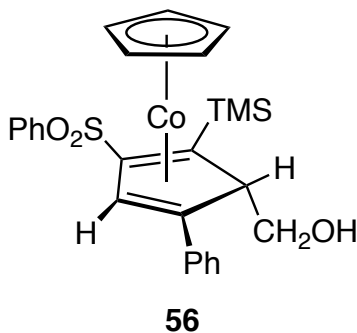
Preparation of (η^5-C$_5$H$_5$)Co[η^4-C(TMS)=C(SO$_2$Ph)CH=C(Ph)CH(CH$_2$OH)] **(56)**: 419.7mg (0.7622 mmol) of (η^5-C$_5$H$_5$)Co[η^4-C(TMS)=C(SO$_2$Ph)CH=C(p-C$_6$H$_4$CMe$_3$)CH(CO$_2$Et] (**8**-*exo*) were dissolved in dry toluene and bubbled with argon for 10 minutes. Then added 2.81 mL (3.37 mmol, 1.2 M in toluene) of DIBAL-H under -78°C while keep it stirring. Some foaming in the red solution was observed during the

addition. The reaction was stirred at -78°C for 2 hours, then at 0°C for four hours. Then

quenched it with 3.2 mL MeOH and extracted three times with a saturated sodium

potassium tartrate solution (30 mL each time). The organic layer was dried with

magnesium sulfate. Via chromatography on silica gel with 30% EtOAc/hexane, 349.2

mg (yield = 90.1%) of **56** was obtained as a slight air sensitive red crystalline solid after

recrystallization from toluene/hexane; Decomposition Temperature 79-80°C; IR

(CH$_2$Cl$_2$) 3519, 3058, 2954, 2899, 2861, 1446, 1120, 1244 cm^{-1}, ^{1}H NMR (CDCl$_3$, 400

MHz) δ 0.24 (s, 9H), 0.46 (dd, 1H, J = 4.8 Hz, 7.6 Hz), 2.51 (m, 1H), 2.67 (m, 1H), 3.57

(t, 1H, J = 4.4 Hz), 4.72 (s, 5H), 6.22 (s, 1H), 7.1-8.2 (m, 10H); ^{13}C{^{1}H} NMR (CDCl$_3$,

125 MHz) δ 1.4, 41.4, 58.4, 60.6, 66.8, 83.3, 104.0, 126.0, 126.4, 127.8, 129.4, 129.5,

133.4, 139.8, 142.8. HRMS for [C$_{26}$H$_{29}$CoO$_3$SSiNa]$^+$: 531.0831 (Theo. Mass), 531.0841

(Mass Measured), Delta (1.9 ppm). Elemental Analysis: C% (61.40); H% (5.75). Found:

C% (61.27); H% (6.14).

57
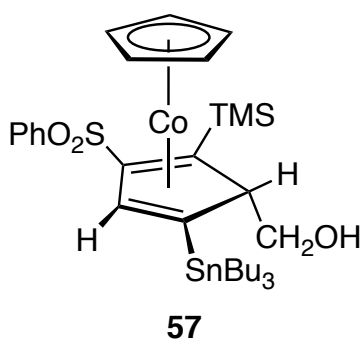
Preparation of (η^5-C$_5$H$_5$)Co[η^4-C(TMS)=C(SO$_2$Ph)CH=C(SnBu$_3$)CH(CH$_2$OH)] (57):

194.3 mg (0.254 mmol) of (η^5-C$_5$H$_5$)Co[η^4-C(TMS)=C(SO$_2$Ph)CH=C(SnBu$_3$)CH(CO$_2$Et]

(**9**-*exo*)   were dissolved in dry toluene and bubbled with argon for 10 minutes. Then

added 1.53 mL (1.53 mmol, 1.0 M in toluene) of DIBAL-H under -78°C while keep it

stirring. Some foaming in the red solution was observed during the addition. The

reaction was stirred at -78°C for 2 hours, then at 0°C for four hours. Then quenched it

with 2 mL MeOH and extracted three times with a saturated sodium potassium tartrate

solution (15 mL each time). The organic layer was dried with magnesium sulfate. Via

chromatography on silica gel with 10% EtOAc/hexane, 168.8 mg (yield = 92.1%) of **57**

was obtained as a slightly air sensitive red oil; IR (CDCl$_3$) 3522, 2956, 2925, 2845,

1443, 1302, 1246, 1149, 1082, 1027, 841, 802, 719 cm^{-1}, ^{1}H NMR (CDCl$_3$, 400 MHz) δ

0.14 (s, 9H), 0.25 (t, 1H, J = 6 Hz), 0.92 (m, 15H), 1.2-1.6 (m, 12H), 2.24 (m, 1H), 2.28

(m, 1H), 2.86 (t, 1H, J = 4.8 Hz), 4.95 (s, 5H), 5.82 (s, 1H), 7.56 (m, 3H), 8.08 (d, 2H, J

= 7.2 Hz); ^{13}C{^{1}H} NMR (CDCl$_3$, 125 MHz) δ 1.2, 10.6, 13.9, 27.6, 29.3, 40.2, 49.4, 66.0,

68.1, 81.3, 89.1, 103.8, 127.4, 129.2, 133.1, 142.9. HRMS for [C$_{32}$H$_{51}$CoO$_3$SSiSnNa]$^+$:

745.1579 (Theo. Mass), 745.1582 (Mass Measured), Delta (0.4 ppm).

61

Preparation of (η^5-C$_5$H$_5$)Co[η^5-C(TMS)C(SO$_2$Ph)CHC(Me)CH]BF$_4$ (61): 36 mg (0.0804

mmol) of complex **51** were dissolved in 20 mL diethyl ether and bubbled with argon for

10 minutes in a round bottom flask. Then added 0.0355 mL (0.2412 mmol) of HBF$_4$·Et$_2$O

into the solution slowly while keep it stirring. The color of the solution changed from red

to yellow gradually. After stirred it for 2 hours, pull off the solvent to obtain an orange

residue. Via chromatography on silica gel with 20% MeOH/Dichloromethane, 35.4 mg

(yield = 88%) of **61** was gained as an air stable orange crystalline solid after

recrystallization from acetone/hexane; mp 177-178°C; IR (CH$_2$Cl$_2$) 3639, 3561, 3117,

2956, 2898 cm^{-1}, ^{1}H NMR (CDCl$_3$, 400 MHz) δ 0.44 (s, 9H), 2.29 (s, 3H), 5.87 (s, 1H),

5.96 (s, 5H), 6.14 (s, 1H), 7.55-8.0 (m, 5H); ^{13}C{^{1}H} NMR (CDCl$_3$, 125 MHz) δ 0.6, 13.8,

87.7, 88.5, 93.1, 94.4, 109.6, 109.8, 128.2, 130.3, 135.3, 139.0. HRMS for

[C$_{20}$H$_{24}$CoO$_2$SSi]$^+$: 415.0593 (Theo. Mass), 415.0591 (Mass Measured), Delta (-0.5

ppm). Elemental Analysis: C% (47.82); H% (4.82). Found: C% (47.56); H% (4.81).

Ar = p-C$_6$H$_4$NMe$_2$

62
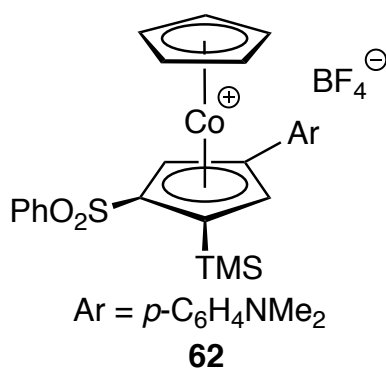
Preparation of $(\eta^5\text{-}C_5H_5)Co[\eta^5\text{-}C(TMS)C(SO_2Ph)CHC(p\text{-}C_6H_4NMe_2)CH]BF_4$ (62): 100.3 mg (0.182 mmol) of complex **54** were dissolved in 30 mL diethyl ether and bubbled with argon for 10 minutes in a round bottom flask. Then added 0.25 mL (1.68 mmol) of $HBF_4 \cdot Et_2O$ into the solution slowly while keeping it stirring. The color of the solution changed from red to clear gradually and some orange suspensions crashed out. After stirred it for 24 hours at room temperature, orange residue was obtained by pouring out the solvent. Via chromatography on silica gel with 15% Acetone/DCM, 92.4 mg (yield = 83.4%) of **62** was gained as an air stable purple crystalline solid after recrystallization from slow evaporation of methyl-ethyl ketone; mp 298°C; IR (CDCl$_3$) 3639, 3097, 2953, 2898, 2859, 1601, 1463, 1443, 1371, 1327, 1202, 1055, 841, 724, 685 cm^{-1}, ^{1}H NMR (CDCl$_3$, 500 MHz) δ 0.47 (s, 9H), 3.06 (s, 6H), 5.70 (s, 5H), 6.35 (s, 1H), 6.47 (s, 1H), 6.73 (d, 2H, J = 9.2 Hz), 7.71 (m, 5H), 7.96 (d, 2H, J = 7.6 Hz); ^{13}C{^{1}H} NMR (CDCl$_3$, 125 MHz) δ 0.4, 40.3, 79.9, 85.2, 87.6, 94.4, 108.5, 112.3, 112.9, 113.4, 127.9, 129.9, 130.0, 134.9, 139.2, 152.8. HRMS for $[C_{27}H_{31}CoNO_2SSi]^+$: 520.1171 (Theo. Mass), 520.1165 (Mass Measured), Delta (-1.2 ppm). Elemental Analysis: C% (53.39); H% (5.14). Found: C% (53.57); H% (5.54).

Ar = p-C$_6$H$_4$CMe$_3$

63

Preparation of (η^5-C$_5$H$_5$)Co[η^5-C(TMS)C(SO$_2$Ph)CHC(*p*-C$_6$H$_4$CMe$_3$)CH]BF$_4$ (63):

1164.7 mg (0.2919 mmol) of **55** were dissolved in 30 mL diethyl ether and bubbled with argon for 10 minutes in a round bottom flask. Then added 0.129 mL (0.8757 mmol) of HBF$_4$·Et$_2$O into the solution slowly while keeping it stirring. The color of the solution changed from red to clear gradually and some yellow suspensions crashed out. After stirred it for 24 hours, yellow residue was obtained by filtering the solvent. By washing the yellow residue with hexane couple of times, 157.4 mg (yield = 86.9%) of **63** was gained as an air stable yellow crystalline solid after recrystallization from acetonitrile/hexane; mp 263°C; IR (CH$_2$Cl$_2$) 3109, 3085, 2961, 2907, 2868, 1609, 1461, 1415, 1147 cm^{-1}, ^{1}H NMR (CD$_3$CN, 500 MHz) δ 0.45 (s, 9H), 1.37 (s, 9H), 5.72 (s, 5H), 6.19 (s, 1H), 6.81 (s, 1H), 7.5-8.1 (m, 9H); ^{13}C{^{1}H} NMR (CD$_3$CN, 125 MHz) δ 0.0, 31.1, 35.6, 85.3, 88.6, 88.9, 95.0, 109.4, 110.2, 125.8, 127.4, 128.8, 129.0, 130.9, 136.0, 139.8, 156.1. HRMS for [C$_{29}$H$_{34}$CoO$_2$SSi]$^+$: 533.1375 (Theo. Mass), 533.1377 (Mass Measured), Delta (0.4 ppm). Elemental Analysis: C% (56.14); H% (5.52). Found: C% (52.64); H% (5.25).

64
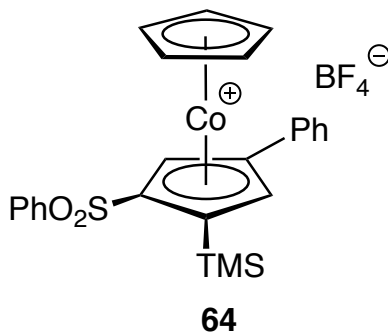
Preparation of (η^5-C$_5$H$_5$)Co[η^5-C(TMS)C(SO$_2$Ph)CHC(Ph)CH]BF$_4$ (64): 349.2 mg

(0.6866 mmol) of **56** were dissolved in 100 mL diethyl ether and bubbled with argon for

10 minutes in a round bottom flask. Then added 0.303 mL (2.06 mmol) of HBF$_4$·Et$_2$O

into the solution slowly while keeping it stirring. The color of the solution changed from

red to clear gradually and some yellow suspensions crashed out. After stirred it for 24

hours, yellow residue was obtained by filtering the solvent. By washing the yellow

residue with hexane couple of times, 326.1 mg (yield = 84.2%) of **64** was gained as an

air stable yellow crystalline solid after recrystallization from acetonitrile/hexane; mp

243°C; IR (CH$_2$Cl$_2$) 3131, 3109, 3098, 2895, 1453, 1330, 1168 cm^{-1}, ^{1}H NMR (CD$_3$CN,

400 MHz) δ 0.45 (s, 9H), 5.73 (s, 5H), 6.21 (s, 1H), 6.83 (s, 1H), 7.5-8.1 (m, 10H);

^{13}C{^{1}H} NMR (CD$_3$CN, 125 MHz) δ 0.1, 85.8, 88.8, 89.3, 95.3, 105.9, 109.1, 110.5,

128.9, 129.2, 130.5, 131.0, 132.4, 136.1, 139.9. HRMS for [C$_{25}$H$_{26}$CoO$_2$SSi]$^+$: 447.0749

(Theo. Mass), 447.0747 (Mass Measured), Delta (-0.4 ppm). Elemental Analysis: C%

(53.21); H% (4.64). Found: C% (53.06); H% (4.68).
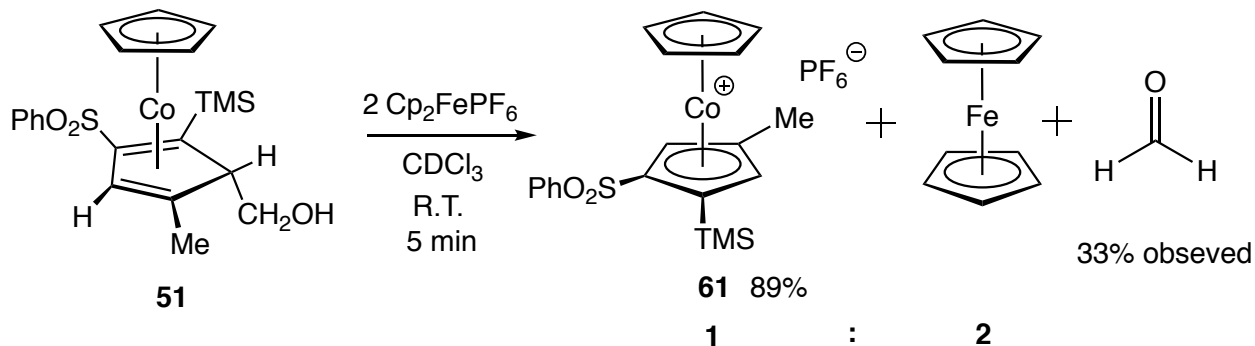
NMR tube reaction of 51 with ferrocenium hexaflourophosphate to produce 61 with formaldehyde: 4.1 mg (0.009 mmol) of **51** and 9.0 mg (0.027 mmol) of ferrocenium hexaflourophosphate were added into a Teflon top NMR tube. Around 1.2 ml of CDCl$_3$ was distilled into the NMR tube on the Schlenk line and argon gas was used to fill the rest empty space of the tube. After shaking the tube on Vortex Mixer for 5 minutes, most of the ferrocenium hexaflourophosphate disappeared and the solution turned to yellow. TMS and Cp peak of the starting material were completely consumed and a new TMS and Cp peak of complex **61** appeared at 0.437 ppm and 5.908 ppm, respectively. The ferrocene which comes from the reduced ferrocenium hexaflourophosphate appeared at 4.160. The ratio of ferrocene and new Cp is integrated as 2.00 and NMR yield is 88.7%. Formaldehyde with a yield of 33% was also observed in the solution (9.74 ppm in ^{1}H NMR and 195 ppm in ^{13}C NMR).

74
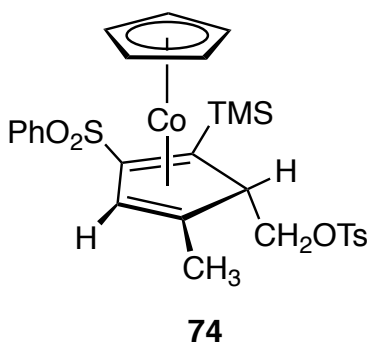
Preparation of (η^5-C$_5$H$_5$)Co[η^4-C(TMS)=C(SO$_2$Ph)CH=C(Me)CH(CH$_2$OTs)] (74): 221.7 mg (0.4965 mmol) of complex **51**, 0.7571 g (3.971 mmol) of tosyl chloride and 0.4852 g (3.972 mmol) of 4-Dimethylaminopyridine were added into a round bottom flask with

10mL dry chloroform. The flask was purged with argon and stirred for overnight at room temperature. Via chromatography on silica gel with 25% EtOAc/hexane, 229.5 mg (yield = 77.03%) of **74** was obtained as an air stable black crystalline solid after recrystallization from chloroform/hexane at -15°C. mp 154-155 °C; IR (CDCl$_3$) 3066, 2946, 2892, 1597, 1446, 1357, 1295, 1245, 1171, 1093 cm^{-1}; ^{1}H NMR (CDCl$_3$, 400 MHz) δ 0.05 (s, 9H), 1.21 (s, 3H), 2.43 (s, 3H), 2.54 (dd, 1H, J = 6.8 Hz, 9.6 Hz), 2.86 (dd, 1H, J = 4.8 Hz, 9.6 Hz), 2.95 (dd, 1H, J = 2 Hz, 6.4 Hz), 4.87 (s, 5H), 5.43 (s, 1H), 7.1-8.1 (m, 9H); ^{13}C{^{1}H} NMR (CDCl$_3$, 125 MHz) δ 1.0, 18.3, 21.8, 38.5, 59.2, 60.1, 71.6, 81.1, 82.3, 102.1, 127.3, 127.9, 129.3, 129.9, 132.7, 133.0, 142.6, 144.9. HRMS for [C$_{28}$H$_{33}$CoO$_5$S$_2$SiNa]$^+$: 623.0763 (Theo. Mass), 623.0761 (Mass Measured), Delta (-0.3 ppm).

75
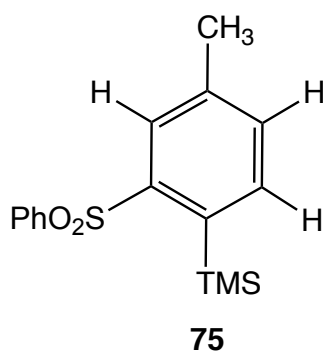
Preparation of trimethyl(4-methyl-2-(phenylsulfonyl)phenyl)silane (75): 229.5 mg (0.3824 mmol) of complex **74** were added into a reaction tube with 10mL dry chloroform. The tube was purged with argon and heat at 75°C in oil bath for 24 hours.

After filtering out the solid and using the rest soluble materials doing chromatography on silica gel with 10% EtOAc/hexane, 82 mg (yield = 70.04%) of **75** was obtained as an air stable pale yellow oil. IR (CDCl$_3$) 3065, 2951, 2898, 2360, 2337, 1596, 1446, 1304, 1260, 1244, 1155, 1138, 1107, 1082, 1038, 841, 755 cm^{-1}; ^{1}H NMR (CDCl$_3$, 400 MHz) δ 0.41 (s, 9H), 2.34 (s, 3H), 7.34 (dm, 1H, ^{HH}J = 7.6 Hz), 7.49 (m, 2H), 7.56 (m, 1H), 7.61 (m, 1H), 7.68 (d, 1H, J = 7.6 Hz), 7.81 (m, 2H); ^{13}C{^{1}H} NMR (CDCl$_3$, 125 MHz) δ 1.6, 21.2 127.3 129.1, 131.0, 132.9, 133.1, 136.8, 137.2, 140.0, 142.7, 145.4. HRMS for [C$_{16}$H$_{20}$O$_2$SSiNa]$^+$: 327.0845 (Theo. Mass), 327.0846 (Mass Measured), Delta (0.3 ppm).

82
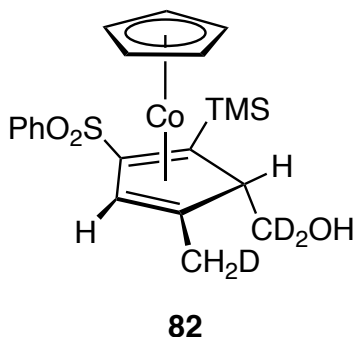
Preparation of (η^5-C$_5$H$_5$)Co[η^4-C(TMS)=C(SO$_2$Ph)CH=C(CH$_2$D)CH(CD$_2$OH)] (82): 428 mg (0.803 mmol) of (η^5-C$_5$H$_5$)Co[η^4-C(TMS)=C(SO$_2$Ph)CH=C(CH$_2$OCH$_3$)CH(CO$_2$Et)] (**52**-*exo*) were dissolved in dry toluene and bubbled with argon for 10 minutes. Then added 13.8 mL (9.66 mmol, 0.7 M in toluene, 98 atom %D) of DIBAL-D under -78° while keep it stirring. Some foaming in the red solution was observed during the addition. The reaction was stirred at -78°C for 2 hours, then at 0˚C for four hours. Then quenched it

with 5 mL MeOH and extracted three times with a saturated sodium potassium tartrate solution (30 mL each time). The organic layer was dried with magnesium sulfate. After chromatography on silica gel with 30% EtOAc/hexane, 256.0 mg (yield = 68.6%) of **82** was obtained as an air stable black crystalline solid via recrystallization from toluene/hexane; IR (CH$_2$Cl$_2$) 3523, 3089, 3070, 2950, 2896, 2249, 2180, 2093, 1440 cm^{-1}, ^{1}H NMR (CDCl$_3$, 400 MHz) δ 0.16 (s, 9H), 0.32 (s, 1H), 1.26 (t, 2H, J =2.0 Hz), 2.87 (s, 1H), 4.87 (s, 5H), 5.44 (s, 1H), 7.5-8.1 (m, 5H); ^{13}C{^{1}H} NMR (CDCl$_3$, 125 MHz) δ 1.5, 17.8 (t, J = 77.5 Hz), 39.1, 61.0, 65.2 (m), 81.1, 82.1, 102.3, 127.5, 129.3, 133.1, 142.8. By comparing with unlabeled sample (**51**), the deuteration analysis shows that D3 = 97.7%, D2 = 2.3% and D1 and D0 are essentially 0%. HRMS for [C$_{21}$H$_{24}$D$_3$CoO$_3$SSi]$^+$ (MH$^+$): 450.1043 (Theo. Mass), 450.1040 (Mass Measured), Delta (0.7 ppm).

83
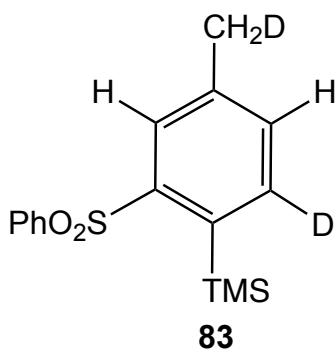
Preparation of trimethyl(4-methyl-2-(phenylsulfonyl)phenyl)silane-d_2 (83): 150 mg (0.323 mmol) of complex **82**, 93 mg (0.488 mmol) of tolyl chloride and 60 mg (0.491 mmol) of 4-Dimethylaminopyridine were added into a reaction tube with 6 mL dry chloroform. The flask was purged with argon and stirred for 12 hours at room

temperature. Then heat the reaction tube in oil bath at 75 °C for 24 hours. Via chromatography on silica gel with 10% EtOAc/hexane, 60 mg (yield = 60.6%) of **83** was obtained as an air stable pale-yellow oil. IR (CDCl$_3$) 3067, 2948, 2895, 2356, 2331, 1594, 1479, 1446, 1302, 1241 cm^{-1}; ^{1}H NMR (CDCl$_3$, 400 MHz) δ 0.41 (s, 9H), 2.33 (m, 2H), 7.34 (s, 1H), 7.49 (m, 2H), 7.56 (m, 1H), 7.61 (m, 1H), 7.81 (m, 2H); ^{13}C{^{1}H} NMR (CDCl$_3$, 125 MHz) δ 1.6, 21.1 (m), 127.2, 129.1, 131.0, 132.9, 133.0, 136.5 (t, J = 98.5 Hz), 137.1, 140.0, 142.6, 145.4. By comparing with unlabeled sample (**75**), the Deuteration analysis shows that D2 = 84.6%, D1 = 15.4% and D0 is essentially 0%. HRMS for [C$_{16}$H$_{18}$D$_2$O$_2$SSiNa]$^+$: 324.1417 (Theo. Mass), 324.1418 (Mass Measured), Delta (0.3 ppm).

G. Appendix
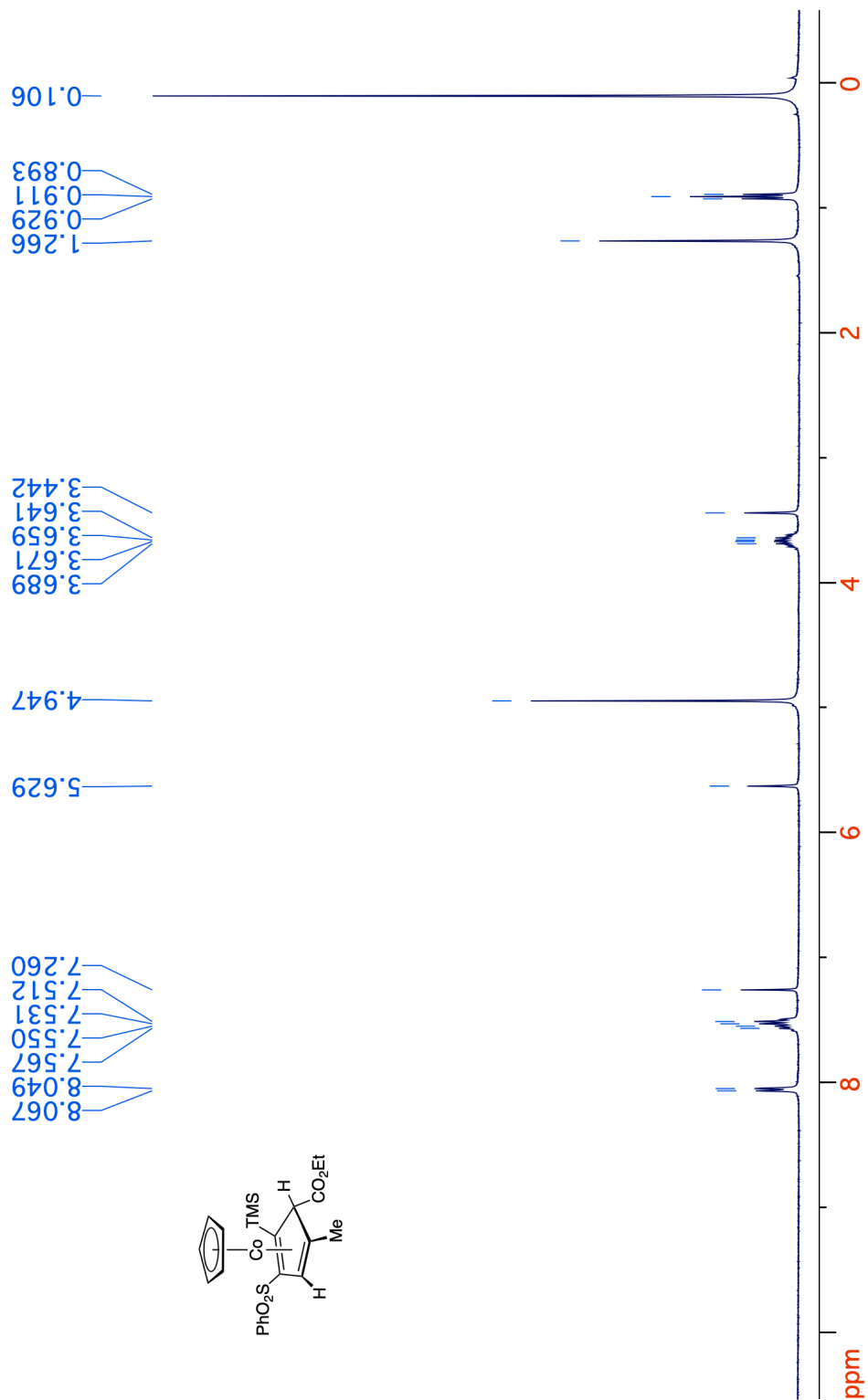
Figure 3-23. ^{1}H NMR spectrum (400 MHz, CDCl$_3$) of **4**-*exo.*
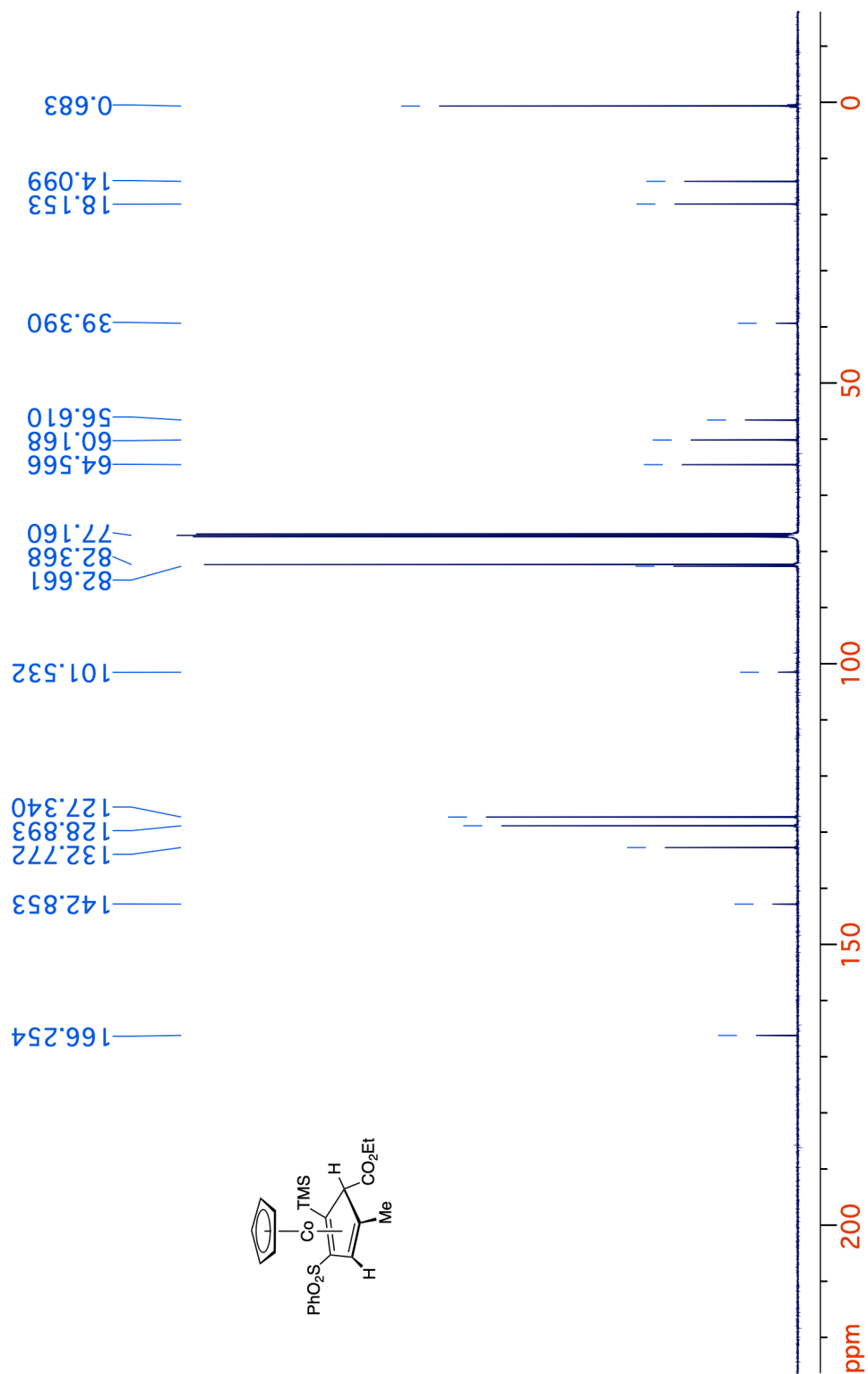
Figure 3-24. $^{13}C\{^1H\}$ NMR spectrum (125 MHz, CDCl$_3$) of **4**-*exo.*

Peak labels: 0.683, 14.099, 18.153, 39.390, 56.610, 60.168, 64.566, 77.160, 82.368, 82.661, 101.532, 127.340, 128.893, 132.772, 142.853, 166.254
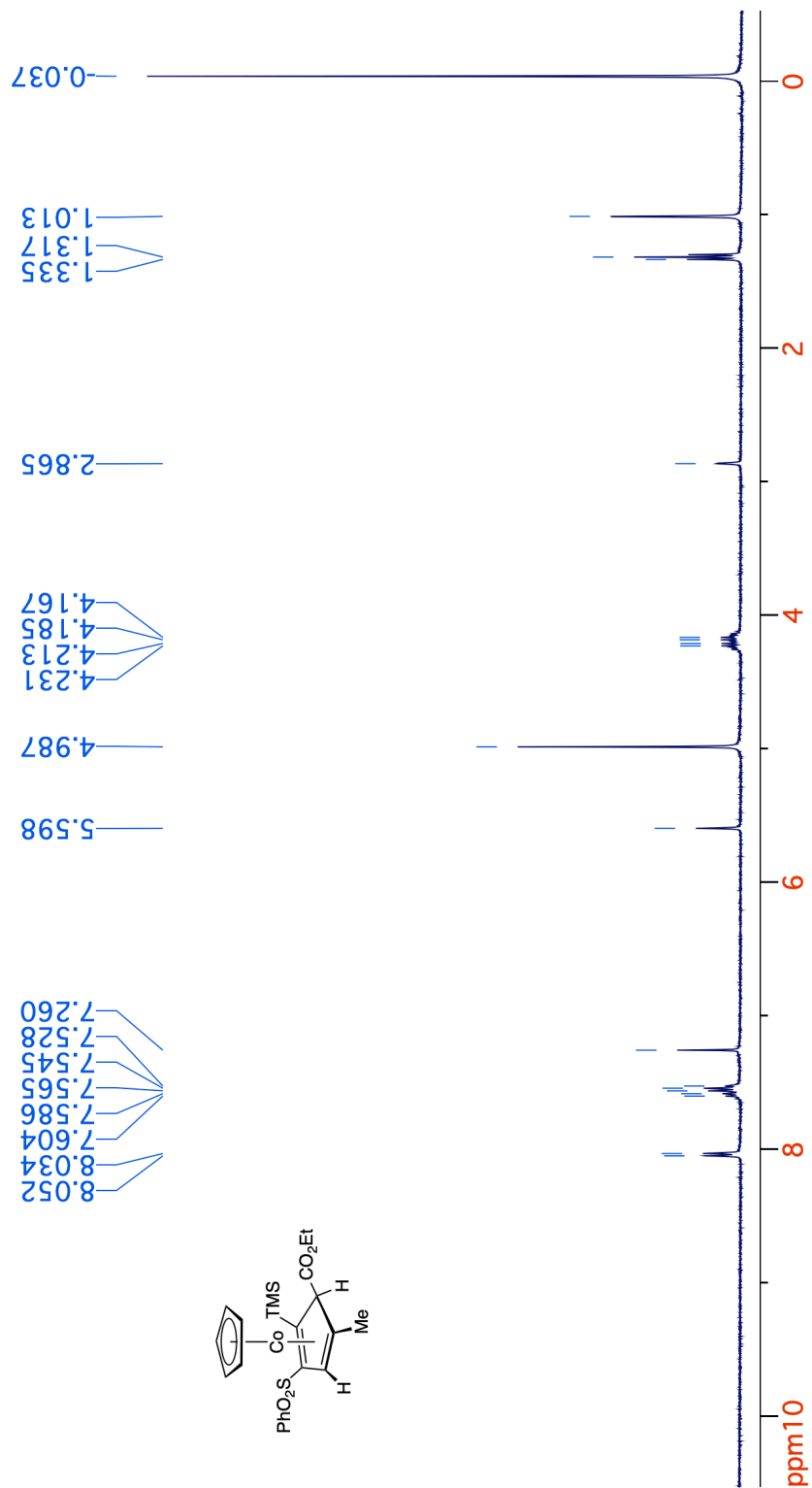
Figure 3-25. ^{1}H NMR spectrum (400 MHz, CDCl$_3$) of **4**-*endo.*
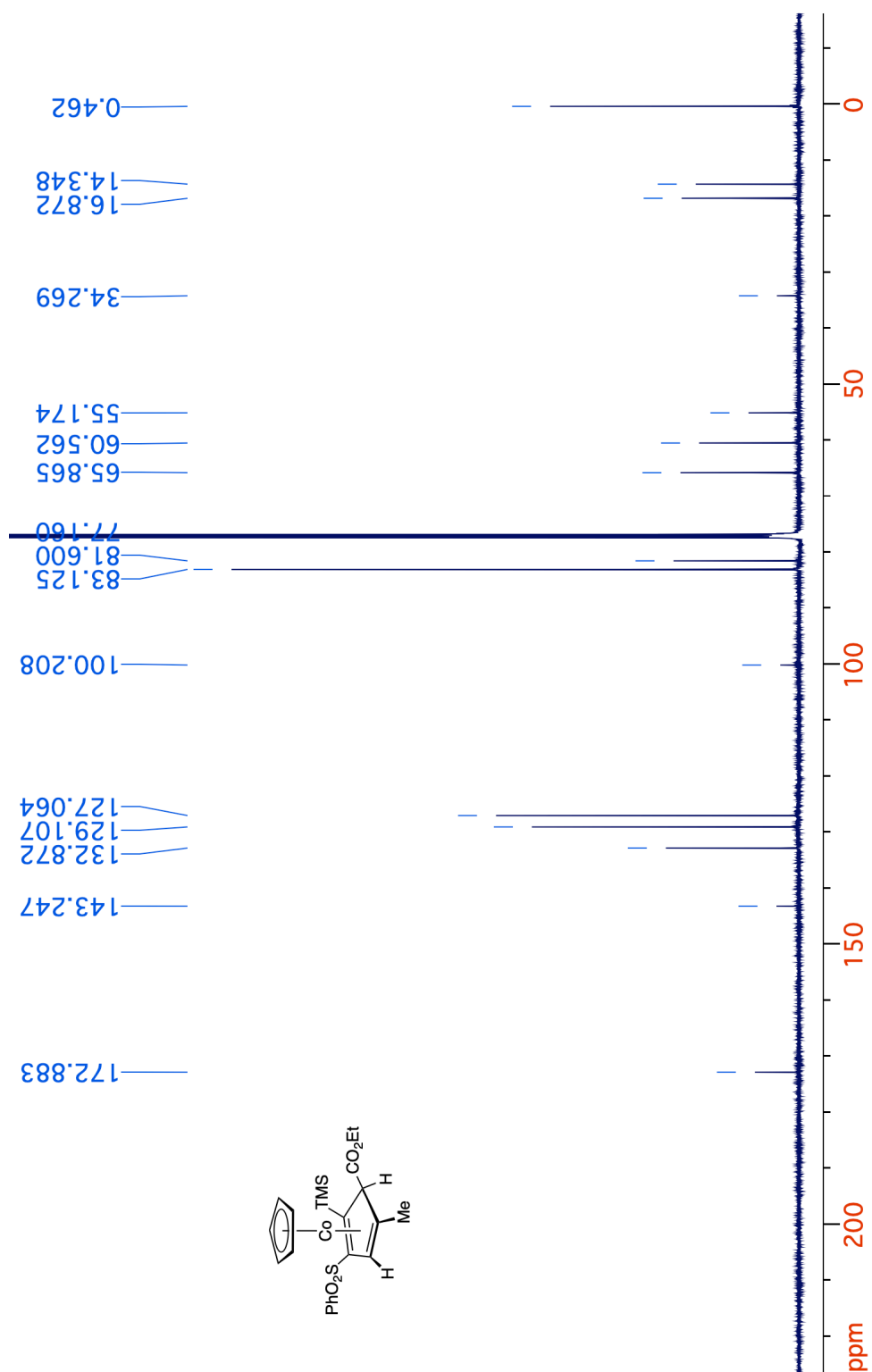
Figure 3-26. $^{13}C\{^1H\}$ NMR spectrum (125 MHz, CDCl$_3$) of **4**-*endo.*

Peaks labeled on spectrum:
0.462
14.348
16.872
34.269
55.174
60.562
65.865
77.160
81.600
83.125
100.208
127.064
129.107
132.872
143.247
172.883
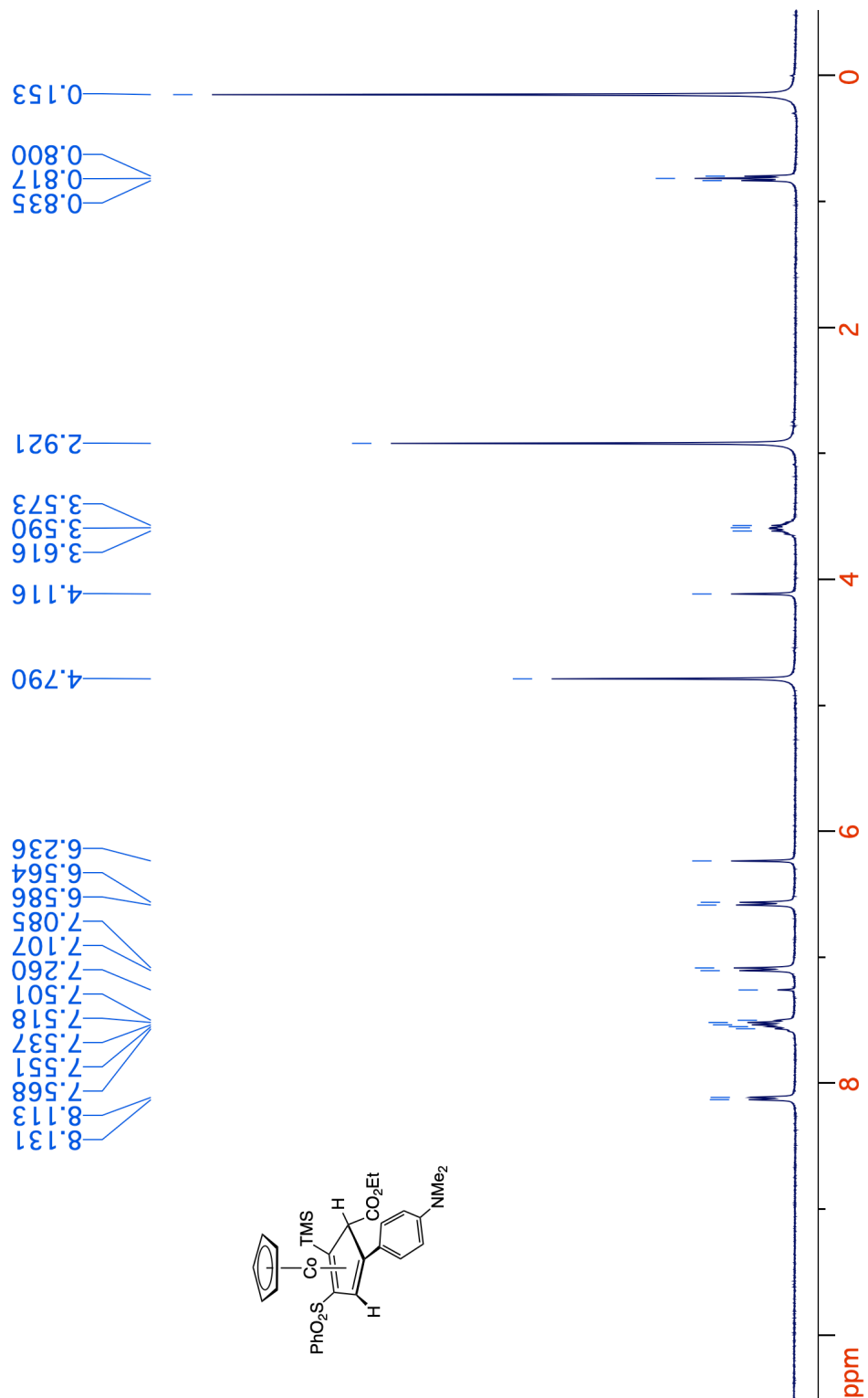
Figure 3-27. ^{1}H NMR spectrum (400 MHz, CDCl$_3$) of **5**-*exo*.

0.633
14.016
38.813
40.516
59.081
60.259
61.316
77.160
78.422
83.032
101.910
112.840
126.722
127.524
128.914
132.785
142.788
148.905
165.916
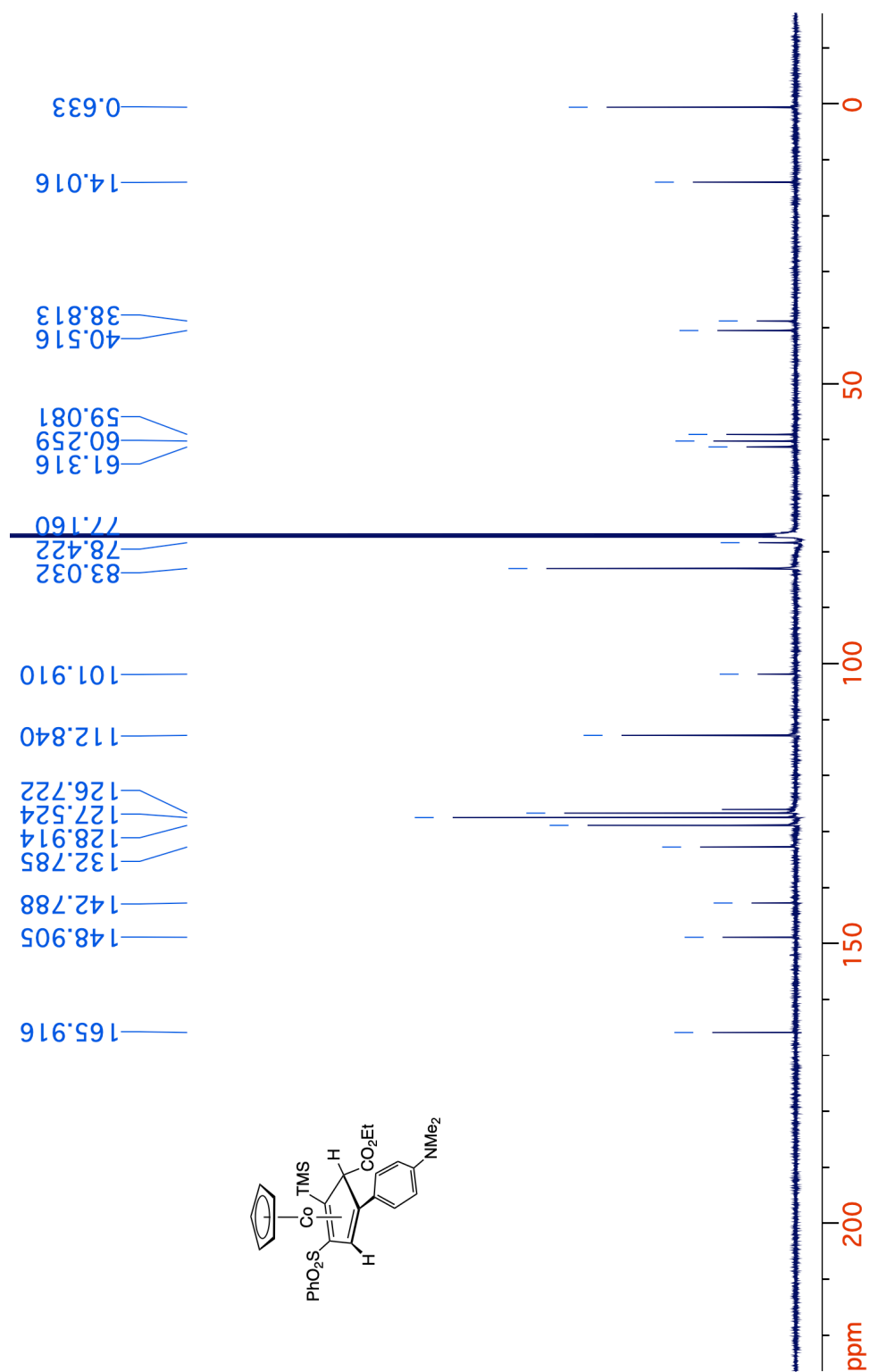
Figure 3-28. ^{13}C{^{1}H} NMR spectrum (125 MHz, CDCl$_3$) of **5**-*exo.*
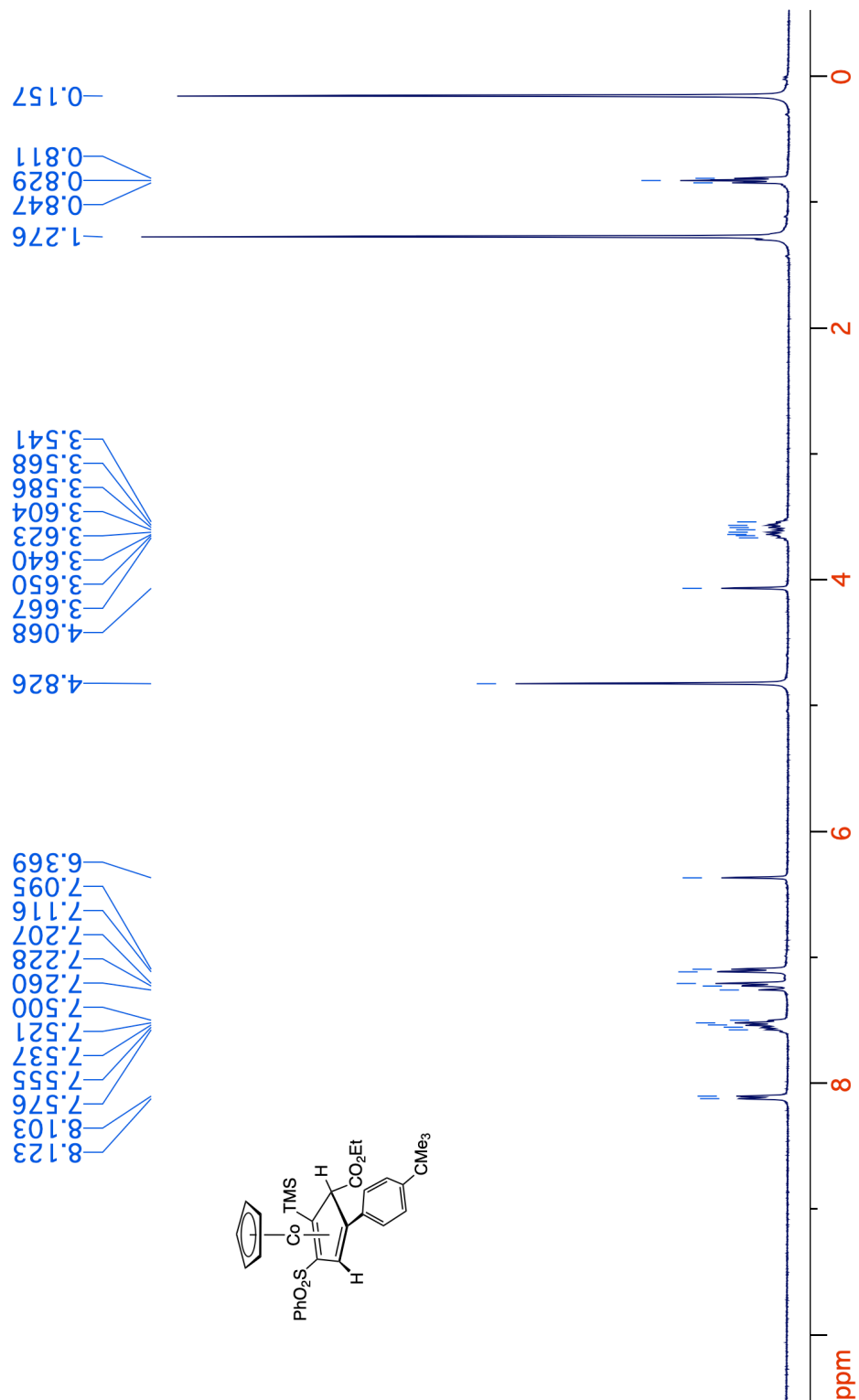
Figure 3-29. ^{1}H NMR spectrum (400 MHz, CDCl$_3$) of **6**-*exo.*
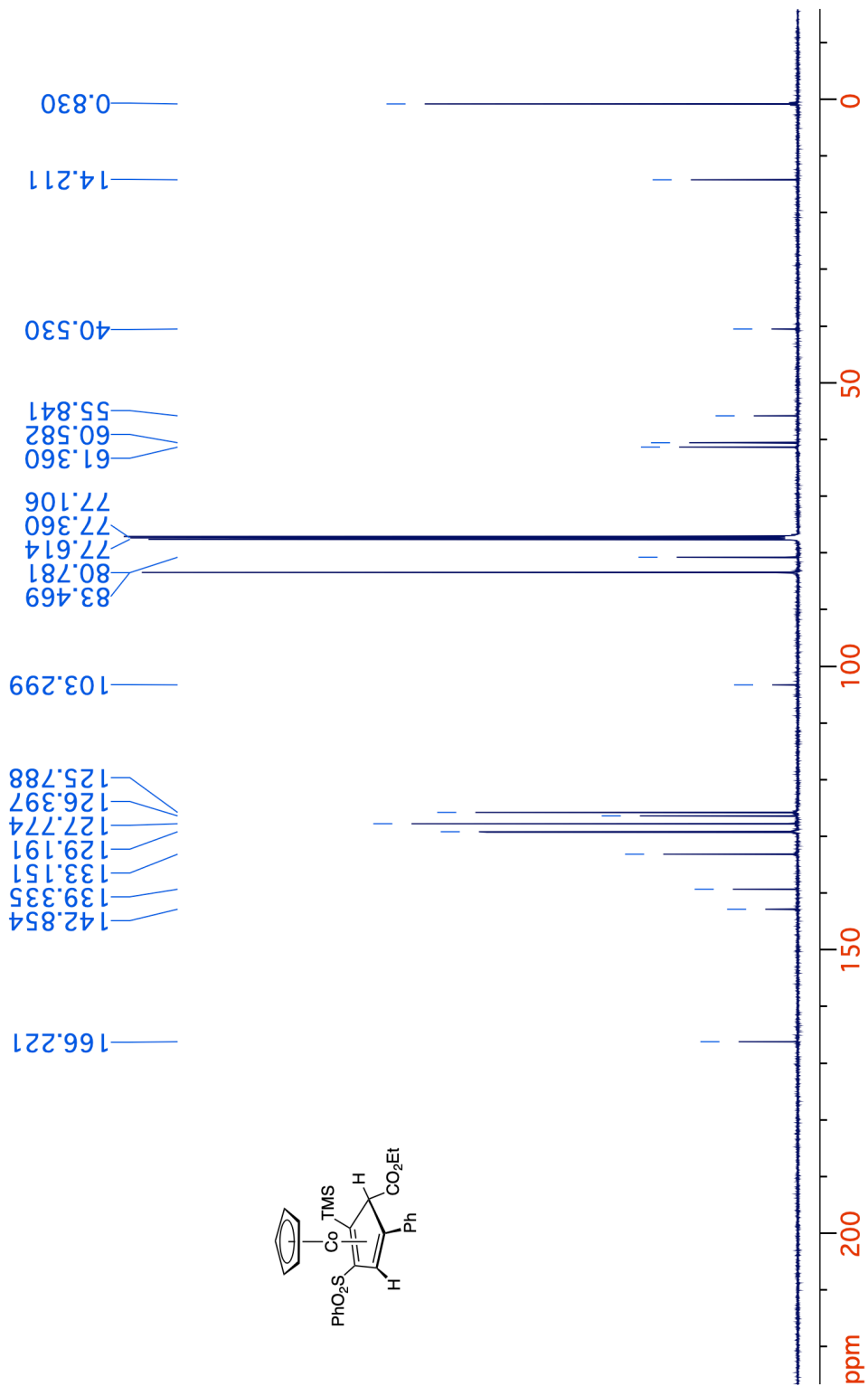
Figure 3-30. $^{13}C\{^1H\}$ NMR spectrum (125 MHz, CDCl$_3$) of **6**-*exo.*
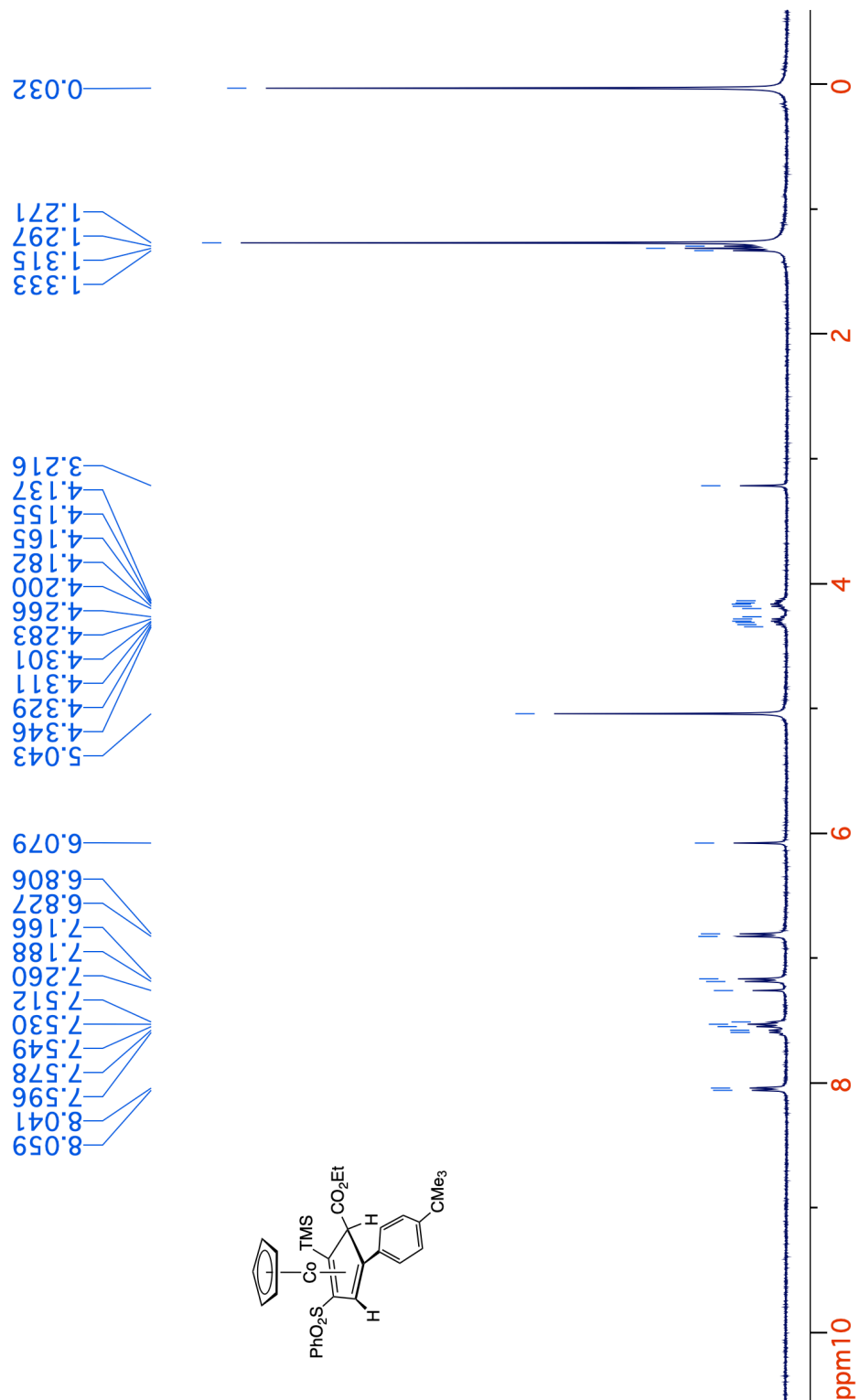
Figure 3-31. ^1H NMR spectrum (400 MHz, CDCl$_3$) of **6**-*endo.*
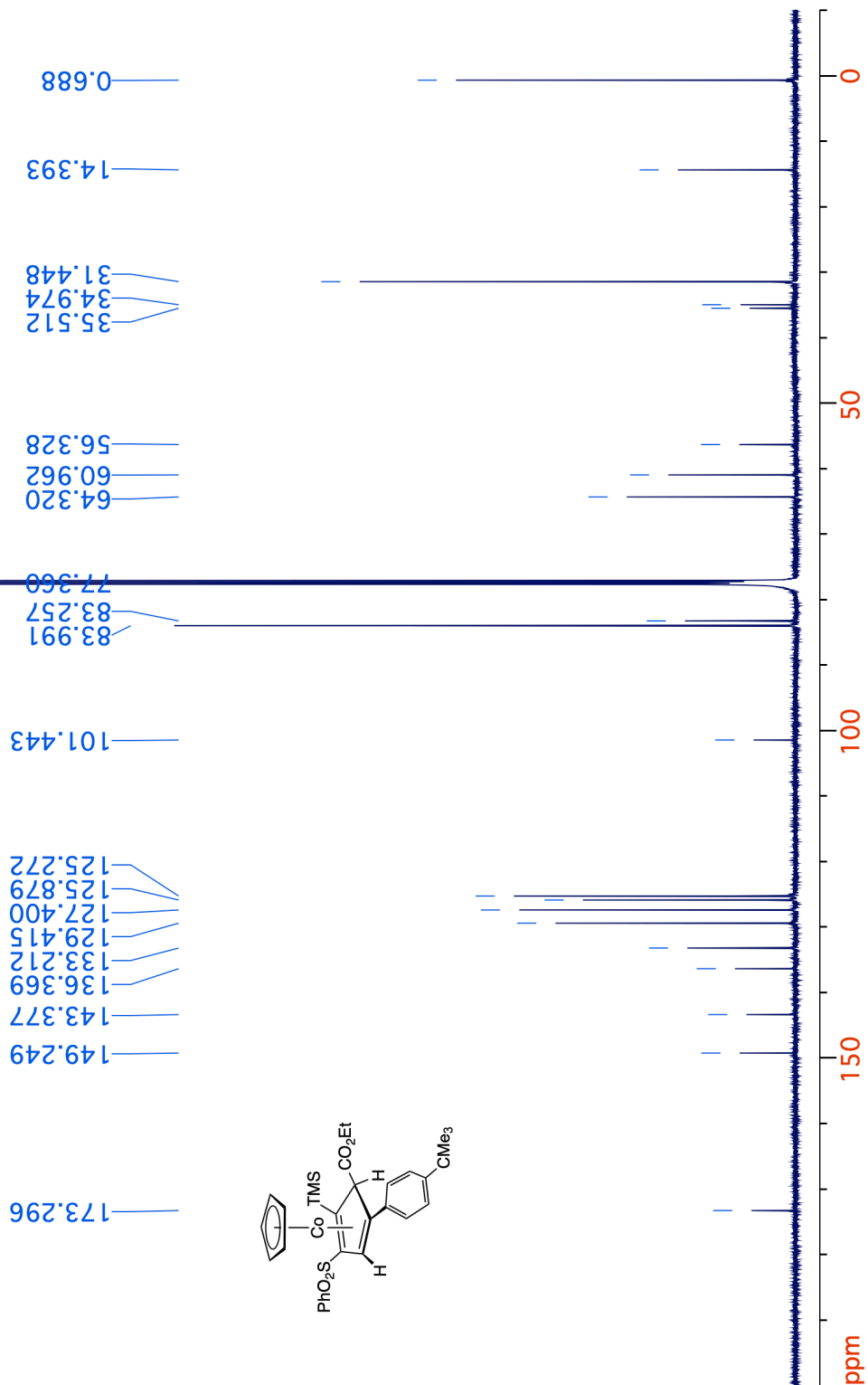
Figure 3-32. $^{13}C\{^1H\}$ NMR spectrum (125 MHz, CDCl$_3$) of **6**-*endo.*

340
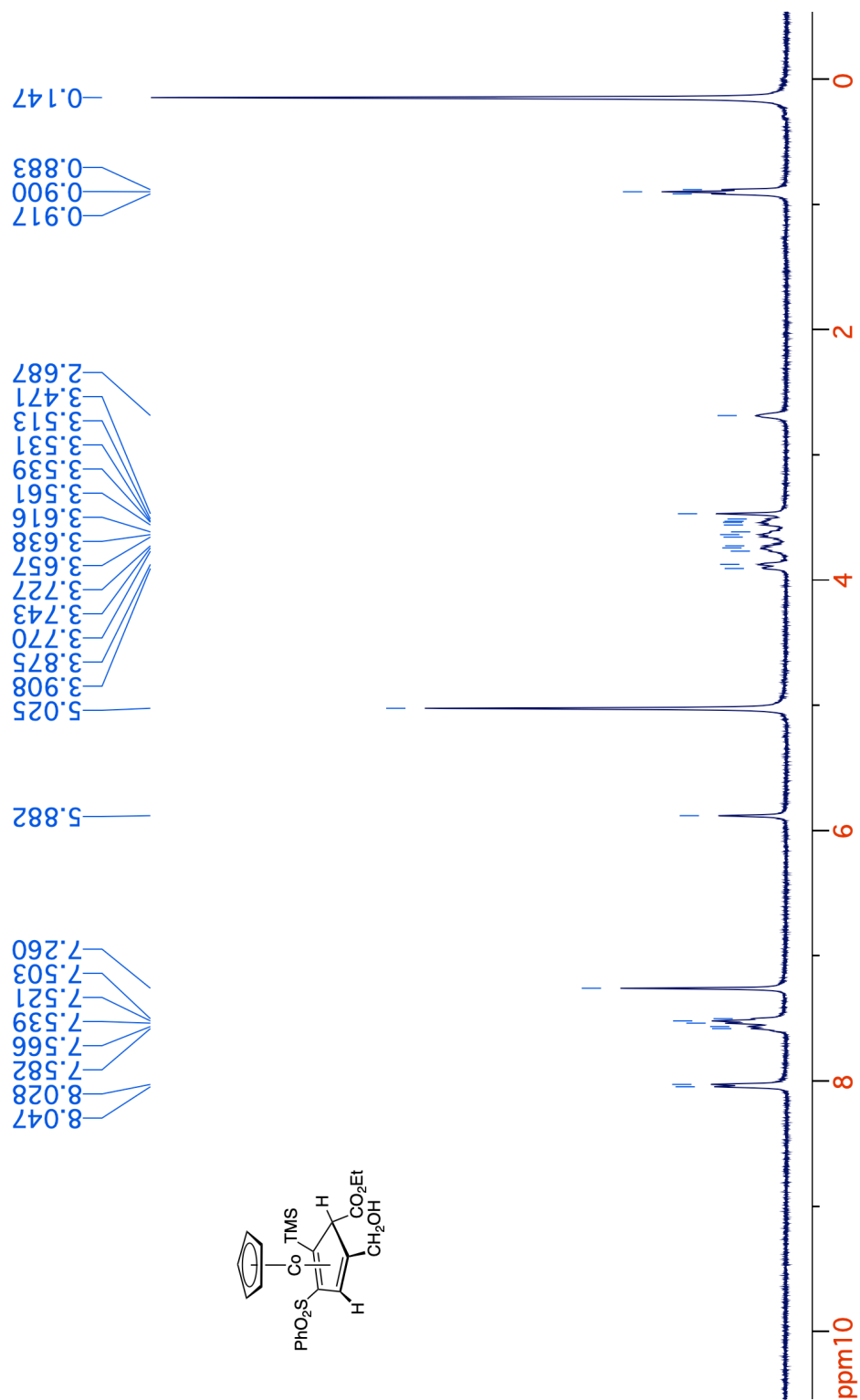
Figure 3-33. ^{1}H NMR spectrum (400 MHz, CDCl$_3$) of **7**-*exo.*
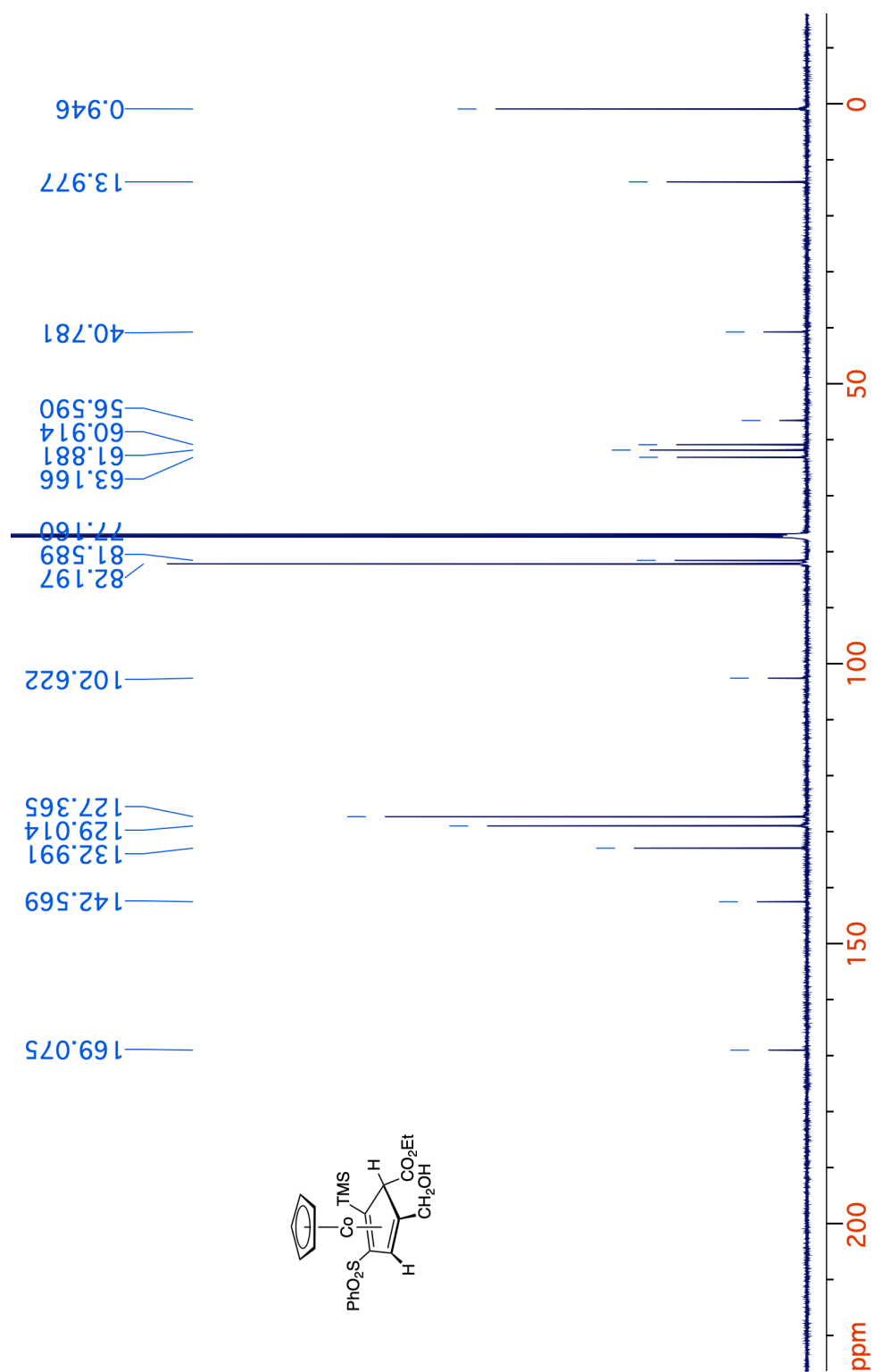
Figure 3-34. $^{13}C\{^1H\}$ NMR spectrum (125 MHz, CDCl$_3$) of **7**-*exo.*

Peaks (ppm):
0.163
0.817
0.834
0.852
3.592
3.610
3.620
3.638
4.082
4.814
6.416
7.199
7.260
7.516
7.534
7.552
7.569
7.586
8.118
8.135

Figure 3-35. ^{1}H NMR spectrum (400 MHz, CDCl$_3$) of **8**-*exo.*
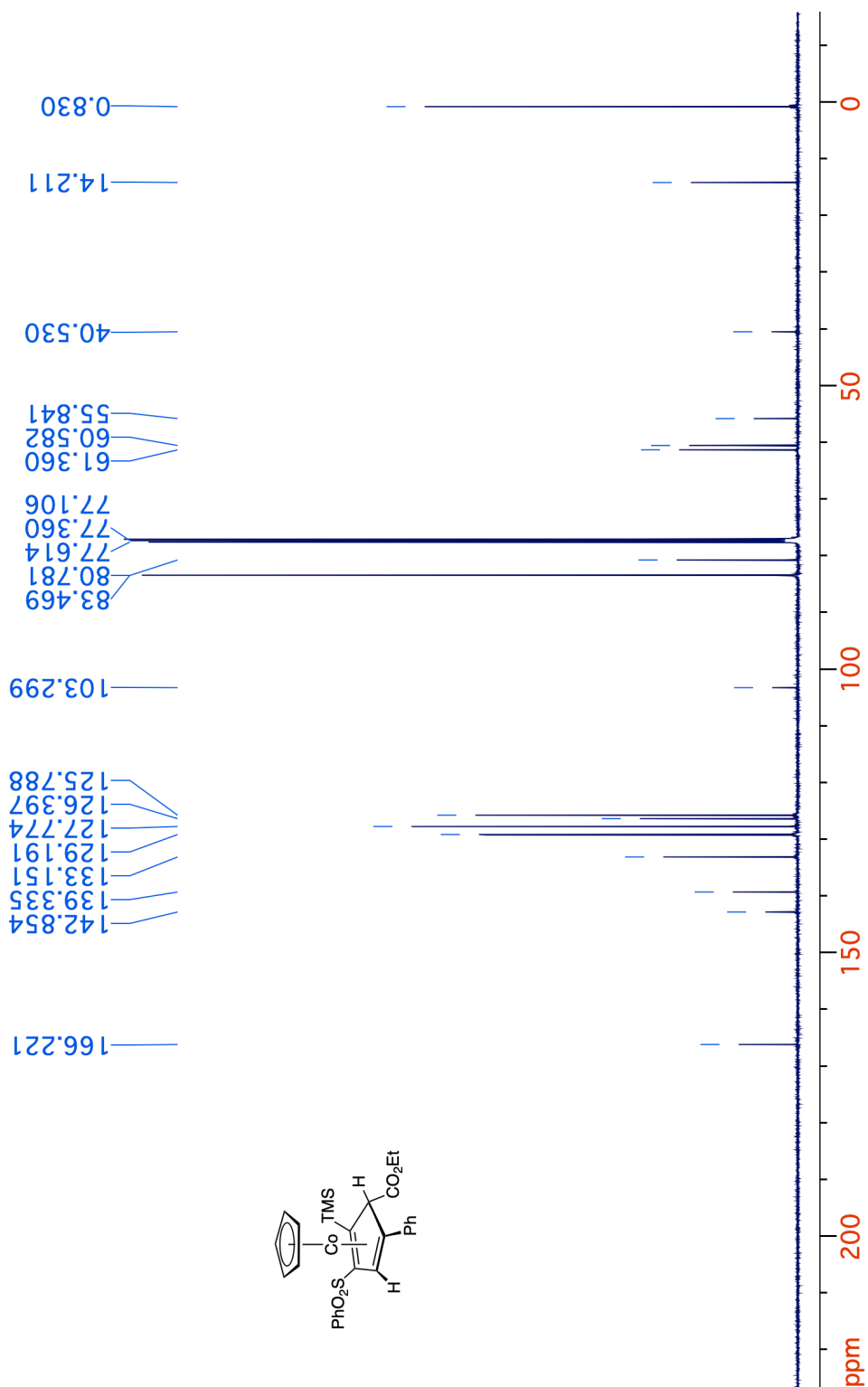
Figure 3-36. $^{13}C\{^1H\}$ NMR spectrum (125 MHz, CDCl$_3$) of **8**-*exo.*

0.830
14.211
40.530
55.841
60.582
61.360
77.106
77.360
77.614
80.781
83.469
103.299
125.788
126.397
127.774
129.191
133.151
139.335
142.854
166.221
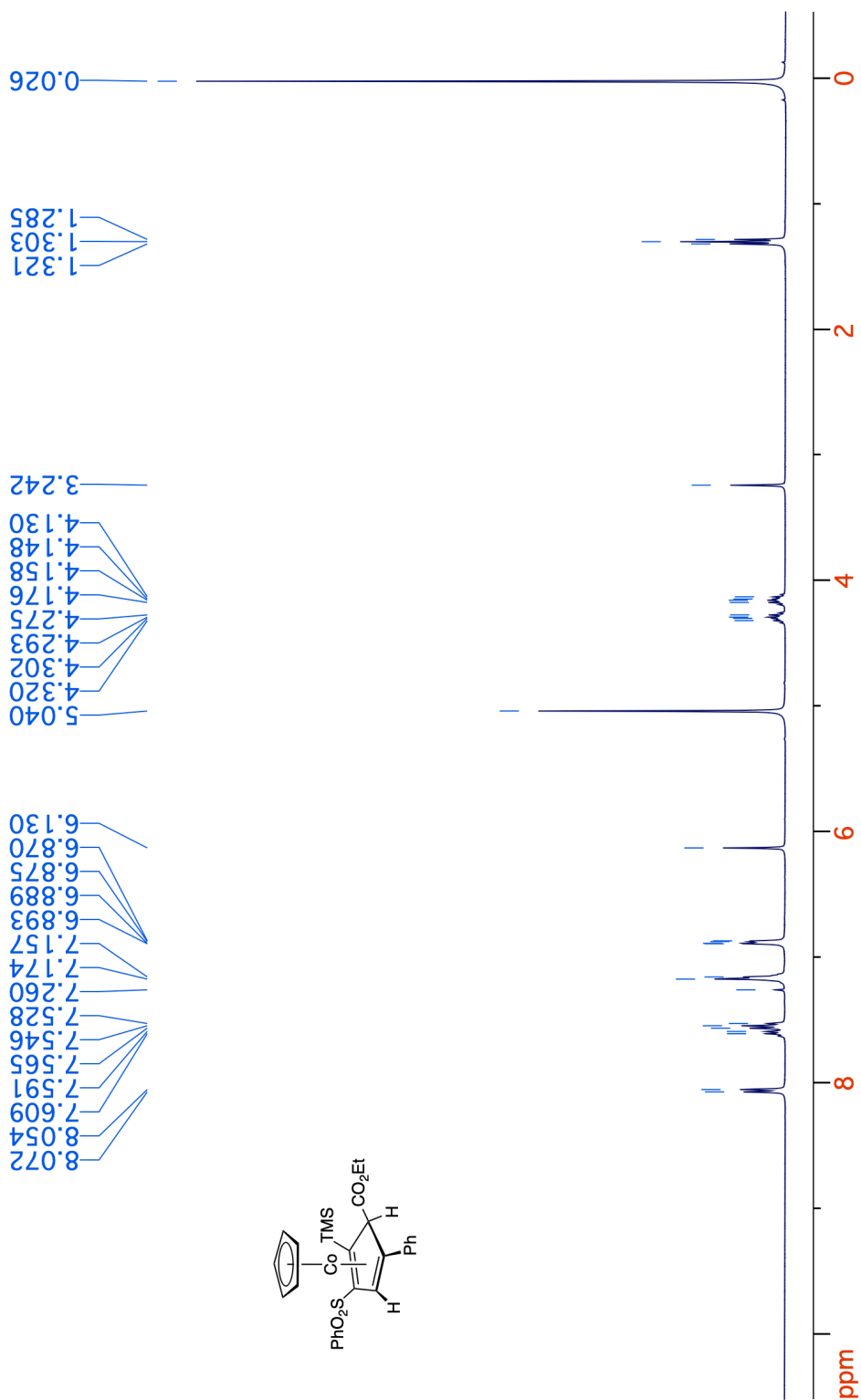
Figure 3-37. ^{1}H NMR spectrum (400 MHz, CDCl$_3$) of **8**-*endo.*
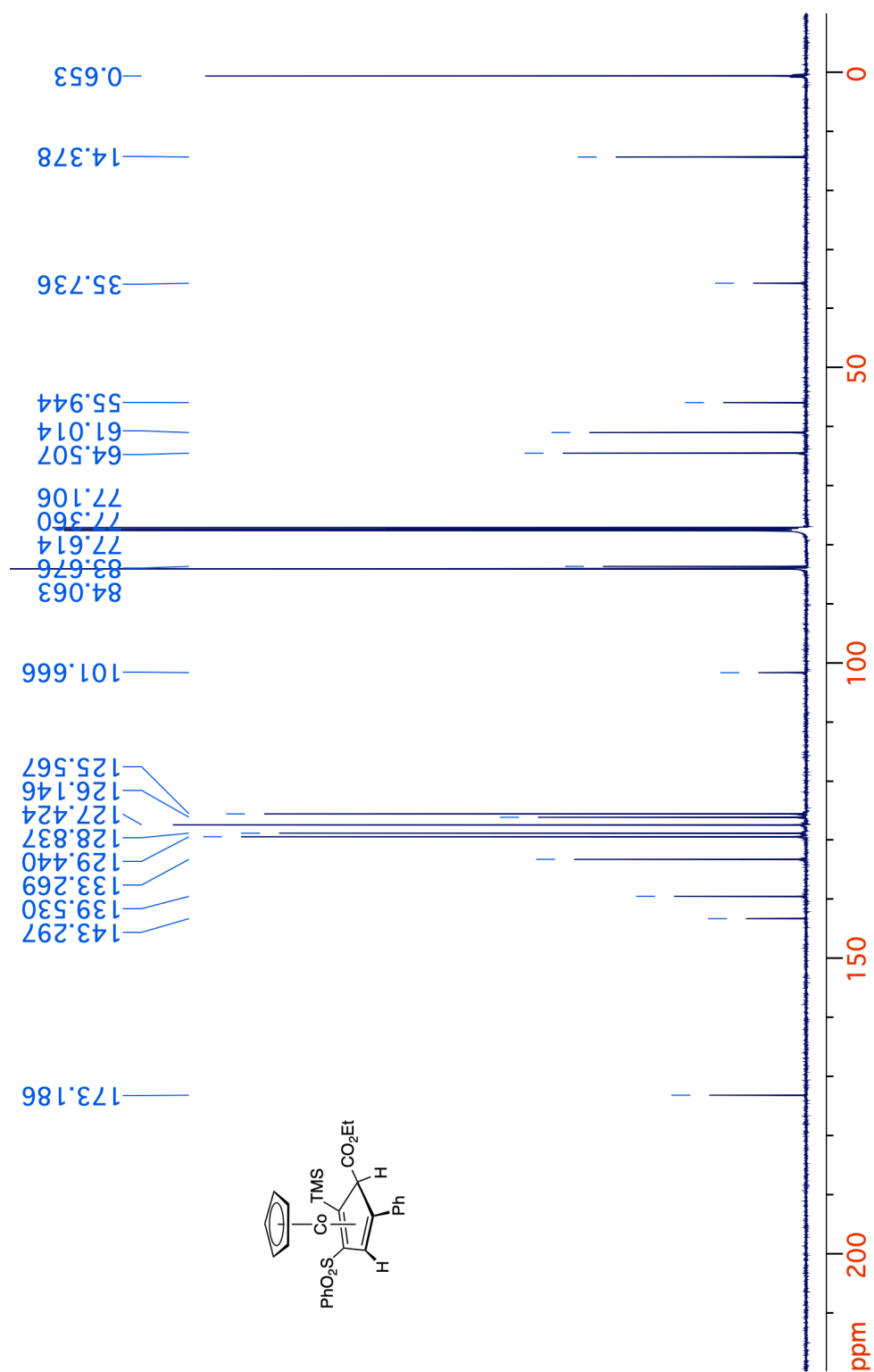
Figure 3-38. $^{13}C\{^1H\}$ NMR spectrum (125 MHz, CDCl$_3$) of **8**-*endo.*

Peaks labeled (ppm):
-0.653, 14.378, 35.736, 55.944, 61.014, 64.507, 77.106, 77.360, 77.614, 83.676, 84.063, 101.666, 125.567, 126.146, 127.424, 128.837, 129.440, 133.269, 139.530, 143.297, 173.186

Figure 3-39. ^{1}H NMR spectrum (400 MHz, CDCl$_3$) of **9**-*exo.*
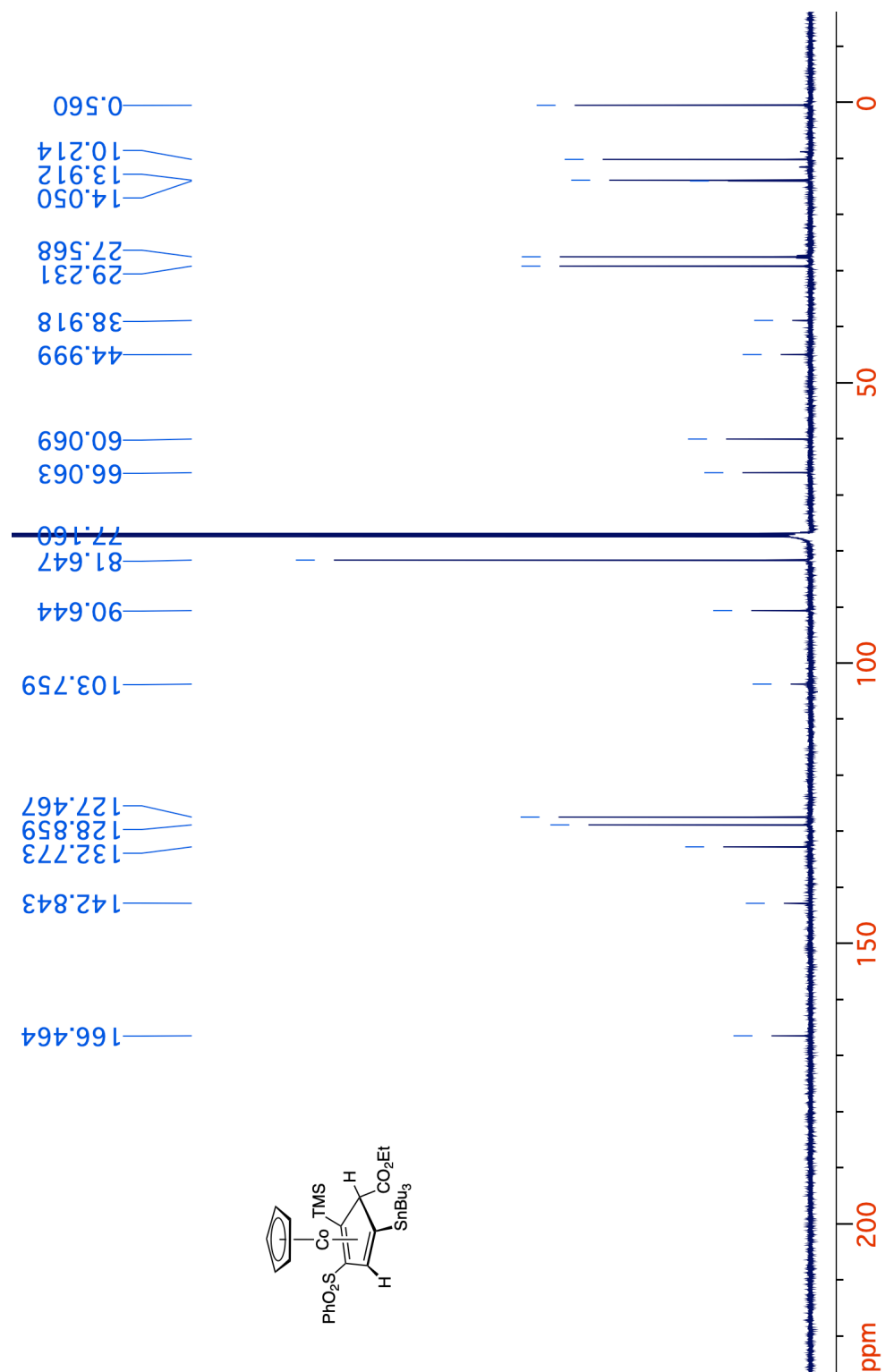
Figure 3-40. $^{13}C\{^{1}H\}$ NMR spectrum (125 MHz, CDCl$_3$) of **9**-*exo*.
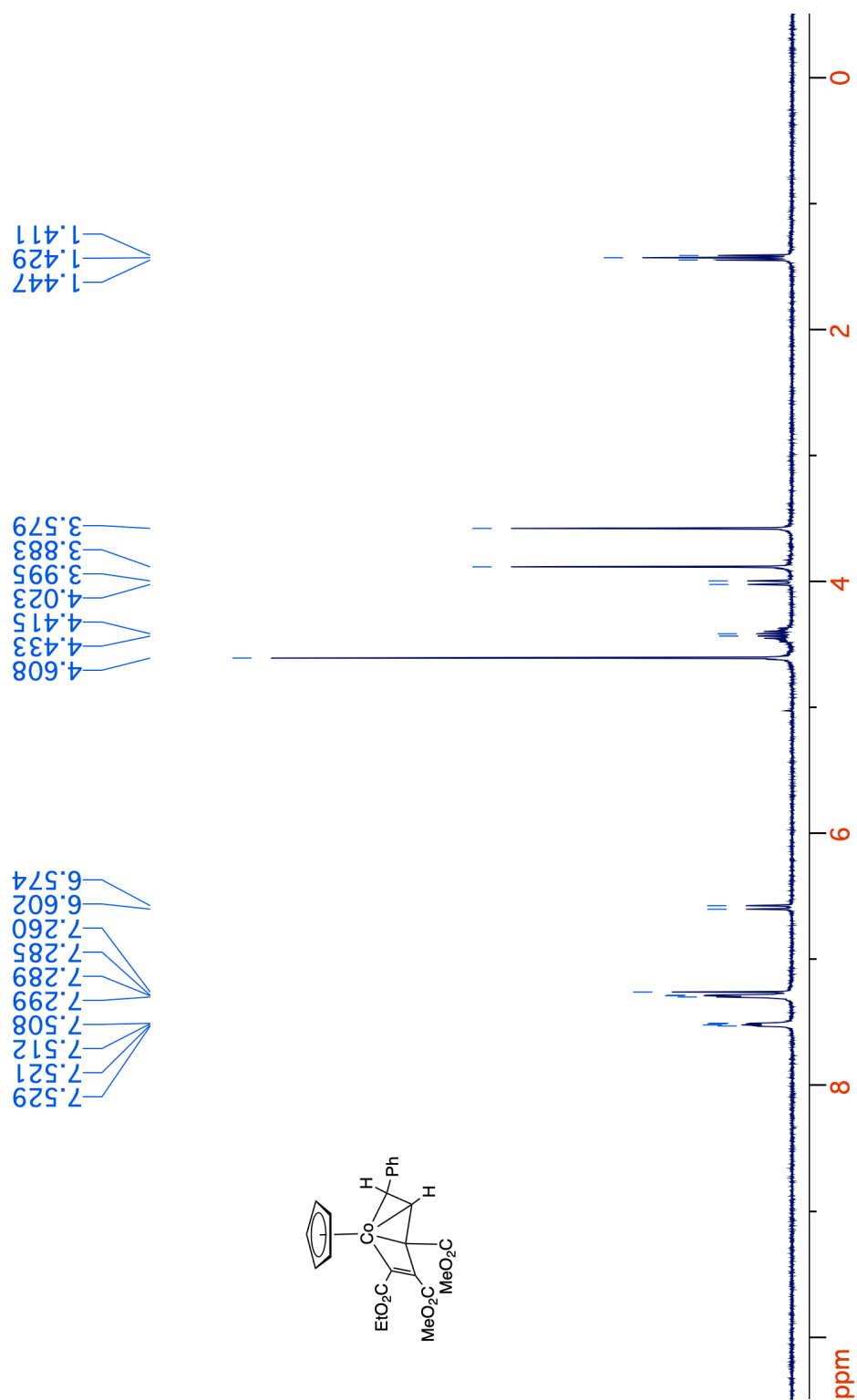
Figure 3-41. ^{1}H NMR spectrum (400 MHz, CDCl$_3$) of **16**.

349

14.910

47.540
51.402
52.794
60.967
65.791

77.160

86.483
91.304

118.383
127.112
127.131
129.408

142.130

156.292
160.644

173.535
173.862
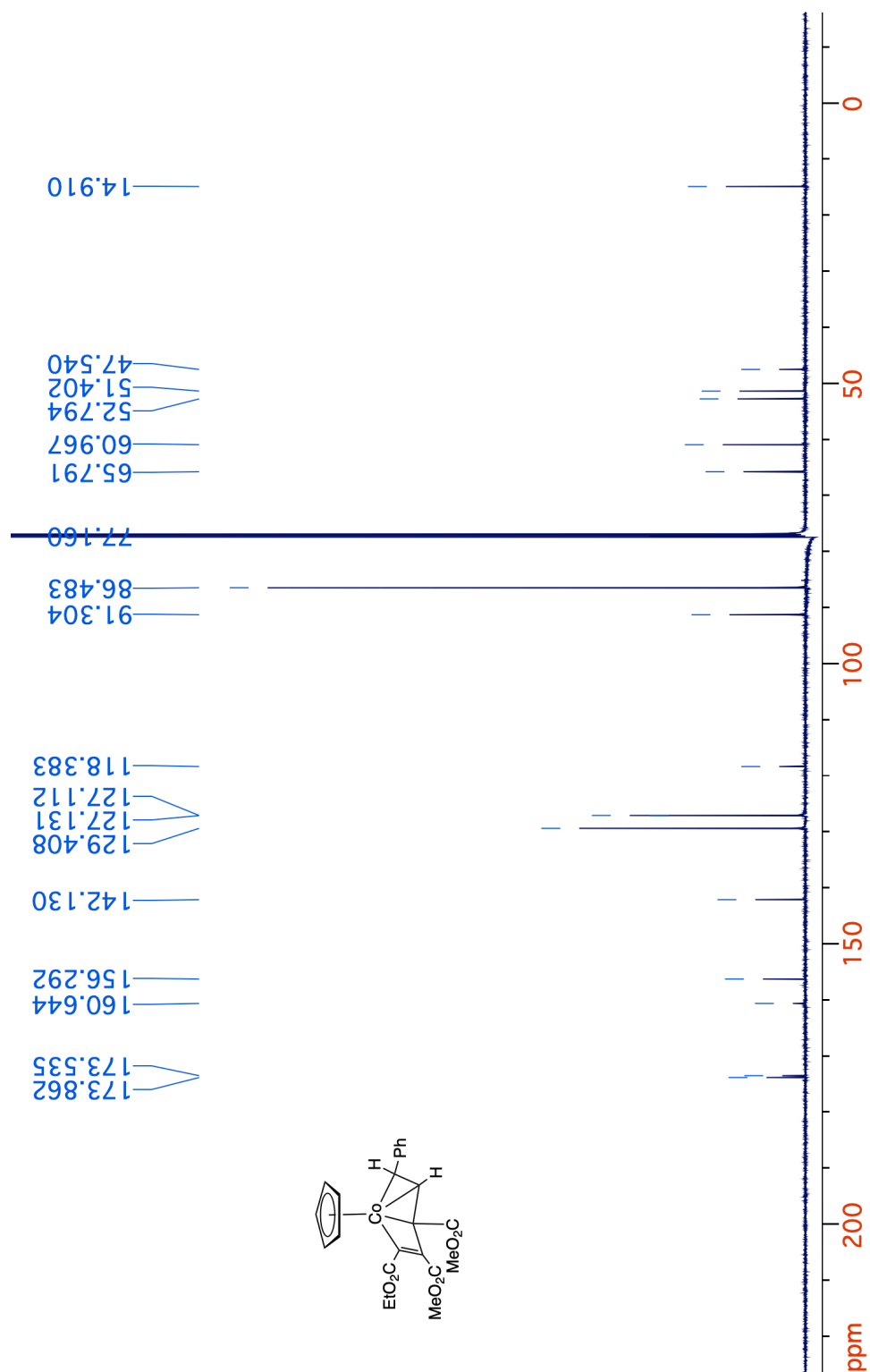
Figure 3-42. $^{13}C\{^1H\}$ NMR spectrum (125 MHz, CDCl$_3$) of **16**.
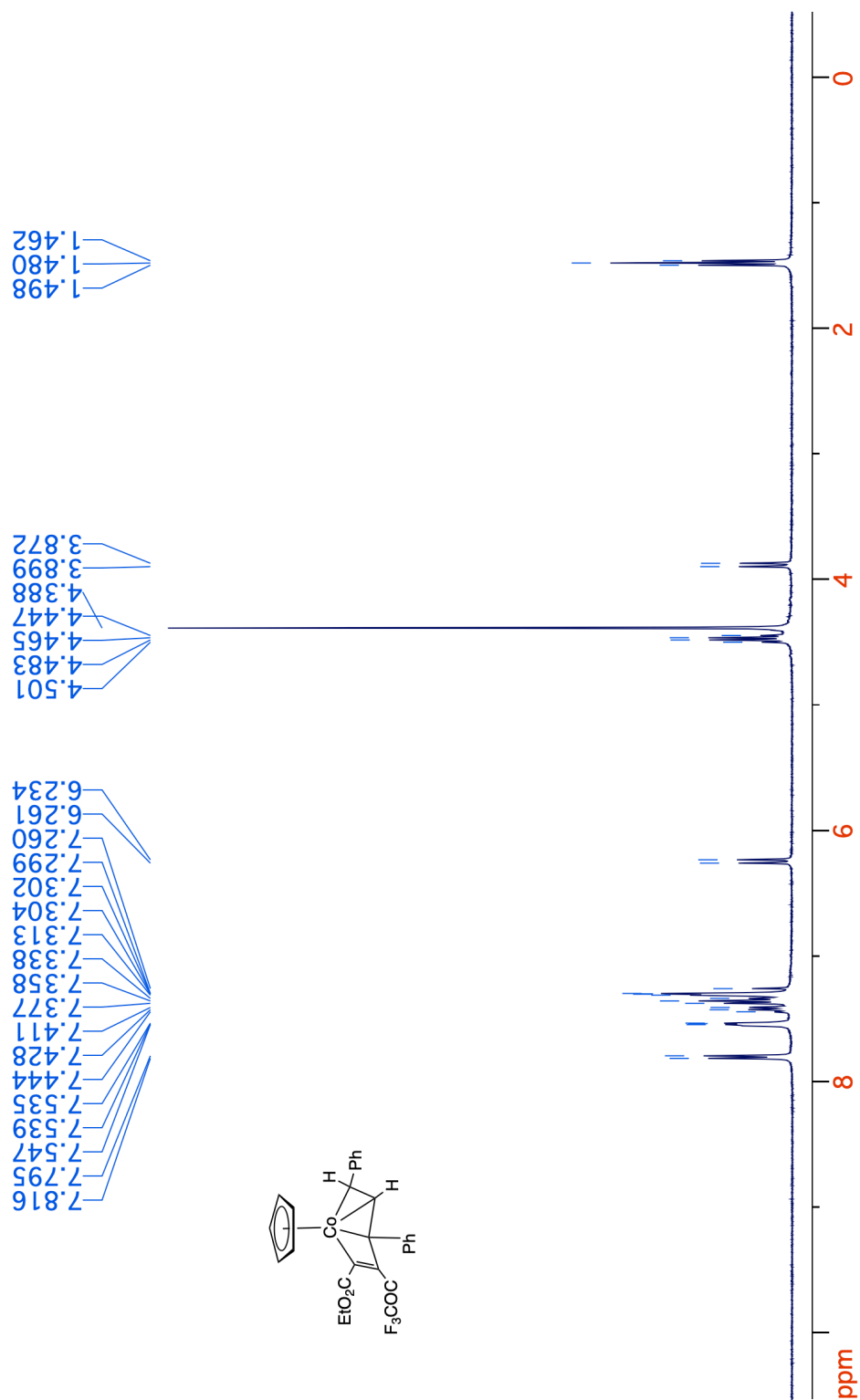
Figure 3-43. ^{1}H NMR spectrum (400 MHz, CDCl$_3$) of **23**.

1.462
1.480
1.498

3.872
3.899
4.388
4.447
4.465
4.483
4.501

6.234
6.261
7.260
7.299
7.302
7.304
7.313
7.338
7.358
7.377
7.411
7.428
7.444
7.535
7.539
7.547
7.795
7.818

351
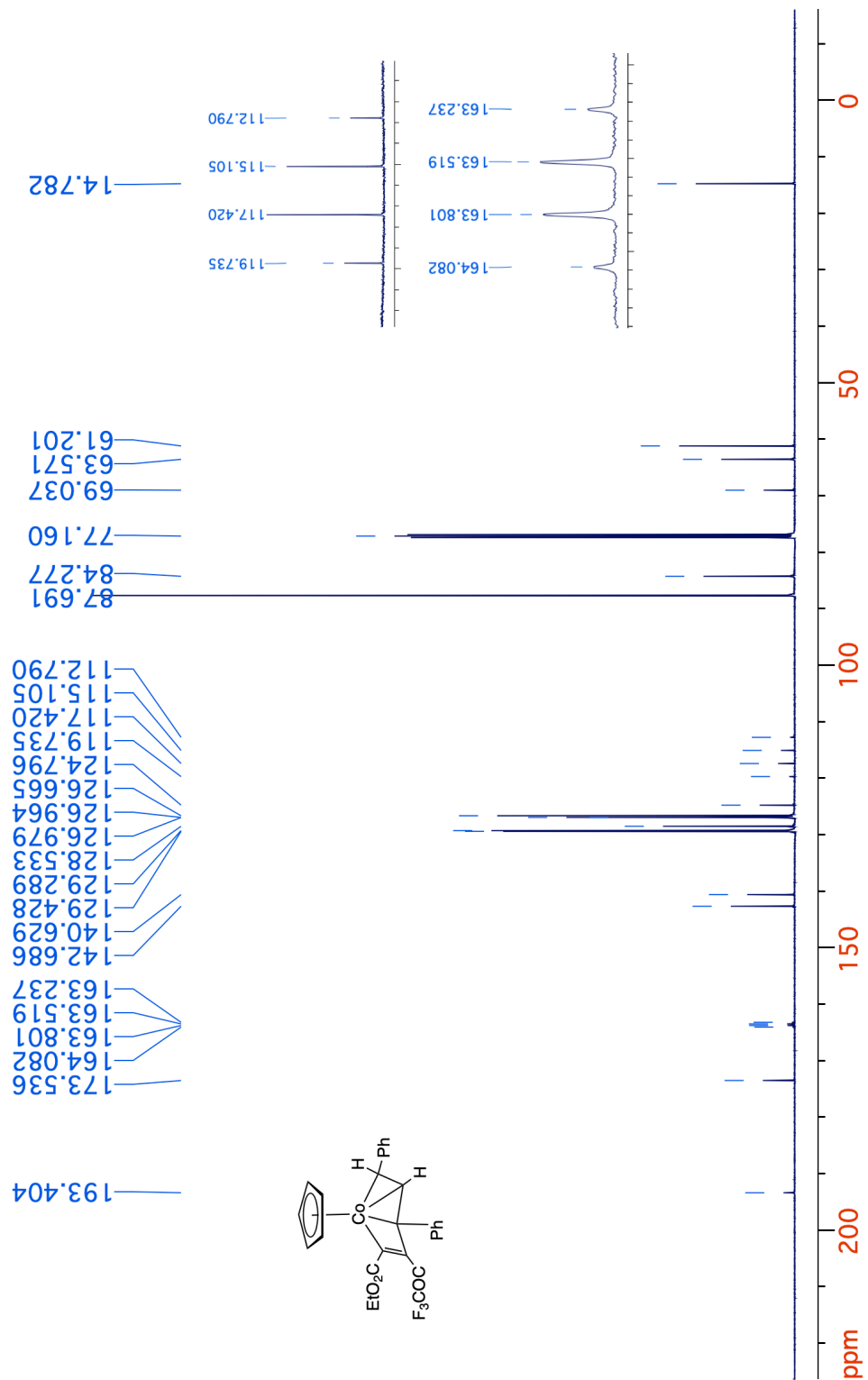
Figure 3-44. $^{13}C\{^1H\}$ NMR spectrum (125 MHz, CDCl$_3$) of **23**.

Peaks labeled: 14.782, 61.201, 63.571, 69.037, 77.160, 84.277, 87.691, 112.790, 115.105, 117.420, 119.735, 124.796, 126.665, 126.964, 126.979, 128.533, 129.289, 129.428, 140.629, 142.686, 163.237, 163.519, 163.801, 164.082, 173.536, 193.404

Inset peaks: 112.790, 115.105, 117.420, 119.735; 163.237, 163.519, 163.801, 164.082

1.054
1.071
1.089

3.863
3.872
3.881
3.883
3.890
3.901
3.908
3.919
3.926
3.937
3.946
4.447
4.573

6.144
7.260
7.278
7.282
7.289
7.295
7.412
7.416
7.423
7.429
7.480
7.484
7.497
7.504
7.884
7.889
7.897
7.901
7.908

Figure 3-45. ^{1}H NMR spectrum (400 MHz, CDCl$_3$) of **24**.
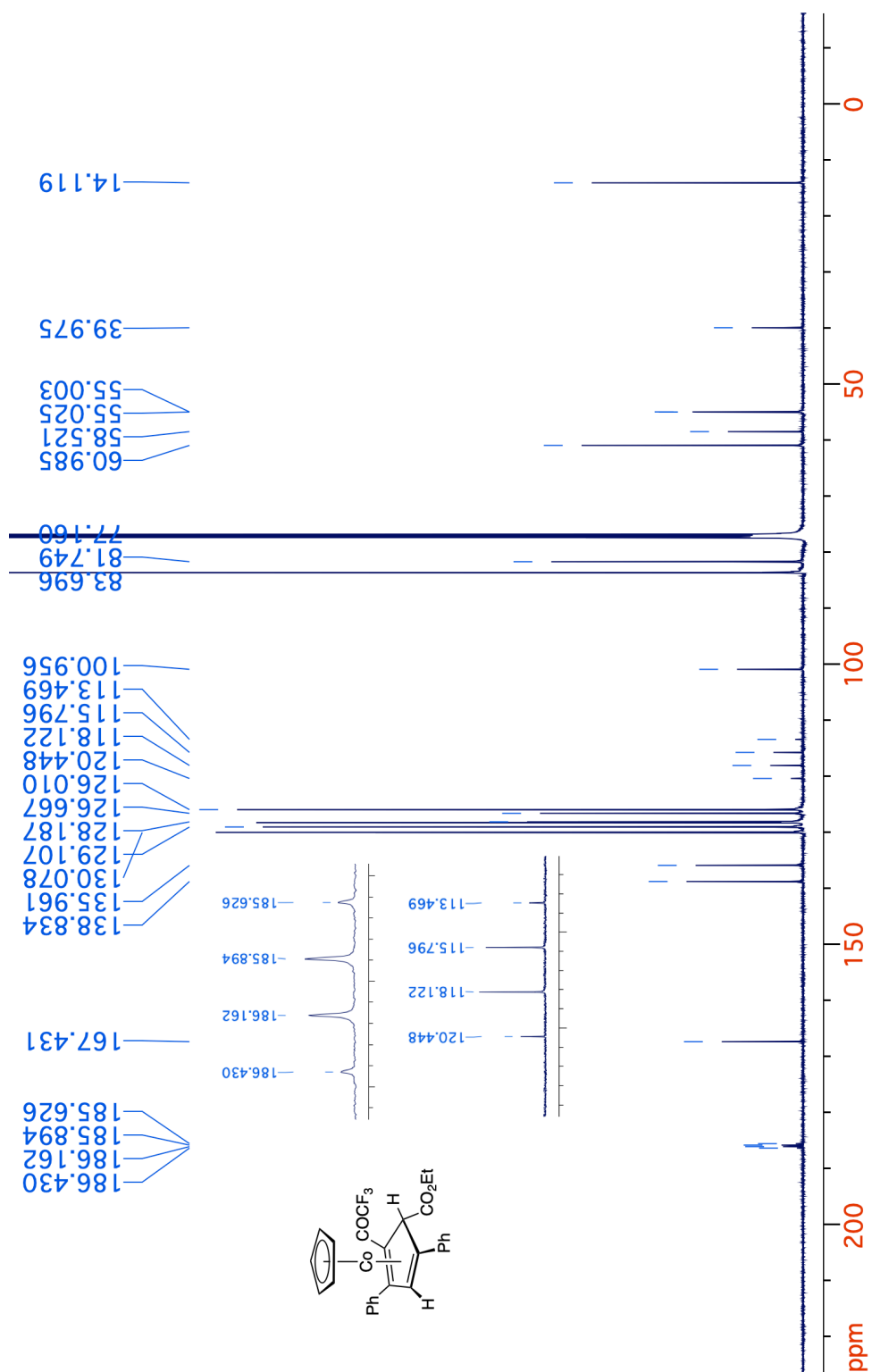
Figure 3-46. $^{13}C\{^1H\}$ NMR spectrum (125 MHz, CDCl$_3$) of **24**.

354

0.119

3.285
3.314

3.914

4.559

6.328
6.357
6.826
6.845
7.109
7.127
7.146
7.166
7.185
7.202
7.260
7.649
7.668
7.689
7.738
7.756
7.774
8.088
8.108
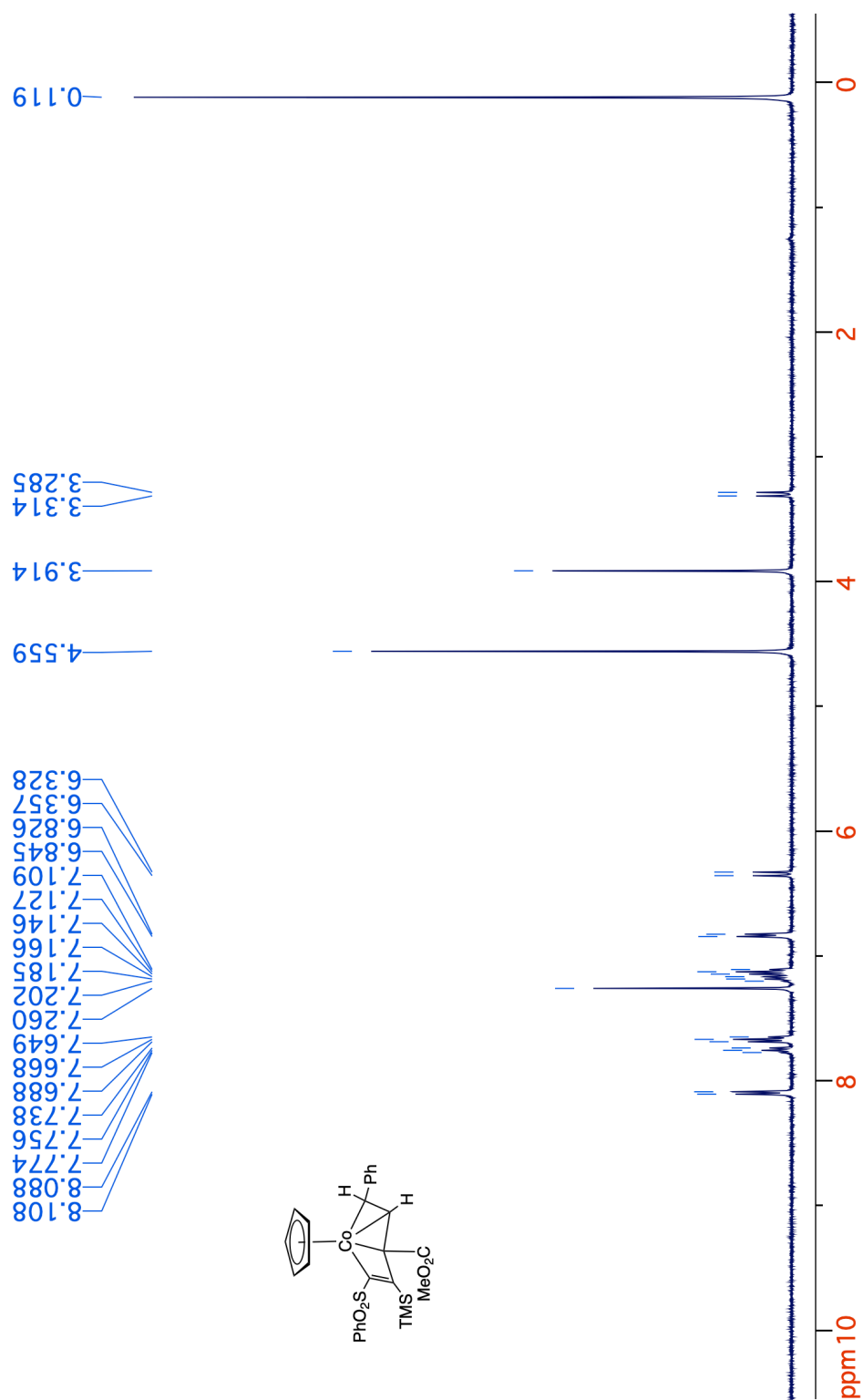
Figure 3-47. ^{1}H NMR spectrum (400 MHz, CDCl$_3$) of **39**.

355
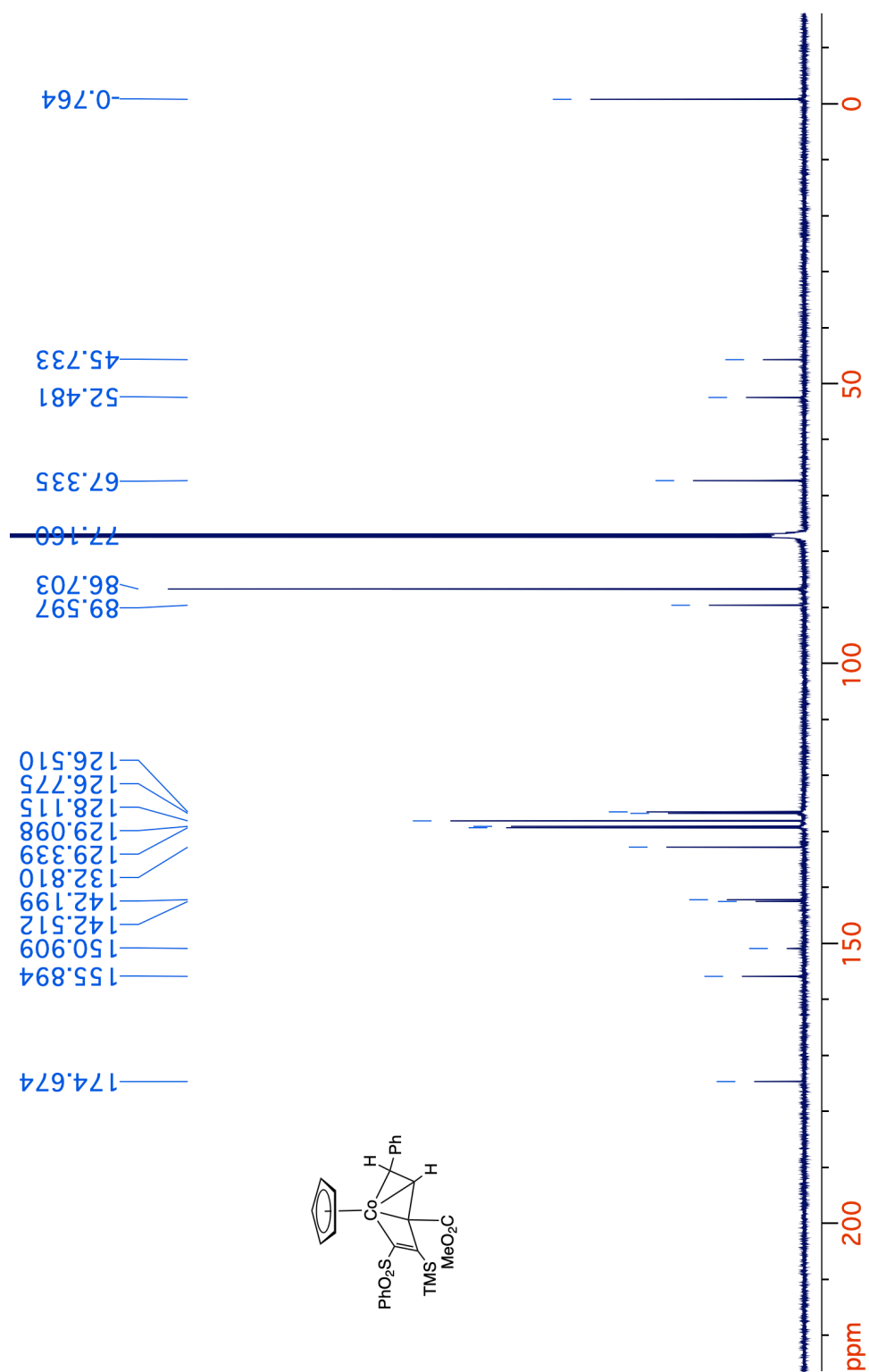
Figure 3-48. $^{13}C\{^1H\}$ NMR spectrum (125 MHz, CDCl$_3$) of **39**.
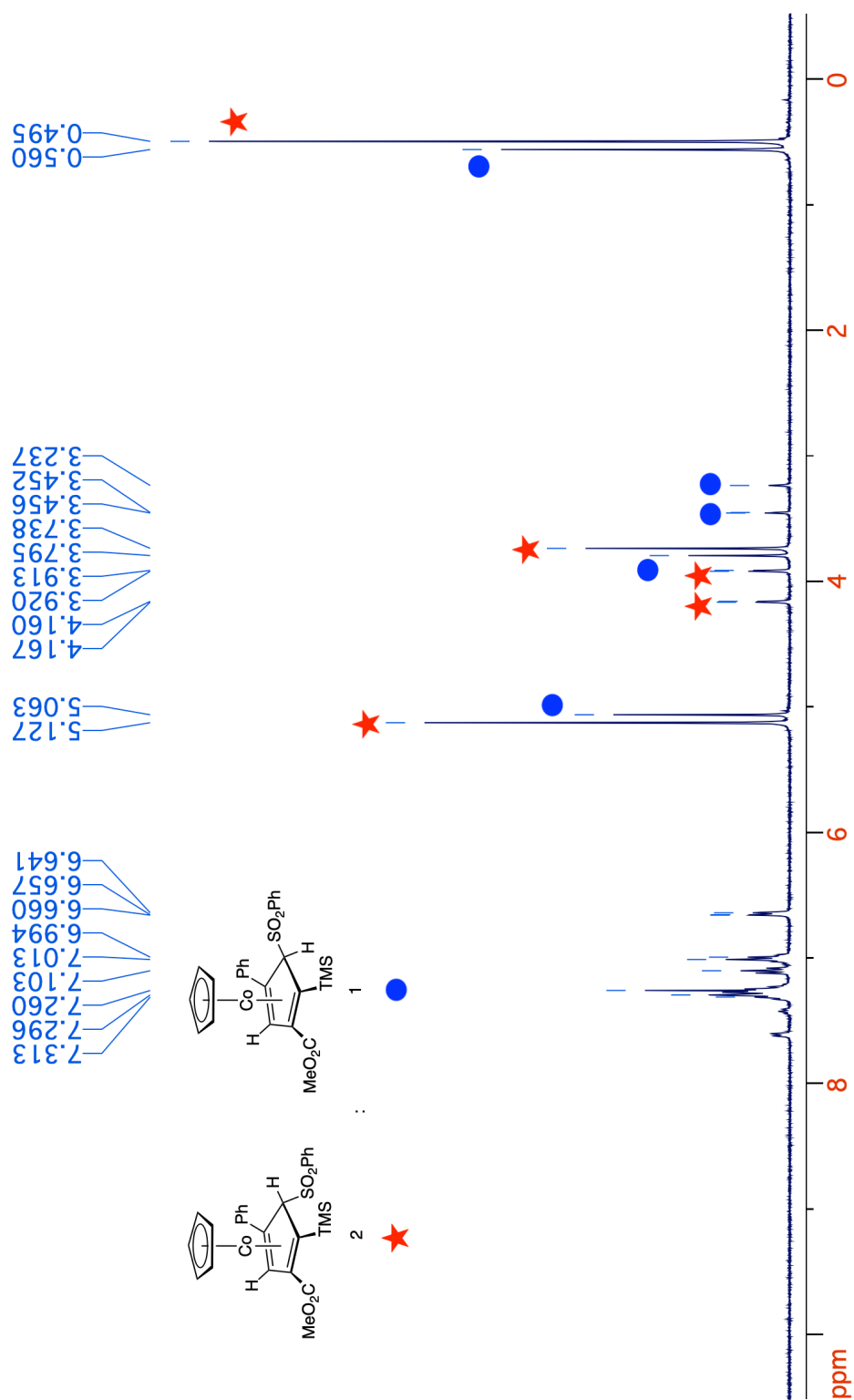
Figure 3-49. ^{1}H NMR spectrum (400 MHz, CDCl$_3$) of 2 : 1 mixture of **41**-*exo* and **41**-*endo*.

357
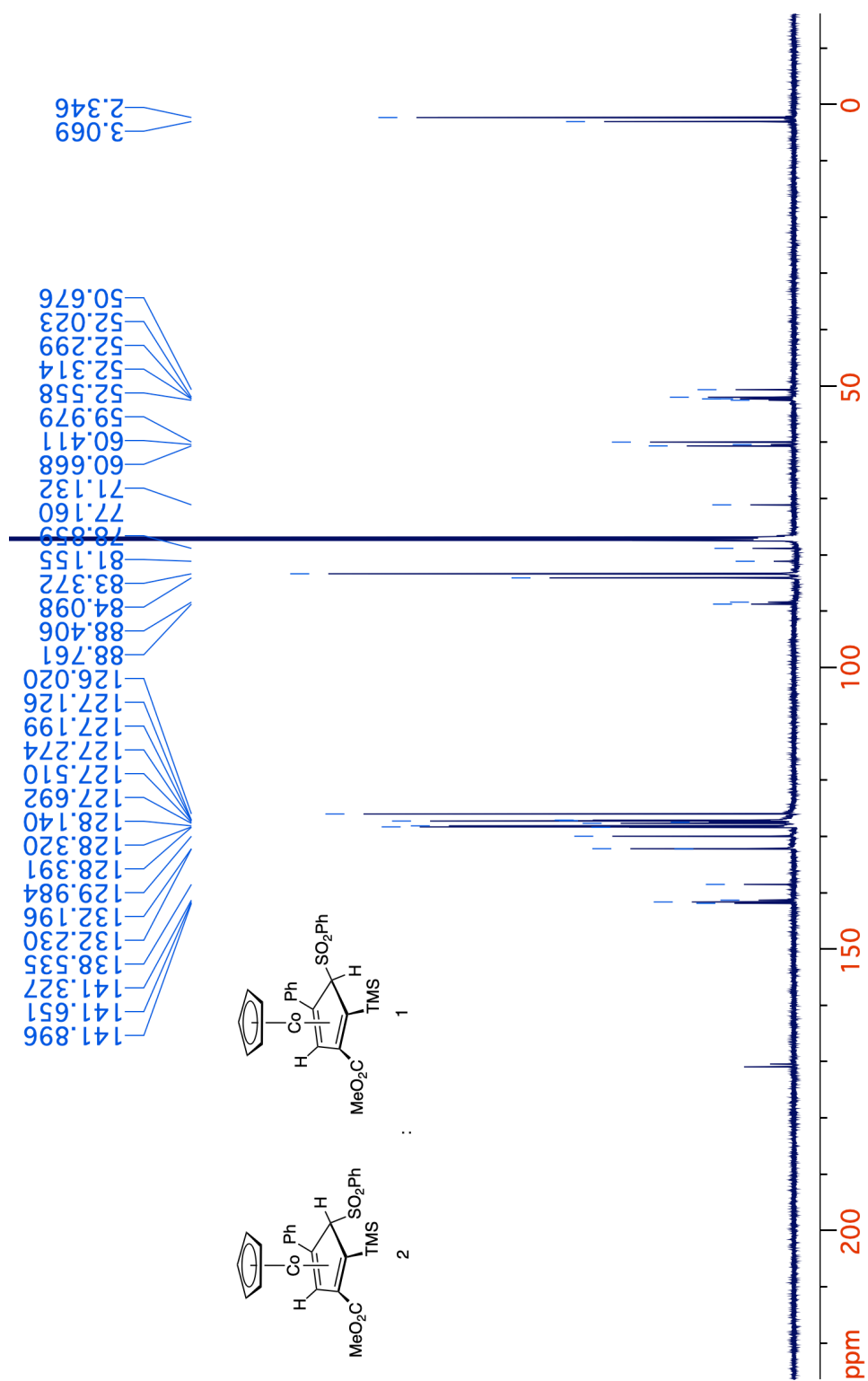
Figure 3-50. $^{13}C\{^1H\}$ NMR spectrum (125 MHz, CDCl$_3$) of 2 : 1 mixture of **41**-*exo* and **41**-*endo*.
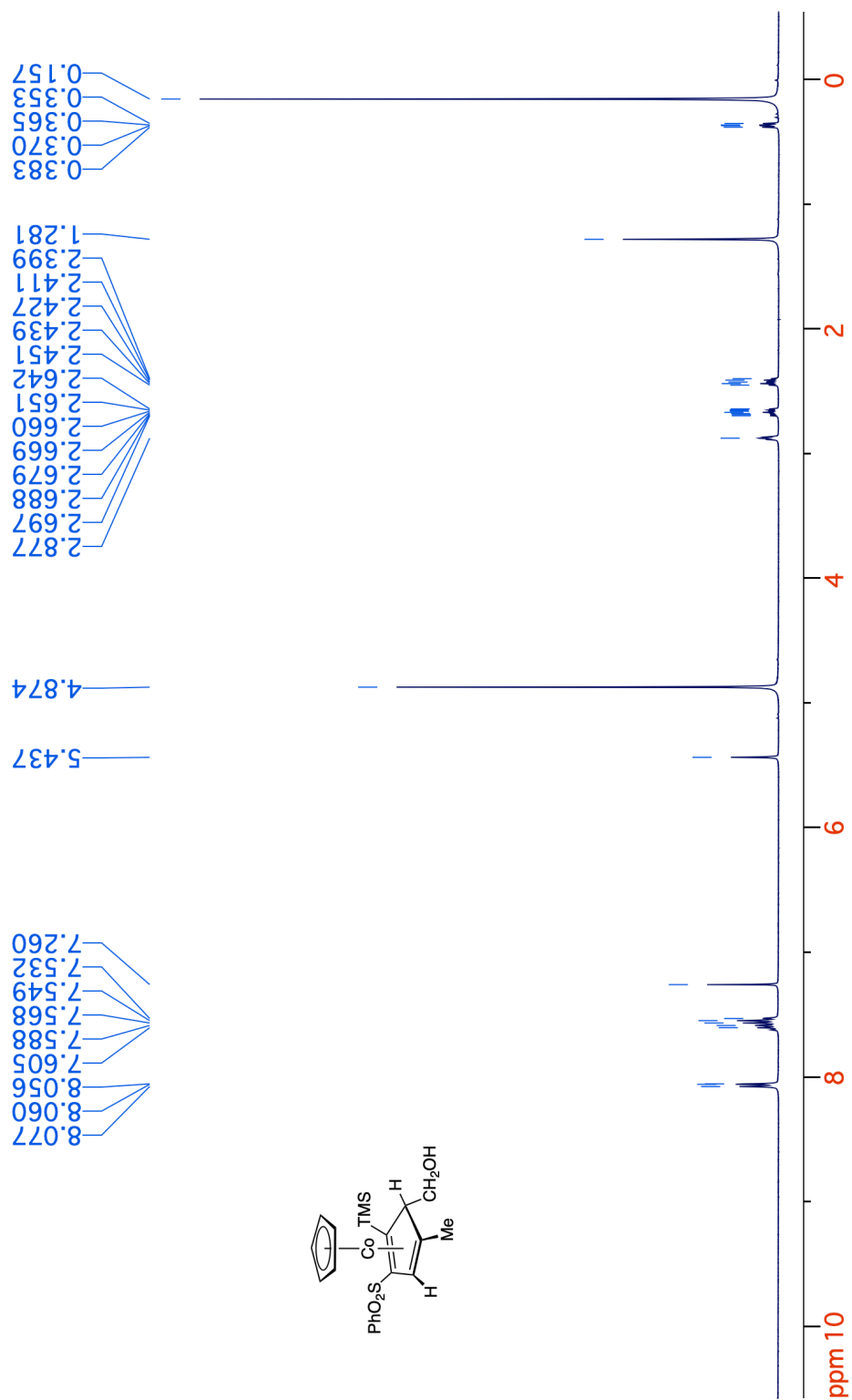
Figure 3-51. ^{1}H NMR spectrum (400 MHz, CDCl$_3$) of **51**.
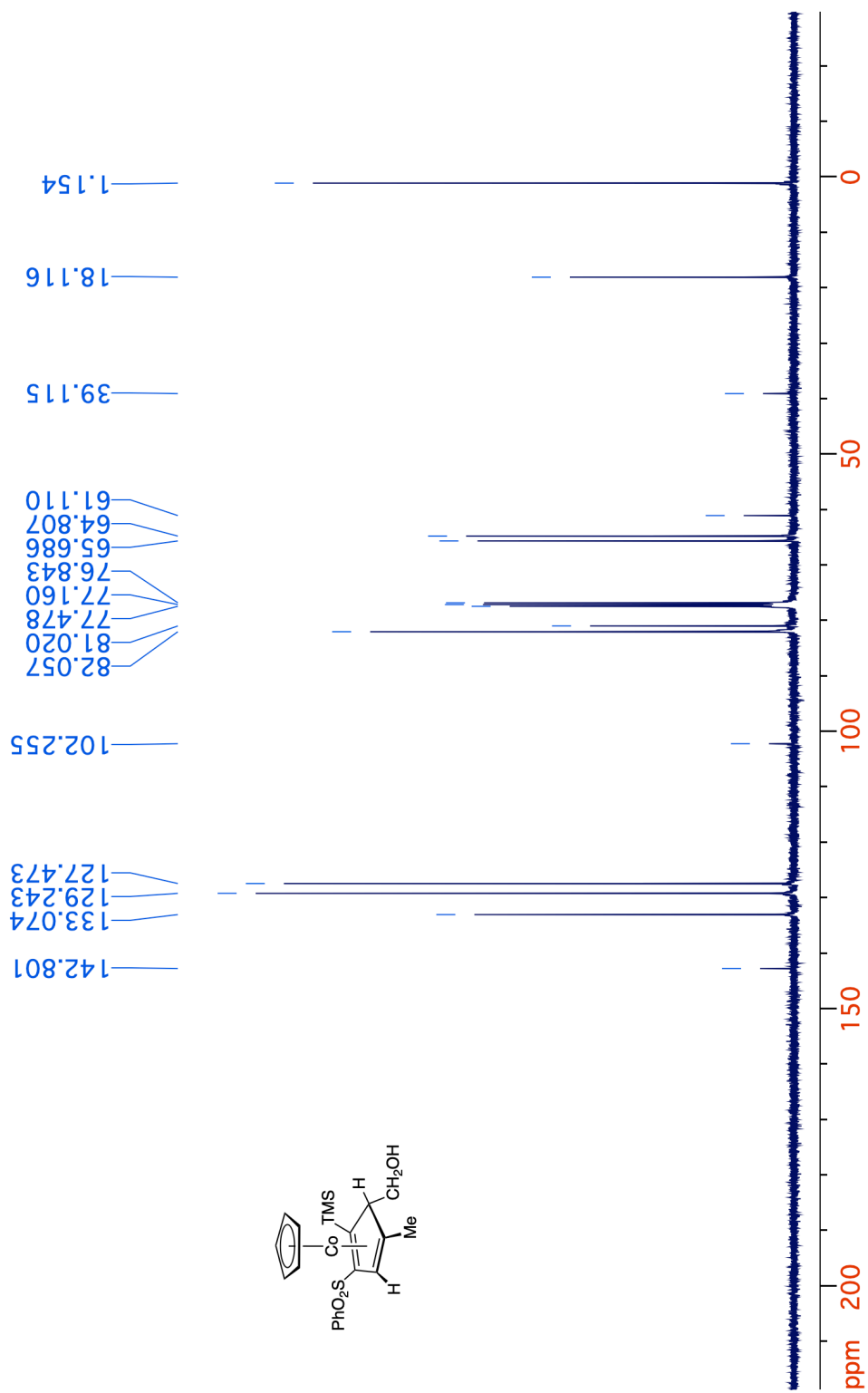
Figure 3-52. $^{13}C\{^1H\}$ NMR spectrum (125 MHz, CDCl$_3$) of **51**.
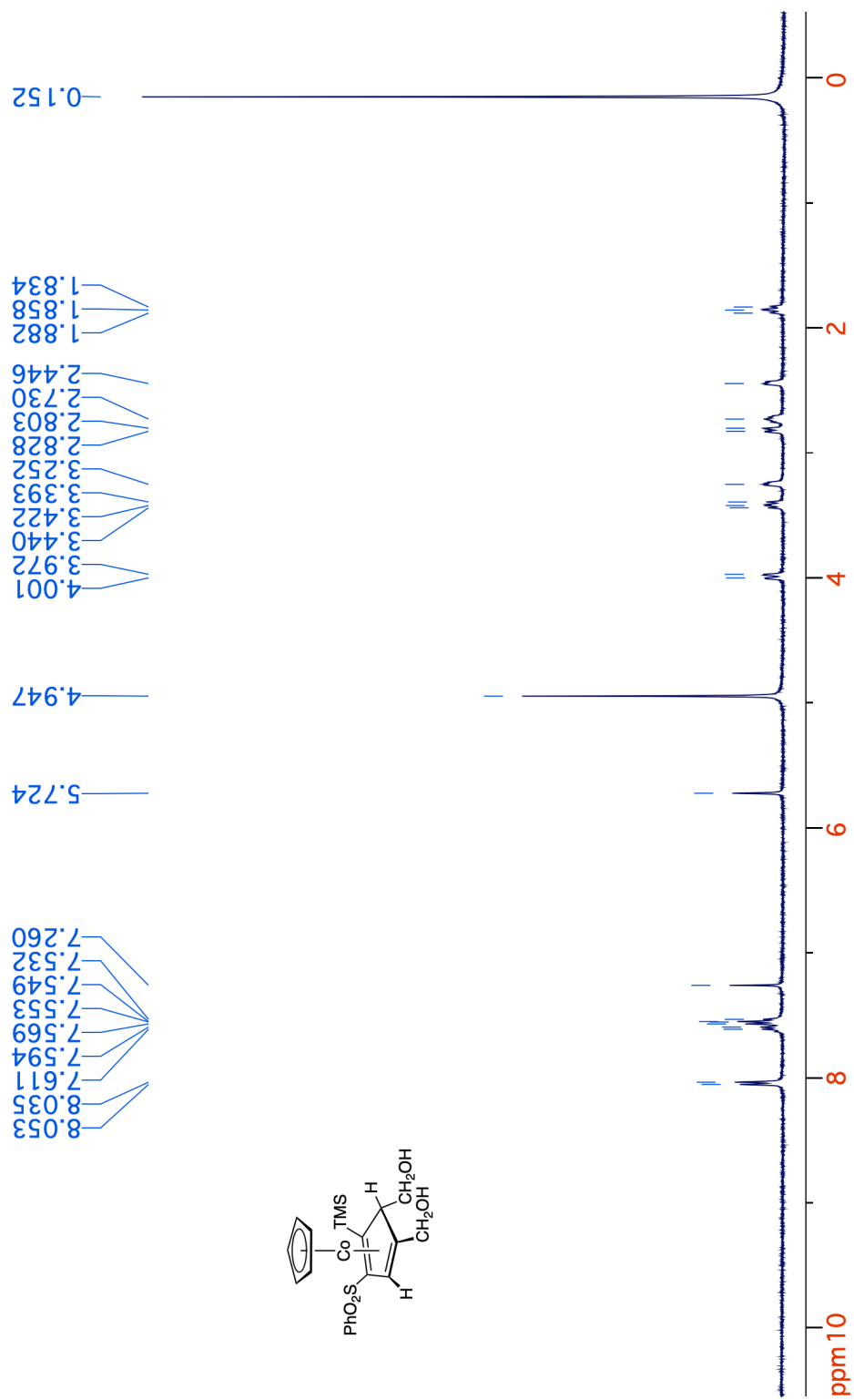
Figure 3-53. ^{1}H NMR spectrum (400 MHz, CDCl$_3$) of **53**.
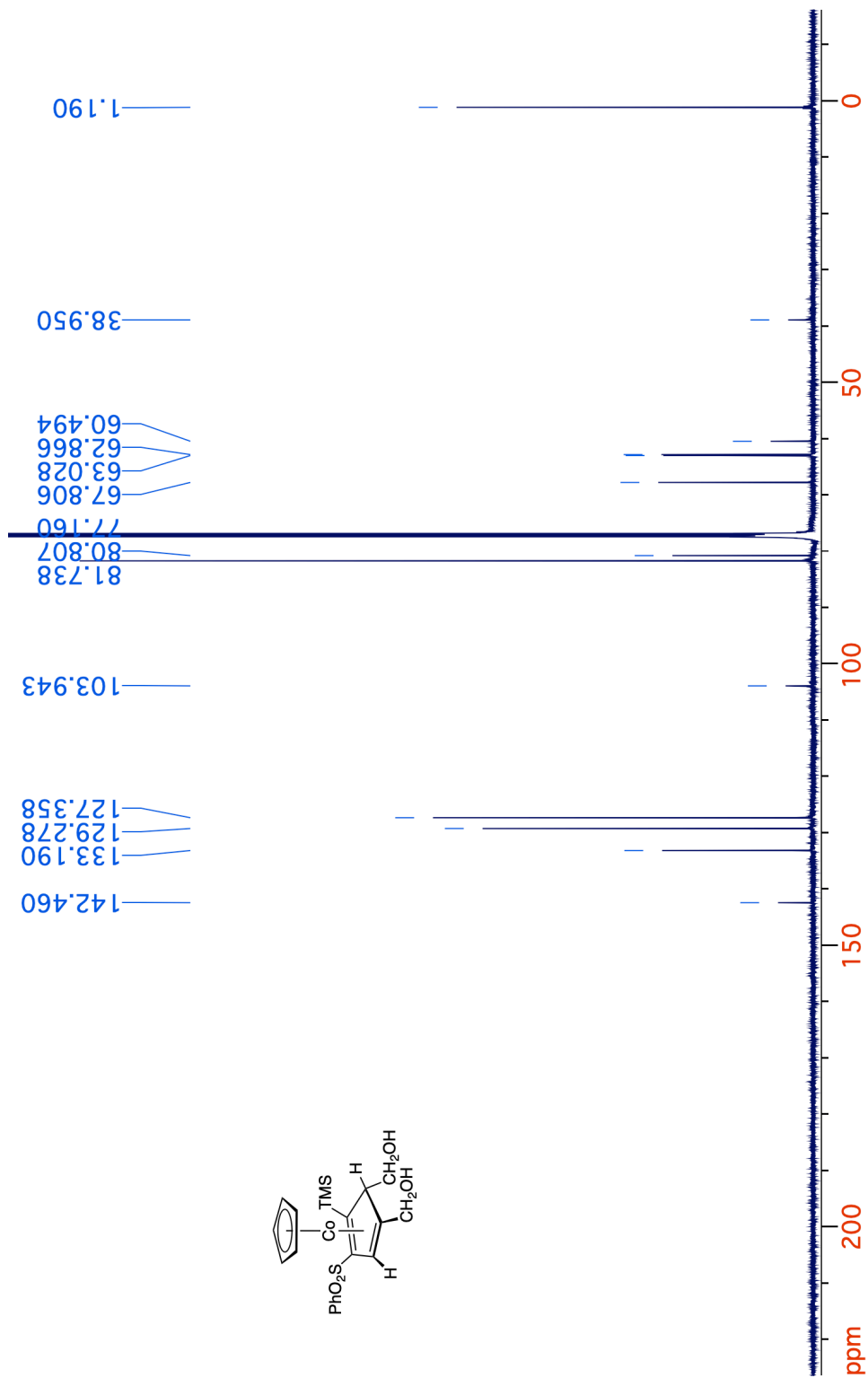
Figure 3-54. $^{13}C\{^{1}H\}$ NMR spectrum (125 MHz, CDCl$_3$) of **53**.
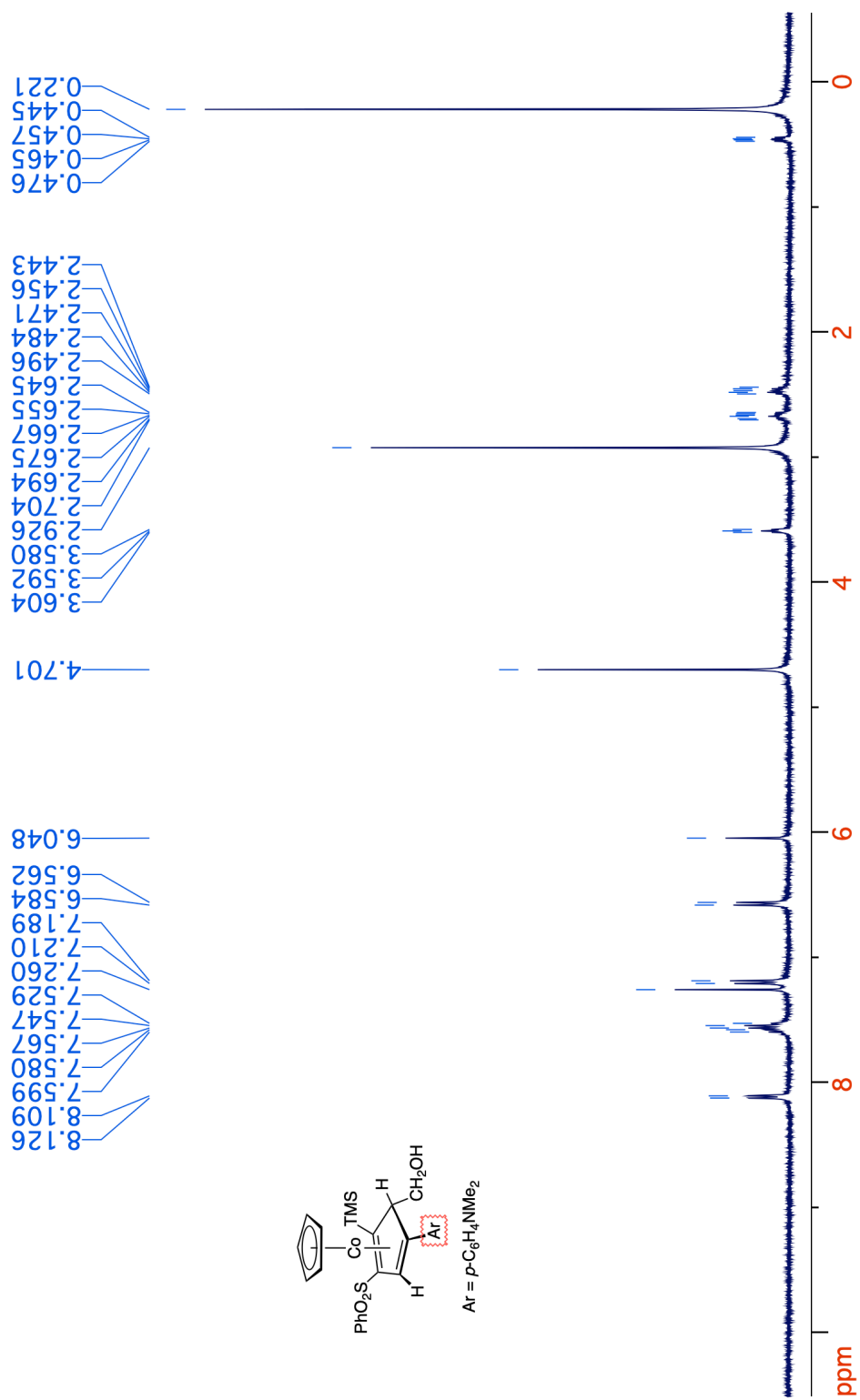
Figure 3-55. ^1H NMR spectrum (400 MHz, CDCl$_3$) of **54**.
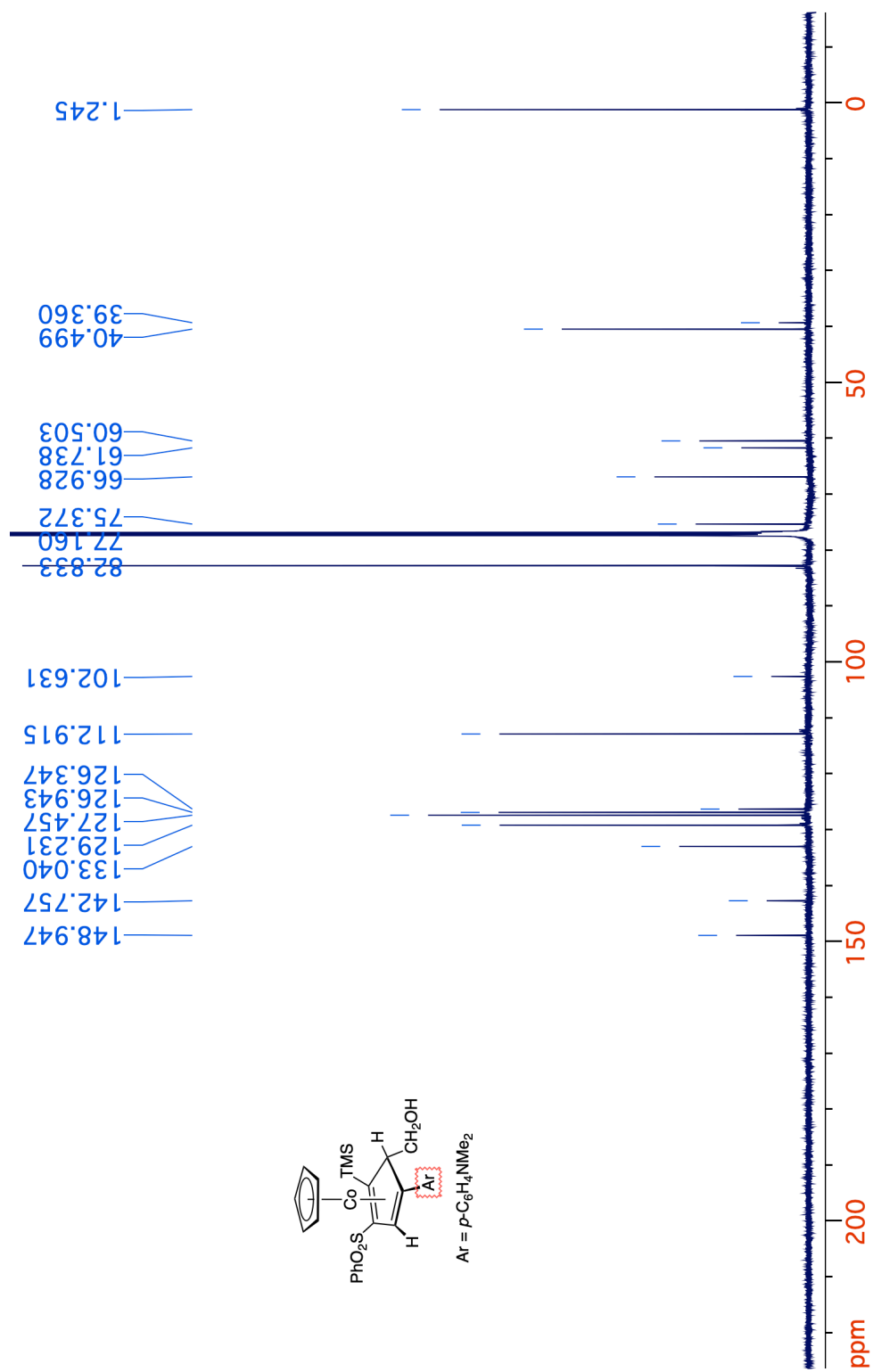
Figure 3-56. $^{13}C\{^1H\}$ NMR spectrum (125 MHz, CDCl$_3$) of **54**.
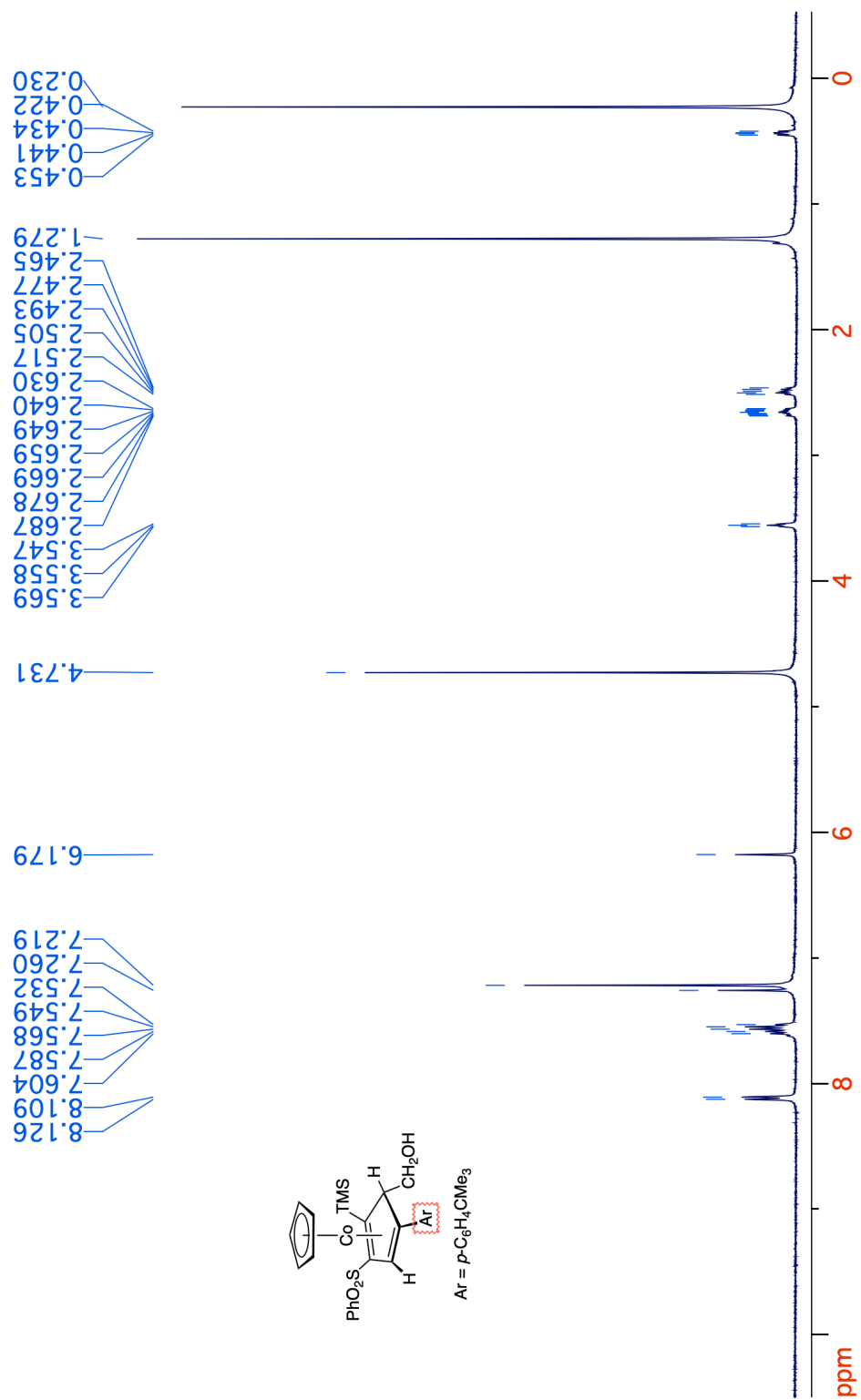
Figure 3-57. ^{1}H NMR spectrum (400 MHz, CDCl$_3$) of **55**.
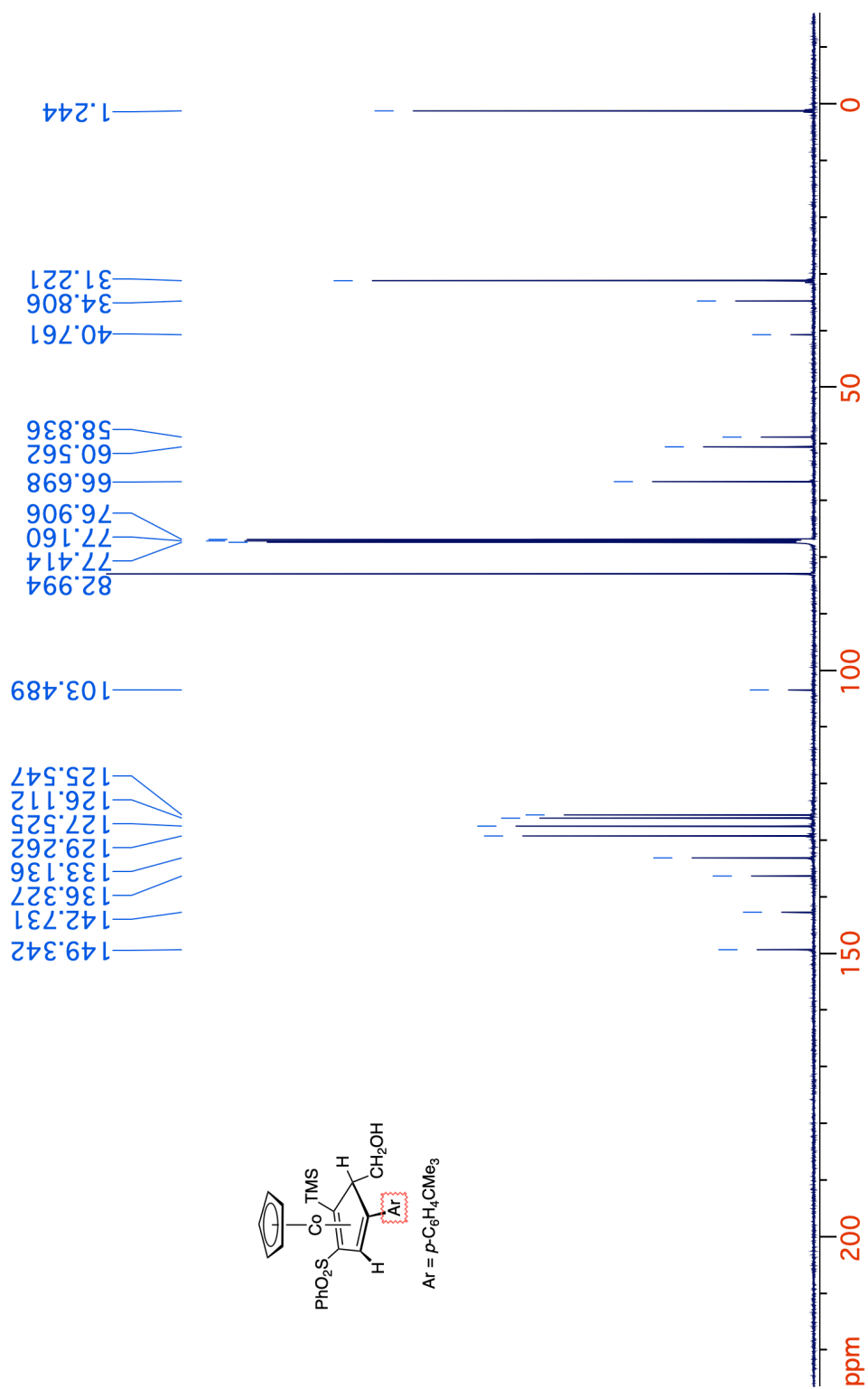
Figure 3-58. $^{13}C\{^1H\}$ NMR spectrum (125 MHz, CDCl$_3$) of **55**.

Figure 3-59. ^{1}H NMR spectrum (400 MHz, CDCl$_3$) of **56**.
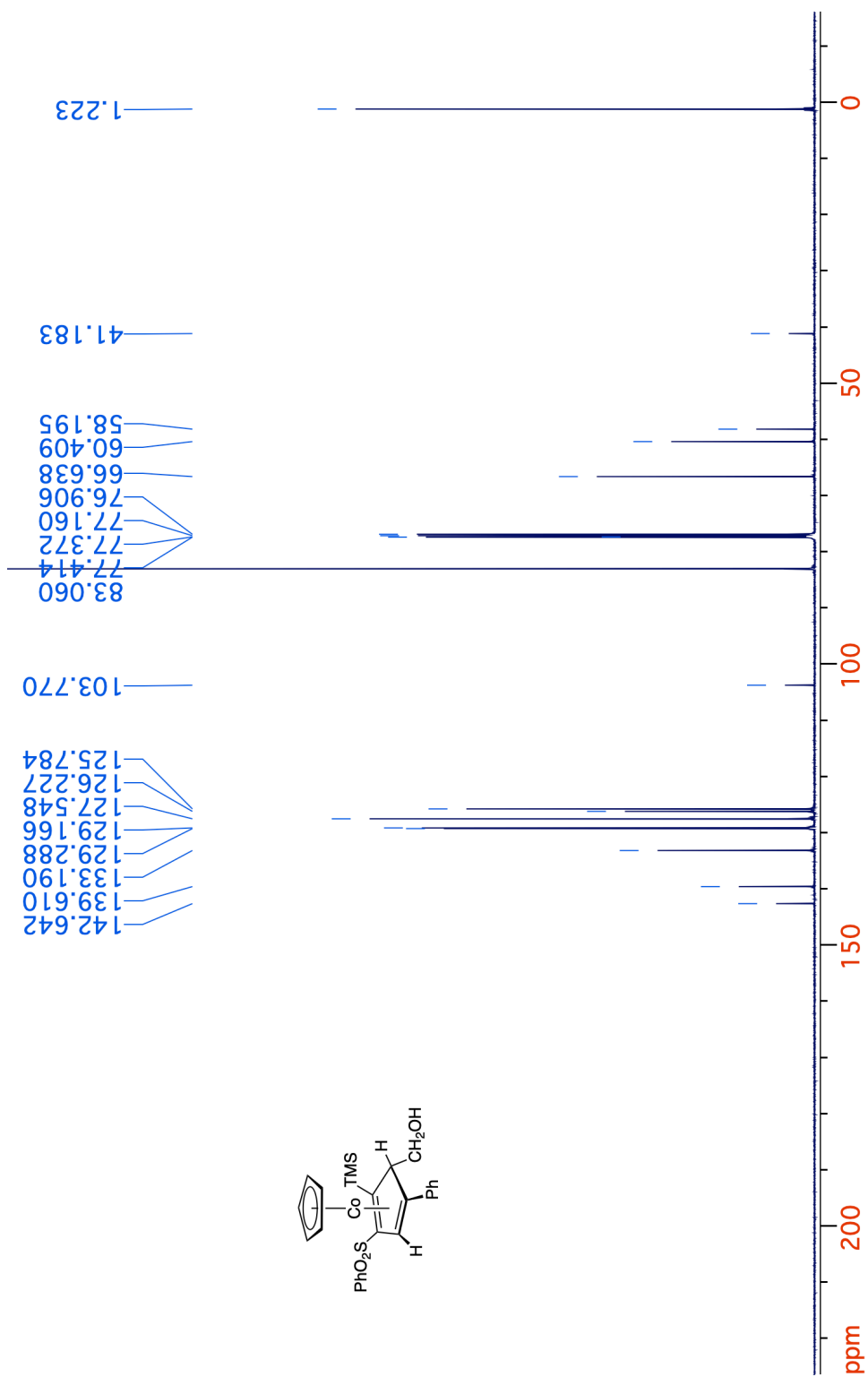
Figure 3-60. $^{13}C\{^{1}H\}$ NMR spectrum (125 MHz, CDCl$_3$) of **56**.
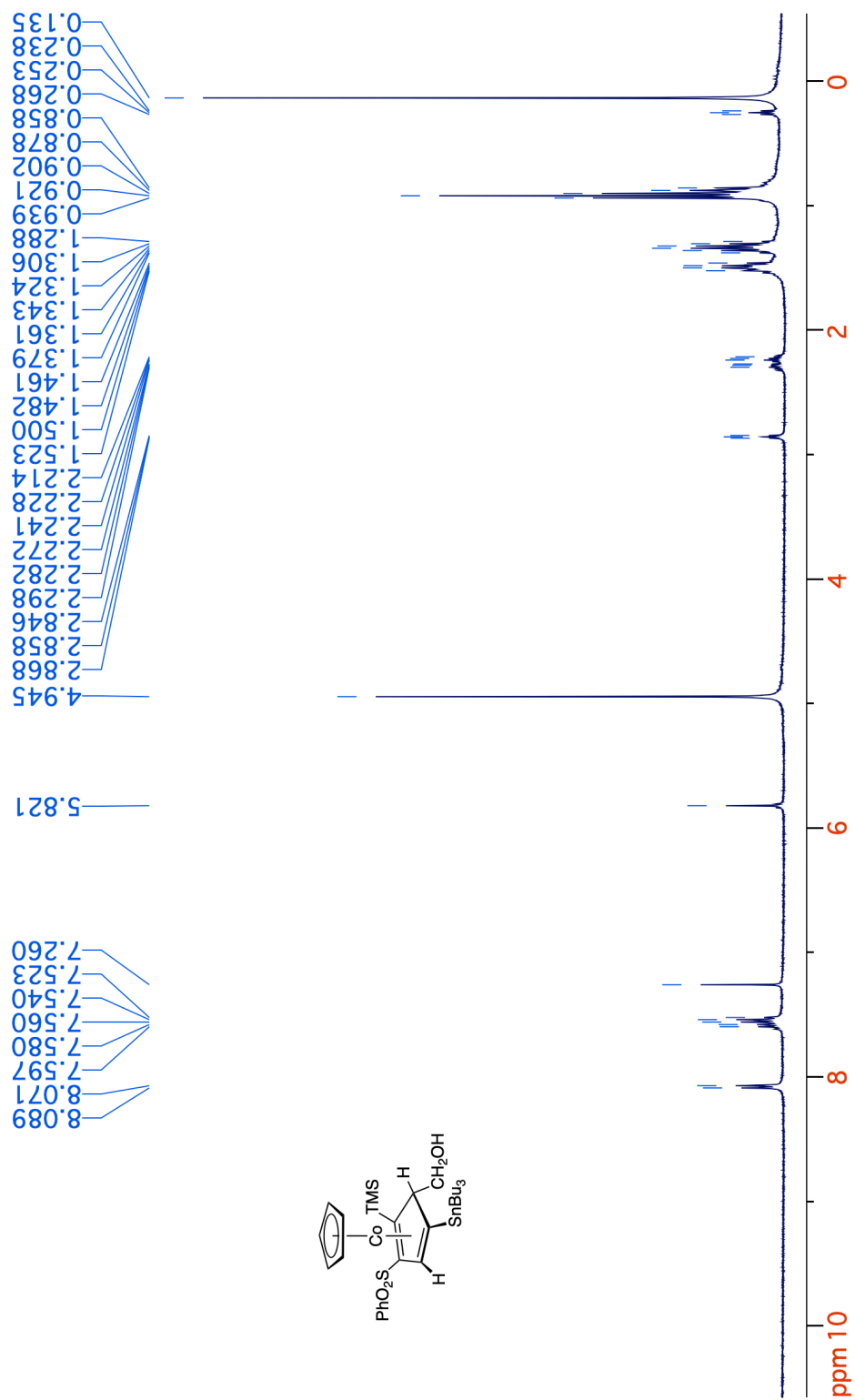
Figure 3-61. ^{1}H NMR spectrum (400 MHz, CDCl$_3$) of **57**.

369
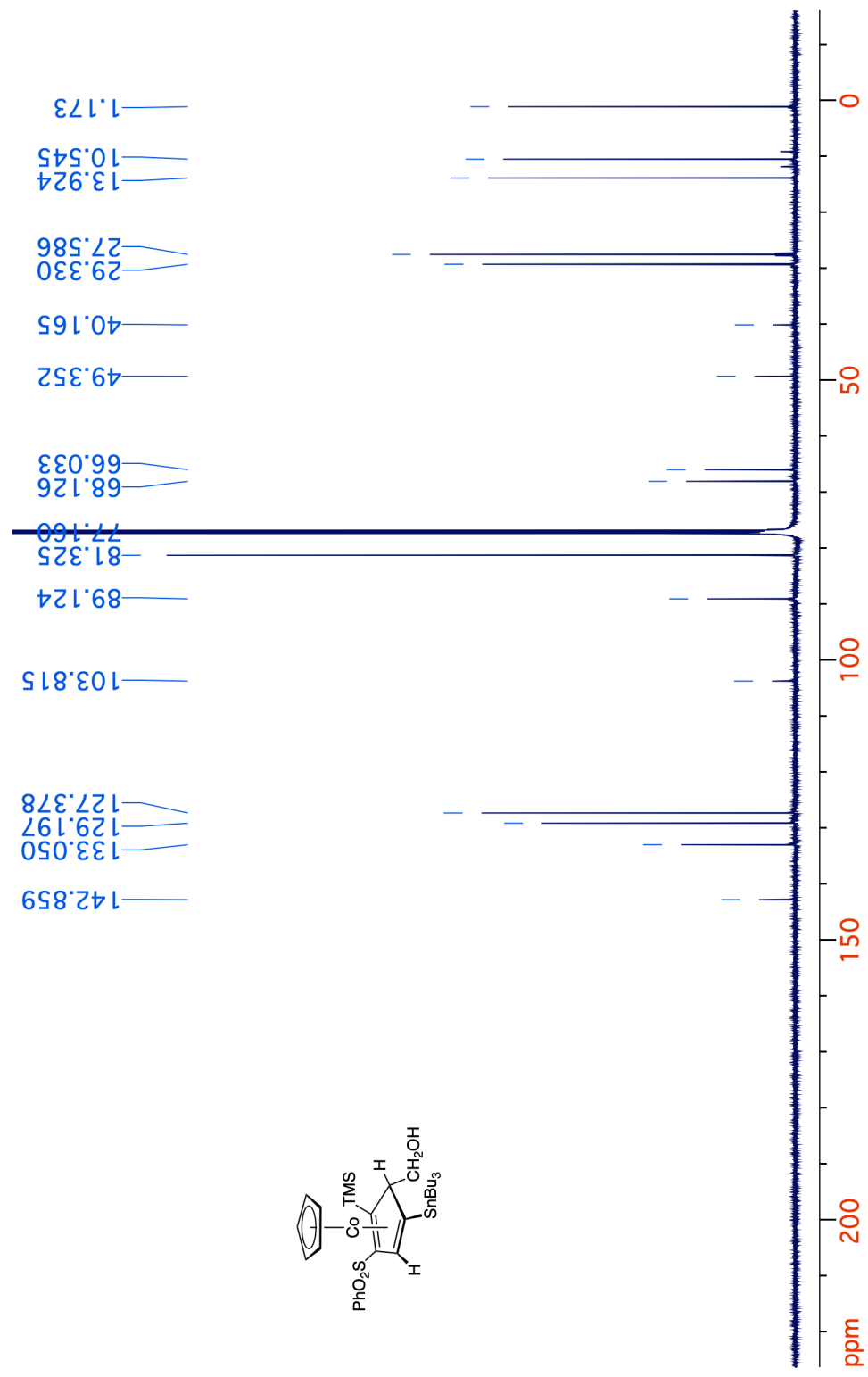
Figure 3-62. $^{13}C\{^{1}H\}$ NMR spectrum (125 MHz, CDCl$_3$) of **57**.

Peak labels (ppm): 1.173, 10.545, 13.924, 27.586, 29.330, 40.165, 49.352, 66.033, 68.126, 77.160, 81.325, 89.124, 103.815, 127.378, 129.197, 133.050, 142.859
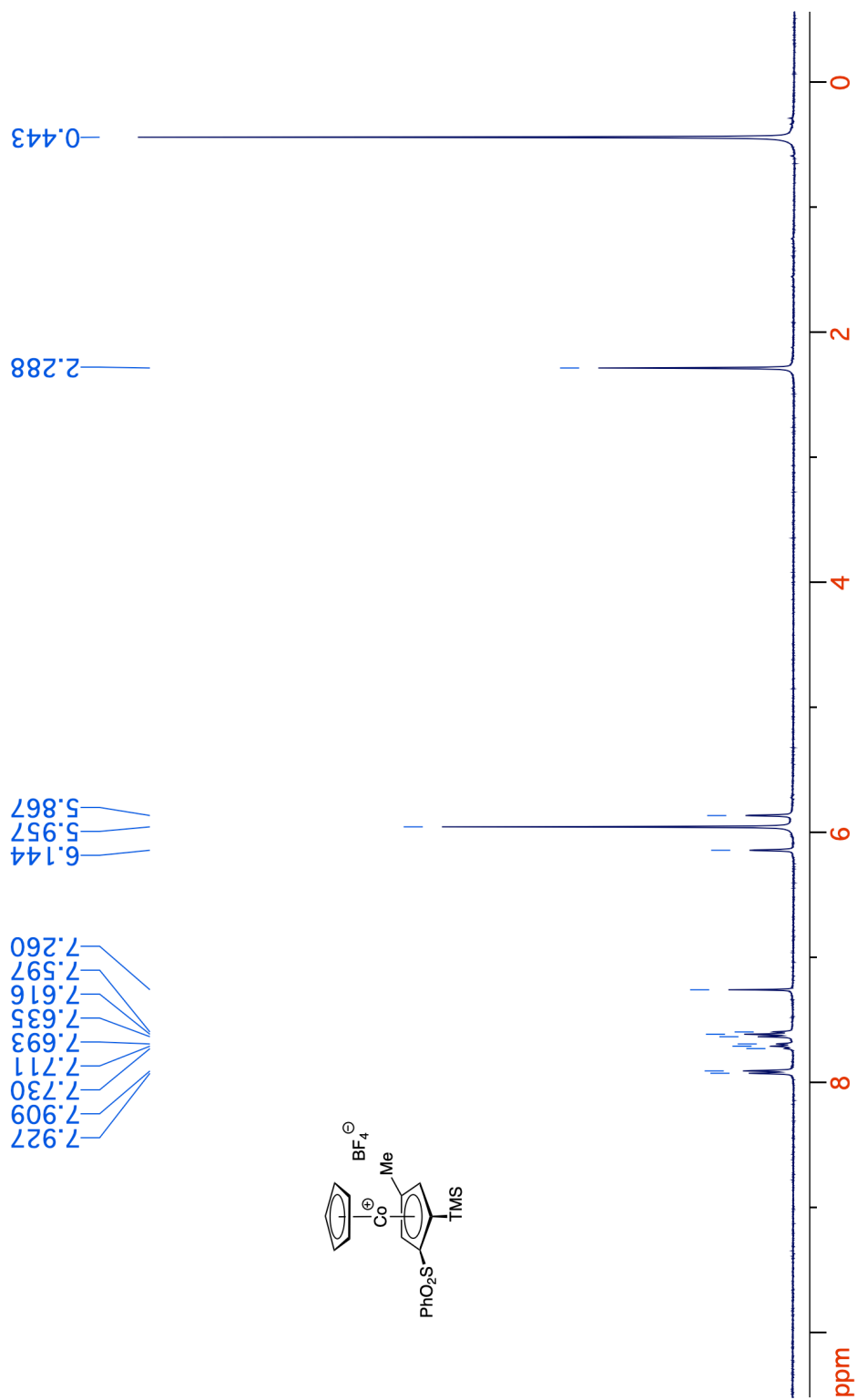
Figure 3-63. ^{1}H NMR spectrum (400 MHz, CDCl$_3$) of **61**.

371
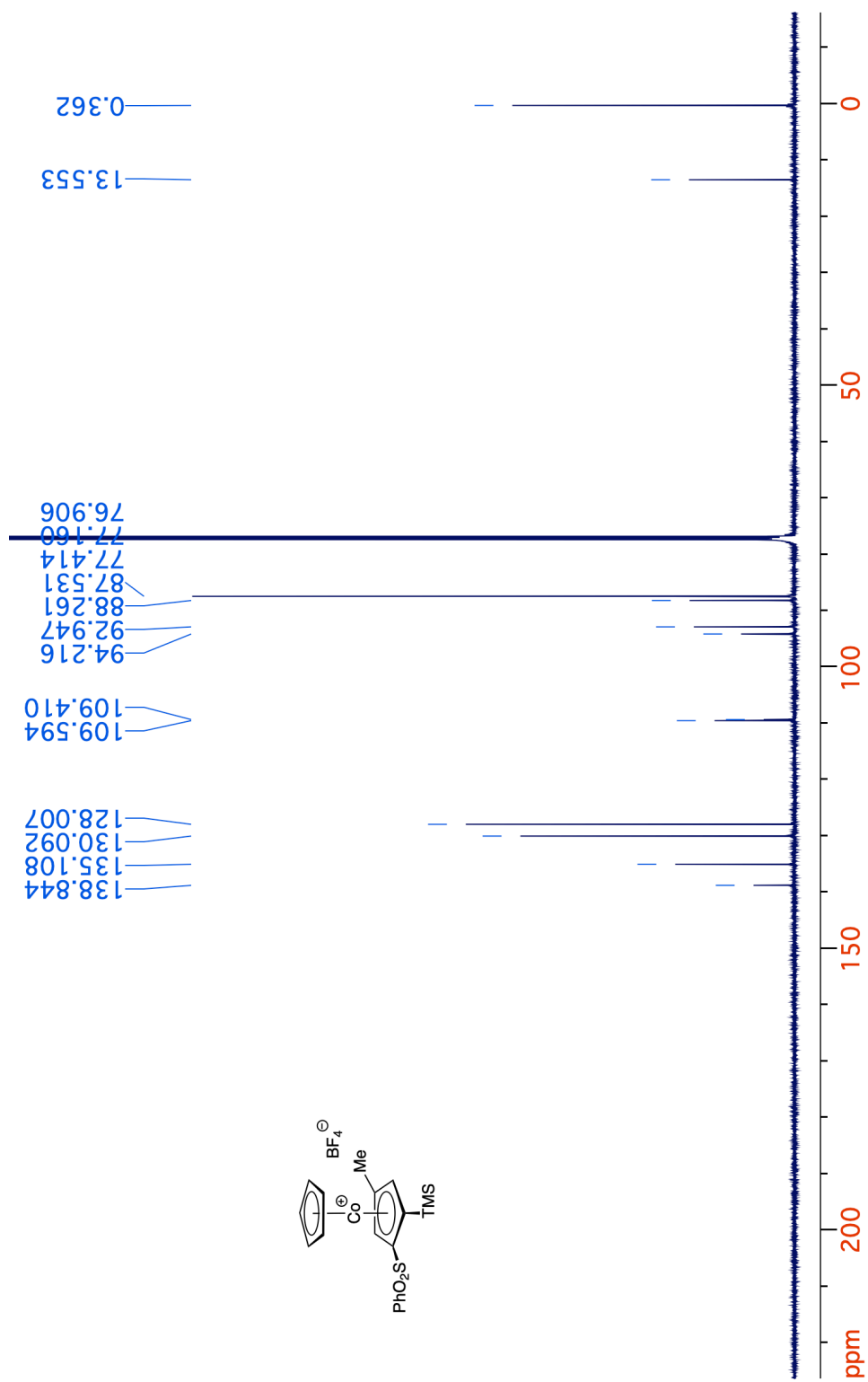
Figure 3-64. $^{13}C\{^{1}H\}$ NMR spectrum (125 MHz, CDCl$_3$) of **61**.
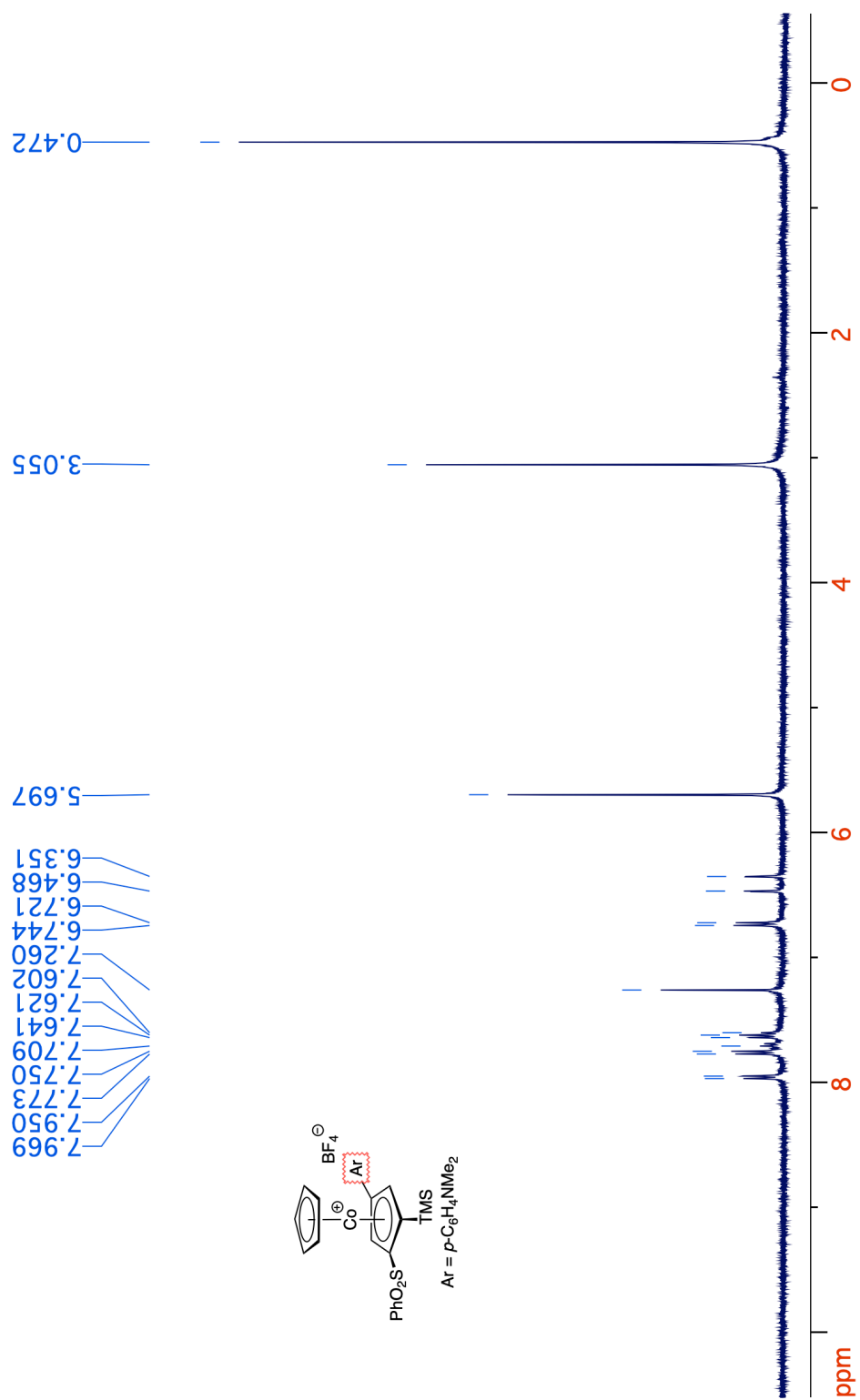
Figure 3-65. ^{1}H NMR spectrum (400 MHz, CDCl$_3$) of **62**.
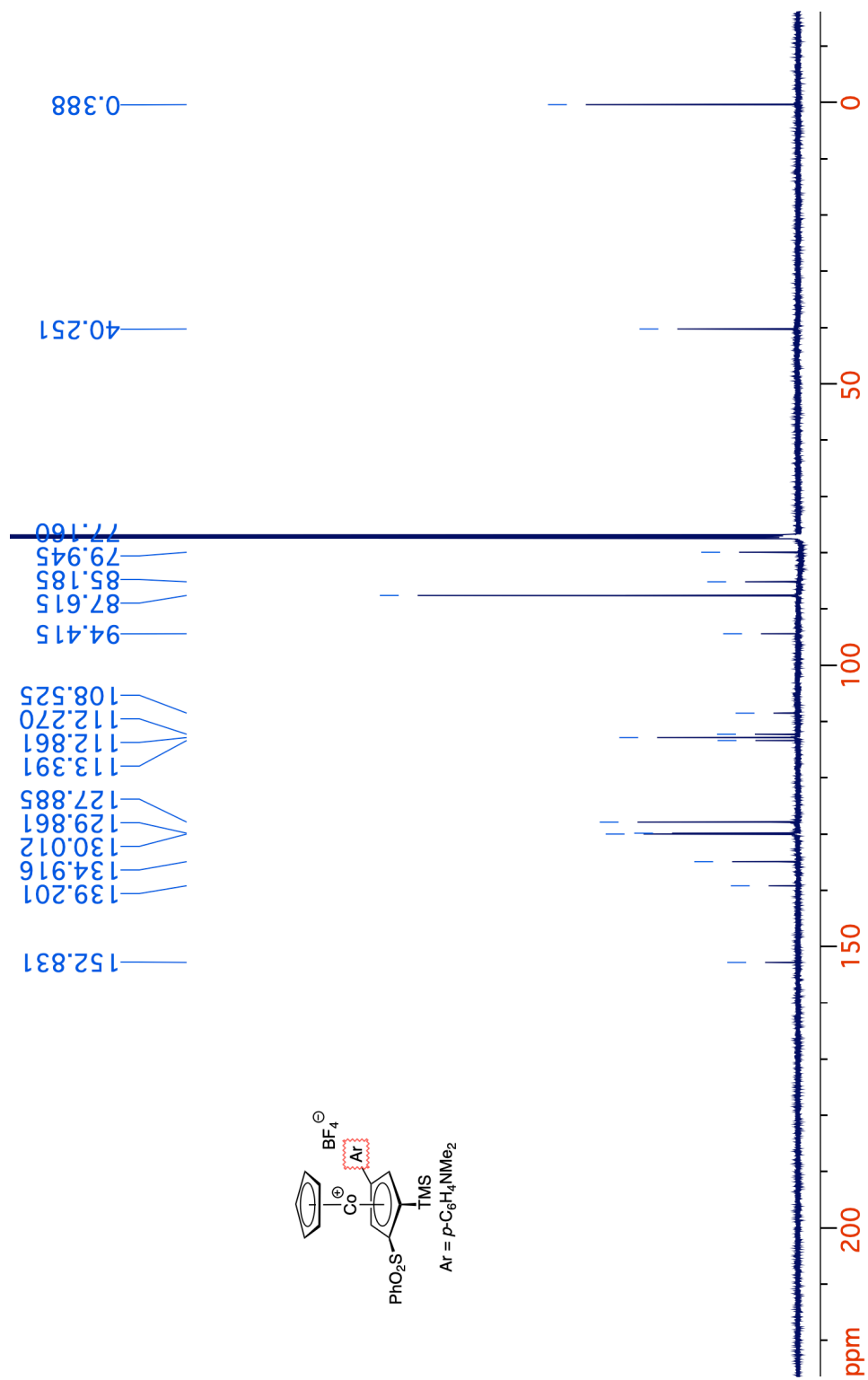
Figure 3-66. $^{13}C\{^1H\}$ NMR spectrum (125 MHz, CDCl$_3$) of **62**.

Peak labels:
0.388
40.251
77.160
79.945
85.185
87.615
94.415
108.525
112.270
112.861
113.391
127.885
129.861
130.012
134.916
139.201
152.831

Structure labels: BF$_4$, Ar, Co, TMS, PhO$_2$S, Ar = p-C$_6$H$_4$NMe$_2$
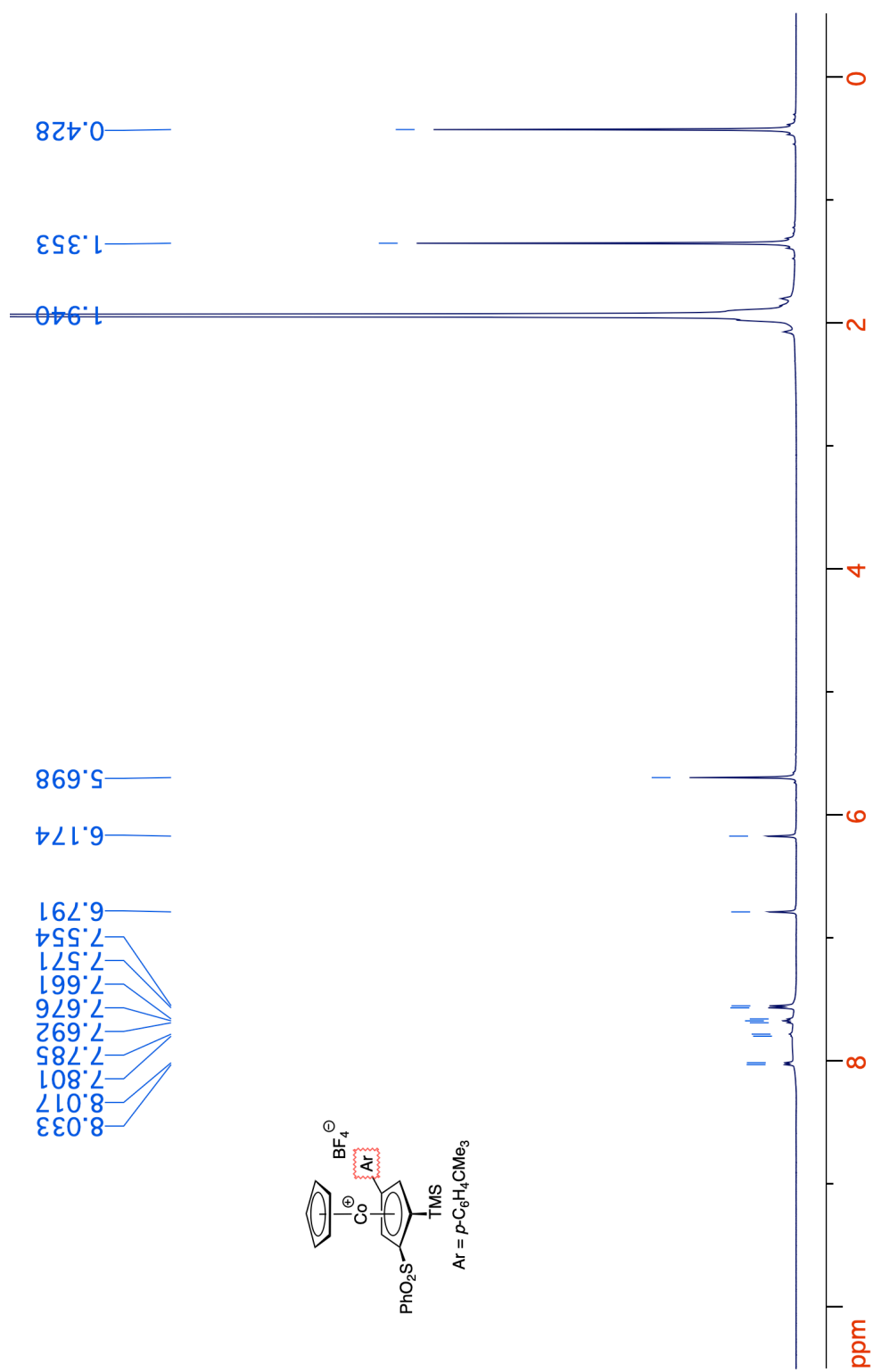
Figure 3-67. ^{1}H NMR spectrum (400 MHz, CD$_3$CN) of **63**.
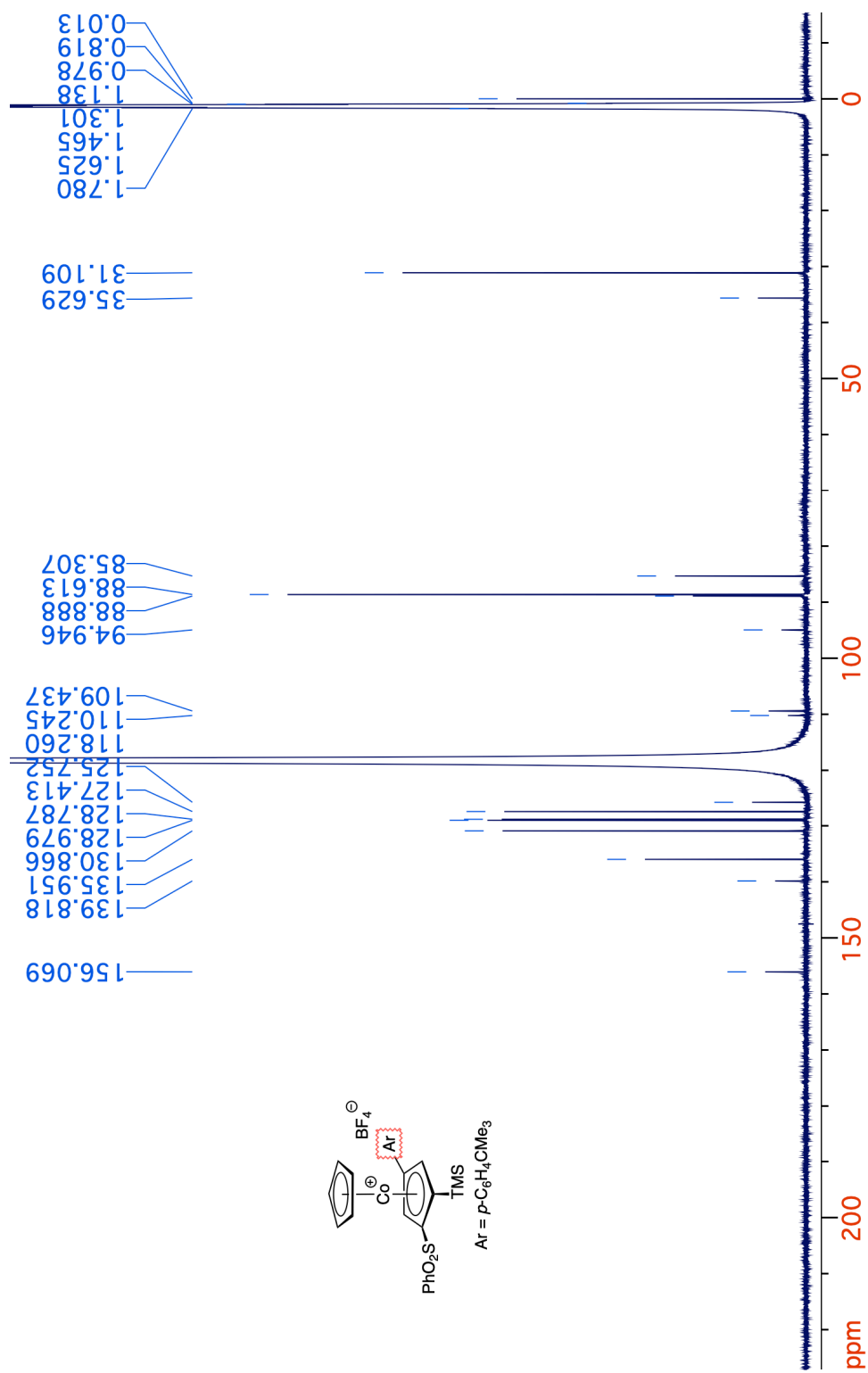
Figure 3-68. $^{13}C\{^1H\}$ NMR spectrum (125 MHz, CD$_3$CN) of **63**.
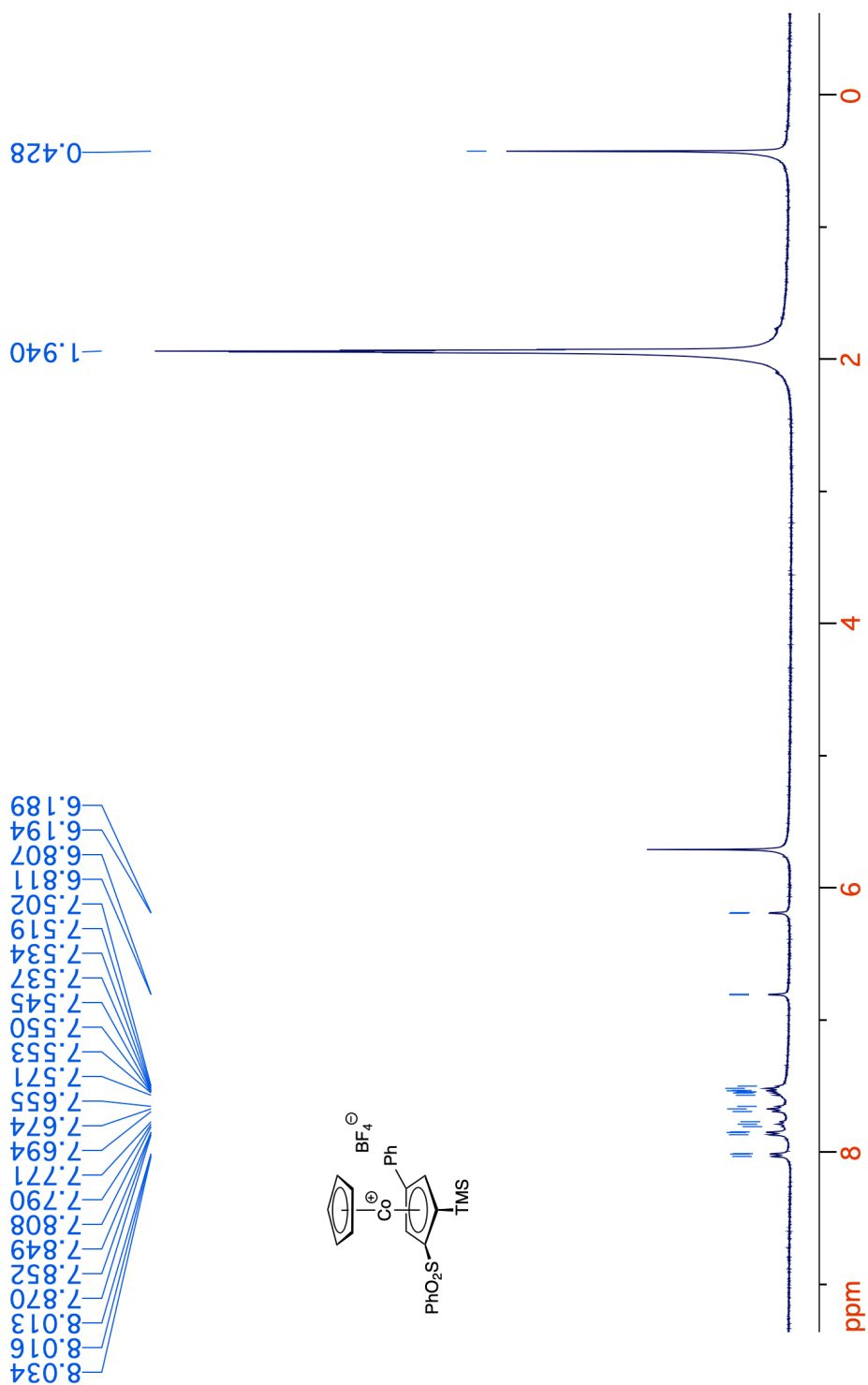
Figure 3-69. ^{1}H NMR spectrum (400 MHz, CD$_3$CN) of **64**.
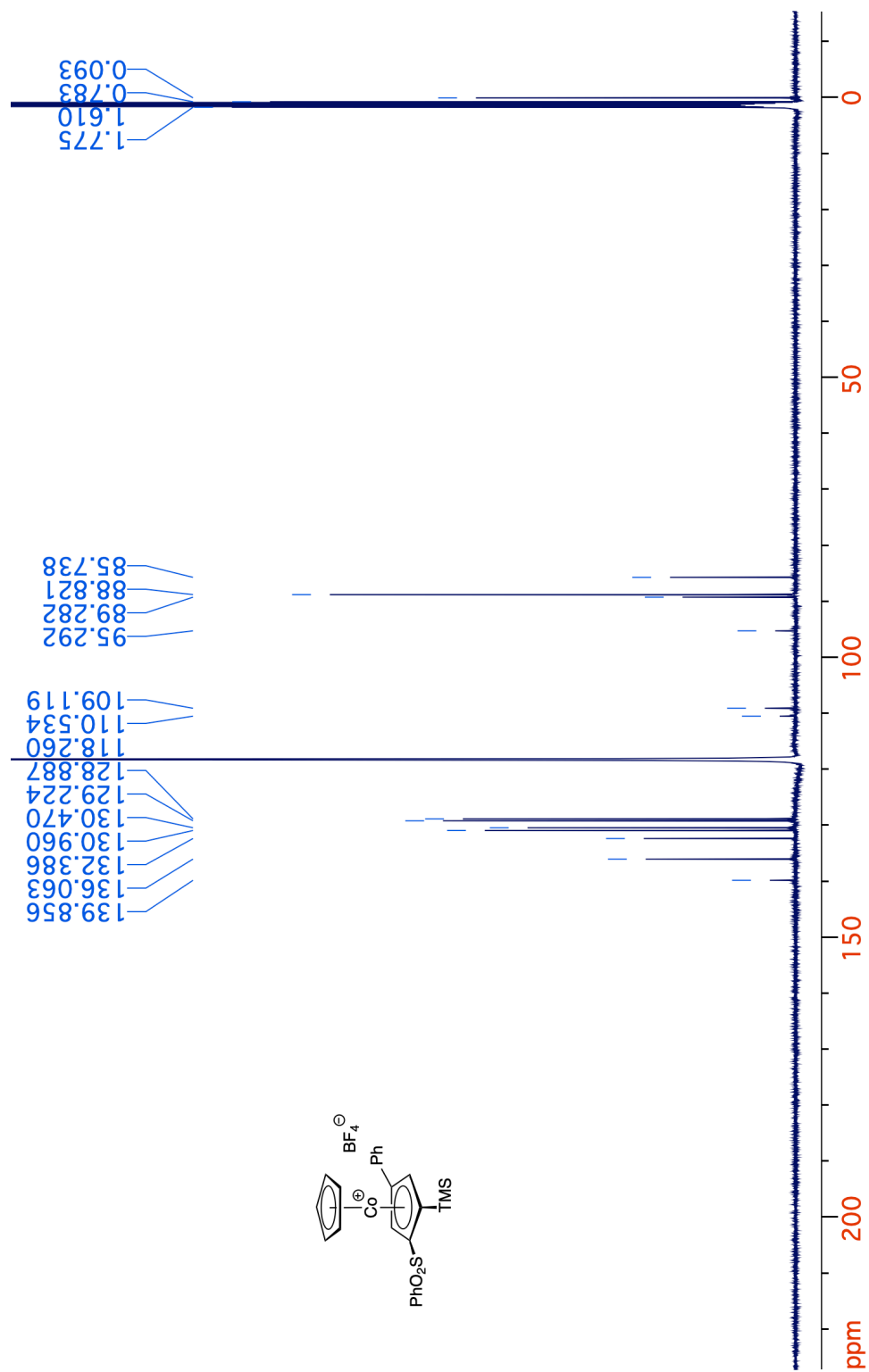
Figure 3-70. $^{13}C\{^1H\}$ NMR spectrum (125 MHz, CD$_3$CN) of **64**.
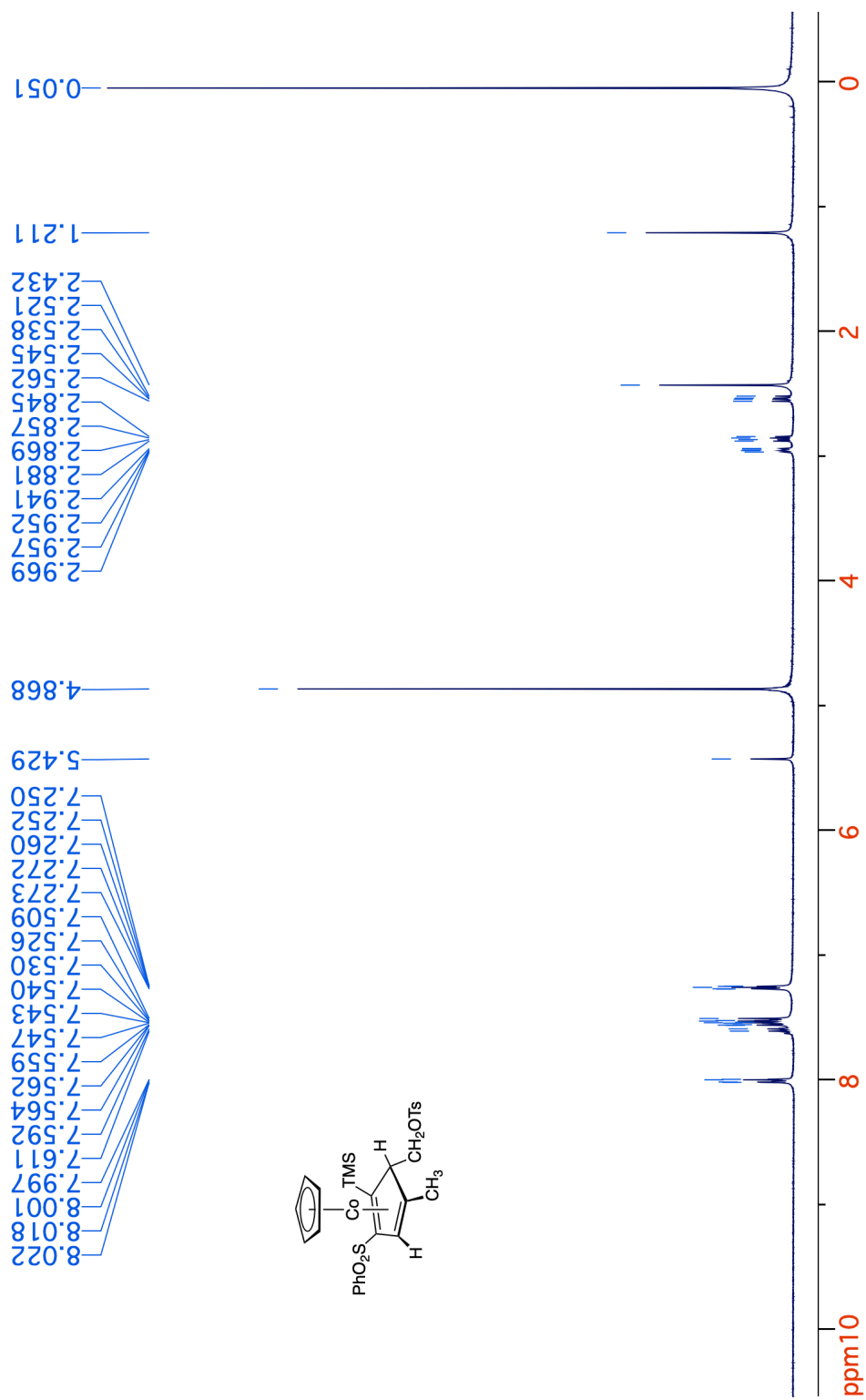
Figure 3-71. ^{1}H NMR spectrum (400 MHz, CDCl$_3$) of **74**.
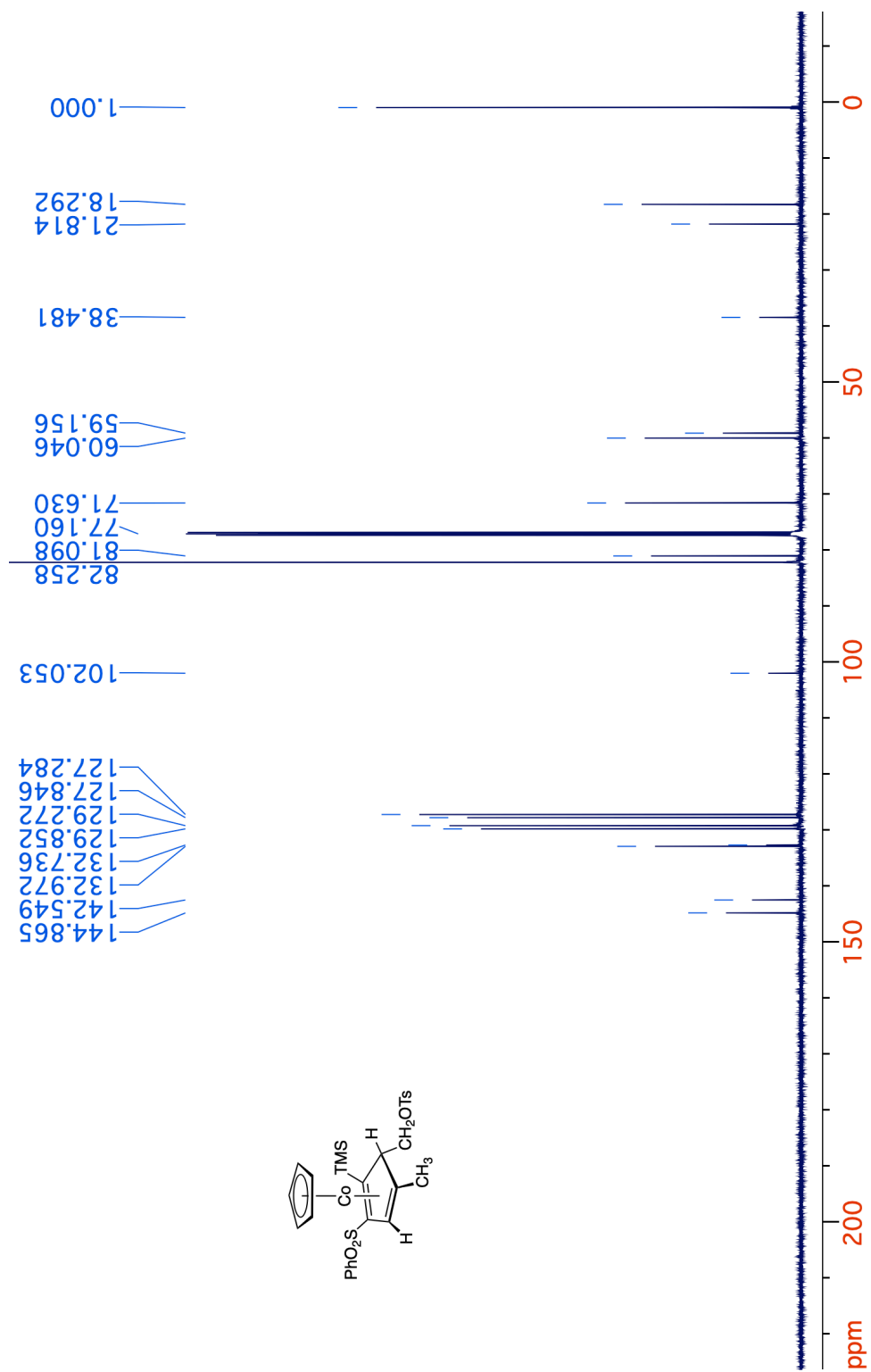
Figure 3-72. $^{13}C\{^{1}H\}$ NMR spectrum (125 MHz, CDCl$_3$) of **74**.

Figure 3-73. ^{1}H NMR spectrum (400 MHz, CDCl$_3$) of **75**.
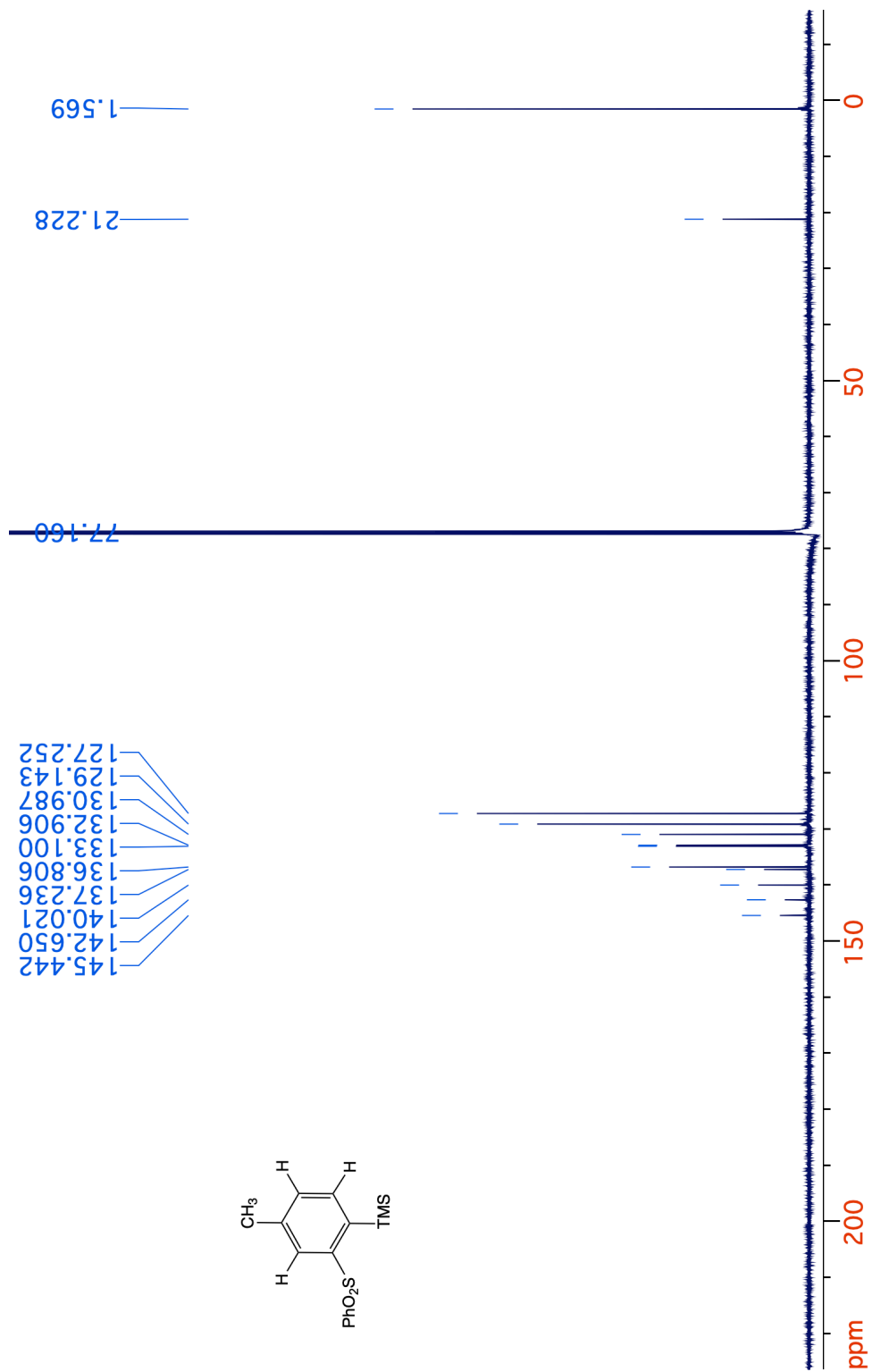
Figure 3-74. $^{13}C\{^1H\}$ NMR spectrum (125 MHz, CDCl$_3$) of **75**.
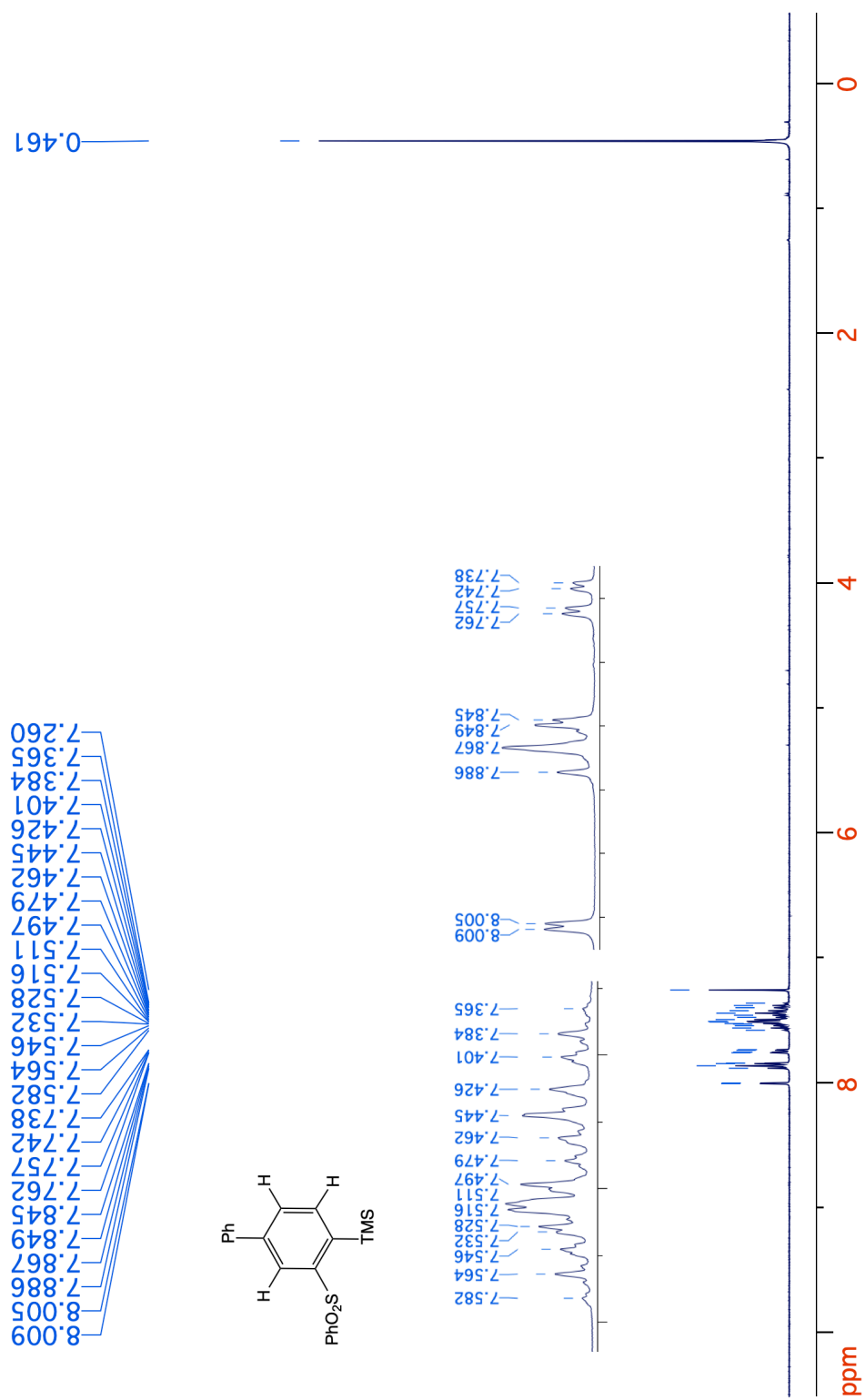
Figure 3-75. ¹H NMR spectrum (400 MHz, CDCl₃) of **78**.
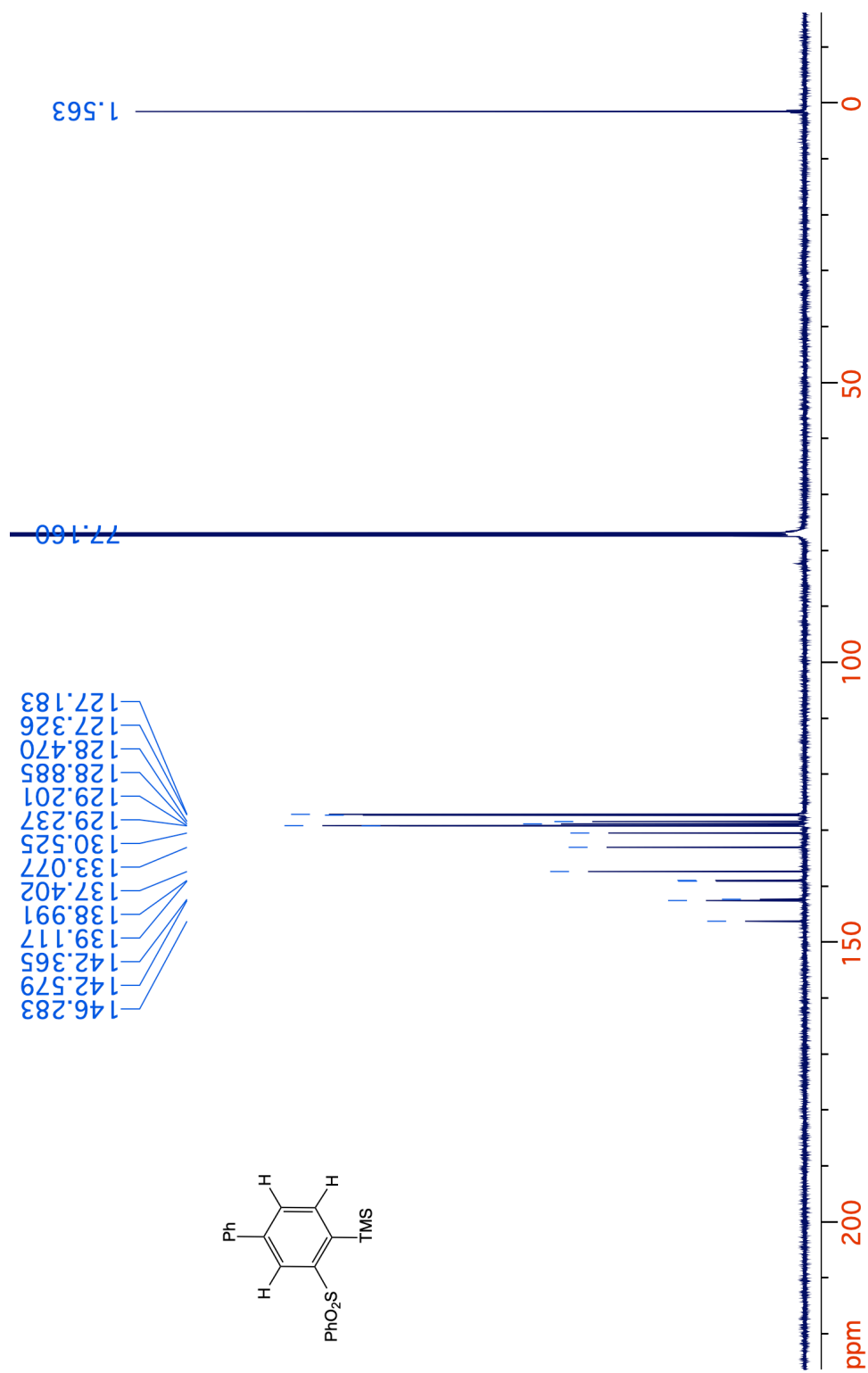
Figure 3-76. $^{13}C\{^1H\}$ NMR spectrum (125 MHz, CDCl$_3$) of **78**.

0.393

1.361
1.377
1.378
1.394
1.396

3.980
3.996
3.998
4.013
4.015
4.032

7.023
7.030
7.044
7.051
7.260
7.261
7.297
7.301
7.489
7.491
7.509
7.541
7.544
7.560
7.578
7.581
7.680
7.701
7.807
7.827
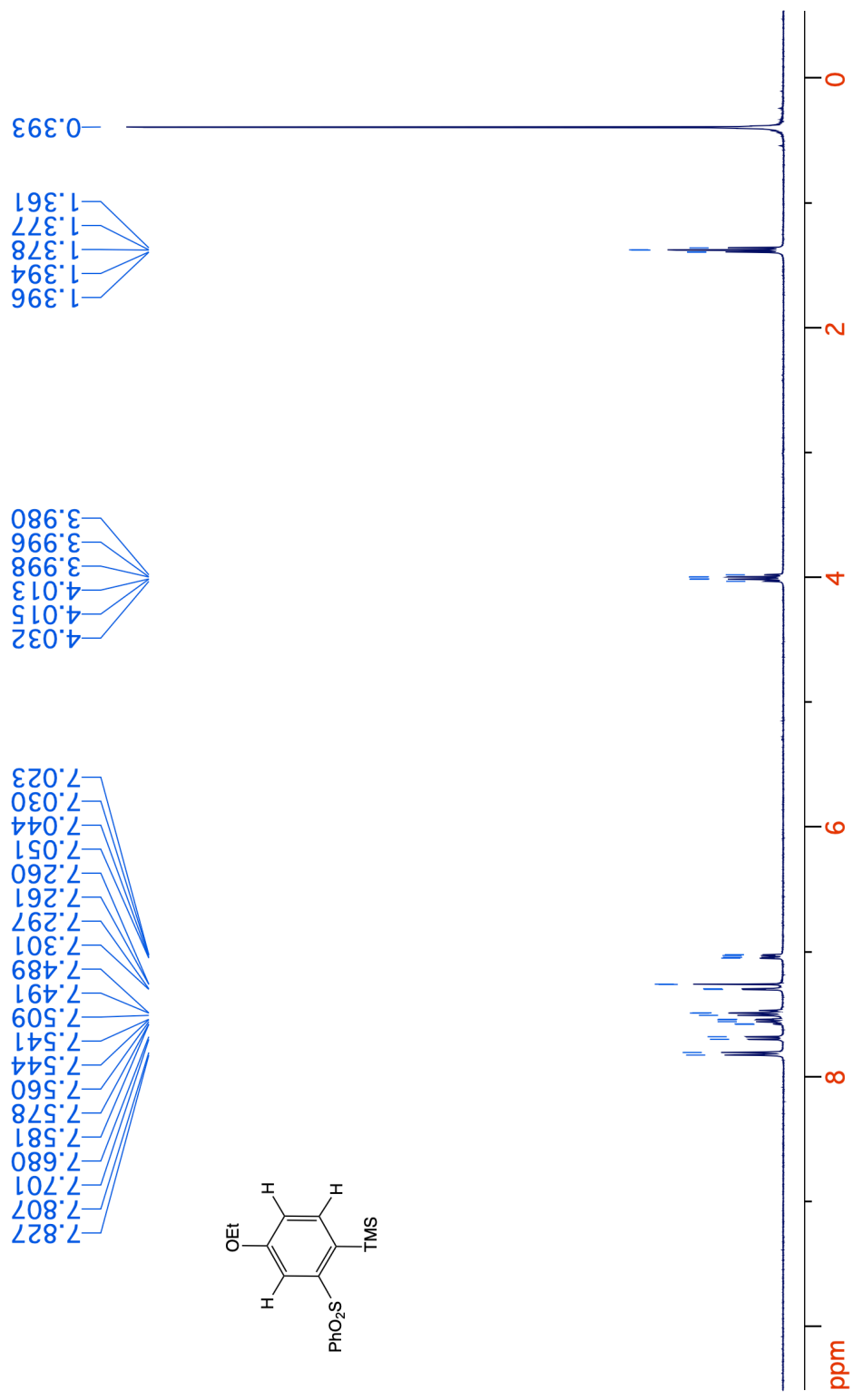
Figure 3-77. ^{1}H NMR spectrum (400 MHz, CDCl$_3$) of **79**.

385
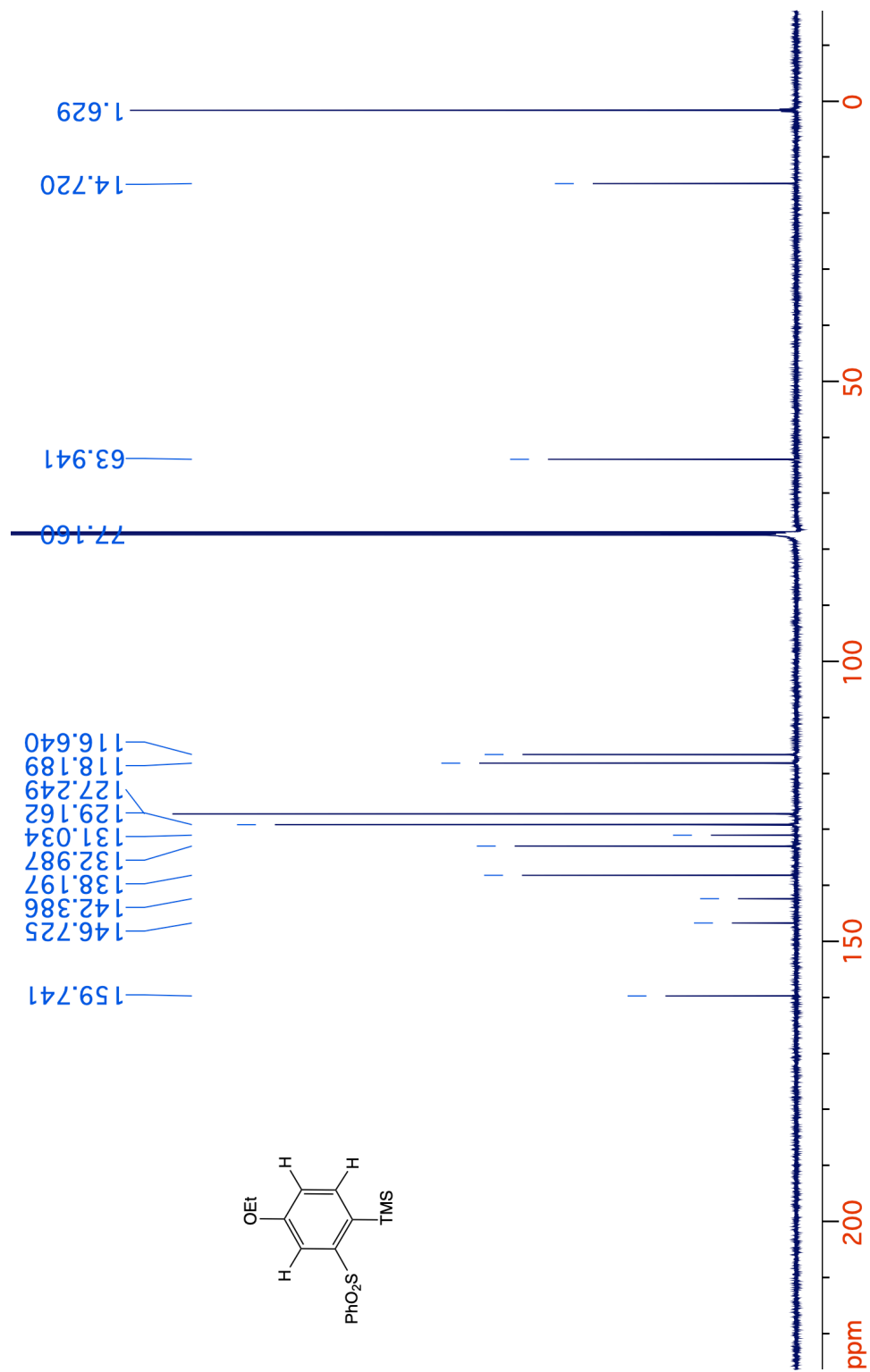
Figure 3-78. $^{13}C\{^1H\}$ NMR spectrum (125 MHz, CDCl$_3$) of **79**.

1.629
14.720
63.941
77.160
116.640
118.189
127.249
129.162
131.034
132.987
138.197
142.386
146.725
159.741
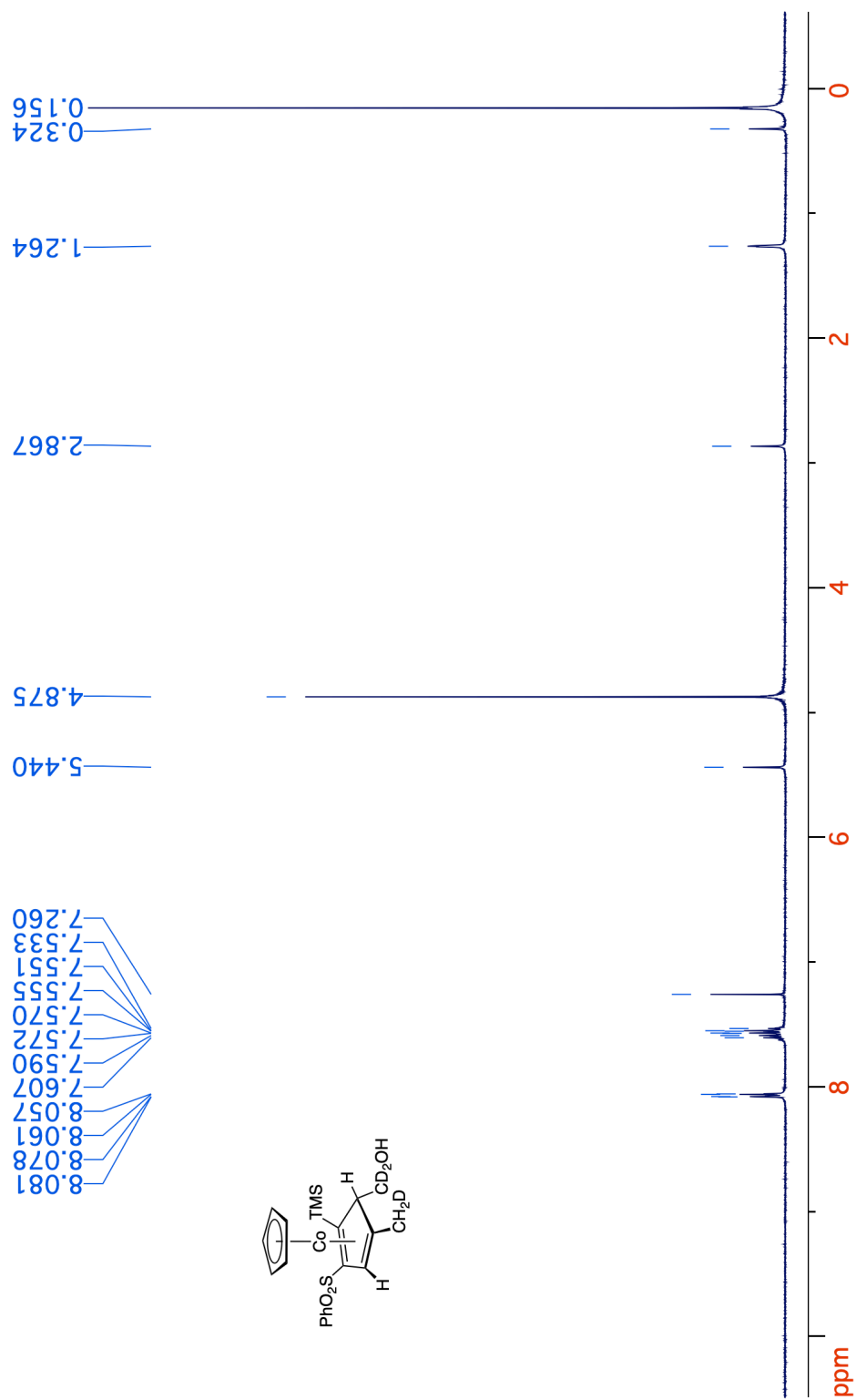
Figure 3-79. ^{1}H NMR spectrum (400 MHz, CDCl$_3$) of **82**.
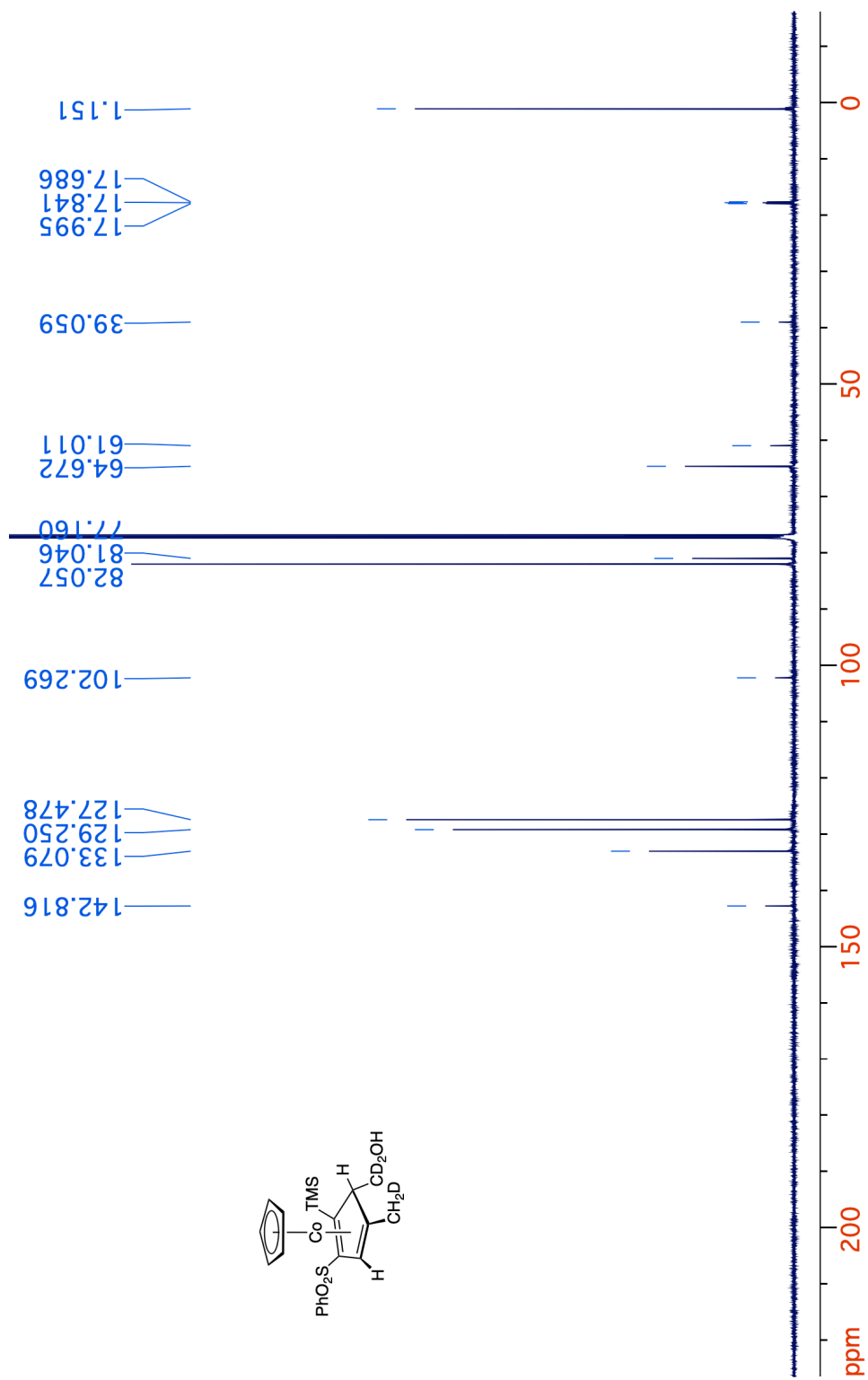
Figure 3-80. $^{13}C\{^1H\}$ NMR spectrum (125 MHz, CDCl$_3$) of **82**.
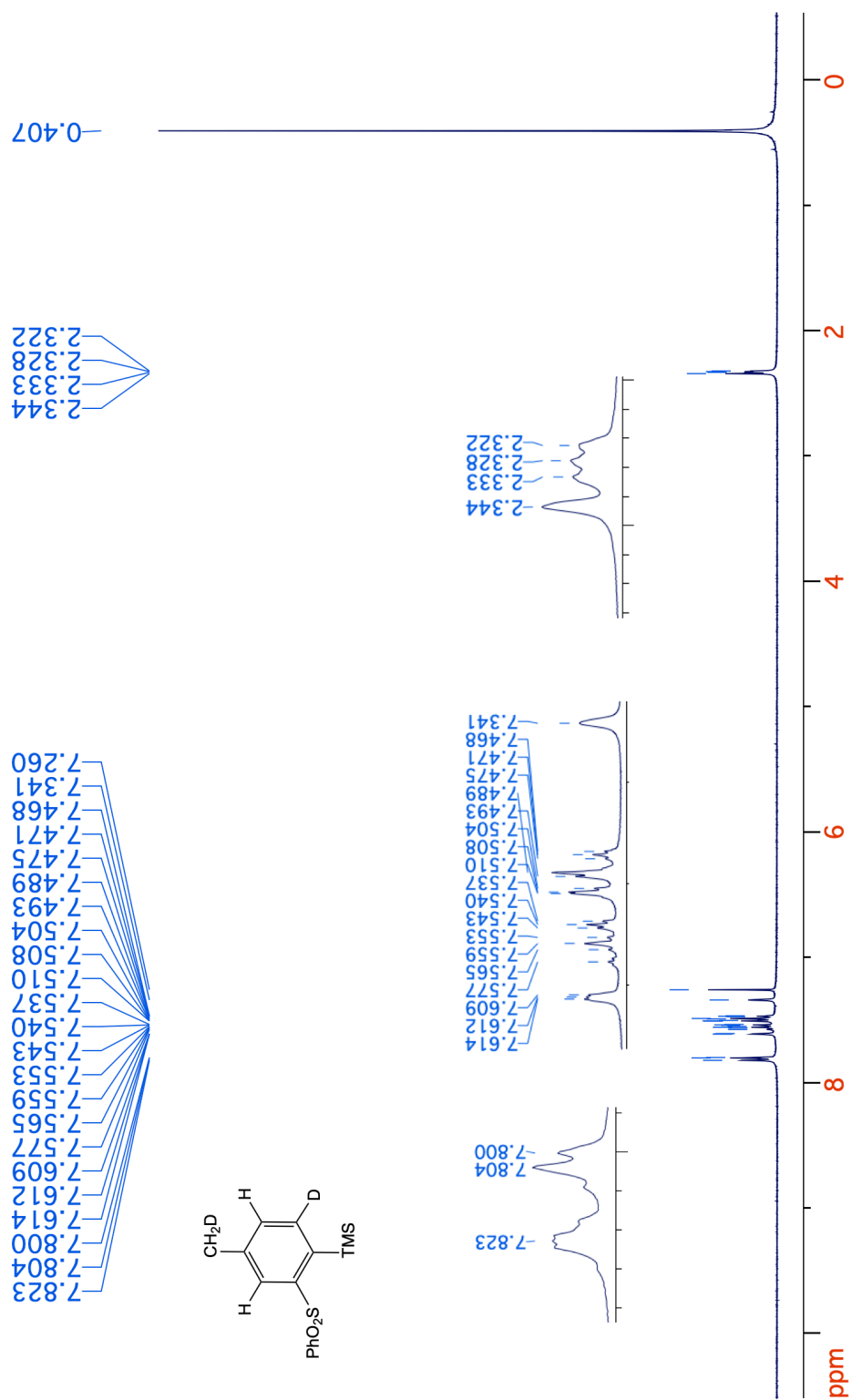
Figure 3-81. ^{1}H NMR spectrum (400 MHz, CDCl$_3$) of **83**.
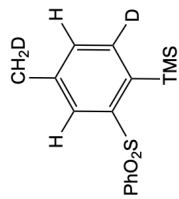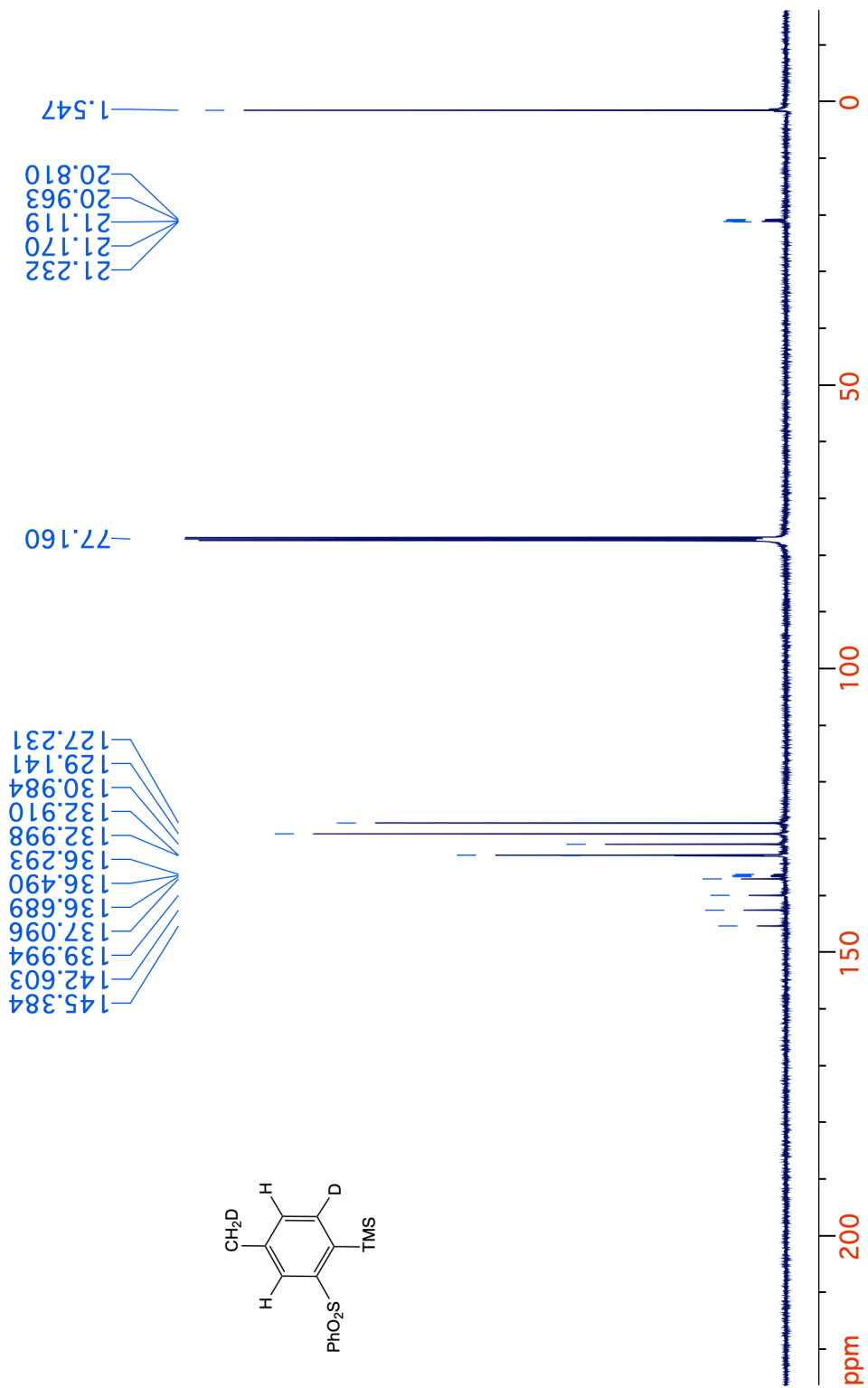
Figure 3-82. $^{13}C\{^1H\}$ NMR spectrum (125 MHz, CDCl$_3$) of **83**.

390
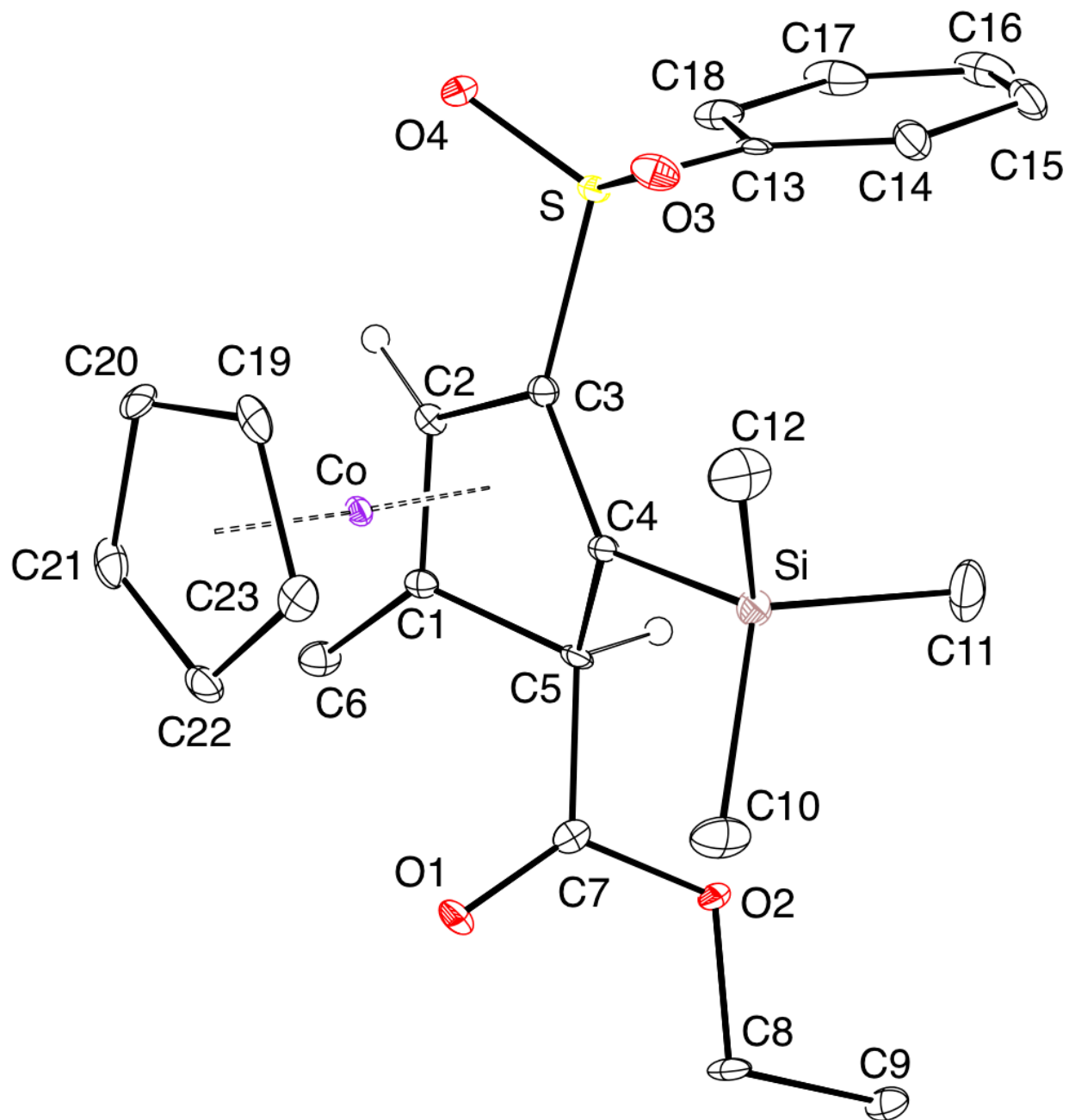
Figure 3-83. ORTEP view of complex **4**-*endo*. Ellipsoids shown at 30% probability. Most hydrogens are omitted for clarity.

Table 3-16. Crystal data and structure refinement for complex **4**-*endo*.

Identification code	RLH3172
Empirical formula	C23 H29 Co O4 S Si
Molecular formula	C23 H29 Co O4 S Si
Formula weight	488.54
Temperature	100.0 K
Wavelength	0.71073 Å
Crystal system	Monoclinic
Space group	P 1 21/c 1
Unit cell dimensions	a = 13.4968(16) Å $\alpha = 90°$.
	b = 7.5472(8) Å $\beta = 92.229(4)°$.
	c = 22.596(3) Å $\gamma = 90°$.
Volume	2299.9(5) Å^3
Z	4
Density (calculated)	1.411 Mg/m^3
Absorption coefficient	0.916 mm^{-1}
F(000)	1024
Crystal size	0.275 x 0.053 x 0.047 mm^3
Crystal color, habit	Dark Red Needle
Theta range for data collection	2.397 to 25.363°.
Index ranges	-15<=h<=16, -8<=k<=9, -27<=l<=27
Reflections collected	34687
Independent reflections	4172 [R(int) = 0.0834, R(sigma) = 0.0618]
Completeness to theta = 25.000°	99.1 %
Absorption correction	Semi-empirical from equivalents
Max. and min. transmission	0.0916 and 0.0632
Refinement method	Full-matrix least-squares on F^2
Data / restraints / parameters	4172 / 0 / 276
Goodness-of-fit on F^2	1.040
Final R indices [I>2sigma(I)]	R1 = 0.0413, wR2 = 0.0799
R indices (all data)	R1 = 0.0729, wR2 = 0.0885
Extinction coefficient	n/a
Largest diff. peak and hole	0.418 and -0.360 e.Å^{-3}
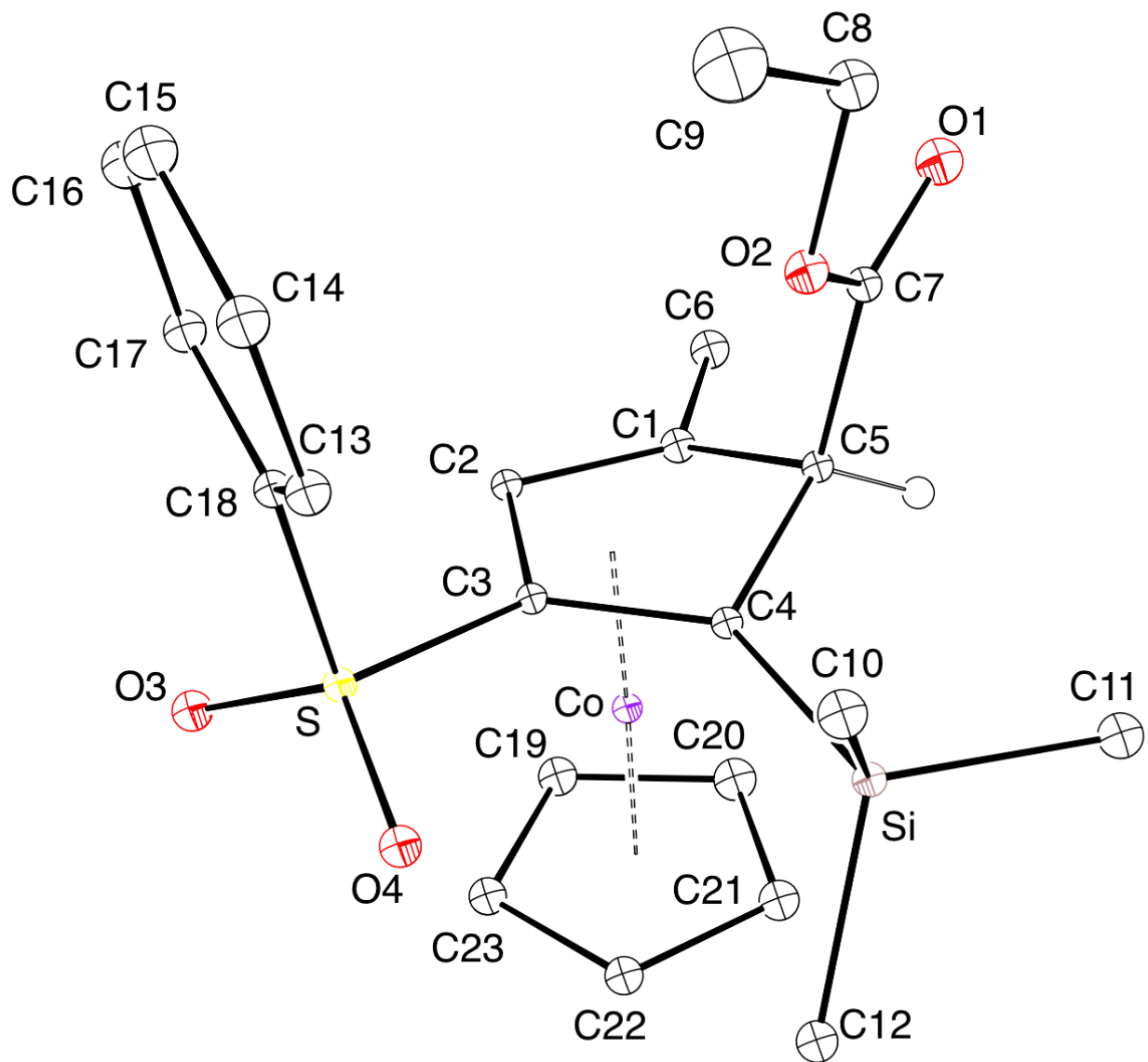
Figure 3-84. ORTEP view of complex **4**-*exo*. Ellipsoids shown at 30% probability. Most hydrogens are omitted for clarity.

Table 3-17. Crystal data and structure refinement for complex **4**-*exo*.

Identification code	PQ_0286
Empirical formula	C23 H29 Co O4 S Si
Molecular formula	C23 H29 Co O4 S Si
Formula weight	488.54
Temperature	100 K
Wavelength	0.71073 Å
Crystal system	Triclinic
Space group	P-1
Unit cell dimensions	a = 8.0451(4) Å α = 93.161(2)°.
	b = 10.2823(5) Å β = 95.413(2)°.
	c = 13.9360(7) Å γ = 99.585(2)°.
Volume	1128.70(10) Å^3
Z	2
Density (calculated)	1.437 Mg/m^3
Absorption coefficient	0.933 mm^{-1}
F(000)	512
Crystal size	0.33 x 0.22 x 0.11 mm^3
Crystal color, habit	Dark Red Block
Theta range for data collection	2.407 to 26.394°.
Index ranges	-9<=h<=10, -12<=k<=12, -17<=l<=11
Reflections collected	17416
Independent reflections	4612 [R(int) = 0.0339, R(sigma) = 0.0313]
Completeness to theta = 25.000°	99.9 %
Absorption correction	Semi-empirical from equivalents
Max. and min. transmission	0.0932 and 0.0681
Refinement method	Full-matrix least-squares on F^2
Data / restraints / parameters	4612 / 0 / 276
Goodness-of-fit on F^2	1.034
Final R indices [I>2sigma(I)]	R1 = 0.0261, wR2 = 0.0603
R indices (all data)	R1 = 0.0330, wR2 = 0.0638
Extinction coefficient	n/a
Largest diff. peak and hole	0.392 and -0.313 e.Å^{-3}
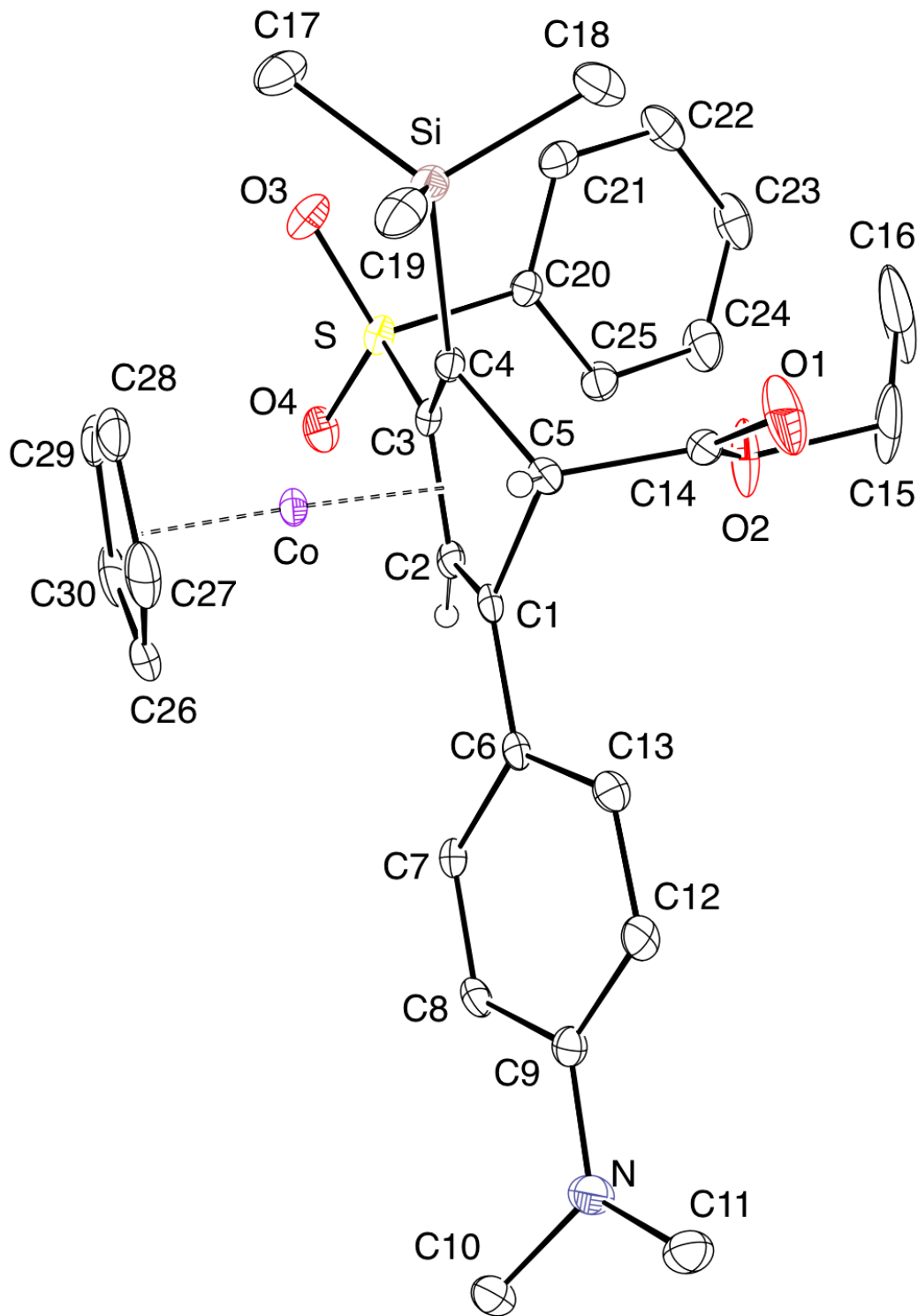
Figure 3-85. ORTEP view of complex **5**-*exo*. Ellipsoids shown at 30% probability. Most hydrogens are omitted for clarity.

Table 3-18. Crystal data and structure refinement for complex **5**-*exo*.

Identification code	RLH3140
Empirical formula	C30 H36 Co N O4 S Si
Molecular formula	C30 H36 Co N O4 S Si
Formula weight	593.68
Temperature	100 K
Wavelength	0.71073 Å
Crystal system	Monoclinic
Space group	P 1 21/n 1
Unit cell dimensions	a = 9.9138(7) Å α = 90°.
	b = 25.5906(18) Å β = 95.532(2)°.
	c = 11.2910(8) Å γ = 90°.
Volume	2851.2(3) Å^3
Z	4
Density (calculated)	1.383 Mg/m^3
Absorption coefficient	0.753 mm^{-1}
F(000)	1248
Crystal size	0.293 x 0.271 x 0.054 mm^3
Crystal color, habit	Red Plate
Theta range for data collection	2.212 to 25.619°.
Index ranges	-11<=h<=12, -30<=k<=31, -13<=l<=12
Reflections collected	38677
Independent reflections	5315 [R(int) = 0.0877, R(sigma) = 0.0604]
Completeness to theta = 25.000°	100.0 %
Absorption correction	Semi-empirical from equivalents
Max. and min. transmission	0.0916 and 0.0590
Refinement method	Full-matrix least-squares on F^2
Data / restraints / parameters	5315 / 30 / 360
Goodness-of-fit on F^2	1.059
Final R indices [I>2sigma(I)]	R1 = 0.0475, wR2 = 0.0924
R indices (all data)	R1 = 0.0791, wR2 = 0.1027
Extinction coefficient	n/a
Largest diff. peak and hole	0.469 and -0.290 e.Å^{-3}

Figure 3-86. ORTEP view of complex **7**-*exo*. Ellipsoids shown at 30% probability. Most hydrogens are omitted for clarity.

Table 3-19. Crystal data and structure refinement for complex **7**-*exo*.

Identification code	RLH3153
Empirical formula	C23 H31 Co O6 S Si
Molecular formula	C23 H29 Co O5 S Si, H2 O
Formula weight	522.56
Temperature	100.0 K
Wavelength	0.71073 Å
Crystal system	Monoclinic
Space group	P 1 21/c 1
Unit cell dimensions	a = 17.283(4) Å $\quad$ α = 90°.
	b = 16.874(4) Å $\quad$ β = 97.070(4)°.
	c = 8.4432(19) Å $\quad$ γ = 90°.
Volume	2443.6(9) Å^3
Z	4
Density (calculated)	1.420 Mg/m^3
Absorption coefficient	0.873 mm^{-1}
F(000)	1096
Crystal size	0.186 x 0.117 x 0.095 mm^3
Crystal color, habit	Reddish Orange Block
Theta range for data collection	1.693 to 25.398°.
Index ranges	-20<=h<=13, -20<=k<=20, -10<=l<=10
Reflections collected	20682
Independent reflections	4477 [R(int) = 0.0333, R(sigma) = 0.0261]
Completeness to theta = 25.000°	100.0 %
Absorption correction	Semi-empirical from equivalents
Max. and min. transmission	0.0916 and 0.0653
Refinement method	Full-matrix least-squares on F^2
Data / restraints / parameters	4477 / 3 / 305
Goodness-of-fit on F^2	1.022
Final R indices [I>2sigma(I)]	R1 = 0.0304, wR2 = 0.0734
R indices (all data)	R1 = 0.0401, wR2 = 0.0784
Extinction coefficient	n/a
Largest diff. peak and hole	0.381 and -0.331 e.Å^{-3}

Figure 3-87. ORTEP view of complex **8**-*endo*. Ellipsoids shown at 30% probability. Most hydrogens are omitted for clarity.

399

Table 3-20. Crystal data and structure refinement for complex **8**-*endo*.

Identification code	RLH3175
Empirical formula	C28 H31 Co O4 S Si
Molecular formula	C28 H31 Co O4 S Si
Formula weight	550.61
Temperature	100.0 K
Wavelength	0.71073 Å
Crystal system	Triclinic
Space group	P-1
Unit cell dimensions	a = 7.5848(2) Å α = 102.6270(10)°.
	b = 12.2189(3) Å β = 97.0260(10)°.
	c = 15.2124(5) Å γ = 104.7290(10)°.
Volume	1306.69(6) Å^3
Z	2
Density (calculated)	1.399 Mg/m^3
Absorption coefficient	0.815 mm^{-1}
F(000)	576
Crystal size	0.315 x 0.269 x 0.247 mm^3
Crystal color, habit	Dark Red Block
Theta range for data collection	2.537 to 25.411°.
Index ranges	-9<=h<=9, -14<=k<=14, -18<=l<=18
Reflections collected	32469
Independent reflections	4806 [R(int) = 0.0450, R(sigma) = 0.0255]
Completeness to theta = 25.000°	99.9 %
Absorption correction	Semi-empirical from equivalents
Max. and min. transmission	0.0916 and 0.0612
Refinement method	Full-matrix least-squares on F^2
Data / restraints / parameters	4806 / 0 / 320
Goodness-of-fit on F^2	1.042
Final R indices [I>2sigma(I)]	R1 = 0.0262, wR2 = 0.0628
R indices (all data)	R1 = 0.0322, wR2 = 0.0658
Extinction coefficient	n/a
Largest diff. peak and hole	0.411 and -0.304 e.Å^{-3}

Figure 3-88. ORTEP view of complex **8**-*exo*. Ellipsoids shown at 30% probability. Most hydrogens are omitted for clarity.

Table 3-21. Crystal data and structure refinement for complex **8**-*exo*.

Identification code	RLH3176
Empirical formula	C28 H31 Co O4 S Si
Molecular formula	C28 H31 Co O4 S Si
Formula weight	550.61
Temperature	100.0 K
Wavelength	0.71073 Å
Crystal system	Monoclinic
Space group	P 1 21/c 1
Unit cell dimensions	a = 16.003(3) Å $\quad$ α = 90°.
	b = 16.012(3) Å $\quad$ β = 104.637(10)°.
	c = 10.400(2) Å $\quad$ γ = 90°.
Volume	2578.6(9) Å^3
Z	4
Density (calculated)	1.418 Mg/m^3
Absorption coefficient	0.826 mm^{-1}
F(000)	1152
Crystal size	0.146 x 0.131 x 0.027 mm^3
Crystal color, habit	Red Plate
Theta range for data collection	1.830 to 25.525°.
Index ranges	-19<=h<=19, -19<=k<=19, -12<=l<=12
Reflections collected	29413
Independent reflections	4717 [R(int) = 0.0657, R(sigma) = 0.0454]
Completeness to theta = 25.000°	99.9 %
Absorption correction	Semi-empirical from equivalents
Max. and min. transmission	0.0916 and 0.0441
Refinement method	Full-matrix least-squares on F^2
Data / restraints / parameters	4717 / 0 / 320
Goodness-of-fit on F^2	1.030
Final R indices [I>2sigma(I)]	R1 = 0.0373, wR2 = 0.0886
R indices (all data)	R1 = 0.0557, wR2 = 0.0972
Extinction coefficient	n/a
Largest diff. peak and hole	0.497 and -0.480 e.Å^{-3}
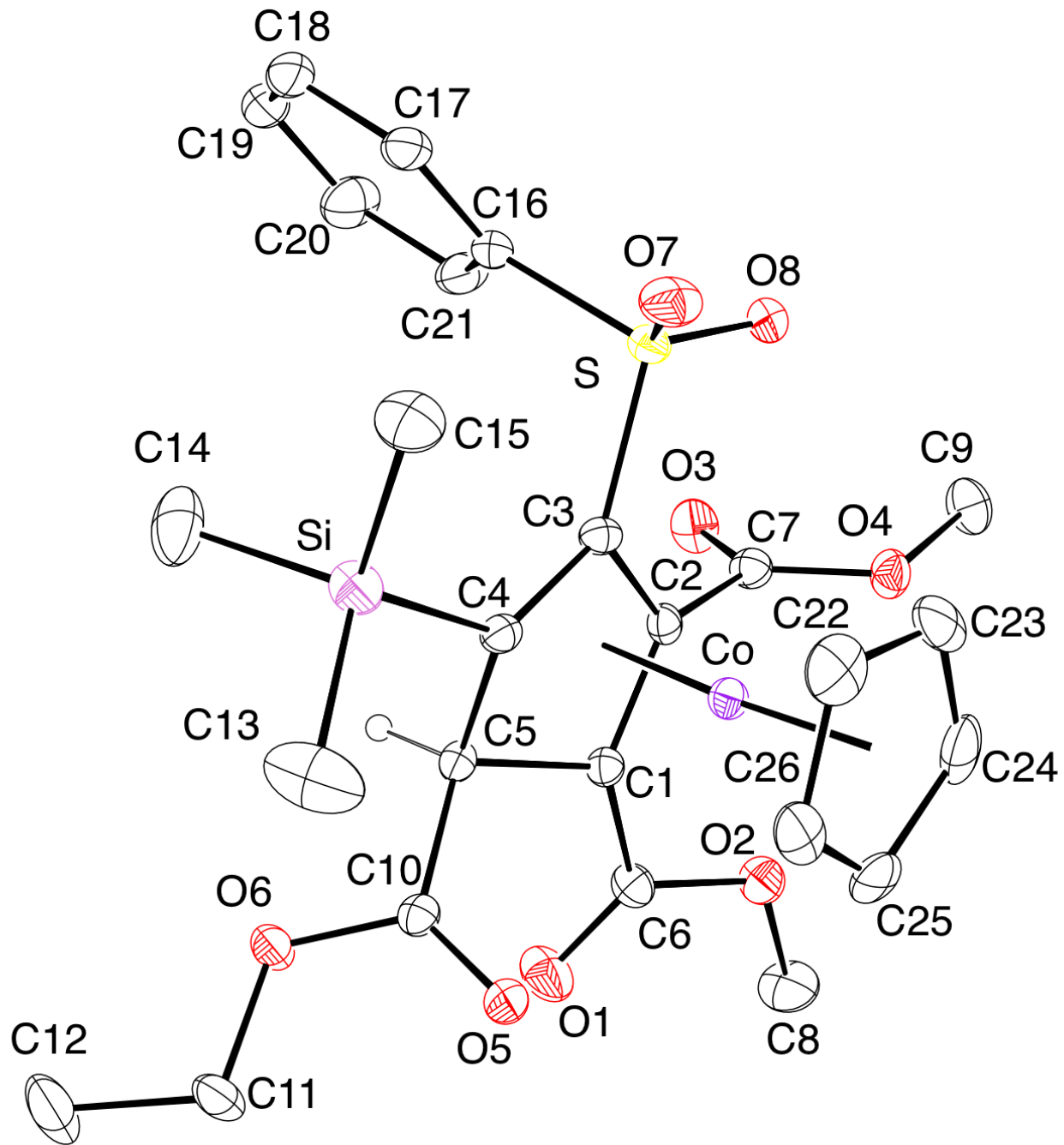
Figure 3-89. ORTEP view of complex **10**-*endo*. Ellipsoids shown at 30% probability. Most hydrogens are omitted for clarity.

Table 3-22. Crystal data and structure refinement for complex **10**-*endo*.

Identification code	oconn_pq_0753_0m_a
Empirical formula	C H0.25 Br0 Co0.25 O0.25 S0.25 Si0.25
Formula weight	46.03
Temperature	100.0 K
Wavelength	0.71073 Å
Crystal system	Monoclinic
Space group	P 1 21 1
Unit cell dimensions	a = 10.737(6) Å α = 90°.
	b = 12.991(7) Å β = 116.593(9)°.
	c = 11.016(6) Å γ = 90°.
Volume	1374.1(13) Å^3
Z	4
Density (calculated)	0.223 Mg/m^3
Absorption coefficient	0.359 mm^{-1}
F(000)	90
Crystal size	0.15 x 0.13 x 0.04 mm^3
Theta range for data collection	2.067 to 25.315°.
Index ranges	-12<=h<=12, -13<=k<=15, -13<=l<=13
Reflections collected	7707
Independent reflections	4458 [R(int) = 0.0245]
Completeness to theta = 25.242°	100.0 %
Absorption correction	None
Max. and min. transmission	0.2590 and 0.2251
Refinement method	Full-matrix least-squares on F^2
Data / restraints / parameters	4458 / 1 / 340
Goodness-of-fit on F^2	0.983
Final R indices [I>2sigma(I)]	R1 = 0.0286, wR2 = 0.0592
R indices (all data)	R1 = 0.0325, wR2 = 0.0608
Absolute structure parameter	0.030(9)
Extinction coefficient	n/a
Largest diff. peak and hole	0.231 and -0.218 e.Å^{-3}
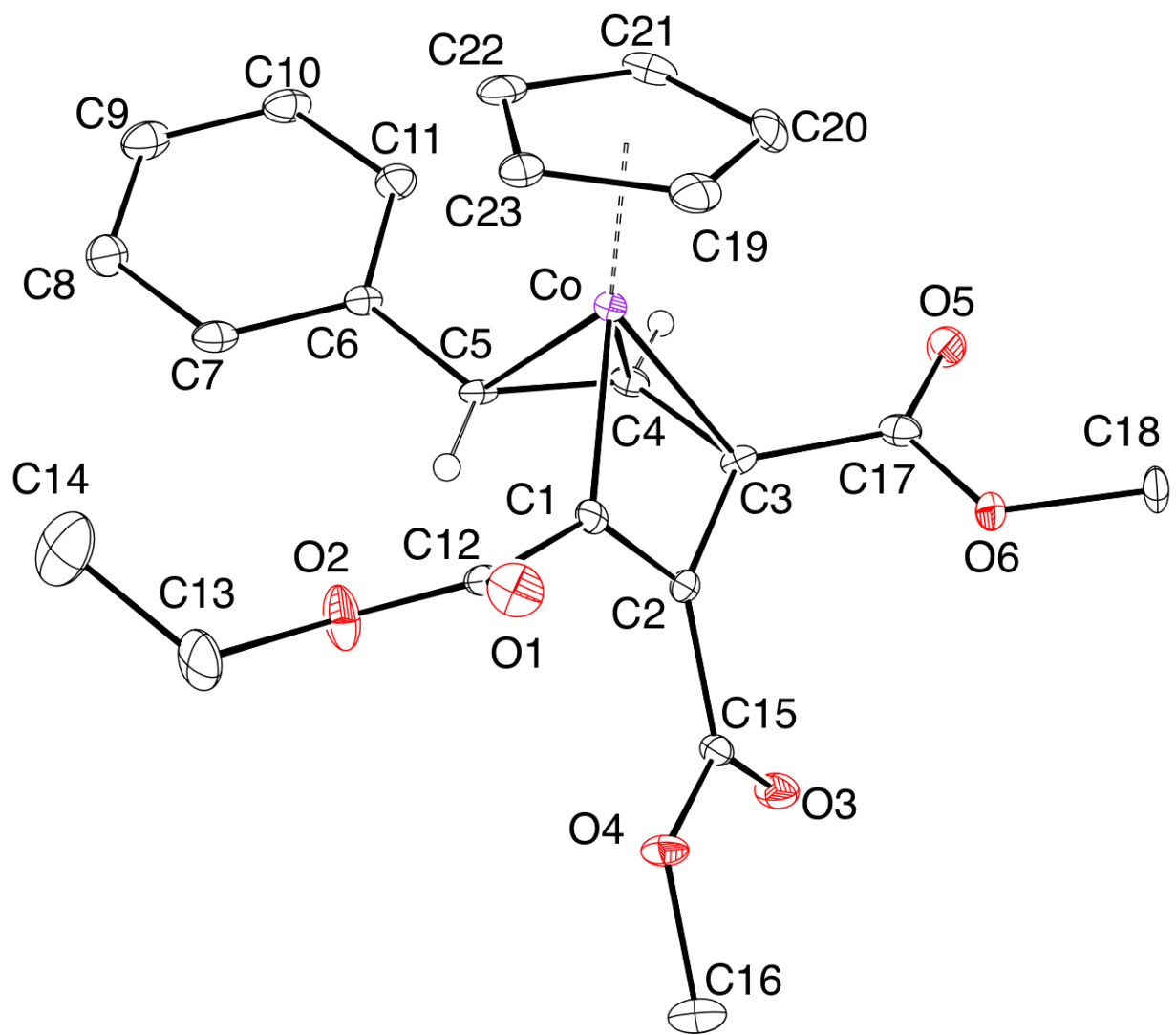
Figure 3-90. ORTEP view of complex **16**. Ellipsoids shown at 30% probability. Most hydrogens are omitted for clarity.

Table 3-23. Crystal data and structure refinement for complex **16**.

Identification code	pq_418
Empirical formula	C30 H31 Co O6
Formula weight	546.48
Temperature	100.0 K
Wavelength	0.71073 Å
Crystal system	Monoclinic
Space group	P 1 21 1
Unit cell dimensions	a = 7.1764(2) Å $\quad$ $\alpha = 90°$.
	b = 21.2149(8) Å $\quad$ $\beta = 91.2800(10)°$.
	c = 8.7511(3) Å $\quad$ $\gamma = 90°$.
Volume	1331.99(8) Å^3
Z	2
Density (calculated)	1.363 Mg/m^3
Absorption coefficient	0.686 mm^{-1}
F(000)	572
Crystal size	0.15 x 0.12 x 0.1 mm^3
Theta range for data collection	1.920 to 26.749°.
Index ranges	-9<=h<=7, -26<=k<=26, -11<=l<=10
Reflections collected	20891
Independent reflections	5597 [R(int) = 0.0291]
Completeness to theta = 26.000°	99.8 %
Absorption correction	Semi-empirical from equivalents
Max. and min. transmission	0.3775 and 0.3524
Refinement method	Full-matrix least-squares on F^2
Data / restraints / parameters	5597 / 46 / 339
Goodness-of-fit on F^2	1.100
Final R indices [I>2sigma(I)]	R1 = 0.0426, wR2 = 0.1125
R indices (all data)	R1 = 0.0439, wR2 = 0.1131
Absolute structure parameter	0.04(2)
Extinction coefficient	n/a
Largest diff. peak and hole	0.900 and -0.907 e.Å^{-3}
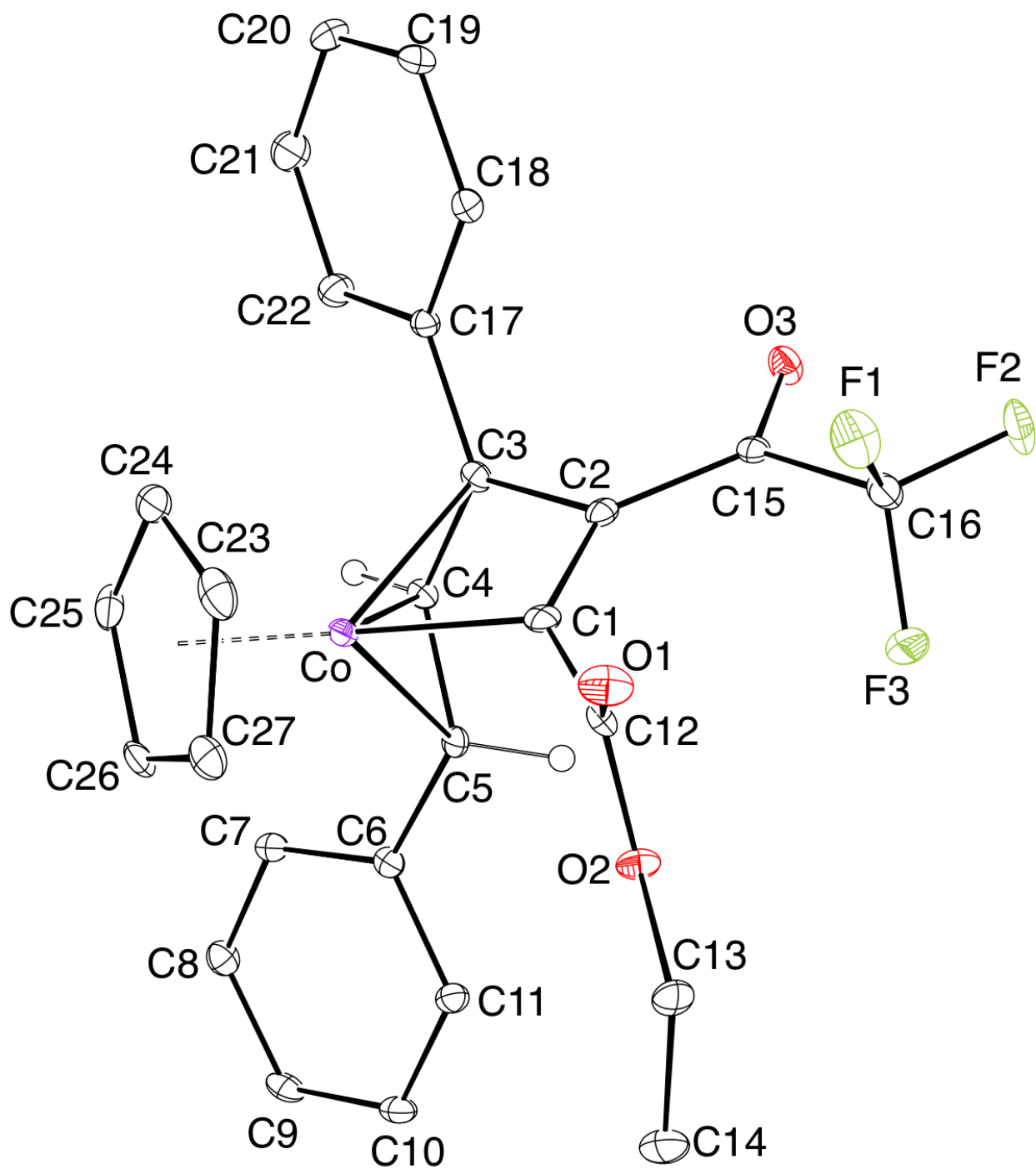
Figure 3-91. ORTEP view of complex **23**. Ellipsoids shown at 30% probability. Most hydrogens are omitted for clarity.

Table 3-24. Crystal data and structure refinement for complex **23**.

Identification code	pq_0468_a
Empirical formula	C27 H22 Co F3 O3
Formula weight	510.37
Temperature	100.0 K
Wavelength	0.71073 Å
Crystal system	Triclinic
Space group	P-1
Unit cell dimensions	a = 8.9793(5) Å α = 72.445(2)°.
	b = 10.2679(6) Å β = 81.977(2)°.
	c = 13.7765(8) Å γ = 67.563(2)°.
Volume	1118.91(11) Å^3
Z	2
Density (calculated)	1.515 Mg/m^3
Absorption coefficient	0.820 mm^{-1}
F(000)	524
Crystal size	0.253 x 0.217 x 0.062 mm^3
Theta range for data collection	2.717 to 25.318°.
Index ranges	-10<=h<=10, -8<=k<=12, -16<=l<=16
Reflections collected	16167
Independent reflections	4081 [R(int) = 0.0427]
Completeness to theta = 25.000°	99.8 %
Absorption correction	Semi-empirical from equivalents
Max. and min. transmission	0.2590 and 0.2276
Refinement method	Full-matrix least-squares on F^2
Data / restraints / parameters	4081 / 0 / 308
Goodness-of-fit on F^2	1.022
Final R indices [I>2sigma(I)]	R1 = 0.0373, wR2 = 0.0674
R indices (all data)	R1 = 0.0568, wR2 = 0.0727
Extinction coefficient	n/a
Largest diff. peak and hole	0.421 and -0.372 e.Å^{-3}
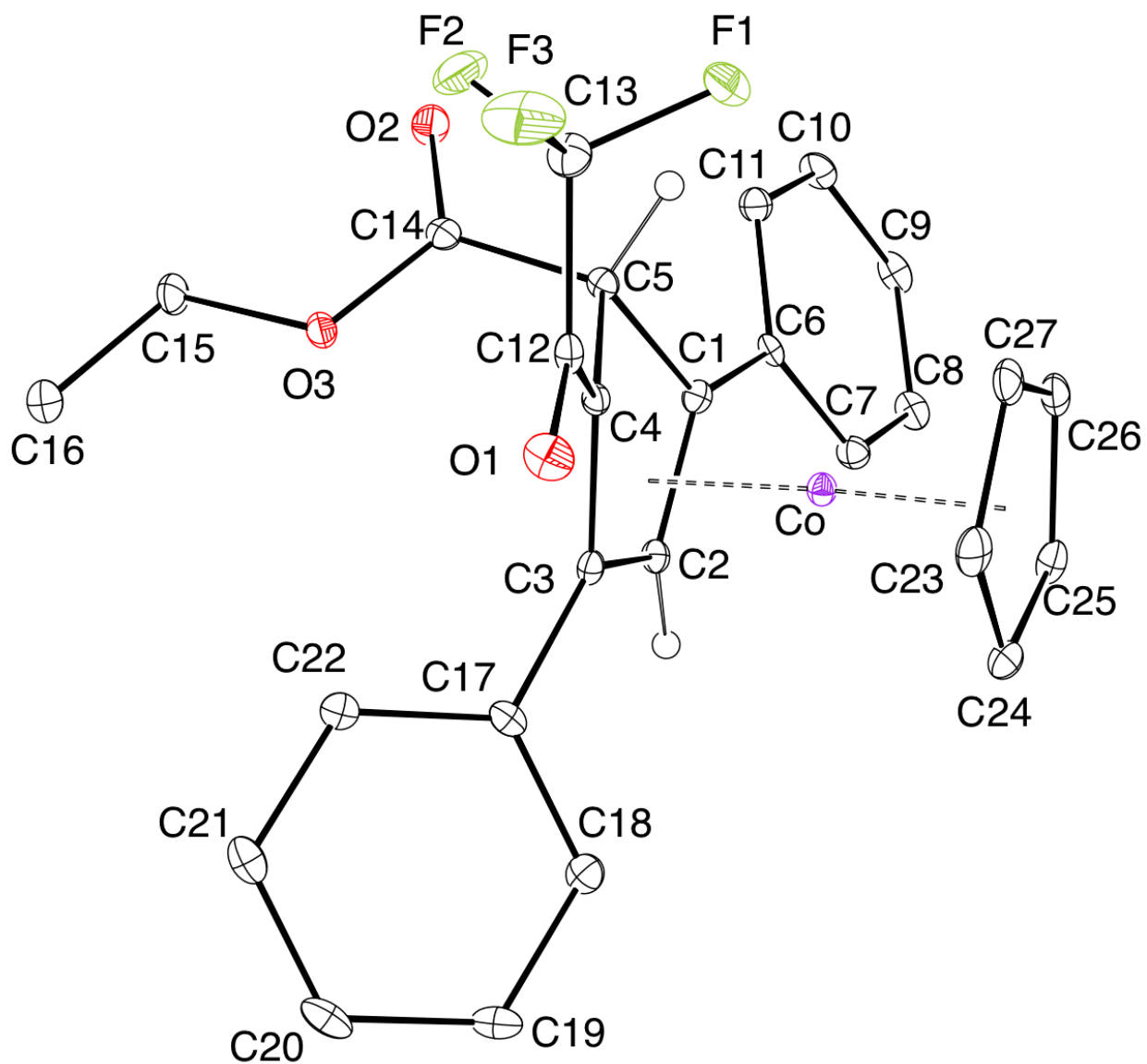
Figure 3-92. ORTEP view of complex **24**. Ellipsoids shown at 30% probability. Most hydrogens are omitted for clarity.

Table 3-25. Crystal data and structure refinement for complex **24**.

Identification code	PQ_434
Empirical formula	C27 H22 Co F3 O3
Molecular formula	C27 H22 Co F3 O3
Formula weight	510.37
Temperature	100 K
Wavelength	0.71073 Å
Crystal system	Triclinic
Space group	P-1
Unit cell dimensions	a = 9.1159(10) Å $\quad\alpha$ = 98.129(4)°.
	b = 10.9174(13) Å $\quad\beta$ = 107.555(4)°.
	c = 12.9484(15) Å $\quad\gamma$ = 110.538(4)°.
Volume	1105.6(2) Å^3
Z	2
Density (calculated)	1.533 Mg/m^3
Absorption coefficient	0.830 mm^{-1}
F(000)	524
Crystal size	0.217 x 0.095 x 0.091 mm^3
Crystal color, habit	Dark Red Block
Theta range for data collection	2.297 to 26.394°.
Index ranges	-11<=h<=9, -13<=k<=13, -15<=l<=16
Reflections collected	20324
Independent reflections	4454 [R(int) = 0.0459, R(sigma) = 0.0487]
Completeness to theta = 25.000°	99.9 %
Absorption correction	Semi-empirical from equivalents
Max. and min. transmission	0.2602 and 0.2314
Refinement method	Full-matrix least-squares on F^2
Data / restraints / parameters	4454 / 0 / 308
Goodness-of-fit on F^2	1.019
Final R indices [I>2sigma(I)]	R1 = 0.0355, wR2 = 0.0653
R indices (all data)	R1 = 0.0521, wR2 = 0.0711
Extinction coefficient	n/a
Largest diff. peak and hole	0.431 and -0.326 e.Å^{-3}
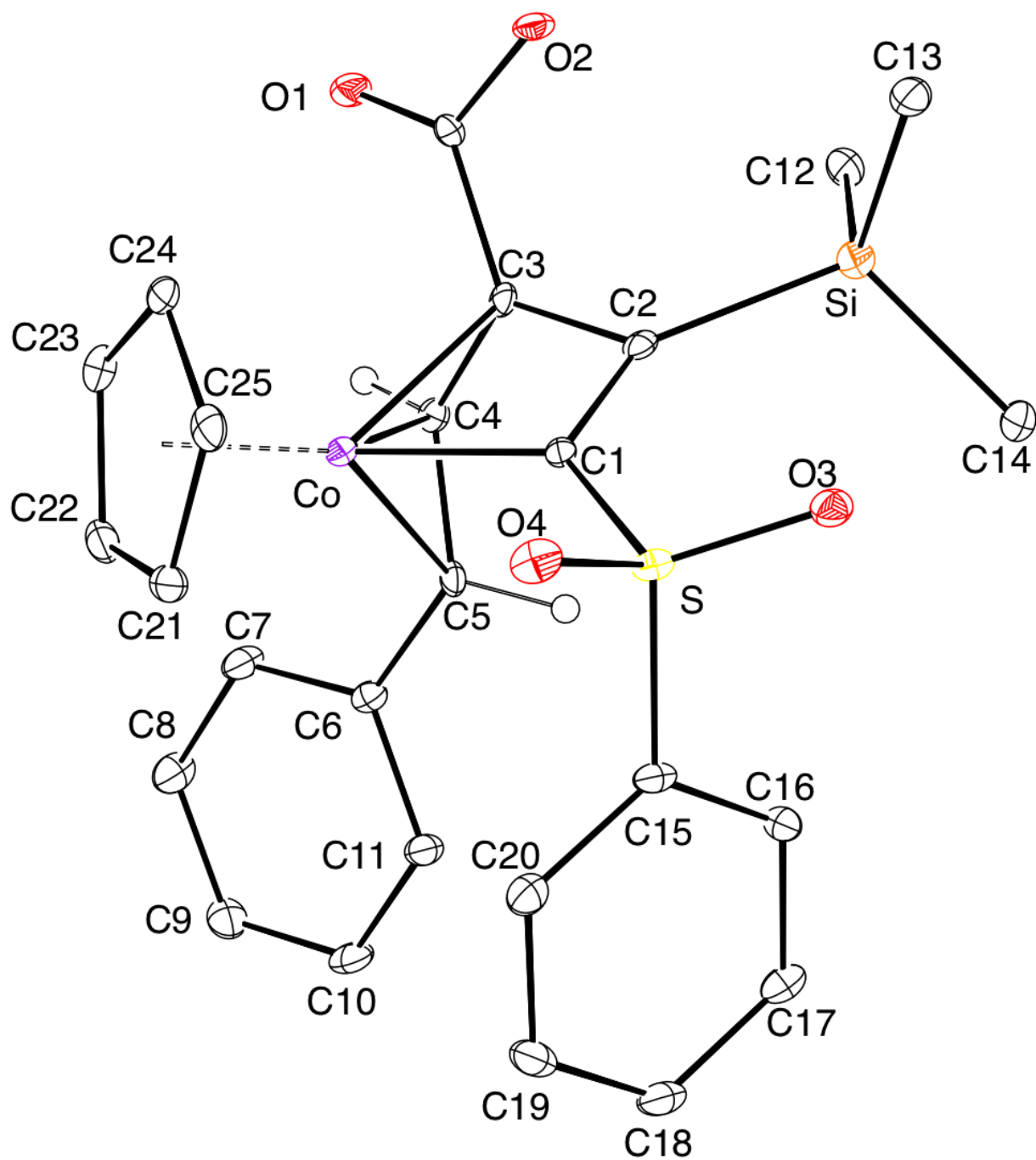
Figure 3-93. ORTEP view of complex **39**. Ellipsoids shown at 30% probability. Most hydrogens are omitted for clarity.

Table 3-26. Crystal data and structure refinement for complex **39**.

Identification code	pq644
Empirical formula	C27 H29 Co O4 P S
Formula weight	539.46
Temperature	100.0 K
Wavelength	0.71073 Å
Crystal system	Monoclinic
Space group	C 1 2/c 1
Unit cell dimensions	a = 37.417(6) Å $\quad$ α = 90°.
	b = 7.8228(12) Å $\quad$ β = 95.854(4)°.
	c = 34.219(5) Å $\quad$ γ = 90°.
Volume	9964(3) Å^3
Z	16
Density (calculated)	1.438 Mg/m^3
Absorption coefficient	0.869 mm^{-1}
F(000)	4496
Crystal size	0.237 x 0.221 x 0.071 mm^3
Theta range for data collection	1.196 to 25.350°.
Index ranges	-44<=h<=44, -9<=k<=9, -36<=l<=41
Reflections collected	35286
Independent reflections	9132 [R(int) = 0.0702]
Completeness to theta = 25.242°	100.0 %
Absorption correction	Semi-empirical from equivalents
Max. and min. transmission	0.7453 and 0.6290
Refinement method	Full-matrix least-squares on F^2
Data / restraints / parameters	9132 / 0 / 621
Goodness-of-fit on F^2	1.008
Final R indices [I>2sigma(I)]	R1 = 0.0431, wR2 = 0.0860
R indices (all data)	R1 = 0.0732, wR2 = 0.0962
Extinction coefficient	n/a
Largest diff. peak and hole	0.467 and -0.543 e.Å^{-3}
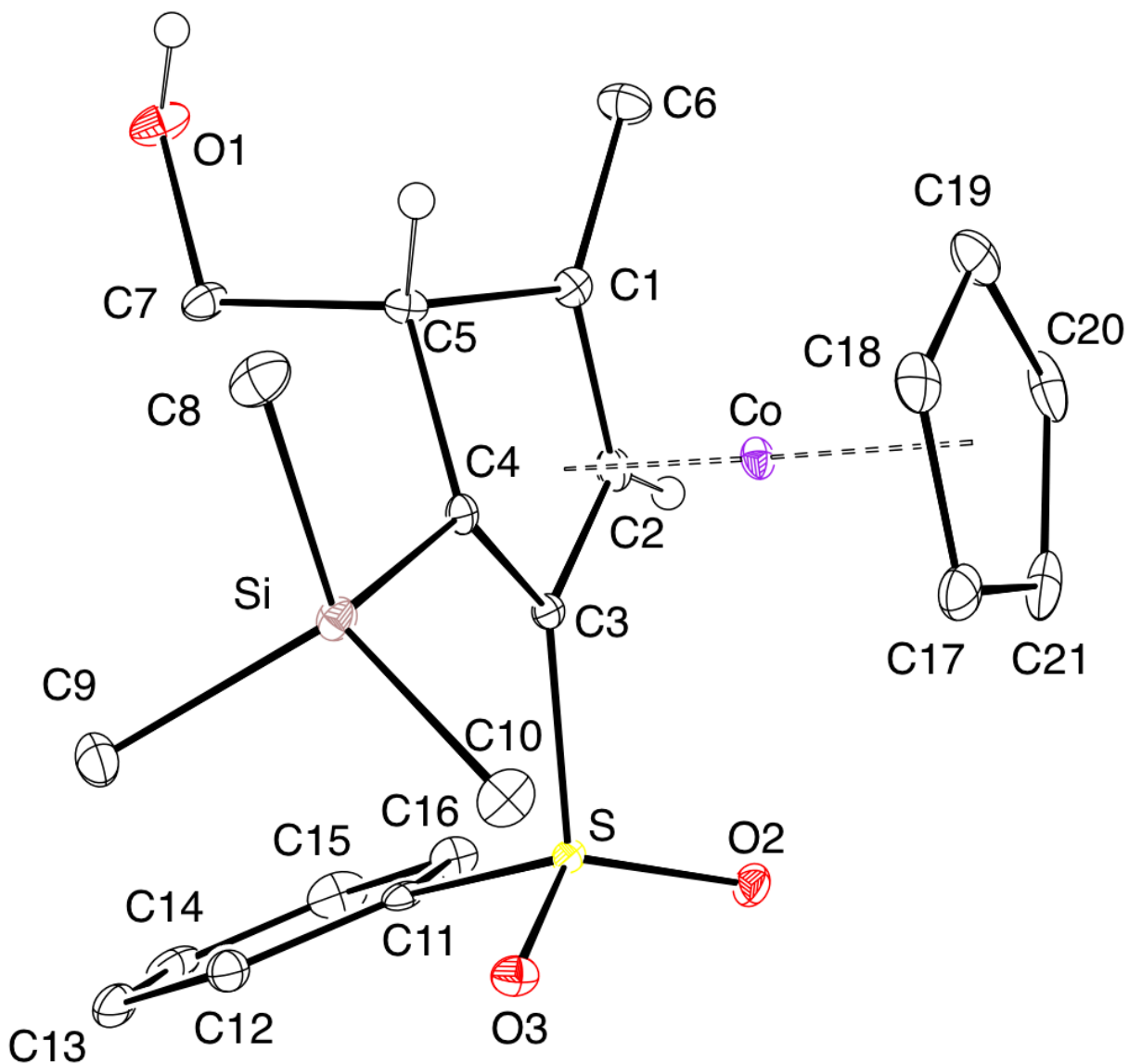
Figure 3-94. ORTEP view of complex **51**. Ellipsoids shown at 30% probability. Most hydrogens are omitted for clarity.

Table 3-27. Crystal data and structure refinement for complex **51**.

Identification code	RLH3152
Empirical formula	C21 H27 Co O3 S Si
Molecular formula	C21 H27 Co O3 S Si
Formula weight	446.50
Temperature	100.0 K
Wavelength	0.71073 Å
Crystal system	Monoclinic
Space group	P 1 21/c 1
Unit cell dimensions	a = 7.9154(3) Å α = 90°.
	b = 16.9766(5) Å β = 92.005(2)°.
	c = 15.5158(5) Å γ = 90°.
Volume	2083.68(12) Å^3
Z	4
Density (calculated)	1.423 Mg/m^3
Absorption coefficient	1.000 mm^{-1}
F(000)	936
Crystal size	0.356 x 0.317 x 0.295 mm^3
Crystal color, habit	Dark Red Block
Theta range for data collection	2.399 to 25.387°.
Index ranges	-9<=h<=7, -20<=k<=20, -18<=l<=18
Reflections collected	23113
Independent reflections	3831 [R(int) = 0.0481, R(sigma) = 0.0343]
Completeness to theta = 25.000°	99.9 %
Absorption correction	Semi-empirical from equivalents
Max. and min. transmission	0.0916 and 0.0587
Refinement method	Full-matrix least-squares on F^2
Data / restraints / parameters	3831 / 1 / 252
Goodness-of-fit on F^2	1.038
Final R indices [I>2sigma(I)]	R1 = 0.0310, wR2 = 0.0716
R indices (all data)	R1 = 0.0428, wR2 = 0.0766
Extinction coefficient	n/a
Largest diff. peak and hole	0.439 and -0.294 e.Å^{-3}
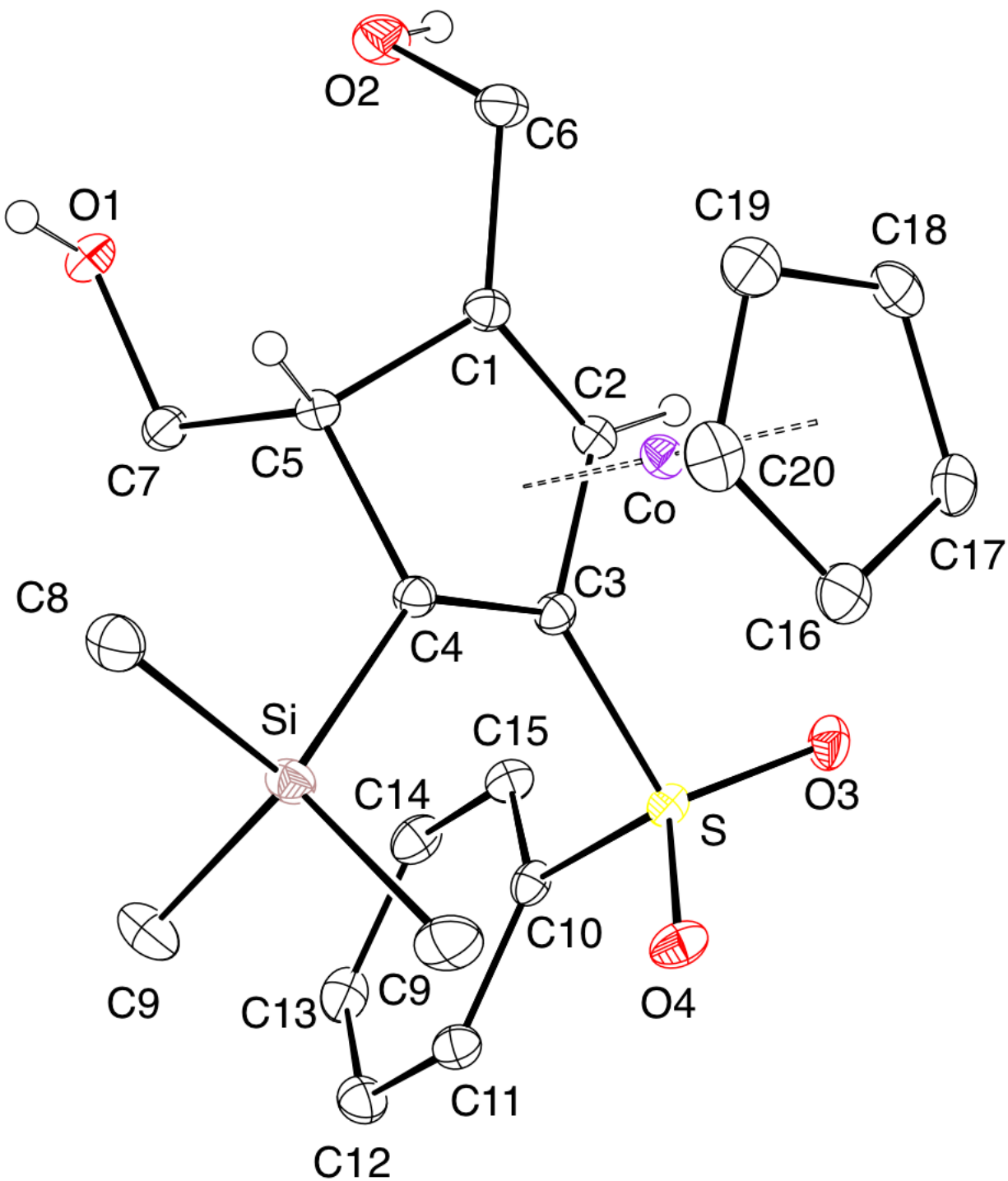
Figure 3-95. ORTEP view of complex **53**. Ellipsoids shown at 30% probability. Most hydrogens are omitted for clarity.

Table 3-28. Crystal data and structure refinement for complex **53**.

Identification code	RLH3158
Empirical formula	C21 H27 Co O4 S Si
Molecular formula	C21 H27 Co O4 S Si
Formula weight	462.50
Temperature	100 K
Wavelength	0.71073 Å
Crystal system	Orthorhombic
Space group	Pbcn
Unit cell dimensions	a = 33.5075(10) Å $\quad \alpha = 90°$.
	b = 8.7316(3) Å $\quad \beta = 90°$.
	c = 14.5845(5) Å $\quad \gamma = 90°$.
Volume	4267.0(2) Å^3
Z	8
Density (calculated)	1.440 Mg/m^3
Absorption coefficient	0.982 mm^{-1}
F(000)	1936
Crystal size	0.204 x 0.055 x 0.033 mm^3
Crystal color, habit	Red Needle
Theta range for data collection	2.410 to 25.380°.
Index ranges	-40<=h<=40, -9<=k<=10, -17<=l<=14
Reflections collected	26676
Independent reflections	3923 [R(int) = 0.0323, R(sigma) = 0.0196]
Completeness to theta = 25.000°	99.9 %
Absorption correction	Semi-empirical from equivalents
Max. and min. transmission	0.0916 and 0.0683
Refinement method	Full-matrix least-squares on F^2
Data / restraints / parameters	3923 / 2 / 264
Goodness-of-fit on F^2	1.038
Final R indices [I>2sigma(I)]	R1 = 0.0277, wR2 = 0.0702
R indices (all data)	R1 = 0.0318, wR2 = 0.0732
Extinction coefficient	n/a
Largest diff. peak and hole	0.401 and -0.254 e.Å^{-3}
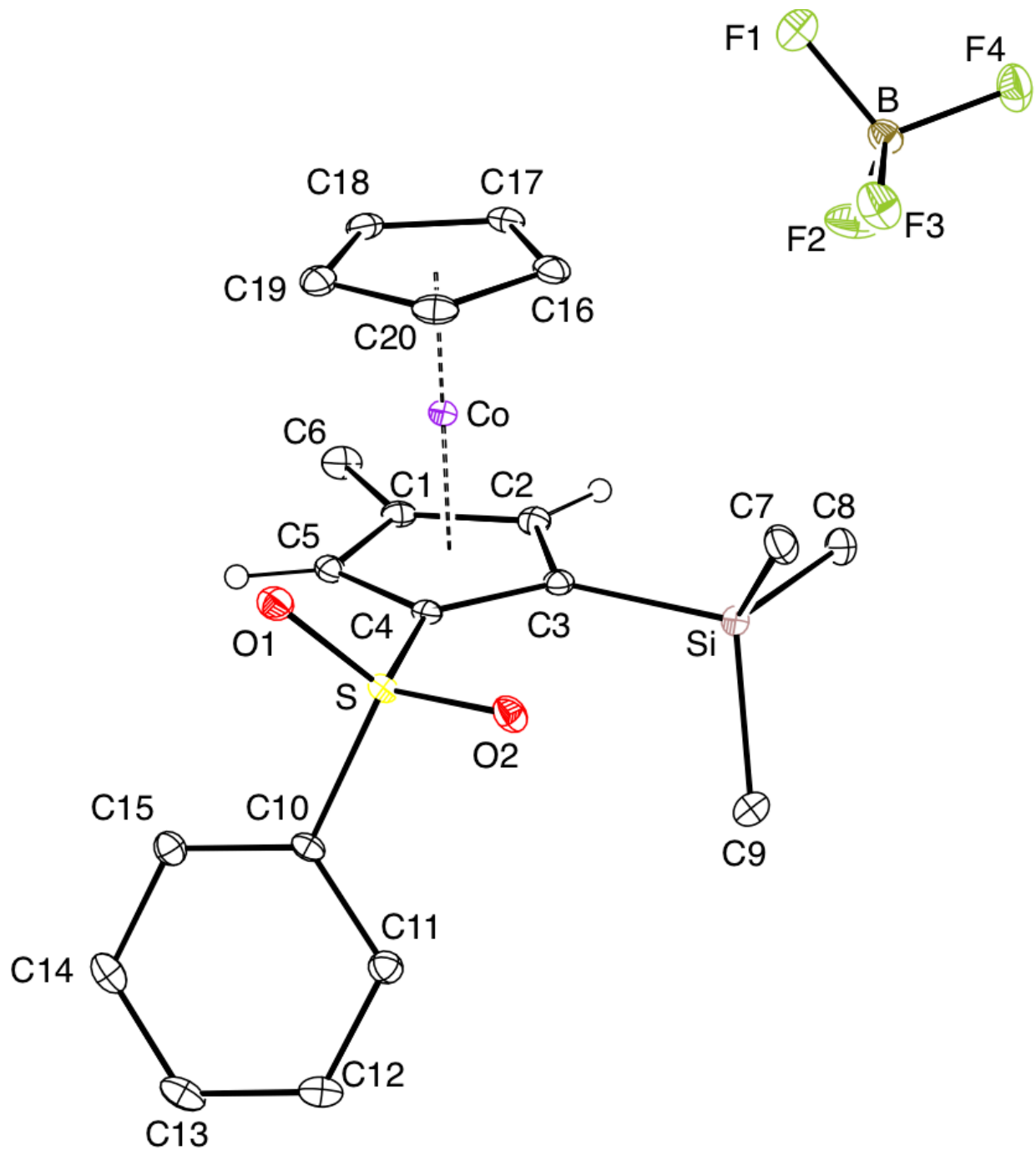
Figure 3-96. ORTEP view of complex **61**. Ellipsoids shown at 30% probability. Most hydrogens are omitted for clarity.

Table 3-29. Crystal data and structure refinement for complex **61**.

Identification code	RLH3168
Empirical formula	C20 H24 B Co F4 O2 S Si
Formula weight	502.28
Temperature	100.0 K
Wavelength	0.71073 Å
Crystal system	Triclinic
Space group	P-1
Unit cell dimensions	a = 7.3583(18) Å $\quad$ α = 86.398(8)°.
	b = 9.281(2) Å $\quad$ β = 77.369(8)°.
	c = 16.083(4) Å $\quad$ γ = 87.055(8)°.
Volume	1068.9(4) Å^3
Z	2
Density (calculated)	1.561 Mg/m^3
Absorption coefficient	1.006 mm^{-1}
F(000)	516
Crystal size	0.134 x 0.117 x 0.095 mm^3
Theta range for data collection	2.599 to 25.509°.
Index ranges	-8<=h<=8, -11<=k<=11, -19<=l<=19
Reflections collected	31602
Independent reflections	3914 [R(int) = 0.0292]
Completeness to theta = 25.000°	99.8 %
Absorption correction	Semi-empirical from equivalents
Max. and min. transmission	0.0916 and 0.0671
Refinement method	Full-matrix least-squares on F^2
Data / restraints / parameters	3914 / 0 / 275
Goodness-of-fit on F^2	1.084
Final R indices [I>2sigma(I)]	R1 = 0.0236, wR2 = 0.0615
R indices (all data)	R1 = 0.0240, wR2 = 0.0619
Extinction coefficient	n/a
Largest diff. peak and hole	0.450 and -0.263 e.Å^{-3}
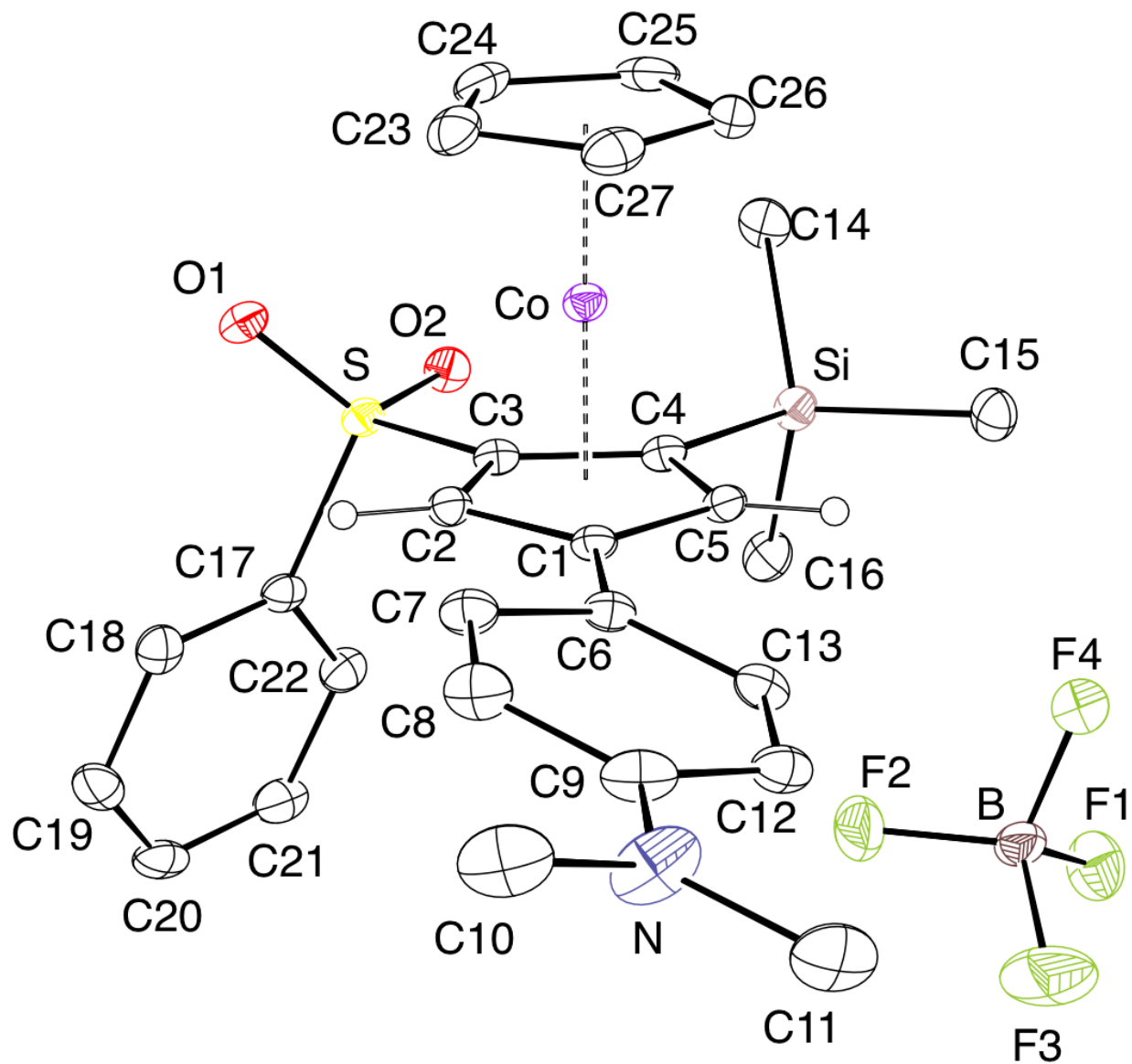
Figure 3-97. ORTEP view of complex **62**. Ellipsoids shown at 30% probability. Most hydrogens are omitted for clarity.

Table 3-30. Crystal data and structure refinement for complex **62**.

|	
Identification code	ocon142_0m_a
Empirical formula	C27 H33 B Co F4 N O3 S Si
Formula weight	625.43
Temperature	100.0 K
Wavelength	0.71073 Å
Crystal system	Triclinic
Space group	P-1
Unit cell dimensions	a = 7.442 Å α = 88.36°.
	b = 9.094 Å β = 80.38°.
	c = 21.524 Å γ = 86.87°.
Volume	1433.7 Å^3
Z	2
Density (calculated)	1.449 Mg/m^3
Absorption coefficient	0.769 mm^{-1}
F(000)	648
Crystal size	0.32 x 0.3 x 0.08 mm^3
Theta range for data collection	1.920 to 26.375°.
Index ranges	-9<=h<=8, -11<=k<=8, -26<=l<=24
Reflections collected	8915
Independent reflections	5779 [R(int) = 0.0250]
Completeness to theta = 26.000°	99.6 %
Absorption correction	Semi-empirical from equivalents
Max. and min. transmission	0.2603 and 0.2028
Refinement method	Full-matrix least-squares on F^2
Data / restraints / parameters	5779 / 0 / 360
Goodness-of-fit on F^2	1.060
Final R indices [I>2sigma(I)]	R1 = 0.0515, wR2 = 0.1218
R indices (all data)	R1 = 0.0650, wR2 = 0.1291
Extinction coefficient	n/a
Largest diff. peak and hole	0.788 and -0.723 e.Å^{-3}
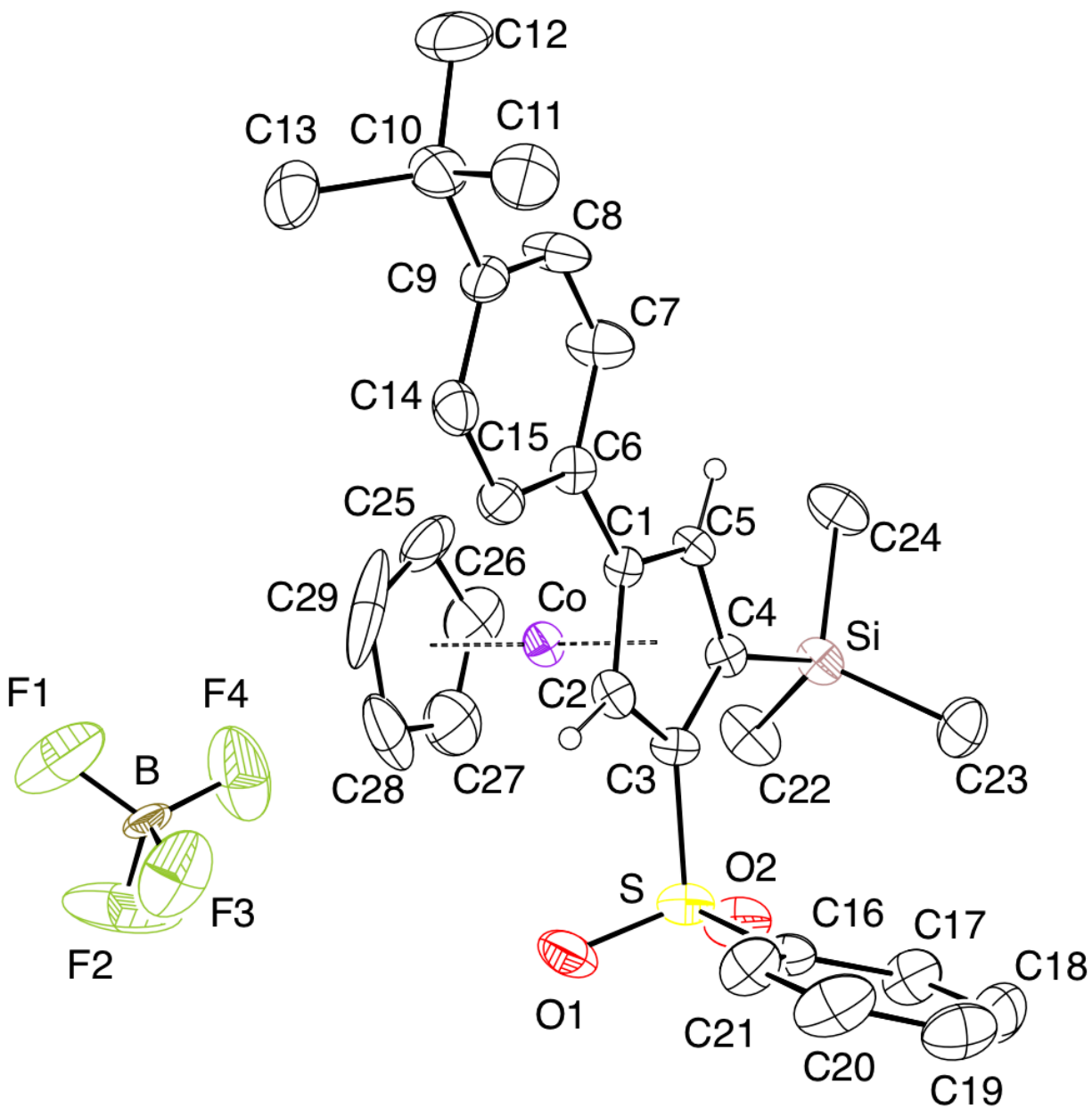
Figure 3-98. ORTEP view of complex **63**. Ellipsoids shown at 30% probability. Most hydrogens are omitted for clarity.

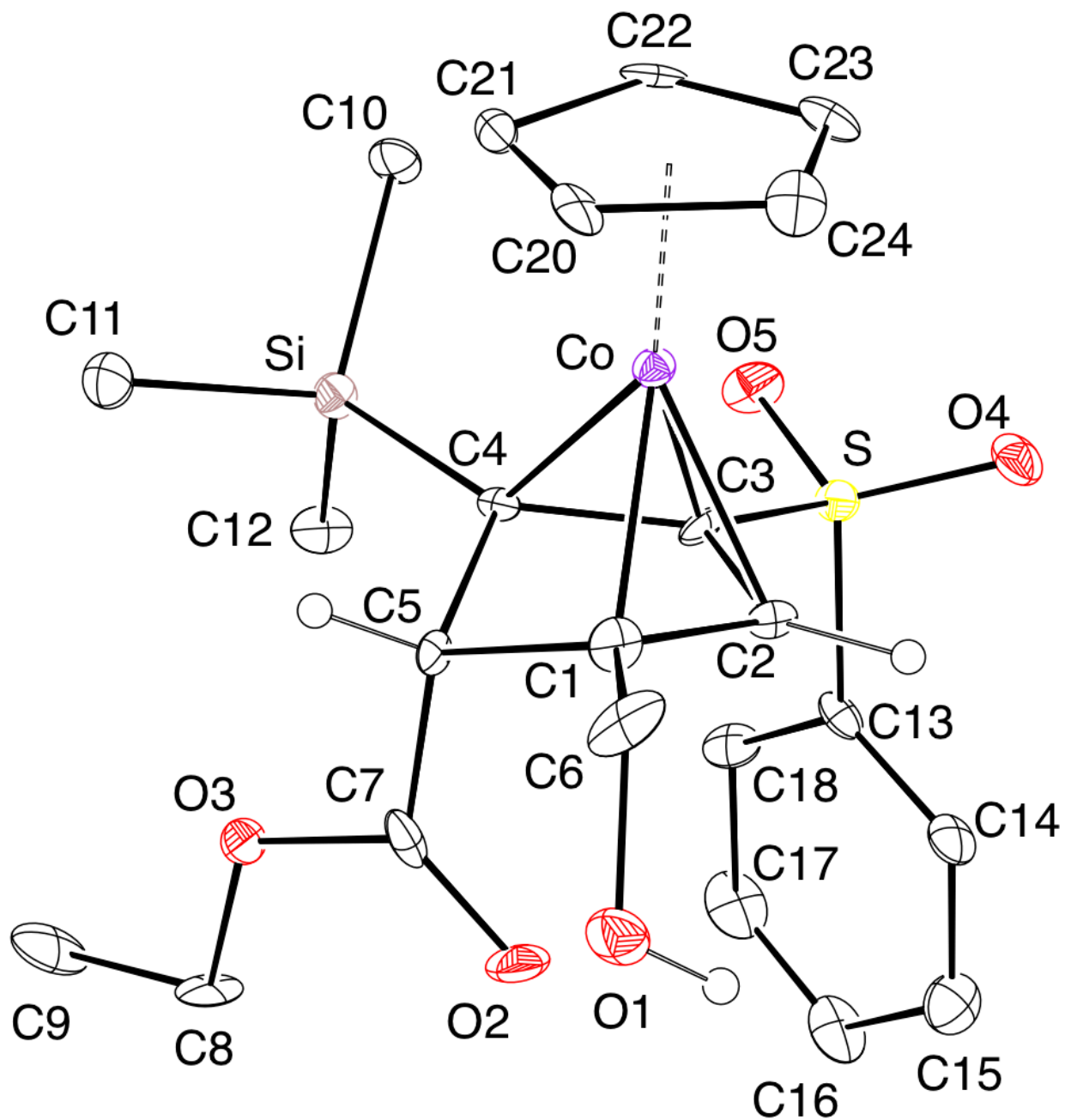**Table 3-31**. Crystal data and structure refinement for complex **63**.

Identification code	rlh3181
Empirical formula	C29.50 H0 B0.25 Co F0.25 O14.50 S2 Si0
Formula weight	716.80
Temperature	100.0 K
Wavelength	0.71073 Å
Crystal system	Triclinic
Space group	P-1

Unit cell dimensions

$a = 11.415(2)$ Å $\quad \alpha = 90°.$

$b = 11.353(2)$ Å $\quad \beta = 97.358(7)°.$

$c = 22.495(4)$ Å $\quad \gamma = 90°.$

Volume	2891.2(9) Å^3
Z	4
Density (calculated)	1.647 Mg/m^3
Absorption coefficient	0.816 mm^{-1}
F(000)	1422
Crystal size	0.42 x 0.35 x 0.07 mm^3
Theta range for data collection	0.913 to 25.458°.
Index ranges	-13<=h<=13, -13<=k<=13, -27<=l<=26
Reflections collected	43232
Independent reflections	10518 [R(int) = 0.1010]
Completeness to theta = 26.000°	92.5 %
Absorption correction	None
Max. and min. transmission	0.7452 and 0.2702
Refinement method	Full-matrix least-squares on F^2
Data / restraints / parameters	10518 / 0 / 715
Goodness-of-fit on F^2	2.172
Final R indices [I>2sigma(I)]	R1 = 0.1653, wR2 = 0.3625
R indices (all data)	R1 = 0.2015, wR2 = 0.3767
Extinction coefficient	n/a
Largest diff. peak and hole	6.929 and -0.673 e.Å^{-3}
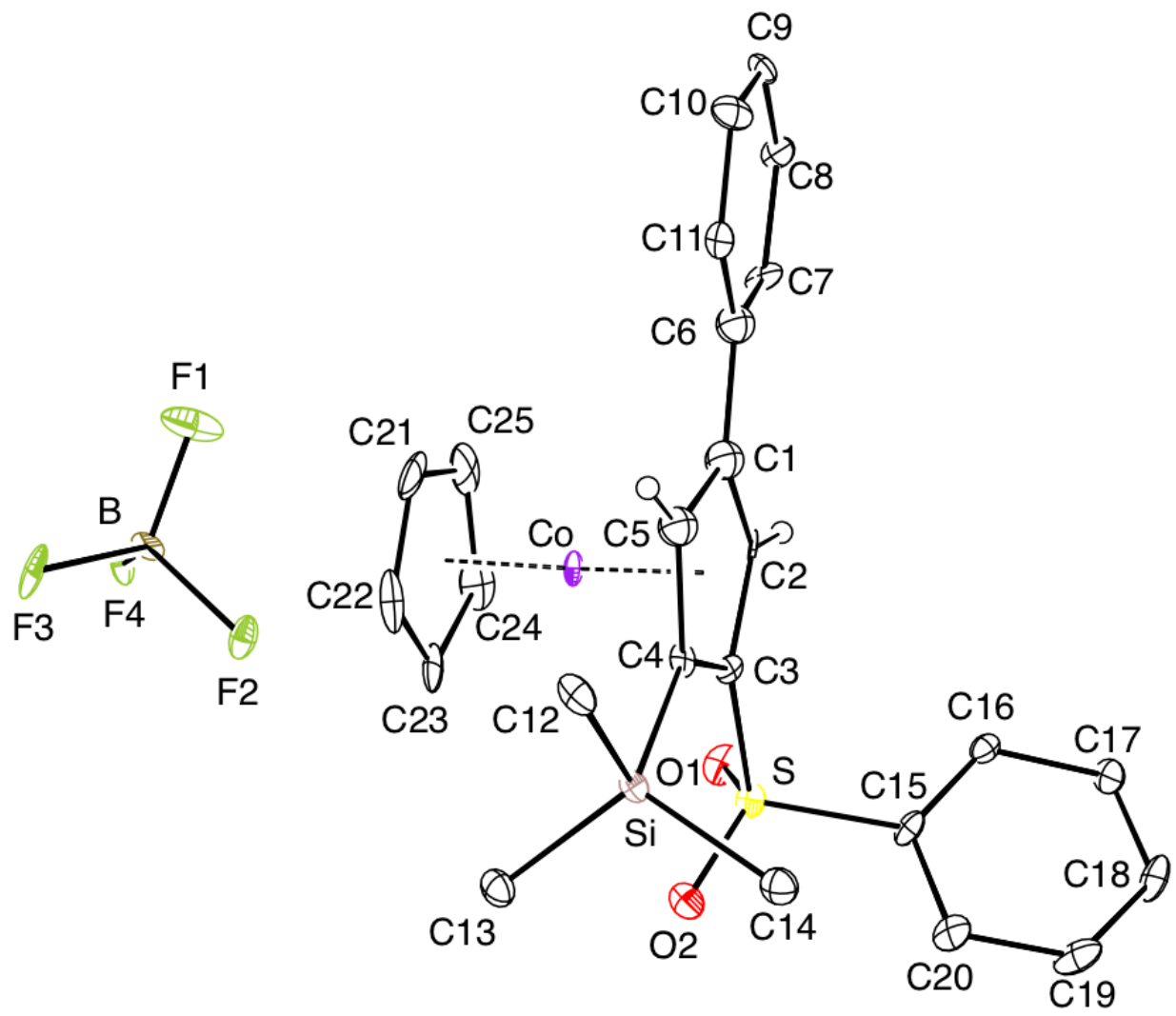
Figure 3-99. ORTEP view of complex **64**. Ellipsoids shown at 30% probability. Most hydrogens are omitted for clarity.

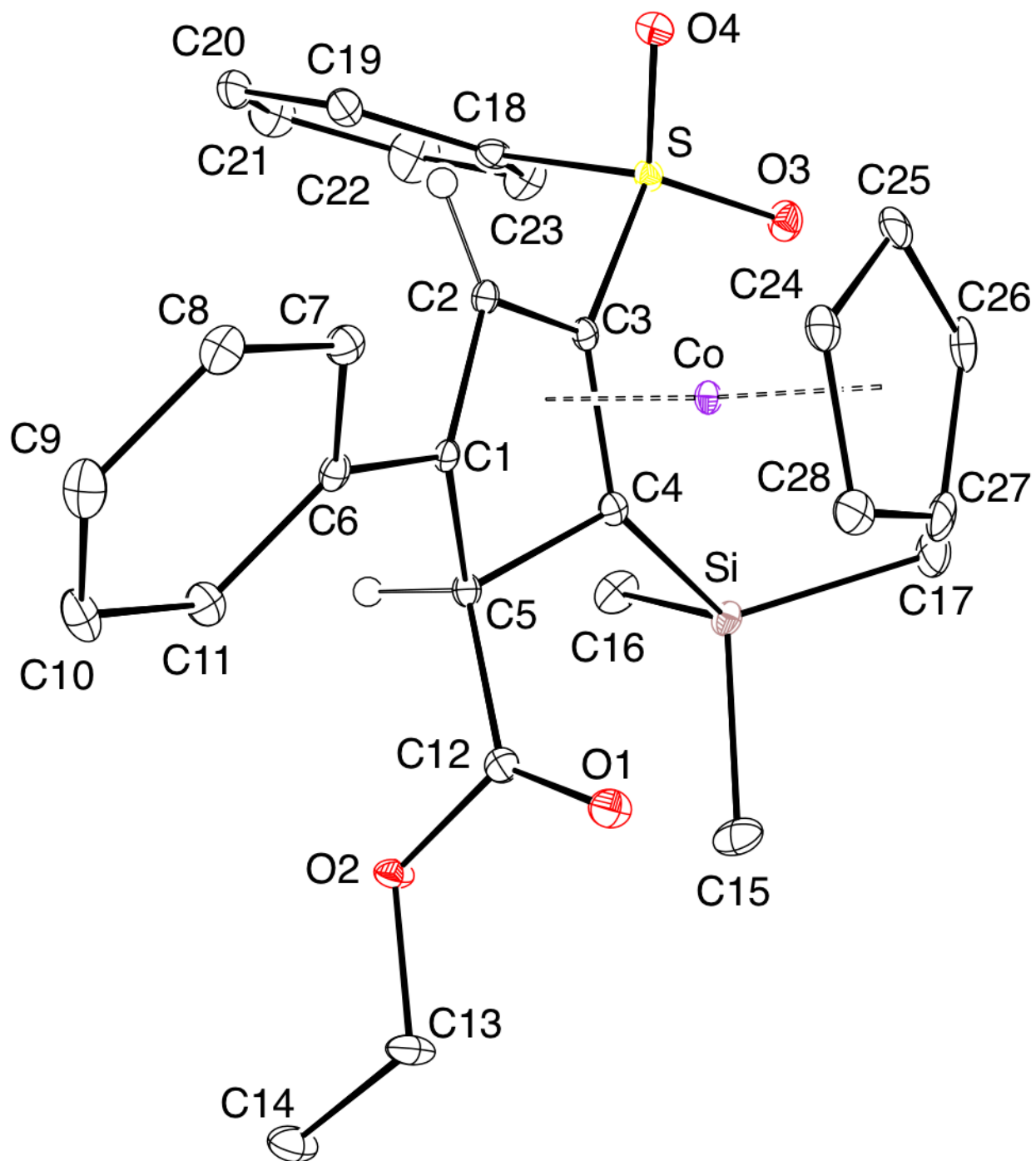**Table 3-32**. Crystal data and structure refinement for complex **64**.

Identification code	rlh3178
Empirical formula	C25 H26 B Co F4 O2 S2 Si0.25
Formula weight	575.34
Temperature	100.0 K
Wavelength	0.71073 Å
Crystal system	Monoclinic
Space group	$P2_1/n$
Unit cell dimensions	a = 6.926(3) Å $\quad\quad\alpha = 90(8)°$.
	b = 6.280(3) Å $\quad\quad\beta = (8)°$.
	c = 22.340(11) Å $\quad\quad\gamma = 89.994(6)°$.
Volume	2520(2) Å^3
Z	4
Density (calculated)	1.516 Mg/m^3
Absorption coefficient	0.910 mm^{-1}
F(000)	1182
Crystal size	0.22 x 0.25 x 0.07 mm^3
Theta range for data collection	1.773 to 25.748°.
Index ranges	-13<=h<=13, -14<=k<=13, -25<=l<=25
Reflections collected	53208
Independent reflections	9484 [R(int) = 0.1378]
Completeness to theta = 26.000°	95.6 %
Absorption correction	None
Max. and min. transmission	0.7452 and 0.4607
Refinement method	Full-matrix least-squares on F^2
Data / restraints / parameters	9484 / 0 / 637
Goodness-of-fit on F^2	2.102
Final R indices [I>2sigma(I)]	R1 = 0.1455, wR2 = 0.3366
R indices (all data)	R1 = 0.1840, wR2 = 0.3468
Extinction coefficient	n/a
Largest diff. peak and hole	6.062 and -1.102 e.Å^{-3}
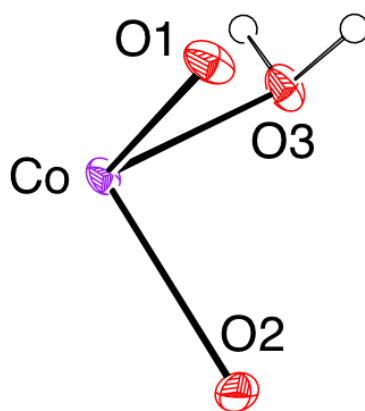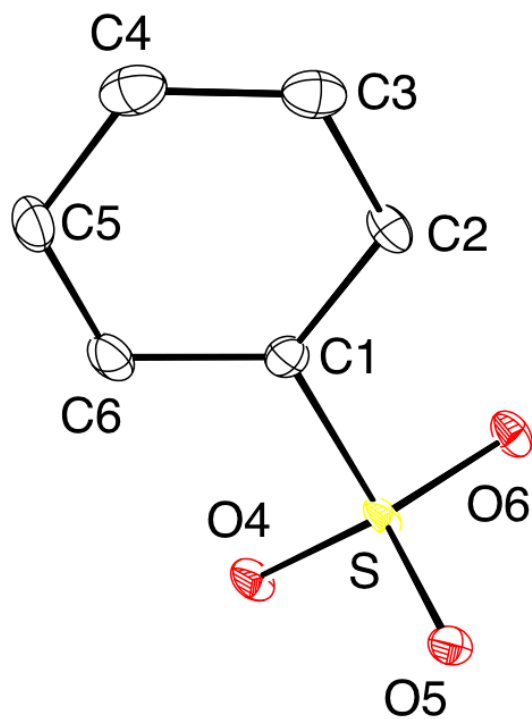
Figure 3-100. ORTEP view of complex **66**. Ellipsoids shown at 30% probability. Most hydrogens are omitted for clarity.

425

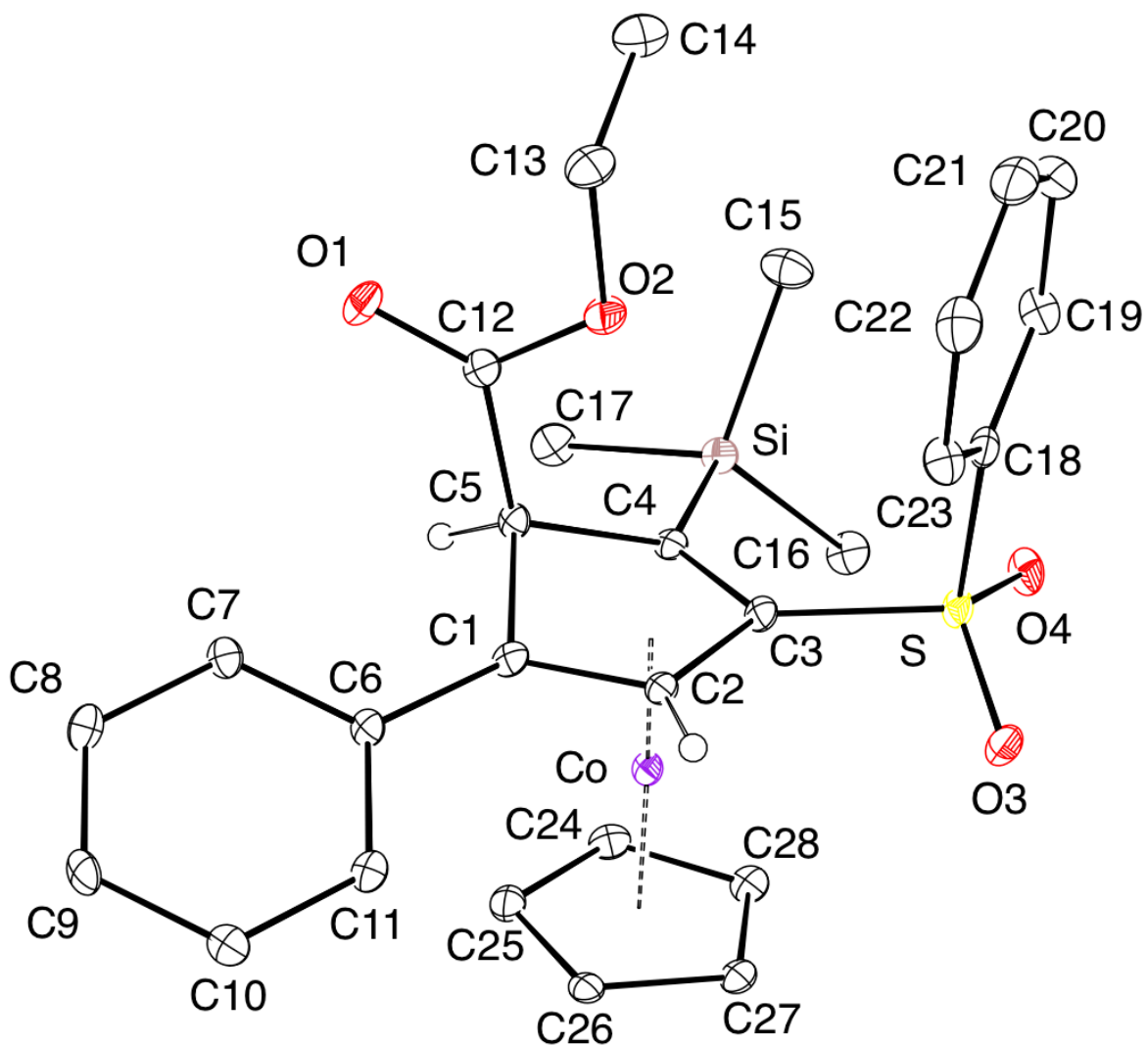**Table 3-33**. Crystal data and structure refinement for complex **66**.

Identification code	66_PQ_P21b
Empirical formula	C3 H3.5 Co0.25 O3 S0.25
Formula weight	118.33
Temperature	100.0 K
Wavelength	0.71073 Å
Crystal system	Triclinic
Space group	P-1
Unit cell dimensions	a = 10.789(5) Å α = 90(8)°.
	b = 11.535(6) Å β = 95.916(8)°.
	c = 20.896(10) Å γ = 90(8)°.
Volume	966.6(8) Å^3
Z	8
Density (calculated)	1.6260 Mg/m^3
Absorption coefficient	0.910 mm^{-1}
F(000)	483.5
Crystal size	0.32 x 0.37 x 0.08 mm^3
Theta range for data collection	1.773 to 25.748°.
Index ranges	-7<=h<=8, -7<=k<=7, -16<=l<=27
Reflections collected	3176
Independent reflections	1847 [R(int) = 0.0406]
Completeness to theta = 26.000°	95.0 %
Absorption correction	None
Max. and min. transmission	0.7452 and 0.4607
Refinement method	Full-matrix least-squares on F^2
Data / restraints / parameters	1847 / 0 / 124
Goodness-of-fit on F^2	1.176
Final R indices [I>2sigma(I)]	R1 = 0.0717, wR2 = 0.1790
R indices (all data)	R1 = 0.0988, wR2 = 0.2030
Extinction coefficient	n/a
Largest diff. peak and hole	0.90 and -1.07 e.Å^{-3}
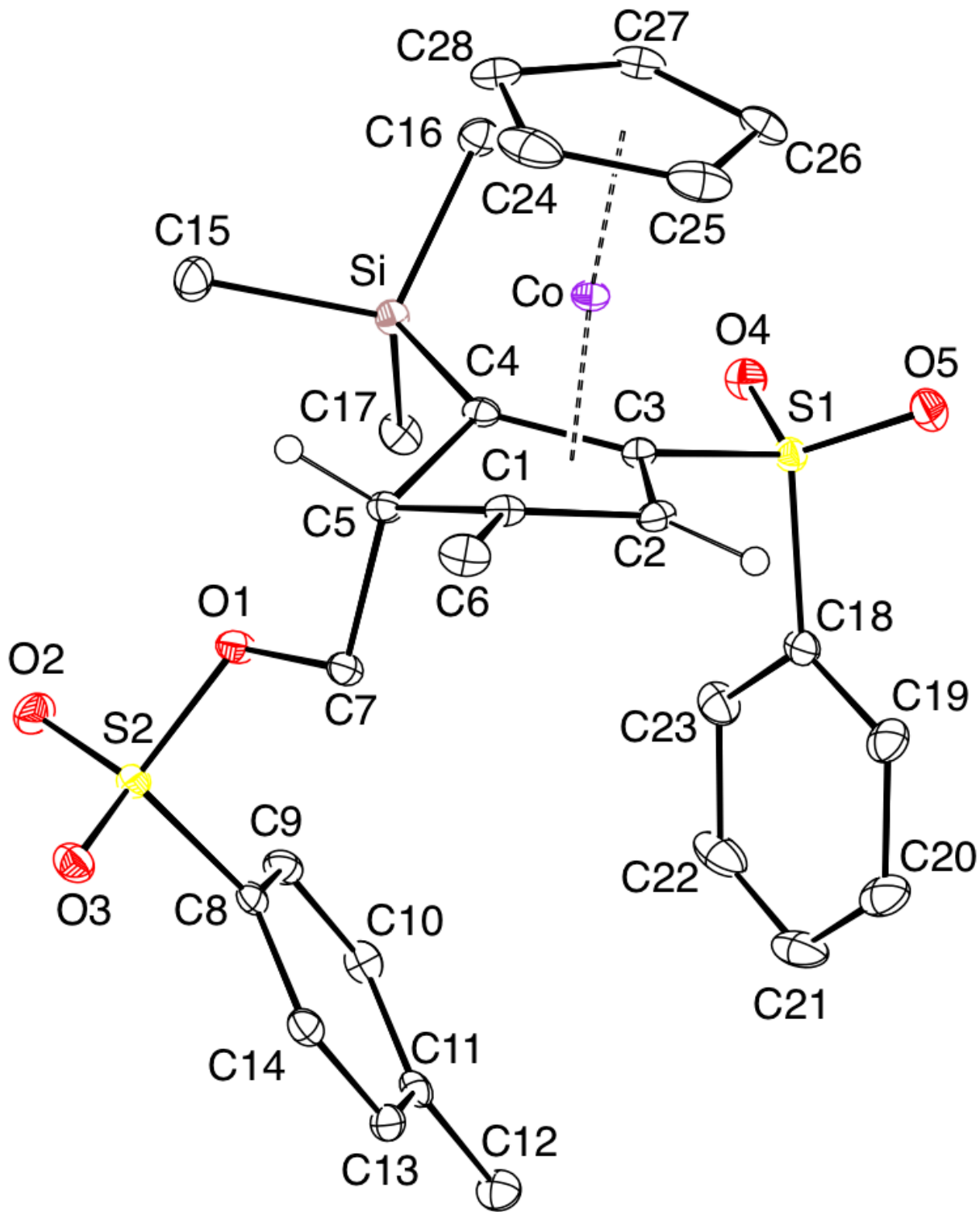
Figure 3-101. ORTEP view of complex **74**. Ellipsoids shown at 30% probability. Most hydrogens are omitted for clarity.

427

Table 3-34. Crystal data and structure refinement for complex **74**.

|	
Identification code	PQ_276
Empirical formula	C28 H33 Co O5 S2 Si
Molecular formula	C28 H33 Co O5 S2 Si
Formula weight	600.68
Temperature	100.0 K
Wavelength	0.71073 Å
Crystal system	Monoclinic
Space group	P 1 21/n 1
Unit cell dimensions	a = 8.8867(2) Å $\quad$ α = 90°.
	b = 21.2699(4) Å $\quad$ β = 104.9710(10)°.
	c = 15.0203(3) Å $\quad$ γ = 90°.
Volume	2742.76(10) Å^3
Z	4
Density (calculated)	1.455 Mg/m^3
Absorption coefficient	0.859 mm^{-1}
F(000)	1256
Crystal size	0.135 x 0.127 x 0.106 mm^3
Crystal color, habit	Red Block
Theta range for data collection	1.915 to 25.357°.
Index ranges	-10<=h<=10, -25<=k<=25, -14<=l<=18
Reflections collected	24878
Independent reflections	5023 [R(int) = 0.0311, R(sigma) = 0.0203]
Completeness to theta = 25.000°	99.9 %
Absorption correction	Semi-empirical from equivalents
Max. and min. transmission	0.0916 and 0.0676
Refinement method	Full-matrix least-squares on F^2
Data / restraints / parameters	5023 / 0 / 339
Goodness-of-fit on F^2	1.052
Final R indices [I>2sigma(I)]	R1 = 0.0273, wR2 = 0.0730
R indices (all data)	R1 = 0.0296, wR2 = 0.0748
Extinction coefficient	n/a
Largest diff. peak and hole	0.415 and -0.289 e.Å^{-3}

Acknowledgement

H. References

1. (a) Matyjaszewski, K.; Xia, J. Atom transfer radical polymerization. *Chem. Rev.* **2001**, *101*, 2921-2990. (b) Kamigaito, M.; Ando, T.; Sawamoto, M. Metal-catalyzed living radical polymerization. *Chem. Rev.* **2001**, *101*, 3689-3746. (c) Wang, B.; Zhuang, Y.; Luo, X.; Xu, S.; Zhou, X. Controlled/"living" radical polymerization of MMA catalyzed by cobaltocene. *Macromolecules* **2003**, *36*, 9684-9686.

2. Gandon, V.; Aubert, C.; Malacria, M. Recent progress in cobalt-mediated [2+ 2+ 2] cycloaddition reactions. *Chem. Commun*. **2006**, 2209-2217.

3. (a) Pauson, P. L.; Khand, I. U. Uses of Cobalt-Carbonyl Acetylene Complexes in Organic Synthesis. *Ann. N. Y. Acad. Sci.* **1977**, *295*, 2-14. (b) Blanco-Urgoiti, J.; Añorbe, L.; Pérez-Serrano, L.; Domínguez, G.; Pérez-Castells, J. The Pauson–Khand reaction, a powerful synthetic tool for the synthesis of complex molecules. *Chem. Soc. Rev.* **2004**, *33*, 32-42.

4. O'Connor J. M.; Fong, B. S.; Ji, H. L.; Hiibner, K.; Rheingold, A. L. A New Metal-Mediated Cyclization: Conversion of a Metallacyclobutene and Alkyne Substrates to η^4-Cyclopentadiene Products. *J. Am. Chem. Soc*. **1995**, *117*, 8029-8030.

5. See chapter 1 section D: η^4-Cyclopentadiene Complexes.

6. (12) (a) Szajek, L. P.; Shapley, J. R. Unexpected Synthesis of CpIr(η^4-C$_5$H$_6$) and a ^{1}H and ^{13}C NMR Comparison with its Cobalt and Rhodium Congeners. *Organometallics* **1991**, *10*, 2512-2515; (b) El Murr, N.; Dusausoy, Y.; Sheats, J. E.; Agnew, M. Electrochemical Behaviour and X-ray Structure of (η^5-Cyclopentadienyl)(4-5-η^2-methoxycarbonylcyclopent-4-en-1,3-ylene)cobalt. *J. Chem. Soc., Dalton Trans.* **1979**, 901-905.

7. Cenzano-Fong, B. Doctoral Dissertation, Synthesis and Reactivity of Late Metal Metallacyclobutene Complex and Eta(4)-Cyclopentadiene Cobalt Compounds. University of California, San Diego, CA, USA, **1997**.

8. O'Connor, J. M.; Baldridge, K. K.; Vélez, C. L.; Rheingold, A. L.; Moore, C. E. Chemistry at the Alkyne–Carbene Intersection: A Metallacyclobutene-η^3-Vinylcarbene Equilibration. *J. Am. Chem. Soc.* **2013**, *135*, 8826-8829.

9. Bunker, K. Doctoral Dissertation, Late-Metal Metallacyclobutenes: Synthesis, Isolation, and Reactivity Studies of Cobaltacyclobutenes. University of California, San Diego, CA, USA, **2003**.

10. O'Connor, J. M.; Ji, H.; Iranpour, M.; Rheingold, A. L. Formation of a Stable Metallacyclobutene Complex from α-Diazocarbonyl and Alkyne Substrates. *J. Am. Chem. Soc.* **1993**, *115*, 1586-1588.

11. Kim, J. Y.; Park, S. H.; Ryu, J.; Cho, S. H.; Kim, S. H.; Chang, S. Rhodium-catalyzed intermolecular amidation of arenes with sulfonyl azides via chelation-assisted C–H bond activation. *J. Am. Chem. Soc.* **2012**, *134*, 9110-9113.

12. Loy, N. S.; Singh, A.; Xu, X.; Park, C. M. Synthesis of Pyridines by Carbenoid-Mediated Ring Opening of 2H-Azirines. *Angew. Chem. Int. Ed.* **2013**, *52*, 2212-2216.

13. (a) Štěpnička, P. The Multifaceted Chemistry of Ferrocene. Eur. J. *Inorg. Chem.* **2016**, 215-216. (b) Heinze, K.; Lang, H. Thematic issue "Ferrocene-Beauty and Function. *Organometallics* **2013**, *32*, 5623-5625. (c) Ferrocenes: Ligands, Materials and Biomolecules; Stepnicka, P., Ed.; Wiley: Chichester, U.K., **2008**. (d) Ferrocenes: Homogeneous Catalysis, Organic Synthesis, Materials Science; Togni, A., Hayashi, T., Eds.; VCH: Weinheim, Germany, **1995**. (e) Hailes, R. L. N.; Oliver, A. M.; Gwyther, J.; Whittell, G. R.; Manners, I. *Chem. Soc. Rev.* **2016**, *45*, 5358-5407. (f) Astruc, D. Eur. J. *Inorg. Chem.* **2017**, *2017*, 6-29. (g) Molina, P.; Tárraga, A.; Alfonso, M. *Dalton Trans.* **2014**, *43*, 18-29.

14. (a) Nguyen, P.; Go´mez-Elipe, P.; Manners, I. *Chem. Rev.* **1999**, *99*, 1515-1548. (b) Manners, I. Synthetic Metal-Containing Polymers; Wiley-VCH: Weinheim, **2004**. (c) Korczagin, I.; Lammertink, R. G. H.; Hempenius, M. A.; Golze, S.; Vancso, G. *J. Adv.*

Polym. Sci. **2006**, *200*, 91-117. (d) Hudson, R. D. A. *J. Organomet. Chem*. **2001**, *47*, 637-639.

15. Herberich, G. E.; Bauer, E.; Schwarzer, J. Untersuchungen zur reaktivität organometallischer komplexe III. Über die reaktion von dicyclopentadienylkobalt mit halogenmethanen. *J. Organomet. Chem.* **1969**, *17*, 445-452.

16. Bunz, U. H. F. Cyclobutadiene-cyclopentadienylcobalt is a 18-e neutral system. *Top. Curr. Chem*. **1999**, *201*, 131–160.

17. (a) Carraher Jr, C. E.; Sheats, J. E. Synthesis of organometallic polymers by the interfacial technique. XXVI. Synthesis of poly [bis (oxycarbonylcyclopentadienyl)-cobalt (III)(dicyclopentadienyltitan (IV)) hexafluorophosphate]. *Makromol. Chem.* **1973**, *166*, 23-29. (b) Pittman Jr, C. U.; Ayers, O. E., Suryanarayanan, B.; McManus, S. P.; Sheats, J. E. Organometallic polymers, 28 Condensation polymerization of cobalticinium salts. *Makromol. Chem*. **1974**, *175*, 1427-1437. (c) Mayer, U. F.; Gilroy, J. B.; O'Hare, D.; Manners, I. Ring-opening polymerization of 19-electron [2] cobaltocenophanes: a route to high-molecular-weight, water-soluble polycobaltocenium polyelectrolytes. *J. Am. Chem. Soc*. **2009**, *131*, 10382-10383.

18. (a) Albada, B.; Metzler-Nolte, N. Highly potent antibacterial organometallic peptide conjugates. *Acc. Chem. Res.* **2017**, *50*, 2510-2518. (b) Chantson, J. T.; Falzacappa, M. V. V; Crovella, S.; Metzler-Nolte, N. Antibacterial Activities of Ferrocenoyl- and Cobaltocenium-Peptide Bioconjugates. *J. Organomet. Chem*. **2005**, *690*, 4564−4572.

19. Vanicek, S.; Kopacka, H.; Wurst, K.; Müller, T.; Schottenberger, H.; Bildstein, B. Chemoselective, Practical Synthesis of Cobaltocenium Carboxylic Acid Hexafluorophosphate. *Organometallics* **2014**, *33*, 1152-1156.

20. Vanicek, S.; Kopacka, H.; Wurst, K.; Müller, T.; Hassenrück, C.; Winter, R. F.; Bildstein, B. Monofunctionalized Cobaltocenium Compounds by Dediazoniation Reactions of Cobaltoceniumdiazonium Bis (hexafluorophosphate). *Organometallics* **2016**, *35*, 2101-2109.

21. Jochriem, M.; Bosch, D.; Kopacka, H.; Bildstein, B. Direct Amination of Cobaltocenium Hexafluoridophosphate via Vicarious Nucleophilic Substitution. *Organometallics* **2019**.

22. (a) Wolter-Steingrube, A.; Bugenhagen, B. E.; Herrmann, C.; Heck, J. Synthesis and Molecular Structures of Monosubstituted Pentamethylcobaltocenium Cations. *Eur. J. Inorg. Chem.* **2014**, *2014*, 4115-4122. (b) Wolter-Steingrube, A.; Cordsen, K.; Heck, J. Nucleophilic Substitution in the Nitrocobaltocenium Ion. *Eur. J. Inorg. Chem.* **2017**, *2017*, 1314-1319.

23. (a) Sheats, J. E.; Rausch, M. D. *J. Org. Chem*. **1970**, *35*, 3245–3249. (b) Sheats, J. E.; Carraher, J. C. E.; Pittman, J. C. P.; Zeldin, M.; Currell, B. Inorganic and Metal-

Containing Polymeric Materials; Plenum: New York, **1985**. (c) Peckham, T. J.; Go´mez-Elipe, P.; Manners, I. In Metallocenes. Synthesis, ReactiVity, Applications; Togni, A., Halterman, R. L., Eds.; Wiley- VCH: Weinheim, **1998**; p 7563. (d) Astruc, D.; Ornelas, C.; Ruiz, J. *Acc. Chem. Res*. **2008**, *41*, 841–856. (e) Ornelas, C.; Ruiz, J.; Astruc, D. *Organometallics* **2009**, *28*, 2716–2723. (f) Casado, C. M.; Gonzalez, B.; Cuadrado, I.; Alonso, B.; Moran, M.; Losada, J. *Angew. Chem., Int. Ed*. **2000**, *39*, 2135–2138.

24. (a) Szajek, L. P.; Shapley, J. R. Unexpected Synthesis of CpIr(η^4-C$_5$H$_6$) and a ^{1}H and ^{13}C NMR Comparison with its Cobalt and Rhodium Congeners. *Organometallics* **1991**, *10*, 2512-2515; (b) El Murr, N.; Dusausoy, Y.; Sheats, J. E.; Agnew, M. Electrochemical Behaviour and X-ray Structure of (η-Cyclopentadienyl)(4-5-η^2-methoxycarbonylcyclopent-4-en-1,3-ylene)cobalt. *J. Chem. Soc., Dalton Trans.* **1979**, 901-905.

25. (a) Green, M. L.; H.; Pratt, L.; Wilkinson, G. A New Type of Transition Metal-Cyclopentadiene Compound. *J. Chem. Soc.* **1959**, 3753-3767. (b) El Murr, N.; Laviron, E.; Dabard, R. Chemical and Electrochemical Oxidation of Some Cyclopentadiene Cyclopentadienyl Cobalt. *J. Organomet. Chem.* **1974**, *67*, C77-C80; (c) El Murr, N.; Laviron, E. Electrochemistry of Organometallic Compounds. I. Electrosynthesis of Cyclopentadiene Cyclopentadienyl Cobalt Substitutes. *Can. J. Chem.* **1976**, *54*, 3350-3356; (d) El Murr, N.; Laviron, E. Electrochemistry of Organometallic Compounds. II. New Pathway to Substituted Cobalticinium Substitutes. *Can. J. Chem.* **1976**, *54*, 3357-3363.(e) Leonova, E. V.; Malkov, A. V.; Kochetkova, N. O.; Sokolova, A. N.; Rukhlyada, N. N. Sulfuric Acid as a Hydride Ion Acceptor in Cobalt(I) Cyclopentadiene Complexes. *Izv. Akad. Nauk SSSR, Ser. Khim.* **1984**, *3,* 727-728. (f) Malikov, A. V.; Leonova, E. V.; Kochetkova, N. S.; Sergeev, V. A. The Interaction of the Cobaltocenium Cation with Nucleophiles. *Metalloorganicheskoi Khimiya* **1988**, *1*, 357-363; (g) Leonova, E. V.; Malikov, A. V.; Kochetkova, N. S.; Sergeev, V. A. Oxidative Elimination of Hydride from the Cobalt Complexes (η^4-*exo*-RC$_5$H$_4$)CoCp. *Metalloorganicheskoi Khimiya* **1988**, *1*, 137-141.

26. Cotton, F. A.; Daniels, L. M.; Wilkinson, C. C. A highly disordered cobaltocenium salt. *Acta Cryst*. **2001**, *57*, 529-530.

27. Connelly, N. G.; Geiger, W. E. Chemical redox agents for organometallic chemistry. *Chem. Rev.* **1996**, *96*, 877-910.

28. Vanicek, S.; Kopacka, H.; Wurst, K.; Vergeiner, S.; Oehninger, L., Ott, I.; Bildstein, B. Cobaltocenium Carboxylate Transition Metal Complexes: Synthesis, Structure, Reactivity, and Cytotoxicity. *Zeitschrift für anorganische und allgemeine Chemie*, **2015**, *641*, 1282-1292.

29. Vanicek, S.; Kopacka, H.; Wurst, K.; Vergeiner, S.; Kankowski, S.; Schur, J.; Ott, I. Cobaltoceniumethynyl gold (I) as an unusual heterodinuclear bioorganometallic fragment to study the biological properties of alkynyl gold complexes. *Dalton Trans.* **2016**, *45*, 1345-1348.

30. Romero, A.; Ramos, E.; Ares, I.; Castellano, V.; Martínez, M.; Martínez-Larrañaga, M. R.; Martínez, M. A. Fipronil sulfone induced higher cytotoxicity than fipronil in SH-SY5Y cells: protection by antioxidants. *Toxicol. lett*. **2016**, *252*, 42-49.

31. Chen, F.; Wang, T.; Jiao, N. Recent advances in transition-metal-catalyzed functionalization of unstrained carbon–carbon bonds. *Chem. Rev.*, **2014**, *114*, 8613-8661.

32. (a) Herberich, G. E.; Greiss, G.; Heil, H. F. Untersuchungen zur reaktivität organometallischer komplexe V. Zum sterischen verlauf der pseudocarboniumumlagerung der cyclopentadienyl [5-exo-(α-halogenalkyl) cyclopentadien] kobalt-komplexe. *J. Organomet. Chem*. **1970**, *22*, 723-730. (b) Herberich, G. E.; Schwarzer, J. Die Ringerweiterung der Cyclopentadienyl-[5-exo-halogenmethyl-cyclopentadien]-kobalt-Komplexe. *Chem. Ber*. **1970**, *103*, 2016-2023. (c) Herberich, G. E.; Schwarzer, J. Solvolytic Ring Expansion in a Transition Metal π-Complex. *Angew. Chem., Int. Ed*. 1969, *8*, 143-144.

33. (a) Dzwiniel, T. L.; Stryker, J. M. Cobalt-Mediated Two-Carbon Ring Expansion of Five-Membered Rings. Electrophilic Carbon-Carbon Bond Activation in the Synthesis of Seven-Membered Rings. *J. Am. Chem. Soc.* **2004**, *126*, 9184-9185. (b) Dzwiniel, T. L.; Etkin, N.; Stryker, J. M. Carbon-Carbon Bond Activation by Electrophilic Complexes of Cobalt: Anomalous [3 + 2 + 2] Allyl/Alkyne Cycloaddition Reactions and [5 + 2] Cyclopentenyl/Alkyne Insertion-Ring Expansion Reactions. *J. Am. Chem. Soc.* **1999**, *121*, 10640-10641.

34. Murakami, M.; Makino, M.; Ashida, S.; Matsuda, T. Construction of carbon frameworks through β-carbon elimination mediated by transition metals. *Bull. Chem. Soc. Jpn.* **2006**, *79*, 1315-1321.

35. Ten Brink, G. J.; Arends, I. W. C. E.; Sheldon, R. A. The Baeyer-Villiger reaction: New developments toward greener procedures. *Chem. Rev.* **2004**, *104*, 4105-4124.

CHAPTER 4

Acid - Induced Liberation of Polysubstituted Cyclopentadiene Ligands from

Cyclopentadienyl Cobalt: A [2 + 2 + 1] Cycload-dition Route Toward 1,2,4-Trisubstituted

Cyclopentadienes[a]

a. Qin, P.; Holland, R. L.; Bunker, K. D.; O'Connor, J. M.; Baldridge, K. K.; Rheingold, A. L. *J. Org. Chem*. **2019**, *84*, 13992-14004.

A. Abstract
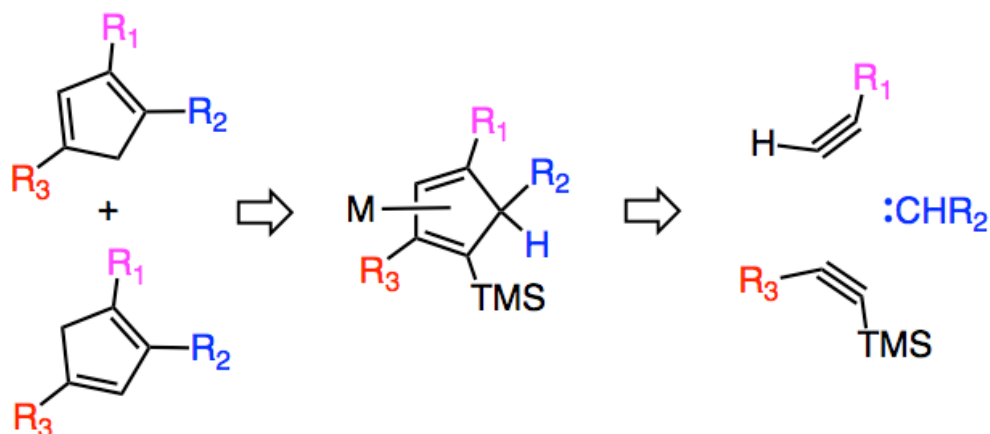
Here we report that trifluoroacetic acid (TFAH) induces demetallation and protodesilylation of the cyclopentadiene ligand in cobalt-η^4-cyclopentadiene complexes of general formula [(η^5-C$_5$H$_5$)Co(η^4-exo-C(TMS)=C(SO$_2$Ph)CH=CRCH(CO$_2$Et))] (**1-*Ph***, R = Ph; **1-*Ar^tBu***, R = *p*-C$_6$H$_4$^{t}Bu; **1-*ArNMe$_2$***, R = *p*-C$_6$H$_4$NMe$_2$; and **1-*Me***, R = Me). The trisubstituted cyclopentadiene products are isolated as a mixture of two tautomers, [(CH$_2$C(SO$_2$Ph)=CHC(CO$_2$Et)=CR)] (**8-*R-A***) and [(CH=C(SO$_2$Ph)CH$_2$C(CO$_2$Et)=CR)] (**8-*R-B***). The *endo* isomer, [(η^5-C$_5$H$_5$)Co(η^4-*endo*-C(TMS)=C(SO$_2$Ph)CH=CPhCH(CO$_2$Et))] (**1-*Ph-endo***), also undergoes demetallation and protodesilylation to give **8**-*Ph-A* and **8**-*Ph-B* in excellent yield. The cobalt-cyclopentadiene complex, [(η^5-C$_5$H$_5$)Co(η^4-*exo*-C(TMS)=C(SO$_2$Ph)CH=C(CO$_2$Me)CH(CO$_2$Et))] (**1-*CO$_2$Me***), undergoes demetallation and protodesilylation upon treatment with TFAH to give a hydrogen-bonded fulvenol (**8-*CO$_2$Me***). Liberation of the ethoxy-substituted cyclopentadiene ligand of [(η^5-C$_5$H$_5$)Co(η^4-*exo*-C(TMS)=C(SO$_2$Ph)CH=C(OEt)CH(CO$_2$Et))] (**1-*OEt***) leads to formation of a

cyclopentenone derivative (**11**). Thermolysis of the **8-*Ph-A*/8-*Ph-B*** in the presence of maleimide leads to a highly functionalized Diels-Alder adduct; whereas **8-*Ph-A*/8-*Ph-B*** serve as precursors to trisubstituted ruthenocenes by *in situ* deprotonation and reaction with $[(\eta^5\text{-}C_5R_5)Ru(NCMe)_3]PF_6$ (**16-*H*,** R = H; **16-*Me*,** R = Me).

B. Introduction

Cyclopentadienes and cyclopentadiene derivatives serve as important precursors to substituted cyclopentadienyl ligands,[1] novel materials,[2] and a vast array of complex cyclic and polycyclic compounds.[3] Promising new applications for cyclopentadienes have also emerged in the field of chemical biology.[4] Despite the scientific importance of this remarkable compound class, synthetic routes toward multifunctional cyclopentadienes remain limited.[5] A potentially powerful retrosynthetic approach toward polysubstituted cyclopentadienes (**I**) involves ligand dissociation from metal-η^4-cyclopentadiene complexes (**II**), which in turn are accessed via metal-mediated [2 + 2 + 1] cycloaddition of two alkynes and a carbene (Figure 4-1).[6-8]
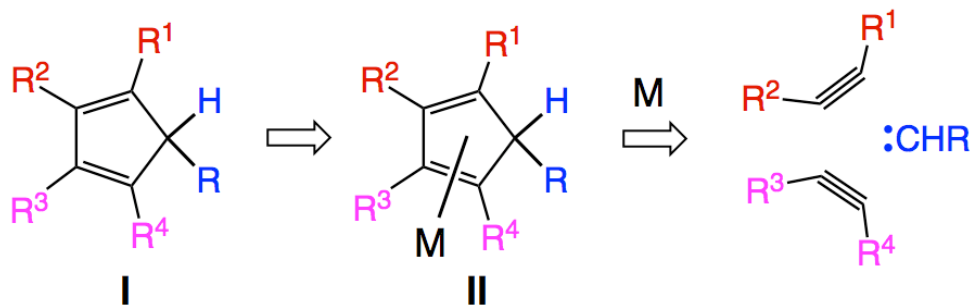
Figure 4-1. A [2 + 2 + 1] cycloaddition route toward highly substituted cyclopentadienes.

We previously developed methods for the synthesis of highly substituted cobalt-η^4-cyclopentadiene complexes from the stepwise cycloaddition of two alkynes and a carbene.[8] For example, access to tetrasubstituted cyclopentadiene complexes, [(η^5-C$_5$H$_5$)Co(η^4-*exo*-C(TMS)=C(SO$_2$Ph)CH=C(R)CH(CO$_2$Et))] (**1-R**), is readily achieved via conversion of the cobalt-alkyne complex, [(η^5-C$_5$H$_5$)Co(PPh$_3$)(η^2-TMSC≡CSO$_2$Ph)] (**2**),[9] and ethyl diazoacetate to cobaltacyclobutene [(η^5-C$_5$H$_5$)(PPh$_3$)Co(κ^2-C(SO$_2$Ph)=C(TMS)CH(CO$_2$Et))] (**3**),[10] followed by reaction with a second alkyne (Scheme 4-1).[8b,11] The sequence of transformations involves a [2 + 1] cycloaddition followed by alkyne incorporation thereby resulting in a formal [2 + 2 + 1] cycloaddition for the combined steps.
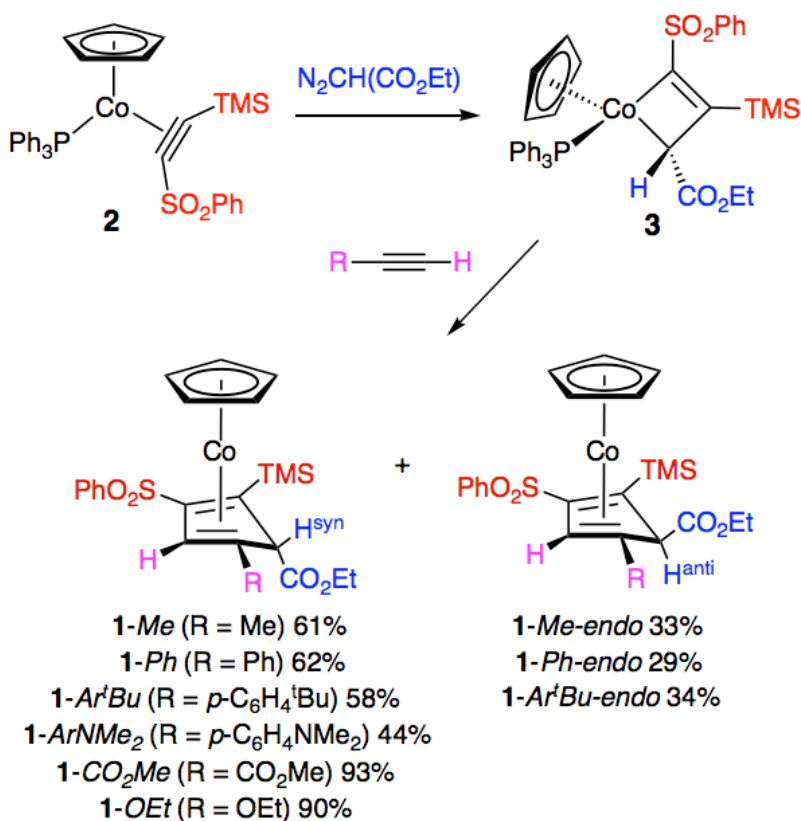
Scheme 4-1. A cobalt-mediated [2 + 2 + 1] route to η^4-cyclopentadiene complexes.

437

Herein we report that the cyclopentadiene ligand in [(η^5-C$_5$H$_5$)Co(η^4-*exo*-C(TMS)=C(SO$_2$Ph)CH=C(R)CH(CO$_2$Et))] (**1**-*Ph*, R = Ph), as well as that in the new cyclopentadiene complexes, **1**-*Ar^{t}Bu* (R = *p*-C$_6$H$_4$^{t}Bu), **1**-*ArNMe$_2$* (R = *p*-C$_6$H$_4$NMe$_2$) and **1**-*Me* (R = Me), are liberated from cobalt in excellent yield upon treatment with trifluoroacetic acid (TFAH). In each case the liberated cyclopentadiene exists as a mixture of two tautomers, [CH$_2$C(SO$_2$Ph)=CHC(CO$_2$Et)=CR] and [CH=C(SO$_2$Ph)CH$_2$C(CO$_2$Et)=CR], whose relative stabilities are established by computation for R = Ph and R = *p*-C$_6$H$_4$NMe$_2$. In the case of R = Ph, the highest energy tautomer, [CH(SO$_2$Ph)CH=C(CO$_2$Et)=CPh=CH], is trapped as its Diels-Alder adduct upon reaction with maleimide at 100 °C. Alternatively, deprotonation of the cyclopentadiene tautomers (R = Ph), followed by reaction with [(η^5-C$_5$R$_5$)Ru(NCMe)$_3$]PF$_6$ (R = H; R = Me) provides access to the trisubstituted ruthenocenes, [(η^5-C$_5$R$_5$)Ru(η^5-C(SO$_2$Ph)CHC(CO$_2$Et)C(Ph)CH)]PF$_6$ (R = H; R = Me). In the case of **1**-*CO$_2$Me* (R = CO$_2$Me),[8b] the liberated cyclopentadiene exists as a hydrogen-bonded fulvenol tautomer; whereas reaction of **1**-*OEt* (R = OEt)[8b] with TFAH liberates the cyclopentadiene ligand as a trisubstituted cyclopentenone.

C. Results and Discussion

1. Synthesis and characterization of (η^5-C$_5$H$_5$)Co(η^4-(cyclopentadiene) complexes, 1-*R*

Synthesis of the desired η^4-cyclopentadiene complexes, **1**-*R*, was readily accomplished by heating cobaltacyclobutene **3** with the corresponding alkyne at 70 °C in toluene (Scheme 4-1). Both **1**-*CO_2Me*[8b] and **1**-*OEt*[8b,c] were generated as the *exo* diastereomer; whereas, **1**-*Ph*,[8b] **1**-*Ar^tBu*, and **1**-*Me* were formed as separable mixtures of *exo* and *endo* stereoisomers. In general, it was found that the *exo* complexes are air-stable, with the *endo* diastereomers being slightly air-sensitive, as indicated by slight decomposition of the *endo* isomers upon chromatography in the air. The greater instability of the *endo* isomer relative to the *exo* isomer may be related to greater steric congestion in the former. For the synthesis of **1**-*ArNMe_2*, a ^{1}H NMR analysis of the crude reaction mixture indicated the formation of a 1 : 1 ratio of *exo* : *endo* isomers, however the *endo* isomer decomposed upon attempted isolation, resulting in isolation of only the slightly air-sensitive *exo* isomer.

The assigned *exo/endo* stereochemistry for **1**-*R* is based on the observation that the ^{1}H NMR chemical shift for the $(sp^3)CH^{syn}$ hydrogens in *exo* isomers appear downfield (δ 3.44 – 4.12) of the $(sp^3)CH^{anti}$ resonances for the corresponding *endo* isomers (δ 2.86 – 3.24).[12] Regioselectivity is readily established by the chemical shift of the $(sp^2)CH$ cyclopentadiene ring-hydrogen. For example, in the ^{1}H NMR spectrum (CDCl_3) of the parent complex, $[(\eta^5\text{-}C_5H_5)Co(\eta^4\text{-}C_5H_6)]$ (**4**-*H*), the vinyl-hydrogens α to the sp^3 ring-carbon resonate at δ 2.48 (s, 2H) whereas the vinyl-hydrogens β to the sp^3 ring-carbon are observed at 5.37 (s, 2H).[12a] For the ten cobalt-cyclopentadiene complexes described in this study, the cyclopentadiene vinyl-hydrogens resonate as singlets between δ 5.6 – 6.6 in CDCl_3.

2. Literature reactions of cobalt-η^4-cyclopentadiene complexes with Brønsted acids.

The reactivity of cobalt-η^4-cyclopentadiene complexes toward Brønsted acids have a long and complicated history. Sixty years ago, Wilkinson and coworkers reported that $[(\eta^5\text{-}C_5H_5)Co(\eta^4\text{-}C_5H_6)]$ (**4**-*H*) acts as a hydride source upon treatment with aqueous HCl to give the cobaltocenium cation (**5**-*H*; eq 1).[13] El Murr later reported that $[(\eta^5\text{-}C_5H_4Me)Co(\eta^4\text{-}C_5H_5Me)]$ (**6**-*Me-endo*) undergoes reaction with $HClO_4$ to give the dimethyl cobalticinium salt **7** (eq 2); whereas exposure of the *exo* monomethyl cyclopentadiene complex **4**-*Me* to $HClO_4$ results in decomposition and formation of C_5H_6 and C_5H_5Me (eq 3).[14] Surprisingly, the diester derivative **6**-*CO$_2$Me-endo* was found to be stable under similar conditions (eq 4).[14] Still later, Leonova described the conversion of **4**-*Me*, and related alkyl analogues (**4**-*R*; R = Et, ^{i}Pr, etc.), to cobalticinium cations (**5**-*R*) upon treatment with H_2SO_4 (eq 5).[15,16] The authors noted that outside an optimal H_2SO_4 concentration range, **4**-*Me* underwent partial decomposition leading to a decreased yield of **5**-*Me*. Based on the earlier work of El Murr (eq 3), we speculate that this decomposition may involve formation of C_5H_5R. More recently, Leonova found that reaction of H_2SO_4 with **4**-*R* (R = CH_2CN, $SiPh_3$, NEt_2, etc.) led to loss of the cyclopentadiene substituent to form cobaltocenium **5**-*H* (eq 6).[16] The authors noted the formation of inorganic cobalt salts in cases where the **5**-*H* yield was low suggests a decomposition pathway that may involve loss of the cyclopentadiene ligand.

$$\text{4-}H \xrightarrow{\text{HCl (aq)}} \text{5-}H \quad \text{Cl}^{\ominus} \tag{1}$$

$$\text{6-}Me\text{-}endo \xrightarrow{\text{HClO}_4} \text{7} \quad \text{ClO}_4{}^{\ominus} \tag{2}$$

$$\text{4-}Me \xrightarrow{\text{HClO}_4} \text{C}_5\text{H}_6 + \text{C}_5\text{H}_5\text{Me} \tag{3}$$

$$\text{6-}CO_2Me\text{-}endo \xrightarrow{\text{HClO}_4} \text{no reaction} \tag{4}$$

$$\text{4-}R \xrightarrow[\substack{R = Me, Et, \\ {}^iPr, {}^tBu, Bz}]{\text{H}_2\text{SO}_4} \text{5-}R \quad \text{HSO}_4{}^{\ominus} \tag{5}$$

$$\text{4-}R \xrightarrow[\substack{R = CH_2CN, \\ SiPh_3, NEt_2 \\ CH_2CO_2Et, \\ etc}]{\text{H}_2\text{SO}_4} \text{5-}H \quad \text{HSO}_4{}^{\ominus} + RH \tag{6}$$

441
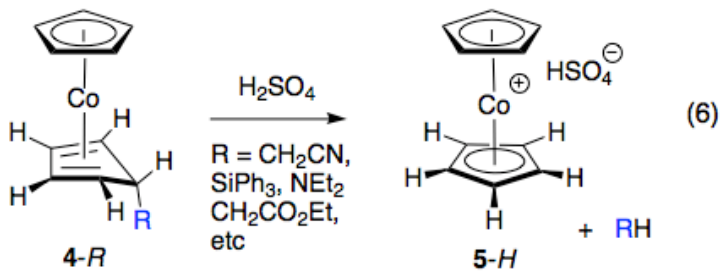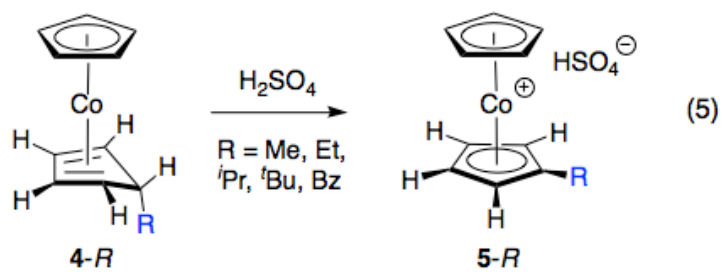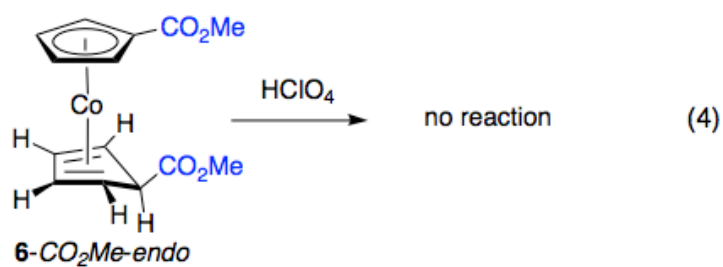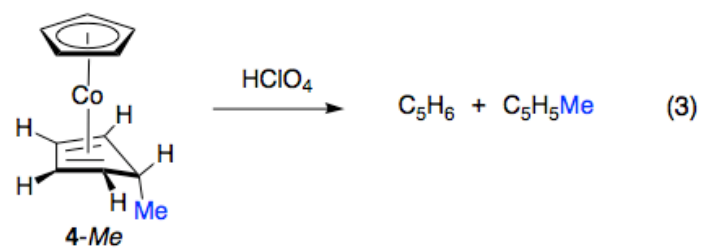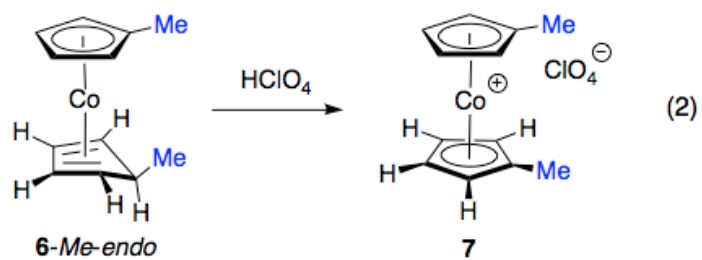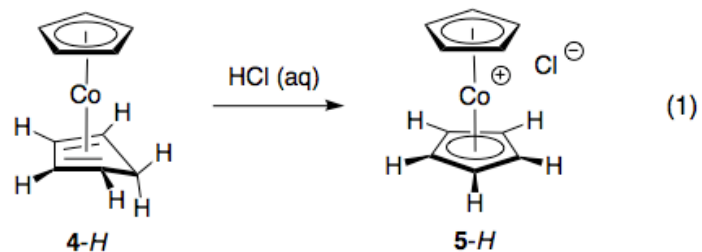
3. Reactions of the *exo*-η^4-cyclopentadiene complexes, 1-*R* (R = Ph, *p*-C$_6$H$_4$^{t}Bu, *p*-C$_6$H$_4$NMe$_2$, Me, CO$_2$Me, OEt), with trifluoroacetic acid (TFAH)

The transformations shown in eq 1 – 6 established four fundamentally different outcomes for the reactions of cobalt-cyclopentadiene derivatives with Brønsted acids: a) loss of a cyclopentadiene hydrogen to give a cobaltocenium salt (eq 1, 2, 4); b) loss of the cyclopentadiene ligand (eq 3); c) no reaction (eq 4);[17] and d) loss of a cyclopentadiene ring-substituent to give a cobaltocenium salt (eq 6). Reactions of highly substituted cobalt-η^4-cyclopentadiene complexes with Brønsted acids have not been reported prior to the work described herein. One might anticipate that the presence of substituents flanking the sp^3-ring-carbon, as in cyclopentadiene complexes **1**-*R*, may sterically inhibit cobaltocenium formation. In addition, the presence of an electron withdrawing sulfone substituent is expected to reduce the hydridic character of the cyclopentadiene (sp^3)C-H bond, again favoring demetallation over cobaltocenium formation.

Indeed, the reactions of **1**-*R* (R = Ph, *p*-C$_6$H$_4$^{t}Bu, *p*-C$_6$H$_4$NMe$_2$, Me) with trifluoracetic acid (TFAH) led to high yields of the corresponding trisubstituted cyclopentadienes, **8**-*R*, with no evidence for formation of cobaltocenium salts (Scheme 4-2). In each case **8**-*R* was formed as a mixture of two tautomers.
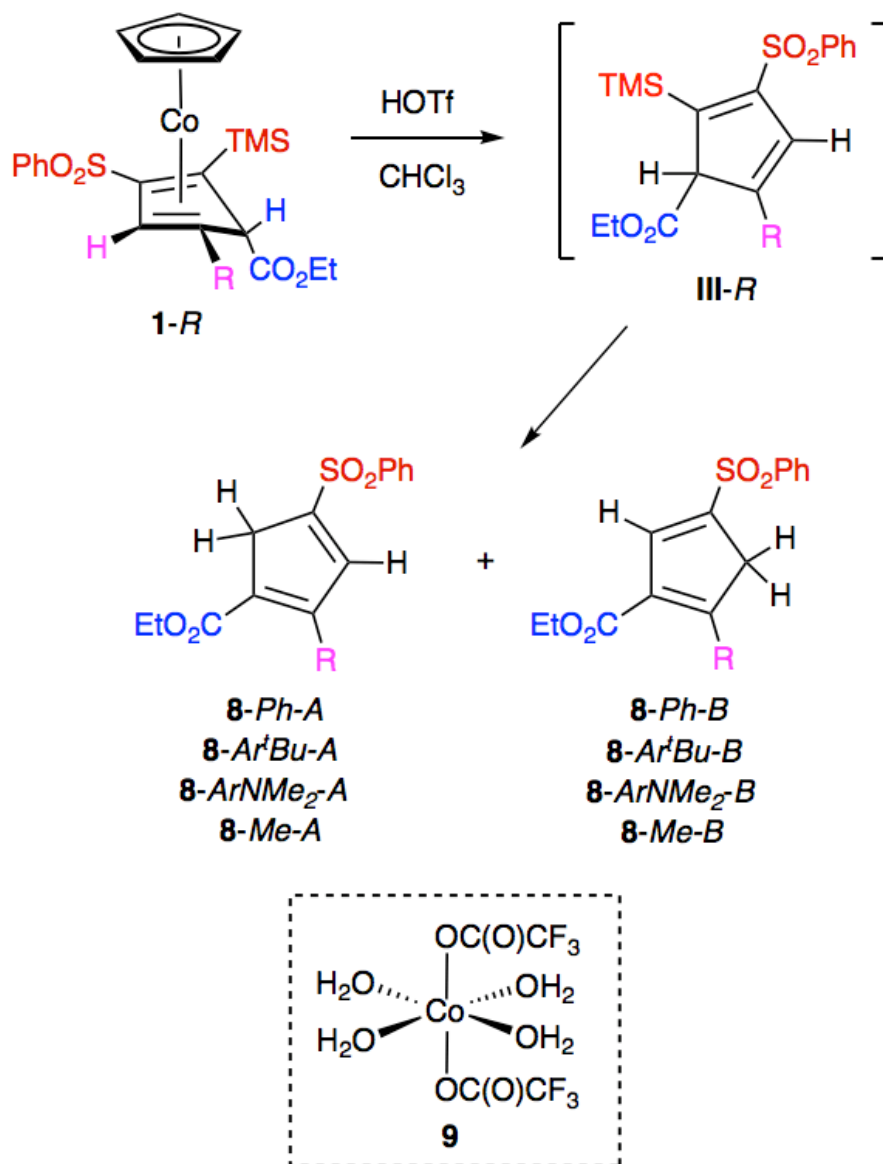
Scheme 4-2. Reaction of **1**-*Ph* and trifluoroacetic acid (TFAH).

In a preliminary small-scale experiment, a CDCl₃ solution of **1**-*Ph* (4 mg, 0.007 mmol), trifluoroacetic acid (TFAH; 0.131 mmol), and 1,3,5-tri-tert-butylbenzene (internal standard), was monitored by ^{1}H NMR spectroscopy. Within ten minutes at ambient temperature, the resonances for **1**-*Ph* were no longer present and a new set of downfield singlets at δ 5.00 (1H, C*H*CO₂Et) and 6.74 (1H, =C*H*-) indicated the formation

of demetallated tetrasubstituted cyclopentadiene **III**-*Ph* (Scheme 2). For comparison, the (sp^3)CH hydrogen resonance for [CPh=CPhCPh=CPhCH(CO$_2$Et)] is observed at δ 5.07 (s, 1H) in chloroform-*d*.[18] A larger scale reaction was carried out in an attempt to isolate **III**-*Ph*, however workup of the reaction mixture led to protodesilylation and formation of a 1.0 : 0.9 ratio of cyclopentadiene tautomers, **8**-*Ph-A* and **8**-*Ph-B*, in 96% combined yield (Scheme 2). An attempt to prepare **III**-*Ph* by reaction of **1**-*Ph* (0.020 mmol) with iodine (0.104 mmol) also resulted in a nearly quantitative NMR yield of **III**-*Ph*.[19] Upon exposure of the reaction solution to air, **III**-*Ph* was converted to **8**-*Ph-A* and **8**-*Ph-B* in 87% combined yield. Fortunately, the clean formation of **III**-*Ph* permitted the acquisition of ^{13}C NMR (CDCl$_3$) data on the crude reaction mixture, and the observation of a doublet of triplets for the carbonyl carbon resonance at δ 167.9 ($^2J_{CH}$ = 10.8 Hz, $^3J_{CH}$ = 3.1 Hz, C*H*CO$_2$Et) established the structure of **III**-*Ph* to be that of the tautomer with a hydrogen and ethoxycarbonyl substituent at the sp^3-ring-carbon. Thus, demetallation of **1**-*Ph-exo* to **III**-*Ph* occurs without 1,5-prototropic shifts,[20] and protodesilylation[21] to give **8**-*Ph-A*/**8**-*Ph-B* occurs without migration of the phenyl, sulfonyl, or ester substituents.[20] The isolated mixture of cyclopentadienes **8**-*Ph-A* and **8**-*Ph-B* was characterized by NMR spectroscopy and an X-ray crystallographic analysis confirmed the structural assignments. The absence of a high field TMS hydrogen resonance and the presence of two overlapping methylene hydrogen resonances at δ 3.80 (s, 4H) in the ^{1}H NMR (CDCl$_3$) spectrum confirmed that protodesilylation had occurred and established that both isomers lacked a substituent at the sp^3-ring-carbon. Integration of methyl hydrogen triplets at δ 1.18 ($^3J_{HH}$ = 7.2 Hz) and 1.25 ($^3J_{HH}$ = 7.2 Hz) established a 1.0 : 0.9 ratio for **8**-*Ph-A* : **8**-*Ph-B*.
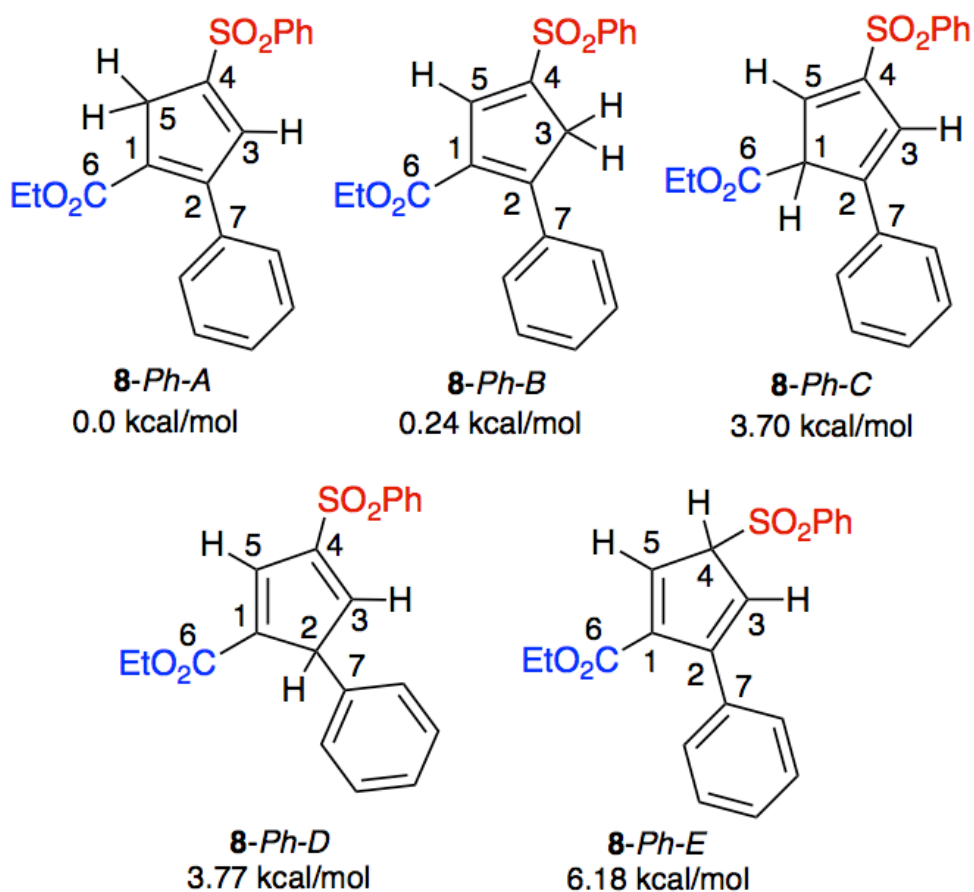
Figure 4-2. B97D/Def2-TZVPP(trichloromethane) relative energetics for five **8-*Ph*** tautomers.

Because the spectroscopic data did not reveal which structure corresponded to the major product, we resorted to computation to establish the relative energetics of the five tautomers that might arise from [1,5]-H sigmatropic shifts in **8-*Ph*** (Figure 4-2, Table 1). The finding that **8-*Ph-A*** is slightly more stable than **8-*Ph-B*** ($\Delta G° = 0.24$ kcal/mol) leads us to tentatively assign structure **8-*Ph-A*** to the major isomer. The other three tautomers (*C* – *E*) are > 3.46 kcal/mol higher in energy than **8-*Ph-A*/8-*Ph-B***, consistent with the experimental observation of only isomers *A* and *B*. The greater stability of **8-*Ph-A*/8-*Ph-B*** relative to tautomers *C* – *E* is presumably a consequence of the more

highly substituted diene unit in the former. The high energy of tautomer **8**-*Ph-E* relative to that of tautomers *C* and *D* may be due in part to greater stability of a vinyl sulfone relative to conjugated phenyl and ester groups. Additionally, greater negative hyperconjugation[22] involving the sp^3–C – sulfur bond compared to the sp^3–C – ester or sp^3–C – phenyl bonds may play a role in the high energy of **8**-*Ph-E* since the sulfone is a much stronger inductively electron-withdrawing group than phenyl or ethyl carboxylate (Hammett constants: SO_2Ph, σ_m = 0.62; σ_p = 0.68; ethyl carboxylate, σ_m = 0.37; σ_p = 0.45; and phenyl, σ_m = 0.06; σ_p = -0.01.[23]

Orange crystals grown from a $CHCl_3$/hexanes solution of the **8**-*Ph-A*/**8**-*Ph-B* mixture at – 20 °C, were subjected to an X-ray crystallographic analysis (Figure 4-3, Table 4-1). The structural data indicate that two isomers of **8**-*Ph* co-crystallized, resulting in a disordered structure consisting of 50% occupancy of the three ring hydrogens of **8**-*Ph-A* (H3-A, H5-A, H5'-A, shown in fuschia color) and the three ring hydrogens of **8**-*Ph-B* (H5-B, H3-B, H3'-B, shown in salmon color). The structural data thus confirm that the ring substituents are arranged in a 1,2,4-substitution pattern. Both isomers have vinyl sulfone and α,β-unsaturated ester substructures, as required by the NMR data. The C(1) – C(2) bond distance of 1.364(3) Å is significantly shorter than the C(3) – C(4) and C(4) – C(5) distances of 1.411(3) and 1.421(3), respectively, and carbons C(1), C(2), C(3), C(4), and C(5) comprise a nearly planar five-membered ring, with the largest deviation from the plane at C(4) (0.004(1) Å). The conformation about the C(2) – C(7) and C(1) – C(6) bonds, as represented by C(1)–C(2)–C(7)–C(8) and the C(2)–C(1)–C(6)–O(1) torsion angles of 21.4(4)° and –21.5(3)°, respectively, permit delocalization of the phenyl and ester π-electrons across the C(1) – C(2) double bond.

The reactions of **1**-*Ar^tBu* and **1**-*Me* with TFAH also led to essentially 1 : 1 ratios of **8**-*Ar^tBu-A*/**8**-*Ar^tBu-B* (1.0 : 0.9) and **8**-*Me-A*/**8**-*Me-B* (1.0 : 1.0); whereas reaction of **1**-*ArNMe₂* and TFAH gave a 1.0 : 0.6 ratio of **8**-*ArNMe₂-A* : **8**-*ArNMe₂-B*. Computation once again found that **8**-*ArNMe₂-A* is more stable than **8**-*ArNMe₂-B* ($\Delta G° = -0.31$ kcal/mol).

Table 4-1. Distances (Å) and angles (deg) from the X-ray crystallographic data for **8**-*Ph-A*/**8**-*Ph-B*, and calculated data for **8**-*Ph-A-calc*, **8**-*Ph-B-calc*, **8**-*Ph-C-calc*, **8**-*Ph-D-calc*, **8**-*Ph-E-calc*, **8**-*ArNMe₂-A-calc*, **8**-*ArNMe₂-B-calc*, and **8**-*Ph-anion-calc*.

	8-*Ph-A/B*	**8**-*Ph-A-calc*	**8**-*ArNMe₂-A-calc*	**8**-*Ph-B-calc*	**8**-*ArNMe₂-B-calc*	**8**-*Ph-C-calc*	**8**-*Ph-D-calc*	**8**-*Ph-E-calc*	**8**-*Ph-anion*
C(1)-C(2)	1.364(3)	1.376	1.384	1.378	1.392	1.518	1.516	1.488	1.452
C(1)-C(5)	1.475(3)	1.507	1.509	1.460	1.454	1.511	1.357	1.355	1.413
C(1)-C(6)	1.489(3)	1.474	1.467	1.485	1.478	1.538	1.471	1.485	1.454
C(2)-C(3)	1.498(3)	1.465	1.466	1.511	1.519	1.362	1.506	1.358	1.398
C(2)-C(7)	1.481(3)	1.470	1.459	1.461	1.445	1.459	1.528	1.469	1.469
C(3)-C(4)	1.421(3)	1.353	1.352	1.499	1.500	1.458	1.353	1.494	1.426
C(4)-C(5)	1.411(3)	1.496	1.497	1.354	1.356	1.351	1.460	1.494	1.407
C(4)-S	1.745(2)	1.760	1.759	1.752	1.743	1.773	1.773	1.864	1.723
S-C(9)	1.767(2)	1.811	1.794	1.795	1.796	1.792	1.791	1.790	1.723
C(6)-O(1)	1.212(2)	1.223	1.227	1.218	1.222	1.213	1.223	1.219	1.229
S-O(3)	1.442(2)	1.458	1.458	1.458	1.459	1.457	1.457	1.458	1.465
S-O(4)	1.437(2)	1.457	1.458	1.459	1.461	1.458	1.457	1.456	1.466
C(10)-N	-	-	1.369	-	1.366	-	-	-	-
C(6)-C(1)-C(2)-C(7)	-5.7(3)	-5.6	-9.4	-9.0	-12.1	62.2	61.5	-12.6	14.1
C(1)-C(2)-C(7)-C(8)	-21.4(4)	-40.2	-32.2	-35.0	-25.1	8.4	52.9	-37.0	35.2
C(4)-S-C(9)	103.9(1)	103.0	103.1	103.2	103.4	102.2	101.8	102.8	104.8
θ(sp³C)-X[a]	-	-	-	-	-	143.5	142.7	147.6	-
fold angle[b]	-	1.50	2.03	0.48	0.76	+0.08	-1.04	-1.48	-

In order to compare reactivity of the same cobalt-cyclopentadiene complex toward three different Brønsted acids we examined the reactions of **1**-*Me* with H_2SO_4, $HClO_4$ and TFAH in CDCl₃. Of the three acids, TFAH gave the highest yield of **8**-*Me-*

A/**8**-*Me-B* (94%); whereas perchloric acid gave an 86% yield. The reaction with sulfuric acid generated a mixture of uncharacterized products with no evidence for **III**-*Me* or **8**-*Me-A*/**8**-*Me-B*. Although it is not clear why TFAH is the most effective acid we do note that acid strength does not appear to be the major factor since $HClO_4$ has a pK_a of -10.0 and TFAH has a pK_a of -0.25,[24] and both give good yields of cyclopentadiene products.
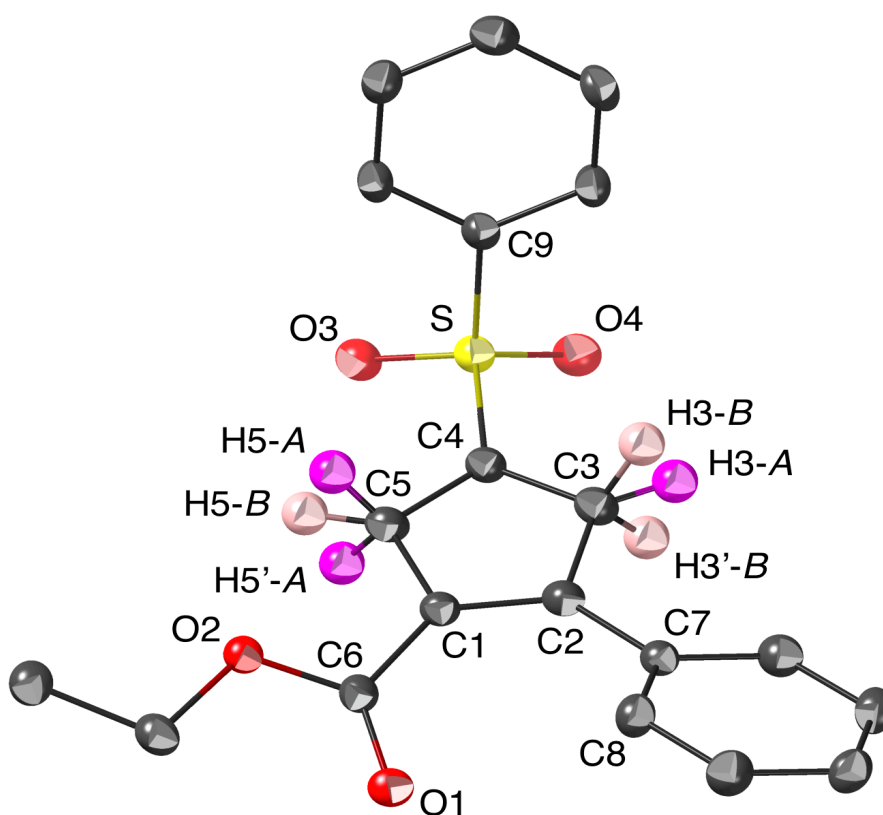
Figure 4-3. ORTEP drawing of the disordered structure for **8**-*Ph-A*/**8**-*Ph-B*, showing 50% occupancy of the two isomers, with fuschia colored hydrogen atoms (H5-A, H5'-A, H3-A) shown for **8**-*Ph-A*. All other hydrogen atoms are omitted for clarity.

The workup procedure for all four reactions of **1**-*R* (R = Ph, *p*-$C_6H_4^tBu$, *p*-$C_6H_4NMe_2$, Me) with TFAH involved evaporation of the volatiles to remove residual TFAH. Subsequent addition of chloroform to the residue led to the formation of a small

amount of insoluble red material and a red oil that coated the walls of the flask. In order to isolate the cyclopentadiene products, the chloroform solution was decanted away from the red oil and filtered through Celite. In the case of **8**-*Ar^tBu-A*/**8**-*Ar^tBu-B*, the red oil that remained in the flask was exposed to air overnight which led to the formation of red crystals that were analyzed by X-ray crystallography, thereby revealing the red byproduct to be the known tetra(aquo) complex [Co(H$_2$O)$_4$(OC(=O)CF$_3$)$_2$] (**9**; Scheme 2).[25]

When a CDCl$_3$ solution of **1**-*CO$_2$Me* and TFAH was monitored by ^{1}H NMR spectroscopy at ambient temperature, the resonances for **1**-*CO$_2$Me* were replaced by a new set of resonances attributed to fulvenol **8**-*CO$_2$Me* (92% NMR yield; Scheme 4-3). Of particular note was a downfield singlet at δ 19.8 (1H) assigned to the enol hydroxyl hydrogen and downfield multiplets at δ 7.46 (m, 5 H) and 7.93 (m, 2H) that integrated for seven hydrogens. The ^{1}H NMR spectrum of the isolated compound in C$_6$D$_6$ exhibited an enol OH resonance at δ 19.78 (s, 1H), a methyl singlet at 3.11, and two vinyl hydrogen resonances at 7.73 (d, $^4J_{HH}$ = 2.4 Hz, 1H) and 7.83 ($^4J_{HH}$ = 2.4 Hz, 1H). For comparison, the ^{1}H NMR spectrum (CDCl$_3$) of fulvenol **10** (Scheme 3) exhibits a hydroxyl hydrogen resonance at δ 19.70, a methyl hydrogen singlet at 4.01 (6H), and a vinyl hydrogen resonance at 7.63 (s, 2H).[26,27]
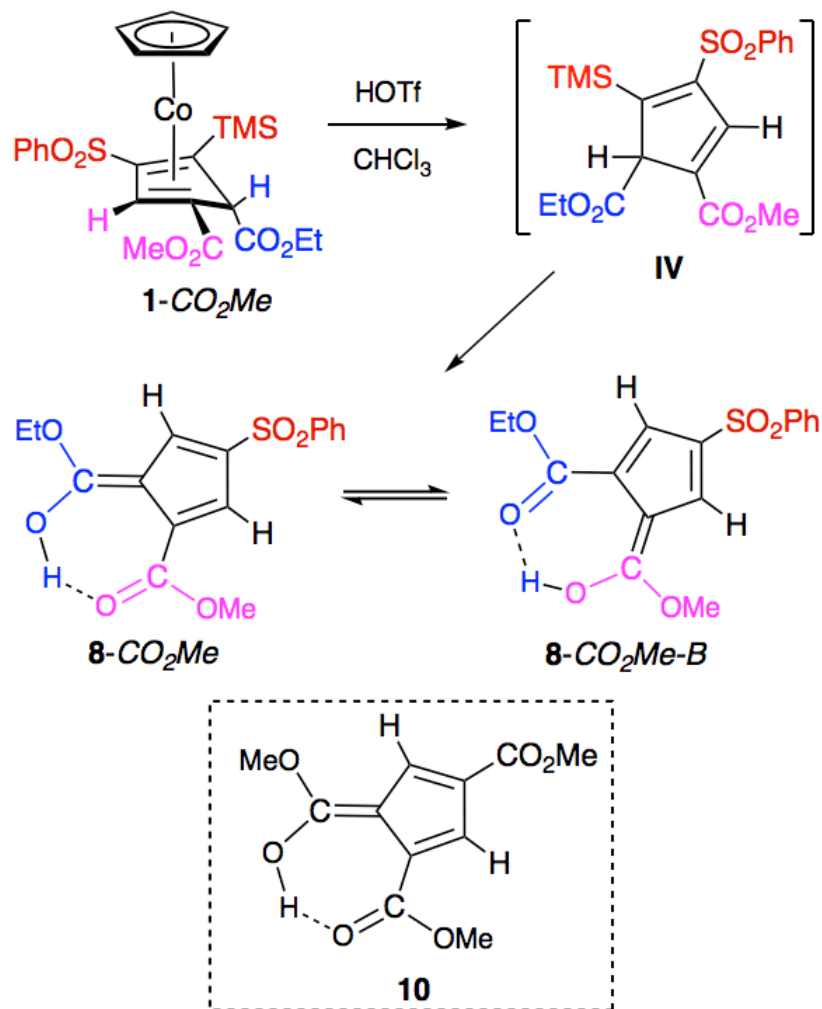
Scheme 4-3. Reaction of **1**-*CO₂Me* and trifluoroacetic acid. Proposed intermediate IV was not observed.

The spectroscopic data for **8**-*CO₂Me* are consistent with the structures of both **8**-*CO₂Me* and tautomer **8**-*CO₂Me-B*, or a rapidly interconverting mixture of the two (Scheme 4-3). A crystallographic analysis established the solid-state structure to be that of **8**-*CO₂Me* (Figure 4-4). The H^b hydrogen atom was refined and the $O(5) - H^b$ and $O(1) - H^b$ distances determined to be 1.353 and 1.115 Å, respectively. The short $O(1) - H^b$ distance relative to that for $O(5) - H^b$, as well as a 1.272(2) Å $C(6) - O(1)$ and a 1.249(2) $C(1) - O(5)$ distance are indicative of a highly asymmetric hydrogen bond.[28]

The hydrogen bond angle of O(1) – H^b– O(5) is slightly bent at 171.2(20)^o, with an O(1)····O(5) distance of 2.460(2) Å. The solid-state structure of **10**, exhibits a symmetric hydrogen bond due to the large experimental error associated with the O – H bond distances.[26] Four of the carbon – carbon bond distances in the five-membered ring of **8**-*CO₂Me* are of similar length: C(1) – C(2) (1.399(2)), C(2) – C(3) (1.386(2)), C(3) – C(4) (1.396(2)), and C(4) – C(5) (1.388(2)), whereas the C(1) – C(5) distance is significantly longer at 1.438(2) Å. A similar pattern of carbon – carbon bond distances was observed for the solid-state structure of **10**.[26] We attribute the longer C(1) – C(5) distance to pi-electron delocalization across the O(1) – C(6) – C(5) – C(4) – C(3) – C(2) – C(1) – C(7) – O(5) that results in less double bond character at the C(1) – C(5) bond.
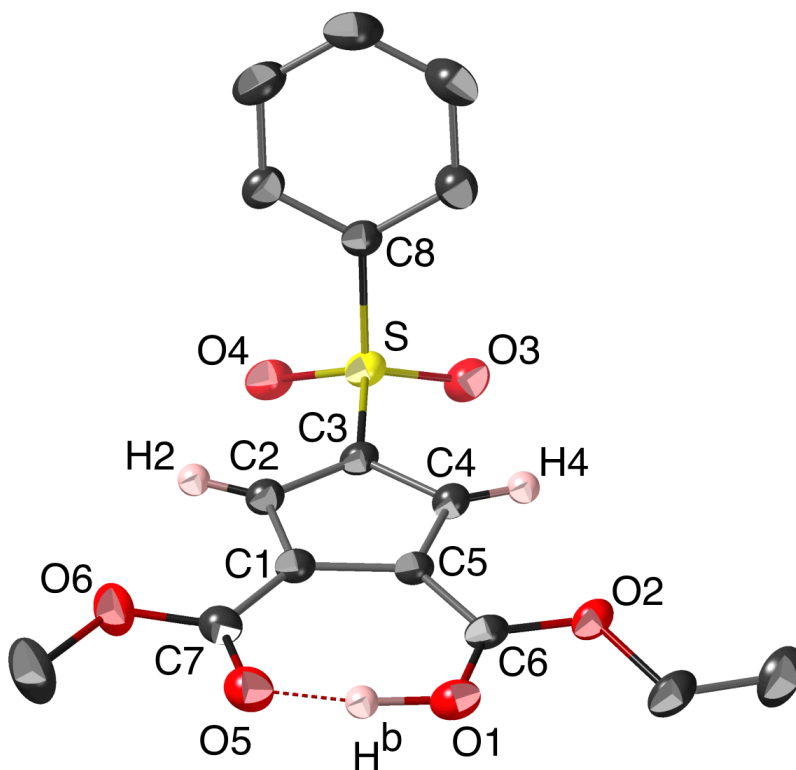
Figure 4-4. ORTEP drawing of **8**-*CO₂Me*.
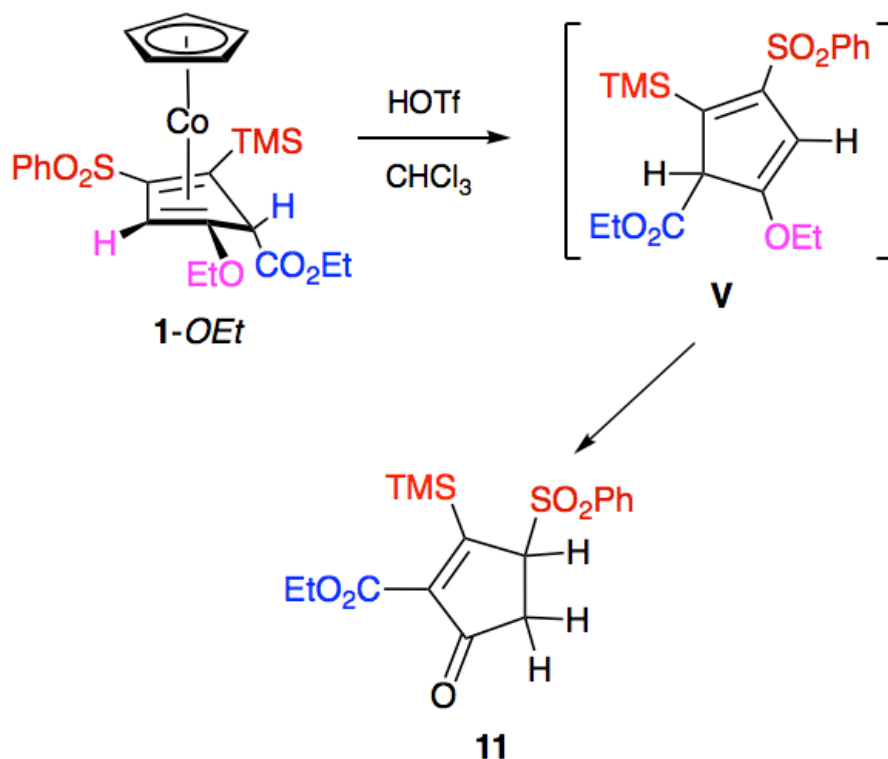
Scheme 4-4. Conversion of 1-*OEt* and TFAH to cyclopentenone **11**.

Reaction of the ethoxy-substituted cyclopentadiene complex [(η^5-C$_5$H$_5$)Co(η^4-*exo*-C(TMS)=C(SO$_2$Ph)CH=C(OEt)CH(CO$_2$Et))] (**1-OEt**) and TFAH resulted in a distinctly different outcome compared to that observed for the other cyclopentadiene complexes described herein (Scheme 4-4). Stirring a CHCl$_3$ solution of **1-OEt** and TFAH at ambient temperature for 6 h led to a gradual change of the solution color from red to dark brown and eventually to light orange. As was observed for the other reactions of **1-R** with TFAH, a red oil (presumably cobalt byproduct **9**) was observed upon evaporation of the volatiles and dissolving the residue in CHCl$_3$. Decanting the chloroform from the flask and subjecting the solution to a chromatographic workup led to isolation of cyclopentenone **11** in 99% yield.[8c,29] The ^{1}H NMR spectrum of **11** revealed

the presence of the TMS substituent and the loss of the ethyl group. An X-ray crystallographic analysis confirmed that **11** was a cyclopentenone derivative (Figure 4-5). We attribute the fact that protodesilylation did not occur to rapid hydrolysis of the presumed cyclopentadiene intermediate **V** to **11**.
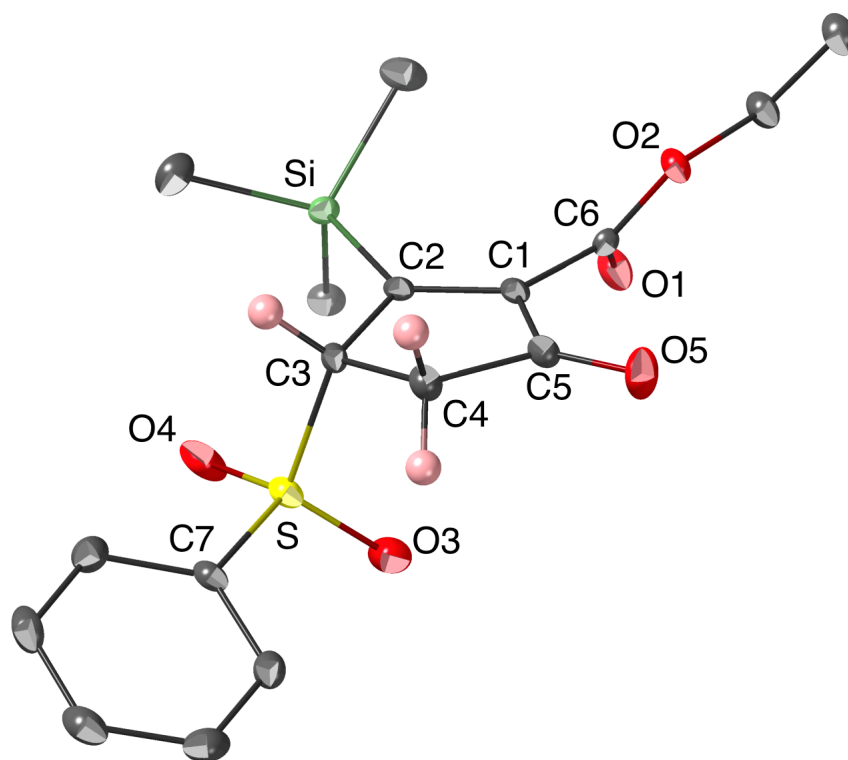
Figure 4-5. ORTEP drawing of **11** with phenyl and ethyl hydrogens omitted for clarity. Selected bond distances (Å): C(1)–C(2), 1.349(3); C(1)-C(5), 1.488(3); C(1)-C(6), 1.494(3); C(2)–C(3), 1.535(3); C(2)-Si, 1.913(2); C(3)–C(4), 1.530(3); C(3)-S, 1.808(2); C(4)–C(5), 1.517(3); C(5)–O(5), 1.209(2); C(6)–O(1), 1.206(2).

4. Reaction of 1-*Ph-endo* with trifluoroacetic acid

El Murr's observation that **6**-*Me-endo* underwent reaction with perchloric acid to give cobaltocenium cation **7** (eq 2), whereas **4**-*Me* underwent reaction under similar conditions to give methylcyclopentadiene (eq 3), suggested that *endo/exo*

stereochemistry may strongly influence partitioning between cyclopentadiene release and hydride loss. We therefore examined the reaction of **1**-*Ph-endo* with TFAH in chloroform and found that the reaction outcome was like that observed for the *exo* isomer **1**-*Ph* (Scheme 4-5). Thus, reaction of **1**-*Ph-endo* with TFAH in chloroform at ambient temperature led to a 92% isolated yield of **8**-*Ph-A* and **8**-*Ph-B* in a 1.0 : 0.9 ratio. A similar reaction of **1**-*Ph-endo* with iodine in CDCl$_3$ resulted in only a 40% yield of **8**-*Ph-A* and **8**-*Ph-B* at 100% conversion. Thus, both *endo* and *exo* isomers of **1**-*Ph* undergo acid-induced demetallation in high yield, with no evidence for formation of a cobaltocenium cation; and demetallation with TFAH provides a superior demetallation yield than does iodine.
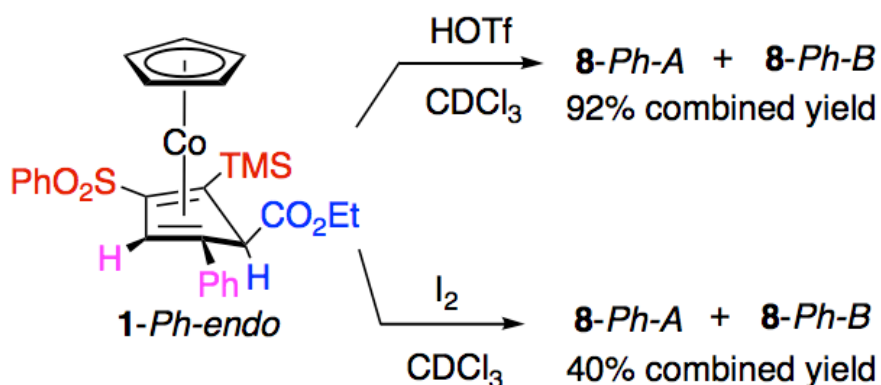
Scheme 4-5. Reaction of **1**-*Ph-endo* and trifluoroacetic acid compared to reaction with iodine.

5. Reactivity studies on 8-*Ph*

In order to establish the basic reactivity patterns of **8**-*Ph*, we examined its deuterium exchange chemistry, thermal stability, Diels-Alder reactivity, and utility as a precursor to trisubstituted cyclopentadienyl ligands in metallocenes.
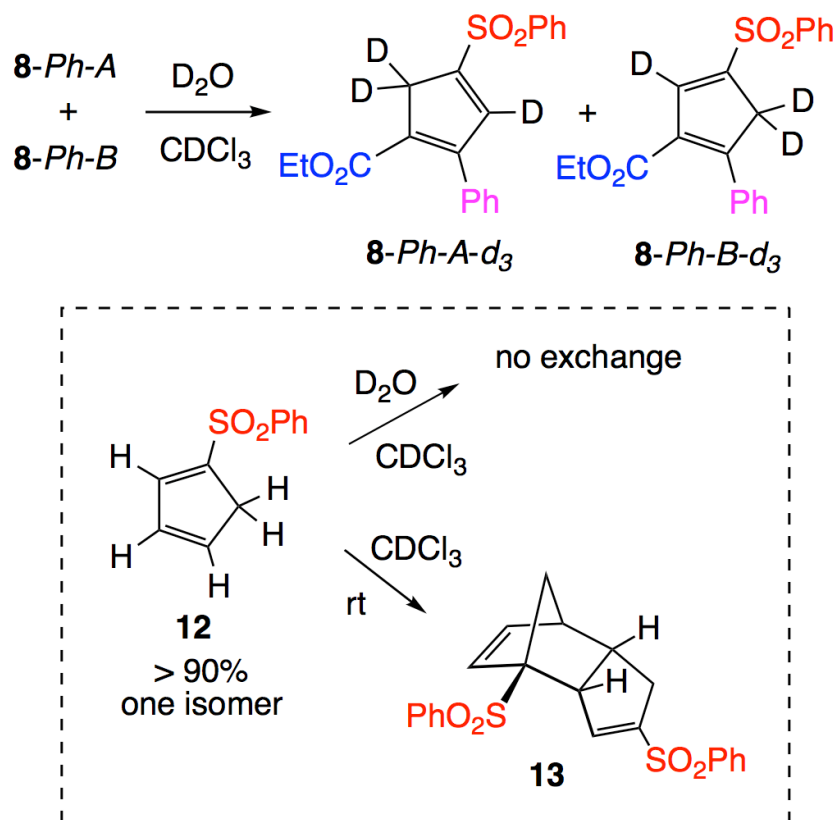
Scheme 4-6. Deuterium exchange occurs in **8-*Ph*** at ambient temperature, unlike literature compound **12**, which does not undergo exchange under similar conditions.

Treatment of the mixture of **8-*Ph-A*** and **8-*Ph-B*** with D₂O in CDCl₃ led to slow incorporation of deuterium into the ring hydrogen positions over the course of 12 h to give **8-*Ph-A-d₃*** and **8-*Ph-B-d₃***, as indicated by a decrease in the intensity of the δ 3.80 methylene hydrogen resonances and the vinyl-hydrogen resonances at 7.37 and 7.65 (Scheme 4-6). An accurate integration of the latter two resonances was not possible due to extensive overlap with the aromatic hydrogen signals. The deuterium exchange reaction presumably involves deprotonation of **8-*Ph-A*** and **8-*Ph-B*** to give the cyclopentadienide, **8-*Ph-anion*** (Figure 4-6). The electrophilic HOMO plot for **8-*Ph-anion*** indicates the highest probability for attack by an electrophile is at C(2), C(3), and C(5)

455

(Figure 4-6). Protonation at C(2) would lead to the higher energy tautomer **8**-*Ph-D* (3.77 kcal/mol calc), however, regardless of the site of protonation, [1,5]-H shifts would ultimately result in exchange of hydrogen for deuterium at C(3) and C(5). The deuterium exchange chemistry of **8**-*Ph* contrasts with that of 1-(phenylsulfonyl)cyclopentadiene (**12**) which undergoes rapid deuterium exchange with D_2O in DMSO-d_6 even under neutral conditions, but fails to exchange with D_2O in $CDCl_3$ (Scheme 4-6).[30,31] Not surprisingly, unlike **12** which dimerizes at ambient temperatures to give Diels-Alder adduct **13**,[30] the more highly substituted and electron deficient **8**-*Ph* is self-orthogonal[4b] at ambient temperature.
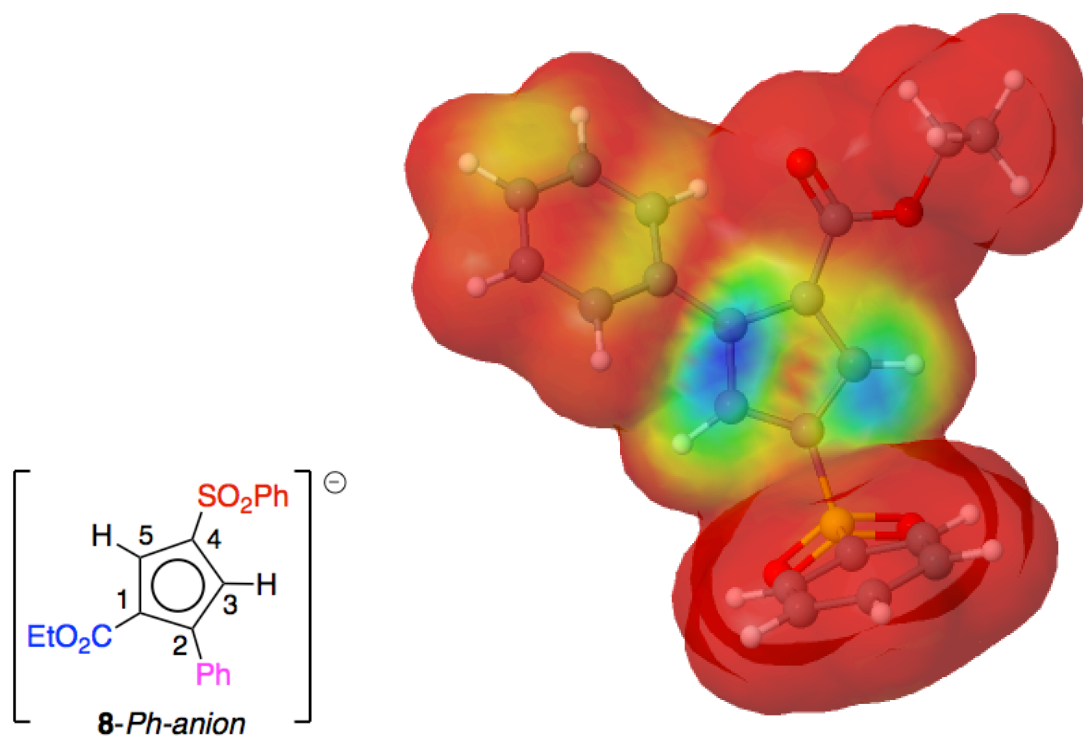
Figure 4-6. *Left panel:* Deprotonation of **8**-*Ph* gives cyclopentadienide, **8**-*Ph-anion*. *Right Panel:* Electrophilic HOMO frontier density plot for **8**-*Ph-anion*. Blue indicates the regions with the highest probability for attack of an electrophile in the absence of steric effects.
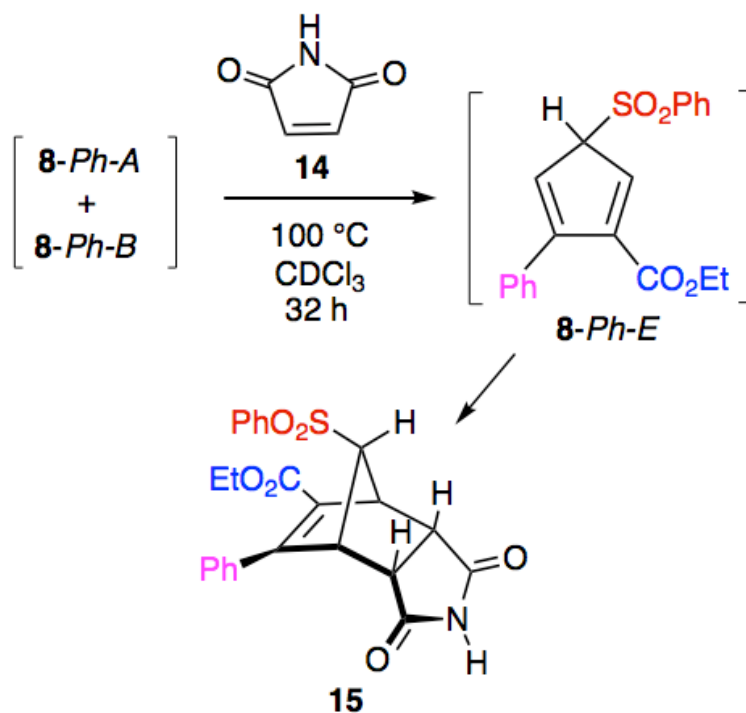
Scheme 4-7. Thermal reaction of **8**-*Ph* with maleimide (**14**) gives Diels-Alder adduct **15**.

Dienyl sulfones are notable for exhibiting dual electron demand behavior toward dienophiles in Diels-Alder reactions.[32] In addition to the strong electron-withdrawing phenylsulfone substituent present in **12**, cyclopentadiene **8**-*Ph* bears an electron-withdrawing ester, and an inductively electron-withdrawing phenyl substituent. Thus, it was not clear if highly electron deficient **8**-*Ph* would be capable of participating in a normal electron demand Diels-Alder reaction. In addition to typical electronic considerations found in acyclic 1,3-dienes, sigmatropic shifts are a major impediment to the use of substituted cyclopentadienes in Diels-Alder reactions since the various tautomers often lead to mixtures of cycloadducts.[20,33] In order to determine the selectivity of **8**-*Ph* toward an electron deficient dienophile, a chloroform-*d* solution of **8**-*Ph-A*/**8**-*Ph-B* (0.014 mmol) and excess maleimide (**14**; 0.049 mmol), with 1,4-

bis(trimethylsilyl)benzene as an internal standard, was heated at 100 °C (Scheme 4-7).

After 30 h, a ^{1}H NMR spectrum of the sample indicated complete consumption of **8**-*Ph*

and the formation of at least five products, based on the presence of five triplets ($^3J_{HH}$ =

7.0 – 7.2 Hz, CH$_3$) between δ 0.87 and 1.34. Of these resonances, one at δ 1.19 ($^3J_{HH}$

= 7.2 Hz) indicated formation of a single major product (**15**; 49.4% yield). A larger scale

reaction was carried out, and chromatographic workup led to the isolation of **15** as a

white solid in 43% yield.
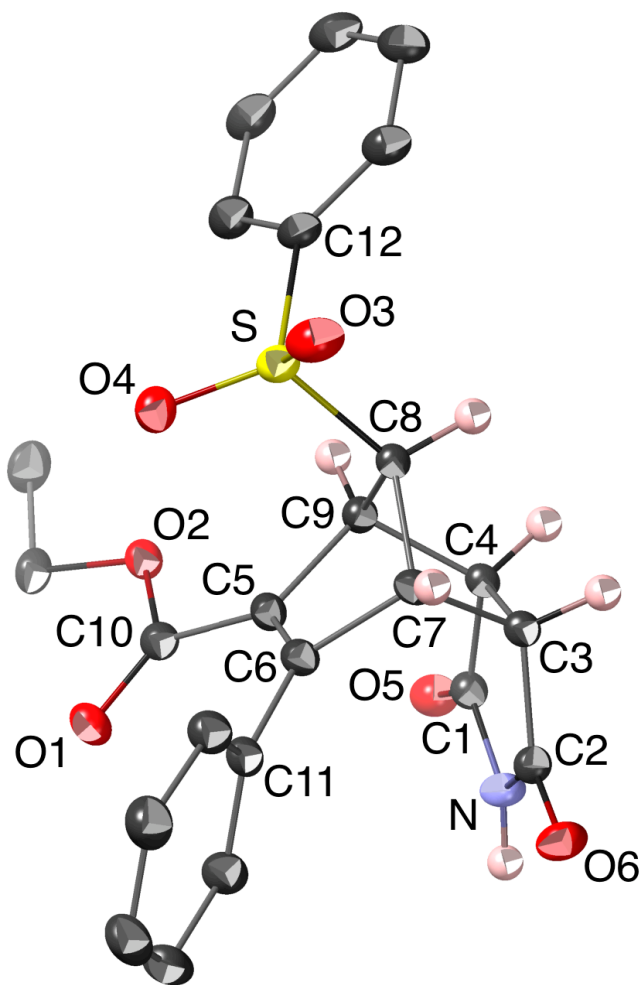
Figure 4-7. ORTEP drawing of **15** with phenyl and ethyl hydrogens omitted for clarity.
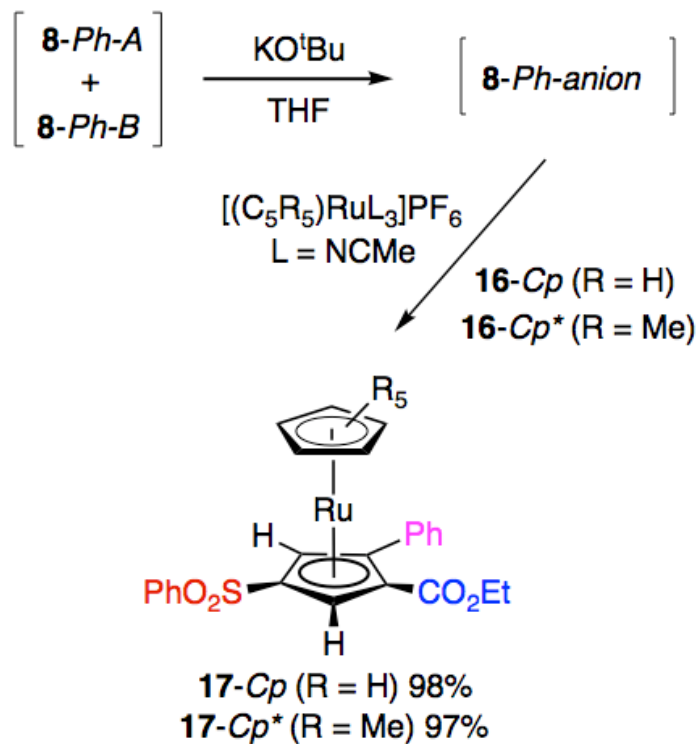
Scheme 4-8. Conversion of **8**-*Ph* to $[(\eta^5\text{-}C_5R_5)Ru(\eta^5\text{-}1,2,4\text{-}C_5H_2(Ph)(SO_2Ph)(CO_2Et)]$ (**17**-*Cp*, R = H; **17**-*Cp**, R = Me).
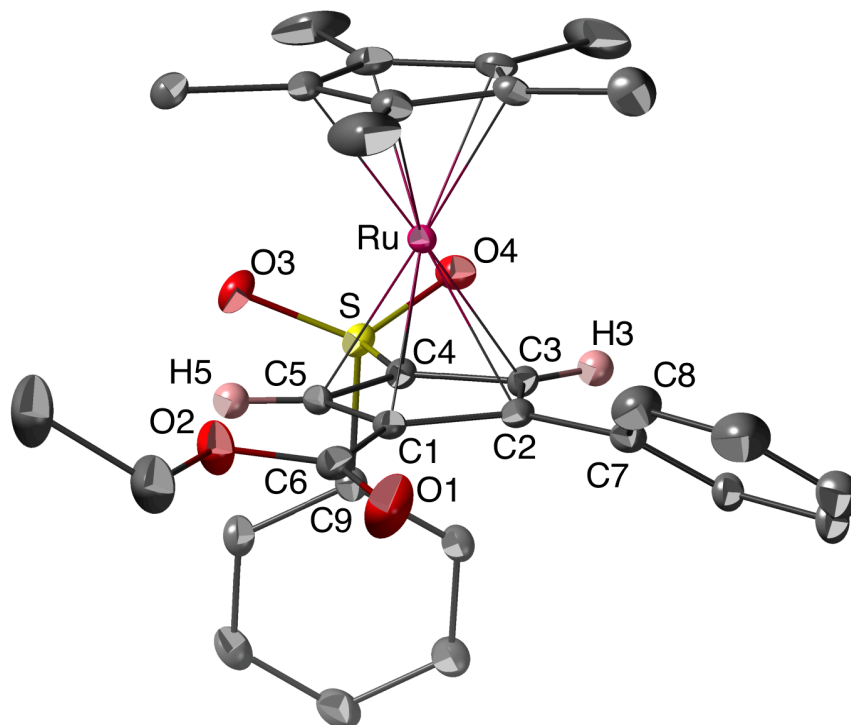
Figure 4-8. ORTEP drawing of **17**-*Cp**. All hydrogen atoms except H(3) and H(5) are omitted for clarity.

In an effort to establish proof of principle for conversion of trisubstituted cyclopentadienes **8**-*Ph-A* and **8**-*Ph-B* to a trisubstituted cyclopentadienyl metal complex, the **8**-*Ph* mixture was converted to the cyclopentadienide **8**-*Ph-anion* which was then allowed to react with $[(C_5R_5)Ru(NCMe)_3]PF_6$ (**16**-*Cp*, R = H; **16**-*Cp**, R = Me; Scheme 4-8).[34] A chromatographic workup of the reaction mixtures led to isolation of the corresponding chiral ruthenocene derivatives, $[(\eta^5\text{-}C_5R_5)Ru(\eta^5\text{-}1,2,4\text{-}C_5H_2(Ph)(SO_2Ph)(CO_2Et)]$ (**17**-*Cp*, R = H; **17**-*Cp**, R = Me) in nearly quantitative yield. In the ^{1}H NMR spectrum (CD$_3$CN) of **17**-*Cp*, the two cyclopentadienyl ring hydrogens of the substituted ligand resonate significantly downfield (δ 5.38 and 5.58) of the cyclopentadienyl hydrogen resonance at 4.80 (s, 5H). For **17**-*Cp** the ring hydrogens of the substituted cyclopentadienyl ligand resonate at δ 5.05 (s, 1H) and 5.12 (s, 1H) in CD$_3$CN solvent. A search for Cp*RuCp' derivates in the Cambridge Crystallographic Data Base found 115 hits of which there were no mononuclear Cp*RuCp' structures wherein Cp' has a 1,2,4-substitution pattern. The solid-state structure of **17**-*Cp** was determined by X-ray crystallography in order to determine the effect of the electron-withdrawing substituents on the bonding parameters (Figure 4-8). The pentamethylcyclopentadienyl to cyclopentadienyl distance of 3.579(4) Å is shorter than the 3.625(3) distance in Cp*RuCp,[35] with the Ru-Cp* distance (1.769(4)) significantly longer than the Cp'Ru distance (1.811(1)). The trisubstituted ligand exhibits a slightly longer C(1) – C(2) distance (1.448(3) Å) than the other carbon – carbon distances which average l.426(2) Å.

D. Conclusions

In summary, the work presented herein demonstrates the the use of Brønsted acids for demetallation of highly substituted cyclopentadiene ligands from CpCo, without formation of cobaltocenium byproducts. The fact that CpCo(η^4-cyclopentadiene) complexes are readily accessible from CpCo – mediated cyclization of two alkynes and ethyldiazoacetate makes the combination of [2 + 2 + 1] cyclization and acid-promoted demetallation an intriguing regioselective approach toward trisubstituted cyclopentadiene (**VI**), fulvenol (**VII**), and cyclopentenone (**VII**) compounds that have unusual substitution patterns and functionality (Figure 4-9). The trisubstituted cyclopentadienes **8-Ph-A,B** have also been shown to serve as precursors to trisubstituted cyclopentadienyl ligands and Diels-Alder adducts.
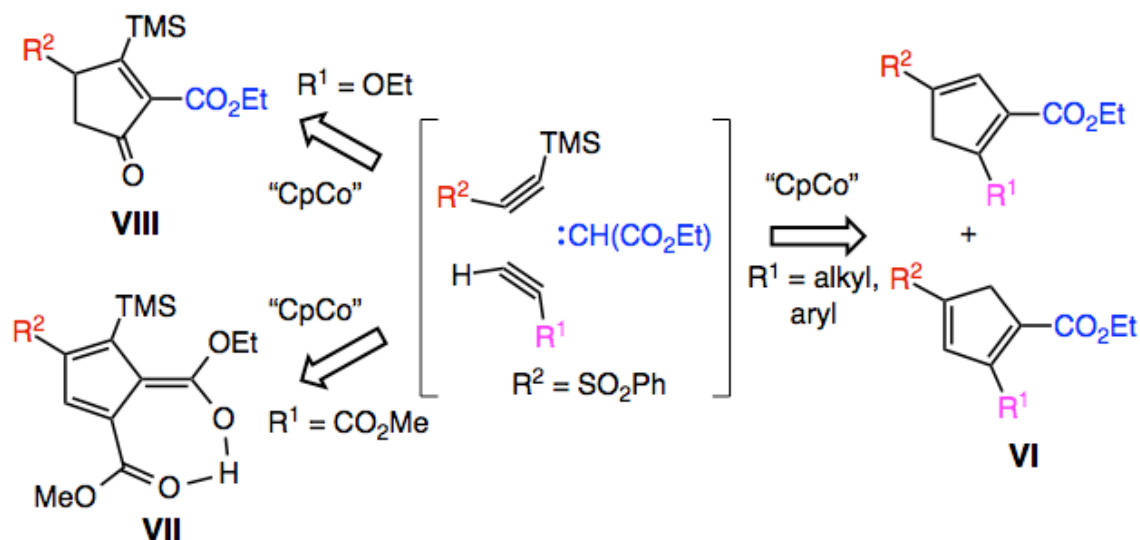
Figure 4-9. Regioselective conversion of two alkynes and a carbene to cyclopentadiene (**VI**), fulvenol (**VII**), and cyclopentenone (**VIII**) products.

E. Experimentals

1. General Information

All manipulations were carried out under an atmosphere of dry dinitrogen using standard Schlenk or glovebox techniques. NMR-scale reactions were performed under a dry dinitrogen atmosphere in 5 mm J-Young NMR tubes equipped with a Teflon needle-valve adapter using freshly degassed solvents (freeze/pump/thaw procedure). Chloroform-*d* was dried and stored over calcium hydride under a dinitrogen atmosphere. Toluene and hexanes were dried on columns of activated alumina using a J. C. Meyer (formerly Glass Contour) solvent purification system. Flash column chromatographic purifications were performed using silica gel (60 Å, particle size 43-60 μm, 230-400 mesh, EMD Chemicals). Combustion analysis was performed by NuMega laboratories of San Diego, CA (USA) or MIDWEST MICROLAB of Indianapolis, IN (USA).

2. Instrumentation

NMR spectra were recorded on Varian Mercury 300 (^{1}H, 300 MHz; ^{13}C, 75.5 MHz), Varian Mercury 400 (^{1}H, 400 MHz; ^{13}C, 100.7 MHz), Jeol ECA 500 (^{1}H, 500 MHz) or Varian VX 500 (^{1}H, 500 MHz; ^{13}C, 125 MHz) spectrometers. ^{1}H and ^{13}C{^{1}H} NMR chemical shifts (δ) are reported in parts per million (ppm) relative to tetramethylsilane (^{1}H and ^{13}C, δ = 0.00 ppm), with reference to the residual proton or carbon resonance

for CDCl$_3$ (^{1}H, δ 7.26 ppm; ^{13}C, δ 77.16 ppm) or acetone-d_6 (^{1}H, δ = 2.05 ppm; ^{13}C, δ = 29.84 ppm). IR spectra of isolated compounds were recorded on a Thermo-Nicolet iS10 FTIR spectrometer at room temperature. High-resolution mass spectra were recorded at the University of California, San Diego Mass Spectrometry Facility on an Agilent 6230 Accurate-Mass TOFMS instrument by using positive ion mode. Melting points are uncorrected and were recorded on a Stanford Research Systems EZ-Melt apparatus.

3. Computational Methods

The structural and energetic analyses of the molecular systems described in this study were carried out with the B97-D density functional method.[36] All calculations employ an ultrafine grid with the Def2-TZVPP basis set.[37] Full geometry optimizations were performed and uniquely characterized via second derivatives (Hessian) analysis to establish stationary points and effects of zero point energy. Effects of solvation were taken into account using the COSab method,[38,39] using a dielectric in accord with experiment and solvent radii from Klamt.[40] Visualization and analysis of structural and property results were obtained using WEBMO.[41]

4. Synthesis

8-*Ph-A*   **8**-*Ph-B*
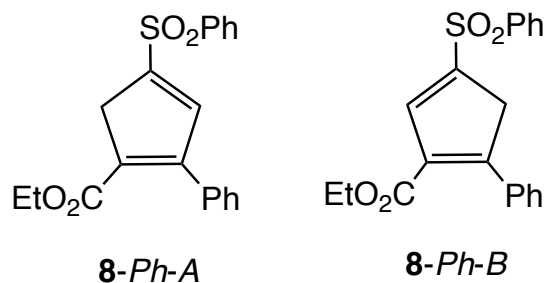
Preparation of [(CH₂C(SO₂Ph)=CHC(CO₂Et)=CR)] (8-*Ph-A*) and [(CH=C(SO₂Ph)CH₂C(CO₂Et)=CR)] (8-*Ph-B*): Trifluoroacetic acid (5 mL) was added to a chloroform solution (20 mL) of **1**-*Ph* (480 mg, 0.872 mmol). After stirring the solution at ambient temperature for 6 h, the solution color changed from red to dark brown and then to orange. The volatiles were evaporated under vacuum to remove residual TFAH, and chloroform (50 mL) was added, leading to the formation of a red oil coating the walls of the flask and a small amount of insoluble red material (cobalt byproducts). The oil and insoluble material were removed by decanting and filtration of the solution through Celite. The chloroform was removed under vacuum, diethyl ether (50 mL) was added, and after stirring for 10 min the solution was again filtered through Celite. Chromatography (silica gel, 30% EtOAc/hexanes) led to the isolation of a 1.0 : 0.9 mixture of **8**-*Ph-A*/**8**-*Ph-B* as a pale yellow solid (294.8 mg, 95.5% yield). Recrystallization from CHCl₃/hexanes at −20 °C gave **8**-*Ph-A*/**8**-*Ph-B* as an air-stable orange crystalline solid. mp 104-105 °C; IR (CDCl₃) 3062, 2981, 2934, 2903, 1710, 1591, 1532, 1488, 1446, 1316 cm⁻¹. ¹H NMR (CDCl₃, 400 MHz): δ 1.18 (t, 3H, *J* = 7.2 Hz), 1.25 (t, 3H, *J* = 7.2 Hz), 3.80 (overlapping singlets, 4H), 4.15 (q, 2H, *J* = 7.2 Hz), 4.22 (q, 2H, *J* = 7.2 Hz), 7.0-8.1 (m, 22H). ¹³C{¹H} NMR (CDCl₃, 125 MHz): δ 14.2, 14.2, 42.9, 45.9, 60.9, 61.2, 127.8, 128.0, 128.2, 128.3, 128.9, 128.9, 129.3, 129. 6, 129.6, 129.8, 130.5, 133.5, 133.6, 133.8, 133.9, 134.6, 140.4, 140.9, 143.0, 143.0, 144.5, 148.5, 152.2, 160.7, 163.1, 163.4. HRMS (ESI-TOF) *m/z*: [M-H]- Calcd for C₂₀H₁₇O₄S 353.0853; Found 353.0852.
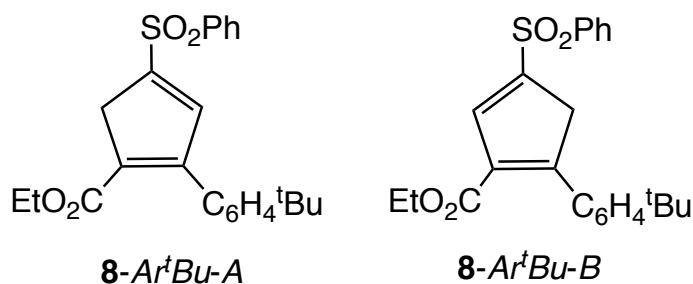
8-Ar^t^Bu-A   **8-Ar^t^Bu-B**

Preparation of [(CH$_2$C(SO$_2$Ph)=CHC(CO$_2$Et)=CR)] (8-Ar^{t}Bu-A, R = p-C$_6$H$_4$^{t}Bu) and [(CH=C(SO$_2$Ph)CH$_2$C(CO$_2$Et)=CR)] (8-Ar^{t}Bu-B, R = p-C$_6$H$_4$^{t}Bu): Trifluoroacetic acid (5 mL) was added to a chloroform solution (20 mL) of **1-Ar^{t}Bu** (262 mg, 0.432 mmol). After stirring the solution at ambient temperature for 6 h, the solution color changed from red to dark brown and then to orange. The volatiles were evaporated under vacuum to remove residual TFAH, and chloroform (40 mL) was added, leading to the formation of a red oil coating the walls of the flask and a small amount of insoluble red material (cobalt byproducts). The oil and insoluble material were removed by decanting and filtration of the solution through Celite. The chloroform was removed under vacuum, diethyl ether (50 mL) was added, and after stirring for 10 min the solution was again filtered through Celite. Chromatography (silica gel, 20% EtOAc/hexanes) led to the isolation of a 1.0 : 0.9 mixture of **8-Ar^{t}Bu-A/8-Ar^{t}Bu-B**, as an air-stable orange oil (171.0 mg, 96.5% yield). IR (CDCl$_3$) 3067, 2964, 2903, 2867, 1716, 1590, 1501, 1446, 1363, 1302, 1210, 1158 cm^{-1}. ^{1}H NMR (CDCl$_3$, 400 MHz): δ 1.20 (t, 3H, J = 7.2 Hz), 1.27 (t, 3H, J = 7.2 Hz), 1.31 (s, 9H), 1.33 (s, 9H), 3.79 (overlapping singlet, 4H), 4.16 (q, 2H, J = 7.2 Hz), 4.24 (q, 2H, J = 7.2 Hz), 7.0-8.1 (m, 20H). ^{13}C{^{1}H} NMR (CDCl$_3$, 125 MHz): δ 14.2, 14.2, 31.3, 31.4, 35.0, 35.0, 43.0, 45.7, 60.8, 61.1, 125.2, 125.3, 127.8, 128.0, 128.8, 128.8, 129.5, 129.6, 129.8, 130.5, 130.8, 133.5, 133.8, 133.9, 140.5, 141.0, 142.4, 143.3, 144.7,

148.3, 152.2, 152.7, 153.3, 161.0, 163.2, 163.5. HRMS (ESI-TOF) *m/z*: [M+Na]+ Calcd for $C_{24}H_{26}O_4SNa$ 433.1444; Found 433.1445.
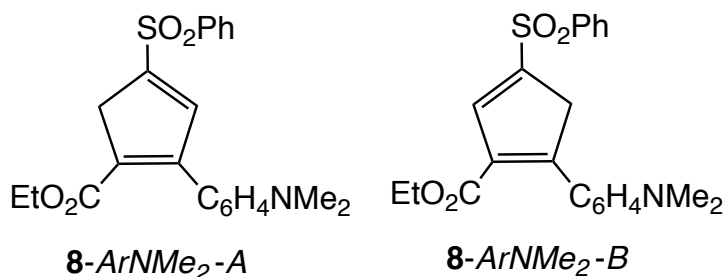
8-*ArNMe₂*-A   **8**-*ArNMe₂*-B

Preparation of [(CH₂C(SO₂Ph)=CHC(CO₂Et)=CR)] (8-*ArNMe₂*-A, R = *p*-C₆H₄NMe₂)

and [(CH=C(SO₂Ph)CH₂C(CO₂Et)=CR)] (8-*ArNMe₂*-B, R = *p*-C₆H₄NMe₂):

Trifluoroacetic acid (5 mL) was added to a chloroform solution (15 mL) of **1**-*ArNMe₂* (197.0 mg, 0.332 mmol). After stirring the solution at ambient temperature for 3 h, the solution color changed from red to light orange. The volatiles were evaporated under vacuum to remove residual TFAH, and chloroform (30 mL) was added, leading to the formation of a red oil coating the walls of the flask and a small amount of insoluble red material (cobalt byproducts). The oil and insoluble material were removed by decanting and filtration of the solution through a glass microfiber filter. The chloroform was removed under vacuum and diethyl ether (50 mL) was added, leading resulting in a yellow-green solution color. After stirring for 2 min the solution was again filtered through a glass microfiber filter. Evaporation of the volatiles led to the isolation of a mixture consisting of a 1.0 : 0.6 mixture of **8**-*ArNMe₂*-A/**8**-*ArNMe₂*-B, as green air-sensitive oil (129.0 mg, 97.5% yield). IR (CDCl₃) 3064, 2981, 2895, 1710, 1679, 1605, 1499, 1440, 1365, 1304, 1199, 1152, cm⁻¹. For **8**-*ArNMe₂*-A: ¹H NMR (CDCl₃, 400 MHz): δ 1.31 (t,

3H, J = 7.2 Hz), 3.02 (s, 6H), 3.80 (s, 2H), 4.26 (q, 2H, J = 6.8 Hz), 6.7-8.1 (m, 10H).

For **8**-*ArNMe₂-B*: ¹H NMR (CDCl₃, 400 MHz): δ 1.24 (t, 3H, J = 7.2 Hz), 3.05 (s, 6H), 3.77 (s, 2H), 4.17 (q, 2H, J = 6.8 Hz), 6.7-8.1 (m, 10H). For **8**-*ArNMe₂-A*/**8**-*ArNMe₂-B* mixture: ¹³C{¹H} NMR (CDCl₃, 125 MHz): δ 14.3, 14.4, 41.9, 43.0, 43.5, 45.2, 60.9, 61.0, 113.7, 116.0, 124.9, 127.7, 127.8, 128.0, 128.6, 129.5, 129.7, 131.0, 131.0, 133.3, 133.4, 133.9, 140.2, 140.5, 141.0, 144.1, 144.2, 147.2, 148.6, 149.5, 151.3, 160.8, 163.4, 163.5. HRMS (ESI-TOF) m/z: [M+Na]+ Calcd for $C_{22}H_{23}NO_4SNa$ 420.1240; Found 420.1235.

8-*Me-A*   **8**-*Me-B*
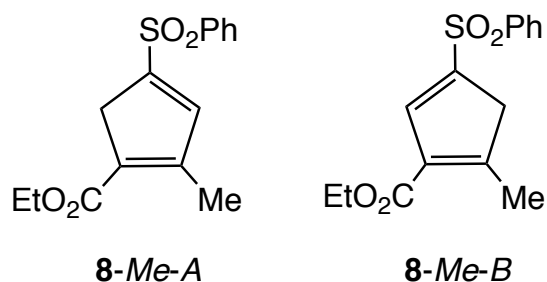
Preparation of **[(CH₂C(SO₂Ph)=CHC(CO₂Et)=CMe)]** **(8-*Me-A*)** **and** **[(CH=C(SO₂Ph)CH₂C(CO₂Et)=CMe)]** **(8-*Me-B*)**:   Trifluoroacetic acid (3.5 mL) was added to a chloroform solution (15 mL) of **1**-*Me* (206 mg, 0.422 mmol). After stirring the solution at ambient temperature for 8 h, the solution color changed from red to brown and then to orange. The volatiles were evaporated under vacuum to remove residual TFAH, and chloroform (30 mL) was added, leading to the formation of a red oil coating the walls of the flask and a small amount of insoluble red material (cobalt byproducts). The oil and insoluble material were removed by decanting and filtration of the solution through Celite. The chloroform was removed under vacuum, diethyl ether (50 mL) was

467

added, and after stirring for 10 min the solution was again filtered through Celite. Chromatography (silica gel, 25% EtOAc/hexanes) led to the isolation of a 1 : 1 mixture of **8**-*Me-A*/**8**-*Me-B* as a white solid (116.0 mg, 94.1% yield). Recrystallization from CHCl$_3$/hexanes at −20 °C gave **8**-*Me-A*/**8**-*Me-B* as an air-stable white solid. IR (CDCl$_3$) 3089, 3070, 2995, 1718, 1530, 1443, 1307, 1241, 1146 cm^{-1}. ^{1}H NMR (CDCl$_3$, 400 MHz): δ 1.30 (t, 3H, J = 7.2 Hz), 1.34 (t, 3H, J = 7.2 Hz), 2.35 (s, 3H), 2.40 (s, 3H), 3.41 (s, 2H), 3.55 (s, 2H), 4.22 (q, 2H, J = 7.2 Hz), 4.27 (q, 2H, J = 7.2 Hz), 7.0-8.1 (m, 12H); ^{13}C{^{1}H} NMR (CDCl$_3$, 125 MHz): δ 14.4, 14.5, 15.4, 16.4, 41.7, 46.9, 60.6, 60.8, 127.7, 127.9, 129.5, 129.6, 130.9, 133.4, 133.7, 135.1, 140.6, 141.1, 141.2, 142.6, 145.3, 148.2, 151.8, 163.2, 163.9, 164.0. HRMS (ESI-TOF) *m/z*: [M+Na]+ Calcd for C$_{15}$H$_{16}$O$_4$SNa 315.0662; Found 315.0658.

9
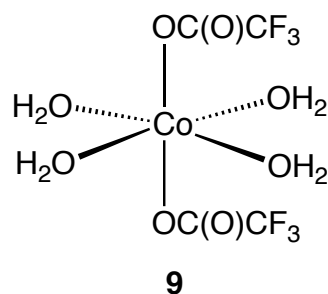
Preparation of [Co(H$_2$O)$_4$(OC(=O)CF$_3$)$_2$] (9)*: Trifluoroacetic acid (5 mL) was added to a chloroform solution (20 mL) of **1**-*Ar^{t}Bu* (262 mg, 0.432 mmol). After stirring the solution at ambient temperature for 6 h, the solution color changed from red to dark brown and then to orange. The volatiles were evaporated under vacuum to remove residual TFAH, and chloroform (40 mL) was added, leading to the formation of a red oil coating the walls of the flask. The solution was decanted away from the oil and the oil crystallized

upon standing overnight. Previously reported **9** was isolated as an air-stable red crystalline solid (5 mg, 61.6% yield). IR (KBr) 3411, 1710, 1679, 1632, 1457, 1435 cm^{-1}. At attempt at obtaining a mass spectrum failed. The structure was confirmed by X-Ray crystallography (see supporting information).

11
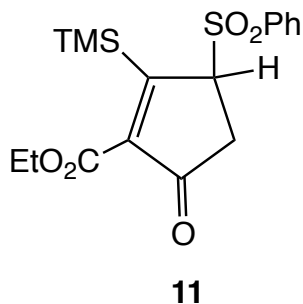
Preparation of Ethyl 5-oxo-3-((phenylperoxy)thio)-2-(trimethylsilyl)cyclopent-1-ene-1-carboxylate (11): Trifluoroacetic acid (5 mL) was added to a chloroform solution (20 mL) of **1**-*OEt* (353 mg, 0.681 mmol). The solution was stirred at ambient temperatures for 6 h, during which time the color changed from red to dark brown and then to light orange in color. The volatiles were evaporated under vacuum to remove residual HFA, and chloroform (50 mL) was added, leading to the formation of a red oil coating the walls of the flask and a small amount of insoluble red material (cobalt byproducts). The oil and insoluble material were removed by decanting and filtration of the solution through Celite. Chromatography (silica gel, 30% EtOAc/hexanes) led to the isolation of **11** as a white solid (248.0 mg, yield = 99.4% yield). Recrystallization from CHCl$_3$/hexanes at −20 °C gave **11** as an air-stable white crystalline solid. mp 148-149 °C; IR (CDCl$_3$) 3614, 3545, 3059, 2981, 1746, 1723, 1621, 1446, 1307, 1209 cm^{-1}. ^{1}H NMR (CDCl$_3$, 400 MHz): δ 0.44 (s, 9H), 1.35 (t, 3H, J = 7.2 Hz), 2.61 (m, 2H), 4.30 (m,

2H), 4.71 (dd, 1H, J_1 = 6.8 Hz, J_2 = 1.6 Hz), 7.5-8.0 (m, 5H). $^{13}C\{^{1}H\}$ NMR (CDCl$_3$, 125 MHz): δ 0.8, 14.2, 39.1, 61.9, 68.3, 129.5, 129.8, 134.8, 135.1, 151.0, 163.5, 175.7, 198.6. HRMS (ESI-TOF) *m/z*: [M+H]+ Calcd for C$_{17}$H$_{23}$O$_5$SSi 367.1030; Found 367.1024.

15
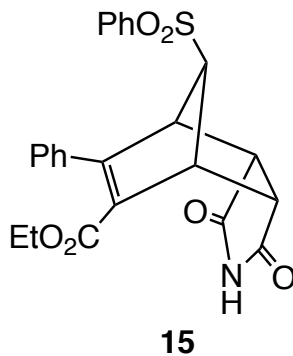
Diels-Alder reaction of 8-*Ph-A*/8-*Ph-B* and maleimide (15): A CDCl$_3$ solution (50 mL) of **8-*Ph-A*/8-*Ph-B*** (265 mg, 0.748 mmol) and maleimide (363 mg, 3.741 mmol) was heated at 100 °C for 32 h, after which time a chromatographic workup (silica gel, 25% EtOAc/hexanes) led to isolation of **15** (145 mg, 42.9% yield) as a white solid. Recrystallization from chloroform/hexanes led to a white crystalline solid. mp 219 °C; IR (CD$_3$CN) 3245, 3078, 2981, 1768, 1721, 1446, 1299, 1263, 1182, 1149 cm^{-1}. ^{1}H NMR (CDCl$_3$, 400 MHz): δ 1.19 (t, 3H, J = 7.2 Hz), 3.56 (m, 3H), 4.06 (m, 3H), 4.20 (m, 1H), 7.0-8.0 (m, 11H). $^{13}C\{^{1}H\}$ NMR (CDCl$_3$, 125 MHz): δ 14.1, 46.6, 47.4, 49.4, 53.5, 61.0, 83.7, 126.6, 128.1, 128.7, 129.5, 129.6, 130.6, 132.1, 134.3, 139.0, 152.5, 162.5, 173.6. HRMS (ESI-TOF) *m/z*: [M+Na]+ Calcd for C$_{24}$H$_{21}$NO$_6$SNa 474.0982; Found 474.0980.
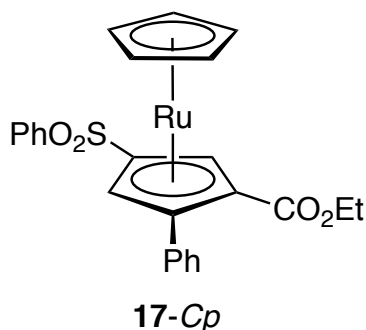
17-Cp

[(η^5-C₅H₅)Ru(η^5-C(SO₂Ph)CHC(CO₂Et)CHC(Ph))] (17-Cp): A THF solution (25 mL) of

8-*Ph-A*/**8**-*Ph-B* (236 mg, 0.666 mmol) and KO*t*Bu (75 mg, 0.669 mmol) was stirred

under a nitrogen atmosphere at ambient temperature for 15 min. The volatiles were

evaporated, and the residue re-dissolved in THF (30 mL) before adding

[(C₅H₅)Ru(NCMe)₃]PF₆ (**16**-*Cp*; 240 mg, 0.553 mmol). After stirring at ambient

temperature for 20 min the volatiles were removed in vacuo and the residue dissolved in

chloroform (15 mL). The mixture was filtered through a glass pipette packed with

aluminum oxide to give **17**-*Cp* (283 mg, 98.5% yield) as a yellow solid. Recrystallization

from toluene/hexanes at –20 °C afforded **17**-*Cp* as air-stable yellow crystals. mp 149

°C; IR (CDCl₃) 3103, 3062, 2978, 1724, 1446, 1318, 1224, 1158, 1118 cm⁻¹. ¹H NMR

(CD₃CN, 400 MHz): δ 1.14 (t, 3H, *J* = 7.2 Hz), 4.08 (m, 2H), 4.80 (s, 5H), 5.38 (s, 1H),

5.58 (s, 1H), 7.0-8.0 (m, 10H). ¹³C{¹H} NMR (CD₃CN, 125 MHz): δ 14.3, 61.4, 73.4,

76.3, 76.6, 78.0, 95.3, 98.2, 128.0, 128.3, 128.5, 130.4, 132.0, 134.4, 135.0, 143.0,

168.2. HRMS (ESI-TOF) *m/z*: [M+Na]+ Calcd for C₂₅H₂₂O₄RuSNa 543.0181; Found

543.0176. Anal. Calcd for C₂₅H₂₂O₄RuS: C, 57.79; H, 4.27. Found C, 57.30; H, 4.65.
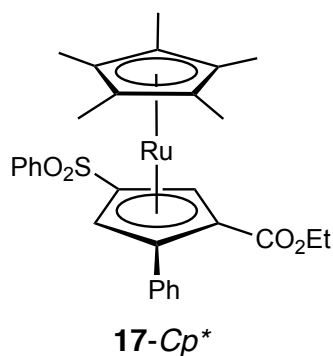
17-*Cp**

[(η^5-C₅Me₅)Ru(η^5-C(SO₂Ph)CHC(CO₂Et)CHC(Ph))] (17-Cp*): A THF solution (25 mL) of **8**-*Ph-A*/**8**-*Ph-B* (231 mg, 0.649 mmol) and KO^{t}Bu (74 mg, 0.660 mmol) was stirred under a nitrogen atmosphere at ambient temperature for 15 min. The volatiles were evaporated, and the residue re-dissolved in THF (30 mL) before adding [(C₅Me₅)Ru(NCMe)₃]PF₆ (**16**-*Cp**; 280 mg, 0.554 mmol). After stirring at ambient temperature for 20 min the volatiles were removed in vacuo and the residue dissolved in chloroform (15 mL). The mixture was filtered through a glass pipette packed with aluminum oxide to give **17**-*Cp** (318 mg, 97.3% yield) as a white solid. Recrystallization from toluene/hexanes at –20 °C afforded **17**-*Cp** as air-stable white crystals. mp 195 °C; IR (CDCl₃) 3098, 3059, 2978, 2906, 1718, 1599, 1476, 1446, 1374, 1321, 1160, 1118 cm^{-1}, ^{1}H NMR (CD₃CN, 400 MHz): δ 1.20 (t, 3H, J = 7.2 Hz), 1.81 (s, 15H), 4.11 (m, 2H), 5.05 (s, 1H), 5.12 (s, 1H), 7.0-8.0 (m, 10H). ^{13}C{^{1}H} NMR (CD₃CN, 125 MHz): δ 10.8, 14.5, 61.2, 76.0, 77.7, 77.8, 90.0, 95.1, 97.0, 127.6, 128.0, 128.4, 130.4, 130. 8, 134.0, 134.5, 144.4, 167.5. HRMS (ESI-TOF) *m/z*: [M+H]+ Calcd for C₃₀H₃₃O₄RuS 591.1145; Found 591.1140. Anal. Calcd for C₃₀H₃₂O₄RuS: C, 61.10; H, 5.47. Found C, 60.94; H, 5.09.

F. Appendix
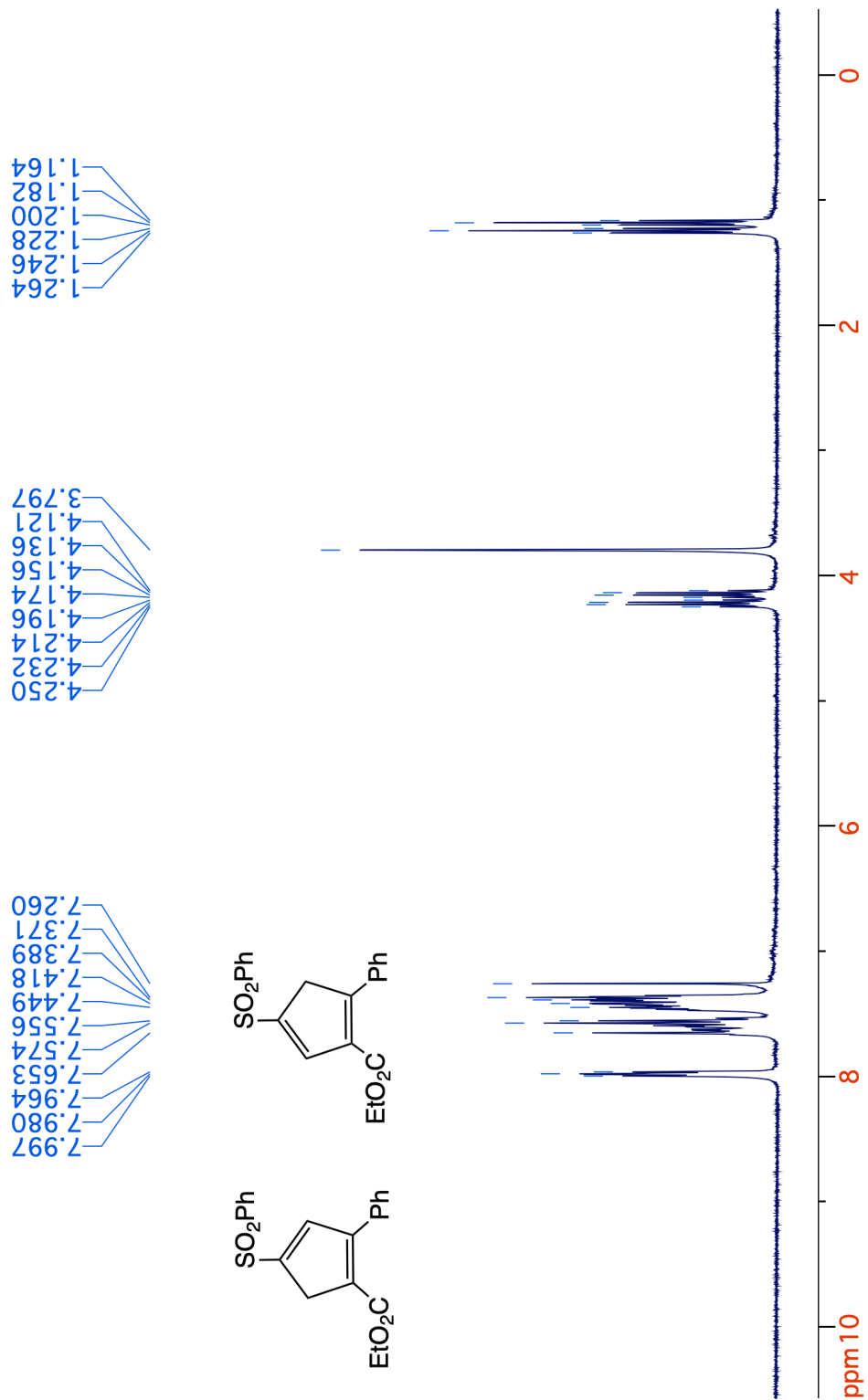
Figure 4-10. ^{1}H NMR spectrum (400 MHz, CDCl$_3$) of **8**-*Ph-A* and **8**-*Ph-B*.
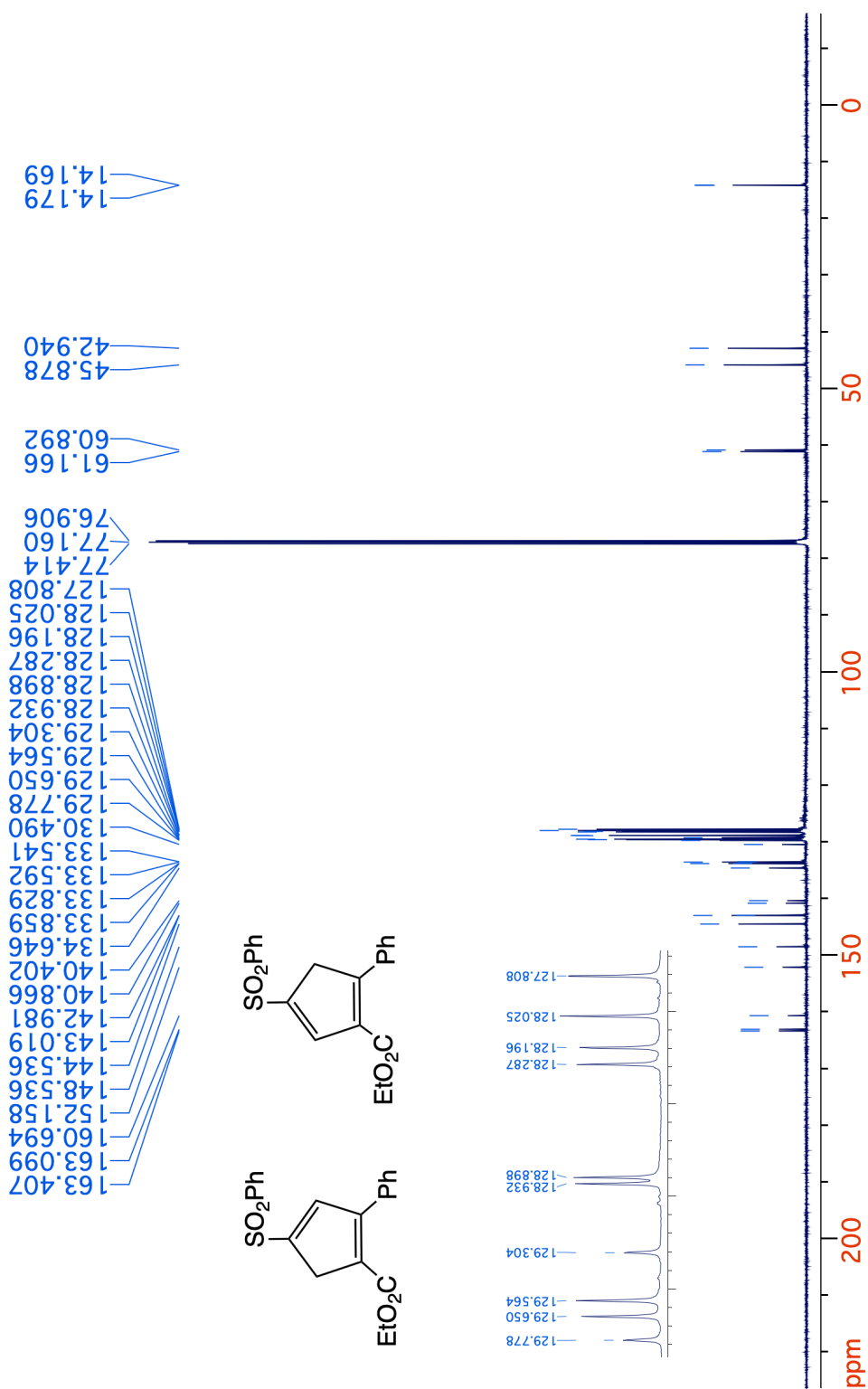
Figure 4-11. $^{13}C\{^1H\}$ NMR spectrum (125 MHz, CDCl$_3$) of **8**-*Ph-A* and **8**-*Ph-B*.

474
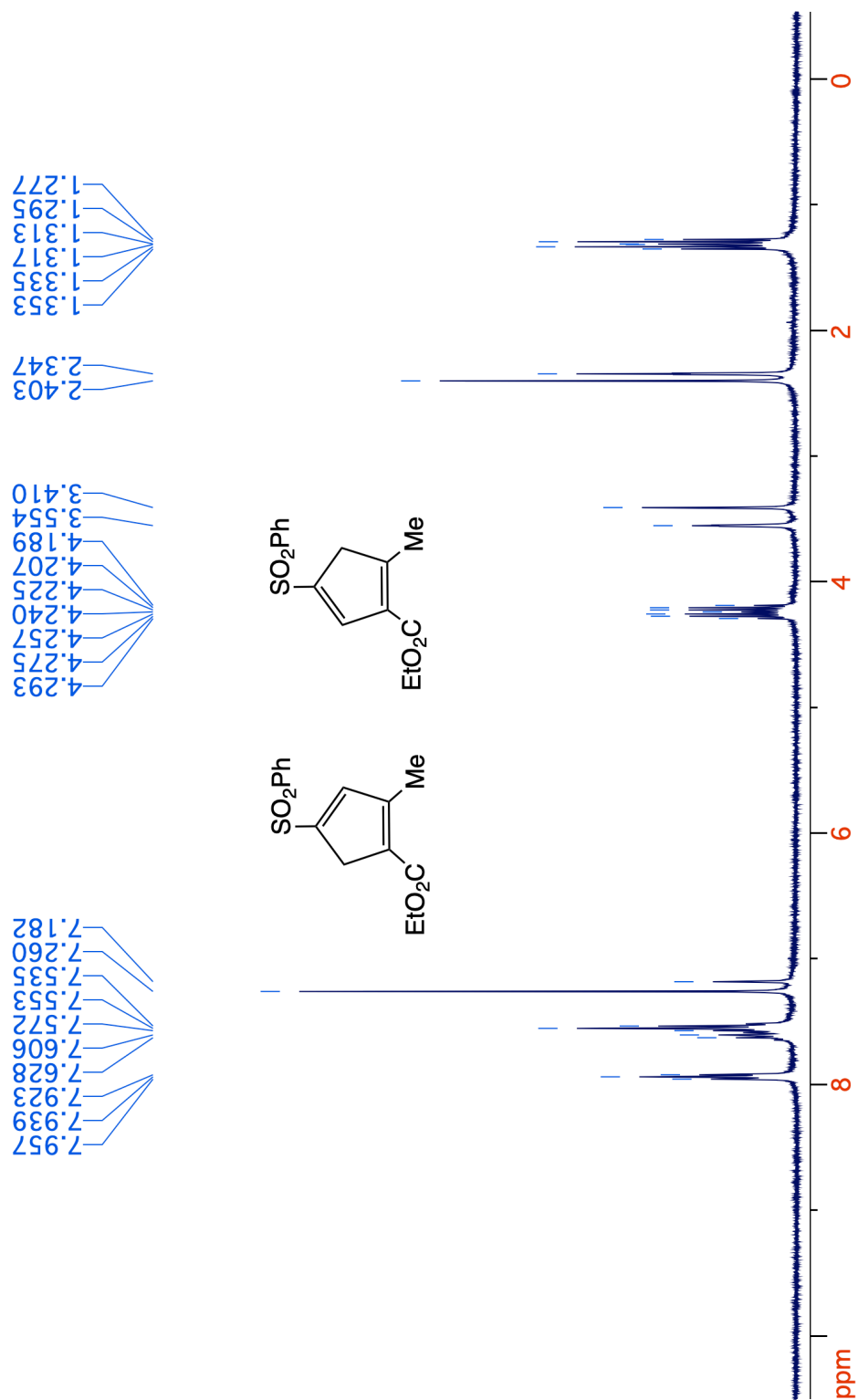
Figure 4-12. ^{1}H NMR spectrum (400 MHz, CDCl$_3$) of **8-*Me-A*** and **8-*Me-B***.

475

14.431
14.456
15.375
16.445

41.713
46.896

60.579
60.784

76.906
77.160
77.414

127.700
127.942
129.471
129.573
130.908
133.404
133.721
135.108
140.551
141.105
141.250
142.576
145.293
148.237
151.790
163.228
163.869
164.000

SO₂Ph

Me

EtO₂C

SO₂Ph

Me

EtO₂C
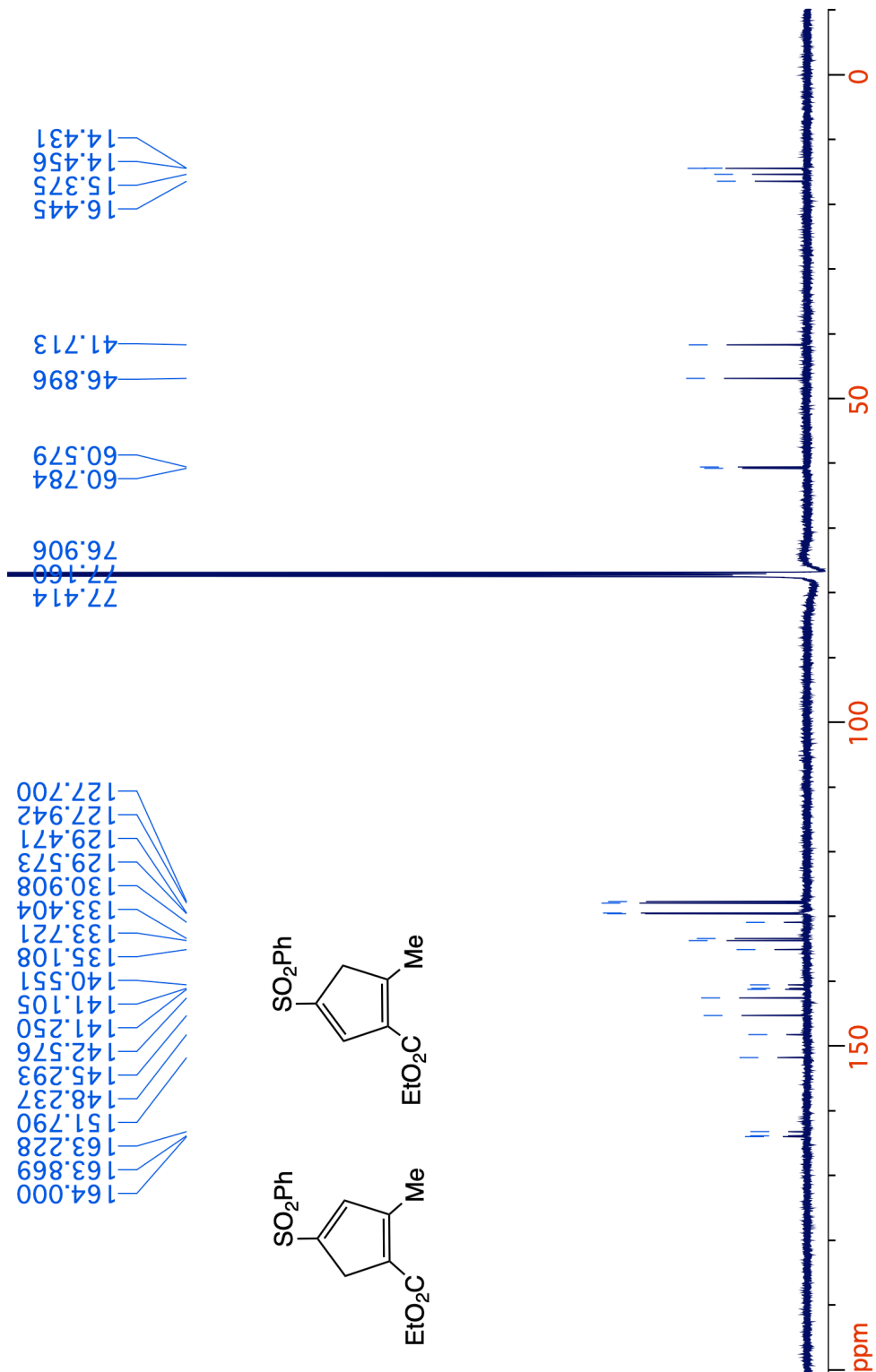
Figure 4-13. $^{13}C\{^1H\}$ NMR spectrum (125 MHz, CDCl₃) of **8**-*Me-A* and **8**-*Me-B*.
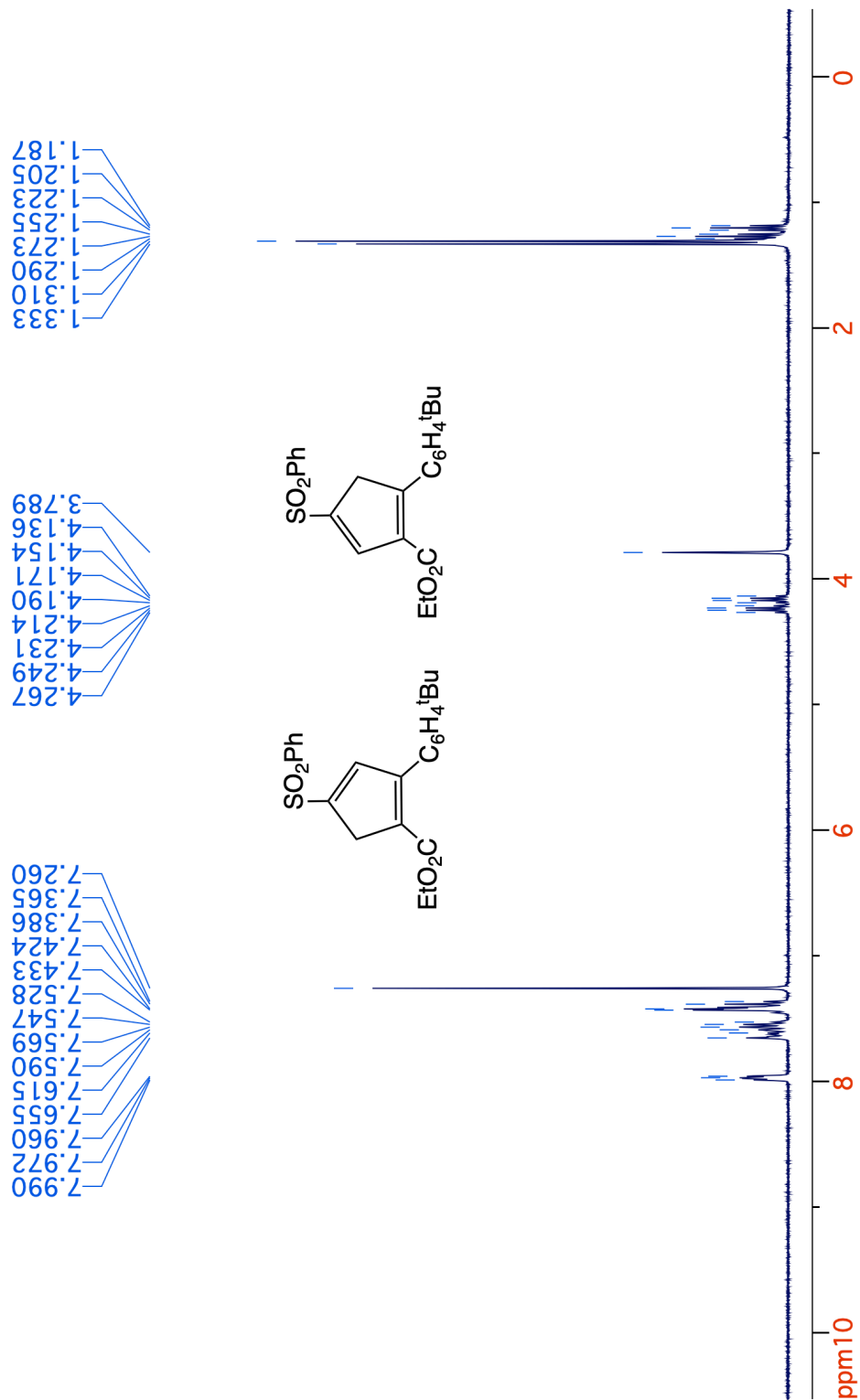
Figure 4-14. ^{1}H NMR spectrum (400 MHz, CDCl$_3$) of **8-*Ar^tBu*-A** and **8-*Ar^tBu*-B**.
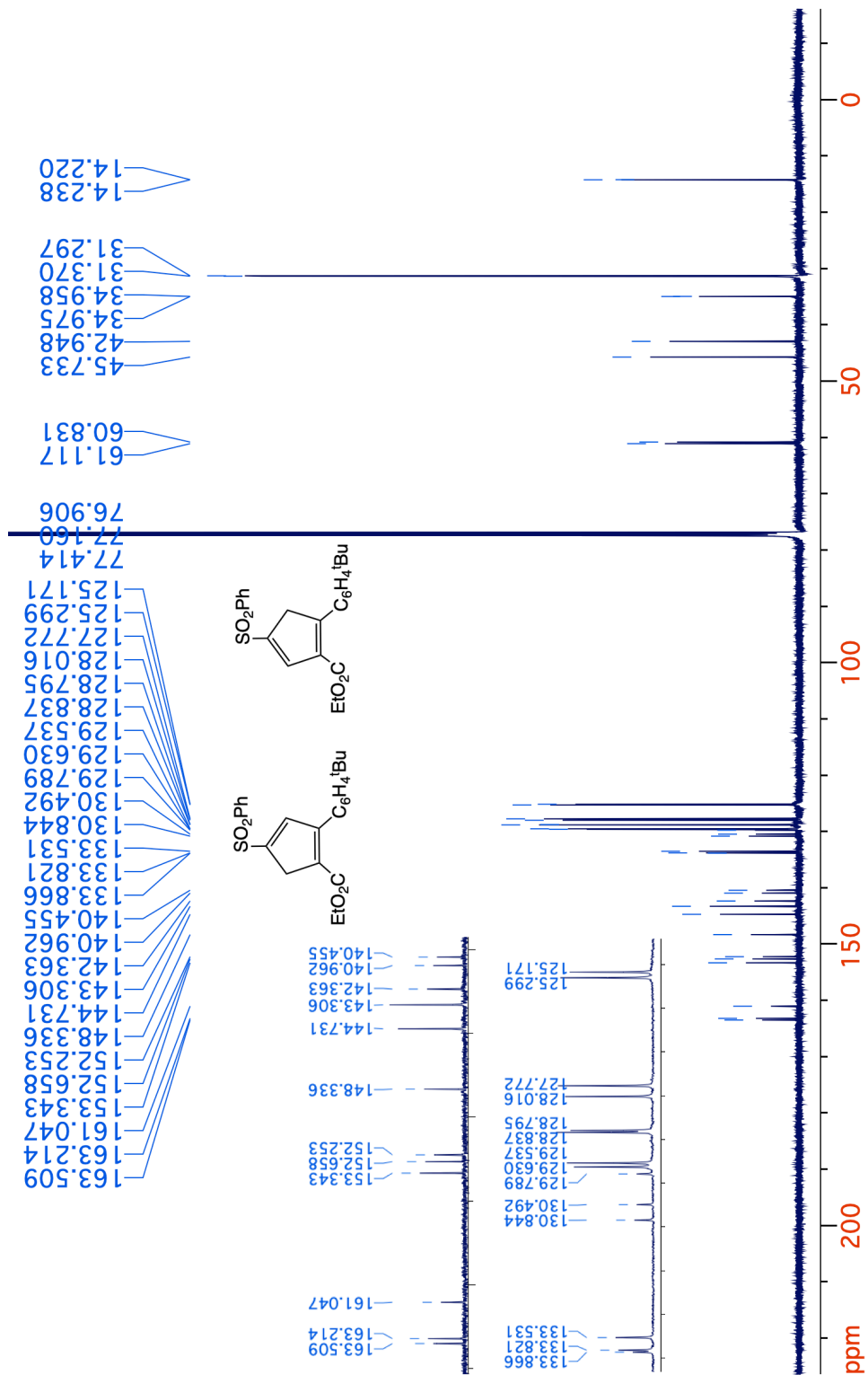
Figure 4-15. $^{13}C\{^1H\}$ NMR spectrum (125 MHz, CDCl$_3$) of **8**-*Ar^{t}Bu-A* and **8**-*Ar^{t}Bu-B*.
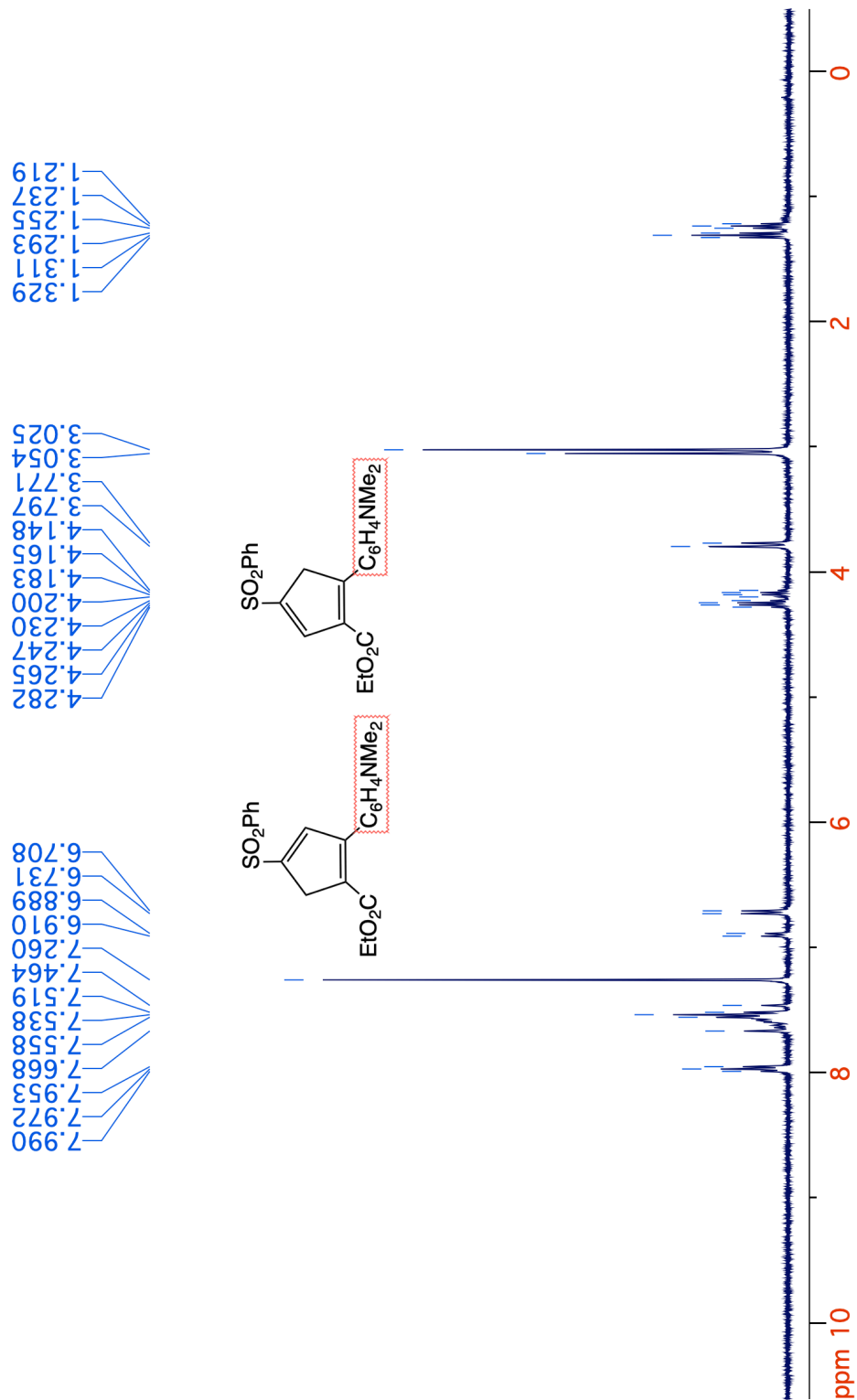
Figure 4-16. ^{1}H NMR spectrum (400 MHz, CDCl$_3$) of **8-*ArNMe$_2$-A*** and **8-*ArNMe$_2$-B***.
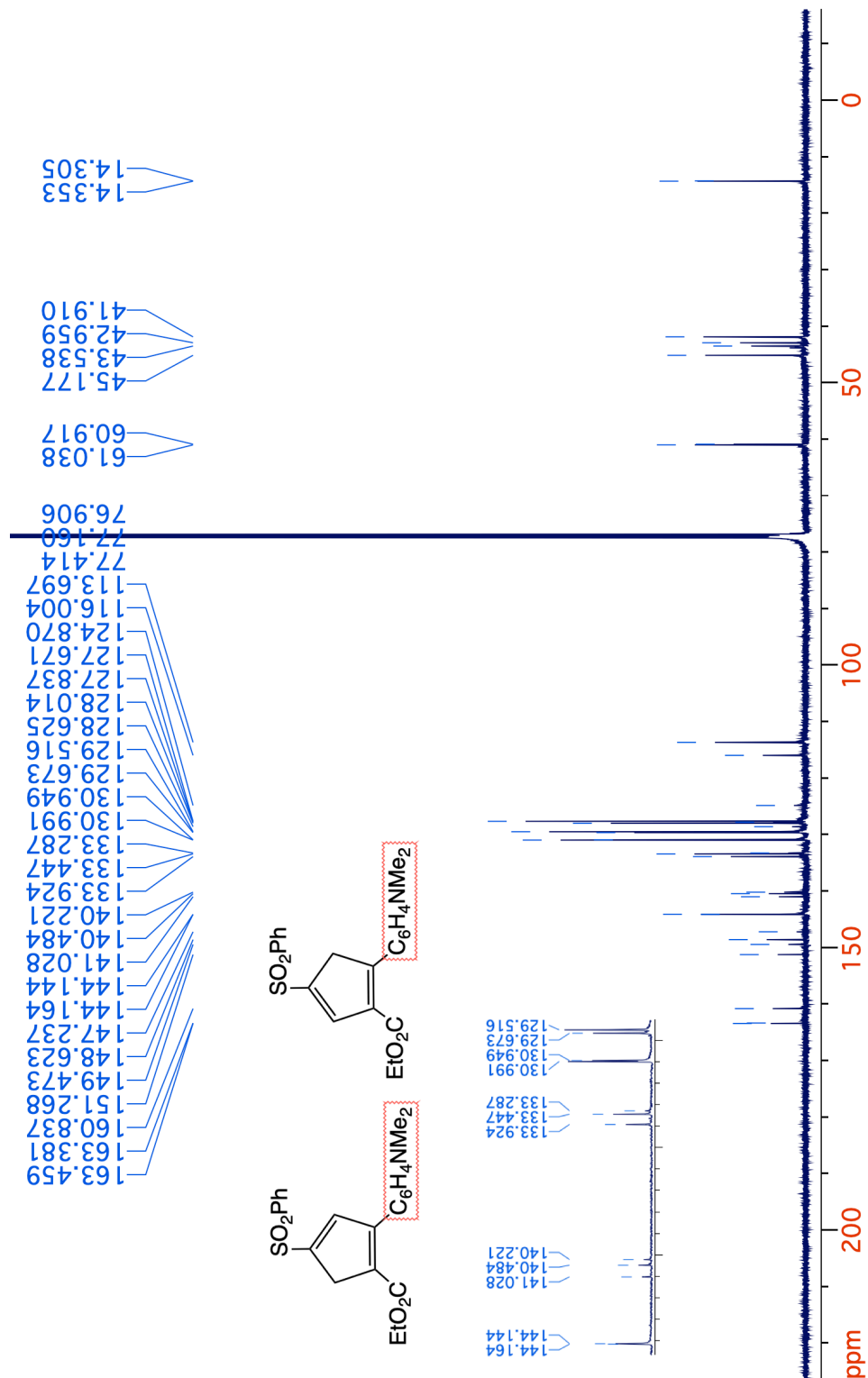
Figure 4-17. $^{13}C\{^1H\}$ NMR spectrum (125 MHz, CDCl$_3$) of **8-*ArNMe$_2$-A*** and **8-*ArNMe$_2$-B***.
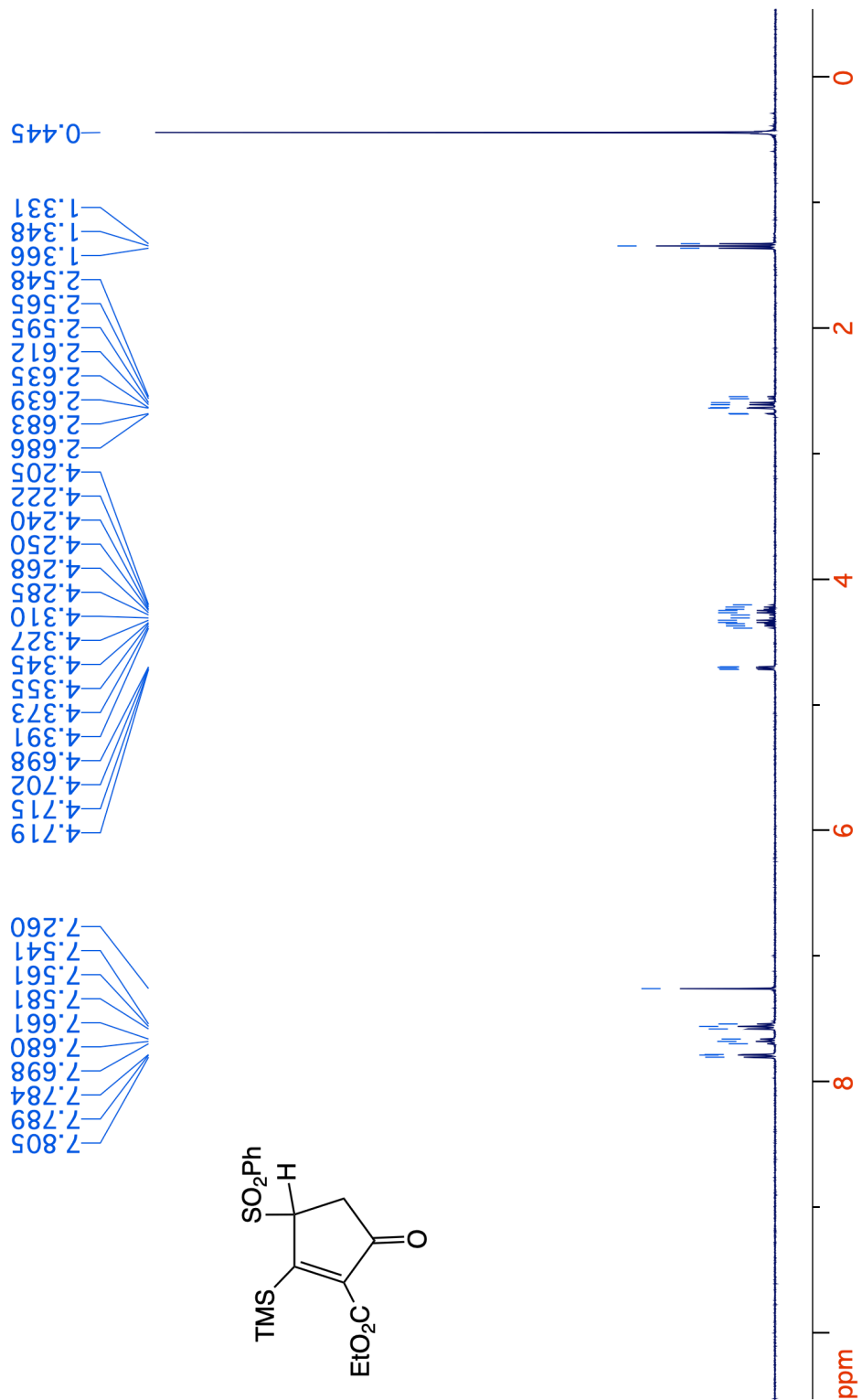
Figure 4-18. ^{1}H NMR spectrum (400 MHz, CDCl$_3$) of **11**.
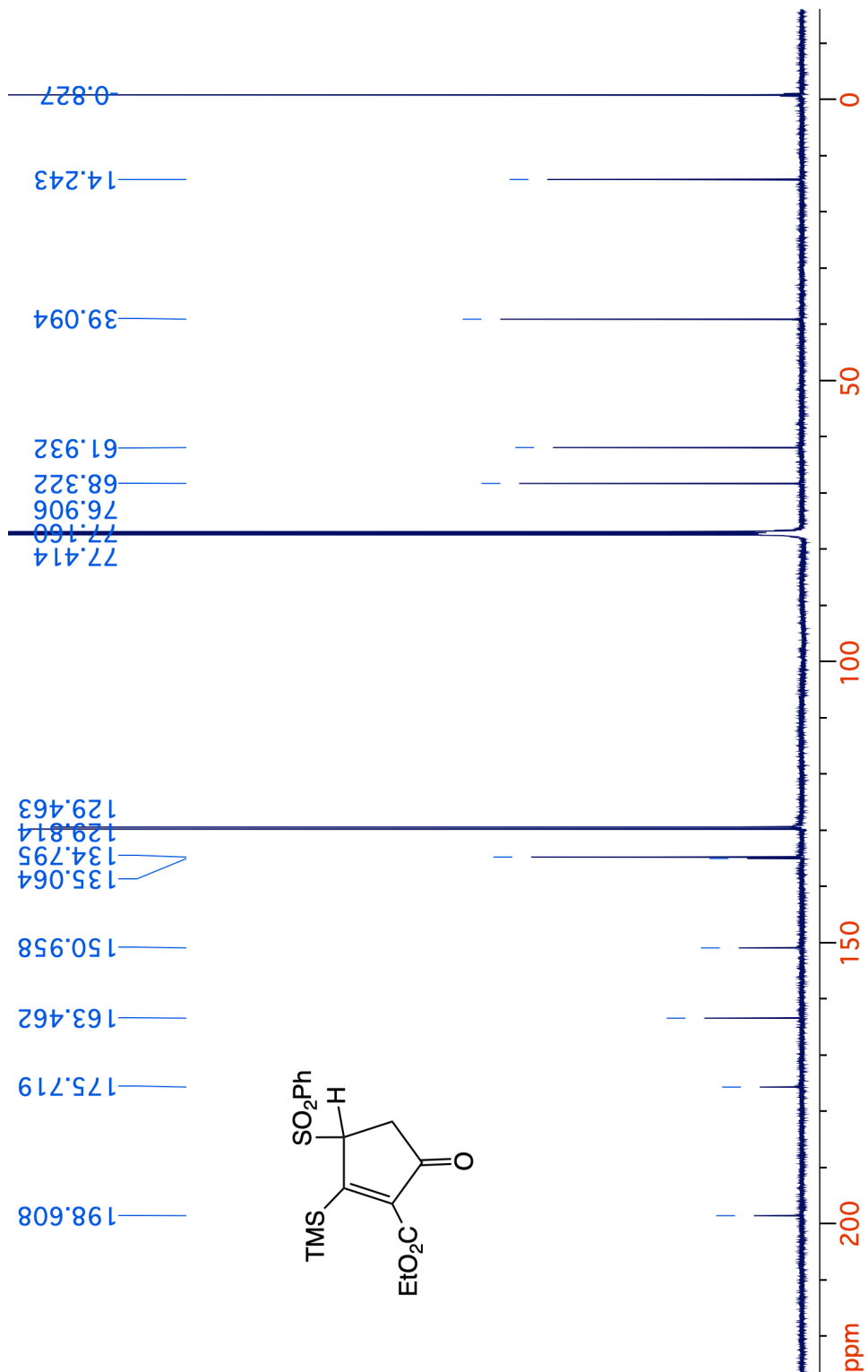
Figure 4-19. $^{13}C\{^1H\}$ NMR spectrum (125 MHz, CDCl$_3$) of **11**.
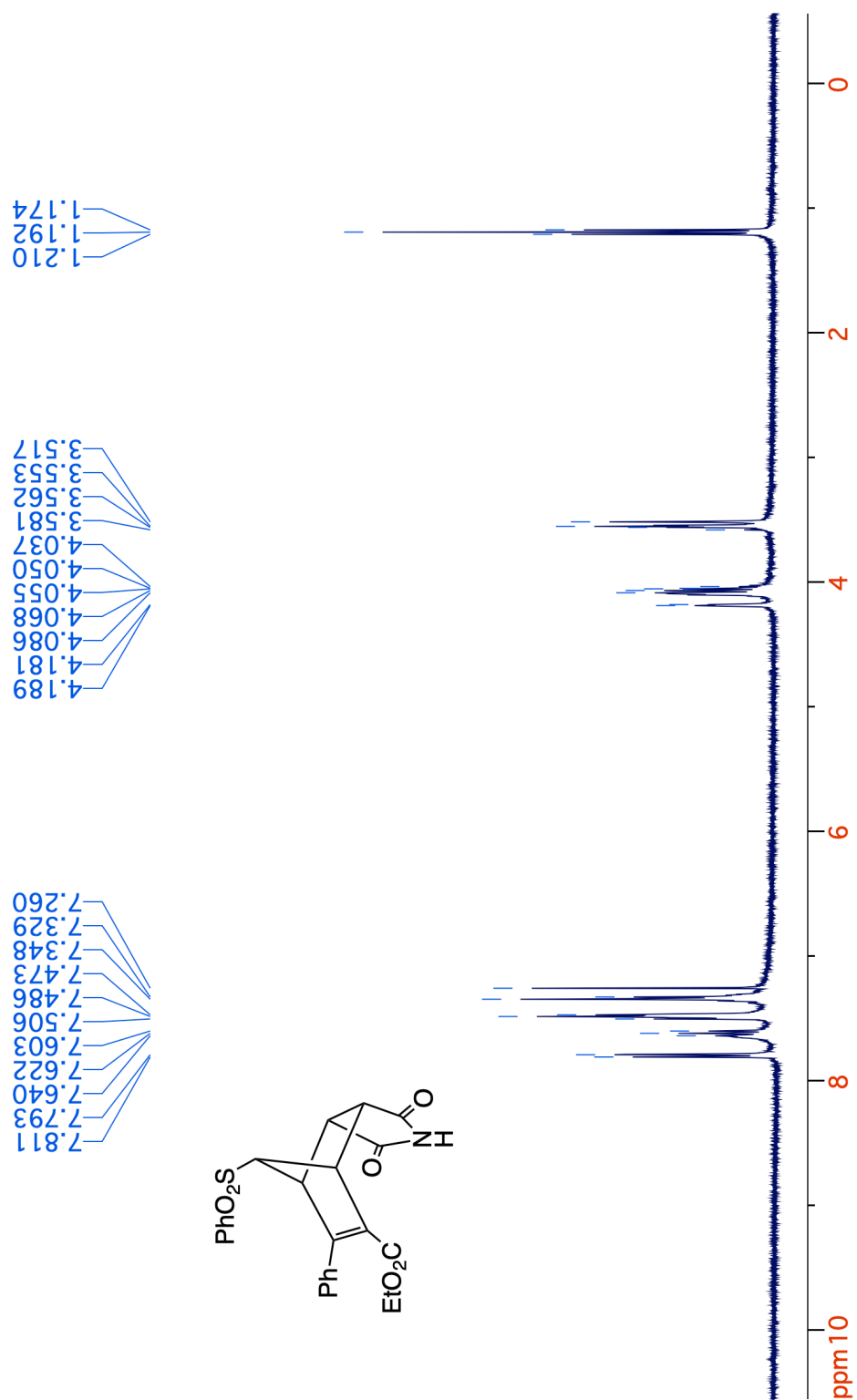
Figure 4-20. ^{1}H NMR spectrum (400 MHz, CDCl$_3$) of **15**.

483
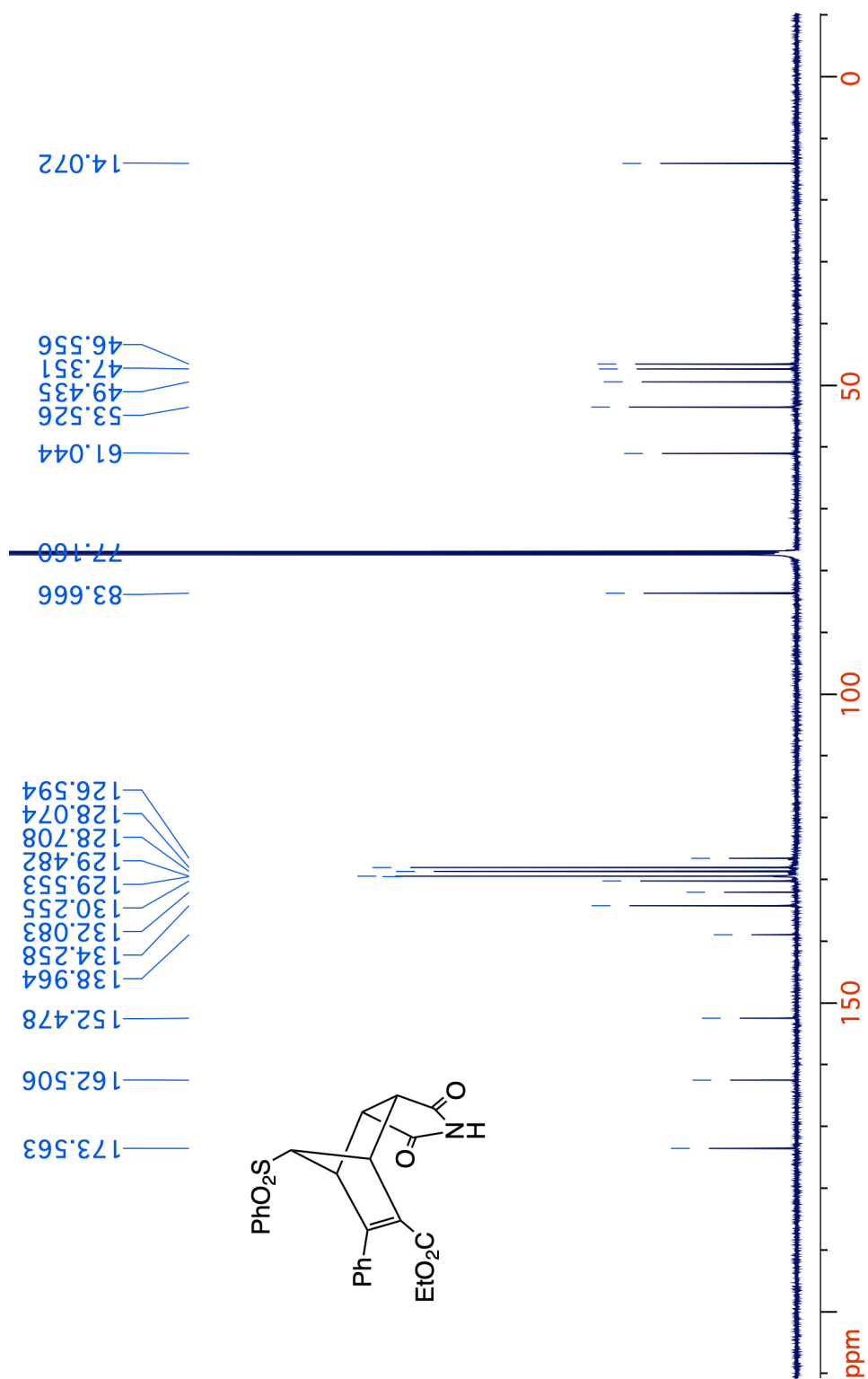
Figure 4-21. $^{13}C\{^1H\}$ NMR spectrum (125 MHz, CDCl$_3$) of **15**.

Peaks labeled: 14.072, 46.556, 47.351, 49.435, 53.526, 61.044, 77.160, 83.666, 126.594, 128.074, 128.708, 129.482, 129.553, 130.255, 132.083, 134.258, 138.964, 152.478, 162.506, 173.563
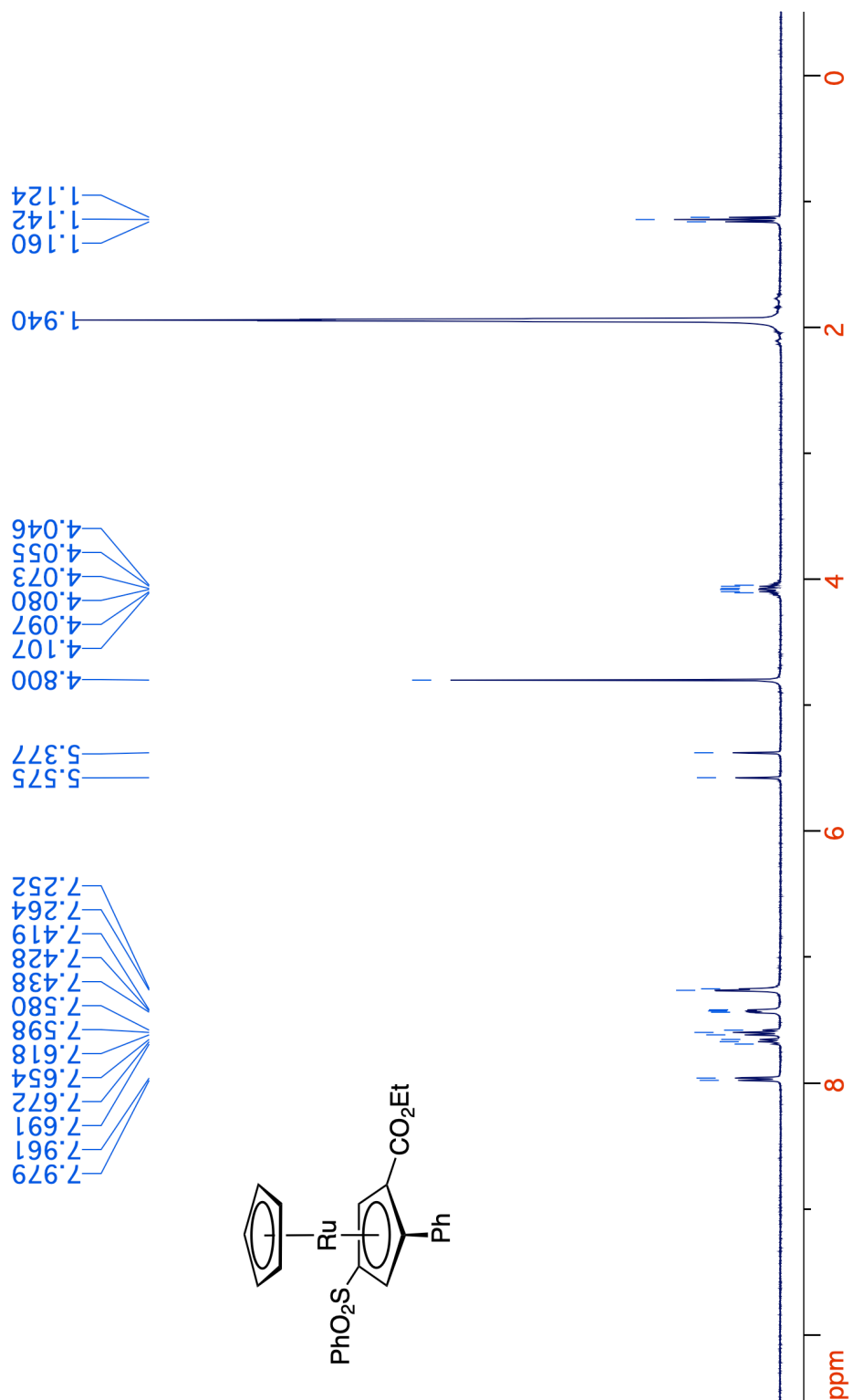
Figure 4-22. ^{1}H NMR spectrum (400 MHz, CD$_3$CN) of **17**-*Cp*.

485
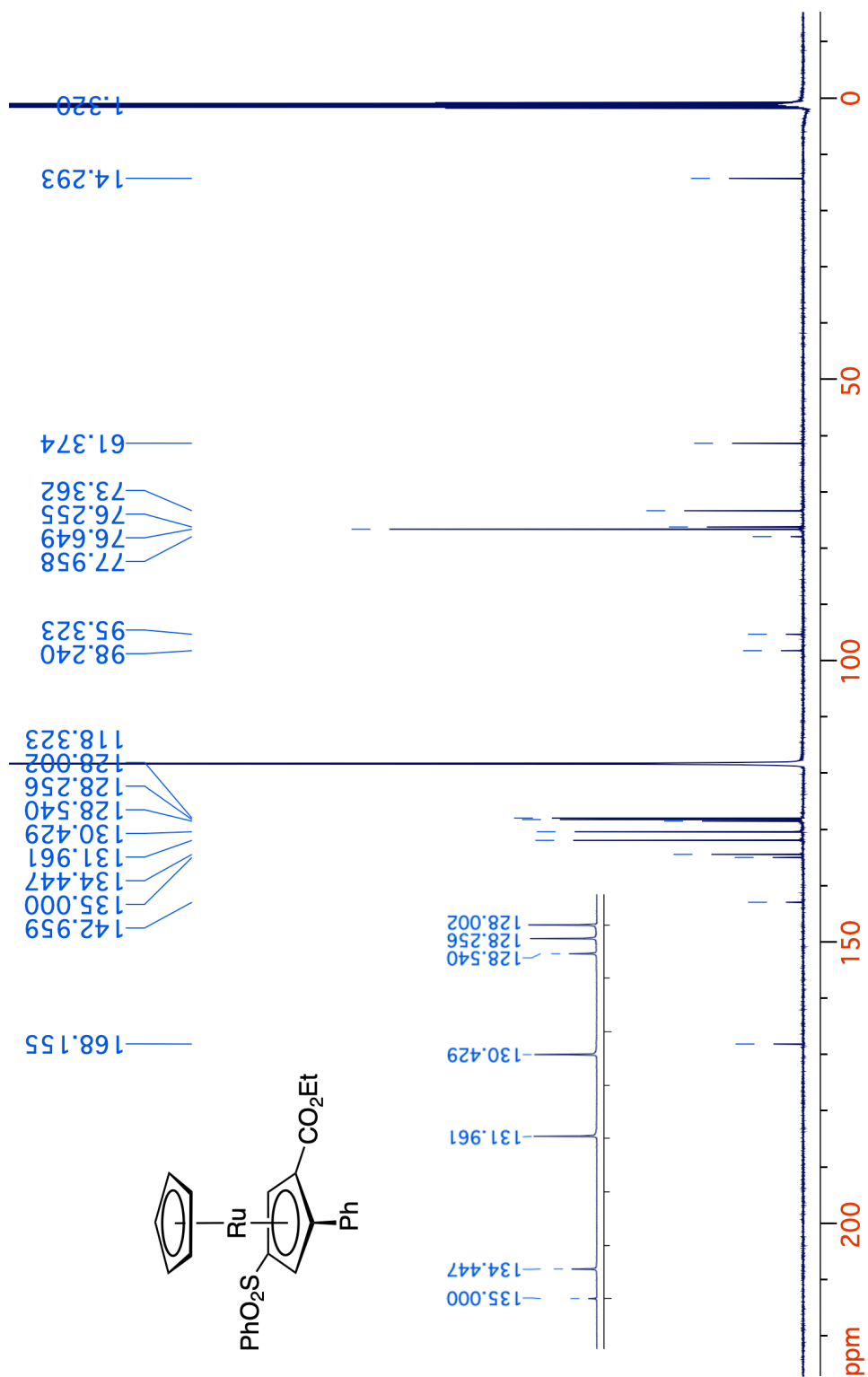
Figure 4-23. $^{13}C\{^1H\}$ NMR spectrum (125 MHz, CD$_3$CN) of **17**-*Cp*.

486
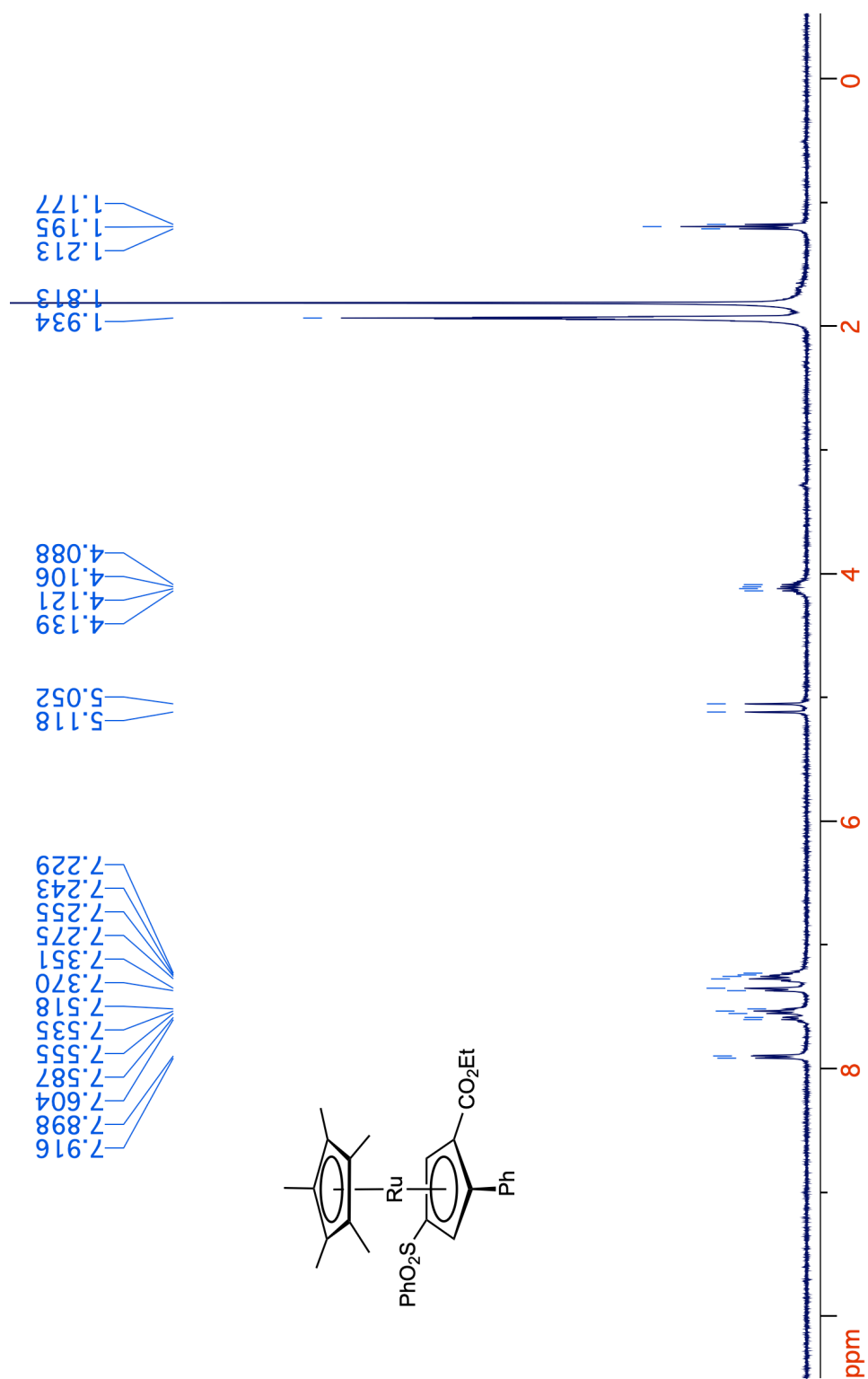
Figure 4-24. ^{1}H NMR spectrum (400 MHz, CD$_3$CN) of **17**-*Cp**.
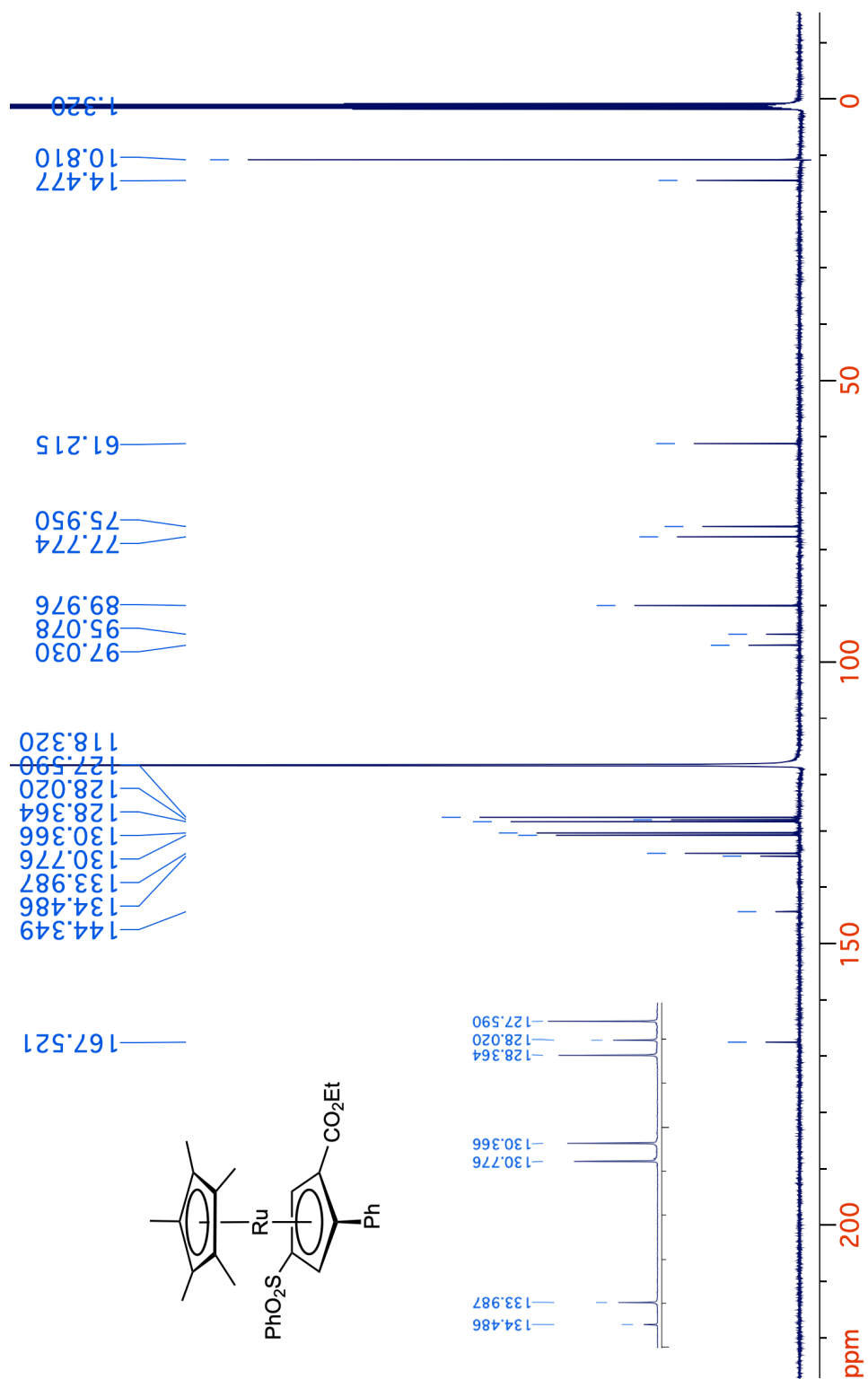
Figure 4-25. $^{13}C\{^1H\}$ NMR spectrum (125 MHz, CD$_3$CN) of **17**-*Cp**.
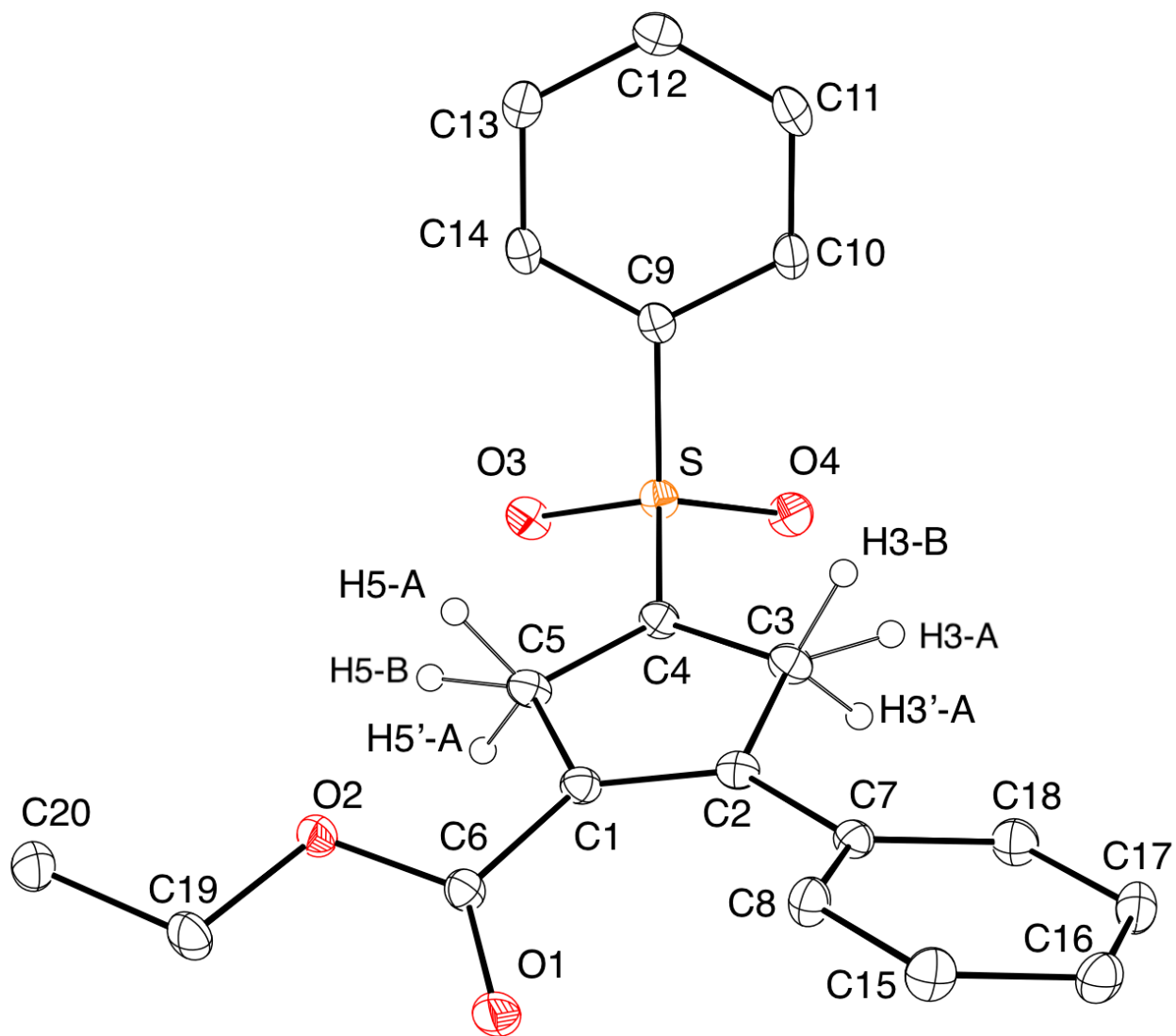
Figure 4-26. ORTEP view of **8**-*Ph-A/***8**-*Ph-B*. Ellipsoids shown at 30% probability. Most hydrogens are omitted for clarity.

Table 4-2. Crystal data and structure refinement for **8**-*Ph-A/***8**-*Ph-B*.

Identification code	PQ_0313
Empirical formula	C20 H18 O4 S
Molecular formula	C20 H18 O4 S
Formula weight	354.40
Temperature	100.0 K
Wavelength	0.71073 Å
Crystal system	Monoclinic
Space group	P 1 21/n 1
Unit cell dimensions	a = 11.0617(8) Å $\alpha = 90°$.
	b = 10.3249(8) Å $\beta = 104.003(3)°$.
	c = 15.3097(11) Å $\gamma = 90°$.
Volume	1696.6(2) Å^3
Z	4
Density (calculated)	1.388 Mg/m^3
Absorption coefficient	0.213 mm^{-1}
F(000)	744
Crystal size	0.297 x 0.086 x 0.074 mm^3
Crystal color, habit	Light Yellow Needle
Theta range for data collection	2.737 to 25.381°.
Index ranges	-13<=h<=13, -8<=k<=12, -18<=l<=18
Reflections collected	11890
Independent reflections	3094 [R(int) = 0.0352, R(sigma) = 0.0363]
Completeness to theta = 25.000°	99.6 %
Absorption correction	Semi-empirical from equivalents
Max. and min. transmission	0.0916 and 0.0635
Refinement method	Full-matrix least-squares on F^2
Data / restraints / parameters	3094 / 0 / 227
Goodness-of-fit on F^2	1.059
Final R indices [I>2sigma(I)]	R1 = 0.0406, wR2 = 0.0894
R indices (all data)	R1 = 0.0541, wR2 = 0.0952
Extinction coefficient	n/a
Largest diff. peak and hole	0.376 and -0.344 e.Å^{-3}
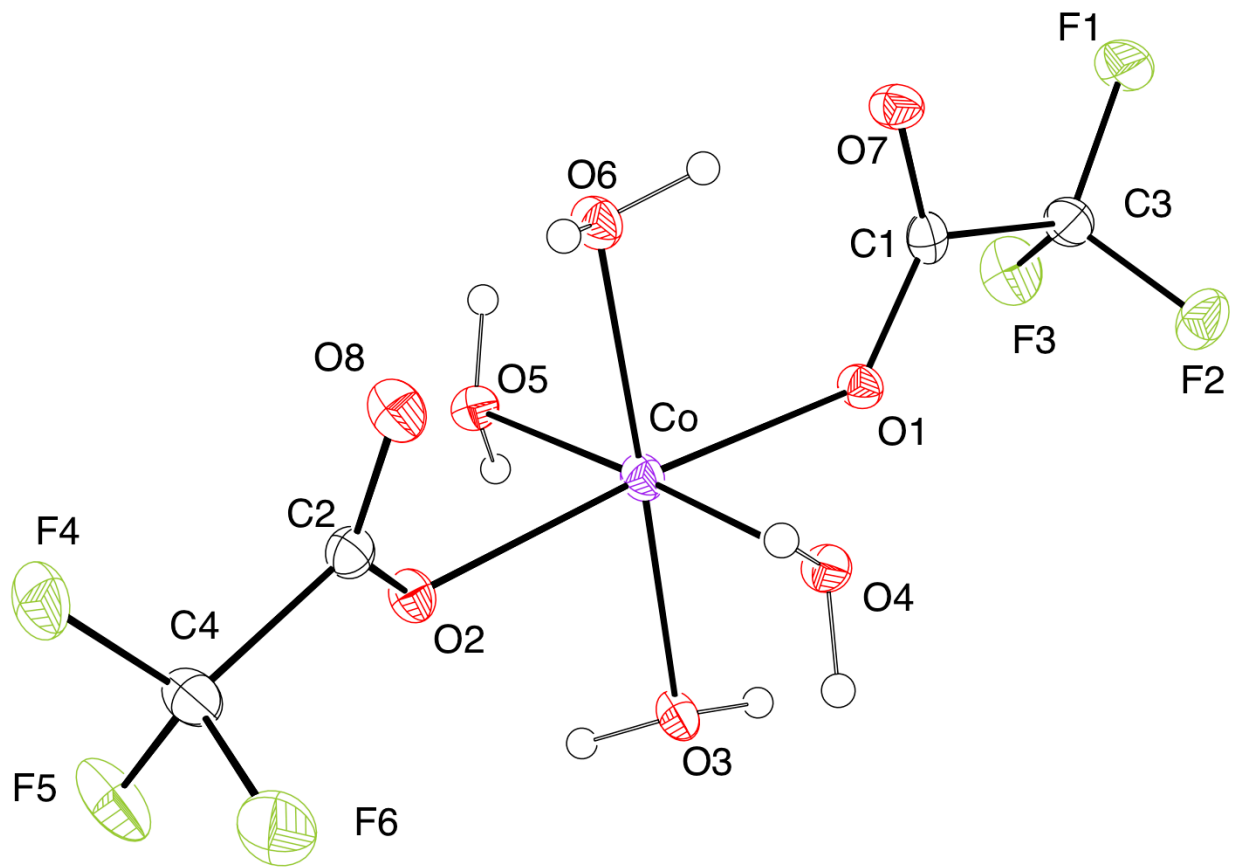
Figure 4-27. ORTEP view of complex **9**. Ellipsoids shown at 30% probability. Most hydrogens are omitted for clarity.

Table 4-3. Crystal data and structure refinement for complex **9**.

Identification code	PQ_0331
Empirical formula	C4 H8 Co F6 O8
Molecular formula	C4 H8 Co F6 O8
Formula weight	357.03
Temperature	100.0 K
Wavelength	0.71073 Å
Crystal system	Triclinic
Space group	P-1
Unit cell dimensions	a = 8.1249(14) Å $\quad$ α = 75.059(12)°.
	b = 9.0422(14) Å $\quad$ β = 64.690(11)°.
	c = 9.2650(15) Å $\quad$ γ = 71.468(11)°.
Volume	577.49(18) Å^3
Z	2
Density (calculated)	2.053 Mg/m^3
Absorption coefficient	1.603 mm^{-1}
F(000)	354
Crystal size	0.131 x 0.054 x 0.042 mm^3
Crystal color, habit	Red Needle
Theta range for data collection	2.400 to 25.389°.
Index ranges	-9<=h<=9, -10<=k<=10, -11<=l<=11
Reflections collected	4179
Independent reflections	4179 [R(int) = ?, R(sigma) = 0.0667]
Completeness to theta = 25.000°	100.0 %
Absorption correction	Semi-empirical from equivalents
Max. and min. transmission	0.091642 and 0.061194
Refinement method	Full-matrix least-squares on F^2
Data / restraints / parameters	4179 / 0 / 177
Goodness-of-fit on F^2	1.057
Final R indices [I>2sigma(I)]	R1 = 0.0551, wR2 = 0.1087
R indices (all data)	R1 = 0.0784, wR2 = 0.1202
Extinction coefficient	n/a
Largest diff. peak and hole	0.532 and -0.572 e.Å^{-3}
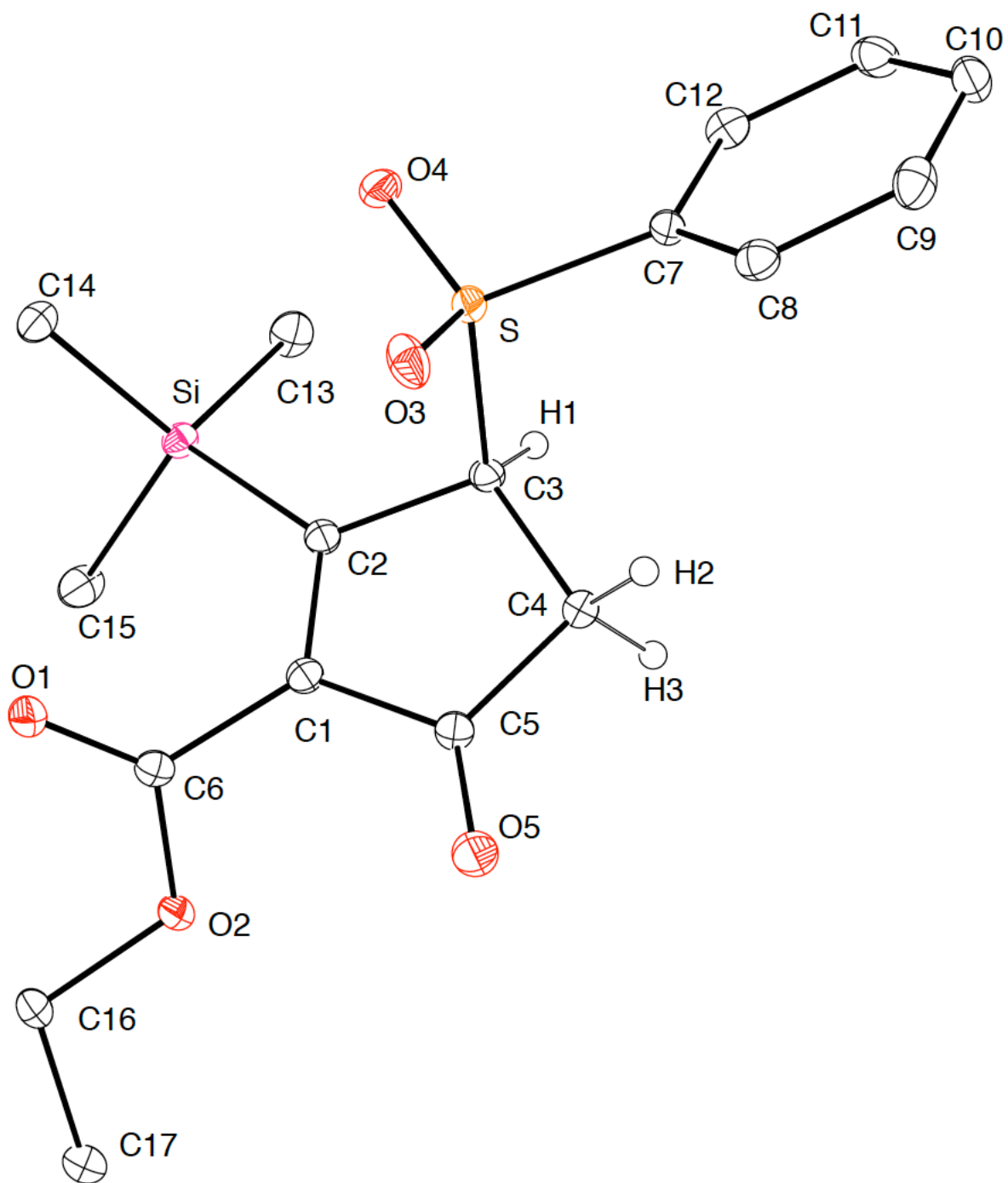
Figure 4-28. ORTEP view of **11**. Ellipsoids shown at 30% probability. Most hydrogens are omitted for clarity.

Table 4-4. Crystal data and structure refinement for **11**.

Identification code	PQ_0323
Empirical formula	C17 H22 O5 S Si
Molecular formula	C17 H22 O5 S Si
Formula weight	366.49
Temperature	100.0 K
Wavelength	0.71073 Å
Crystal system	Monoclinic
Space group	P 1 21/c 1
Unit cell dimensions	a = 15.5019(8) Å $\quad$ α = 90°.
	b = 8.5732(5) Å $\quad$ β = 107.173(2)°.
	c = 14.4028(8) Å $\quad$ γ = 90°.
Volume	1828.81(18) Å^3
Z	4
Density (calculated)	1.331 Mg/m^3
Absorption coefficient	0.265 mm^{-1}
F(000)	776
Crystal size	0.346 x 0.317 x 0.294 mm^3
Crystal color, habit	Colorless Block
Theta range for data collection	2.745 to 25.786°.
Index ranges	-18<=h<=14, -10<=k<=10, -16<=l<=17
Reflections collected	31136
Independent reflections	3508 [R(int) = 0.0467, R(sigma) = 0.0274]
Completeness to theta = 25.000°	100.0 %
Absorption correction	Semi-empirical from equivalents
Max. and min. transmission	0.0921 and 0.0667
Refinement method	Full-matrix least-squares on F^2
Data / restraints / parameters	3508 / 0 / 221
Goodness-of-fit on F^2	1.051
Final R indices [I>2sigma(I)]	R1 = 0.0349, wR2 = 0.0845
R indices (all data)	R1 = 0.0456, wR2 = 0.0905
Extinction coefficient	n/a
Largest diff. peak and hole	0.398 and -0.377 e.Å^{-3}
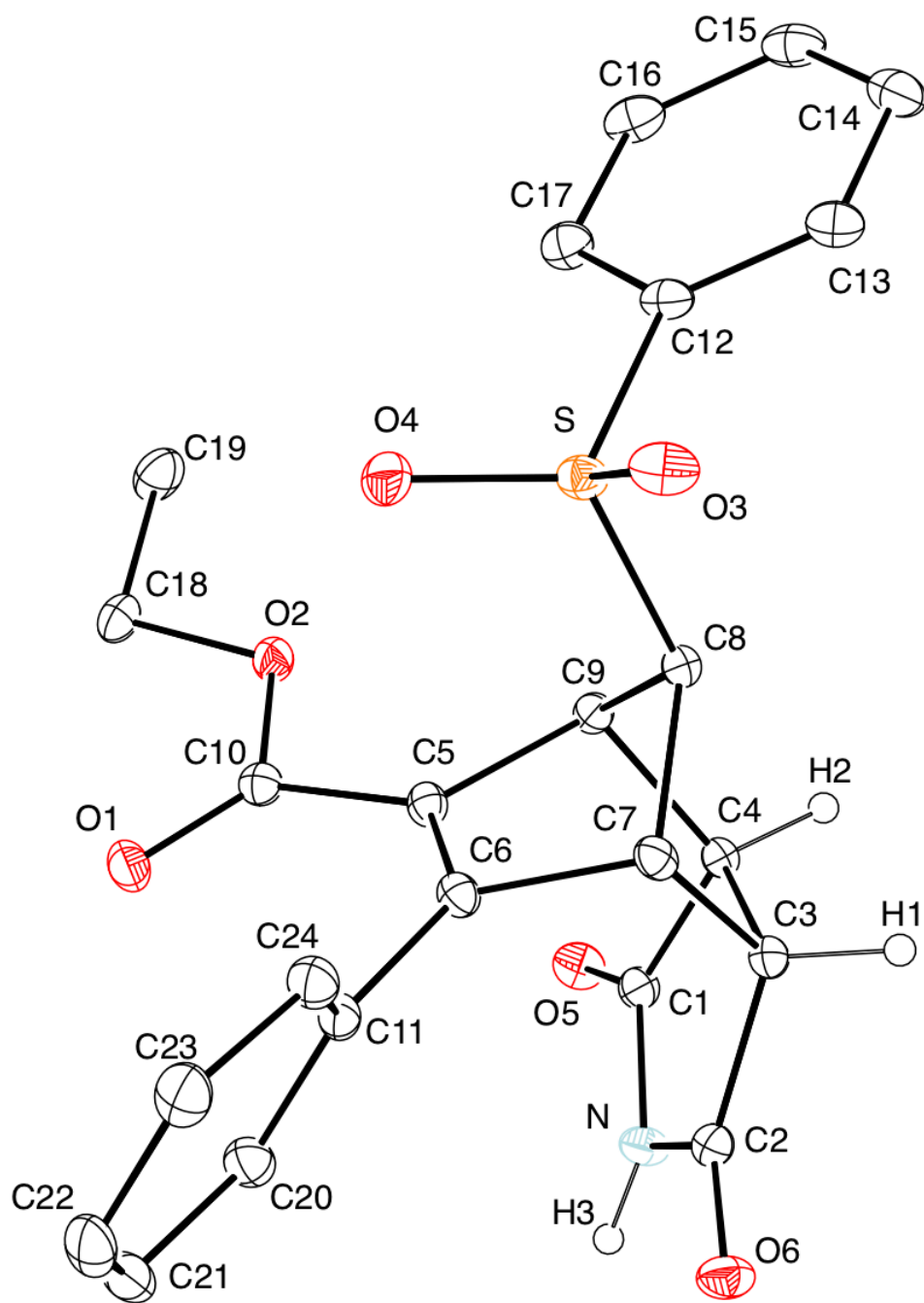
Figure 4-29. ORTEP view of **15**. Ellipsoids shown at 30% probability. Most hydrogens are omitted for clarity.

Table 4-5. Crystal data and structure refinement for **15**.

Identification code	PQ_0388
Empirical formula	C24 H21 N O6 S
Molecular formula	C24 H21 N O6 S
Formula weight	451.48
Temperature	100.0 K
Wavelength	0.71073 Å
Crystal system	Triclinic
Space group	P-1
Unit cell dimensions	a = 7.5692(2) Å α = 69.5260(10)°.
	b = 11.1619(3) Å β = 76.8910(10)°.
	c = 13.8735(4) Å γ = 78.4190(10)°.
Volume	1059.96(5) Å^3
Z	2
Density (calculated)	1.415 Mg/m^3
Absorption coefficient	0.195 mm^{-1}
F(000)	472
Crystal size	0.267 x 0.242 x 0.165 mm^3
Crystal color, habit	Colorless Block
Theta range for data collection	1.590 to 26.384°.
Index ranges	-9<=h<=8, -13<=k<=13, -16<=l<=17
Reflections collected	14618
Independent reflections	4315 [R(int) = 0.0293, R(sigma) = 0.0281]
Completeness to theta = 25.000°	100.0 %
Absorption correction	Semi-empirical from equivalents
Max. and min. transmission	0.0932 and 0.0695
Refinement method	Full-matrix least-squares on F^2
Data / restraints / parameters	4315 / 0 / 290
Goodness-of-fit on F^2	1.027
Final R indices [I>2sigma(I)]	R1 = 0.0406, wR2 = 0.0966
R indices (all data)	R1 = 0.0488, wR2 = 0.1029
Extinction coefficient	n/a
Largest diff. peak and hole	0.478 and -0.353 e.Å^{-3}

Figure 4-30. ORTEP view of complex **17**-*Cp**. Ellipsoids shown at 30% probability. Most hydrogens are omitted for clarity.

Table 4-6. Crystal data and structure refinement for complex **17**-*Cp**.

Identification code	OCon_PQ389
Empirical formula	C30 H32 O4 Ru S
Molecular formula	C30 H32 O4 Ru S
Formula weight	589.68
Temperature	100.0 K
Wavelength	0.71073 Å
Crystal system	Monoclinic
Space group	P 1 21/c 1
Unit cell dimensions	a = 15.5730(11) Å $\alpha = 90°.$
	b = 15.4582(11) Å $\beta = 106.128(2)°.$
	c = 11.9655(9) Å $\gamma = 90°.$
Volume	2767.1(3) Å^3
Z	4
Density (calculated)	1.415 Mg/m^3
Absorption coefficient	0.675 mm^{-1}
F(000)	1216
Crystal size	0.217 x 0.153 x 0.131 mm^3
Crystal color, habit	Light Yellow Rod
Theta range for data collection	1.361 to 26.431°.
Index ranges	-19<=h<=19, -19<=k<=19, -14<=l<=13
Reflections collected	58579
Independent reflections	5688 [R(int) = 0.0661, R(sigma) = 0.0376]
Completeness to theta = 25.000°	100.0 %
Absorption correction	Semi-empirical from equivalents
Max. and min. transmission	0.2468 and 0.2041
Refinement method	Full-matrix least-squares on F^2
Data / restraints / parameters	5688 / 152 / 432
Goodness-of-fit on F^2	1.043
Final R indices [I>2sigma(I)]	R1 = 0.0300, wR2 = 0.0743
R indices (all data)	R1 = 0.0383, wR2 = 0.0814
Extinction coefficient	n/a
Largest diff. peak and hole	0.438 and -0.569 e.Å^{-3}

Acknowledgement

Chapter 4 is a full reprint of the publication "Acid-Induced Liberation of Polysubstituted Cyclopentadiene Ligands from Cyclopentadienyl Cobalt: A [2 + 2 + 1] Cycloaddition Route Toward 1, 2, 4-Trisubstituted Cyclopentadienes" Qin, P.; Holland, R. L.; Bunker, K. D.; O'Connor, J. M.; Baldridge, K. K.; Rheingold, A. L. *J. Org. Chem.* **2019**, *84*, 13992-14004. The dissertation author is the first author on this paper.

G. References

1. (a) Janiak, C.; Schumann, H. Bulky or Supracyclopentadienyl Derivatives in Organometallic Chemistry. *Adv. Organomet. Chem.* **1991**, *33*, 291-393; (b) Halterman, R. L. Synthesis and Applications of Chiral Cyclopentadienylmetal Complexes. *Chem. Rev.* **1992**, *92*, 965-994; (c) Enders, M.; Baker, R. W. Synthesis of Aryl- and Heteroaryl-Substituted Cyclopentadienes and Indenes and their Use in Transition Metal Chemistry. *Curr. Org. Chem.* **2006**, *10*, 937-953. (d) Newton, C. G.; Kossler, D.; Cramer, N. Asymmetric Catalysis Powered by Chiral Cyclopentadienyl Ligands. *J. Am. Chem. Soc.* **2016**, *138*, 3953-3941; (e) Patra, M.; Gasser, G. The Medicinal Chemistry of Ferrrocene and its Derivatives. *Nat. Rev. Chem.* **2017**, *1*, article number 0066.

2. (a) Veldman, B.; Kaully, T.; Feller, R. K.; Falcao, E.; Wudl, F. Staudinger's Poly(cyclopentadiene): Sintering Processing of Poly(Diels-Alder Cyclopentadiene). *Macromolecules* **2009**, *42*, 6848-6850; (b) Chen, L.; Mahmoud, S. M.; Yin, X.; Lalancette, R. A.; Pietrangelo, A. Decreasing Aromaticity in π-Conjugated Materials: Efficient Synthesis and Electronic Structure Identification of Cyclopentadiene-Containing Systems. *Org. Lett.* **2013**, *15*, 5970-5973; (c) Bando, Y.; Haketa, Y.; Sakurai, T.; Matsuda, W.; Seki, S.; Takaya, H.; Maeda, H. Ion-Pairing Assemblies based on Pentacyano-substituted Cyclopentadienide as a π-Electron Anion. *Chem. Eur. J.* **2016**, *22*, 7843-7850; (d) Hamilton, J. A.; Pugh, T.; Johnson, A. L.; Kingsley, A. J.; Richards, S. P. Cobalt(I) Olefin Complexes: Precursors for Metal-Organic Chemical Vapor Deposition of High Purity Cobalt Metal Thin Films. *Inorg. Chem.* **2016**, *55*, 7141-7151; (e) Bian, S.; Scott, A. M.; Cao, Y.; Liang, Y.; Osuna, S.; Houk, K. N.; Braunschweig, A. B. Covalently Patterned Graphene Surfaces by a Force-Accelerated Diels-Alder Reaction. *J. Am. Chem. Soc.* **2013**, *135*, 9240-9243.

3. (a) Wilson, P. J.; Wells, J. H. The Chemistry and Utilization of Cyclopentadiene. *Chem. Rev.* **1944**, *34*, 1-50; (b) Winterfeldt, E. Enantiomerically Pure Cyclopentadienes. *Chem. Rev.* **1993**, *93*, 827-843; (c) Nicolaou, K. C.; Snyder, S. A.; Montagnon, T.; Vassilikogiannakis, G. The Diels-Alder Reaction in Total Synthesis. *Angew. Chem. Int. Ed.* **2002**, *41*, 1668-1698; (d) Funel, J.-A.; Abele, S. Industrial Applications of the Diels-Alder Reaction. *Angew. Chem. Int. Ed.* **2013**, *52*, 3822-3863; (e) Herrmann, N.; Vogelsang, D.; Behr, A.; Seidensticker, T. Homogeneously Catalyzed 1,3-Diene Functionalization – A Success Story from Laboratory to Miniplant Scale. *ChemCatChem.* **2018**, *10*, 5342-5365.

4. (a) Yousaf, M. N.; Mrksich, M. Diels-Alder Reaction for the Selective Immobilization of Proteins to Electroactive Self-Assembled Monolayers. *J. Am. Chem. Soc.* **1999**, *121*, 4286-4287; (b) Levandowski, B. J.; Gamache, R. F.; Murphy, J. M.; Houk, K. N. Readily Accessible Ambiphilic Cyclopentadienes for Bioorthogonal Labeling. *J. Am. Chem. Soc.* **2018**, *140*, 6426-6431.

5. Frei, A. Synthetic Routes towards Multifunctional Cyclopentadienes. *Chem. Eur. J.* **2019**, *25*, 7074-7090.

6. For the synthesis of cyclopentadiene derivatives via a chromium-mediated cyclization of two alkynes and a carbene, see: (a) Wu, T.-T.; Flynn, B.; Schirmer, H.; Funke, F.; Müller, S.; Labahn, T.; Nötzel, M.; De Meijere, A. From α,β-Unsaturated Fischer Carbene Complexes to Highly Substituted 3-Ethoxycyclopentadienes, Masked Cyclopentenones. *Eur. J. Org. Chem.* **2004**, 724-748; (b) Wu, Y-T.; Kurahashi, T.; de Meijere, A. Some Recent Applications of Fischer Carbene Metal Complexes in Organic Synthesis. *J. Organomet. Chem.* **2005**, *690*, 5900-5911.

7. For a nickel-mediated [2+2+1] cycloaddition of a chromium carbene with two alkynes, see: Barluenga, J.; Barrio, P.; Riesgo, L.; López, L. A.; Tomás, M. Nickel(0)-mediated [2+2+1] Cyclization of Chromium Carbene Complexes and Internal Alkynes. *Tetrahedron* **2006**, *62*, 7547-7551.

8. (a) O'Connor, J. M.; Pu, L.; Uhrhammer, R.; Johnson, J. A.; Rheingold, A. L. A New Mode of Carbene Reactivity: Coupling with Two Alkynes to Generate Highly Substituted Cyclopentadiene Products. *J. Am. Chem. Soc.* **1989**, *111*, 1889-1891; (b) O'Connor, J. M.; Fong, B. S.; Ji, H-L.; Hiibner, K. A New Metal-Mediated Cyclization: Conversion of a Metallacyclobutene and Alkyne Substrates to η^4-Cyclopentadiene Products. *J. Am. Chem. Soc.* **1995**, *117*, 8029-8030; (c) Compounds **1**-*OEt* and **11** were originally assigned an incorrect substitution pattern in ref. 8b.

9. Baldridge, K. K.; Bunker, K. D.; Velez, C. L.; Holland, R. L.; Rheingold, A. L.; Moore, C. E.; O'Connor, J. M. Structural Characterization of (C$_5$H$_5$)Co(PPh$_3$)(η^2-alkyne) and (C$_5$H$_5$)Co(η^2-alkyne) Complexes of Highly Polarized Alkynes. *Organometallics* **2013**, *32*, 5473-5480.

10. (a) O'Connor, J. M.; H. Ji.; Iranpour, M.; Rheingold, A. L. Formation of a Stable Metallacyclobutene Complex from α-Diazocarbonyl and Alkyne Substrates. *J. Am. Chem. Soc.* **1993**, *115*, 1586-1588. (b) O'Connor, J. M.; Baldridge, K. K.; Vélez, C. L.; Rheingold, A. L.; Moore, C. E. Chemistry at the Alkyne−Carbene Intersection: A Metallacyclobutene − η^3-Vinylcarbene Equilibration. *J. Am. Chem. Soc.* **2013**, *135*, 8826-8829.

11. For alternative routes to polysubstituted cobalt-cyclopentadiene complexes, see: (a) Tane, J. P.; Vollhardt, K. P. C. Cyclopentadienone Complexes as Synthons: Ring- and Regiospecific Nucleophilic Additions to Cobaltocenium Salts – Synthesis of Substituted Cyclopentadiene and Cyclopentenones. *Angew. Chem. Int. Ed. Engl.* **1982**, *21*, 617-618; (b) Buisine, O.; Aubert, C.; Malacria, M. Cobalt(I)-Mediated Cycloisomerization of Enynes: Mechanistic Insights. *Chem. Eur. J.* **2001**, *7*, 3517-3525.

12. (a) Szajek, L. P.; Shapley, J. R. Unexpected Synthesis of CpIr(η^4-C_5H_6) and a ^{1}H and ^{13}C NMR Comparison with its Cobalt and Rhodium Congeners. *Organometallics* **1991**, *10*, 2512-2515; (b) El Murr, N.; Dusausoy, Y.; Sheats, J. E.; Agnew, M. Electrochemical Behaviour and X-ray Structure of (η-Cyclopentadienyl)(4-5-η-2-methoxycarbonylcyclopent-4-en-1,3-ylene)cobalt. *J. Chem. Soc., Dalton Trans.* **1979**, 901-905.

13. Green, M. L.; H.; Pratt, L.; Wilkinson, G. A New Type of Transition Metal-Cyclopentadiene Compound. *J. Chem. Soc.* **1959**, 3753-3767.

14. (a) El Murr, N.; Laviron, E.; Dabard, R. Chemical and Electrochemical Oxidation of Some Cyclopentadiene Cyclopentadienyl Cobalt. *J. Organomet. Chem.* **1974**, *67*, C77-C80; (b) El Murr, N.; Laviron, E. Electrochemistry of Organometallic Compounds. I. Electrosynthesis of Cyclopentadiene Cyclopentadienyl Cobalt Substitutes. *Can. J. Chem.* **1976**, *54*, 3350-3356; (c) El Murr, N.; Laviron, E. Electrochemistry of Organometallic Compounds. II. New Pathway to Substituted Cobalticinium Substitutes. *Can. J. Chem.* **1976**, *54*, 3357-3363.

15. Leonova, E. V.; Malkov, A. V.; Kochetkova, N. O.; Sokolova, A. N.; Rukhlyada, N. N. Sulfuric Acid as a Hydride Ion Acceptor in Cobalt(I) Cyclopentadiene Complexes. *Izv. Akad. Nauk SSSR, Ser. Khim.* **1984**, *3*, 727-728.

16. (a) Malikov, A. V.; Leonova, E. V.; Kochetkova, N. S.; Sergeev, V. A. The Interaction of the Cobaltocenium Cation with Nucleophiles. *Metalloorganicheskoi Khimiya* **1988**, *1*, 357-363; (b) Leonova, E. V.; Malikov, A. V.; Kochetkova, N. S.; Sergeev, V. A. Oxidative Elimination of Hydride from the Cobalt Complexes (η^4-*exo*-RC_5H_4)CoCp. *Metalloorganicheskoi Khimiya* **1988**, *1*, 137-141.

17. It is not clear to the authors why **6**-*CO_2Me-endo* is reported to be less reactive toward protic acid than **4**-*H*, **4**-*Me*, **4**-*R* and all of the cobalt-cyclopentadiene complexes reported herein.

18. O'Connor, J. M.; Johnson, J. A. Selective Oxidation of a Highly-Substituted η^4-Cyclopentadiene Cobalt Complex: Partitioning Between Uncomplexed Diene and Cobalticinium Cation Products. *Synlett* **1989**, 57-58.

19. For oxidative liberation of diene ligands from CpCo upon treatment with iodine, see: (a) Holland, R. L.; O'Connor, J. M.; Bunker, K. B.; Qin, P.; Cope, S. K.; Baldridge, K. K.; Siegel, J. S. Stereospecific Oxidative Demetallation of Highly Functionalized CpCo(1,3-Diene) Complexes: An Experimental and Computational Study. *Synlett* **2015**, *26*, 2243-2246; (b) ref 6b; (c) Knizhnikov, V. A.; Shirokii, V. L.; Sutormin, A. B.; Novikova, M. G.; Maier, N. A.; Ol'dekop, Yu. A. Reactions of Cyclopentadienyl(cyclopentadiene)cobalt with Iodine. *Metalloorganicheskaya Khimiya* **1989**, *2*, 1160-1162; (d) Dahl, T.; Moberg, C. (Trichloromethyl)cyclopentadiene from π-Cyclopentadienyl-[(trichloromethyl)cyclopentadiene]cobalt. *Acta Chemica Scandinavica* **1973**, *27*, 728-228.

20. (a) Spangler, C. W. Thermal [1,*j*] Sigmatropic Rearrangements. *Chem. Rev.* **1976**, *76*, 187-217; (b) Clarke, J.; Fowler, P. W.; Gronert, S.; Keeffe, J. R. Effect of Ring Size and Migratory Groups on [1,*n*] Suprafacial Shift Reactions. Confirmation of Aromatic and Antiaromatic Transition-State Character by Ring-Current Analysis. *J. Org. Chem.* **2016**, *81*, 8777-8788, and references therein.

21. (a) Fleming, I.; Dunoguè, J.; Smithers, R. The Electrohilic Substitution of Allylsilanes and Vinylsilanes. *Organic Reactions* **1989**, *37*, 57-574; (b) Allemann, O.; Duttwyler, S.; Romanato, P.; Baldridge, K. K.; Siegel, J. S. Proton-Catalyzed, Silane-Fueled Friedel-Crafts Coupling of Fluoroarenes. *Science* **2011**, *332*, 574-577.

22. Levandowski, B. J.; Zou, L.; Houk, K. N. Hyperconjugative Aromaticity and Antiaromaticity Control the Reactivities and π-Facial Selectivities of 5-Substituted Cyclopentadiene Diels-Alder Cycloadditions. *J. Org. Chem.* **2018**, *83*, 14658-14666, and references therein.

23. Hansch, C.; Leo, A.; Taft, R. W. A Survey of Hammett Substituent Constants and Resonance and Field Parameters. *Chem. Rev.* **1991**, *91*, 165-195.

24. Guthrie, J. P. Hydrolysis of Esters of Oxy Acids: pK_a Values for Strong Acids; Brønsted Relationship for Attack of Water at Methyl; Free Energies of Hydrolysis of Esters of Oxy Acids; and a Linear Relationship Between Free Energy of Hydrolysis and pK_a Holding over a Range of 20 pK Units. *Can J. Chem.* **1978**, *56*, 2342-2354.

25. Guntlin, C. P.; Zünd, T.; Kravchyk, K. V.; Wörle, M.; Bodnarchuk, M. I.; Kovalenko, M. V. Nanocrystalline FeF_3 and MF_2 (M = Fe, Co, and Mn) from metal trifluoroacetates and their Li(Na)-ion Storage Properties. *J. Mat. Chem. A* **2017**, *5*, 7383-7393, and references therein.

26. (a) Lei, Y. X.; Cerioni, G.; Rappoport, Z. Stable Enols of Carboxylic Esters. The Poly(methoxycarbonyl)cyclopentadiene Systems. *J. Org. Chem.* **2000**, *65*, 4028-4028.

27. For additional fulvenol compounds, see: (a) Seitz, G. Synthesis of Tetramethyl Cyclopentadiene-1,2,3,4-tetracarboxylate. *Angew. Chem. Int. Ed.* **1966**, *5*, 670-671; (b) Kasai, M.; Funamizu, M.; Fujita, K.; Kitahara, Y. Thermal rearrangement of 1-Acyl-2-alkyl-6-hydroxyfulvenes to 1-Acyl-3-alkyl-6-hydroxyfulvenes. *Chem. Lett.* **1975**, 297-300; (c) Lloyd, D.; Preston, N. W. 1,2-Diacylcyclopentadienes (2-Acyl-6-hydroxyfulvenes). *J. Chem. Soc. (C)* **1969**, 2464-2469; (d) Tayyari, S. F.; Laleh, S.; Zahedi-Tabrizi, M.; Vakili, M. Structure, Vibrational Assignments, and NMR Spectroscopy of 1,2-Bis(dichloroacetyl) Cyclopentadiene. *J. Mol. Struct.* **2013**, *1036*, 151-160; (e) Hafner, K.; Kramer, H. E. A.; Musso, H.; Ploss, G.; Schulz, G. the Structure of 6-Hydroxy-Fulvene or Cyclopentadiene-ene-aldehydes. *Chem. Ber.* **1964**, *97*, 2066-2075.

28. Perrin, C. L.; Wu, Y. Symmetry of Hydrogen Bonds in Two Enols in Solution. *J. Am. Chem. Soc.* **2019**, *141*, 4103-4107, and references therein.

29. For a prior report of oxidative demetallation of a CpCo complex bearing an ethoxy-substituted cyclopentadiene ligand to give a cyclopentenone derivative, see ref. 11a.

30. (a) Bridges, A. J.; Fischer, J. W. An Investigation of the Chemistry of Phenylsulphonylcyclopentadiene. *J. Chem. Soc. Perkin Trans. I* **1983**, 2359-2364; (b) Hartke, K.; Gleim, H-U. Disulfonylcyclopentene und Disulfonylcyclopentadiene. *Liebigs Ann. Chem.* **1976**, 716-729.

31. For additional example of arylsulfone-substituted cyclopentadienes, see: (a) Hartke, K.; Lee, K.-H.; Massa, W.; Schwarz, B. Highly Substituted Cyclopentadienes with Arylthio and Arylsulfonyl Groups. *Liebigs Ann. Chem.* **1991**, 243-251; (b) Giblin, G. M. P.; Ramcharitar, S. H.; Simpkins, N. S. Synthesis and Stereoselective Chemistry of a Novel Cyclopentadienyl Sulphone. *Tetrahedron Lett.* **1988**, *29*, 4197-4200; (c) Hartke, K.; Lee, M. H. Reactions of Monosulfonyl-Cyclopentadiene. *Arch. Pharm. (Weinheim)* **1991**, *324*, 373-377; (d) Hartke, K.; Jung, M. H.; Zerbe, H.; Kämpchen, T. Bis(sulfonyl)cyclopentadiene. *Liebigs Ann. Chem.* **1986**, 1268-1280.

32. (a) Bäckvall, J. E.; Juntunen, S. K. 2-(Phenylsulfonyl)-1,3-dienes as Versatile Synthons in Organic Transformations. Multicoupling Reagents and Diels-Alder Dienes with a Dual Electron Demand. *J. Am. Chem. Soc.* **1987**, *109*, 6396-6403; (b) Back, T. G.; Clary, K. N.; Gao, D. Cycloadditions and Cyclizations of Acetylenic, Allenic, and Conjugated Dienyl Sulfones. *Chem. Rev.* **2010**, *110*, 4498-4553.

33. Hudon, J.; Cernak, T. A.; Ashenhurst, J. A.; Gleason, J. L. Stable 5-Substituted Cyclopentadienes for the Diels-Alder Cycloaddition and their Application to the Synthesis of Palau'amine. *Angew. Chem. Int. Ed.* **2008**, *47*, 8885-8888.

34. Muratov, D. V.; Romanov, A. S.; Kudinov, A. R. Non-symmetrically Substituted Ruthenocenes: Synthesis, Structures, and Bond Nature. Electronic Effects of Substituents in Ruthenocene. *Russ. Chem. Bull. Int. Ed.* **2014**, *63*, 2485-2492.

35. Zanin, I. E.; Antipin, M. Yu.; Struchkov, Yu T. Crystal and Molecular Structure of Pentamethylruthenocene [(η^5-C$_5$H$_5$)Ru(η^5-C$_5$Me$_5$)] 123-293 K. Intramolecular Motion in the Crystal According to X-ray Diffraction Data. *Kristallografiya* **1991**, *36*, 420-428.

36. Grimme, S. Semiempirical GGA-type Density Functional Constructed with a Long-range Dispersion Correction. *J. Comput. Chem.,* **2006**, *27*, 1787-1799.

37. Weigend, F.; Ahlrichs, R. Balanced Basis Sets of Split Valence, Triple Zeta Valence and Quadruple Zeta Valence Quality for H to Rn: Design and Assessment of Accuracy. *Phys. Chem. Chem. Phys.*, **2005**, *7*, 3297-3305.

38. Klamt, A.; Schüürmann, G. COSMO: A New Approach to Dielectric Screening in Solvents with Explicit Expressions for the Screening Energy and its Gradient. *J. Chem. Soc. Perkin Trans 2* **1993**, 799-805.

39. Baldridge, K.; Klamt, A. First Principles Implementation of Solvent Effects without Outlying Charge Errors. *J. Chem. Phys.* **1997**, *106*, 6622-6633.

40. Klamt, A.; Jonas, V.; Bürger, T.; Lohrenz, C. W. Refinement and Parametrization of COSMO-RS. *J. Phys. Chem.* **1998**, *102*, 5074-5085.

CHAPTER 5

Photoactivated Transition-Metal Triggers for Ambient Temperature Enediyne and

Dienyne Cyclization: Ruthenium-η^6-Naphthalene Complexes[a]

a. Qin, P.; Cope, S. K.; Steger, H.; Veccharelli, K. M.; Holland, R. L.; Hitt, D. M.; Moore, C. E.; Baldridge, K. K.; O'Connor, J. M. *Organometallics* **2017**, *36*, 3967-3973.

A. Abstract

A persistent challenge confronting potential applications of the Bergman cycloaromatization reaction is the development of methods for spatiotemporal control of diradical formation. Photochemical variants (photo-Bergman cycloaromatizations) have thus far met with limited success, failing completely in the case of acyclic enediynes. Here we describe the development of efficient photoactivated transition-metal complexes that allow for spatiotemporal control of enediyne cycloaromatization at ambient temperatures. This strategy relies on air- and moisture-stable ruthenium naphthalene complexes that undergo photo-chemical dissociation of the naphthalene ligand, thereby generating coordination sites for enediyne binding and cycloaromatization. The same ruthenium-naphthalene complexes also trigger dienyne cyclization under photochemical conditions.

B. Introduction

In a now classic 1972 study, Bergman reported the gas-phase thermal equilibration of deuterium-enriched acyclic enediynes **1** and **2**, and provided evidence for the intermediacy of *para*-aryne **I** (Scheme 5-1).[1] The thermal Bergman cycloaromatization is now the single most powerful and general method for the formation of diradicals from readily available precursors.[2] Efforts to develop photo-Bergman cycloaromatizations for spatiotemporal control of diradical formation have met with only limited success.[3] For example, Bergman and others have found that irradiation

of acyclic enediynes,[4] such as **1** and **3**, results in *cis-trans* equilibration, with no evidence for *para*-aryne formation.[1,5,6]
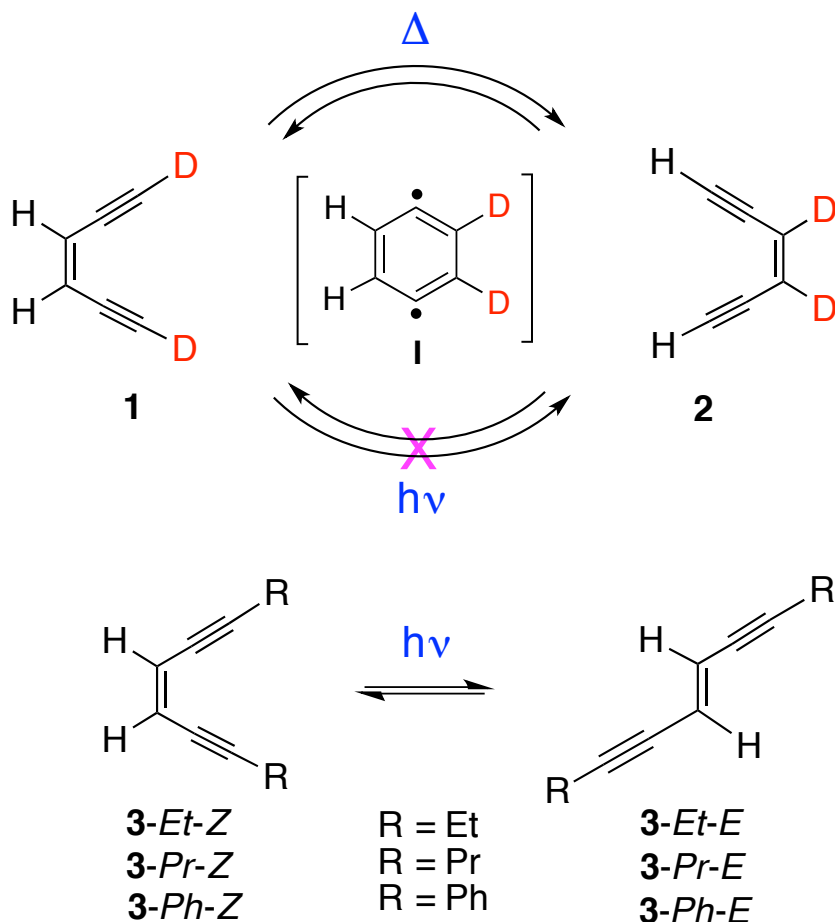
Scheme 5-1. Thermal cycloaromatization of acyclic enediyne **1**. Photolysis of **1** and **3** leads to cis-trans isomerization with no *para*-aryne formation.

Successful examples of photo-Bergman reactions typically proceed in low to moderate yield[7] and require a cyclic alkene in order to prevent *cis-trans* equilibration (eq 1).[3] In addition, nearly all cases reported to date require[8] the presence of conjugating substituents in order to obtain reasonable yields.[7-11] Alternative strategies for photo-initiated cycloaromatization of enediynes at ambient temperature include: a) photochemical enediyne deprotection for in situ generation of a strained-ring enediyne

(eq 2);[12] b) photochemical functional group transformation leading to increased ring-strain in pre-existing enediynes (eq 3);[13,14] and c) the use of metal-coordinated enediynes for photo-induced charge transfer cycloaromatization (eq 4).[15]

R = Me, H• = 1,4-CHD (6%)
R = Ph, H• = 1,4-CHD (44%)
R = Ph, H• = THF (64%)
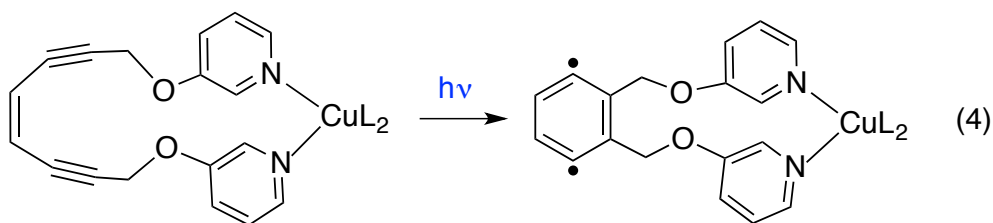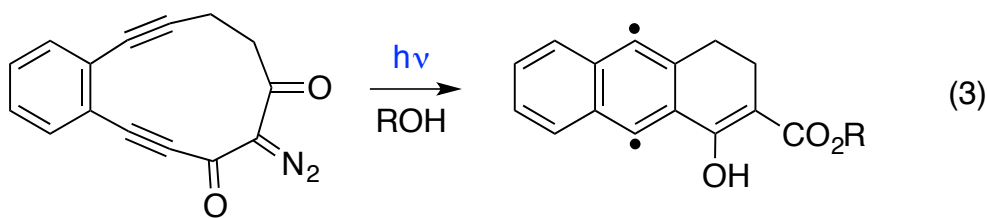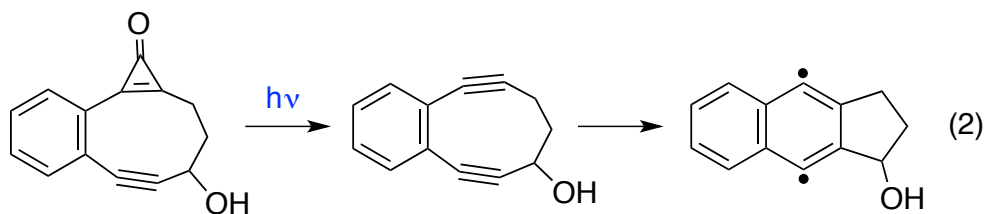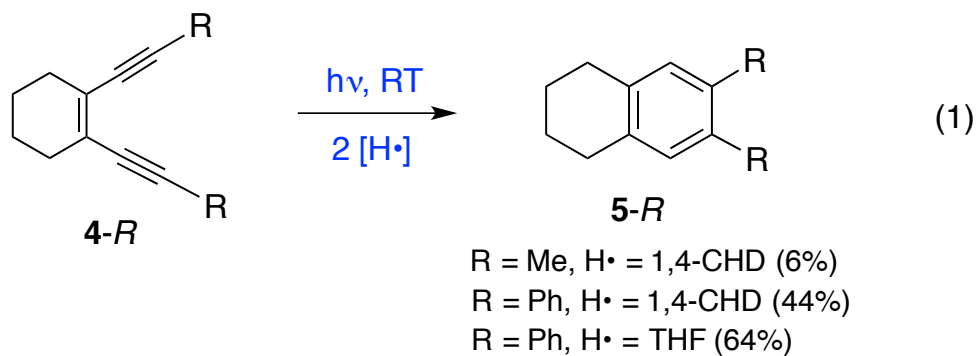
We previously demonstrated that [Cp*Ru(NCMe)$_3$]PF$_6$ cycloaromatizes enediynes in the presence of a hydrogen-atom donor, in the dark, to give [Cp*Ru(η^6-arene)]PF$_6$ complexes.[16] The ruthenium approach is unique in that it triggers the room temperature cycloaromatization of *acyclic* enediynes, such as **3**-*Pr-Z*, which do not undergo either thermal or photochemical cycloaromatization in the absence of ruthenium. The reaction was found to be catalytic in ruthenium under photochemical conditions (Scheme 5-2).[18] Irradiation has two functions, the first is photo-isomerization of the *E*-enediyne to a *Z*-enediyne,[19] and the second is photodissociation of the arene ligand in **6**-*M*. Our current mechanistic hypothesis for this remarkable transformation involves the formation of an [Cp*Ru(η^6-enediyne)]PF$_6$ intermediate (**I**) which cycloaromatizes to the diradical [Cp*Ru(η^6-aryne)]PF$_6$ (**II**; Scheme 5-2).[17] Subsequent hydrogen atom abstraction would then generate the observed ruthenium-arene product. A major limitation of these first generation metal-arene photo-triggers is the inefficient arene photodissociation step. For example, photolysis of isolated **6**-*Ru* in acetonitrile required 48 h of irradiation to achieve 91% conversion to **7** at room temperature.[18]

We now report that ruthenium-naphthalene complexes [(η^5-C$_5$H$_5$)Ru(η^6-napthalene)]PF$_6$ (**8**-*Cp*)[20], [(η^5-C$_5$Me$_5$)Ru(η^6-napthalene)]PF$_6$ (**8**-*Cp**),[21] and [(η^5-C$_5$Me$_4$CF$_3$)Ru(η^6-napthalene)]PF$_6$ (**8**-*Cp*^{*CF3}),[22] function as more efficient photoactivated triggers than **6**-*Ru* for ambient temperature cycloaromatization of enediynes. The results indicate that optimal yields are obtained with a more electron-rich metal center, as in **8**-*Cp**. The same complex serves as a photoactivated trigger for dienyne cyclization at ambient temperature.
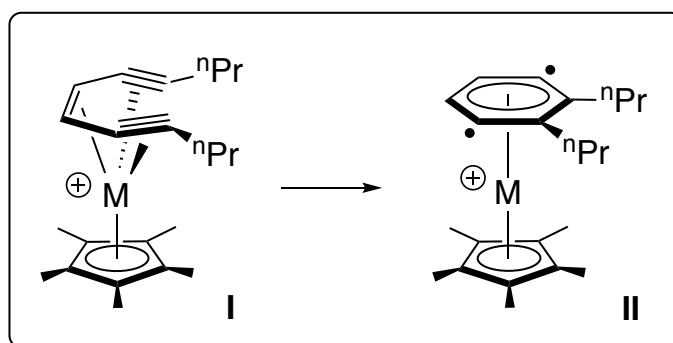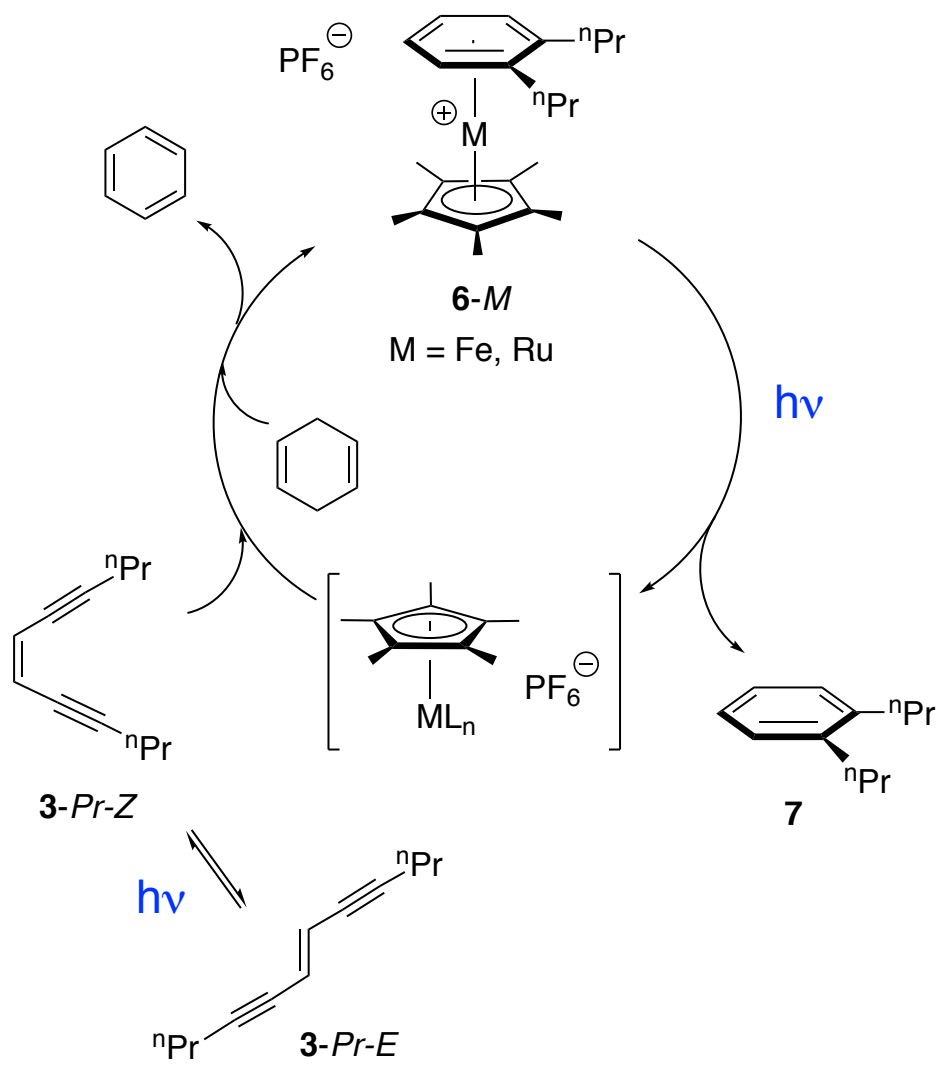
Scheme 5-2. Metal-arene complexes serve as photoactivated Bergman cycloaromatization triggers.

C. Results and Discussions

We were initially attracted to complexes **8**-*Cp* and **8**-*Cp** as promising candidates for photoactivated cyclization triggers by Kudinov's reports that these complexes undergo efficient photochemical exchange of the naphthalene ligand with arenes at room temperature.[23,24] For example, photolysis of acetone solutions containing **8**-*Cp* and three equivalents of *p*-xylene led to a 95% yield of $[(\eta^5\text{-}C_5H_5)Ru(\eta^6\text{-}p\text{-xylene})]PF_6$ (**9**) after only 6 h of irradiation (eq 5),[23a] and irradiation of an acetone solution of **8**-*Cp** and benzene (51 fold excess) for 18 h at room temperature led to a 90% isolated yield of $[(\eta^5\text{-}C_5Me_5)Ru(\eta^6\text{-benzene})]PF_6$.[23d]
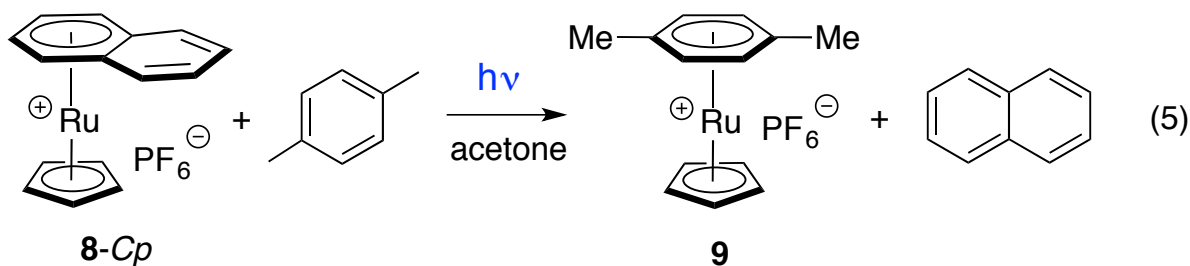
In order to establish the relative rates of benzene and naphthalene photodissociation from ruthenium complexes, we carried out a conversion vs. time study on an NMR-tube sample containing a mixture of $[(\eta^5\text{-}C_5Me_5)Ru(\eta^6\text{-napthalene})]PF_6$ (**8**-*Cp**; 0.024 mmol), $[(\eta^5\text{-}C_5Me_5)Ru(\eta^6\text{-benzene})]PF_6$ (**6**-*Ru-PhH*; 0.019 mmol), and 1,3,5-tri-tert-butylbenzene (internal standard) at 33 – 34 °C in acetonitrile-d_3. The products of are naphthalene, benzene, and $[Cp^*Ru(NCCD_3)_3]PF_6$. Over the first 140 min of photolysis, the rate constant for disappearance of **6**-*Ru-PhH* was 1.54 x 10^{-3} min^{-1},

whereas the rate constant for disappearance of **8**-*Cp** was 6.49 x 10^{-3} min^{-1} (see Appendix section). The 5-fold faster rate for naphthalene photodissociation relative to benzene dissociation is in agreement with qualitative literature observations that naphthalene dissociation from Cp^*Ru^+ occurs more rapidly than does dissociation of non-benzannulated-arene ligands.

We chose (*Z*)-octa-4-en-2,6-diyne (**3**-*Me-Z*) as a representative acyclic enediyne substrate for preliminary studies due to the simplicity of its ^{1}H NMR spectral signature (singlets at δ 1.93 and 5.59 in $CDCl_3$) that permits convenient monitoring of reactions by ^{1}H NMR spectroscopy. Roth et al. previously prepared **3**-*Me* as a 1:1 mixture of *Z:E* isomers and observed equilibration of **3**-*Me* with (*Z*)- and (*E*)-4,5-diethynyl-2-butene in the gas phase; an equilibration that presumably involves a *para*-aryne intermediate.[25] We prepared enediyne **3**-*Me-Z* as a single isomer in 76% isolated yield from a double Sonogashira cross-coupling reaction between *cis*-1,2-dichloroethylene and propyne at room temperature (eq 6).
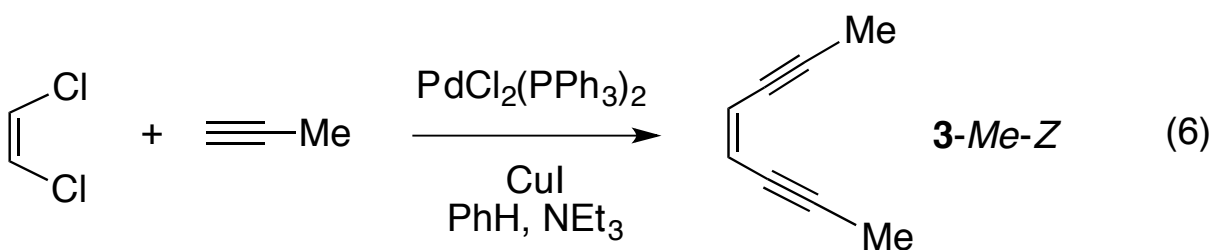
Photolysis of an acetone-d_6 solution containing **8**-*Cp* (29 μmol), **3**-*Me-Z* (29 μmol), 1,4-cyclohexadiene as hydrogen-atom donor (1,4-CHD; 60 μmol), and 1,3,5-tri-*tert*-butylbenzene (internal standard) was carried out in a Rayonett photoreactor

equipped with UV broadband lamps centered at 254 nm (Scheme 5-3). During the course of reaction, the ^{1}H NMR resonances for **3**-*Me-Z* and **8**-*Cp* decreased in intensity and new resonances, attributed to [(η^5-C$_5$H$_5$)Ru(η^6-*o*-xylene)]PF$_6$ (**10**-*Cp*), were observed at δ 2.45 (s, 6H) and 5.45 (s, 5H). After 6 h of irradiation, integration of the spectrum indicated 93% conversion of **8**-*Cp* and an 86% yield of **10**-*Cp*. In a similar fashion, **8**-*Cp** and **3**-*Me-Z*, underwent conversion to the known complex, [(η^5-C$_5$Me$_5$)Ru(η^6-*o*-xylene)]PF$_6$ (**10**-*Cp**)[26] in 91% yield after 6 h of irradiation.
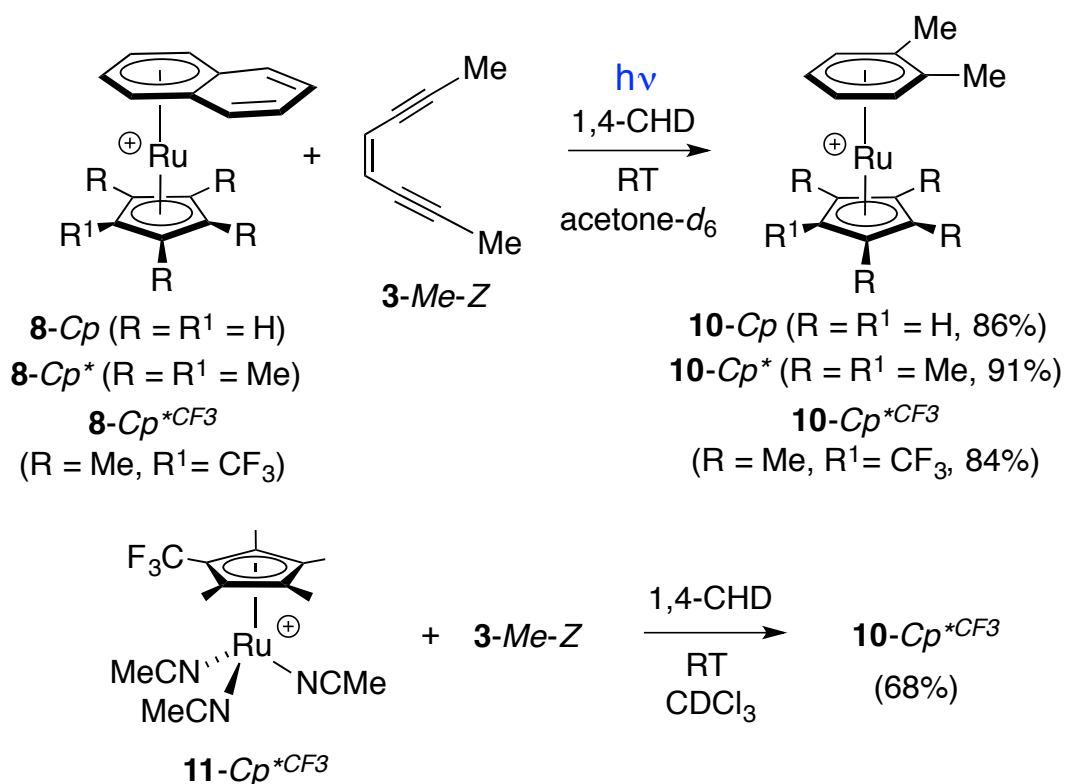
Scheme 5-3. Room Temperature Photoactivated Ruthenium Enediyne Cycloaromatization Triggers (PF$_6^-$ counter-ions not shown).

The higher yield of cycloaromatized product observed with **8**-*Cp** may be the result of either a more electron-rich metal center, or larger cyclopentadienyl ligand

substituents. Butenschön has noted dramatic effects for Ru-catalyzed reactions as a result of cyclopentadienyl ligand modification.[27] In order to address this classic "sterics vs. electronics" question, we examined the use of $[(\eta^5\text{-}C_5Me_4CF_3)Ru(\eta^6\text{-}$napthalene)]PF$_6$ (**8**-*Cp**^{CF3})[22] as a photoactivated cyclization trigger. Gassman previously established that the 1-trifluoromethyl-2,3,4,5-tetramethylcyclopentadienyl ligand (Cp*^{CF3}) exhibits similar electronic properties to the Cp ligand while affording steric bulk that is similar to the Cp* ligand.[28] Furthermore, Mann's observation that photolysis of $[(\eta^5\text{-}C_5Me_4CF_3)Ru(\eta^6\text{-}$napthalene)]PF$_6$ (**8**-*Cp**^{CF3}) in acetonitrile leads to high yields of $[(\eta^5\text{-}C_5Me_4CF_3)Ru(NCMe)_3]PF_6$ (**11**-*Cp**^{CF3}) suggested that the Cp^{CF3} ligand would be stable under photochemical conditions. When an acetone-d_6 solution of **8**-*Cp**^{CF3} (29 μmol), **3**-*Me-Z* (29 μmol), 1,4-CHD (60 μmol), and 1,3,5-tri-*tert*-butylbenzene (internal standard) was subjected to the same reaction conditions used for the reaction of **3**-*Me-Z* with **8**-*Cp* and **8**-*Cp**, **10**-*Cp**^{CF3} was formed in 84% yield at 95% conversion of **8**-*Cp**^{CF3} (Scheme 5-3). This result suggests that the more electron-rich ruthenium center in **8**-*Cp** is responsible for the superior performance of **8**-*Cp** relative to that for **8**-*Cp*. We also examined the thermal reaction of **11**-*Cp**^{CF3} (30 μmol) with **3**-*Me-Z* (30 μmol) in the presence of 1,4-cyclohexadiene (1,4-CHD, 30 μmol) and observed rapid conversion to $[(\eta^5\text{-}C_5Me_4CF_3)Ru(\eta^6\text{-}o\text{-}xylene)]PF_6$ (**10**-*Cp**^{CF3}), but in only 68% NMR yield.
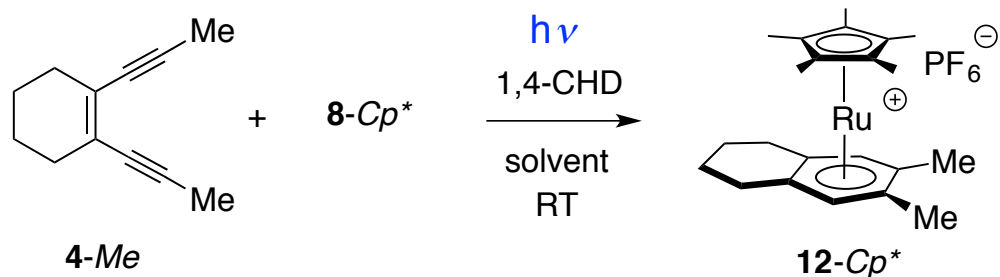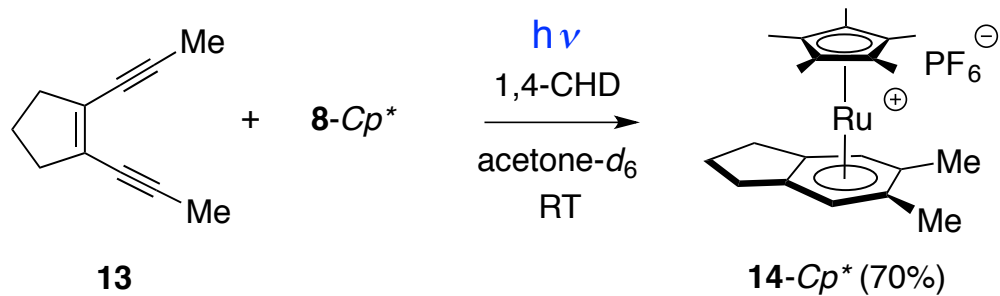
Scheme 5-4. Solvent Effects on Photoactivated Ruthenium Enediyne Cycloaromatization.

Based on the superior performance of **8**-*Cp** with acyclic enediyne **3**-*Me-Z*, we next examined its use as a photoactivated trigger for the cycloaromatizations of tetrasubstituted enediyne **4**-*Me* (Scheme 5-4). In the dark, no reaction was observed between **8**-*Cp** and **4**-*Me* over the course of 48 h at room temperature. Under similar conditions to those employed for the reaction of **8**-*Cp** with **3**-*Me-Z*, photolysis of an acetone-d_6 solution containing **4**-*Me* and **8**-*Cp** led to a 48% yield of **12**-*Cp** after 6 h, and a 75% yield after 48 h (Scheme 5-5). This compares with a 6% yield of cycloaromatized free arene product, **5**-*Me*, generated upon photolysis of **4**-*Me* in the absence of **8**-*Cp** (eq 1).[29] For an additional comparison, the thermal reaction of **4**-*Me*

and $[(\eta^5\text{-}C_5Me_5)Ru(NCMe)_3]PF_6$ (**11**-*Cp**) in the presence of 1,4-CHD led to a 51% yield of **12**-*Cp**. The five-membered ring enediyne **13** for which the critical distance[30] between the methyl substituted *sp*-carbons is 0.4 Å greater than in **4**-*Me* also underwent reaction with **8**-*Cp** in acetone-d_6 to give the known arene complex[17b] **14**-Cp* in 70% yield (Scheme 5-4).
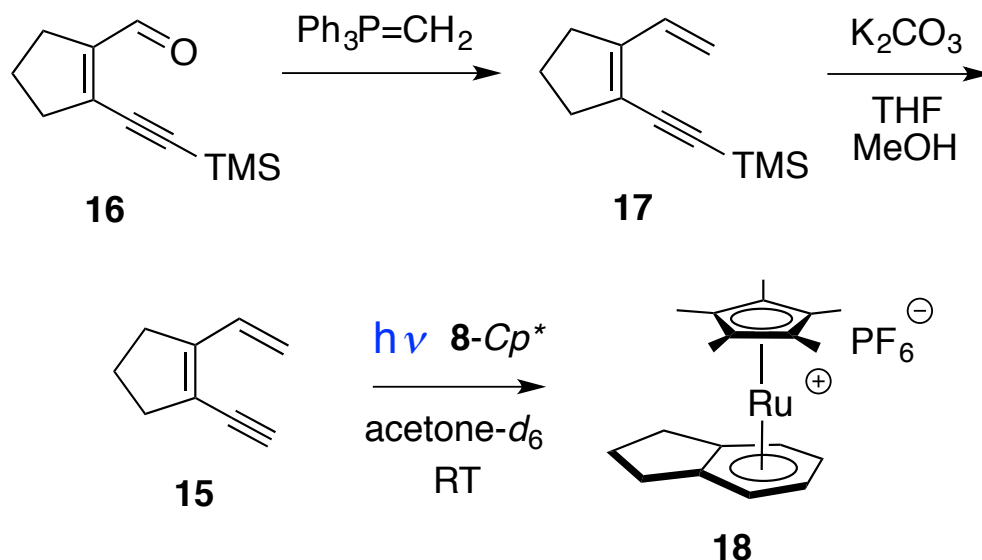
Scheme 5-5. Synthesis and Cycloaromatization of Dienyne **15**.

In order to establish the optimal reaction conditions, we examined the reaction of **4**-*Me* with **8**-*Cp** in a variety of solvents, including THF-d_8, CD_3NO_2, and $CDCl_3$ (Scheme 5-4). While comparable yields of **12**-*Cp** were observed in THF-d_8 and acetone-d_6, the limited solubility of **8**-*Cp** in THF was problematic. In nitromethane-d_3 the yield was only 22%, and even with a larger excess 1,4-CHD (14 equiv) the yield was 46%. The addition of 0.3 equiv. of acetone-d_6 to the nitromethane solvent failed to significantly improve the yield of **12**-*Cp**. Isopropanol is often employed as both

hydrogen-atom donor and solvent for thermal enediyne cycloaromatizations, however **8**-*Cp** exhibits very poor soluble in isopropanol. Thus, acetone proved to be the optimal solvent for the photoactivated cycloaromatization reactions of of **8**-*Cp** when compared to $CDCl_3$, CH_3NO_2, [i]PrOH, and THF.

We previously observed that $[(\eta^5\text{-}C_5Me_5)Ru(NCMe)_3]PF_6$ (**11**-*Cp**) also triggered the cyclization of dienynes at ambient temperature.[17c,31] The mechanism of this reaction differs significantly from that observed for enediynes in that it is a dienyne to arene rearrangement with no H-atom abstraction. Dienyne **15** was prepared from known enynyl aldehyde **16**[32] by conversion to dienyne **17** followed by desilylation (Scheme 5-5). In a control experiment, photolysis of **8**-*Cp** and **15** in acetone-d_6 led to extensive decomposition of the dienyne over the course of 24 h, with no indane product observable by ^{1}H NMR spectroscopic analysis of the crude reaction mixture. We were therefore pleased to find that the use of **8**-*Cp** as a photoactivated trigger for cyclization of **15** led to formation of arene complex $[(\eta^5\text{-}C_5H_5)Ru(\eta^6\text{-}indane)]PF_6$ (**18**) in 60% yield after 24 h of irradiation. Complex **18** was independently prepared from the reaction of **11**-*Cp** and indane.

D. X-ray Crystallographic and Computational Studies

The solid-state structures of **8**-*Cp*CF3* and *o*-xylene complex **10**-*Cp*CF3* were determined by X-ray crystallography (Figure 5-1, Appendix). Within the errors of the measurements the structure of **8**-*Cp*CF3* is nearly identical to the structures reported for **8**-*Cp*20* and **8**-*Cp23b*. In order to establish the structural parameters for a series of

517

Cp*^{CF3}, Cp*, and Cp'Ru complexes, independent of crystal packing forces, BP86/Def2-TZVPP(THF) computational studies were carried out on **8**-*Cp*^{*CF3}-*calc*, **10**-*Cp*^{*CF3}-*calc*, **10**-*Cp*-*calc* (Figure 5-2, Appendix). For the three *o*-xylene complexes, the minor structural variation that exists within the series is manifested primarily in the Ru-Arene^{cnt} distances rather than the Ru-Cp^{cnt} distances. The Ru-Cp^{cnt} distances are within 0.003 Å of one another and approximately 0.1 Å longer than the Ru-Arene^{cnt} distances. Whereas **10**-*Cp*^{*CF3}-*calc* and **10**-*Cp*-*calc* exhibit 1.731 and 1.730 Ru-Arene^{cnt} distances, respectively, the corresponding distance in **10**-*Cp*-*calc* is significantly shorter at 1.714 Å. This variation in metal-arene distance is attributed to less steric congestion in **10**-*Cp*-*calc* due to the absence of Cp-ring-substituents.
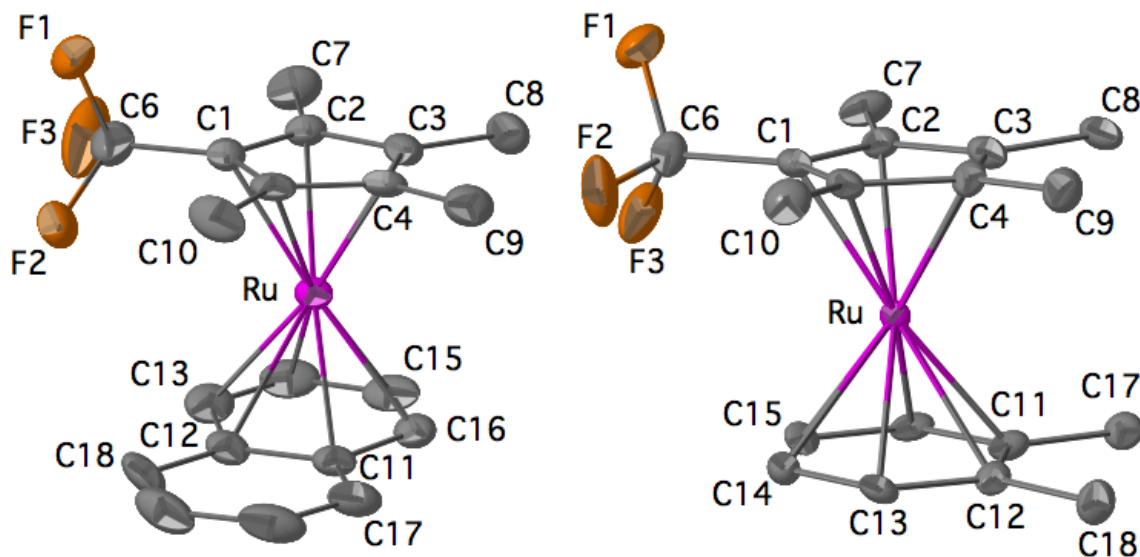
Figure 5-1. ORTEP drawings of the cations for **8**-*Cp*^{*CF3} (left) and **10**-*Cp*^{*CF3} (right). Hydrogen atoms are omitted for clarity.
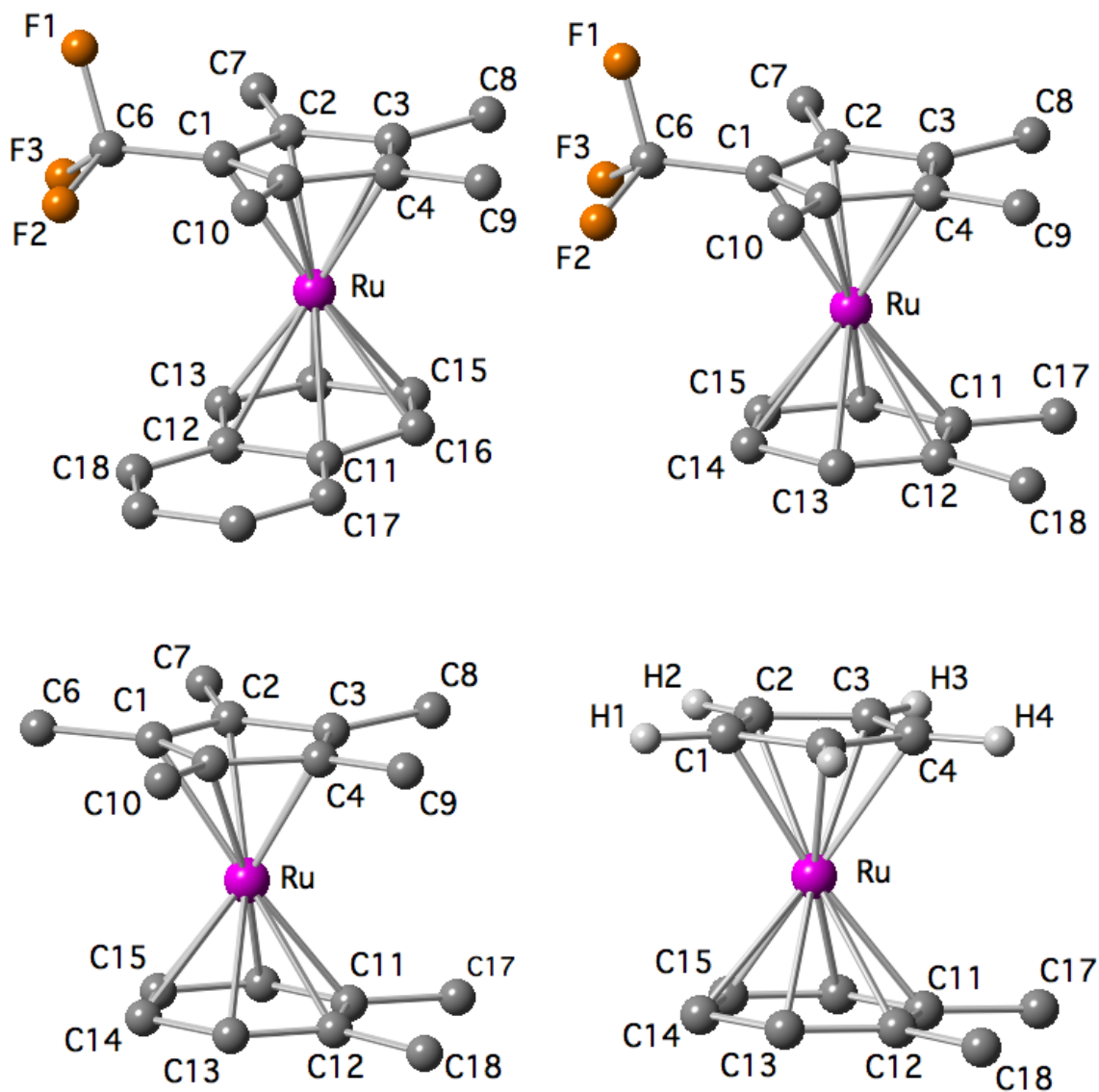
Figure 5-2. Calculated structures for cations of **8**-*Cp**CF3 (upper left) **10**-*Cp**CF3-*calc* (upper right), **10**-*Cp**-*calc* (lower left), and **10**-*Cp*-*calc* (lower right). Hydrogen atoms are omitted for clarity.

E. Conclusions

The ruthenium-naphthalene complexes, **8**-*Cp*, **8**-*Cp**, and **8**-*Cp**CF3 serve as convenient, readily accessible, photoactivated cycloaromatization triggers for both enediynes and dienynes. Use of the most electron-rich **8**-*Cp** provides higher yields

than with either **8**-*Cp* or **8**-*Cp*CF3*.   Advantages of the naphthalene complexes, compared to tris(acetonitrile) analogues such as **11**-*Cp*CF3* and **11**-*Cp**, include greater stability toward air and moisture, higher cyclization yields, and spatiotemporal control of diradical formation. Both disubstituted (**3**-*Me-Z*) and tetrasubstituted enediynes (**4**-*Me* and **13**) undergo room temperature cycloaromatization, however significantly lower yields and longer reaction times are observed in the case of the tetrasubstituted enediynes.

It should be noted that while facile photodissociation of naphthalene from **8** allows for rapid reaction with enediyne substrate, it does not lead to a more efficient catalytic system than in the case of non-benzannulated arene complexes such as **6**-*Ru* (Scheme 5-2). An exception to this would be ruthenium-catalyzed cycloaromatization of benzannulated enediynes, which would generate more labile benzannulated arene ligands. Beyond the development of photocatalytic enediyne cycloaromatizations, it may prove possible to use these photoactivated triggers to initiate free radical alkene polymerization reactions.

F. Experimentals

1. Computational Methods

The structural and energetic analyses of the molecular systems described in this study were carried out using the BP86 density functional,[33,34] with an ultrafine grid, together with the Def2-TZVPP basis set.[35] Effects of solvent were included using

the continuum solvation model based on the original COSMO theory of Klamt modified for *ab initio* theory,[36,37] with a dielectric for THF. Full geometry optimizations were performed and uniquely characterized via second derivative (Hessian) analysis to establish stationary points and effects of zero point energy and thermal corrections. Visualization and analysis of structures was carried out using Avogadro.[38]

2. General Information

All manipulations were performed using standard Schlenk technique or in nitrogen filled Vacuum Atmospheres or MBraun gloveboxes, unless otherwise stated. ^{1}H and ^{13}C NMR spectra were recorded on Varian Mercury 400 MHz, Varian VX 500 MHz, or JOEL ECA 500 MHz instruments. ^{1}H and ^{13}C NMR chemical shifts (δ) are reported in parts per million (ppm). Spectra were referenced to the residual solvent peak. Infrared spectra were obtained on a Nicolet iS10 FT-IR. High-resolution mass spectra analyses were performed at either the mass spectrometer facility at UC San Diego or UC Riverside. Reaction solvents were dried using a solvent dispensing system equipped with two neutral alumina columns under argon atmosphere or by the use of 3 Å activated molecular sieves. NMR-scale reactions were performed in 5 mm J-Young NMR tubes equipped with a Teflon needle valve. All literature compounds were prepared according to the indicated references or purchased from commercial suppliers and used as received.

3. Representative photolysis experiment

An acetone-d_6 solution (1.5 mL) of enediyne **4**-*Me* (4.6 mg, 29 μmol), **8**-*Cp** (14.8 mg, 29 μmol), 1,4-CHD (4.56 mg, 57 μmol), and 1,3,5-tri-*tert*-butylbenzene internal standard, was maintained at rt for 48 h in the dark, after which time a ^{1}H NMR spectrum of the sample indicated that no reaction had occurred. The sample was then irradiated in a Rayonett photo-reactor equipped with UV lamps centered at 254 nm and the progress of reaction was monitored by ^{1}H NMR spectroscopy. After irradiation for 24 h the yield of **12**-*Cp** was determined to be 75% by integration of the ^{1}H NMR spectrum. The product exhibited spectroscopic properties identical to those reported in literature.[25]

4. Relative Rates of of Arene Photodissociation from [(η^5-C$_5$Me$_5$)Ru(η^6-napthalene)]PF$_6$ (8-*Cp**) and [(η^5-C$_5$Me$_5$)Ru(η^6-benzene)]PF$_6$ (6-*Ru-PhH*)

[(η^5-C$_5$Me$_5$)Ru(η^6-napthalene)]PF$_6$ (**8**-*Cp**; 12.0 mg, 0.024 mmol), [(η^5-C$_5$Me$_5$)Ru(η^6-benzene)]PF$_6$ (**6**-*Ru-PhH*; 8.9 mg, 0.019 mmol) and 1,3,5-tri-*tert*-butylbenzene (internal standard) were added to an oven dried J. Young tube. Acetonitrile-d_3 (0.91 mL) was added to the tube, and the solution was degassed via 3 freeze/pump/thaw/degas cycles. An initial ^{1}H NMR spectrum was recorded and the tube was placed in a Rayonette photoreactor equipped with UV broadband lamps centered at 254 nm (33-34 °C). Photolysis was initiated and reaction progress was monitored by interrupting the photolysis every 20 min to record a ^{1}H NMR spectrum. Diagnostic ^{1}H NMR resonances for **6**-*Ru-PhH* (δ 5.76) and **8**-*Cp** (δ 6.49) were integrated relative to internal standard. Product resonances were observed at δ 1.60 {[(η^5-C$_5$Me$_5$)Ru(NCCD$_3$)$_3$]PF$_6$}, δ 7.52, 7.88 (naphthalene), and 7.37 (benzene).

G. Appendix

Table 5-1. Distances (Å) and angles (deg) from the X-ray crystallographic data for 10-*Cp**CF3, and BP86/Def2-TZVPP calculated data for 10-*Cp**CF3-*calc,* 10-*Cp*-calc,* 10-*Cp-calc, and* 8-*Cp**CF3-*calc.*

	10-*Cp**CF3	**10-***Cp**CF3-*calc*	**10-***Cp*-calc*	**10-***Cp-calc*	**8-***Cp**CF3-*calc*
Ru-C1	2.141(5)	2.154	2.201	2.196	2.154
Ru-C2	2.188(5)	2.202	2.200	2.199	2.178
Ru-C3	2.203(5)	2.220	2.202	2.199	2.195
Ru-C4	2.195(4)	2.222	2.202	2.198	2.224
Ru-C5	2.182(5)	2.204	2.201	2.196	2.216
Ru-C11	2.244(4)	2.269	2.267	2.255	2.338
Ru-C12	2.241(4)	2.268	2.267	2.255	2.333
Ru-C13	2.217(5)	2.233	2.228	2.217	2.227
Ru-C14	2.219(4)	2.228	2.232	2.218	2.232
Ru-C15	2.209(5)	2.227	2.232	2.219	2.225
Ru-C16	2.216(5)	2.233	2.228	2.216	2.225
Ru-C1-C6	125.4(3)	128.4	127.6	-	129.5
Ru-C2-C7	127.8(4)	128.9	127.7	-	128.8
Ru-C11-C17	130.6(3)	131.4	131.6	131.1	131.2
Ru-C12-C18	129.4(3)	131.5	131.6	131.0	131.2

Table 5-2. Concentration of **8**-*Cp** and **6**-Ru-*PhH* and their natural logarithms at differet time points during the photolysis experiment.

(mol/L)	0	20 min	40 min	60 min	80 min	100 min	120 min	140 min
[Cp*Ru(C$_{10}$H$_8$)PF$_6$]	0.0266	0.0225	0.0181	0.0164	0.0147	0.0128	0.0116	0.0106
[Cp*Ru(PhH)PF$_6$]	0.0213	0.0207	0.0203	0.0194	0.0189	0.0181	0.0179	0.0172
ln[Cp*Ru(C$_{10}$H$_8$)PF$_6$]	-3.627	-3.794	-4.012	-4.110	-4.220	-4.358	-4.456	-4.547
ln[Cp*Ru(PhH)PF$_6$]	-3.849	-3.878	-3.897	-3.942	-3.969	-4.012	-4.023	-4.063
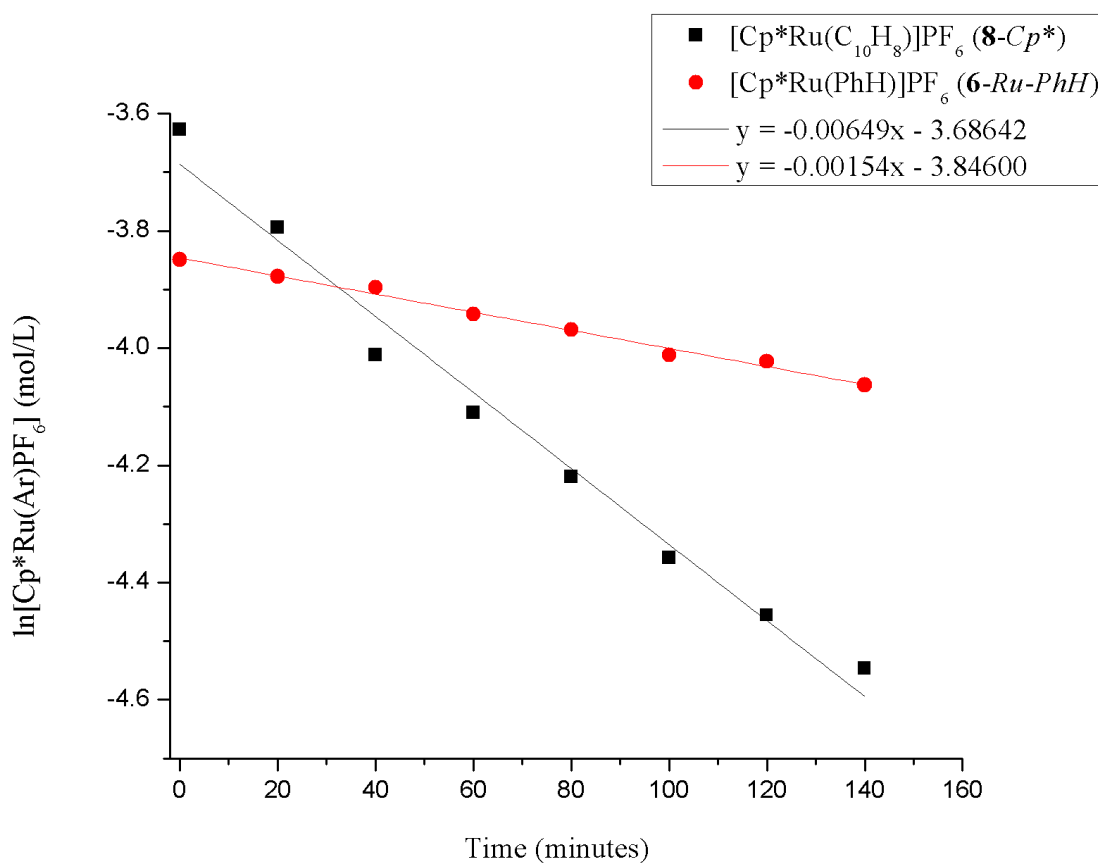
Figure 5-3. Plot of natural logarithm [**8**-*Cp**] and [**6**-*PhH*] vs time.

Acknowledgement

Chapter 5 is a full reprint of the publication "Photoactivated Transition-Metal Triggers for Ambient Temperature Enediyne and Dienyne Cyclization: Ruthenium-η^6-Naphthalene Complexes" Qin, P.; Cope, S. K.; Steger, H.; Veccharelli, K. M.; Holland, R. L.; Hitt, D. M.; Moore, C. E.; Baldridge, K. K.; O'Connor, J. M. *Organometallics*, **2017**, *36*, 3967-3973. The dissertation author is the first author on this paper.

H. References

1. (a) Jones, R. R.; Bergman, R. G. *J. Am. Chem. Soc.* **1972**, *74*, 660-661. (b) Lockhart, T. P.; Mallon, C. B.; Bergman, R. G. *J. Am. Chem. Soc.* **1980**, *102*, 5976-5978. (c) Lockhart, T. P.; Comita, P. B.; Bergman, R. G. *J. Am. Chem. Soc.* **1981**, *103*, 4082-4090. (d) Lockhart, T. P.; Bergman, R. G. *J. Am. Chem. Soc.* **1981**, *103*, 4091-4096.

2. For leading references, see: (a) Nicolaou, K. C.; Wang, Y.; Lu, M.; Mandal, D.; Pattanayak, M. R.; Yu, R.; Shah, A. A.; Chen, J. S.; Zhang, H.; Crawford, J. J.; Pasunoori, L.; Poudel, Y. B.; Chowdari, N. S.; Pan, C.; Nazeer, A.; Gangwar, S.; Vite, G.; Pitsinos, E. N. *J. Am. Chem. Soc.* **2016**, *138*, 8235-8246, and references therein. (b) Bdour, H. M.; Snigdha, R.; Basak, A. *Lett. Drug Design Disc* **2015**, *12*, 545-557. (c) Mohamed, R. K.; Peterson, P. W.; Alabugin, I. V. *Chem. Rev.* **2013**, *113*, 7089-7129. (d) Boerner, L. J. K.; Dye, D. F.; Köpke, T.; Zaleski, J. M. *Coord. Chem. Rev.* **2013**, *257*, 599-620. (e) Peterson, P. W.; Mohamed, R. K.; Alabugin, I. V. *Eur. J. Org. Chem.* **2013**, 2505-2527.

3. For a recent review of the photo-Bergman cyclization, see: *Photochemistry and Photobiology*, 3rd ed.; CRC Press: Boca Raton, FL, 2012; p 549-592.

4. We define "acyclic" here as enediynes where none of the three unsaturated units are located within a ring structure.

5. Kagan, J.; Wang, X.; Chen, X.; Lau, K. Y.; Batac, I. V.; Tuveson, R. W.; Hudson, J. B. *J. Photochem. Photobiol. B.: Biol.* **1993**, *21*, 135-142.

6. For a computational treatment of acyclic enediyne photo-Bergman reactions, see: Clark, A. E.; Davidson, E. R.; Zaleski, J. M. *J Am. Chem. Soc.* **2001**, *123*, 2650-2657.

7. For photo-Bergman cyclizations of strained-ring enediynes that proceed in high yield, see: Funk, R. L.; Young, E. R. R.; Williams, R. M.; Flanagan, M. R.; Cecil, T. L. *J. Am. Chem. Soc.* **1996**, *118*, 3291-3292.

8. We are aware of only two examples where the photo-Bergman reaction succeeds with substrates that lack conjugating substituents, see: Kaneko, T.; Takahashi, M.; Hirama, M. *Angew. Chem. Int. Ed.* **1999**, *38*, 1267-1268.

9. (a) Cambell, I. D.; Eglinton, G. *J. Chem. Soc. C* **1968**, 2120-2121. (b) Evanzahav, A.; Turro, N. J. *J. Am. Chem. Soc.* **1998**, *120*, 1835-1841. (c) Kar, M.; Basak, A. *Chem. Rev.* **2007**, *107*, 2861-2890.

10. Jones, G. B.; Wright, J. M.; Purohit, A. D.; Wyatt, J. K.; Hynd, G.; Fouad, F. *J. Am. Chem.* Soc. **2000**, *122*, 9872-9873.

11. Zhao, Z.; Peacock, J. G.; Gubler, D. A.; Peterson, M. A. *Tetrahedron Lett.* **2005**, *46*, 1373-1375.

12. (a) Poloukhtine, A.; Popik, V. V. *J. Org. Chem.* **2005**, *70*, 1297-1305. (b) Zhegalovaa, N. G.; Popik, V. V. *J. Phys. Org. Chem.* **2011**, *24*, 969-975. (c) Pandithavidana, D. R.; Poloukhtine, A.; Popik, V. V. *J. Am. Chem. Soc.* **2009**, *131*, 351-356.

13. Karpov, G. V.; Popik, V. V. *J. Am. Chem. Soc.* **2007**, *129*, 3792-3793.

14. (a) Nicolaou, K. C.; Dai, W.-M.; Wendeborn, S. V.; Smith, A. L.; Torisawa, Y.; Maligres, P.; Hwang, C.-K. *Angew. Chem. Int. Ed. Engl.* **1991**, *30*, 1032-1036. (b) Wender, P. A.; Zercher, C. K.; Beckham, S.; Haubold, E.-M. *J. Org. Chem.* **1993**, *58*, 5867-5869. (c) Basak, A.; Bdour, H. M.; Shain, J. C.; Mandal, S.; Rudra, K. R.; Nag, S. *Bioorg. Med. Chem. Lett.* **2000**, *10*, 1321-1325.

15. (a) Benites, P. J.; Holmberg, R. C.; Rawat, D. S.; Kraft, B. J.; Klein, L. J.; Peters, D. G.; Thorp, H. H.; Zaleski, J. M. *J. Am. Chem. Soc.* **2003**, *125*, 6434-6446. (b) Kraft, B. J.; Coalter, N. L.; Nath, M.; Clark, A. E.; Siedle, A. R.; Huffman, J. C.; Zaleski, J. M. *Inorg. Chem.* **2003**, *42*, 1663-1672.

16. The $[(\eta^5\text{-}C_5Me_5)Ru(NCMe)_3]$ cation triggers thermal cycloaromatization of enediynes at rt, see: (a) O'Connor, J. M.; Friese, S. J. *Organometallics* **2008**, *27*, 4280-4281. (b) O'Connor, J. M.; Friese, S. J.; Tichenor, M. *J. Am. Chem. Soc.* **2002**, *124*, 3506-3507. (c) O'Connor, J. M.; Lee, L. I.; Gantzel, P.; Rheingold, A. L.; Lam, K-C. *J. Am. Chem. Soc.* **2000**, *122*, 12057-12058.

17. For a related chromium-mediated enediyne cycloaromatization, see: Ylijoki, K. E. O.; Lavy, S.; Fretzen, A.; Kündig, E. P.; Berclaz, T.; Bernardinelli, G.; Besnard, C. *Organometallics* **2012**, *31*, 5396-5404.

18. O'Connor, J. M.; Friese, S. J.; Rodgers, B. L. *J. Am. Chem. Soc.* **2005**, *127*, 16342-16343.

19. Photolysis establishes a photostationary state (equilibrium) between *E*- and *Z*-enediynes. As ruthenium cycloaromatizes the *Z*-enediyne, the *E/Z* equilibrium is re-established. Due to photoisomerization of the enediyne, pure *E*-enediyne should function as a substrate under photochemical conditions.

20. (a) Kündig, E. P.; Monnier, F. R. *Adv. Synth. Catal.* **2004**, *346*, 901-904. (b) Urbaneja, X.; Mercier, A.; Besnard, C.; Kündig, E. P. *Chem. Commun.* **2011**, 47, 3739-3741.

21. Loughrey, B. T.; Cunning, B. V.; Healy, P. C.; Brown, C. L.; Parsons, P. G.; Williams, M. L. *Chem. Asian J.* **2012**, *7*, 112-121.

22. Evju, J. K.; Mann, K. R. *Organometallics* **2002**, *21*, 993-996.

23. (a) Karslyan, E. E.; Perekalin, D. S.; Petrovskii, P. V.; Borisova, A. O.; Kudinov, A. R.; *Russ. Chem. Bull., Int. Ed.* **2009**, *58*, 585-588. (b) Karslyan, E. E.; Perekalin, D. S.; Petrovskii, P. V.; Lyssenko, K. A.; Kudinov, A. R. *Russ. Chem. Bull., Int. Ed.* **2008**, *57*, 2201-2203. (c) Perekalin, D. S.; Karslyan, E. E.; Trifonova, E. A.; Konovalov, A. I.; Loskutova, N. L.; Nelyubina, Y. V.; Kudinov, A. R. *Eur. J. Inorg. Chem.* **2013**, 481-493. (d) Perekalin, D. S.; Shvydkiy, N. V.; Nelyubina, Y. V.; Kudinov, A. R. *Mendeleev Commun.* **2015**, *25*, 29-31.

24. One would anticipate that η^2-enediyne coordination to ruthenium would have a lower energy of activation than η^2-*p*-xylene coordination since the latter requires disruption of aromaticity. For η^2-arene coordination, see: (a) Jones, W. D.; Feher, F. J. *J. Am. Chem. Soc.* **1984**, *106*, 1650-1663. (b) Jones, W. D.; Feher, F. J. *J. Am. Chem. Soc.* **1986**, *108*, 4814. (c) Keane, J. M.; Harman, W. D. *Organometallics* **2005**, *24*, 1786-1798. (d) Harrison, D. P.; Harman, W. D. *Aldrichimica Acta* **2012**, *45*, 45-55.

25. Roth, W. R.; Hopf, H.; Horn, C. *Chem. Ber.* **1994**, *127*, 1781-1795.

26. Masuda, K.; Ohkita, H.; Kurumatani, S.; Itoh, K. *Organometallics* **1993**, *12*, 2221-2226.

27. Butenschön, H. *Angew. Chem. Int. Ed. Engl.* **1994**, *33*, 636-638.

28. (a) Gassman, P. G.; Mickelson, J. W.; Sowa Jr., J. R. *J. Am. Chem. Soc.* **1992**, *114*, 6942-6944. (b) Gassman, P. G.; Sowa Jr., J. R.; Hill, M. G.; Mann, K. R. *Organometallics* **1995**, *14*, 4879-4885.

29. Photolysis of an acetone-d_6 solution containing **4**-*Me* and 1,4-CHD in the absence of ruthenium complex failed to generate cycloaromatization product in sufficient quantities to be observable by ^{1}H NMR spectroscopy.

30. For the effect of "critical distance" on enediyne cycloaromatizations, see: Nicolaou, K. C.; Dai, W.-M.; Hong, Y. P.; Tsay, S.-C.; Baldridge, K. K.; Siegel, J. S. *J. Am. Chem. Soc.* **1993**, *115*, 7944-7953.

31. O'Connor, J. M.; Friese, S. J.; Rodgers, B. L.; Rheingold, A. L.; Zakharov, L. *J. Am. Chem. Soc.* **2005**, *127*, 9346-9347.

32. Wang, K. K.; Liu, B.; Lu, Y. *Tetrahedron Lett.* **1995**, *36*, 3785-3788.

33. Becke, A. D. *Phys. Rev. A: At., Mol., Opt. Phys.*, **1988**, 38, 3098-3100.

34. Perdew, J. P. Phys. Rev. B: Condens. Matter Mater. Phys., **1986**, 33, 8822-8824.

35. Weigend, F.; Ahlrichs, R. *Phys. Chem. Chem. Phys.* **2005**, *7*, 3297-3305.

36. Klamt, A.; Schüürmann, *J. Chem. Soc. Perkin Trans. 2,* 799-805.

37. Baldridge, K.; Klamt, A. *J. Chem. Phys.* **1997**, *106*, 6622–6633.

38. Hanwell, M.; Curtis, D.; Lonie, D.; Vandermeersch, T.; Zurek, E.; Hutchison, G. *J. Cheminform.* **2012**, *4*, 17.

39. Pilling, G. M.; Sondheimer, F. *J. Am. Chem. Soc.* **1971**, *93*, 1970-1977.

CHAPTER 6

Chemo-and Regioselective Ruthenium-catalyzed Cycloaromatization of Conjugated

Dienynes

A. Introduction

Cycloaromatization of conjugated dienynes has been the subject of extensive research since 1969 when Hopf discovered the isomerization of 1,3-hexadien-5-yne to benzene at 274 °C in the gas phase (Scheme 6-1).[1-3] It was proposed that a 6π electrocyclization occurs at high temperature to generate the cyclic eneallene intermediate **2**, that is followed by a 1,2-hydride shift to produce carbene intermediate **3**. A further hydrogen atom shift affords the aromatized product. The readily available dienynes can be synthesized via classic metal-catalyzed cross coupling reactions, such as Heck reaction, Suzuki reaction, and Sonogashira reaction, which provides potential application of this remarkable transformation to assemble functionalized annulated products with new carbon-carbon bonds.[4] However, due to the high temperature it requires in the cyclization process, decomposition and polymerization of the starting materials can be problematic.
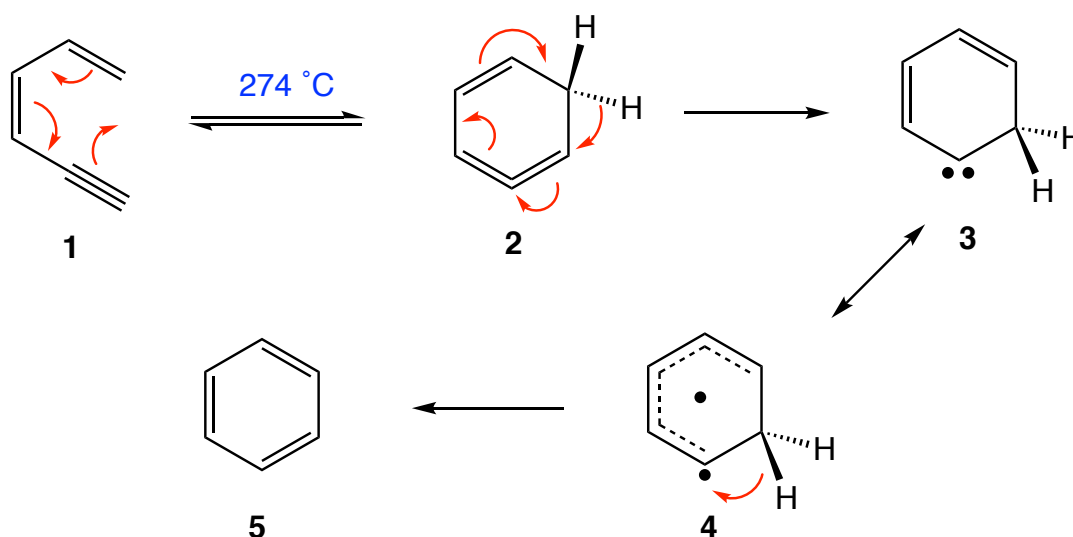
Scheme 6-1. Mechanism of Hopf cyclization.

With the development of organometallic chemistry, people start to seek strategy to lower down the energy of transition state via coordination to transition metals. In 2009, Aguilar group reported a gold-catalyzed cycloaromatization of a dienyne carboxylic acid to generate 2,3-disubstituted phenols at ambient temperature (Scheme 6-2). The reaction has total regioselective control with short reaction time and low catalyst loading.[5] In 2018, Zi reported a rhodium-catalyzed De Novo synthesis of phenols via an oxidative cycloaromatization of conjugated dienynes (Scheme 6-3). The reaction was found bearing a wide substrate scope and functional group tolerance. Late-stage derivatization of natural products with a phenol ring was also achieved by employing this method.[6]
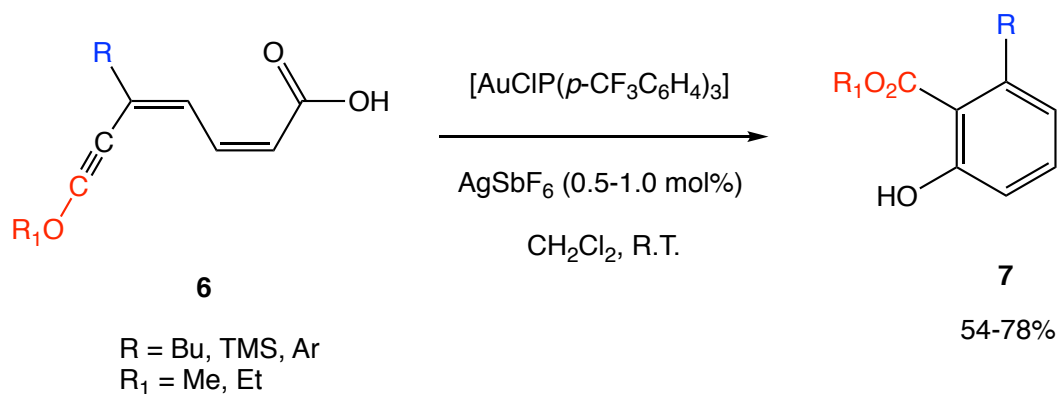
Scheme 6-2. Gold-catalyzed cycloaromatization of dienyne.
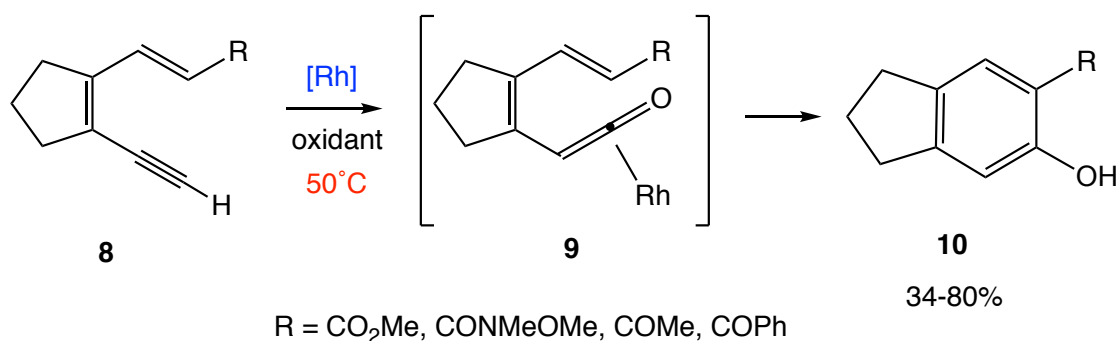
Scheme 6-3. Rhodium-catalyzed cycloaromatization of dienyne.

531

O'Connor lab pioneered in ruthenium-mediated cycloaromatization of conjugated "tri-π" molecules, including dienyne, enediyne, and triene. In 2005, they discovered that dienyne molecule **12** can be cyclized by Cp*Ru(NCMe)$_3$PF$_6$ to form a ruthenium arene product **14** at -10 °C with 52% NMR yield (Scheme 6-4).[7] They proposed that an η^6-dienyne complex **13** that was observed at -60 °C might serve as the intermediate on the way to cyclization. More recently, they reported a stereoselective formation of η^6-arene ruthenium complex via metal-triggered Hopf cycloaromatization, in which a stereocenter was placed on the allylic position of dienyne **15**, and the products were formed with different diastereomeric ratios (Scheme 6-5).[8]
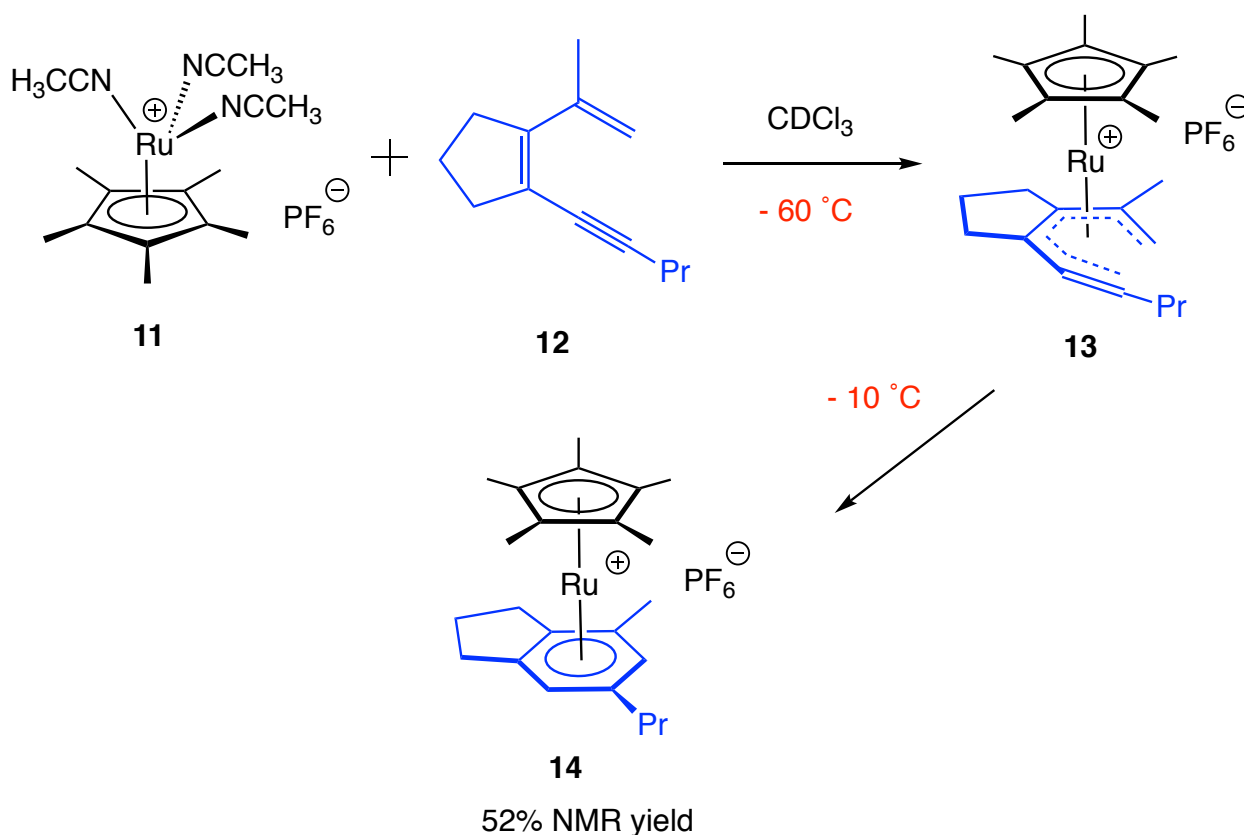
Scheme 6-4. Ruthenium-mediated cycloaromatization of dienyne **12**.
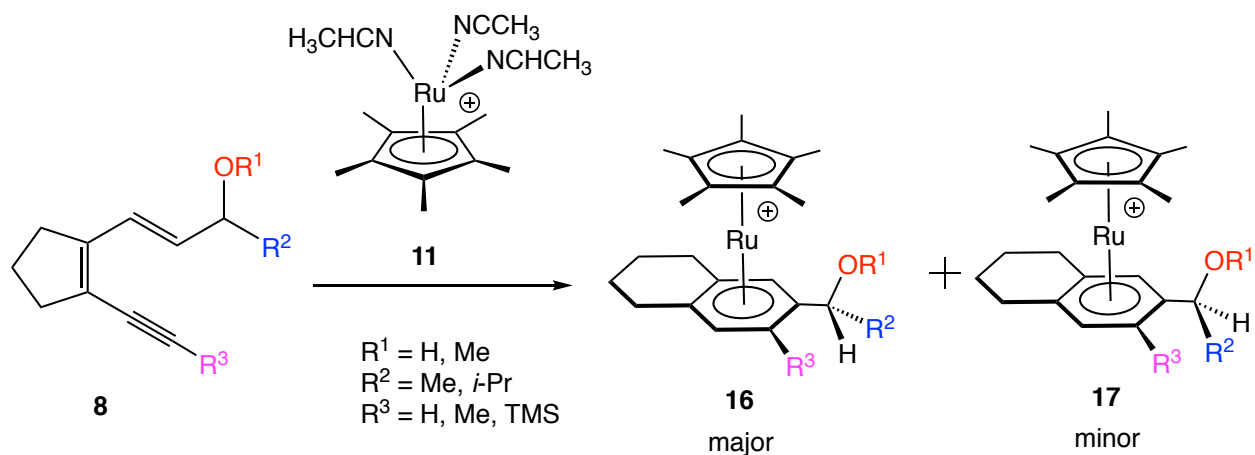
Scheme 6-5. Stereoselective cycloaromatization of dienyne **8**.

Most examples of the cycloaromatization of dienynes shown in the literature are benzannulated, and dienynes without the incorporation of aromatic rings were found less stable and subjected to decomposition upon heating.[3] Also, Hopf found that a 1,2-phenyl shift could occur to generate the *meta*-diphenyl benzene **21** as the major product when heating the phenyl substituted dienyne **18**, which suggests that the bulky phenyl group attached on C6 position might impede the cyclization process (Scheme 6-6).[3a]
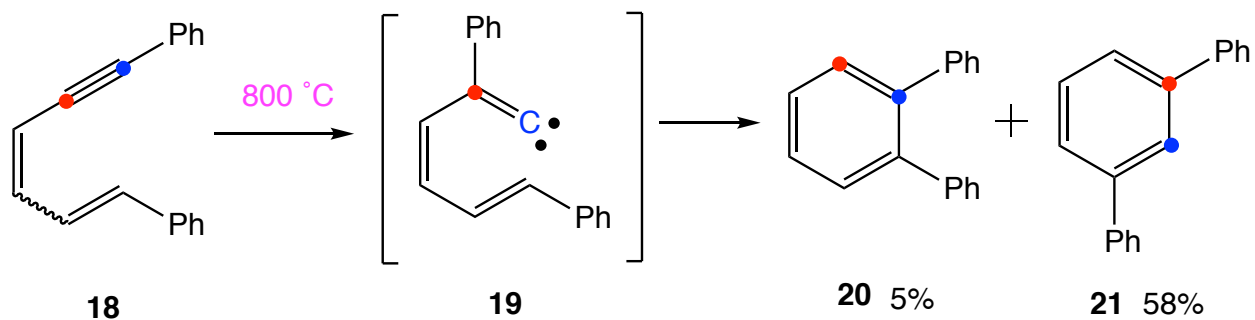
Scheme 6-6. Thermocyclization of phenyl substituted dienyne **18**.

Despite [Cp*Ru]$^+$ moiety is notorious for its high affinity with arenes, here we describe a chemoselective cycloaromatization of conjugated dienynes bearing a phenyl substituent at ambient temperature without competitive complexation to the phenyl substituent or any phenyl group migration. The subsequent photodissociation of the arene ligand provides an ideal synthetic strategy to assemble multi-substituted aromatic molecules with excellent yields. The kinetic studies suggest that the η^6-coordinated dienyne complex may serves as intermediate on the way to cyclization. Furthermore, when dienynes bearing a methyl substituent on the alkene are employed as substrate, different highly regioselective cycloisomerization patterns are observed between the cyclopentenyl dienyne and its cyclohexenyl dienyne analogue.

B. Reversable Formation of Ruthenium η^6-Dienyne Complex

In order to compare with η^6-arene ruthenium complex, firstly, we examined the affinity of dienyne substrate to [Cp*Ru]$^+$ moiety. The substrate we used is a dienyne with a TMS substituent attached on the alkyne that can potentially slow down the cyclization process by the large steric congestion. To synthesize the substrate **26**, we started with the conversion of cyclopentanone to vinyl bromide, followed by a Sonogashira coupling with trimethylsilane acetylene (Scheme 6-7). After a Wittig reaction was conducted with methyl triphenyl phosphonium bromide, molecule **26** can be obtained as clear oil with 88% yield.
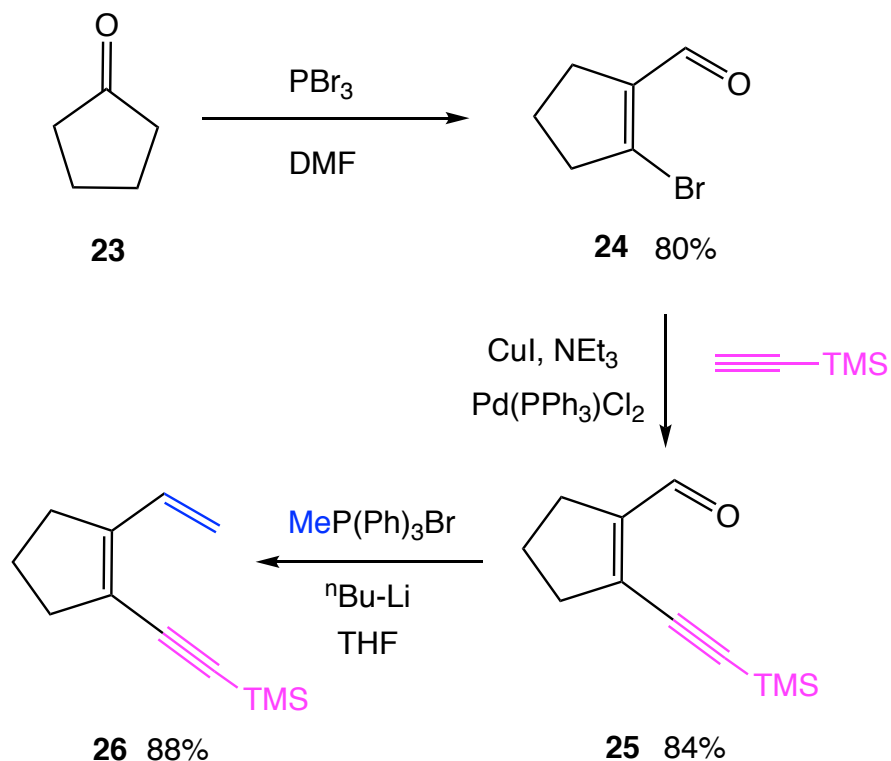
Scheme 6-7. Synthesis of TMS substituted dienyne **26**.

A NMR scale reaction was subsequently carried out between dienyne **26** and Cp*Ru(NCMe)$_3$PF$_6$ (**11**). A chloroform-*d* (1.2 mL) solution of compound **26** (2.1 mg, 0.011 mmol) was treated with complex **11** (5.5 mg, 0.011 mmol) at ambient temperature in a J.Y. NMR tube under inert atmosphere (Scheme 6-8). The reaction mixture was monitored by NMR spectroscopy (400 MHz). After 2 minutes, 70 % of the dienyne **26** was consumed, and a new ruthenium complex was observed based on the characteristic resonances at δ 0.36 (s, 9H, TMS) and 1.82 (s, 15H, Cp*). The coordination of metal center to the terminal alkene in the product is manifested by the three upper field vinyl hydrogen signals at δ 0.65 (dd, 1H, *J* = 9.6 Hz, *J* = 2 Hz, H$_C$), 3.40 (dd, 1H, *J* = 9.6 Hz, *J* = 2 Hz, H$_B$), and 5.13 (t, 1H, *J* = 9.6 Hz, H$_A$), compared to the

corresponding resonances in the free dienyne **26** at δ 5.20 (d, 1H, J = 18 Hz), 5.21 (d, 1H, J = 10.4 Hz), 6.85 (dd, 1H, J = 10.4 Hz, J = 18 Hz).
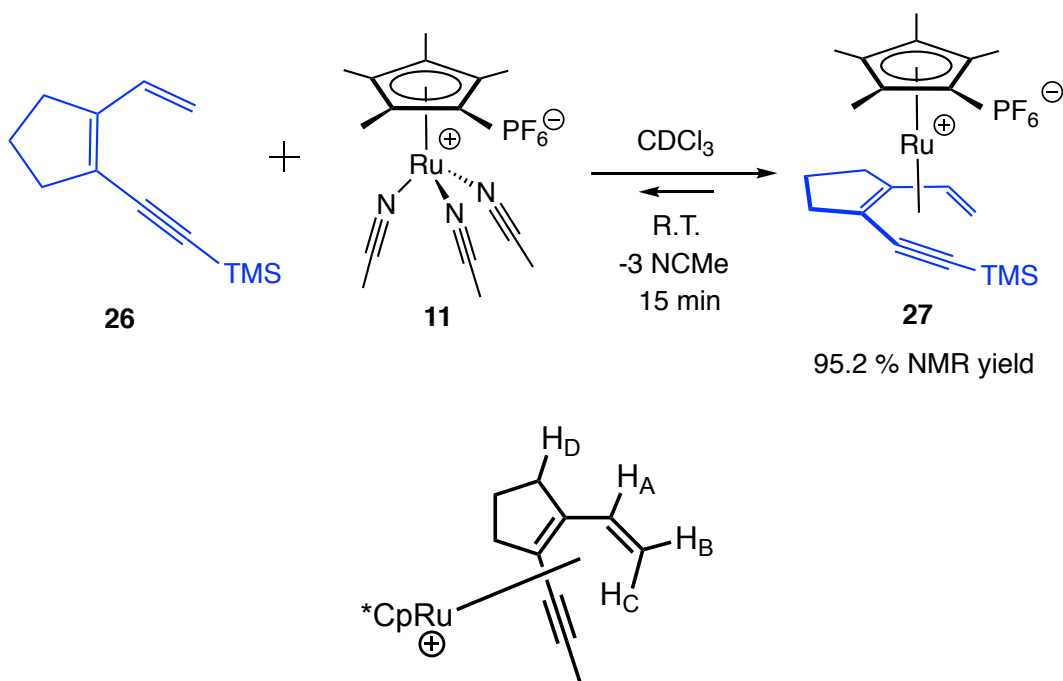
Scheme 6-8. Reaction of dienyne **26** with complex **11**.

The unambiguous assignment of these vinyl hydrogens in the product was confirmed by a NOE NMR experiment, in which the vinyl hydrogen H_A at δ 5.14 was irradiated, obvious NOE effects were observed at δ 3.40 (H_B), 2.72 (methylene-H, H_D), and 1.82 (Cp*). The existence of vinyl hydrogen resonances excludes the η^6-arene ruthenium complex. In the $^{13}C\{^1H\}$ NMR spectrum (125 MHz, CDCl$_3$), the fact that all four vinyl carbon resonances (Δ = 24.4 − 59.1 ppm) and two acetylene carbon resonances (Δ = 9.1 − 10.1 ppm) are more shielded compared to the original free dienyne **26** strongly suggests that the all three conjugated π bonds are coordinated to

the ruthenium. In addition, no acetonitrile ligand was observed binding to the metal center anymore. It was noticed that after 15 minutes, an equilibrium was established between the staring Cp*Ru(NCMe)$_3$PF$_6$ and the product **27**, and the reaction can be moved to completion by distilling out the free acetonitrile and adding fresh CDCl$_3$, which gives a 95.2% NMR yield of the product **27** based on the integration of TMS resonance at δ 0.36 (s, 9H) relative to internal standard.

Complex **27** has been proved to be air sensitive, and it slowly decomposed in chloroform to give some unknow complexes. The X-ray quality crystal of complex **27** was obtained by fast crystallization in chloroform and hexanes at ambient temperature, and the crystallographic analysis reveals a ruthenium η^6-dienyne complex, in which all six carbons of the conjugated dienyne are coordinated to the ruthenium (Figure 6-1). The selected bond distances and angles of complex **27** were allowed to compare to complex **13**, and the data are summarized in Table 6-1. The dienyne moiety of complex **27** is essentially planar with the largest deviation of planarity at C5 (C5 – plane C1-C2-C3-C4-C5-C6 distance, 0.123(3) Å). The metal is located 1.5518(16) Å from the centroid of the dienyne plane, which is 0.2822 Å shorter than the Ru – Cp* centroid distance. The alkyne is substantially bent by the back-donation effect from the metal center, which is manifested by the C4-C5-C6 angle (157.3(4) °) and C5-C6-Si angle (151.0(4) °). The Ru – C6 bond (2.415(4) Å) is significantly elongated compared to the bond distances between ruthenium and rest five carbons (2.189(14) – 2.258(4) Å). The two alkenes are found still well conjugated with a small C1-C2-C3-C4 torsion angle (11.5(5) °). The nonbonding distance between C1 and C6 was measured as 2.949(6) Å. Compared to complex **13** with a propyl group, the steric congestion from the bulky TMS

group in complex **27** is reflected by the longer Ru – C6 bond (Δ = 0.089 Å) and smaller C4-C5-C6 angle (Δ = 5.4 °).
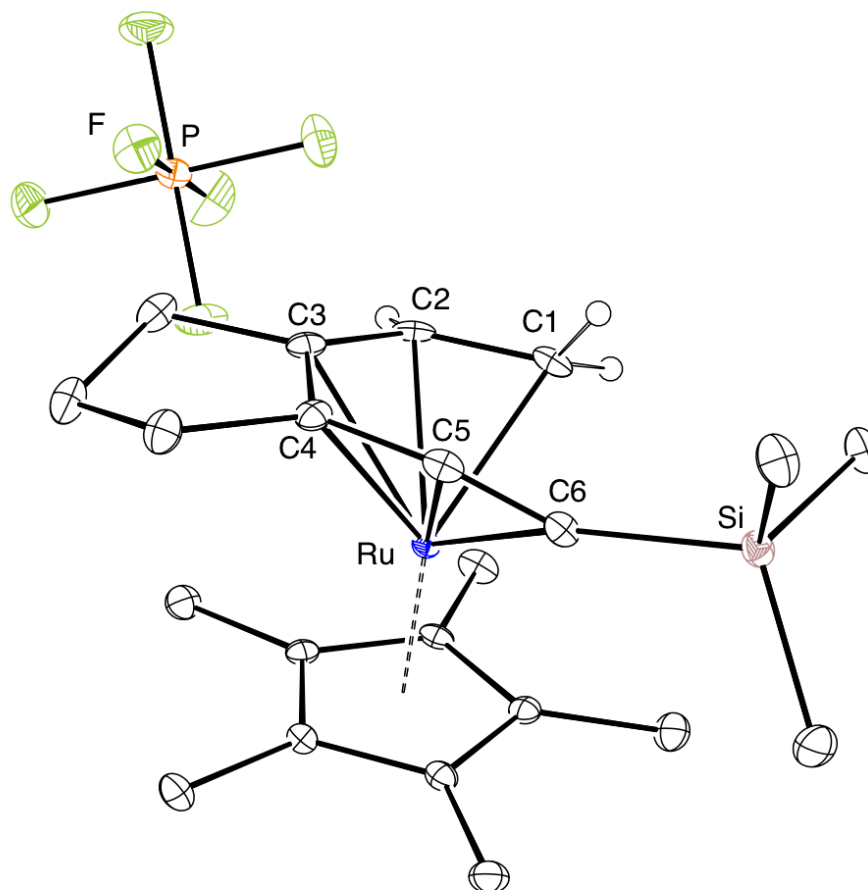
Figure 6-1. ORTEP drawing of **27** with ellipsoids shown at 30% probability.

The isolated complex **27** was subsequently treated with acetonitrile-d_6 solvent at ambient temperature. It was found the dienyne ligand dissociated immediately to generate a 97.2% yield of free dienyne **26** and 98.5% yield of Cp*Ru(NCMe)$_3$PF$_6$-d_9, respectively (Scheme 6-9). In comparison, normally, the dissociation of arene ligand from η^6-arene ruthenium complexes needs to be conducted under photochemical conditions in acetonitrile-d_6 solvent.[9] Despite the [Cp*Ru]$^+$ moiety was demonstrated to

bear high affinity to dienyne substrate by the fast formation of complex **27** with excellent yield, the binding energy between ruthenium and dienyne is still smaller compared to the stronger coordination of arene to ruthenium.

Table 6-1. Seletecd bond distances (Å) and angles (deg) of complex **27** and **13**.

	27	**13**		**27**	**13**
C1 – C2	1.412(6)	1.399(5)	Ru – C4	2.227(4)	2.215(3)
C2 – C3	1.415(6)	1.431(4)	Ru – C5	2.196(4)	2.197(3)
C3 – C4	1.422(5)	1.431(4)	Ru – C6	2.415(4)	2.326(4)
C4 – C5	1.402(6)	1.416(4)	C4-C5-C6	22.7(4)	28.1(4)
C5 – C6	1.233(7)	1.237(5)	C5-C6-Si	29.0(4)	–
Ru – C1	2.202(3)	2.212(4)	Ru – dienyne	1.5518(16)	1.5593(13)
Ru – C2	2.189(4)	2.234(3)	C1-C2-C3-C4	11.5(5)	7.1(4)
Ru – C3	2.258(4)	2.252(3)	Co····C6	2.949(6)	2.797(5)
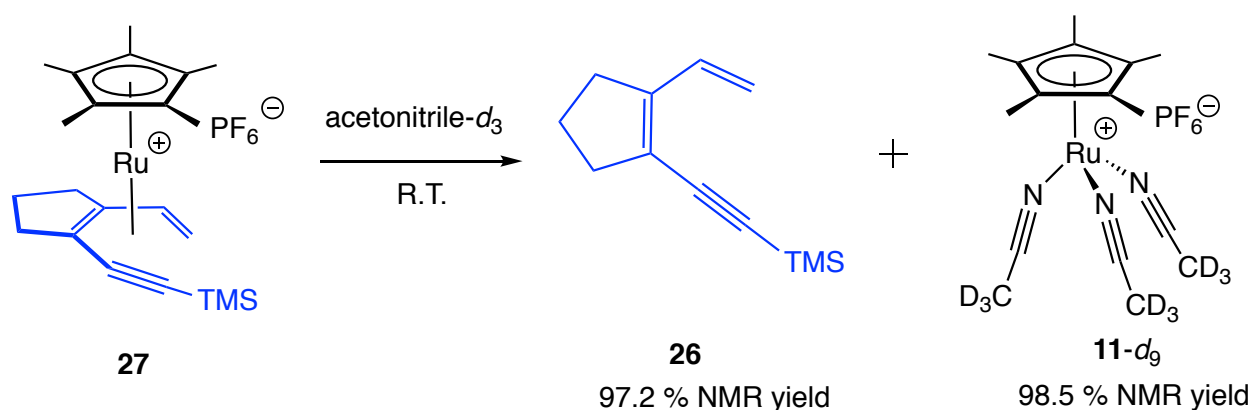
Scheme 6-9. Reaction of complex **27** with acetonitrile.

C. Reaction between Cp*Ru(NCMe)$_3$PF$_6$ and Phenyl Substituted Dienyne

Even though the η^6-arene ruthenium complex is found thermodynamically more favorable than the η^6-dienyne ruthenium complex, the dienyne ligand can still be more kinetically favored due to the higher flexibility, which provides the chance for the [Cp*Ru]$^+$ moiety chemoselectively binds to the dienyne first and triggers the cyclization before the coordination to the arene ligand. The chemoselectivity issues of the reaction between Cp*Ru(NCMe)$_3$PF$_6$ and phenyl substituted dienyne are summarized in Scheme 6-10. While the cyclized product **29** is expected to be more stable than the ruthenium arene complex **30**, the chemoselectivity and distribution of products are dictated by the relative rates of ruthenium-mediated cyclization process and phenyl-complexation process. Furthermore, another selectivity issue would be additional complexation of a [Cp*Ru]$^+$ moiety to the cyclized arene product to form the bimetallic complex **31**.
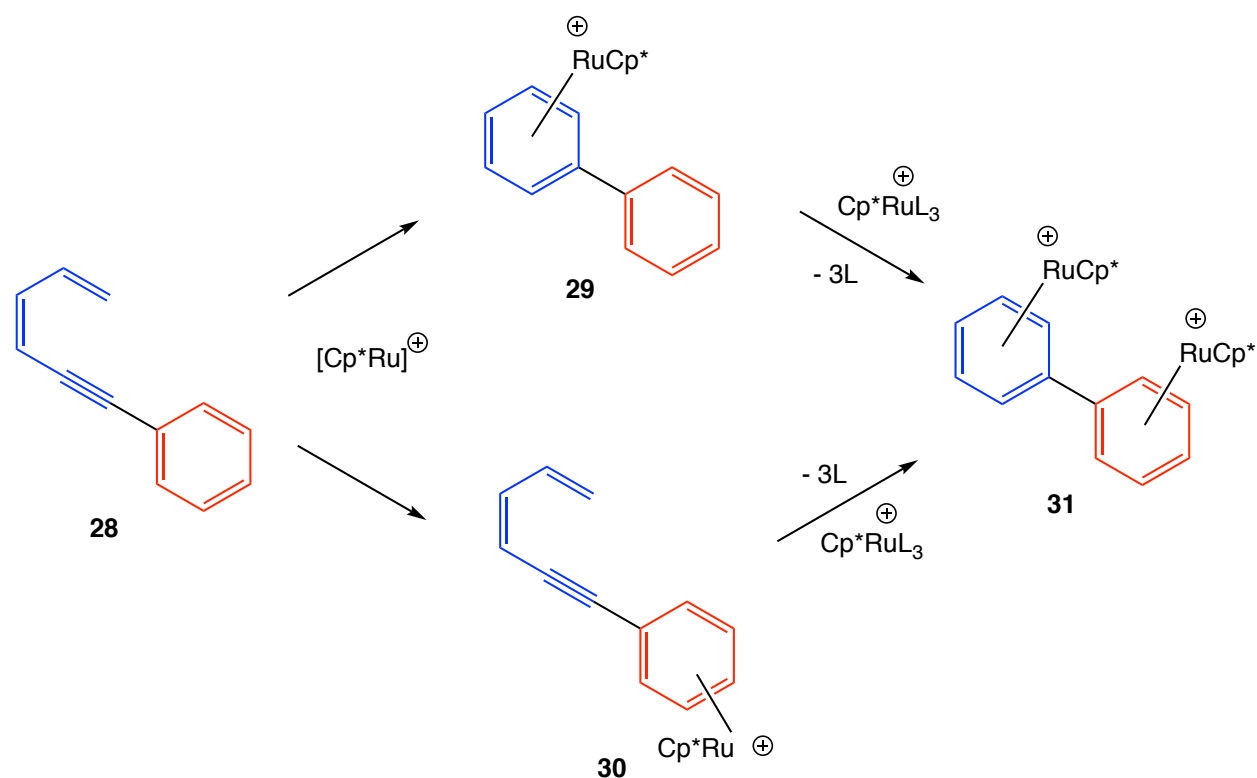
Scheme 6-10. Chemoselectivity issues of reaction between **28** and complex **11**.

In order to examine the chemoselectivity issue, we chose a dienyne substrate bearing a phenyl group on the acetylene carbon to react ruthenium complex **11**. The synthetic method for dienyne **32** is essentially the same as the TMS substituted analogue **26** except for utilizing the phenyl acetylene to conduct the Sonogashira coupling reaction. After aqueous work up and chromatography on silica gel, molecule **32** can be isolated as clear oil with 89% yield.

An NMR scale reaction was subsequently conducted by using dienyne **32** (2.0 mg, 0.01 mmol) and complex **11** (5.3 mg, 0.01 mmol) in CDCl$_3$ solvent with internal standard at ambient temperature under inert atmosphere (Scheme 6-11). After 20 minutes, ^{1}H NMR spectrum (400 MHz, CDCl$_3$) indicates all the dienyne **32** were

consumed, and two products were generated with 24% and 72% NMR yields based on the integration of two new Cp* resonances at δ 1.67 (s, 15H) and 1.70 (s, 15H), respectively. The former was determined as a η^6-dienyne complex owing to the observation of three shielded vinyl hydrogen resonances at δ 1.13 (dd, 1H, J = 10.4 Hz, 2.0 Hz), 3.55 (dd, 1H, J = 9.2 Hz, 2.0 Hz), and 5.18 (t, 1H, J = 9.8 Hz), which is very similar to the patterns of η^6-dienyne complex **27**. Another analogous structure is a pentadienyl ruthenium complex **37** reported by Ernst, which exhibits the three vinyl hydrogen resonances at δ 0.54 (dd, 1H, J = 8.9 Hz, 2.3 Hz), 2.39 (dd, 1H, J = 9.2 Hz, 2.0 Hz), and 4.48 (t, 1H, J = 8.8 Hz), respectively (Figure 6-2).[10]

The major product was assigned as a ruthenium η^6-arene structure **34**, in which the metal center is coordinated to the benzene that is generated from the cycloaromatized dienyne (Scheme 6-11). The assignment of the structure **34** is determined by the three-characteristic shielded arene resonances of the trisubstituted benzene at δ 6.01 (d, 1H, J = 6.0 Hz), 6.22 (d, 1H, J = 6.0 Hz), and 6.36 (s, 1H). It was found that after longer reaction time (40 minutes), all the η^6-dienyne complex **33** disappeared, and 92% NMR yield of η^6-arene complex **34** was obtained. A preparation-scale reaction was also carried out in a similar fashion with 20 mg (0.103 mmol) of **32** and 52 mg (0.103 mmol) of complex **11**, which affords 85% yield of complex **34** as a clear air-stable crystalline solid. In the $^{13}C\{^1H\}$ NMR spectrum (125 MHz, CD_2Cl_2) of the isolated **34**, the observation of 6 upper filed aromatic carbon signals at δ 81.6, 83.4, 84.1, 100.7, 107.9, and 108.0 also supports the hexahapto-arene complexation mode. It was noted that there is no evidence for the formation of dienyne-arene-ruthenium

542

complex **35** or bimetallic complex **36** at ambient temperature during the whole reaction process.
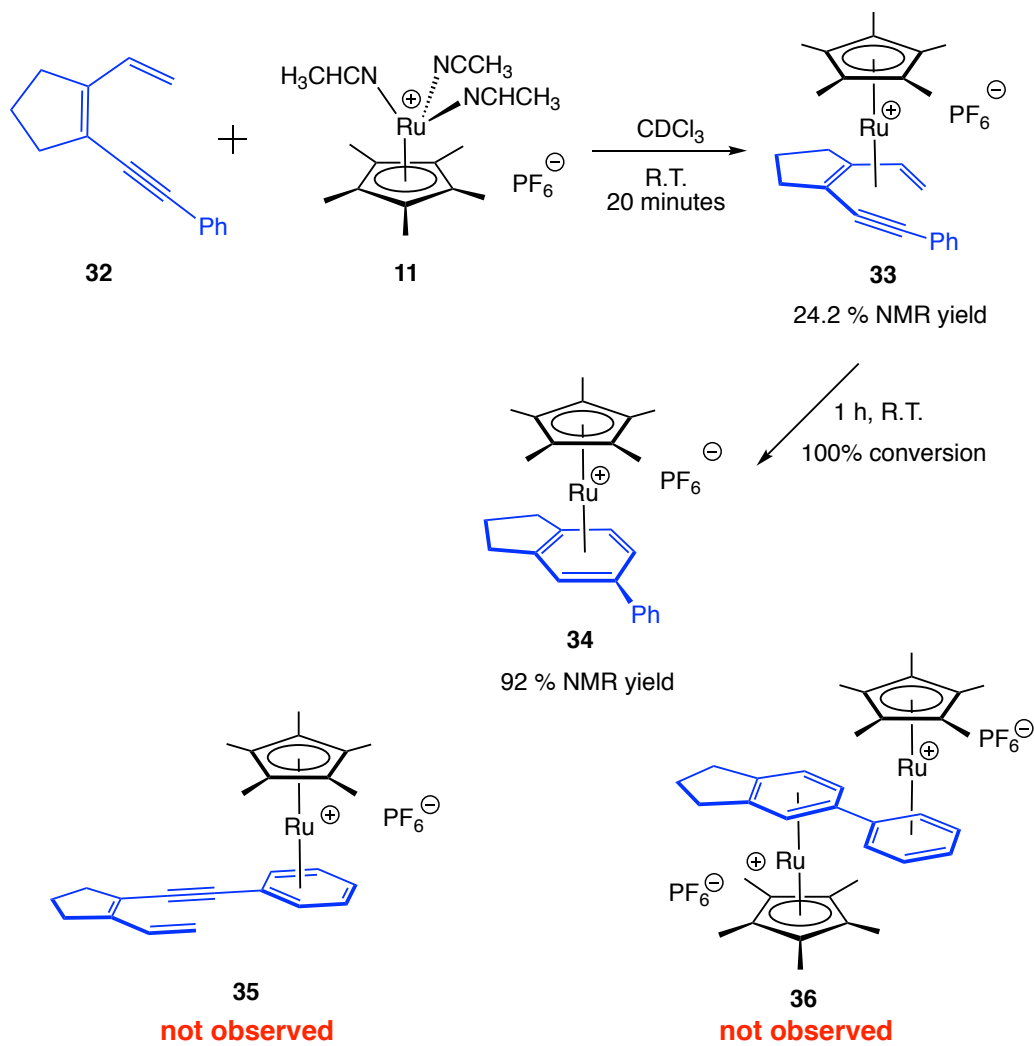
Scheme 6-11. Reaction of complex **11** with dienyne **26**.
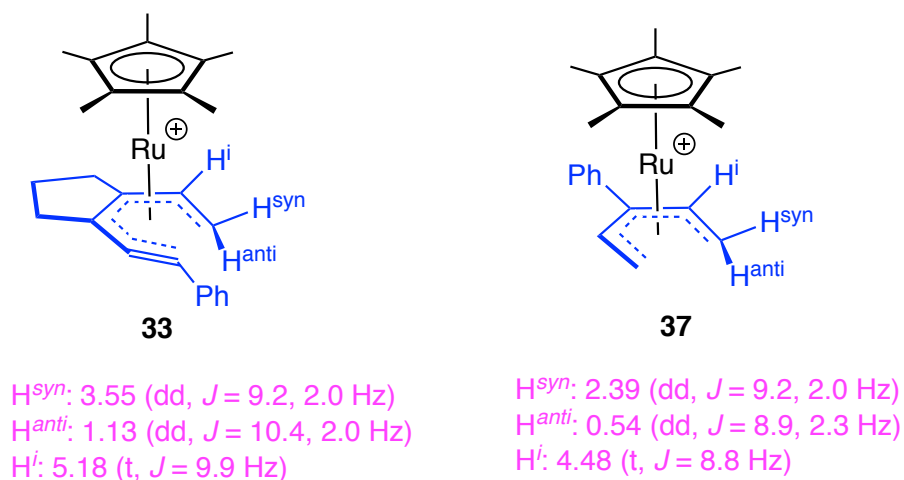
Figure 6-2. Spectroscopic comparison of **33** with **37**.

The crystals of complex **34** were obtained from recrystallization in methylene chloride and hexanes, and the structure of **34** was confirmed by the followed X-ray crystallographic analysis (Figure 6-3). The selected bond distances and angles are summarized in Table 6-2. The average C – C bond distance in the ruthenium-coordinated benzene was measured as 1.419 Å, which is significantly longer than the average C – C bond distance of the unbind benzene (1.371 Å) due to the back-donation effect from the metal center. The annulated five-membered ring is restricted slightly puckered with the largest deviation from planarity on C10 as 0.1341(2) Å (the distance between C10 and mean plane of C3-C4-C11-C10-C9). The inductively electron-withdrawing effect from benzene substituent tunes the Ru – C1 bond distance shorter than the Ru – C3 (Δ = 0.024 Å) and Ru – C4 (Δ = 0.026 Å) bond distances that are adjacent to electron-donating alkyl groups. The distance between ruthenium and arene centroid is measured as 1.7200(4) Å, while a length of 1.8091(4) Å is shown between ruthenium and Cp* centroid. The two phenyl rings are found well conjugated with a small torsion angle of C2-C1-C7-C8 (20.858(5) °).
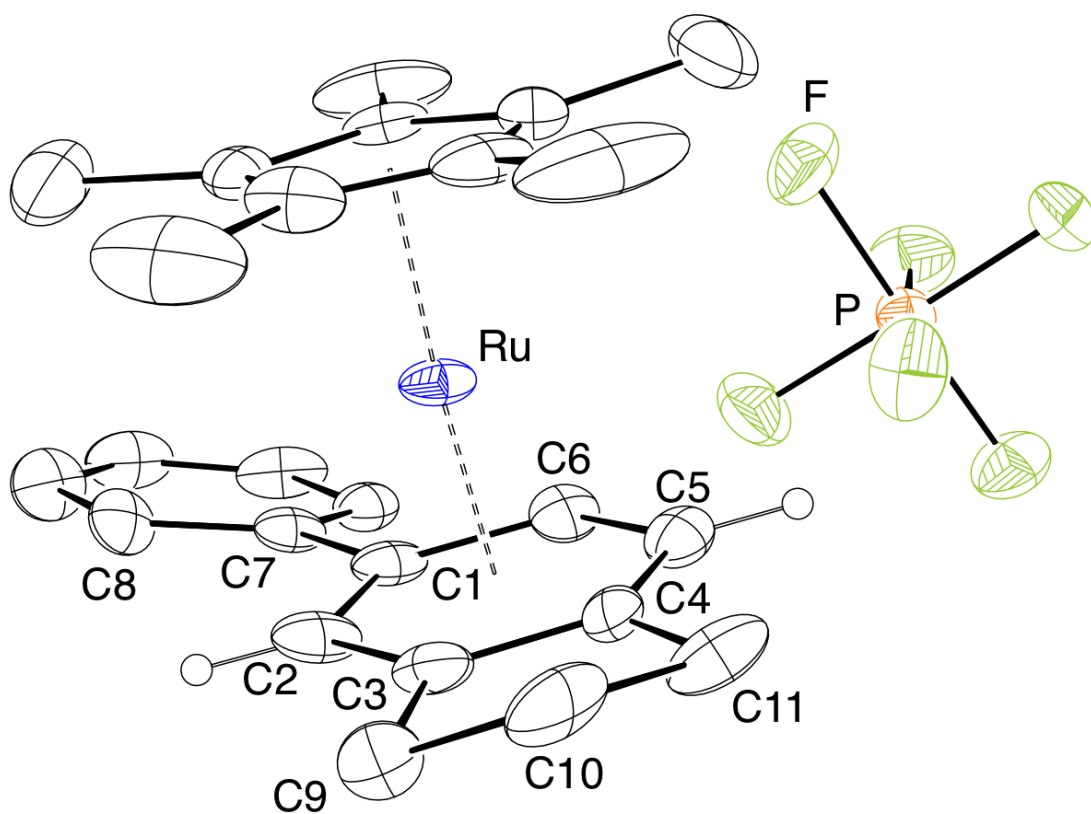
Figure 6-3. ORTEP drawing of **34** with ellipsoids shown at 30% probability.

Table 6-2. Seletecd bond distances (Å) and angles (deg) of complex **34**.

C1 – C2	1.385(2)	Ru – C4	2.237(4)
C2 – C3	1.493(2)	Ru – C5	2.273(4)
C3 – C4	1.398(2)	Ru – C6	2.205(4)
C4 – C5	1.371(2)	C2-C1-C6	119.769(4)
C5 – C6	1.418(2)	C2-C3-C4	118.258(1)
C6 – C1	1.447(2)	C3-C4-C5	124.779(3)
Ru – C1	2.211(5)	Ru – Cp*	1.809(4)
Ru – C2	2.217(4)	Ru – arene	1.720(4)
Ru – C3	2.235(3)	C2-C1-C7-C8	20.858(5)

The formation of η^6-arene complex **34** and no observation of generating complex **35** or bimetallic complex **36** indicate that upon dissociation of acetonitrile ligands, the [Cp*Ru]$^+$ moiety can chemoselectively coordinates to the dienyne faster to trigger the subsequent cycloaromatization without any competition of complexing to phenyl substituent. This unique coordination mode helps lower down the activation barrier, and thus prevent the phenyl shift during the cyclization process. We attribute the different experimental results between the phenyl substituted dienyne and the TMS substituted dienyne to the larger steric hindrance of TMS group, which elongates the C1····C6 nonbonding distance, and thus impedes the cyclization.

In order to isolate the cyclized free arene molecule and retrieve the ruthenium complex **11**, complex **34** was allowed to be photolyzed in a Rayonette photoreactor equipped with UV broadband lamps centered at 254 nm in acetonitrile-d_3 solvent under inert atmosphere. After 2 hours, all the starting complex **34** disappeared, and 95% yield of the free arene molecule **38** was obtained with 97% recovery of the ruthenium complex **11**-d_9 (Scheme 6-12). In comparison, a control experiment was conducted by heating the dienyne substrate **32** at 165 °C in a J.Y. NMR tube for a regular Hopf cyclization (Scheme 6-13). After 7 days, the ^{1}H NMR spectrum (400 MHz, C$_6$D$_6$) of the reaction mixture indicates that all the dienyne **32** was consumed with only 20% yield of the desired arene product **38**. Also, the literature reported pioneering example of synthesis of the same molecule is the cobalt-catalyzed [2 + 2 + 2] cyclotrimerization reaction, which only gave 26% yield of the arene product at 125 °C for 48 hours (Scheme 6-14).[11]
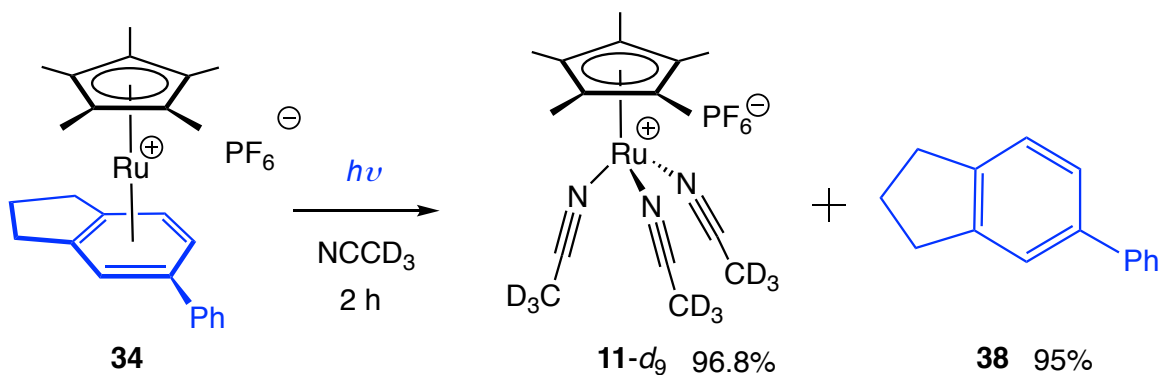
Scheme 6-12. Photolysis of complex **34** in acetonitrile.
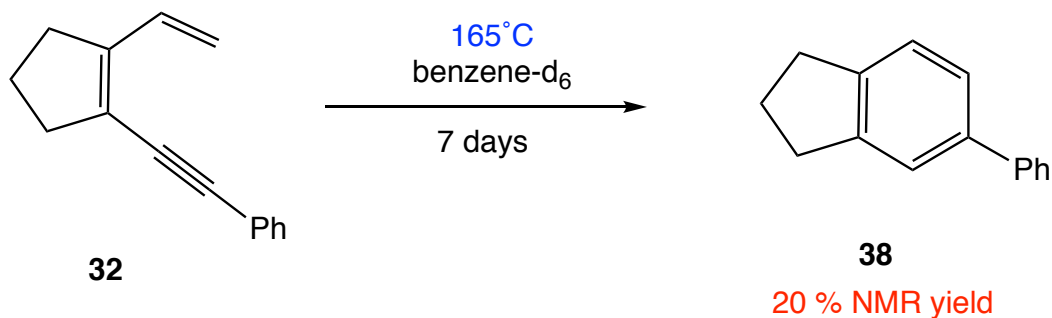
Scheme 6-13. Thermal cyclization of dienyne **32**.
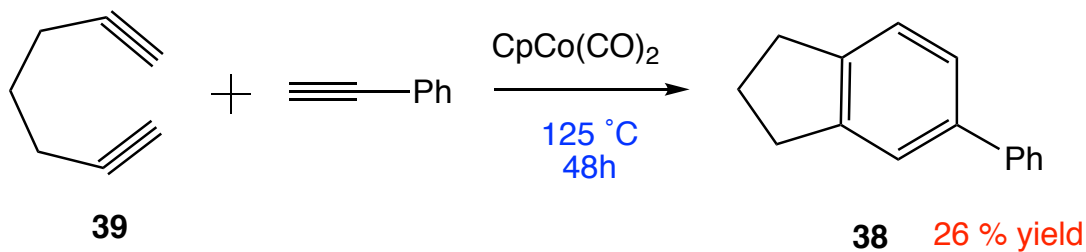
Scheme 6-14. Cobalt-catalyzed [2 + 2 + 2] cyclotrimerization to form **38**.

Furthermore, when the cyclized arene product **38** was treated with one equivalent of Cp*Ru(NCMe)$_3$PF$_6$ in CDCl$_3$ in an NMR tube, the mixture of two ruthenium η^6-arene complexes **34** and **40** were observed with a 1.6 : 1 ratio based on the relative

integration of the two new Cp* resonances (Scheme 6-15). The structure of complex **40** was determined by the diagnostic resonances of the phenyl group that is complexed with ruthenium at δ 5.85 (t, 1H, J = 6.0 Hz), 5.96 (t, 2H, J = 6.0 Hz), and 6.19 (d, 2H, J = 6.0 Hz). The selective complexation result is consistent with what was reported in the literature that ruthenium is thermodynamically more favorable to coordinate to more substituted arene group.[12]
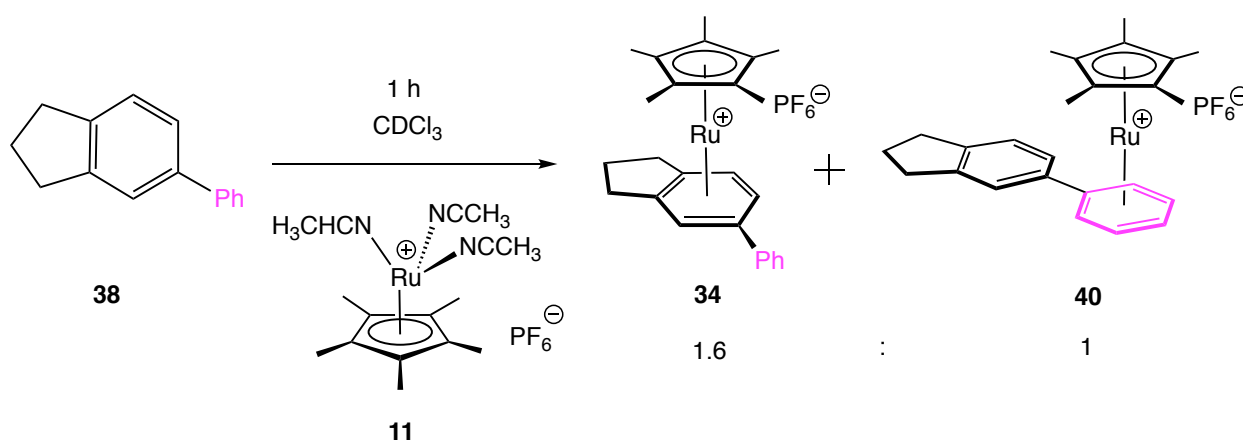
Scheme 6-15. Reaction of complex **11** with arene **38**.

D. Kinetic Studies and Proposed Mechanisms

In principle, on the path to cycloaromatization, three acetonitrile ligands need to dissociate from the Cp*Ru(NCMe)$_3$PF$_6$ complex, which can potentially generate η^2-dienyne complex **41**, η^4-dienyne complex **42**, and η^6-dienyne complex **33** by loss a acetonitrile in sequence (Scheme 6-16). Since the exchange of acetonitrile with π bond of dienyne is fast, rapid equilibrium can be established among these three complexes. The reversable formation of η^6-dienyne complex **33** was confirmed by adding 150

equivalents of acetonitrile after 5 minutes of mixing complex **11** and substrate **32** in CDCl₃, and it was found that 84% of complex **33** converted back to free dienyne **32** and complex **11** immediately. Due to the rapid interconversion, it would be hard to directly determine which hapticity severs as the true intermediate before the rate-limiting cyclization step. In order to answer this question, a kinetic study was carried out to investigate the how the concentration of acetonitrile affects the rate of reaction.
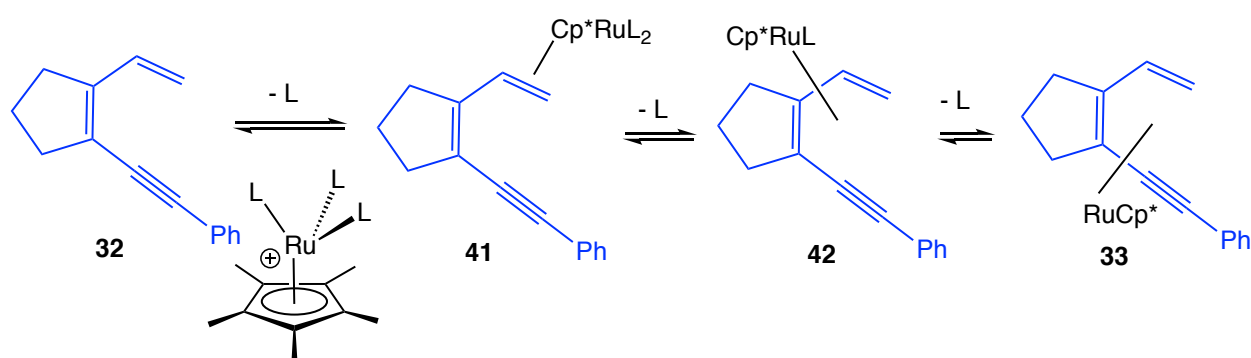
Scheme 6-16. Possible intermadiates for the cyclization of **32**.

Since the reaction of dienyne substrate **32** with complex **11** is very fast at ambient temperature, excess of acetonitrile-d_6 was loaded into the reaction mixture beforehand to tune the reaction rate slow enough to be measured. Also, 16 equivalents of substrate **32** was added to make the reaction pseudo first order to complex **11**.

A general way to conduct the kinetic experiments are described as below (Scheme 6-17): Cp*Ru(NCMe)₃PF₆ (2.0 mg, 0.004 mmol), ((2-vinylcyclopent-1-en-1-yl)ethynyl)benzene (12.5 mg, 0.064 mmol), acetonitrile-d_3 (120 mg, 162 mg, 196 mg, and 233 mg for different entries), and 1,3,5-tri-*tert*-butylbenzene (internal standard) were added to an oven dried J. Young NMR tube. After the NMR tube was frozen at -78

°C and placed under vacuum, acetone-d_6 was distilled into the NMR tube until the whole solution volume is 0.73 mL. The NMR tube was shaken to dissolve all the solid while it is kept cold, and time recording started when the NMR tube was placed into a water bath to warm up. The reaction was subsequently monitored by ^{1}H NMR spectroscopy, and time points were taken while the NMR tube stayed in the NMR equipment at ambient temperature (23 °C). The consumption of Cp*Ru(NCMe)$_3$PF$_6$ was recorded by the integration of Cp* resonance at δ 1.61 (s, 15H) relative to internal standard at δ 1.32 at different time points. The ln[Cp*Ru(NCMe)$_3$PF$_6$]-Time plots were made to calculate to the rate constant k_{obs} for different concentration of acetonitrile-d_3. The table of data and plots with trend lines have been shown below.
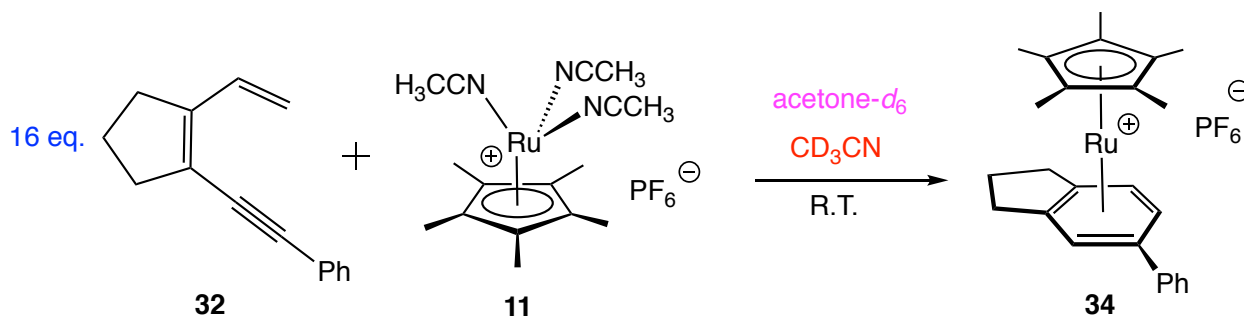
Scheme 6-17. Kinetic experiments of complex **11** with dienyne **32**.

Table 6-3. Concentration of Cp*Ru(NCMe)$_3$PF$_6$ (C$_{11}$) and their natural logarithms at different time points (loading of CD$_3$CN equals 7.744 mol/L).

Time (min)	C$_{11}$ (mol/L)	ln [C$_{11}$]	Time (min)	C$_{11}$ (mol/L)	ln [C$_{11}$]
3.5	4.418	-5.485	35	3.247	-5.730
5	4.136	-5.488	40	3.120	-5.770
6.5	4.087	-5.500	50	2.968	-5.820
8	4.014	-5.518	60	2.726	-5.905
9.5	3.966	-5.531	70	2.570	-5.964
11	3.927	-5.540	80	2.339	-6.058
12.5	3.907	-5.545	90	2.181	-6.128
15	3.810	-5.571	100	1.858	-6.288
20	3.765	-5.582	110	1.719	-6.366
25	3.661	-5.611	120	1.622	-6.424
30	3.518	-5.651	130	1.491	-6.508

$y = -0.0081x - 5.4366$
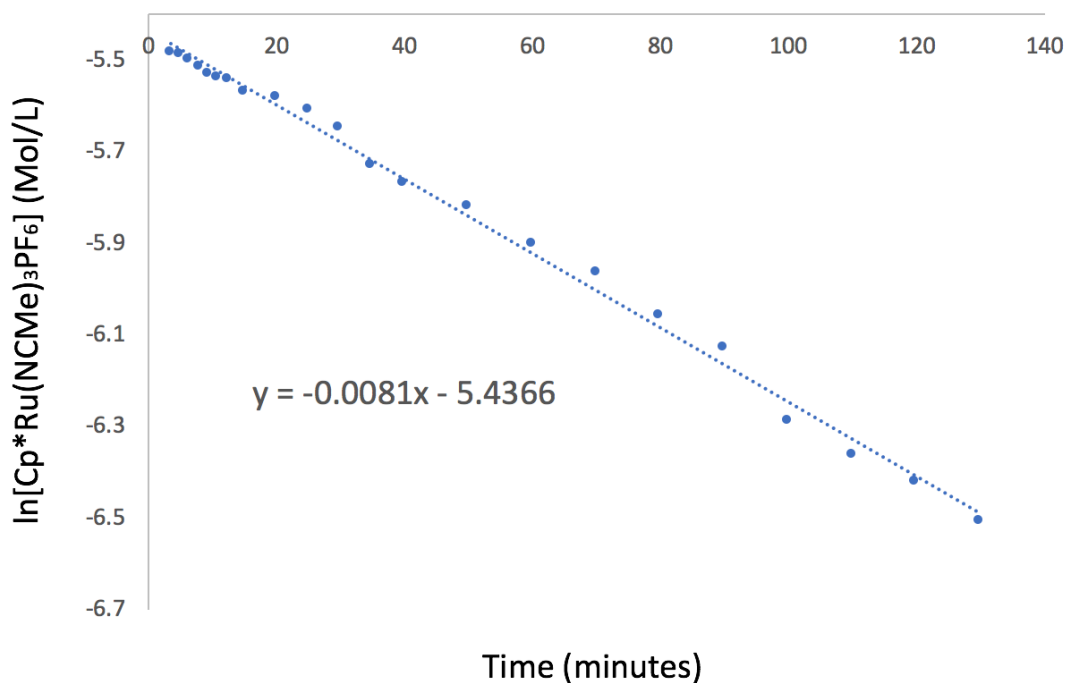
Figure 6-4. Natural logarithm concentration change of Cp*Ru(NCMe)$_3$PF$_6$ with time when the concentration of CD$_3$CN is 7.744 mol/L.

Table 6-4. Concentration of $Cp*Ru(NCMe)_3PF_6$ (C_{11}) and their natural logarithms at different time points (loading of CD_3CN equals 6.514 mol/L).

Time (min)	C_{11} (mol/L)	ln $[C_{11}]$	Time (min)	C_{11} (mol/L)	ln $[C_{11}]$
3	4.450	-5.415	30	2.965	-5.821
4.5	4.251	-5.461	35	2.653	-5.932
6	4.161	-5.482	40	2.541	-5.975
7.5	4.026	-5.515	45	2.427	-6.021
9	3.880	-5.552	50	2.192	-6.123
10.5	3.856	-5.558	60	2.003	-6.213
13.5	3.765	-5.582	70	1.778	-6.332
16.5	3.728	-5.592	80	1.514	-6.493
20	3.376	-5.691	90	1.318	-6.632
25	3.180	-5.751			
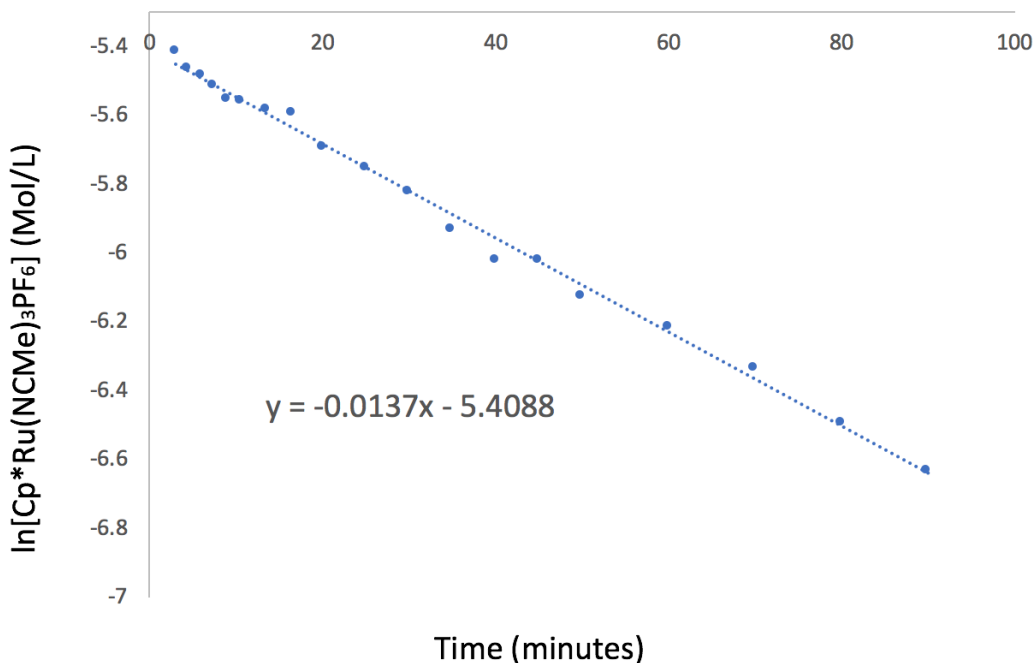
Figure 6-5. Natural logarithm concentration change of $Cp*Ru(NCMe)_3PF_6$ with time when the concentration of CD_3CN is 6.514 mol/L.

Table 6-5. Concentration of Cp*Ru(NCMe)$_3$PF$_6$ (C$_{11}$) and their natural logarithms at different time points (loading of CD$_3$CN equals 5.384 mol/L).

Time (min)	C$_{11}$ (mol/L)	ln [C$_{11}$]	Time (min)	C$_{11}$ (mol/L)	ln [C$_{11}$]
3.5	3.237	-5.733	27	1.745	-6.351
5.5	3.104	-5.775	30	1.742	-6.353
7	3.022	-5.802	35	1.590	-6.444
8.5	2.923	-5.835	38.5	1.486	-6.512
10	2.775	-5.887	40.5	1.373	-6.591
11.5	2.619	-5.945	42.5	1.237	-6.695
13	2.501	-5.991	44.5	1.204	-6.722
14.5	2.452	-6.011	47.5	1.102	-6.811
17.5	2.401	-6.032	51.5	1.028	-6.880
20.5	2.110	-6.161	55	0.928	-6.982
24	1.946	-6.242	60	0.080	-7.121

$y = -0.0241x - 5.6466$
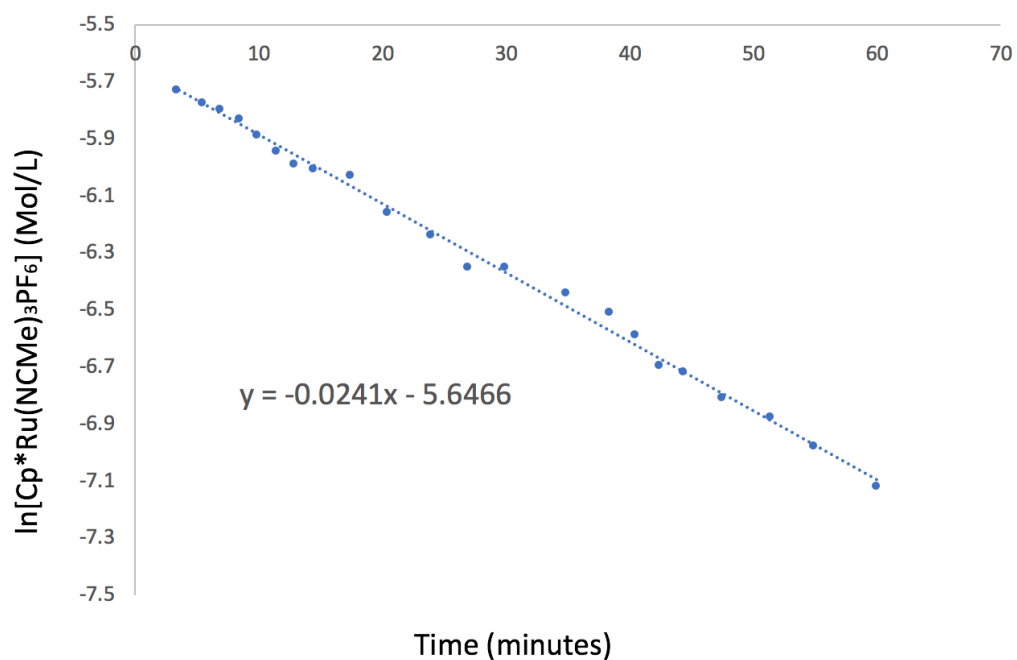
Figure 6-6. Natural logarithm concentration change of Cp*Ru(NCMe)$_3$PF$_6$ with time when the concentration of CD$_3$CN is 5.384 mol/L.

Table 6-6. Concentration of Cp*Ru(NCMe)$_3$PF$_6$ (C$_{11}$) and their natural logarithms at different time points (loading of CD$_3$CN equals 3.990 mol/L).

Time (min)	C$_{11}$ (mol/L)	ln [C$_{11}$]	Time (min)	C$_{11}$ (mol/L)	ln [C$_{11}$]
2.5	2.606	-5.950	16	1.416	-6.560
4	2.405	-6.030	17.5	1.273	-6.666
5.5	2.221	-6.111	19	1.180	-6.742
7	2.048	-6.191	21	1.028	-6.880
8.5	2.009	-6.210	22.5	0.881	-7.034
10	1.834	-6.301	24	0.725	-7.230
11.5	1.747	-6.350	25.5	0.649	-7.341
13	1.695	-6.381	27	0.596	-7.425
14.5	1.534	-6.480			
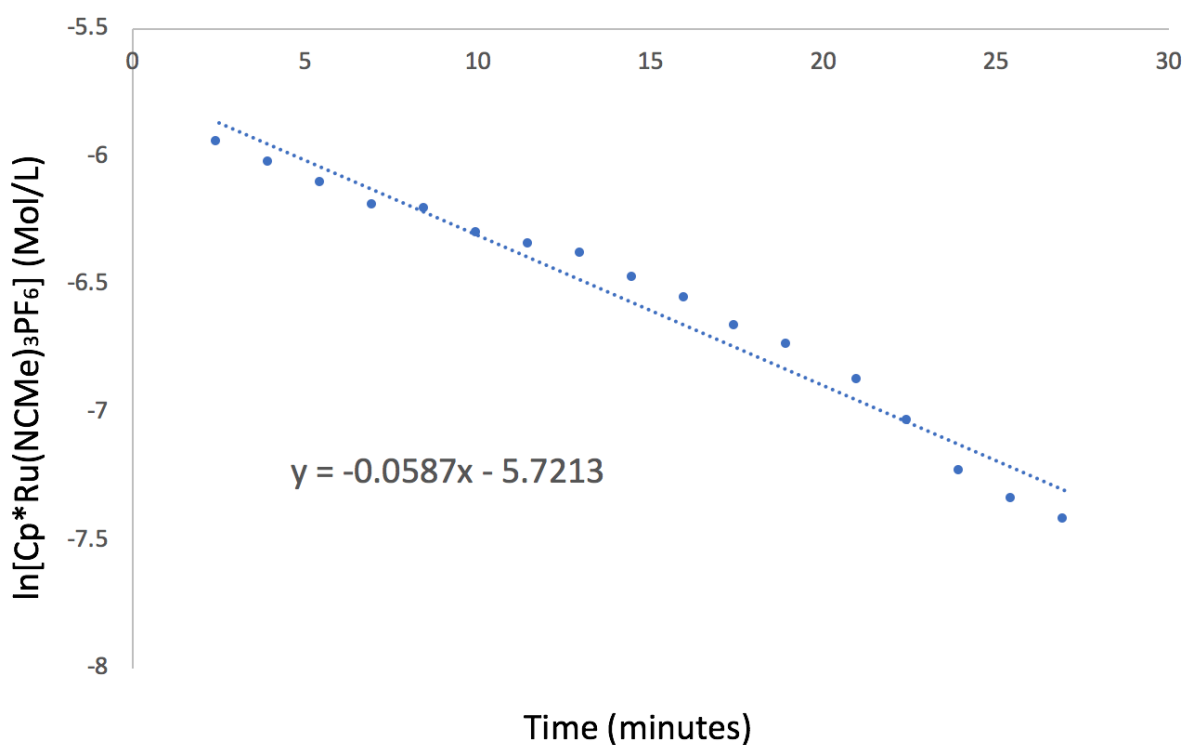
Figure 6-7. Natural logarithm concentration change of Cp*Ru(NCMe)$_3$PF$_6$ with time when the concentration of CD$_3$CN is 3.990 mol/L.

A subsequent plot was made by using $\ln(k_{obs})$ verses $\ln$ [acetonitrile] (Table 6-7, Figure 6-8), which produces a trend line with a slope of -2.9. This result demonstrates that the reaction is inverse third order to the concentration of acetonitrile, which indicates the necessity of losing three acetonitrile ligands before the cyclization step, and thus prove the intermediacy of η^6-dienyne complex **33** on the way to cycloaromatization. The kinetic calculation process has been shown in Scheme 6-17. It should be noted that it is reasonable to assume $k_2 \gg k_{-1}$ since the rate-limiting cyclization step is much slower than the establishment of equilibrium between complex **11** and η^6-dienyne complex **33**.

In addition, the equilibrium constant between complex **11** and complex **33** was calculated as 1050 at ambient temperature, and the corresponding ΔG was calculated as - 4.1 kcal/mol, which also demonstrates the high affinity of dienyne substrate to [Cp*Ru]$^+$ moiety.

Table 6-7. Natural logarithms of k_{obs} at different concentration of CD$_3$CN.

k_{obs} (min^{-1})	ln [k_{obs}]	CD$_3$CN (mol/L)	ln [CD$_3$CN]
0.0081	-4.816	7.744	2.047
0.0137	-4.290	6.514	1.874
0.0241	-3.726	5.384	1.683
0.0587	-2.835	3.990	1.384

$y = -2.8955x + 1.1605$
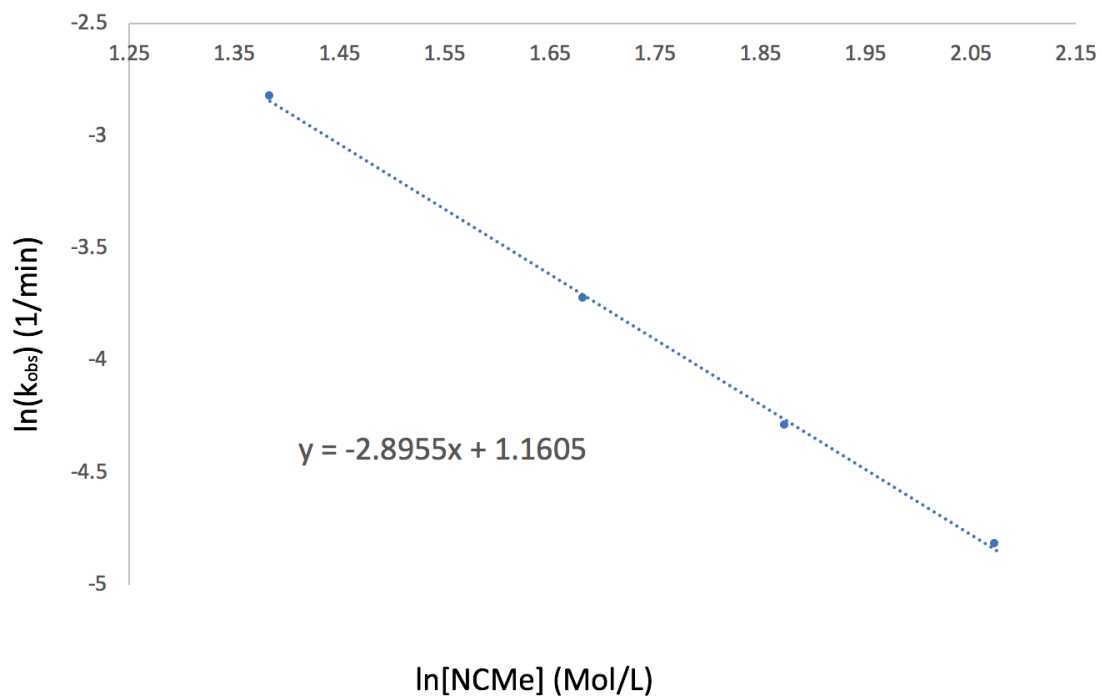
Figure 6-8. Natural logarithm of k_{obs} with natural logarithm of concentration of CD_3CN.
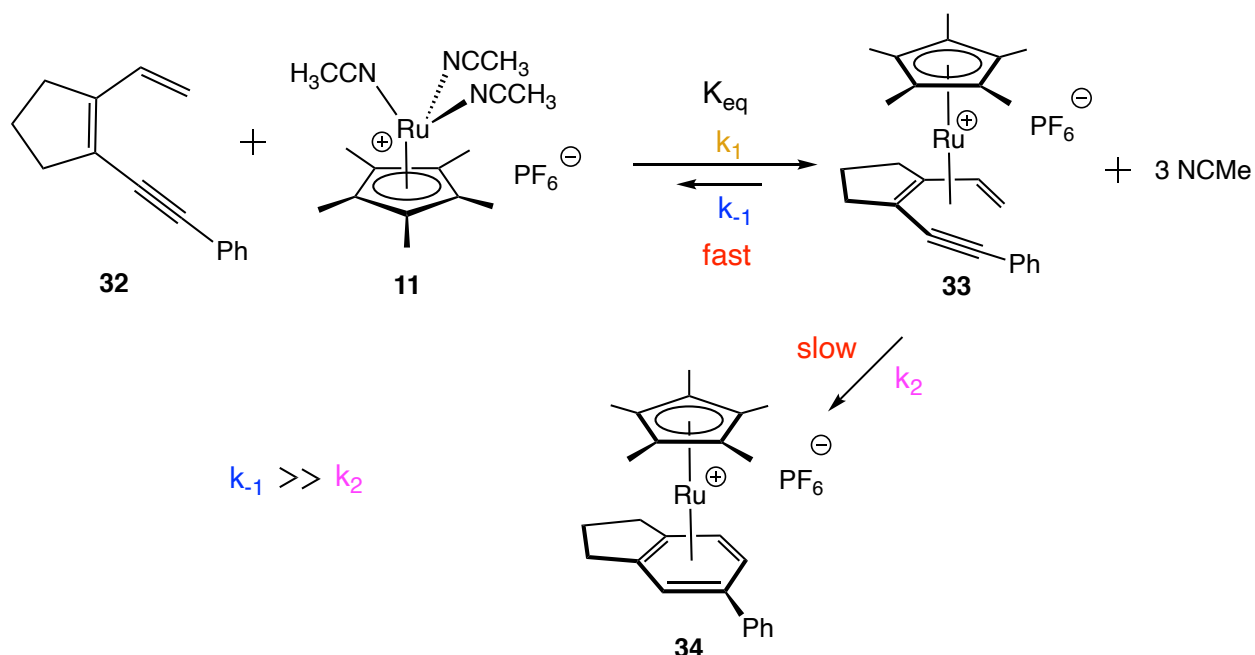
Rate $= k_{obs}[\textbf{11}] = k_2[\textbf{33}]$

$$K_{eq} = \frac{[\textbf{33}] * [NCMe]^3}{[\textbf{32}] * [\textbf{11}]}$$

$\Longrightarrow \quad k_{obs} = k_2 K_{eq}[\textbf{32}] * [NCMe]^{-3}$

$\ln(k_{obs}) = \ln\{k_2 K_{eq}[\textbf{32}]\} - 3\ln[NCMe]$

Scheme 6-17. The kinetic calculation process of dienyne cycloaromatization.

In order to address the relative stabilities of regioismeric dienyne complexes, a computation study was conducted by Professor Kim Baldridge on the three possible η^2-dienyne complexes (Figure 6-9), in which the ruthenium is coordinated to the terminal alkene (**41**), internal alkene (**43**), and alkyne (**44**), respectively. As expected, complex **41** has the lowest energy (0.0 kcal/mol) due to the least steric congestion. It was found

that the structure is more stable when metal binds to alkyne in complex **44** ($\Delta G = 4.20$

kcal/mol) than coordination to internal alkene in complex **43** ($\Delta G = 6.95$ kcal/mol).

41 (0.0 kcal/mol)

43 (6.95 kcal/mol)   **44** (4.20 kcal/mol)
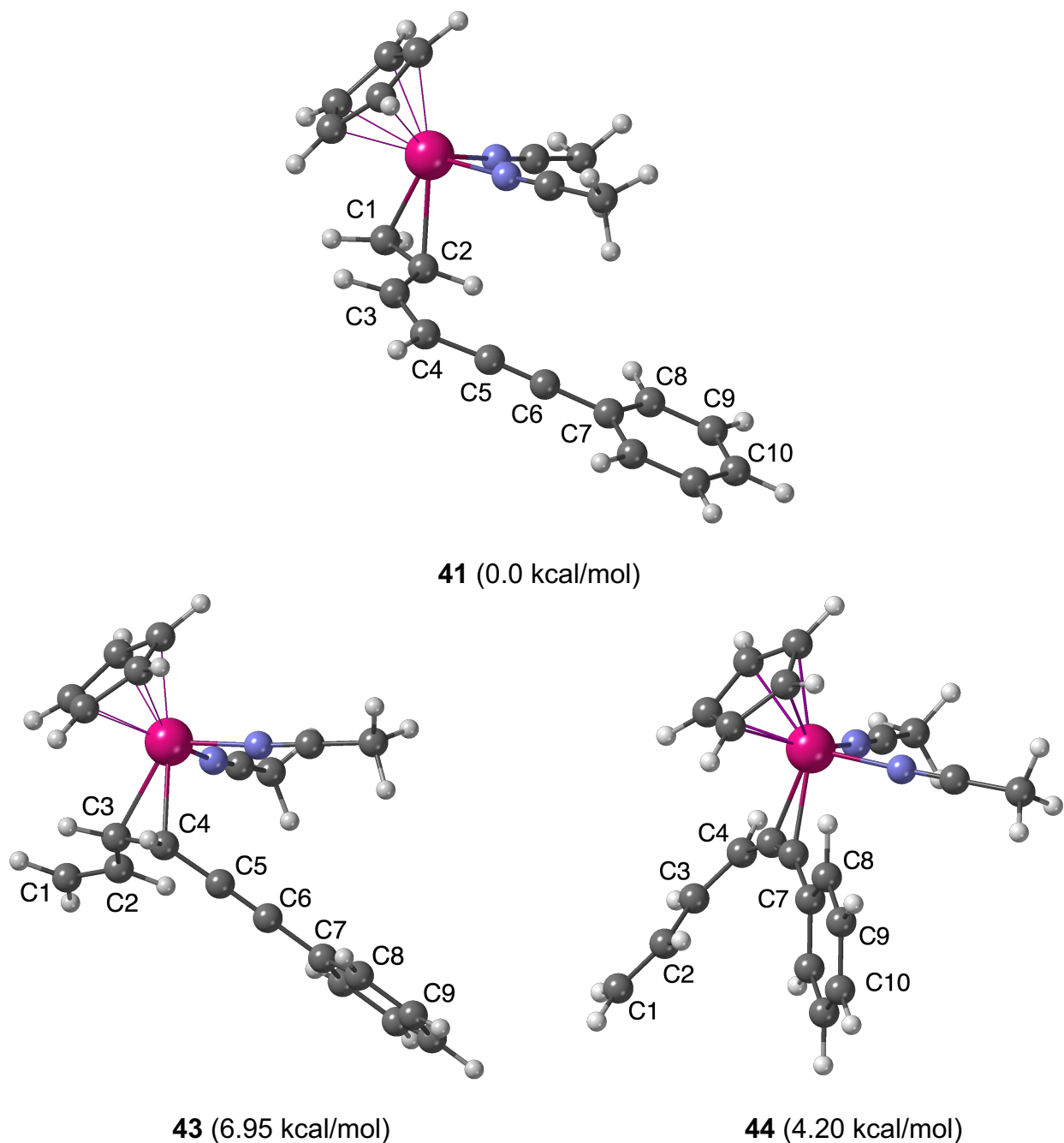
Figure 6-9. Calculated structures for η^6-complex **41**, **43**, and **44**.

Based on the kinetic studies and computational results, the proposed mechanism of ruthenium-mediated cycloaromatization of dienyne is exhibited in Scheme 6-18. Dissociation of the first acetonitrile from complex **11** produces the η^2-complex **41**, that is followed by formation of the η^4-diene complex **42** via the loss of the second acetonitrile. Similar ruthenium η^4-diene complex has been reported in the literature by exchanging a naphthalene ligand of complex [Ru(η^6-C$_{10}$H$_8$)(η^4-1,5-COD)] with a conjugated diene and an acetonitrile.[13] The η^6-dienyne complex **33** can be generated by a further loss of acetonitrile from **42**, and the followed cyclic allene intermediate **45** is stabilized by the coordination to the metal center. After hydride shift, the final η^6-arene product **34** is afforded.
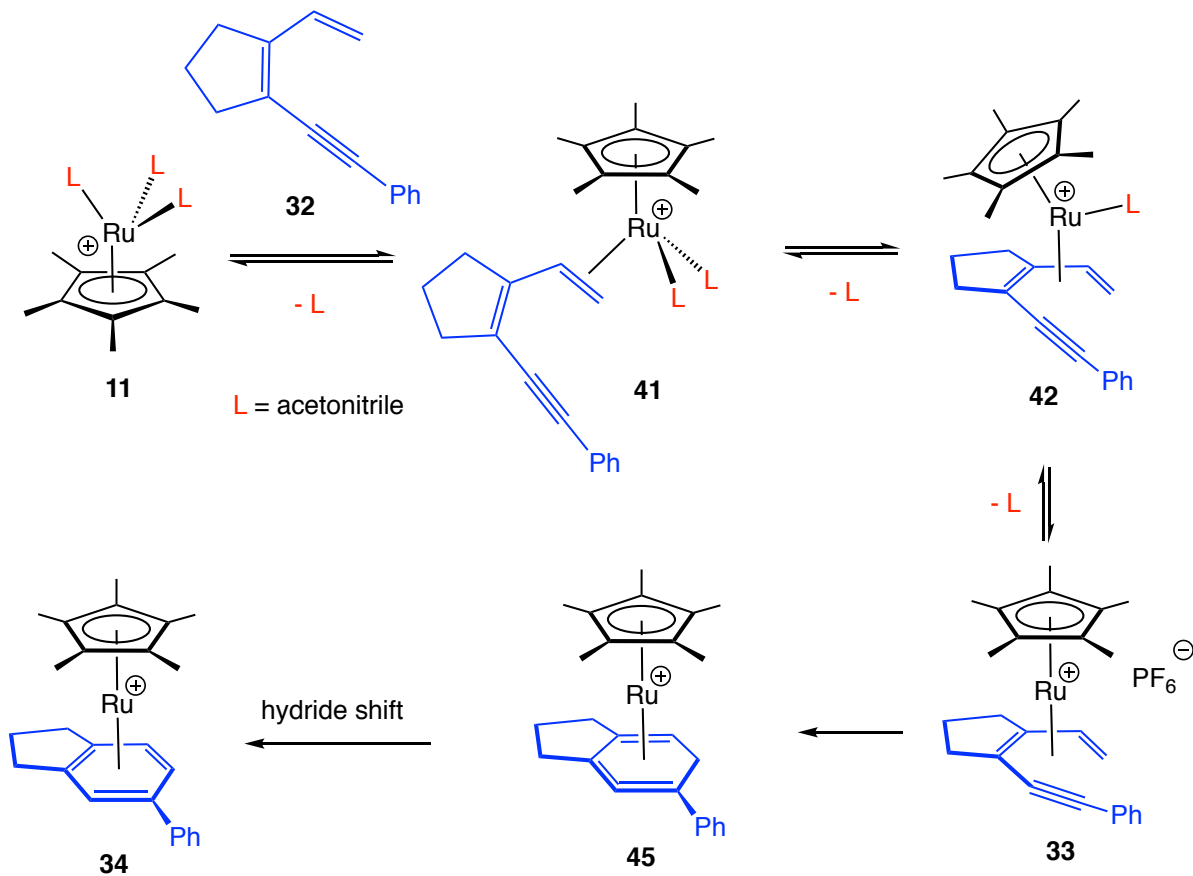
Scheme 6-18. Proposed mechanism for the reaction of complex **11** with dienyne **32**.

E. Regioselective Cycloaromatizations of Methyl Substituted Dienynes

In order to explore the electron effect on the ruthenium-mediated cycloaromatization of dienyne, a halogen incorporated dienyne **46** that was synthesized from the reaction between HCl and 1,2-di(prop-1-yn-1-yl)cyclopent-1-ene was treated with complex **11**. When 152 mg (0.84 mmol) of substrate 46 was mixed with 420 mg (0.83 mmol) of complex **11** in methylene chloride at ambient temperature under nitrogen gas, the solution gradually changed from yellow to clear in one hour (Scheme 6-19). After concentrated and chromatography on silica gel, 96% yield of product can be obtained as clear air-stable solids.
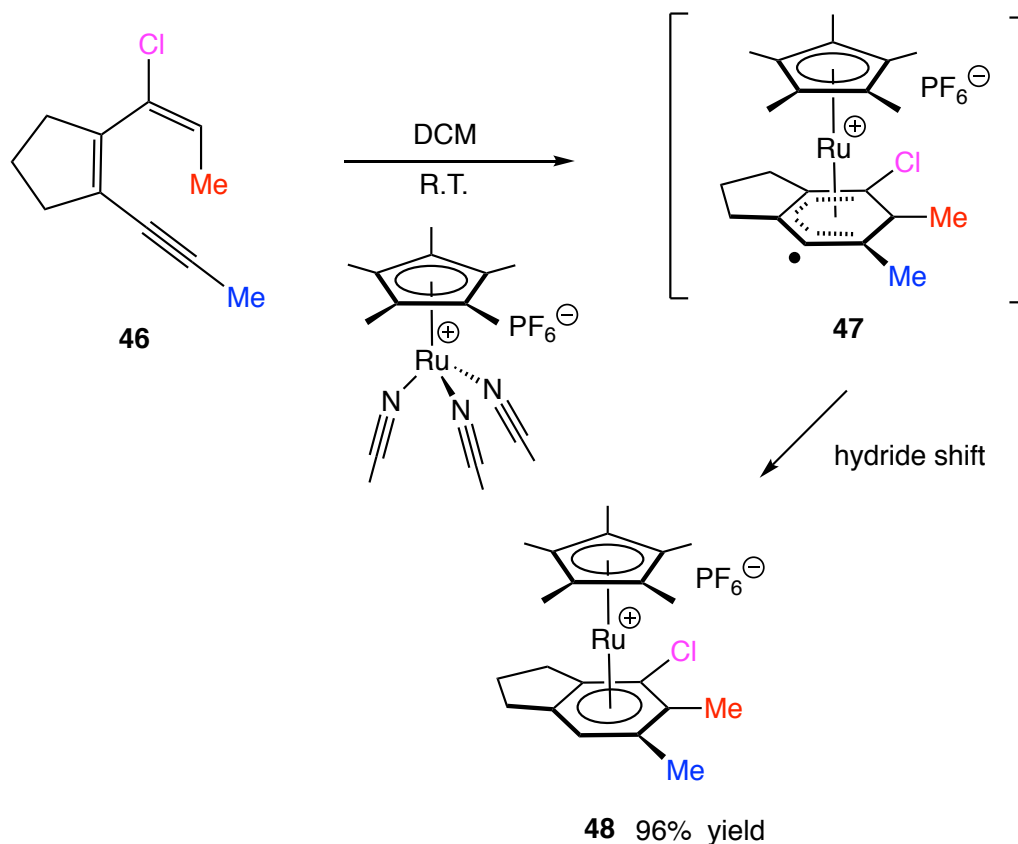
Scheme 6-19. Reaction of complex **11** with dienyne **46**.

560

In the ^{1}H NMR spectrum (400 MHz, CDCl$_3$) of the product, both methyl resonances were observed as singlet at δ 2.18 (s, 3H) and 2.21 (s, 3H). A shielded aromatic hydrogen signal was detected at δ 6.02 (s, 1H). The six down-field aromatic carbon resonances in the ^{13}C{^{1}H} NMR spectrum (125 MHz, CDCl$_3$) at δ 86.35, 97.44, 99.17, 102.89, 106.06, and 107.49 indicate a η^6-arene structure.

The crystals of product **48** were obtained from recrystallization in methylene chloride and hexanes, and the structure was confirmed by X-ray crystallography (Figure 6-10). As anticipated, the product shows a regular Hopf cyclization structure with two methyl groups adjacent to each other. The back bonding of the metal center significantly elongates the carbon – carbon bonds in the six-membered ring with an average length as 1.406 Å (Table 6-8). The electron-withdrawing effect from the chlorine atom tunes the Ru – C1 bond considerably shorter than the Ru – C2 bond (Δ = 0.027 Å). The steric hindrance between chlorine and adjacent alkyl groups is manifested by the greater C6-C1-C2 angle (123.555(9) °) than the C1-C2-C3 angle (117.927(2) °). The distance between ruthenium and arene centroid is measured as 1.7201(5) Å, while the distance between ruthenium and Cp* centroid is detected as 1.8172(5) Å. Very similar to complex **34**, the annulated five-membered ring is slightly pucker at the C8 position with the deviation from planarity as 0.12850(3) Å.
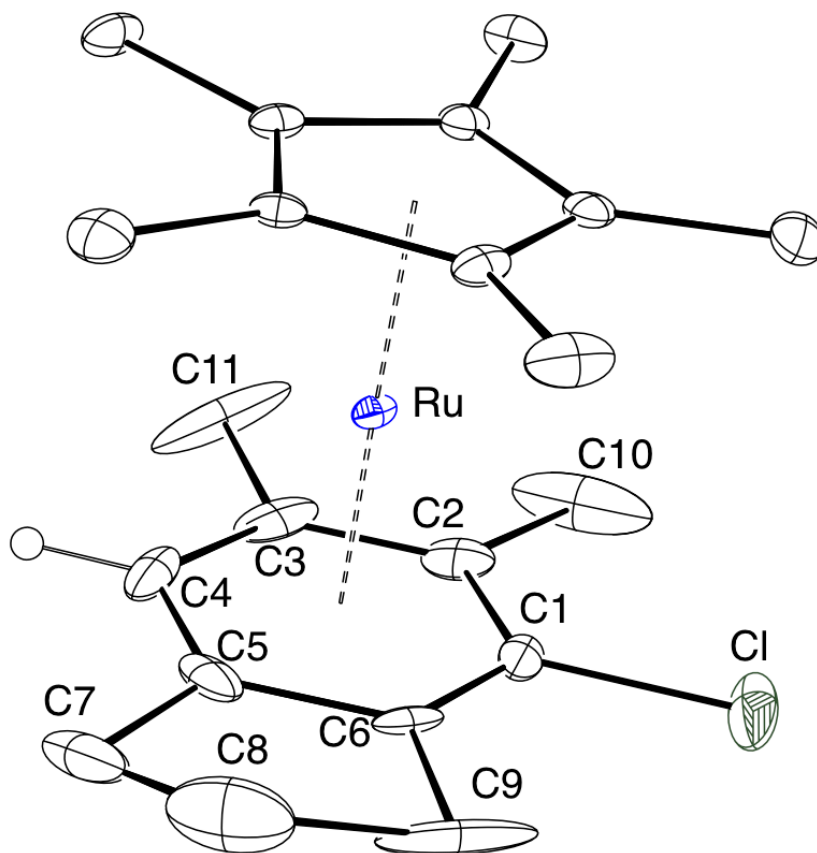
Figure 6-10. ORTEP drawing of **48** with ellipsoids shown at 30% probability.

Table 6-8. Seletecd bond distances (Å) and angles (deg) of complex **48**.

C1 – C2	1.400(5)	Ru – C4	2.211(3)
C2 – C3	1.406(5)	Ru – C5	2.229(4)
C3 – C4	1.394(3)	Ru – C6	2.229(4)
C4 – C5	1.416(3)	C2-C1-C6	123.555(9)
C5 – C6	1.433(3)	C1-C2-C3	117.927(2)
C6 – C1	1.385(3)	C2-C3-C4	120.746(2)
Ru – C1	2.206(4)	C4-C5-C6	119.256(2)
Ru – C2	2.233(4)	Ru – Cp*	1.720(5)
Ru – C3	2.220(3)	Ru – arene	1.817(5)

A photochemical demetallation was subsequently carried out on complex **48** under UV-vis light in acetonitrile-d_3 at ambient temperature, which produced free penta-substituted arene molecule **53** with 95% NMR yield (Scheme 6-20). It was noted that longer irradiation time (40 hours) was needed for the fully demetallation for complex **48** than complex **34** (2 hours), which might be attributed to the stronger Ru – Arene bonds in the former caused by the electron-withdrawing chlorine atom.
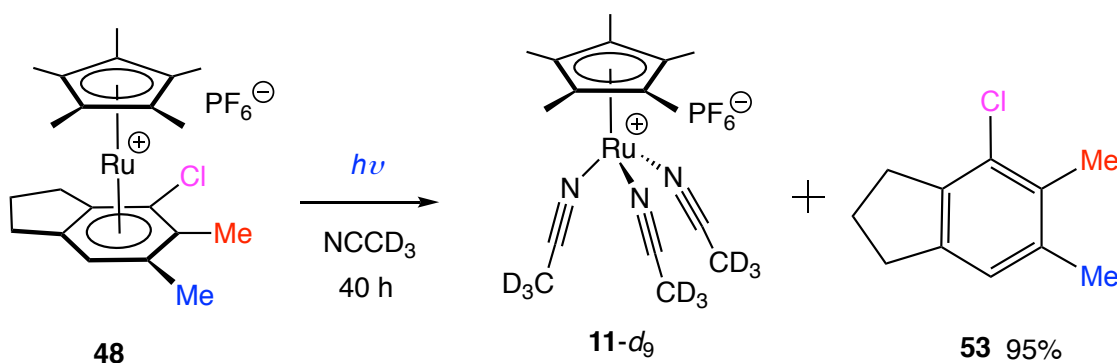
Scheme 6-20. Photolysis of complex **48** in acetonitrile.

In comparison, the reactivity of the six-membered ring annulated dienyne analogue **49** was also examined with complex **11**. When an NMR scale reaction between substrate **49** and complex **11** was carried out in a similar fashion in CDCl$_3$, an unprecedented cycloaromatization mode was observed to produce η^6-arene product **50**, in which the methyl carbon C7 (red) forms a new bond to acetylene carbon C5 (Scheme 6-21). The structure of product **50** was illustrated by the ^{1}H NMR spectrum (400 MHz, CDCl$_3$), which shows an ethyl group at δ 1.24 (t, 3H, J = 7.5 Hz, CH$_2$CH$_3$), 2.23 (dq, 1H, J = 14.6 Hz, 7.5 Hz, CH$_2$CH$_3$), and 2.39 (dq, 1H, J = 14.6 Hz, 7.5 Hz, CH$_2$CH$_3$). Also, two shielded aromatic hydrogen resonances were observed at δ 5.92 (d, 1H, J = 6.0 Hz)

and 5.99 (d, 1H, J = 6.0 Hz). The structural assignment of complex **50** was also confirmed by comparing the ^{1}H and ^{13}C NMR spectra to the authentic sample that was synthesized by Dave Hitt via the reaction between complex **11** and molecule **51**.[14] It is noted that there is no evidence for the formation of any regular Hopf cyclization product **52**.

1.24 (t, 3H, J = 7.5 Hz)
2.23 (dq, 1H, J = 14.6, 7.5 Hz)
2.39 (dq, 1H, J = 14.6, 7.5 Hz)
5.92 (d, 1H, J = 6.0 Hz, Ar-H)
5.99 (d, 1H, J = 6.0 Hz, Ar-H)

1.18 (t, 3H, J = 7.5 Hz)
2.56 (q, 2H, J = 7.5 Hz)
6.94 (d, 1H, J = 8.0 Hz, Ar-H)
7.15 (d, 1H, J = 8.0 Hz, Ar-H)
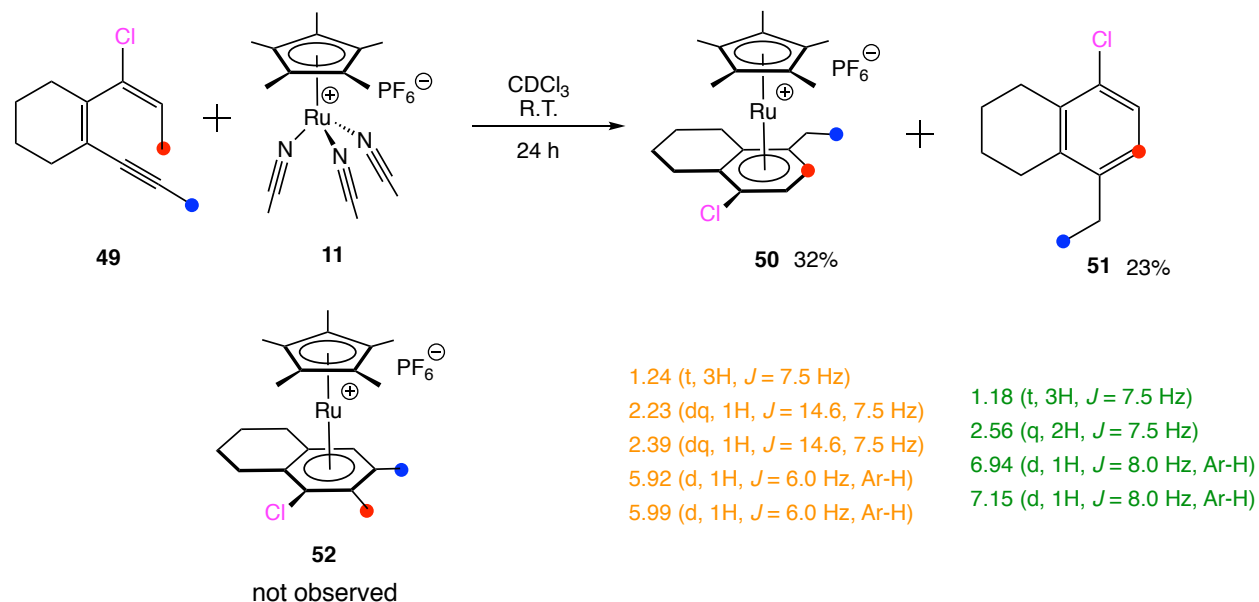
Scheme 6-21. Reaction of dienyne **49** with complex **11** in CDCl$_3$.

Besides the generation of complex **50**, what is even more exciting is the observance of 23% yield of free arene **51** in the reaction mixture. The characteristic resonances of **51** were observed in the ^{1}H NMR spectrum (400 MHz, CDCl$_3$) at δ 1.18 (t, 3H, J = 7.5 Hz, CH$_2$*CH$_3$*), 2.56 (q, 2H, J = 7.5 Hz, *CH$_2$*CH$_3$), 6.94 (d, 1H, J = 8.0 Hz, Ar), and 7.15 (d, 1H, J = 8.0 Hz, Ar). The structure of compound **51** was also confirmed by comparing the spectroscopic data with the authentic sample that was synthesized in Chapter 7. The existence of the free arene indicates that this novel cyclization mode can be potentially catalyzed by ruthenium, which has not been observed in the

ruthenium-mediated Hopf type cyclization of the five-membered ring analogue **46**. In order to furtherly investigate this novel transformation, a series of NMR reactions were conducted with different solvents, ruthenium loadings, and at different temperatures (Scheme 6-22). The NMR reaction results are summarized in Table 6-9.
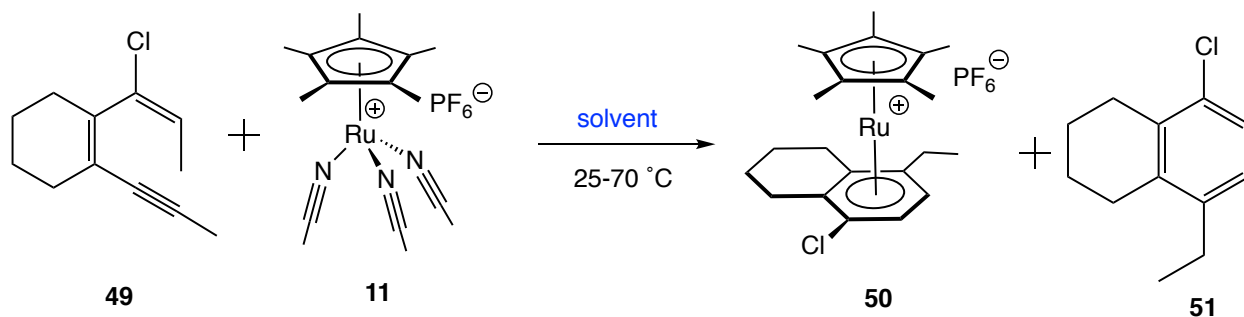
solvent = DCM-d_2, chloroform-d, acetone-d_6, THF-d_8

Scheme 6-22. Reaction of dienyne **49** with complex **11** in different solvent system at variable temperature.

Table 6-9. Different entries of reaction between dienyne **49** and complex **11**.

complex **11** loaded	solvent	time	**49** converted	yield of **50**	yield of **51**
3 eq.	CDCl$_3$	24 h	41%	32.1%	23.3%
6 eq.	CDCl$_3$	40 h	47%	50.4%	0
1 eq.	Acetone-d_6	17 h	100%	54.3%	0
1 eq.	CD$_2$Cl$_2$	10 h	100%	70.5%	0
1 eq.	THF-d_8	10 h	47.5%	30.2%	58.1%
0.2 eq.	THF-d_8	24 h	57.7%	38.7%	50%
0.2 eq. + 3 eq. NCCD$_3$	THF-d_8	7 D	60.4%	32.4%	52.5%
0.2 eq. + 10 eq. NCCD$_3$	THF-d_8	12 D	64.3%	31%	54%

The highest yield of complex **50** (71%) was obtained from CD$_2$Cl$_2$ solvent, however, none of free arene **51** was observed in this scenario. It was found the coordination solvent is the key for the formation of **51**. For instance, when THF-d_8 was employed as solvent, 58% yield of free arene was obtained with 1 equivalent loading of complex **11**. Also, when excess of acetonitrile was added into the reaction mixture, high yield of **51** was observed even with lower loading of complex **11** (0.2 equivalents, 54% yield). However, higher concentration of acetonitrile inhibits the dissociation of acetonitrile ligand from ruthenium, and the low reaction rate can be problematic.

Based on these observations, mechanistically, we proposed that upon the dissociation of three acetonitrile ligands, an η^6-dienyne intermediate **54** can be generated, that is followed by a 1,7-hydride shift to produce the η^6-allene intermediate **55** (Scheme 6-23). A subsequent 6π electron cyclization affords a ruthenium η^6-triene complex **56**. The η^6-arene complex **50** can be generated by a ruthenium-induced hydride shift from complex **56** (path b); whereas the [Cp*Ru]$^+$ moiety can be knocked off by coordination solvent (THF and/or acetonitrile) to give free triene **58** and Cp*RuL$_3$PF$_6$ (L = THF, acetonitrile) (path a). The triene compound **58** can subsequently aromatize in the solution to form the arene **51**, while complex **57** reacts another dienyne substrate to regenerate the η^6-dienyne complex **54**. We attribute the different regioselective cyclization modes of dienyne substrates **49** and **46** to the longer nonbonding distance between the methyl carbon and the acetylene carbon in **46** (Figure 6-11), which is controlled by the adjacent embedded ring size. More computational work is underway to furtherly illustrate this remarkable regioselective cycloaromatizations.
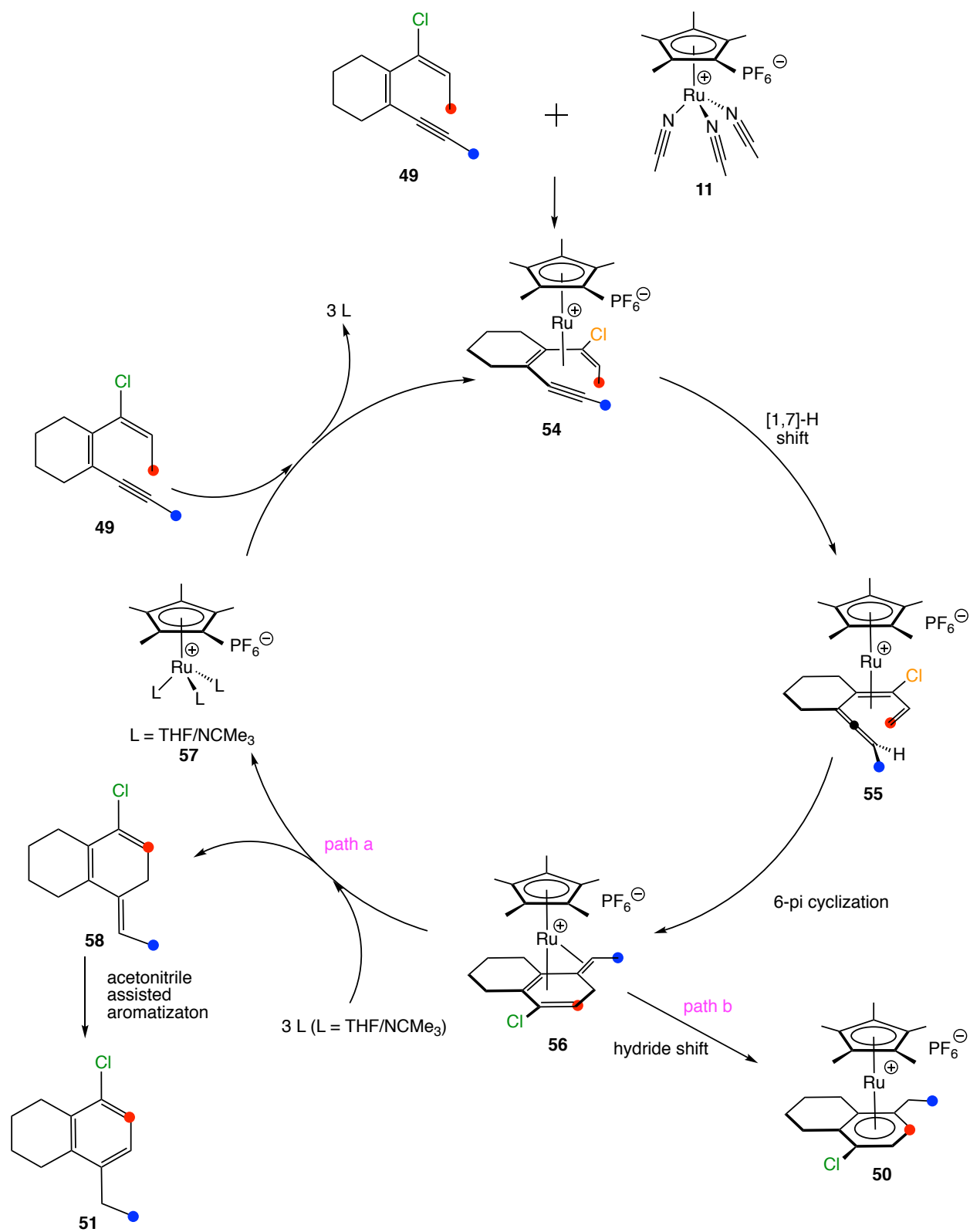
Scheme 6-23. Ruthenium-catalyzed formation of arene **51** and complex **50**.

$d > d$
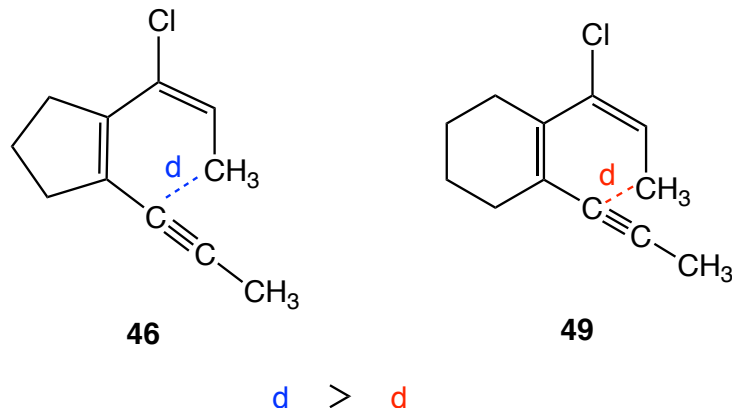
Figure 6-11. Critical nonbonding distance comparison between dienyne **46** and **49**.

F. Conclusions

The reversible formation of complex (η^5-C$_5$Me$_5$)Ru(η^6-trimethyl((2-vinylcyclopent-1-en-1-yl)ethynyl)silane) (**27**) demonstrated the high affinity of dienyne substrate to the [Cp*Ru]$^+$ moiety, and this unique haxahapto coordination mode of conjugated dienyne was studied by X-ray crystallography. Acyclic dienynes bearing phenyl substituent undergo ruthenium-mediated cycloaromatization at ambient temperatures to afford η^6-arene complex in excellent yields, without competitive coordination of metal at the phenyl group. Kinetic studies indicate cyclization rate of dienyne is inverse third order to the concentration of acetonitrile, which demonstrates the intermediacy of η^6-dienyne complex before the rate-limiting cyclization step.

Aside from classic Hopf cyclization, an unprecedented ruthenium-catalyzed highly regioselective cyclization mode was discovered, which is dictated by the adjacent embedded ring size. The readily photodissociation of the arene ligand from ruthenium

products led to the development of synthetic strategy of multisubstituted benzene derivatives.

G. Experimentals

26
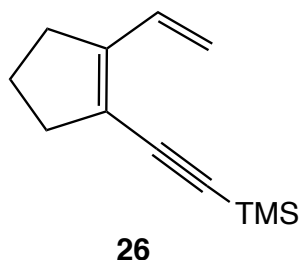
Preparation of trimethyl((2-vinylcyclopent-1-en-1-yl)ethynyl)silane (26): A 2.5 M solution of n-BuLi (1.2 mL, 3 mmol) in hexanes was added to a stirring heterogeneous mixture of methyltriphenylphosphonium bromide (1.07 g, 3 mmol) in THF (200 mL) at -78 ˚C. The resulting yellow solution was allowed to warm to room temperature. Then a solution of 2-((trimethylsilyl)ethynyl)cyclopent-1-ene-1-carbaldehyde (289 mg, 1.5 mmol) in THF (10 mL) was added over 10 min. After stirring at room temperature for 2 h, the reaction mixture was poured over saturated NH_4Cl (200 mL) and extracted with Et_2O three times (200 mL each time). The organic extracts were combined and washed with brine (300 mL), dried over $MgSO_4$, concentrated, purified by flash silica column chromatography (hexanes) to afford dienyne **26** as a clear oil (251 mg, 88% yield). IR (CHCl₃) 3086, 2961, 2846, 2133, 1618, 1432, 1249, 996, 903, 844 cm⁻¹, ¹H NMR (CDCl₃, 400 MHz) δ 0.21 (s, 9H, SiMe₃), 1.40 (m, 2H, CH_2), 2.54 (m, 4H, CH_2), 5.20 (d, 1H, J = 18 Hz), 5.21 (d, 1H, J = 10.4 Hz), 6.85 (dd, 1H, J = 10.4 Hz, J = 18 Hz); ¹³C{¹H}

NMR (CDCl$_3$, 125 MHz) δ 0.28 (SiMe$_3$), 22.43 (CH$_2$), 31.85 (CH$_2$), 37.20 (CH$_2$), 101.07 (*sp-C*), 101.69 (*sp-C*), 116.47 (vinyl-*C*), 122.48 (vinyl-*C*), 132.02 (vinyl-*C*), 149.31 (vinyl-*C*). HRMS for [C$_{12}$H$_{19}$Si]$^+$: 191.1256 (Theo. Mass), 191.1248 (Mass Measured)
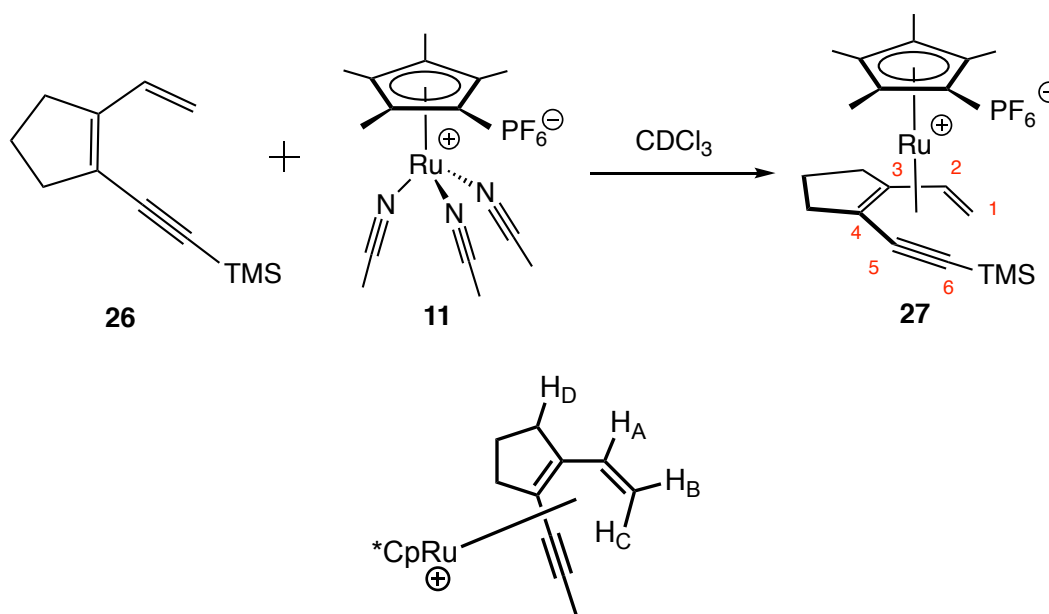
NMR reaction of dienyne 26 with Cp*Ru(NCMe)$_3$PF$_6$ in CDCl$_3$ solvent to form η^6-dienyne complex 27: trimethyl((2-vinylcyclopent-1-en-1-yl)ethynyl)silane (**26**) (2.1 mg, 0.011 mmol), 1,3,5-tri-*tert*-butylbenzene (internal standard) were added to a J.Y. NMR tube. After 1.2 ml of CDCl$_3$ was distilled into the NMR tube, the first ^{1}H NMR spectrum was taken immediately. Then 5.5 mg (0.011 mmol) of Cp*Ru(NCMe)$_3$PF$_6$ was added into the NMR tube under inert atmosphere. After shaking the tube for 2 minutes, a ^{1}H NMR spectrum indicates 70% of the dieneyne was consumed based on the integration of TMS resonance at δ 0.21 relative to internal standard. Acetonitrile resonance was observed at δ 2.01. After waiting for 10 more minutes, the reaction starts to form

equilibrium, and to push the equilibrium move to the desired product, the solvent with acetonitrile were distilled out under vacuum. Then 0.7 ml of CDCl$_3$ was distilled into the NMR tube. ^{1}H NMR spectrum (400 MHz) of the resulting solution indicates all dienyne **26** were consumed, and resonances of **27** were observed at δ 0.36 (s, 9H, SiMe$_3$), 0.65 (dd, 1H, J = 9.6 Hz, J = 2 Hz, H$_C$), 1.82 (s, 15H, Cp*), 1.85 (m, 1H, methylene-H), 2.12 (m, 1H, methylene-H), 2.38 (m, 1H, methylene-H), 2.72 (m, 1H, methylene-H), 2.91 (m, 1H, methylene-H), 3.24 (m, 1H, methylene-H), 3.40 (dd, 1H, J = 9.6 Hz, J = 2 Hz, H$_B$), 5.13 (t, 1H, J = 9.6 Hz, H$_A$), respectively. The assignments of the vinyl hydrogen resonances were confirmed by a NOE NMR experiment, in which the vinyl hydrogen H$_A$ at δ 5.14 was irradiated, obvious NOE effects were observed at δ 3.40 (H$_B$), 2.72 (methylene-H, H$_D$), and 1.82 (Cp*). Resonances of **27** in ^{13}C{^{1}H} NMR spectrum (125 MHz) were observed at δ 0.63 (SiMe$_3$), 10.10 (Cp*), 22.63 (methylene-C), 31.73 (methylene-C), 32.74 (methylene-C), 57.35 (vinyl-C, C1), 91.00 (sp-C, C6), 91.86 (vinyl-C, C2), 92.55 (sp-C, C5), 93.98 (vinyl-C, C4), 98.46 (Cp*), 124.87 (vinyl-C, C3), respectively. Resonances of **27** in ^{13}C NMR spectrum were observed at δ 0.63 (q, J = 121.0 Hz, SiMe$_3$), 10.10 (q, J = 128.7 Hz, Cp*), 22.63 (t, J = 133.1 Hz, methylene-C), 31.69 (t, J = 130.4 Hz, methylene-C), 32.78 (t, J = 128.1 Hz, methylene-C), 57.35 (t, J = 160.3 Hz, vinyl-C, C1), 91.00 (s, sp-C, C6), 91.82 (d, J = 167.1 Hz, vinyl-C, C2), 92.55 (s, sp-C, C5), 93.98 (s, vinyl-C, C4), 98.46 (m, Cp*), 124.87 (s, vinyl-C, C3), respectively. The NMR yield (95.2%) of complex **27** was calculated by the integration of TMS resonance at δ 0.36 (s, 9H, SiMe$_3$) relative to the internal standard at δ 1.33. The X-ray quality crystals were obtained from laying with hexanes.
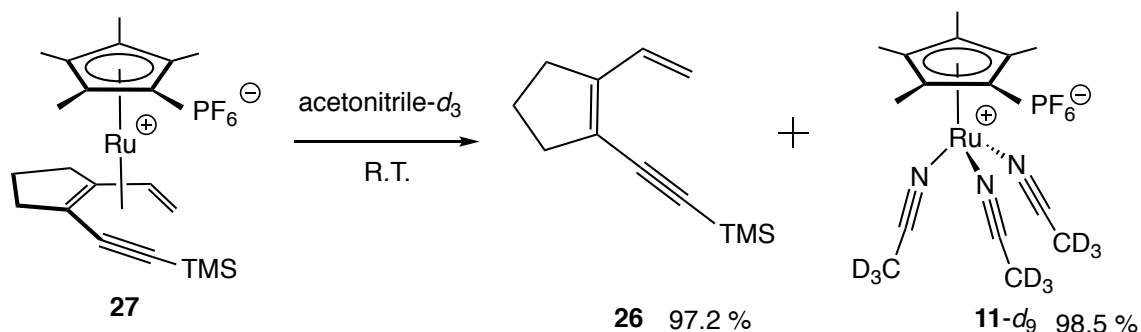
NMR reaction of 27 with acetonitrile-d_3 solvent to form 26 and Cp*Ru(NCMe)$_3$PF$_6$-d_9: complex **27** (2.2 mg, 0.005 mmol), 1,3,5-tri-*tert*-butylbenzene (internal standard) were added to a J.Y. NMR tube. After 0.7 ml of acetonitrile-d_3 was distilled into the NMR tube, the tube was shaken at room temperature for 5 minutes. A followed ^{1}H NMR spectrum indicates all of the **27** were consumed. Cp*Ru(NCMe)$_3$PF$_6$-d_9 was observed at δ 1.60 (s, 15H). Resonances of **26** were observed at δ 0.19 (s, 9H, TMS), 1.93 (m, 4H, methylene-*H*), 2.51 (m, 2H, methylene-*H*), 5.25 (d, 1H, *J* = 10 Hz, vinyl-*H*), 5.27 (d, 1H, *J* = 16.5 Hz, vinyl-*H*), 6.81 (dd, 1H, *J* = 10 Hz, *J* = 16.5 Hz, vinyl-*H*). The NMR yield (97.2%) of **26** and Cp*Ru(NCMe)$_3$PF$_6$-d_9 (98.5%) were calculated by the integration of TMS resonance of **26** at δ 0.19 (s, 9H) and Cp* resonance of Cp*Ru(NCMe)$_3$PF$_6$-d_9 at δ 1.60 (s, 15H) relative to internal standard.

32
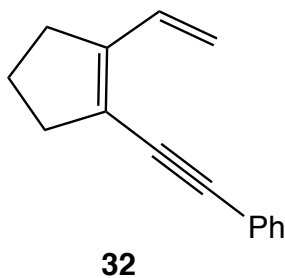
Preparation of dienyne ((2-vinylcyclopent-1-en-1-yl)ethynyl)benzene (32): A 2.5 M solution of n-BuLi (0.62 mL, 1.55 mmol) in hexanes was added to a stirring heterogeneous mixture of methyltriphenylphosphonium bromide (0.55 g, 1.54 mmol) in THF (200 mL) at -78 °C. The resulting yellow solution was subsequently allowed to warm to room temperature. Then a solution of 2-(phenylethynyl)cyclopent-1-ene-1-carbaldehyde (200 mg, 1.02 mmol) in THF (10 mL) was added over 10 min. After stirring at room temperature for 2 h, the reaction mixture was poured over saturated NH$_4$Cl (200 mL) and extracted with Et$_2$O three times (200 mL each time). The organic extracts were combined and washed with brine (300 mL), dried over MgSO$_4$, concentrated, purified by flash silica column chromatography (hexanes) to afford dienyne **32** as a clear oil (177 mg, 89.3% yield). IR (CHCl$_3$) 3078, 3054, 3000, 2950, 2845, 2190, 1618, 1596, 1488, 1571, 1488, 1442, 1249, 1068, 1025 cm^{-1}, ^{1}H NMR (CDCl$_3$, 400 MHz) δ 1.97 (m, 2H, C*H*$_2$), 2.59 (t, 2H, J = 7.6 Hz), 2.67 (t, 2H, J = 7.6 Hz), 5.23 (d, 1H, J = 16.4 Hz), 5.24 (d, 1H, J = 11.6 Hz), 6.97 (dd, 1H, J = 11.6 Hz, J = 16.4 Hz), 7.27-7.50 (m, 5H, Ph); ^{13}C{^{1}H} NMR (CDCl$_3$, 125 MHz) δ 22.5 (*C*H$_2$), 31.9 (*C*H$_2$), 37.3 (*C*H$_2$), 86.1 (*sp-C*), 96.0 (*sp-C*), 116.2 (vinyl-*C*), 122.6 (vinyl-*C*), 123.7 (*C$_i$*-Ph), 128.2 (*C$_p$*-Ph), 128.4 (*C$_o$*-Ph), 131.6 (*C$_m$*-Ph), 132.1 (vinyl-*C*), 148.0 (vinyl-*C*). HRMS (APCI/TOFMS) m/z: [M + H]$^+$ Calcd for [C$_{15}$H$_{15}$]$^+$ 195.1168; Found 195.1169.

34
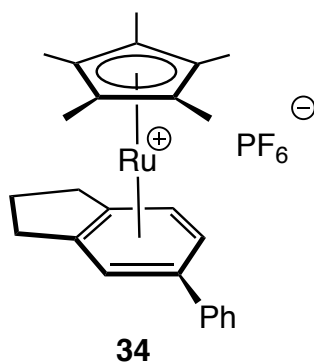
Preparation of (η^5-C$_5$Me$_5$)Ru(η^6-5-phenyl-2,3-dihydro-1H-indene)PF$_6$ complex (34):

20 mg (0.103 mmol) of **32** and 52 mg (0.103 mmol) of Cp*Ru(NCMe)$_3$PF$_6$ were added

into a Schlenk flask under nitrogen. After 10 ml of dry DCM was distilled into the flask

on the high vacuum line, the reaction mixture was allowed to stir at room temperature

for 2 hours under inert atmosphere. The solution was added 150 ml of hexanes to

precipitate out crude **34**. The white precipitates were washed with Et$_2$O (10 ml) twice,

and after recrystallization in DCM and hexanes, 50.4 mg (85.1% yield) of **34** were

obtained as a clear crystalline solid. Mp: 276 ˚C; IR (CH$_2$Cl$_2$) 3114, 3064, 2962, 2912,

1454, 1384, 1032, 883, 840, 771 cm^{-1}, ^{1}H NMR (CD$_2$Cl$_2$, 400 MHz) δ 1.71 (s, 15H, Cp*),

1.82 (m, 1H, methylene-*H*), 2.28 (m, 1H, methylene-*H*), 2.64 (m, 2H, methylene-*H*), 2.79

(m, 2H, methylene-*H*), 5.88 (d, 1H, *J* = 6 Hz, arene-Ru), 6.10 (d, 1H, *J* = 6 Hz, arene-

Ru), 6.28 (s, 1H, arene-Ru), 7.5-7.7 (m, 5H, Ph); ^{13}C{^{1}H} NMR (CD$_2$Cl$_2$, 125 MHz) δ 9.9

(Cp*), 23.5 (*C*H$_2$), 29.3 (*C*H$_2$), 29.8 (*C*H$_2$), 81.6 (arene-Ru), 83.4 (arene-Ru), 84.1

(arene-Ru), 95.5 (Cp*), 100.7 (arene-Ru), 107.9 (arene-Ru), 108.0 (arene-Ru), 127.1

(Ph), 129.9 (Ph), 130.7 (Ph), 132.5 (Ph). HRMS (ESI/TOFMS) m/z: [M − PF$_6$]$^+$ Calcd for

C$_{25}$H$_{29}$Ru 431.1307; Found 431.1317.
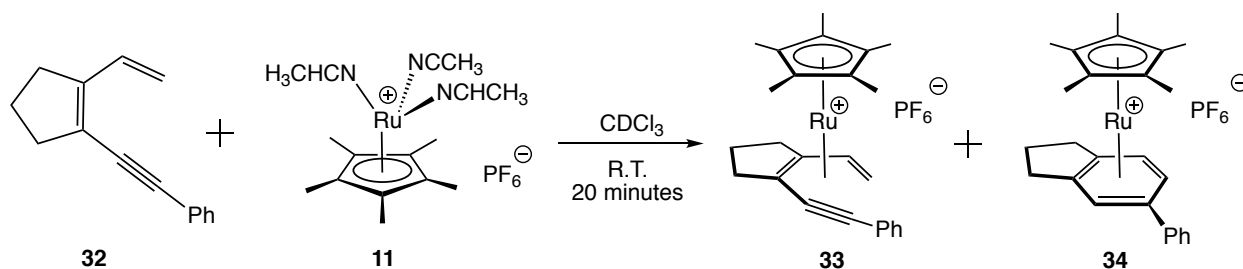
NMR tube reaction of dienyne 32 with Cp*Ru(NCMe)₃PF₆ in CDCl₃ solvent to form

33 and 34: Dienyne **32** (2.0 mg, 0.01 mmol), 1,3,5-tri-*tert*-butylbenzene (internal

standard) were added to a J.Y. NMR tube. After 0.7 ml of CDCl₃ was distilled into the

NMR tube, the first ^{1}H NMR spectrum was taken immediately. Then 5.3 mg (0.01 mmol)

of Cp*Ru(NCMe)₃PF₆ was added into the NMR tube under inert atmosphere. The

resulting reaction mixture was monitored by ^{1}H NMR spectroscopy. After 20 minutes,

the ^{1}H NMR spectrum indicates all dienyne **32** were consumed based on the vinyl

hydrogen resonances at δ 5.22 (d, 1H, *J* = 16.4 Hz), 5.23 (d, 1H, *J* = 11.6 Hz) and 6.96

(dd, 1H, *J* = 11.6 Hz, *J* = 16.4 Hz). Resonances of **33** were observed at δ 1.13 (dd, 1H,

J = 10.4 Hz, *J* = 2 Hz, vinyl-*H*), 1.67 (s, 15H, Cp*), 2.40 (m, 1H, methylene-*H*), 2.80 (m,

1H, methylene-*H*), 3.31 (m, 1H, methylene-*H*), 3.55 (dd, 1H, *J* = 9.2 Hz, *J* = 2 Hz, vinyl-

H), 5.18 (t, 3H, *J* = 9.8 Hz, vinyl-*H*), respectively. Other resonances for **33** cannot be

reported clearly due to peaks overlap. Resonances of **34** were observed at δ 1.70 (s,

15H, Cp*), 1.78 (m, 1H, methylene-*H*), 2.27 (m, 1H, methylene-*H*), 2.66 (m, 2H,

methylene-*H*), 2.97 (m, 2H, methylene-*H*), 6.01 (d, 1H, *J* = 6 Hz, arene-Ru), 6.22 (d, 1H,

J = 6 Hz, arene-Ru), 6.36 (s, 1H, arene-Ru), 7.4-7.7 (m, 5H, Ph), respectively. The NMR

yield of **34** (72%) and NMR yield of **33** (24.2%) were calculated by the integration of

arene hydrogen resonance of **34** at δ 6.22 (d, 1H, J = 6 Hz) and vinyl hydrogen resonance of **33** at δ 3.55 (dd, 1H, J = 9.2 Hz, J = 2 Hz) relative to internal standard.

34   **11**-d_9 96.8%   **38** 95%
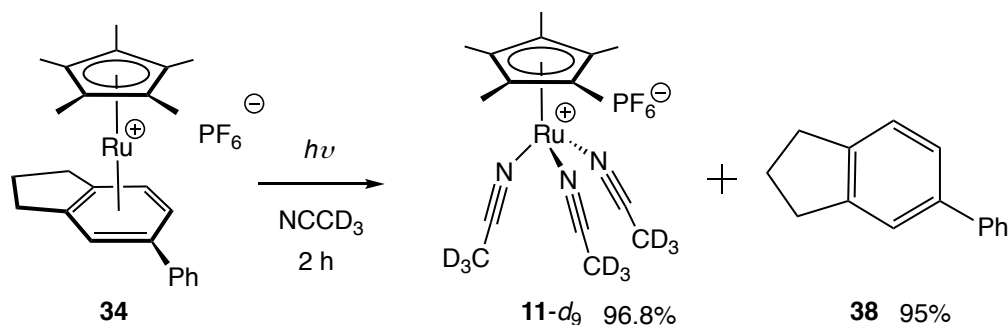
NMR reaction of photolyzing 34 in acetonitrile-d_3 to generate Cp*Ru(NCMe)$_3$PF$_6$-d_9 and 38:   complex **34** (2.0 mg, 0.003 mmol) and 1,3,5-tri-*tert*-butylbenzene (internal standard) were added to a J.Y. NMR tube. After 0.7 ml of acetonitrile-d_3 was distilled into the NMR tube, the resulting solution was subsequently degassed via 3 cycles of freeze/pump/thaw/degas, and then the first ^{1}H NMR spectrum was taken immediately. The J. Young tube was then placed in a Rayonette photoreactor equipped with UV broadband lamps centered at 254 nm. The reaction was subsequently monitored by ^{1}H NMR spectroscopy, and after 2 hours, the ^{1}H NMR spectrum indicates all **34** were consumed based on the Cp* resonance at δ 1.68 (s, 15H). Cp*Ru(NCMe)$_3$PF$_6$-d_9 was observed at δ 1.60 (s, 15H) with a 96.8% yield. Resonances of **38** were observed at δ 2.10 (m, 2H, methylene-H), 2.94 (m, 4H, methylene-H), 7.26-7.62(m, 8H, aromatic-H). The NMR yield (95%) of **38** was calculated by the integration of methylene hydrogen resonance at δ 2.10 (m, 2H, methylene-H) relative to internal standard.
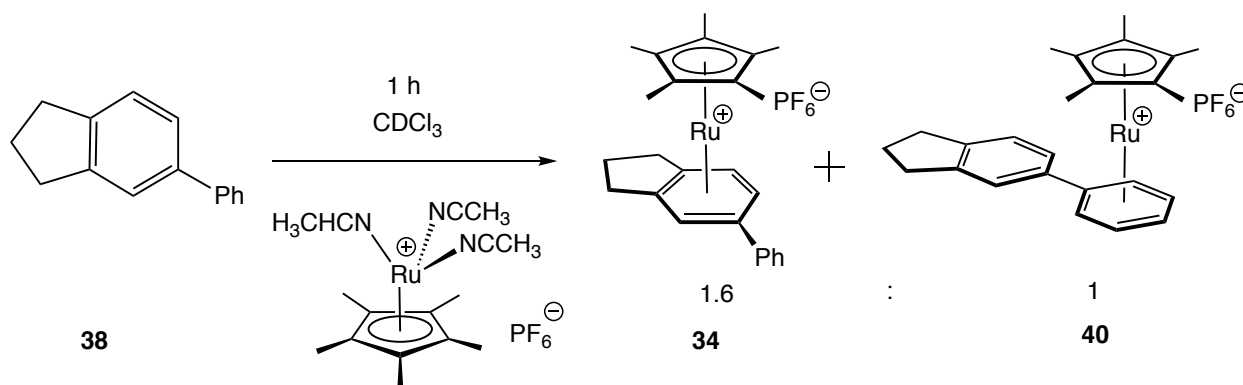
NMR tube reaction of forming mixture of 34 and 40 in CDCl₃: complex **34** (2.2 mg, 0.004 mmol) was added into a J.Y. NMR tube. After 0.7 ml of acetonitrile-d_3 was distilled into the NMR tube, the resulting solution was subsequently degassed via 3 cycles of freeze/pump/thaw/degas, and then the first ¹H NMR spectrum was taken immediately. The J. Young tube was then placed in a Rayonette photoreactor equipped with UV broadband lamps centered at 254 nm. The reaction was subsequently monitored by ¹H NMR spectroscopy, and after 2 hours, the ¹H NMR spectrum indicates all **34** were consumed based on the Cp* resonance at δ 1.68 (s, 15H). Cp*Ru(NCMe)₃PF₆-d_9 was observed at δ 1.60 (s, 15H) , and resonances of **38** were observed at δ 2.10 (m, 2H, methylene-*H*), 2.94 (m, 4H, methylene-*H*), 7.26-7.62 (m, 8H, aromatic-*H*). Then the solvent of the resulting solution was pumped away under vacuum, and 0.7 ml of dry CDCl₃ was distilled into the NMR tube. After one hour, ¹H NMR spectrum indicates that all the Cp*Ru(NCMe)₃PF₆-d_9 were consumed, and complexes **34** and **40** were generated. Diagnostic resonances of **34** were observed at δ 1.71 (s, 15H, Cp*), 6.03 (d, 1H, J = 6.4 Hz, aromatic-*H*), 6.24 (d, 1H, J = 6.4 Hz, aromatic-*H*), 6.33 (s, 1H, aromatic-*H*), and diagnostic resonances of **40** were observed at δ 1.83 (s, 15H, Cp*), 5.85 (t, 1H, J = 6.0 Hz, aromatic-*H*), 5.96 (t, 2H, J = 6.0 Hz, aromatic-*H*), 6.19 (d, 2H, J = 6.0 Hz,

aromatic-*H*). The ratio of **34** and **40** (1.6 : 1) was calculated by the integration of aromatic hydrogen of **34** at δ 6.33 (s, 1H) and aromatic hydrogen of **40** at δ 6.19 (d, 2H, *J* = 6.0 Hz).

48
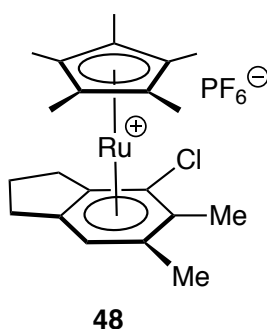
Preparation of (η^5-C$_5$Me$_5$)Ru(η^6-4-chloro-5,6-dimethyl-2,3-dihydro-1H-indene)PF$_6$ (48): 152 mg (0.84 mmol) of (*E*)-1-(1-chloroprop-1-en-1-yl)-2-(prop-1-yn-1-yl)cyclopent-1-ene (**46**) and 420 mg of Cp*Ru(NCMe)$_3$PF$_6$ (0.83 mmol) were added to an oven dried round bottom flask under nitrogen atomosphere. Then 120 ml of dry DCM was added into the flask, and the solution was allowed to stir under nitrogen for 1 hour. The solvent was then evaporated under reduced pressure and chromatography on silica gel with 70% EtOAc/hexane yielded 450 mg (96%) of **48** as an air stable crystalline white solid; Mp: 186°C; IR (DCM) 3093, 2966, 2917, 1475, 1434, 1421, 1384, 1071, 1027, 987, 910 cm^{-1}; ^{1}H NMR (CDCl$_3$, 400 MHz) δ 1.77 (s, 15H, Cp*), 2.18 (s, 3H, Me), 2.21 (s, 3H, Me), 2.25 (m, 2H, methylene-H), 2.64 (m, 1H, methylene-H), 2.78 (m, 1H, methylene-H), 2.90 (m, 1H, methylene-H), 3.04 (m, 1H, methylene-H), 6.02 (s, 1H, methylene-H); ^{13}C{^{1}H} NMR (CDCl$_3$, 125 MHz) δ 8.93 (Cp*), 13.78 (methylene-C), 17.68 (methylene-C), 22.46 (methylene-C), 29.50 (Me), 29.76 (Me), 86.35 (Ar), 94.43 (Cp*), 97.44 (Ar),

99.17 (Ar), 102.89 (Ar), 106.06 (Ar), 107.49 (Ar); HRMS (HR-ESI-TOFMS) for [C$_{21}$H$_{28}$ClRu]$^+$: 417.0920 (Theo. Mass), 417.0919 (Mass Measured), Delta (-0.2 ppm). Elemental Analysis: C% (44.89); H% (5.02). Found: C% (44.50); H% (5.13).
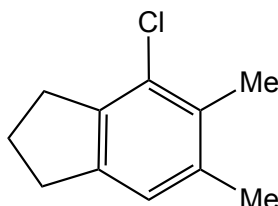
53

Preparation of 4-chloro-5,6-dimethyl-2,3-dihydro-1H-indene (53): To a Teflon-sealed Schlenk flask added 200 mg (0.356 mmol) of complex (η^5-C$_5$Me$_5$)Ru(η^6-4-chloro-5,6-dimethyl-2,3-dihydro-1H-indene)PF$_6$ (**48**) with 100 mL of dry acetonitrile. After the reaction mixture was purged with argon for 15 minutes, the flask was sealed and placed in a Rayonette photoreactor equipped with UV broadband lamps centered at 254 nm. Then 250 mL of diethyl ether was added to the solution to precipitate out the Cp*Ru(NCMe)$_3$PF$_6$ complex, which can be recovered by filtration and washing with hexanes. The rest solution was concentrated, and after chromatography on silica gel with hexanes, 57.2 mg (89% yield) of compound **53** can be obtained as colorless oil. ^{1}H NMR (CDCl$_3$, 400 MHz) δ 2.06 (quintet, 2H, J = 7.2 Hz, methylene-H), 2.27 (s, 3H, Me), 2.29 (s, 3H, Me), 2.92 (q, 4H, J = 7.2 Hz, methylene-H), 6.93 (s, 1H, Ar); ^{13}C{^{1}H} NMR (CDCl$_3$, 125 MHz) δ 16.14 (methylene-C), 21.14 (methylene-C), 24.77 (methylene-C), 32.97 (Me), 33.62 (Me), 124.01 (Ar), 131.17 (Ar), 131.68 (Ar), 136.27 (Ar), 140.26 (Ar),

142.63 (Ar); HRMS (HR-EI) for $[C_{11}H_{13}Cl]^+$: 180.0706 (Theo. Mass), 180.0704 (Mass Measured), Delta (-0.2 ppm).
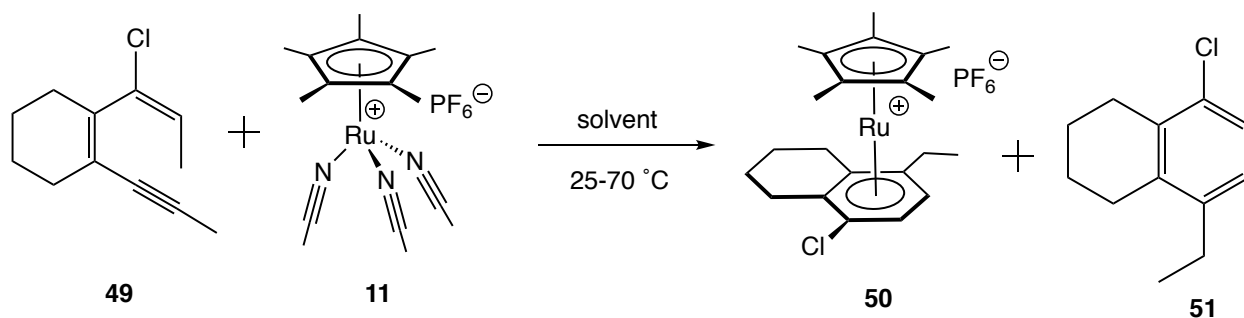
General procedure of NMR reactions between complex 11 and vinyl-chloride 49 to generate (η^5-C$_5$Me$_5$)Ru(η^6-5-chloro-8-ethyl-1,2,3,4-tetrahydronaphthalene)PF$_6$ (48) and 5-chloro-8-ethyl-1,2,3,4-tetrahydronaphthalene (51) in different solvents and conditions: (*E*)-1-(1-chloroprop-1-en-1-yl)-2-(prop-1-yn-1-yl)cyclohex-1-ene (**49**) and 1,3,5-tri-*tert*-butylbenzene (internal standard) were added to an oven dried J. Young tube (quantities of **49** see Table 6-9). Then around 0.75 ml of dry deuterated solvent was distilled into the NMR tube. The resulting solution was subsequently degassed via 3 cycles of freeze/pump/thaw/degas. The first ^{1}H NMR spectrum was taken immediately. The J. Young tube was transferred into a glove box and complex **11** was added (quantities of **11** see Table 6-9). Then the tube was placed into an oil bath at 70°C and the reaction was subsequently monitored by ^{1}H NMR spectroscopy until all vinyl-chloride **49** disappeared based on the vinyl hydrogen peak or until the reaction didn't go any further. Conversion of **49** was calculated based on the integration of the vinyl hydrogen of **49** relative to internal standard. Yield of **50** and **51** were calculated by the integration of aromatic hydrogen of **50** and **51** relative to converted **49**. Here we use

THF-d_8 as an example: After 4 mg (0.02 mmol) of **49**, 10.4 mg (0.02 mmol) of **11**, 1,3,5-tri-*tert*-butylbenzene (internal standard) and 0.6 ml of THF-d_8 were added into the J. Young tube by employing the method mentioned above, the NMR tube was allowed to heat at 70 ˚C in an oil bath, and the reaction was monitored by ^{1}H NMR spectroscopy. After 10 hours, 47.5% of the **49** were consumed based on the integration of the vinyl hydrogen at δ 5.67 (q, 4H, J = 6.8 Hz) relative to internal standard. Complex **50** was observed at δ 1.23 (t, 3H, J = 7.2 Hz), 1.89 (s, 15H, Cp*), 5.99 (d, 1H, J = 6.8 Hz), 6.17 (d, 1H, J = 6.8 Hz) with a 30.2% yield based on the converted **49**. Complex **51** was observed at δ 1.16 (t, 3H, J = 7.2 Hz), 2.56 (q, 2H, J = 7.2 Hz), 2.72 (m, 4H), 6.93 (d, 1H, J = 8.4 Hz), 7.10 (d, 1H, J = 8.4 Hz) with a 58.1% yield based on the converted **49**.

H. Appendix
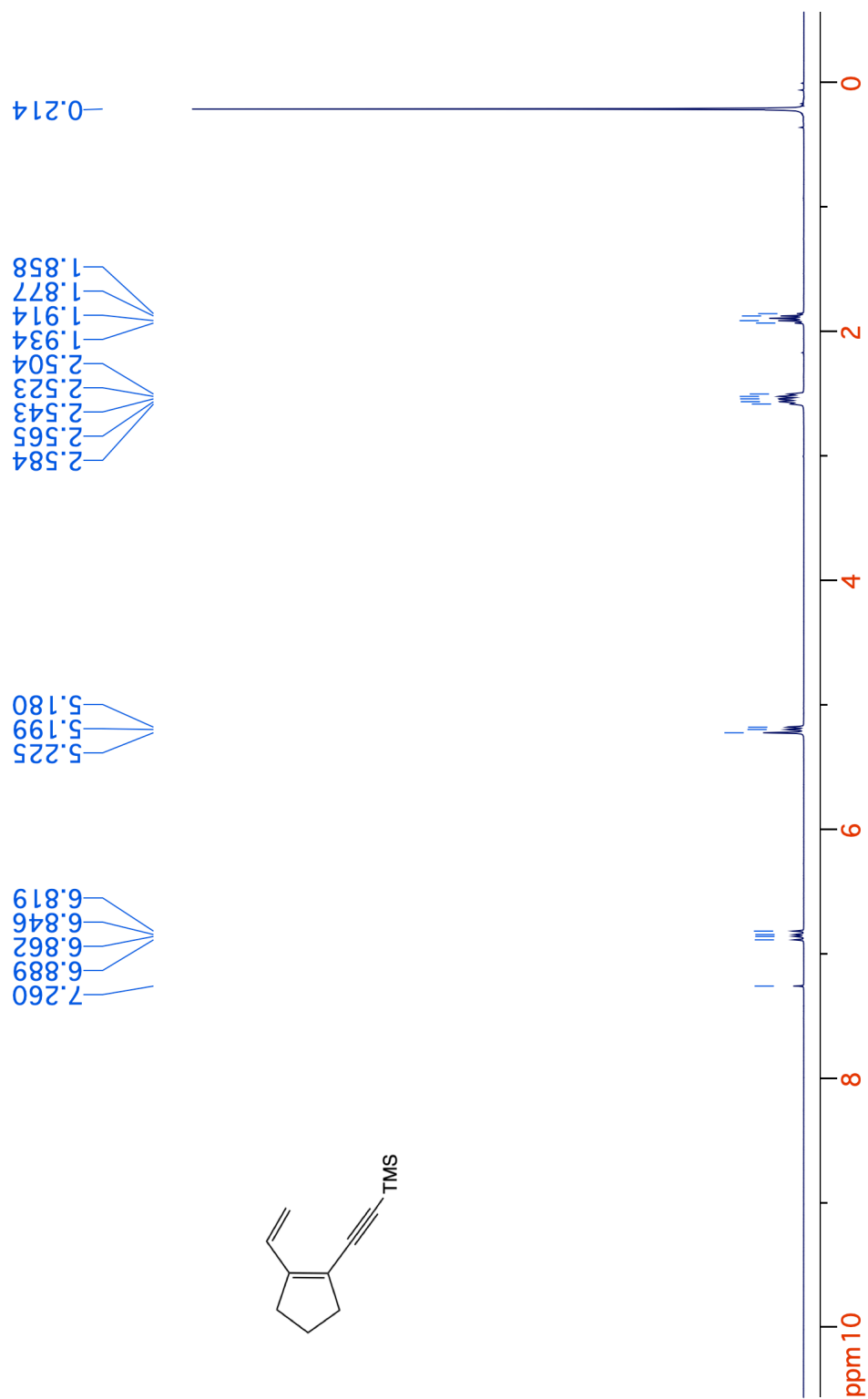
Figure 6-12. ^{1}H NMR spectrum (400 MHz, CDCl$_3$) of **26**.
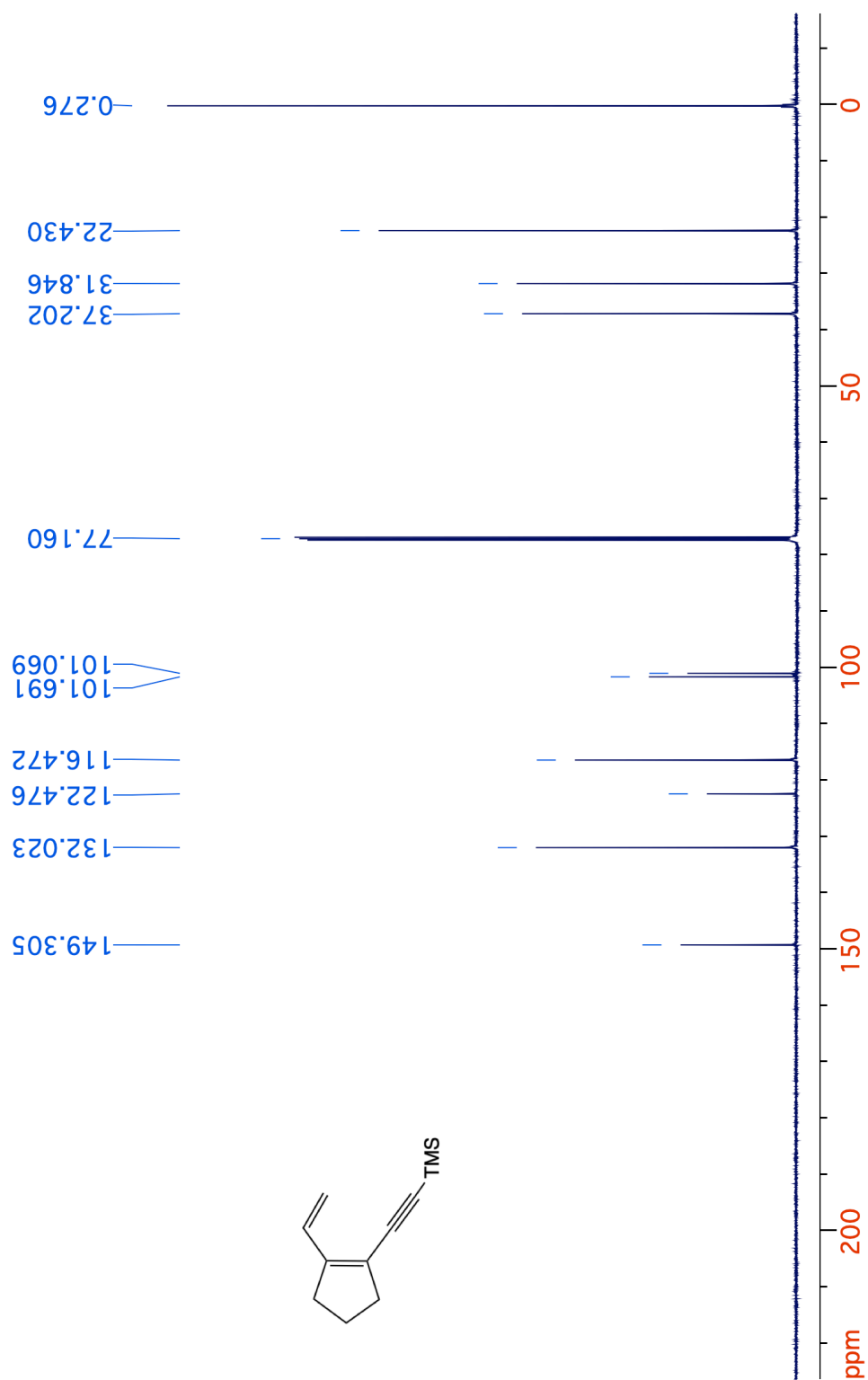
Figure 6-13. $^{13}C\{^1H\}$ NMR spectrum (125 MHz, CDCl$_3$) of **26**.
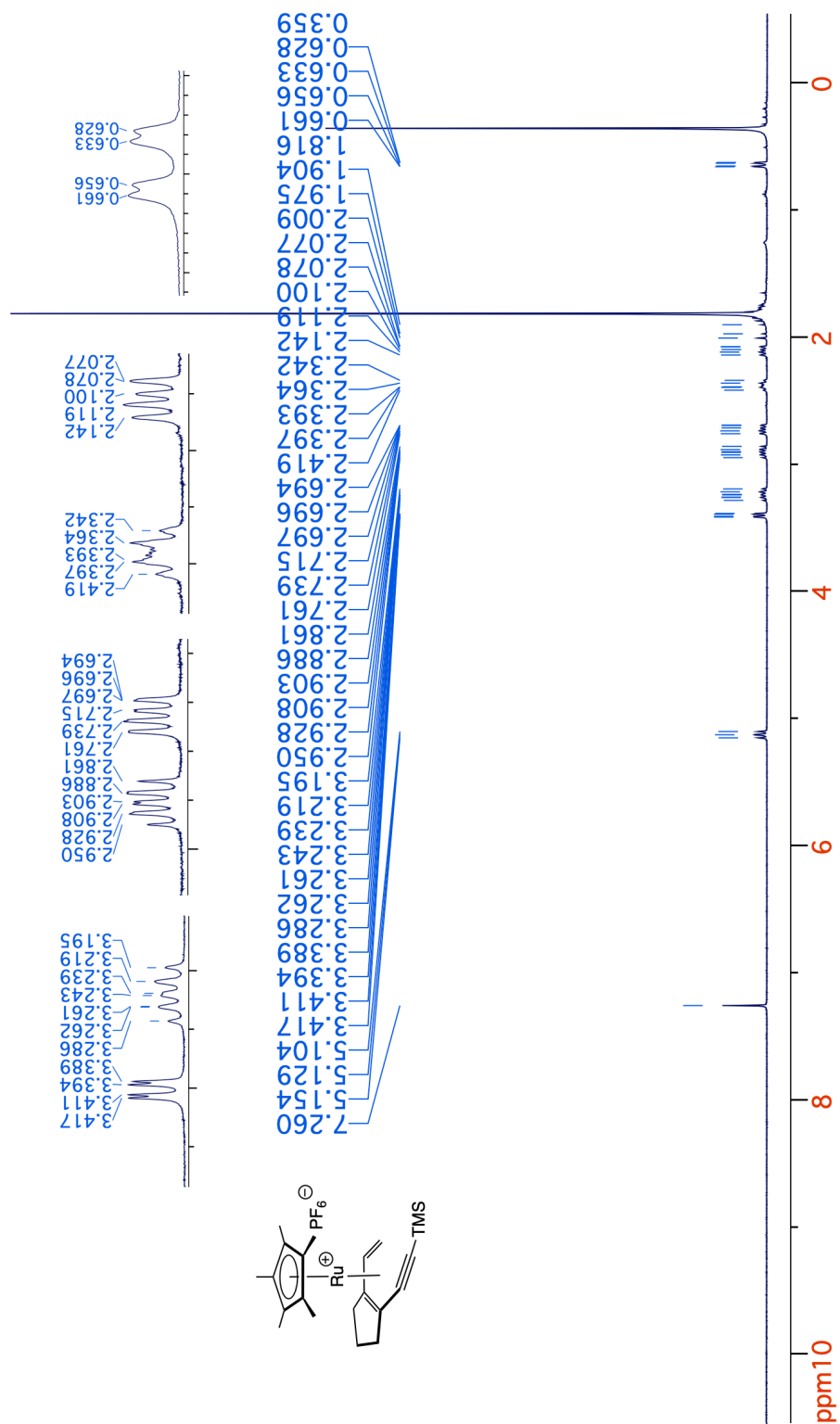
Figure 6-14. ^{1}H NMR spectrum (400 MHz, CDCl$_3$) of **27**.

0.629
10.099
22.630
31.721
32.740
57.340
77.160
90.995
91.810
92.549
93.964
98.460
124.860
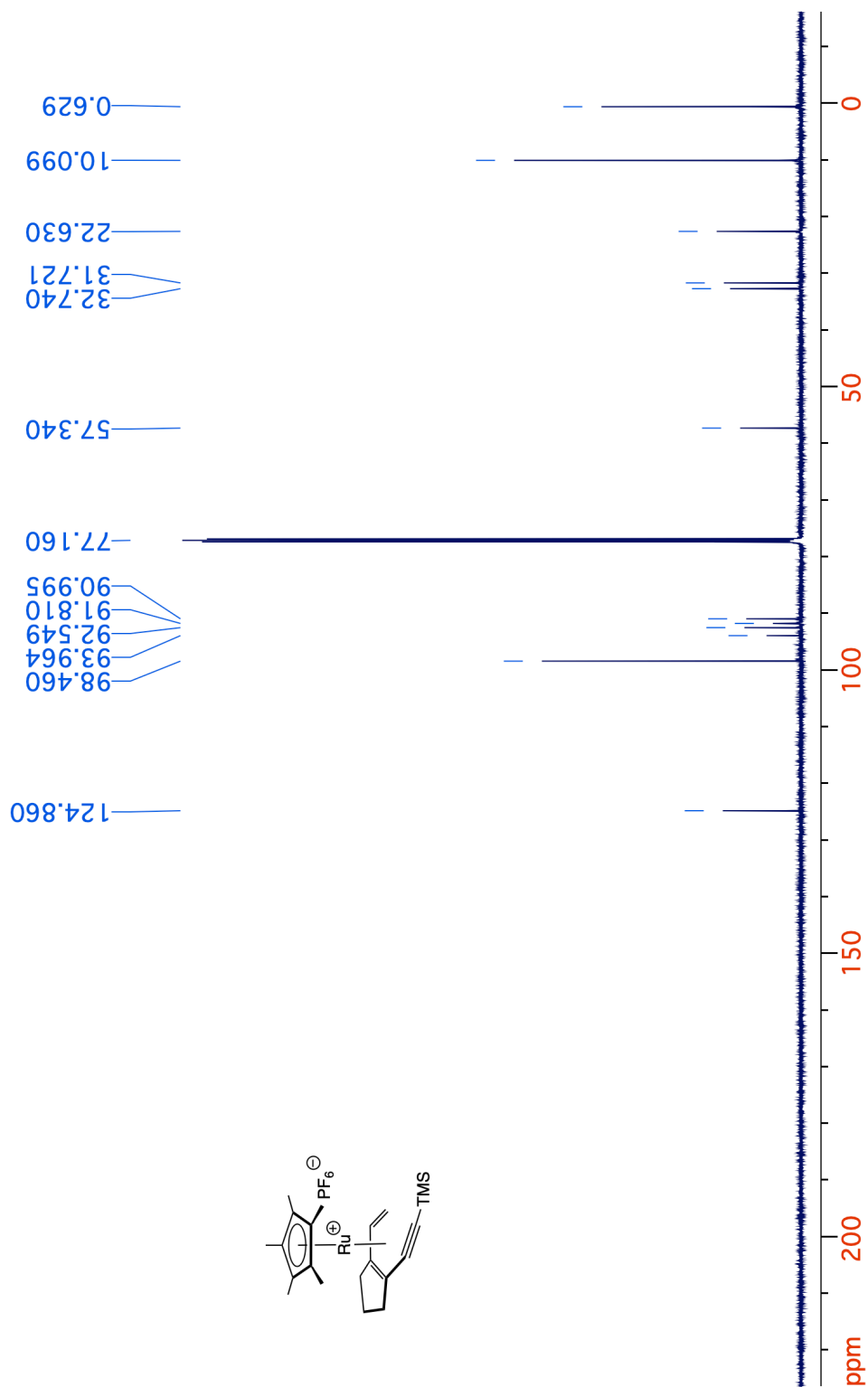
Figure 6-15. $^{13}C\{^1H\}$ NMR spectrum (125 MHz, CDCl$_3$) of **27**.
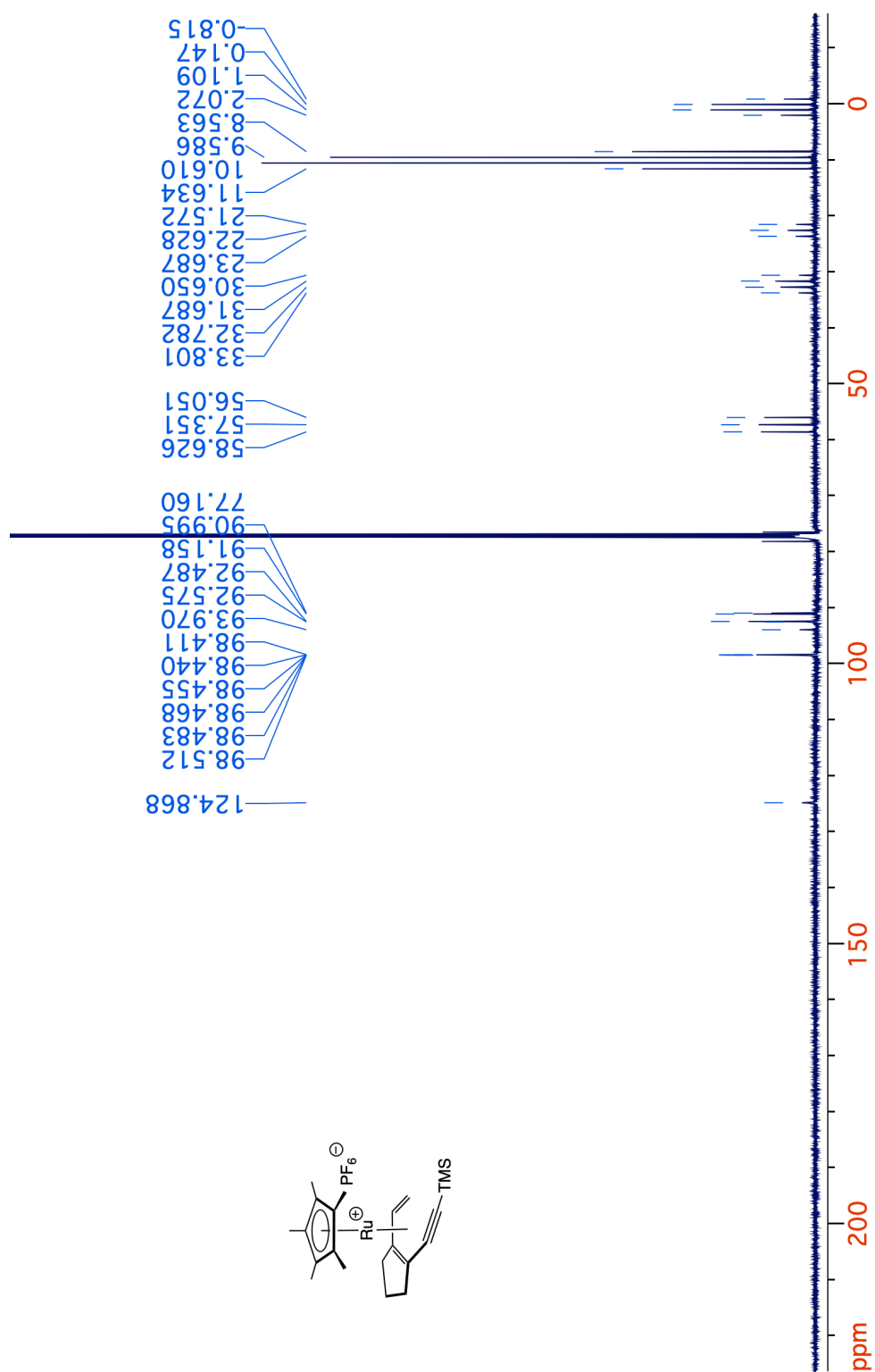
Figure 6-16. ^{13}C NMR spectrum (125 MHz, CDCl$_3$) of **27**.
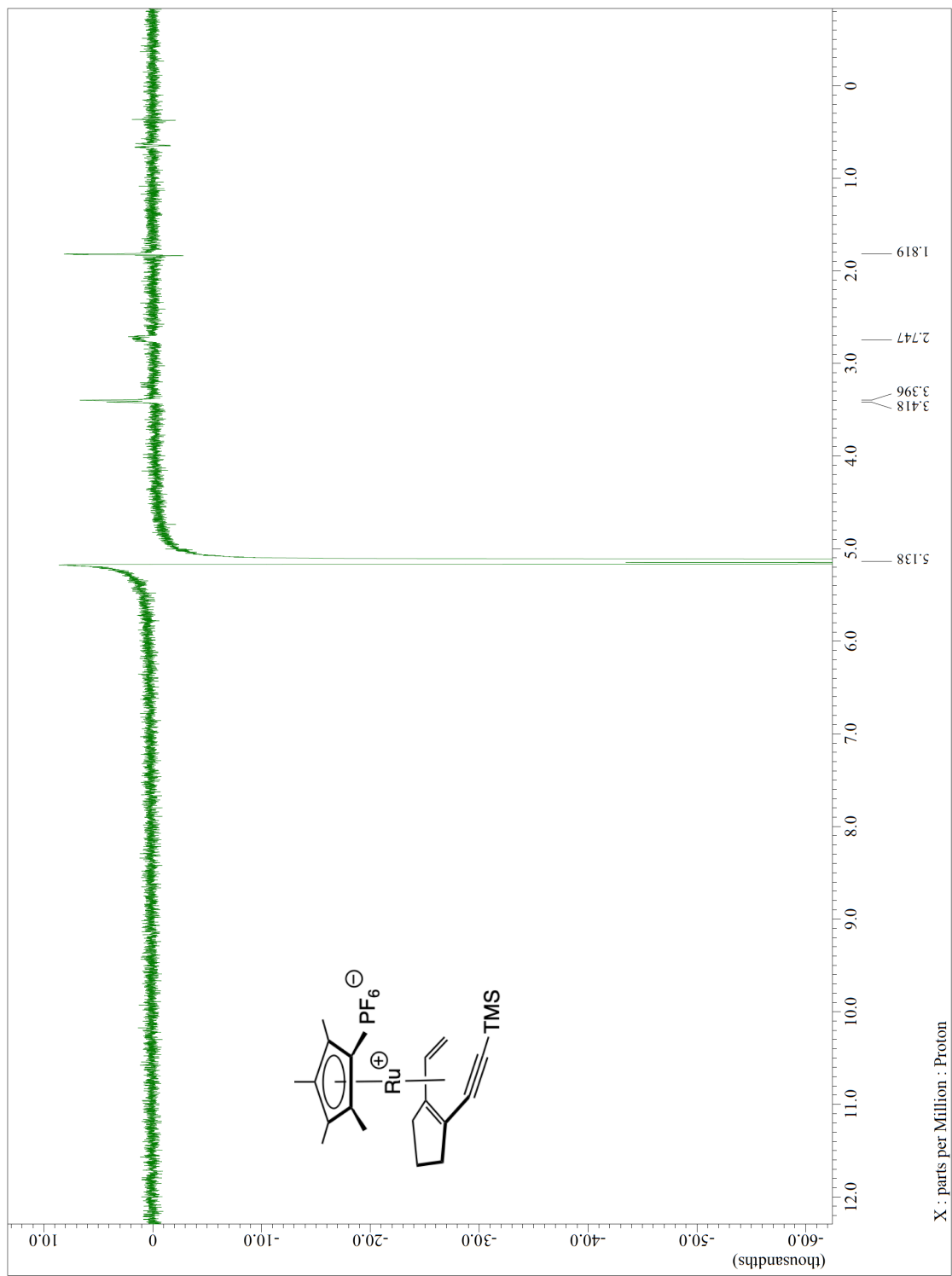
Figure 6-17. NOE NMR spectrum (500 MHz, CDCl₃) of **27** by irradiating vinyl hydrogen at δ 5.14.
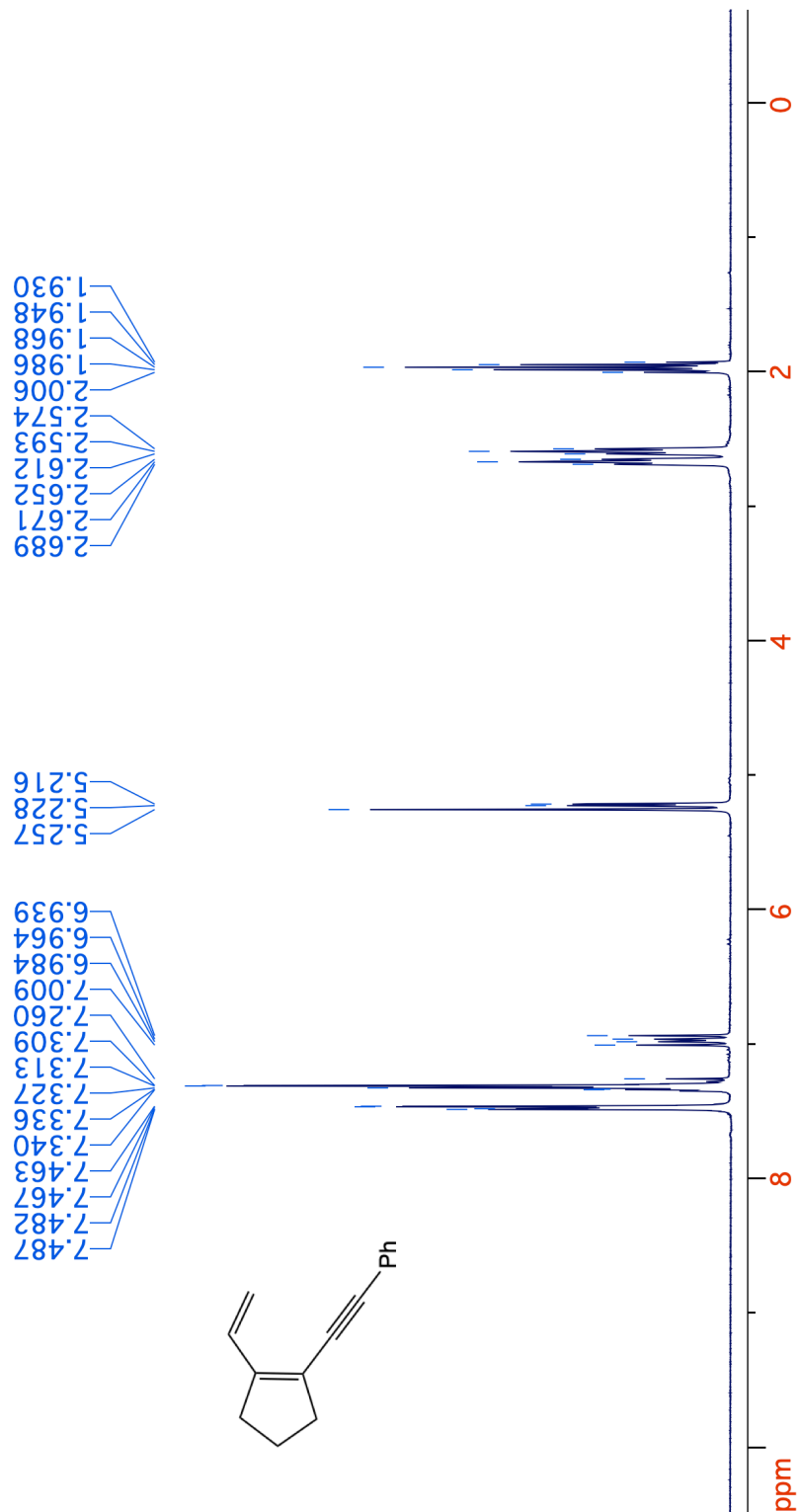
Figure 6-18. ¹H NMR spectrum (400 MHz, CDCl₃) of **32**.
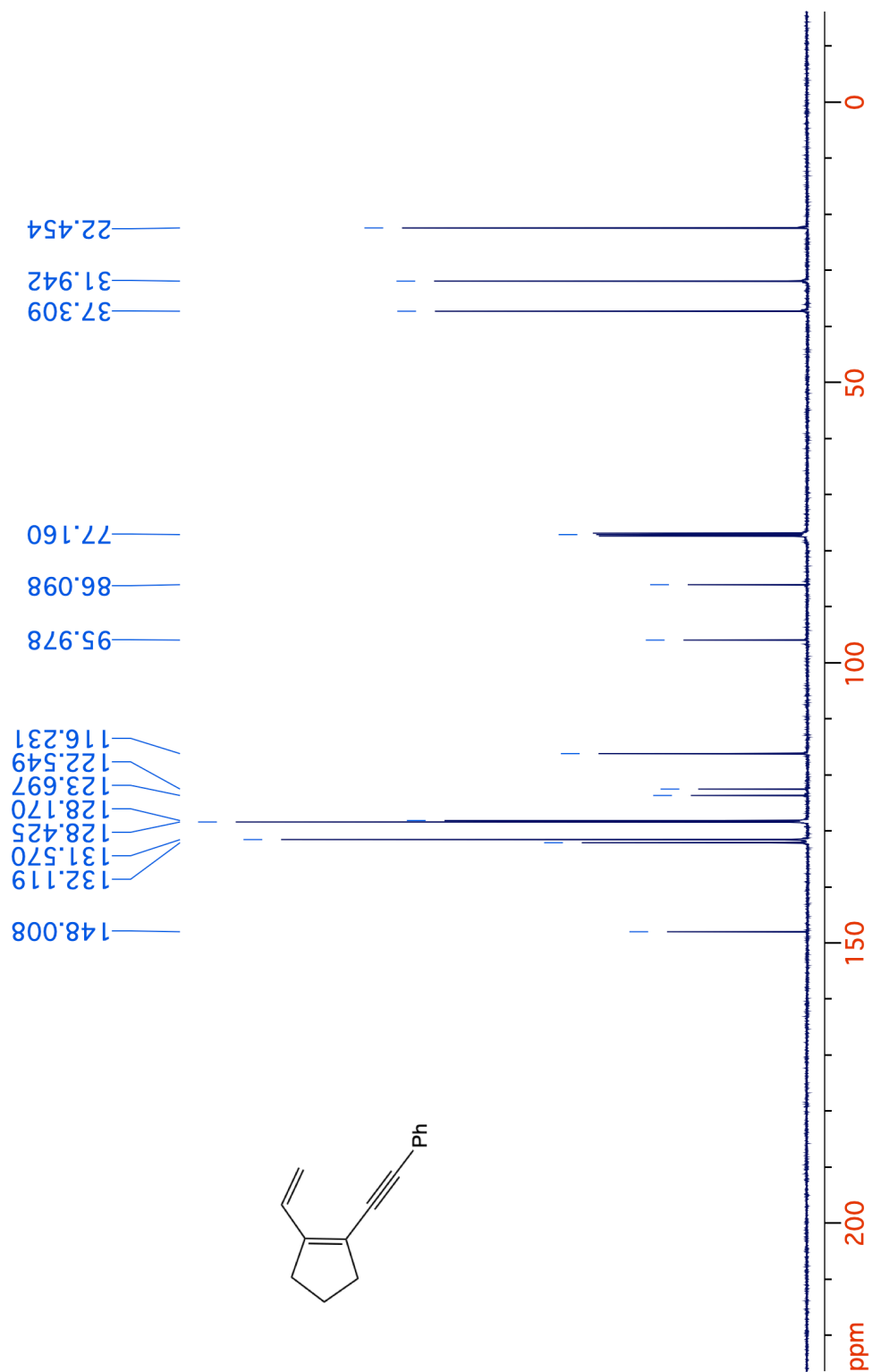
Figure 6-19. $^{13}C\{^1H\}$ NMR spectrum (125 MHz, CDCl$_3$) of **32**.

Peaks: 22.454, 31.942, 37.309, 77.160, 86.098, 95.978, 116.231, 122.549, 123.697, 128.170, 128.425, 131.570, 132.119, 148.008
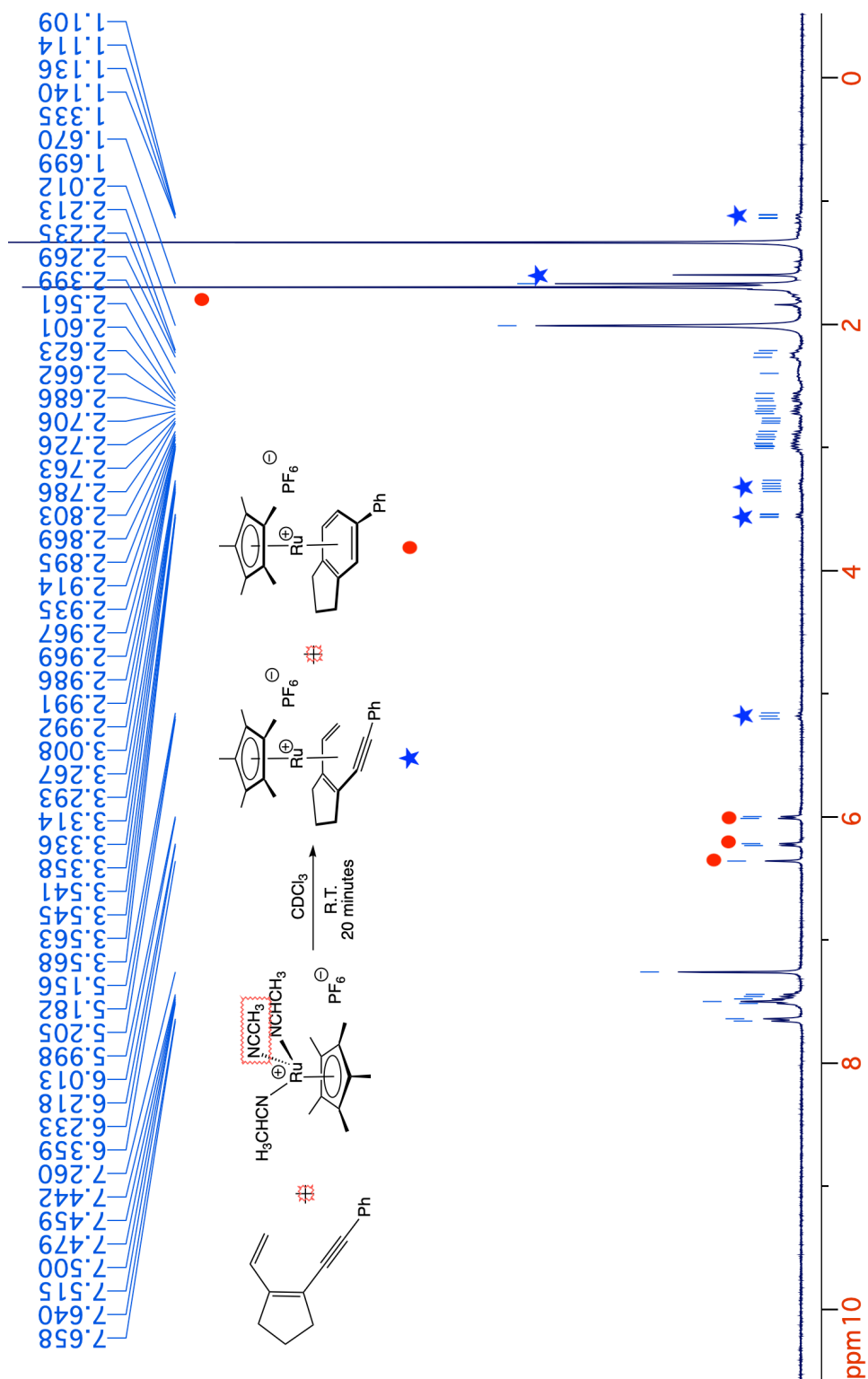
Figure 6-20. ^{1}H NMR spectrum (400 MHz, CDCl$_3$) of crude reaction mixture to form complex **33** and **34**.
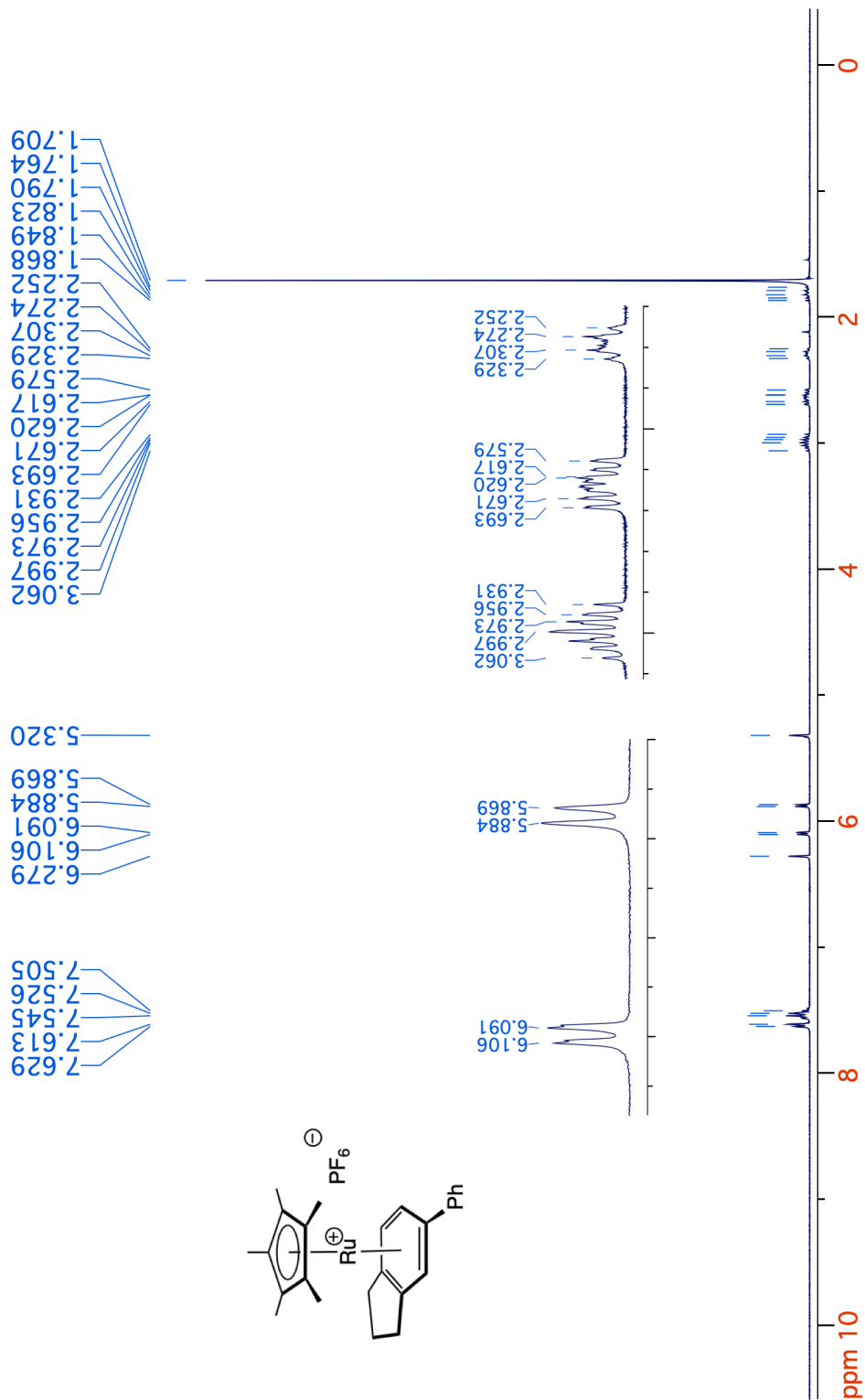
Figure 6-21. ^{1}H NMR spectrum (400 MHz, CD$_2$Cl$_2$) of **34**.
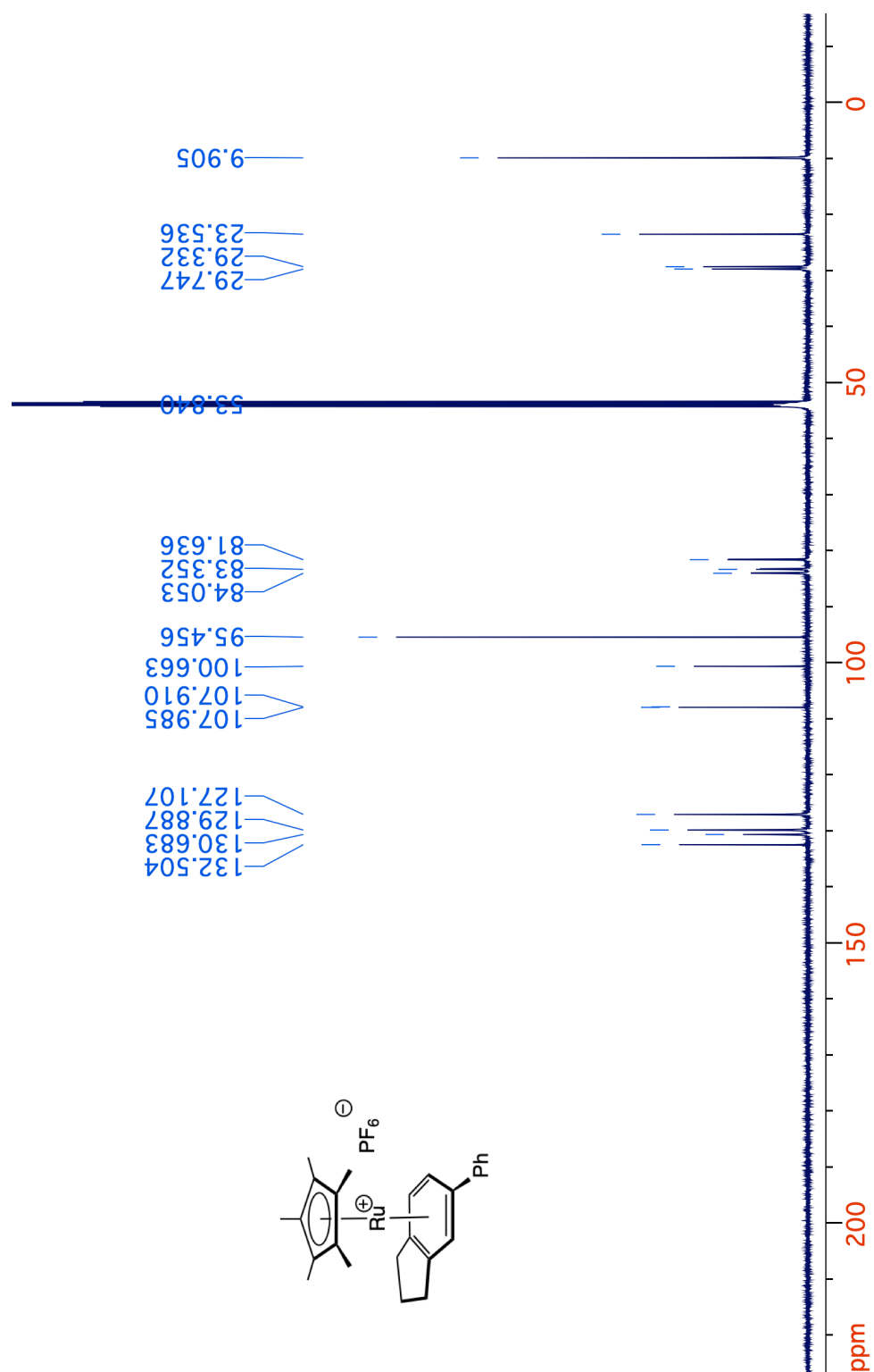
Figure 6-22. $^{13}C\{^1H\}$ NMR spectrum (125 MHz, CD_2Cl_2) of **34**.
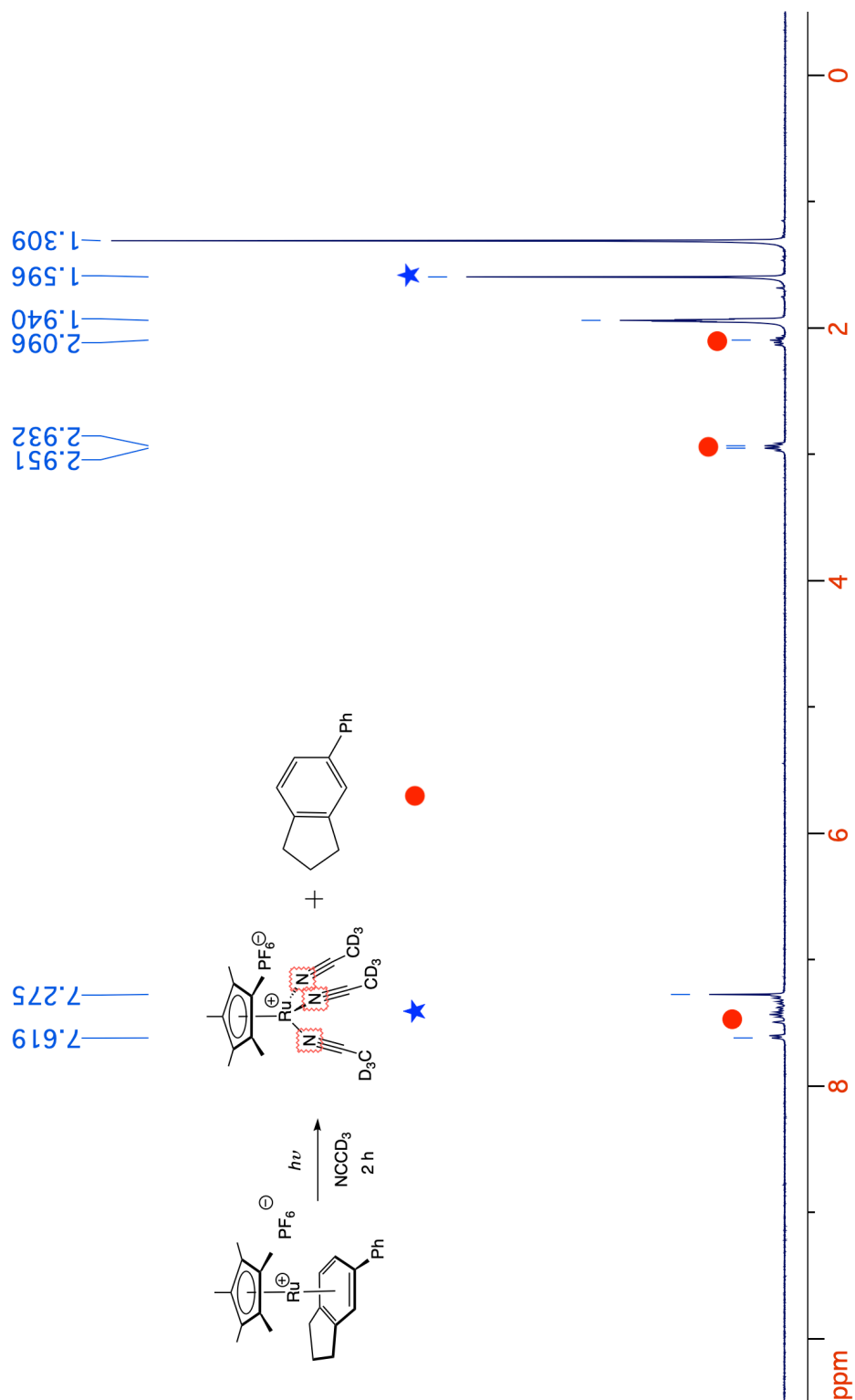
Figure 6-23. ^{1}H NMR spectrum (400 MHz, CD$_3$CN) of crude reaction mixture of photolyzing complex **34** in CD$_3$CN solvent for 2 hours.
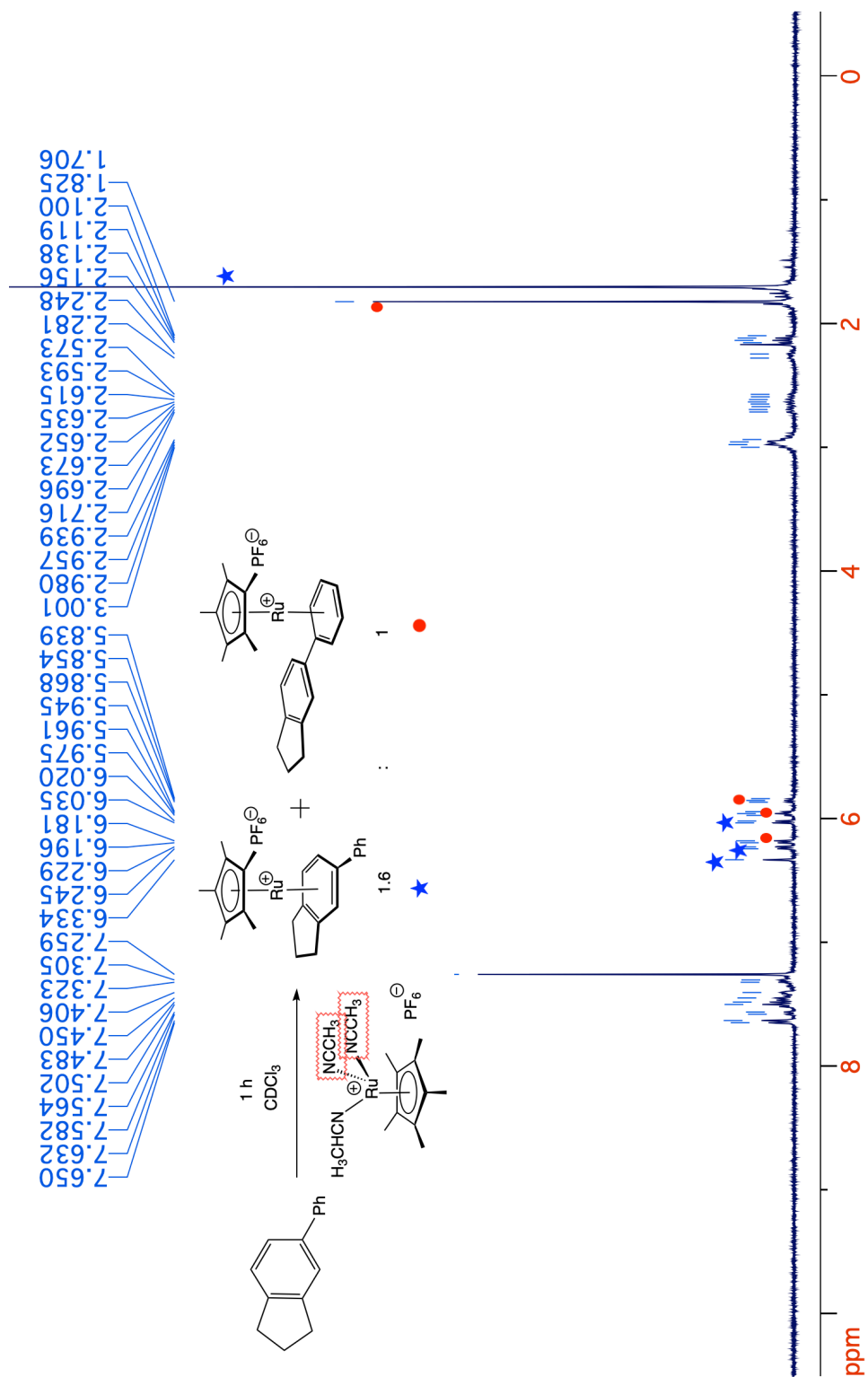
Figure 6-24. ^{1}H NMR spectrum (400 MHz, CDCl$_3$) of crude reaction mixture of forming complex **34** and **40** from arene **38**.
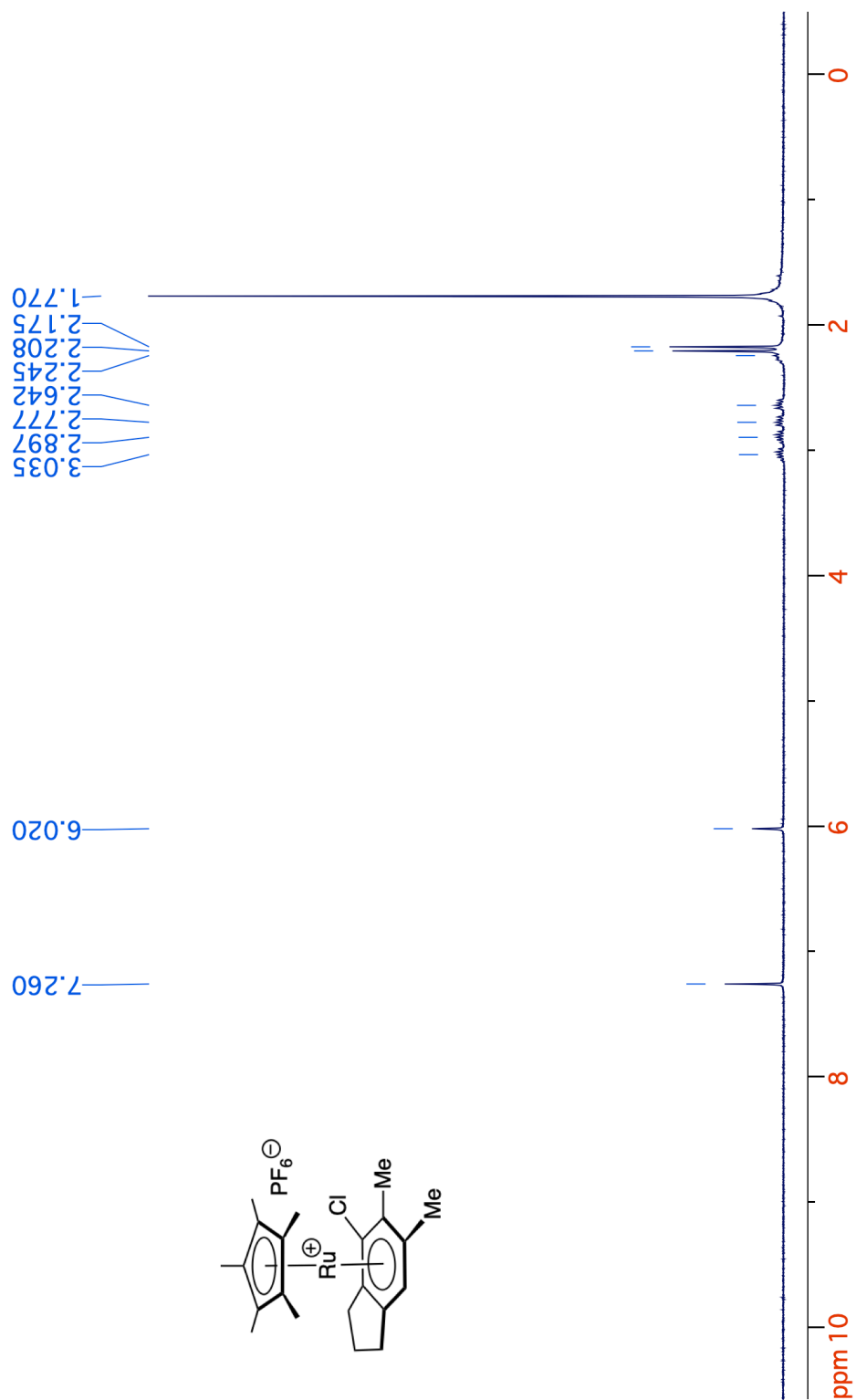
Figure 6-25. ^{1}H NMR spectrum (400 MHz, CDCl$_3$) of **48**.

595
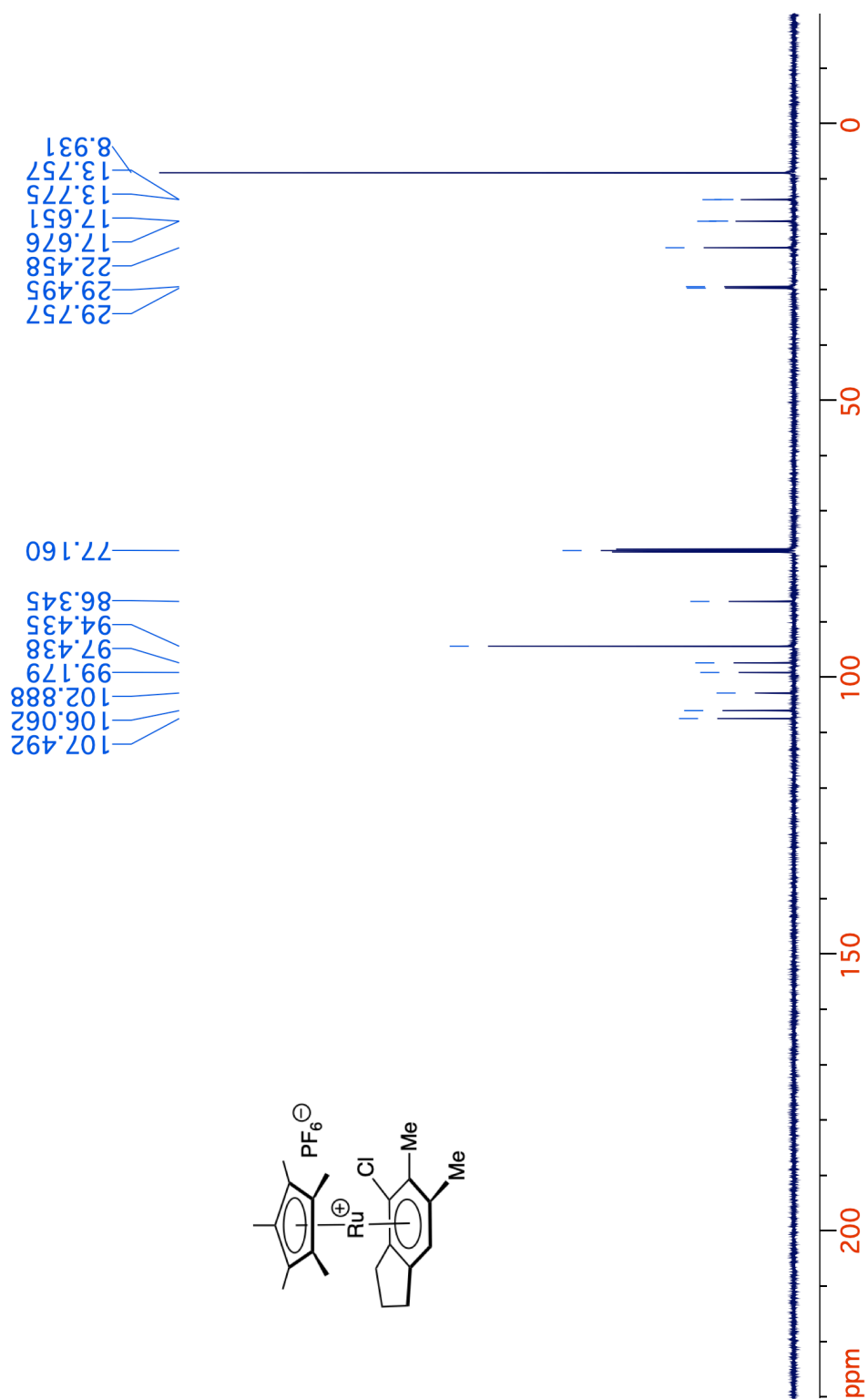
Figure 6-26. $^{13}C\{^1H\}$ NMR spectrum (125 MHz, CDCl$_3$) of **48**.

8.931
13.757
13.775
17.651
17.676
22.458
29.495
29.757

77.160

86.345
94.435
97.438
99.179
102.888
106.062
107.492
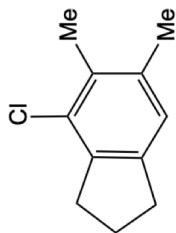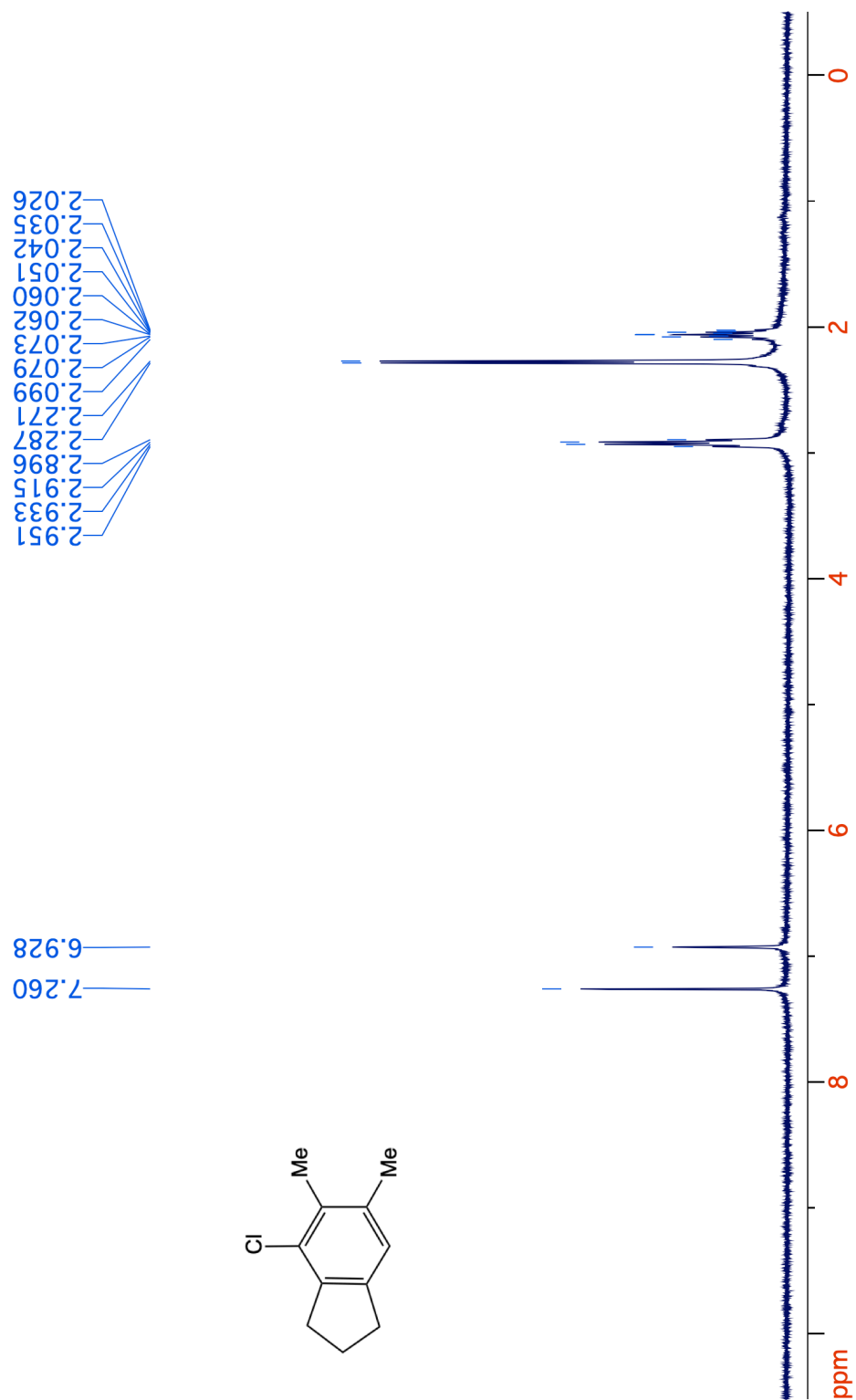
Figure 6-27. ^{1}H NMR spectrum (400 MHz, CDCl$_3$) of **53**.

2.026
2.035
2.042
2.051
2.060
2.062
2.073
2.079
2.099
2.271
2.287
2.896
2.915
2.933
2.951

6.928
7.260

16.139
21.143
24.766
32.973
33.619

77.160

124.013
131.172
131.681
136.274
140.260
142.631
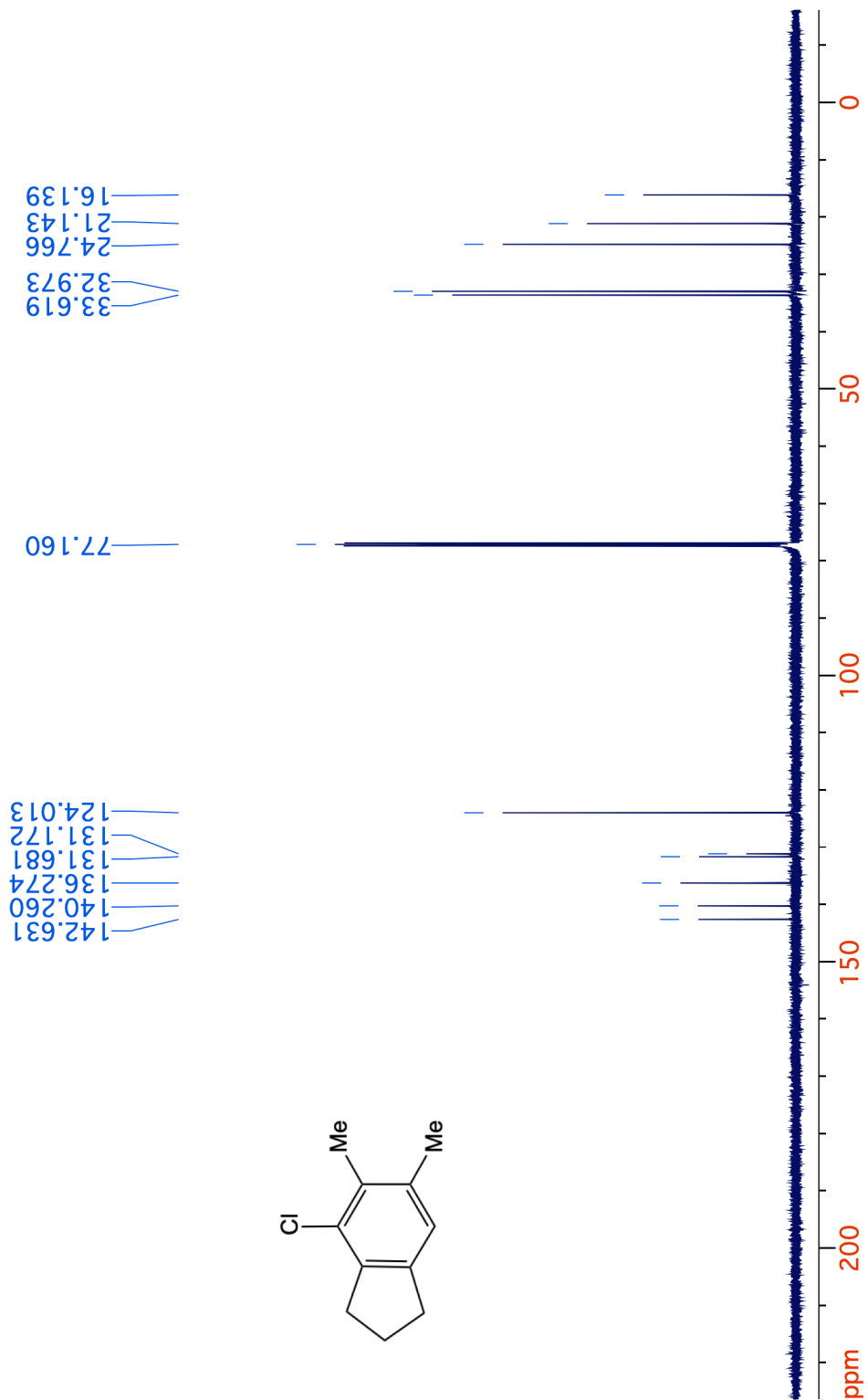
Figure 6-28. $^{13}C\{^1H\}$ NMR spectrum (125 MHz, CDCl$_3$) of **53**.

598
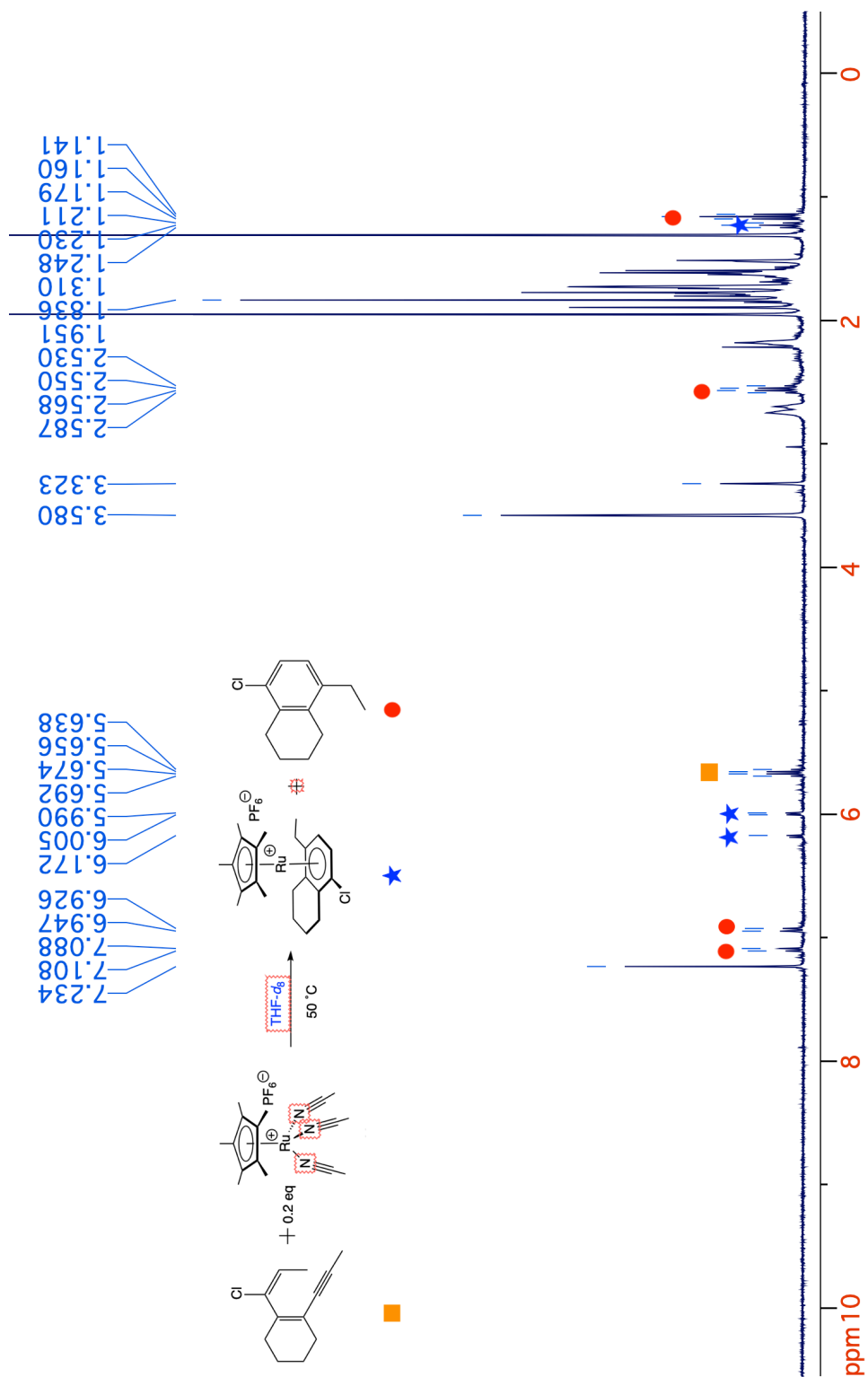
Figure 6-29. ^{1}H NMR spectrum (400 MHz, THF-d_8) of crude reaction mixture of **49** and **11** to form complex **50** and **51**.
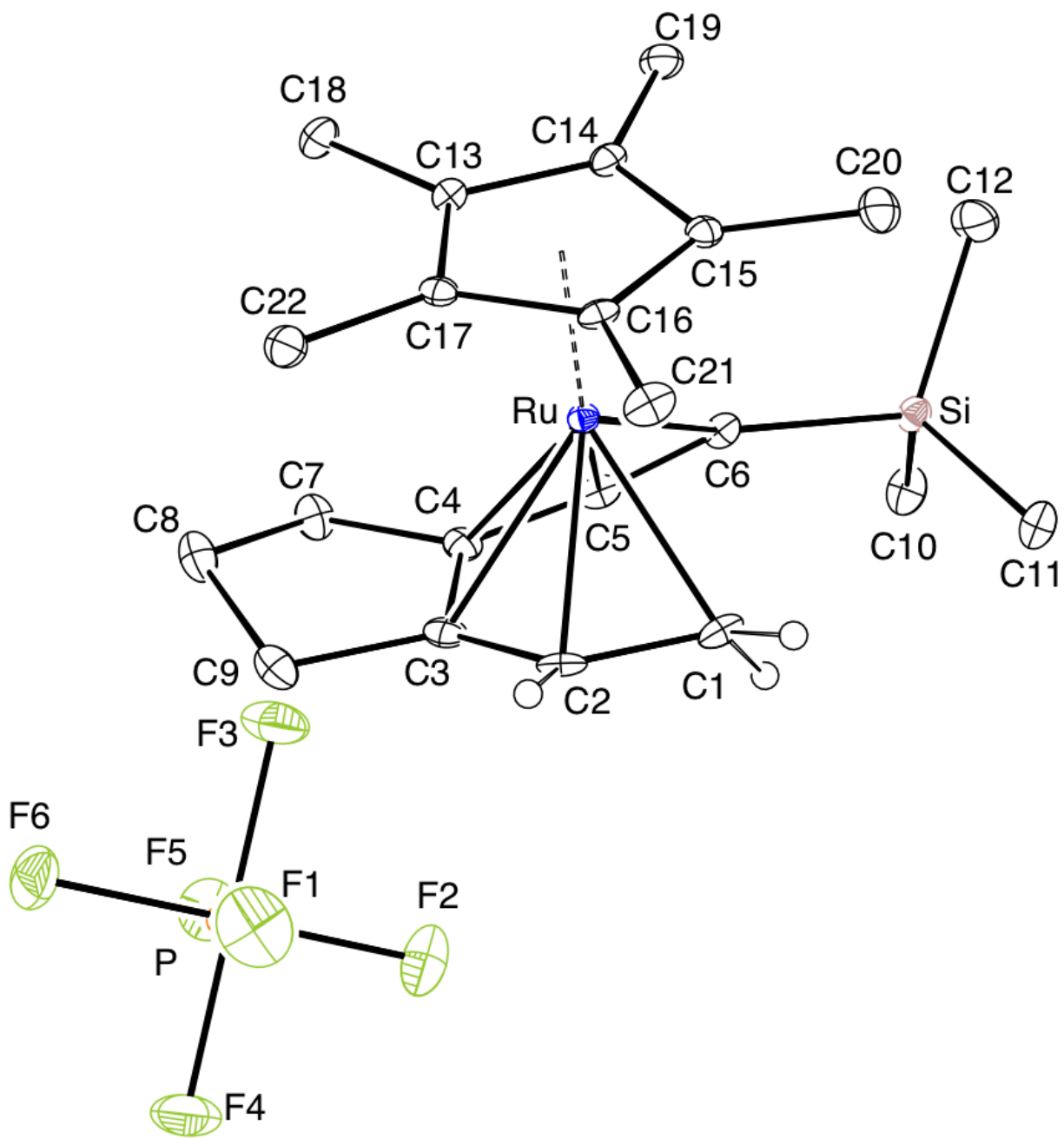
Figure 6-30. ORTEP view of complex **27**. Ellipsoids shown at 30% probability. Most hydrogens are omitted for clarity.

Table 6-10. Crystal data and structure refinement for **27**.

Identification code	pq691_f
Empirical formula	C22 H33 F6 P Ru Si
Formula weight	571.61
Temperature	100.0 K
Wavelength	0.71073 Å
Crystal system	Orthorhombic
Space group	Pca2$_1$
Unit cell dimensions	a = 16.8781(4) Å α = 90°.
	b = 8.8351(2) Å β = 90°.
	c = 16.0308(4) Å γ = 90°.
Volume	2390.51(10) Å^3
Z	4
Density (calculated)	1.588 Mg/m^3
Absorption coefficient	0.827 mm^{-1}
F(000)	1168
Crystal size	0.3 x 0.2 x 0.05 mm^3
Theta range for data collection	2.305 to 26.452°.
Index ranges	-21<=h<=21, -10<=k<=11, -20<=l<=20
Reflections collected	20404
Independent reflections	4895 [R(int) = 0.0273]
Completeness to theta = 25.242°	100.0 %
Absorption correction	None
Max. and min. transmission	0.2602 and 0.2313
Refinement method	Full-matrix least-squares on F^2
Data / restraints / parameters	4895 / 1 / 288
Goodness-of-fit on F^2	1.041
Final R indices [I>2sigma(I)]	R1 = 0.0243, wR2 = 0.0575
R indices (all data)	R1 = 0.0276, wR2 = 0.0593
Absolute structure parameter	0.016(11)
Extinction coefficient	n/a
Largest diff. peak and hole	1.463 and -0.554 e.Å^{-3}
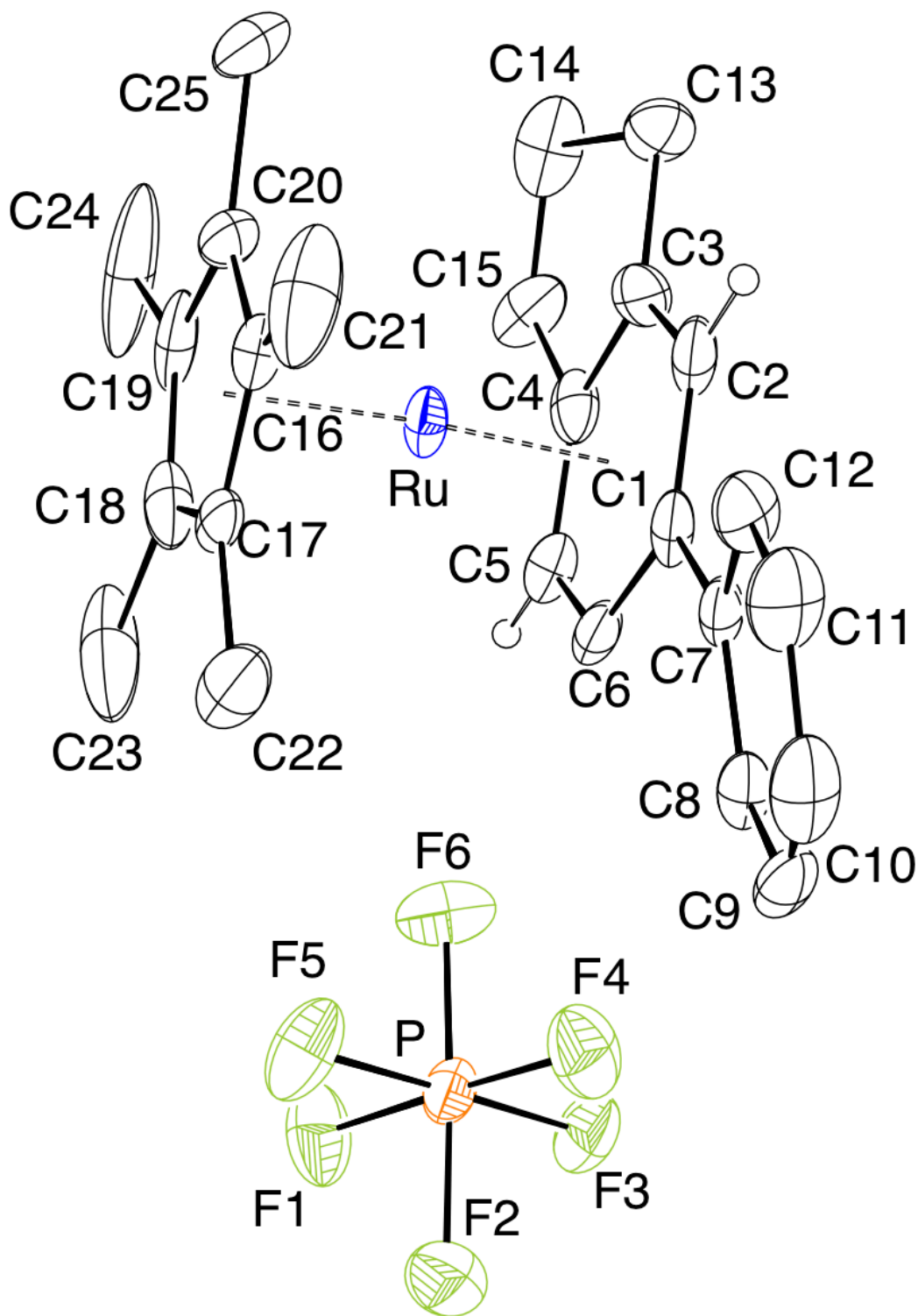
Figure 6-31. ORTEP view of complex **34**. Ellipsoids shown at 30% probability. Most hydrogens are omitted for clarity.

Table 6-11. Crystal data and structure refinement for **34**.

Identification code	pq_0693_a
Empirical formula	C25 H29 F6 P Ru
Formula weight	575.52
Temperature	100.0 K
Wavelength	0.71073 Å
Crystal system	Monoclinic
Space group	P 1 21/c 1
Unit cell dimensions	a = 7.8675(2) Å $\quad\alpha = 90°$.
	b = 17.6877(3) Å $\quad\beta = 95.7910(10)°$.
	c = 17.1052(3) Å $\quad\gamma = 90°$.
Volume	2368.18(8) Å^3
Z	4
Density (calculated)	1.614 Mg/m^3
Absorption coefficient	0.788 mm^{-1}
F(000)	1168
Crystal size	0.4 x 0.5 x 0.03 mm^3
Theta range for data collection	1.661 to 26.041°.
Index ranges	-9<=h<=6, -21<=k<=21, -21<=l<=21
Reflections collected	38826
Independent reflections	4663 [R(int) = 0.0315]
Completeness to theta = 25.242°	100.0 %
Absorption correction	None
Max. and min. transmission	0.2598 and 0.2308
Refinement method	Full-matrix least-squares on F^2
Data / restraints / parameters	4663 / 0 / 227
Goodness-of-fit on F^2	1.348
Final R indices [I>2sigma(I)]	R1 = 0.0761, wR2 = 0.1968
R indices (all data)	R1 = 0.0821, wR2 = 0.2024
Extinction coefficient	n/a
Largest diff. peak and hole	1.732 and -0.637 e.Å^{-3}
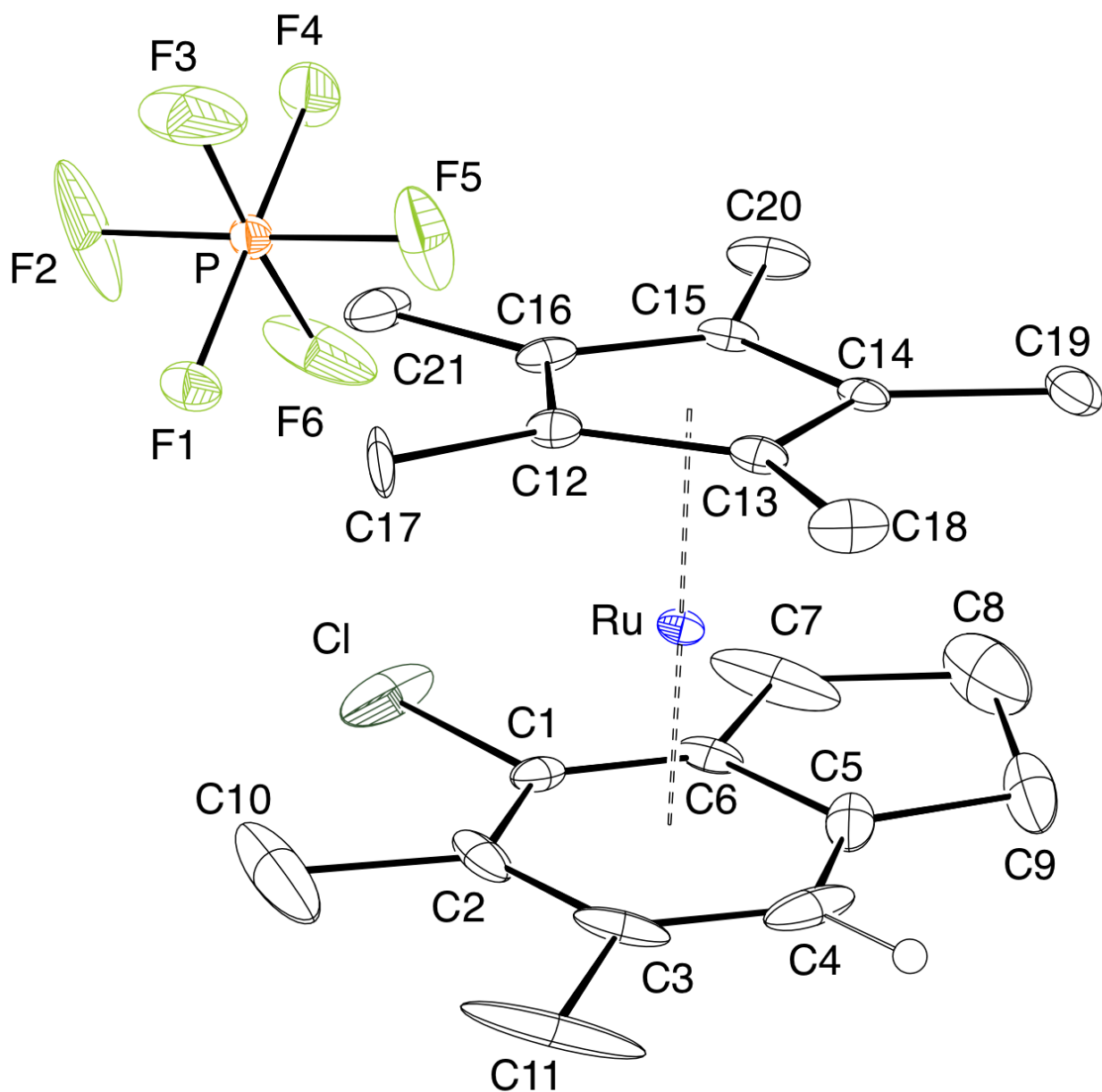
Figure 6-32. ORTEP view of complex **48**. Ellipsoids shown at 30% probability. Most hydrogens are omitted for clarity.

604

Table 6-12. Crystal data and structure refinement for **48**.

Identification code	pq500_a
Empirical formula	C3.14 H3.57 Cl0.14 F0.86 P0.14 Ru0.14
Formula weight	81.56
Temperature	100.0 K
Wavelength	0.71073 Å
Crystal system	Triclinic
Space group	P-1
Unit cell dimensions	a = 8.3847(3) Å α = 77.4680(10)°.
	b = 15.5465(6) Å β = 83.5830(10)°.
	c = 17.3235(7) Å γ = 88.4380(10)°.
Volume	2190.54(15) Å^3
Z	28
Density (calculated)	1.731 Mg/m^3
Absorption coefficient	0.969 mm^{-1}
F(000)	1148
Crystal size	0.4 x 0.3 x 0.04 mm^3
Theta range for data collection	1.211 to 26.376°.
Index ranges	-10<=h<=10, -18<=k<=19, -21<=l<=21
Reflections collected	36751
Independent reflections	8963 [R(int) = 0.0416]
Completeness to theta = 25.242°	100.0 %
Absorption correction	None
Max. and min. transmission	0.4908 and 0.4552
Refinement method	Full-matrix least-squares on F^2
Data / restraints / parameters	8963 / 0 / 571
Goodness-of-fit on F^2	1.045
Final R indices [I>2sigma(I)]	R1 = 0.0840, wR2 = 0.1685
R indices (all data)	R1 = 0.0966, wR2 = 0.1758
Extinction coefficient	n/a
Largest diff. peak and hole	6.678 and -6.641 e.Å^{-3}

Acknowledgement

Chapter 6 contains the material being prepared for the publication "Chemoselective Ruthenium-Catalyzed Cycloisomerization of Conjugated Dienynes". Qin, P.; Steger, H.; O'Connor, J. M.; Baldridge, K. K.; Cope, S. K. The dissertation author is the first author on this paper.

Chapter 6 contains the material being prepared for the publication "Ambient Temperature Aitken Cycloisomerization of Dienynes: Partitioning between Hopf and Aitken Pathways". Hitt, D. M.; Qin, P.; Steger, H.; Baldridge, K. K.; Rheingold, A. L.; O'Connor, J. M. The dissertation author is the co-author on this paper.

I. References

1. Hopf, H.; Musso, H. Preparation of Benzene by Pyrolysis of cis-and trans-1, 3-Hexadien-5-yne. *Angew. Chem. Int. Ed. Engl.* **1969**, *8*, 680-680

2. (a) Nüchter, U.; Zimmermann, G.; Francke, V.; Hopf, H. Thermal Rearrangements, 28. Competing Reaction Pathways in the Thermal Cycloisomerization of 1, 3-Hexadien-5-ynes. *Liebigs Ann./Recueil* **1997**, 1505-1515; (b) Litovitz, A. E.; Carpenter, B. K.; Hopf, H. Computational investigation of the reactivity of a hexadienyne derivative. *Org. Lett.* **2005**, *7*, 507-510; (c) Hopf, H.; Berger, H.; Zimmermann, G.; Nüchter, U.; Jones, P. G.; Dix, J. Formation of Isobenzenes by Thermal Isomerization of 1, 3-hexadiene-5-yne Derivatives. *Angew. Chem. Int. Ed. Engl.* **1997**, *36*, 1187-1190; (d) Christl, M.; Braun, M.; Müller, G. 1, 2, 4-Cyclohexatriene, an Isobenzene, and Bicyclo [4.4. 0] deca-1, 3, 5, 7, 8-pentaene, an Isonaphthalene: Generation and Trapping Reactions. *Angew. Chem. Int. Ed. Engl.* **1992**, *3*, 473-476.

3. For reviews on dienyne cyclization, see: (a) Zimmermann, G. Cycloaromatization of Open and Masked 1, 3-Hexadien-5-ynes- Mechanistic and Synthetic Aspects. *Eur. J. Org. Chem.* **2001**, 457-471; (b) Hitt, D. M.; O'Connor, J. M. Acceleration of conjugated dienyne cycloaromatization. *Chem. Rev.* **2011**, *111*, 7904-7922; (c) Aguilar, E.; Sanz, R.; Fernández-Rodríguez, M.; García-García, P. 1, 3-Dien-5-ynes: Versatile Building

Blocks for the Synthesis of Carbo-and Heterocycles. *Chem. Rev.* **2016**, *116*, 8256-8311.

4. (a) Mainetti, E.; Mouriès, V.; Fensterbank, L.; Malacria, M.; Marco-Contelles, J. The Effect of a Hydroxy Protecting Group on the PtCl$_2$-Catalyzed Cyclization of Dienynes—A Novel, Efficient, and Selective Synthesis of Carbocycles. *Angew. Chem. Int. Ed. Engl.* **2002,** *41*, 2132-2135. (b) Morris, C. L.; Hu, Y.; Head, G. D.; Brown, L. J.; Whittingham, W. G.; Brown, R. C. Oxidative cyclization reactions of trienes and dienynes: Total synthesis of membrarollin. *J. Org. Chem.* **2009**, *74*, 981-988. (c) Meyer, F. E.; Parsons, P. J.; De Meijere, A. Palladium-catalyzed polycyclization of dienynes: surprisingly facile formation of tetracyclic systems containing a three-membered ring. *J. Org. Chem.* **1991**, *56*, 6487-6488.

5. García-García, P.; Fernández-Rodríguez, M. A.; Aguilar, E. Gold-Catalyzed Cycloaromatization of 2, 4-Dien-6-yne Carboxylic Acids: Synthesis of 2, 3-Disubstituted Phenols and Unsymmetrical Bi-and Terphenyls. *Angew. Chem. Int. Ed. Engl.* **2009**, *48*, 5534-5537.

6. Rong, M. G.; Qin, T. Z.; Liu, X. R.; Wang, H. F.; Zi, W. De Novo Synthesis of Phenols and Naphthols through Oxidative Cycloaromatization of Dienynes. *Org. Lett.* 2018, *20*, 6289-6293.

7. O'Connor, J. M.; Friese, S. J.; Rodgers, B. L.; Rheingold, A. L.; Zakharov, L. An η^6-dienyne transition-metal complex. *J. Am. Chem. Soc.* **2005**, *127*, 9346-9347.

8. Hitt, D. M.; Holland, R. L.; Baldridge, K. K.; Cope, S. K.; O'Connor, J. M. Stereoselective Formation of η^6-Arene Ruthenium (II) Complexes via Metal-Triggered Bergman and Hopf Cycloaromatizations. *Organometallics* **2017**, *36*, 4256-4267.

10. Kulsomphob, V.; Turpin, G. C.; Lam, K-C.; Youngkin, C.; Trakarnpruk, W.; Carroll, P.; Rheingold, A. L.; Ernst, R. D. Incorporation of phenyl-substituted pentadienyl ligands in (pentamethylcyclopentadienyl) ruthenium complexes. *J. Chem. Soc., Dalton Trans*. **2000**, 3086-3093.

11. Hillard III, R. L.; Vollhardt, K. P. C. Substituted benzocyclobutenes, indans, and tetralins via cobalt-catalyzed cooligomerization of. Alpha., omega.-diynes with substituted acetylenes. Formation and synthetic utility of trimethylsilylated benzocycloalkenes. *J. Am. Chem. Soc.* **1977**, *99*, 4058-4069.

12. Makhoul, R.; Shaw-Taberlet, J. A.; Sahnoune, H.; Dorcet, V.; Kahlal, S.; Halet, J-F.; Hamon J-R.; Lapinte, C. Complexation of the (η^5-Cp) Ru+ and (η^5-Cp*) Ru$^+$ Arenophiles on Alkynylnaphthalene: Solvent Effect on the Regioselectivity and the Haptotropic Rearrangement. *Organometallics* **2014**, 33, 6023-6032.

13. Hirano, M.; Sakate, Y.; Inoue, H.; Arai, Y.; Komine, N.; Komiya, S.; Wang, X.; Bennett, M. A. Synthesis of conjugated diene complexes of ruthenium (0) derived from

Ru (η^6-naphthalene)(η^4-1,5-COD): Z to E isomerisation of coordinated 1,3-pentadiene. *J. Organomet. Chem.* **2012**, *708*, 46-57.

14. Hitt, M.D. Doctoral Dissertation, Investigations into Novel Modes of Reactivity and Stereoselectivity for the Cycloaromatization of Conjugated Enediynes and Dienynes. University of California, San Diego, CA, USA, **2011**.

CHAPTER 7

Hydrochloric Acid Incorporated Cycloaromatization of Conjugated Enediyne

A. Introduction.

In 1972, Bergman and coworkers reported a self-annulation process of enediyne at high temperature to generate aromatics.[1] They proposed that upon heating enediyne **1**, it can cyclize to form a benzene diradical intermediate **2**, which subsequently abstracts two hydrogen atoms from surrounding hydrogen atom donor to produce benzene (Scheme 7-1). Since then, cycloaromatization of enediynes has been vastly investigated both on the novel mechanism and the potential application to assemble new arenes for organic synthesis. Later on, this the fascinating cyclization mode has also been furtherly explored with directly incorporation of reactive functionality into the arene products by changing different atom donors and reaction conditions.[2,3]
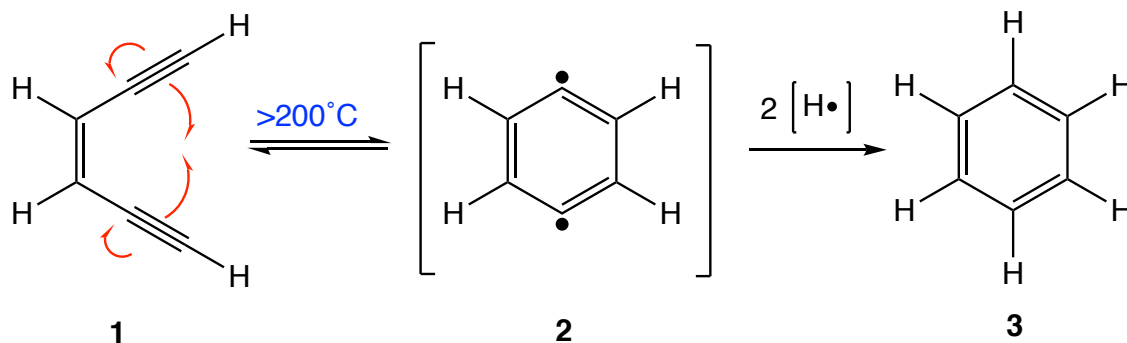
Scheme 7-1. Thermal cycloaromatization of **1**.

However, due to the wild reaction conditions, severe decomposition and/or polymerization of the enediyne starting materials at high temperature can be problematic. In order to lower down the activation barrier of cyclization, O'Connor group discovered that $[(\eta^5\text{-}C_5Me_5)Ru(NCMe)_3]PF_6$ (**6**) can trigger the cycloaromatization of the

acyclic dimethyl substituted enediynes **4** and **5** in CDCl$_3$ at ambient temperature in the presence of cyclohexadiene as hydrogen atom donor to produce ruthenium-η^6-arene products **7** and **8**, respectively (Scheme 7-2).[4,5]
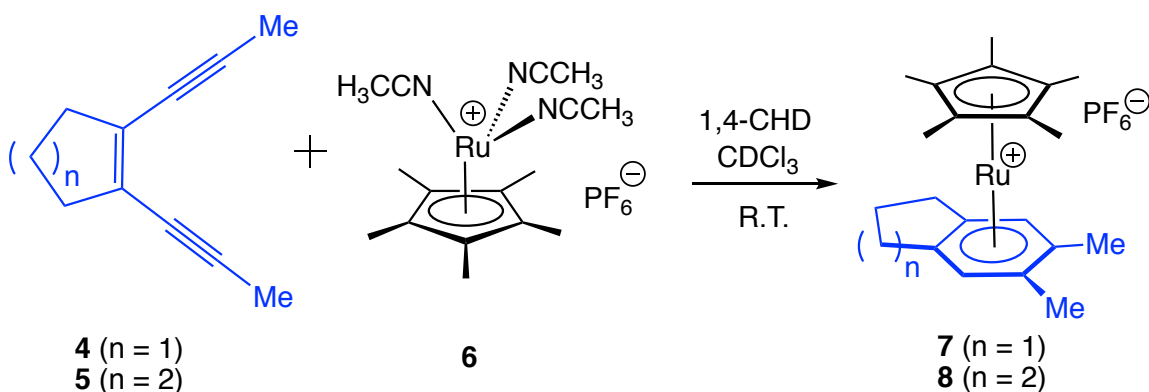
Scheme 7-2. Ruthenium triggered cycloaromatization of enediynes **4** and **5**.

For a comparison, a thermal cyclization of the same enediyne **5** was carried out in CDCl$_3$ without addition of metal complex. However, instead of formation of regular Bergman type product **10**, an unprecedented cyclization mode was discovered to generate the chlorine incorporated arene product **9** (Scheme 7-3). This reaction was firstly explored by previous graduate student Hitt and Cope,[6,7] and then I took part into this project to optimize the reaction yields, purify and characterize products, and conduct some mechanistic studies.
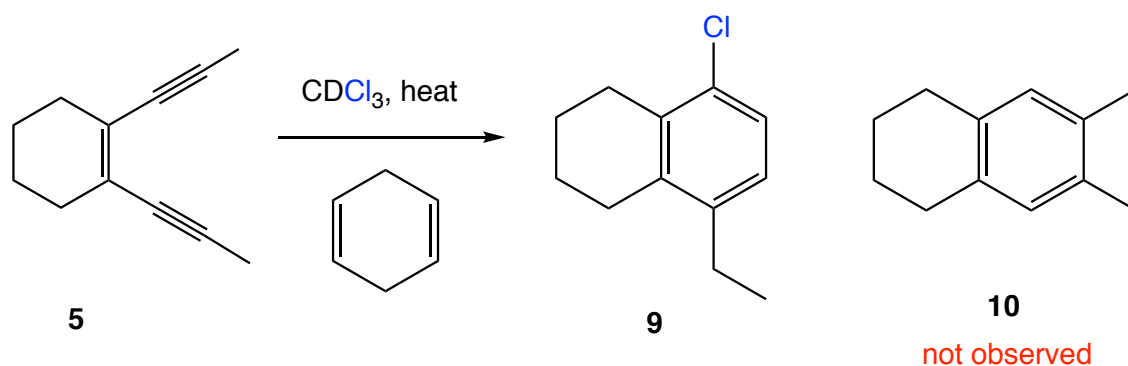
Scheme 7-3. Cycloaromatization of **5** in chloroform with 1,4-CHD.

B. Cycloaromatization of Enediyne in CDCl₃ with 1,4-CHD

In order to explore the best yields of this reaction, firstly, I repeated an NMR scale thermal reaction of enediyne **5**. A chloroform-*d* solution of enediyne (5.1 mg, 0.032 mmol) and 1,4-CHD (21.7 mg, 0.272 mmol) was added into a 5 mm medium-wall NMR tube with 1,3,5-tri-*tert*-butylbenzene as internal standard. After freeze-pump-thaw degas for 3 times, the NMR tube was sealed by propane flame, and then the reaction mixture was heated at 165 °C and monitored by ^{1}H NMR spectroscopy (Scheme 7-4). After 96 hours, all the starting enediyne 5 was consumed, and 86.5% NMR yield of compound **9** was observed based on the characteristic resonances at δ 1.19 ppm (t, 3H, *J* = 7.6 Hz, Me), 2.57 (q, 2H, *J* = 7.6 Hz, C*H₂*CH₃), 6.95 (d, 1H, *J* = 8.4 Hz, Ar), and 7.16 (d, 1H, *J* = 8.4 Hz, Ar). A 7.7% NMR yield of minor product **11** was detected based on the characteristic resonances at δ 2.26 ppm (s, 3H, Me), 2.31 (s, 3H, Me) and 6.81 (s, 1H, Ar). In addition, 1.2 equivalents (relative to the formation of compound **9**) of CHDCl₂ was observed at δ 5.29 ppm (t, J_{HD} = 1.2 Hz). Furthermore, the presence of HCl in the

612

reaction mixture was demonstrated by previous lab member Veccharelli via utilizing

proton sponge in a separate NMR reaction.[8]
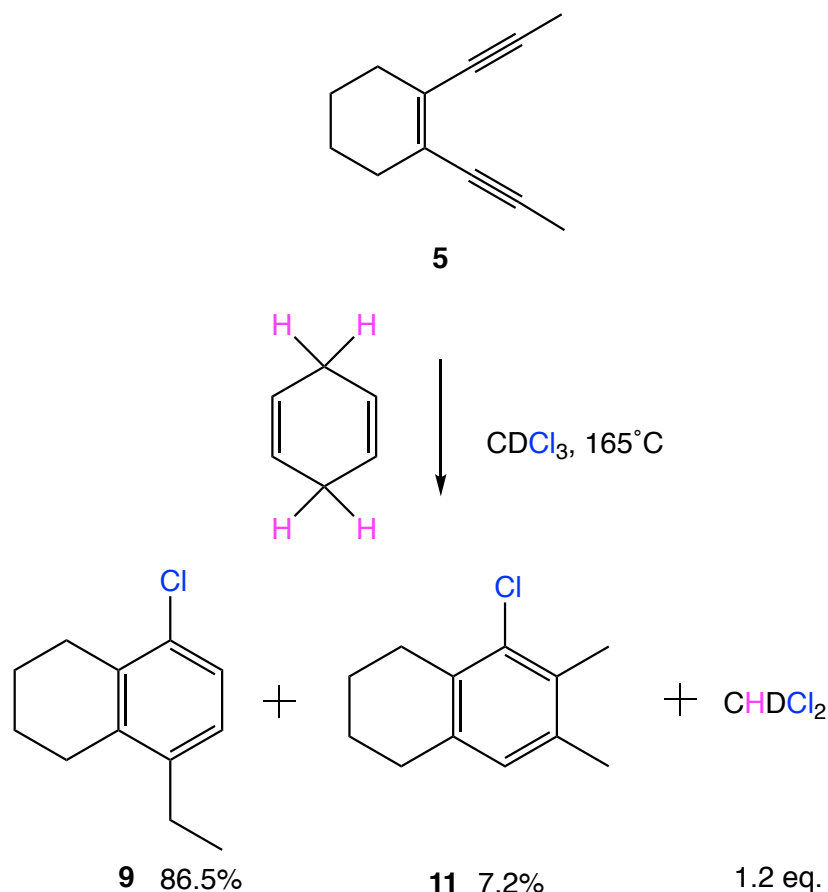
Scheme 7-4. NMR-tube thermal reaction of enediyne **5**.

Two possible mechanisms were proposed for the formation of HCl and $CHDCl_2$.

In mechanism A, trace amount of impurities in the chloroform solvent can generate

small amount of radical **12**,[9,10] which behaves as initiator for the followed radical-chain

mechanism to abstract a hydrogen atom from the 1,4-cyclohexadiene to produce the

cyclohexadienyl radical **13** (Scheme 7-5). Hydrochloric acid can be subsequently

assembled by the hydrogen atom from radical **13** and chlorine atom from CDCl$_3$, with the regeneration of radical intermediate **12**.
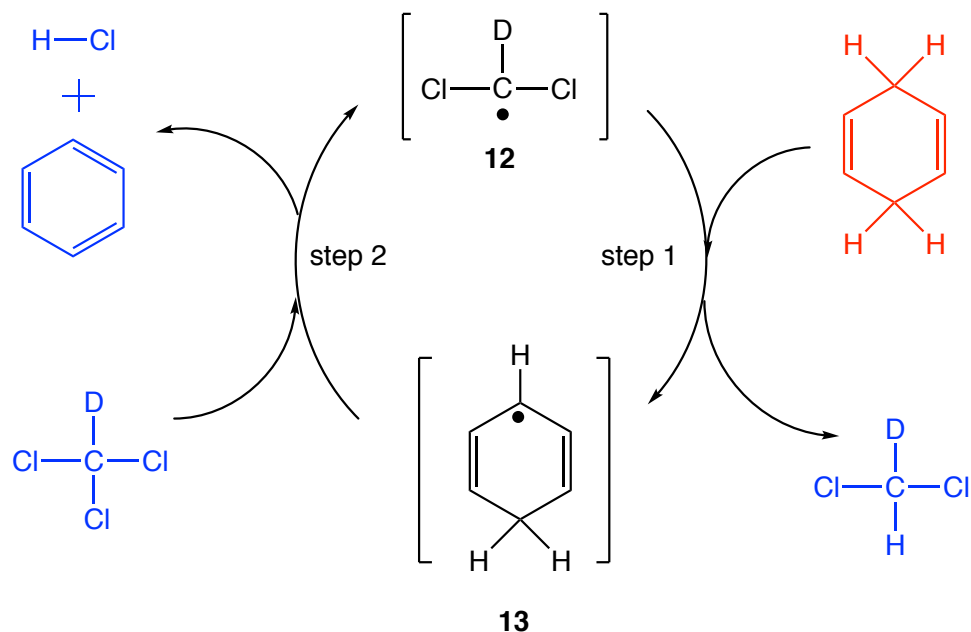
Scheme 7-5. Proposed mechanism A for the formation of HCl.

Alternatively, in mechanism B, after the formation of cyclohexadienyl radical **13**, it could directly abstract a chlorine atom from the solvent to produce the chlorine incorporated cyclohexadiene intermediate **14** and/or **15**, with the formation of dichloromethyl radical **12**. A subsequent elimination of HCl from **14/15** gives the HCl and benzene (Scheme 7-6).
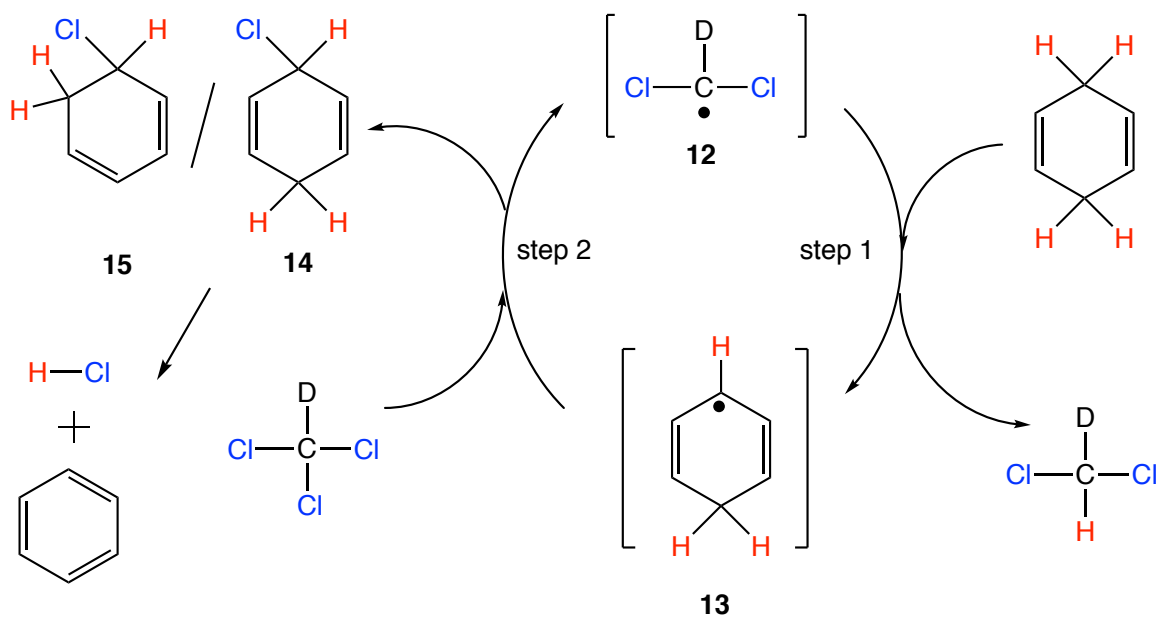
Scheme 7-6. Proposed mechanism B for the formation of HCl.

In order to examine the validity of the two possible mechanisms, a computational study was carried out by Professor Kim Baldridge (Figure 7-1). The result shows that both transition states TS-p$_{3.2}$ and TS-o$_{3.2}$ to form cyclohexadiene **14** and **15** are around 6 kcal/mol higher than the transition state TS$_{2.2}$ in mechanism A, and thus mechanism A should be more reasonable due to the lower activation barrier.
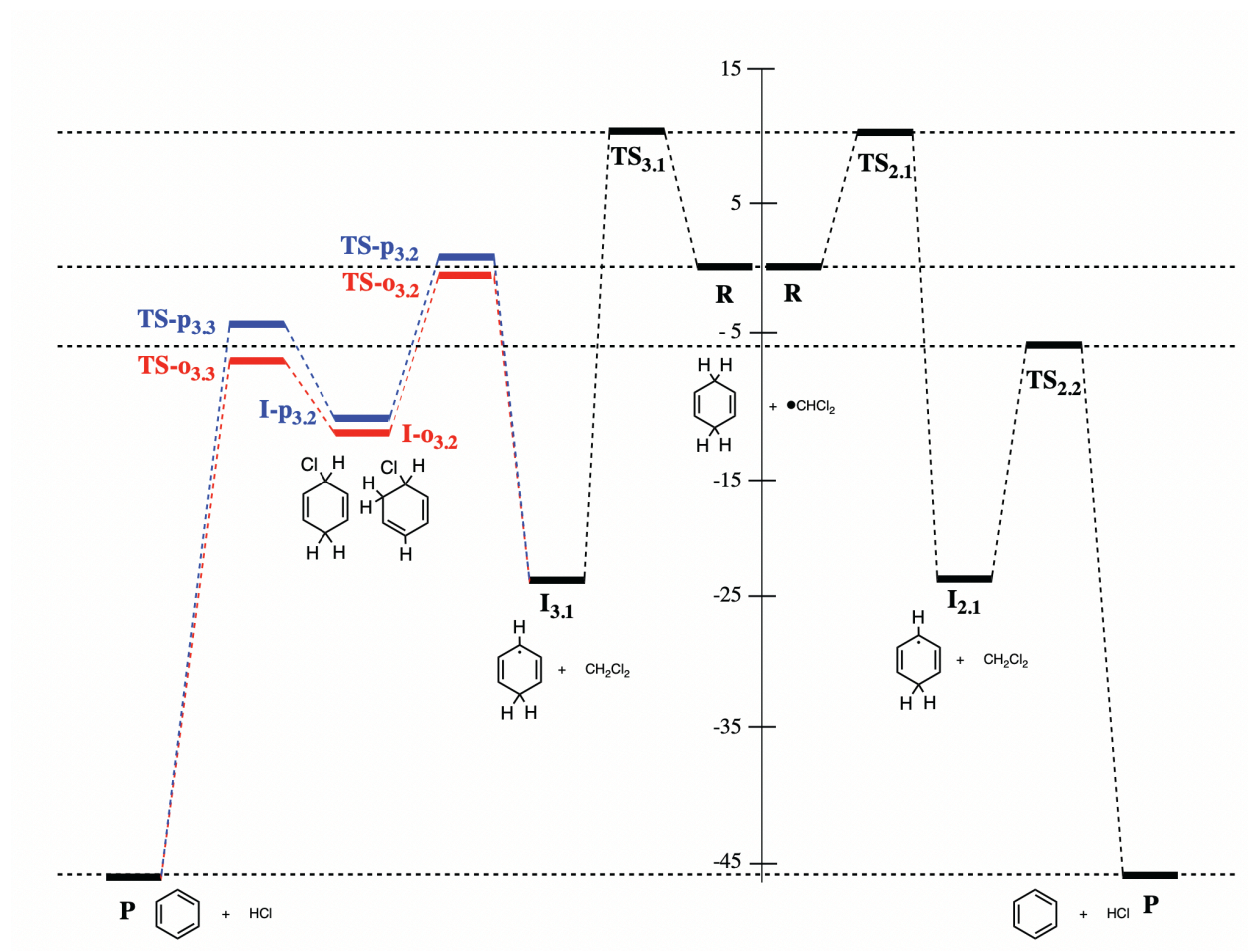
Figure 7-1. Computational studies of mechanisms A and B.

An alternate mechanism to form the arene product **9** without generation of HCl could be that radical **13** reacts with enediyne substrate **5** to produce the vinyl radical intermediate **16**, that is followed by an abstraction of chlorine atom from the solvent to give vinyl chloride **17** and dichloromethyl radical **12** without any generation of HCl (Scheme 7-7). The vinyl chloride **17** can subsequently cycloaromatize to form the arene product **9** (vide infra). However, this mechanism was excluded by the following three NMR tube reactions (Scheme 7-8): a) heating up the mixture of enediyne **5** with 1,4-CHD in the presence of azobisisobutyronitrile (AIBN) in C_6D_6 solvent at 165 °C for 42

days only gives 45% yield of the Bergman type arene product **10**; b) after heating enediyne **5** with AIBN in 1,4-CHD as solvent for 19 days, arene **10** was also the only observed product; c) mixture of enediyne **5** and AIBN was heated in THF-d_8 solvent at 165 °C, which produced **10**-d_2 as the only product after 24 days. If the proposed mechanism is valid, it is expected that arene molecule **18** should be observed as the major product, however, there is no evidence for any formation of **18** in any of these three reactions.
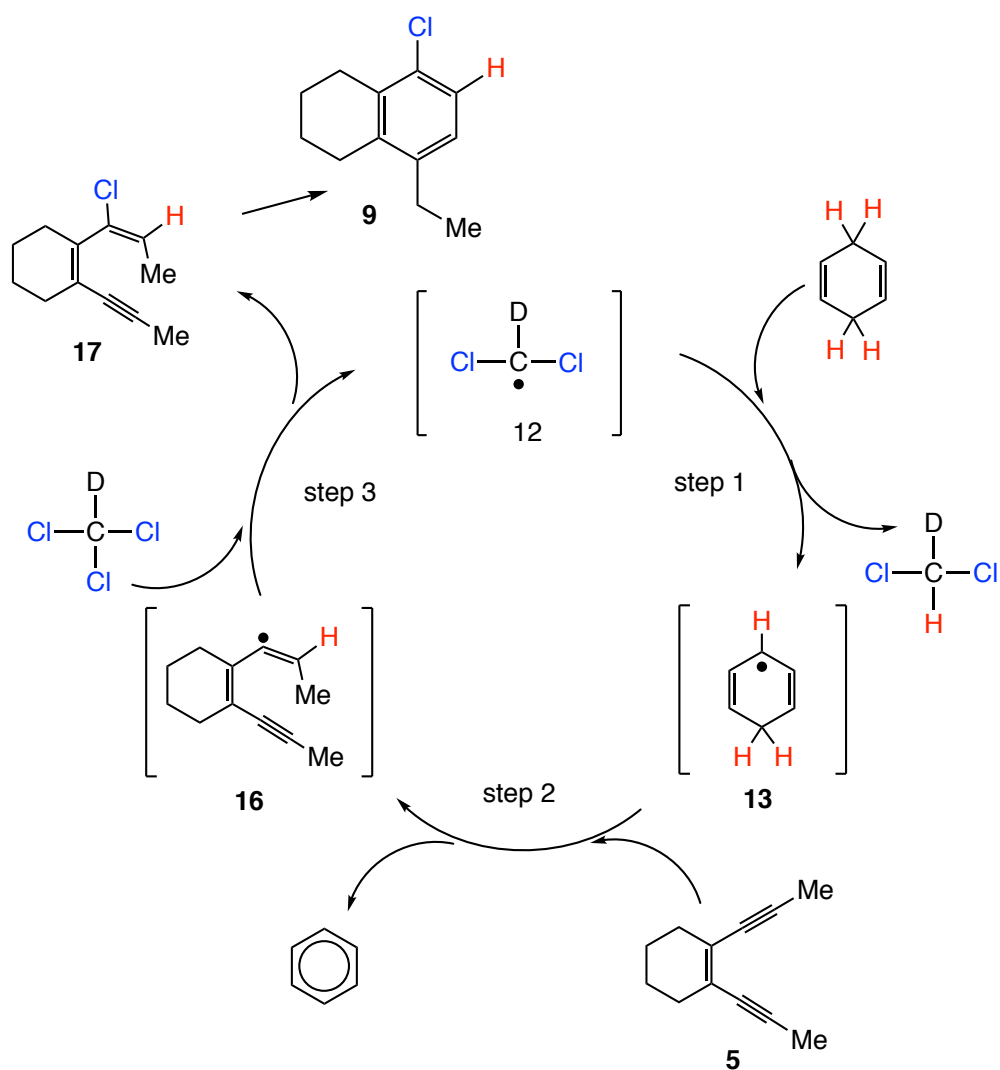
Scheme 7-7. An alternative mechanism without formation of HCl.
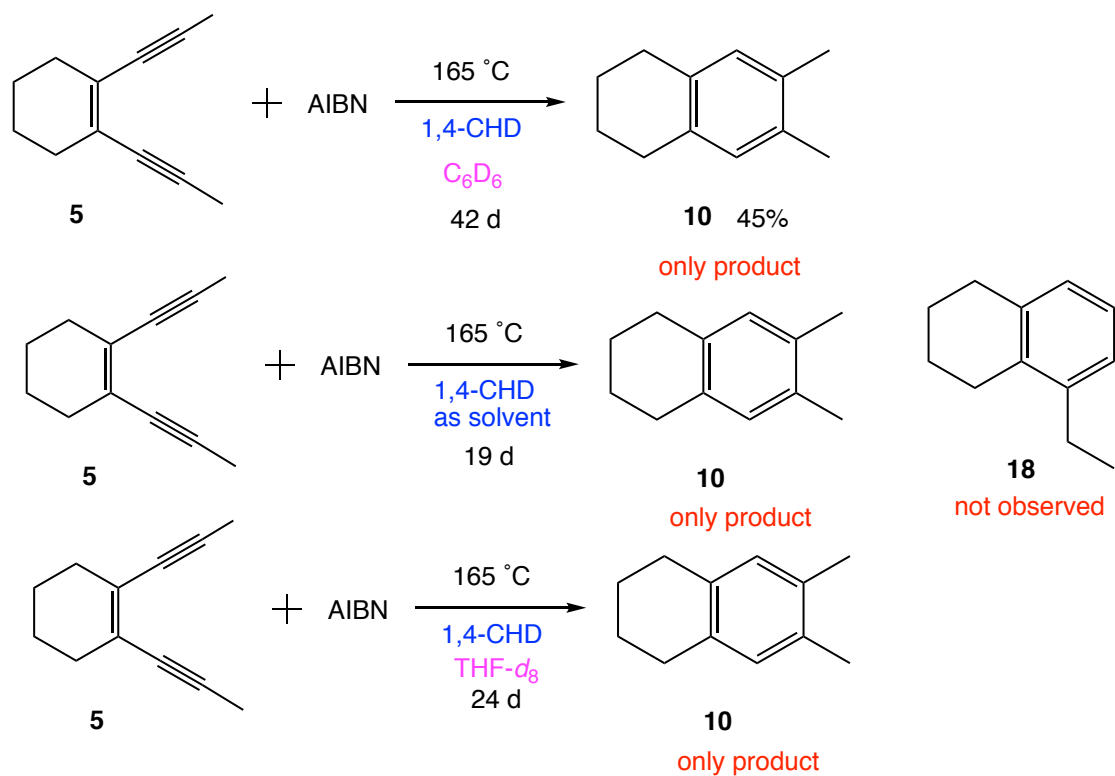
Scheme 7-8. Thermal reaction of 5 under various conditions.

In addition, the intermediacy of HCl in the cyclization process was furtherly demonstrated by a separate NMR tube reaction, in which HCl was added as reagent with enediyne **5** in the absence of 1,4-CHD in chloroform solvent. After heating the reaction mixture at 165 °C for 4 days, similar result was obtained with a 83 : 17 ratio of arene products **9** and **17** (Scheme 7-9).
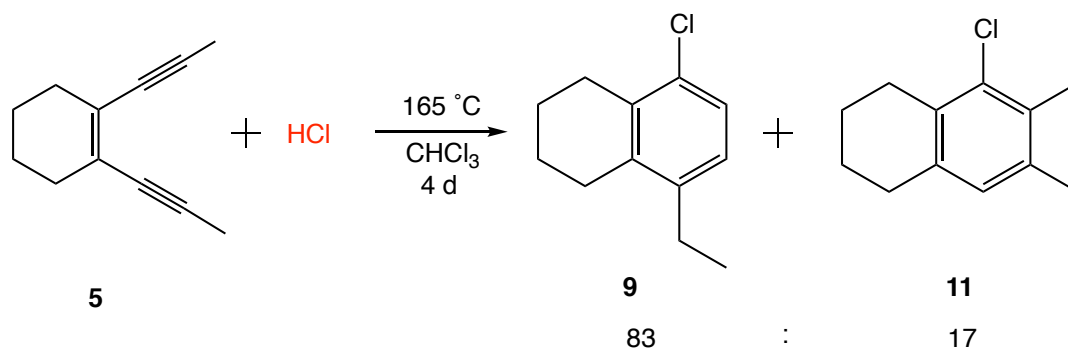
Scheme 7-9. Thermal reaction of enediyne **5** with HCl.

Besides utilizing chloroform as the halogen source, we also examined the reactivities of other haloalkanes towards 1,4-CHD. When (bromomethyl)benzene (**19**), bromocyclohexane (**20**), and 1-bromo-3-methylbutane (**21**) was treated with excess of 1,4-CHD (4 – 6 equivalents) in the presence of 0.6 equivalents of AIBN at 165 °C in a flame-sealed NMR tube for 20 – 48 hours, it was found only the activated haloalkane **19** produce 82% yield of the desired toluene product, while no reaction was observed for **20** or **21** (Scheme 7-10).
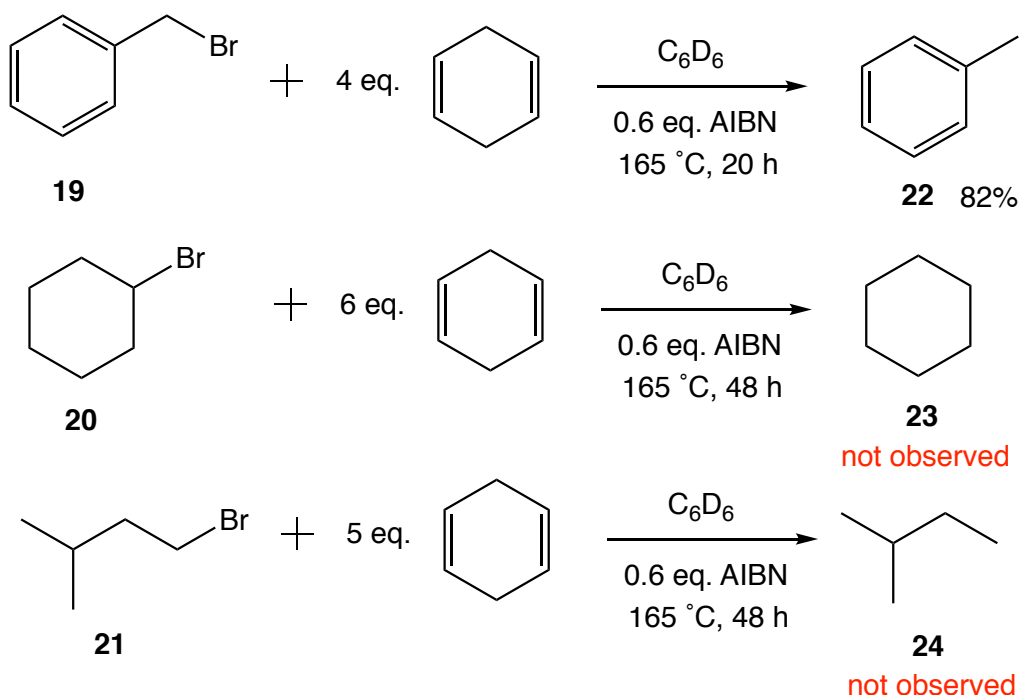
Scheme 7-10. Various haloalkanes reacting with 1,4-CHD.

C. Formation and Cyclization of Vinyl Chloride

The reactivity of enediyne **5** with hydrochloric acid was also examined. 440 mg (2.78 mmol) of enediyne substrate **5** was treated with HCl (2.8 mmol, 2 M in Et$_2$O) in dry chloroform (20 mL) under inert atmosphere, and the reaction mixture was monitored by TLC analysis. After 9 days at ambient temperature, all the starting enediyne was consumed, and then the reaction mixture was subjected to aqueous work up and chromatography on silica gel to give compound **17**-*E* as a clear oil with 85% yield (Scheme 7-11).
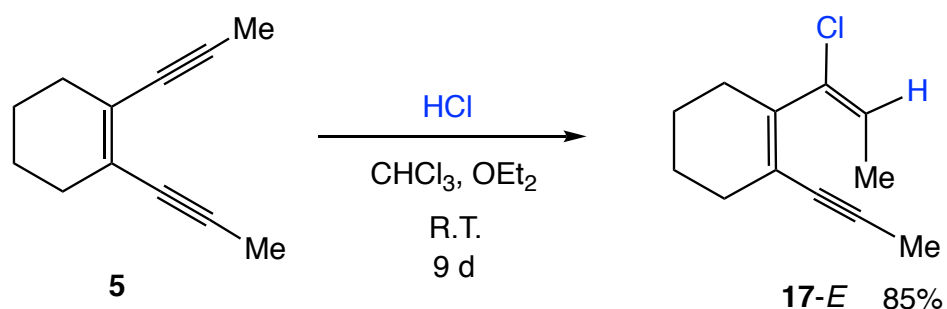
Scheme 7-11. Reaction of **5** with HCl.

It is interesting to notice that the reaction has very high regio-and stereoselectivity. Addition of HCl only occurs on one of the acetylenes even when excess of acid is loaded, and **17**-*E* was obtained exclusively without any evidence for the formation of the *Z* isomer. Some other reaction conditions have been attempted with enediyne **5** and HCl to make the *Z* isomer, such as addition of radical initiator, changing temperature, and adding other mineral acid (Table 7-1). However, none of these reactions produce any of *Z* isomer. An interesting scenario is the reaction in the presence of H_2SO_4, which gives 87.5% isolated yield of **17**-*E* within 5 hours, and thus provides a more ideal synthetic route towards the vinyl chloride.

Table 7-1. Reaction of enediyne **5** with HCl under various reaction conditions.

acid used	other reagents, solvent and temperature	product
HCl in Et_2O	$CHCl_3$, R.T.	only **17**-*E*
HCl in Et_2O	AIBN, $CDCl_3/CHCl_3$, R.T.	only **17**-*E*
HCl in Et_2O	AIBN, 1,4-CHD, $CDCl_3$, 70 °C	only **17**-*E*
HCl in Et_2O	$CHCl_3$, 70 °C	only **17**-*E*
HCl in Et_2O	H_2O_2 (30% in H_2O), $CDCl_3$	only **17**-*E*
aqueous HCl	concentrated H_2SO_4, $CHCl_3$	only **17**-*E*

The vinyl chloride **17**-*E* (300 mg, 1.54 mmol) was subsequently heated at 165 °C in chloroform under nitrogen, and the reaction mixture was monitored by ^{1}H NMR spectroscopy. After 60 hours, the resulting solution was concentrated, and the followed chromatography on silica gel afforded arene product **9** as a clear oil with 96.3% yield (Scheme 7-12). There is no evidence for the formation of the minor product **11** that was observed in the thermal reaction of enediyne **5**.

17-*E*   **9** 96.3%   **11**
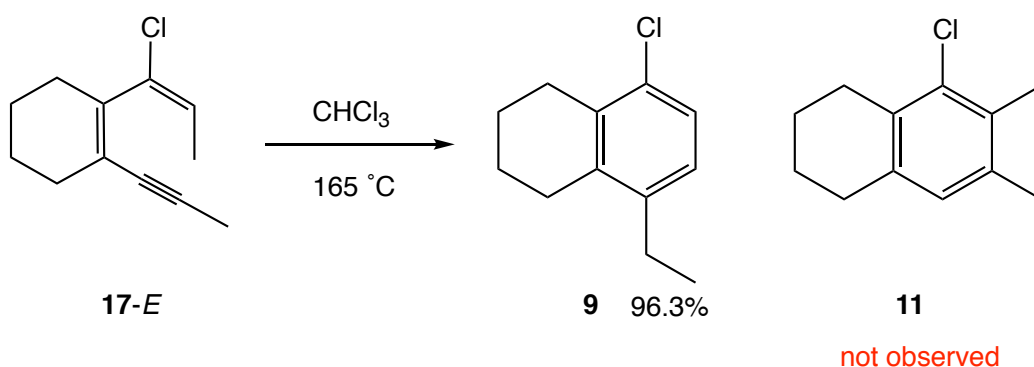
not observed

Scheme 7-12. Thermal reaction of **17**-*E*.

Since thermal cyclization of vinyl chloride **17**-*E* only gives the major arene product **9**, we propose that the minor product **11** of the original thermal reaction of enediyne must come from the unobserved **17**-*Z* that is generated from the acid triggered isomerization of **17**-*E* at high temperature (Scheme 7-13). In order to verify this proposal, an NMR tube reaction was carried out with the isolated vinyl chloride **17**-*E* and a nonnucleophilic acid (trifluoroacetic acid) at 165 °C (Scheme 7-14). As expected, both major and minor arene products **9** and **11** were observed with 81 : 19 ratio, which is very similar to what was observed in the thermal reaction of enediyne **5**. However, we are not sure about which isomer is favored in the equilibrium.
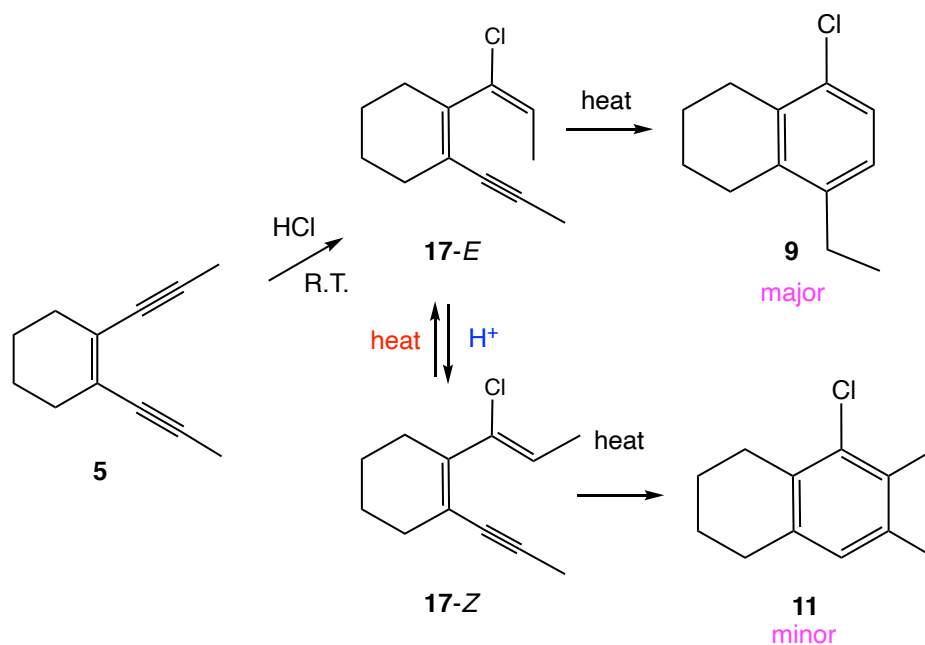
Scheme 7-13. Formation of major product **9** and minor product **11**.
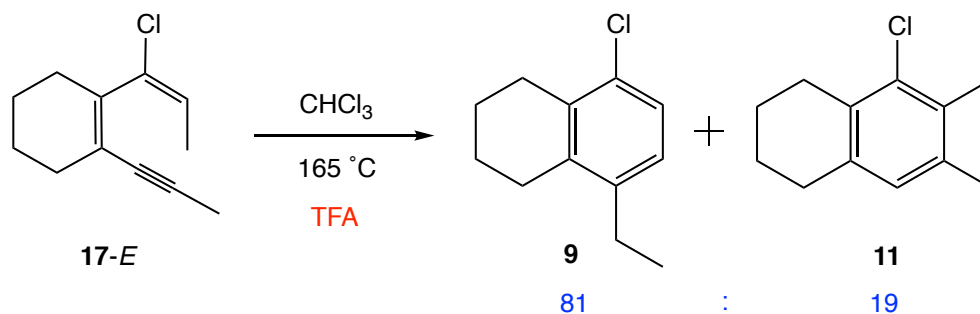
Scheme 7-14. Thermal reaction of **17**-*E* in the presence of TFA.

When the same type of reactions was carried out on the five-membered ring enediyne analogue **4** under very similar reaction conditions, the results of the products were essentially the same. Only the *E* isomer (**25**-*E*) of vinyl chloride was obtained with 85.5% yield when treating **4** with hydrochloric acid at ambient temperature, and the arene product **26** was generated exclusively (89% yield) without any competition of minor product formation when heating **25**-*E* at 165 °C (Scheme 7-15).
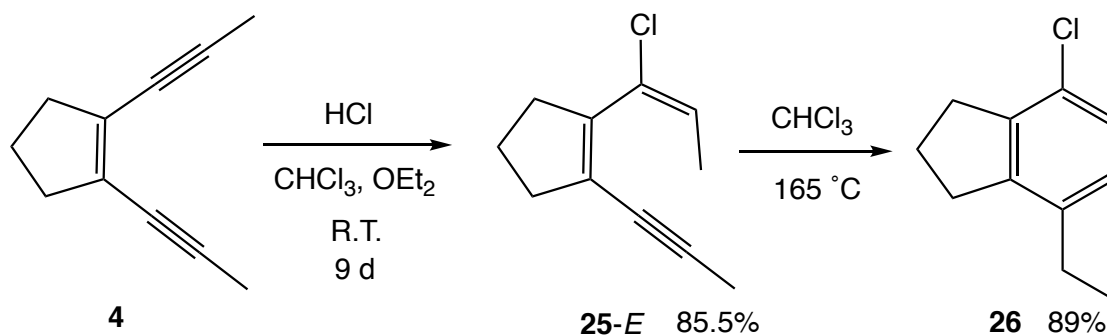
Scheme 7-15. Synthesis of **25**-*E* and **26** from enediyne **4**.

In addition, a photochemical reaction was carried out on **17**-*E* to see if a cyclization or isomerization process can be triggered by the light. However, surprisingly, upon irradiating the benzene-d_6 solution of **17**-*E* in a Rayonette photoreactor equipped with UV broadband lamps centered at 254 nm, 42% yields of the enediyne **5** was observed as the only product after 12 hours. There is no evidence for the formation of **17**-*Z* or arene product **9** (Scheme 7-16).
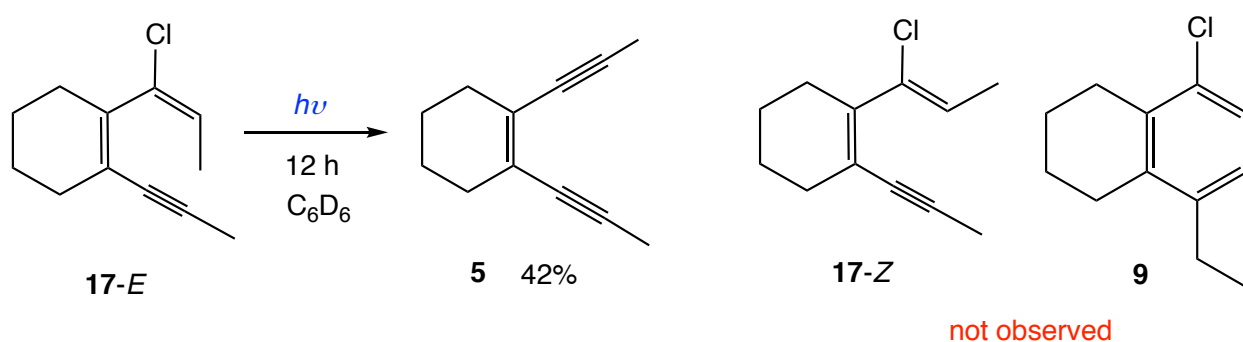
Scheme 7-16. Photolyze in **17**-*E* C_6D_6.

D. Deuterium Labelling Study

1. Formation of Major and Minor Arene products

In order to explore the mechanism and regioselective connectivity of this novel cyclization process, a deuterium labelling study was conducted by enriching the two methyl groups on enediyne **5**, which is synthesized from deprotonation of terminal enediyne **27** followed by methylation with iodomethane-d_3 (Scheme 7-17). The deuterium labeled vinyl chloride **28**-*E* can be made in a similar fashion to **17**-*E*, with the treatment of **5**-d_6 with HCl in Et$_2$O/chloroform at ambient temperature.
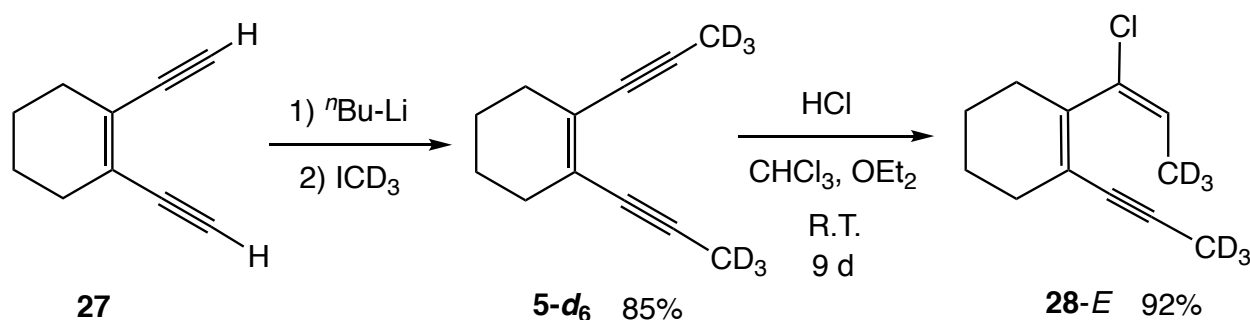
Scheme 7-17. Synthesis of **5**-d_6 and **28**-*E*.

The isolated vinyl chloride **28**-*E* (0.298 g, 1.48 mmol) was subsequently heated in a Schlenk flask in CDCl$_3$ at 165 °C for 7 days (Scheme 7-18). After aqueous work up and chromatography on silica gel, 88.6% yield of product was obtained as clear oil. A GC-MS analysis of the product indicates that it is a 66 : 34 ratio of mixture of **29** with 6 deuteriums and **30** with 5 deuteriums. Compare the ^{1}H NMR (CDCl$_3$, 500 MHz) spectrum of the product to the protio analogue **9**, the aromatic hydrogen at δ 6.95 (d,

1H, J = 8.2 Hz) is no longer present, and the more deshielded aromatic hydrogen at δ 7.15 changes from a doublet to a singlet, which indicates that the cyclization is constructed by a new bond forming between C1 and C6. The methyl resonance at δ 1.19 (t, 3H, J = 7.6 Hz) is gone, while 0.34 H is integrated on the C7 methylene position, which is consistent with the GC-MS results that 30% of compound **30** was generated from the loss of deuterium. As required by the ^{1}H NMR spectrum, the missing deuterium resonances were observed in the ^{2}H NMR (CHCl$_3$, 500 MHz) at δ 1.19 (s, 3D), 2.57 (s, 1.66D), 7.03 (s, 1D). In the ^{13}C{^{1}H} NMR (CDCl$_3$, 500 MHz) spectrum, the two carbons of ethyl group were observed as multiplets at δ 13.3 (m), 24.9 (m), and the aromatic C1 was detected coupled with deuterium at δ 125.8 (t, J_{DC} = 24.2 Hz).
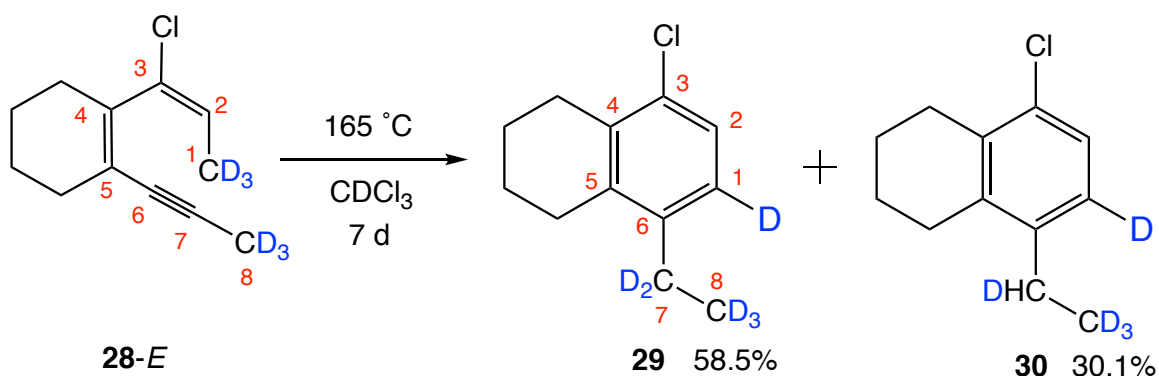
Scheme 7-18. Thermal reaction of **28**-*E*.

Based on the connectivity information provided by the spectroscopic data, we proposed a mechanism for the cyclization process as shown in Scheme 7-19. Upon heating the vinyl chloride **17**-*E*, a 1,7-hydride shift occurs to generate the allene intermediate **31**. Despite the 1,7-hydride shift is found very rare for dienynes,[11] The activation barrier for the 1,7-hydride shift was calculated as 25.8 kcal/mol by Professor

Kim Baldridge, which is in good agreement with the experimental results. A subsequent 6π electrocyclization of **31** give a triene intermediate **32**, that is followed by an aromatization to produce final arene product **9**.
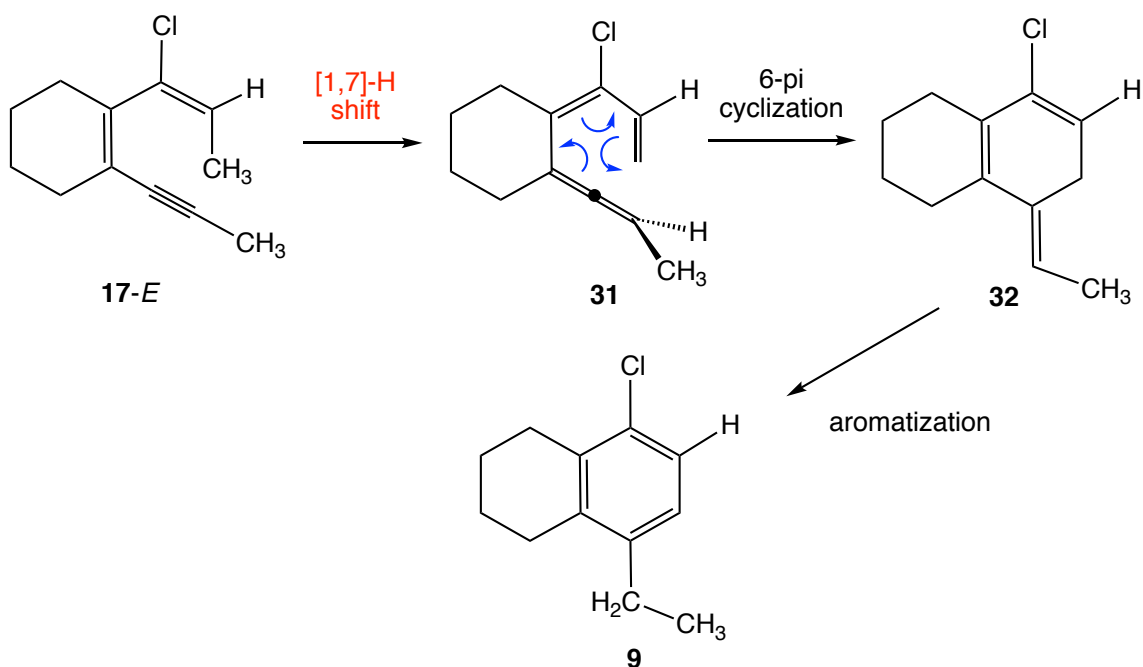
Scheme 7-19. Proposed mechanism for the formation of **9**.

The loss of deuterium on the methylene position in the minor product **30** must be caused by the last aromatization step, which suggests that the rearrangement should go through an intermolecular fashion. The intermolecular process is supported by a crossover experiment, in which a 1 : 1 ratio of **17**-*E* and **28**-*E* was mixed and heated at 165 °C for 7 days in CDCl₃ (Scheme 7-20). A GC-MS analysis of the crude reaction mixture indicates the components of the products as: D0% is 40% (**9**); D1% is 11% (**36**); D5% is 30% (**30**); D6% is 18% (**29**). The intermolecular pathway is manifested by the massive existence of compound **36** and **30**, which are generated from deuterium

scrambling. The experimental results are also consistent with the fact that the intramolecular concerted antarafacial 1,3-hydride shift is impossible in the last step due to the transition state topology.
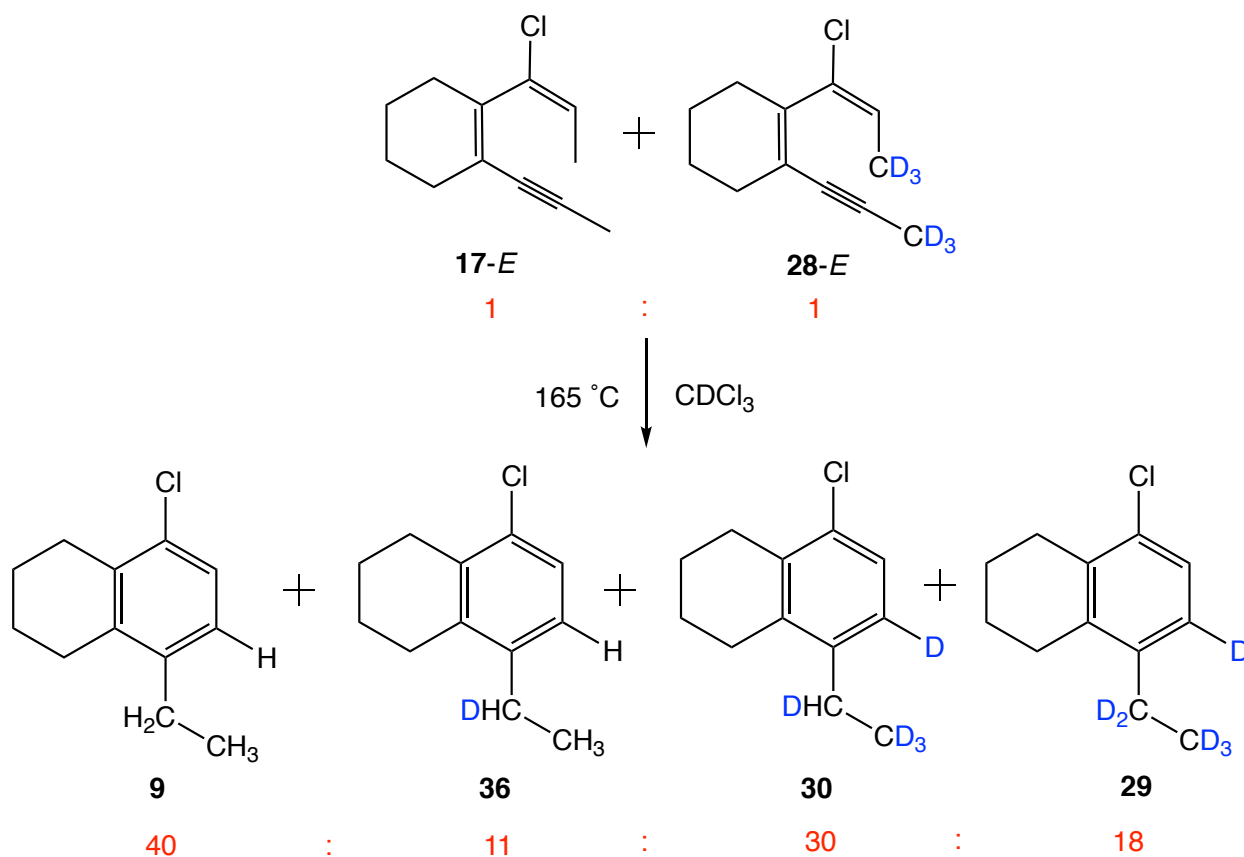
Scheme 7-20. Crossover experiment between **17**-*E* and **28**-*E*.

There are three possible two-step mechanisms for the aromatization step, as shown in Scheme 7-21. It can be realized by a deprotonation-protonation (I), protonation-deprotonation (II), or radical pathway. In order to examine the three possible mechanisms, a few NMR tube reactions were carried out.
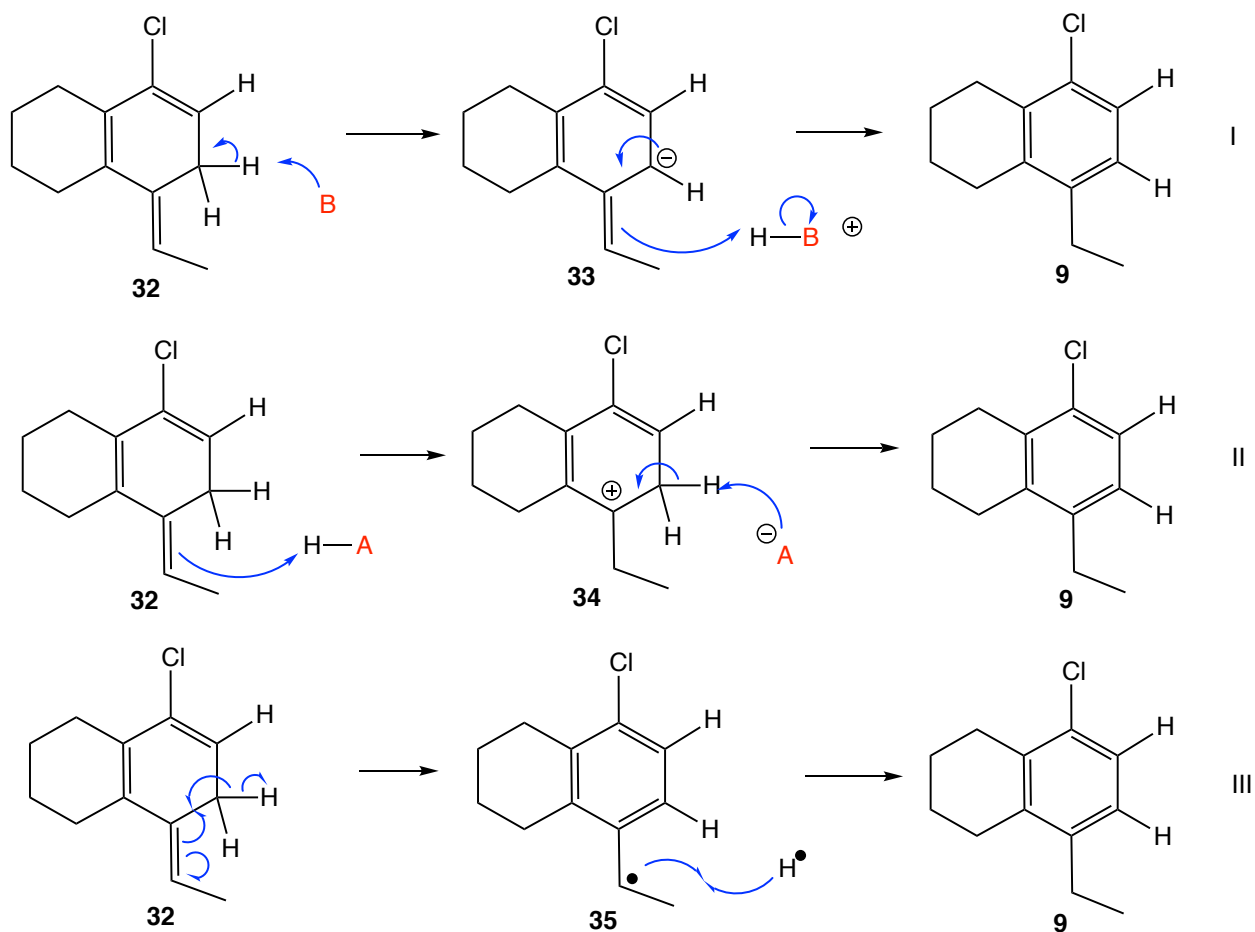
Scheme 7-21. Three possible mechanisms for the aromatization.

In the first one, the solvent was changed to freshly distilled benzene-d_6 that was dried and purified in sodium benzophenone ketyl mixture to exclude any possible acid or base in the solution. When the reaction is finished, a GC-MS analysis gives 78 : 26 ratio of the compound **29** and **30**, which is very similar to what was observed in the CDCl$_3$ solvent (Scheme 7-22). The second reaction was carried out in the presence of 0.2 equivalents of diisopropylamine to scavenge any trace amount of acid in the solution, however, the GC-MS analysis also gives a 76 : 24 ratio of compound **29** and **30**, which excludes the protonation-deprotonation mechanism. In the third reaction, one

equivalent of D_2O was loaded in the reaction mixture, and the deprotonation-protonation mechanism was excluded by the fact that there is no net increment of the ratio of compound **29** in the resulting product. The most persuasive evidence for the proposed radical mechanism is the addition of 25 equivalents of 1,4-CHD in the fourth reaction, which tunes molecule **29** to be the minor product with a ratio of 25 : 75 relative to compound **30**. We ascribe the drastic change of product distribution to the fact that the deuterated analogue of radical intermediate **35** can abstract a hydrogen atom from 1,4-CHD to produce more of **30**. In addition, further analysis of the GC-MS spectrum of crude reaction mixture from the first reaction provides the evidence of existence of molecule **37** and **38**, which can explain the proton source for the formation of **30**.
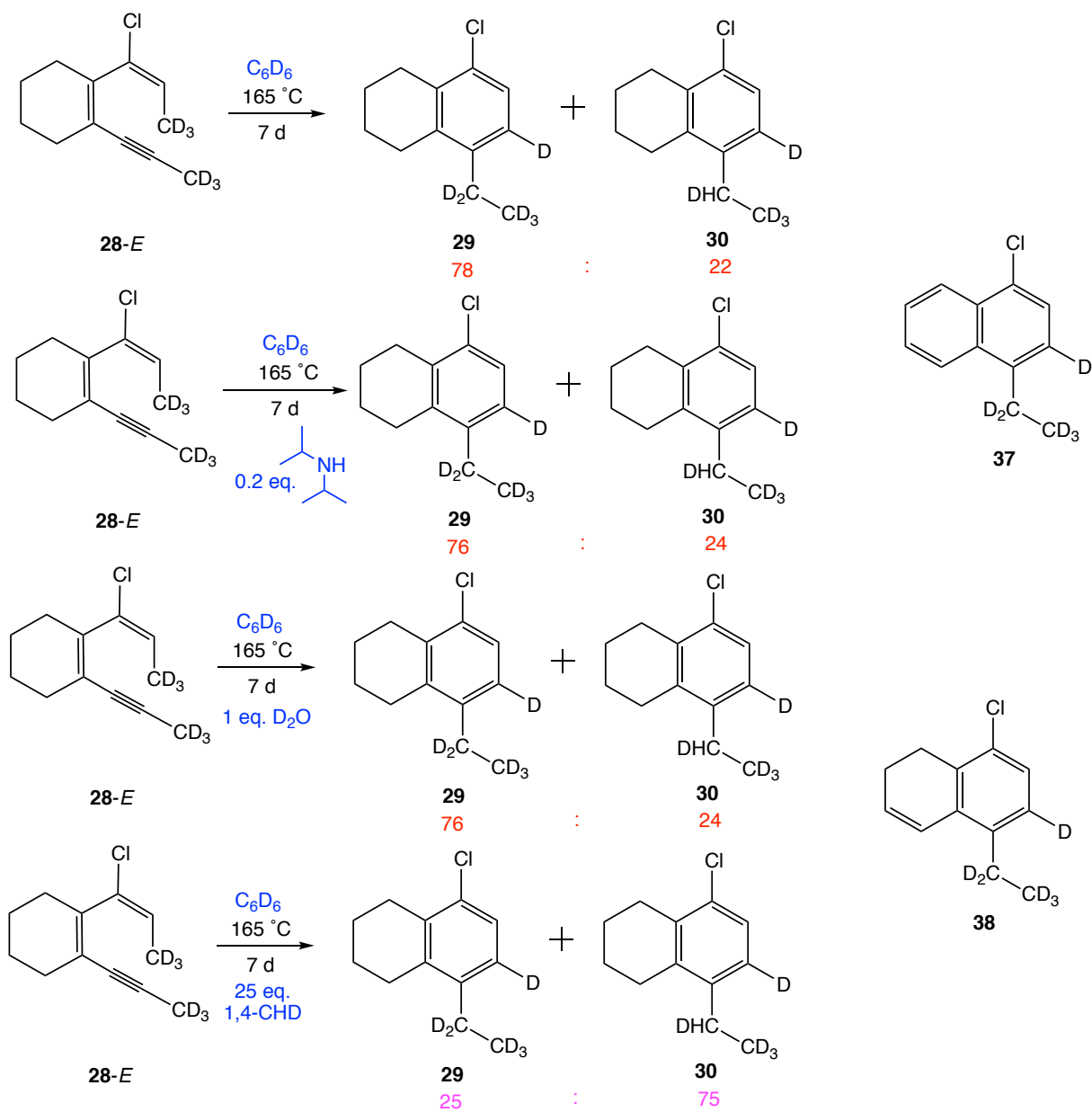
Scheme 7-22. NMR reaction evidences for the radical mechanism.

2. Kinetic Isotope Effect Study

In order to explore the effects of deuterium on the relative cycloaromatization rate

of vinyl chloride, a kinetic isotope effect study was carried out by utilizing **17**-*E* and **28**-*E*

in two separate NMR tube reactions under similar reaction conditions side by side (Scheme 7-23). The reaction mixtures were heated at 165 °C and monitored by ^{1}NMR spectroscopy. The time points were taken every 30 minutes at early stage (7.5 hours). The concentration of **17**-*E* and **28**-*E* were calculated by the integration of internal standard relative to vinyl hydrogen at 5.72 ppm (q, 1H, *J* = 7.2 Hz) and 5.71 ppm (s, 1H), respectively. The kinetic data are summarized and shown in Table 7-2, and the natural logarithm concentration change of the two vinyl chlorides with time are plotted in Figure 7-2. The trend lines of the natural logarithm concentration decay of the two compounds give a rate constant 0.081 h^{-1} for **17**-*E* and a rate constant 0.037 h^{-1} for **28**-*E*. This 2.2-fold faster reaction rate of the all protio vinyl chloride analogue **17**-*E* is consistent with the primary isotope effect that exists in the proposed mechanism.
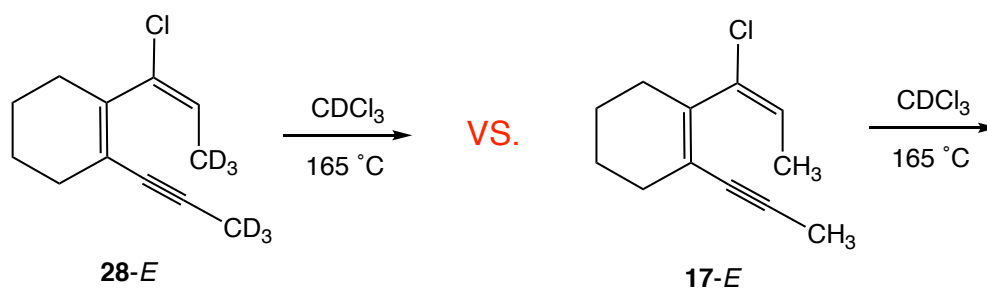
Scheme 7-23. Kinetic isotope effect study of vinyl chloride **17**-*E* and **28**-*E*.

Table 7-2. Kinectic data of isotope effect study of vinyl chloride **17**-*E* and **28**-*E*.

mol/L	0	0.5 h	1 h	1.5 h	2 h	2.5 h	3 h	3.5 h
[**17**-*E*]	0.0910	0.0876	0.0840	0.0813	0.0761	0.0728	0.0708	0.0694
[**28**-*E*]	0.0851	0.0830	0.0814	0.0796	0.0788	0.0778	0.0765	0.0745
ln [**7**-*E*]	-2.397	-2.435	-2.477	-2.509	-2.576	-2.620	-2.649	-2.667
ln [**28**-*E*]	-2.464	-2.489	-2.508	-2.531	-2.540	-2.553	-2.571	-2.598
	0	0.5 h	1 h	1.5 h	2 h	2.5 h	3 h	3.5 h
[**17**-*E*]	0.0910	0.0876	0.0840	0.0813	0.0761	0.0728	0.0708	0.0694
[**28**-*E*]	0.0851	0.0830	0.0814	0.0796	0.0788	0.0778	0.0765	0.0745
ln [**7**-*E*]	-2.397	-2.435	-2.477	-2.509	-2.576	-2.620	-2.649	-2.667
ln [**28**-*E*]	-2.464	-2.489	-2.508	-2.531	-2.540	-2.553	-2.571	-2.598
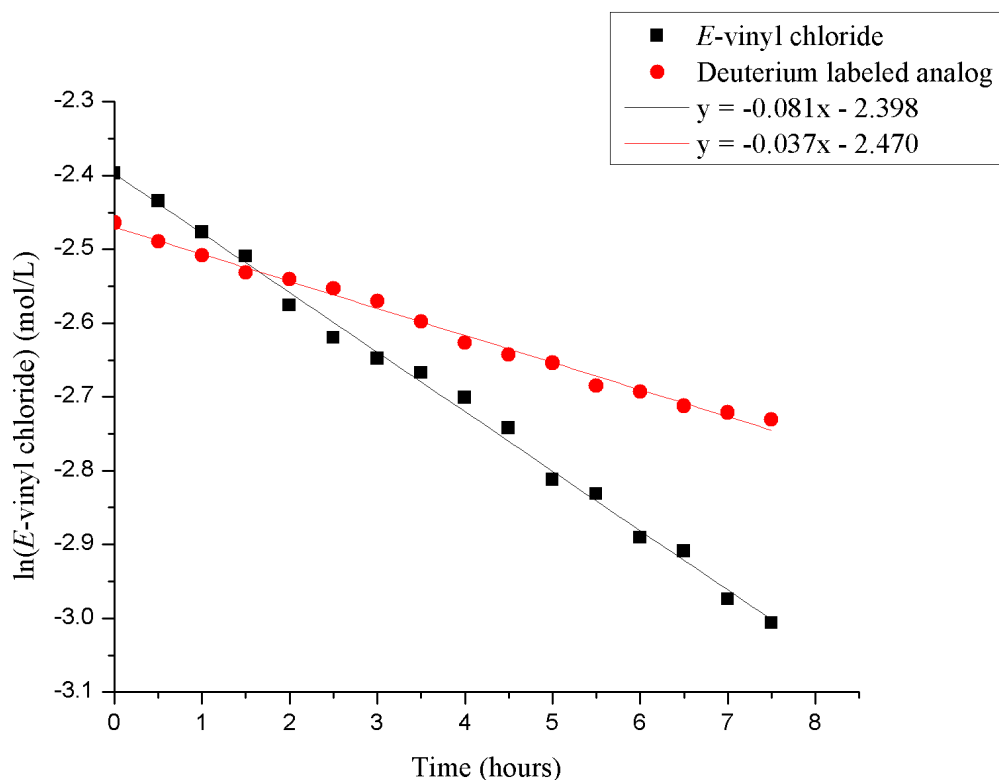
Figure 7-2. Natural logarithm concentration change of **17**-*E* and **28**-*E* with time and calculated rate constant.

E. Conclusions

In summary, continued from the exploration of an unprecedented cycloaromatization of enediynes that was discovered by previous graduate students, the two vinyl chlorides and two arene products (both with five-membered ring and six-membered ring) were resynthesized in a modified higher yieled synthetic pathway. All the four compounds were successfully purified and fully characterized. The mechanism of vinyl chloride formation that includes the generation of HCl in situ was demonstrated by computational studies and a series of NMR tube reactions. A deuterium labelling study furtherly uncovered the radical pathway of the aromatization process, and the subsequent kinetic study illustrated the 2.2-fold primary isotope effect on the rate-limiting cyclization step of the proposed mechanism.

F. Experimentals
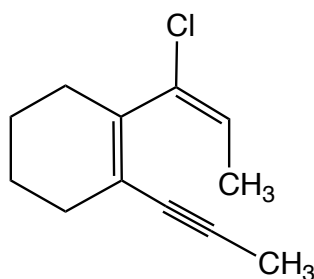
17-*E*

Preparation of (*E*)-1-(1-chloroprop-1-en-1-yl)-2-(prop-1-yn-1-yl)cyclohex-1-ene (17-*E*): Enediyne 1,2-di(prop-1-yn-1-yl)cyclohex-1-ene (**5**) (440 mg, 2.78 mmol) was added into a Teflon topped Schlenk flask. After the Schlenk flask was frozen by liquid nitrogen

and then placed under vacuum, 20 ml of dry $CDCl_3$ was distilled into the Schlenk flask. Then the empty space was filled with argon. The Schlenk flask was placed under -10˚C and 1.4 ml of HCl (2.8 mmol, 2 M in Et_2O) was syringed in while keeping stirring the solution. The clear solution turned to light green. Then the solution was allowed to warm up to room temperature and was kept stirring for 5 days, during which time the reaction was monitored by NMR. After 5 days, the ratio of enediyne **5** and **17**-*E* was 1: 1.54. Then 2.8 ml of HCl (5.6 mmol, 2 M in in Et_2O) was syringed in at -10˚C and solution was allowed to stir for 4 more days at room temperature. Resulting solution was concentrated and after chromatography on silica with hexane, 460 mg (85 % yield) of **17**-*E* was obtained as clear oil. IR ($CHCl_3$) 2934, 2859, 2231, 1650, 1614, 1435, 1319, 1228, 1152, 951 cm^{-1}, ^{1}H NMR ($CDCl_3$, 400 MHz) δ 1.62 (d, 3H, *J* = 7.2 Hz, Me), 1.64 (m, 4H, methylene-*H*), 1.95 (s, 3H, Me), 2.21 (m, 4H, methylene-*H*), 5.72 (q, 1H, *J* = 7.2 Hz, vinyl-*H*); ^{13}C{^{1}H} NMR ($CDCl_3$, 125 MHz) δ 4.7, 15.3, 22.2, 22.4, 27.7, 30.6, 79.7, 88.7, 121.2, 124.3, 131.9, 137.6. HRMS for $[C_{12}H_{16}Cl]$+: 195.0940 (Theo. Mass), 195.0932 (Mass Measured).

9
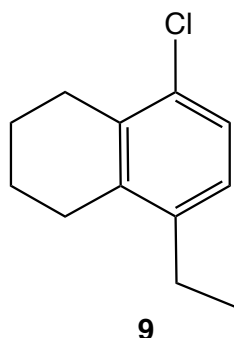
Preparation of 5-chloro-8-ethyl-1,2,3,4-tetrahydronaphthalene (9): Vinyl chloride **17-**

E (300 mg, 1.54 mmol) was added into a Teflon topped Schlenk flask. After the Schlenk

flask was frozen by liquid nitrogen and then placed under vacuum, around 10 ml of dry

chloroform-D was distilled into the Schlenk flask. The resulting solution was

subsequently degassed via 3 cycles of freeze/pump/thaw/degas. Then the Schlenk flask

was sealed and put into an oil bath at 165°C. After 2.5 days, solution was concentrated

and after chromatography on silica with hexane, 289 mg (96.3 % yield) of **9** was

obtained as clear oil. IR (CHCl$_3$) 2937, 2859, 1582, 1458, 1435, 1177, 1141, 955, 896,

819 cm^{-1}; ^{1}H NMR (CDCl$_3$, 400 MHz) δ 1.19 (t, 3H, *J* = 7.6 Hz), 1.80 (m, 4H), 2.57 (q,

2H, *J* = 7.6 Hz), 2.65-2.79 (m, 4H), 6.95 (d, 1H, *J* = 8.2 Hz), 7.15 (d, 1H, *J* = 8.2 Hz);

^{13}C{^{1}H} NMR (CDCl$_3$, 125 MHz) δ 14.4, 22.7, 22.9, 25.5, 26.7, 28.0, 126.1, 126.2, 132.3,

134.8, 137.3, 140.9. HRMS (EI) for [C$_{12}$H$_{15}$Cl]+: 194.0862 (Theo. Mass), 194.0858

(Mass Measured).

5   **9** 86.5%   **11** 7.2%   1.2 eq.
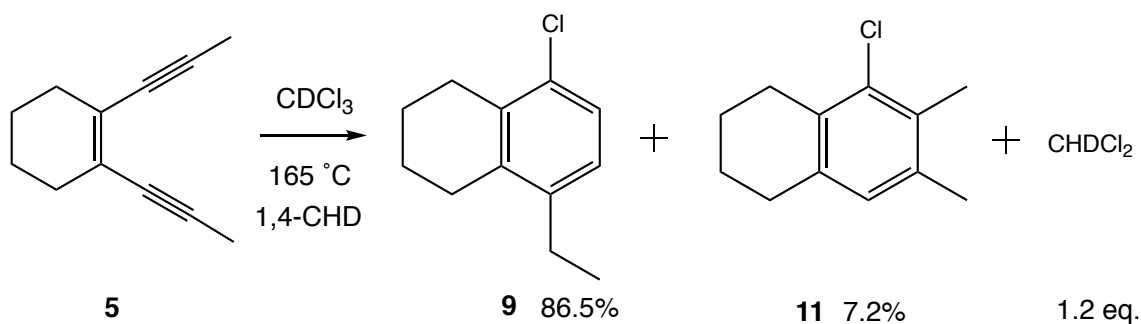
NMR tube reaction of endiyne 5 with 1,4-CHD in CDCl₃ solvent to form arene products and CHDCl₂: Enediyne **5** (5.1 mg, 0.032 mmol), 1,4-cyclohexadiene (21.7 mg, 0.272 mmol) and 1,3,5-tri-*tert*-butylbenzene (internal standard) were added to a 5 mm medium wall NMR tube. After the NMR tube was frozen by liquid nitrogen and then placed under vacuum, 0.65 ml of CDCl₃ was distilled into the NMR tube. The resulting solution was subsequently degassed via 3 cycles of freeze/pump/thaw/degas. Then the NMR tube was sealed by propane flame. An initial ^{1}H NMR spectrum was taken immediately. The NMR tube was submerged into an oil bath at 165°C and the reaction was monitored by ^{1}H NMR spectroscopy. After 4 days, the resonance of enediyne **5** at δ 2.03 ppm (s, 6H, Me) was no longer present and new ^{1}H NMR resonances for **9** were observed at δ 1.19 ppm (t, 3H, J = 7.6 Hz, Me), 1.80 (m, 4H), 2.57 (q, 2H, J = 7.6 Hz), 2.65-2.79 (m, 4H), 6.95 (d, 1H, J = 8.4 Hz), 7.16 (d, 1H, J = 8.4 Hz). Percent yield was calculated from integration of the internal standard relative to the Me resonance of **9** at 1.19 ppm. (86.5% yield). A minor product **11** was observed at δ 2.26 ppm (s, 3H), 2.31 (s, 3H), 6.81 (s, 1H) with a 7.7% yield. 1.2 equivalents of CHDCl₂ also observed at δ 5.289 ppm (t, J_{HD} = 1.2 Hz.
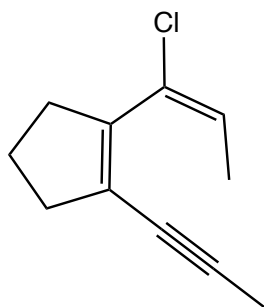
25-*E*

Preparation of (*E*)-1-(1-chloroprop-1-en-1-yl)-2-(prop-1-yn-1-yl)cyclopent-1-ene (25-*E*): 10 mL of concentrated sulfuric acid and 20 mL of hydrochloric acid was mixed in a 250 mL flask, and the mixed acid was allowed to cool down to ambient temperature. Then enediyne 1,2-di(prop-1-yn-1-yl)cyclopent-1-ene (**4**) (502 mg, 3.48 mmol) was slowly added into the acid mixture while keeping stirring. After 6 hours, the reaction mixture was cooled down in an ice bath, and 200 mL of ice water was slowly added into the flask to quench the reaction. After extraction with diethyl ether 200 mL (3 times), concentrated and chromatography on silica gel with hexanes, 506 mg of **25-*E*** can be obtained as clear oil with 80.5% yield. IR (CHCl$_3$): 2943, 2916, 2850, 2226, 1720, 1604, 1438, 1356, 1311, 1159, 1114 cm^{-1}; ^{1}H NMR (CDCl$_3$, 400 MHz) δ 1.69 (d, 3H, *J* = 7.2 Hz, Me), 1.91 (m, 2H, methylene-*H*), 2.00 (s, 3H, Me), 2.57 (m, 4H, methylene-*H*), 5.81 (d, 1H, *J* = 7.2 Hz, vinyl-*H*); ^{13}C{^{1}H} NMR (CDCl$_3$, 125 MHz) δ 4.7, 16.0, 22.6, 35.5, 37.9, 76.5, 93.1, 125.1, 125.8, 127.7, 141.7; HRMS (EI) for [C$_{11}$H$_{13}$Cl]+: 180.0706 (Theo. Mass), 180.0702 (Mass Measured).

26
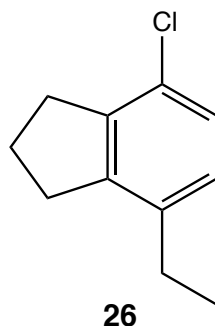
Preparation of 4-chloro-7-ethyl-2,3-dihydro-1H-indene (26): Vinyl chloride **25**-*E* (200 mg, 1.107 mmol) was added into a Teflon topped Schlenk flask. After the Schlenk flask was frozen by liquid nitrogen and then placed under vacuum, around 10 ml of dry chloroform-*d* was distilled into the Schlenk flask. The resulting solution was subsequently degassed via 3 cycles of freeze/pump/thaw/degas. Then the Schlenk flask was sealed and put into an oil bath at 165˚C. After 48 hours, solution was concentrated and after chromatography on silica with hexane, 178 mg (89 % yield) of **26** was obtained as clear oil. IR (CHCl$_3$) 2956, 2931, 2872, 1590, 14471, 1438, 1412, 1309, 1170, 1127, 1063, 896 cm^{-1}; ^{1}H NMR (CDCl$_3$, 400 MHz) δ 1.18 (t, 3H, *J* = 7.6 Hz, Me), 2.09 (m, 2H, methylene-*H*), 2.56 (q, 2H, *J* = 7.6 Hz, C*H*$_2$CH$_3$), 2.95 (m, 4H, methylene-*H*), 6.92 (d, 1H, *J* = 8.0 Hz, Ar), 7.08 (d, 1H, *J* = 8.2 Hz, Ar); ^{13}C{^{1}H} NMR (CDCl$_3$, 125 MHz) δ 14.5, 24.2, 26.2, 32.1, 32.6, 126.5, 127.0, 128.1, 138.4, 142.1, 144.3; HRMS (EI) for [C$_{11}$H$_{13}$Cl]+: 180.0706 (Theo. Mass), 180.0704 (Mass Measured).
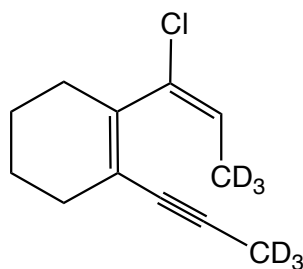
28-*E*

Preparation of (*E*)-1-(1-chloroprop-1-en-1-yl-3,3,3-d₃)-2-(prop-1-yn-1-yl-d₃)cyclohex-1-ene (28-*E*): Enediyne 1,2-di(prop-1-yn-1-yl)cyclohex-1-ene (**5**) (460 mg, 2.80 mmol) was added into a Teflon topped Schlenk flask. After the Schlenk flask was frozen by liquid nitrogen and then placed under vacuum, 10 ml of dry $CDCl_3$ was distilled into the Schlenk flask. Then the empty space was filled with argon. The Schlenk flask was placed under -10°C and 5.6 ml of HCl (11.2 mmol, 2 M in Et_2O) was syringed in while keeping stirring the solution. The clear solution turned to light green slowly. Then the solution was allowed to warm up to room temperature and was kept stirring for 5 days. Resulting solution was concentrated and after chromatography on silica with hexane, 517 mg (92 % yield) of **28-*E*** was obtained as clear oil. IR ($CHCl_3$) 2933, 2860, 2838, 2229, 2118, 2101, 2062, 1645, 1614, 1449, 1435, 1320, 1232 cm^{-1}, ^1H NMR ($CDCl_3$, 400 MHz) δ 1.64 (m, 4H), 2.21 (m, 4H), 5.71 (s, 1H); ^2H NMR ($CHCl_3$, 500 MHz) δ 1.62 (s, 3D), 1.95 (s, 3D); $^{13}C\{^1H\}$ NMR ($CDCl_3$, 125 MHz) δ 4.0 (m), 14.5 (m), 22.1, 22.4, 27.7, 30.6, 79.8, 88.6, 121.2, 124.2, 132.0, 137.6.

165 ˚C
CDCl₃ → wait

Cl

CD₃
CD₃

28-E

165 °C
CDCl₃
7 d

Cl
D
D₂C CD₃

29 58.5%

+

Cl
D
DHC CD₃

30 30.1%
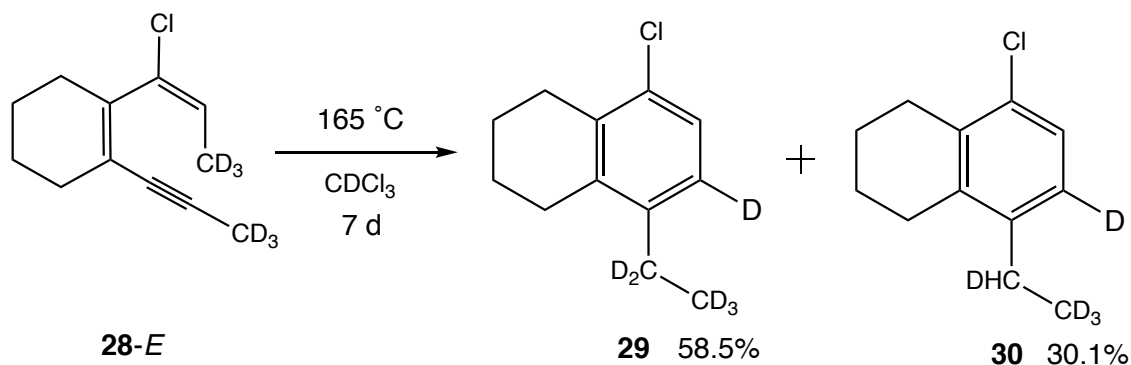
Preparation of 29 and 30 from 28-E: Vinyl chloride **28**-*E* (298 mg, 1.48 mmol) was added into a Teflon topped Schlenk flask. After the Schlenk flask was frozen by liquid nitrogen and then placed under vacuum, around 10 ml of dry chloroform-D was distilled into the Schlenk flask. The resulting solution was subsequently degassed via 3 cycles of freeze/pump/thaw/degas. Then the Schlenk flask was sealed and put into an oil bath at 165°C. After one week, the resulting solution was concentrated and after chromatography on silica with hexane, 264 mg (88.6 % yield) of mixture of **29** and **30** (66:34) were obtained as clear oil. IR (CHCl₃) 2935, 2862, 2223, 2131, 2071, 1563, 1452, 1433, 1394, 1325, 1153, 1055, 1000 cm⁻¹, ¹H NMR (CDCl₃, 500 MHz) δ 1.79 (m, 4H), 2.52 (s, 0.34H), 2.73 (m, 4H), 7.15 (s, 1H); ²H NMR (CHCl₃, 500 MHz) δ 1.19 (s, 3D), 2.57 (s, 1.66D), 7.03 (s, 1D); ¹³C{¹H} NMR (CDCl₃, 125 MHz) δ 13.3 (m), 22.7, 22.9, 24.9 (m), 26.7, 28.0, 125.8 (t, J_{DC} = 24.2 Hz), 126.1, 132.3, 134.8, 137.3, 140.7. MS (EI) for [C₁₂H₉D₆Cl]: 200.1 (Theo. Mass), 200.1 (Mass Measured); MS (EI) for [C₁₂H₁₀D₅Cl]: 199.1 (Theo. Mass), 199.1 (Mass Measured); Calculated deuterium enrichment from MS data: D5% is 34.0% and D6% is 66.0%

641
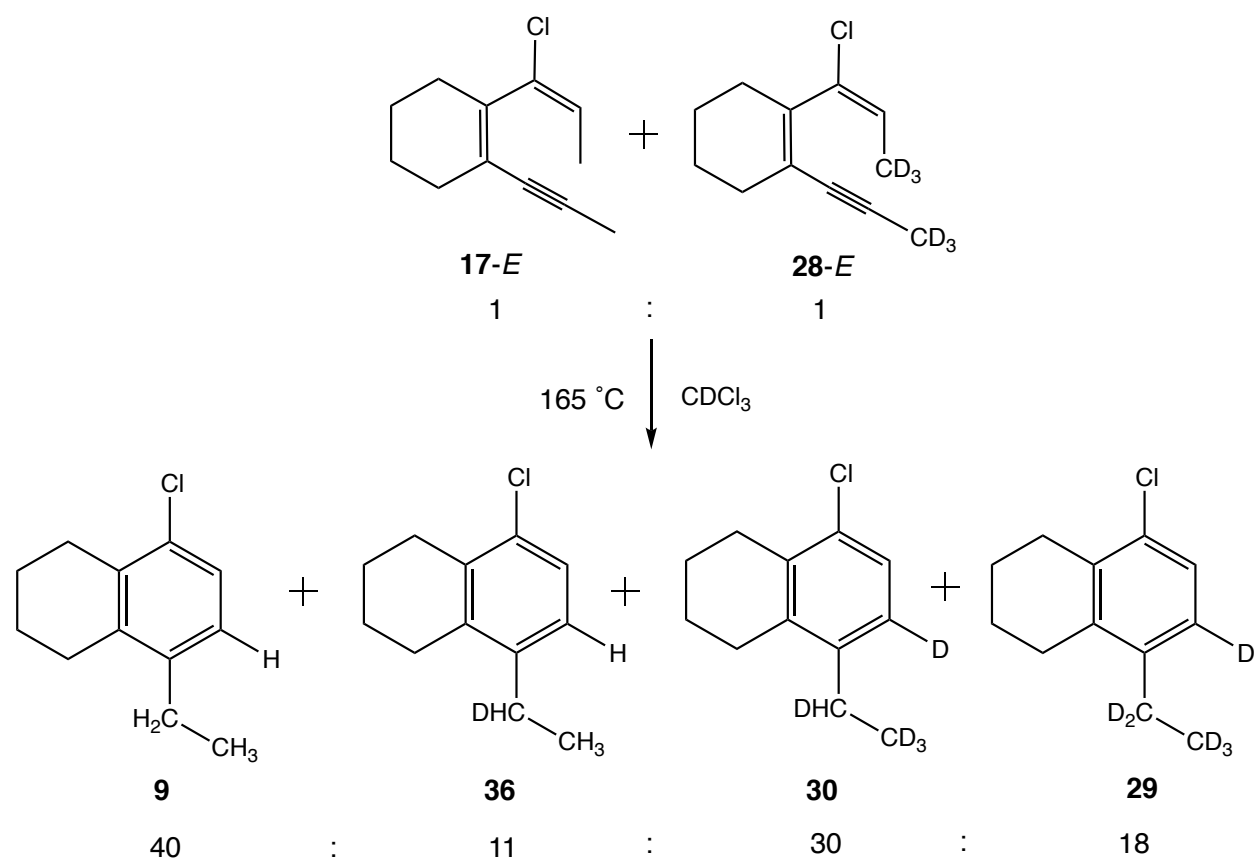
Crossover experiment between vinyl chloride 17-*E* and 28-*E*: Vinyl chloride **28**-*E* (155 mg, 0.77 mmol) and **17**-*E* (150 mg, 0.77 mmol) were added into a Teflon topped Schlenk flask. After the Schlenk flask was frozen by liquid nitrogen and then placed under vacuum, around 10 ml of dry chloroform-D was distilled into the Schlenk flask. The resulting solution was subsequently degassed via 3 cycles of freeze/pump/thaw/degas. Then the Schlenk flask was sealed and put into an oil bath at 165°C. After one week, the resulting solution was concentrated and after chromatography on silica with hexane, 278 mg (91.1 % yield) of products were obtained as clear oil. Deuterium enrichment were calculated by using Mass Spectroscopy (EI): D0% is 40%; D1% is 11%; D5% is 30%; D6% is 18%.
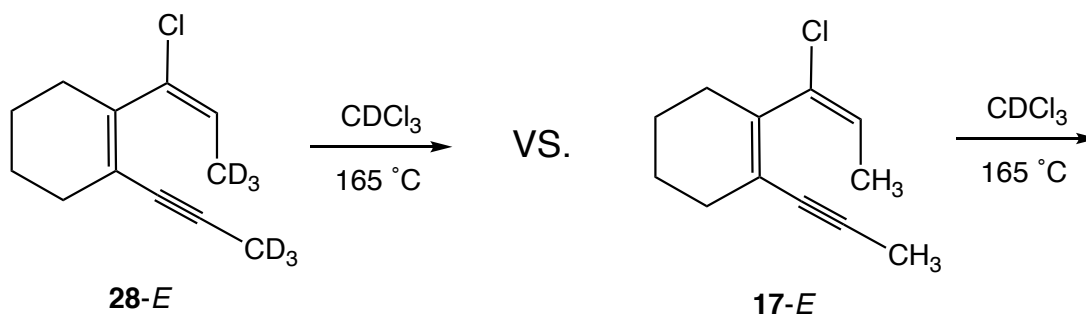
Kinetic isotope effect study (thermal cyclization of 17-*E* and 28-*E* in CDCl₃ solvent): **17**-*E* (7.8 mg, 0.040 mmol), and 1,3,5-tri-*tert*-butylbenzene (internal standard) were added to 5 mm medium wall NMR tube. After the NMR tube was frozen by liquid nitrogen and then placed under vacuum, 0.44 ml of dry CDCl₃ was distilled into the NMR tube. The resulting solution was subsequently degassed via 3 cycles of freeze/pump/thaw/degas. Then the NMR tube was sealed by propane flame. **28**-*E* (7.5 mg, 0.038 mmol) was prepared by using the same way with 0.44 ml of dry CDCl₆ in another 5 mm medium wall NMR tube. The two initial ¹H NMR spectra were taken immediately. The two NMR tubes were submerged into an oil bath side by side at 165˚C. The reactions were subsequently monitored by ¹H NMR spectroscopy and time points were taken at every 30 minutes until 7.5 hours. The concentration of **17**-*E* and **28**-*E* were calculated by the integration of internal standard relative to vinyl hydrogen at 5.72 ppm (q, 1H, *J* = 7.2 Hz) and 5.71 ppm (s, 1H), respectively. The ln (*E*-vinyl chloride)-Time plots were made to calculate to the rate constant. The rate constant of **17**-*E* is 0.081 h⁻¹ while the rate constant of **28**-*E* is 0.037 h⁻¹.

G. Appendix
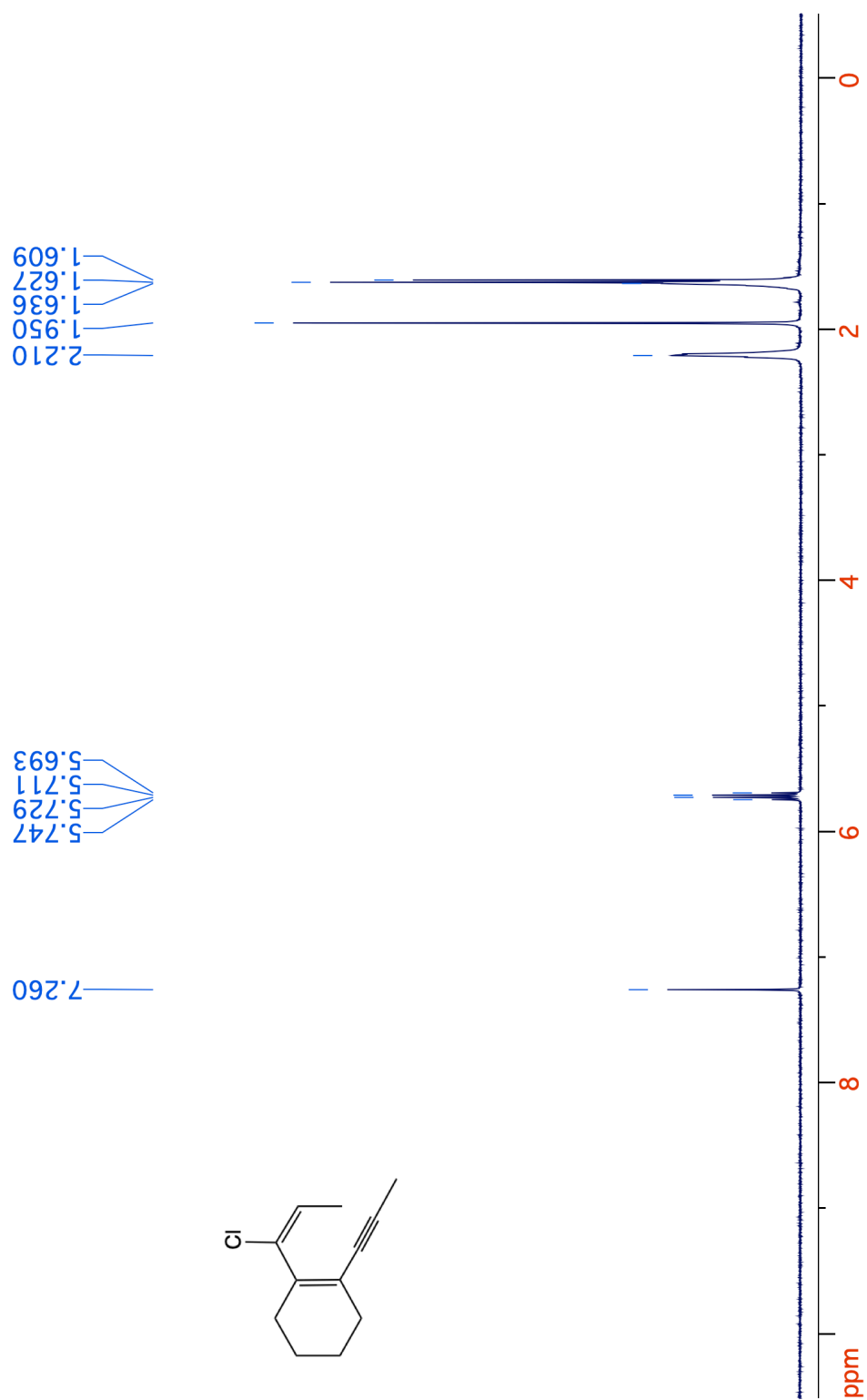
Figure 7-3. ^{1}H NMR spectrum (400 MHz, CDCl$_3$) of **17**-*E*.

4.685
15.262
22.151
22.358
27.702
30.630

77.160
79.713
88.697

121.240
124.256
131.958
137.618
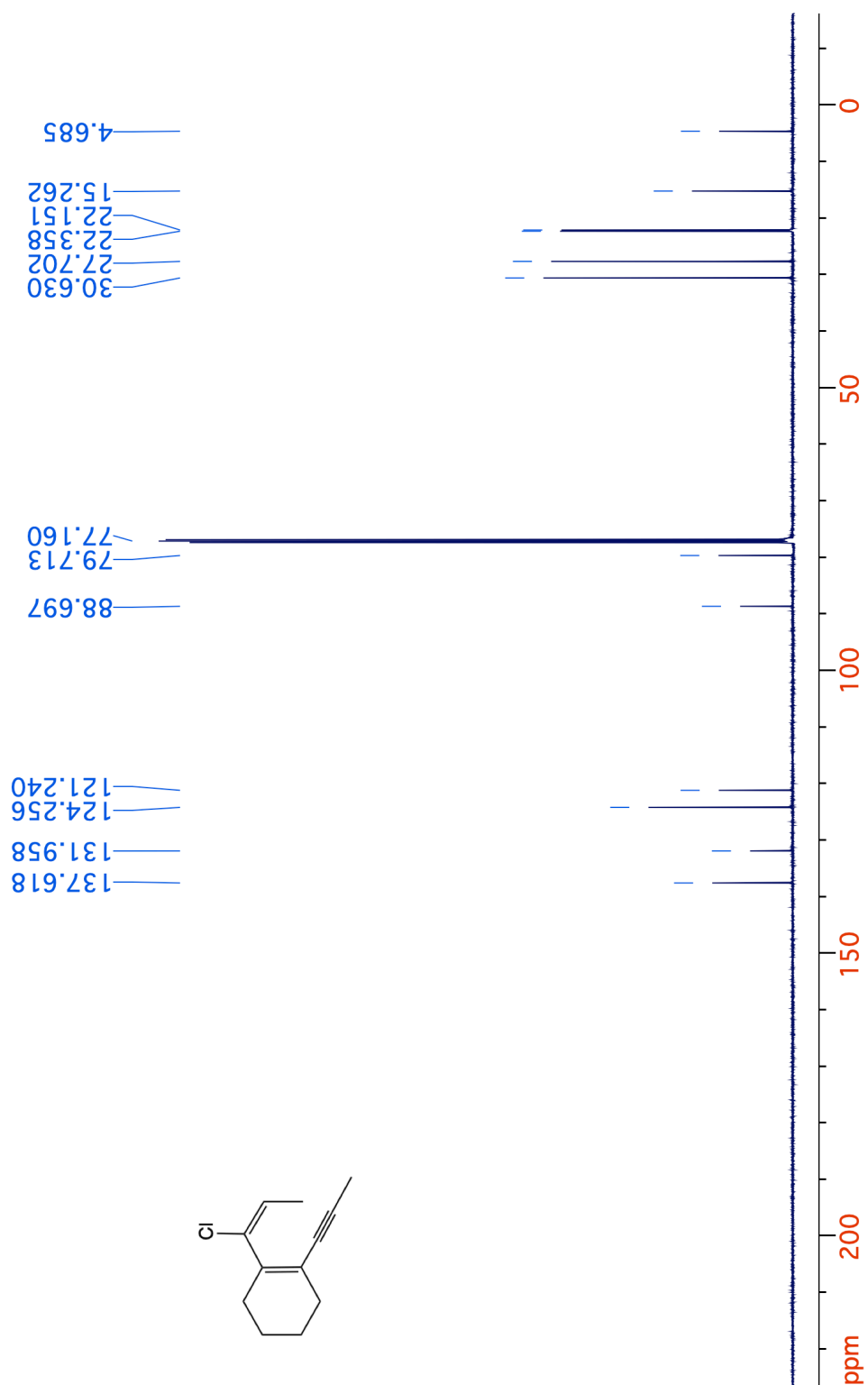
Figure 7-4. $^{13}C\{^1H\}$ NMR spectrum (125 MHz, CDCl$_3$) of **17**-*E*.
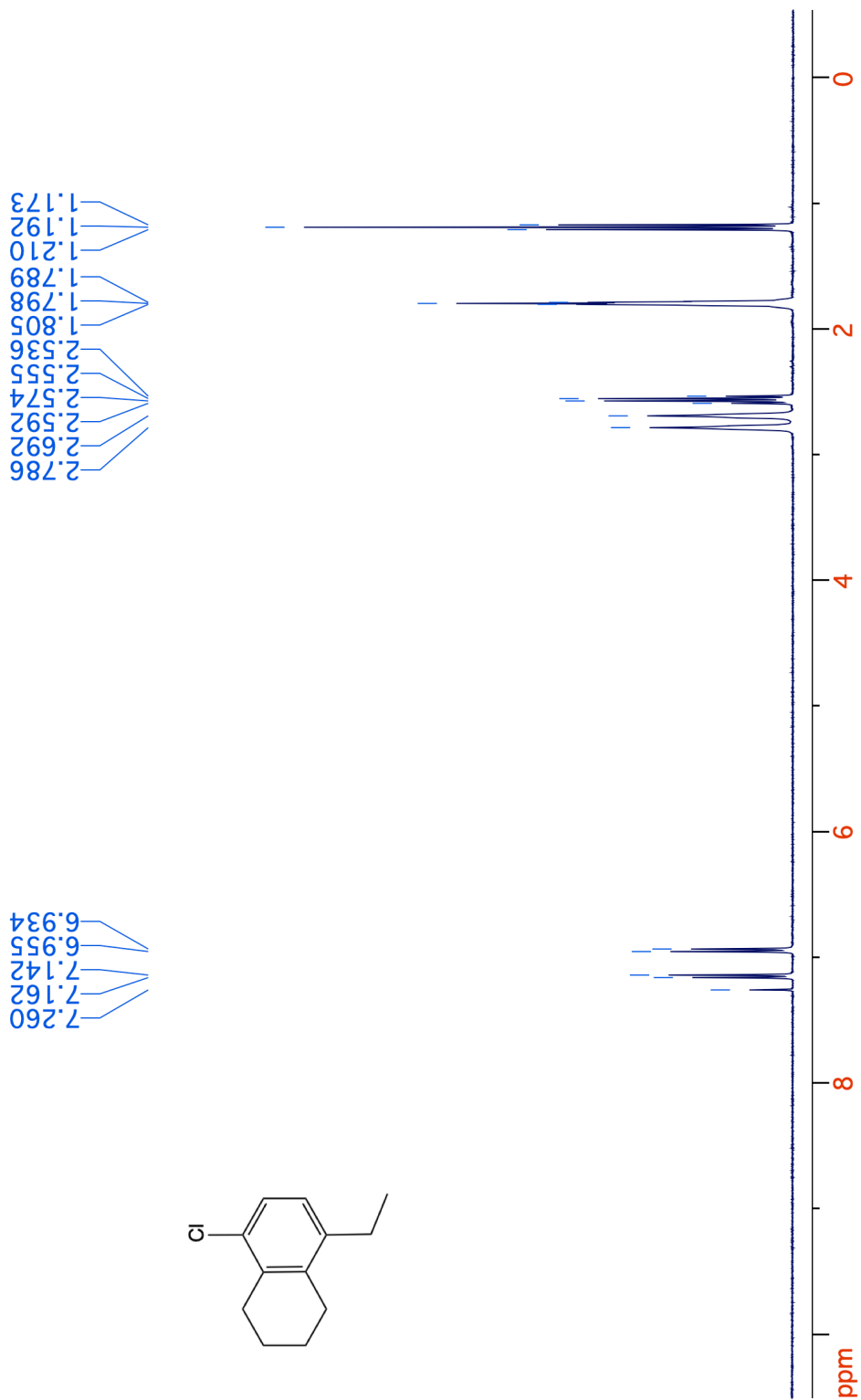
Figure 7-5. ^{1}H NMR spectrum (400 MHz, CDCl$_3$) of **9**.
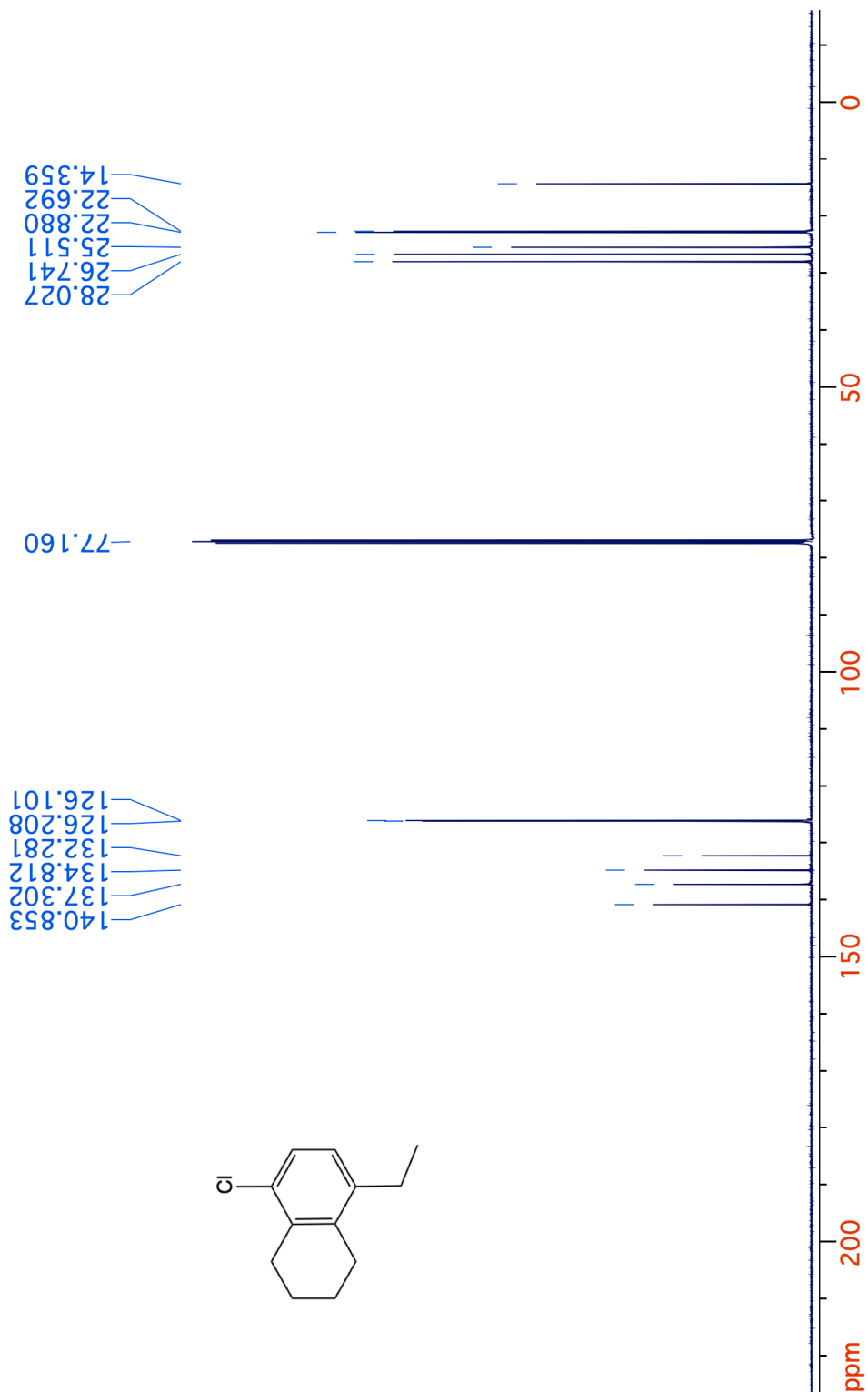
Figure 7-6. $^{13}C\{^1H\}$ NMR spectrum (125 MHz, CDCl$_3$) of **9**.

Peaks labeled: 14.359, 22.692, 22.880, 25.511, 26.741, 28.027, 77.160, 126.101, 126.208, 132.281, 134.812, 137.302, 140.853
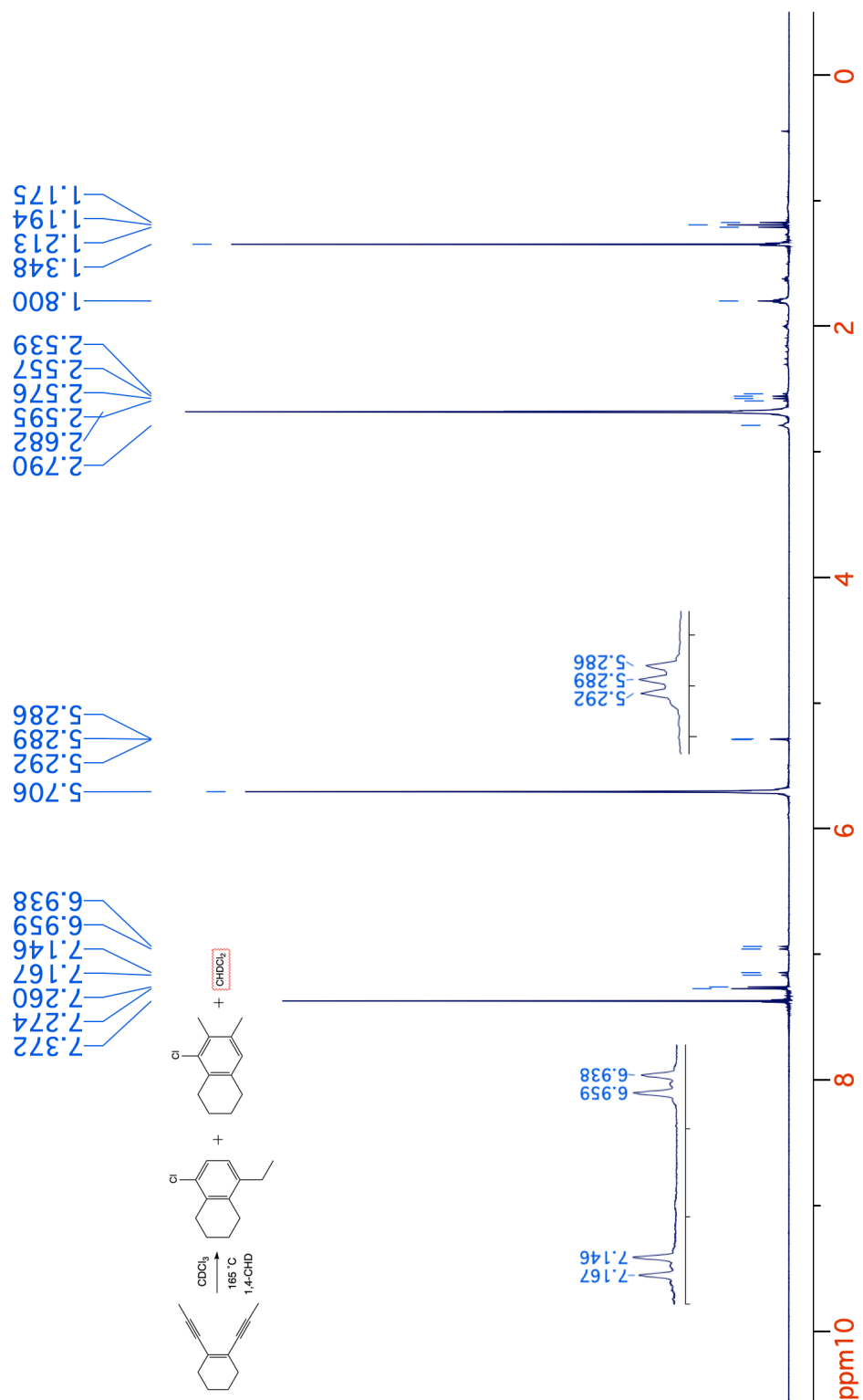
Figure 7-7. ^1H NMR spectrum (400 MHz, CDCl$_3$) of curde thermal reaction of **5** in CDCl$_3$ with the presence of 1,4-CHD.

648
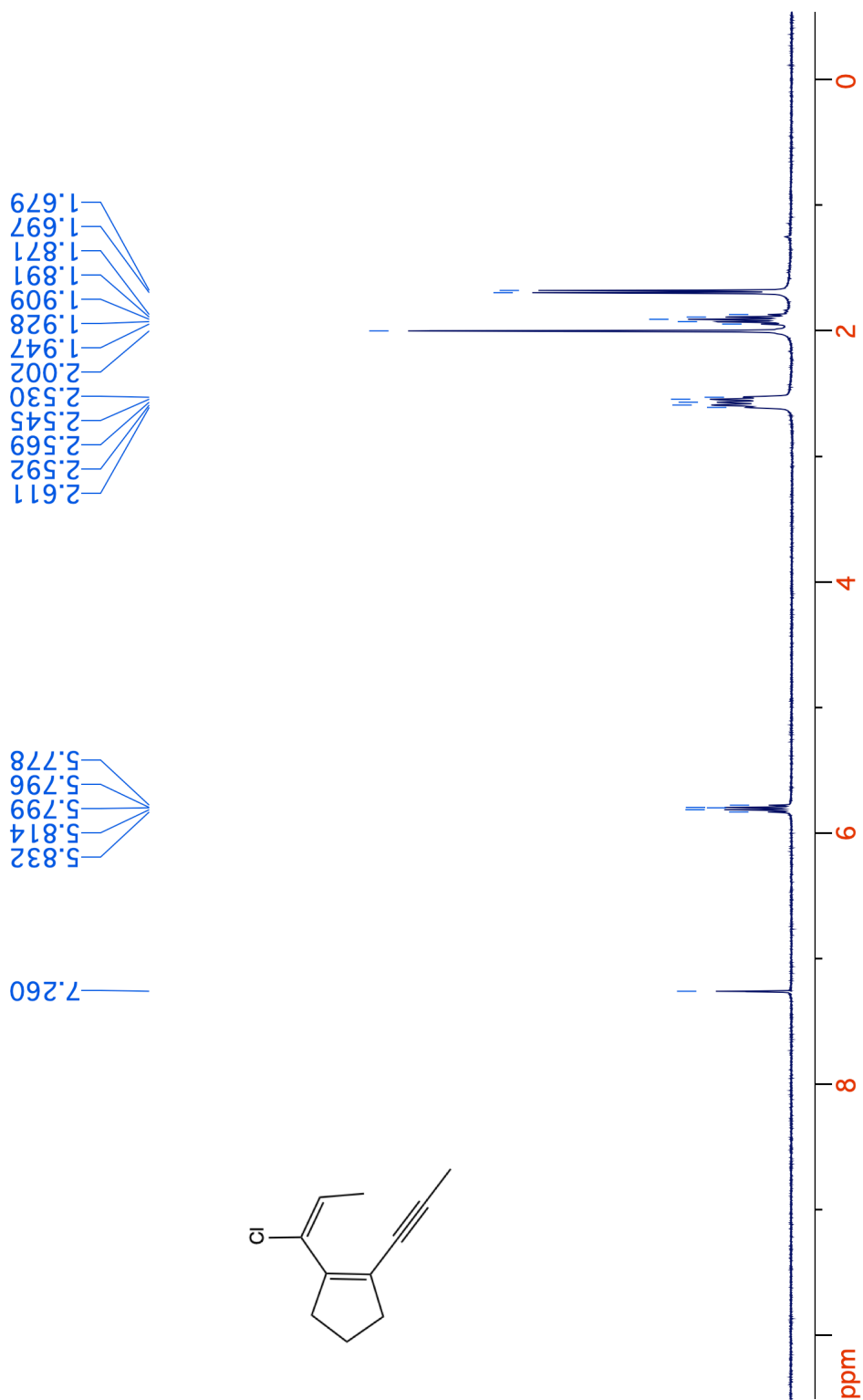
Figure 7-8. ^{1}H NMR spectrum (400 MHz, CDCl$_3$) of **25**-*E*.
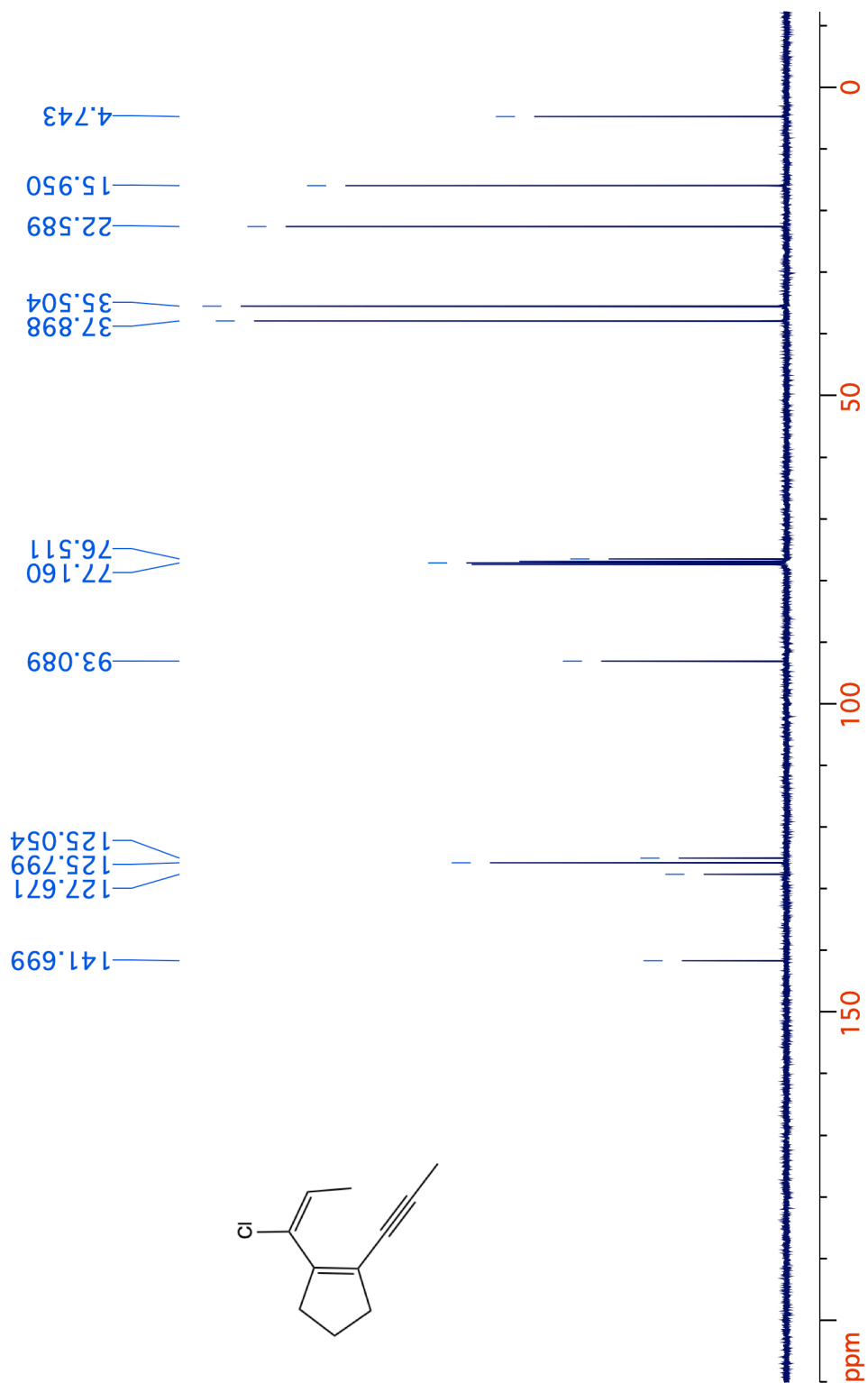
Figure 7-9. $^{13}C\{^1H\}$ NMR spectrum (125 MHz, CDCl$_3$) of **25**-*E*.
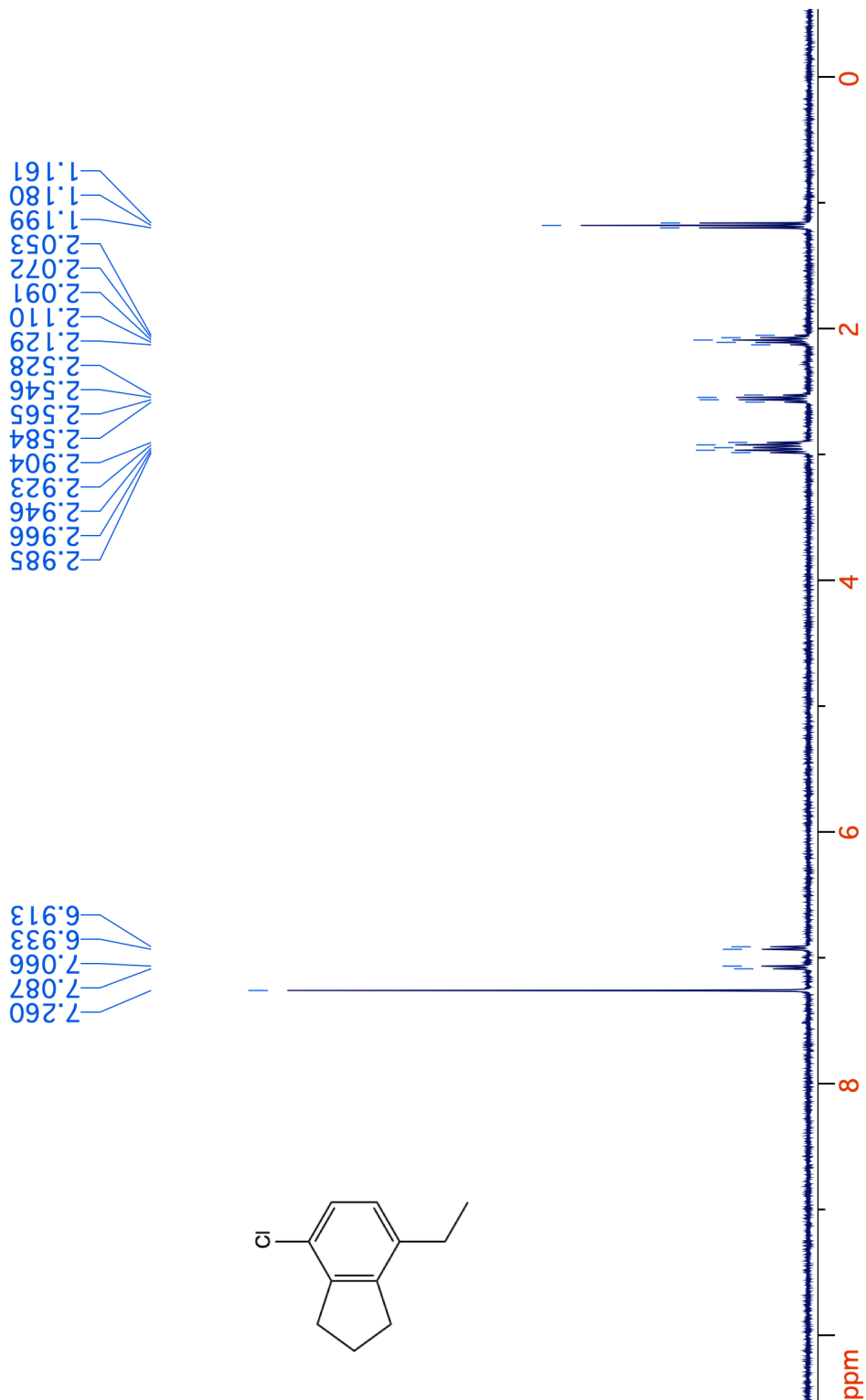
Figure 7-10. ^{1}H NMR spectrum (400 MHz, CDCl$_3$) of **26**.

7.161
7.180
7.199
2.053
2.072
2.091
2.110
2.129
2.528
2.546
2.565
2.584
2.904
2.923
2.946
2.966
2.985

6.913
6.933
7.066
7.087
7.260
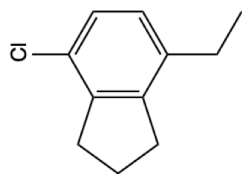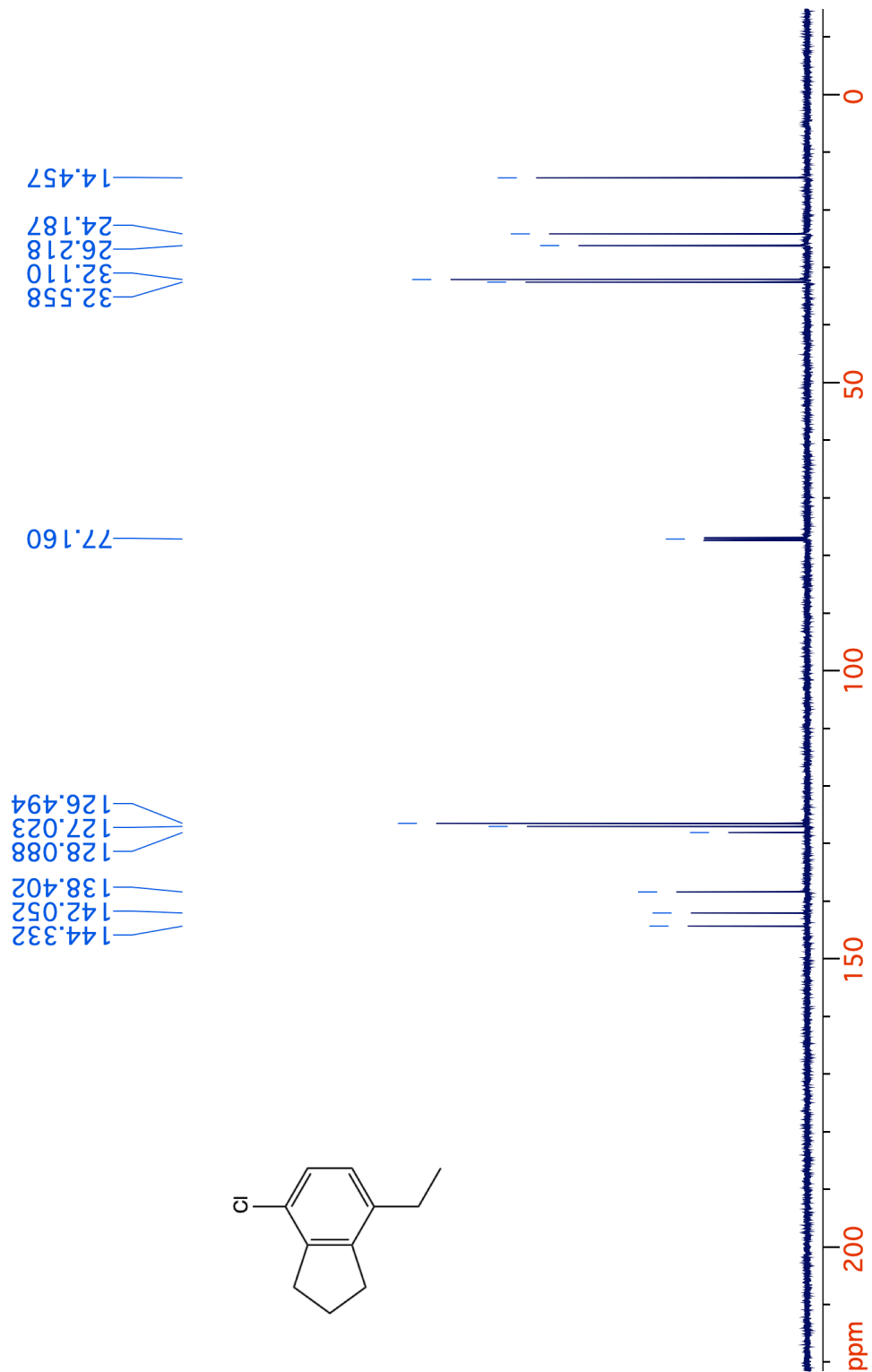
Figure 7-11. $^{13}C\{^1H\}$ NMR spectrum (125 MHz, CDCl$_3$) of **26**.

652
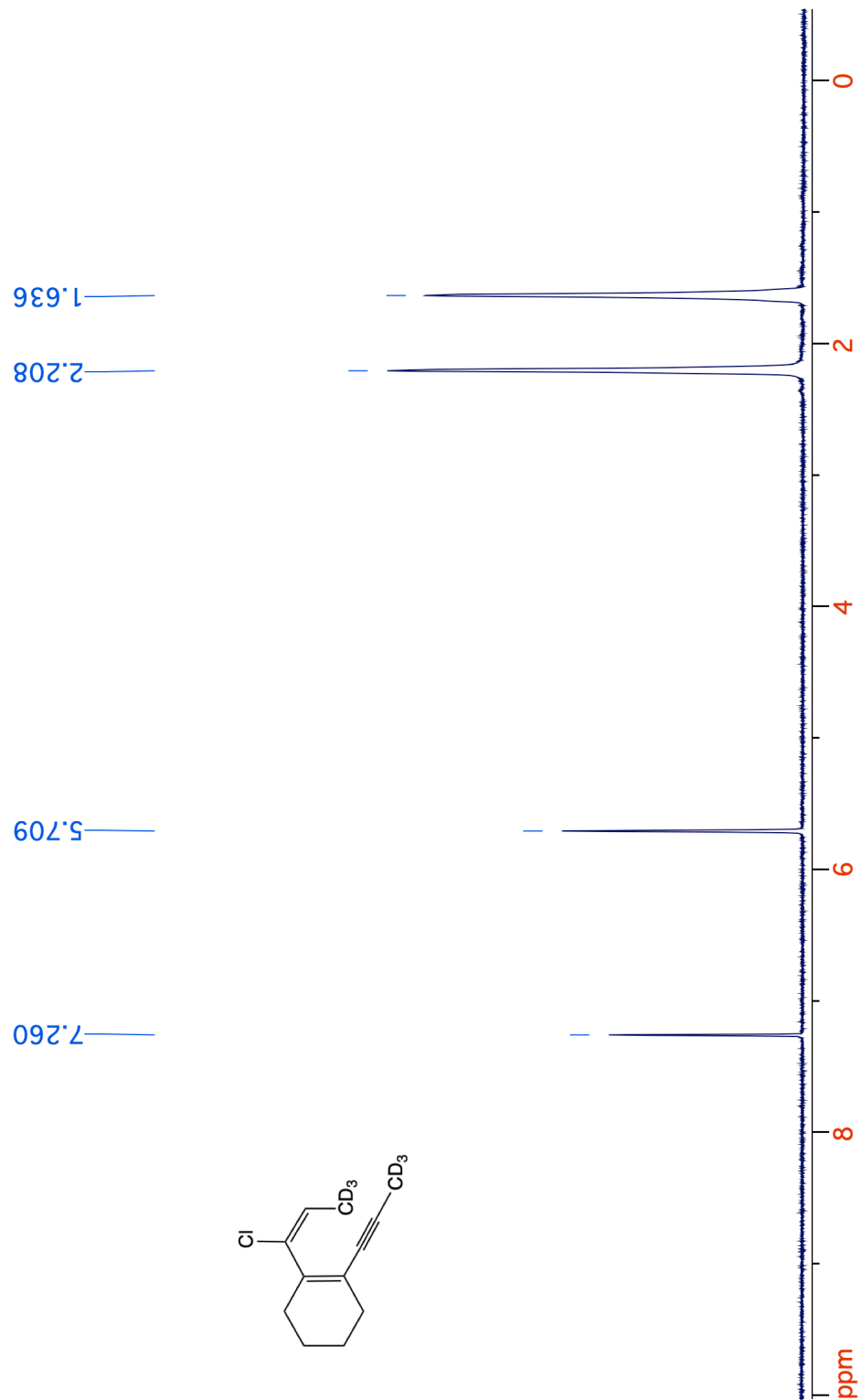
Figure 7-12. ^{1}H NMR spectrum (400 MHz, CDCl$_3$) of **28**-*E*.

1.636

2.208

5.709

7.260

CD$_3$

CD$_3$

Cl
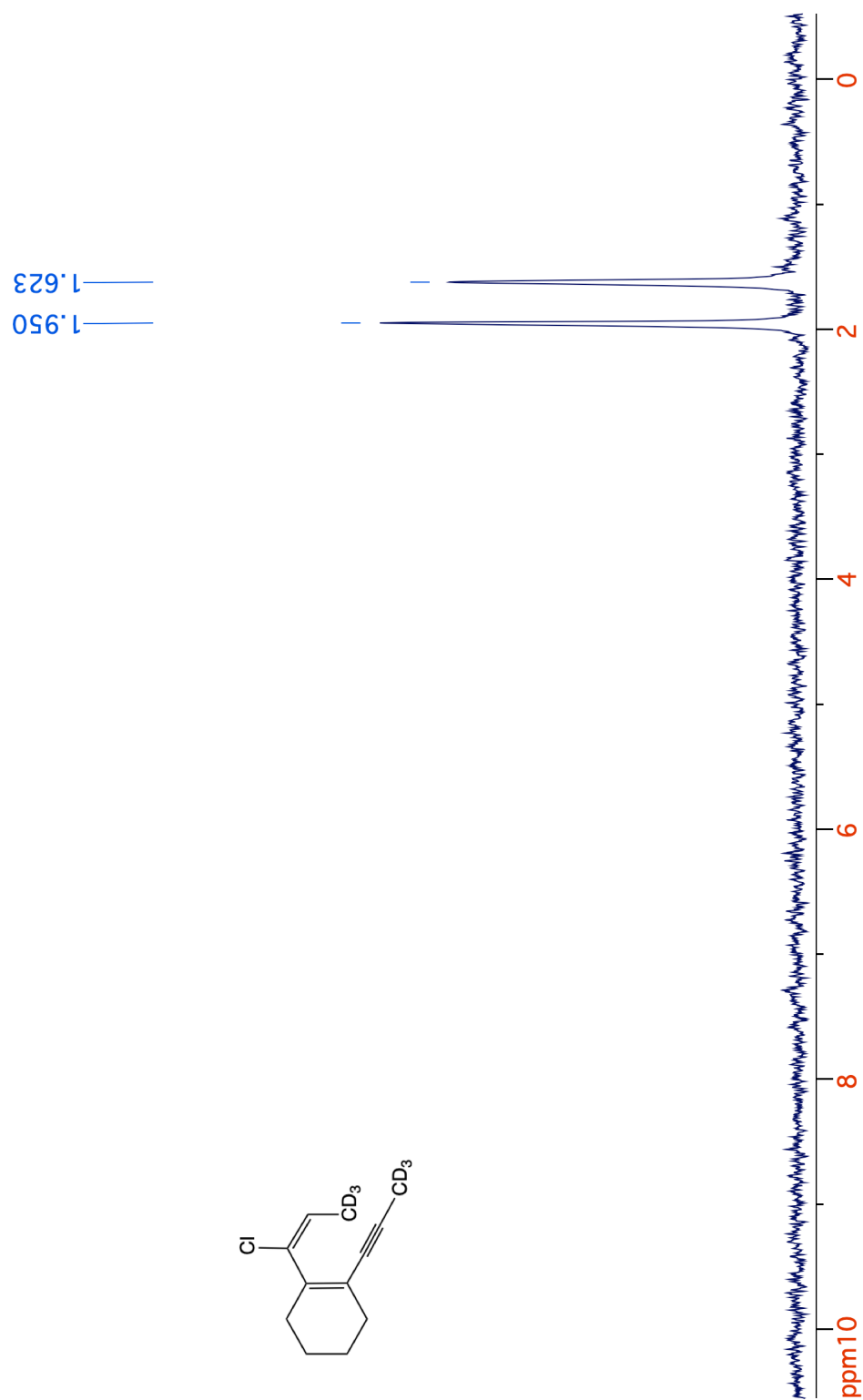
Figure 7-13. ^{2}H NMR spectrum (500 MHz, CHCl$_3$) of **28**-*E*.

654
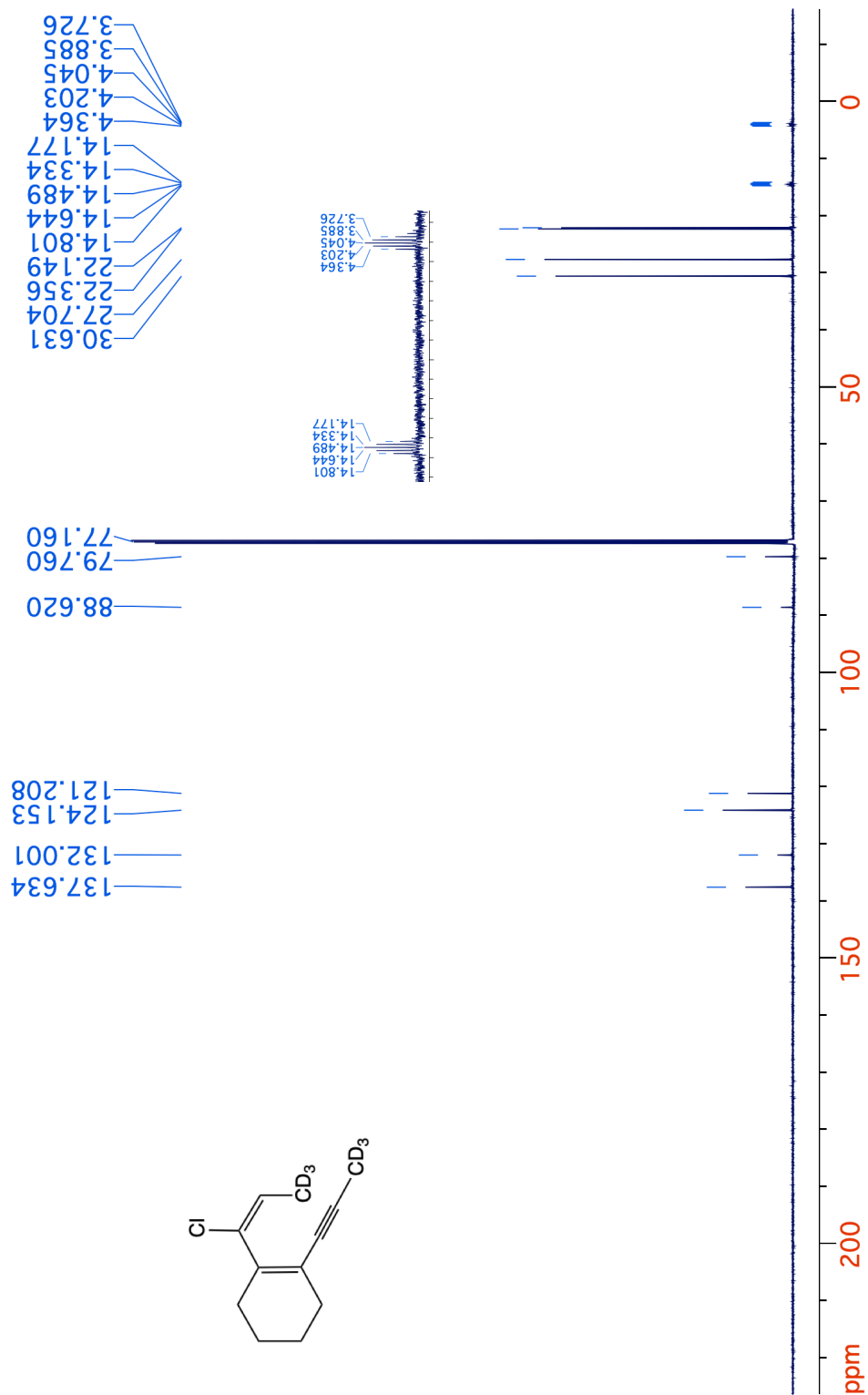
Figure 7-14. $^{13}C\{^1H\}$ NMR spectrum (125 MHz, CDCl$_3$) of **28**-*E*.

Acknowledgement

Chapter 7 contains the material being prepared for the publication "Enediyne Cycloaromatization with Incorporation of Chlorine from Chloroform and Hydrogen from 1,4-Cyclohexadiene". Qin, P.; O'Connor, J. M.; Baldridge, K. K.; Perrin, C. L.; Hitt, D. M.; Veccharelli, K. M.; Cope, S. K.; Holland, R. L.; Raub, A. The dissertation author is the first author on this paper.

H. References

1. Jones, R. R.; Bergman, R. G. *p*-Benzyne. Generation as an intermediate in a thermal isomerization reaction and trapping evidence for the 1, 4-benzenediyl structure. *J. Am. Chem. Soc.* **1972**, *94*, 660-661.

2. Perrin, C. L.; Rodgers, B. L.; O'Connor, J. M. Nucleophilic addition to ap-benzyne derived from an enediyne: a new mechanism for halide incorporation into biomolecules. *J. Am. Chem. Soc.* **2007**, *129*, 4795-4799.

3. Lo, C. Y.; Kumar, M. P.; Chang, H. K.; Lush, S. F.; Liu, R. S. Regioselective Haloaromatization of 1, 2-Bis (ethynyl) benzene via Halogen Acids and $PtCl_2$. Platinum-Catalyzed 6-π Electrocyclization of 1,2-Bis (1-haloethenyl) benzene Intermediates. *J. Org. Chem.* **2005**, *70*, 10482-10487.

4. O'Connor, J. M.; Friese, S. J.; Tichenor, M. Ruthenium-mediated cycloaromatization of acyclic enediynes and dienynes at ambient temperature. *J. Am. Chem. Soc.* **2002**, *124*, 3506-3507.

5. O'Connor, J. M.; Friese, S. J.; Rodgers, B. L. A transition-metal-catalyzed enediyne cycloaromatization. *J. Am. Chem. Soc.* **2005**, *127*, 16342-16343.

6. Hitt, M.D. Doctoral Dissertation, Investigations into Novel Modes of Reactivity and Stereoselectivity for the Cycloaromatization of Conjugated Enediynes and Dienynes. University of California, San Diego, CA, USA, **2011**.

7. Cope, S.K. Doctoral Dissertation, Ruthenium-Mediated Cycloaromatization of Tri-Pi Systems. University of California, San Diego, CA, USA, **2015**.

8. Veccharelli, K.M. Doctoral Dissertation, Conjugated Tri-Pi Systems: Investigations into Hexahapto Metal Complexes of Acyclic Conjugated Trienes and Novel Cycloaromatization Reaction of Nitrogen-Containing Enediynes. University of California, San Diego, CA, USA, **2017**.

9. Gao, Y.; DeYonker, N. J.; Garrett III, E. C.; Wilson, A. K.; Cundari, T. R.; Marshall, P. Enthalpy of formation of the cyclohexadienyl radical and the C-H bond enthalpy of 1,4-cyclohexadiene: An experimental and computational re-evaluation. *The J. Phys. Chem. A* **2009**, *113*, 6955-6963.

10. James, D. G. L.; Suart, R. D. Kinetic study of the cyclohexadienyl radical. Part 3.- Mutual interaction and thermal decomposition. *Trans. Faraday Soc.* **1968**, *64*, 2752-2769.

11. Lian, J. J.; Lin, C. C.; Chang, H. K.; Chen, P. C.; Liu, R. S. Thermal and Metal-Catalyzed Cyclization of 1-Substituted 3,5-Dien-1-ynes via a [1,7]-Hydrogen Shift: Development of a Tandem Aldol Condensation-Dehydration and Aromatization Catalysis between 3-En-1-yn-5-al Units and Cyclic Ketones. *J. Am. Chem. Soc.* **2006**, *128*, 9661-9667.

CHAPTER 8

Ruthenium-catalyzed 6π Electrocyclization of Conjugated Trienes

A. Introduction

Concerted 6π electrocyclization of conjugated trienes is a well-known fundamental organic annulation process, which has been extensively studied in the past 50 years since Lewis and Steiner reported the kinetic and mechanistic studies on a thermal cyclization of (Z)-hexa-1,3,5-triene (**1**) to 1,3-cyclohexadiene (**2**) in 1964 (Scheme 8-1).[1] Six years later, Woodward and Hoffmann formulated the principle of conservation of orbital symmetry,[2] which dictates the cyclization mode of conjugated π systems under different reaction conditions. For instance, triene **3** undergoes cyclization in a disrotatory fashion to give cyclohexadiene **4** with two R groups *syn* to each other under thermal condition; whereas a conrotatory ring closure can selectively occur on triene **3** to produce diastereomer **5** under photochemical condition (Scheme 8-2). Since then, 6π electrocyclization of conjugated triene has been attracted considerable attentions from synthetic community for the potential powerful application to construct new C – C bond in annulation reactions with high stereoselectivity. However, due to the high temperature it requires to overcome the activation barrier, decomposition and polymerization of the substrates that leads to low yield of desired products can be problematic.
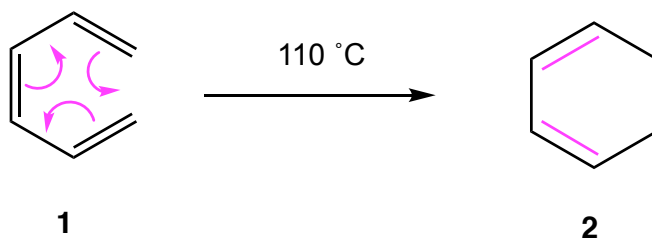
Scheme 8-1. Thermal cyclization of conjugated triene **1**.
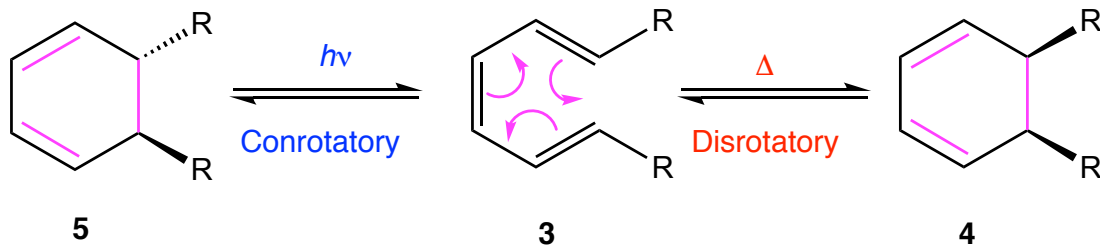
Scheme 8-2. Cyclization of triene **3** under thermal and photochemical conditions.

With the development of organometallic chemistry, metals have been attempted to coordinate and stabilize the transition state of the cyclization process. However, very limited success has been achieved so far, and a representative example of metal-catalyzed 6π electrocyclization of conjugated triene reported by Bergman and Trauner in 2008.[3] The strategy they employed is utilizing the coordination of a Lewis acid (Me$_2$AlCl) to the carbonyl oxygen of ester group to tune it more electron deficient, and thus lower down the energy of transition state (Scheme 8-3). According to their kinetic study, a 11-fold rate acceleration was achieved with one equivalent of catalyst loading in their system at 50 °C. Tantillo made a comment in a followed computational work that acceleration would likely involve direct interactions between a promoter and the electrons that rearrange.[20]
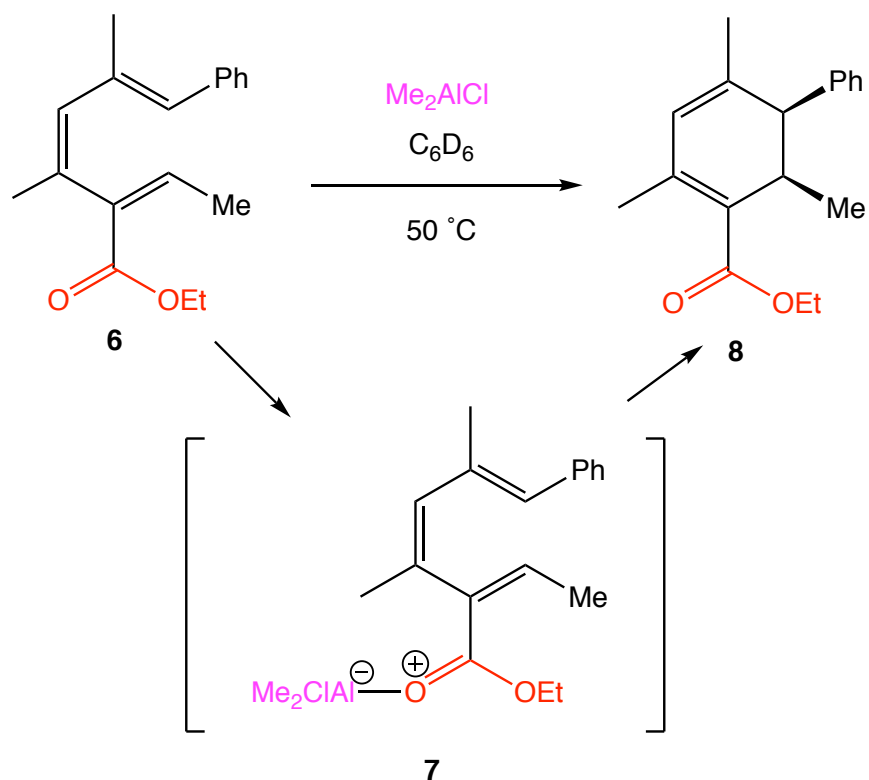
Scheme 8-3. Me$_2$AlCl catalyzed cycliztion of triene **6**.

In the literature, however, no successful example of electrostatic acceleration via transition metal-π interaction has been reported so far. For instance, Vollhardt reported that when a triene was heated with CpCo(PPh$_3$)$_2$, only η^2/η^4-metal complex was obtained under thermal or photochemical conditions, without any observation of 6π electrocyclization (Scheme 8-4).[21]

Brookhart found that extra heat is needed to trigger the cyclization of 1,3,5,7-cyclononatetraene when iron is coordinated, which is compared to the readily 6π electrocyclization at ambient temperature without participation of metal. The result suggests that in this scenario, the metal-π interaction even stabilizes the substrate and *retards* the cyclization process (Scheme 8-5).[22]
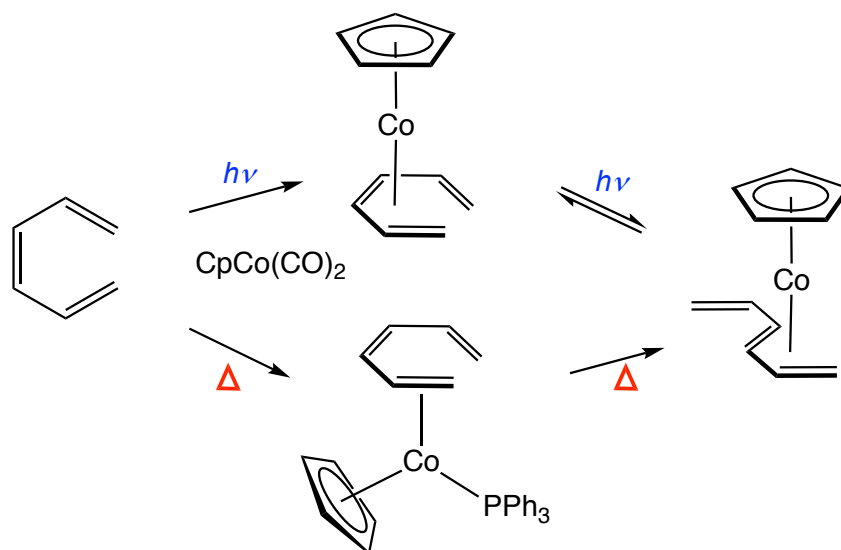
Scheme 8-4. Reaction of triene and CpCo(CO)$_2$ under different conditions.
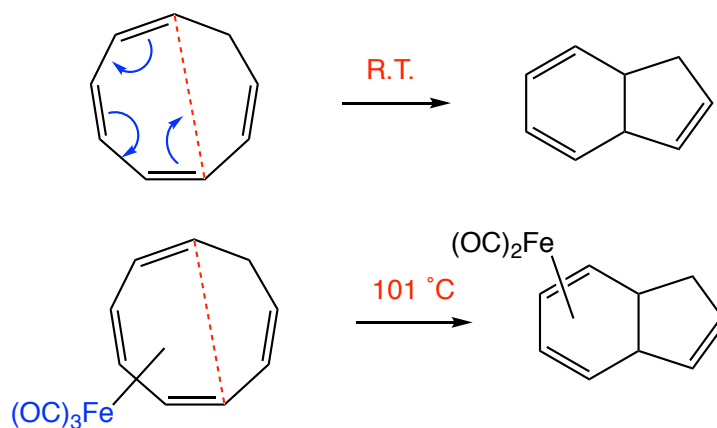
Scheme 8-5. Cylization of 1,3,5,7-cyclononatetraene.

Notably, Chaudret group discovered that the reaction of 1,3,5-hexatriene with [Cp*Ru$^+$], generated *in situ* through protonation of [Cp*Ru(OMe)]$_2$ by CF$_3$SO$_3$H, leads to formation of ruthenium-η^6-arene complex **10** and hydrogen gas at ambient temperature with quantitively yield (Scheme 8-6).[4] They ascribe the driving force of the this

remarkable transformation to the thermodynamic stability of the ruthenium-arene bond in complex **10**. However, they didn't provide any mechanistic studies or speculated mechanisms in this work.
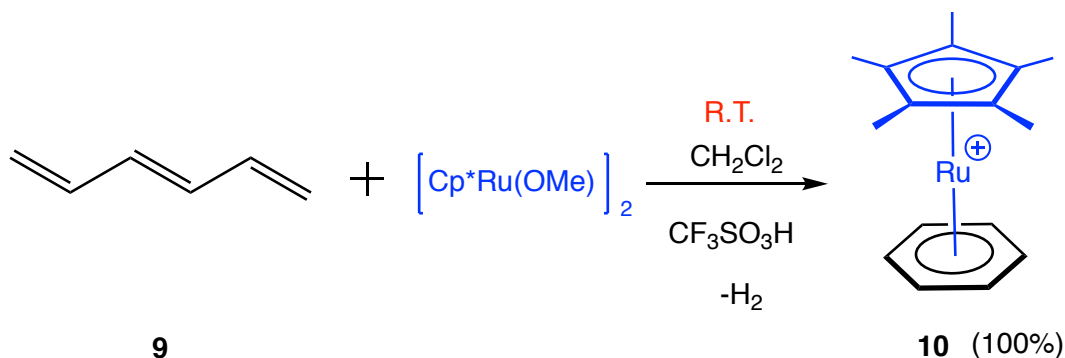
Scheme 8-6. Ruthenium-mediated cycloaromatization of triene **9**.

Stryker and coworkers reported a ruthenium-mediated aromatization of η^4-cyclohexadiene complex **11** via the activation of carbon – carbon bond with loss of a methane (Scheme 8-7).[5] By comparing Sryker result to Chaudret work, we postulate that a ruthenium-η^4-cyclohexadiene complex might also serve as the intermediate on the way to η^6-arene complex **10** in Chaudret system, in which a ruthenium-mediated cyclization of 1,3,5-hexatriene is involved.
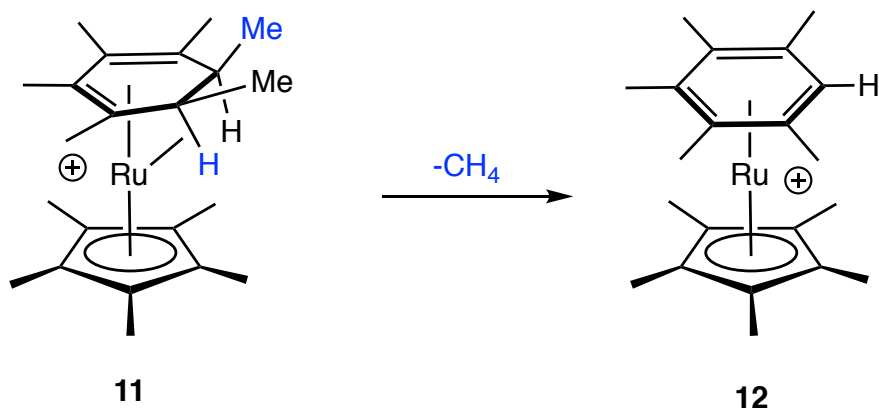
Scheme 8-7. Aromatize complex **11** by loss of a methane.

Inspired by our previous success on the ruthenium-mediated cycloaromatization of conjugated enediynes[6,7,8] and dienynes[9], here, an exploration of CpRu(NCMe)$_3$PF$_6$ (**13**) triggered cycloaromatization of acyclic conjugated trienes was carried out, which generates the ruthenium-η^6-arene product with excellent yield (88 – 92%) at ambient temperature within several hours. Mechanistic study at low temperature allows for the observation and isolation of various intermediates. Furthermore, the first example of transition-metal-catalyzed 6π electrocyclization was discovered by employing a more sterically hindered triene substrate.

B. Reactions of Dimethyl-substituted Trienes with Complex 13

1. Synthesis of Triene Substrates

In this work, three dimethyl-substituted acyclic isomeric conjugated trienes **14** (*ZZ*), **15** (*EE*), and **16** (*EZ*) (Figure 8-1) were synthesized and employed as substrates to react with CpRu(NCMe)$_3$PF$_6$ (**13**). The reason to choose these trienes is based on the three following considerations: a) the annulated six-membered ring can lock the *Z* configuration of the internal alkene, which is required for the followed cyclization process; 2) the size of methyl substituent is relatively small compared to other bulkier functional groups that could potentially impede the cyclization step;[10] 3) it would be a good comparison by utilizing all the three isomers as substrate for the exploration of stereochemistry and mechanistic studies.
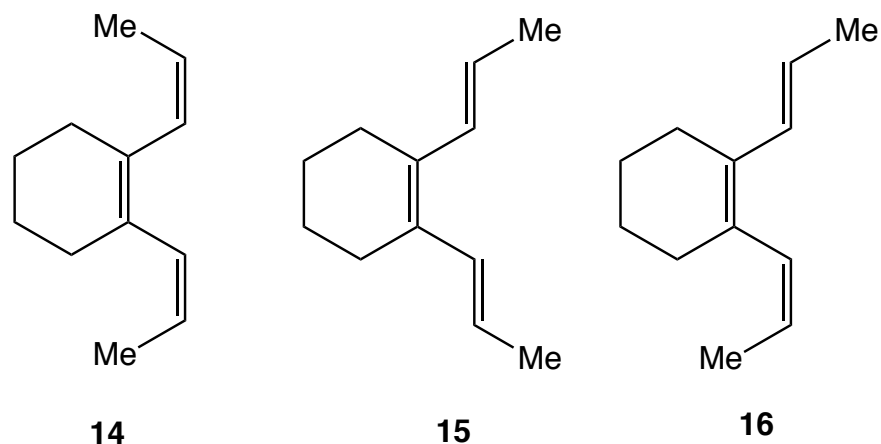
Figure 8-1. The three isomeric dimethyl-substituted trienes **14**, **15**, and **16**.

The synthesis of all three dimethyl-substituted trienes are shown in Scheme 8-8. The *ZZ* isomer **14** was made from a double Lindlar reduction of enediyne **17** that was made from the modified procedure in literature.[8,11] The synthesis of *EZ* isomer **16** starts from a literature known molecule 2-((trimethylsilyl)ethynyl)cyclohex-1-ene-1-carbaldehyde (**18**),[12] followed by 5 steps, including Wittig reaction, photochemical isomerization, desilylation, methylation, and Lindlar reduction. The *EE* isomer **15** can be prepared from an iodine-catalyzed isomerization of **16** in benzene solution with a 45% isolated yield. It was noted that the concertation of **16**, reaction time, and the amount of iodine loading are all curtail factors for the success of this reaction to get a decent yield (see experimental section). Other attempts to synthesize **15** all failed, such as photochemical isomerization of **16** and dissolving-metal reduction of enediyne **17**, due to the massive decomposition or polymerization of the starting materials. All the three isomeric trienes (**14**, **15**, **16**) were isolated and purified by flash chromatography on silica gel with hexanes, and the resulting colorless oil can be stored under -20 °C for a few weeks without decomposition.
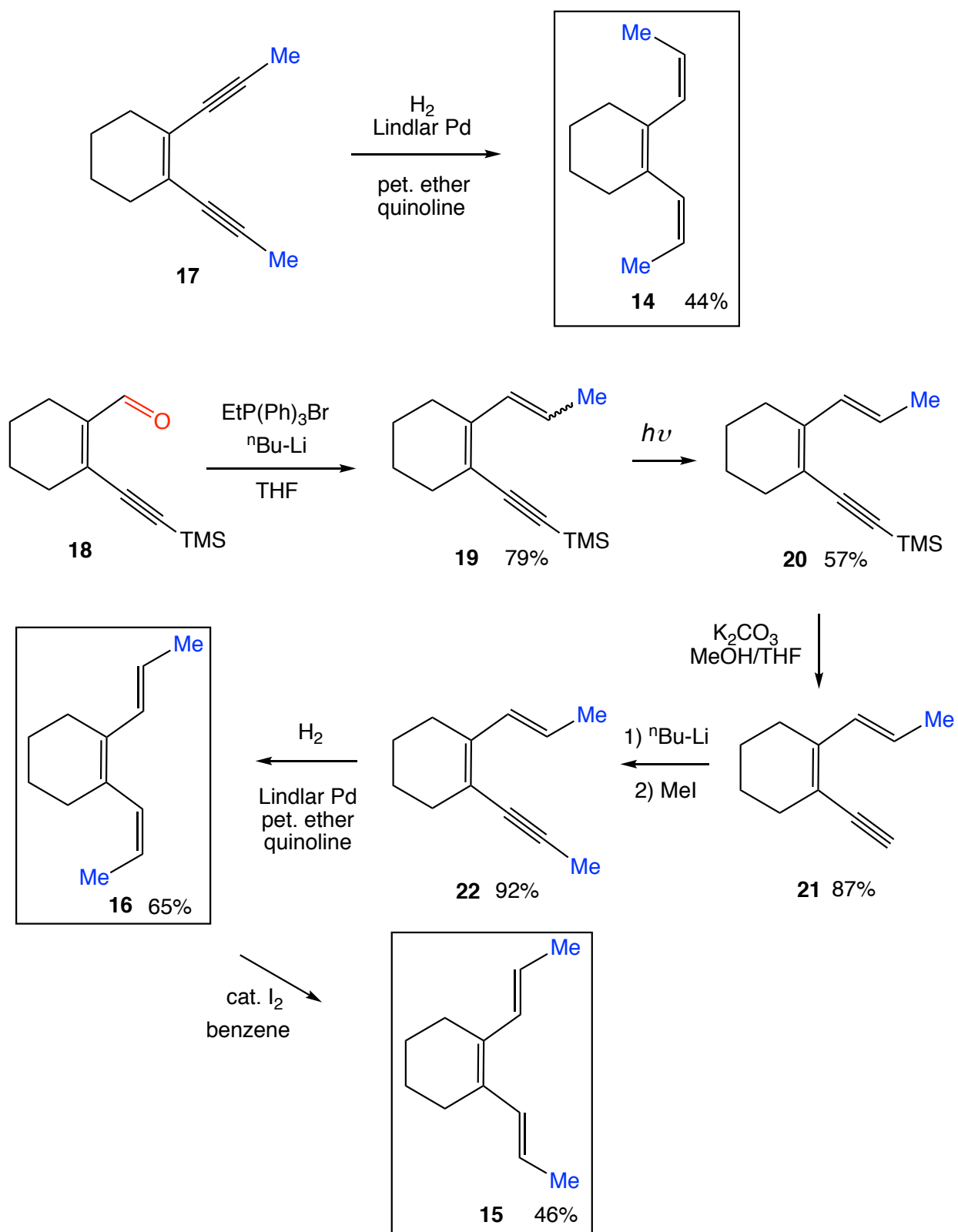
Scheme 8-8. Synthesis of trienes **14**, **15**, and **16**.

2. The Reaction of Triene 14 with Complex 13

The first triene we examined is the *ZZ* isomer **14**. When a CD_2Cl_2 solution of **14** (4.8 mg, 0.03 mmol) was treated 12.8 mg (0.03 mmol) of complex **13** in an NMR tube under inert atmosphere at ambient temperature, the color of the solution gradually changed from yellow to clear. After 100 minutes, the ^1H NMR spectrum (400 MHz) indicates that all starting triene **14** was consumed, and a product with 92.6% NMR yield was observed based on the new methyl and Cp resonances at δ 2.30 (s, 6H) and 5.11 (s, 5H), respectively (Scheme 8-9).
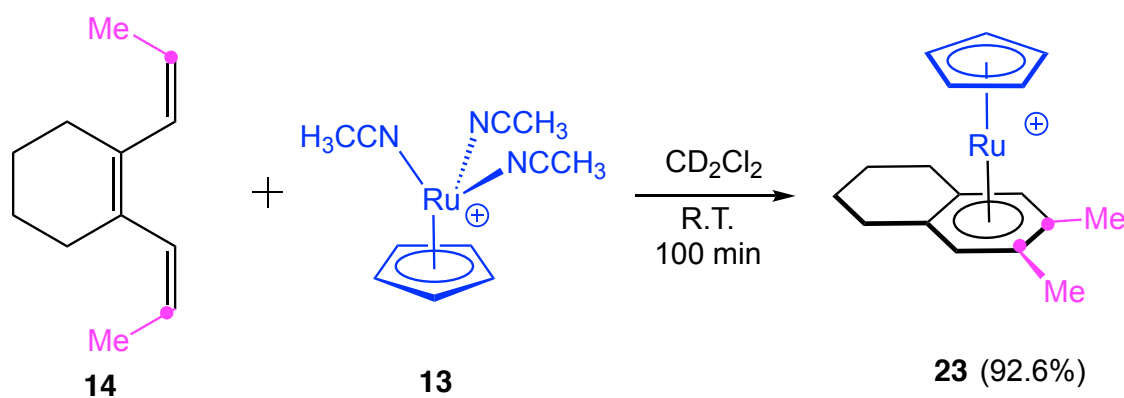
Scheme 8-9. Reaction of tirene **14** with complex **13**.

In a preparation-scale reaction, 1.5 equivalents of triene **14** was treated with complex **13** in a similar fashion. After crystallization from the crude reaction mixture with diethyl either and methylene chloride, 83.5% yield of product **23** was obtained as colorless solid. In the ^1H NMR spectrum (400 MHz, CD_2Cl_2) of the isolated product, all the vinyl hydrogens disappeared, and a shielded aromatic hydrogen resonance was observed at δ 6.01 (s) with the integration of 2 relative to the 5 hydrogens of Cp ligand.

The characteristic eight methylene-hydrogen signals of the six-membered ring are still present. Three shielded aromatic carbon resonances exist in the $^{13}C\{^1H\}$ NMR spectrum at δ 87.5, 100.7, and 102.5, respectively. The structure of the product was confirmed by X-ray crystallography, which reveals a ruthenium-η^6-arene complex (Figure 8-2). The result is consistent with what Chaudret observed in their linear triene system.
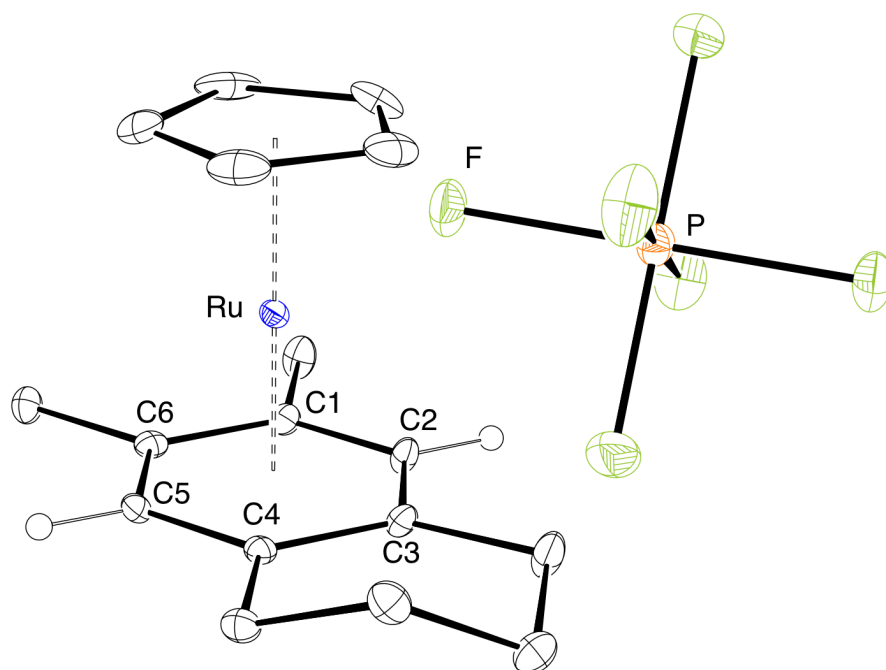
Figure 8-2. ORTEP drawing of complex **23** with ellipsoids shown at 30% probability.

In order to explore the mechanism, a variable temperature NMR tube reaction was carried out. A 1 : 1 ratio of triene **14** and complex **13** was dissolved in acetone-d_6 at -78 °C with 1,3,5-tri-*tert*-butylbenzene as internal standard, and the reaction mixture was monitored by ^{1}NMR that was equipped with a nitrogen-cooled cold probe (Scheme 8-10). When increase the temperature to -45 °C and stayed for 45 minutes, it was observed that 98% of the complex **13** disappeared, and an intermediate with a new Cp

resonance was detected at δ 5.26 (s, 5H, Cp). The existence of two methyl signals at δ 1.77 (d, 3H, J = 5.5 Hz), and 1.48 (d, 3H, J = 6.5 Hz) suggests that the structure of the intermediate is no longer symmetric. Four shielded vinyl hydrogen resonances were observed at δ 4.02 (d, 1H, J = 9.0 Hz), 4.51 (d, 1H, J = 9.5 Hz), 4.75 (m, 1H), and 5.13 (m, 1H), respectively, which indicates that the two terminal alkenes are both coordinated to ruthenium, and thus excludes the η^2-triene structure. It was noted that a singlet with 3 hydrogen located at δ 2.55 matches the typical range of ruthenium-binding acetonitrile.[13] The intermediate was observed gradually disappeared when slowly increasing the temperature, and after staying 120 minutes at ambient temperature, complex **23** was obtained with 91.6% NMR yield.
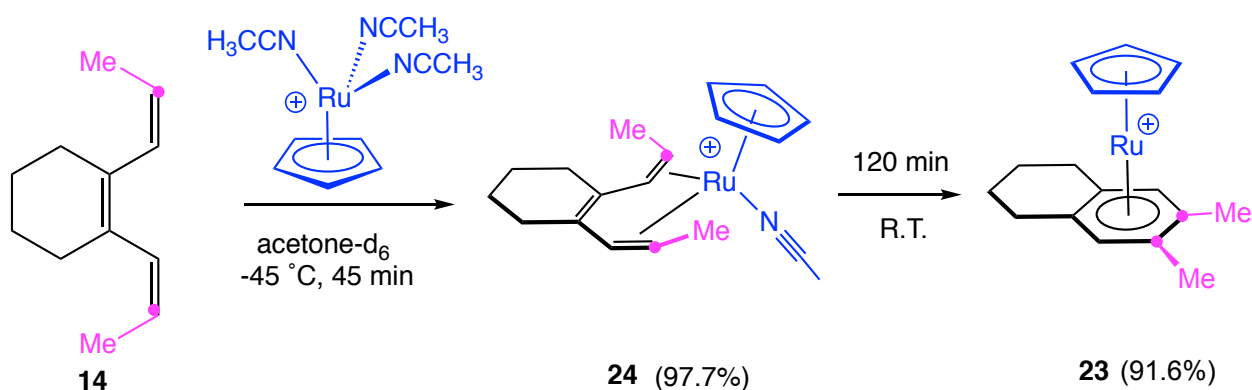
Scheme 8-10. Variable temperature NMR reaction of triene **14** with complex **13**.

The X-ray quality crystals of the intermediate **24** was successfully obtained by distilling dry hexanes into the reaction mixture in a separate tube of the same set up after 45 minutes at -45 °C. The followed X-ray crystallographic analysis reveals **24** as an unsymmetrical ruthenium-η^4-triene structure, in which the metal center is coordinated

to the two alkenes bearing methyl groups without any isomerization of the alkenes (Figure 8-3). The structure of ruthenium-η^4-1,3-diene complexes have been widely studied and reported in the literature,[14] however, to our best knowledge, this is the first example of ruthenium binding to two alternate alkenes in conjugated triene systems. As anticipated, the C1 – C2 (1.411(6) Å) and C5 – C6 (1.382(6) Å) bond distances are significantly longer than the C3 – C4 (1.316(6) Å) bond due the back-donation effect from the ruthenium (Table 8-1). The metallacyclopentene ring that is assembled by atom C2, C3, C4, C5, and Ru is essentially planar with the largest deviation from planarity on C4 (Δ_{max} = 0.060(3) Å, the distance between C4 and mean plane C2-C3-C4-C5-Ru). The steric congestion between two methyl groups are released by their relative *anti* positions with respect to the metallacyclopentene. In comparison, a similar structure that was reported by Kirchner exhibits a flatter metallacyclopentene ring (Δ_{max} = 0.018(3) Å, Figure 8-4),[15] which could be attributed to the released torsion strain in complex **25** that is caused by one less coordination of alkene. The steric hindrance between the methyl group on C6 and Cp ligand is manifested by the longer Ru – C6 bond (2.273(4) Å) than Ru – C1 bond (2.217(4) Å). The three alkenes are found no longer conjugated due to the large torsion angle of C3-C4-C5-C6 (72.2(5) °) and C1-C2-C3-C4 (70.3(5) °). The nonbonding C1⋯C6 distance is measured as 3.885(6) Å.
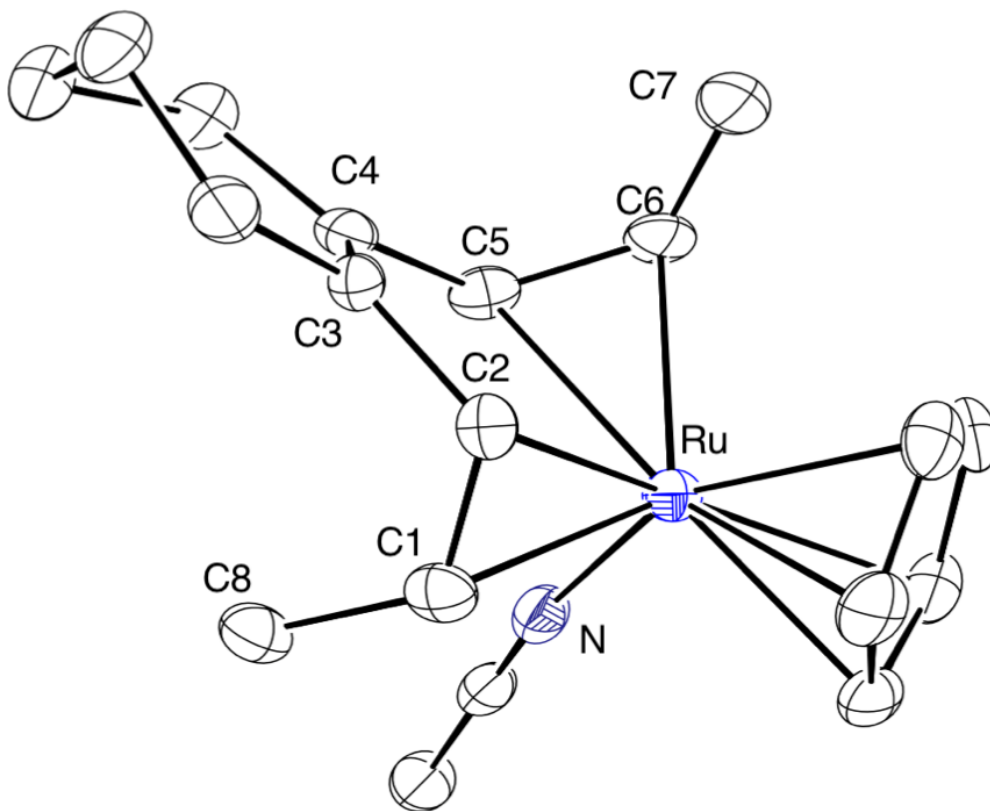
Figure 8-3. ORTEP drawing of complex **24** with ellipsoids shown at 30% probability.

Table 8-1. Seletecd bond distances (Å) and angles (deg) of complex **24**.

C1 – C2	1.411(6)	Ru – C2	2.240(4)
C2 – C3	1.482(6)	Ru – C5	2.308(4)
C3 – C4	1.316(6)	Ru – C6	2.273(4)
C4 – C5	1.487(6)	C2-Ru-C6	74.85(16)
C5 – C6	1.382(6)	C3-C4-C5-C6	72.2(5)
Ru – N	2.064(4)	C1-C2-C3-C4	70.3(5)
Ru – C1	2.217(4)	C1····C6	3.885(6)
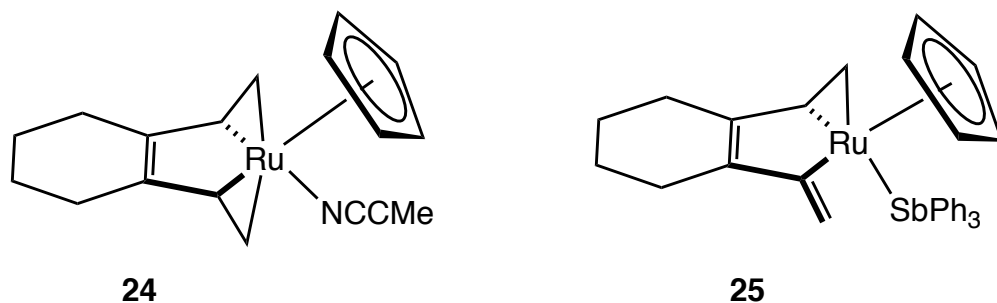
Figure 8-4. Comparison of structure **24** and **25**.

A computational study was carried out to compare the relative stability of the unsymmetrical intermediate **24** and the symmetrical analogue **26**, as shown in Figure 8-5. The calculated energy of the symmetrical complex **26** is 3.4 kcal/mol higher than the unsymmetrical analogue **24**, which is consistent with the experimental results. The nonbonding C1····C6 distance in the symmetrical structure **26** is detected much shorter (Δ = 0.103 Å).
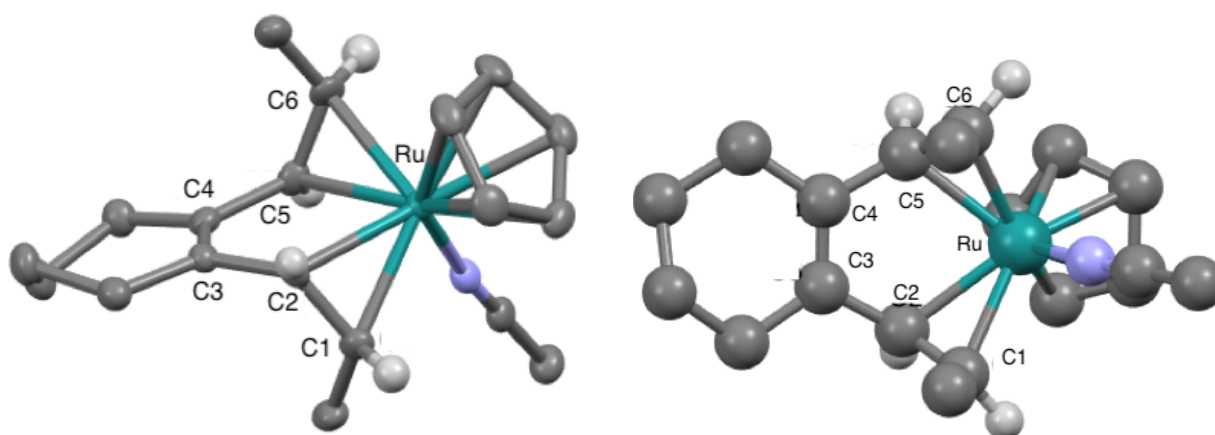
Figure 8-5. Computational structures of complex **24** (left) and **26** (right).

3. The Reaction of Triene 15 with Complex 13

Both an NMR tube reaction at ambient temperature and a variable temperature NMR tube reaction between triene **15** and complex **13** were also conducted in a similar fashion. For the ambient temperature scenario, one equivalent of triene was treated with complex **13** in methylene chloride under inert atmosphere. After 70 minutes, when the reaction is finished, the same ruthenium-arene complex **23** was obtained with 87.3% NMR yield based on the integration of Cp resonance at δ 5.11 (s, 5H) relative to internal standard (Scheme 8-11).
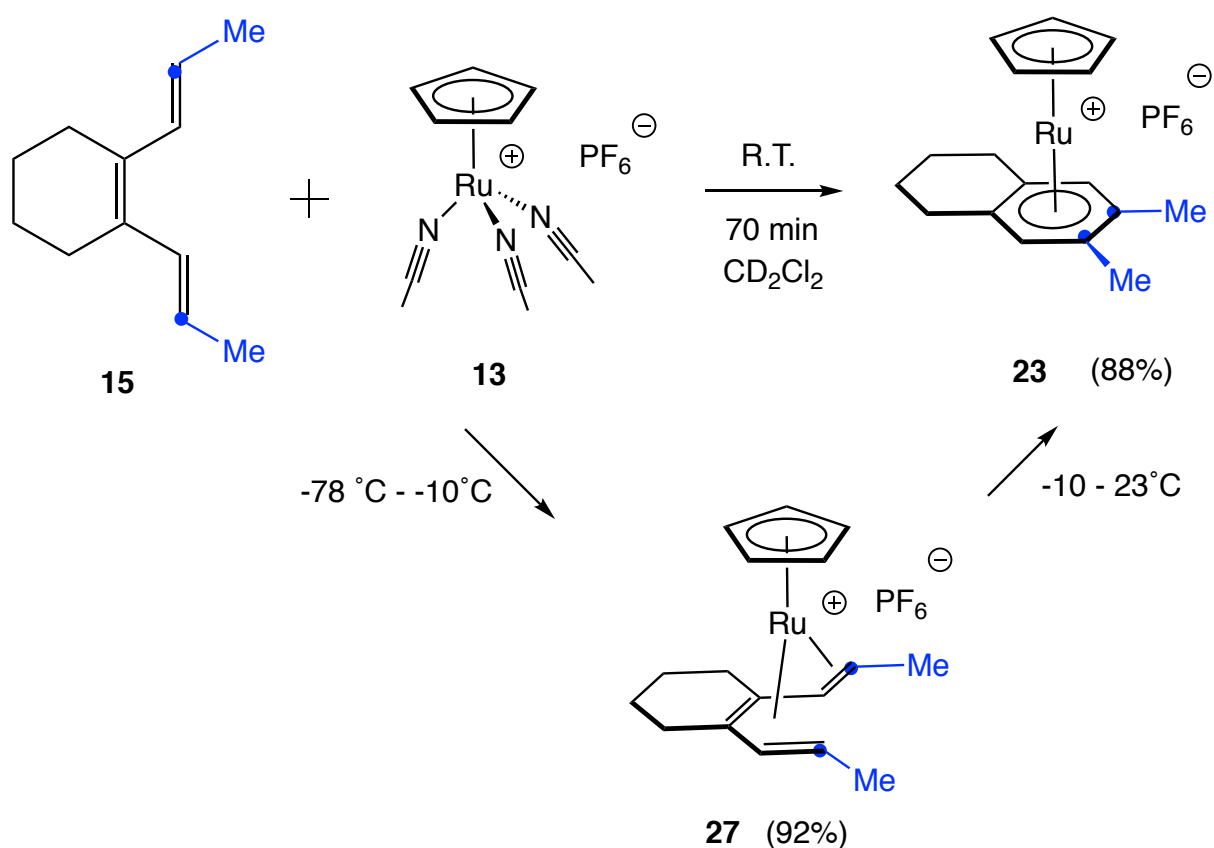
Scheme 8-11. Reaction of triene **15** with complex **13**.

For the variable temperature NMR reaction, after mixing triene **15** and complex **13** at -78 °C in CD_2Cl_2, the reaction mixture starts to be monitored by ^1H NMR spectroscopy from -60 °C. It was found when the temperature reached -20 °C, a new intermediate appeared, and the maximum yield (92%) of the intermediate was obtained at -10 °C for 20 minutes based on the integration of the new Cp resonance at δ 5.13 (s, 5H) relative to internal standard. The observance of two new methyl resonances at δ 1.66 (d, 3H, J = 6.0 Hz) and 2.07 (d, 3H, J = 6.0 Hz) indicate that the structure is also unsymmetrical. There is no acetonitrile found coordinated to the metal center anymore. In the $^{13}C\{^1H\}$ NMR spectrum (500 MHz), six shielded vinyl carbon resonances were observed at δ 91.1, 105.5, 100.5, 113.0, 91.2, and 65.0, respectively, which indicates that all three double bonds are binding to ruthenium through a η^6-cooridnation mode. After increasing the temperature to 23 °C and staying for 70 minutes, all the intermediate disappeared, and ruthenium-arene complex **23** was observed with 88% NMR yield.

The intermediate **27** was successfully isolated by distilling dry hexanes into the reaction mixture in a separate tube of the same set up after 7 hours at -20 °C. The single crystal was also obtained and subsequently studied by X-ray crystallography, which gives an unsymmetrical ruthenium-η^6-triene structure with a s-*cis* conformation on diene moiety C1-C2-C3-C4 and a s-*trans* conformation on diene moiety C3-C4-C5-C6 (Figure 8-6). Despite a few examples of ruthenium-η^6-triene structures can be found in the literature,[16] this is the first observation of a ruthenium coordinated to an acyclic conjugated triene. Compared to Ru – C1 bond, the Ru – C6 bond is considerably longer (Δ = 0.138 Å), and the corresponding weaker back-donation effects of metal center to

alkene C5=C6 than alkene C1=C2 is manifested by the shorter C5 – C6 bond (1.368(7)

Å) compared to C1 – C2 bond (1.418(10) Å) (Table 8-2). The significant conjugation of

the s-*cis* diene moiety is reflected by the small torsion angle of C1-C2-C3-C4 (7.4(11) °);

whereas the two double bonds of the s-*trans* diene are essentially localized with a large

torsion angle of C3-C4-C5-C6 (56.1(6) °). Carbon C6 is found off the mean plane C1-

C2-C3-C4-C5 by 0.893(10) Å, and the angle between bond C5 – C6 and the plane

normal is measured as 45.1(4) °. The nonbonding C1····C6 distance is detected as

3.431(8) Å.
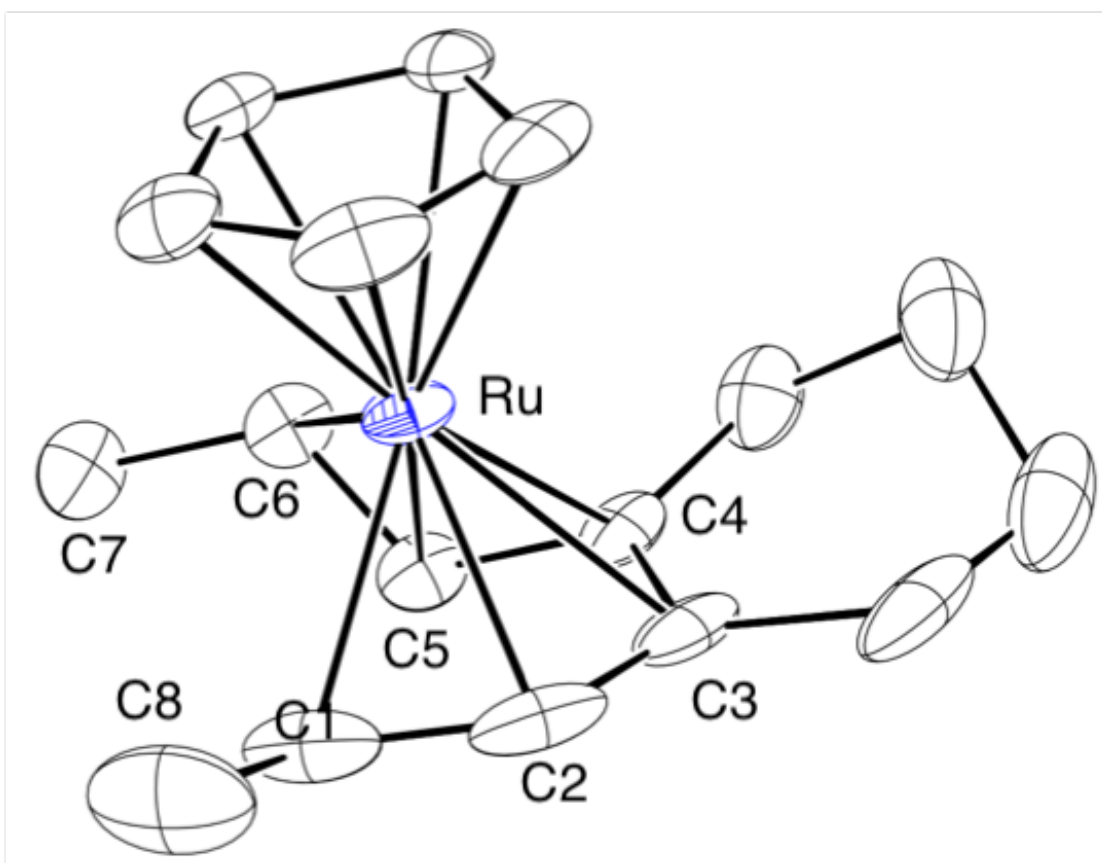
Figure 8-6. ORTEP drawing of complex **27** with ellipsoids shown at 30% probability.

Table 8-2. Seletecd bond distances (Å) and angles (deg) of complex **27**.

C1 – C2	1.418(10)	Ru – C3	2.254(5)
C2 – C3	1.428(9)	Ru – C4	2.177(5)
C3 – C4	1.437(7)	Ru – C5	2.196(5)
C4 – C5	1.450(7)	Ru – C6	2.362(5)
C5 – C6	1.368(7)	C3-C4-C5-C6	56.1(6)
Ru – C1	2.224(6)	C1-C2-C3-C4	7.4(11)
Ru – C2	2.178(5)	C1····C6	3.431(8)

In order to get the unambiguous NMR assignments of complex **27**, some 2D NMR data (HSQC, HMBC, and COSY; 500 MHz, methylene-d_2) were subsequently acquired at ambient temperature (Figure 8-7 and Table 8-3). The results of acquisitions are consistent with the unsymmetrical η^6-bounded structure. Two methyl doublets were observed in correlation with two vinyl hydrogens at δ 3.65 and 6.13, respectively. The other two vinyl hydrogens located at δ 2.22 and 5.12 exhibit close proximity to C3 at δ 105.5 and C6 at δ 91.2 in HSQC, which is in agreement with the shielding effect from metal center. The presence of an unusual upfield vinyl carbon C7 at δ 65.0 that is in one bond correlation with vinyl hydrogen at δ 3.65 might be ascribed to the short Ru-C distances (2.231 Å) relative to its counterpart C3 (2.393 Å). HMBC correlations of the δ 6.13 proton resonance with the C1 at δ 20.4, C3 at δ 105.5, and C4 at δ 100.5 is in good consistence with the structure, in which H2 is twisted farthest from the metal center, and it also supports the assigned connectivity among C1, C2, C3, and C4.
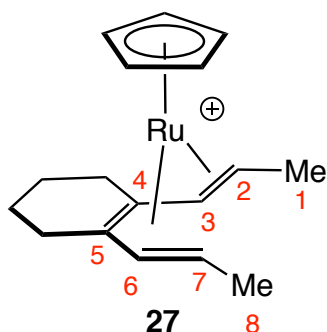
Figure 8-7. Numbering of complex **27** for NMR assignments.

Table 8-3. 2D-NMR spectroscopic data of complex **27**.

¹H (ppm)	HSQC ¹³C correlation (ppm)	HMBC ¹³C correlation (ppm)	COSY ¹H correlation (ppm)
1.68 (d, 3H, J = 5.6 Hz, H8)	23.9 (C8)	65.0 (C7), 91.2 (C6)	3.65 (H7)
2.09 (d, 3H, J = 5.6 Hz, H1)	20.4 (C1)	91.1 (C2), 105.5 (C3)	6.13 (H2)
2.22 (d, 1H, J = 13.2 Hz, H3)	105.5 (C3)	91.1 (C2), 100.5 (C4), 113.0 (C5)	6.13 (H2)
3.65 (m, 1H, H7)	65.0 (C7)	23.9 (C8), 91.2 (C6), 113.0 (C5)	1.68 (H8), 5.12 (H6)
5.12 (d, 1H, J = 10.0 Hz, H6)	91.2 (C6)	23.9 (C8), 100.5 (C4)	3.65 (H7)
6.13 (m, 1H, H2)	91.1 (C2)	20.4 (C1), 100.5 (C4), 105.5 (C3)	2.09 (H1), 2.22 (H3)

One might expect that 3.431 Å is too long to directly form a new bond between C1 and C6 for the followed cyclization step. Indeed, the isolated complex **27** was found stable in the CD₂Cl₂ solvent at ambient temperature under inert atmosphere for a few days. Only when heating up the CD₂Cl₂ solution of **27** at 50 °C, complex **23** was

observed to generate, and quantitively yield was obtained after 5 hours (Scheme 8-12). In comparison, a rapid conversion of **27** to complex **23** was observed in acetone-d_6 solvent at ambient temperature with 98% NMR yield. Based on these observations, we proposed that a coordination ligand, such as acetonitrile and acetone, is needed for an isomerization to shorten the C1····C6 nonbonding distance, in which the s-*trans* conformation of C3-C4-C5-C6 in **28** is converted to a s-*cis* conformation to form **29** (Scheme 8-13).
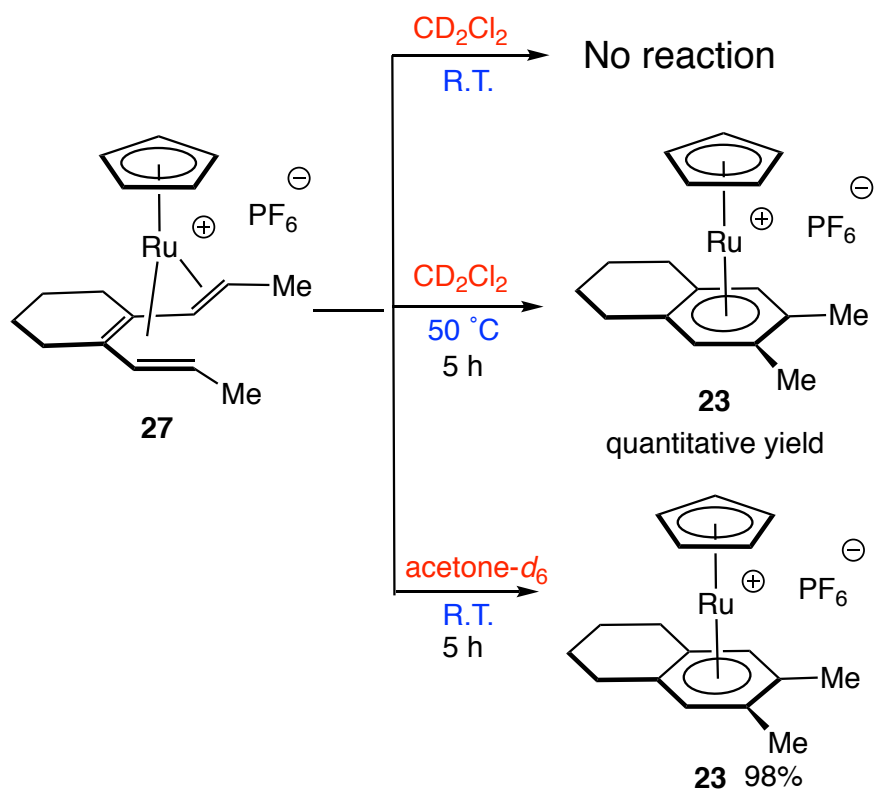
Scheme 8-12. Reation of complex **27** under different conditions.

678
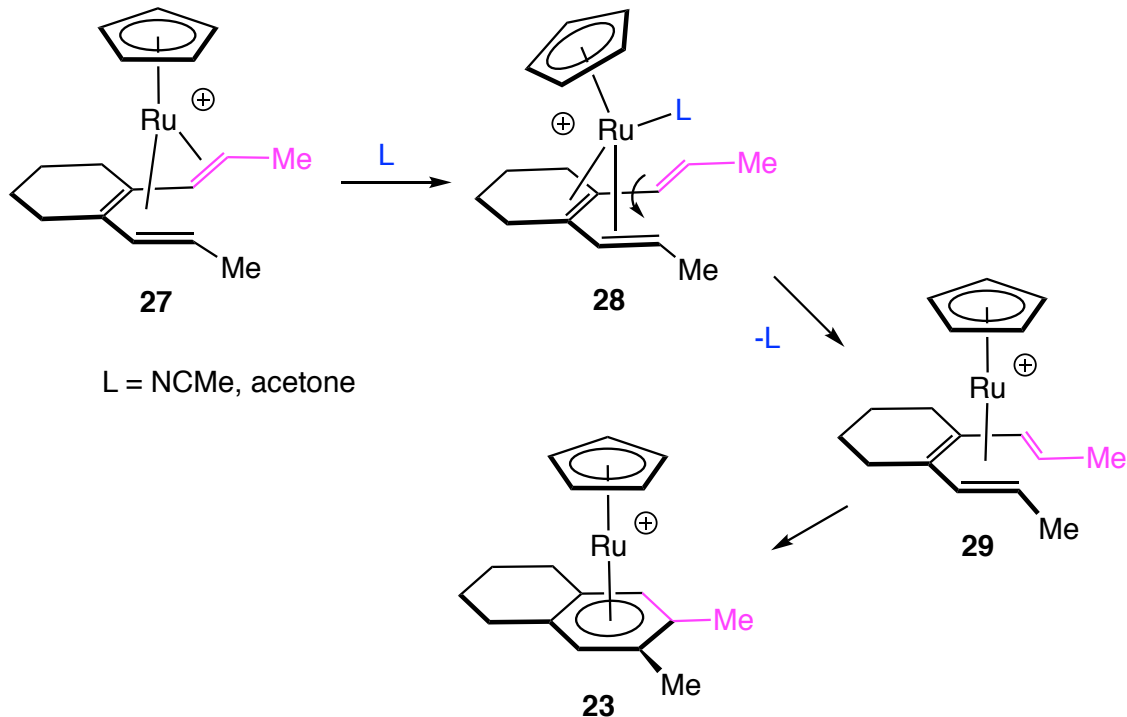
Scheme 8-13. Cooridnation ligand-assited isomerization of complex **27**.

4. The Reaction of Triene 16 with Complex 13

A similar variable temperature NMR reaction was conducted between triene **16** and complex **13**. Different from the other two triene isomers, interestingly, more intermediates were able to be observed at low temperature (Scheme 8-14). The first intermediate observed is a η^4-triene **30** with a maximum yield of 20.2% after 30 minutes at -20 °C, which was characterized by the two methyl groups at δ 1.45 (d, 3H, J = 6.0 Hz) and 1.82 (d, 3H, J = 6.0 Hz), an acetonitrile resonance at δ 2.44 (s, 3H), and four shielded vinyl hydrogen signals at δ 3.75 (d, 1H, J = 13 Hz), 4.38 (d, 1H, J = 10 Hz), and 4.62 (m, 2H), respectively.
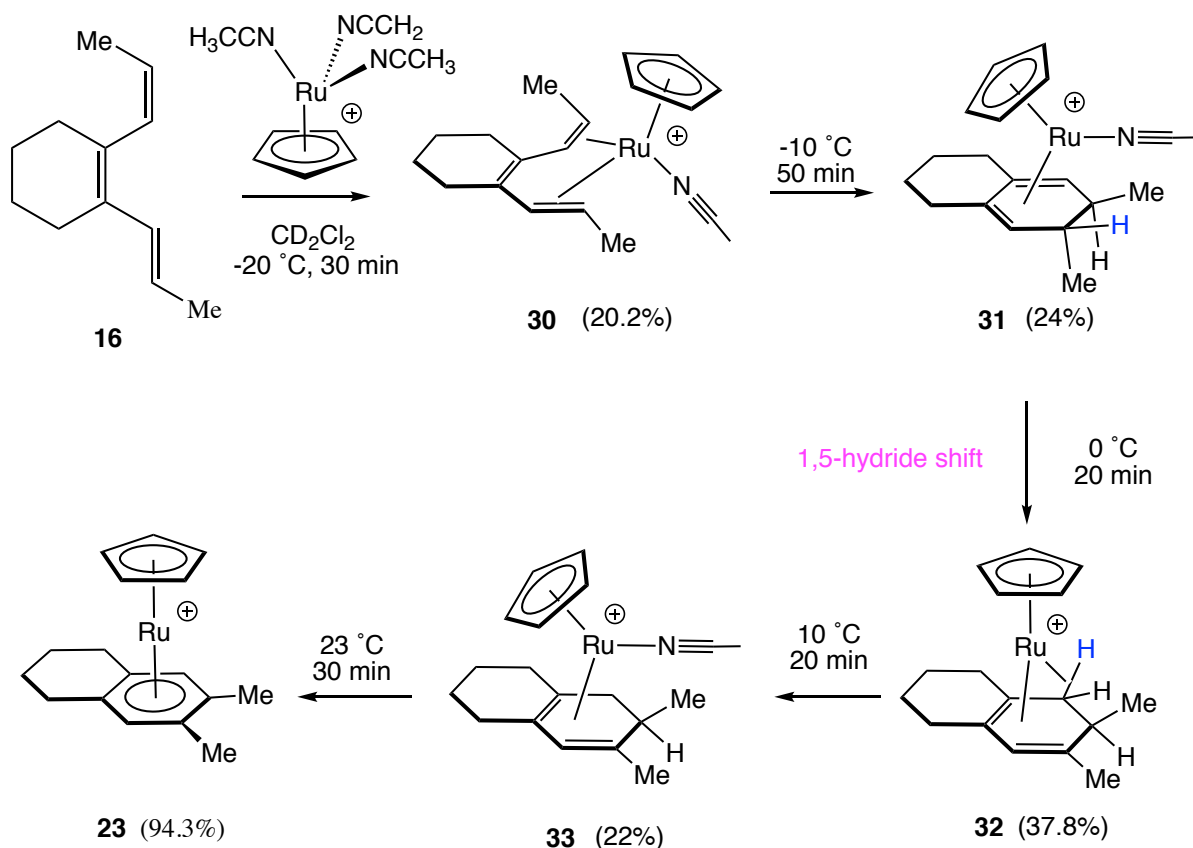
Scheme 8-14. Variable temperature NMR reaction of triene **16** with complex **13**.

After increasing the temperature to -10 °C and keeping for 50 minutes, the second intermediate **31** was observed and characterized as a ruthenium-η^4-cyclohexadiene complex. The coordinated acetonitrile resonance was detected at δ 2.57 (s, 3H). The two methyl groups were found at δ 0.92 (d, 3H, J = 6.0 Hz) and 1.24 (d, 3H, J = 6.0 Hz), respectively, which are more shielded compared to the intermediate **30** due to the change of hybridization of the two adjacent ring carbons from sp^2 to sp^3. The unsymmetrical structure of **31** indicates that the ruthenium-mediated cyclization also proceeds in the expected thermal disrotatory fashion. The two vinyl hydrogens of

31 were observed at δ 5.37 (bs, 2H). The small coupling between vinyl hydrogen and methylene hydrogen is typically found in cyclohexadiene substructures.[17]

More strikingly, an agostic-ruthenium intermediate **32** was observed at 0 °C with a 37.8% maximum yield. The agostic-H resonance was detected at δ -7.9 (t, 1H, J = 16 Hz), and the splitting pattern is ascribed to a geminal coupling and a vicinal coupling with the same coupling constant. We proposed that intermediate **32** is generated through a ruthenium-mediated 1,5-hydride sift from complex **31** (Scheme 8-15), which is in excellent agreement with the mechanism Sryker proposed.[5] The methyl group attached on the tertiary carbon was observed at δ 0.90 (d, 3H, J = 7.0 Hz), while the more deshielded methyl group that is attached on the vinyl carbon was exhibited as a singlet at δ 1.81 (s,3H). The relative *anti* position of the agostic hydrogen with the adjacent tertiary hydrogen is manifested by the large coupling constant (16 Hz), which furtherly demonstrates the stereochemistry of intermediate **31** and the disrotatory ring-closure fashion of the triene.
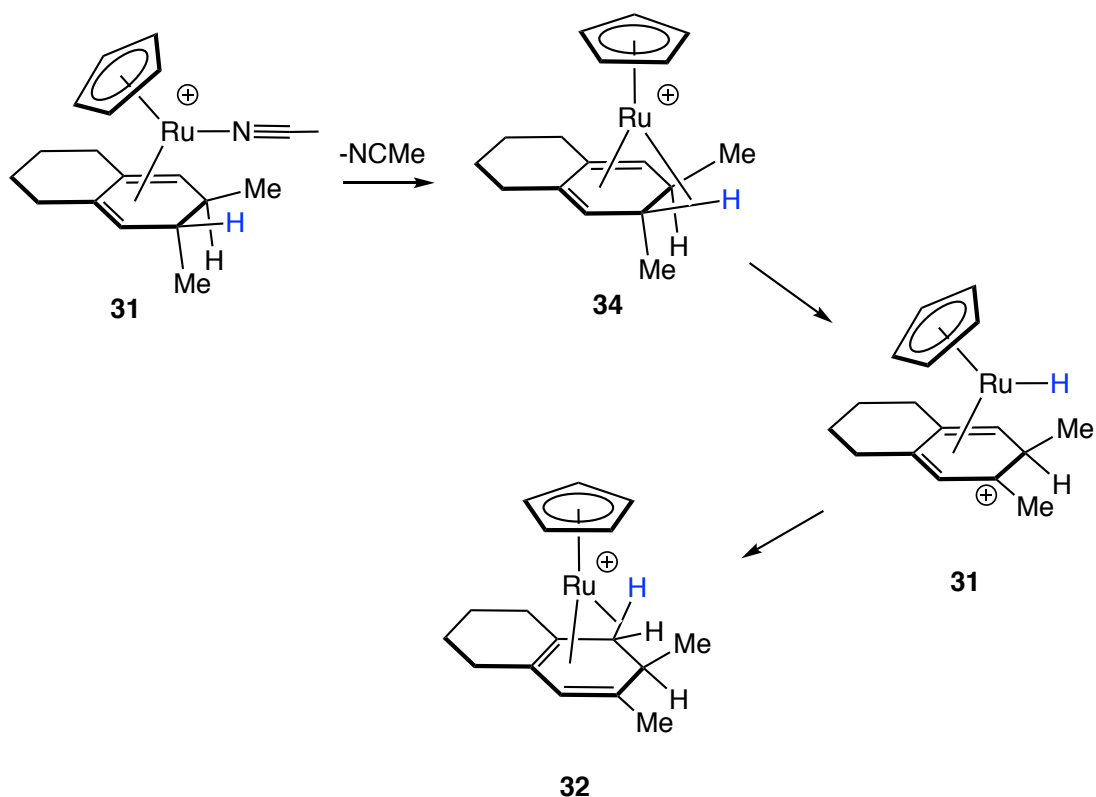
Scheme 8-15. Formation of complex **32** from **31**.

The fourth intermediate **33** was observed at 10 °C for 20 minutes with a 22% maximum yield. The structure of **33** was deduced as an η^4-cyclohexadiene complex, and the characteristic resonances were observed as: δ 0.92 (d, 3H, J = 7.0 Hz, Me), 1.75 (s 3H, Me), 2.63 (s, 3H, NCMe), and 4.60 (s, 1H, vinyl-H). After reaching 23 °C for 30 minutes, all the intermediates disappeared, and ruthenium-arene product **23** was obtained with 94.3% NMR yield.

Based on the observations in the variable temperature NMR experiments of all three triene isomers, the mechanism of ruthenium-mediated cycloaromatization of trienes was proposed and shown in Scheme 8-16. Here we used *EZ* isomer **16** as example. Upon the dissociation two acetonitrile ligands, ruthenium coordinates to the

two terminal alkenes to generate the η^4-triene intermediate **30**, that is followed by a further replacement of one acetonitrile ligand to give η^6-triene intermediate **36**. After a metal-mediated 6π electrocyclization, η^4-cyclohexadiene intermediate **34** can be produced. A subsequent 1,5-hydride shift affords the intermediate **32** with an agostic interaction, in which the exceedingly acidic agostic hydrogen can be easily deprotonated by any base present in the solution (such acetonitrile) to generate the η^5-cyclohexadienyl complex **37**. The loss of a hydride on the tertiary carbon gives the final ruthenium-arene product **32** with a hydrogen gas.
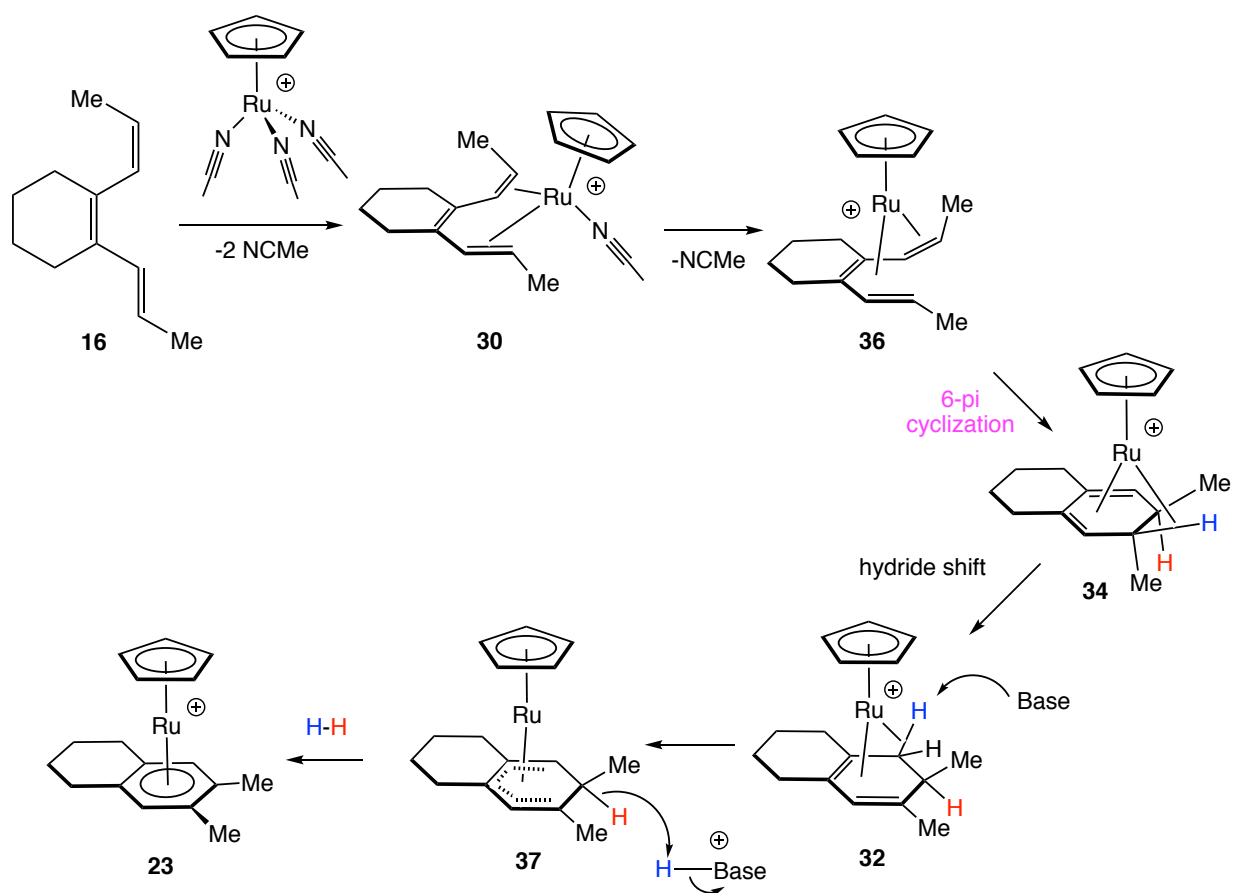
Scheme 8-16. Proposed mechanism for the formation of complex **23**.

5. Control experiments without addition of metal

In order to compare the results from ruthenium incorporated cyclization of trienes, the three dimethyl-substituted triene isomers were also examined under classic thermal and photochemical conditions. For instance, when the *ZZ* isomer **14** was heated in an NMR tube at 130 °C in benzene-d_6 solvent for one hour, a rapid formation of *EZ* isomer **16** was observed with a 97% yield (Scheme 8-17). After longer reactions time was executed (9 days), a maximum yield (22%) of the desired cyclohexadiene **38** was obtained. The characteristic resonances of **38** were observed at δ 1.01 (d, 6H, *J* = 6.0 Hz, Me) and 5.31 (bs, 2H, vinyl-H) in the ^{1}H NMR (400 MHz, C_6D_6) of the crude reaction mixture. The spectroscopic data was also compared to the authentic sample that was synthesized from a preparation-scale reaction. However, slow isomerization was observed on **38** to produce the diene molecule **39** after longer reaction time, and a maximum yield (52%) of **39** was observed after 29 days. The characteristic resonances of **39** were observed at δ 0.92 (d, 3H, *J* = 6.4 Hz, Me), 0.99 (d, 3H, *J* = 7.2 Hz, Me), 5.22 (bs, 1H, vinyl-*H*), and 5.44 (bs, 1H, vinyl-*H*), respectively. When the thermolysis of triene **15** was carried out at 130 °C in benzene-d_6 solvent, only slowly decomposition and/or polymerization of the starting material was observed without any evidence for the formation of desired cyclohexadiene product.
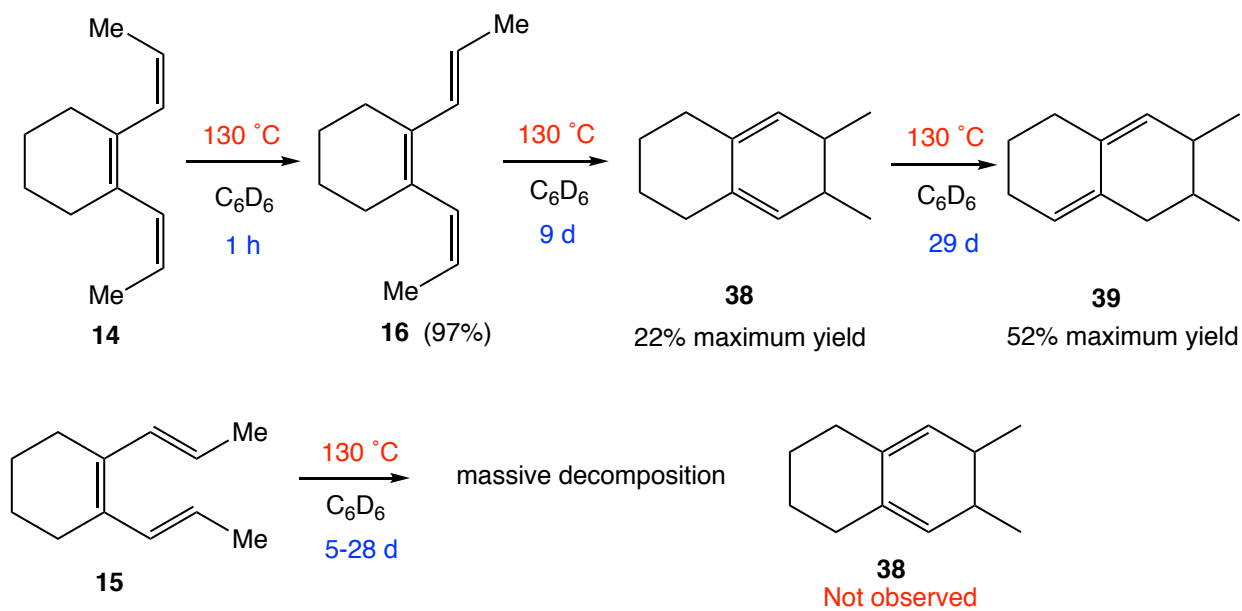
Scheme 8-17. Thermal reactions of dimethyl-substituted trienes.

For the photochemical condition, triene samples were dissolved in acetone-d_6 in an NMR tube, and the solution was placed in a Rayonette photoreactor equipped with UV broadband lamps that is centered at 254 nm. The reaction mixture was subsequently monitored by using ^{1}H NMR (400 MHz) spectroscopy. The results show that both the *ZZ* isomer **14** and *EZ* isomer **16** were isomerized to *EE* isomer **15** under photochemical condition at early reaction stage (Scheme 8-18). However, massive decomposition and/or polymerization of the substrate was observed after longer irradiation time, and there is no evidence for the formation of desired cyclohexadiene.
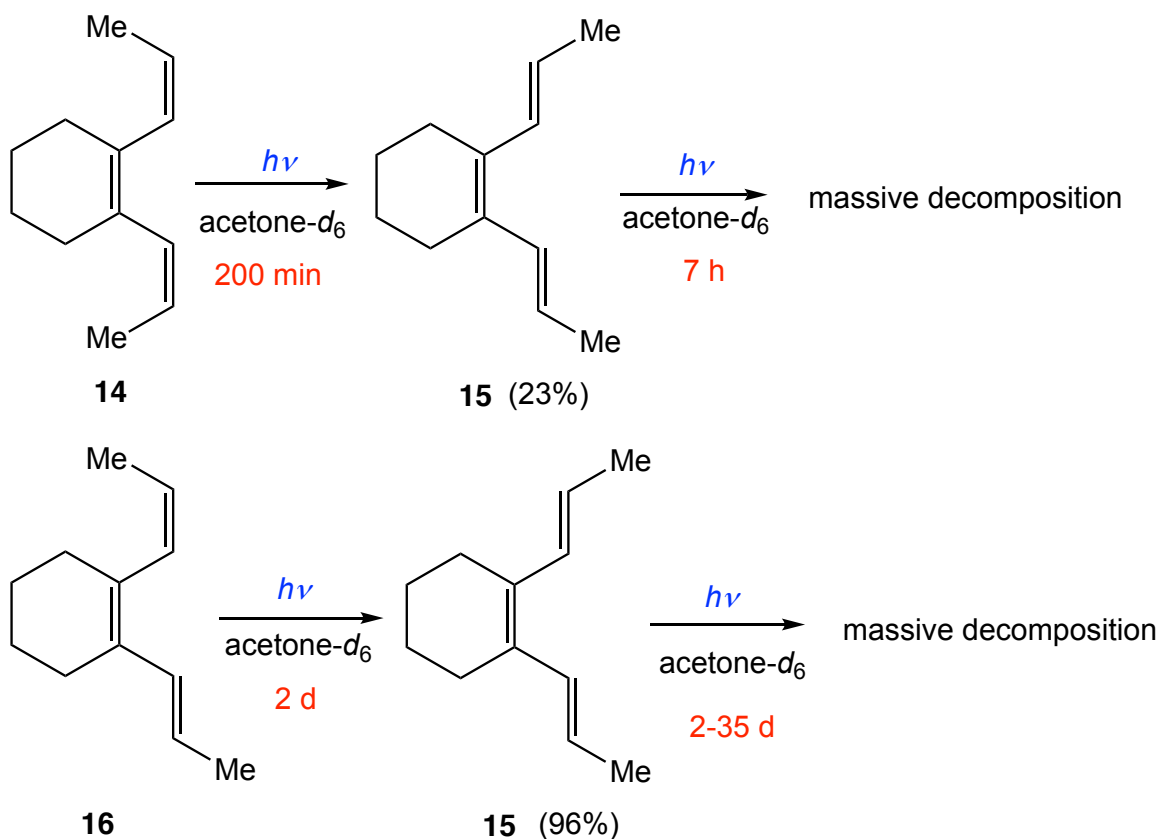
Scheme 8-18. Reactions of dimethyl-substituted trienes under photochemical condition.

The remarkable different results in the absence of ruthenium in these control experiments demonstrates the prominent advantage of the transition-metal-assisted stabilization of transition state on the way to cyclizations.

C. Reactions of Diester-substituted Trienes with Complex 13

In order to explore the electron effects from the substituents on the cyclization process, the triene **40** with two electron-withdrawing ester groups was also examined with complex **13**. Triene **40** (*EE*) is prepared from a simple two-fold Heck reaction on

the vinyl dibromide **42** that is synthesized from a modified procedure in literature by using cyclohexanone as the starting material (Scheme 8-19).[18]
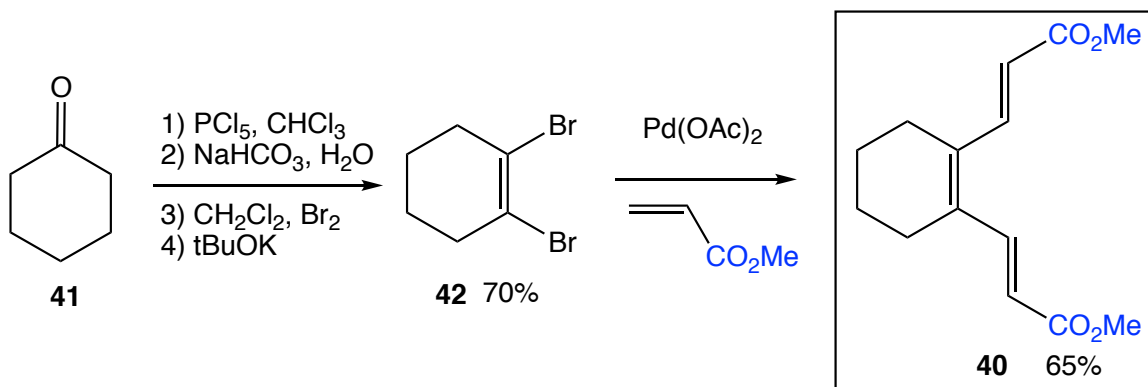
Scheme 8-19. Synthesis of triene **40**.

When triene **40** was treated with complex **13** in CD$_2$Cl$_2$ solvent at ambient temperature for 5 minutes (Scheme 8-20), a new Cp signal (71.2% yield) with four shielded vinyl hydrogen resonances were observed at δ 5.40 (s, 5H,Cp), 5.88 (d, 1H, J = 9.6 Hz), 5.70 (d, 1H, J = 12 Hz), 3.64 (d, 1H, J = 9.6 Hz), and 3.36 (d, 1H, J = 12 Hz), respectively, which indicates that the cyclization has not occurred yet. The existence of two methyl ester resonances at δ 3.75 (s, 3H) and 3.90 (s, 3H) suggests the unsymmetrical coordination mode of the product. The η^6-triene substructure of complex **43** is manifested by the six shielded carbon resonances in ^{13}C{^{1}H} NMR spectrum (400 MHz) at δ 67.4, 90.2, 91.2, 105.8, 111.0, and 118.7, respectively.
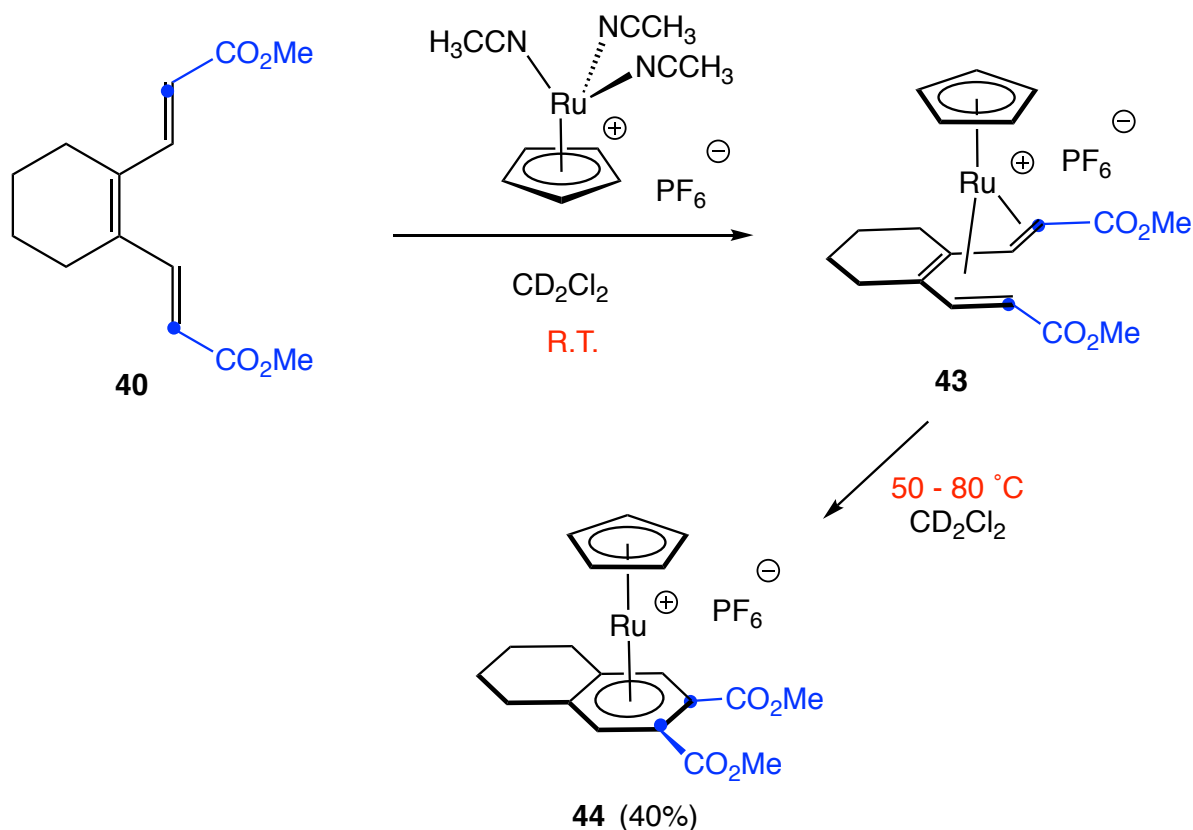
Scheme 8-20. Reaction of triene **40** with complex **13**.

It was noted that complex **43** is more stable compared to the dimethyl-substituted analogue **27**, and no cycloaromatization was observed at ambient temperature in two days unless heating the solution at 50 – 80 °C, which eventually gave the corresponding ruthenium-arene product **44** with a 40% yield (Scheme 8-20). We attribute the exceedingly stable structure of complex **43** to the strong electron-withdrawing effect of the two ester groups that strengthens the π-back bonding between the alkenes and metal center.

Complex **43** was successfully isolated by layering diethyl ether to the reaction mixture, and the crystals was subsequently allowed for X-ray crystallographic analysis. As anticipated, the structure of **43** was revealed as an unsymmetrical η^6-triene complex

(Figure 8-8). The selected bond angles and distances are summarized in Table 8-4. A s-*cis* conformation shows on the C1-C2-C3-C4 diene moiety, while a s-*trans* conformation exists on the C3-C4-C5-C6 diene moiety. Carbon C6 is found off the mean plane C1-C2-C3-C4-C5 by 0.954(5) Å, and the angle between bond C5 – C6 and the plane normal is measured as 42.5(3) °. The Ru – C6 bond is found significantly longer the Ru – C1 bond (Δ = 0.099 Å). The two ester groups are found well delocalized with the two alkenes with a small torsion angle of O2-C8-C1-C2 (3.4(4) °) and O1-C7-C6-C5 (3.3(3) °), respectively. The two double bonds of the s-*trans* diene substructure are no longer conjugated due to the large dihedral angle of C3-C4-C5-C6 (58.3(3) °). Compared to dimethyl-substituted analogue **27**, the Ru – C1 bond and Ru – C6 bond in complex **43** are considerably shorter (Δ = 0.035 Å, 0.074 Å), which might be ascribed to the electron-withdrawing effect of the ester group that fortifies the ruthenium-carbon bonds. The nonbonding C1····C6 distance is detected as 3.356(4) Å.
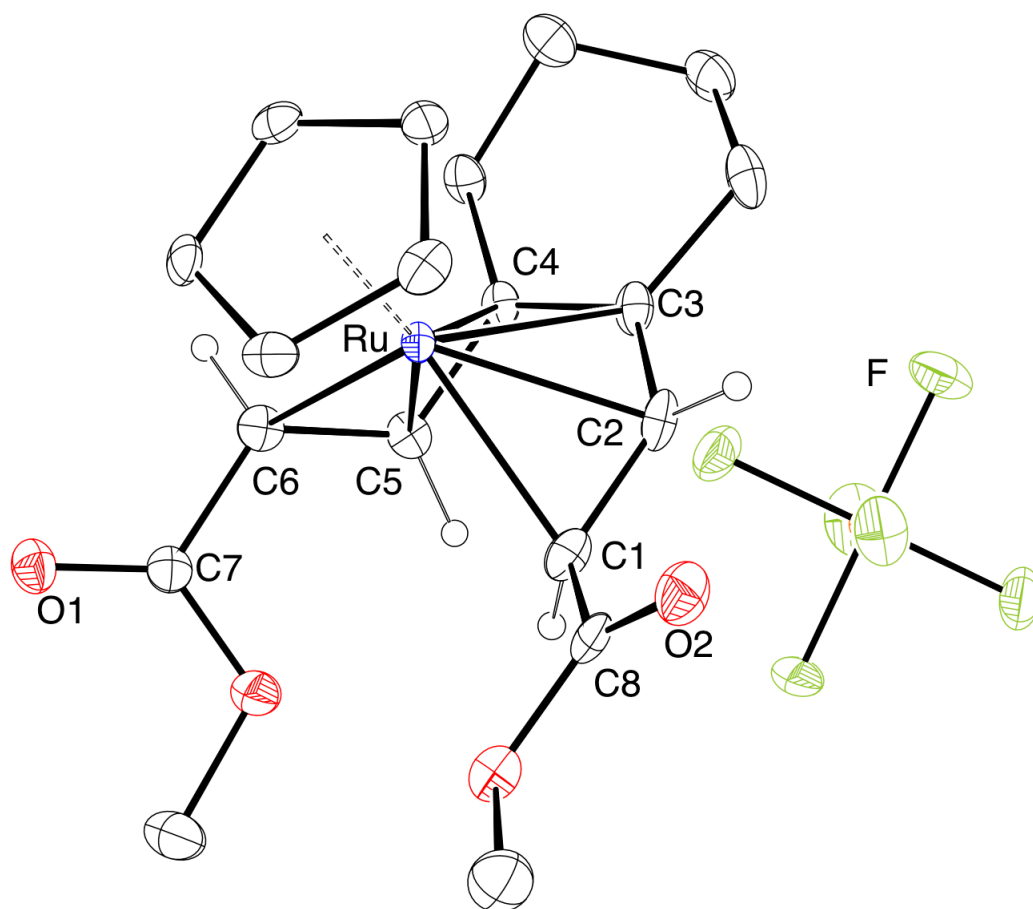
Figure 8-8. ORTEP drawing of complex **43** with ellipsoids shown at 30% probability.

Table 8-4. Seletecd bond distances (Å) and angles (deg) of complex **43**.

C1 – C2	1.409(5)	Ru – C5	2.179(3)
C2 – C3	1.438(5)	Ru – C6	2.288(3)
C3 – C4	1.422(4)	C1-C2-C3	128.8(3)
C4 – C5	1.437(4)	C4-C5-C6	121.1(3)
C5 – C6	1.370(5)	O1-C7-C6-C5	3.3(3)
Ru – C1	2.189(3)	O2-C8-C1-C2	3.4(4)
Ru – C2	2.162(3)	C1-C2-C3-C4	9.9(4)
Ru – C3	2.280(3)	C3-C4-C5-C6	58.3(3)
Ru – C4	2.205(3)	C1····C6	3.356(4)

D. Ruthenium-catalyzed 6π Electrocyclization of Trimethyl-substituted Trienes

1. Reactions with Stoichiometric Amount of Ruthenium

Since a hydrogen gas needs to be extruded from the two terminal vinyl hydrogens in the aromatization process of the dimethyl-substituted triene scenario, one might expect that the aromatization can be impeded if replace the vinyl hydrogen with an alkyl group, and thus the reaction can stop at the cyclohexadiene stage. Based on this proposal, the reactivities of two isomeric trimethyl-substituted trienes (**48**, *Z*; **49**, *E*) were examined towards ruthenium complexes.

The triene substrate **48** was synthesized by employing commercially available cyclohenxanone as starting material to execute Sonogashira coupling, Lindlar hydrogenation, and Wittig reaction in succession (Scheme 8-21). The *E* isomer **49** can be prepared from the thermal isomerization of **48** at 130 °C in benzene solvent for 6 hours with an 88% yield. Both trimethyl-substituted triene isomers can be isolated and purified by flash chromatography as a colorless oil, and they can be stored under -20 °C for a few weeks without any decomposition.
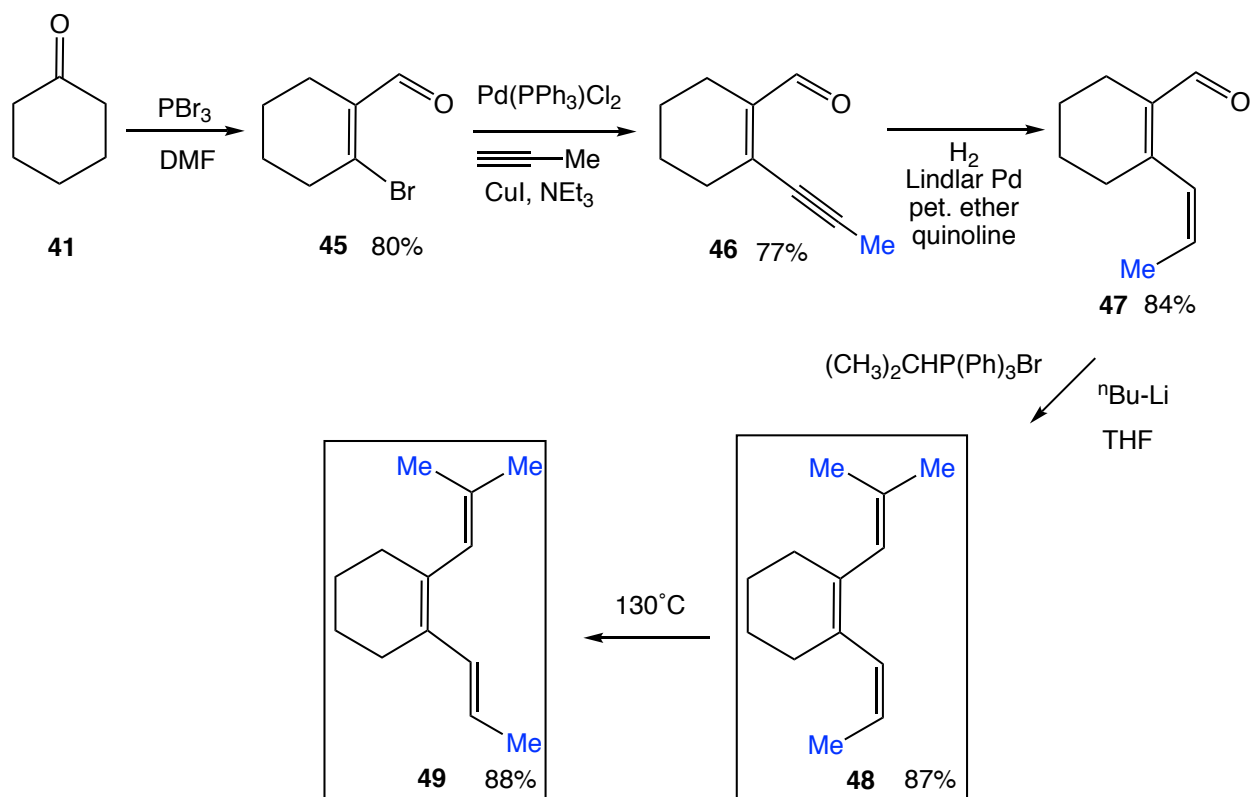
Scheme 8-21. Synthesis of trienes **48** and **49**.

A CD$_2$Cl$_2$ solution of triene **48** was treated with stoichiometric amount of complex **13** at ambient temperature, and reaction was monitored by ^{1}H NMR spectrum (400 MHz). After 90 minutes, 76% yield of ruthenium-η^4-cyclohexadiene complex **50** was observed (Scheme 8-22). The diagnostic agostic-hydrogen resonance of **50** was detected at δ -8.03 (d, 1H, J = 18 Hz), and three methyl signals were observed at δ 0.50 (s, 3H), 1.30 (s, 3H), and 1.61 (s, 3H), respectively. As anticipated, complex **50** is more stable than the dimethyl-substituted analogue **32**, and only 30% of **50** was converted to the ruthenium-arene product **23** after 3 days at ambient temperature. In addition, when the *E* isomer **49** was treated with complex **13** in a similar fashion, the same intermediate **50** and final product **23** were observed (Scheme 8-22). The formation of **50** from *E*

isomer **49** can be explained by the coordination of ruthenium to the opposite face to the cyclohexadiene after the cyclization process, in which the dissociation of the cyclized substrate is involved (vide infra).
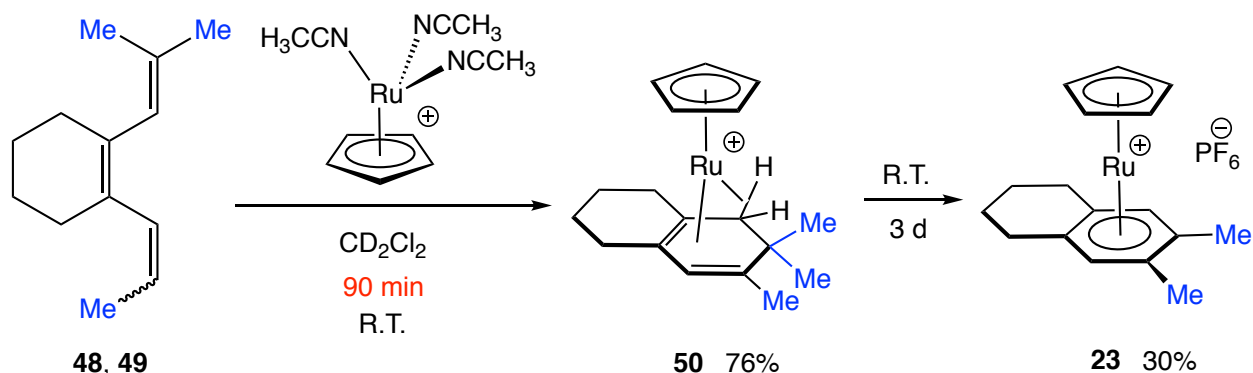
Scheme 8-22. Reaction of triene **48** and **49** with complex **13**.

More electron rich Cp*Ru(NCMe)$_3$PF$_6$ (**54**) was also examined with the triene substrate **48** at ambient temperature in CD$_2$Cl$_2$ solvent (Scheme 8-23). After 7 hours, the agostic complex **51** was obtained with a maximum yield of 88.5%, and the characteristic resonances were observed at δ -8.39 (d, 1H, J = 19 Hz, agostic-H), 0.48 (s, 3H, Me), 1.15 (s, 3H, Me), and 1.38 (s, 3H, Me) in the ^{1}H NMR spectrum. In the ^{13}C{^{1}H} NMR spectrum (500 MHz), the four shielded vinyl carbon signals were detected at δ 83.4, 92.0, 93.5, and 94.6, respectively. The significantly slower formation rate of **51** than **50** might be attributed to the more sluggish ruthenium-mediated 1,5-hydride shift in the Cp*Ru scenario. However, it was noted that complex **51** is more stable than **50**, and there is no evidence for any consumption of **51** in the reaction mixture after 24 hours. Complex **51** was subsequently treated with dry acetonitrile-d_3 in an NMR tube. A rapid dissociation of the cyclohexadiene **52** was observed to regenerate the

Cp*Ru(NCMe)$_3$PF$_6$-d_9 with quantitative yield, which allows for the isolation of **52** by precipitating out the ruthenium complex with diethyl ether.
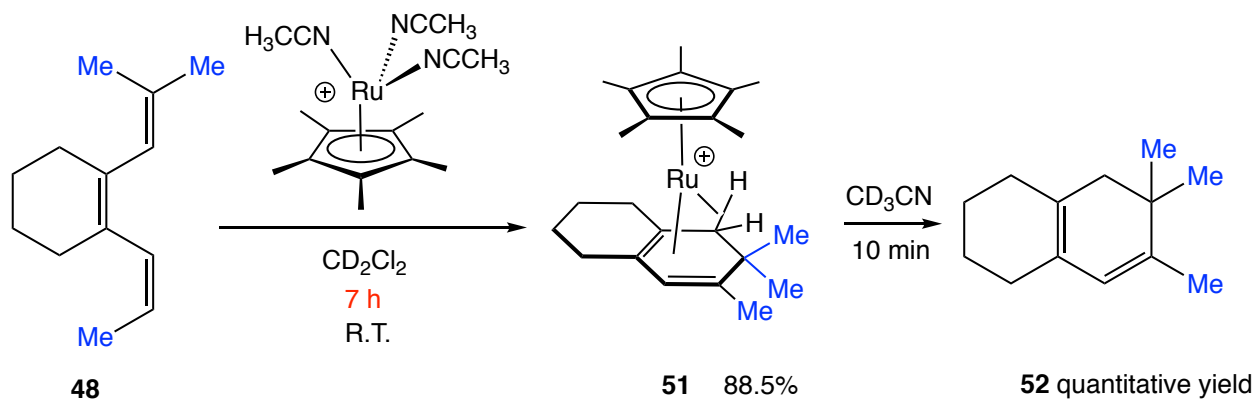
Scheme 8-23. Formation of **51** and **52** from triene **48**.

2. Ruthenium-catalyzed 6π Electrocyclizations

It was noted that when excess of triene **48** was loaded in the reaction with complex **13**, before the formation of agostic complex **50**, a new set of resonances were observed at δ 0.77 (s, 3H, Me), 0.90 (d, 3H, J = 7.2 Hz, Me), 0.97 (s, 3H, Me) 5.13 (s, 1H, vinyl-H), and 5.14 (bs, 1H, vinyl-H) with the consumption of triene **48**. After isolation and characterization of the molecule, we were pleased to find that these new forming signals belong to the free cyclohexadiene **53**, which suggests that triene **48** has been cyclized in a catalytic fashion.

A lower ruthenium loading (5 mol%) was subsequently examined with **48**, and it was found that cyclohexadiene **53** can be generated with 70.5% NMR yield in 100 minutes at ambient temperature (Scheme 8-24). To our best knowledge, this is the first

example of transition-metal catalyzed 6π electrocyclization of conjugated triene. The *E* isomer **49** was also allowed to react complex **13** (5 mol%) in a similar fashion, and 100 minutes, 67% yield of **53** was obtained with 79% conversion of the substrate. In addition, a very similar catalytic behavior was observed when the more electron-rich analogue Cp*Ru(NCMe)$_3$PF$_6$ (**54**) was employed as catalyst (5 mol% loading), which gave a 74% yield of **53** after 75 minutes at ambient temperature (Scheme 8-25).
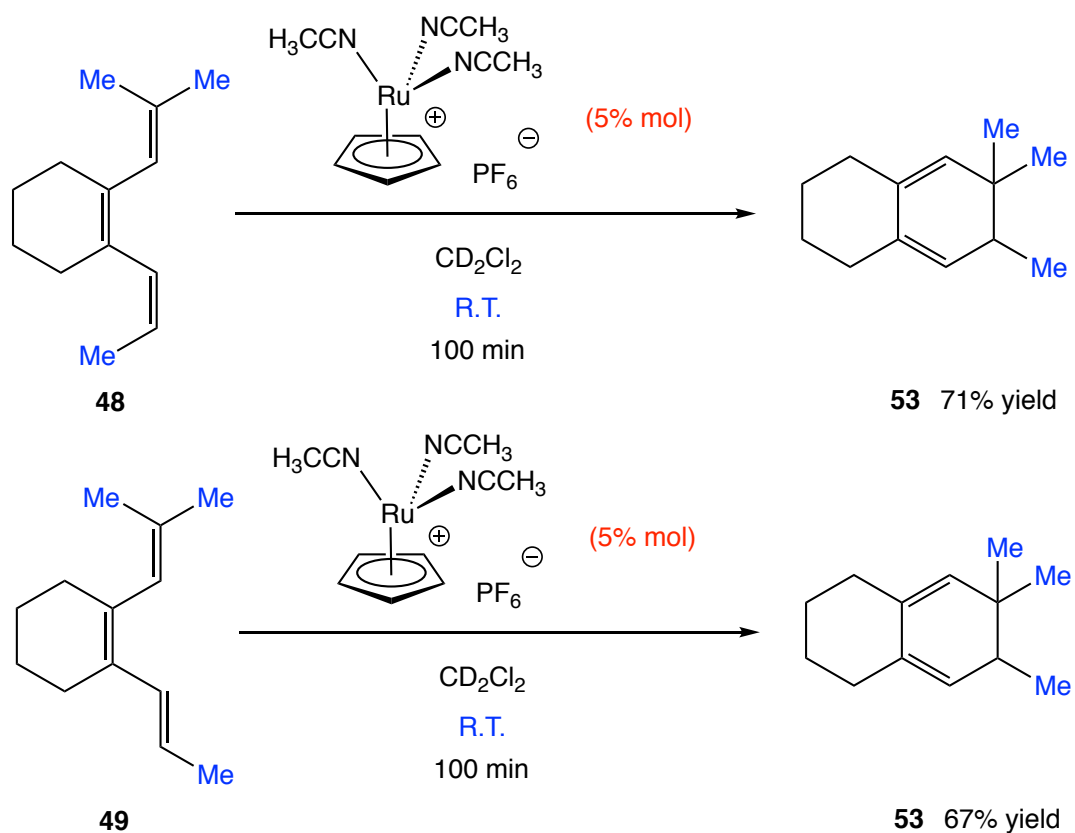
Scheme 8-24. Catalytic cyclization of triene **48** and **49** via complex **13**.
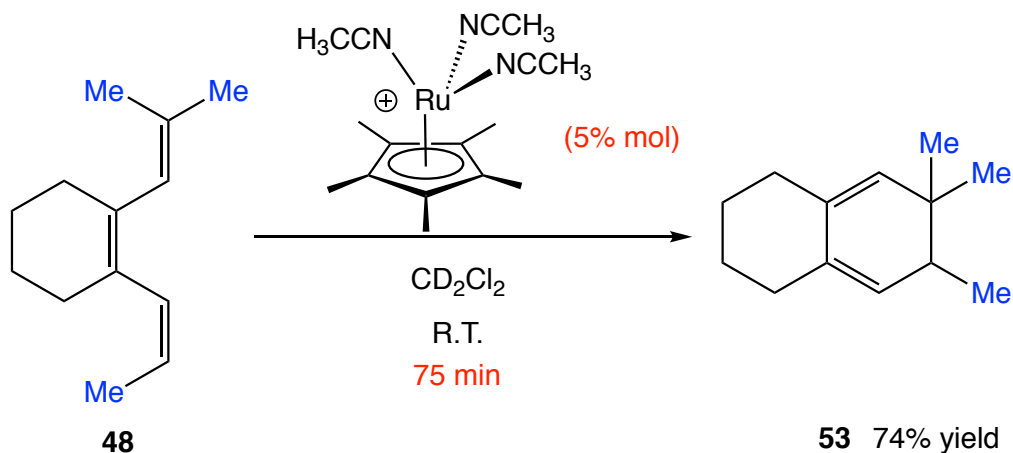
Scheme 8-25. Catalytic cyclization of triene **48** via complex **54**.

Mechanically, we proposed that upon the dissociation of three acetonitrile ligands from complex **13**, the [CpRu]$^+$ moiety can be rapidly trapped by the triene substrate **48** to generate the η^6-triene intermediate **54** (Scheme 8-26), which contrasts to the Lewis acid-base coordination mode between oxygen and aluminum in Bergman's system.[3] The subsequent ruthenium-mediated 6π electron cyclization process occurs to produce η^4-cyclohexadiene intermediate **55** with the incorporation of an acetonitrile. Similar ruthenium-acetonitrile η^4-diene complex has been reported in the literature by exchanging a naphthalene ligand of complex [Ru(η^6-C$_{10}$H$_8$)(η^4-1,5-COD)] with a conjugated diene and an acetonitrile.[19] The steric hindered labile trimethyl substituted cyclohexadiene can quickly dissociate with the replacement of another triene substrate coordinating to the ruthenium to regenerate the η^6-triene complex **54**. However, in the absence of free triene, a slow 1,5-hydride shift could occur to produce complex **50** with an agostic interaction, as required by the ^{1}H NMR spectrum. The free acetonitrile in the solution can behave as base to do the deprotonation on the agostic proton, that is

followed by a fragmentation of a methyl anion to generate η^6-arene product **23**. The process from **50** to **23** is in high agreement to what Stryker proposed in their cyclohexadienyl ruthenium system.[5]
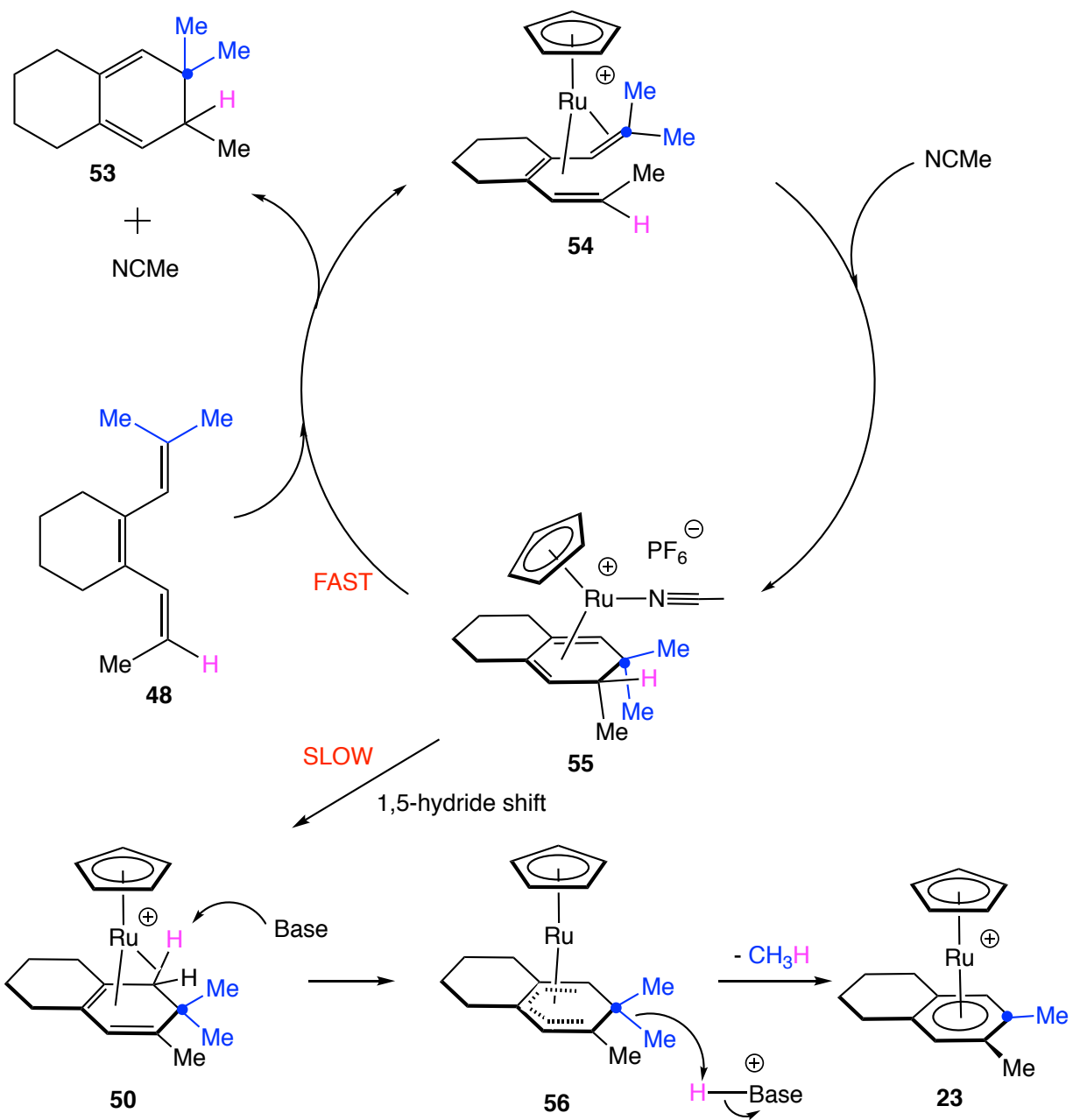
Scheme 8-26. Proposed mechanism of catalytic cycle and formation of complex **23**.

In comparison, classic thermal and photochemical conditions were also examined on the two trimethyl-substituted triene isomers for cyclization. The *Z* isomer **48** was heated in a flame-sealed NMR tube in benzene-d_6 solvent at 130 °C. After 6 hours, ^{1}H NMR spectrum indicates 89% yield of *E* isomer **49** was obtained (Scheme 8-27). However, decomposition of **49** was observed after longer reaction time in the followed 15 days, and there is no evidence for the formation of desired cyclohexadiene **53**. Under photochemical condition, the acetone-d_6 solution of *Z* isomer **48** was irradiated in a Rayonette photoreactor equipped with UV broadband lamps that is centered at 254 nm. It was found that triene **49** was slowly generated via the isomerization of **48**, and the maximum yield (7%) of cyclohexadiene **53** was obtained after 2 hours. However, when longer reaction time was executed, massive decomposition of both triene starting material and cyclohexadiene **53** was observed.
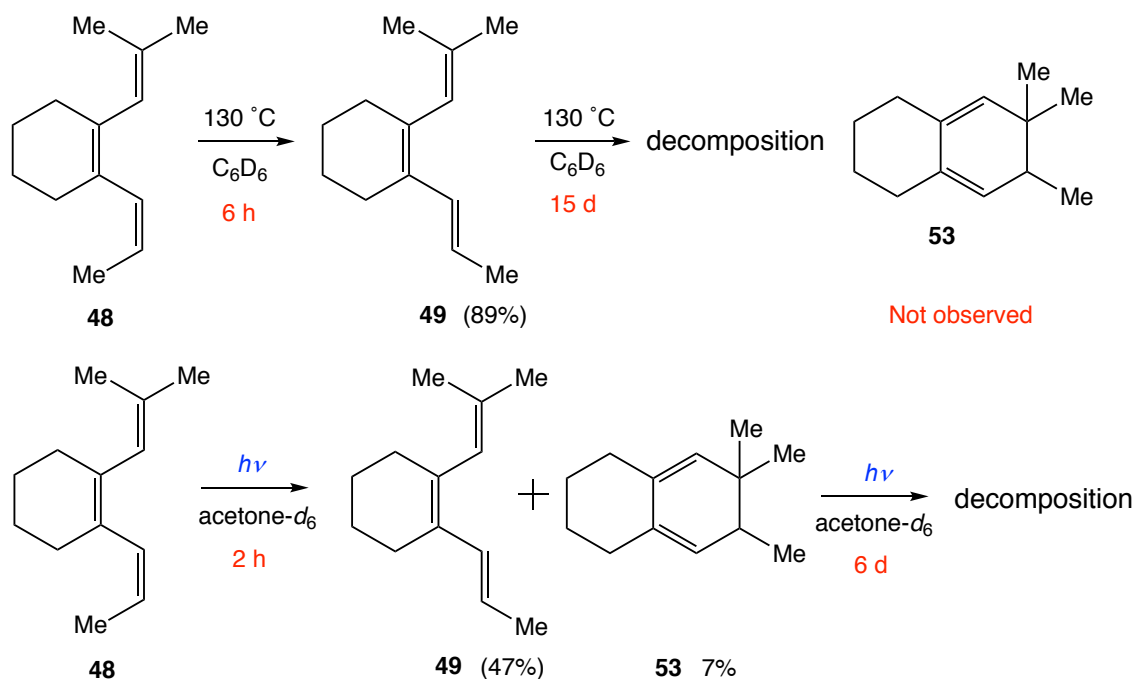
Scheme 8-27. Reactions of **48** and **49** under thermal and photochemical conditions.

698

3. Kinetic studies

The kinetic studies have been carried out between trimethyl substituted triene **49** and CpRu(NCMe)$_3$PF$_6$ (**13**) in methylene chloride-d_2 at ambient temperature. The decay of substrate concentration with different catalyst loadings (0.0025 – 0.0225 mol/L) is shown in Figure 8-9, which demonstrates the first-order kinetic feature of triene **49** via the excellent agreement with exponential fits. The prominent catalytic-trunover character of this reaction is manifested by the drastic change on reaction rate when increase the concentration of complex **13** from 0.04 equivalents ($t_{1/2}$ = 3466 s) to 0.36 equivalents ($t_{1/2}$ = 385 s) at ambient temperature. In comparison, when Me$_2$AlCl was employed by Bergman to catalyze the cyclization of an ester substituted triene, a half life of 21 minutes was observed with stoichiometric loading of catalyst at 50 °C.[3] The plot of natural logarithm of rate constant (k_{obs}) versus natural logarithm of complex **13** concentration at sub-stoichiometric catalyst loadings is shown in Figure 8-11, and the slope of trend line is measured as 0.998, which indicates the reaction is also first order to the ruthenium catalyst.
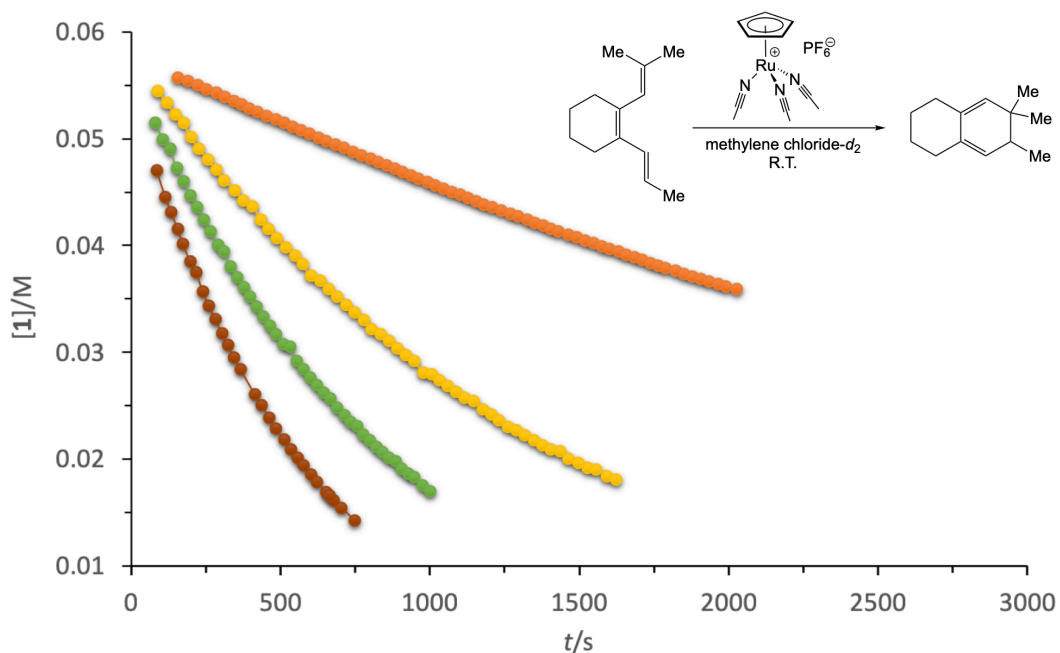
Figure 8-9. Kinetic plots (with first order exponential decay fits) and half lives of the electrocyclization of **49** at room temperature in the presence of CpRu(NCMe)$_3$PF$_6$. orange: 0.04 equivalents of CpRu(NCMe)$_3$PF$_6$, $t_{1/2}$ = 3466 s; yellow: 0.16 equivalents of CpRu(NCMe)$_3$PF$_6$, $t_{1/2}$ = 990 s; green: 0.24 equivalents of CpRu(NCMe)$_3$PF$_6$, $t_{1/2}$ = 578 s; brown: 0.36 equivalents of CpRu(NCMe)$_3$PF$_6$, $t_{1/2}$ = 385 s.

Table 8-5. k_{obs} at different concentrations of CpRu(NCMe)$_3$PF$_6$.

[CpRu(NCMe)$_3$PF$_6$] (mol / L)	k_{obs} (s^{-1})
0.0025	0.0002
0.01	0.0007
0.015	0.0012
0.0225	0.0018
0.0275	0.0022
0.0325	0.0026
0.0375	0.0029
0.0426	0.0031
0.0476	0.0033
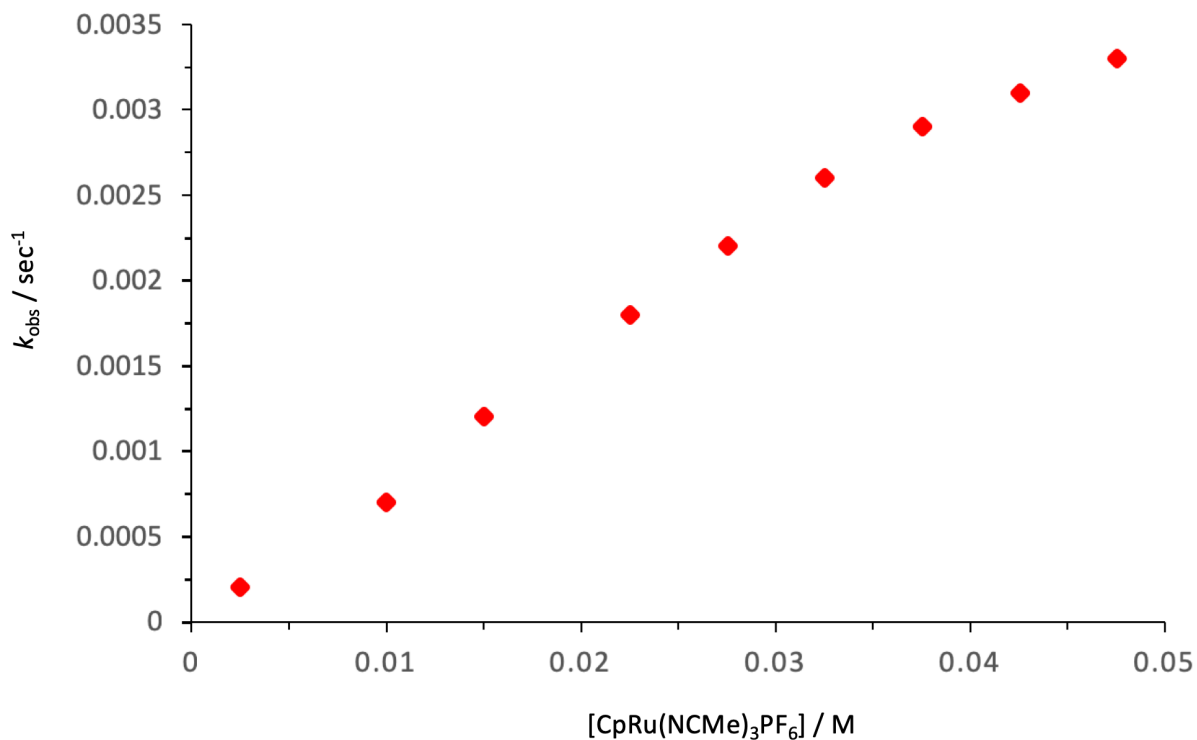
Figure 8-10. k_{obs} with different concentrations of CpRu(NCMe)$_3$PF$_6$.

Table 8-6. Natural logarithms of [CpRu(NCMe)$_3$PF$_6$] with natural logarithms of k_{obs} at sub-stoichiometric catalyst loadings.

ln [CpRu(NCMe)$_3$PF$_6$]	ln k_{obs}
-5.990	-8.517
-4.604	-7.264
-4.199	-6.725
-3.793	-6.320
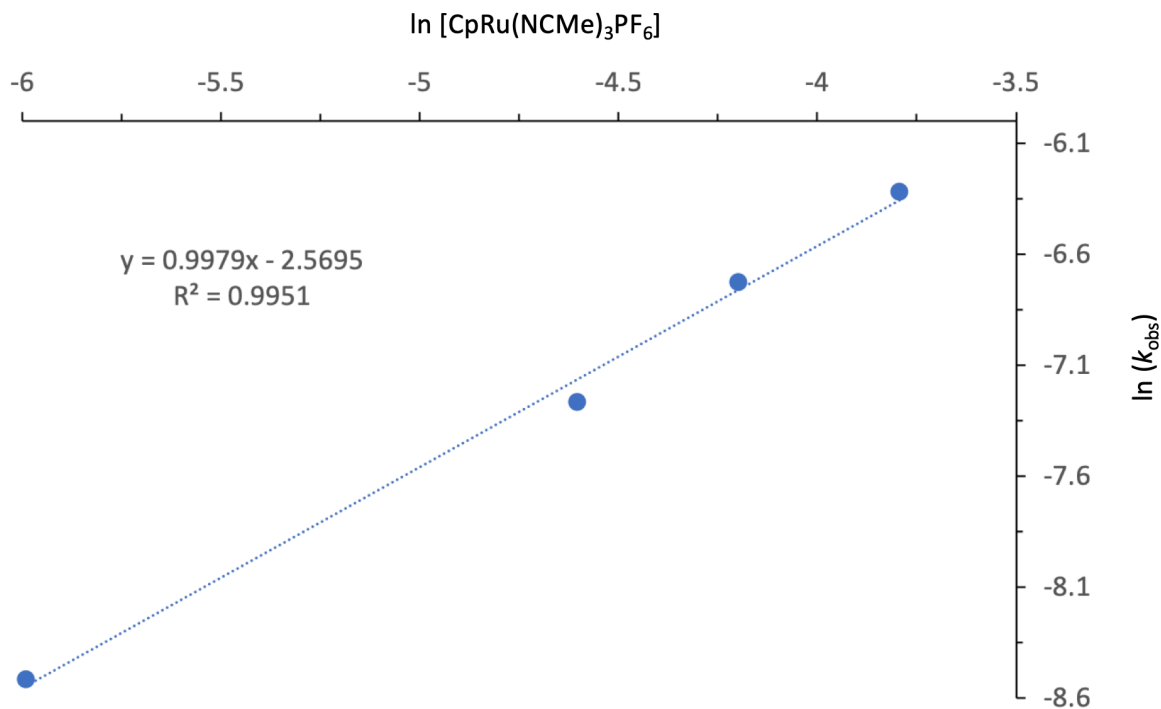
Figure 8-11. Natural logarithms of [CpRu(NCMe)$_3$PF$_6$] with natural logarithms of k_{obs} at sub-stoichiometric catalyst loadings.

E. Conclusions

Three isomeric dimethyl substituted acyclic conjugated trienes were cycloaromatized by CpRu(NCMe)$_3$PF$_6$ at ambient temperature to generate the same ruthenium η^6-arene product **23** with excellent yields within a few hours, in which a metal-mediated 6π electrocyclization is involved.

Isolation of intermediates from different triene substrates at low temperature affords η^4-triene complex **24** and hexahapto intermediate **27** with unprecedented coordination modes of transition metal with the conjugated tri-π system, which sheds light on the mechanisms behind the cyclization process.

702

The first example of transition metal catalyzed 6π electrocyclization was discovered by employing trialkyl-substituted trienes, which contrasts with the low yield and long reaction time under classical thermal or photochemical conditions. The followed kinetic studies indicate that the reaction is both first order to the substrate and catalyst. It also furtherly demonstrates the drastic change of the reaction rates brought by different catalyst loadings.
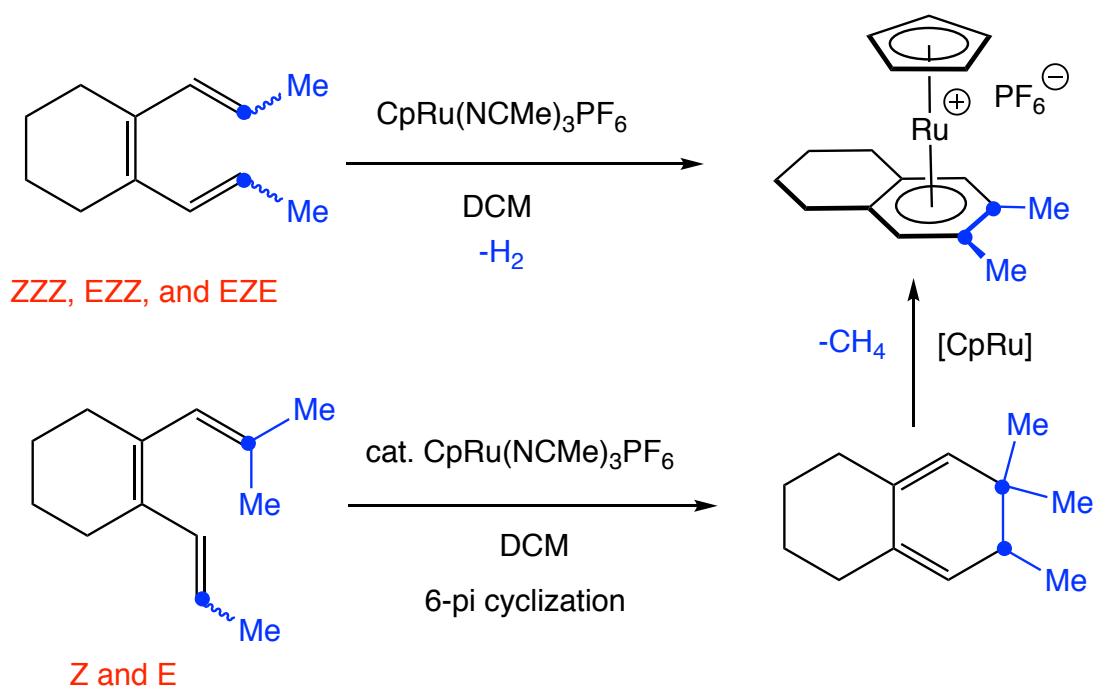
Scheme 8-28. Ruthenium-catalyzed 6π electrocyclization of conjugated trienes and followed aromatization.

F. Experimentals

1. General Information

All the organometallic reagents were handled under inert gas atmosphere or using the standard Schlenk technique, unless otherwise noted. All glassware was oven dried before use. All the dry solvents were flushed through an aluminum column under inert gas atmosphere via a J. C. Meyer (formerly Glass Contour) solvent purification system. The commercially available acetonitrile-d_3, chloroform-d, methylene chloride-d_2 were refluxed over CaH_2 for two days and freeze-pump-thaw to degas. Benzene-d_6 was dried over sodium/benzophenone ketyl and freshly distilled prior to use. Acetone-d_6 was dried in activated molecular sieves for 2 hours before distilled into a dry Schlenk flask. NMR-scale reactions were performed under a dry dinitrogen atmosphere in 5 mm J-Young style NMR tubes equipped with a Teflon needle-valve adapter using freshly degassed solvents (freeze/pump/thaw procedure). Flash column chromatographic purifications were performed using silica gel (60 Å, particle size 43-60 μm, 230-400 mesh, EMD Chemicals). Combustion analysis was performed by NuMega laboratories of San Diego, CA (USA) or MIDWEST MICROLAB of Indianapolis, IN (USA).

2. Instrumentation

Solution ^1H and $^{13}C\{^1H\}$ NMR were recorded on Varian Mercury 300 (^1H, 300 MHz; ^{13}C, 75.5 MHz), Varian Mercury 400 (^1H, 400 MHz; ^{13}C, 100.7 MHz), Varian

VX500 (^{1}H, 500 MHz; ^{13}C, 125 MHz) or JEOL ECA500 (^{1}H, 500 MHz; ^{13}C, 126 MHz) spectrometer. ^{1}H and ^{13}C{^{1}H} NMR chemical shifts (δ) were reported in parts per million (ppm), which is referenced to the residual proton resonance of CDCl$_3$ (^{1}H, δ 7.26; ^{13}C, δ 77.16), CD$_3$CN (^{1}H, δ 1.94; ^{13}C, δ 118.26), benzene-d_6 (^{1}H, δ 7.16; ^{13}C, δ 128.06), acetone-d_6 (^{1}H, δ 2.05; ^{13}C, δ 29.84) and methylene chloride (^{1}H, δ 5.32; ^{13}C, δ 53.84). Coupling constants J are given in Hertz as positive values regardless of their real individual signs. NMR multiplicities are abbreviated as follows: s = singlet, d = doublet, t = triplet, q = quartet, sept = septet, m = multiplet, bs = broad singlet. The IR spectra of the isolated compounds were recorded on a Thermo-Nicolet iS10 FTIR spectrometer at room temperature. The mass spectra were recorded at the UC San Diego Mass Spectrometry Laboratory on an Agilent 6230 Accurate-Mass TOFMS instrument by using positive ion mode. Single crystal X-ray diffraction data were collected on Bruker Apex diffractometers using Mo-Kα radiation (λ = 0.71073 Å) or Cu-Kα radiation (λ = 1.54178 Å) at the UC San Diego Crystallography Facility. Melting points were measured with an electrothermal *EZ*-Melt apparatus.

3. Preparation and Characterization Data

21
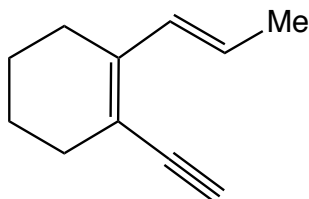
Preparation of (*E*)-1-ethynyl-2-(prop-1-en-1-yl)cyclohex-1-ene (21): 2.9 g of anhydrous K_2CO_3 was added to a stirring solution of (*E*)-trimethyl((2-(prop-1-en-1-yl)cyclohex-1-en-1-yl)ethynyl)silane (**20**) (1.47 g) in THF/MeOH (70 ml, 1:1) at 23 °C. After stirring at 23 °C for 1.5 hours, 100 mL of water was introduced, and the reaction mixture was extracted with pentane (3 x 70 mL). The organic extract was dried over anhydrous $MgSO_4$, concentrated, and purified by flash silica column chromatography (pentane) to afford **21** as a colorless oil (0.86 g, 5.8 mmol, 86.5% yield). IR (film, cm^{-1}) 3032, 2931, 2085, 1638, 1585, 1446, 1374, 964. ^{1}H NMR (400 MHz, CDCl$_3$) δ 1.63 (m, 4H, methylene-*H*), 1.83 (d, 3H, *J* = 6.4 Hz, Me), 2.24 (m, 4H, methylene-*H*), 3.23 (s, 1H, C≡C-*H*), 5.81 (m, 1H, vinyl-*H*), 6.81 (d, 1H, *J* = 16 Hz, vinyl-*H*) ^{13}C{^{1}H} NMR (125 MHz, CDCl$_3$) δ 18.8 (Me), 22.2 (methylene-*C*), 22.5 (methylene-*C*), 25.3 (methylene-*C*), 30.6 (methylene-*C*), 81.5 (C≡*C*-H), 84.4 (*C*≡C-H), 115.9 (vinyl-*C*), 126.0 (vinyl-*C*), 131.5 (vinyl-*C*), 142.3 (vinyl-*C*), HRMS (HR-APCI) m/z: [M+H]$^+$ Calcd for [C$_{11}$H$_{15}$]$^+$ 147.1168; Found 147.1169.

22
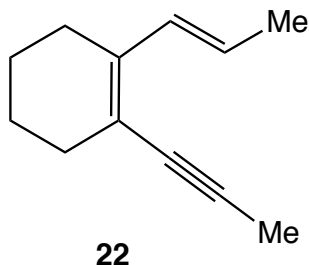
Preparation of (*E*)-1-(prop-1-en-1-yl)-2-(prop-1-yn-1-yl)cyclohex-1-ene (22): 3.48 mL of n-butyllithium (2.5 M in hexane) was added dropwise into a stirring solution of (*E*)-1-ethynyl-2-(prop-1-en-1-yl)cyclohex-1-ene (**21**) (0.86 g, 5.8 mmol) in THF (110 mL) at -78

°C. After stirring at -78°C for 2 hours, 0.722 mL of iodomethane (11.6 mmol) was introduced. The reaction mixture was allowed to stir for 4.5 hours while slowly warming up to 23 °C, the reaction was poured over sat. aq. NH$_4$Cl (60 mL) and extracted with hexanes (3 x 60 mL). The organics extracts were successively washed with water (50 mL)/ brine (50 mL), dried over MgSO$_4$, concentrated, and purified by flash silica column chromatography (hexanes) to afford **22** as a colorless oil (0.87 g, 5.425 mmol, 92% yield).IR (film, cm^{-1}) 3031, 2927, 2858, 2222, 1639, 1589, 1446, 1434, 1373, 968. ^{1}H NMR (400 MHz, CDCl$_3$) δ 1.61 (m, 4H, methylene-*H*), 1.82 (d, 3H, *J* = 6.4 Hz, Me), 2.04 (s, 3H, Me), 2.20 (m, 4H, methylene-*H*), 5.73 (m, 1H, vinyl-*H*), 6.79 (d, 1H, *J* = 15.6 Hz, vinyl-*H*). ^{13}C{^{1}H} NMR (125 MHz, CDCl$_3$) δ 4.8 (C≡C-*Me*), 18.8 (C=C-*Me*), 22.4 (methylene-*C*), 22.7 (methylene-*C*), 25.2 (methylene-*C*), 31.1 (methylene-*C*), 80.2 (C≡*C*-Me), 90.1 (*C*≡C-Me), 117.6 (vinyl-*C*), 124.6 (vinyl-*C*), 131.8 (vinyl-*C*), 139.1 (vinyl-*C*),. HRMS (HR-APCI) m/z: [M+H]$^+$ Calcd for [C$_{12}$H$_{17}$]$^+$ 161.1325; Found 161.1326.

16
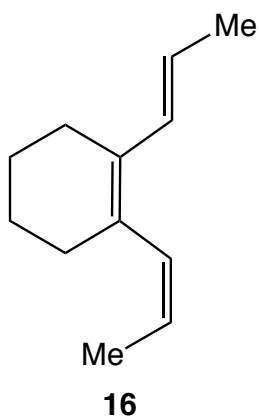
Preparation of 1-((*E*)-prop-1-en-1-yl)-2-((*Z*)-prop-1-en-1-yl)cyclohex-1-ene (16): H$_2$ (1 atm) was bubbled through a stirring mixture of quinoline (0.0638 mL, 0.54 mmol) and

Lindlar Pd (0.612 g, 0.29 mmol) in hexanes (100 mL) at 23 °C for 10 minutes, and then (E)-1-(prop-1-en-1-yl)-2-(prop-1-yn-1-yl)cyclohex-1-ene (**22**) (0.87 g, 5.43 mmol) was introduced. After stirring at 23 °C under hydrogen atmosphere (1 atm) for 12 hours, the reaction mixture was filtered through celite, concentrated, and purified by flash column chromatography (hexanes) to afford **16** as a colorless oil (0.575 g, 3.55 mmol, 65% yield). IR (film, cm^{-1}) 3032, 2923, 2858, 1994, 1639, 1608, 1446, 1373, 972. ^{1}H NMR (400 MHz, CDCl$_3$) δ 1.53 (d, 3H, J = 7.2 Hz, Me), 1.64 (m, 4H, methylene-H), 1.76 (d, 3H, J = 6.4 Hz, Me), 2.05 (m, 2H, methylene-H), 2.18 (m, 2H, methylene-H), 5.55 (m, 1H, vinyl-H), 5.62 (m, 1H, vinyl-H), 5.87 (d, 1H, J =11.2 Hz, vinyl-H), 6.31 (d, 1H, J = 15.6 Hz, vinyl-H),. ^{13}C{^{1}H} NMR (125 MHz, CDCl$_3$) δ 14.9 (Me), 18.8 (Me), 22.97 (methylene-C), 22.99 (methylene-C), 25.4 (methylene-C), 30.7 (methylene-C), 121.9 (vinyl-C), 125.9 (vinyl-C), 129.8(vinyl-C), 130.9 (vinyl-C), 131.8 (vinyl-C), 132.1 (vinyl-C). HRMS (HR-APCI) m/z: [M+H]$^+$ Calcd for [C$_{12}$H$_{19}$]$^+$ 163.1481; Found 163.1482.

15
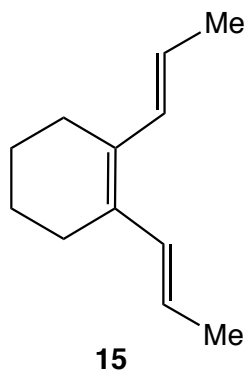
Preparation of 1,2-di((E)-prop-1-en-1-yl)cyclohex-1-ene (15): Iodine (2 mg, 0.008 mmol) was added into a Schlenk flask with 1-((E)-prop-1-en-1-yl)-2-((Z)-prop-1-en-1-yl)cyclohex-1-ene (**16**) (300 mg, 1.85 mmol). Then 40 mL of dry benzene-d_6 was

distilled into the flask. After stirring the reaction mixture for 24 hours at 23 °C, the reaction was concentrated, and iodine was sublimed off via high vacuum. The crude product was purified by flash column chromatography (hexanes) to afford **15** as a colorless oil (220 mg, 1.36 mmol, 73.5% yield). IR (film, cm^{-1}) 3042, 1666, 1455, 1256, 958. ^{1}H NMR (400 MHz, C$_6$D$_6$) δ 1.52 (m, 4H, methylene-*H*), 1.72 (d, 6H, *J* = 6.4 Hz, Me), 2.22 (m, 4H, methylene-*H*), 5.64 (m, 2H, vinyl-*H*), 6.94 (d, 2H, *J* = 15.2 Hz, vinyl-*H*). ^{13}C{^{1}H} NMR (125 MHz, CDCl$_3$) δ 19.0 (Me), 23.1 (methylene-*C*), 26.9 (methylene-*C*), 123.3 (vinyl-*C*), 129.9 (vinyl-*C*), 130.7 (vinyl-*C*). HRMS (HR-APCI) m/z: [M+H]$^+$ Calcd for [C$_{12}$H$_{19}$]$^+$ 163.1481; Found 163.1481.

NOTE: It was found that the concentration of starting material **16**, reaction time, and the amount of iodine loadings are all crucial for the success of this reaction to get a decent yield. The ideal loading of **16** was discovered as around 0.04 M. Heavily decompositions of starting material was observed if it is too concentrated, and diminished yields can be caused by the extended reaction time when the solution is too diluted. In addition, a tiny piece of iodine is enough to catalyze the isomerization, and it was found that too much iodine in the solution can also significantly drop down the yields.

14

Preparation of 1,2-di((Z)-prop-1-en-1-yl)cyclohex-1-ene (14): H_2 (1 atm) was bubbled through a stirring mixture of quinoline (0.114 mL, 0.97 mmol) and Lindlar 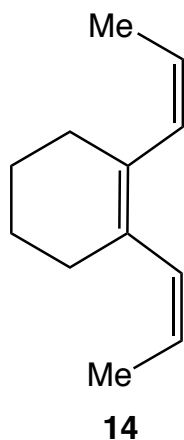Pd (1.097 g, 0.51 mmol) in hexanes (110 mL) at 23 °C for 10 minutes, and then 1,2-di(prop-1-yn-1-yl)cyclohex-1-ene (0.77 g, 4.86 mmol) was introduced. After stirring at 23 °C under hydrogen atmosphere (1 atm) for 12 hours, the reaction mixture was filtered through celite, concentrated, and purified by flash column chromatography (hexanes) to afford **14** as a colorless oil (0.35 g, 2.16 mmol, 44% yield). IR (film, cm^{-1}) 3000, 2930, 2858, 1641, 1437, 1365, 1034, 968. ^1H NMR (400 MHz, C_6D_6) δ 1.52(m, 4H, methylene-*H*), 1.63 (d, 6H, *J* = 6Hz, Me), 2.18 (m, 4H, methylene-*H*), 5.43 (m, 2H, vinyl-*H*), 6.03 (d, 2H, *J* = 10.8 Hz vinyl-*H*). $^{13}C\{^1H\}$ NMR (125 MHz, CDCl$_3$) δ 15.3 (Me), 23.1 (methylene-*C*), 30.1 (methylene-*C*), 124.3 (vinyl-*C*), 131.4 (vinyl-*C*), 132.0 (vinyl-*C*). HRMS (HR-APCI) m/z: [M+H]$^+$ Calcd for [$C_{12}H_{19}$]$^+$ 163.1481; Found 163.1480.

Me Me

48
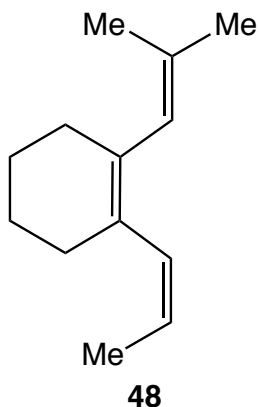
Preparation of (*Z*)-1-(2-methylprop-1-en-1-yl)-2-(prop-1-en-1-yl)cyclohex-1-ene (48): Isopropyltriphenyl phosphonium iodide (6.47g, 14.9 mmol) was added into an oven-dried 250 mL flask under N_2 with dry THF (175 mL). The suspension was cooled down to -78˚C in a dry ice / acetone bath, and then 5.19 mL of n-butylithium (2.5 M in hexane) was added dropwise. The resulting solution was stirred while warming to 0 °C. Then (*Z*)-2-(prop-1-en-1-yl)cyclohex-1-ene-1-carbaldehyde (**47**) (1.49 g, 9.9 mmol) was added dropwise at 0 °C. The resulting solution was allowed to stir at 0˚C for 30 minutes and 3 more hours at 23 °C. The reaction mixture was quenched with sat. aq. NH_4Cl (50 mL) and extracted with hexanes (3 x 100 mL). The organic extract was washed with brine (100 mL), dried with anhydrous $MgSO_4$, concentrated, and purified by flash column chromatography (hexanes) to afford **48** as a clear oil (1.52 g, 8.62 mmol, 87% yield). IR (film, cm^{-1}) 2999, 2918, 2852, 2727, 2663, 1992, 1665, 1640, 1446, 1375, 1275, 1206, 1127, 1036. ^1H NMR (400 MHz, CDCl$_3$) δ 1.54 (s, 3H, Me), 1.62 (m, 4H, methylene-*H*), 1.63 (d, 3H, *J* = 7.2 Hz, Me), 1.72 (s, 3H, Me), 2.07 (m, 2H, methylene-*H*), 2.20 (m, 2H, methylene-*H*), 5.33 (m, 1H, vinyl-*H*), 5.58 (s, 1H, vinyl-*H*), 5.86 (d, 1H, *J* = 11.6 Hz, vinyl-*H*). $^{13}C\{^1H\}$ NMR (125 MHz, CDCl$_3$) δ 15.3 (Me), 19.9 (Me), 23.1

(methylene-*C*), 23.3 (methylene-*C*), 26.1 (Me), 30.0 (methylene-*C*), 30.5 (methylene-*C*), 123.3 (vinyl-*C*), 126.6 (vinyl-*C*), 130.9 (vinyl-*C*), 131.7 (vinyl-*C*), 132.8 (vinyl-*C*), 133.2 (vinyl-*C*). HRMS (HR-APCI) m/z: [M+H]$^+$ Calcd for [C$_{13}$H$_{21}$]$^+$ 177.1638; Found 177.1639.

49
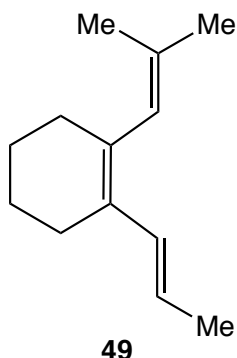
Preparation of (*E*)-1-(2-methylprop-1-en-1-yl)-2-(prop-1-en-1-yl)cyclohex-1-ene (49): 800 mg of (*Z*)-1-(2-methylprop-1-en-1-yl)-2-(prop-1-en-1-yl)cyclohex-1-ene (**48**) (4.54 mmol) was added into an oven dried 100 mL Schlenk flask. The flask was frozen by dry ice / acetone and then placed under vacuum. After 15 mL of dry benzene-*d*$_6$ was distilled into the tube under vacuum, the Schlenk flask was degassed via 3 cycles of freeze/pump/thaw/degas. The resulting solution was heated at 130 °C for 6 hours, then concentrated and purified by flash column chromatography (hexanes) to afford **49** as a clear oil (0.7 g, 4.0 mmol, 87.5% yield). IR (film, cm^{-1}) 3027, 2909, 2850, 1580, 1533, 1439, 958. ^{1}H NMR (400 MHz, CDCl$_3$) δ 1.51 (s, 3H, Me), 1.61 (m, 4H, methylene-*H*), 1.76 (d, 3H, *J* = 6.4 Hz, Me), 1.79 (s, 3H, Me), 2.00 (m, 2H, methylene-*H*), 2.16 (m, 2H, methylene-*H*), 5.57 (m, 1H, vinyl-*H*), 5.60 (s, 1H, vinyl-*H*), 6.27 (d, 1H, *J* = 16.0 Hz, vinyl-*H*). ^{13}C{^{1}H} NMR (126 MHz, CDCl$_3$) δ 18.9 (Me), 19.7 (Me), 23.32 (methylene-*C*), 23.33 (methylene-*C*), 25.6 (Me), 25.7 (methylene-*C*), 31.3 (methylene-*C*), 121.4 (vinyl-

C), 126.7 (vinyl-*C*), 130.0 (vinyl-*C*), 132.7 (vinyl-*C*), 133.3 (vinyl-*C*), 133.9 (vinyl-*C*).

HRMS (HR-APCI) m/z: [M+H]$^+$ Calcd for [C$_{13}$H$_{21}$]$^+$ 177.1638; Found 177.1641.
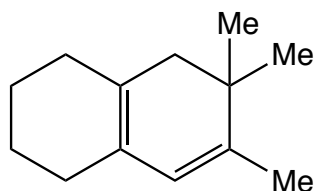
52

Preparation of 6,6,7-trimethyl-1,2,3,4,5,6-hexahydronaphthalene (52): 18 mg (0.10 mmol) of triene **48** and 50 mg of Cp*Ru(NCMe)$_3$PF$_6$ (0.10 mmol) were added into an oven dried Schlenk flask with 10 mL of dry methylene chloride. After stirring the reaction mixture at ambient temperature under inert atmosphere for 20 hours, methylene chloride was distilled out and 15 mL of dry acetonitrile was distilled into the flask. After stirring the resulting solution for 20 minutes, 50 mL of dry hexanes was poured into the flask to precipitate out the ruthenium complex. The followed filtration, concentration, and chromatography on silica gel with hexanes affords 14.5 mg (80.5%) of **52** as colorless oil. IR (film, cm^{-1}) 2998, 2924, 2850, 1458, 1445, 1369, 816. ^{1}H NMR (400 MHz, CDCl$_3$) δ 0.93 (s, 6H, Me), 1.61 (m, 4H, methylene-*H*), 1.71 (s, 3H, Me), 1.87 (bs, 2H, methylene-*H*), 1.97 (m, 4H, methylene-*H*), 5.38 (s, 1H, vinyl-*H*). ^{13}C{^{1}H} NMR (125 MHz, CDCl$_3$) δ 18.6 (Me), 23.2 (methylene-*C*), 23.3 (methylene-*C*), 25.9 (Me), 28.1 (methylene-*C*), 30.3 (methylene-*C*), 34.4 (methylene-*C*), 45.3 (methylene-*C*), 123.3 (vinyl-*C*), 125.9 (vinyl-*C*), 127.3 (vinyl-*C*), 140.6 (vinyl-*C*). HRMS (HR-APCI) m/z: [M+H]$^+$ Calcd for [C$_{13}$H$_{21}$]$^+$ 177.1638; Found 177.1638.
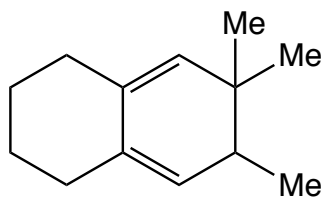
53

Preparation of 6,6,7-trimethyl-1,2,3,4,6,7-hexahydronaphthalene (53): 0.14 g of (*Z*)-1-(2-methylprop-1-en-1-yl)-2-(prop-1-en-1-yl)cyclohex-1-ene **(48)** (0.79 mmol) was added into an oven dried 100 mL Schlenk flask with CpRu(NCMe)$_3$PF$_6$ (68 mg, 0.16 mmol). Then 8 mL of dry DCM was distilled into the tube, and the reaction mixture was allowed to stir at 23 °C for 40 minutes. The solution was poured into hexanes (100 mL), and the resulting solution was passed through a short plug of Celite followed by a short plug of silica gel with hexanes / EtOAc (50 : 50, 100 mL) as eluant. Then the solution was concentrated, and purified by flash column chromatography (hexanes) to afford **53** as a colorless oil (0.13 g, 0.74 mmol, 92% yield). IR (film, cm^{-1}) 2958, 2925, 2854, 1737, 1459, 1435, 1369, 1369, 1244, 818. ^{1}H NMR (400 MHz, CDCl$_3$) δ 0.77 (s, 3H, Me), 0.91 (d, 3H, *J* = 7.2 Hz, Me), 0.98 (s, 3H, Me), 1.46 (m, 2H, methylene-*H*), 1.62 (m, 2H, methylene-*H*), 2.10 (m, 1H, C*H*Me), 2.22 (m, 4H, methylene-*H*), 5.13 (s, 1H, vinyl-*H*), 5.14 (bs, 1H, vinyl-*H*). ^{13}C{^{1}H} NMR (125 MHz, CDCl$_3$) δ 14.3 (Me), 20.5 (Me), 24.99 (methylene-*C*), 25.02 (methylene-*C*), 28.3 (methylene-*C*), 30.8 (methylene-*C*), 31.0 (methylene-*C*), 34.2 (methylene-*C*), 39.3 (methylene-*C*), 126.7 (vinyl-*C*), 132.5 (vinyl-*C*), 132.9 (vinyl-*C*), 133.3 (vinyl-*C*).   HRMS (HR-APCI) m/z: [M+H]$^+$ Calcd for [C$_{13}$H$_{21}$]$^+$ 177.1638; Found 177.1640.

23
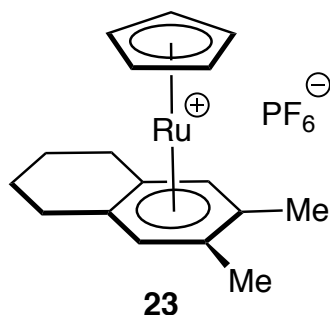
Preparation of (η^5-cyclopentadienyl) (η^6-6,7-dimethyl-1,2,3,4-tetrahydro-naphthalene)Ru hexafluorophosphate (23): 56 mg of 1,2-di((Z)-prop-1-en-1-yl)cyclohex-1-ene (**14**) (0.35 mmol) and CpRu(NCMe)$_3$PF$_6$ (100mg, 0.23 mmol) were added into an oven dried 100 ml schlenk flask. The flask was frozen by dry ice acetone and then placed under vacuum. After 20 ml of dry methylene chloride was distilled into the flask under vacuum, the flask was degassed via 3 cycles of freeze/pump/thaw/degas. Then the reaction mixture was allowed to stir at room temperature for 2 hours followed by layered with Et$_2$O (80 ml) to afford **23** as a colorless flake crystal (90.5 mg, 83.5% yield). mp: 266.7 °C. IR (film, cm^{-1}) 3113, 3082, 2939, 1473, 1454, 1433, 1416, 1391, 1038, 1005, 945, 837. ^{1}H NMR (400 MHz, CD$_2$Cl$_2$) δ 1.73 (m, 2H, methylene-*H*), 1.83 (m, 2H, methylene-*H*), 2.30 (s, 6H, Me), 2.62 (m, 2H, methylene-*H*), 2.78 (m, 2H, methylene-*H*), 5.11 (s, 5H, Cp), 6.01 (s, 2H, aromatic-*H*). ^{13}C{^{1}H} NMR (125 MHz, CD$_2$Cl$_2$) δ 18.7 (Me), 22.5 (methylene-*C*), 28.1 (methylene-*C*), 81.3 (Cp), 87.5 (Ar), 100.7 (Ar), 102.5 (Ar). HRMS (HR-ESI/TOFMS) m/z: [M-PF$_6$]$^+$ Calcd for [C$_{17}$H$_{21}$Ru]$^+$ 327.0686; Found 327.0682.
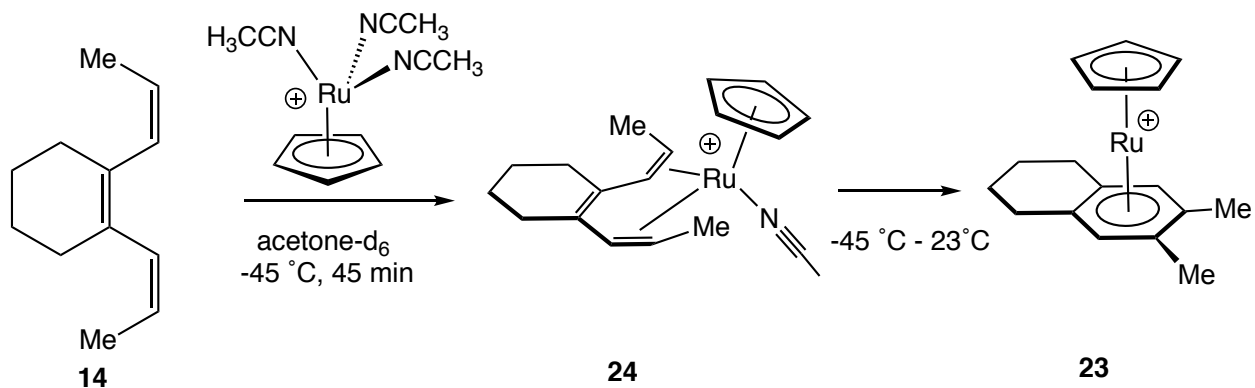
NMR tube reaction of 1,2-di((Z)-prop-1-en-1-yl)cyclohex-1-ene (14) with CpRu(NCMe)₃PF₆ in acetone-d₆ : 1,2-di((Z)-prop-1-en-1-yl)cyclohex-1-ene (**14**) (2.4 mg, 0.015 mmol) and CpRu(NCMe)₃PF₆ (6.4 mg, 0.015 mmol) were added into an oven dried J.Y. NMR tube with 1,3,5-tri-tert-butylbenzene as internal standard. The tube was frozen by liquid nitrogen and then placed under vacuum. After 0.45 mL of dry acetone-d_6 was distilled into the tube under vacuum, the tube was degassed via 3 cycles of freeze/pump/thaw/degas. The NMR tube was kept at -60 °C in the JEOL ECA500 NMR instrument equipped with a nitrogen-cooled Cold Probe, and an initial ¹H NMR spectrum was recorded immediately. Then the reaction mixture was monitored by ¹H NMR spectroscopy at -45 °C. After 45 minutes, ¹H NMR spectrum indicates that 73% of CpRu(NCMe)₃PF₆ were consumed based on the Cp resonance at δ 4.34 (s, 5H), and resonances of complex **24** were observed at δ 1.48 (d, 3H, J = 6.5 Hz, Me), 1.73 (m, 2H, methylene-H), 1.77 (d, 3H, J = 5.5 Hz, Me), 2.55 (s, 3H, NCMe), 4.02 (d, 1H, J = 9.0 Hz, vinyl-H), 4.51 (d, 1H, J = 9.5 Hz, vinyl-H), 4.75 (m, 1H, vinyl-H), 5.13 (m, 1H, vinyl-H), 5.26 (s, 5H, Cp), respectively. The yield (97.7%) of **24** is calculated based on the integration of Cp resonance at δ 5.26 (s, 5H) relative to converted CpRu(NCMe)₃PF₆.

Then the reaction mixture was allowed to warmed up slowly, and during that process, the consumption of **24** was observed, and a new set of resonances of complex **23** was observed at δ 1.80 (m, 4H, methylene-*H*), 2.38 (s, 6H, Me), 2.80 (m, 4H, methylene-*H*), 5.37 (s, 5H, Cp), and 6.27 (s, 2H, Ar). After keeping the reaction at room temperature for 120 minutes, all the intermediate **24** were consumed based on the Cp resonance at δ 5.26 (s, 5H), and the yield (91.6%) of **23** was calculated based on the integration of Cp resonance at δ 5.37 (s, 5H) relative to internal standard. To crystalize the intermediate **24**, a similar reaction was conducted: 1,2-di((Z)-prop-1-en-1-yl)cyclohex-1-ene (**14**) (4.8 mg, 0.03 mmol) and CpRu(NCMe)$_3$PF$_6$ (12.84 mg, 0.03 mmol) were added into an oven dried J.Y. NMR tube. After 0.7 ml of the dry acetone was distilled into the tube at -78 °C, the reaction mixture was allowed to keep at -45 °C for 45 minutes. Then dry hexanes (2 mL) was distilled into the NMR tube at -78 °C, and the tube was kept at -40 °C for several days to introduce crystallization of **24**, which was suitable for X-ray crystallography analysis.

NOTE: The reaction with loadings of 1,2-di((Z)-prop-1-en-1-yl)cyclohex-1-ene (**14**) (2.5 mg, 0.015 mmol) and CpRu(NCMe)$_3$PF$_6$ (6.3 mg, 0.015 mmol) in dry acetone (0.45 mL) was also conducted at room temperature with 1,3,5-tri-tert-butylbenzene as internal standard. The reaction mixture was monitored by ^{1}H NMR spectroscopy. After 10 minutes, the integrations of Cp resonances at δ 5.24 (s, 5H) and 5.37 (s, 5H) indicate a 1 : 0.96 ratio of **23** to **24**. After 100 minutes, all of the **24** were consumed, and the yield (90.4%) of **13** was calculated based on the integration of Cp resonance at δ 5.37 (s, 5H) relative to internal standard.
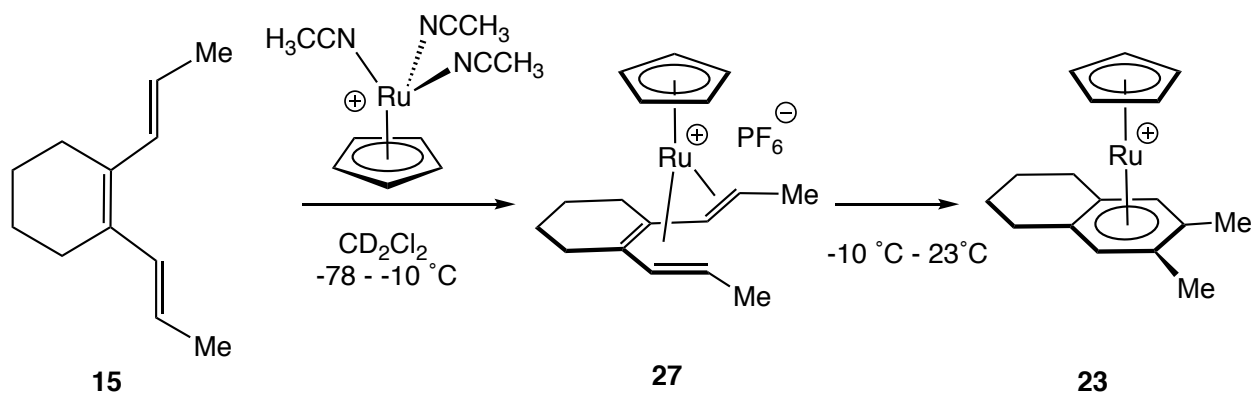
NMR tube reactions of 1,2-di((*E*)-prop-1-en-1-yl)cyclohex-1-ene (15) with CpRu(NCMe)$_3$PF$_6$ in methylene chloride-d_2 : 1,2-di((*E*)-prop-1-en-1-yl)cyclohex-1-ene (**15**) (1.9 mg, 0.012 mmol) and CpRu(NCMe)$_3$PF$_6$ (5.0 mg, 0.012 mmol) were added into an oven dried J.Y. NMR tube with 1,3,5-tri-tert-butylbenzene as internal standard. The tube was frozen by liquid nitrogen and then placed under vacuum. After 0.65 mL of dry methylene chloride-d_6 was distilled into the tube under vacuum, the tube was degassed via 3 cycles of freeze/pump/thaw/degas. The NMR tube was kept at -60 °C in the JEOL ECA500 NMR instrument equipped with a nitrogen-cooled Cold Probe, and an initial ^{1}H NMR spectrum was recorded immediately. Then the reaction mixture was monitored by ^{1}H NMR spectroscopy at -20 °C for 2.5 hours, and 20 more minutes at -10 °C. ^{1}H NMR spectrum indicates that 85% of CpRu(NCMe)$_3$PF$_6$ were consumed based on the Cp resonance at δ 4.25 (s, 5H), and resonances of complex **27** were observed at δ 1.66 (d, 3H, *J* = 6.0 Hz, Me), 1.73 (m, 2H, methylene-*H*), 2.07 (d, 3H, *J* = 6.0 Hz, Me), 2.98 (d, 1H, *J* = 17.0 Hz, methylene-*H*), 3.61 (m, 1H, vinyl-*H*), 5.10 (1H, vinyl-*H*), 5.13 (s, 5H, Cp), 6.07 (m, 1H, vinyl-*H*), respectively. The yield (92%) of **27** is calculated based on the integration of Cp resonance at δ 5.13 (s, 5H) relative to converted

CpRu(NCMe)$_3$PF$_6$. Then the reaction mixture was allowed to warmed up slowly, and during that process, the consumption of **27** was observed, and a new set of resonances of complex **23** was observed at δ 1.73 (m, 2H, methylene-*H*), 1.83 (m, 2H, methylene-*H*), 2.30 (s, 6H, Me), 2.62 (m, 2H, methylene-*H*), 2.78 (m, 2H, methylene-*H*), 5.11 (s, 5H, Cp), and 6.01 (s, 2H, Ar). After keeping the reaction at room temperature for 70 minutes, all the intermediate **27** were consumed based on the Cp resonance at δ 5.13 (s, 5H), and the yield (88%) of **23** was calculated from the integration of Cp resonance at δ 5.11 (s, 5H) relative to internal standard. To crystalize the intermediate **27**, a similar reaction was conducted: 1,2-di((*E*)-prop-1-en-1-yl)cyclohex-1-ene (**15**) (2.0 mg, 0.012 mmol) and CpRu(NCMe)$_3$PF$_6$ (5.0 mg, 0.012 mmol) were added into an oven dried J.Y. NMR tube. After 0.7 ml of the dry methylene chloride was distilled into the tube at -78 °C, the reaction mixture was allowed to keep at -20 °C for 7 hours. Then dry hexanes (2 mL) was distilled into the NMR tube at -78 °C, and the tube was kept at -20 °C for several days to introduce crystallization of **27**, which was suitable for X-ray crystallography analysis. For the isolation of **27** as powder, a larger scale NMR reaction was conducted in a similar fashion: 1,2-di((*E*)-prop-1-en-1-yl)cyclohex-1-ene (**15**) (6.0 mg, 0.037 mmol) and CpRu(NCMe)$_3$PF$_6$ (12.0 mg, 0.029 mmol) were added into an oven dried J.Y. NMR tube. After 1.4 ml of the dry methylene chloride was distilled into the tube at -78 °C, the reaction mixture was allowed to keep at -20 °C for 7 hours. Then most of the methylene chloride was pumped away followed by distilling in 4 mL of dry diethyl ether at -20 °C to crush out **27** as yellow powder, which was filtered and washed with cold hexanes under nitrogen to give 11.9 mg of **27** (87% yield). ^{1}H NMR analysis indicates the presence of trace amount of **23** (less than 5%).

Characterization of 27: IR (film, cm^{-1}) 3116, 2940, 2870, 2309, 2201, 1535, 1430, 1380, 1296,1035, 955, 708. ^{1}H NMR (400 MHz, CD$_2$Cl$_2$) δ 1.33 (m, 1H, methylene-*H*), 1.68 (d, 3H, *J* = 5.6 Hz, Me), 1.75 (m, 1H, methylene-*H*), 1.79 (m, 1H, methylene-*H*), 1.93 (m, 2H, methylene-*H*), 2.09 (d, 3H, *J* = 5.6 Hz, Me), 2.22 (d, 1H, *J* = 13.2 Hz, vinyl-*H*), 2.30-2.48 (m, 2H, methylene-*H*), 3.00 (m, 1H, methylene-*H*), 3.65 (m, 1H, vinyl-*H*), 5.12 (1H, vinyl-*H*), 5.14 (s, 5H, Cp), 6.13 (m, 1H, vinyl-*H*). ^{13}C{^{1}H} NMR (125 MHz, CDCl$_3$) δ 20.4 (Me), 21.8 (methylene-*C*), 22.5 (methylene-*C*), 23.9 (Me), 28.2 (methylene-*C*), 30.9 (methylene-*C*), 65.0 (*C*HCH$_3$), 86.9 (Cp), 91.1 (*C*HCH$_3$), 91.2 (*C*CCH$_3$), 100.5 (ring vinyl-*C*), 105.5 (*C*CCH$_3$), 113.0 (ring vinyl-*C*). HRMS (HR-ESI-TOFMS) m/z: [M]$^+$ Calcd for [C$_{17}$H$_{23}$Ru]$^+$ 323.0870; Found 323.0854.
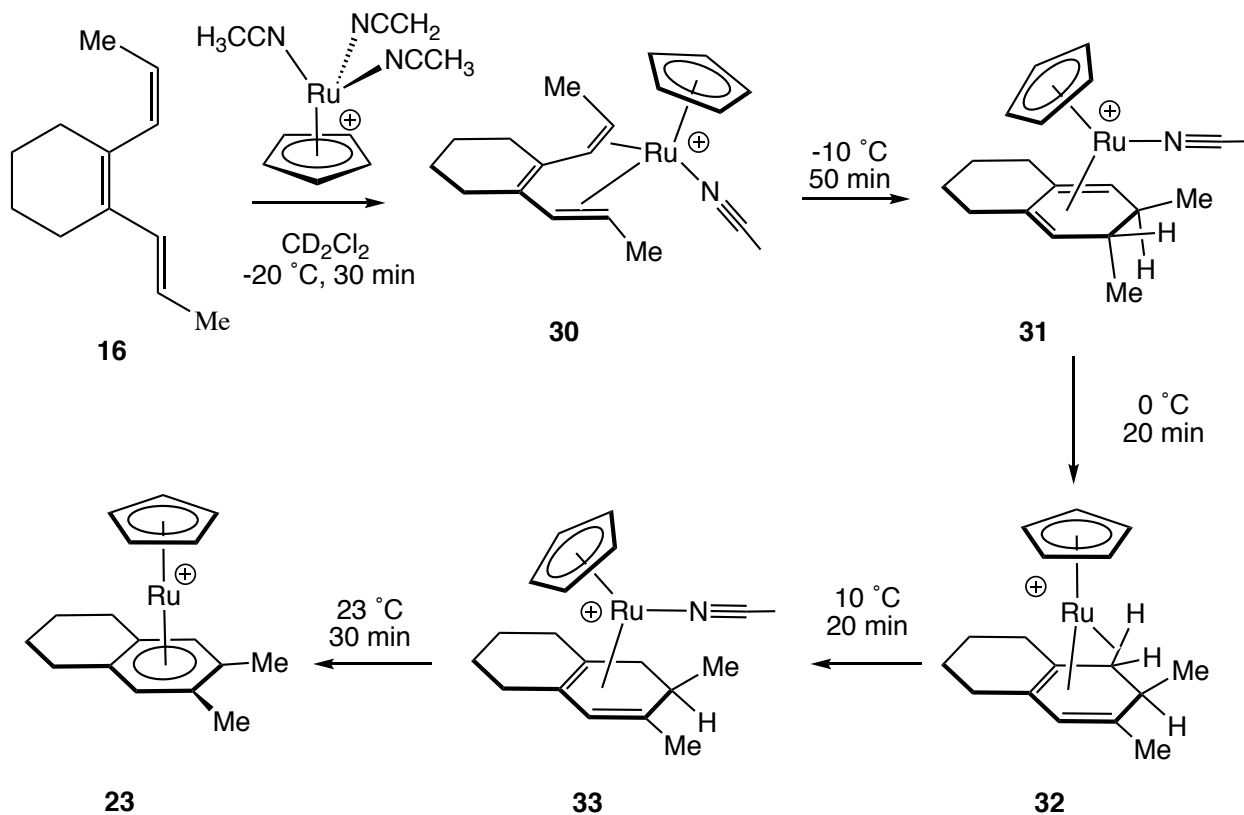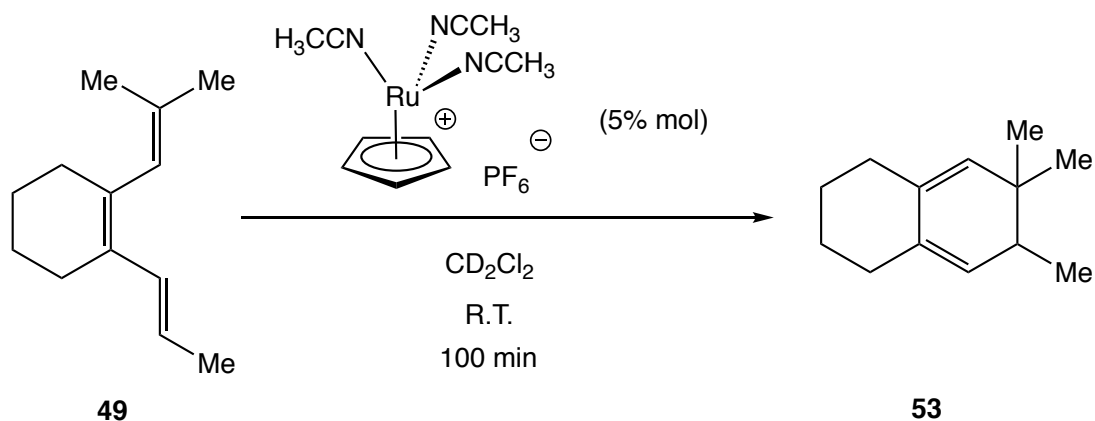
NMR reaction of CpRu(NCMe)₃PF₆ with 1-((*E*)-prop-1-en-1-yl)-2-((*Z*)-prop-1-en-1-yl)cyclohex-1-ene (16) at low temperature in methylene chloride-*d*₂: 5 mg (0.031 mmol) of 1-((*E*)-prop-1-en-1-yl)-2-((*Z*)-prop-1-en-1-yl)cyclohex-1-ene and 10 mg (0.023 mmol) of CpRu(NCMe)₃PF₆ were added into an oven dried J.Y. NMR tube. The tube was frozen by liquid nitrogen immediately and then placed under vacuum. After 0.75 mL of dry CD₂Cl₂ was distilled into the tube under vacuum, the tube was degassed via 3 cycles of freeze/pump/thaw/degas. The NMR tube was kept at -60 °C in the JEOL ECA500 NMR instrument equipped with a nitrogen-cooled Cold Probe, and an initial ¹H NMR spectrum was recorded immediately. Then the reaction mixture was monitored by ¹H NMR spectroscopy while slowly increasing temperature. After 30 minutes at -20 °C, a new set of resonances of intermediate **30** were observed at δ 1.45 (d, 3H, *J* = 6 Hz, Me), 1.82 (d, 3H, *J* = 6 Hz, Me), 2.44 (s, 3H, NCMe), 3.75 (d, 1H, *J* = 13 Hz, vinyl-*H*), 4.38 (d, 1H, *J* = 10 Hz, vinyl-*H*), 4.62 (m, 2H, vinyl-*H*), 4.97 (s, 5H, Cp). The yield (20.2%) of **30** at this point was calculated based on the integration of Cp resonance at δ 4.97 (s, 5H) relative to internal standard. Then the reaction was allowed to stay at -20 °C for 300 minutes and then warmed up to -10 °C for 50 minutes, a new set of resonances of intermediate **31** were observed at δ 0.92 (d, 3H, *J* = 6.5 Hz, Me), 1.24 (d, 3H, *J* = 6.5 Hz, Me), 2.57 (s, 3H, NCMe), 5.00 (s, 5H, Cp), 5.37 (bs, 2H, vinyl-*H*). The yield (24.0%) of **31** at this point was calculated based on the integration of Cp resonance at δ 5.00 (s, 5H) relative to internal standard. The reaction mixture was then allowed to stay at -5 °C for 20 minutes and 0 °C for another 20 minutes, a new set of resonances of **32** was observed at δ -7.90 (t, 1H, *J* = 16.0 Hz, agnostic-*H*), 0.90 (d, 3H, *J* = 7.0 Hz, Me), 1.81 (s, 3H, Me), 5.18 (s, 5H, Cp), 5.25 (s, 1H, vinyl-*H*). The yield

(37.8%) of **32** at this point was calculated based on the integration of Cp resonance at δ 5.18 (s, 5H) relative to internal standard. Then the reaction mixture was allowed to stay at 5 °C for 20 minutes and 10 °C for another 20 minutes, a new set of resonances of **33** was observed at δ 0.92 (d, 3H, J = 7.0 Hz, Me), 1.75 (s, 3H, Me), 2.63 (s, 3H, NCMe), 4.60 (s, 1H, vinyl-H), 4.95 (s, 5H, Cp). The yield (22.0%) of **33** at this point was calculated based on the integration of Cp resonance at δ 4.95 (s, 5H) relative to internal standard. Then the reaction mixture was warmed up to 23 °C. After 30 minutes, all the intermediate resonances disappeared, and resonances of complex **23** were observed at δ 1.73 (m, 2H, methylene-H), 1.83 (m, 2H, methylene-H), 2.30 (s, 3H, Me), 2.62 (m, 2H, methylene-H), 2.78 (m, 2H, methylene-H), 5.11 (s, 5H, Cp), 6.01 (s, 2H, arene-H). The yield of **23** (94.3%) was calculated by the integration of Cp resonance at δ 5.11 (s, 5H) relative to internal standard.

NMR reaction of CpRu(NCMe)₃PF₆ catalyzed 6-π cyclization of (Z)-1-(2-methylprop-1-en-1-yl)-2-(prop-1-en-1-yl)cyclohex-1-ene (48) in methylene chloride-d_2: 40 mg of **48** (0.227 mmol) and 5 mg of CpRu(NCMe)₃PF₆ (0.0115 mmol) were
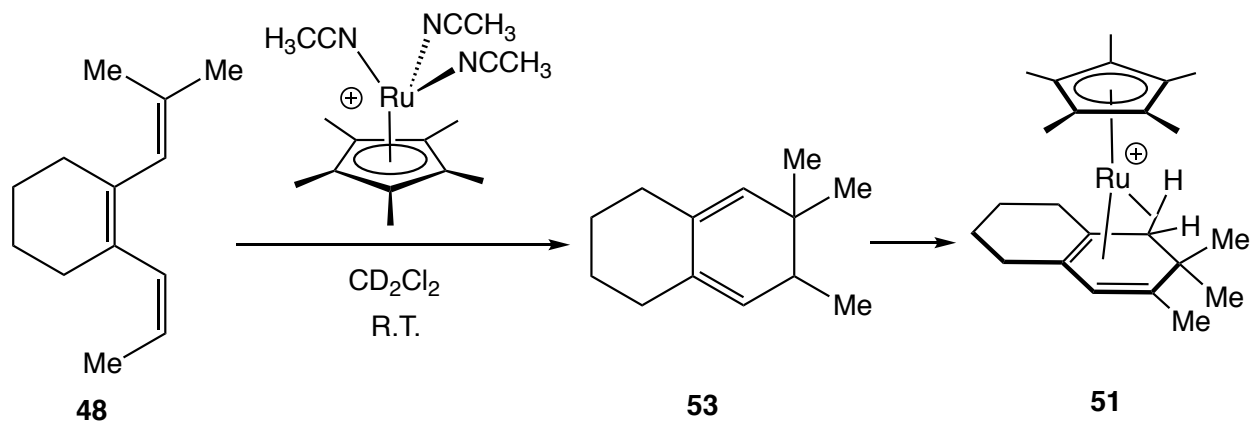
added into an oven dried J.Y. NMR tube with 1,3,5-tri-tert-butylbenzene as internal standard. The NMR tube was immediately frozen by dry ice / acetone and placed under vacuum. 0.8 mL of dry methylene chloride-d_2 was distilled into the NMR tube, and the tube was vortexed to dissolve all the solids while kept cold. After the tube was degassed via 3 cycles of freeze/pump/thaw/degas, an initial ^{1}H NMR spectrum was recorded immediately, and then the reaction mixture was monitored by ^{1}H NMR spectroscopy at room temperature. After 100 minutes, 83% of **48** were consumed based on the integration of the vinyl hydrogen resonance at δ 5.84 (d, 1H, J = 11.6 Hz), and the resonances of **53** were observed at δ 0.77 (s, 3H, Me), 0.90 (d, 3H, J = 7.2 Hz, Me), 0.97 (s, 3H, Me), 1.45 (m, 2H, methylene-H), 1.61 (m, 2H, methylene-H), 2.0-2.3 (m, 5H, methylene-H and CHMe), 5.13 (s, 1H, vinyl-H), 5.14 (bs, 1H, vinyl-H), respectively. The yield (70.5%) of **53** is calculated by the integration of methyl resonance at δ 0.77 (s, 3H) relative to internal standard.

NOTE: Longer reaction time can cause some decomposition of the desired product (**53**). It might have been polymerized or oligomerized to some unknown molecules. In addition, if increase the loading of ruthenium catalyst to 20 mol%, all the triene **48** can be consumed in 30 minutes with quantitively yield of **53**.

NMR reaction of CpRu(NCMe)₃PF₆ catalyzed 6-π cyclization of (E)-1-(2-methylprop-1-en-1-yl)-2-(prop-1-en-1-yl)cyclohex-1-ene (49) in methylene chloride-d₂: The same amount of **49**, CpRu(NCMe)₃PF₆ and solvent were employed as starting materials to conduct the same procedure described above. After 100 minutes, 79% of **49** were consumed based on the integration of the vinyl hydrogen resonance at δ 6.26 (d, 1H, J = 15.2 Hz). The yield (67%) of **53** is calculated by the integration of methyl resonance at δ 0.77 (s, 3H) relative to internal standard.

NOTE: Longer reaction time can also cause some decomposition of the desired product (**53**). It might have been polymerized or oligomerized to some unknown molecules. In addition, if increase the loading of ruthenium catalyst to 20 mol%, all the triene **49** can be consumed in 30 minutes with quantitively yield of **53**.

NMR reaction of Cp*Ru(NCMe)₃PF₆ with (*Z*)-1-(2-methylprop-1-en-1-yl)-2-(prop-1-en-1-yl)cyclohex-1-ene (48) to form (η^5-petamethylcyclopentadienyl)(η^6-6,6,7-trimethyl-1,2,3,4,5,6-hexahydronaphthalene) Ru(II) hexafluorophosphate (51) in methylene chloride-*d₂*: 3.5 mg (0.0198 mmol) of **48** and 5 mg of Cp*Ru(NCMe)₃PF₆ (0.01 mmol) were added into an oven dried J.Y. NMR tube with 1,3,5-tri-tert-butylbenzene as internal standard. The NMR tube was immediately frozen by dry ice / acetone and placed under vacuum. After 0.65 mL of dry methylene chloride-*d₂* was distilled into the NMR tube, the tube was degassed via 3 cycles of freeze/pump/thaw/degas, and an initial ¹H NMR spectrum was recorded immediately, and then the reaction mixture was monitored by ¹H NMR spectroscopy at room temperature. After 10 minutes, all of **48** were consumed based on the methyl peak at δ 1.53 (s, 3H), and the resonances of **53** were observed at δ 0.77 (s, 3H, Me), 0.90 (d, 3H, *J* = 7.2 Hz, Me), 0.97 (s, 3H, Me), 1.45 (m, 2H, methylene-*H*), 1.61 (m, 2H, methylene-*H*), 2.0-2.3 (m, 5H, methylene-*H* and C*H*Me), 5.13 (s, 1H, vinyl-*H*), 5.14 (bs, 1H, vinyl-*H*), respectively. After 7 hours, the maximum amount of **51** was obtained, and the resonances of **51** were observed at δ -8.39 (d, 1H, J = 18 Hz, agostic-*H*), 0.48 (s,

3H, Me), 1.15 (s, 3H, Me), 1.38 (s, 3H, Me), 1.53 (d, 1H, , J = 20 Hz, CHCMe$_2$), 1.64 (m, 1H, methylene-H), 1.79 (s, 15H, Cp*), 1.98 (m, 2H, methylene-H), 2.42 (m, 2H, methylene-H), 2.57 (m, 1H, methylene-H), 2.68 (m, 1H, methylene-H), 3.06 (m, 1H, methylene-H), 4.60 (s, 1H, vinyl-H). The carbon resonances of **51** in ^{13}C{^{1}H} NMR (125 MHz, CD$_2$Cl$_2$) were observed at δ 10.1 (Cp*), 17.2 (methylene-C), 22.1 (methylene-C), 22.3 (methylene-C), 25.1 (methylene-C), 26.7 (Me), 29.4 (Me), 29.5 (Me), 47.6 (CHCMe$_2$), 83.4 (vinyl-C), 92.0 (vinyl-C), 93.5 (vinyl-C), 94.6 (Cp*), 108.4 (vinyl-C). The NMR yield (88.5%) of **51** was calculated by the integration of methyl resonance at δ 0.48 relative to internal standard at δ 1.32.

General methods of the kinetic studies of CpRu(NCMe)$_3$PF$_6$ with (*E*)-1-(2-methylprop-1-en-1-yl)-2-(prop-1-en-1-yl)cyclohex-1-ene at room temperature in methylene chloride-*d*$_2$ solvent: (*E*)-1-(2-methylprop-1-en-1-yl)-2-(prop-1-en-1-yl)cyclohex-1-ene (10.0 mg, 0.0567 mmol), CpRu(NCMe)$_3$PF$_6$ (1 mg, 4 mg, 6 mg, 9 mg, 11 mg, 13 mg, 15 mg, 17 mg and 19 mg for different entries), and 1,3,5-tri-*tert*-butylbenzene (internal standard) were added to an oven dried J. Young NMR tube. After

the NMR tube was frozen at -78 ˚C and placed under vacuum, methylene chloride-d_2 was distilled into the NMR tube until the total solution volume is 920 μL. The NMR tube was shaken to dissolve all the solid while it was kept cold, and time recording started when the NMR tube was placed into a water bath to warm up to 23 ˚C. The reaction was subsequently monitored by ^{1}H NMR spectroscopy, and time points were taken while the NMR tube stayed in the NMR equipment at room temperature (23 ˚C). The consumption of (E)-1-(2-methylprop-1-en-1-yl)-2-(prop-1-en-1-yl)cyclohex-1-ene was recorded by the integration of vinyl hydrogen resonance at δ 6.26 (d, 1H, J = 16 Hz) relative to internal standard at δ 7.24. The [triene]-Time plots fit the first order exponential decay. The ln [triene]-Time plots were made to calculate to the rate constant k_{obs} and half lives for different concentration of CpRu(NCMe)$_3$PF$_6$. The ln (k_{obs})-ln [Cp*Ru(NCMe)$_3$PF$_6$] plot was made to produce a straight line with a slope of 0.998, which indicates the reaction is first order to CpRu(NCMe)$_3$PF$_6$.

G. Appendix
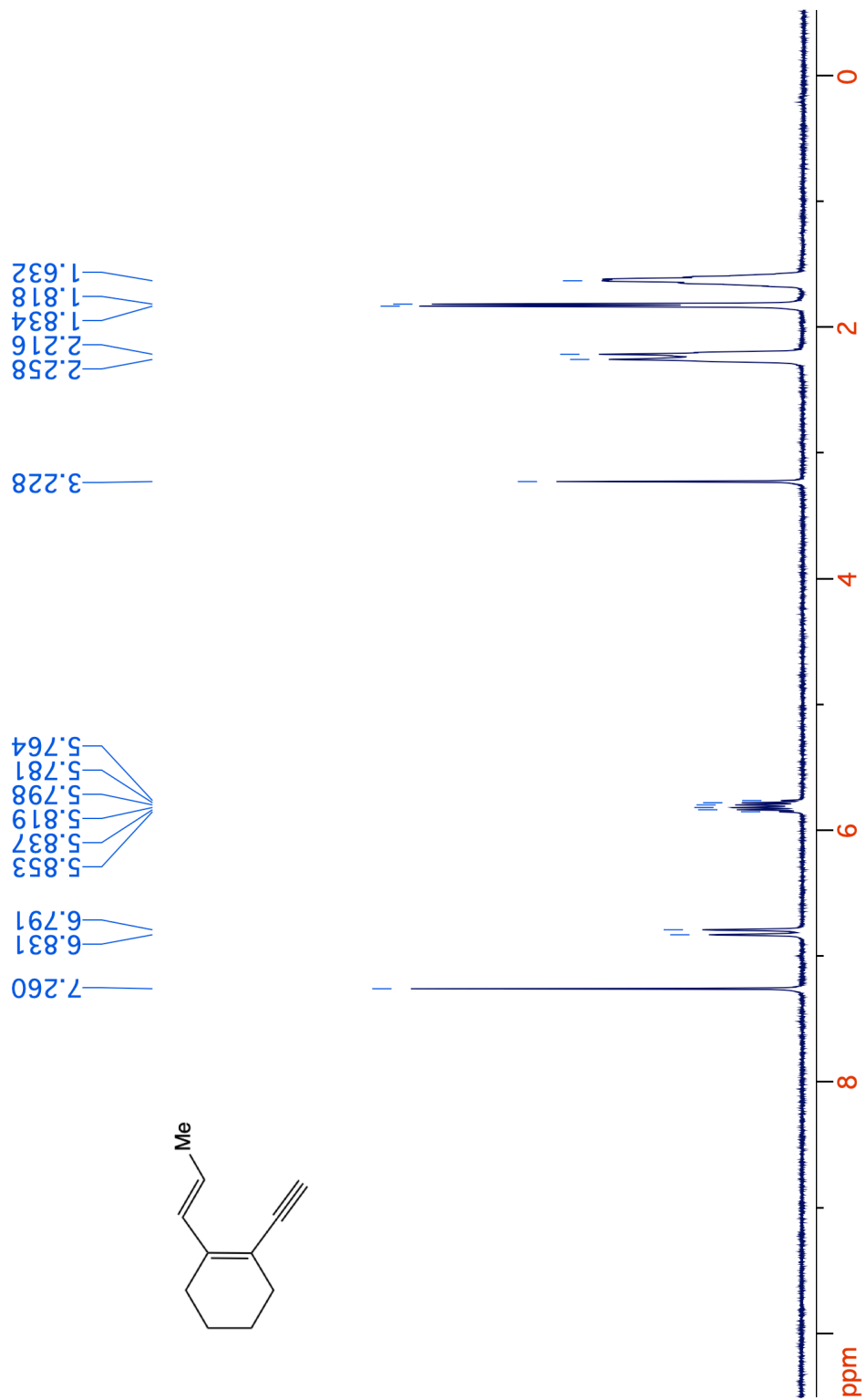
Figure 8-12. ^{1}H NMR spectrum (400 MHz, CDCl$_3$) of **21**.
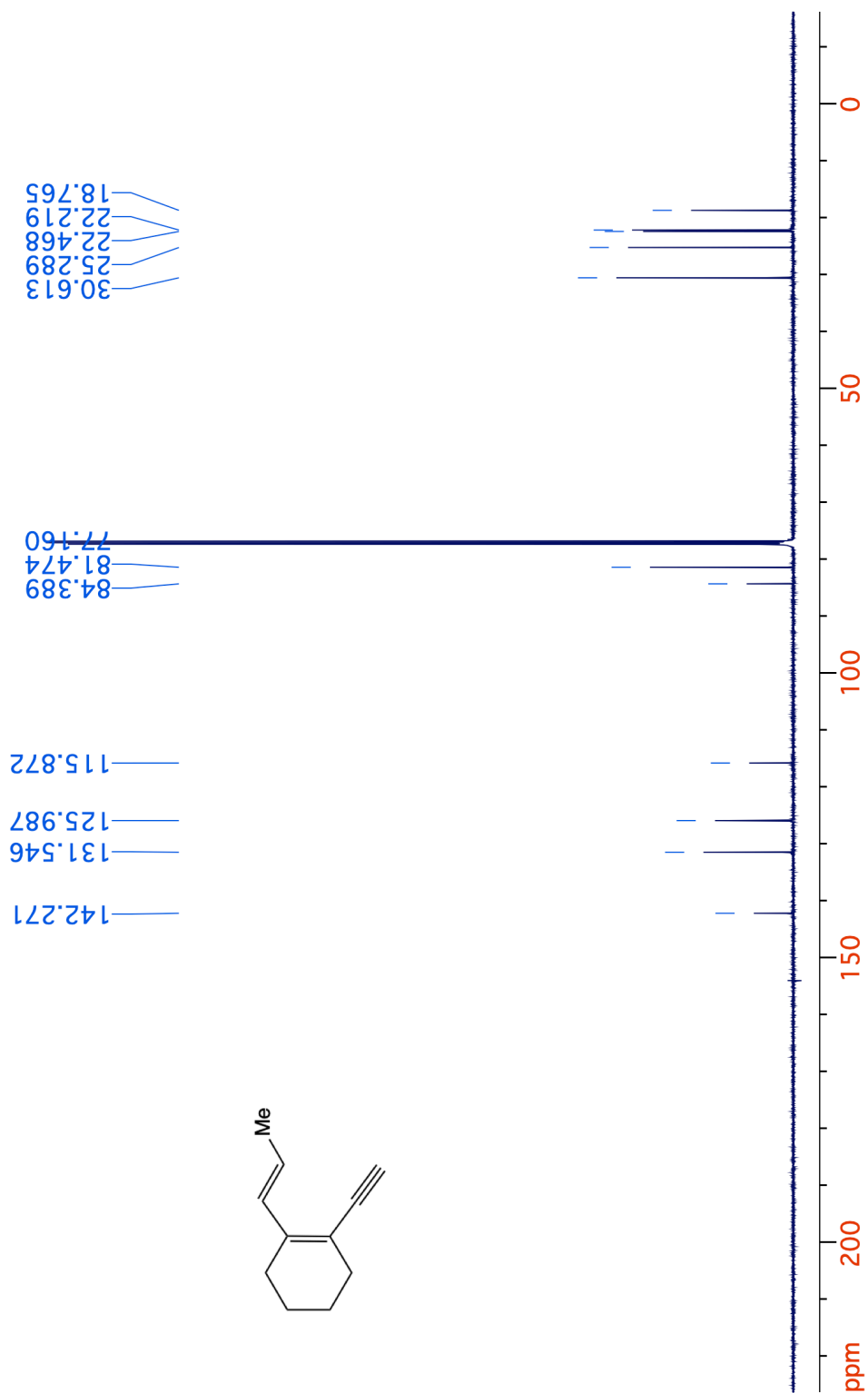
Figure 8-13. $^{13}C\{^1H\}$ NMR spectrum (125 MHz, CDCl$_3$) of **21**.

Peak labels (from spectrum):
- 18.765
- 22.219
- 22.468
- 25.289
- 30.613
- 77.160
- 81.474
- 84.389
- 115.872
- 125.987
- 131.546
- 142.271
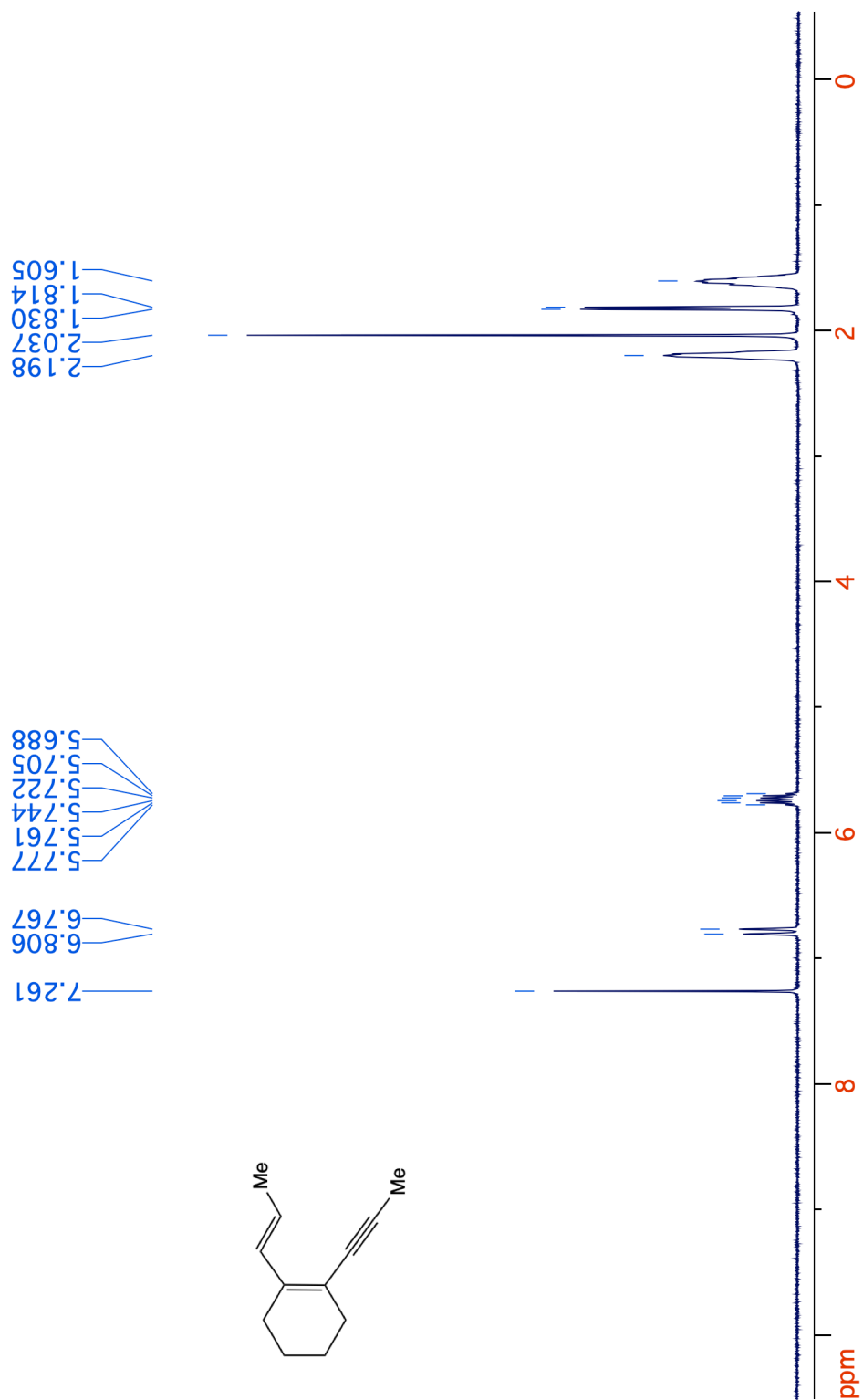
Figure 8-14. ^{1}H NMR spectrum (400 MHz, CDCl$_3$) of **22**.
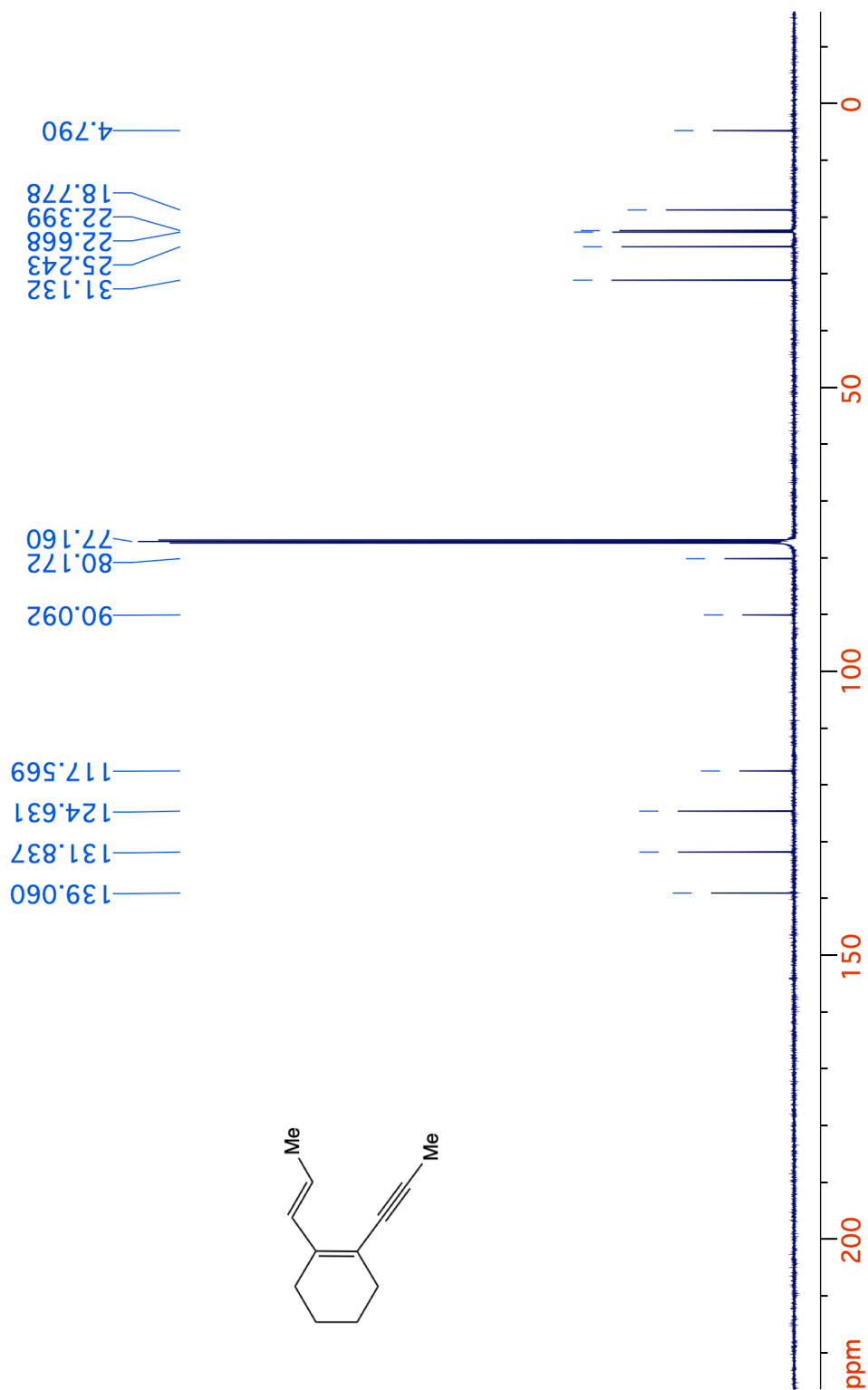
Figure 8-15. $^{13}C\{^1H\}$ NMR spectrum (125 MHz, CDCl$_3$) of **22**.

Peaks labeled: 4.790, 18.778, 22.399, 22.668, 25.243, 31.132, 77.160, 80.172, 90.092, 117.569, 124.631, 131.837, 139.060

1.523
1.618
1.633
2.176

5.385
5.403
5.420
5.432
5.449
5.467
6.014
6.041

7.160
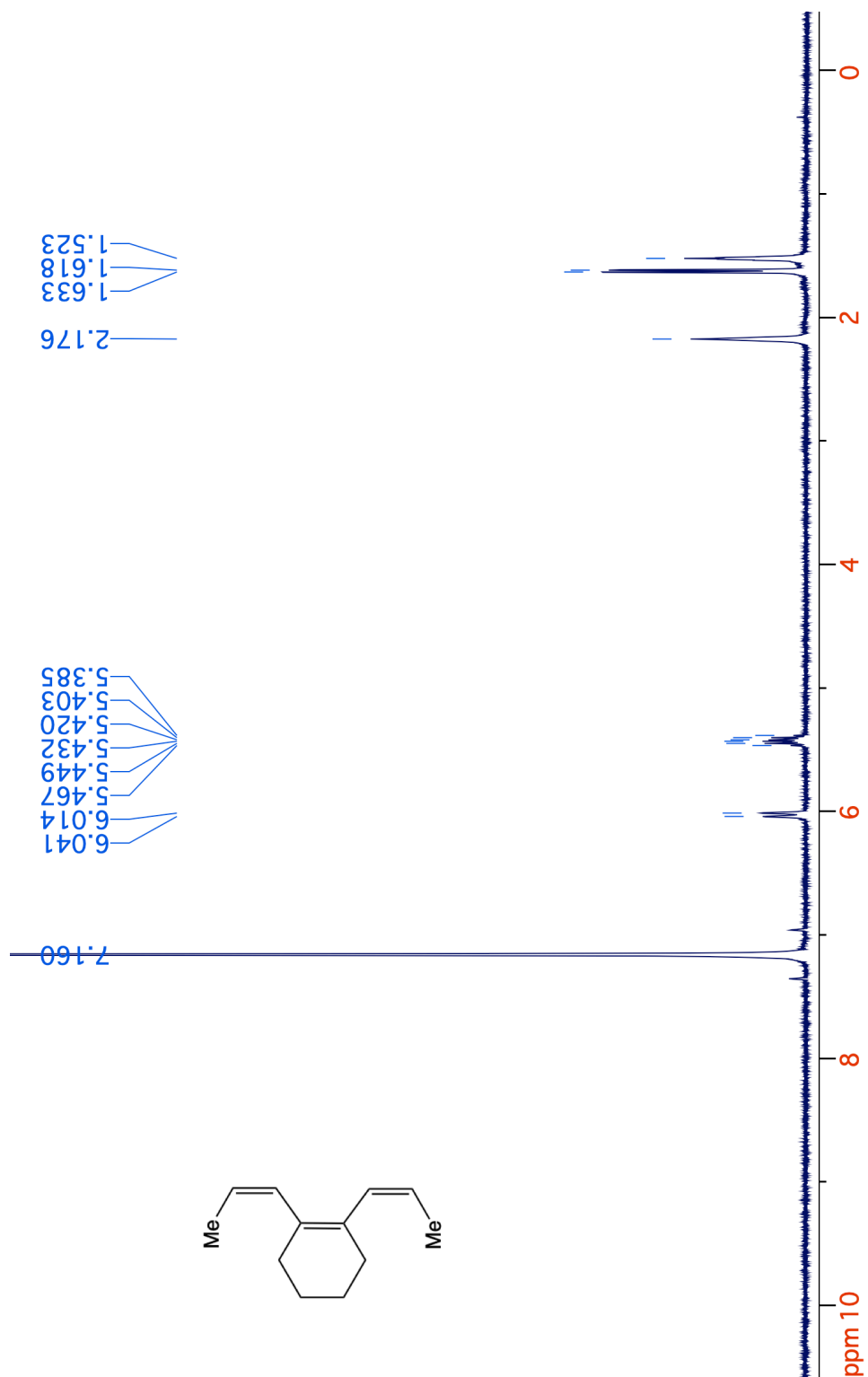
Figure 8-16. ¹H NMR spectrum (400 MHz, C₆D₆) of **14**.

15.271
23.077
30.099
77.160
124.266
131.433
131.987
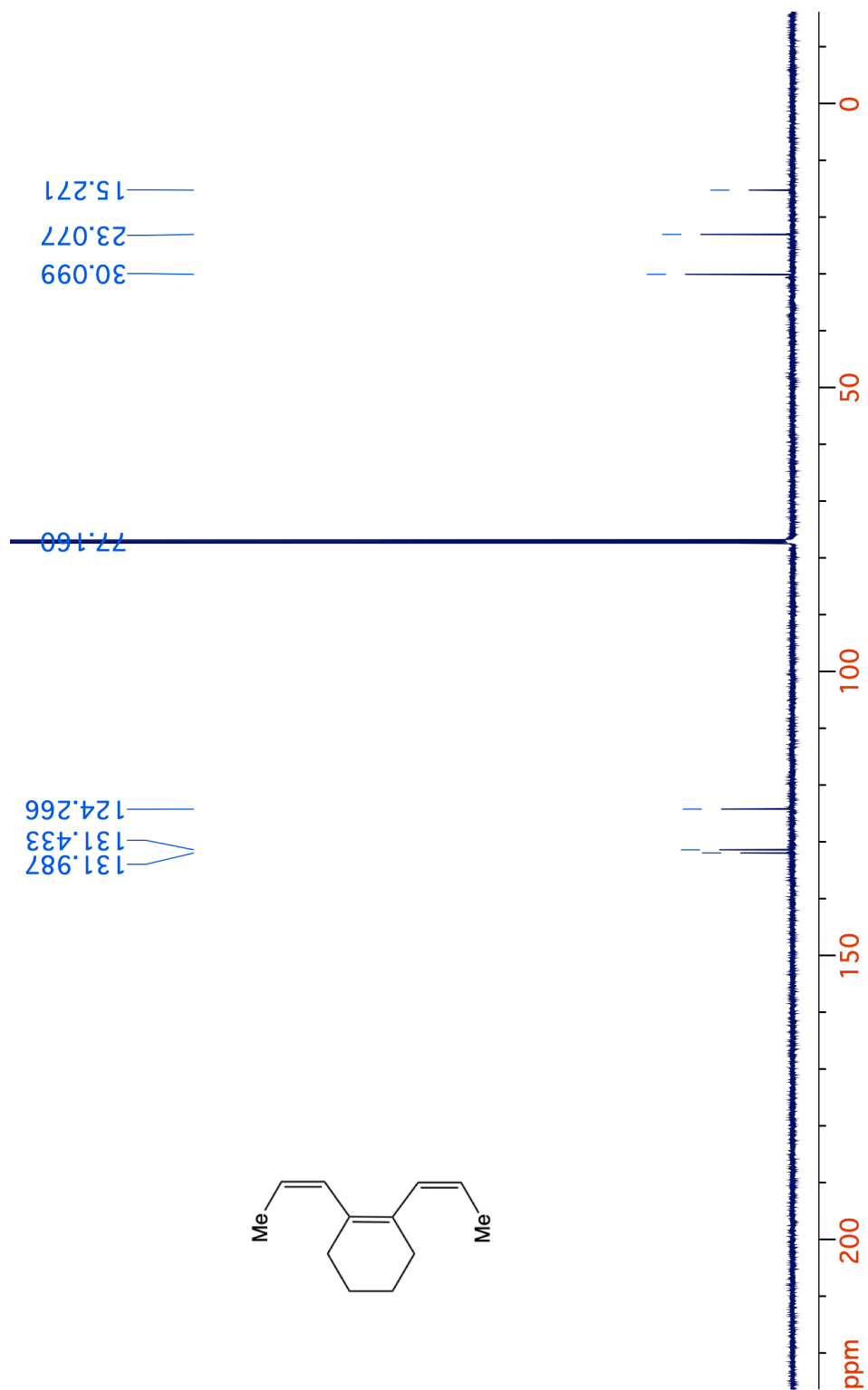
Figure 8-17. $^{13}C\{^1H\}$ NMR spectrum (125 MHz, CDCl$_3$) of **14**.
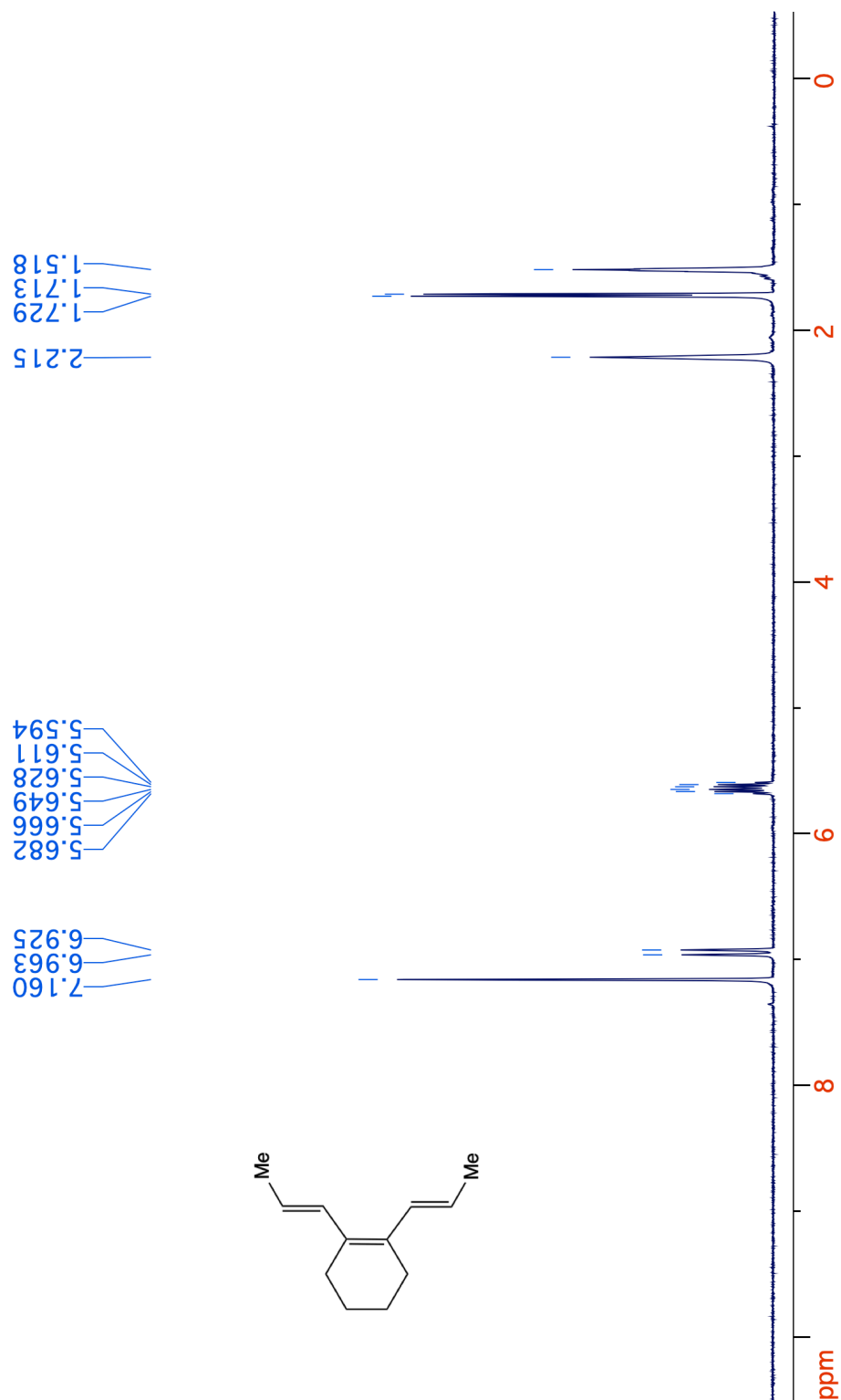
Figure 8-18. ^{1}H NMR spectrum (400 MHz, C$_6$D$_6$) of **15**.
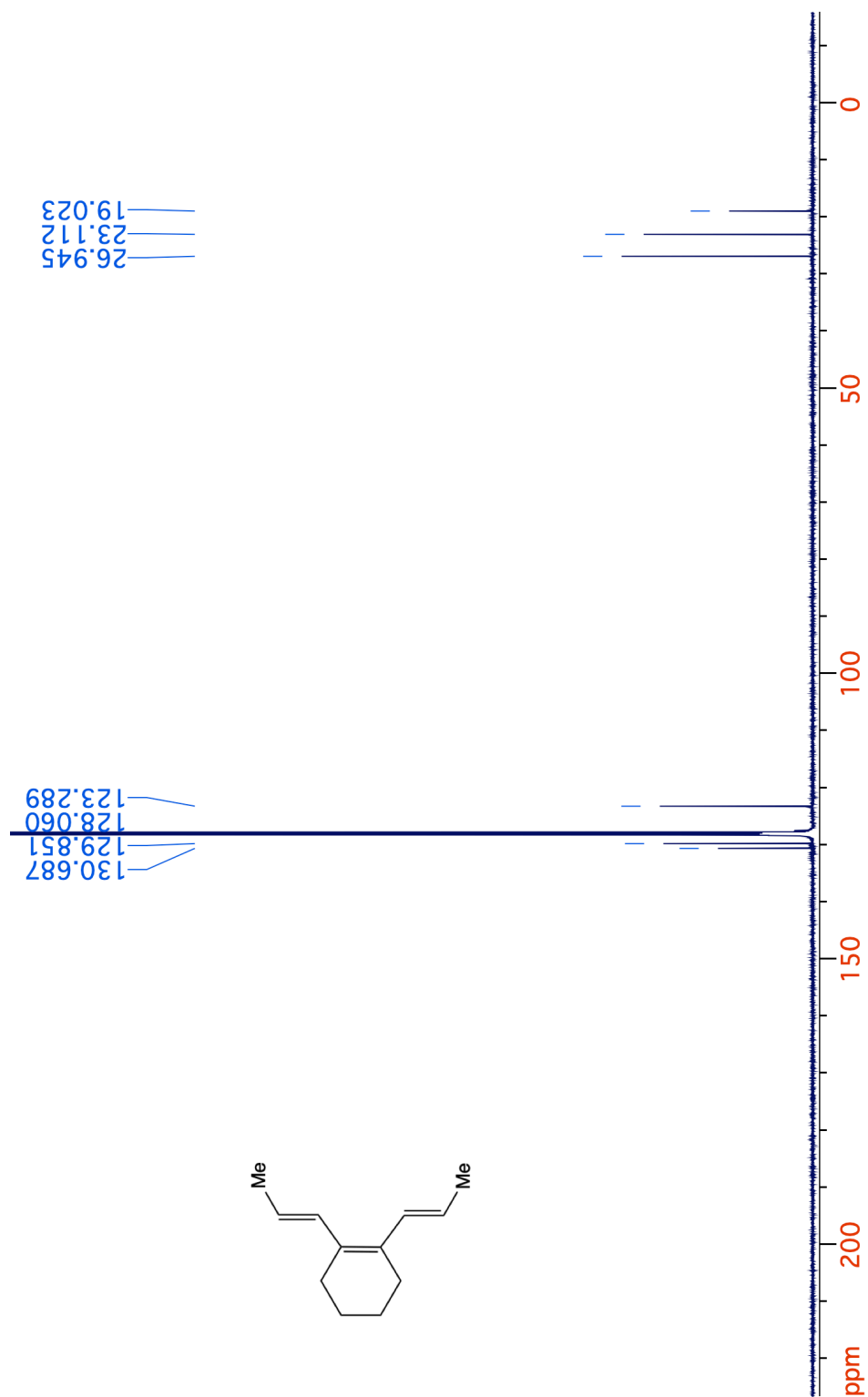
Figure 8-19. $^{13}C\{^1H\}$ NMR spectrum (125 MHz, C_6D_6) of **15**.

19.023
23.112
26.945

123.289
128.060
129.851
130.687
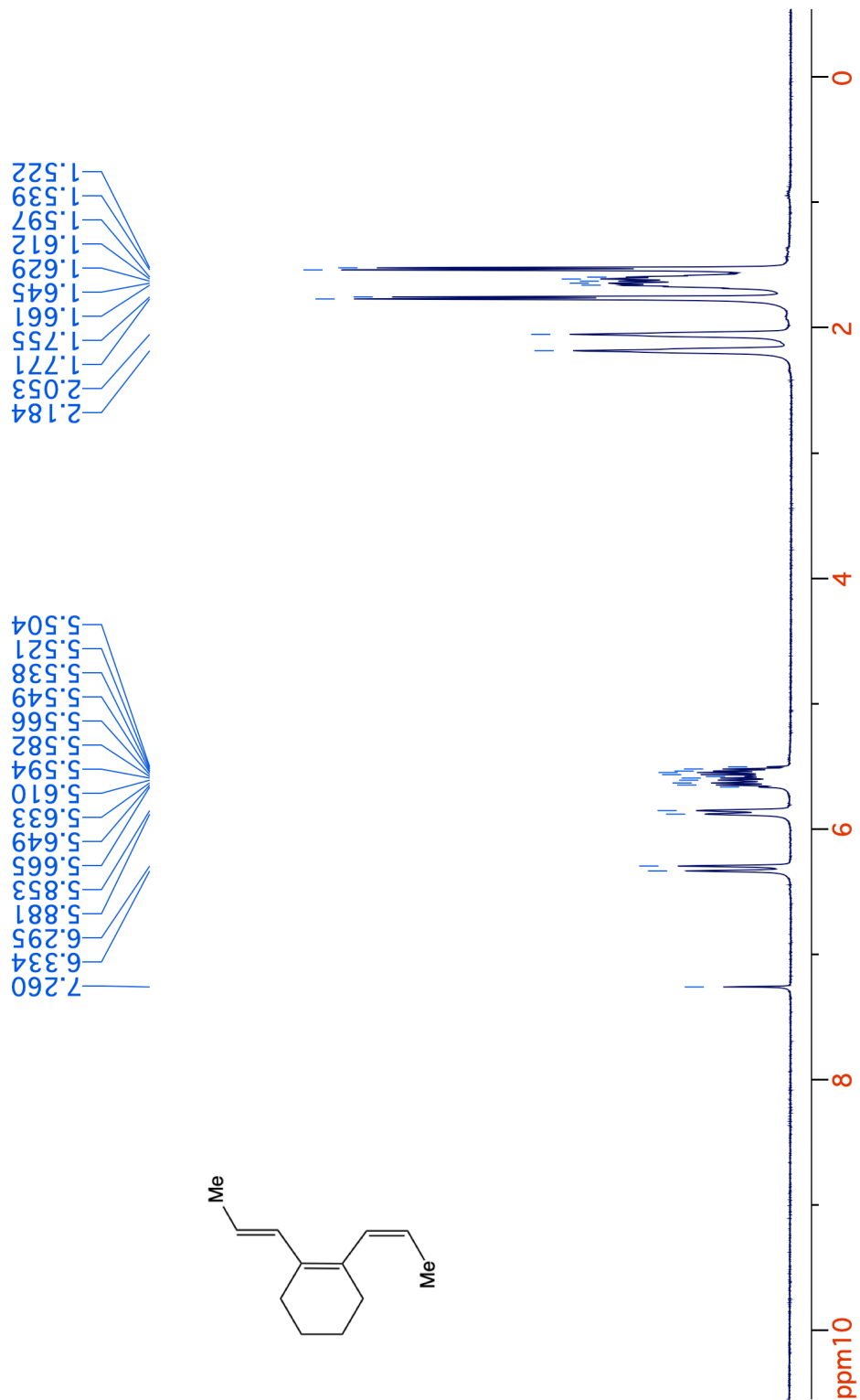
Figure 8-20. ^{1}H NMR spectrum (400 MHz, CDCl$_3$) of **16**.
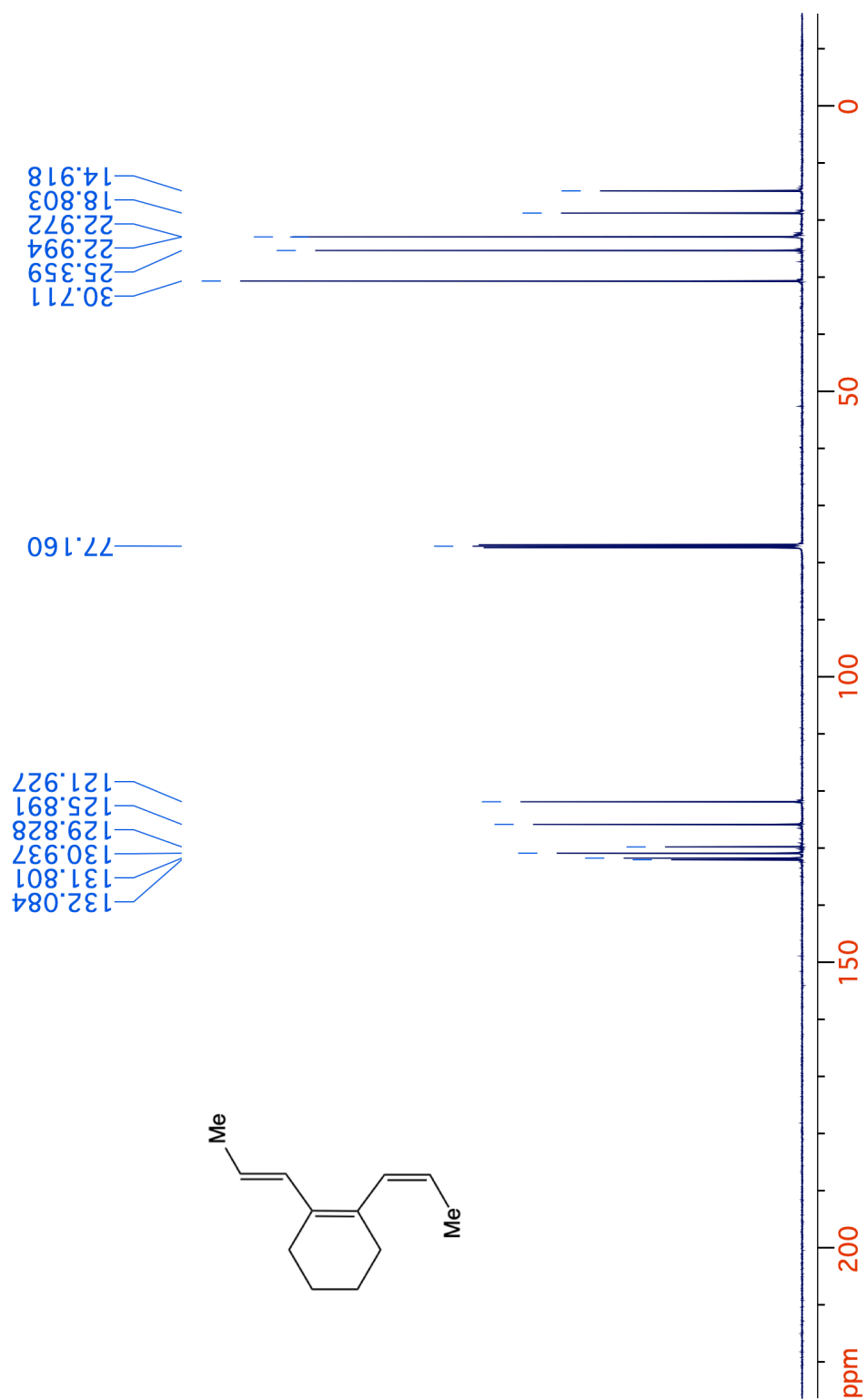
Figure 8-21. $^{13}C\{^1H\}$ NMR spectrum (125 MHz, CDCl$_3$) of **16**.
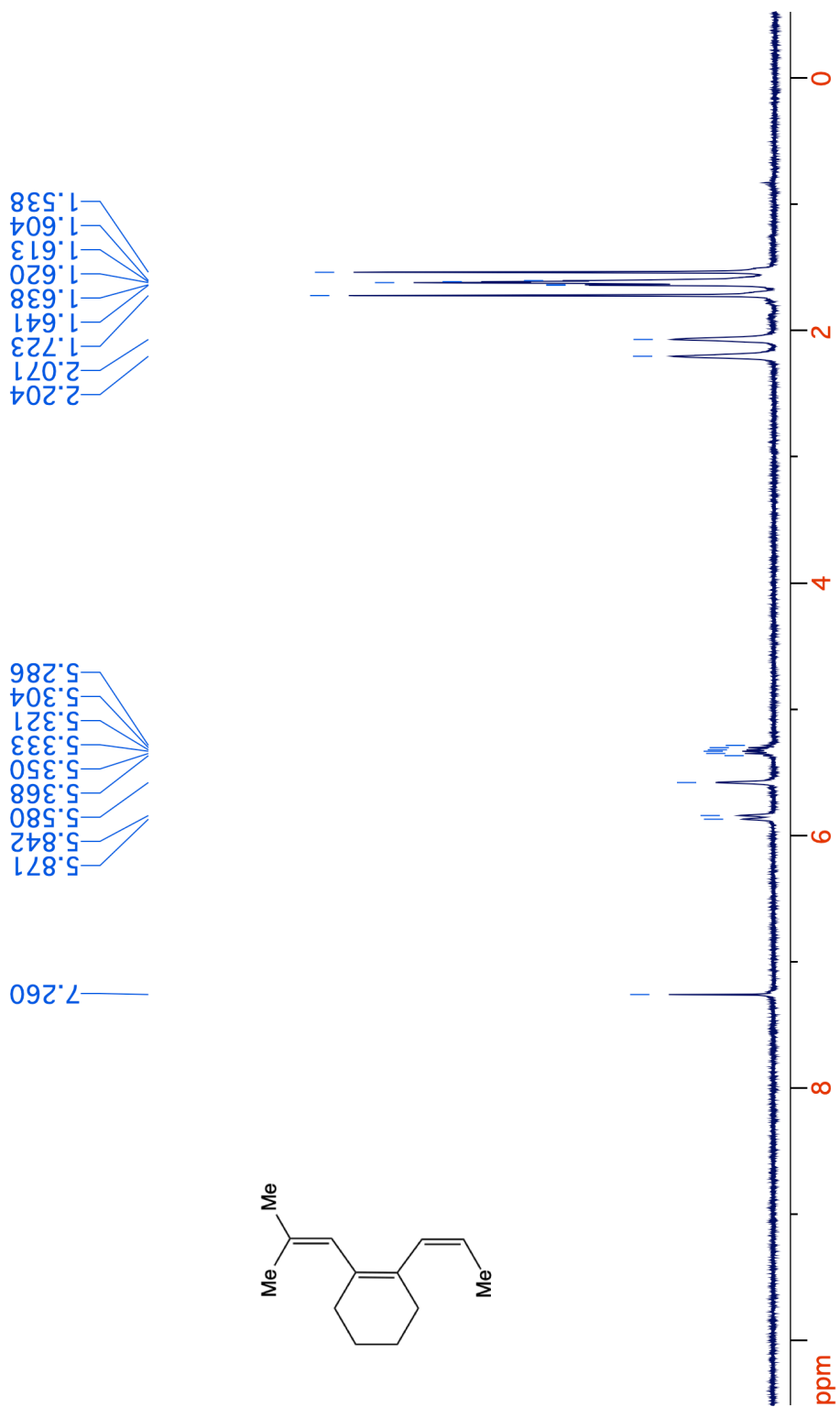
Figure 8-22. ^{1}H NMR spectrum (400 MHz, CDCl$_3$) of **48**.
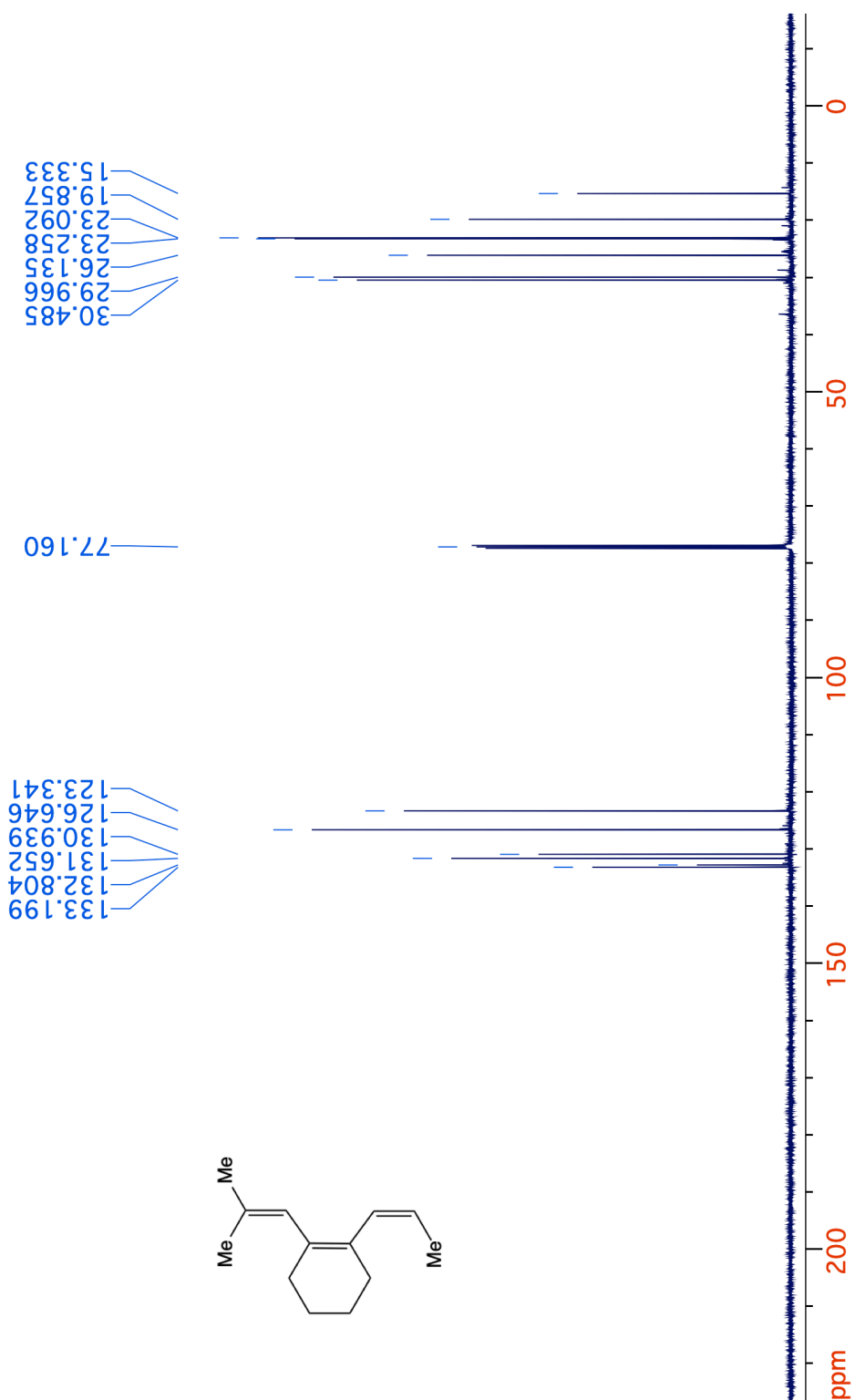
Figure 8-23. $^{13}C\{^1H\}$ NMR spectrum (125 MHz, CDCl$_3$) of **48**.
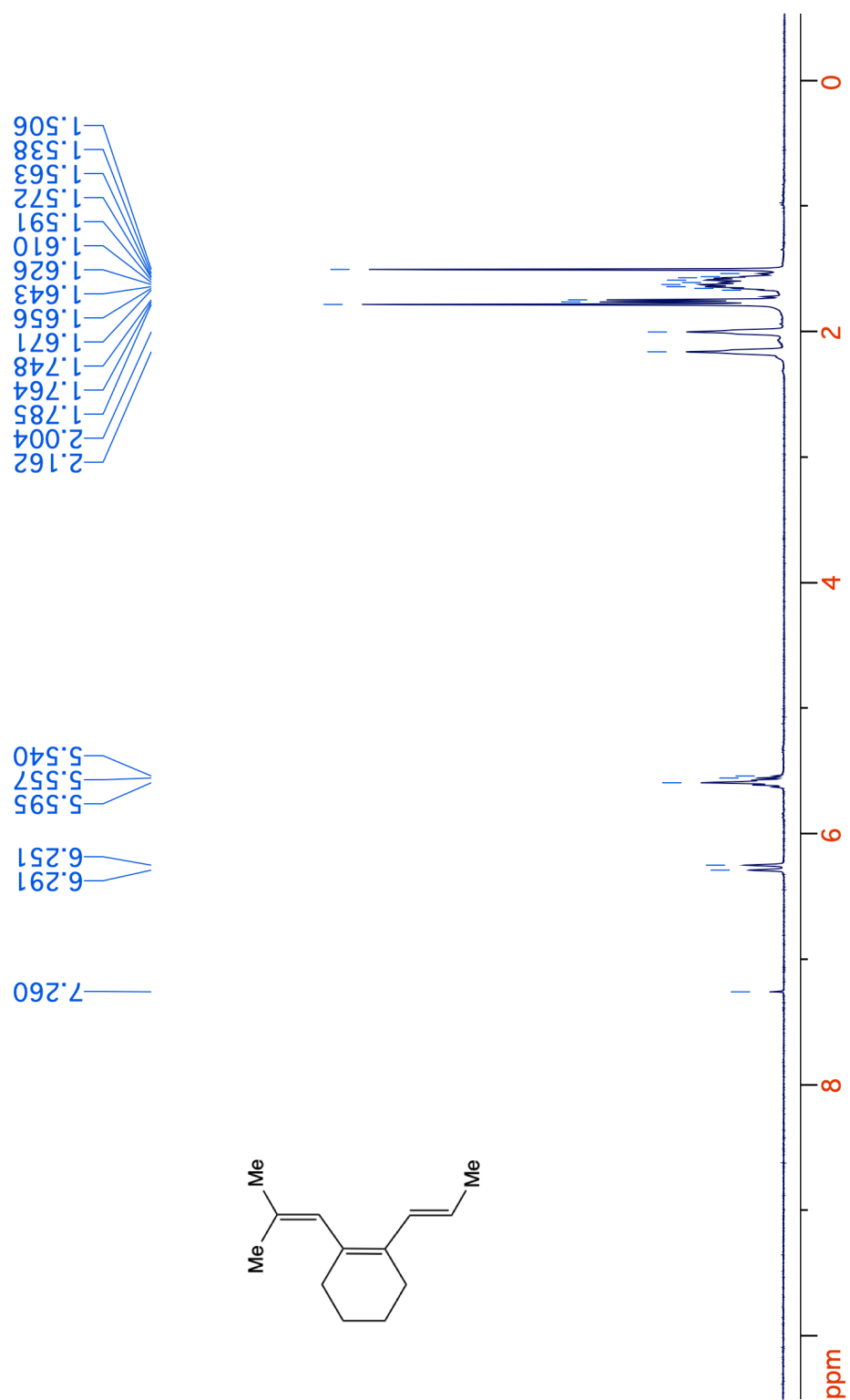
Figure 8-24. ^{1}H NMR spectrum (400 MHz, CDCl$_3$) of **49**.

740
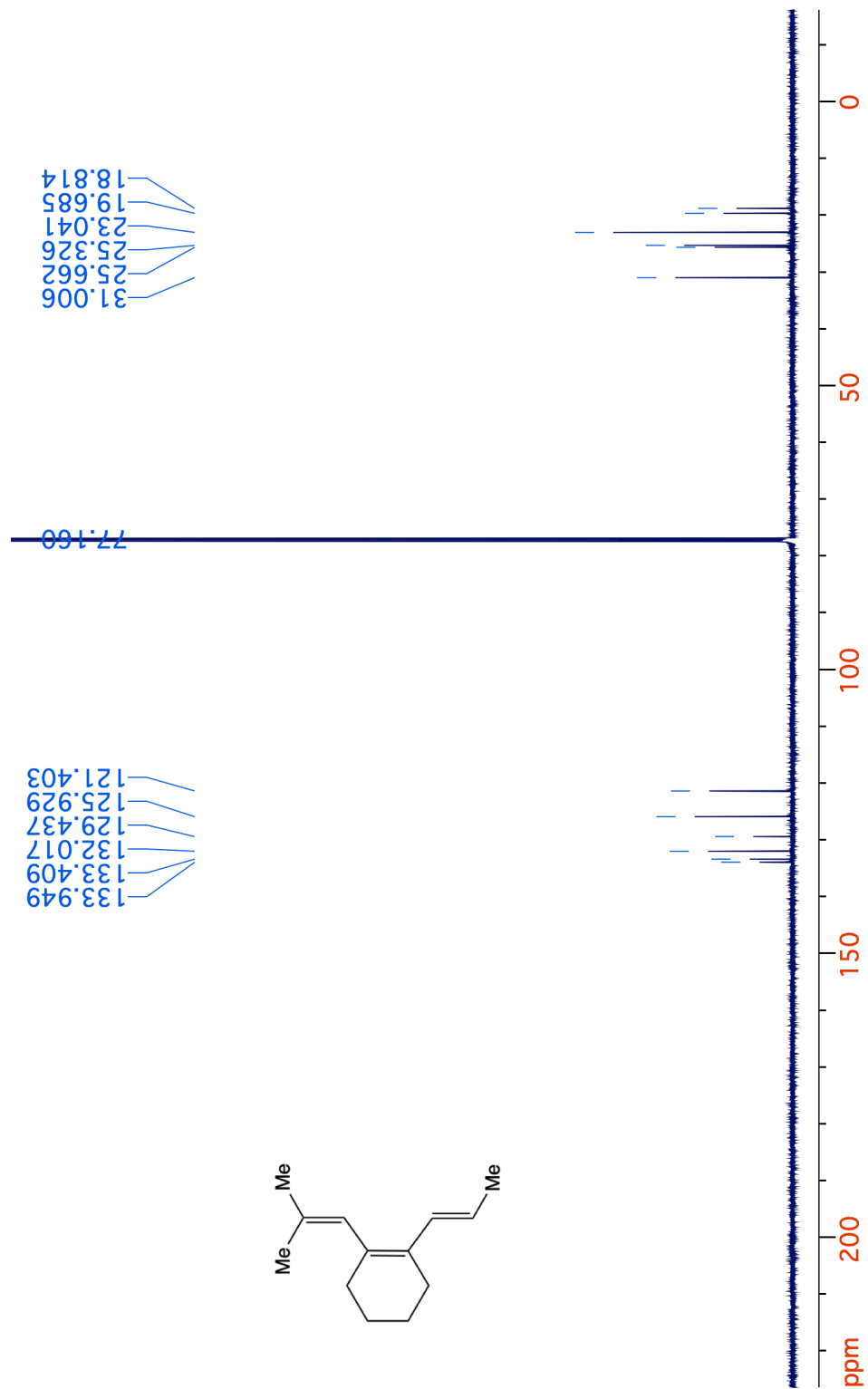
Figure 8-25. $^{13}C\{^1H\}$ NMR spectrum (125 MHz, CDCl$_3$) of **49**.
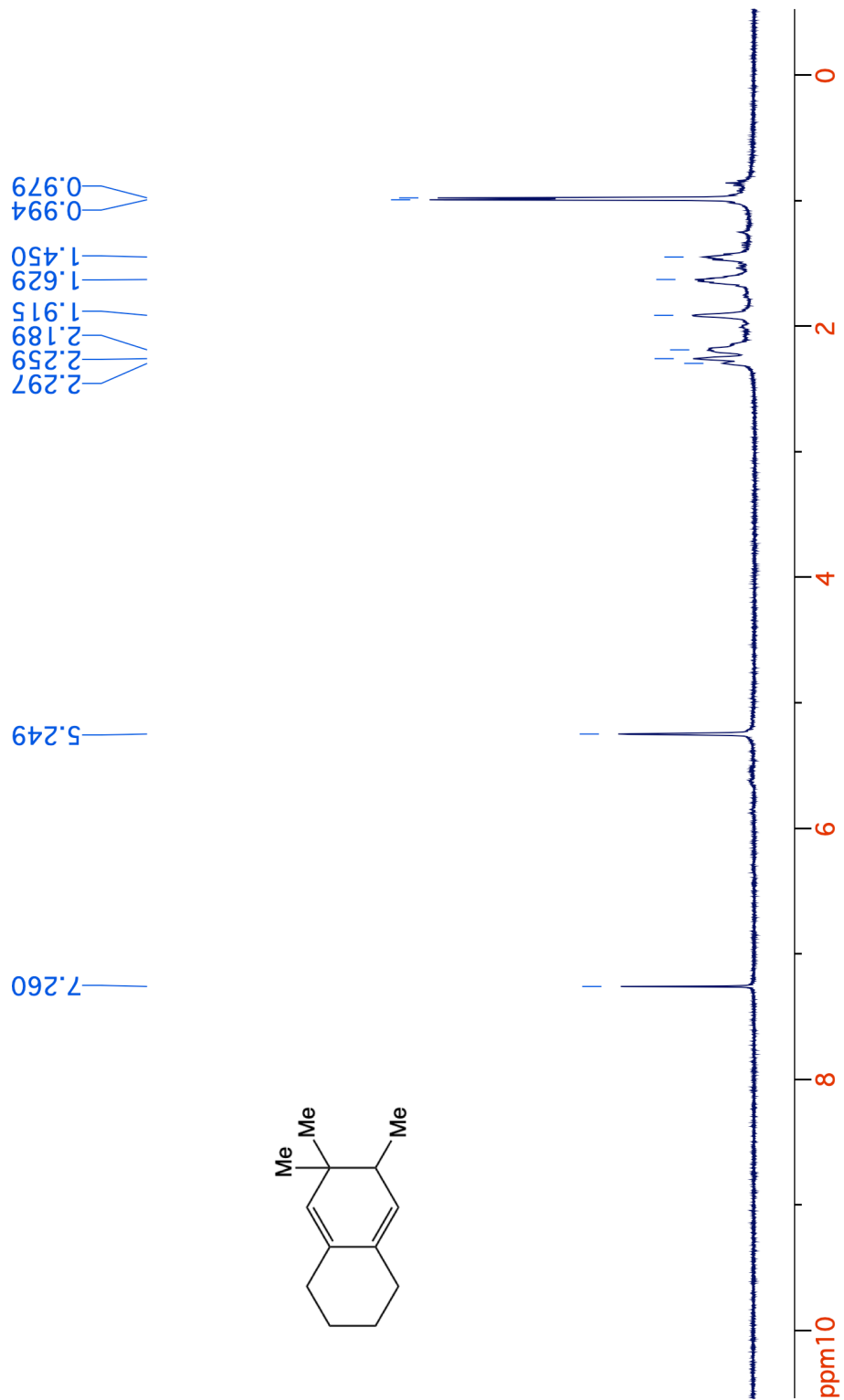
Figure 8-26. ^{1}H NMR spectrum (400 MHz, CDCl$_3$) of **53**.
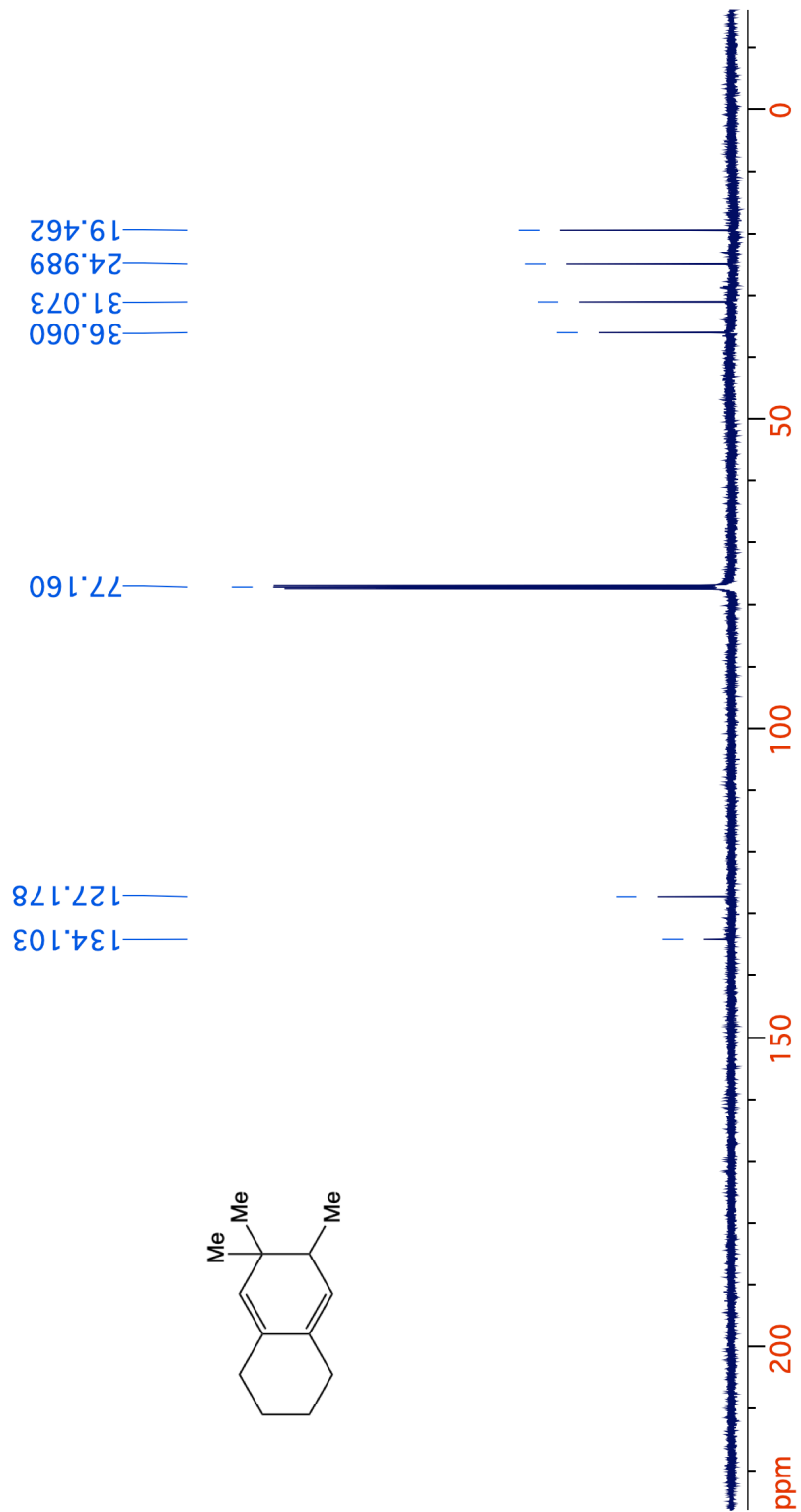
Figure 8-27. $^{13}C\{^1H\}$ NMR spectrum (125 MHz, CDCl$_3$) of **53**.
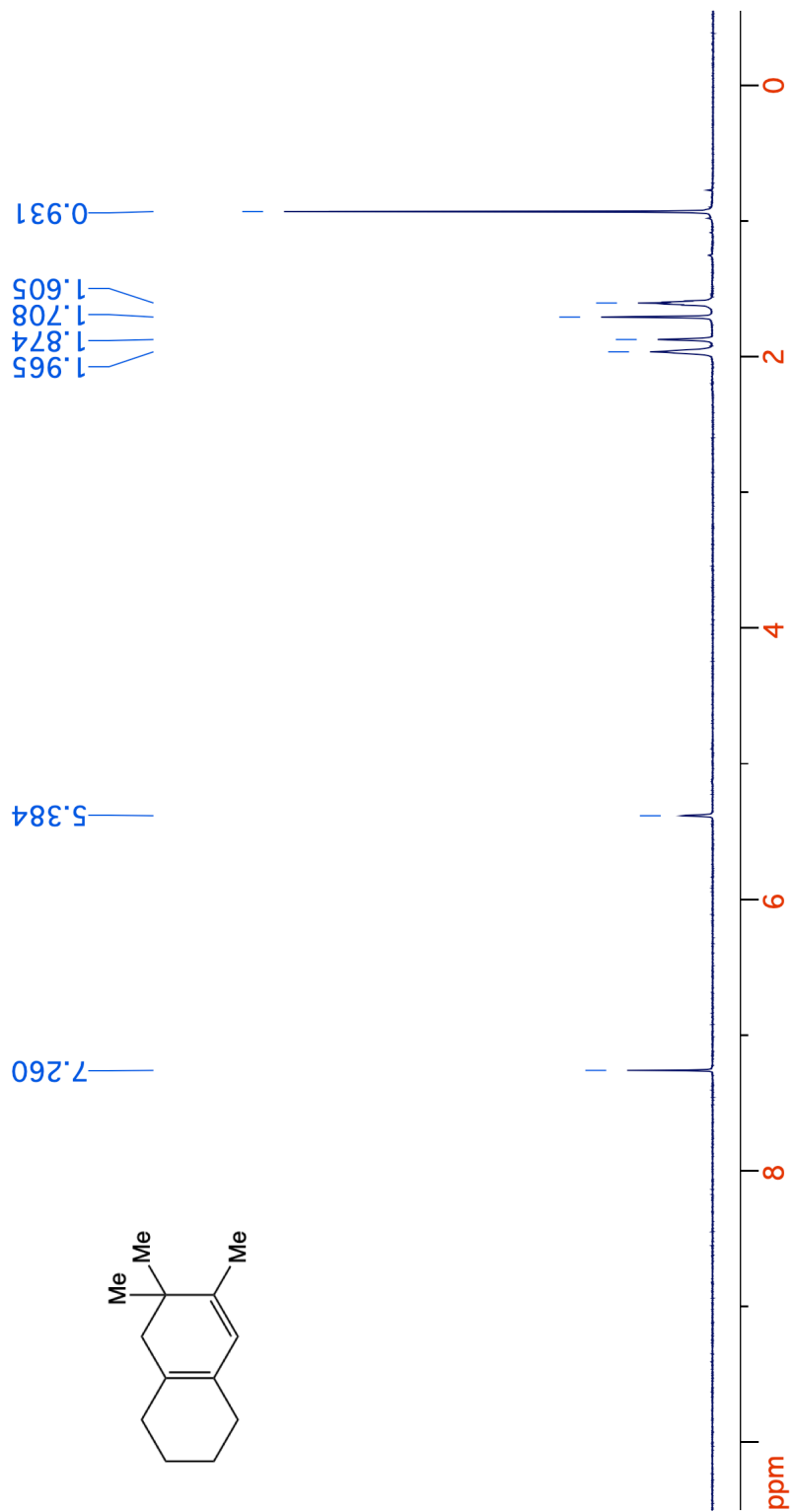
Figure 8-28. ^{1}H NMR spectrum (400 MHz, CDCl$_3$) of **52**.
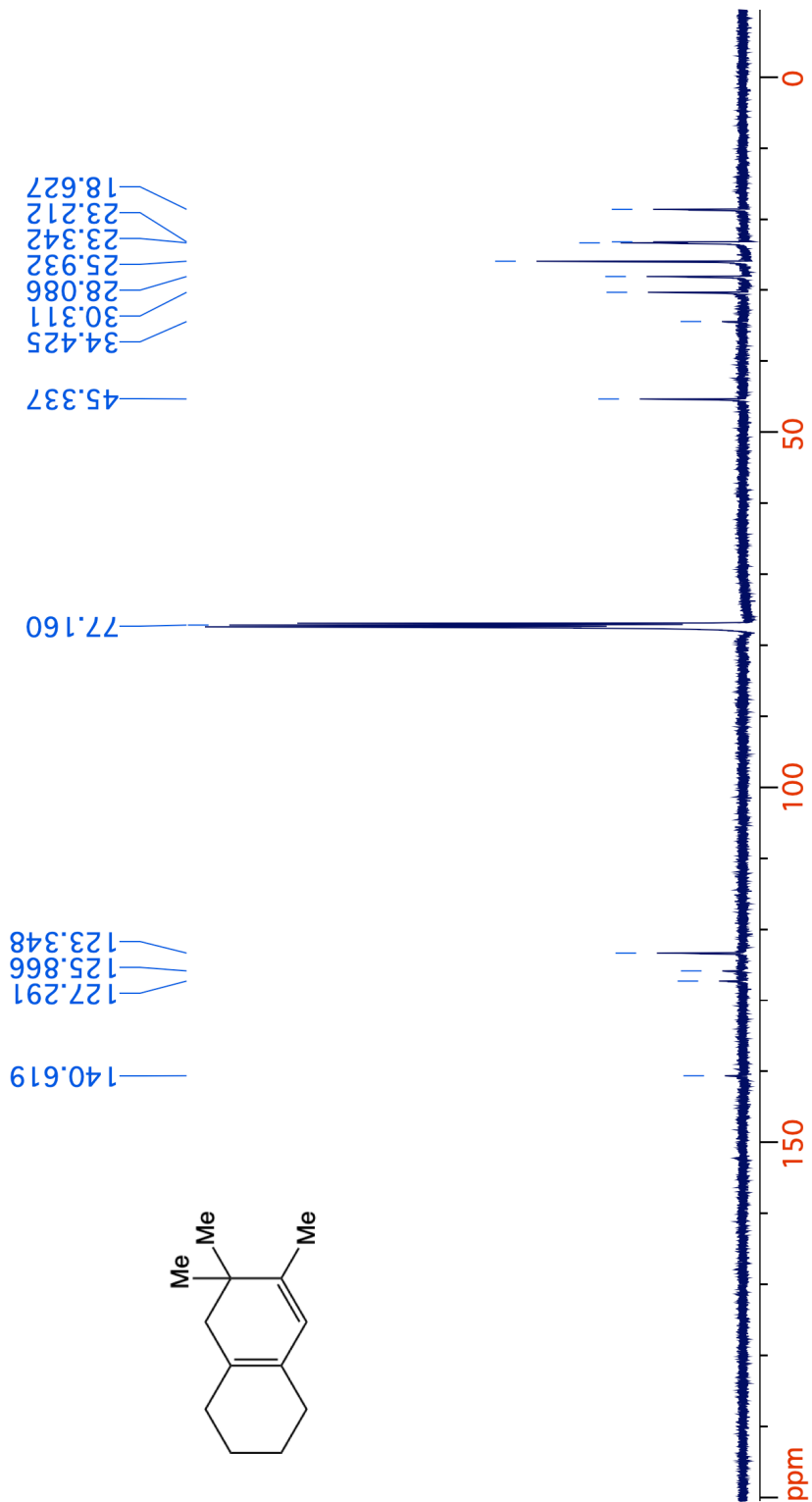
Figure 8-29. $^{13}C\{^1H\}$ NMR spectrum (125 MHz, CDCl$_3$) of **52**.
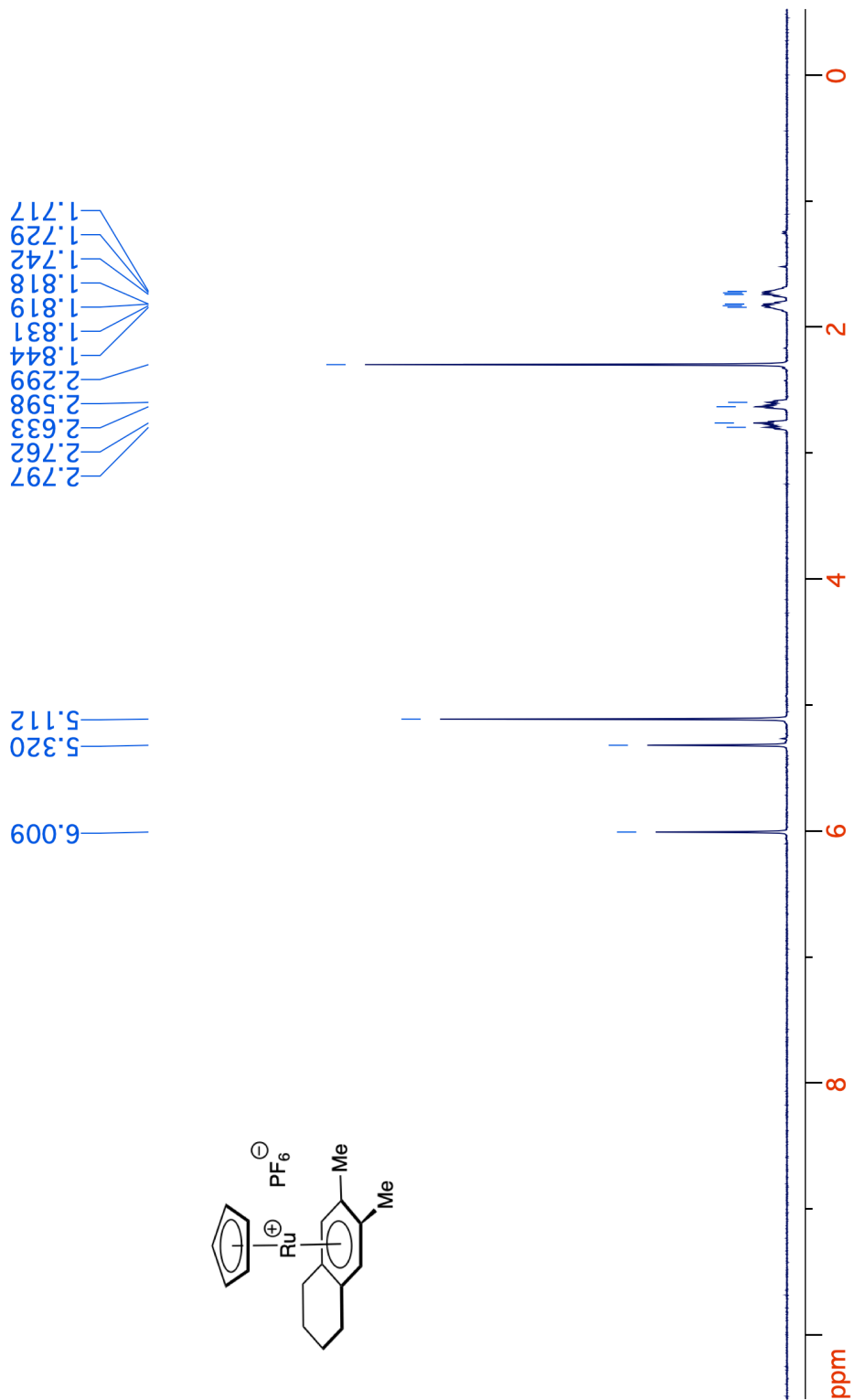
Figure 8-30. ^{1}H NMR spectrum (400 MHz, CD$_2$Cl$_2$) of **23**.
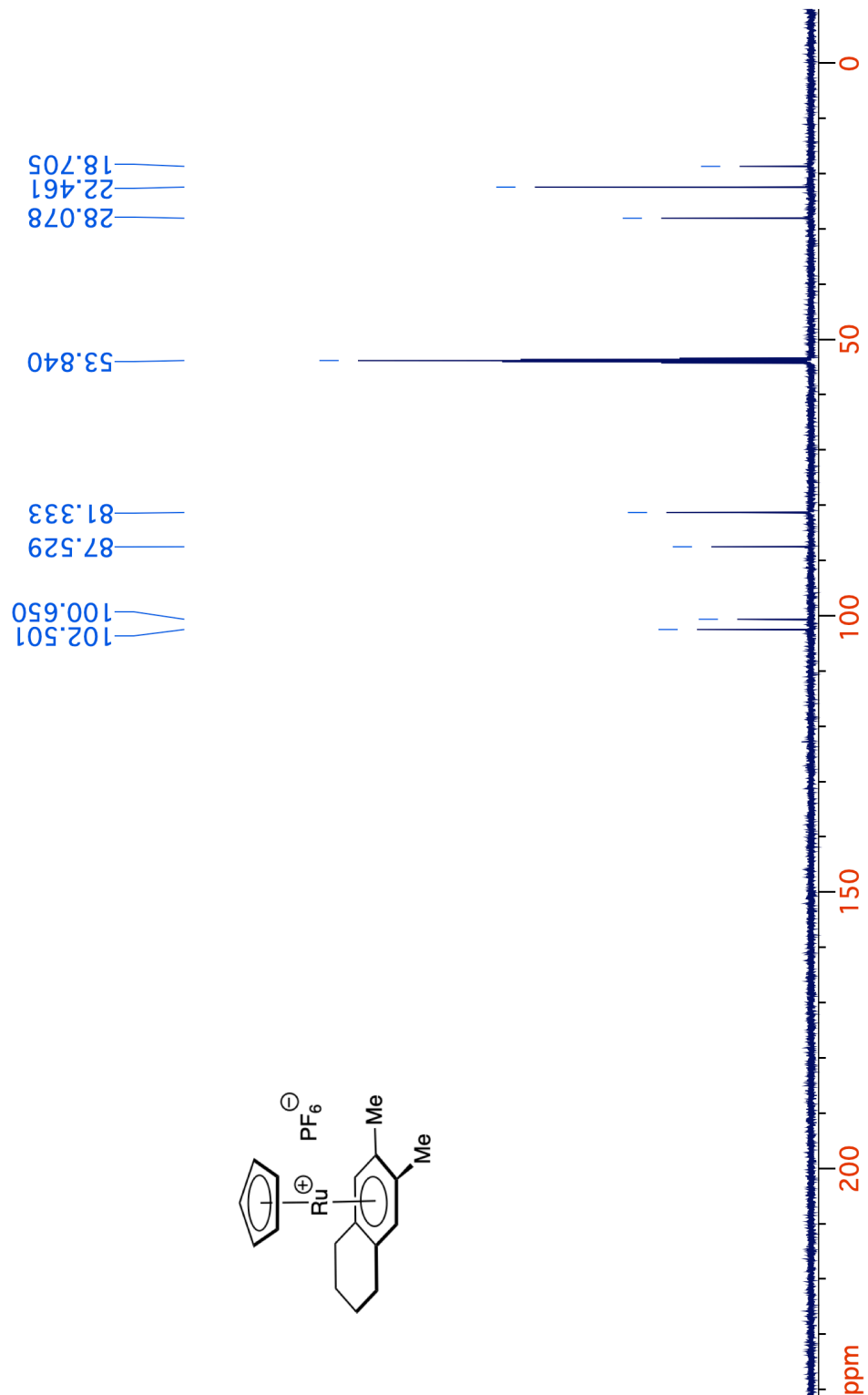
Figure 8-31. $^{13}C\{^1H\}$ NMR spectrum (125 MHz, CD_2Cl_2) of **23**.

Peak labels: 18.705, 22.461, 28.078, 53.840, 81.333, 87.529, 100.650, 102.501
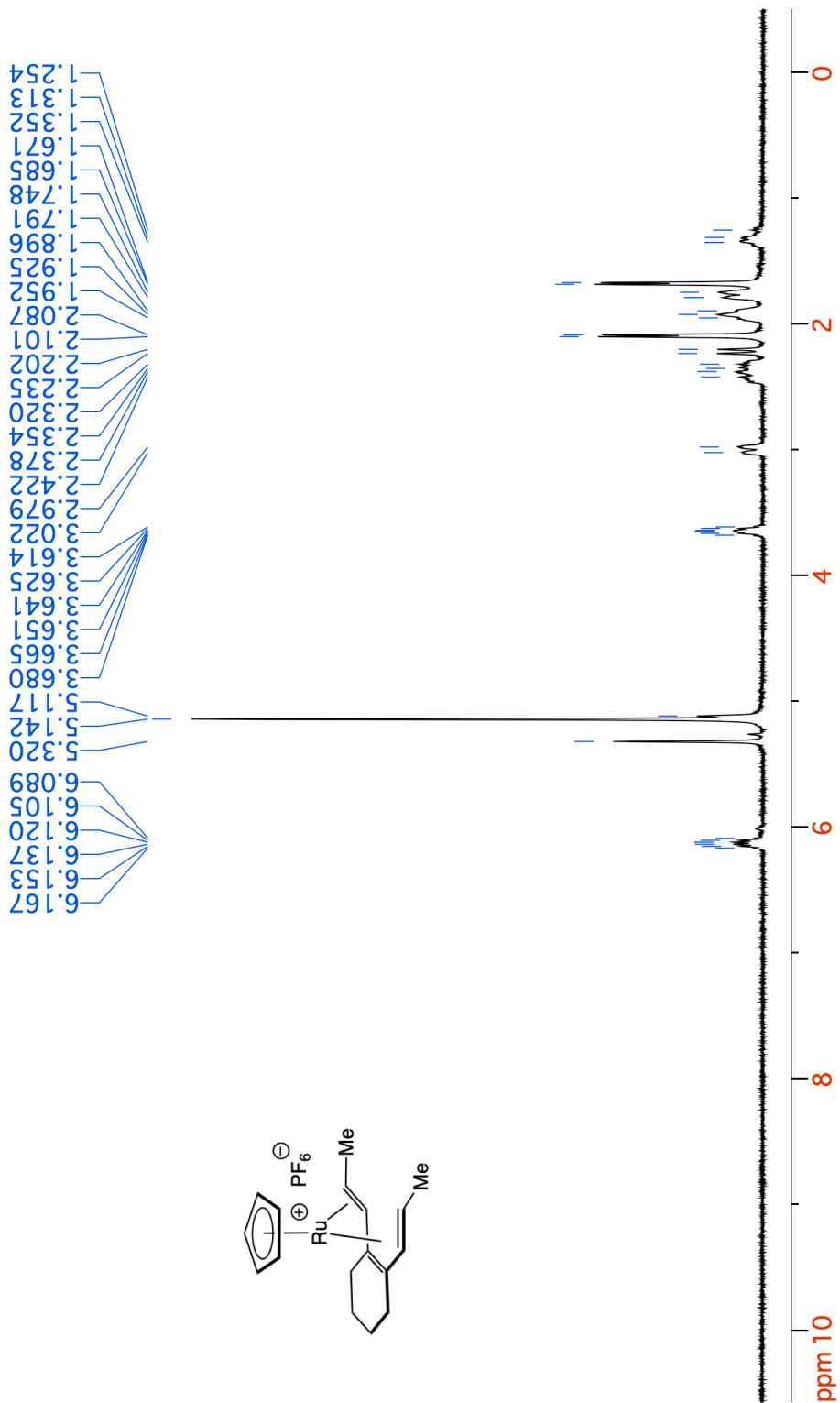
Figure 8-32. ^{1}H NMR spectrum (400 MHz, CD$_2$Cl$_2$) of **27**.
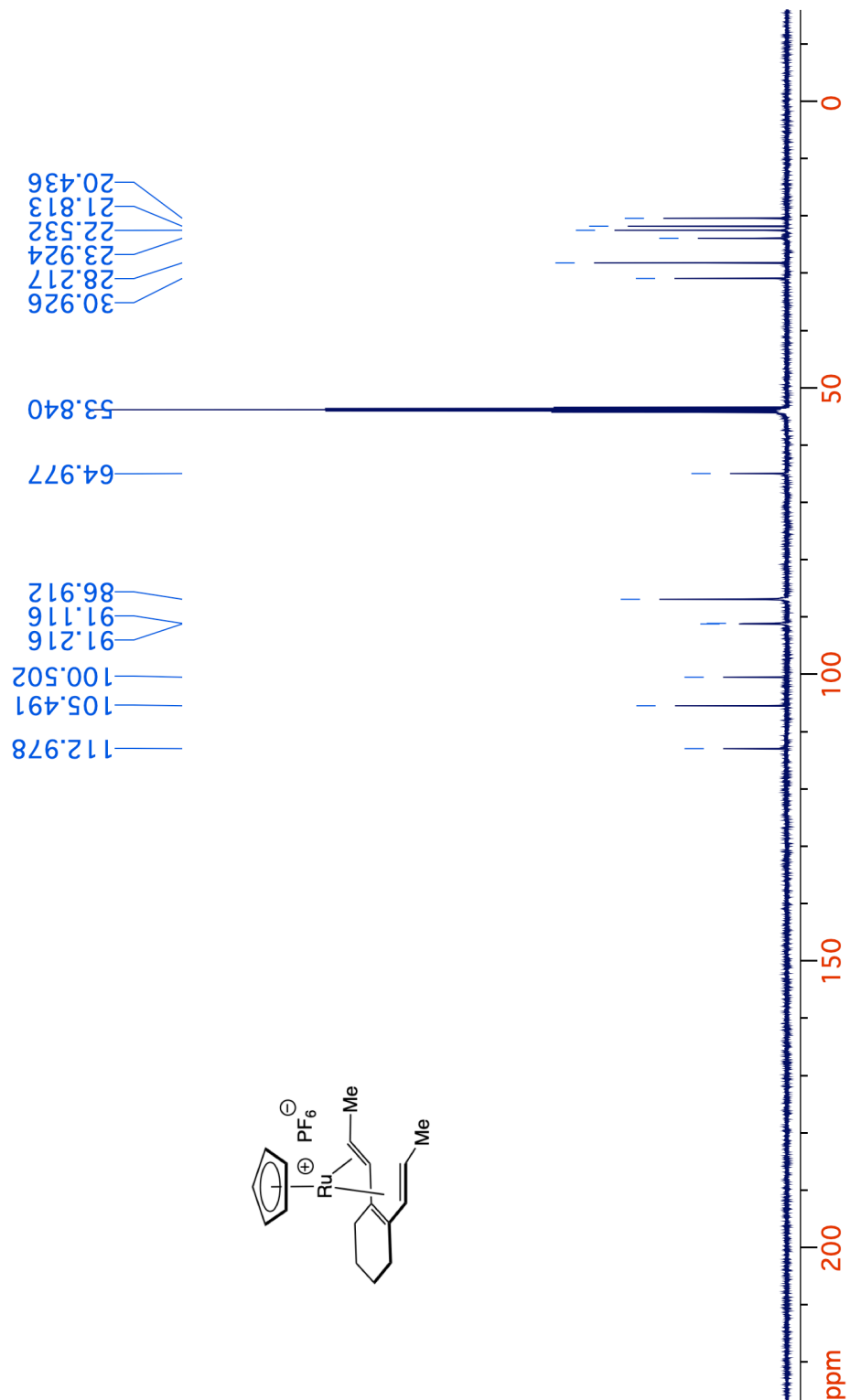
Figure 8-33. $^{13}C\{^1H\}$ NMR spectrum (125 MHz, CD_2Cl_2) of **27**.

Peak labels: 20.436, 21.813, 22.532, 23.924, 28.217, 30.926, 53.840, 64.977, 86.912, 91.116, 91.216, 100.502, 105.491, 112.978
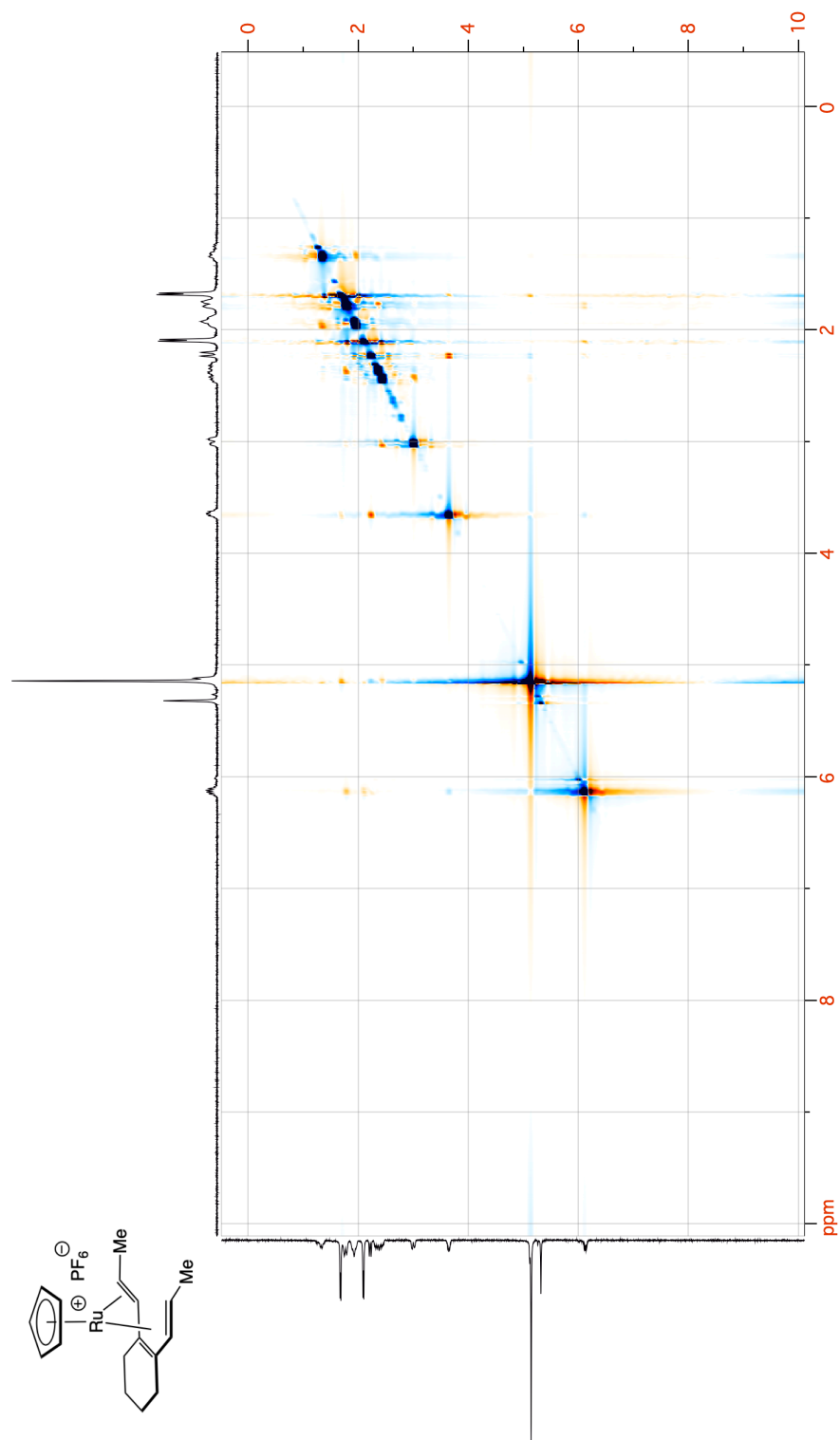
Figure 8-34. 2D NOSEY spectrum (500 MHz, CD_2Cl_2) of **27**.
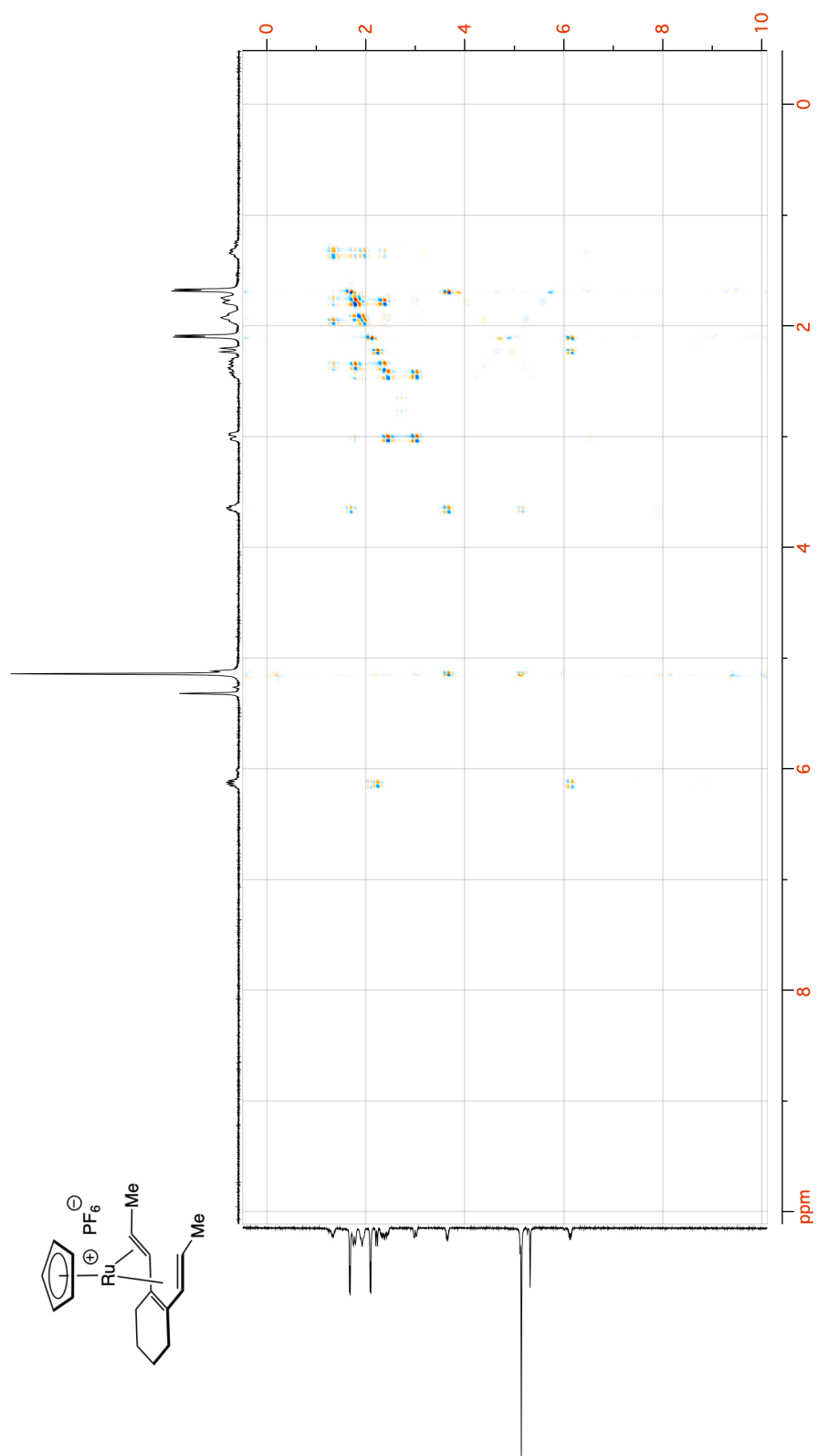
Figure 8-35. COSEY spectrum (500 MHz, CD$_2$Cl$_2$) of **27**.
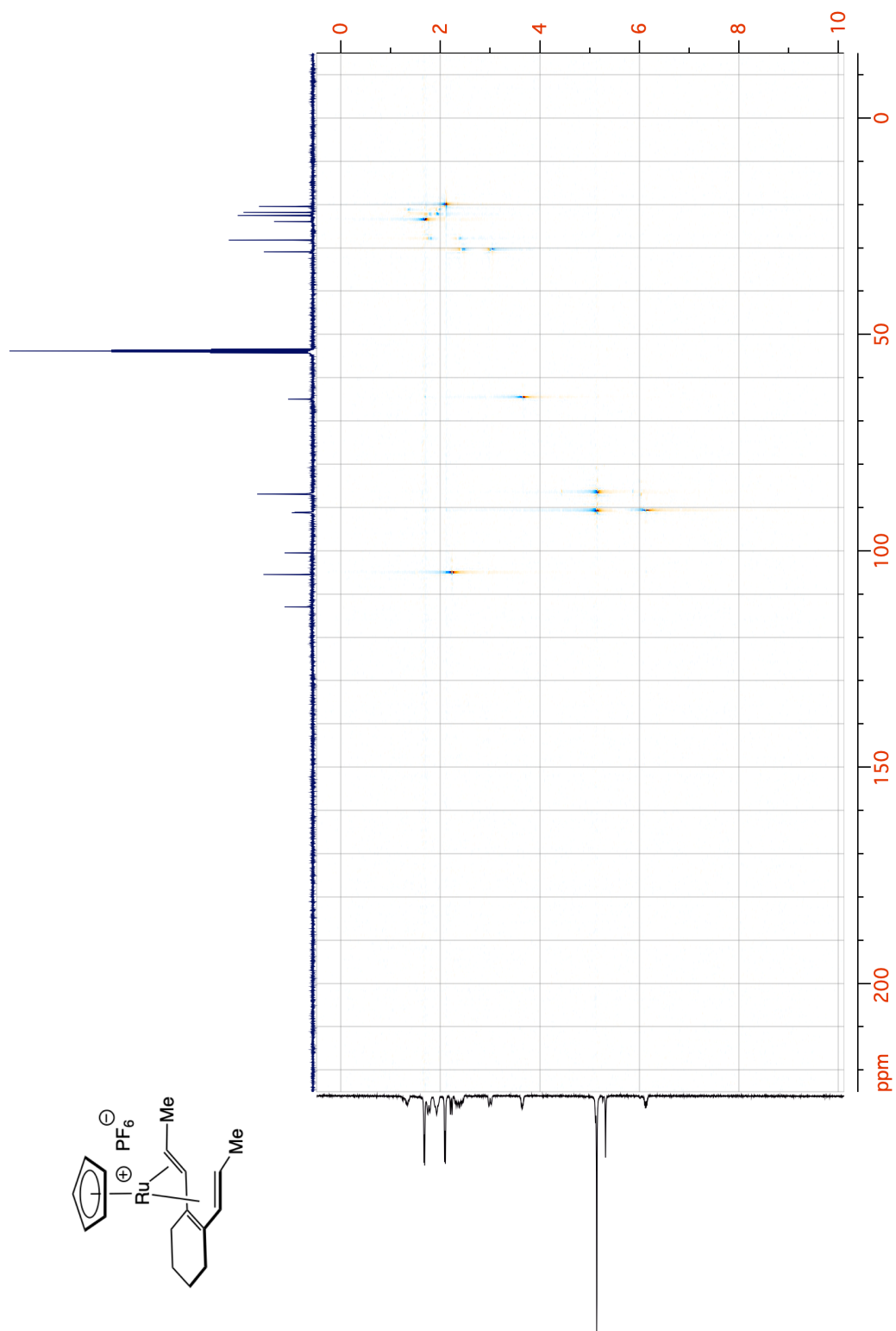
Figure 8-36. HSQC spectrum (500 MHz, CD_2Cl_2) of **27**.
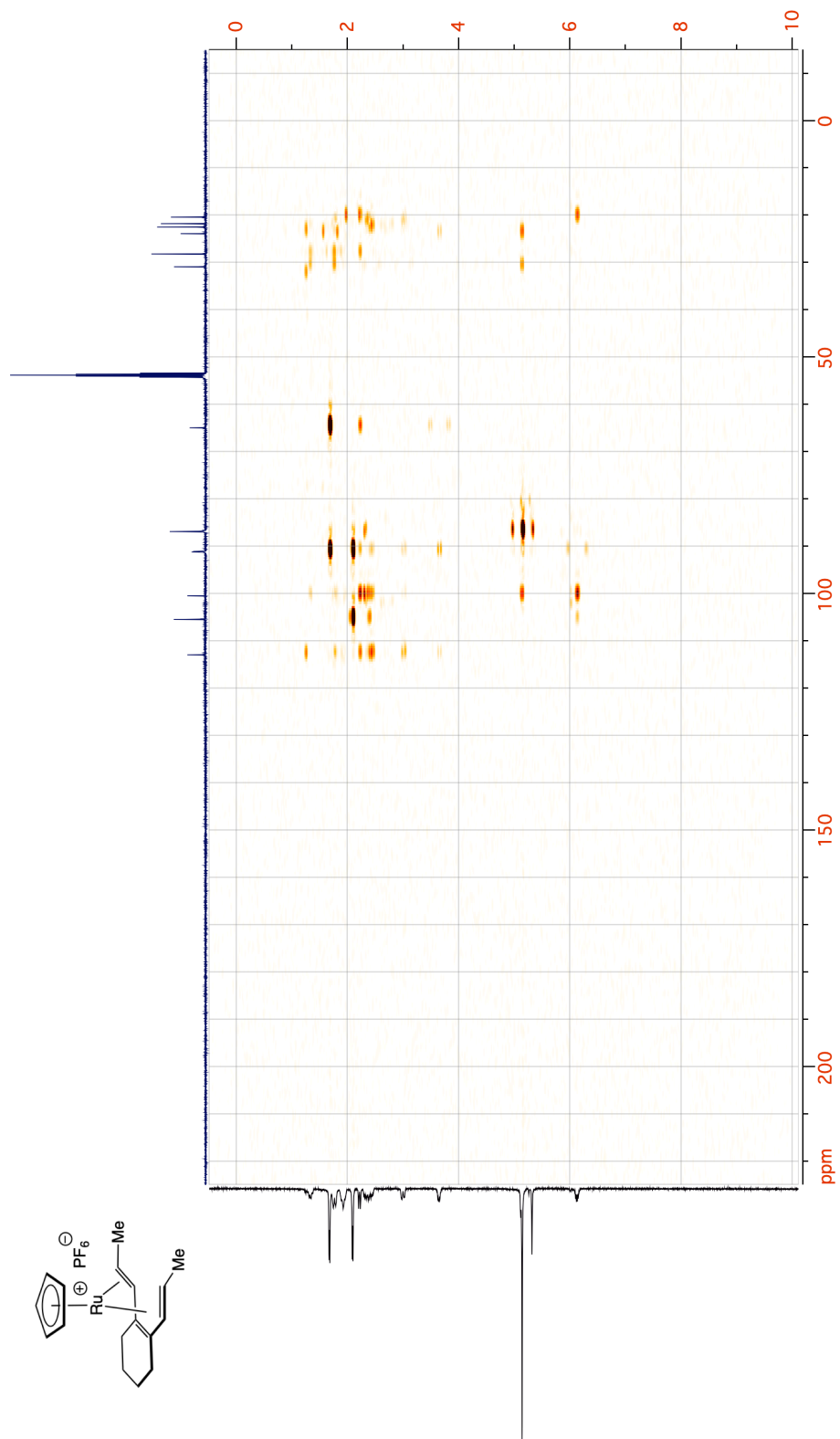
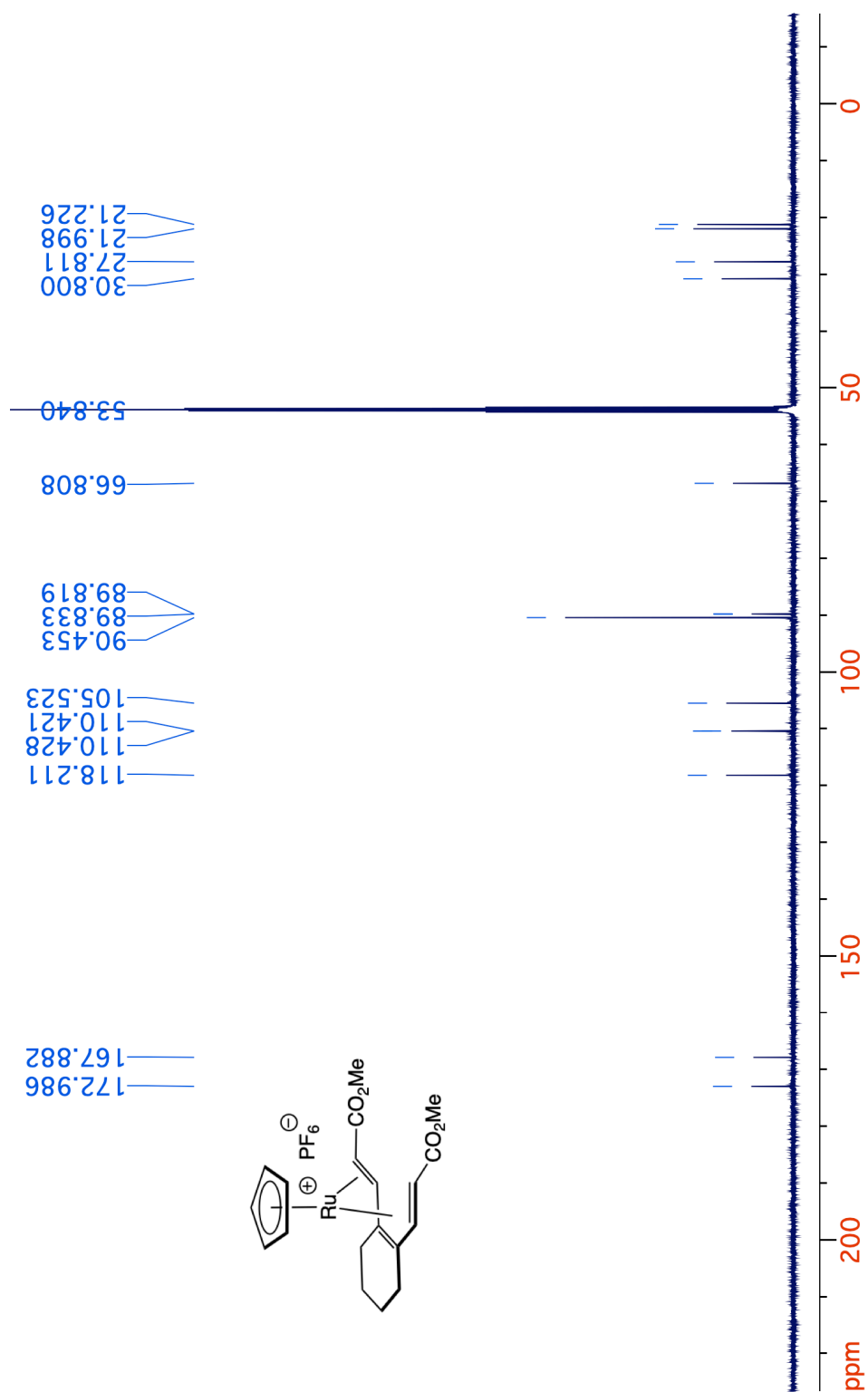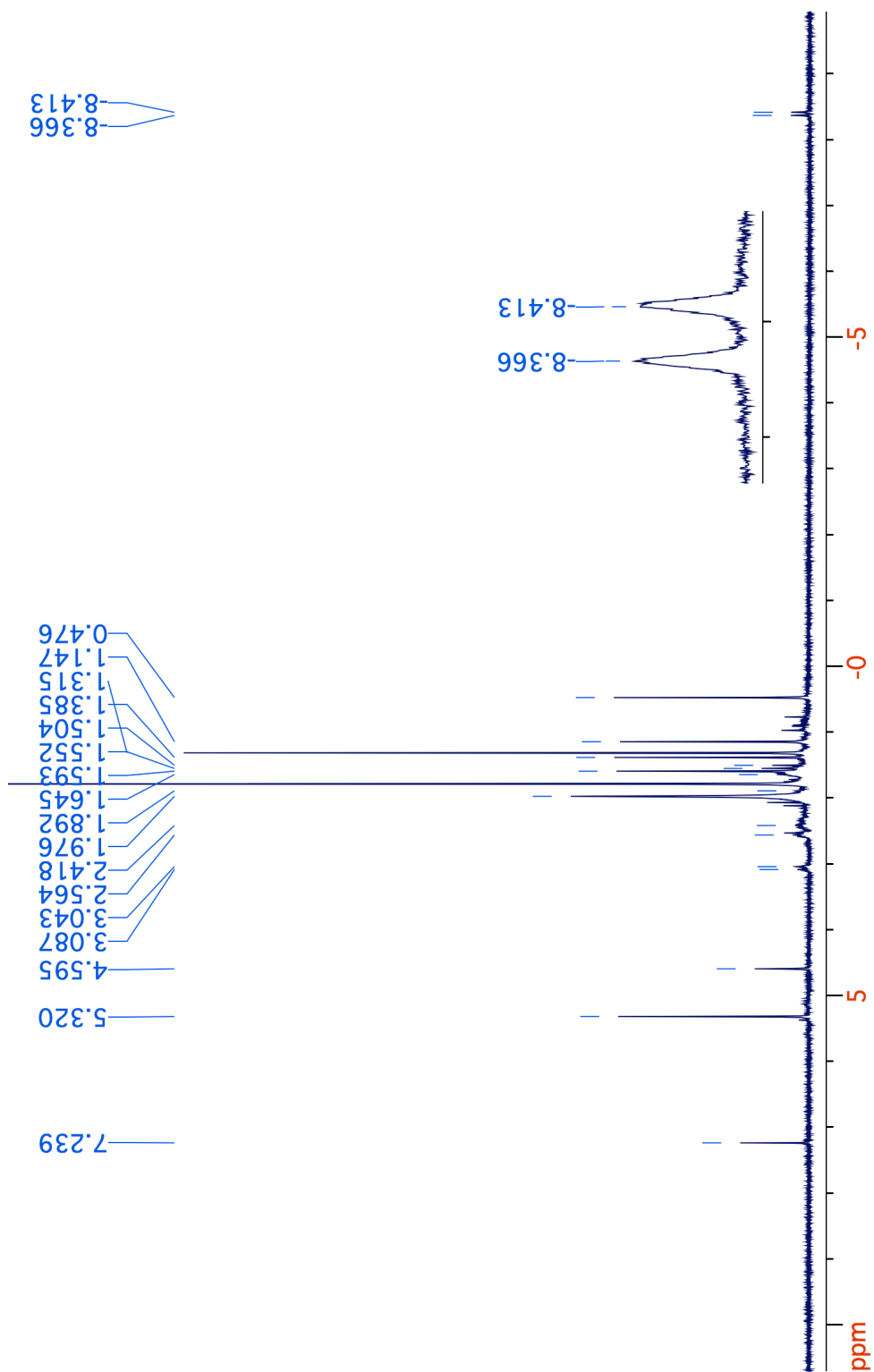**Figure 8-37**. HMBC spectrum (500 MHz, CD$_2$Cl$_2$) of **27**.
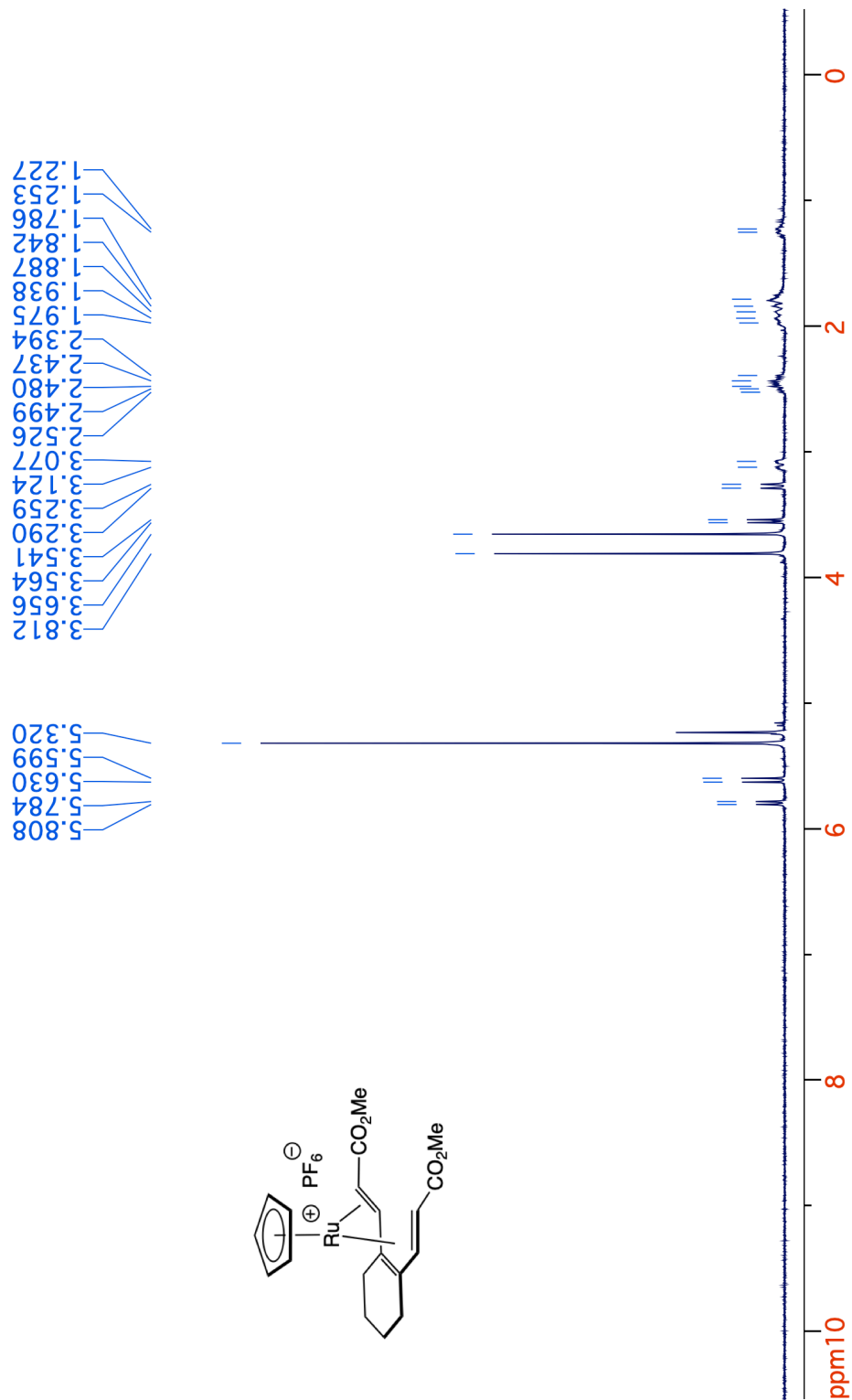
Figure 8-38. ^{1}H NMR spectrum (400 MHz, CD_2Cl_2) of **43**.

Figure 8-39. $^{13}C\{^1H\}$ NMR spectrum (125 MHz, CD_2Cl_2) of **43**.

21.226
21.998
27.811
30.800
53.840
66.808
89.819
89.833
90.453
105.523
110.421
110.428
118.211
167.882
172.986

Figure 8-40. ^{1}H NMR spectrum (400 MHz, CD$_2$Cl$_2$) of crude reation mixture to form **51**.
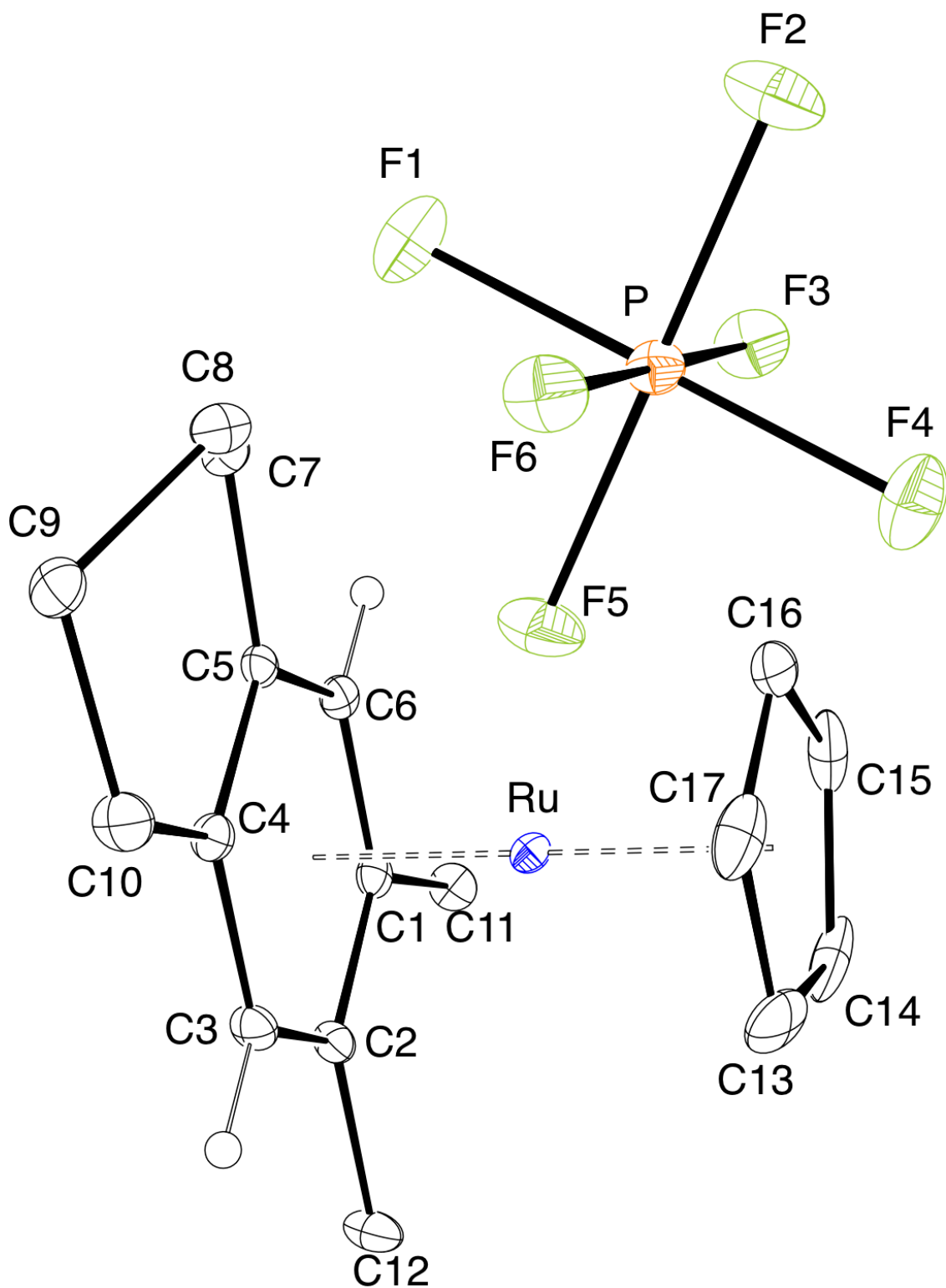
Figure 8-41. ORTEP view of complex **23**. Ellipsoids shown at 30% probability. Most hydrogens are omitted for clarity.

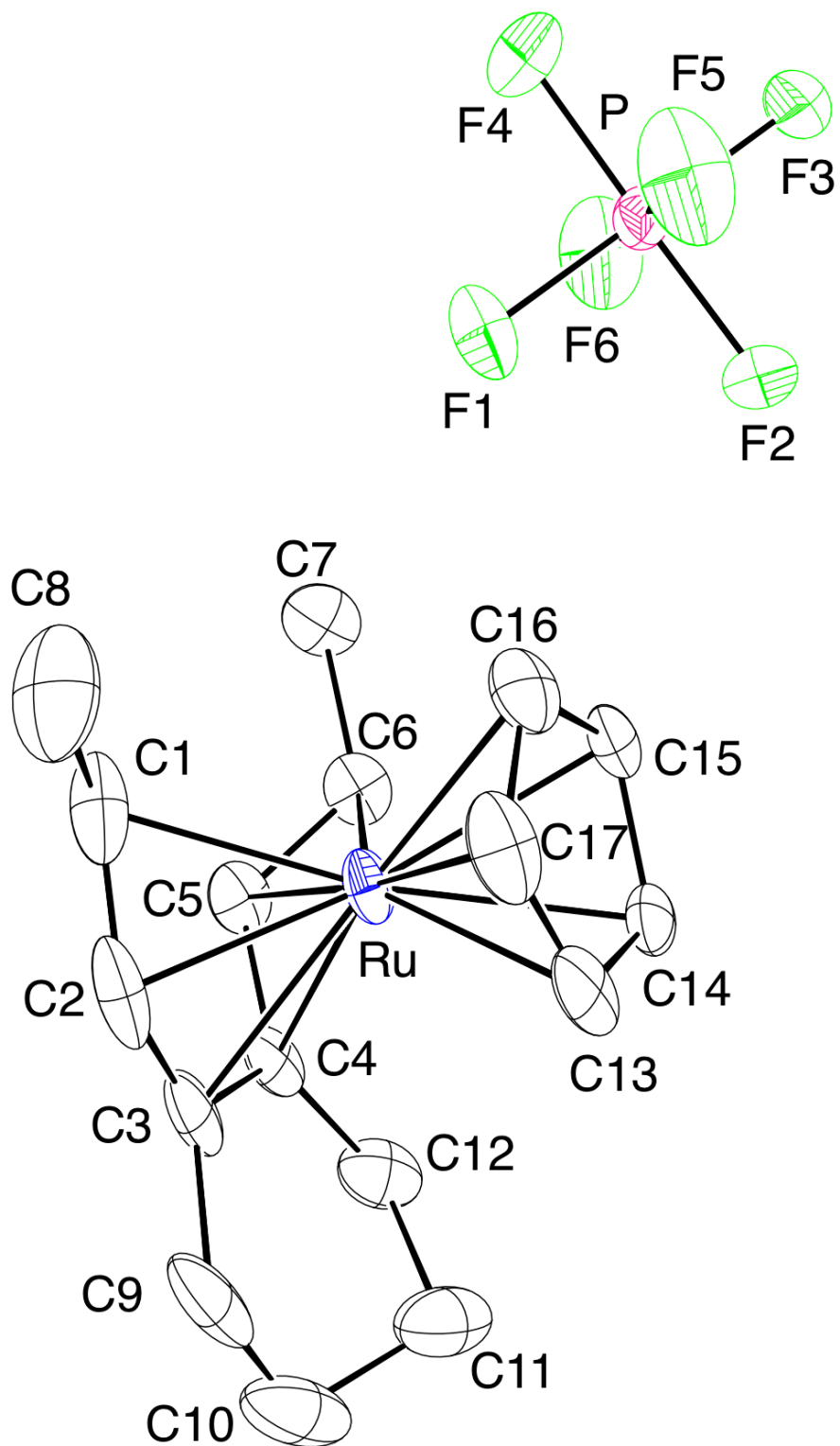**Table 8-7**. Crystal data and structure refinement for complex **23**.

Identification code	law179
Empirical formula	C17 H21 F6 P Ru
Formula weight	471.38
Temperature	100.0 K
Wavelength	0.71073 Å
Crystal system	Monoclinic
Space group	P 1 21/n 1
Unit cell dimensions	a = 12.4179(15) Å $\quad$ $\alpha = 90°$.
	b = 10.8090(13) Å $\quad$ $\beta = 112.154(3)°$.
	c = 14.0326(18) Å $\quad$ $\gamma = 90°$.
Volume	1744.5(4) $Å^3$
Z	4
Density (calculated)	1.795 Mg/m^3
Absorption coefficient	1.047 mm^{-1}
F(000)	944
Crystal size	0.15 x 0.095 x 0.05 mm^3
Theta range for data collection	2.451 to 26.022°.
Index ranges	-15<=h<=15, -13<=k<=8, -17<=l<=17
Reflections collected	12406
Independent reflections	3435 [R(int) = 0.0389]
Completeness to theta = 25.242°	99.9 %
Absorption correction	Semi-empirical from equivalents
Max. and min. transmission	0.4908 and 0.4609
Refinement method	Full-matrix least-squares on F^2
Data / restraints / parameters	3435 / 0 / 228
Goodness-of-fit on F^2	1.037
Final R indices [I>2sigma(I)]	R1 = 0.0259, wR2 = 0.0548
R indices (all data)	R1 = 0.0389, wR2 = 0.0606
Extinction coefficient	n/a
Largest diff. peak and hole	0.495 and -0.435 e.$Å^{-3}$
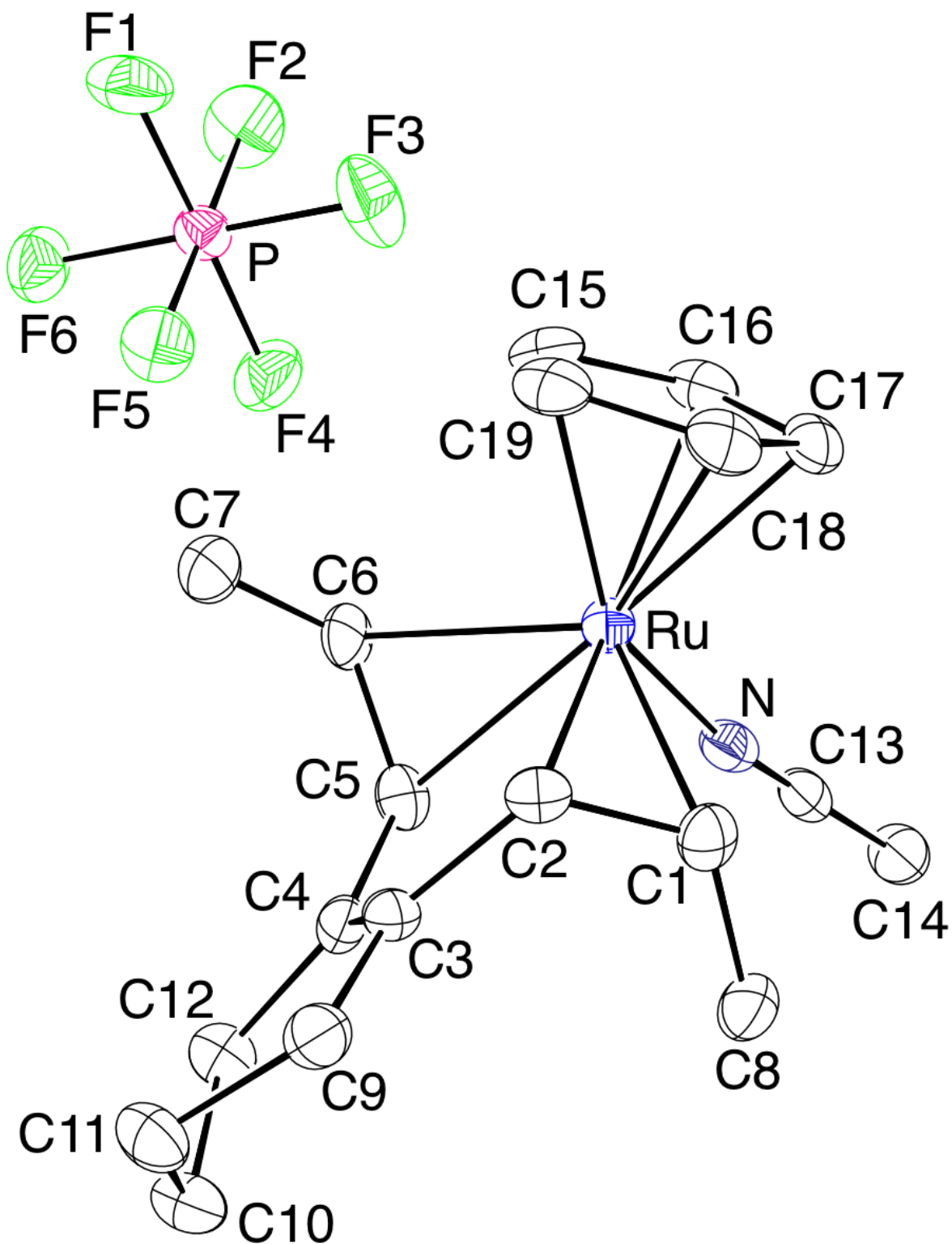
Figure 8-42. ORTEP view of complex **24**. Ellipsoids shown at 30% probability. Most hydrogens are omitted for clarity.

Table 8-8. Crystal data and structure refinement for complex **24**.

|	
Identification code	oconn_law_194_a
Empirical formula	C19 H26 F6 N P Ru
Formula weight	514.45
Temperature	100.0 K
Wavelength	0.71073 Å
Crystal system	Monoclinic
Space group	P 1 21/n 1
Unit cell dimensions	a = 7.9543(4) Å $\quad$ α = 90°.
	b = 21.9813(10) Å $\quad$ β = 101.531(2)°.
	c = 11.8304(7) Å $\quad$ γ = 90°.
Volume	2026.75(18) Å^3
Z	4
Density (calculated)	1.686 Mg/m^3
Absorption coefficient	0.910 mm^{-1}
F(000)	1040
Crystal size	0.25 x 0.2 x 0.15 mm^3
Theta range for data collection	1.986 to 25.419°.
Index ranges	-9<=h<=9, -19<=k<=25, -14<=l<=14
Reflections collected	12971
Independent reflections	3672 [R(int) = 0.0613]
Completeness to theta = 25.242°	98.6 %
Absorption correction	Semi-empirical from equivalents
Max. and min. transmission	0.2590 and 0.2158
Refinement method	Full-matrix least-squares on F^2
Data / restraints / parameters	3672 / 0 / 256
Goodness-of-fit on F^2	1.017
Final R indices [I>2sigma(I)]	R1 = 0.0421, wR2 = 0.0801
R indices (all data)	R1 = 0.0823, wR2 = 0.0922
Extinction coefficient	n/a
Largest diff. peak and hole	0.844 and -0.518 e.Å^{-3}

Figure 8-43. ORTEP view of complex **27**. Ellipsoids shown at 30% probability. Most hydrogens are omitted for clarity.

Table 8-9. Crystal data and structure refinement for complex **27**.

Identification code	oconn_law_238_0m_a_a_sq
Empirical formula	C35 H46 Cl2 D2 F12 P2 Ru2
Formula weight	1033.72
Temperature	100.0 K
Wavelength	0.71073 Å
Crystal system	Monoclinic
Space group	P 1 21/n 1
Unit cell dimensions	a = 15.520(5) Å $\qquad \alpha = 90°$.
	b = 15.706(5) Å $\qquad \beta = 110.448(4)°$.
	c = 18.633(6) Å $\qquad \gamma = 90°$.
Volume	4256(2) Å^3
Z	4
Density (calculated)	1.613 Mg/m^3
Absorption coefficient	0.988 mm^{-1}
F(000)	2072
Crystal size	0.25 x 0.2 x 0.15 mm^3
Theta range for data collection	1.477 to 25.327°.
Index ranges	-18<=h<=18, -14<=k<=18, -22<=l<=22
Reflections collected	34605
Independent reflections	7772 [R(int) = 0.0364]
Completeness to theta = 25.242°	100.0 %
Absorption correction	Semi-empirical from equivalents
Max. and min. transmission	0.2590 and 0.2304
Refinement method	Full-matrix least-squares on F^2
Data / restraints / parameters	7772 / 4 / 472
Goodness-of-fit on F^2	1.036
Final R indices [I>2sigma(I)]	R1 = 0.0466, wR2 = 0.1200
R indices (all data)	R1 = 0.0572, wR2 = 0.1284
Extinction coefficient	n/a
Largest diff. peak and hole	3.031 and -1.247 e.Å^{-3}
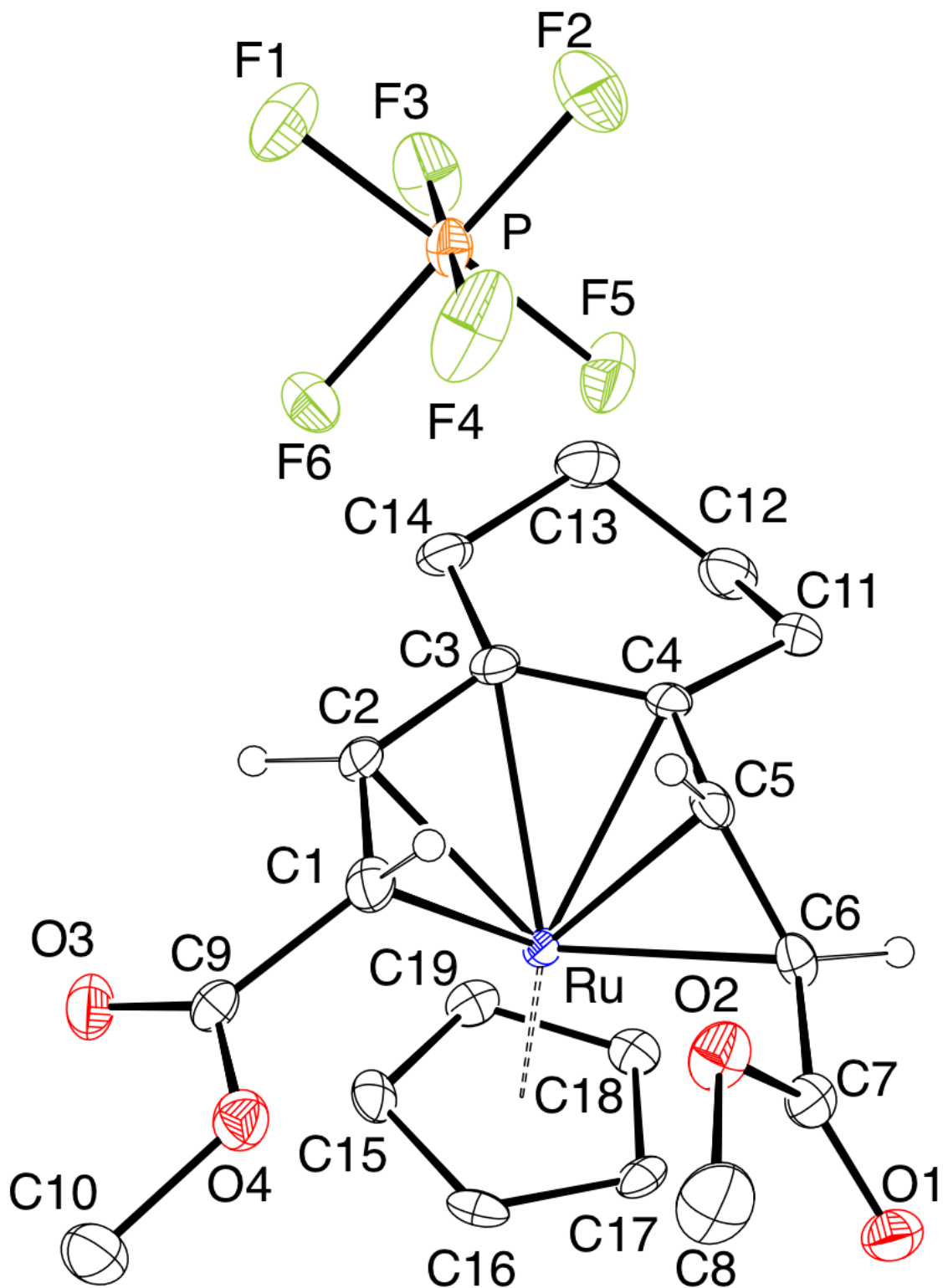
Figure 8-44. ORTEP view of complex **43**. Ellipsoids shown at 30% probability. Most hydrogens are omitted for clarity.

763

Table 8-10. Crystal data and structure refinement for complex **43**.

Identification code	law192
Empirical formula	C19 H23 F6 O4 P Ru
Formula weight	561.41
Temperature	100.0 K
Wavelength	0.71073 Å
Crystal system	Monoclinic
Space group	P 1 21/c 1
Unit cell dimensions	a = 8.0225(4) Å α = 90°.
	b = 14.1183(7) Å β = 101.393(2)°.
	c = 19.1718(10) Å γ = 90°.
Volume	2128.69(19) Å^3
Z	4
Density (calculated)	1.752 Mg/m^3
Absorption coefficient	0.887 mm^{-1}
F(000)	1128
Crystal size	0.055 x 0.05 x 0.04 mm^3
Theta range for data collection	1.804 to 26.369°.
Index ranges	-10<=h<=9, -14<=k<=17, -23<=l<=23
Reflections collected	24638
Independent reflections	4337 [R(int) = 0.0689]
Completeness to theta = 25.242°	100.0 %
Absorption correction	None
Refinement method	Full-matrix least-squares on F^2
Data / restraints / parameters	4337 / 0 / 282
Goodness-of-fit on F^2	1.022
Final R indices [I>2sigma(I)]	R1 = 0.0334, wR2 = 0.0823
R indices (all data)	R1 = 0.0472, wR2 = 0.0870
Extinction coefficient	n/a
Largest diff. peak and hole	0.808 and -0.603 e.Å^{-3}

Acknowledgement

Chapter 8 contains the material that is accepted for the publication "Transition-Metal Catalysis of Triene 6π Electrocyclization: The π-Complexation Strategy Realized". *Angew. Chem. Int. Ed.* **2020**, *accepted.* Qin, P.; Wang, L. A.; O'Connor, J. M.; Baldridge, K. K.; Li, Y.; Tufekci, B.; Chen, J.; Rheingold, A. L. The dissertation author is the first author on this paper.

H. References

1. Lewis, K. E.; Steiner, H. 588. The kinetics and mechanism of the thermal cyclisation of hexa-1-cis-3,5-triene to cyclohexa-1,3-diene. *J. Chem. Soc.* **1964**, 3080-3092.

2. Woodward, R.B.; Hoffmann, R. "Conservation of Orbital Symmetry," Verlag Chemie, Weinhiem, **1970**.

3. Bishop, L. M.; Barbarow, J. E.; Bergman, R. G.; Trauner, D. Catalysis of 6π electrocyclizations*. Angew. Chem. Int. Ed*. **2008**, 8100.

4. Carreno, R.; Chaudret, B.; Labroue, D.; Sabo-Etienne, S. Reactivity of ruthenium fragment Cp* Ru$^+$ with acyclic unsaturated hydrocarbons: a novel catalytic carbon-carbon bond activation reaction. *Organometallics* **1993**, *12*, 13-14.

5. Older, C. M.; Stryker, J. M. The Mechanism of Carbon-Carbon Bond Activation in Cationic 6-Alkylcyclohexadienyl Ruthenium Hydride Complexes. *J. Am. Chem. Soc*. **2000**, *122*, 2784-2797.

6. O'Connor, J. M.; Friese, S. J.; Rodgers, B. L. A transition-metal-catalyzed enediyne cycloaromatization. *J. Am. Chem. Soc.* **2005**, *127*, 16342-16343.

7. O'Connor, J. M.; Friese, S. J.; Tichenor, M. Ruthenium-mediated cycloaromatization of acyclic enediynes and dienynes at ambient temperature. *J. Am. Chem. Soc.* **2002**, *124*, 3506-3507.

8. Qin, P.; Cope, S. K.; Steger, H.; Veccharelli, K. M.; Holland, R. L.; Hitt, D. M.; Moore, C. E.; Baldridge, K. K.; O'Connor, J. M. Photoactivated Transition-Metal Triggers for

Ambient Temperature Enediyne and Dienyne Cyclization: Ruthenium-η^6-Naphthalene Complexes. *Organometallics* **2017**, *36*, 3967-3973.

9 O'Connor, J. M.; Friese, S. J.; Rodgers, B. L.; Rheingold, A. L.; Zakharov, L. An η^6-dienyne transition-metal complex. *J. Am. Chem. Soc*. **2005**, *127*, 9346-9347.

10. Veccharelli, K.M. Doctoral Dissertation, Conjugated Tri-Pi Systems: Investigations into Hexahapto Metal Complexes of Acyclic Conjugated Trienes and Novel Cycloaromatization Reaction of Nitrogen-Containing Enediynes. University of California, San Diego, CA, USA, **2017**.

11. Shu, C.; Shi, C. Y.; Sun, Q.; Zhou, B.; Li, T. Y.; He, Q.; Lu, X.; Liu, R. S.; Ye, L. W. Generation of Endocyclic Vinyl Carbene Complexes via Gold-Catalyzed Oxidative Cyclization of Terminal Diynes: Toward Naphthoquinones and Carbazolequinones. *ACS Catal.* **2018**, *9*, 1019-1025.

12. Odedra, A.; Datta, S.; Liu, R. S. Ruthenium-Catalyzed Cyclization of 2-Alkyl-1-ethynylbenzenes via a 1,5-Hydrogen Shift of Ruthenium-Vinylidene Intermediates. *J. Org. Chem.* 2007, *72*, 3289-3292.

13. (a) Chang, C. W.; Lin, Y. C.; Lee, G. H.; Wang, Y. Reactions of Ruthenium Cyclopropenyl Complexes Containing Pentamethyl cyclopentadienyl Ligands. *Organometallics* **2000**, *19*, 3211-3219. (b) Lundgren, R. J.; Rankin, M. A.; McDonald, R.; Stradiotto, M. Neutral, cationic, and zwitterionic ruthenium (II) atom transfer radical addition catalysts supported by P, N-substituted indene or indenide ligands. *Organometallics,* **2007**, *27*, 254-258. (c) Pavlik, S.; Jantscher, F.; Dazinger, G.; Mereiter, K.; Kirchner, K. Reactions of Ruthenium-Aminophosphane Complexes with Diynes: P-N Bond Activation and Formation of Novel Phosphaallyl, Azaallyl, and Aminocarbene Complexes. *Eur. J. Inorg. Chem.* **2006**, *2006* 1006-1021. (d) Duraczyńska, D.; Nelson, J. H. Phosphaallyl complexes of Ru (II) derived from dicyclohexylvinylphosphine (DCVP). *Dalton Trans.* **2005**, 92-103. (e) Lynam, J. M.; Milner, L. M.; Mistry, N. S.; Slattery, J. M.; Warrington, S. R.; Whitwood, A. C. [Ru(η^5-C$_5$H$_5$)(η^6-C$_{10}$H$_8$)]PF$_6$ as a catalyst precursor for the one-pot direct C–H alkenylation of nitrogen heterocycles. *Dalton Trans.* **2014**, *43*, 4565-4572.

14. For selected ruthenium-η^4-1,3-diene complexes: (a) Cadenbach, T.; Gemel, C.; Bollermann, T.; Fischer, R. A. Syntheses and Crystal Structures of Ruthenium and Rhodium Olefin Complexes Containing GaCp. *Inorg. Chem.* **2009**, *48*, 5021-5026. (b) Sato, H.; Bender, M.; Chen, W.; Krische, M. J. Diols, α-ketols, and diones as 22$_\pi$ components in [2 + 2 + 2] cycloadditions of 1, 6-diynes via ruthenium (0)-catalyzed transfer hydrogenation. *J. Am. Chem. Soc.* **2016**, *138*, 16244-16247. (c) Sánchez-Castro, M. E.; Paz-Sandoval, M. A. Comparative study of the reactivity of (Cp* RuCl)$_4$ and (Cp* RuCl$_2$)$_2$ with silylated dienyl Ligands. *Organometallics*, **2008**, *27*, 6083-6089. (d) Hull Jr, J. W.; Gladfelter, W. L. Synthesis, structure, and reactivity of Ru (. eta. 6-C$_6$Me$_6$)[. eta. 4-C$_6$Me$_4$(CH$_2$)$_2$]. An unusual transition-metal o-xylylene complex. *Organometallics*, **1982**, *1*, 1716-1718. (e) Hull Jr, J. W.; Gladfelter, W. L. eta.

4-Bonding in (arene) ruthenium complexes of octamethylnaphthalene. *Organometallics*, **1984**, *3*, 605-613. (f) Cotton, F. A.; Eiss, R. Stereochemically nonrigid organometallic molecules. XXIII. Crystal and molecular structures of (cyclooctatetraene) tricarbonylruthenium. *J. Am. Chem. Soc.* **1969**, *91*, 6593-6597.

15. Becker, E.; Mereiter, K.; Puchberger, M.; Schmid, R.; Kirchner, K. Metallacyclopentatriene-Butadienyl Carbene Rearrangement in the Oxidative Coupling of Alkynes Mediated by [RuCp(SbR$_3$)(CH$_3$CN)$_2$]$^+$ (R= Ph, n-Bu). *Organometallics*, **2003**, *22*, 2124-2133.

16. For selected ruthenium-η^6-triene structures: (a) Itoh, K.; Oshima, N.; Jameson, G. B.; Lewis, H. C.; Ibers, J. A. Structures, spectroscopy, and a mechanism of formation of linked-norbornadiene complexes of ruthenium (II). Interaction of ruthenium (II) with alicyclic hydrogen atoms. *J. Am. Chem. Soc.* **1981**, *103*, 3014-3023. (b) Planas, J. G.; Marumo, T.; Ichikawa, Y.; Hirano, M.; Komiya, S. Carbon–oxygen and carbon–sulfur bond activation of vinyl esters, ethers and sulfides by low valent ruthenium complexes. *J. Chem. Soc. Dalton Trans.* **2000**, 2613-2625. (c) Ball, R. G.; Kiel, G. Y.; Takats, J.; Krueger, C.; Raabe, E.; Grevels, F. W.; Moser, R. Dicarbonyltris (. eta. 2-trans-cyclooctene) ruthenium. Synthesis and molecular structure of the first stable M(CO)$_2$(olefin)$_3$ type compound. *Organometallics* **1987**, *6*, 2260-2261. (d) Suzuki, T.; Shiotsuki, M.; Wada, K.; Kondo, T.; Mitsudo, T. A. Syntheses and structures of novel zerovalent ruthenium monodentate amine complexes. *J. Chem. Soc. Dalton Trans.* **1999**, 4231-4237. (e) Grellier, M.; Vendier, L.; Sabo-Etienne, S. Ruthenium complexes carrying hydride, dihydrogen, and phosphine ligands: reversible hydrogen release. *Angew. Chem. Int. Ed.* **2007**, *46*, 2613-2615. (f) Steed, J. W.; Tocher, D. A.; Rogers, R. D. Ruthenium-mediated cyclodimerisation of buta-1,3-diene. *Chem. Commun.* **1996**, 1589-1590. (g) Itoh, K.; Masuda, K.; Fukahori, T.; Nakano, K.; Aoki, K.; Nagashima, H. Stoichiometric and catalytic dimerization of conjugated dienes with (C$_5$R$_5$) Ru (diene)$^+$. *Organometallics* **1994**, *13*, 1020-1029.

17. Aubert, C.; Gandon, V.; Han, S.; Johnson, B. M.; Malacria, M.; Schömenauer, S.; Vollhardt, K. P; Whitener, G. D. Cyclopentadienylcobalt-Mediated Intermolecular Cycloaddition of α, ω-Diynes to (Cyclo) alkenes: Synthesis of Linearly Fused Oligocycles and Extension to Enantiomerically Pure (6aR, 10aR)-Dihydroanthracyclinones. *Synthesis* **2010**, *2010*, 2179-2200.

18. Voigt, K.; von Zezschwitz, P.; Rosauer, K.; Lansky, A.; Adams, A.; Reiser, O.; de Meijere, A. The Twofold Heck Reaction on 1,2-Dihalocycloalkenes and Subsequent 6π-Electrocyclization of the Resulting (*E, Z, E*)-1,3,5-Hexatrienes: A New Formal {2 + 2 + 2}-Assembly of Six-Membered Rings. *Eur. J. Org. Chem.* **1998**, *1998*, 1521-1534.

19. Hirano, M.; Sakate, Y.; Inoue, H.; Arai, Y.; Komine, N.; Komiya, S.; Wang, X.; Bennett, M. A. Synthesis of conjugated diene complexes of ruthenium (0) derived from Ru (η^6-naphthalene)(η^4-1,5-COD): Z to E isomerisation of coordinated 1,3-pentadiene. *J. Organomet. Chem.* **2012**, *708*, 46-57.

20. Tantillo, D. J. Using theory and experiment to discover catalysts for electrocyclizations. *Angew. Chem. Int. Ed*. **2009**, *48*, 31-32.

21. King Jr, J. A.; Vollhardt, K. P. C. Thermally and photochemically induced vinyl-hydrogen activation of [η^4-1,2:3,4-(trans-1,3,5-hexatriene)](η^5-cyclopentadienyl) cobalt: Regio-and stereospecific hydrogen migrations. *J. Organomet. Chem*. **1994**, *470*, 207-222.

22. Brookhart, M.; Davis, E. R.; Harris, D. L. Low-temperature protonation of cyclooctatetraeneiron tricarbonyl and methylcyclooctatetraeneiron tricarbonyl. Generation and observation of cyclooctatrienyliron tricarbonyl cations. *J. Am. Chem. Soc*. **1972**, *94*, 7853-7858.